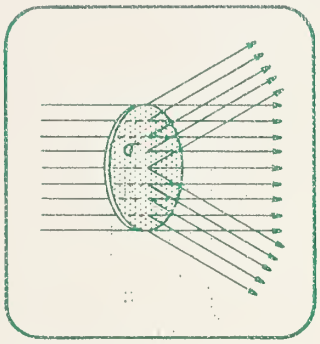

Neutron Cross Sections and Technology

Proceedings of a Conference

Washington, D.C.
March 4-7, 1968

NBS Special Publication 299
Volume I

U.S. DEPARTMENT OF COMMERCE / NATIONAL BUREAU OF STANDARDS

U.S. DEPARTMENT OF COMMERCE
C. R. Smith, Secretary
NATIONAL BUREAU OF STANDARDS
A. V. Astin, Director

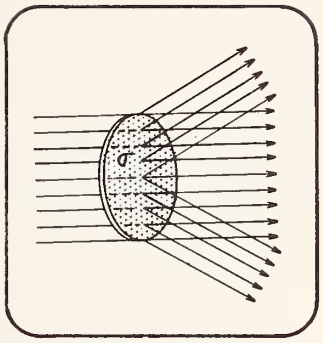

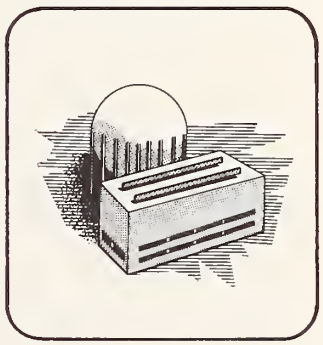

Neutron Cross Sections and Technology

Proceedings of a Conference

Washington, D.C.
March 4-7, 1968

Edited by
D. T. Goldman
Center for
Radiation
Research
National Bureau of Standards
Washington, D.C., 20234

U.S. National Bureau of Standards, Special Publication 299, - Issued SEPT. 1968

Volume I, Sessions A-D, Pages 1-640

For sale by the Superintendent of Documents, U.S. Government Printing Office, Woshington, D.C. 20402 – Price $10.50 per set of 2 volumes

Abstract

The Second Conference on Neutron Cross Sections and Technology was held in Washington, D.C. on March 4-7, 1968. Papers from this Conference have been published in two volumes, as follows: Volume I, Sessions A-D, pages 1-640; Volume II, Sessions E-H, pages 641-1337. These volumes contain the texts of the invited and contributed papers of the Conference. Topics covered include: The need for neutron data in fields of science and technology; standard data and flux measurements; the determination of neutron cross sections by theoretical and experimental techniques; a presentation of recently measured data and their utilization in a variety of applications.

Key words: cross sections, neutrons, nuclear data, nuclear technology, reactors.

Library of Congress Catalog Card Number: 68-60083

Foreword

The National Bureau of Standards, along with the other sponsoring institutions, has been most gratified with the conduct of this second in a series of conference designed to bring neutron cross section measurers and users together. The first conference was entitled, "Neutron Cross Section Technology," and was held in Washington, D. C., March 22-24, 1966. Its success prompted the "Second Conference on Neutron Cross Sections and Technology," held in Washington, D. C., on March 4-7, 1968.

The sponsors generally, and the Center for Radiation Research particularly, are keenly interested in promoting effective coupling between basic and applied radiation research. These conferences have proved to be a most successful exercise in the transfer of technology. We look forward to more of these symposia in the future. For this recent one, we wish to acknowledge the very capable manner in which the General Chairman, Dr. David T. Goldman, of the Center for Radiation Research, conducted the conference.

Carl O. Muehlhause, Director
Center for Radiation Research
National Bureau of Standards

Preface

These are the proceedings of the Second Conference on Neutron Cross Sections and Technology held at the Shoreham Hotel in Washington, D. C., 1968. The meeting was sponsored by the Atomic Energy Commission, the National Bureau of Standards, the American Physical Society, and the Reactor Physics and Shielding Divisions of the American Nuclear Society. There were 320 registrants of whom approximately 20% came from outside the United States.

The purpose of this conference, as elucidated in its prospectus, was to provide a common meeting area for the exchange of information among nuclear scientists and engineers interested in neutron cross sections. The program was designed to consider aspects of neutron cross sections in the following sequence: the need for accurate measurements; their determination by theoretical and experimental techniques; and their applications. As indicated in the Table of Contents, the conference was divided into eight sessions, each lasting a half day. Each session consisted of two or three invited talks, which are distinguishable in these pages by their greater length, and contributed papers. No attempt was made to record the comments and questions following each oral presentation in order to retain informality at the meeting. By requesting one speaker to summarize several papers dealing with a single topic, it was possible to avoid simultaneous sessions and yet present over half of the more than one hundred contributed papers. There is, however, no distinction made between those presented orally and those accepted for publication only. The report of the panel summarizing the contents of the meeting was recorded verbatim and subsequently edited. It is suggested that the reader turn to these pages first to receive an impression of the general flavor of the meeting, prior to turning to specific research contributions.

Following a well established custom for the rapid dissemination of the proceedings of scientific conferences, it was decided to publish this volume by direct photoreproduction of manuscripts provided by the authors. The editor would like to acknowledge the cooperation of the authors who provided a suitable copy promptly, thereby assisting the speedy publication of these proceedings. Any errors appearing herein are, however, the responsibility of the editor, though effort was made to avoid them by retyping where necessary.

The editor, who also functioned as Conference Chairman, would like to thank the members of the Program Committee who were responsible for arranging the choice of speakers, the selection of contributed papers, and an initial review of the manuscripts. They responded immediately to any request from the chairman. The success of the conference was due to the Committee members, many of whom also functioned as session chairmen, to the speakers, and, most important of all, to the attendees who provided well attended sessions complete with stimulating discussions. The

experience provided by the initial conference and its Chairman, Professor W. W. Havens, Jr., and the example of its Proceedings, CONF-660303 (1966) edited by P. Hemmig were of extreme value. The most delightful and informative speech delivered by Congressman Craig Hosmer of California, Ranking minority member on the Joint Committee on Atomic Energy, following the Conference banquet was one of the high points of the meeting. The talk entitled, "The Scientific Establishment, Where Is It Headed?" provided many points for future discussions and will be published in PHYSICS TODAY.

Appreciation is expressed to the sponsoring organizations without whose encouragement and financial assistance this Conference would not have taken place.

The editor gratefully acknowledges the assistance of the NBS Office of Technical Information and Publications and secretarial assistance of Mrs. Sue Damron and Miss Wanda Hein in the preparation of these proceedings.

March 1968

David T. Goldman
National Bureau of Standards

Contents, Volume I

Contents, Volume II

Papers from Sessions E, F, G, and H - Pages 641 through 1341

CONFERENCE CHAIRMAN

David T. Goldman, National Bureau of Standards

PROGRAM COMMITTEE:

J. R. Beyster, Gulf General Atomic
R. C. Block, Rensselaer Polytechnic Institute
D. Bogart, National Aeronautics and Space Administration
R. S. Caswell, National Bureau of Standards
F. Feiner, Cornell University
J. L. Fowler, Oak Ridge National Laboratory
D. T. Goldman, National Bureau of Standards
H. Goldstein, Columbia University
P. Greebler, General Electric--Advanced Products Operations
E. Haddad, Atomic Energy Commission
D. R. Harris, Bettis Atomic Power Laboratory
W. W. Havens, Columbia University
A. Hemmendinger, Los Alamos Scientific Laboratory
P. B. Hemmig, Atomic Energy Commission
J. C. Hopkins, Los Alamos Scientific Laboratory
M. H. Kalos, New York University
S. Pearlstein, Brookhaven National Laboratory
J. L. Russell, Gulf General Atomic
A. B. Smith, Argonne National Laboratory

ARRANGEMENTS COMMITTEE

E. H. Eisenhower, National Bureau of Standards
F. J. Shorten, National Bureau of Standards

Session A

THE NEED FOR AND USE OF NEUTRON DATA IN FIELDS OF BASIC AND APPLIED SCIENCE

Chairman

J. R. BEYSTER
Gulf General Atomic

THE ROLE OF NEUTRONS IN ASTROPHYSICAL PHENOMENA*

WILLIAM A. FOWLER

California Institute of Technology, Pasadena, California 91109

ABSTRACT

Although yeoman work has been done by Macklin and Gibbons at Oak Ridge on neutron capture cross sections in the ~ 1 to ~ 100 keV range for application to the s-process of nucleosynthesis in stars, yet much research in this and related fields is still needed. Many important isotopic cross sections are still unmeasured. At Los Alamos Seeger has continued his important studies of the properties of the unstable neutron-rich nuclei but more experimental and theoretical work is required to reach an understanding of the r-process of nucleosynthesis. At Rice University Clayton has analyzed the empirical data needed to reach a more complete understanding of the chronology of nucleosynthesis in the Galaxy. At the California Institute of Technology studies continue on reactions such as $C^{13}(\alpha,n)$ which serve as sources of neutrons in stars. The situation as of March, 1968 is reviewed with especial emphasis being placed on the correlation of astrophysical and geochemical observations with predictions based on experiment and theory in neutron physics.

*Supported in part by the National Science Foundation [GP-7976, formerly GP-5391] and the Office of Naval Research [Nonr-220(47)].

1. INTRODUCTION

Neutrons play many roles in the drama of astrophysical phenomena. Along with protons they are one of the fundamental building blocks from which all nuclei can be synthesized.[1] Charged particle reactions are impeded by Coulomb barriers and become ineffective in nucleosynthesis beyond the iron-group nuclei. Unhampered by Coulomb barriers, neutrons build the heavy nuclei.

Two years ago at the First Conference on Neutron Cross Sections and Technology, George I. Bell [1] discussed in some detail the two processes by which nuclei are synthesized by the multiple capture of neutrons in stars, supernovae, and other astronomical objects. These two processes are (1) the s-process in which the neutron captures are slow (s) compared to the intervening beta decays and (2) the r-process in which the neutron captures are rapid compared to the beta decays. In the r-process, photo-ejection of neutrons plays an important role in near equilibrium with neutron captures. Since Bell's paper discussed the detailed operation of the two processes as well as the experimental situation in regard to the relevant neutron cross-section measurements as of early 1966, I will not attempt a fundamental discussion of the theory of the two processes. I will instead concentrate on an up-dating of the experimental information on cross sections and binding energies still needed for correlation with observations on elemental and isotopic abundances in meteorites, the sun and other stars. In addition, I will discuss a recent suggestion concerning the site of the s-process and, finally, the recently suggested role of neutrons in explosive nucleosynthesis.

2. MULTIPLE NEUTRON CAPTURE IN STELLAR NUCLEOSYNTHESIS

The separation of heavy element synthesis by multiple neutron capture into the s- and r-processes was first clearly demonstrated by Burbidge, Burbidge, Fowler & Hoyle [2] who noted double abundance peaks at the magic neutron numbers N = 50, 82 and 126. The double peaks associated with N = 82 are illustrated in Fig. 1 and are discussed in the caption. B^2FH [2] pointed out that the path of the s-process proceeded through the valley of nuclear stability while the r-process proceeded along the neutron-rich slope of this valley. They also pointed out that the rare proton-rich nuclei (low mass isotopes of the elements) could not be produced by neutron capture processes and attributed their production to the p-process involving the capture of protons or the photo-ejection of neutrons. The p-process was taken to be much less probable than neutron capture under astrophysical circumstances. The s-process path is illustrated in Fig. 2, taken from Clayton, Fowler, Hull & Zimmerman [3], for the case of the synthesis of the isotopes of tin. CFHZ [3] chose tin as a particularly good example because it has a large number of isotopes, namely ten. These isotopes have not been chemically

[1] Inside nuclei, neutrons and protons may exist part of the time in their "excited states" which high-energy physicists identify as coequal "elementary particles." However, under astrophysical circumstances it is neutrons and protons and the very stable combination of two neutrons and two protons, the alpha particle, which are the principal transfer agents in the nuclear transmutations by which nucleosynthesis occurs. Thus cross sections involving these particles are the *sine qua non* in the application of nuclear physics to astrophysical phenomena.

fractionated since their nucleosynthesis and thus tell us the true results of this nucleosynthesis. As shown in Fig. 3, CFHZ [3] pointed out that the relative abundance of the ten tin isotopes clearly indicated the operation of the s-, r-, and p-processes.

3. THE S-PROCESS

Conclusive quantitative confirmation in the case of the s-process, to which we will now turn, came from the brilliant experimental measurements of Macklin & Gibbons and their collaborators [4] at Oak Ridge who measured neutron capture cross sections, often employing isotopically pure targets, in the energy range from ~ 1 keV to above 100 keV. The results of Macklin, Inada & Gibbons [5] for neutron capture cross sections for seven of the isotopes of tin at 30 keV are given in Table 1. The energy, 30 keV, corresponds to $T \sim 3.5 \times 10^8$ °K which is a reasonable estimate for the temperature at which s-process neutrons become available in stars. The operation of the s-process is governed by the set of differential equations

$$dN_A/dt = -\varphi_n(\sigma_A N_A - \sigma_{A-1} N_{A-1}) \qquad (1)$$

where φ_n is the neutron flux, N_A is the abundance of the stable isobar at atomic mass A on the s-process path and σ_A is its neutron capture cross section. This equation assumes that the beta decay lifetimes of unstable isobars at A are short compared to their neutron capture lifetimes. Solutions of this set of equations for a number of possible neutron exposure distributions, $\rho(\tau) \propto \tau^{-n}$, where τ is the time integrated neutron flux ($d\tau = \varphi_n dt$), are shown in Fig. 4 taken from Seeger, Fowler & Clayton.[2]

TABLE 1

σN for TIN ISOTOPES

Nucleus	Process	σ (30 keV) (mb)	N(abundance) $\frac{\text{isotope}}{\text{element}}$	σN	N_r	$\sigma N_s = \sigma(N - N_r)$
Sn 116	s	92 ± 19	0.142	13.1	0	13.1
117	sr	390 ± 82	0.076	29.5	~ 0.040	13.9
118	sr	59 ± 12	0.240	14.2	~ 0.045	11.5
119	sr	243 ± 51	0.086	20.9	~ 0.040	11.1
120	sr	35 ± 7	0.330	11.5	~ 0.045	10.0
122	r	23 ± 5	0.047	1.1	0.047	--
124	r	23 ± 4	0.060	0.8	0.060	--

[2] These solutions assume that the seed nucleus was Fe^{56}, the most abundant of the iron-group nuclei. The results are to a certain extent independent of the seed nucleus or nuclei assumed. It has been suggested by Amiet and Zeh, in a paper submitted to this conference, that r-process nuclei are the seeds for the p-process. Since r-process nuclei have an abundance distribution which decreases with A it would be expected that a fit to the observations might be obtained with a larger n than for Fe^{56}, or the iron-group nuclei, as seeds. This is being investigated by D. D. Clayton, J. G. Peters, and myself.

The ledges in this figure correspond to $\sigma_A N_A \sim$ constant, which will be the case when dN_A/dt is small compared to either of the two terms on the right-hand side of Eq. 1. This occurs when the cross sections are reasonably large. The precipices occur when magic-N nuclei with small cross sections hold up the flow of the s-process so that dN_A/dt is comparable to $\sigma_{A-1}N_{A-1}$(magic N) and $\sigma_A N_A$ for the next nucleus and subsequent nuclei are correspondingly smaller along a new ledge.

The tin isotopes studied by MG [4] fall on the ledge between A $\sim$ 90, N = 50 and A $\sim$ 138, N = 82. Thus σN_s, where N_s is the s-process abundance relative to total Sn, should be roughly constant or slightly decreasing for those isotopes of tin produced in the s-process as determined in Fig. 2. Table 1 shows that this is indeed the case after correction for small r-process contributions, $N_s = N - N_r$, is made. The r-process contribution is estimated from the abundance of the r-only isotopes, Sn^{122} and Sn^{124}. For these isotopes, it will be noted that σN bears no relation to $\sigma N \sim \sigma N_s$ for Sn^{116} to Sn^{120} as should be the case where $N_s = 0$, $N = N_r$. Note that relative isotopic abundances to total elemental Sn and not absolute solar-system abundances have been used in this analysis.

SFC [6] used cross sections determined by MG [4], or systematic estimates where experimental values were not available, plus solar-system abundances compiled from meteorite determinations by Urey [7] and others to produce a curve for $f_A = \sigma_A N_A$ vs. A similar to that shown in Fig. 5. This figure is actually taken from Seeger & Fowler [8]. It clearly gives an observational demonstration of the ledge and precipice structure from which parameters characteristic of the s-process exposure of solar-system material are determinable. The apparent cut-off in the power law $\rho(c) \propto \tau^{-3.2}$ at $\tau_{max} = 1.35 \times 10^{27}$ neutrons cm^{-2} will be referred to in the sequel.

Danziger [9] used the abundances he observed in γ Pavonis and other stars to show that the neutron exposure for the material in these stars was in general different than that in the sun. Nevertheless the ledge and precipice structure for the σN curves for these stars is clearly shown in Fig. 6 taken from Danziger's paper.

The analysis by MG [4] of the σN_s product for tin isotopes was complicated by the necessity of making an r-process correction to obtain $N_s = N - N_r$. For this reason MG [4] measured the cross sections for samarium which has two s-only isotopes, Sm^{148} and Sm^{150}, and for tellurium which has three s-only isotopes (excluding possible very small p-process contributions), Te^{122}, Te^{123} and Te^{124}. The results are shown in Tables 2 and 3 where it will be apparent that the relative σN are the same for the s-only isotopes of Sm and of Te respectively, and that the other σN products show considerable spread as is expected since r-process contributions, where possible, to Sm and Te isotopic abundances are quite substantial and not small as in the case of Sn.

The σN_s behavior on a precipice is illustrated quantitatively in Tables 4 and 5 for Sr and Zr respectively where, after corrections for small r-process contributions are made, a decrease of σN_s with A is unmistakably indicated. This is also indicated in Fig. 7 which represents an up-dating of Fig. 5 to be discussed in more detail later. In Fig. 7 σN_s for Sr and Zr are plotted using solar-system abundances rather than relative isotopic abundances and the drop in σN_s from Sr^{86} through Zr^{94} is quite marked. At this point we might remark parenthetically that it is fair to raise some question concerning either the neutron capture cross section or the

TABLE 2

σN for SAMARIUM ISOTOPES

Nucleus	Process	σ (30 keV) (mb)	N(abundance) isotope/element	σN
Sm 144	p	150 ± 70	0.031	5 ± 2
147	rs	1170 ± 190	0.150	175 ± 28
148	s	257 ± 50	0.112	28.9 ± 5.6
149	rs	1620 ± 280	0.138	224 ± 39
150	s	370 ± 72	0.074	27.4 ± 5.3
152	rs	410 ± 70	0.267	110 ± 19
154	r	325 ± 60	0.227	74 ± 14

TABLE 3

σN for TELLURIUM ISOTOPES

Nucleus	Process	σ (30 keV) (mb)	N(abundance) isotope/element	σN
Te 122	s	248 ± 40	0.0246	6.1 ± 1.0
123	s	842 ± 80	0.0087	7.3 ± 0.7
124	s	167 ± 25	0.0461	7.7 ± 1.2
125	sr	458 ± 60	0.0699	32.0 ± 4.2
126	sr	89 ± 15	0.1871	16.6 ± 2.8
128	r	33 ± 10	0.3179	10.5 ± 3.2
130	r	14 ± 5	0.3448	4.8 ± 1.7

TABLE 4

σN for STRONTIUM ISOTOPES

Nucleus	Process	σ (30 keV) (mb)	N(abundance) isotope/element	σN	N_r EST	$\sigma N_s = \sigma(N - N_r)$
Sr 86	s	75 ± 15	0.0986	7.4 ± 1.5	0	7.4 ± 1.5
87	sr	108 ± 20	0.0702	7.6 ± 1.4	0.007	6.8 ± 1.2
88	sr	6.9 ± 1.7	0.8256	5.7 ± 1.4	0.078	5.2 ± 1.3

TABLE 5

σN for ZIRCONIUM ISOTOPES

Nucleus	Process	σ (30 keV) (mb)	N(abundance) $\frac{\text{isotope}}{\text{element}}$	σN	N_r EST	$\sigma N_s = \sigma(N - N_r)$
Zr 90	$s_m r$	11 ± 3	0.515	5.7 ± 1.5	0.030	5.3 ± 1.5
91	sr	59 ± 10	0.112	6.6 ± 1.1	0.025	5.2 ± 0.9
92	sr	34 ± 6	0.171	5.8 ± 1.0	0.030	4.8 ± 0.8
94	sr	21 ± 4	0.174	3.7 ± 0.7	0.028	3.1 ± 0.6
96	r	41 ± 12	0.028	1.1 ± 0.3	0.028	--

meteoritic abundance for Y^{89}, the only isotope of yttrium, for which σN_s is substantially less than its correct position on the precipice between Sr^{89} and Zr^{90}.

As noted above, Fig. 7 is an up-dating to early 1968 of Fig. 5, vintage 1966. New measurements for σ and new determinations for N_s have been included. In addition there are included points based on cross-section estimates made by Macklin & Gibbons (private communication) in connection with new and urgent theoretical calculations now being undertaken by Seeger (private communication). These estimates (see caption of Fig. 7 for identification) are based on the best available systematics and theory of nuclear capture cross sections but seem to yield discrepant σN_s values in a number of cases. Thus new measurements are needed and these have been summarized in Table 5. In addition to difficulties concerning germanium, barium and osmium we note that special emphasis should be placed on isotopic measurements in cadmium which has eight isotopes and is similar to tin in this context. The new cross section estimates which lower the ledge between A = 140 and A = 200 should be checked by actual measurement. The cross section for Y^{89} should probably be remeasured although there is a good chance that its abundance in meteorites relative to Sr and Zr is not correctly known.

Lead is the last element mentioned in Table 6 and, although r-process contributions to lead abundances are substantial, this section will be concluded with a discussion of this element. Lead is interesting in that it has georadiogenic contributions from the decay of natural radioactivity since the formation of the solar system. It is believed that these contributions can be eliminated by using the abundances observed in iron meteorites which contain little uranium and thorium. However, cosmoradiogenic contributions from radioactive decay of r-process nuclei during galactic nucleosynthesis prior to the formation of the solar system are not eliminated in this way. Thus the calculation of r-process contributions for the lead isotopes is fairly complicated and is related to that for uranium and thorium discussed in the next section.

In Table 7 the situation in regard to lead isotopic abundances and cross sections is presented. The relative isotopic abundances in iron meteorites have been normalized to the total lead abundance observed spectroscopically in the sun by Helliwell [10]. More recent determinations by Mutschlecner [11], Grevesse, Blanquet & Boury [12] and Ross, Aller & Mohler [13] average

TABLE 6

NEUTRON CAPTURE CROSS SECTIONS NEEDED
FOR CLARIFICATION OF S-PROCESS

Nuclei	Remarks
All Fe-Cr Isotopes	Required for Cu-Ni synthesis.
Ge 70, 72, 73, 74	Reverse trend in σN but discrepancy in Ge 74 measurements.
Cd 106 to 116	Eight isotopes, five s-process. Similar to tin.
Ba 130 to 138	Current estimates for σ yield reverse trend in σN.
Os 186, 187, 188	Current estimates yield high σN. Cosmochronology: Re 187 → Os 187.
Pb 208	Present error ($\sigma = 3^{+1}_{-2}$) leaves cosmochronology uncertain.

TABLE 7

LEAD ABUNDANCES (Si = 10^6 SCALE)

	Iron Meteorites	N_r	N_s	σ (mb)	σN_s
Pb 204	0.05	0	0.05	43	2.2
206	0.47	0.24	0.23	9.6	2.2
207	0.52	0.33	0.19	8.7	1.6
208	1.46	0.12	1.34	3^{+1}_{-2}	4^{+2}_{-3}
	2.50				

Solar Pb	2.5	Helliwell (1961)
	$1.4^{+2.1}_{-0.8}$	Mutschlecner (1963)
	1.8	Grevesse, Blanquet & Boury (1967)
	3.2	Ross, Aller & Mohler (1967)

Nota Bene: Total Pb > 1.6 for $N_s(207) > 0$

out to Helliwell's value. This value, lead/silicon = 2.5×10^{-6}, is considerably greater than that found in ordinary chondritic meteorites and is even somewhat greater than the value, 1.6×10^{-6}, found in the Orgueil meteorite (7) which is a carbonaceous chondrite. The r-process abundances, N_r, are determined quite independently of the observed abundances through r-process calculations normalized as discussed in the next section. Considerable confidence can be placed in these r-process values. The resulting $N_s = N - N_r$ values are multipled by the cross sections from MG [4] to obtain σN_s. Clayton & Rassbach [14] show that the SF [8] neutron exposure with cut-off cannot account for these σN_s-values which look much more like equilibrium values (σN_s = constant) characteristic of a substantial exposure

with $\tau > 2.50 \times 10^{27}$ neutrons cm^{-2}. This may indicate that r-process nuclei in the N = 126 peak near A = 195 have served as seeds for the s-process. To reach a clearer understanding of the situation a more accurate cross section for Pb^{208} is required. Although MG [4] give the Maxwellian averaged cross section at kT = 30 keV as 2.9 mb, in a private communication they point out that the error is (+1,-2) mb. Finally in this connection there is one point which must be emphasized. Because the r-process contributions are fairly well established a lower limit on the overall lead abundance can be obtained by setting the s-process contribution to Pb^{207}, for example, equal to zero. This leads to total Pb > 1.6 on the Si = 10^6 scale. Observational values below this number are suspect and should be investigated carefully for reliability. In fact $N_s(Pb^{207})$ is certainly not zero and a reliable lower limit in round numbers is Pb ≥ 2. This corresponds to log Pb ≥ 1.8 on the astronomical scale on which log H = 12, log Si = 7.5.

4. THE SITE OF THE S-PROCESS

During the past year R. H. Sanders [15] has suggested a promising site for the s-process. He suggests that neutrons will be produced by interactions among the light nuclei and captured by heavy seed nuclei in the helium burning shells of "mild" Population II stars during their red giant stage of stellar evolution. Population II stars are those old stars formed early in the history of the Galaxy when the primordial gas contained few heavy elements. Those remaining now have masses equal to or less than that of the sun (low mass stars age very slowly) and their counterparts, which formed with greater mass, are thought to have evolved to the point where they slowly (planetary nebulae) or rapidly (supernovae) ejected much of their mass into the interstellar medium. This ejected mass contained new elements synthesized during the evolution of these stars. From the interstellar medium, laden with nuclear debris, young Population I stars such as the sun are thought to have formed. Mild Population II stars are intermediate in this scheme of things and do contain some heavy elements, particularly the iron group, inherited from extreme Population II stars.

Sanders' ideas are illustrated very schematically and not to scale in Fig. 8. Schwarzschild & Härm [16] showed that helium burning in low mass Population II stars eventually leads to an inert C^{12} core surrounded by a helium burning shell in which C^{12} is being produced via 3 $He^4 \rightarrow C^{12}$. They found this shell burning to be thermally unstable and to lead to flashes or relaxation oscillations in which the large nuclear energy generated led to convective instability and consequent large scale mixing. This mixing reached through inert, unburned helium previously produced by 4 $H^1 \rightarrow He^4$ into the outer region containing unburned hydrogen. Sanders points out that the hydrogen mixed down to the outer parts of the helium burning shell in which C^{12} is being produced will rapidly react at the ambient temperature of 10^8 °K according to $C^{12}(p,\gamma)N^{13}(e^+\nu)C^{13}$ to produce C^{13}. The half life of the N^{13} is only 10 minutes and it will beta decay rather than react with additional protons. In fact, if too many protons are not injected into the outer layer of the helium burning shell, the C^{12} will consume the protons and the C^{13} will survive to mix still deeper to temperatures as high as 2×10^8 °K. There it can interact with helium to release neutrons in the reaction $C^{13}(\alpha,n)O^{16}$. These neutrons are captured by heavy seed nuclei such as Fe^{56} to form still heavier elements by $Fe^{56}(n,\gamma)Fe^{57}(n,\gamma)Fe^{58}(n,\gamma)Fe^{59}$ $(e^-\bar{\nu})Co^{59}(n,\gamma)Co^{60}(e^-\bar{\nu})Ni^{60}(n,\gamma)Ni^{61}$..... These capture reactions are indeed the beginning of the s-process which terminates by re-cycling involving alpha and beta radioactivity in the lead and bismuth isotopes:

$Pb^{206}(n,\gamma)Pb^{207}(n,\gamma)Pb^{208}(n,\gamma)Pb^{209}(e^{-}\bar{\nu})Bi^{209}(n,\gamma)Bi^{210}(e^{-}\bar{\nu})Pb^{210}(\alpha)Pb^{206}$.... The heavy elements are mixed outward by the convection and are eventually dispersed into the interstellar medium in the eventual disruption of the star. Thus proceeds the s-process and Sanders adduces quantitative arguments to show that sufficient heavy elements are produced in "mild" Population II stars to account for the abundances observed in Population I stars.

Critical to the above argument is the rate of the $C^{13}(\alpha,n)O^{16}$ reaction. Fortunately this has recently been measured in our laboratory by my former student, C. N. Davids [17], whose results are shown in Fig. 9. It would seem that all is well with the s-process!

5. THE R-PROCESS

The abundances due to the r-process are not correlated at all with neutron capture cross sections as is illustrated in Fig. 10 taken from CFHZ [3]. On the other hand these abundances are thought to be proportional to the beta decay lifetimes of neutron-rich progenitor nuclei which lie in the r-process capture path. The problems associated with the estimation of the binding energies and beta decay lifetimes of these nuclei will be discussed at this Conference by P. A. Seeger and so discussion of r-process theory will be omitted here and correlations with observations will be stressed.

By the use of the σN_s curve in Fig. 5 and of cross section measurements for σ it is possible to determine many unknown values for N_s. Subtraction from solar-system abundance N then yields N_r. For nuclei bypassed in the s-process, $N_s = 0$ and $N_r = N$ directly. In this way Fig. 11 was prepared by SFC [6]. The abundance peaks characteristic of the r-process at $A \sim 80$ ($N = 50$), $A \sim 130$ ($N = 82$) and $A \sim 195$ ($N = 126$) are clearly apparent and can be accounted for quantitatively by the detailed theory of the r-process. In simple terms the peaks arise from the relatively long lifetimes of the magic N progenitors in the r-process path. Of considerable interest is the broad hump among the rare earth elements near $A \sim 160$. This has been ascribed to the additional stability and longer lifetimes of deformed nuclei between the closed shells at $N = 82$ and $N = 126$. Clayton & Fowler [18] used s- and r-process calculations to calculate abundances in this region for comparison with observations on rare earth abundances in meteorites made by Schmitt, Smith, Lasch, Mosen, Olehy & Vasilevskis [19]. The motivation for this particular comparison lies in the fact that rare earth elements will have been relatively less fractionated since nucleosynthesis than other elements. The comparison is shown in Table 8 where it will be noted that the "absolute" calculations of CF [18] need only be normalized by a factor 0.7 to give agreement with SSLMOV [19] to within a factor better than 2 in all cases.

It is believed that a deformation hump similar to that observed in the rare earths will occur around $A \sim 250$ in between the closed shells at $N = 126$ and $N = 184$. This hump will occur in the abundances for nuclei which are the progenitors of Th^{232}, U^{235} and U^{238}, the parents of the natural radioactive series. Thus it is salutary to have good agreement between observation and theory in the rare earth region.

Several groups of authors have extended the r-process calculations into the trans-bismuth region where this process alone operates since the s-process terminates by alpha decay re-cycling in the lead and bismuth isotopes. The

TABLE 8

COMPARISON OF OBSERVED AND CALCULATED ABUNDANCES OF RARE EARTHS
(Si = 10^6 SCALE)

Element	Average in 12 Chondrites[a]	Calculated ($\times$ 0.7)[b]	Ratio
La	0.39	0.49	1.3
Ce	1.05	0.82	0.8
Pr	0.16	0.12	0.7
Nd	0.66	0.54	0.8
Sm	0.23	0.42	1.8
Eu	0.081	0.104	1.3
Gd	0.33	0.29	0.9
Tb	0.054	0.058	1.1
Dy	0.31	0.31	1.0
Ho	0.075	0.059	0.8
Er	0.21	0.25	1.2
Tm	0.032	0.042	1.3
Yb	0.18	0.27	1.5
Lu	0.031	0.025	0.8
	3.8	3.8	

[a] SSLMOV [19]
[b] CF [18] [$0.7 \times (N_r + N_s)$]

motivation is to calculate the expected abundances of thorium and uranium which have important bearing on the chronology of nucleosynthesis. In the calculation of the abundance of Th^{232}, U^{235} and U^{238} produced by the r-process it must be recalled, as first pointed out by B^2FH [2], that these nuclei have progenitors at atomic masses other than A = 232, 235 and 238 respectively. For example, in the case of U^{235}, alpha decay follows beta decay for all nuclei produced at A = 239, 243, 247, 251, and 255. Thus the abundances produced at these mass numbers contribute on a relatively short time scale to the U^{235} abundance. This sequence of progenitors terminates at A = 255 since the beta stable nucleus at A = 259 is thought to decay by spontaneous fission rather than by alpha decay. The consequences for the total abundance of U^{235} are shown in the middle column of Table 9 prepared by Hoyle & Fowler [20]. Similar arguments apply to the calculation of the abundances of Th^{232} and U^{238} although slight complications arise as noted in the table at A = 248, 250 and 252 where both alpha decay and spontaneous fission occur. The normalization indicated in the table was determined empirically by HF [20] by comparing similar calculations by them with observations in the region A $\sim$ 120 to 180.

It must be noted that the calculations for the Th^{232}, U^{235} and U^{238} require a chronological model of nucleosynthesis in the Galaxy prior to the formation of the solar system since these nuclei decay even while they are being produced. HF [20] used the continuous synthesis model extending back to an assumed origin of the Galaxy some 12×10^9 years ago as first proposed by Fowler & Hoyle [21] and subsequently discussed by Fowler [22] and Clayton [23]. In addition the exponential decay since the origin of the solar system must be taken into account as is done in the last line of Table 9 to obtain present day abundances. These r-process abundances are

TABLE 9

TH AND U ABUNDANCES PRODUCED IN THE R-PROCESS (Si = 10^6 SCALE)

Th^{232}		U^{235}		U^{238}	
A	Yield	A	Yield	A	Yield
232	0.078	235	0.074	238	0.098
236	0.083	239	0.114	242	0.157
240	0.142	243	0.143	246	0.134
244	0.148	247	0.117	250(0.10α)	0.012
248 (0.89α)	0.110	251	0.109		
252 (0.86α)	0.101	255	0.105		
Sum (each r-event)	0.662		0.662		0.401
Normalized	0.20 ± 0.07		0.20 ± 0.07		0.12 ± 0.04
4.6×10^9 yr ago	0.16 ± 0.05		0.02 ± 0.007		0.068 ± 0.023
Now	0.13 ± 0.04		$(2.4\pm0.8)\times10^{-4}$		0.034 ± 0.011

TABLE 10

THORIUM & URANIUM ABUNDANCES (Si = 10^6 SCALE)

	Th	U
Ordinary Chondrites Urey (1964)	0.027 ± 0.004	0.009 ± 0.003
Carbonaceous Chondrites Morgan & Lovering (1967)	0.040 ± 0.009	0.012 ± 0.004
R-Process Calculations Hoyle & Fowler (1963) Seeger, Fowler & Clayton (1965)	 0.13 ± 0.04 0.20 ± 0.05	 0.034 ± 0.011 0.049 ± 0.012
Solar Spectroscopy Grevesse, Blanquet & Boury (1967)	0.12 ± 0.03	Difficult to observe

entered in Table 10 for comparison with observations on meteorites and the sun. Quite independent calculations by SFC [6] are also entered as an indication of the overall uncertainties in the r-process abundances. The two sets agree within their estimated uncertainties (± 25 to 30%). On the other hand the r-process abundances are definitely larger than the thorium and uranium abundances listed in Table 10 for ordinary chondrites, U [7], and for carbonaceous chondrites, Morgan & Lovering [24]. This discrepancy has constituted a major problem for some years in regard to nucleocosmochronology and the radioactive content and heating of the earth and moon as discussed, for example, by HF [20].

For numerous reasons uranium and thorium are difficult to observe spectroscopically in the sun. Recently, GBB [12] have identified one thorium line in the sun and find the value entered in Table 10.

This value is in agreement with the r-process prediction but clearly more observations are needed. It must also be stressed, however, that more information on the masses, binding energies and beta decay lifetimes of neutron-rich nuclei are needed in the r-process calculations and P. A. Seeger will speak to this need when he addresses this Conference.

6. EXPLOSIVE NUCLEOSYNTHESIS

Gamow's "big bang" during the early stages of the expanding universe is the prototype of explosive nucleosynthesis. Wagoner, Fowler & Hoyle [25] have recently repeated the early calculations of Fermi & Turkevich [26] on nucleosynthesis in the "big bang" using modern nuclear reaction rate data. They confirm the original conclusion that elements beyond helium cannot be produced in "big bang". At the same time they found that some heavy element production will occur in the explosion of supermassive stars ($M \gtrsim 10^3\ M_\odot$). This result has been confirmed and verified by Wagoner [27]. A typical example of the abundances resulting from the explosion of a star with mass equal to $\sim 10^3\ M_\odot$ is shown in Fig. 12. The abundances produced show a marked similarity to solar-system abundances in relative proportions but are all low relative to helium in the solar system. This is not as discouraging as it might seem since old Population II stars are deficient in the heavy elements but do show relative proportions similar to solar-system abundances. Population II stars may well have inherited their small but definite amounts of heavy elements from very rapid contamination of the primordial gas of the Galaxy by debris from rapidly evolving supermassive stars.

Wagoner's results are critically dependent on cross-section estimates for a number of neutron induced reactions as listed in Table 11. It will

TABLE 11

NEUTRON REACTION CROSS SECTIONS NEEDED IN EXPLOSIVE NUCLEOSYNTHESIS

Reaction	Q (MeV)	Resonances E_r(cm,keV),J^π	Reaction	Q (MeV)	Resonances E_r(cm,keV),J^π
$Li^6(n,\gamma)Li^7$	7.253	222, $\frac{5}{2}^-$	$C^{13}(n,\gamma)C^{14}$	8.176	147, 1^+ or 2^+
$Be^9(n,\gamma)Be^{10}$	6.815	562, 3^- 733, 2^+	$N^{14}(n,\gamma)N^{15}$	10.835	470, 600,
$B^{10}(n,\gamma)B^{11}$	11.456	220, $\frac{5}{2}^+$ or $\frac{7}{2}^+$ 490, $\frac{3}{2}^-$ or $\frac{5}{2}^+$	$O^{16}(n,\gamma)O^{17}$	4.143	409, $\frac{3}{2}^-$
			$O^{17}(n,\gamma)O^{18}$	8.046	160, 2^+ 233, 3^-
$B^{11}(n,\gamma)B^{12}$	3.369	18, $\leq 3^+$ 390, 2^+	$O^{18}(n,\gamma)O^{19}$	3.956	150,
$C^{12}(n,\gamma)C^{13}$	4.947	560 ?	$Ne^{20}(n,\gamma)Ne^{22}$	6.760	540,
$Be^7(n,\alpha)He^4$	18.991	~ 0, 2^- 150, 3? 320, 3^+	$O^{17}(n,\alpha)C^{14}$	1.819	160, 2^+ 233, 3^-

All (n,γ), (n,α) & (n,p) multiresonance reactions for nuclei with $A > 20$ over the energy range 10 keV to 3 MeV.

be noted that the (n,γ) and (n,α) cross sections at certain specific low lying resonances in nuclei from Be^7 to Ne^{20} are urgently needed. Above Ne^{20} level densities become large and Maxwellian averaged cross sections for kT $\sim$ 10 keV to 3 MeV are needed for (n,γ), (n,α) and (n,p) reactions. Neutron physicists have much to do before the origin of the heavy element abundances in the first stars which formed in the Galaxy is understood.

7. OMISSIONS

Lack of space and time has prevented discussion of the following topics:

(1) The lifetime of the neutron. The recent redetermination of this basic physical datum, 10.80 ± 0.16 min, by Christensen, Nielsen, Bahnsen, Brown & Rustach [28] differs by more than the combined probable errors from the previously accepted value, 11.7 ± 0.3 min, due to Sosnovsky, Spivak, Prokofiev, Kutikov & Dobrinin [29]. This change increases the square of the axial vector coupling constant of the weak interaction by approximately 10%. In turn the rate of the pp-reaction in the sun and other stars is increased by the same amount. Bahcall & May [30] show that the central temperature of the sun is thereby decreased and the probability of detecting B^8 neutrinos from the sun is lowered by 30%. New, independent measurements are urgently needed to resolve the disparity in the Danish-Russian results.

(2) The primary and secondary effects of neutrons in spallation processes on the surfaces of stars.

(3) The production of neutrons in flares on the surface of the sun and the possibility of detection of these neutrons in satellites and space probes.

(4) The role of neutron stars in astronomy and the possibility of detecting such objects.

8. EPILOGUE

In this paper an appeal has been made for additional measurements on neutron interaction cross sections and binding energies for a variety of nuclei in order to lead to further clarification of the operation of the s-process and the r-process in stars and supernova and of the role of neutrons in explosive nucleosynthesis. This has been done in full awareness of the dangers expressed so succinctly by Abe Zarem, a good friend since our graduate student days at Caltech, in the following passage:

> "The terrible tragedies of science are the horrible murders of beautiful theories by ugly facts."

This paper is dedicated to Robert G. Thomas (1923-1956) who contributed so much to our understanding of nuclear interactions throughout his lifetime both as a graduate student in our laboratory and as a staff member at the Los Alamos Scientific Laboratory.

313-475 O-68—3

The author wishes to acknowledge assistance in the work leading to the preparation of this paper from N. Bahcall, G. R. Caughlan, D. D. Clayton, G. J. Michaud, J. G. Peters, J. Rasmussen, P. A. Seeger, R. V. Wagoner, and B. A. Zimmerman.

9. REFERENCES

(After the first reference in the text these papers are referred to by B [1], B^2FH [2], etc. etc.)

1. G. I. Bell, Cross Sections for Nucleosynthesis in Stars and Bombs, Proceedings of the First Conference on Neutron Cross Sections and Technology, Washington, D.C. (1966). Also Rev. Mod. Phys. 39, 59 (1967).
2. E. M. Burbidge, G. R. Burbidge, W. A. Fowler & F. Hoyle, Rev. Mod. Phys. 29, 547 (1957); Science 124, 611 (1956).
3. D. D. Clayton, W. A. Fowler, T. E. Hull & B. A. Zimmerman, Ann. Phys. 12, 331 (1961).
4. R. L. Macklin & J. H. Gibbons, Rev. Mod. Phys. 37, 166 (1965); Phys. Rev. 159, 1007 (1967); Science 156, 1039 (1967); Astrophys. J. 149, 577 (1967); Astrophys. J. 150, 721 (1967).
5. R. L. Macklin, T. Inada & J. H. Gibbons, Nature 194, 1272 (1962).
6. P. A. Seeger, W. A. Fowler & D. D. Clayton, Astrophys. J. Suppl. No. 97, 11, 121 (1965).
7. H. C. Urey, Rev. Geophys. 2, 1 (1964). For later results see Qu. Jour. Roy. Astron. Soc. 8, 23 (1967).
8. P. A. Seeger & W. A. Fowler, Astrophys. J. 144, 822 (1966).
9. I. J. Danziger, Astrophys. J. 143, 527 (1966).
10. T. M. Helliwell, Astrophys. J. 133, 566 (1961).
11. P. Mutschlecner, Thesis, University of Michigan (1962).
12. N. Grevesse, G. Blanquet & A. Boury, Proceedings of Conference on "Origin & Distribution of the Elements," Paris (1967).
13. J. Ross, L. H. Aller & O. C. Mohler, Proc. Nat. Acad. Sci. 59, 1 (1968).
14. D. D. Clayton & M. E. Rassbach, Astrophys. J. 148, 69 (1967).
15. R. H. Sanders, Astrophys. J. 150, 971 (1967).
16. M. Schwarzschild & R. Härm, Astrophys. J. 150, 961 (1967).
17. C. N. Davids, Nucl. Phys. in press (1968).
18. D. D. Clayton & W. A. Fowler, Ann. Phys. 16, 51 (1961).
19. R. A. Schmitt, R. H. Smith, J. E. Lasch, A. W. Mosen, D. A. Olehy & J. Vasilevskis, Geochim & Cosmochim. Acta 27, 577 (1963).
20. F. Hoyle & W. A. Fowler, Isotopic and Cosmic Chemistry, Chapter 30, ed. H. Craig, S. Miller & G. J. Wasserburg (North-Holland Publishing Co., Amsterdam, 1963).
21. W. A. Fowler & F. Hoyle, Ann. Phys. 10, 280 (1960).
22. W. A. Fowler, Proceedings of the Rutherford Jubilee International Conference (Heywood & Co., Ltd., London, 1961) p. 640.
23. D. D. Clayton, J. Geophys. Res. 68, 3715 (1963).
24. J. W. Morgan & J. F. Lovering, Nature 213, 873 (1967).
25. R. V. Wagoner, W. A. Fowler & F. Hoyle, Astrophys. J. 148, 3 (1967).
26. E. Fermi & A. Turkevich, quoted in R. A. Alpher & R. C. Herman, Rev. Mod. Phys. 22, 153 (1950).
27. R. V. Wagoner, Astrophys. J. in press (1968).
28. C. J. Christensen, A. J. Nielsen, A. Bahnsen, W. K. Brown & B. M. Rustach, Phys. Letters 26B, 11 (1967).
29. A. N. Sosnovsky, P. E. Spivak, Y. A. Prokofiev, I. E. Kutikov & Y. P. Dobrinin, Nucl. Phys. 10, 395 (1959).
30. J. N. Bahcall & R. M. May, Astrophys. J. in press (1968).

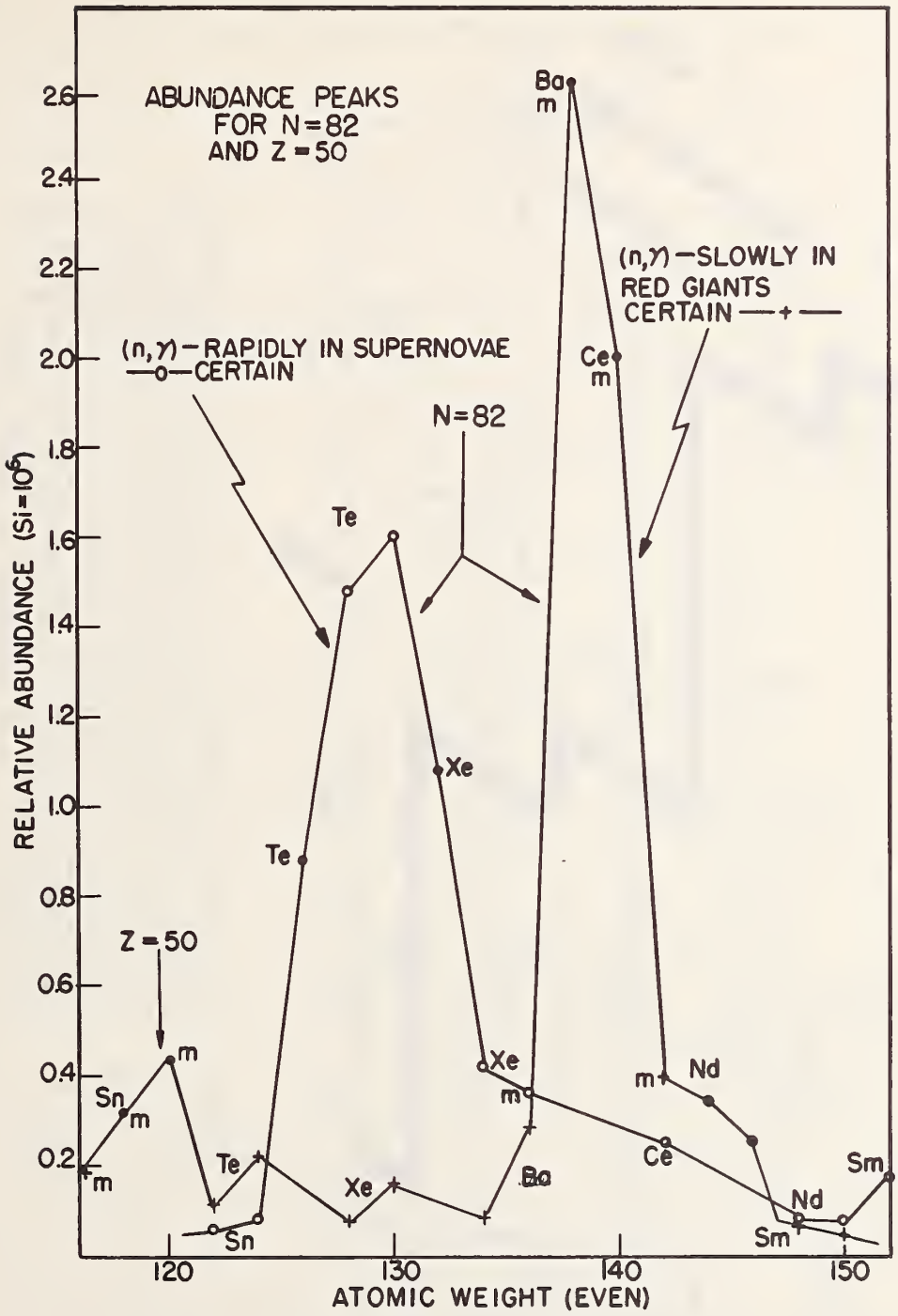

Fig. 1. The even-A abundance peaks near A = 130 and 138. The peak near A = 138 is ascribed to the s-process in which $_{56}Ba_{82}^{138}$ and $_{58}Ce_{82}^{140}$, for example, are actually in the path of nucleosynthesis. Their large abundance is attributed to their small neutron capture cross section which follows that both are nuclei with a closed neutron shell (N = 82). The peak near $_{52}Te_{78}^{130}$ is attributed to the r-process in which the progenitor, before beta decay, of $_{52}Te_{78}^{130}$ was $_{48}Cd_{82}^{130}$ which calculations show should have a longer beta decay lifetime and thus a greater abundance than its immediate neighbors on the path of r-process synthesis.

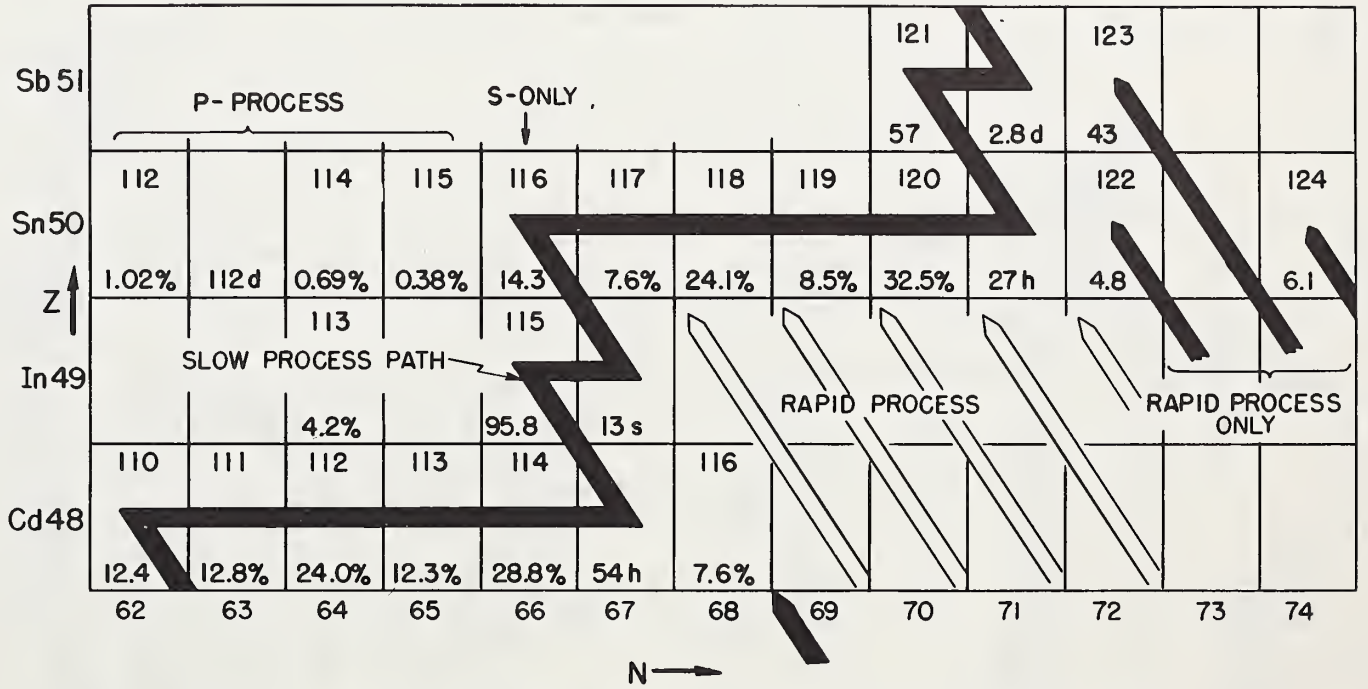

Fig. 2. The s-process path through the isotopes of tin. The neutron number increases by units of one on a slow time scale until negative beta activity occurs and the path moves to the isobar of higher Z. This path can be determined from empirical evidence on the beta stability of nuclei. Note that the path bypasses the p-process and the r-process nuclei. The r-process nuclei are the end products of an isobaric beta-decay chain as shown at the far right from neutron-rich progenitors produced in an intense neutron flux. The p-process nuclei are produced by subjecting a small fraction of s- and r-process nuclei to an intense proton or photon flux.

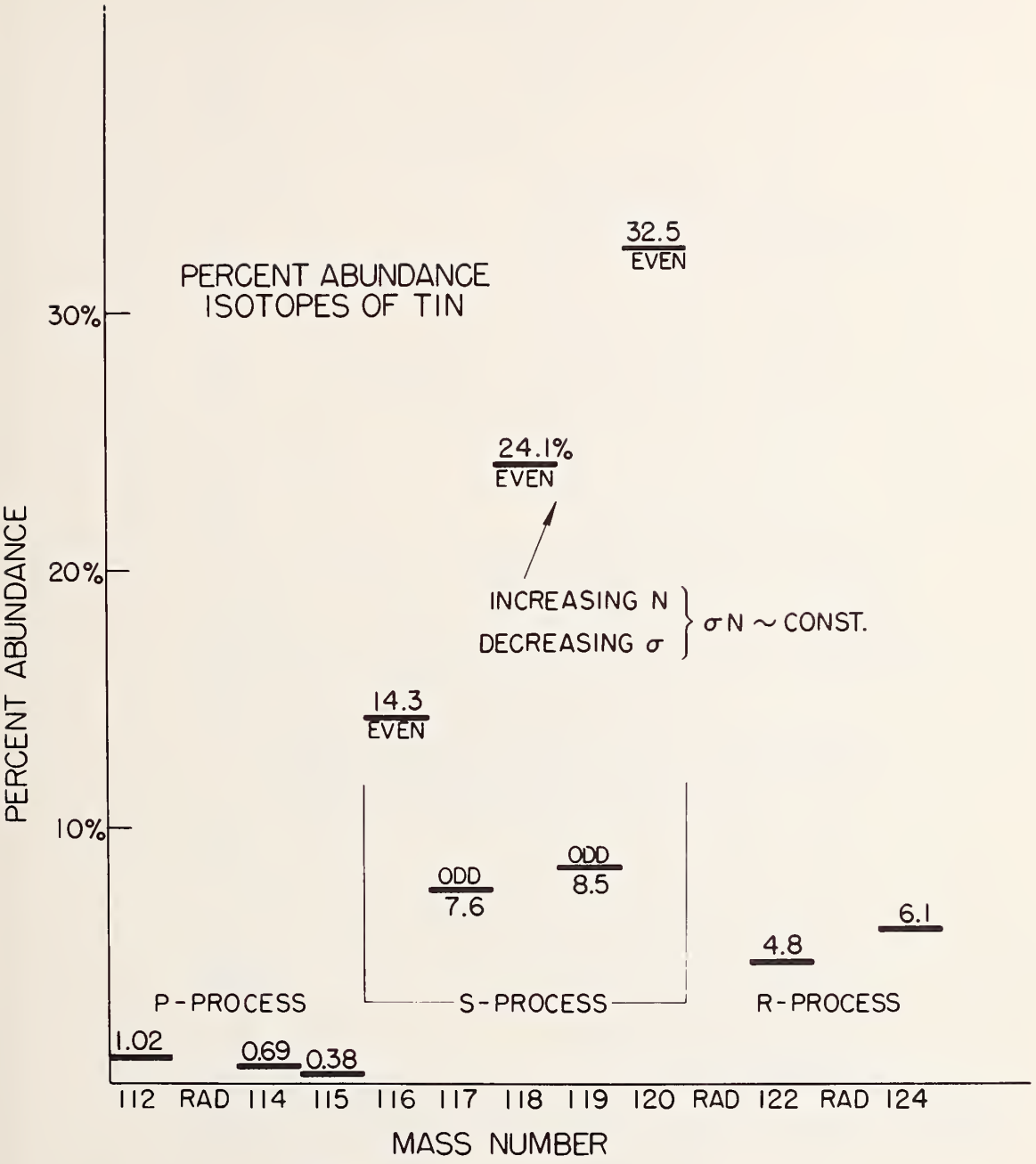

Fig. 3. Abundance evidence for the operation of three separate processes, p, s, and r, in the formation of the stable isotopes of the element tin. The first three isotopes can only be produced in the relatively rare p-process involving charged particles (protons) or radiation and their abundances are seen to be quite small. The next five isotopes are produced by neutron capture at a slow rate (s-process) and exhibit the regularity expected for this process-decreasing capture cross section, hence increasing abundance, with increasing mass number. The last two isotopes are produced only by neutron captures at a rapid rate (r-process) and the discontinuity between the s-process and the r-process is quite apparent.

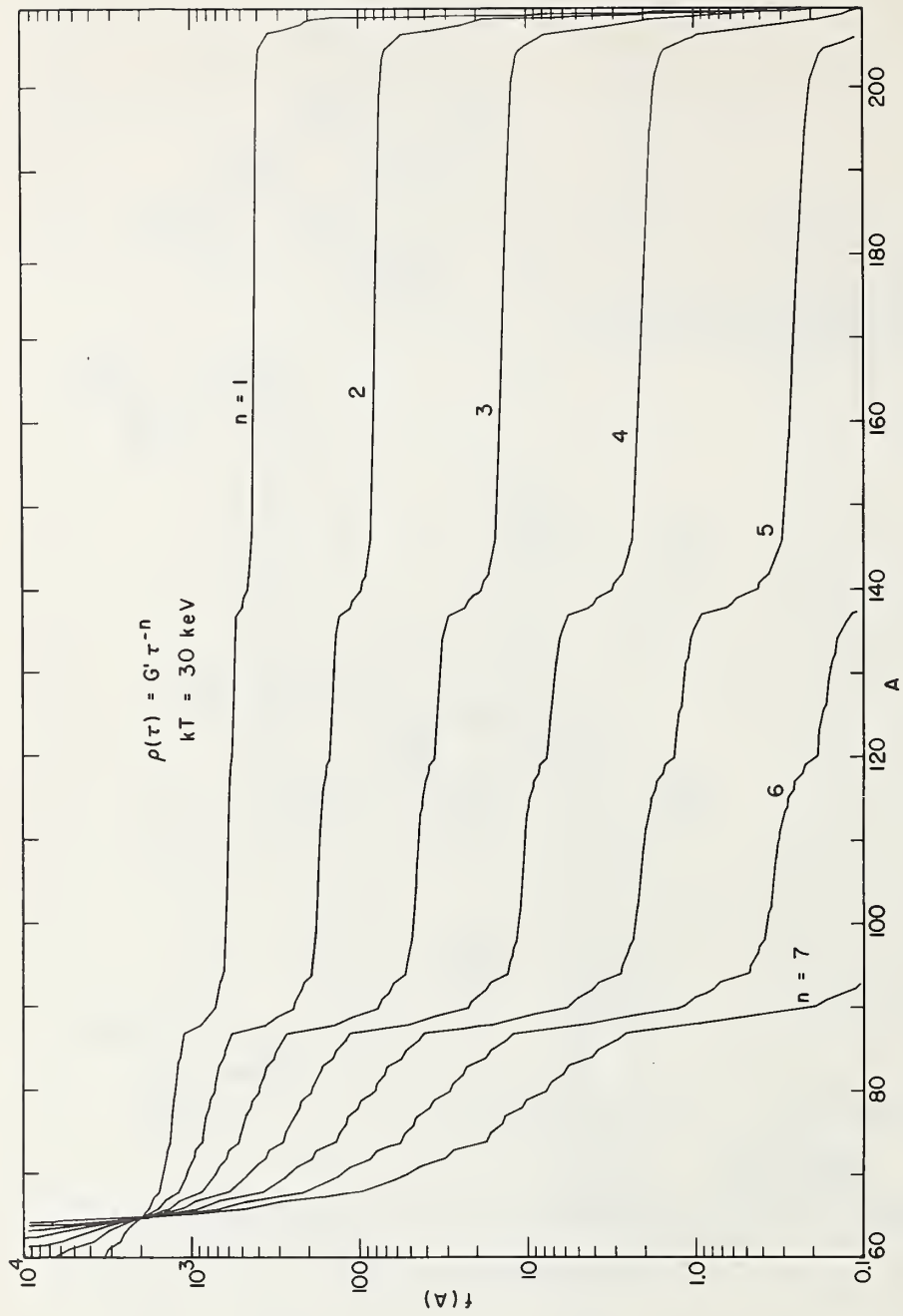

Fig. 4. The product $f(A) = \sigma_A N_A$ calculated for various neutron exposure distributions, $\rho(\tau) \propto \tau^{-n}$, n = 1 to 7. These calculations assume that Fe^{56} was the seed nucleus. Note the ledge and precipice nature of the solutions and compare with observations in Fig. 5.

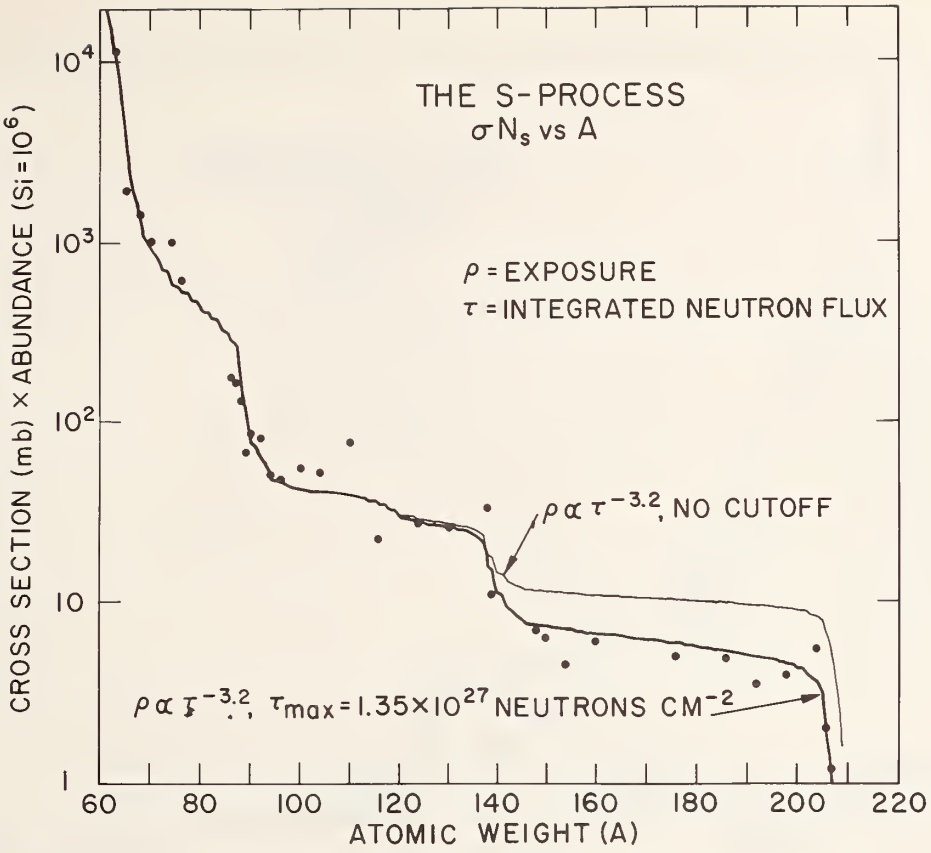

Fig. 5. Neutron capture cross section (σ) at 30 keV times the solar-system abundance attributable to the s-process (N_s). See SFC [6] for details of experimental points. The heavy curve is that calculated for exposures to integrated neutron flux given by $\rho \propto \tau^{-3}$. The light-curve is that calculated without cutoff in τ.

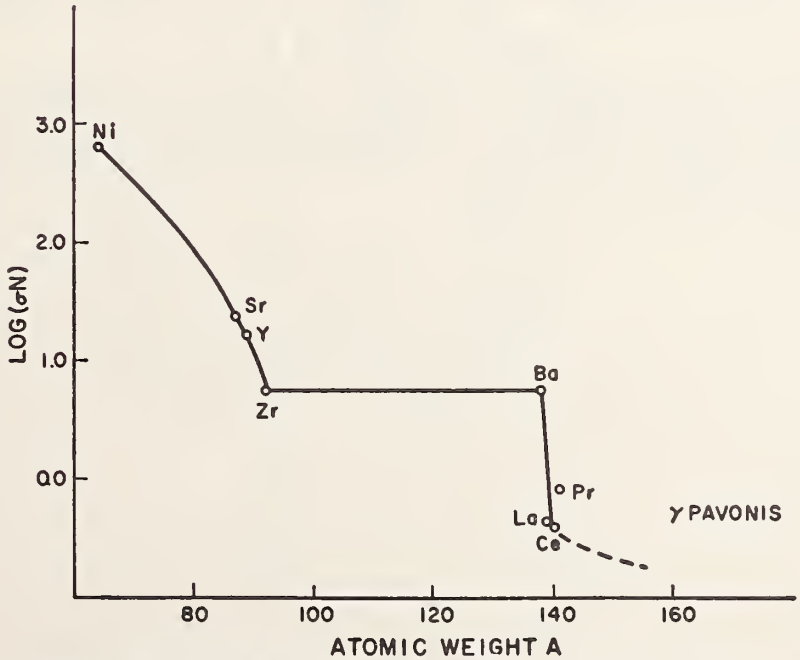

Fig. 6. Plot of log Nσ versus atomic mass A for a number of different stellar objects.

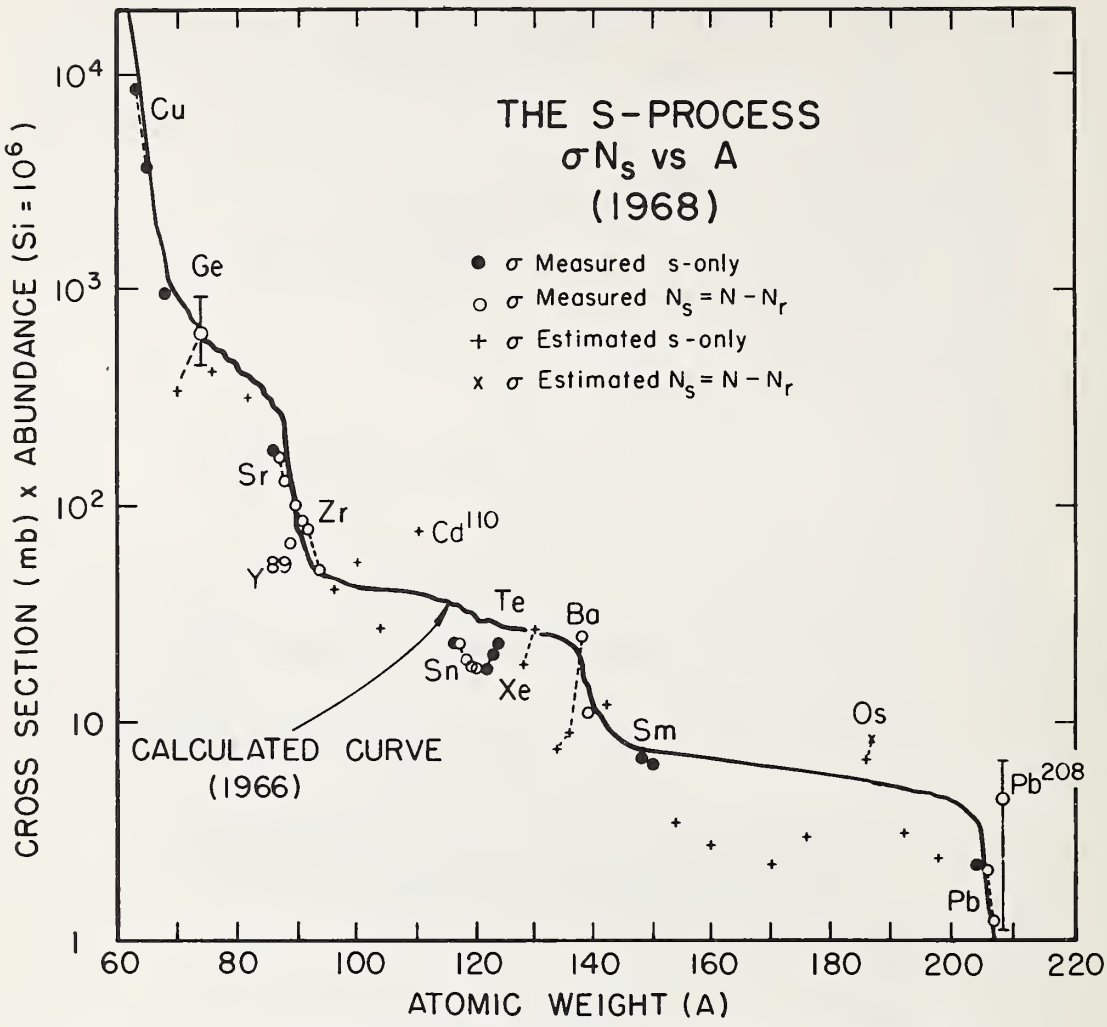

Fig. 7. Fig. 5 (1966) updated to early 1968. The points are designated by ● for an s-only nucleus with measured cross section, by o for an s > r nucleus with measured cross section, by + for an s-only nucleus with estimated cross section, and by x for an s > r nucleus with estimated cross section.

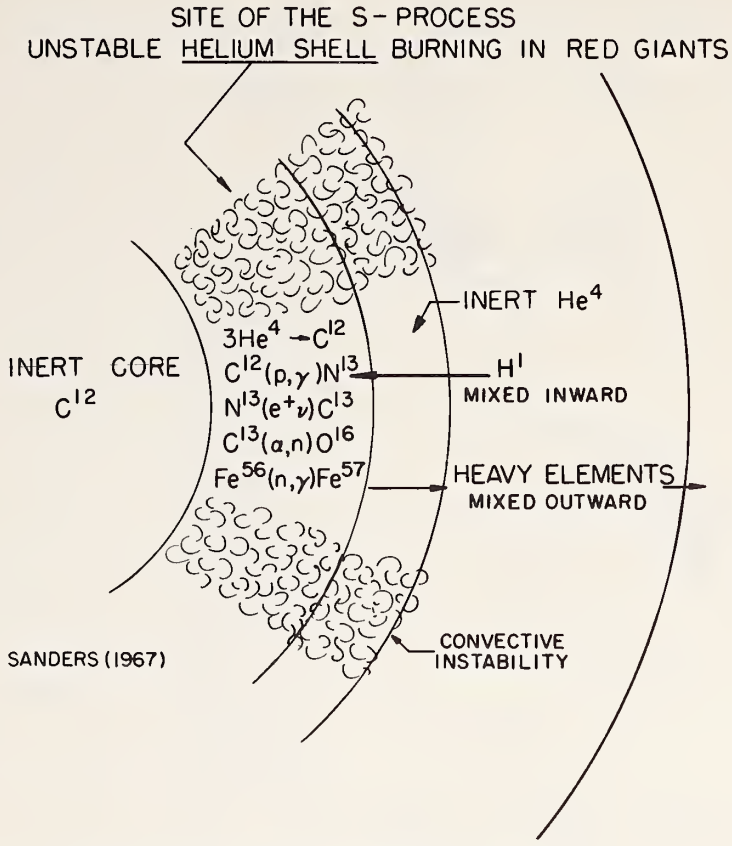

Fig. 8. The site of the s-process discussed in the text.

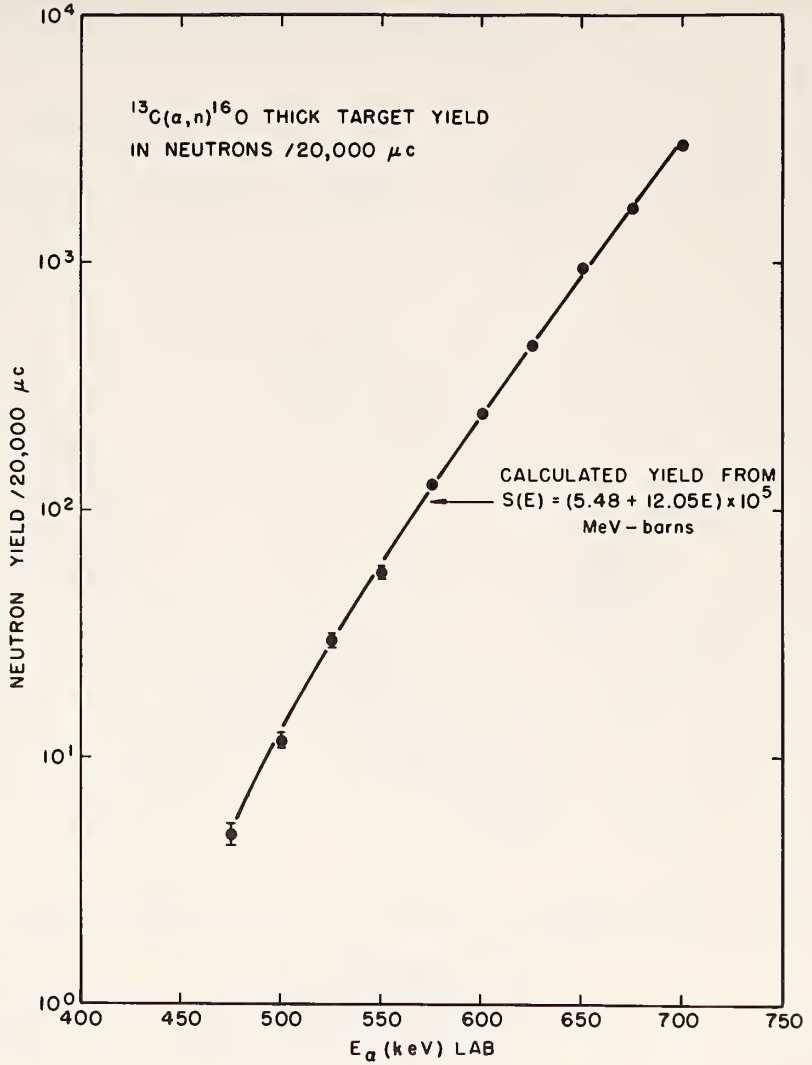

Fig. 9. Yield of the $C^{13}(\alpha,n)O^{16}$ reaction versus energy. The experimental data, Davids [17], is fitted to a curve derived from $\sigma = S(E)E^{-1} \exp(-20.77\ E^{-1/2})$ with $S(E) = (5.48 + 12.05E) \times 10^5$ MeV barns and with center-of-momentum energy E in MeV.

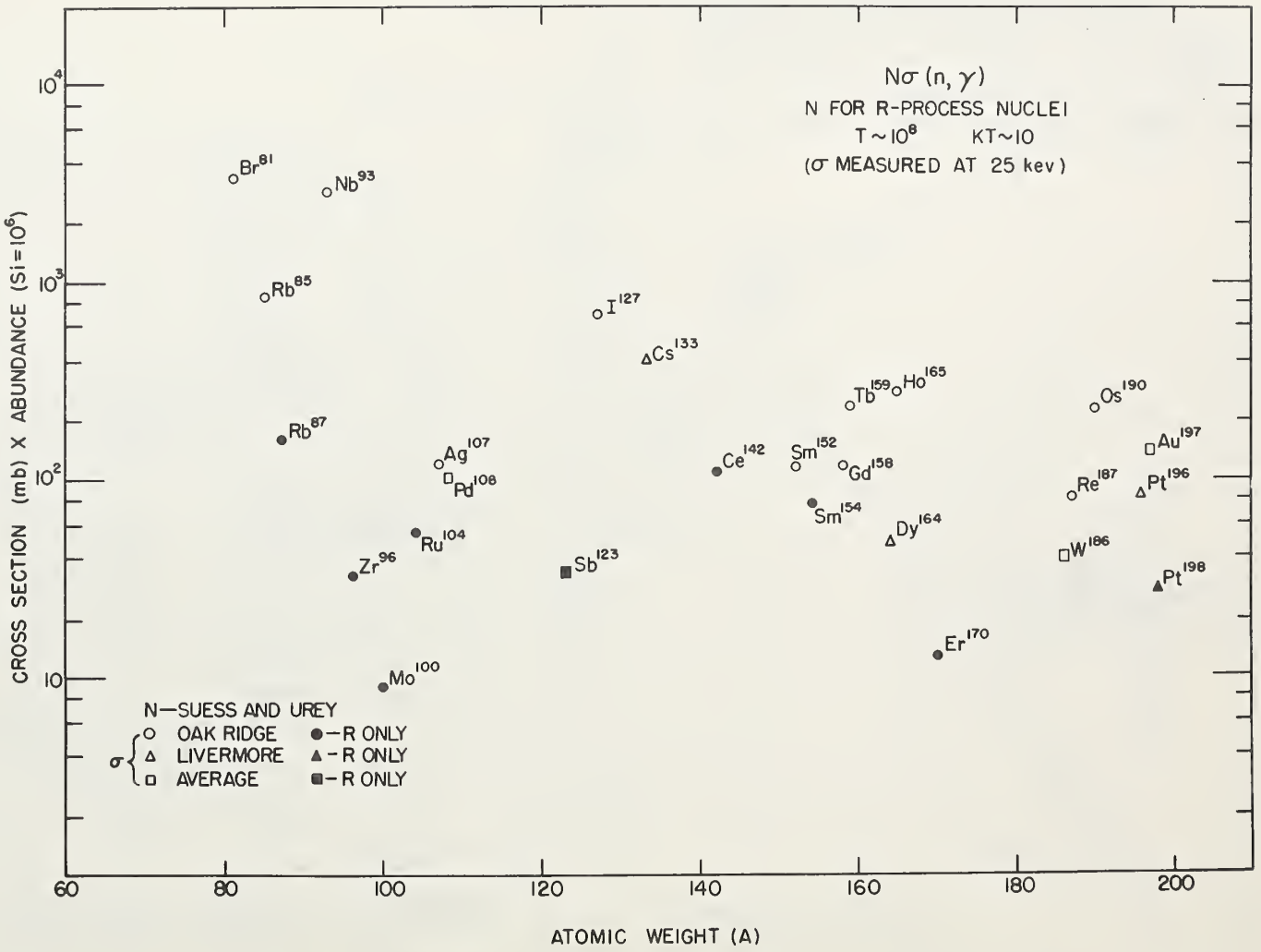

Fig. 10. The product σN for r-process nuclei similar to that shown for the s-process nuclei shown in Fig. 5. The fluctuations in σN for these nuclei are expected and show that the smooth variation indicated in Fig. 5 is not wholly accidental.

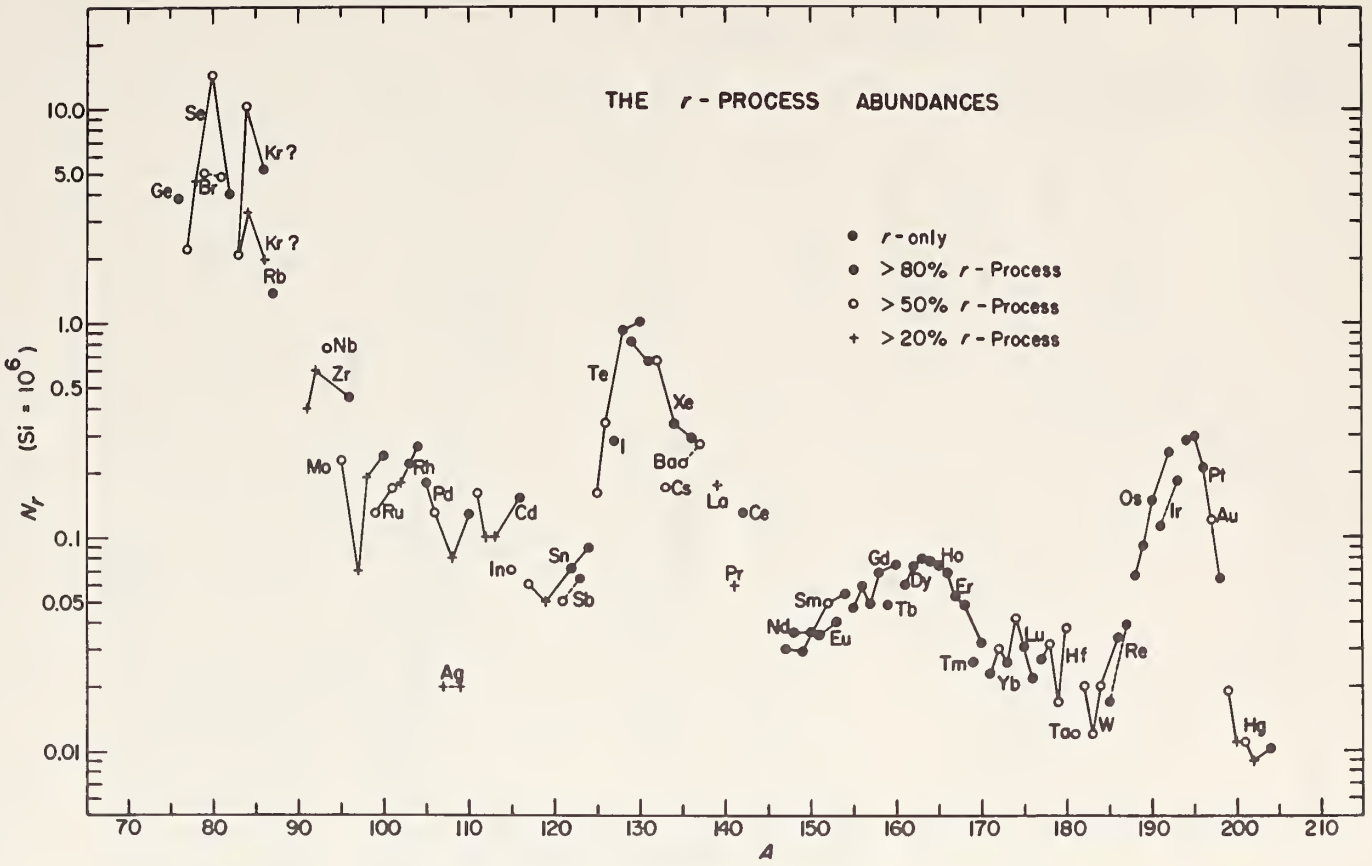

Fig. 11. Solar-system r-process abundances. Abundances of isotopes produced in the r-process are plotted after subtraction of the contribution by the s-process. Isotopes of a given element are joined by lines (solid line = even Z, dashed line = odd Z).

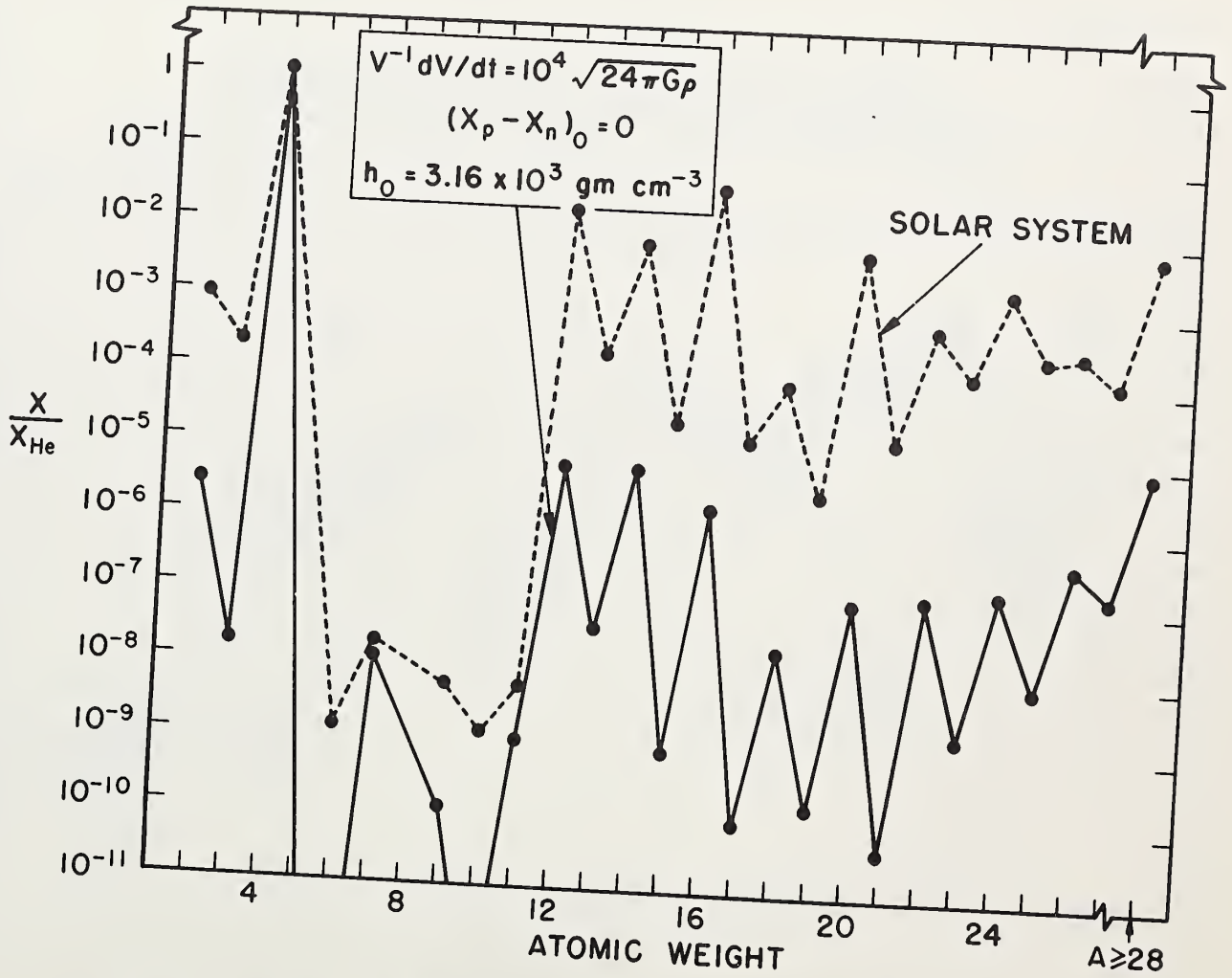

Fig. 12. Abundances by mass relative to He^4 produced in the rapid explosion of a star of mass $\sim 10^3\ M_\odot$ for which the parameter determining the adiabat along which expansion occurs is $h_o = \rho T_9^{-3} = 10^{3.5}$ gm cm^{-3} where ρ is the density and T_9 is the temperature in 10^9 ^oK.

Cosmic Abundances and the Extrapolation of Nuclear Systematics*

Philip A. Seeger
Los Alamos Scientific Laboratory, University of California
Los Alamos, New Mexico 87544

Abstract

The semi-empirical atomic mass law is a well-known way of representing nuclear systematics near the valley of beta stability. The fine structure of the mass surface provides evidence of nuclear shell effects and deformations. In order to calculate the abundances of nuclides synthesized by rapid neutron capture (r-process) in astrophysical events, nuclear systematics must be extrapolated to the extreme neutron-rich area of the N,Z-plane, and the details of shell and deformation effects become paramount.

A mass law with correction terms based on the Nilsson model is presented and shown to be adequate for simplified calculations of the r-process. Equilibrium nuclear deformations are also found.

Of the major processes of nucleosynthesis[1] which have produced the isotopes present in the material of the solar system, only the r-process, or neutron capture on a rapid time scale, deals with nuclides whose properties cannot be measured in the laboratory. Figure 1 displays the solar-system abundances of the r-process. The figure results from subtracting the abundances attributed to other processes from the experimental measurements; they are generally the most neutron-rich isotopes. At temperatures found in stellar interiors, charged-particle reactions are highly unlikely to occur on high-Z elements because of the Coulomb barrier, and we therefore hypothesize that the elements heavier than iron are synthesized principally by neutron captures on "seed" nuclei in the iron group. If so, the structure of the abundance distribution should reflect nuclear properties which depend on neutron number; this is in fact clearly seen in the s-process, which produces abundance peaks for nuclei with magic numbers of neutrons by capture on a slow time scale. It is attractive to hypothesize that the three major peaks in Fig. 1 at A = 80, A = 130, and A = 195 result from neutron magic numbers 50, 82, and 126 respectively. This implies that the path of the capture chain lies so far to the neutron-rich side of the valley of β-stability that the nuclides cannot be produced by current laboratory techniques, including fission.

A calculated capture path is plotted vs N and Z in Fig. 2. The valley of β-stability is indicated by the line labeled "s-process", and the r-process path is shown by symbols indicating the relative isotopic

---

*Work performed under the auspices of the U. S. Atomic Energy Commission

abundances of each element during the active phase of the process. The r-process hypothesis [2] is that the captures occur in a high density neutron bath at a high enough temperature that a steady state exists between γ-rays, neutrons, and nuclei of each value of Z, with β-decay to the next higher Z (at a rate very slow compared to (n,γ) and (γ,n) rates) providing for motion of material along the path. After the temperature and neutron density are turned off, the existing nuclides β-decay isobarically toward β-stability, producing finally the neutron-rich stable isotopes we observe. In the calculation shown, the temperature is 1.8×10^9 °K and the neutron density is 5×10^{26} per cm^3.

The calculation of steady states requires a knowledge of neutron binding energies, and the flow rate depends on β-decay energies. It is therefore necessary to extrapolate the semi-empirical atomic mass law to large neutron excesses. In the same manner that measured binding energies show the effects of nuclear shell structure and deformations near β-stability, the structure of the abundance distribution of r-process nuclides shows that the same fine structure of the mass surface must extrapolate into the neutron-rich region. It can be seen in Fig. 2 that the abundance peaks can indeed be related to neutron magic numbers. Also note that in the region of A~160 the path passes through a region of deformed (non-spherical) nuclei. The mass law used must contain an adequate representation of shell and deformation effects for the calculated abundances to fit the data. It has been found [3] that the results are very dependent on the structure of the mass law used, while being relatively insensitive to assumptions concerning β-decay rates, initial seed nuclei, and nuclear level densities. Therefore this work has led to further study of the mass law.

In order for a mass law to be extrapolated confidently, it must be based as firmly as possible on theory or at least on a good model, and have as few arbitrary constants as possible. To be useful for calculations over such a large part of the N-Z plane as needed for the r-process, it must be simple enough that computer time is not prohibitive. The simplest usable nuclear shell model is the Nilsson model. [4] The level diagrams shown in Figs. 3 and 4 as a function of nuclear quadrupole deformation are each functions of only two parameters. There is an additional radius parameter to convert from harmonic oscillator units to energy units but this is the same radius parameter used to calculate Coulomb energy. The essential features to observe in these diagrams are the gaps which define the magic numbers of nucleons for spherical shapes, and the rarefactions which occur between magic numbers for deformed shapes; both classes of features result in a net increase in binding energy compared to a uniform distribution of levels.

Strutinsky [5] has given a recipe for comparing a level diagram to the liquid-drop nuclear model, and this has made it possible to develop a mass law from the Nilsson model.[6] Any model can be expected to go over into the liquid-drop model for an infinite number of particles, and Strutinsky approximates this procedure for finite nuclei by spreading each discrete level into a Gaussian with width from 0.5 to 0.9 harmonic oscillator units. This leads to overlapping of all levels, and eliminates

fine structure. The liquid-drop part of the Nilsson model is not correct because the model gives an accurate representation only of those levels near the Fermi level; the harmonic oscillator potential used is not adequate for low-lying or highly excited levels. Thus the best mass law is obtained by applying shell structure as a correction to the well known liquid-drop model mass law. [7]

The correction terms are found in a consistent manner by comparing the discrete level diagrams to the smoothed out versions of the same levels. Figure 5 gives the amount of extra binding energy for a number of nuclei. Also shown in the figure is the calculated even-odd binding energy difference based on the Bardeen-Cooper-Schrieffer model. The range of the correction is 16 MeV, being maximum for doubly magic ^{208}Pb, and quite negative for the mid-shell regions of rare earths and actinides. In those regions, however, the most stable nuclear shape is found to be deformed rather than spherical; the calculated deformations and deformation energies are shown in Fig. 6. Note that although the calculation gives some large deformations for lighter nuclei, only in the rare earths and actinides does a great increase in binding energy result from deformation.

The deviations of the resulting mass law, with five liquid-drop parameters determined by least-squares adjustment to known masses and six model parameters selected on the basis of other physical evidence, are shown in Fig. 7. Systematic deviations remain, and are subject to further study. Also, we expect to extend the calculations to include greater deformations and additional deformation shapes, in order to study fission barriers.

Finally, this mass law [8] and many others [3] have been used in the r-process calculations. Figure 8 is the best fit obtained to abundances between A = 76 and A = 130; it was made with a mass law containing shell but not deformation terms. This new mass law does not fit as well, probably because of the spurious calculated deformations seen in Fig. 6 and also indicated in Fig. 2. For A>130, however, as seen in Fig. 9, only this mass law and a similar one by Myers and Swiatecki [9] have descriptions of deformations adequate to give the observed hump shape around A = 160.

The r-process does provide a qualitative test of mass laws in the extreme neutron-rich region by showing inadequacies and by indicating the need for proper shell and deformation terms.

References

[1] E. M. Burbidge, G. R. Burbidge, W. A. Fowler, and F. Hoyle, Rev. Mod. Phys. 29, 547 (1957).

[2] P. A. Seeger, W. A. Fowler, and D. D. Clayton, Astrophys. J. Suppl. XI, 121 (1965).

[3] P. A. Seeger, Arkiv Fysik 36, 495 (1967).

[4] S. G. Nilsson, Mat. Fys. Medd. Dan. Vid. Selsk 29, No. 16 (1955).

[5] V. M. Strutinsky, Nucl. Phys. A95, 420 (1967).

[6] P. A. Seeger, "A Model-Based Mass Law and a Table of Binding Energies," Los Alamos Scientific Laboratory Report LA-3751, Sept. 11, 1967.

[7] H. A. Bethe and R. F. Bacher, Rev. Mod. Phys. 8, 82 (1936).

[8] P. A. Seeger in Proceedings of the Third International Conference on Atomic Masses, R. C. Barber, ed. (University of Manitoba Press, Winnipeg, 1968).

[9] W. D. Myers and W. J. Swiatecki, Nucl. Phys. 81, 1 (1966).

313-475 O-68—4

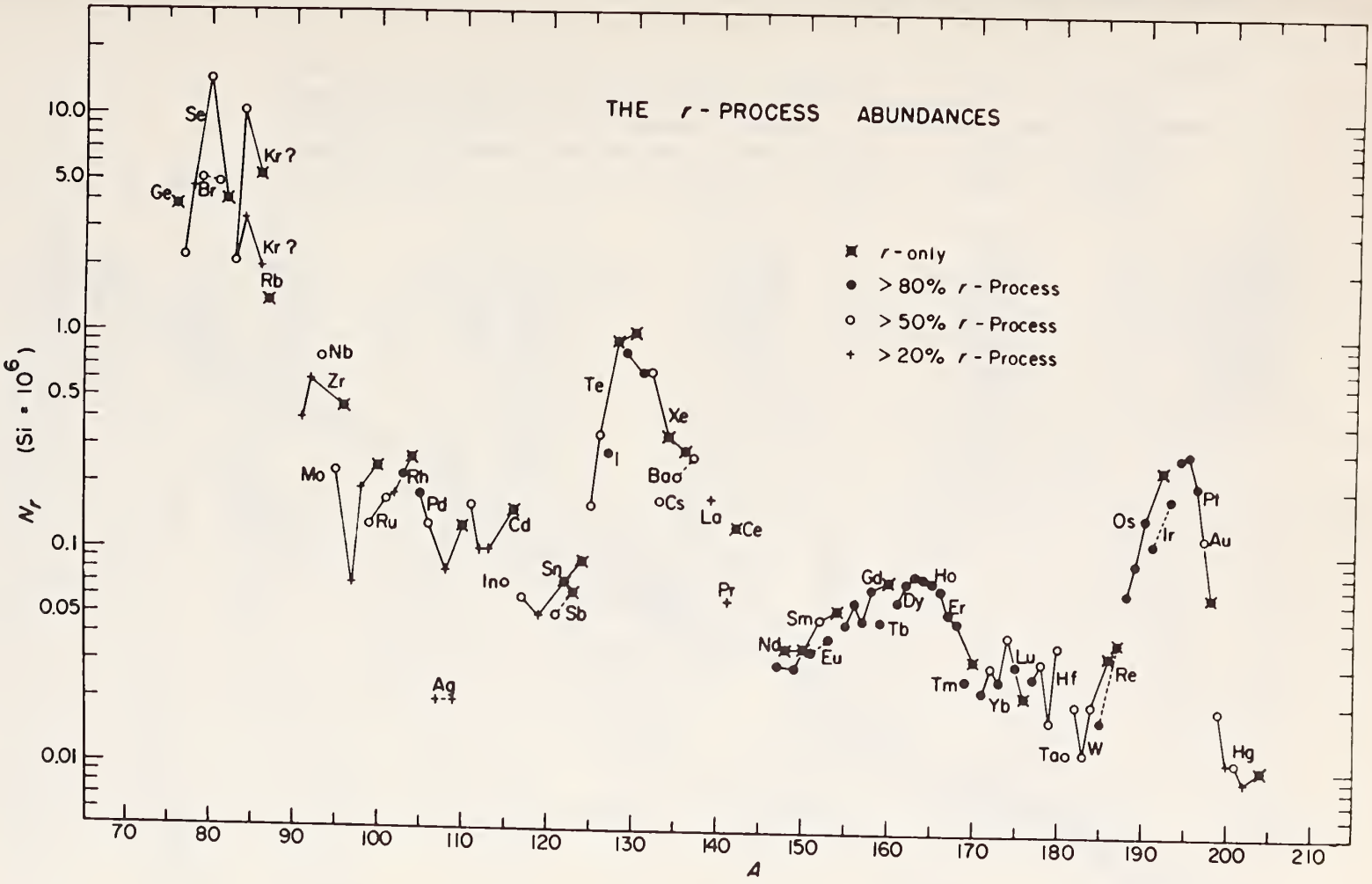

Fig. 1. Solar-system r-process abundances. Contributions from other nucleosynthesis processes have been subtracted from abundances determined principally from meteorites.

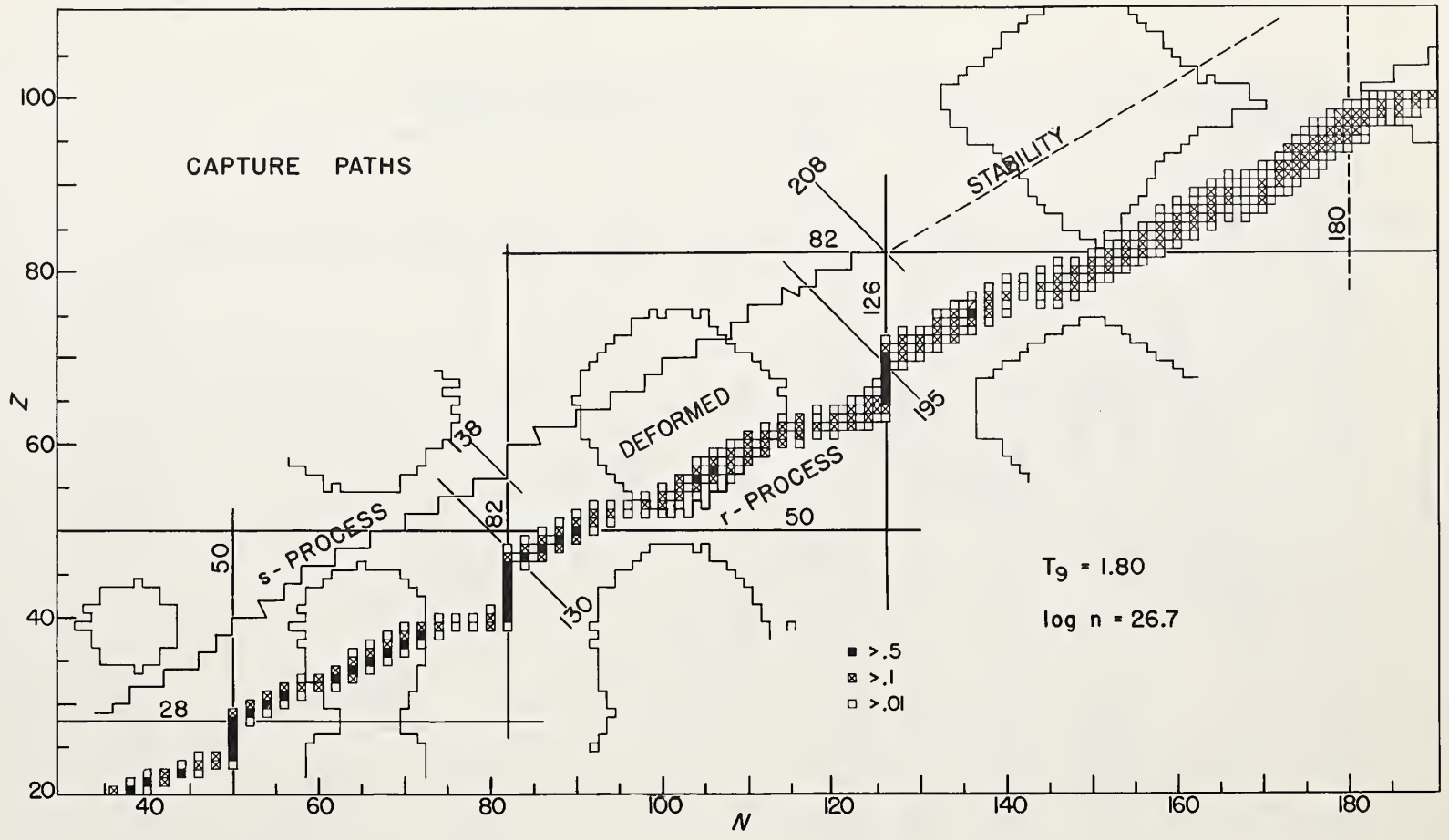

Fig. 2. Capture paths of the s- and r-processes. Magic neutron and proton numbers are shown, and regions in which the calculated equilibrium nuclear deformations are greater than $\varepsilon = 0.2$ are outlined. Abundance peaks associated with magic neutron numbers occur at A = 90, 138, and 208 in the s-process, and at A = 78, 130, and 195 in the r-process

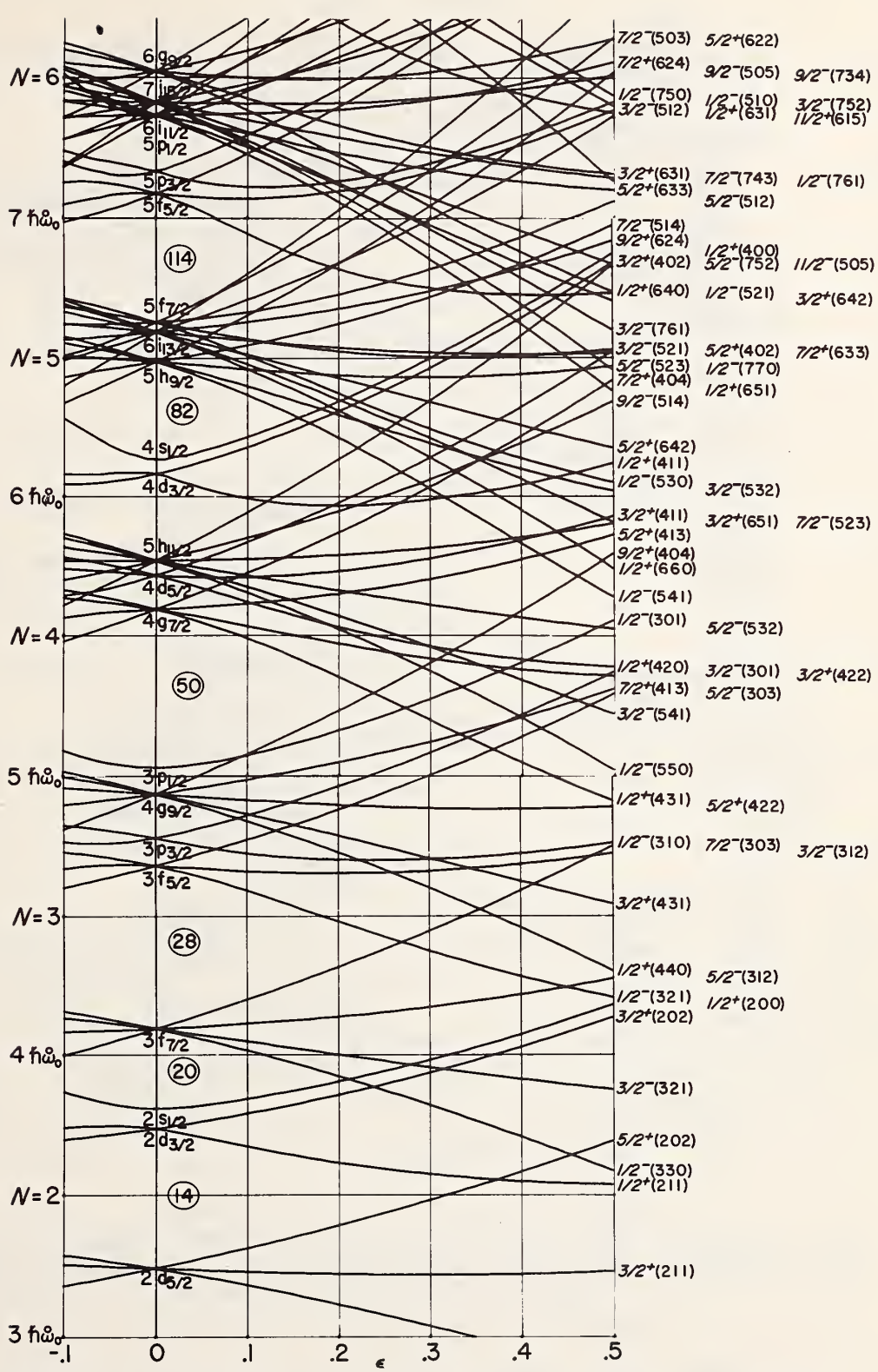

Fig. 3. Nilsson level diagram for protons; energy in harmonic oscillator units vs deformation. Quantum numbers N, ℓ, and j are indicated at zero deformation, and the asymptotic quantum numbers $\Omega^{\pi}(N\ n_z\ \Lambda)$ at the right edge.

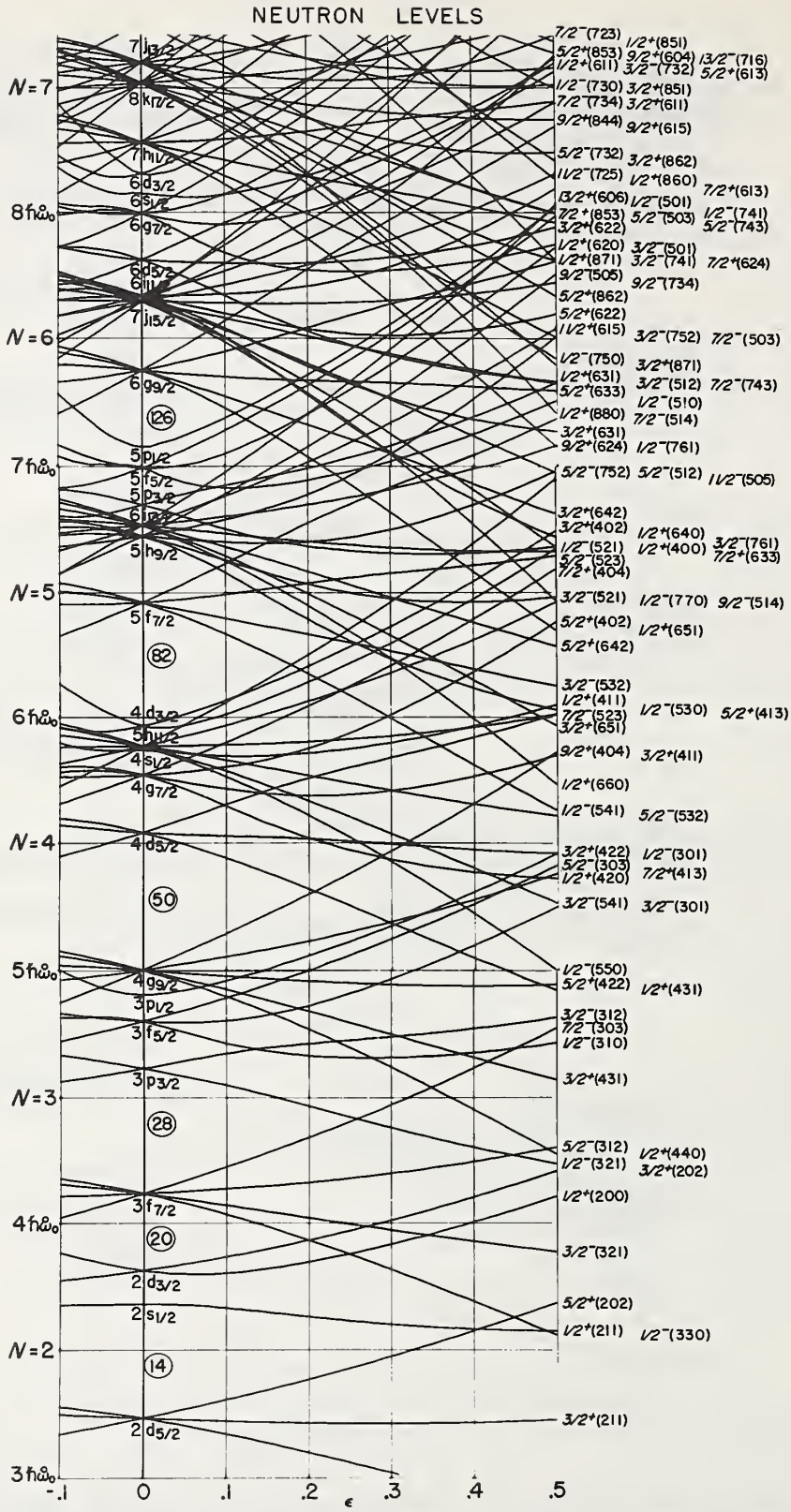

Fig. 4. Nilsson level diagram for neutrons; see Fig. 3.

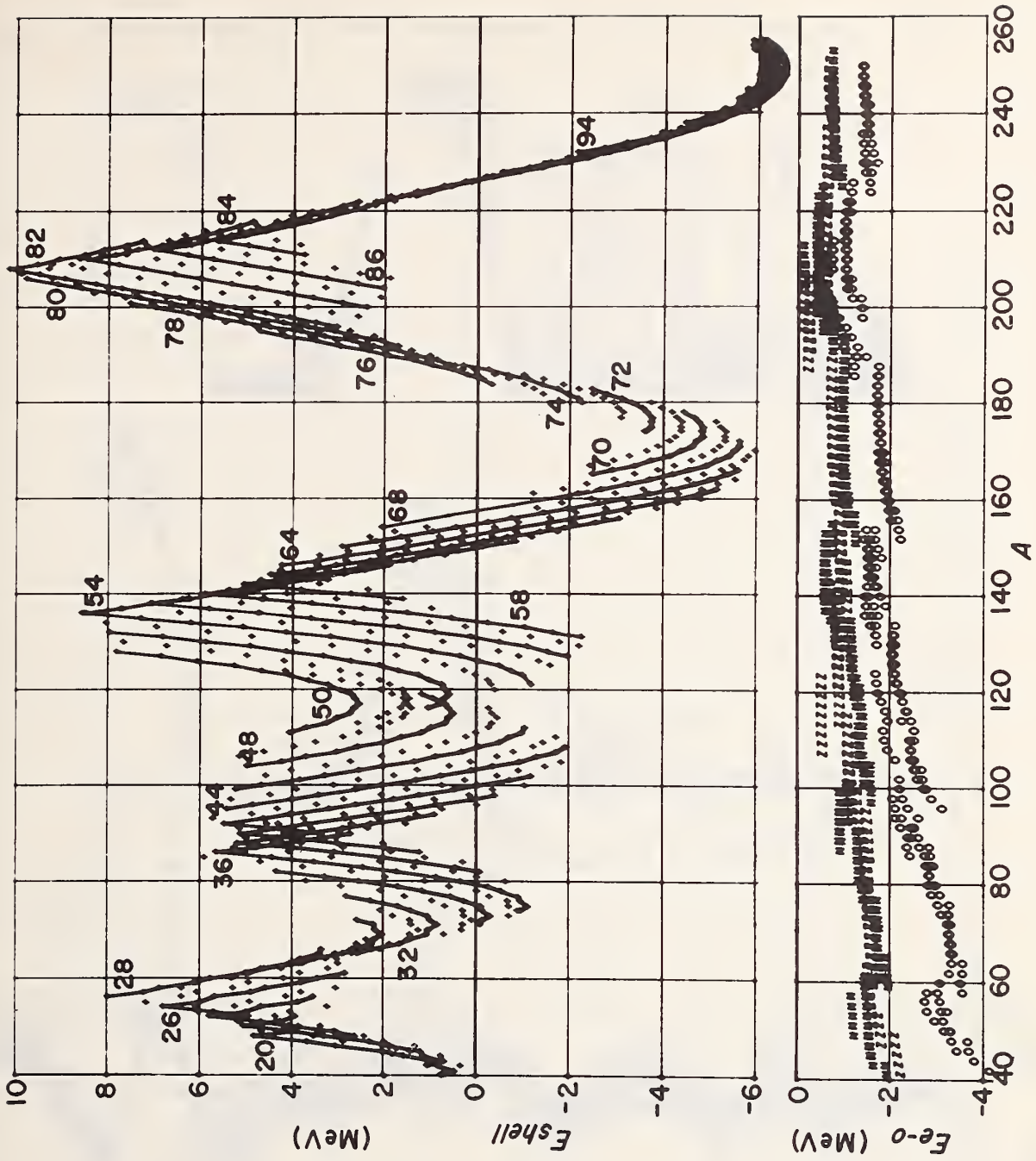

Fig. 5. Shell and even-odd energies vs A. On the upper plot, points for each even Z are connected. On the lower plot, the symbols N, Z, and O refer to odd N, odd Z, and odd-odd nuclei, respectively.

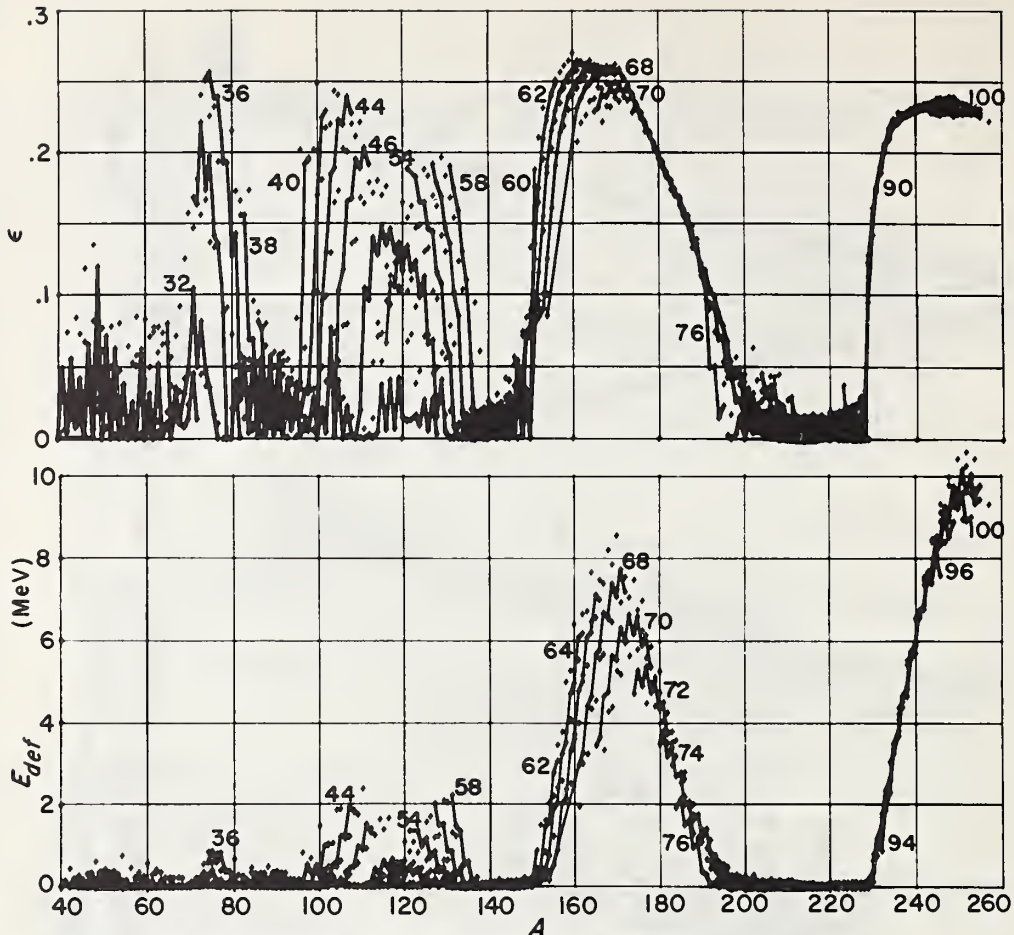

Fig. 6 Equilibrium deformation and energy of deformation. Points for even Z are connected.

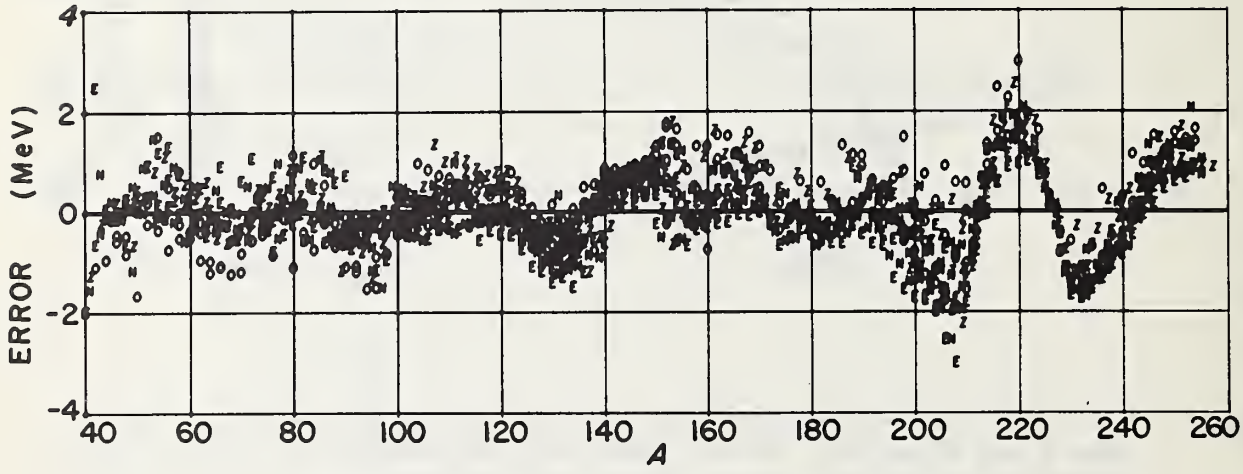

Fig. 7. Errors of binding energies calculated with the new mass law.

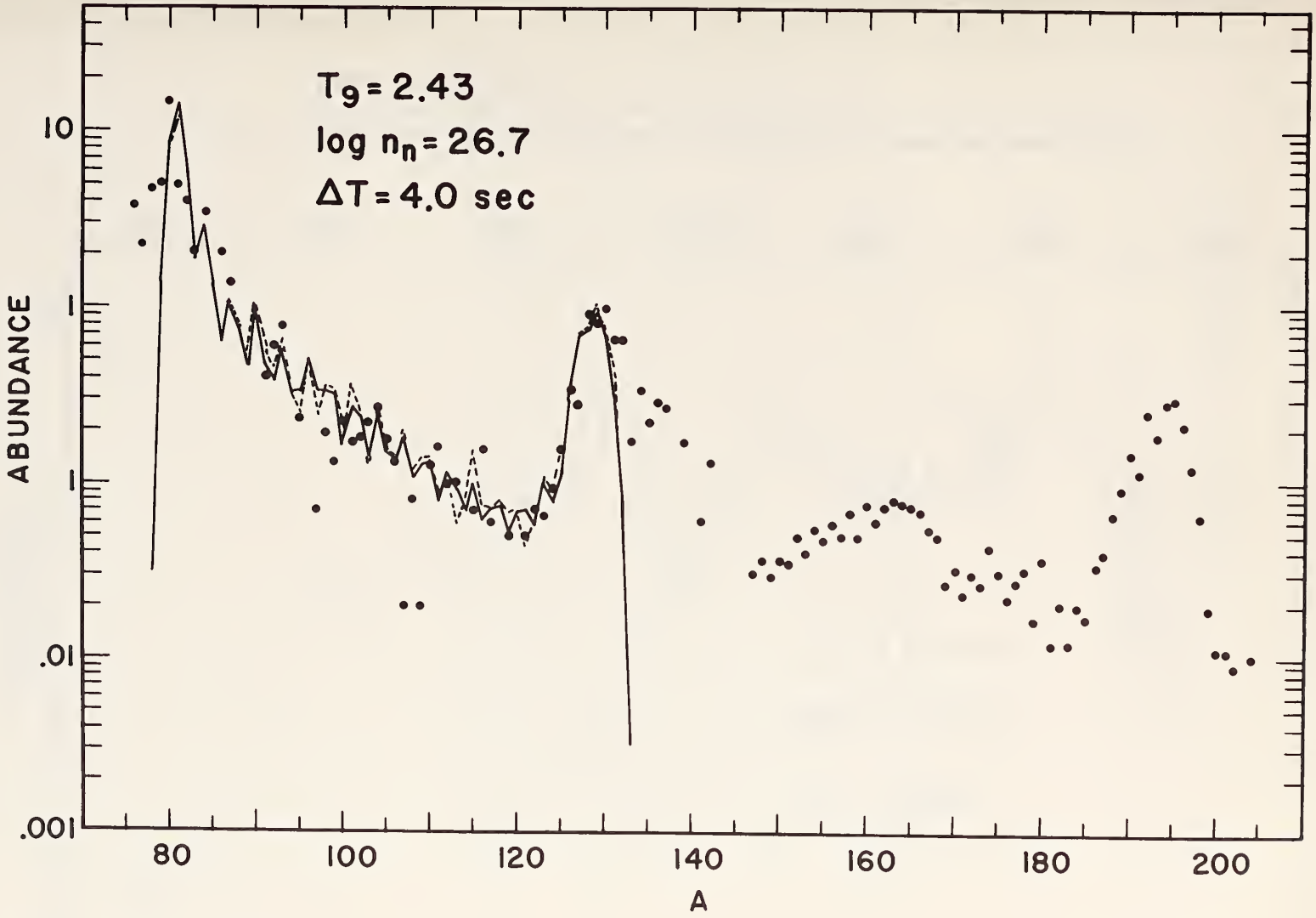

Fig. 8. Comparison of calculated and experimental abundances; best fit for A<130. The fit was made using a mass law without deformation terms.

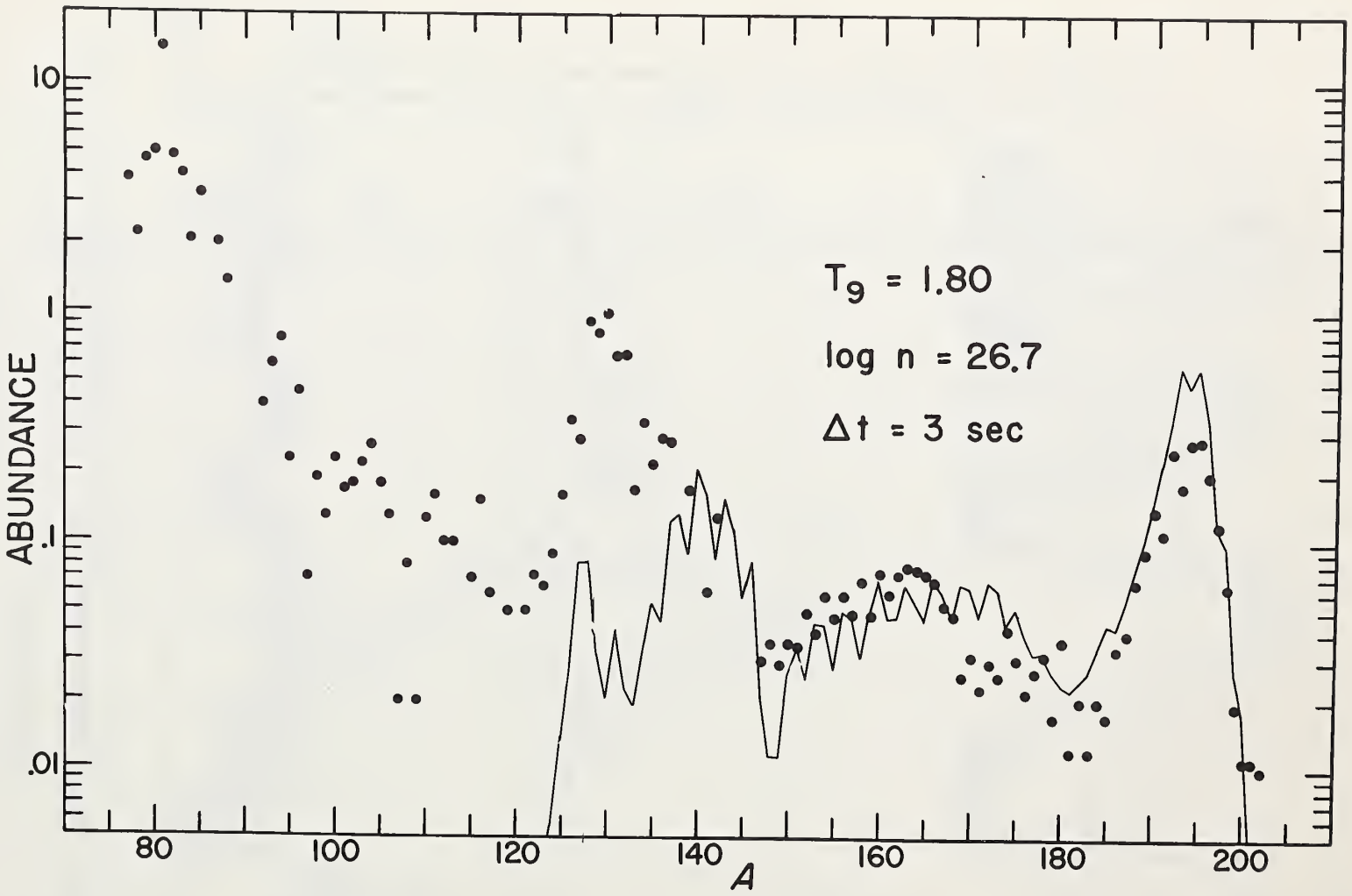

Fig. 9. Comparison of calculated and experimental abundances above A~130. Use of the new mass law permits calculation of the "deformation hump" around A~160.

THE FIELD OF SHIELDING TECHNOLOGY

Herbert Goldstein

Columbia University
New York, New York 12180

ABSTRACT

Neutron cross sections are required as input for transport calculations of various integral quantities required for shielding design as, for example, fast neutron doses. A survey is presented of the information currently available on the sensitivity of these shielding calculations to changes in the input cross sections. The discussion is concentrated on the total cross section, the energy spectrum of neutrons from inelastic scattering and the representation of the angular distribution of elastically scattered neutrons. Evidence is presented for the need for high accuracy measurements of total cross sections in the regions of minima. In non-hydrogenous shields where the nuclei are so heavy that inelastic scattering is the primary moderating mechanism, the details of the secondary neutron energy distribution may greatly influence the shielding performance. Finally, it is concluded that insofar as the scalar flux in homogeneous media is concerned, limited representations of the anisotropy of elastic scattering may be adequate.

1. Introduction

The relation between neutron cross sections and the technology of nuclear energy can be represented by a highly symbolic equation:

$$\underset{\sim}{k} = \underset{\sim\sim}{B}\underset{\sim}{\sigma} \qquad (1)$$

A set of nuclear cross sections and other microscopic data, denoted by $\underset{\sim}{\sigma}$, is manipulated in a mathematically complicated process symbolized by the operator $\underset{\sim}{B}$ (so designated in honor of the Boltzmann equation). The result is a body of integral or macroscopic data, indicated as $\underset{\sim}{k}$, of direct use in nuclear design. Under discussion here is a particular subset of $\underset{\sim}{k}$, that which is involved in shielding against nuclear radiation from a fission or fusion source. This subset includes such quantities and effects as neutron dose in and outside of shields, neutron source densities for secondary gamma radiation, heating rates, radiation damage, activation of shields and components, attenuation of neutrons through ducts and around barriers, etc. There is a corresponding shielding subset of microscopic data, $\underset{\sim}{k}$, distinguished from the general set for reactor technology by the emphasis on fast cross sections ($\sim$ 2MeV and above) and on light nuclei (Fe or lighter and especially on the group Li through O).

We are concerned at this Conference not so much with the individual subsets $\underset{\sim}{\sigma}$ and $\underset{\sim}{k}$ as with what may be called the variational derivative (to carry the symbolism further):

$$\frac{\delta \underset{\sim}{k}}{\delta \underset{\sim}{\sigma}}$$

i.e. the effect on the integral quantities of changes in the input microscopic data. It is the information symbolized by this derivative which is needed to say how accurately and in what detail the input neutron cross sections must be supplied to obtain given accuracy in the shielding information. Reactor physicists have worried for some time about such "sensitivity" calculations, but less attention has been paid to this question in the shielding field. For one thing, it is only just now that we have confidence we can perform correctly and in adequate detail the complicated process denoted by $\underset{\sim}{B}$. With the advent of the "third-generation" computers this is becoming increasingly feasible, and scattered information is appearing on cross section sensitivities. While the symbolism of a variational

derivation implies a perturbation calculation, such as has been employed in reactor physics in similar questions, all the shielding sensitivity calculations have been done so far by brute force repeated computations with different input data.

The available information on the variational derivative now permits some meaningful statements to be made on the sensitivity question for three types of input cross sections:

1. Total cross section, $\sigma_{nT}(E)$

2. The spectrum of inelastically scattered neutrons, $\sigma_{n,n'}(E;E')$

3. The angular distribution of elastically scattered neutrons, $\sigma_{n,n}(E;\theta)$

The emphasis or interest in cross section types implied by this list is quite different from that provided by the shielding requests listed in the latest "Request Compilation" [1]. An analysis of the first and second priority requests identifiable with shielding needs leads to the following distribution:

50% of the requests are for cross sections leading to gamma ray production, e.g. $\sigma_{n,n\gamma}(E;E_\gamma)$, $\sigma_{n,\gamma}(E,E_\gamma)$ etc.

30% of the requests are for cross sections involved in secondary neutron production, e.g. $\sigma_{n,n'}(E;E')$

18% of the requests are for elastic scattering cross sections, $\sigma_{n,n}(E;\theta)$

2% of the requests, i.e. 1 request, is for a total cross section.

Gamma ray production cross sections are not included in the following discussion not because they are unimportant, but because the sensitivity problem for this type of cross section is so difficult to grapple with that almost nothing is known about it. What little has been done is practically all contained in the subsequent paper by Yost et al [2]. On the other hand the emphasis on total cross sections in the request list probably reflects the time lag in the compilation of the list; the knowledge acquired recently on the sensitivity of shielding properties to total cross section phenomena has not yet influenced the character of the cross section requests.

2. Total Cross Section Effects

In our preoccupation with methods of measuring details of differential cross sections and of using them in calculations there is a tendency to overlook the dominant importance of the total collision cross section in determining neutron attenuation. After all, any collision a neutron makes is likely to have a marked effect on its chance of penetrating through a shield. To the zeroth approximation the penetration probably is therefore exponential with the total cross section appearing in the exponent. Because of this exponential behavior slight errors in the total cross section have an effect on the uncertainty in the penetrating flux that grows approximately linearly with distance. A 2% error in the total cross section (and few fast total cross sections are known this well for light nuclei) can produce a 20% variation in the flux after only 10 mfp -- an uncertainty which is only barely tolerable for some applications.

Of course, not all features of the total cross section curve are equally important. Some aspects of the total cross section as a function of energy are of little concern to the neutron shielder, others are vital. In the resonance region the pattern of emphasis for neutron shielding is almost the inverse of the relative interests of the nuclear physicist. With well separated resonances, the theoretical or experimental nuclear physicist will concentrate on the resonance curve itself to extract from it resonance parameters -- energy, widths, peak cross section etc. The small inter-resonance cross section is usually considered, if at all, to obtain the magnitude of a nonresonant 'background.' But for shielding the predominant phenomena are indicated not so much by the cross section curve as by the transmission curve, and most of the neutrons penetrating a sample are those falling between the resonances. Once a sample is thick enough to be black to the resonances, the details of the resonance parameters are unimportant. Rather, we want to know accurately what happens between resonances.

If the total cross section happens, further, to have a dip in the curve, as e.g. by destructive interference between potential scattering and a resonance, then the shielding properties of that element may depend dramatically on the characteristics of this "window" in the cross section. A striking case in point is the 2.37MeV anti-resonance in ^{16}O, the importance of which was first pointed out by Straker and Clifford at the Oak Ridge National Laboratory [3]. The cross section curve in the vicinity of this energy is shown at the bottom of Fig. 1, based primarily on the predictions of a phenomenological model

of Slaggie and Reynolds [4]. The dip results from destructive interference between an $S_{1/2}$ resonance and a potential scattering whose phase shift happens to be close to 90° at that energy. As a consequence, the presence of the resonance is marked only by the dip, which is about 120 keV wide. The cross section at the lowest point is almost entirely the result of D-wave potential scattering, and has a magnitude that may be variously estimated from 50-150 mb, i.e. about 10% of the cross section on either side of the dip. The upper curve in Fig. 1 is a portion of the infinite medium flux spectrum in pure oxygen for a fission source as calculated by O. Ozer at Columbia [6]. As would be expected for a scattering antiresonance, the effect of the dip appears as a peak in the spectrum at the same energy; the product of the flux spectrum and the total cross section would be almost flat. At large distances from a neutron source the situation is quite different. Ozer [6] has calculated by the moments method the spectrum of neutrons at various distances from a 16 cm radius fission source immersed in an infinite sea of oxygen of the same density as the oxygen in water (about 25% less than the density of liquid oxygen). Fig. 2 shows the spectrum in the 2-3 MeV region for various distances. The cross section dip still manifests itself by a narrow peak. But in addition there is an ever increasing disparity between the flux above and below the dip. At 2 m from the source, the flux at energies below the dip is not quite a factor of 10 larger than that above; by a distance 6 m the ratio has increased to over a factor of 10^4!

Clearly, the scalar flux below 2.4 MeV at large distances is dominated by source neutrons with energies close to the cross section minimum, so that the neutrons penetrate to great depths before eventually making a scattering collision. In confirmation of this analysis, Ozer [6] has calculated the fast neutron dose (a weighted energy integral of the flux above 100 keV) in oxygen as a function of depth both for the cross section curve in Fig. 1 and for a cross section set in which the dip was made much shallower. The results for both sets are shown in Fig. 3. Below about 2 m depth the two curves are not far different. At greater depths the two curves diverge markedly as the effect of the "window" becomes dominant. By 6 m the two doses differ by about 4 orders of magnitude. In effect none of the properties of the cross section curve (nor of the source distribution) are of any consequence except for the narrow region a few tenths of an MeV wide, encompassing the minimum.

Admittedly the oxygen example is artificial. Thick shields of pure oxygen are unlikely to occur in practice, and even small admixtures of other elements will dethrone this particular cross section phenomenon from its position of

importance. But there are other single elements more likely to constitute the main component of a shield for which interference "holes" have significant effects, e.g. iron, aluminum and sodium. And in other elements there are shallower but broader cross section minima, e.g. in beryllium, carbon and nitrogen, which play a role in neutron penetration much out of proportion to their insignificant appearance. It is in the neighborhood of these cross section features that it is important to fix the total cross section to within 2%.

3. Effect of Secondary Neutron Spectra from Inelastic Scattering

Inelastic scattering has always been acknowledged as an important determinant of neutron attenuation in many practical shields. After all, it is this phenomenon which makes iron a better moderator than hydrogen for, say, 6 MeV neutrons. But it has often been stated that what is significant about inelastic scattering is the total cross section for its occurrence; the energy distribution of the secondary neutrons resulting from the process is relatively unimportant. A qualitative argument can be given to justify this statement in shields where hydrogen is an effective component. At energies where inelastic scattering is large, say around 5 MeV or higher in the lighter nuclei, the energy loss in an inelastic collision is large -- most of the secondary neutrons have an energy of 2 MeV or less. At these low energies the hydrogen cross section is much larger than at the incident energy, and the secondary neutron is not likely to travel far from the location of birth before it collides with a hydrogen nucleus. This collision in turn will still further reduce the mean-free-path of the neutron and curb its chance of wandering far in space. The rate of penetration of the source neutrons will therefore in the main be determined by the collision rate of the faster neutrons, and the inelastic neutrons will appear as an equilibrium swarm (a "buildup") accompanying the dominant fast neutrons. The exact details of the spectrum of neutrons from inelastic scattering are then unimportant so long as the neutrons have indeed lost a good deal of energy.

A graphic illustration of the underlying premise in this argument is afforded by some calculations of Hansen and Sandmeier [5]. These authors computed the effect on the spectrum of neutrons in air 825 m from a point isotropic 14 MeV source when the nitrogen inelastic cross section is replaced by elastic scattering. The fractional change observed in the spectrum is shown in Fig. 4. It is clear that the main effect of inelastic scattering is to reduce the flux near the source energy by

almost a factor of 5 and to distribute these neutrons over an energy region from 2 MeV down. If this were a hydrogenous medium these lower energy neutrons would penetrate only feebly compared to the source neutrons. But in air the relaxation length of these secondary neutrons is not greatly different from those at source energies, and the exact energy distribution can effect the overall rate of attenuation. Straker [7] has calculated the effect of treating inelastic scattering in air either as absorption or as elastic scattering for 14 MeV source neutrons in air. Fig. 5 shows the resultant fast dose curves out to 1400 m from the source. Clearly, the secondary neutrons from inelastic scattering cannot be neglected; at 1000m the dose for the correct treatment of inelastic scattering is over ten times higher than the curve for which inelastic scattering is treated as an absorption. But the point here is that the secondary neutrons do not just form a "buildup" in spatial equilibrium with the higher energy elastically scattered neutrons. The slopes of the two lower curves differ by 25% at large distances, showing that the secondary neutrons form a component of the spectrum increasing in magnitude with distance. Because of the energy variation of the oxygen and nitrogen cross sections below 3 MeV, it is expected that the exact significance of the secondary component will be sensitive to the assumed energy distribution of inelastic scattering, although no detailed calculations have yet been made.

An even more striking illustration of sensitivity to the energy distribution after inelastic scattering is provided by calculations of Grimstone and collaborators in England [8]. They examined the spectrum of neutrons from a 6 MeV point source at a distance of 60 cm in iron. Inelastic scattering here provides the only significant slowing down mechanism. Calculations were done initially using the moments method code RENUPAK and its associated data library, with the resultant spectrum indicated by the solid line in Fig. 6. At the same time the solid histogram spectrum was calculated with the Monte Carlo code McNid using a 1957 evaluation of iron cross sections prepared at Aldermaston. Around 4 MeV the two spectra differ by more than a factor of 10. To show that the differences are not the result of the change in calculational method, the Monte Carlo results were recalculated with the same cross sections utilized in the moments method. The results, indicated by the dashed histogram, agreed within expected statistical fluctuations with the moments method. A glance at the spectra from inelastic scattering at 6 MeV used in the various calculations (shown in the inset in Fig. 6) clearly indicates the reason for the discrepancies. The energy distribution of the moments method (denoted as 'NDA Data') represents an early (and probably incorrect) attempt to put in the effect of transitions to low-lying levels which are consider-

ably more dense than statistical considerations would predict. As a result the data led to a flux spectrum with many more high energy neutrons than did the AWRE Data which used primarily a Maxwellian distribution with a temperature around 1 MeV. Even relatively modest changes in the input data, as evidenced by the set marked 'DFN 36 Data' in Fig. 6 have a significant effect on the resultant spectrum (the dotted histogram). To calculate the neutron shielding properties of nonhydrogenous shields composed of materials like iron it is obviously important to know closely not only the magnitude of inelastic scattering, but also the shape of the energy distribution of the scattered neutrons.

Representations of the Angular Distribution of Elastic Scattering

Many methods of solving numerically the transport equation naturally lead to an expansion of the angular distribution of elastic scattering in terms of Legendre polynomials. If ω_c is the cosine of the scattering angle in the C.M. system the expansion appears in the form:

$$\sigma_n(E,\omega_c) = \sigma_n(E) \sum_{k=0} \frac{2k+1}{4\pi} f_k(E) P_k(\omega_c) \qquad (2)$$

At the high energies of interest in shielding (up to 18 MeV) the elastic scattering is so highly anisotropic that a large number of terms are needed to represent the angular distribution faithfully. To retain all the terms required to depict $\sigma_n(E,\omega_c)$ in detail greatly complicates the transport calculation, and requires a high order of accuracy in the cross section measurement. A large body of experience indicates that for shielding purposes it is grossly inadequate to truncate the expansion in Eq. (2) at the k = 1 term, i.e. linear anisotropy. But the question naturally arises, how far does one have to go? Is there some value of k > 1 beyond which the terms can be neglected?

For some time evidence has been accumulating that for a wide range of circumstances it is adequate for shielding purposes to truncate k = 3. Thus, H.A. Sandmeier and collaborators at Los Alamos [9] calculated the flux in air from a 14 MeV point source by an anisotropic discrete ordinate method. Expanding the scattering integral in a fashion roughly analogous to Eq. (2) they found that terms involving P_4 and higher made a negligible contribution to the scalar flux at 825 meters. The

expansion of the scattering integral is described as only roughly analogous, because in fact a double summation is involved. If $J(r,E,\mu)$ represents the inscattering term in the integro-differential Boltzmann equation, then one can consider J as an expansion of the form

$$J(r,E,\mu) = \sum_{k,\ell} \frac{2\ell+1}{4\pi} A_{\ell k}(r,E) P_\ell(\mu). \quad (3)$$

The coefficients $A_{\ell k}$ are integrals over the scattering energy E' which except for constant factors, have the form

$$A_{\ell k}(r,E) \propto \int dE' \frac{E'}{E} \Sigma_s(E') N_\ell(r,E') P_\ell(\omega_L) P_k(\omega_c) f_k(E'). \quad (4)$$

Here N_ℓ is the coefficient in the expansion of the angular flux:

$$N(r,E,\mu) = \sum_{\ell} \frac{2\ell+1}{4\pi} N_\ell(r,E) P_\ell(\mu), \quad (5)$$

and ω_L is the cosine of the scattering angle in the laboratory system. In the integral, of course both ω_L and ω_c are functions of E/E' as determined by the mass of the target nucleus. It should also be noted that in the limit of infinitely heavy mass $E' \to E$, $\omega_L \to \omega_c$ and the integral reduces to the orthogonality integral for Legendre polynomials, i.e. vanishes except for the diagonal terms $k = \ell$. For most actual circumstances the $A_{\ell k}$ coefficients remain roughly diagonal, though decreasingly so as ℓ,k increase.

The two summations in the expansion of J are naturally truncated in various ways in the different methods of integrating the Boltzmann equation. In the moments method, for example, the natural truncation is in k. On the other hand in the codes using the discrete ordinates method the series is naturally truncated in ℓ, k being allowed to go as high as the input data provides. Because of the approximate diagonality of $A_{\ell k}$ either truncation should be expected to have roughly the same effect on the calculated flux. (Neither summation index should be confused with the order of angular quadrature which may be taken to quite high precision independently of the maximum values of k or ℓ). In the work of Sandmeier et al the maximum value of k was kept at 9, and the maximum ℓ was varied. No significant effect was found in the case quoted for ℓ above 3.

313-475 O-68—5

Ozer [6] has recently systematically examined the effect of various truncation procedures on the scalar flux out to 15 mfp in homogeneous media. For a fission source in water, using the ANISN discrete ordinate code, the maximum difference between truncating ℓ at 3 compared to $\ell = 5$ was at most 1% for all spectrum energies. It might be argued that this was to be expected in water where hydrogen plays such an important role. Calculations were therefore performed by the moments method for a 14 MeV source in lead. At the farthest distance truncation at $k = 3$ instead of $k = 8$ changed the flux by about 4% near source energies, and almost negligibly everywhere else. But here too it might be countered that at these energies the chief moderating process in lead is inelastic scattering whose anisotropy is usually neglected. A series of calculations were therefore carried out for a 10 MeV point source in oxygen. The energy is sufficiently high for the elastic angular distribution to be sharply anisotropic, but inelastic scattering is still not overly important. From the results with both the moments and the discrete-ordinates techniques it can be concluded that the series for J can be truncated at either k or ℓ equal to 3 with no more than a 5% error at the deepest penetration studied.

Finally, an artificial monoenergetic case was studied in which half the cross section was absorption and half was scattering in the forward direction only, i.e. a delta function at $\omega = 1$. Since the scattering so assumed does not affect the neutron motion at all, the flux from a plane isotropic source in this medium would be the well known E_1 function. Fig. 7, taken from Ozer, shows the ratio to E_1 of the scalar flux as calculated by ANISN for various maximum values of $k = \ell$, out to 10 mfp (in terms of the absorption cross section). Because of some difficulty experienced in treating the exact source geometry the ANISN predictions for a pure absorber differed from the E_1 function by small amounts of less than 1%. For a maximum $k = 5$ the results were indistinguishable from the exact case. With maximum $k = 4$ the error was always $\pm 2\%$ or less, while for an expansion through $k = 3$ the difference kept below $\pm 3\%$, but it looked as if it was beginning to fail disastrously at the maximum penetration. As the delta function provides the greatest anisotropy it seems safe to state as a general conclusion that for calculating the scalar flux in a homogeneous medium out to 15 mfp or less the highest term that need be retained in the Legendre polynomial expansion of the elastic scattering angular distribution is P_5, and for many applications P_3 will suffice.

Now, a P_3 or even P_5 expansion is a pretty poor representation of the elastic angular distribution for, say, lead at 14 MeV or oxygen at 10 MeV. Why then is the conclusion valid? There seems qualitatively to be two factors working in our favor

here. First it will be noted that for given k or ℓ the coefficient $A_{\ell k}$ has its maximum value around ℓ = k, and that the integral for A_{kk} involves the product of $f_k N_k$. Either of these expansion coefficients f_k or N_k may fall of quite slowly with k (i.e. both the scattering cross section and the flux may be quite anisotropic) but the product $f_k N_k$ will fall off with increasing k faster than either of them separately. Secondly, the structure of the transport equation is such that the scalar flux is mainly determined by the terms in J for ℓ small, i.e. ≤ 3. (This is equivalent to saying that a P_3 spherical harmonic solution to the Boltzmann equation is not too bad). The higher terms merely add refinements especially not too close to boundaries. Both these factors indicate that the interesting terms in the scattering integral are for k and ℓ small. A practical conclusion appears to be that measurements of the angular distribution for applications to neutron technology should concentrate on obtaining as well as possible the first 3 or so terms in the Legendre polynomial expansion, and not worry if these terms by themselves do not provide an adequate representation of the actual angular distribution or if they predict negative cross sections at some angles.

One word of warning should be sounded. The evidence presented above refers only to the scalar flux in homogeneous media, and the conclusion drawn may not be valid under other circumstances. The qualitative arguments on the significance of the various $A_{\ell k}$ terms, for example, obviously applies only to consideration of the scalar flux. Where the complete angular flux is desired, especially at backward angles, there is some evidence that higher expansion terms in the elastic cross section play a significant role.

The investigations of the sensitivity of shielding quantities to various cross section phenomena -- the "variational derivative" mentioned at the start of this paper -- are clearly still in their infancy. Every question answered raises more questions worthy of study. But equally clearly what has been accomplished so far underlines the usefulness of these investigations both to the shielder and to the measurer of cross sections.

4. REFERENCES

[1] WASH 1078 "Compilation of Requests for Nuclear Cross Section Measurements," A.B. Smith, ed. June 1967

[2] "Sensitivity of Gamma-Ray Dose Calculations to the Energy

Dependence of Gamma-Ray Production Cross Sections," K.J. Yost and M. Solomito. Paper, this Conference.

[3] Clifford, C.E. et al. Nucl. Sci. Eng. 27, 299-307 (1967), also Straker, E.A. and M.B. Emmett, Trans. Am. Nucl. Soc. 10, 392 (1967).

[4] Slaggie, E.L. and J.T. Reynolds, KAPL-M 6452, 1965.

[6] Ozer, O. Columbia U. Doctoral Thesis, 1968, also Ozer, O. and H. Goldstein, paper to be presented at the ANS Meeting, Toronto, June 1968.

[5] Hansen, G.E., and H.A. Sandmeier, La-3810, Dec. 7, 1967.

[7] Straker, E.A. ORNL-TM-1547, Aug. 9, 1966.

[8] Grimstone, M. et al. Paper RS/1.3/7 presented at the International Conference on the Physics Problems of Reactor Shielding, Harwell, September 1967.

[9] Sandmeier, H.A. et al. LA-3415, Nov. 1965, reported in part also in Bell, G.I. et al. Nucl. Sci. Eng. 28, 367 (1967)

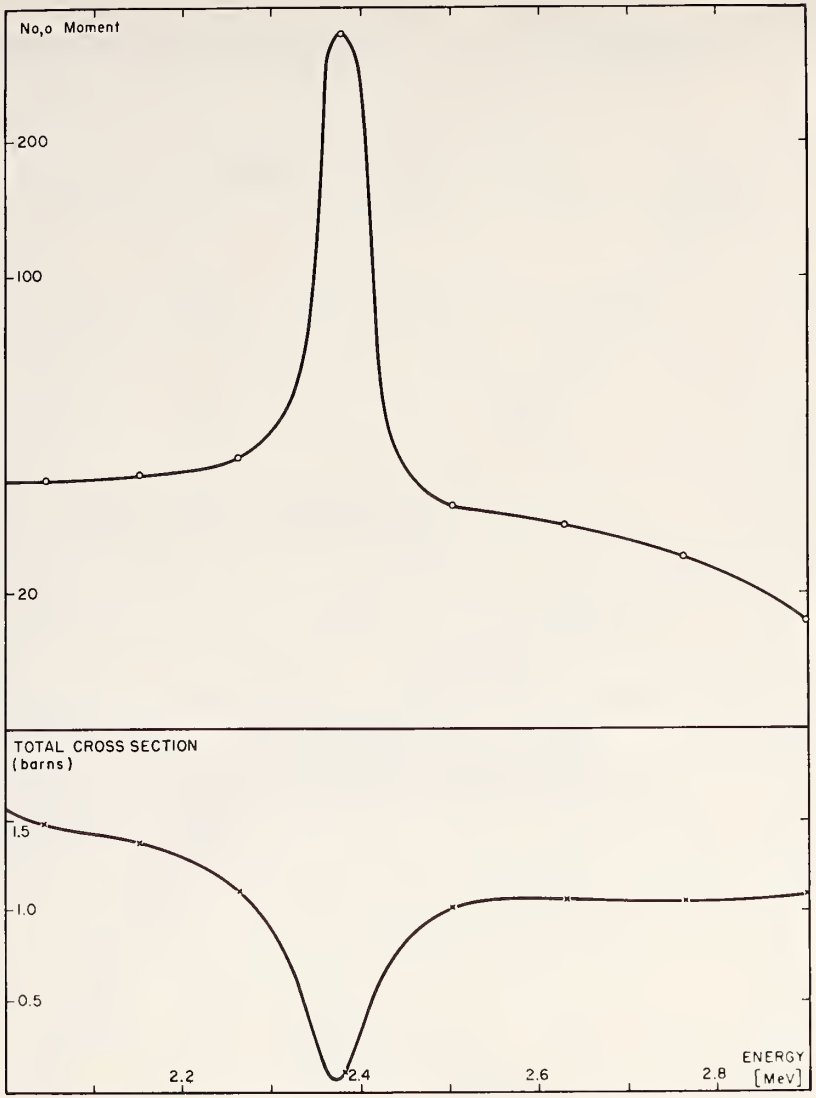

Fig. 1: Total cross section of oxygen from 2.2 to 2.9 MeV and infinite medium spectrum from a fission source in the same energy range. After Ozer, Ref. 6.

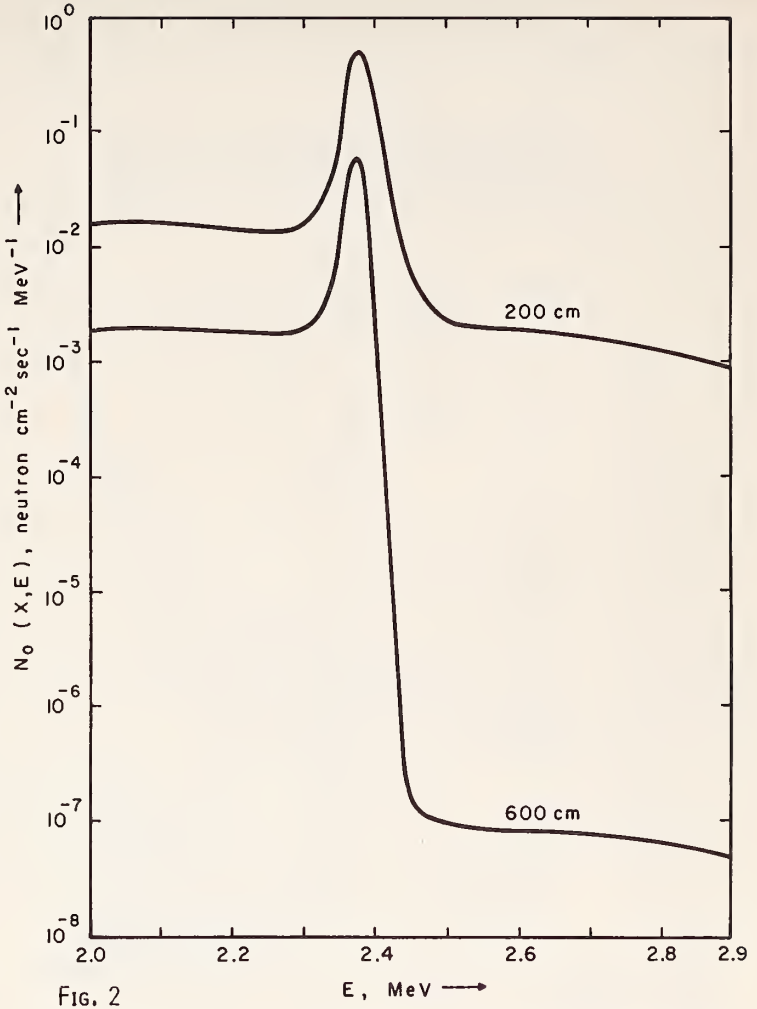

FIG. 2

Neutron Spectra in Oxygen, Plane Fission Source, Oxygen Density as in Water. (From O. Ozer, Ref. 6)

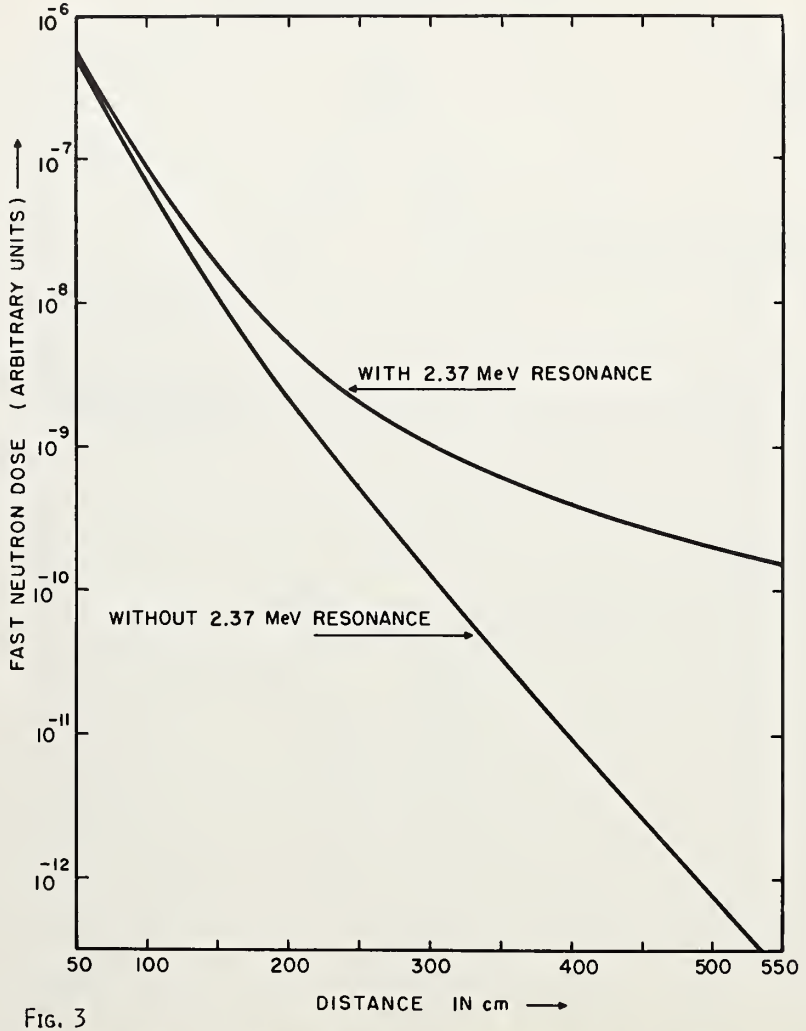

FIG. 3

Fast Neutron Dose from a Fission Source 16cm in Radius in an Infinite Medium of Oxygen, Density as in H_2O (From O. Ozer, Ref. 6)

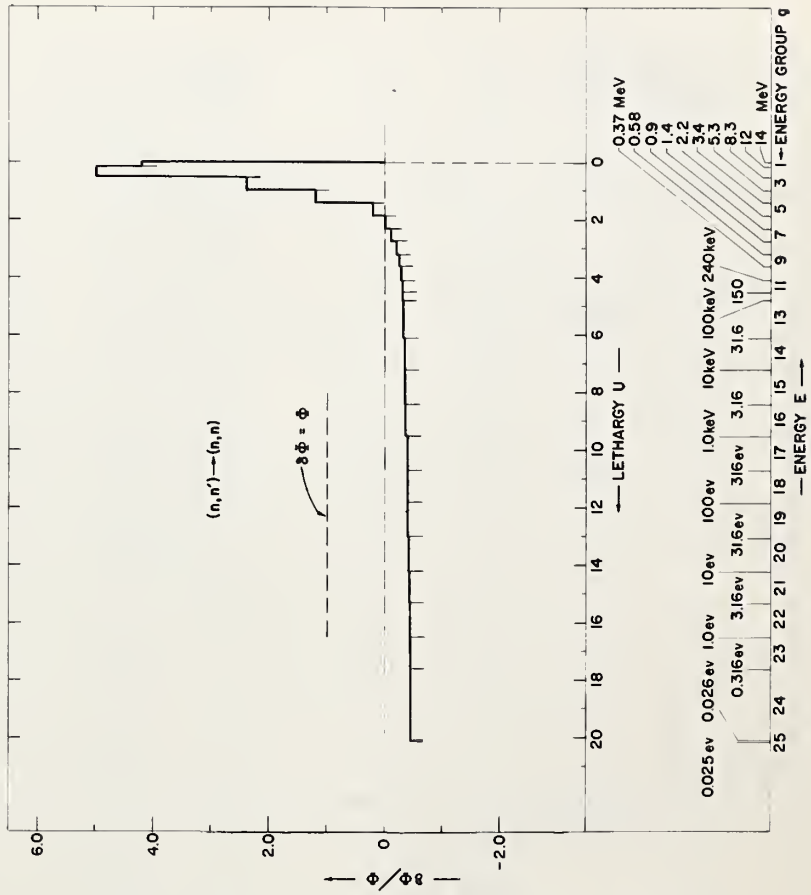

Fig. 4: Change in the flux spectrum at 825 m in air when the inelastic cross section in nitrogen is treated as elastic scattering; 14 MeV point isotropic source. (From G.E. Hansen and H.A. Sandmeier, LA-3810).

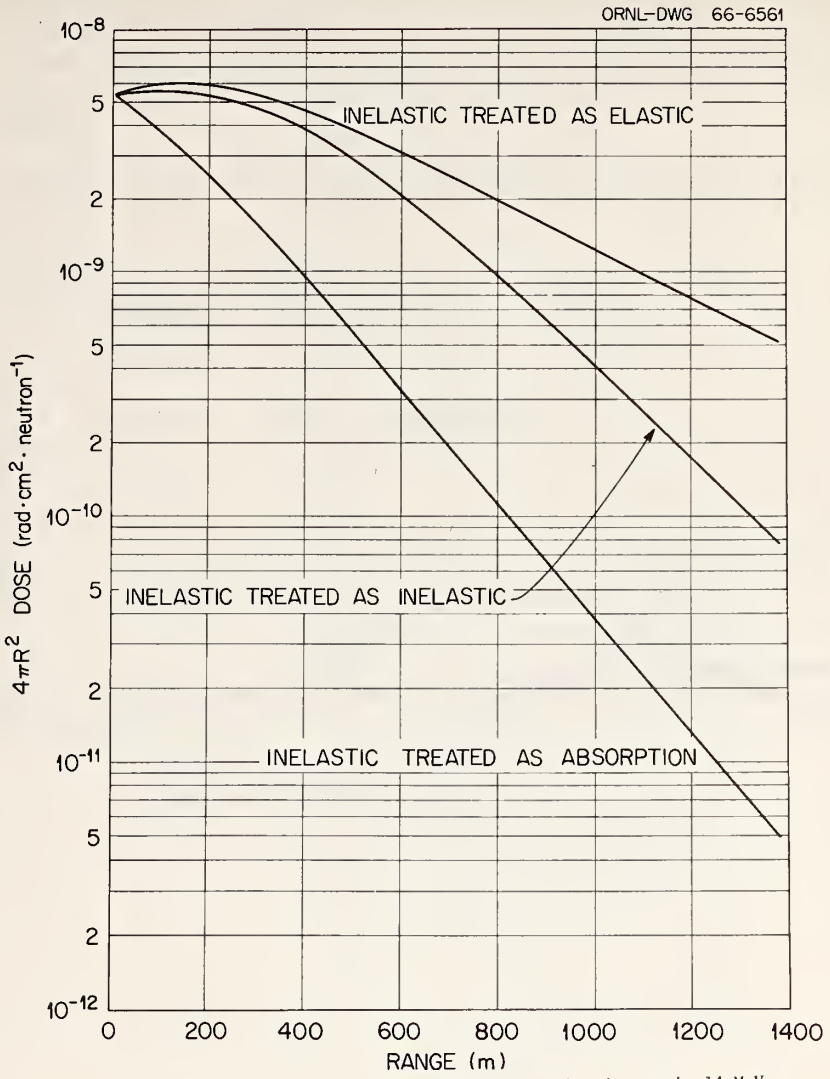

Fig. 5: Fast neutron dose in air from a point isotropic 14 MeV source for different treatments of inelastic scattering. (From E.A. Straker, Ref. 7).

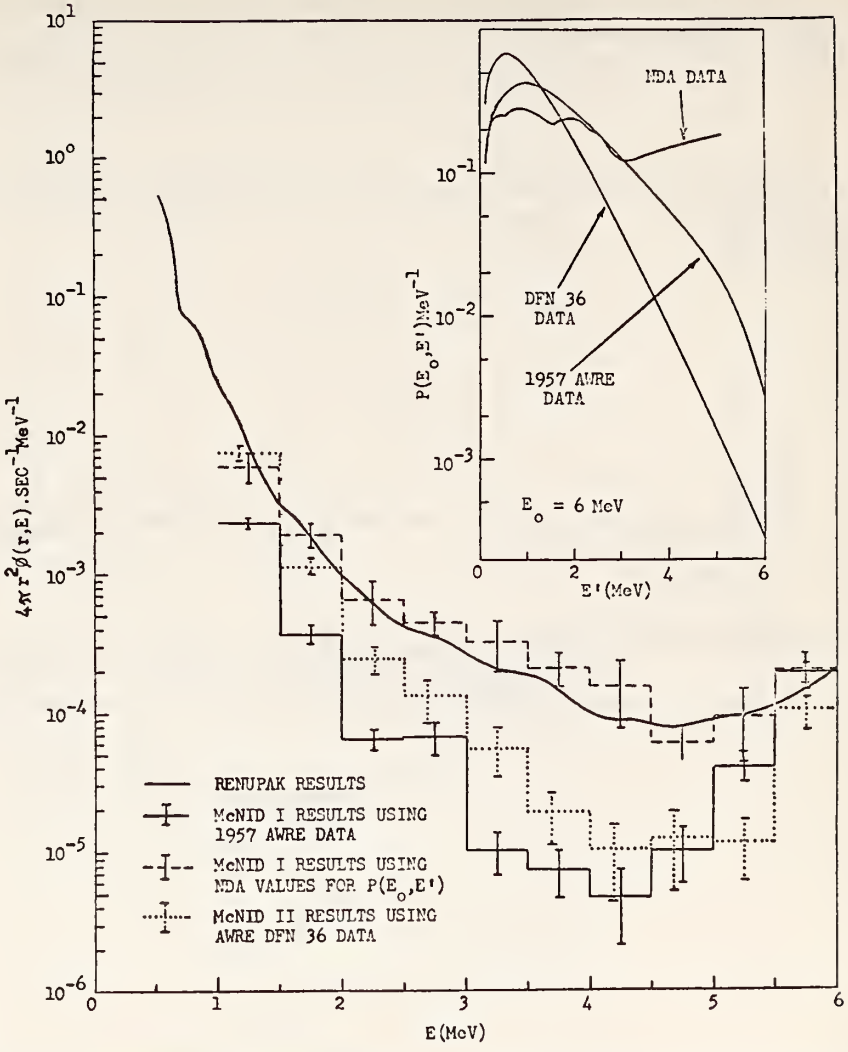

FIG. 6 DIFFERENTIAL NEUTRON SPECTRUM IN IRON AT 60 CM FROM A 6 MeV POINT ISOTROPIC SOURCE OF STRENGTH 1 NEUTRON/SEC

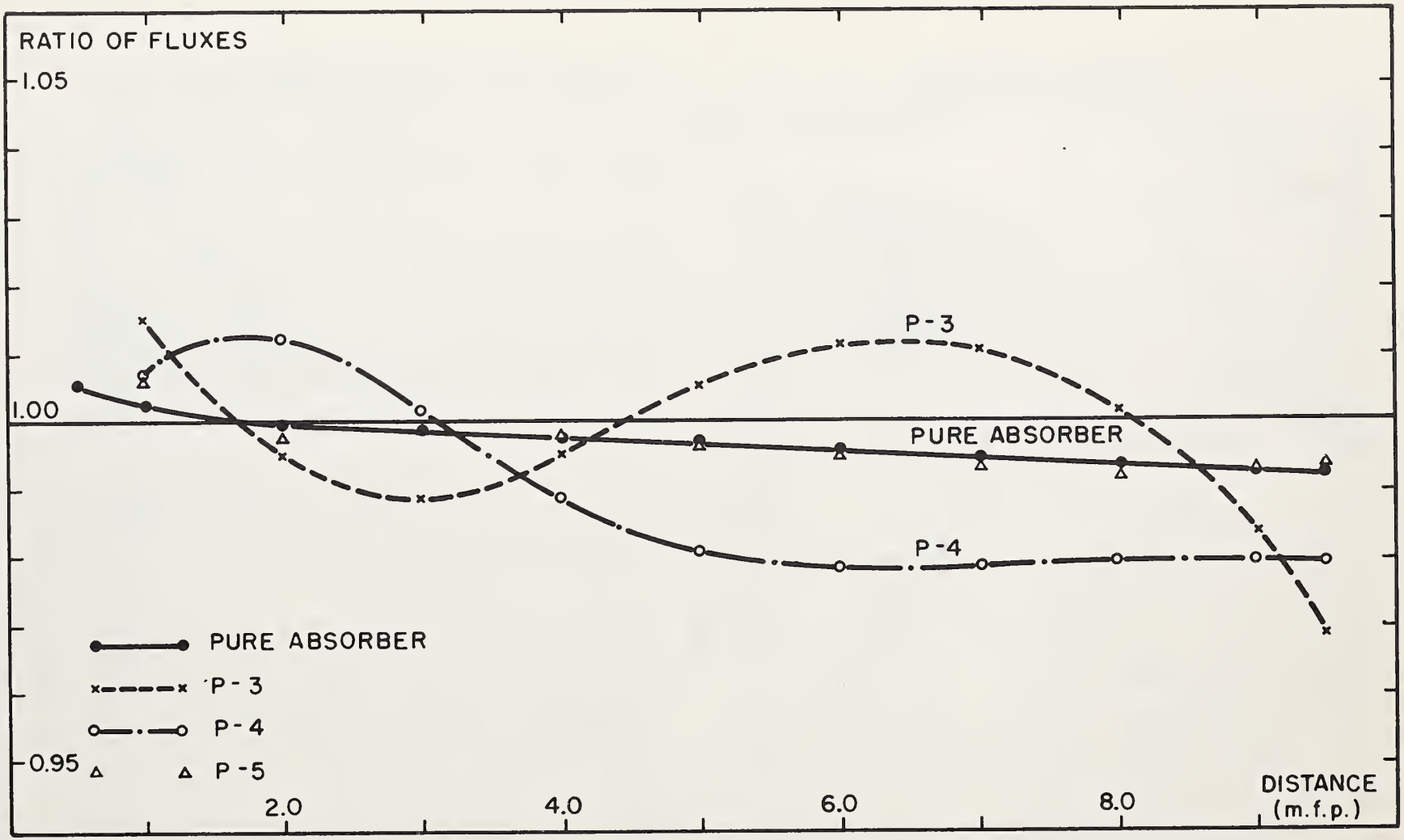

FIG. 7

Comparison of fluxes calculated with different order approximations to the scattering function for the case of forward scattering. (From O. Ozer, Ref. 6)

SENSITIVITY OF GAMMA-RAY DOSE CALCULATIONS TO THE ENERGY DEPENDENCE OF GAMMA-RAY PRODUCTION CROSS SECTIONS*

K. J. Yost and M. Solomito
Oak Ridge National Laboratory
Oak Ridge, Tennessee 37830

Abstract

The dependence of neutron-capture gamma-ray spectra on capture neutron energy is of particular importance in the design of optimized reactor shields. The heretofore common practice of assuming that neutron-capture gamma-ray spectra are invariant to neutron energy is expected to be an unacceptable approximation for a shield material exhibiting strong resonance characteristics. The importance of adequately predicting gamma-ray yields from the capture of non-thermal neutrons for a particular shield is clearly a function of (a) the relative magnitudes of thermal and non-thermal neutron capture rates in regions of the shield contributing substantially to the surface capture gamma dose rate, (b) the magnitude of the capture gamma dose rate as compared to other sources of gamma radiation, and (c) the extent to which the capture gamma dose rate is sensitive to changes in the shape of the capture gamma-ray spectrum. Each of these questions has been investigated in detail for three SNAP 10A core-laminated tungsten, lithium hydride shield configurations. Results indicate that, depending upon the shield in question, non-thermal neutron capture accounts for 90% to ~ 100% of the capture gamma dose rate in tungsten, that capture gammas in tungsten constitute a far larger component of the surface gamma dose rate than do either primary or tungsten inelastic scattering gammas, and that capture gamma dose sensitivity to the shape of the capture spectrum is strongly dependent upon shield configuration.

****

In order that we may view the present work in the proper perspective it should be noted that it represents but one phase of a larger effort designed to determine the implications for shielding technology of the energy dependence of neutron-capture gamma-ray spectra [1]. In addition to the gamma transport to be discussed we have two other major endeavors in progress. One of these is an experimental program being carried out at General Atomic which presently involves preparation for the measurement of capture gamma-ray spectra in tungsten for neutron energies in the thermal to 100 keV range. Our data requirements are such that for the foreseeable future we must rely upon some method for supplementing existing capture gamma-ray data. A third major effort has thus been devoted to the development of a method for the

*Research sponsored by the U. S. Atomic Energy Commission under contract with the Union Carbide Corporation.

prediction of neutron-capture gamma-ray spectra to an accuracy consistent with the requirements of capture gamma-ray production cross sections. To date we have developed a spin, parity, and radiative transition matrix element sensitive gamma-ray cascade model, and are currently formulating a method designed to provide for the model such cascade parameters as spin branching ratios and multipole transition probabilities [2].

It has in the past been common practice in coupled neutron-gamma-ray shield calculations to base capture gamma-ray production cross sections for all neutron energies on the thermal capture spectrum. The impact on shield calculations of gamma-ray spectrum capture state dependence can thus be put in the form of the following question: What is the effect on such quantities as shield surface capture-gamma dose and capture-gamma heating of specifically accounting for the energy dependence of capture gamma-ray spectra as opposed to ascribing a thermal spectrum to the capture of neutrons of all energies?

The calculation of energy sensitive neutron-capture gamma-ray production cross sections can be illustrated in terms of the following definitions:

$N_k \equiv$ number of capture resonances in kth neutron group;

$\sigma_j^k(E) \equiv$ neutron capture cross section corresponding to the jth resonance in the kth neutron group;

$$\sigma_T^k(E) \equiv \sum_{j=1}^{N_k} \sigma_j^k(E);$$

$Y_j^k(i) =$ yield for the ith gamma group/histogram bin for the jth resonance of the kth neutron group.

The group-averaged yield of the ith gamma group for the kth neutron group is given by

$$\bar{Y}^k(i) = \frac{\int_{E_{k+1}}^{E_k} dE' \sum_{j=1}^{N_k} Y_j^k(i)\, \sigma_j^k(E')\, \varphi(E')}{\int_{E_{k+1}}^{E_k} \sigma_T^k(E')\, \varphi(E')\, dE'} \qquad (1)$$

where $\varphi(E')$ denotes the neutron flux and E_k and E_{k+1} the upper and lower boundaries, respectively, of the kth neutron group. Given appropriate nuclear level spacing, the thermal capture gamma-ray spectrum for a particular nucleus represents in essence the de-excitation of a single neutron capture state. The relation of this spectrum to a neutron group-averaged or "composite" spectrum with neutron group-averaged yields given by Eq. 1 determines the associated differences in calculated gamma dose and heating.

In the course of the present investigation it became evident that some assessment of the consequences of capture spectrum energy dependence had to be made before either the aforementioned theoretical or experimental efforts had progressed to the point that the required data were available. For this reason our approach was based upon a technique which made it feasible to calculate shield surface gamma-ray dose rates corresponding to a wide range of assumptions regarding the composite capture spectrum. The method involves generating a curve of capture gamma dose rate normalized to the emission of a single photon of energy, E, vs. E. Such a "dose profile" can be constructed in either of two ways: (a) by a series of capture gamma-ray dose calculations each based upon a unit gamma yield for one gamma group, and zero yields for all others, or (b) by integrating the product of a flux-to-dose conversion ratio weighted gamma-ray adjoint or importance function defined with respect to shield penetration and the neutron capture rate over appropriate regions of phase space. For the present investigation we used the former method primarily because the computer programming required to implement the latter is still in progress. The calculations were performed with the one-dimensional discrete ordinates code, ANISN. In this analysis the shield surface dose corresponding to a unit yield for the ith gamma group and zero for all other groups, $\underline{D}(i)$, multiplied by a measured or calculated yield for the ith gamma group, $\overline{Y}(i)$ and summed over i gives the total capture gamma surface dose rate, D_T. Symbolically,

$$D_T = \sum_{i=1}^{N_\gamma} \overline{Y}(i)\, D(i) \qquad (2)$$

where

$$\overline{Y}(i) = \frac{\sum_k \overline{Y}^k(i) \int_{E_{k+1}}^{E_k} \sigma_T(E')\, \varphi(E')\, dE'}{\int_{\text{all } E} \sigma_T(E')\, \varphi(E')\, dE'}$$

The foregoing method has been applied to three SNAP-10A core-laminated tungsten-lithium hydride shield configurations. Figures 1 and 2 illustrate dose profiles for the indicated shields. The importance of accounting explictly for gamma-ray spectrum shape dependence on capture neutron energy is obviously a function of the relative magnitudes of the thermal and non-thermal capture rates. Non-thermal neutron capture constituted from 92% (for the four-region shield) to 99.7% (for the five-region shield) of the total capture rate in tungsten for the three-shield configurations.

Table 1 exhibits absolute and relative contributions to a shield surface gamma-ray dose rate composed of primary, tungsten capture, and tungsten inelastic scattering gamma rays for the shields of Figs. 1 and 2. The capture gamma dose rate is based upon the thermal capture spectrum for

natural tungsten reported in Vol. III of the Reactor Handbook [3]. In each case capture gammas constitute by far the largest component of the "total" gamma-ray dose rate.

In order to determine limiting values of the capture-gamma dose rate for the shields of Figs. 1 and 2, Eq. 2 was used in conjunction with the appropriate dose profiles to calculate dose rates based upon a wide range of assumptions regarding capture spectra properly averaged with respect to capture neutron energy. These spectra were generated for cascade multiplicities, m, in the range $1 \leq m \leq 4$ consistent with a composite, natural tungsten binding energy of 6.2 MeV. The spectrum "generating functions" for given values of m are as follows:

$$D(N), \quad m = 1$$

$$\sum_{i=1}^{\left[\frac{N}{2}\right]} \left[Y(N-i)\, D(N-i) + Y(i)\, D(i) \right], \quad m = 2$$

$$\sum_{i=\left[\frac{N}{3}\right]}^{N-2} \left\{ Y(i)\, D(i) + \sum_{j=\left[\frac{N-i}{2}\right]}^{N-i-1} \left[Y(j)\, D(j) + Y(N-i-j)\, D(N-i-j) \right] \right\}, \quad m = 3 \qquad (3)$$

$$\sum_{i=\left[\frac{N}{4}\right]}^{N-3} \left\{ Y(i)\, D(i) + \sum_{j=\left[\frac{N-i}{3}\right]}^{N-i-2} \left[Y(j)\, D(j) + \sum_{k=\left[\frac{N-i-j}{2}\right]}^{N-i-j-1} \left(Y(k)\, D(k) + Y(N-i-j-k)\, D(N-i-j-k) \right) \right] \right\}, \quad m = 4,$$

where N denotes the number of gamma groups, Y(i) the neutron energy averaged gamma yield per capture for the ith gamma group, and D(i) is as defined in conjunction with Eq. 2. The sums extend over gamma groups 0.1 MeV in width. The composite binding energy represents an abundance, level density, and resonance strength weighted average of the binding energies of the four isotopes found in appreciable measure in natural tungsten. Table 2 exhibits maximum and minimum surface capture gamma dose rates as a function of m for each shield configuration. For purposes of comparison the dose rate corresponding to the thermal capture spectrum is also shown. The

difference between maximum and minimum capture gamma dose rates for the four-region optimized shield is significantly smaller than is the case for the other two configurations. This appears to be a consequence of a substantial neutron flux peaking at the tungsten-lithium hydride interface of the four-region shield which results in a relatively larger uncollided component of the surface capture gamma-ray flux.

The foregoing calculations indicate that the importance of neutron-capture gamma-ray spectrum variation with capture neutron energy is strongly dependent upon shield configuration. In particular, the ratio of the maximum to the minimum capture gamma dose rates varied from 1.25 for the four-region shield to 4.10 for the six-region shield. Gamma rays with energies of 1 MeV or less can be largely neglected in surface dose calculations. They are, of course, correspondingly more important for heating calculations than higher-energy photons. Capture gammas are a controlling factor in shield design relative to primary or core gammas for all three of the shield configurations. The non-thermal neutron capture rate dominated the total neutron capture rate in the tungsten regions of each of the shields considered. Finally, in lieu of reliable experimental or calculated non-thermal capture spectra, we estimate from the foregoing calculations that the surface capture gamma dose rate based upon the thermal capture spectrum is high for all three shields; by as much as 20% for the four-region shield and 50% for the five- and six-region shields.

References

1. K. J. Yost,"The Calculation of Neutron-Capture Gamma-Ray Spectra," Invited Paper presented at the 1967 Winter Meeting of the American Nuclear Society in a special session, Gamma-Ray Production and Transport - I, to be published as T.I.E. report.

2. K. J. Yost, "A Method for the Calculation of Neutron-Capture Gamma-Ray Spectra," to be published in Nuclear Science and Engineering.

3. Reactor Handbook, Vol. III, Part B. Shielding, E. P. Blizard and L. S. Abbott, Eds., 2nd ed., p. 46, Interscience, New York, 1962.

Table 1. Components of Shield Surface Dose Rates Composed of Core, Tungsten Capture, and Tungsten Inelastic Scattering Gamma Rays

Shield Type	Gamma-Ray Dose Rate at Shield Surface (r/hr)			
	Capture Gamma Rays	Core Gamma Rays	Inelastic Gamma Rays	Total
Optimized Shield I (4 Region)	3.31×10^{-11}	Negligible	5.60×10^{-13}	3.366×10^{-11}
Percent of Total	98.3%	Negligible	1.7%	
Optimized Shield II (6 Region)	2.15×10^{-11}	3.2×10^{-12}	3.18×10^{-13}	2.502×10^{-11}
Percent of Total	85.9%	12.8%	1.3%	
5-Region Shield	5.00×10^{-12}	5.0×10^{-14}	1.12×10^{-13}	5.162×10^{-12}
Percent of Total	96.8%	1.0%	2.2%	

Table 2. Limiting Values of Tungsten Surface Capture Gamma-Ray Dose Rates as a Function of Cascade Multiplicity Compared to Thermal [3] Capture Spectrum Dose Rates

Multiplicity	Dose Rate ($r/hr/cm^3 \times 10^{-11}$)		
	Maximum	Minimum	Thermal
Four-Region Optimized Shield			
1	2.96	2.96	3.62
2	3.40	2.96	
3	3.56	2.95	
4	3.68	2.95	
Six-Region Optimized Shield			
1	1.73	1.73	1.98
2	2.34	1.61	
3	2.29	1.33	
4	2.24	0.57	
Five-Region Outer W Sleeve Shield			
1	0.50	0.50	0.53
2	0.59	0.42	
3	0.59	0.36	
4	0.58	0.25	

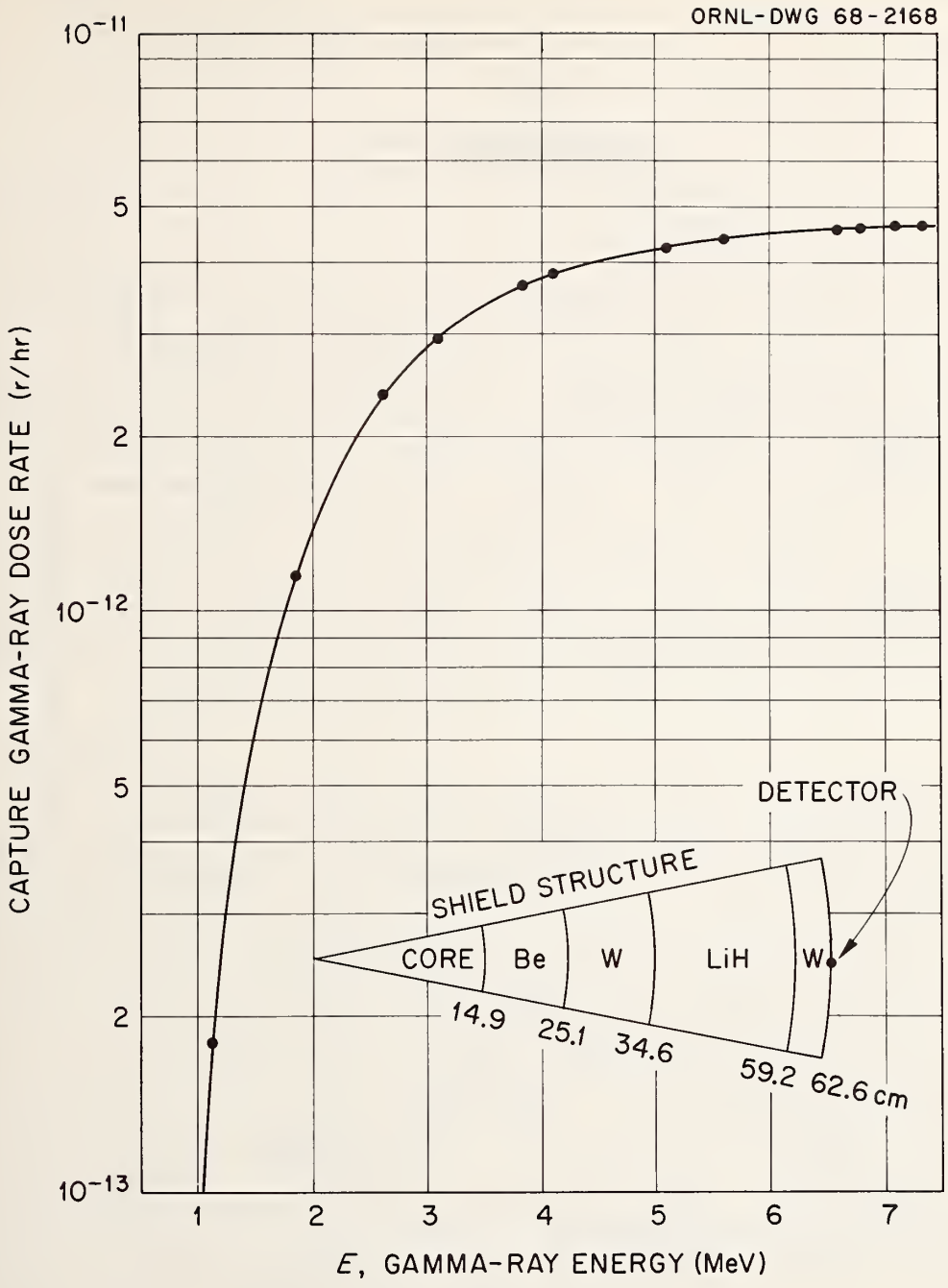

FIG. 1 Capture Gamma-Ray Dose Rate Normalized to one Gamma Ray of Energy E per Neutron Capture.

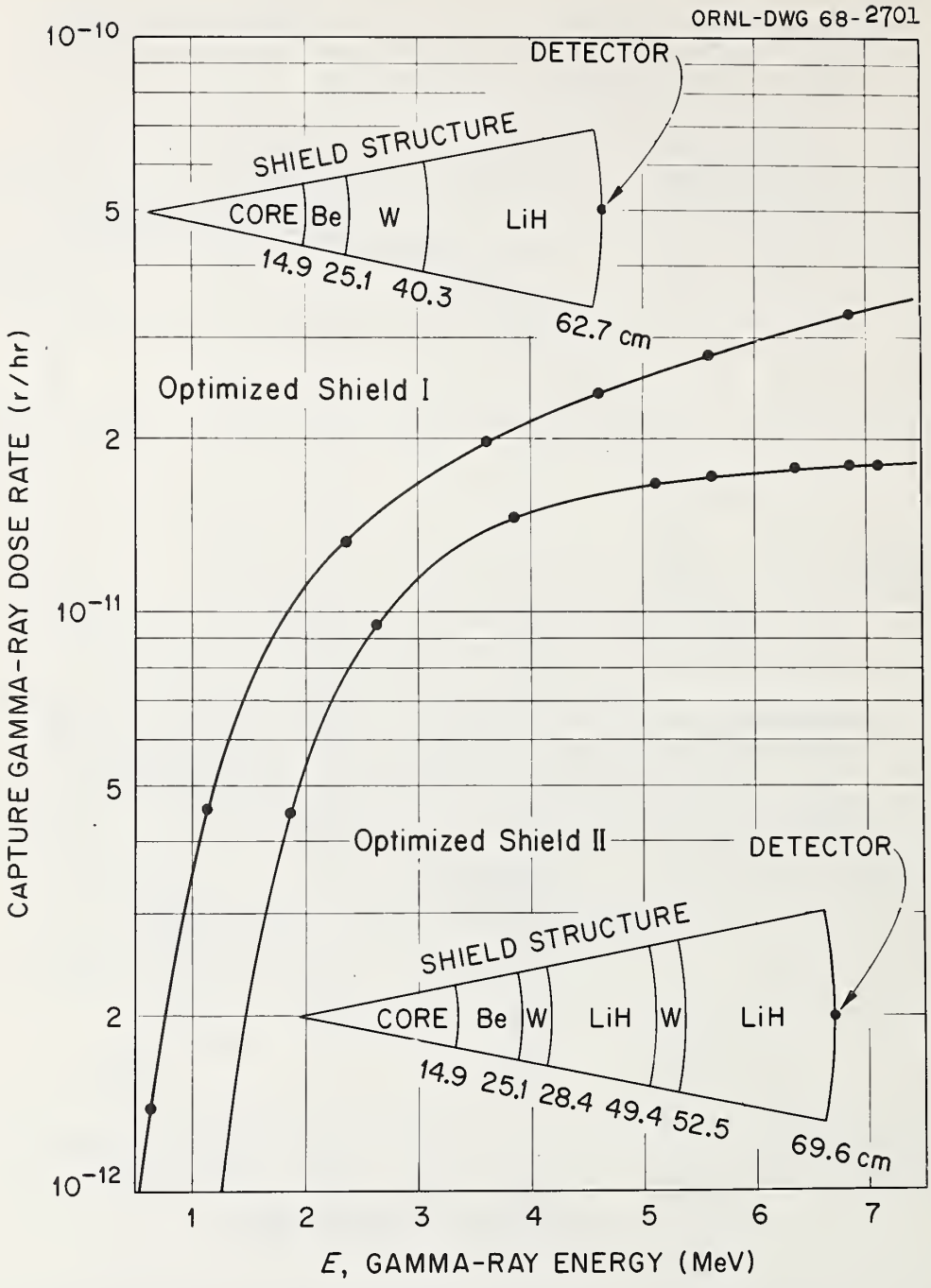

FIG. 2 Capture Gamma-Ray Dose Rate Normalized to one Gamma Ray of Energy E per Neutron Capture

Temperature Dependence of the Average Transmission of Tungsten Between 2 keV and 2 MeV Neutron Energy*

F. H. Fröhner**, J. L. Russell, Jr., and J. C. Young

Gulf General Atomic
San Diego, California 92112

Abstract

The average transmission of natural tungsten for neutrons with energies between 2 keV and 2 MeV was measured at room temperature and at 755°K. Below 100 keV a marked temperature dependence was observed. Around 10 keV the average transmission of the heated sample was about 16% lower than that measured at room temperature with a sample thickness of roughly one mean free path. The reason is the resonance structure of the total cross section of tungsten in this energy region. The Monte Carlo self-shielding code SESH was used to calculate the effect from level statistics (strength functions, mean level spacings, Wigner and Porter-Thomas distributions). It was found that in order to reproduce the data one has to use strength functions which are considerably higher than published values, and correspondingly small effective nuclear radii.

1. Measurement

Recent results of neutron spectrum measurements in large tungsten spheres [1] indicate an appreciable temperature effect. Such an effect can be understood on the basis of the temperature dependence of self-shielding by Doppler-broadened resonances. In order to test this hypothesis the average transmission of natural tungsten was measured in good geometry at room temperature (293°K) and, with a heated sample, at 755°K. The General Atomic electron linac was used to produce short bursts of neutrons, and time-of-flight data were taken on a 50 m flight path in the energy region between 400 eV and 2 MeV. The sample thickness was 0.153 nuclei/barn corresponding to roughly one mean free path in this energy range. After self-shielding corrections had been applied to the transmission data average total cross sections could be calculated (see next section). The agreement with average total cross sections by Whalen and Meadows [2] and by Tabony, Bilpuch and Seth [2] is good (see Fig. 1) for 293°K. Below about 200 keV, however, a marked temperature effect was observed. Around 5 keV, for instance, the average transmission is roughly 16% lower at 755°K than at 293°K, as shown in Fig. 2.

* Work supported by the U. S. Atomic Energy Commission.

** Present address: Kernforschungszentrum Karlsruhe, Institut für Angewandte Kernphysik.

313-475 O-68—6

2. Calculation

The average transmission can be written as

$$\left\langle e^{-n\sigma} \right\rangle = e^{-n\langle\sigma\rangle} \left\langle e^{-n(\sigma-\langle\sigma\rangle)} \right\rangle, \qquad (1)$$

where σ is the total cross section (weighted average over all isotopes) and n is the sample thickness in nuclei/barn. The angular brackets denote energy averages of the form

$$\left\langle f(E) \right\rangle = \int w(E,E') f(E') dE' \quad , \qquad (2)$$

where the weight function w(E,E') (normalized to unity) contains essentially the instrumental resolution and the energy dependence of the neutron flux. The second factor on the right-hand side of Eq. 1 is the self-shielding correction. For thin samples or for smooth cross sections it approaches unity.

At the energies of interest here the tungsten resonances are well separated from each other. This means that in each level sequence of importance the resonance widths (natural widths) are normally much smaller than the spacings between neighbor levels of the same sequence (same spin and parity). In this case the cross section can be written as a sum of Breit-Wigner single-level terms, and the average can be found as

$$\left\langle o(E) \right\rangle = 2\pi^2 \lambda\lambda_1 \sum_1 (2l+1) S_l v_l \cos 2\xi_l + 4\pi\lambda^2 \sum_1 (2l+1) \sin^2 \xi_l, \qquad (3)$$

where $2\pi\lambda$ is the CMS wave length of the neutron, $2\pi\lambda_1$ is the wave length for E = $\frac{1}{3}$ eV, v_l and ξ_l are hard-sphere penetration factors and phase shifts, [3] and S_l is the strength function of the l-th partial wave. S_l was assumed to be independent of the resonance spin J.

The average cross section is seen to be temperature-independent. This shows that the temperature dependence of the average transmission must be contained in the self-shielding correction factor.

A calculation of the average transmission at a given energy E involves an energy average according to Eq. 2 or, equivalently, an average over the cross section distribution if the weight function w(E,E') is so broad that many resonances contribute to the average. Analytical expressions for the average transmission can only be derived with drastic and questionable simplifications, but as Bogart and Semler [4] showed it is straightforward to generate cross section samples by Monte Carlo techniques starting from level statistics, i. e. from the Wigner and Porter-Thomas distributions. Average transmission and capture data are being interpreted at General Atomic by a self-shielding code, SESH, [5] which was written along these

lines. Starting from level statistics this code generates representative cross samples according to the following scheme:

For a large number of energies E' near E "resonance environments" are created as illustrated in Fig. 3. The distances between resonances are found by sampling the Wigner distribution [6], the widths from the Porter-Thomas distribution [7]. Radiation widths are taken as constant from resonance to resonance. Contributions from abl important resonance sequences (spin-parity combinations) and isotopes are added to yield the total cross section. The fact that large level spacings contain more energies E' (receive more neutrons) is properly taken into account.

The SESH code was used to calculate the self-shielding corrections indicated in Fig. 1 and the average transmissions shown in Fig. 2. Mean level spacings and radiation widths were taken from BNL 325 [2], s-wave strength functions from Seth's compilation [8]. For the p-wave strength function values between 0 and 10^{-4} were used, however, the results were not very sensitive to S_1 below 100 keV. Partial waves with $l > 1$ contributed only slightly to the potential scattering cross section and were neglected. Above 100 keV the calculated values began to deviate from the experimental data. The reason is inelastic scattering, which becomes important above 100 keV but was neglected in the calculations. Below 5 keV, on the other hand, fluctuations due to partially resolved resonances become noticeable. Therefore only the range from 5 keV and 100 keV was used in fitting the data. The fit was achieved by adjusting the effective nuclear radius R' ($\xi_0 = R'/\lambda$), i. e. the potential scattering cross section. The result, R' = 7.3 fm, is listed in Table 1 together with the input quantities. The resulting fit is shown in Figs. 1 and 2.

It is seen that the calculated temperature effect is only about 70% of the measured effect. A slight improvement is possible by raising the s-wave strength functions by about 30%, i. e. to the upper limits given by the error bars in Seth's compilation, and by lowering R' by a corresponding amount to 6 fm. However, the resulting temperature effect is still about 20% too small. In order to improve the agreement between experiment and calculation one has to use much higher strength function values.

3. Conclusion

The temperature dependence of the average transmission of tungsten was measured and calculated. For a sample thickness corresponding to one mean free path the effect is appreciable: At 5 keV neutron energy the average transmission is about 16% lower at 755°K than at 293°K. Monte Carlo calculations of the average transmission reproduced the energy dependence quite well but the temperature effect was underestimated by about 25%. In order to remove this discrepancy one has to assume much higher s-wave strength functions and much lower effective nuclear radii at 10 keV than those which are known from the resolved-resonance region (below 1 keV). At this stage it is difficult to say whether this result actually indicates large strength function variations within 10 keV (intermediate structure) or whether there are other effects, including unknown systematic errors in the experiment or the calculation. Some of the ambiguities in the present analysis could be removed by the use of separated isotopes in a measurement

of the temperature dependence of the average transmission of tungsten.

TABLE 1

Input quantities for self-shielding calculation

A	$S_0 \cdot 10^4$	$S_1 \cdot 10^4$	D_0 (eV)	D_1 (eV)	Γ_γ (eV)	R' (fm)
182	2.9	1.0	42	14	0.063	7.3
183	2.0	1.0	13	5.8	0.083	7.3
184	2.6	1.0	80	27	0.057	7.3
186	1.8	1.0	56	19	0.072	7.3

4. References

1. S. C. Cohen, J. L. Russell, Jr., J. C. Young, Trans. ANS, 10 (1967)2

2. Goldberg et al. (ed.), Report BNL 325, 2nd Edition, Supplement No. 2, Vo. IIC (August 1966)

3. A. M. Lane and R. G. Thomas, Rev. Mod. Phys. 30 (1958)257

4. D. Bogart and T. T. Semler, USAEC Report CONF-660303, Book 1, p. 502 (1966),
   D. Bogart, Nucl. Data for Reactors, Vo. I, p. 503, Vienna 1967

5. F. H. Fröhner and D. Naliboff, Report GA-8380 (1968)

6. E. P. Wigner, Report ORNL-2309, p. 59 (1959)

7. C. E. Porter and R. G. Thomas, Phys. Rev. 104 (1956) 483

8. K. K. Seth, Nucl. Data A2 (1966) 299

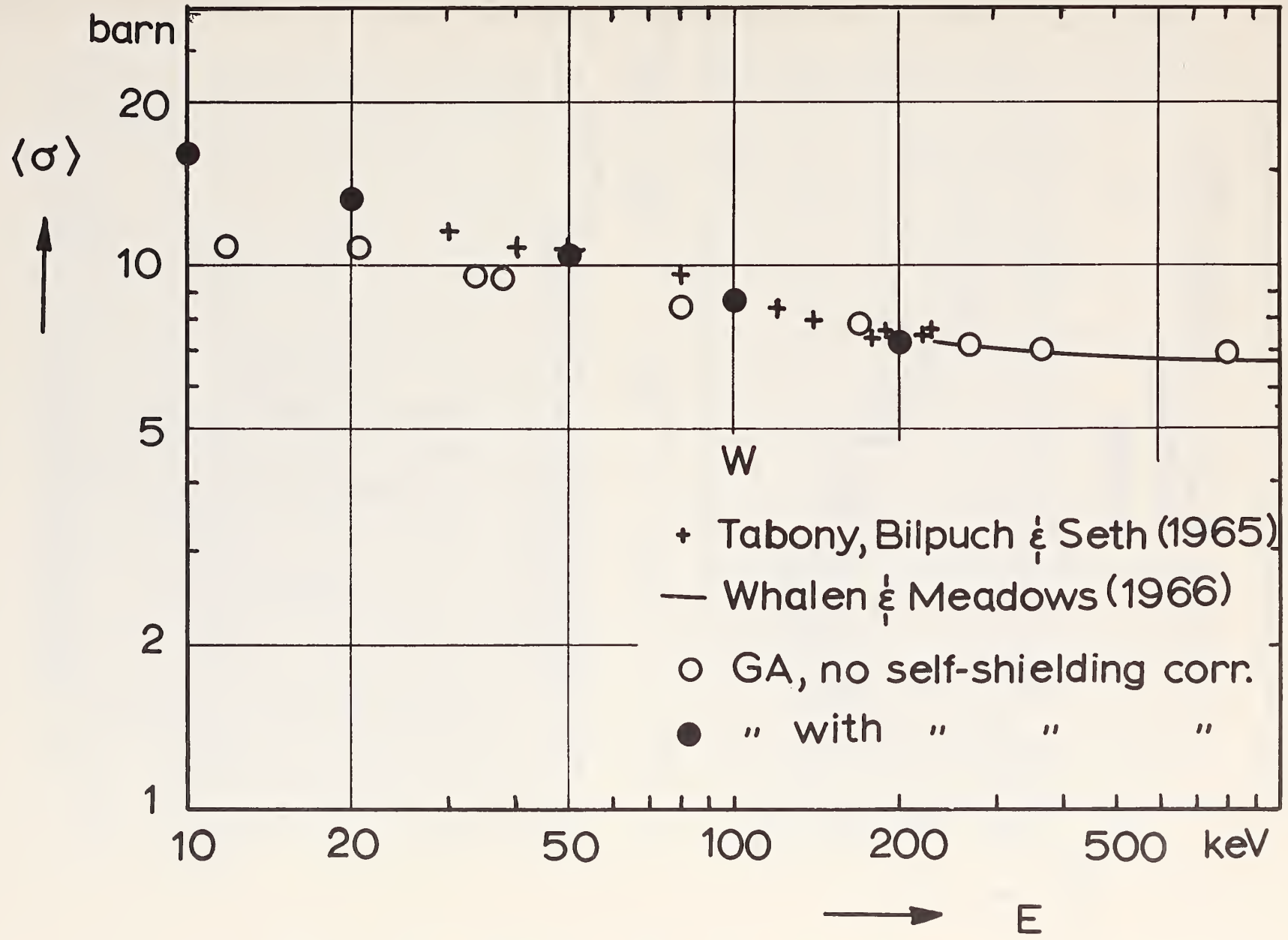

Fig. 1. Average total cross section versus neutron energy.

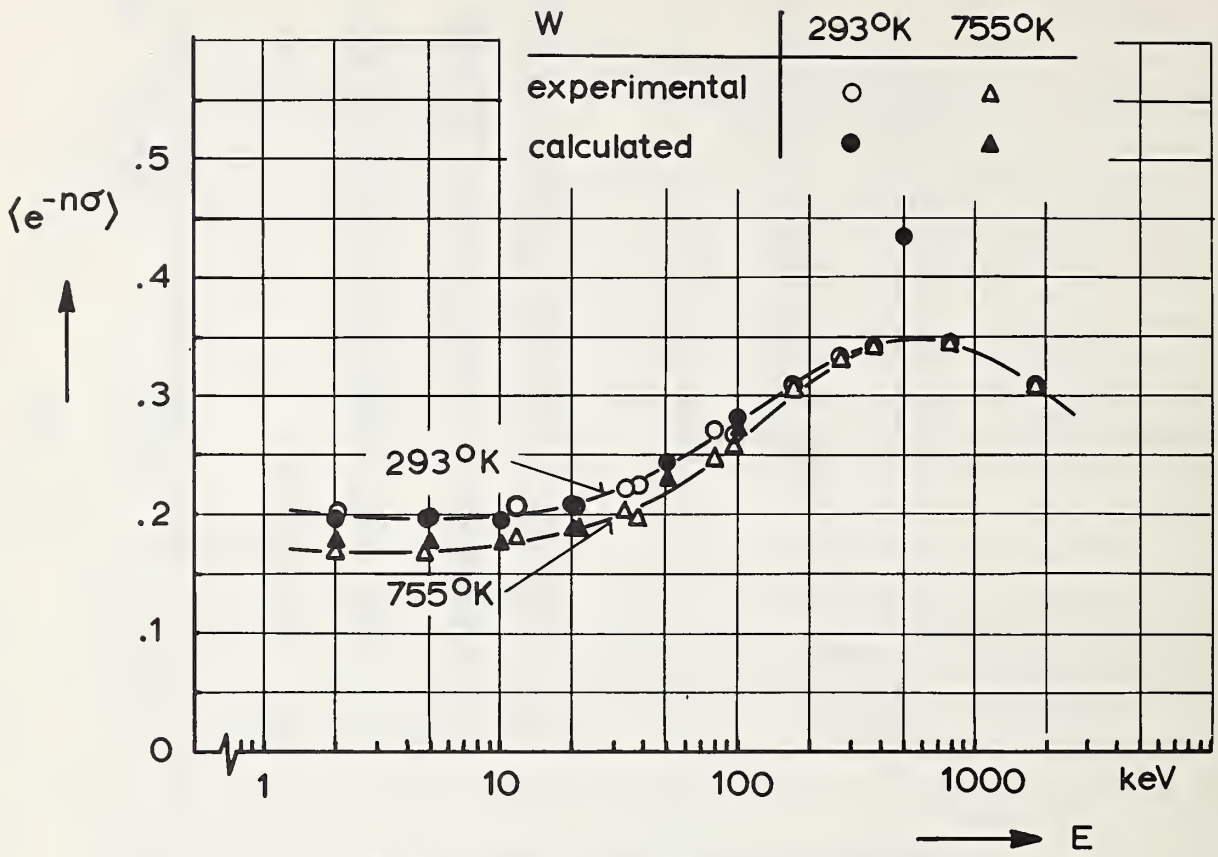

Fig. 2. Average transmission versus neutron energy for two temperatures. The calculated values were obtained by a Monte Carlo calculation with the input numbers of Table 1.

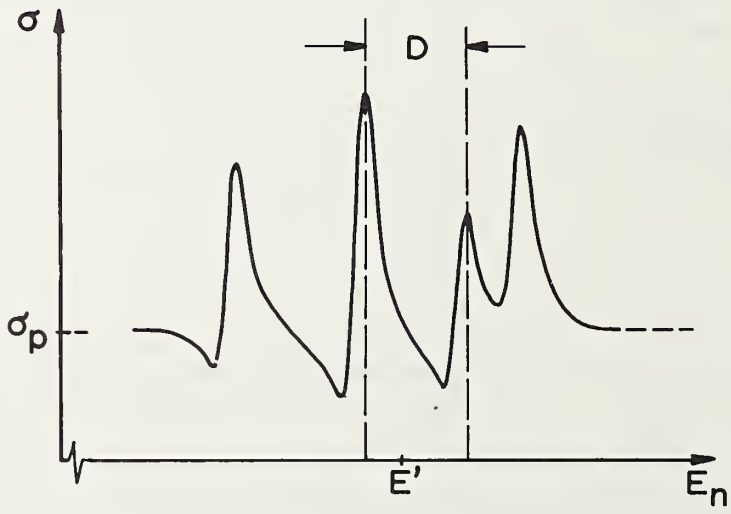

Fig. 3. Illustration of a resonance "environment" at energy E', constructed with two resonance pairs and central interval D.

NEUTRON CROSS SECTIONS: THE FIELD OF RADIATION DAMAGE*

M. S. Wechsler
Solid State Division, Oak Ridge National Laboratory
Oak Ridge, Tennessee 37830

ABSTRACT

Theoretical and experimental aspects of radiation damage are reviewed with special emphasis on the roles of neutron cross section and energy spectrum. Radiation damage to metals is due to the production of lattice defects (atom displacements) caused by collision or recoil events or the introduction of foreign atoms by transmutation reactions. Non-metals are also affected by ionization and electronic excitation. The basic theory of displacement production is outlined, which leads to an over-estimate of the neutron radiation damage in comparison to that observed experimentally. Various elaborations on the basic theory leading to reduced displacement production are then described. These include ionization losses, anisotropy of neutron scattering, forward scattering in the collision cascade, channeling and focusing, and dynamic and thermal annealing. Other special factors are displacements due to inelastic neutron scattering and capture (n,γ) recoils. Finally, the consequences of radiation damage are discussed. Two types of radiation embrittlement are of particular importance in reactor technology: grain boundary embrittlement in fuel cladding alloys and the increase in the ductile-brittle transition temperature in ferritic pressure-vessel steels.

1. Introduction

True solids are characterized by a regular periodic arrangement of atoms in a crystal lattice. "Radiation damage" refers to the deviations from regular periodicity introduced as a result of the bombardment by high-energy particles or electromagnetic radiations. The lattice defects introduced upon neutron irradiation are essentially of two types, lattice displacements and transmuted atoms. When the impinging particle strikes a lattice atom, sufficient energy and momentum may be transferred to displace the lattice atom from its lattice site, thus producing an interstitial atom (or, simply, an "interstitial") at the in-between place where the struck atom comes to rest and a vacant lattice site (a "vacancy") at the point where it originated. For neutron irradiation particularly, the struck atom (or "primary knock-on") may have sufficient energy to displace additional atoms upon subsequent collisions ("secondary knock-ons"), resulting in a kind of displacement cascade as the energy of the primary knock-on is partitioned among other atoms in the crystal. The interstitials and vacancies thus produced may combine with one another, either during the initial formation of the displacement cascade or as a result of thermal motion. If an interstitial and a vacancy recombine, they are mutually annihilated, but if defects of like species become aggregated, then multiple interstitials and vacancies are formed. The outcome is therefore a rather complicated distribution of single and multiple interstitials and vacancies.

*Research sponsored by the U. S. Atomic Energy Commission under contract with Union Carbide Corporation.

The other type of radiation damage, transmuted atoms, are in some respects simpler to deal with. All solids, especially metals, always contain foreign atoms, at least in part-per-million concentrations. The transmutation products are added to the solid's original burden of impurities. Of course, in some respects the transmuted atoms need to be given separate consideration. For one thing, they are usually radioactive and the solid will require special handling. Also, cases arise where an innocuous or even beneficial impurity in a material is transmuted into a harmful one. An example is boron in steel, where the boron-10 isotope undergoes an (n, α) reaction with a thermal-neutron cross section of more than 4000 barns. Since the boron tends to be segregated at grain boundaries, the helium produced will be segregated there. Serious practical consequences of helium produced from this source are found in connection with steels for reactor fuel cladding in thermal reactors. Similar problems arise in fast neutron environments due to (n,p) and (n,α) reactions with various elements in structural materials.

While most of the displacement damage is due to the collision processes sketched above, lattice atoms may receive energy from another source upon neutron irradiation sufficient to displace them from their lattice sites. This is the energy due to atom recoil upon the emission of a capture gamma ray when a neutron is absorbed. The recoil energy is often high enough to create several displacements.

In addition to the lattice defects produced upon irradiation, there are effects due to ionization and electronic excitation. In metals, these effects are mostly minor, since charge anomalies are rapidly dissipated, and energy transferred to the metal from this source is converted into heat. However, in non-metals trapped charges can be retained and this gives rise to optical absorption (color centers), contributions to paramagnetic susceptibility and resonance, and extrinsic semiconductivity and photoconductivity. These are important tools in the study of radiation damage, but we shall confine our attention henceforth to lattice effects. For further information on electronic effects, the reader is referred to the books [1-3] and proceedings [4-5] on radiation damage and to the reviews and papers referenced there. We have said that ionization and electronic excitation do not play a prominent role in radiation damage to metals. While this is largely true, electronic effects do enter in the mechanism of energy loss of energetic knock-ons in metals. This will be mentioned further in the next section.

It is the purpose of this brief review to survey the current status of knowledge concerning radiation damage, with particular emphasis on matters that depend on neutron cross sections and on the energy distribution of the neutron radiation environment. In the next section, we describe the basic theory of radiation damage. Then a brief sketch is given of the reasons why the simple theory is considered inadequate. Finally, some consequences of radiation damage are discussed that are important in reactor technology.

2. The Basic Theory of Radiation Damage

For damage due to neutron collisions, the process starts, of course, when a high-energy neutron collides with a lattice atom. The likelihood of transfer of energy T (within unit energy interval at T) by a neutron of energy E is expressed by the differential scattering cross section, $\sigma_T^!(E,T)$. The next question is: If energy T is transferred, what is the probability that the atom will be displaced? This is given by the displacement probability function, $p(T)$. Finally, given that the atom is displaced and becomes a primary knock-on, how many secondary displacements will ensue as the burst of energy introduced by the projectile neutron is spread out and apportioned in the lattice? For this we need a multiplication factor, $\nu(T)$. These factors are then used to form the

displacement cross section:

$$\sigma_d(E) = \int_0^{T_m(E)} \nu(T)\, p(T)\, \sigma_T'(E,T)\, dT \qquad (1)$$

The upper limit, $T_m(E)$, is the maximum transferred energy (head-on collision between the neutron and the lattice atom); its value, dictated by conservation of energy and momentum, is

$$T_m(E) = 4AE/(1+A)^2 = \alpha E \qquad (2)$$

where A is the mass number of the struck atom and $\alpha = 4A/(1+A)^2$. If the incident radiation has a spectrum of energies such that $\phi'(E)\,dE$ is the flux of neutrons with energies between E and E + dE, then the displacement production rate is

$$K = \int_0^\infty \phi'(E)\, \sigma_d(E)\, dE \qquad (3)$$

For the most part, neutrons interact only with the nuclei of atoms and the scattering is largely isotropic in the center of mass system. In this case the differential cross section $\sigma_T'(E,T)$ is independent of T, all energy transfers from zero to $T_m(E)$ being equally likely. Hence to this isotropic approximation we may write

$$\sigma_T'(E,T) = \begin{cases} \sigma_s(E)/T_m(E) = \sigma_s(E)/\alpha E, & T \leqq T_m \\ 0, & T > T_m \end{cases} \qquad (4)$$

where $\sigma_s(E)$ is the total scattering cross section. It is convenient to define a primary energy distribution function [6,7]

$$\kappa(E,T) = \sigma_T'(E,T)/\sigma_s(E)$$

which for the isotropic case becomes simply

$$\kappa(E,T) = \begin{cases} 1/\alpha E, & T \leqq T_m \\ 0, & T > T_m \end{cases} \qquad (5)$$

For a particular target element, the relative effectiveness of various neutron spectra in producing damage is seen roughly by comparing the functions averaged over the excitation function $\sigma_s(E)\,\phi'(E)$, i.e., weighted by the number of interactions per second per atom at energy E. This gives*

$$\bar{\kappa}(T) \equiv \overline{\kappa(E,T)}^E = \frac{\int_0^\infty \kappa(E,T)\, \sigma_s(E)\, \phi'(E)\, dE}{\int_0^\infty \sigma_s(E)\, \phi'(E)\, dE} \qquad (6)$$

*Strictly speaking, when $\bar{\kappa}(T)$'s are compared for spectra that differ greatly at energies below T_d/a, where $T_d \cong 25$ ev (see below), the lower limits should be T_d/a.

A knowledge of the primary energy distribution function $\kappa(E,T)$, also permits the calculation of the average energy transferred by a neutron of energy E, i.e.

$$\bar{T}(E) = \int_0^{T_m(E)} K(E,T)\, T\, dT \tag{7}$$

We now wish to illustrate the forms of $\bar{\kappa}(T)$ and $\bar{T}(E)$ for several simple cases.

The simplest case to consider is that of isotropic neutron scattering, although as indicated below corrections for forward scattering become significant at higher energies and for heavier atoms. In this case, Eqs. (5), (6) and (7) give

$$\bar{K}(T) = \frac{\int_{T/\alpha}^{\infty} \frac{1}{\alpha E}\, \sigma_s(E)\, \phi'(E)\, dE}{\int_0^{\infty} \sigma_s(E)\, \phi'(E)\, dE} \tag{8}$$

and

$$\bar{T}(E) = \frac{\alpha E}{2} \tag{9}$$

Furthermore, if we assume that σ_s is constant, then $\bar{\kappa}(T)$ and $\bar{T}(E)$ may be evaluated for various analytical forms of $\phi'(E)$. Also, the $\bar{T}(E)$ may be averaged over the spectrum, i.e.

$$\bar{\bar{T}} = \frac{\int_0^{\infty} \bar{T}(E)\, \phi'(E)\, dE}{\int_0^{\infty} \phi'(E)\, dE}$$

For monoenergetic neutrons at energy E_f

$$\bar{K}(T) = \begin{cases} \frac{1}{\alpha E_f}, & T \leq \alpha E_f \\ 0, & T > \alpha E_f \end{cases} \tag{10}$$

as shown in Fig. 1, and $\bar{\bar{T}} = \alpha E_f/2$. A case of more frequent interest is the fission spectrum. If the Cranberg expression [8]

$$\phi'(E) = \phi \frac{2}{E_f} \left(\frac{E}{\pi E_f}\right)^{1/2} \exp\left(-\frac{E}{E_f}\right) \tag{11}$$

is used, we find

$$\bar{K}(T) = \frac{2}{\alpha E_f}\, \mathrm{erfc}\left(\sqrt{T/\alpha E_f}\right) \tag{12}$$

where

$$erfc(x) = \frac{2}{\sqrt{\pi}} \int_x^{\infty} \exp(-t^2)\,dt$$

and $\bar{\bar{T}} = 3\alpha E_f/4$. For U^{235} fission, $E_f \cong 1.3$ Mev. Fig. 1 shows that $\bar{\kappa}(T)$ decreases monotonically with increasing T for the fission spectrum.

The actual neutron spectrum varies, of course, from one reactor type to another and from place to place within a given reactor. Several representative spectra are shown in Fig. 2. In Fig. 3, the $\bar{\kappa}(T)$ functions are shown for Fe as calculated from Eq. (8) using the $\sigma_s(E)$ values from the ORNL GAM-2 library [9]. For the TREAT (graphite-moderated) and HFIR (water-moderated) reactors, the slowing-down spectrum (region $E \lesssim 10$ kev, where $\phi'(E) \cong \phi_o/E$ or where $\phi'(u) \cong \phi_o = \text{const.}$, Fig. 2) gives rise to $\bar{\kappa}(T) \propto T^{-1}$, upper left corner of Fig. 3. Therefore, the number of primary knock-ons with T less than, say, 1 kev is quite large. On the other hand, for the fission spectrum or for a fast reactor like the DFR the $\bar{\kappa}(T)$ is quite constant for T's below 1 kev.

Plots of $\bar{\kappa}(T)$ such as those in Fig. 3 give an indication only of the likelihood of transferring energy T in neutron-atom collisions. Although there remain questions of corrections due to anisotropy of neutron scattering and contributions due to inelastic scattering, the principles underlying the calculation of κ or σ_T' are fairly well understood. However, the treatment of the $p(T)$ and $\nu(T)$ factors in Eq. (1) are not on such firm ground. In the usual approach $p(T)$ is approximated by a step function (dashed curve, Fig. 4) which defines the "displacement threshold energy", T_d. However, it is realized that there must be a range of T's over which $p(T)$ rises from 0 to 1 (solid curve, Fig. 4.), and, furthermore, the probability of displacement will depend on the direction of motion of the struck atom relative to the crystal axes. The T_d's are determined chiefly by electron-irradiation experiments [3] where the energy and direction of the incident beam may be controlled. The damage rate as indicated by electrical resistivity increase upon irradiation is measured as a function of electron energy and the result is compared with theory. The T_d giving the best agreement between observed and calculated damage rates is then chosen as the correct one. The theory of electron-irradiation damage differs from what is sketched here for neutrons chiefly in the differential scattering cross section, $\sigma_T'(E,T)$. For electrons one deals with relativistic Rutherford scattering for which low energy transfers become highly preferred so that most of the electron collisions produce no more than one displacement, i.e., $\nu(T) = 1$. However, it should be realized that even for a well-collimated electron beam and for an infinitessimally thin sample (so that energy degradation in the sample may be neglected), the directions of motion of the struck atoms to be displaced will vary from the angle corresponding to T_d to that for a head-on collision ($\bar{\theta} = 180°$ in the center-of-mass system). The result of these considerations is that the experiment gives an effective T_d, which is unavoidably some kind of average over direction. The general magnitudes of T_d lie in the range 10-50 ev, and 25 ev is generally taken as a reasonable representative value. The values given by Lucasson and Walker [10] for Cu, Ag, Ni, and Fe are 22, 28, 24, and 24 ev, respectively.

The displacement multiplication function, $\nu(T)$, probably represents the most uncertain factor in radiation damage theory. This springs from the fact that at this stage in the damage process ion-ion interactions are taking place in a crystalline environment and the appropriate interaction potentials are not at all well known. In the

simplest form of the theory of displacement cascades, $\nu(T)$ is taken to be

$$\nu(T) = \begin{cases} 0, & T < T_d \quad (13A) \\ 1, & T_d \leq T \leq 2T_d \quad (13B) \\ T/2T_d, & 2T_d \leq T \leq T_i \quad (13C) \\ T_i/2T_d, & T_i < T \quad (13D) \end{cases}$$

The first of Eqs. (13) incorporates the sharp threshold $p(T)$ and Eq. (13B) allows for the idea that an atom with energy between T_d and $2T_d$ may transfer enough energy to displace another atom but it will itself be trapped at the lattice site, thus producing no additional displacements. Equation (13C) is a consequence of the assumption of hard-sphere collisions in which all energy transfers are equally likely, as may be demonstrated in several ways (cf. Chadderton, [11] pp. 26-30). One simple approach is as follows: Since no further displacements are produced when T falls below $2T_d$, consider the energies of atoms when they first fall below $2T_d$. Half of them will lie between 0 and T_d and these will not have contributed any displacements, and half will lie between T_d and $2T_d$ giving rise to one displacement each. By the assumption of equally-likely transferred energies, each of the two groups will contain $T/2T_d$ atoms and thus this number of displacements is produced. Equation (13D) is intended to account for loss of energy due to ionization and electronic excitation at higher energies, which makes no contribution to displacement production. The ionization cutoff energy is not a precise quantity, but it is estimated to be given roughly by the mass number of the target atoms in kilovolts [2], i.e.

$$T_i \cong A \text{ (kev)}$$

We see from Fig. 3 that most of the primary energies lie below this value for Fe ($T_i \cong 56$ kev). As the mass number decreases, the average primary energy at first increases due to the increase in α (Eq. 2), but a point is reached where T_i becomes so low that, upon further decrease in A, the average primary energy effective for producing displacements decreases again. Fig. 5 shows the average effective primary energy as a function of A for the fission spectrum; it reaches a maximum at about A = 70.

3. Elaborations on the Basic Theory

For a number of reasons the basic theory is believed to be inadequate, but it is difficult to put the theory to a rigorous test. The principal experimental method for the determination of displacement production rates is the measurement of the increase in electrical resistivity during irradiation at low temperatures where the radiation-produced defects are immobile. For reactor irradiations of copper at close to liquid helium temperature, the basic theory (excluding ionization losses) predicts a displacement production rate that is greater than that observed experimentally by a factor of about 10 [Ref. 13]. Various factors may be cited to account for the over-prediction:

1. Ionization losses: When ionization losses are included as indicated in

Eq. (13), the discrepancy is reduced to a factor of about 6 [Ref. 12]. However, it is realized that the assumption of a sharp ionization cut-off energy, T_i, is a crude approximation since the shift from energy loss to the electronic system at high energies to energy loss by atom recoil at low energies must occur over a range of energies. Lindhard et al. [14] have given a more elaborate treatment of this energy division as a function of energy and mass number.

2. Anisotropy of neutron scattering: To include anisotropy in the formulation, the differential scattering cross section is expanded in terms of Legendre polynomials $P_\ell(\cos\bar{\theta})$ where $\bar{\theta}$ is the scattering angle in the center-of-mass system. Thus,

$$\sigma_T'(E,T) = \sum_{\ell=0}^{\infty} B_\ell(E)\, P_\ell(\cos\bar{\theta}) \qquad (14)$$

where T and $\bar{\theta}$ are related by $T = T_m \sin^2(\bar{\theta}/2)$ and the normalization is such that

$$\sigma_s(E) = \int_0^{T_m(E)} \sigma_T'(E,T)\, dT = 2B_0$$

As a measure of the anisotropy, we may use B_1/B_0 which, as Leibfried [6] has pointed out, can be set equal to

$$\frac{B_1}{B_0} = \left(\frac{R}{\lambda\!\!\!^{-}}\right)^2$$

where R is the nuclear radius, $R \cong 1.5 \times 10^{-13}$ cm $\times A^{1/3}$, and $\lambda\!\!\!^{-}$ is the deBroglie wavelength of the neutron, $\lambda\!\!\!^{-} = \hbar/(2mE)^{1/2}$. For a 20% deviation from isotropy, i.e. for $B_1/B_0 = 0.2$, the neutron energy must not exceed E_s where

$$E_s \cong 2A^{-2/3} \text{ (in Mev)}$$

In Fig. 6 E_s is plotted versus A. Even for A as low as 10, E_s is only about 0.4 Mev, and thus we may expect anisotropy to be a significant factor in most reactor irradiations. According to Holmes [13] and Wollenberger [15], for Cu in a graphite reactor spectrum like that for the TREAT reactor the theoretical over-prediction of the damage is reduced to a factor of about 4.5 due to the combined effects of ionization losses and anisotropy. The reduction in the average transferred energy due to anisotropy is shown for iron in Fig. 7 taken from the paper by Sheely [16].

3. Atomic scattering in the collision cascade: The expression given in Eqs. (13) for the multiplication factor, $\nu(T)$, assumes that the atom-atom interactions are hard-sphere collisions, but it is realized that this is a rather poor approximation. Robinson [17, 18] has indicated several improved representations of the scattering law. In the first approach, the scattering probability function is expanded in a series of Legendre polynomials similar to the expansion in Eq. (14) for the neutron scattering. A second method is to express the scattering probability function as an inverse power function of the energy transferred T', i.e. as $1/(T')^n$. The exponent n is allowed to range from n=0 (isotropic scattering) to n=2 (Rutherford scattering). The third procedure is to employ hard-sphere scattering in which the distance of closest approach is made energy-dependent by matching the actual potential in value and

slope by an analytic potential such as the screened Coulomb potential [6,7,17]. This last procedure tends to be most accurate for large energy transfers and tends to discount those near the displacement threshold energy. However, any of the above-mentioned representations of the scattering law could account for the remaining discrepancy between theoretical and experimental damage rates.

4. Channeling and focusing: In the foregoing it was assumed that the moving atoms engage in a series of random two-body collisions, with no account taken of the crystalline structure of the medium. Yet, several mechanisms exist in which energy may be lost in sub-threshold interactions due to the regular arrangement of atoms in the solid. In channeling, the moving atom is deflected into an open channel between atom rows, where it undergoes a series of glancing collisions with the atoms that make up the walls of the channel. The subject was reviewed recently by Datz et al. [19]. One evidence of channeling is the anomalously high penetration of ions bombarded upon single crystals as compared to amorphous forms of the same material [20,21]. Oen and Robinson [22] and Robinson [17,18] have given theoretical expressions for $\nu(T)$ which include an energy-independent channeling probability. A probability of 7 or 8 percent is sufficient to reduce $\nu(T)$ by a factor of two. The reduction in radiation damage due to channeling was verified experimentally by Noggle and Oen [23] by observing damage clusters by transmission electron microscopy in single crystal gold films irradiated with 51-Mev iodine ions. The number of damage clusters was about 14 times less for films aligned so as to produce channeling than for unaligned films. However, in order to observe this reduction in damage due to channeling, the ion beam must be aligned along the direction of the channel to within one or two degrees. Thus it seems unlikely that many recoiling atoms will emerge from a lattice site in a direction appropriate for channeling. For one thing, neighboring atoms should tend to block the struck atoms from the channels. The term "focusing" refers to the transmission of energy and momentum (or mass in a series of replacement collisions) down atom rows in a series of correlated collisions. In a manner similar to channeling, focusing may fritter energy away in sub-threshold collisions. However, in contrast to channeling focusing is a low energy event.

5. Dynamic and thermal annealing: As the term "displacement cascade" suggests, many of the defects produced upon neutron irradiation are concentrated in a dense cluster or zone. The energy of an isolated interstitial-vacancy is about 5 ev, whereas, as we have said, the displacement threshold energy is about 25 ev. Thus, a large fraction of the energy expended in producing a displacement is contributed to thermal vibrations which may cause an instantaneous dynamic annealing. Furthermore, the possibility exists that the interstitial may be situated so close to the vacancy that it is mechanical unstable and will recombine with it athermally. This will also cause a loss of energy to thermal vibrations. These factors have not been widely considered quantitatively because of their difficulty, although some treatments are available [6, 7,24,25]. Of course, thermal annealing takes place above about 30°K for many metals. This type of annealing has been studied extensively from the point of view of identifying the defects that are mobile as a function of temperature [3,13].

While on the whole the elaborations on the basic theory tend to reduce the predicted amount of radiation damage, there are several additional mechanisms by which atomic displacements could take place. One of these is inelastic scattering. Although inelastic scattering generally requires high neutron energies where the reactor neutron population is low, the scattering is largely isotropic and thus the average transferred

energy may be high. The expression for the transferred energy is [16,26]

$$T = \frac{\alpha}{2}\left\{E - \cos\bar{\theta}\left[E(E+Q/\mu_2)\right]^{1/2}\right\} + Q\mu_1$$

where Q is excitation energy of the reaction and μ_1 and μ_2 are the reduced masses of the neutron and target atom, respectively. Sheely [16] has shown that the inelastic scattering contribution to the displacement damage in iron is appreciable above about 1 Mev.

Another special source of radiation damage is that due to atom recoil upon capture gamma-ray emission following thermal neutron absorption. The recoil energy is given by

$$T = E_\gamma^2/2Mc^2$$

where E_γ is the capture gamma-ray energy, M is the mass of the recoiling atom, and c is the speed of light. For iron the maximum E_γ is about 10 Mev so the recoil energy may be as high as 10^3 ev. The capture gamma rays are emitted with energies over a spectrum of values. For the spectrum given by Troubetskoy and Goldstein [27,28] , the average T is about 390 ev. In a reactor spectrum in which the thermal neutron and fast neutron populations are roughly equal, the displacements due to (n, γ) recoil would obviously be swamped out by those due to fast neutron collisions. However, Coltman et al. [12,29] have used a highly thermalized neutron environment to study the isolated effects of (n,γ) recoil damage.

4. The Consequences of Radiation Damage

Radiation damage is seen most graphically by transmission electron microscopy. Fig. 8 shows a photomicrograph of a niobium sample irradiated at about 50°C to 2×10^{18} neutrons/cm^2 (E > 1 Mev) [30]. The black spots are defect clusters about 80 Å in diameter. The density is about 5×10^{15} defect clusters per cm^3, which corresponds to a defect cluster production cross section of 0.04 barns. By contrast the neutron scattering cross section for niobium at 1 Mev is about 7 barns. Thus on the average only one primary collision in about 200 produces a defect cluster. Defect clusters have been observed by transmission electron microscopy in many irradiated solids [31], and much effort is being devoted toward determining the nature of the defect clusters (e.g. whether they are of interstitial or vacancy type; whether they are nucleated homogeneously or heterogeneously) and how they influence physical and mechanical properties.

The effect of radiation on mechanical properties is particularly important in connection with the structural integrity of materials for nuclear reactors. Metals and alloys are hardened and embrittled by radiation. The radiation hardening is indicated by an increase in yield stress that appears to be proportional to the square root of the neutron fluence at low fluences, but then exhibits a saturation effect upon further exposure [32,33,34]. The radiation embrittlement is manifested in several ways [35,36], but from the practical point of view we may delineate two areas: high-temperature embrittlement of face-centered metals, particularly reactor fuel cladding alloys, and low-temperature embrittlement of body-centered cubic metals, particularly reactor pressure-vessel steels. The cladding alloys are typically austenitic

stainless steels or nickel-base alloys, and at their operating temperatures (up to about 700°C) the fracture mode is intergranular, i.e. the ductility is limited by cohesion at the grain boundaries. The decrease in ductility upon irradiation is thought to be due to the helium produced by (n, α) reactions, and possibly hydrogen by (n,p) reactions. Trace amounts of boron are a major source of helium in thermal reactors at low exposures through the ^{10}B (n, α) reaction [37]. However, after high exposure enough helium or hydrogen is produced by fast (n, α) or (n, p) reactions to be a serious problem also. In fact, numerous bubbles are observed in stainless steel after irradiation to about 10^{22} neutrons/cm^2 in fast reactors [38,39], a matter of some concern to the fast breeder reactor programs in the United States and elsewhere. In some cases, the bubble volume is greater than can be predicted on the basis of helium and hydrogen production. However, the predictions are based on cross sections largely derived from nuclear systematics [40], which may be seriously in error as a paper in these proceedings has pointed out [41]. These considerations indicate the need for further work on (n,p) and (n, α) cross sections and better determinations of the reactor neutron spectra.

The radiation embrittlement of reactor pressure-vessel steels is associated with the ductile-brittle transition phenomenon characteristic of body-centered cubic metals generally and exemplified by ferritic pressure-vessel steels. Above the ductile-brittle transition temperature, the steel fractures by shear absorbing large amounts of energy, but below this temperature the fracture mode is cleavage involving rather little energy absorption. For the type of steel used in most water-cooled reactor pressure vessels today, the transition temperature is in the region -20° to 10°C as indicated by notch-impact tests. Upon irradiation the transition temperature is increased, which enhances the susceptibility to catastrophic brittle fracture. However, the magnitude of the increase is quite variable. For example, a wide variety of pressure-vessel steels shows an increase of 50° to 150°C upon irradiation below 260°C to 10^{19} neutrons/cm^2, E > 1 Mev (See Fig. 5.8 of Ref. 42). The results for a single grade of steel indicate less scatter (for ASTM A-212-B or A-302-B steel, an increase of 100° to 150°C for 10^{19} neutrons/cm^2). It is possible to enumerate various materials and radiation parameters that may be responsible for the apparent variability in the radiation embrittlement [43]. One factor is the difference in neutron spectrum from one experiment to another. Sheely [16] has taken spectral differences into account by calculating the displacement production rate for irradiations in several types of reactors. When the increase in transition temperature upon irradiation is plotted versus the calculated number of displacements instead of the integral neutron fluence about 1 Mev, the data exhibit considerably less scatter.

The sudden massive failure of welded steel structures due to the inherent low-temperature brittleness of ferritic steels is now a well-documented phenomenon [44]. The danger to the public safety represented by such a failure in a reactor pressure vessel is a matter of recurrent discussion, as indicated for example by recent letters of the Advisory Committee of Reactor Safeguards to the AEC [45,46]. A better understanding of the mechanism of radiation embrittlement in reactor pressure-vessel steels would help to minimize this danger, and neutron physicists can play a role in achieving this by providing more complete and accurate information concerning neutron scattering cross sections and neutron spectra.

The assistance of J. D. Jenkins in providing calculations of neutron spectra and primary energy distribution functions is gratefully acknowledged. I also appreciate the efforts of O. S. Oen, who read the manuscript and made helpful comments.

5. REFERENCES

1. D. S. Billington and J. H. Crawford, Jr., Radiation Damage in Solids, Princeton, N. J., 1961.
2. G. J. Dienes and G. H. Vineyard, Radiation Effects in Solids, Interscience, N.Y., 1957.
3. James W. Corbett, Electron Radiation Damage to Semiconductors and Metals, Academic Press, N. Y., 1966. (Solid State Physics, Suppl. 7)
4. R. Strumane, J. Nihoul, R. Gevers, and S. Amelinekx, The Interaction of Radiation with Solids, North Holland Publishing Company, Amsterdam, 1964.
5. D. S. Billington, Editor, Radiation Damage in Solids, Academic Press, 1962.
6. G. Leibfried, Bestrahlungseffekte in Festkörpern, Teubner, Stuttgart, 1965.
7. G. Leibfried, "Introduction into Radiation Damage Theory," p. 1 in The Interaction of Radiation with Solids, North Holland Publishing Company, Amsterdam, 1964.
8. L. Cranberg, G. Frye, N. Nereson, and L. Rosen, "Fission Neutron Spectrum for U^{235}," Phys. Rev. 103, 662 (1956).
9. J. D. Jenkins, private communication.
10. P. G. Lucasson and R. M. Walker, "Production and Recovery of Electron-Induced Radiation Damage in a Number of Metals," Phys. Rev. 127, 485 (1962).
11. L. T. Chadderton, Radiation Damage to Crystals, John Wiley and Sons, New York, 1965.
12. R. R. Coltman, C. E. Klabunde, D. L. McDonald, and J. K. Redman, "Reactor Damage in Pure Metals," J. Appl. Phys. 33, 3509 (1962).
13. D. K. Holmes, "Radiation Damage in Non-Fissionable Metals," p. 147 in The Interaction of Radiation with Solids, North Holland Publishing Company, Amsterdam, 1964.
14. J. Lindhard, V. Nielsen, M. Scharff, and P. V. Thompson, "Integral Equations Governing Radiation Effects. Notes on Atomic Collisions, III," Mat. Fys. Medd. Dan. Vid. Selsk. 33, No. 10, 1-42 (1963).
15. H. Wollenberger, "The Energy Distributions of Primary Atoms in Copper Produced by Fast Mono-Energetic and Reactor Neutrons," p. 249 in Radiation Damage in Solids, Vol. I, International Atomic Energy Agency, Vienna, 1962.
16. W. F. Sheely, "Correlation of Radiation Damage to Steel with Neutron Spectrum," Nucl. Sci. and Engring. 29, 165 (1967).
17. M. T. Robinson, "The Influence of the Scattering Law on the Radiation Damage Displacement Cascade," Phil. Mag. 12, 741 (1965).
18. M. T. Robinson, "The Influence of the Scattering Law on the Radiation Damage Displacement Cascade, II," Phil. Mag., in press.
19. S. Datz, C. Erginsoy, G. Leibfried, and H. O. Lutz, "Motion of Energetic Particles in Crystals," Ann. Rev. Nucl. Sci. 17, 129 (1967).
20. B. Domeij, F. Brown, J. A. Davies, G. R. Piercy, and E. V. Kornelsen, "Anomalous Penetration of Heavy Ions of Kev Energies in Monocrystalline Tungsten," Phys. Rev. Letters 12, 363 (1964).

313-475 O-68—7

21. G. R. Piercy, F. Brown, J. A. Davies, and M. McCargo, "Experimental Evidence for the Increase of Heavy Ion Ranges by Channeling in Crystalline Structure," Phys. Rev. Letters 10, 399 (1963).
22. O. S. Oen and M. T. Robinson, "The Effect of Channeling on Displacement Cascade Theory," Appl. Phys. Letters 2, 83 (1963).
23. T. S. Noggle and O. S. Oen, "Reduction in Radiation Damage due to Channeling of 51-Mev Iodine Ions in Gold," Phys. Rev. Letters 16, 395 (1966).
24. R. Von Jan, "Defektverteilung in Verlagerungskaskaden (I)," Phys. Stat. Sol. 6, 925 (1964).
25. R. Von Jan, "Defektverteilung in Verlagerungskaskaden (II)," Phys. Stat. Sol. 7, 299 (1964).
26. J. Monahan, "Kinematics of Neutron-Producing Reactions," p. 49 in Fast Neutron Physics, Part I, edited by J. B. Marion and J. L. Fowler, Interscience Publ., 1960.
27. E. Troubetskoy and H. Goldstein, "A Compilation of Information on Gamma-Ray Spectra Resulting from Thermal-Neutron Capture," ORNL-2904, May 17, 1960.
28. E. Troubetskoy and H. Goldstein, "Gamma Rays from Thermal Neutron Capture," Nucleonics 18, 171 (1960).
29. R. R. Coltman, C. E. Klabunde, and J. K. Redman, "Survey of Thermal Neutron Damage in Metals," Phys. Rev. 156, 715 (1967).
30. R. P. Tucker and S. M. Ohr, "Direct Observation of Neutron Irradiation Damage in Niobium," Phil. Mag. 16, 643 (1967).
31. M. J. Makin (editor), The Nature of Small Defect Clusters, in two volumes, AERE-R 5269, 1966.
32. M. J. Makin, "Radiation Damage in Face-Centered Cubic Metals and Alloys," in Radiation Effects, Gordon and Breach Science Publishers Inc., New York, 1968.
33. S. M. Ohr, R. P. Tucker, and M. S. Wechsler, "Radiation Hardening in B.C.C. Metals Niobium and Iron," Proceedings of the International Conference on Strength of Metals and Alloys, Japan Inst. of Metals, 1968.
34. M. S. Wechsler, R. P. Tucker, and S. M. Ohr, "Fluence Dependence of Radiation Hardening in Polycrystalline Niobium," p. 66 in Radiation Metallurgy Section, Solid State Division Progress Report, ORNL-4246, 1968.
35. M. S. Wechsler, "Radiation Embrittlement of Metals and Alloys," pp. 296-345 in The Interaction of Radiation with Solids, ed. by R. Strumane et al., North Holland Publishing Co., Amsterdam, 1964.
36. J. O. Stiegler and J. R. Weir, "Effects of Radiation on Ductility," Chap. 12 in Ductility, American Society for Metals, 1968.
37. D. R. Harries, "Neutron Irradiation Embrittlement of Austenitic Stainless Steels and Nickel Base Alloys," J. Brit. Nucl. Energy Soc. 5 (1), 74-87 (January 1966).
38. C. Cawthorne and E. J. Fulton, "The Influence of Irradiation Temperature on the Defect Structures in Stainless Steel," pp. 446-460 in The Nature of Small Defect Clusters, ed. by M. J. Makin, AERE-R 5269, 1966.
39. J. O. Stiegler, E. E. Bloom, and J. R. Weir, "Electron Microscopy of Irradiated EBR-II Fuel Cladding," Proceedings of ANS Meeting, June 1968.
40. H. Alter and C. E. Weber, "The Production of Hydrogen and Helium in Metals During Reactor Irradiation," J. Nucl. Mater. 16, 68 (1965).

41. J. Weitman and N. Åverhög, "Helium Production Cross Section Measurements," p.125 in Proceedings of the Second Conference on Neutron Cross Sections and Technology, 1968.
42. G. D. Whitman, G. C. Robinson, and A. W. Savolainen, Technology of Steel Pressure Vessels for Water-Cooled Nuclear Reactors, ORNL-NSIC-21, December 1967.
43. M. S. Wechsler, "Radiation Damage to Pressure Vessel Steels," Nucl. Safety 8, 461 (1967).
44. C. F. Tipper, The Brittle Fracture Story, Cambridge University Press, 1962.
45. "Text of ACRS Letter to AEC," Nucleonics 24, 17 (1966). Also Nucl. Safety 7 (2), 260 (1965-66).
46. Letter, ACRS to the Chairman of AEC, Nucl. Safety 8, 277 (1967).

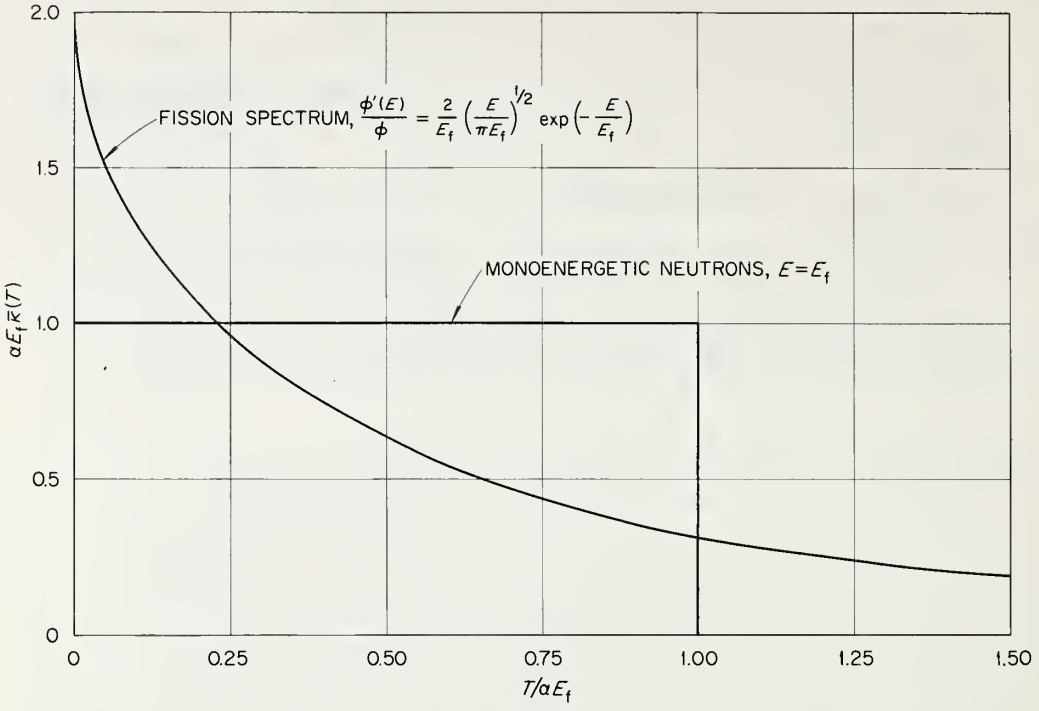

Fig. 1. The Primary Energy Distribution Function $\kappa(T)$ (times αE_f) for Monoenergetic Neutrons of Energy E_f and for a Fission Spectrum (after Leibfried [6]).

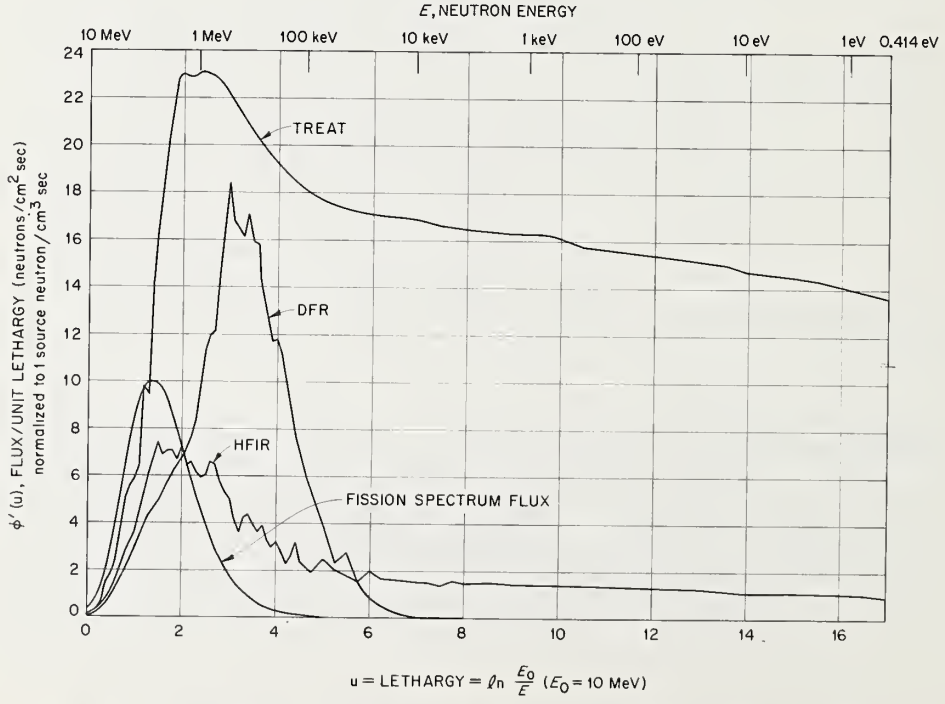

Fig. 2. Representative Neutron Spectra for Several Reactors and for the Fission Spectrum (after Jenkins [9]).

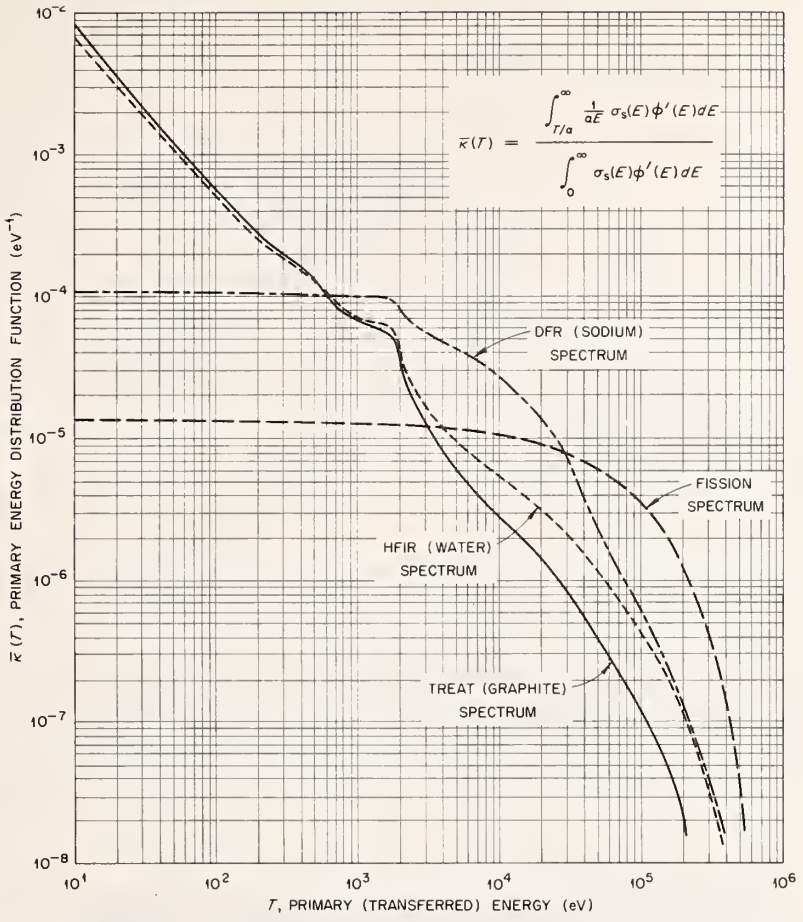

Fig. 3. Primary Energy Distribution Function versus Primary (Transferred) Energy for Iron for Elastic Isotropic Scattering for Various Reactor Spectra (after Jenkins [9]) .

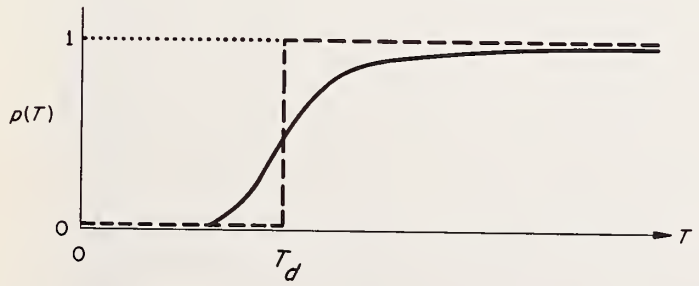

Fig. 4. Displacement Probability Function vs Primary Energy.

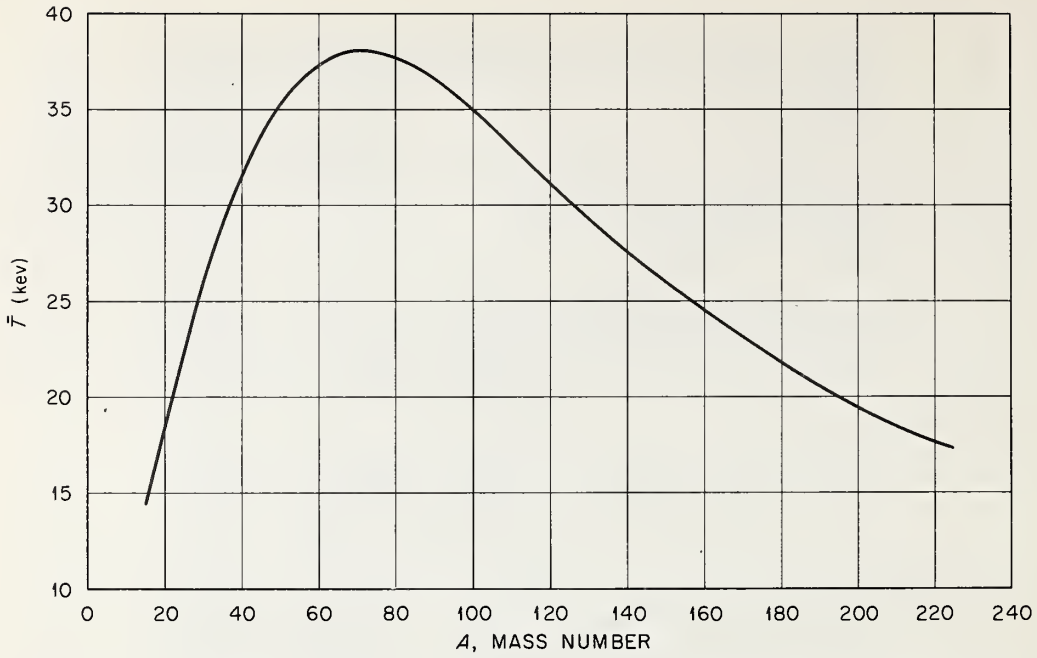

Fig. 5. Average Effective Primary Energy for the Fission Spectrum versus Mass Number with Corrections for Ionization (after Coltman et al. [12]) .

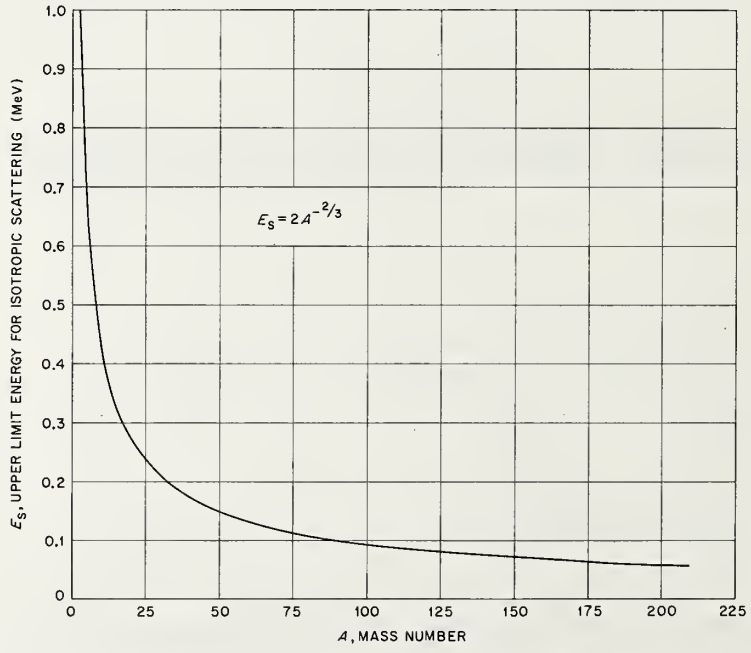

Fig. 6. Upper Limit Energy for Isotropic Neutron Scattering versus Mass Number (after Leibfried [6]) .

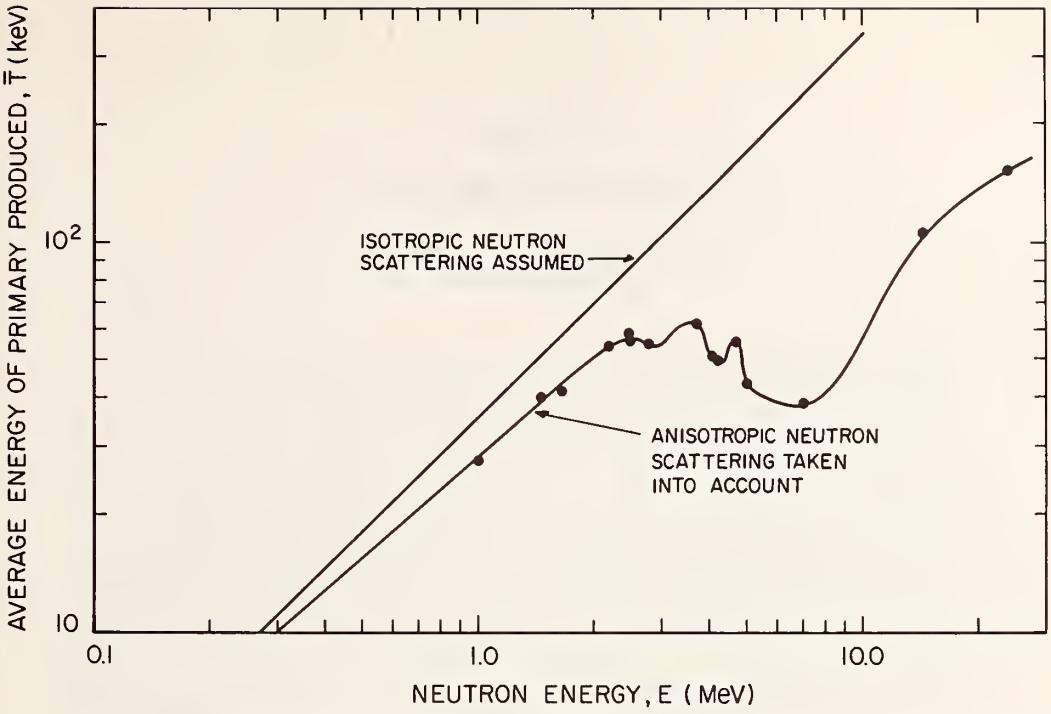

Fig. 7. The Average Primary Energy versus Neutron Energy for Iron Assuming Isotropic Neutron Scattering and taking Anisotropy into Account (after Sheely [16]).

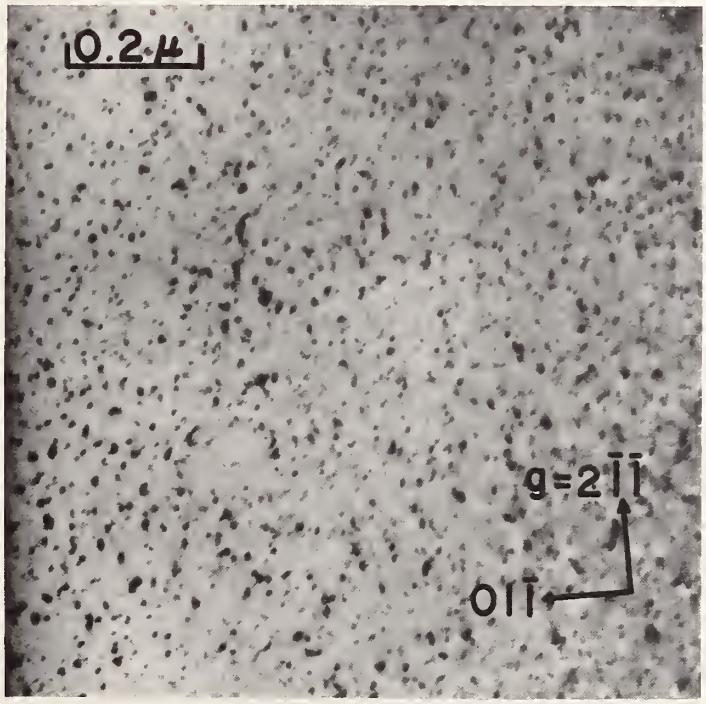

Fig. 8. Transmission Electron Micrograph showing Defect Clusters in Irradiated Niobium (after Tucker and Ohr [30]).

Production of s-Nuclei from e- and r-Seed Nuclei by a Fixed Neutron Flux.

J. P. Amiet and H. D. Zeh

Institut für Theoretische Physik

Universität Heidelberg
German Federal Republic

Abstract

The s-process of nucleo-synthesis assumes that part of the nuclei with A > 62 are produced in a slow neutron capture chain from iron seed-nuclei (e-nuclei) in red giant stars. Experimental data of neutron capture cross sections support the first part of this hypothesis. We want to point out, however, that better agreement with the best data available to us may be obtained in a simpler way. Starting with the iron group nuclei and in addition with the nuclei which may be produced by β^--decay ("r-nuclei") as a seed we are able to approximately reproduce the empirical abundances by irradiating the seed nuclei by a uniform neutron flux. The agreement may be improved if part of the s-abundances are assumed to have been present already in the seed. This result indicates that the s-process is only a secondary process, thus shifting the main burden of nuclear synthesis to the production of the seed nuclei.

The abundance distribution (1,2) of heavy nuclei ($A \gtrsim 63$) definitely shows the existence of at least three abundance groups. The most abundant group consists of just those nuclei which can be produced by β^--decay from nuclei lying on the neutron-rich side of the mass valley. The second group contains the nuclei which are shielded against β^--decay but which may be produced by neutron capture if the time between two capture processes is large compared to β-decay times.

The property of the second group gives information about its history. The correlation (3) between abundances and neutron capture cross sections which exists for this group strongly supports the assumption of a slow neutron capture process ("s-process"). This empirical correlation has become definite with the determination of Maxwell-averaged capture cross sections for several pure isotopes (4). It states that the products σH of cross sections and abundances form a smooth function of atomic weight A(fig. 1).

It has already been noted by B^{2}FH (5) that this curve shows a steep decrease in the neighborhood above iron and a slow decrease for heavier nuclei. More recent data (2) show a definite kink at A 76. Since these authors assumed that all s-nuclei were produced from iron as a seed, they originally suggested two different neutron fluxes J_n for the two parts of the curve. This suggestion was not adequate, since the irradiation of the iron peak nuclei by a uniform flux essentially shifts it towards the right instead of producing a slowly varying distribution. It has hence been proposed that the empirical curve can be explained (6) by mixing many "cooking pots" with different flux histories J_n, using some probability distribution $p(J_n)$. However, plausible distributions (i.e., Gaussian) are not able to describe the empirical curve for both small and large values of A-56. The success of this theory therefore hinges on the selection of rather artificial probability distributions.

Since it is to be expected that the neutron-rich nuclei ("r-nuclei") as well as the iron group nuclei ("e-nuclei") were produced under much more extreme conditions (5,7) than the s-nuclei considered in this paper, it is natural to assume that both were already present in the seed. Fig. 2 shows the results of irradiating this seed with several uniform neutron fluxes. It is shown how structures present in the seed are smoothed and how a kink may be understood as arising from the two components of the seed.

Fig. 1 compares one of these calculated curves with the empirical points and with one of the curves given by Clayton et al. (6). Whereas the latter does not adequately explain the increase towards iron, our curve is too low to the right of magic neutron numbers. As is indicated by the broken line of fig. 1 this shortcoming may be avoided if some of the s-abundance is assumed to have been already present in the seed. This latter curve is not quite consistent, however, since the s-nuclei of the seed cannot have had the same flux history as the present ones. A detailed analysis of the best parameters will be published elsewhere (8). The empirical values for Zr (based on ref. (2)) are too large compared to any existing theory.

More measured and Maxwell averaged neutron capture cross sections of pure isotopes are needed to distinguish between the different theories or parameters, and to answer the question whether the flux history of the heavy nuclei has been the same as that needed to produce the nuclei with $22 > A \geq 44$ (5).

---

(1) H. E. Suess and H. C. Urey, Rev. Mod. Phys. 28 (1956) 53

(2) H. C. Urey, Harold Jeffreys Lecture, delivered at Burlington House, 1966

(3) R. A. Alpher, Phys. Rev. 74 (1948) 1577

(4) R. L. Macklin and J. H. Gibbons, Astroph. J. 149 (1967)577

(5) E. M. Burbidge, G. R. Burbidge, W. A. Fowler and F. Hoyle, Rev. Mod. Phys. 29 (1957) 547

(6) D. D. Clayton, W. A. Fowler, T. E. Hull and B. Zimmerman, Ann. Phys. (N.Y.) 12 (1961) 331

(7) J. P. Amiet and H. D. Zeh, Phys. Lett. 25B (1967) 305

(8) J. P. Amiet and H. D. Zeh, Z. Physik (to be published).

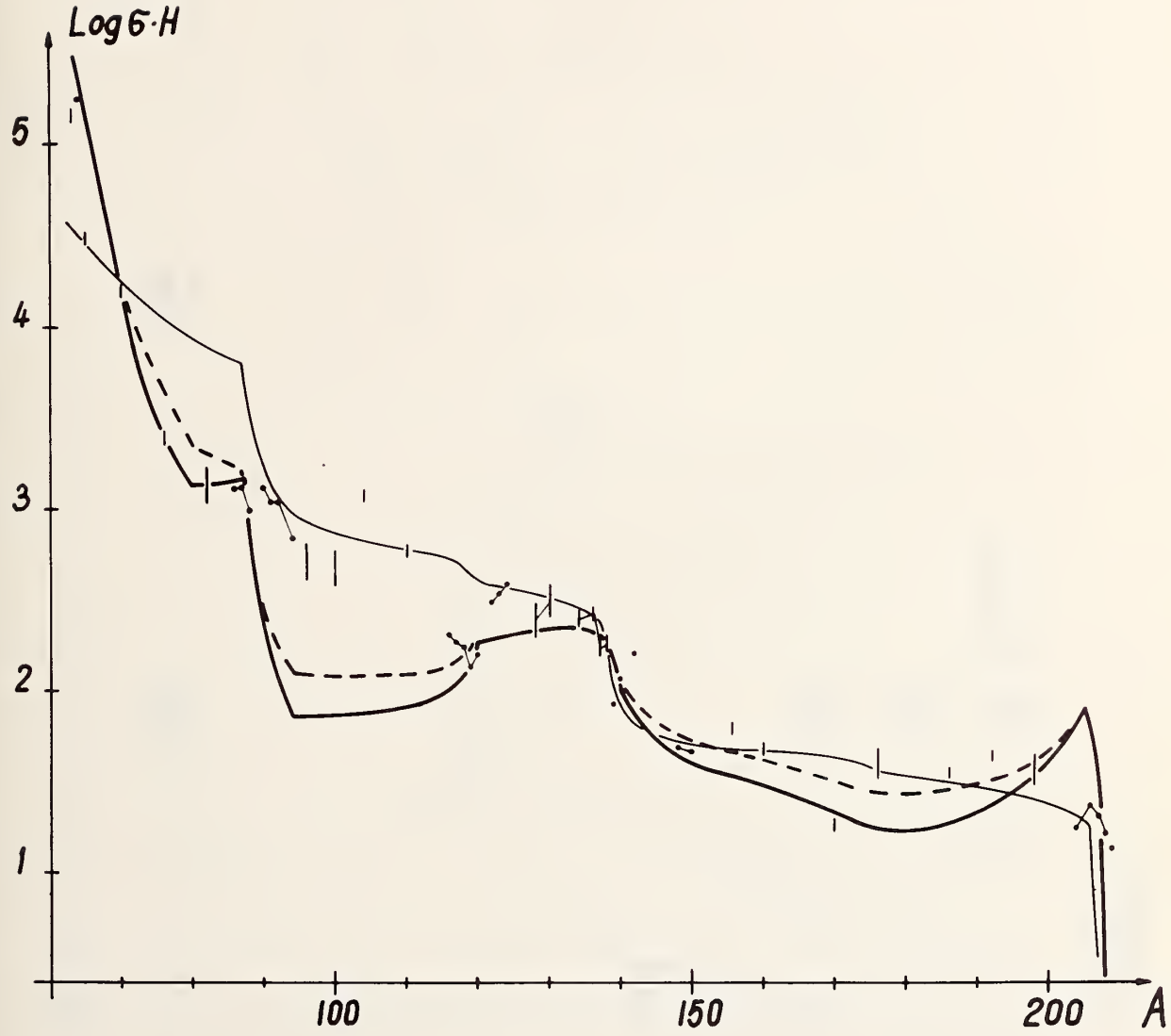

Figure 1: Empirical values of σH are plotted as points if σ (averaged for kT = 30 keV - ref. (4)) has been measured, as small vertical bars if σ has been estimated, and by large bars if σ and H have both been estimated. The measured abundances H are meteoritic data taken from ref. (2). The heavy line shows values calculated with a uniform flux J_n = .12 neutrons /mb from e- and r- seed nuclei. The broken line is obtained with the same flux if 20% of the s nuclei are added to the seed. The thin line represents results of ref. (6) obtained with a weight function $\exp(-J_n/.17)$.

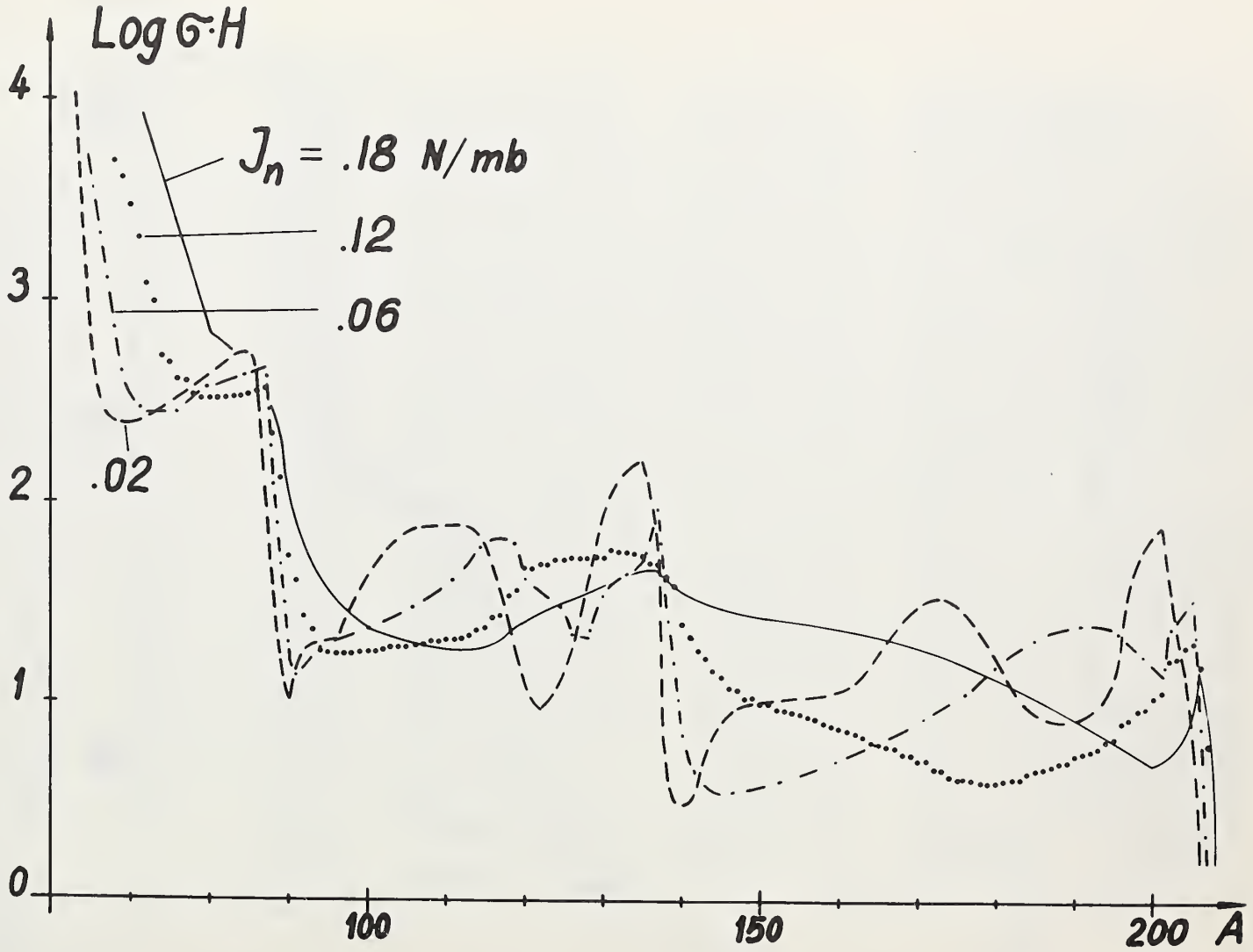

Figure 2: Values of σH obtained by irradiating e- and r- nuclei with different uniform neutron fluxes J_n.

Session B

STANDARD DATA, FLUX MEASUREMENTS, AND ANALYSIS

Chairman

R. S. CASWELL
National Bureau of Standards

NEUTRON FLUX MEASUREMENTS

R. Batchelor

Atomic Weapons Research Establishment

Aldermaston, Berkshire, England

1. Introduction

The problem of neutron flux measurement is basic to most neutron cross-section measurements. The experimenter can only escape it when he can perform a transmission type measurement i.e. when he measures the ratios of two fluxes with and without sample interposed between the neutron source and detector. Usually the transmission measurement is performed in good, linear geometry in which case the cross-section measured is the total cross-section. Occasionally the so-called sphere transmission method is used where the sample takes the form of a spherical shell surrounding either the source or the detector. In this case the measured flux ratio can be interpreted in terms of the total absorption cross-section.

The neutron flux measurement is very often avoided, or at least apparently so, by measuring a cross-section relative to another cross-section. However we note that in such cases it is the second cross-section which is essentially giving the flux. It is interesting to note that there has been a tendency to refer to this type of cross-section measurement as a ratio measurement if the precision of the second cross-section value is poor, whereas if the precision is good we have tended to call the measurement an absolute measurement. For example if an experimenter has measured the Pu^{241} fission cross-section by measuring Pu^{241} and U^{235} fission rates in the same flux we have usually referred to the measurement as a ratio measurement. However, if instead of a U^{235} fission counter, a proton recoil counter is used, we have tended to regard the measurement as an absolute one. One can understand the reason how this has grown up. It is that the H(n,p) happens to be a cross-section that can be measured by the transmission method whereas U^{235} (n,f) cross-section cannot be dealt with in this way. In this presentation I shall avoid this issue and deal first with flux measurements based directly on cross-section values--the so called standard cross-sections--and then deal with other methods, which can conveniently be called absolute methods, in which a knowledge of a cross-section, if required at all, is not the prime basis of the method.

In this paper we shall not be concerned with flux measurements in the general sense but will concentrate on the application to neutron cross-section measurement. We shall attempt to cover the energy region from thermal up to about 14 MeV although we shall concentrate mostly on the intermediate and fast regions. Because I believe that at this conference we are emphasizing the differential measurement, I shall also concentrate most of my remarks on the measurement of a unidirectional mono-energetic flux.

2. Flux Measurements based on Neutron Cross-sections

In the following paper Dr. Gibbons will review the state of Standard cross-sections, some of these cross-sections being the ones on which we base our flux measurements. In the measurement of flux, F(E), based on the standard reaction A(n,B)a the number of reactions counted by the detector is equal to $F(E)\ \sigma(E)\ C(E)n$ where n is the number of A atoms present, $\sigma(E)$ is the cross-section at energy E and C(E) is a correction factor arising from one or more causes e.g. counts lost below bias, multiple scattering. The product $\sigma(E)\ C(E)$ is essentially equal to the efficiency of the detector. Because it is usually difficult to obtain an accurate value of C(E), the experimenter usually tries to arrange for its value to be as close as possible to unity.

To the fast neutron physicist working in the region above 100 keV, by far the most important standard cross-section is the H(n,p). This is a cross-section which can be determined experimentally by transmission measurements and one which is also amenable to calculation. (The present status of this cross-section, and its suitability as a primary standard has recently been discussed by Hopkins[1]). Consequently the cross-section is known to about 1% accuracy. However what is usually required is not the total cross-section but the differential cross-section generally at 0° (for emission of protons). Below about 6 MeV the reaction is isotropic in the CM system but above this energy anisotropy begins to appear and it increases with increasing energy. At 14 MeV the uncertainty in the 0° differential cross-section is at least 2%, enough to be a significant contribution to the overall error in a flux measurement.

I will not have the time to deal in detail with all the methods of flux determination based on the H(n,p) cross-section. Most of the methods rely on the detection of the knock on protons rather than the scattered neutrons although a well known case where the latter is used is in the measurement of fast neutron scattering cross-sections by the time of flight technique. To measure the flux passing through the sample under investigation, the latter is replaced by a polythene sample of similar $n\sigma x$ and the number of neutrons scattered by the hydrogen is measured, usually at an angle of about 45°. The energy resolution is

sufficient to be able to resolve out neutrons scattered by the carbon present in the sample. Since the hydrogen scattered neutrons have a different energy from the neutrons scattered by the original sample, the efficiency response of the neutron detector as a function of neutron energy must be known. Because of the sensitive variation of scattered neutron energy with angle, the H(n,p) reaction is not suitable for very low incident neutron energies (below a few hundred keV) and either the C(n,n) or the Pb(n,n) is used as the standard.

There are two basic methods of using the H(n,p) cross-section by observation of the recoil protons, the first where hydrogen or hydrogenous material forms the sensitive material of the actual proton counter e.g. the gas in a gas counter, and the second where the hydrogenous material is separate from and not an integral part of the actual detector of the protons.

The main instruments belonging to the first class are the gas filled proportional counter and the organic scintillator. The former has in fact proved to be a very precise tool for the energy region 40 keV to 2 or perhaps 3 MeV. Figure 1 shows a diagram of the counter recently used by White[2] for the measurement of the fission cross-section of U^{235}. It is based on an original design of Skyrme et al.[3] The important point to notice is that the sensitive volume of the counter is accurately defined by the use of field tubes held at the correct potential with respect to the wire so that if the gas pressure and composition is known the effective number of hydrogen atoms in the neutron beam is likewise known. Multiple scatter effects in the gas are very small although wall and end effects can be large and have to be allowed for very carefully. Figure 2 shows the pulse height spectra obtained by White for various incident neutron energies, the wall effect being the reason for the slope of each plateau. The wall effect can be reduced by increasing the pressure of hydrogen or using a heavier gas such as methane, although it appears to be impractical to make if sufficiently small for energies greater than about 3 MeV. The diagrams also show how the observed spectra can be fitted to theoretical curves--in these cases obtained with the aid of a Monte Carlo programme. With no wall and end effects all these curves would be flat topped. It is easy to see that for neutrons below 40 keV energy the instrument will not be very useful because only a small fraction of the recoil proton distribution is observable above background due mainly to the presence of γ-radiation. To reduce this lower limit one must either reduce γ-background--usually not practicable--or use some form of discrimination against γ-rays. Bennett[4] has shown that a γ-ray pulse can be rejected from the rate of rise of the pulse relative to the rate of rise of a proton pulse but as far as I know this technique has not been applied by anyone making a flux measurement. However, Bennett has been able to make measurements on neutrons down to 1 keV energy. In his measurements with a proportional counter White[2] was able to achieve an

313-475 O-68—8

accuracy on flux of between 1.5 and 2%, the dominant contribution being that involved in fitting the theoretical pulse height spectrum to the observed curve. Thus this method is capable of quite high accuracy but I doubt if it has much more development potential and it is a tedious and difficult technique to use. However it would be extremely valuable if it could be developed for use at say 5 to 10 keV along the lines used by Bennett.

Also belonging to the first category is the organic scintillation counter, useful for neutrons in the MeV region. Although simple to set up and use--the basic ingredients are an organic scintillator of known size containing a known amount of hydrogen--it has proved to be very difficult to obtain the high accuracy which has been obtained with the proportional counter. The reasons are (a) the light output for electrons is much greater than that for protons thus making the counter very efficient for γ-rays, which are always present as background, (b) the response to protons is not a linear function of energy and (c) multiple scattering effects, which can be quite large in large scintillators. The sensitivity to γ-rays, effect (a), can be reduced by pulse shape discrimination--see e.g. ref. 5, but care has to be taken when applying this technique because it can reduce the neutron sensitivity by an unknown amount. Whereas in the case of the proportional counter only the wall and end effects distort the pulse height distribution from a rectangular shape, in the case of the organic scintillator both the complicated effects (b) and (c) contribute to the distortion. There is therefore a greater error in fitting an observed pulse height distribution to the calculated one. Figure 3 shows pulse distributions for a thin stilbene crystal and it illustrates the difficulties one runs into because of effect (b). The non linear response for protons means that the pulse distribution rises steeply at low pulse height and this type of distribution is clearly difficult to fit precisely. Details of this method of flux measurement have been discussed by Swartz and Owen[6] although since their review there has been further work carried out on the theoretical calculation of pulse height distributions, mainly using the Monte Carlo method to deal with the multiple scattering problem--see e.g. Batchelor et al.[7]

Also belonging to this category is the photographic plate detector, but this is rarely used for absolute flux measurements because it is tedious to apply and also because of the difficulty of knowing the effective number of hydrogen atoms present.

Turning now to the second category of instruments based on proton recoil detection i.e. those with the hydrogenous target separated from the nuclear counter, we find a variety of forms. The target, which must be thin enough to allow the protons to escape with very little energy loss, is a solid one such as polythene. The detector is usually arranged to detect the

protons emitted in the direction of the incident neutrons. The favorite detector used in the past was a CsI scintillator but now there is a tendency to use semiconductor counters at least for energies below about 5 MeV. Another important variable is the angle subtended by the foil at the counter. Since it is usually necessary to make the device as effecient as possible the solid angle is made as large as possible especially at low neutron energies since the effective thickness of the polythene foil must then be very small in order to keep the fraction of the proton energy lost in the foil small. Fortunately this bad geometry is practicable at low energies. An early sample of this type of counter was that used by Diven[8] who detected all the recoil protons i.e. into 2π solid angle, by an argon/CO_2 filled proportional counter. More recently White[2] following the original design of Dearnaley and Whitehead[9] used a semiconductor counter arranged as shown in Fig. 4 and obtained the recoil spectrum of Fig. 5 for neutrons of 2.25 MeV energy. Here again the solid curve is the theoretical fit. Note that this curve exhibits only a slight bump towards the high pulse height region. As the solid angle subtended by the foil at the counter is increased this bump will of course get progressively closer to a peak i.e. the counter gets more selective, until one reaches the limit of a real proton recoil telescope, which is very suited to flux measurements at higher energies, say greater than 5 MeV. The decreased efficiency arising because of the much reduced solid angle can be partially compensated by the use of a thicker foil. This "better" geometry is a practical necessity at high energies in order to eliminate the severe backgrounds from e.g. neutron reactions in the active element of the counter. What is done to reduce background is to insert one, or possibly two, dE/dx counters between the foil and detector and their outputs are put into coincidence with the output of the proton counter. In this way one identifies the protons emitted from the foil in the direction of the main counter and excludes events resulting from neutron interactions in the main counter, for example. Clearly this type of detector is much more difficult to set up and use than the poor geometry type of counter and in consequence it is harder to achieve high accuracy. However with great care one can make flux measurements with these instruments to between 3 and 5%.

We see therefore that instruments based on proton recoil methods cover the fast neutron range with quite good accuracy and the limit on precision is presently well above the error on the H(n,p) cross-section. Although there is no fundamental reason why the techniques can't be improved to the point where the H(n,p) cross-section error is dominant, I believe it will be extremely difficult to realize in practice.

For less precise work, say 5% or worse accuracy, the fast neutron physicist need not use the above tedious methods based on the H(n,p) cross-section. Instead he could choose a reaction

which leads to an active product e.g. $S^{32}(n,p)$ which would be suitable above 2 MeV. Alternatively he might choose a reaction which can be recorded event by event in a pulse counter, and probably the most convenient type of reaction to choose is a fission reaction. Above 1 MeV the $U^{238}(n,f)$ is probably the most suitable since a counter based on this reaction would not be sensitive to background neutrons of low energy which can arise from wall scattering etc. Below 1 MeV one would need to use either $U^{235}(n,f)$ or $Pu^{239}(n,f)$. The latter has some attraction since its cross-section appears to be nearly constant over a wide energy range and it turns out to be a little easier to assay a Pu^{239} foil than a U^{235} foil. Unlike the H(n,p) cross-section, fission cross-sections in the fast neutron region are not very accurately known--presently errors are 3% at best in some energy regions for some nuclei, but more usually 5-10%--and the overall errors on flux measurements are likely to be dominated by the errors in the cross-section. Since the techniques of fission foil assay are now getting very precise[10] and a fission ionisation chamber is such a straightforward instrument, this method of flux measurement could be developed into a very precise method if the errors on fission cross-sections could be reduced.

Fission reactions are clearly unsuitable for flux measurements in the resonance region where a smoothly varying cross-section is required. The obvious reactions to consider for this region are $He^3(n,p)$, $Li^6(n,\alpha)$, $B^{10}(n,\alpha)$ and $B^{10}(n,\alpha\gamma)$ and detectors based on these cross-sections can take on many forms. As yet the first reaction has not gained a great deal of popularity amongst cross-section measurers probably because of the early historical development of counters based on the $B^{10}(n,\alpha)$ reaction.

For laboratory work in the resonance region with white sources the $B^{10}(n,\alpha)$, $B^{10}(n,\alpha\gamma)$ and $Li^6(n,\alpha)$ reactions are used. Rarely does one find that absolute measurements are made; rather relative flux measurements are made so that it is only necessary to know the variation of detection efficiency with neutron energy. Where fission cross-sections are being measured the data obtained are usually normalized to the known values of the cross-sections at thermal energies. In the case of capture cross-section measurements this technique cannot be used (simply because the relative measurements do not extend low enough in energy) and in those cases a technique called the "black resonance technique"[11] is used to establish the product of neutron flux F(E) and detector efficiency $\varepsilon(E)$ at a few selected energies. The basis of this method is to select a resonance which is completely black to the incident neutrons where the capture yield is equal (apart from small corrections) to the product of $F(E)\varepsilon(E)$ and the ratio of capture width to total width. If this ratio is accurately known then $F(E)\varepsilon(E)$ can be obtained at the resonance energy E. Typically errors on the product obtained by this method are $\pm$ 2%.

Detectors based on the B^{10} and Li^{6} reactions should ideally have an efficiency curve which closely follows the shape of the cross-section energy curve. As we will see in Dr. Gibbons' talk we can be fairly sure that the cross-sections follow a $\frac{1}{v}$ behavior at least up to 1 keV, but an area of doubt creeps in around 10 keV. The way to make the detector efficiency follow the cross-section is to use a very small amount of material in the neutron beam and this is one of the reasons why BF_3 counters are so popular. If the counter is chosen so that the product of the number of atoms of B^{10} and the $B^{10}(n,\alpha)$ cross-section is less than 0.05 then the efficiency is proportional to the cross-section to within 2% in the energy region below 229 ev, the first resonance in copper (the material used in the construction of the counter). At higher energies the resonances can cause trouble, but perhaps more important, the counters are not fast enough in response to give the overall energy resolutions required. Detectors based on the $B^{10}(n,\alpha\gamma)$ reaction can also be made such that the efficiency is closely proportional to the cross-section by placing a thin block of B^{10} in the neutron beam and allowing the 478 keV γ-rays to be detected by either a NaI scintillator or a Moxon-Rae type counter.[11] Multiple scattering of neutrons in the B^{10} block is the major effect which causes the shape of the efficiency curve to depart from the shape of the cross-section curve and the effect increases with increasing neutron energy. However in the case of a block 3" diameter, total mass 3.4g the multiple scattering correction has been calculated to be only 2.4% at 100 keV.[12]

The popular counter based on the $Li^{6}(n,\alpha)$ reaction is the lithium loaded glass scintillator but unfortunately multiple scatter corrections are more important in this case because materials other than lithium (oxygen 55%, silicon 16%) are present in the glass which is exposed in the neutron beam. Multiple scatter corrections have been treated by Zetterstrom et al,[13] J. Cameron et al[14] and the Harwell group (unpublished).

An interesting use of the $Li^{6}(n,\alpha)$ reaction for resonance energy flux measurements is in the application to cross-section measurements using underground explosions.[15] Here a thin lithium foil is exposed in the neutron beam and the tritons and α-particles emitted at selected angles are detected by semiconductor counters operating in the current mode.[16] Care has to be taken over the corrections for energy losses of the emitted charged particles in the lithium foil and in any dead surface layers of the semiconductor detectors.

We should note that in the thermal region some cross-sections are known very accurately e.g. B^{10}(n,absorption), $U^{235}(n,f)$.[17] Flux measurements in the thermal region based on these cross-sections are relatively straightforward and accurate.

3. Neutron Flux Measurements using Associated Particle/activity Methods

In this section we deal with a method of flux measurement which is absolute in the strict sense of the word. We turn to the neutron source itself and strive to distinguish the emission of a neutron by the detection of a charged particle or radioactive nucleus produced in the same reaction, i.e. for a reaction A(B,n)C, we measure the number of C nuclei produced, this being equal to the number of neutrons emitted. The advantage of the method lies in the fact that it is usually easier to monitor the number of C nuclei than the number of neutrons.

The first serious application of this method was the counting of the α-particles emitted in the T(d,n)α reaction, the emitted neutrons being in the region of 14 MeV energy. The α-particles are counted in a well defined geometry by a proportional counter, scintillation counter or a semi-conductor counter. It is relatively easy to achieve a 2% accuracy on the 14 MeV neutron flux but with extreme care one can nearly achieve 1/2%.[18] For this very precise work attention has to be paid to such details as the carbon and deuterium build up on the surface of the tritium target and also the distribution of tritium in the target itself. One also needs to make sure the tritium target used is not too old since the tritium decay produce He^3 also reacts with the incident deuterons to give contaminant α-particles (without associated neutrons) via the He^3(d,p) reaction. These α-particles could be quite close in energy to the genuine particles from the T(d,n)α reaction. There can be little doubt that this method has proved to be an extremely valuable method for measuring the flux of 14 MeV neutrons.

Unfortunately the D(d,n)He^3 reaction (which is a copious source of neutrons around 2.5 MeV) has not proved to be so amenable to this technique, mainly because the He^3 recoil particle energy is very close to the energy of the T recoil nucleus emitted in the competing reaction D(d,p)T. This reaction has about equal probability as the neutron producing reaction. Consequently to be effective the particle counter needs to have extremely good energy resolution. However this particular difficulty has been removed by the development of semiconductor counters with thin windows.[19] Even so the method has not yet been widely used and all the difficulties involved in precision measurements have not been discussed.

The T(p,n)He^3 reaction is proving to be even more difficult to be monitored by the associated particle technique. However it is certainly worthwhile trying because of the possibility of bringing the technique to bear on the very important 100 keV neutron energy region. Low energy neutrons are emitted in the backward direction in association with He^3 particles of higher energy in the forward direction. The fact that one needs to detect these He^3 particles in the forward direction, raises many difficult problems. First,

contrary to the T(d,n) reaction where a tritium target on a thick backing can be used, a thin target backing in the transmission position must be used. Second there is a copious yield of scattered protons and recoil tritons in the forward direction and some method of discrimination against these particles must be used in order to count the He^3 particles reliably. Fort and Leroy[20] have managed to overcome most of these problems using the apparatus shown in Figure 6. A combination of electrostatic and magnetic analysis is used to discriminate against coulomb scattered protons and a semi-conductor counter is used to detect the He^3 particles. In a measurement of the $Li^6(n,\alpha)$ cross-section in the energy region 150 keV to 300 keV Fort and Leroy used this technique to measure flux and claimed an accuracy of about ± 3%, a major contribution to this error being one of 2% from the uncertainty in the correction for coulomb scattering in the target. The type of target used was a titanium film with absorbed tritium backed with a thin layer of copper. Further improvements in the technique, both in improving the accuracy and extending to lower energies, can be expected if better tritium films could be made available. Targets of about 100 $\mu g/cm^2$ of titanium or preferably 30 $\mu g/cm^2$ of Li, with absorbed tritium are required.

We should note that the associated particle method essentially gives a measure of the neutron flux in a particular direction since the associated particles are detected in a particular direction. In other words a neutron beam is defined and it is sometimes very useful to take coincidence measurements between the particle and neutron detectors.[19] Also provided only the neutrons within the beam are used the estimation of flux does not depend on any knowledge of the angular distribution of the reaction products. This is not the case for the associated activity method which we will now discuss. Rather than the detection of recoil particles in a particular direction the activity method relies on the measurement of the total number of residual nuclei produced. Apart from the obvious requirement that the residual nuclei are radioactive with a convenient half life, it is also desirable that for each radioactive nucleus formed only one neutron of a fixed energy is emitted. These restrictions narrow the choice down to a few reactions but they have turned out to be important because they provide neutrons in the important energy region 10 to 100 keV. Reactions for which the associated activity method have been used are $Li^7(p,n)Be^7$,[21] the $V^{51}(p,n)Cr^{51}$ and the $Cu^{65}(p,n)Zn^{65}$.[22] In all the applications so far experimenters have avoided the requirement of knowing the angular distributions of the reaction products by quite ingenious ways. In his work with the $Li^7(p,n)Be^7$ reaction Ponitz made use of the fact that all neutrons are emitted in the forward direction at the threshold energy of the reaction. In fact he adjusted the proton energy to be above 2 keV above threshold such that the neutrons are emitted within a forward cone of half angle 12°. The neutron energy at the cone edge is about 30 keV and between 43.2 and 18.7 keV at 0°. Care had to be taken to ensure that all the emitted neutrons were used in the cross-section measurement. The Be^7 activity is measured by counting the 478 keV γ-rays from the first excited state of Li^7

which is fed in 12% of the Be^7 decays. Uncertainty in this branching ratio is presently the main contributor to the overall error of about 3% on flux (bear in mind however that there is a large spread in neutron energy). It has been suggested that if the error on the Be^7 branching ratio could be brought down to ± 1/2%, the error on flux could be reduced below ± 1%.

In the cases of the $V^{51}(p,n)$ and $Cu^{65}(p,n)$ reactions Harris et al completely surrounded the source with a sample of the material whose cross-section was being measured (this technique is not feasible in the case of the $Li^7(p,n)$ reaction because the neutron energy varies greatly with angle). The $V^{51}(p,n)$ reaction was used in the energy range 12 keV to 680 keV, the latter energy being close to the upper limit since the first excited state of Cr^{51} is at 775 keV. The $Cu^{65}(p,n)$ reaction was used for measurements at 39 keV neutron energy. This reaction has a very restricted range of usefulness since the first excited state of Zn^{65} is at 54 keV. The accuracies obtained on flux using these reactions have been several percent.

4. Methods based on Standard Sources

A potentially very accurate way of knowing a neutron flux is to use a calibrated source produced by radiation from a radioactive isotope (as distinct from accelerator produced radiation). Sources produced by some (γ,n) reactions are the most useful since the neutrons are approximately monoenergetic. The source which has been mostly used so far is the Sb Be source giving predominantly 24 keV neutrons and the Na^{24} Be, giving 220 keV neutrons, is also receiving attention. The favored method of calibrating these sources is the manganese sulphate bath method about which much has been written and an accuracy of ± 0.6% on source strength has been claimed.[23] Other methods have been used, but are not so convenient. These are the so-called Boron pile[24] and the oil bath method.[18] The former is a stack of graphite with BF_3 counters arranged within the stack, and a measurement of the BF_3 counting rate is made for the neutron source placed in the centre of the stack. The neutron efficiency of the pile is measured by replacing the source with a gridded ionization chamber containing deuterium in the form of tetra-deutero-methane. Monoenergetic γ-rays are allowed to fall on the chamber through a hold in the pile and hence produce neutrons by the $D(\gamma,n)p$ reaction. The number of neutron counts per proton pulse in the ion chamber is a direct measure of the neutron efficiency. In the oil bath method the source is placed in a large bath of oil and the neutron density in the oil is measured by moving small BF_3 counters throughout the bath and integrating the observed $B^{10}(n,\alpha)$ reaction rate. The device is calibrated by replacing the source with a T(d,n) source which is itself monitored by means of the associated particle method.

Despite the attractions of being able to measure the total neutron output very accurately and also knowing that there must be very little, if any, anisotropy in emission from the source, there are of course some difficulties in using calibrated photo-neutron sources for cross-section measurements. One is that along with the flux of neutrons there is a high energy γ-flux about four orders of magnitude greater in intensity and this introduces a very serious background problem. In fact it restricts measurements to a few reactions which either produce very high energy particles, e.g. fission, or which produce radioactive nuclei which are readily detected. Another is that unless one is prepared to work with very strong γ-sources, the neutron source strength is quite modest (and of course decreases noticeably with time). Consequently, to overcome the low source strength, measurements usually have to be made in poor geometry. Finally, there are uncertainties about the neutron spectrum from the source since the neutrons are moderated by the presence of the beryllium and there is the possibility of "satellite" neutron groups being emitted because of weak unsuspected γ-ray decays in the γ-source material. Nevertheless the method has been used to obtain very precise (2-3%) data on fission cross-sections[25] and a few capture cross-sections[26] at 24.8 keV.

5. Flux Measurements using "Flat" Response detectors

We now turn to the group of instruments generally known as flat response detectors. By flat response we mean that the neutron efficiency of the device is constant, or at least fairly constant, with energy. An important feature of these instruments is that they are not designed to give any information at all on the energy of the neutrons incident on them. The efficiency of some can be calculated accurately but others have to be calibrated in fluxes measured by other methods e.g. by use of standard sources, associated particle method.

Most flat response detectors are basically 4π detectors and hence are not very convenient for measuring neutron beam flux. An important exception is the long counter, originally suggested by Hanson and McKibber,[27] and which is an extremely useful instrument for work not requiring the highest accuracy. The departures from flat response are quite considerable with this instrument and in addition the efficiency is not a smooth function of energy due to the influence of resonances in the carbon cross-section (see Ref. 28 for a summary).

Detectors which are basically 4π detectors can be adapted for use with a collimated beam but as yet very little work along these lines has been done despite the fact that the instruments are potentially capable of good accuracy. Three of these devices

have already been mentioned: the manganese sulphate bath, the boron pile and the oil bath. To measure the flux of a collimated beam of neutrons it is necessary to allow the beam to pass through a re-entrant tube to the centre of the detector. Where necessary all, or a known part, of the incident beam can be scattered into the detector by e.g. a carbon scatterer placed in the centre. Without using a scattering block Ponitz[21] has used the manganese sulphate bath to measure the forward flux of 30 keV and 64 keV neutrons emitted at the thresholds of the $Li^7(p,n)$ and T(p,n) reactions, respectively. The geometry used is shown in Figure 7. At 30 keV the accuracy claimed is better than 2%, the dominant error being one due to leakage of neutrons from the spherical Mn SO_4 bath. This error could be reduced if a larger bath is used.

Conde et al[29] have used the scattering block method in conjunction with a giant scintillator tank with some success. The giant scintillator usually takes the form of a large sphere (up to 1 metre diameter) containing a liquid scintillator loaded with cadmium or gadolinium. So far the main application has been to $\overline{\nu}$ measurements when a fission source is placed in the centre and the total number of neutron capture pulses (random in time because of the moderation process) per fission event is recorded. For $\overline{\nu}$ work the instrument is calibrated by placing a Cf^{252} spontaneous fission source (for which $\overline{\nu}$ is accurately known) in the centre. However the absolute efficiency as a function of neutron energy has been measured by allowing the incident neutrons to be scattered by hydrogen in a plastic scintillator placed in the centre of the tank and measuring the number of delayed neutron counts per knock-on proton count.[30] To measure an unknown flux Conde et al allowed the beam to be scattered by a lead scatterer, the fraction of the beam which was scattered being measured by the transmission technique. The authors claimed that flux could be measured absolutely to an accuracy of 2-3% in the important energy region below 500 keV.

Under this heading of flat response detectors three other instruments must be mentioned. The first is the so-called wax castle (see e.g. Richmond[31]) in which BF_3 counters are positioned in a hydrogenous moderating assembly in order to produce a reasonable flat response over a wide energy range. However a better response can be obtained by using graphite instead of wax since the diffusion length of thermal neutrons is much greater in this material. A fairly recent instrument based on graphite is the graphite sphere constructed by Macklin.[32] Finally we should mention the so-called grey neutron detector described by Ponitz.[33] A diagram of this detector is shown in Figure 8. The principle of operation is that the neutrons are slowed down and captured by the hydrogen to give 2.2 MeV γ-rays, some of which are detected by the NaI detector. Departures from flat response are due to neutrons leaking from the sphere and γ-ray absorption in the sphere.

6. Backgrounds

It would be improper to conclude this review without mentioning the vexed question of neutron background in relation to flux measurements. The presence of background neutrons having energies different from the main beam is one of the main reasons why most flux measurements are tedious and time-consuming and have to be carried out with great care. Of course the background question does not arise with flux measurements based on methods not involving the use of a neutron detector e.g. the associated particle method, but attention still has to be paid to backgrounds in the actual cross-section measurement.

Backgrounds arise from two main causes.

(a) In the case of accelerator produced sources they can be produced by the charged particle beam hitting materials other than the actual target material. This source of background is relatively easy to deal with since it can be measured directly by removing the target material.

(b) Neutrons can be scattered by any material present in the experimental room including the walls of the room. If the flux measuring device happens to be energy selective then there will automatically be some discrimination against this form of background. Otherwise these backgrounds are difficult to deal with and it is definitely good practice to try to reduce them to a minimum when planning the experiment. This is particularly true if the neutron detector is much more sensitive to low than high energy neutrons, e.g. a "$\frac{1}{v}$" detector, since the scattered neutrons are likely to have much lower energies than those in the main beam. Table I shows just how serious this problem is; it gives recent data obtained by White[34] on the calculated and measured backgrounds in various fission chambers and a flat response detector. White based his measurements on plots of the count rate in the detector v the inverse square distance from the source, the usual method of dealing with room scattered background.

Clearly there are no hard and fast rules regarding the background problem. Each case has to be treated on its own, taking due account of the energy sensitivity of the detector and its environment. For accurate flux measurements however the problem is extremely important.

7. Conclusions

The measurement of neutron flux is not a field in which we can expect rapid progress. There are very few, if any, new ideas to be found in the materials which I have presented. However I think it is noticeable that during the last few years we have seen considerable progress in the application and development of techniques to the point where we now have many reliable and accurate methods of measuring flux. At a few selected energies, certainly at 14 MeV and thermal, maybe one or two more, we believe we can measure flux to better than ± 1% accuracy. In some of the intermediate regions we have techniques which can probably achieve ± 2% accuracy on flux and several of these techniques still have development potential. There remain a few sticky energy regions, and in particular I would pick out the one around 10 keV, where we need much more work not only to get good accuracy but to get confidence in our results.

Table I

Calculated and measured relative backgrounds in fission counters and a ^{10}B neutron detector at 20 cm from 24 keV and 120 keV neutron sources.

Neutron Energy	Effective distance of walls (cm)	Background %							
		Detector Nubide	U^{233}	U^{234}	U^{235}	Np^{237}	Pu^{239}	B^{10}	Flat Response Detector
24	4.2	Calculated	27		24		36		2.1
		Measured	43		31		19		
120	4.5	Calculated	14	7	13	0	18	52	1.8
		Measured	9	4	16	0	15	56	
120	4.9	Calculated			10				1.5
		Measured			8				

8. References

1. J. C. Hopkins, Report No. LADC 8781 (1967).

2. P. H. White, Journal of Nuclear Energy Parts A/B 19, 325 (1965).

3. T. H. R. Skyrme, P. R. Tunniliffe and A. G. Ward, Rev. Sci. Inst. 23, 204 (1952).

4. E. F. Bennett, Nuclear Science and Engineering 27, 16 (1967).

5. F. D. Brooks, Nucl. Inst. and Methods 4, 151, (1959).

6. C. D. Swartz and G. E. Owen, Fast Neutron Physics Vol. 1, p. 233, Interscience Publishers (1960).

7. R. Batchelor, W. B. Gilboy, J. B. Parker and J. H. Towle, Nucl. Inst. and Methods, 13, 70 (1961).

8. B. C. Diven, Phys. Rev. 105, 1350 (1957).

9. G. Dearnaley and A. B. Whitehead, AERE Report No. R.3662 (1961).

10. European American Nuclear Data Committee Report No. EANDC 53 "S" (1965).

11. M. C. Moxon and E. R. Rae, Nucl. Inst. and Methods 24, 445 (1963).

12. M. C. Moxon, Private Communication.

13. H. O. Zetterström, S. Schwarz and L. G. Stromberg, Nucl. Inst. and Methods 42, 277 (1966).

14. J. Cameron, L. M. Harrison and J. B. Parker, Nucl. Inst. and Methods, 56, 45 (1967).

15. A. Hemmendinger, Physics Today, August 1965, p. 17.

16. A. Hemmendinger, M. G. Gilbert and A. Moat, IEEE Trans. on Nuclear Science, February 1965, p. 304.

17. Neutron Cross-Sections BNL 325 Second Edition.

18. P. Fieldhouse, E. R. Culliford and D. S. Mather, J. Nuclear Energy 21, 131 (1967).

19. L. F. C. Monier, G. E. Tripard and B. L. White, Nucl. Inst. and Methods, 45, 282 (1966).

20. E. Fort and J. L. Leroy, IAEA Conference on Nuclear Date--Microscopic Cross-Sections and other Basic Data for Reactors, Paper No. CN 23/67, Paris (1966).

21. W. Ponitz, J. Nuclear Energy Parts A/B 20, 825 (1966).

22. K. K. Harris, H. A. Grench, R. G. Johnson and F. J. Vaughn, Nuclear Physics 69, 37 (1965).

23. E. J. Axton, P. Cross and J. C. Robertson, J. Nuclear Energy Parts A/B, 19, 409 (1965).

24. D. W. Colvin and M. G. Sowerby, Proceedings of the IAEA Symposium on the Physics and Chemistry of Fission, Salzburg Vol. 2, p. 25 (1965).

25. J. L. Perkin, P. H. White, P. Fieldhouse, E. J. Axton, P. Cross and J. C. Roberton, J. Nuclear Energy Parts A/B 19, 423 (1965).

26. J. B. Ryves, J. C. Robertson, E. J. Axton, I. Goodier and A. Williams, J. Nuclear Energy Parts A/B 20, 249 (1966).

27. A. O. Hanson and J. L. McKibben, Phys. Rev. 72, 673 (1947).

28. W. D. Allen, Fast Neutron Physics Vol. 1, p. 362, Interscience Publishers (1960).

29. H. Conde, S. Schwarz and N. Starfelt, European-American Nuclear Data Committee Report No. EANDC 33, p. 136 (1963).

30. I. Asplund-Nilson, H. Conde and N. Starfelt, Nuclear Science and Engineering 16, 124 (1963).

31. R. Richmond, AERE Report No. R/R 2097 (1956).

32. R. L. Macklin, Nucl. Inst. and Methods 1, 335 (1957).

33. W. P. Ponitz, Nucl. Inst. and Methods 58, 39 (1968).

34. P. H. White, Nucl. Inst. and Methods 39, 256 (1966).

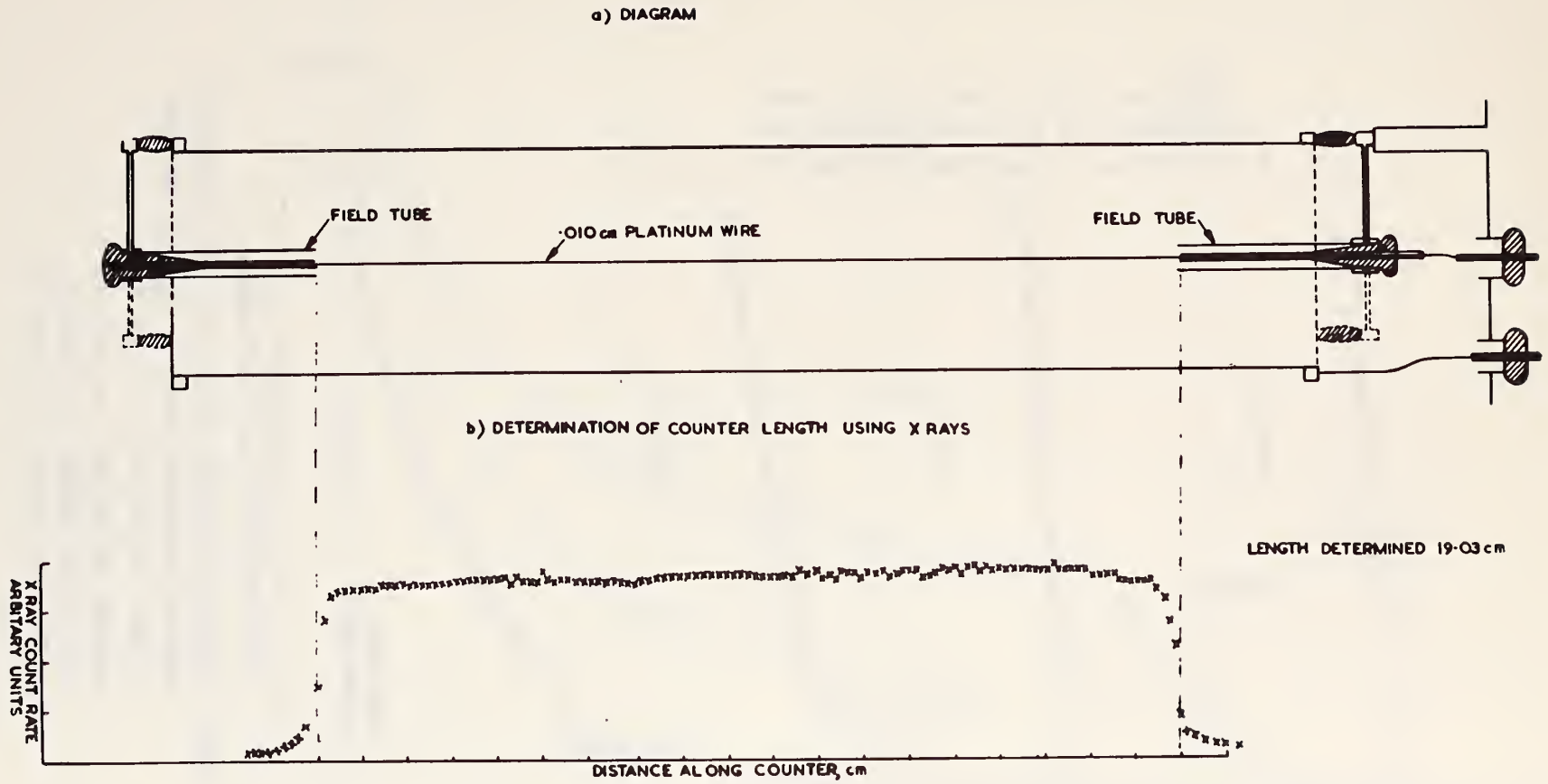

FIGURE 1. PROPORTIONAL RECOIL COUNTER USED BY WHITE (REF. 2)

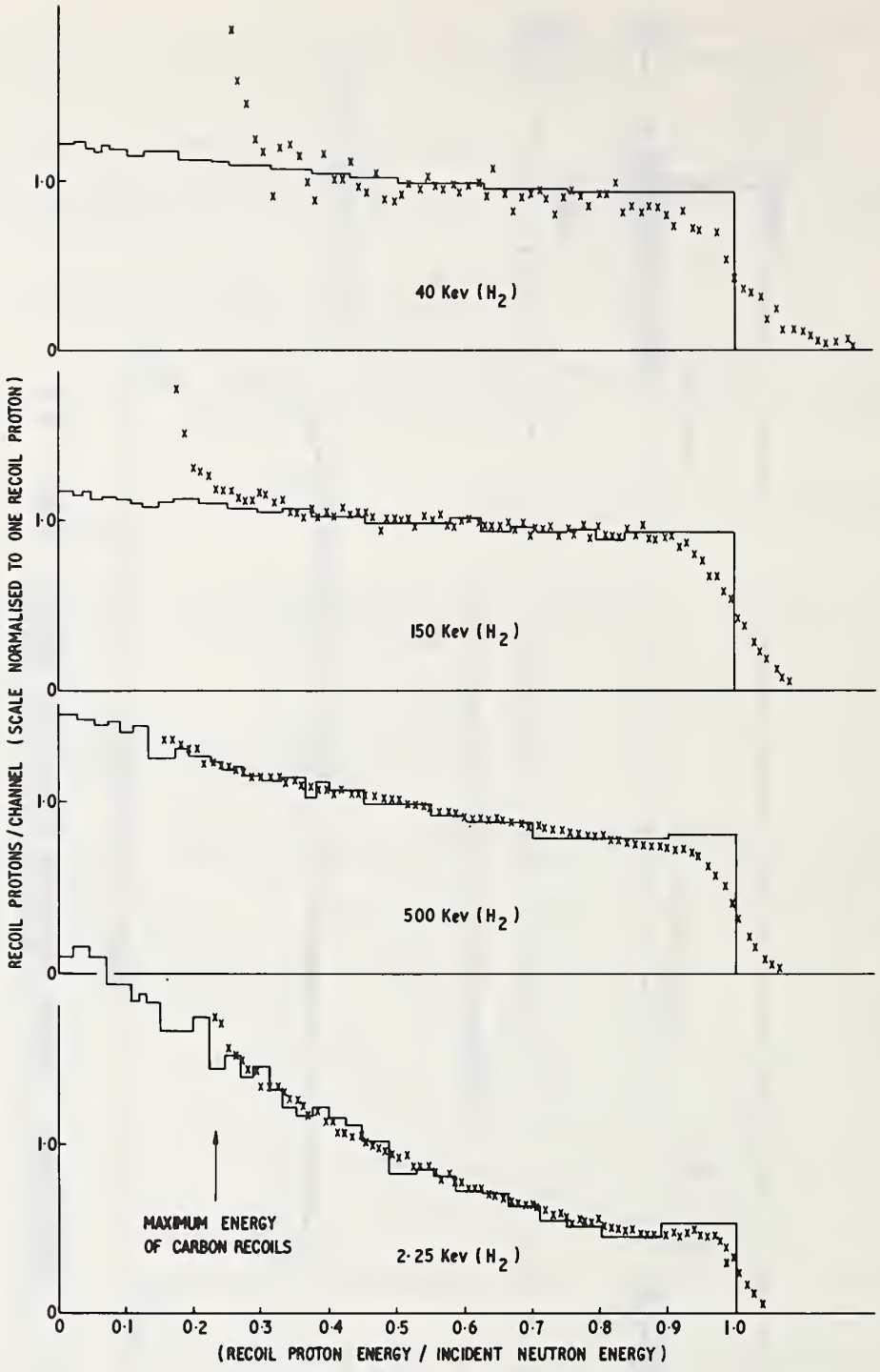

FIGURE 2. RECOIL PROTON SPECTRA FROM THE GAS FILLED PROPORTIONAL COUNTER. X EXPERIMENTAL POINTS — COMPUTED HISTOGRAM.

1st CURVE GAS PRESSURE 20cm Hg OF H_2

2nd CURVE GAS PRESSURE 40cm Hg OF H_2

3rd CURVE GAS PRESSURE 97cm Hg OF H_2

4th CURVE GAS PRESSURE 110cm Hg OF CH_4

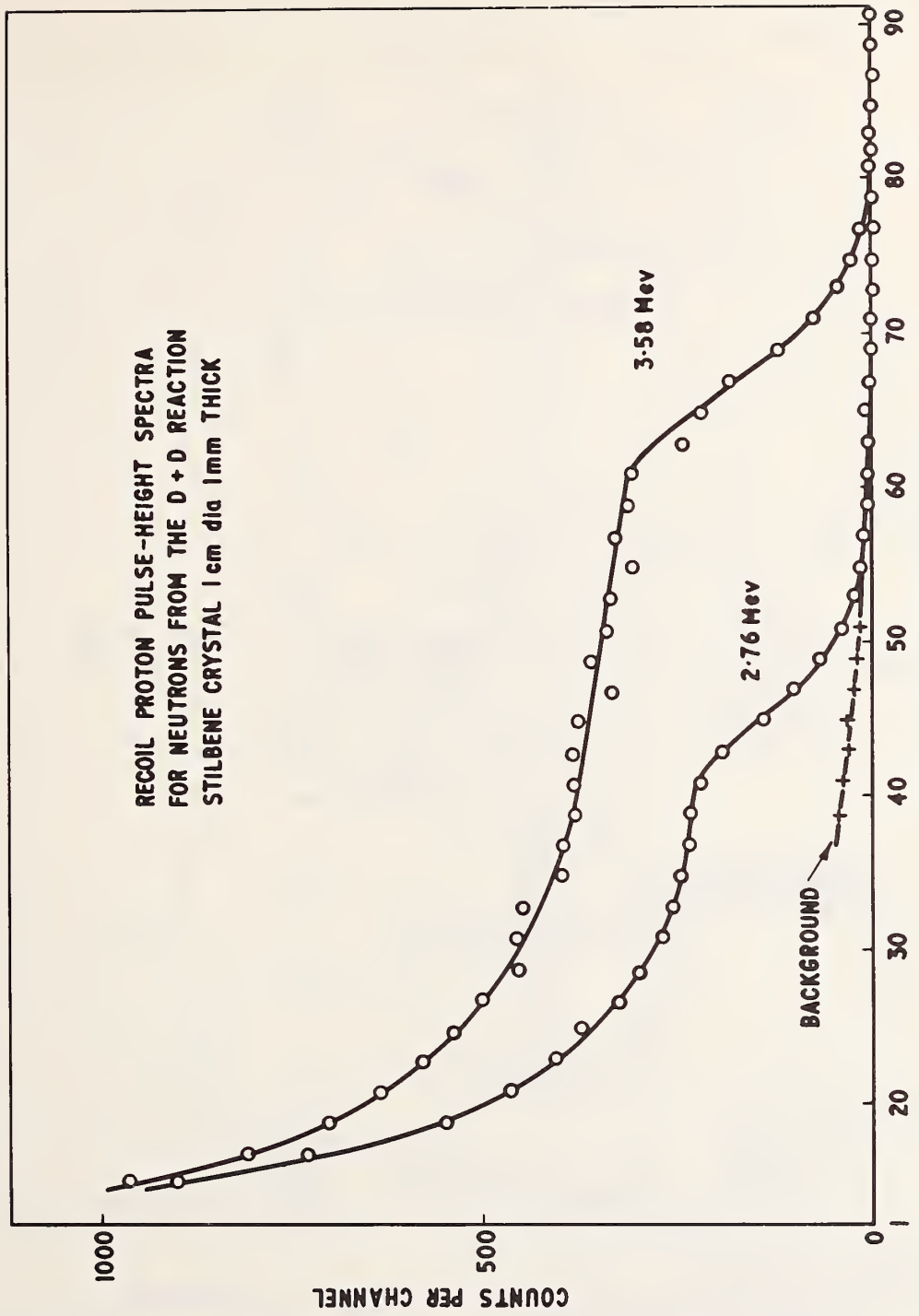

FIGURE 3. EXPERIMENTAL PULSE HEIGHT SPECTRA FOR D-D NEUTRONS ON A STILBENE CRYSTAL 1 cm DIAMETER, 1mm THICK.

313-475 O-68—9

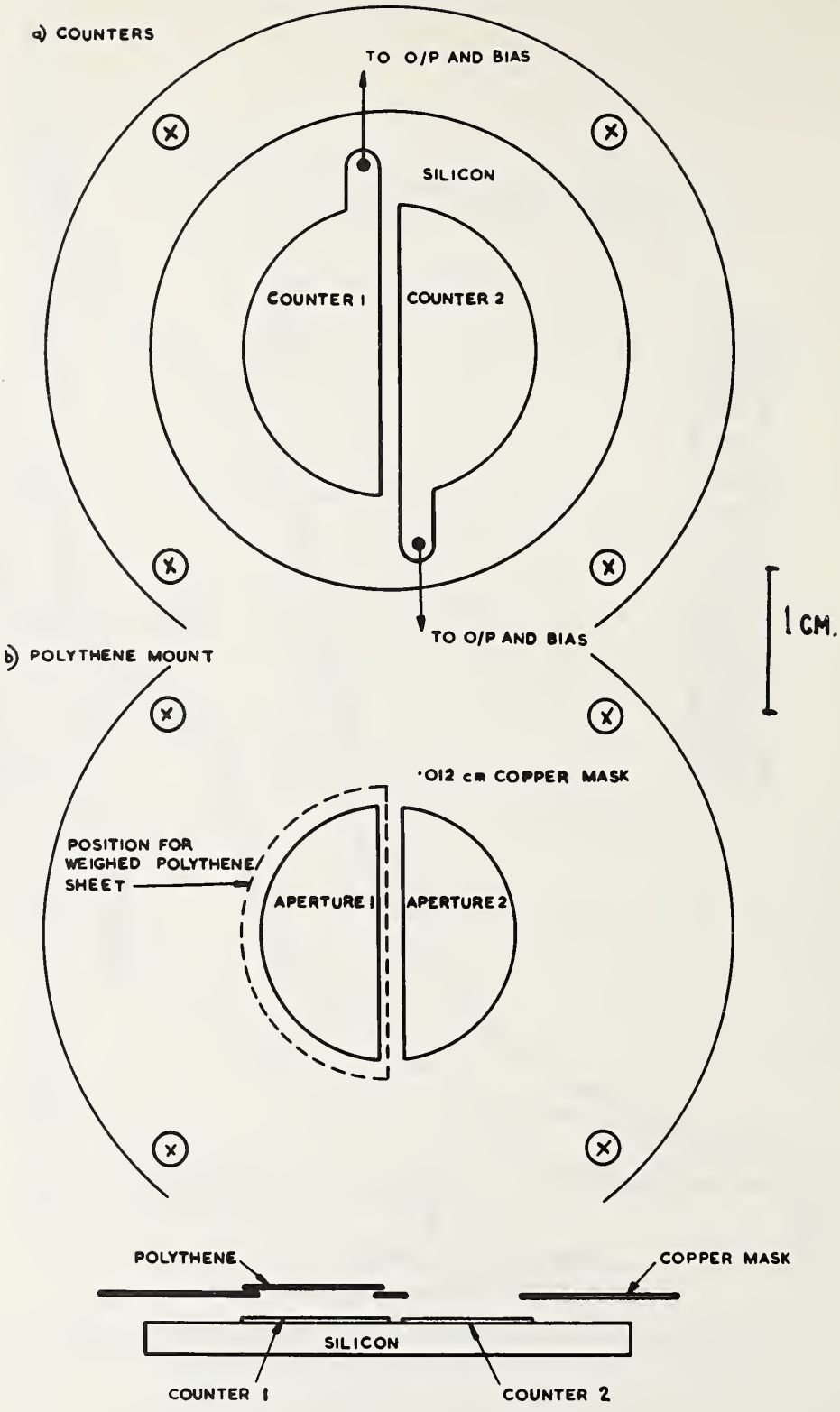

FIGURE 4. SILICON SURFACE BARRIER PROTON COUNTER USED BY WHITE (REF 2).

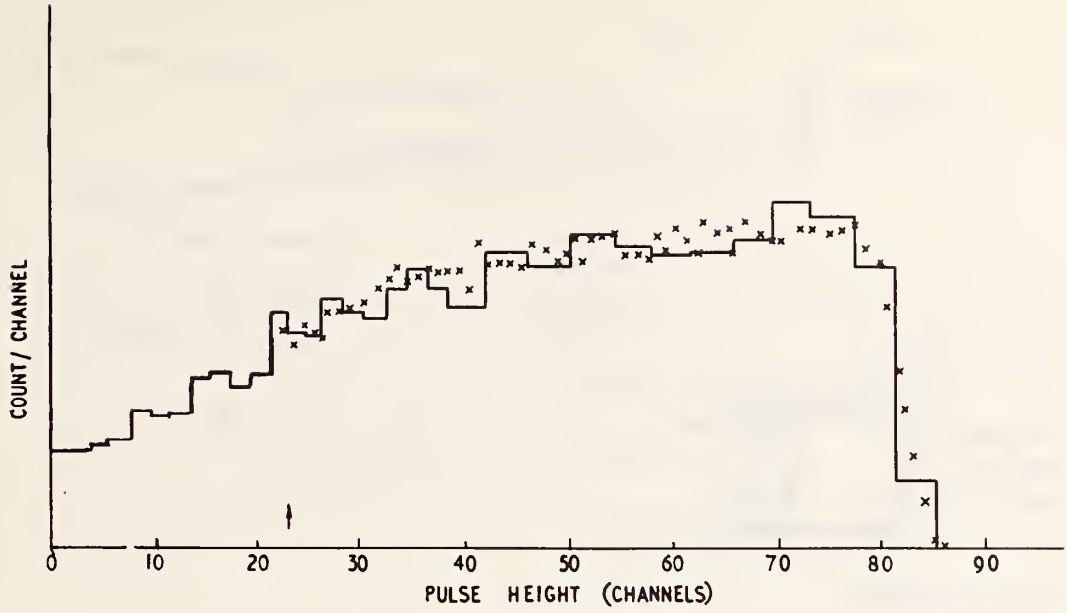

FIGURE 5. RECOIL PROTON SPECTRUM FROM A SEMICONDUCTOR RECOIL COUNTER AT 2·25 Mev NEUTRON ENERGY

x EXPERIMENTAL POINTS

— HISTOGRAM COMPUTED ON A SAMPLE OF 100,000 NEUTRONS

↑ MAXIMUM CARBON RECOIL ENERGY

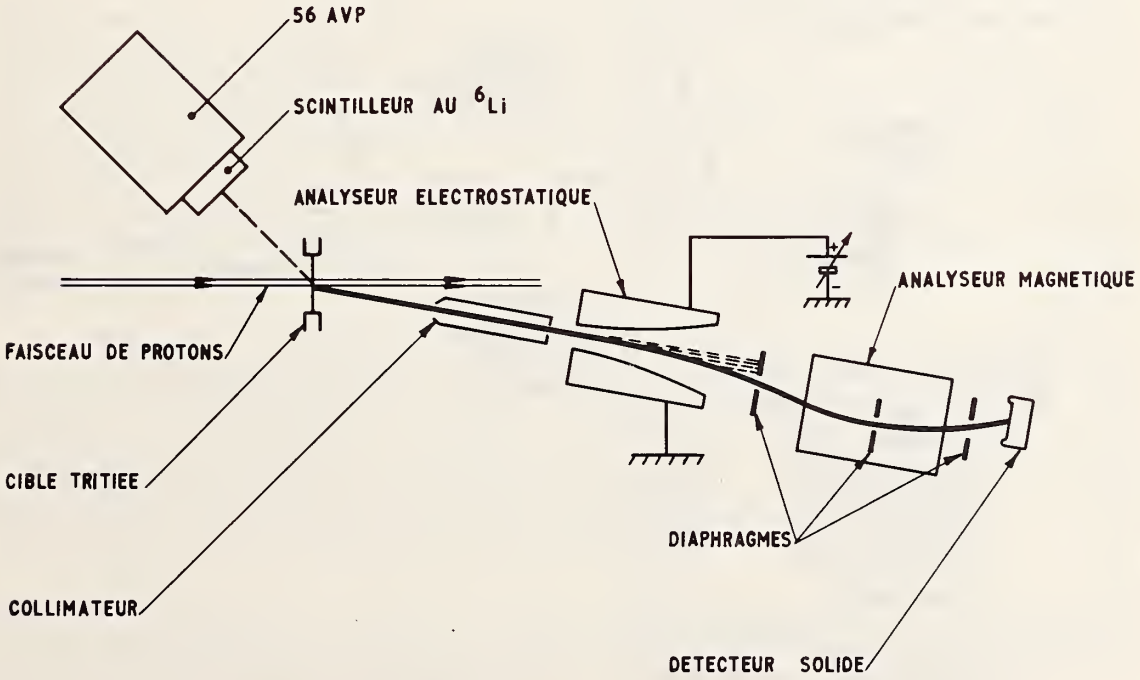

FIGURE 6. EXPERIMENTAL ARRANGEMENT USED BY FORT AND LEROY FOR MONITORING THE T(p,n) REACTION.

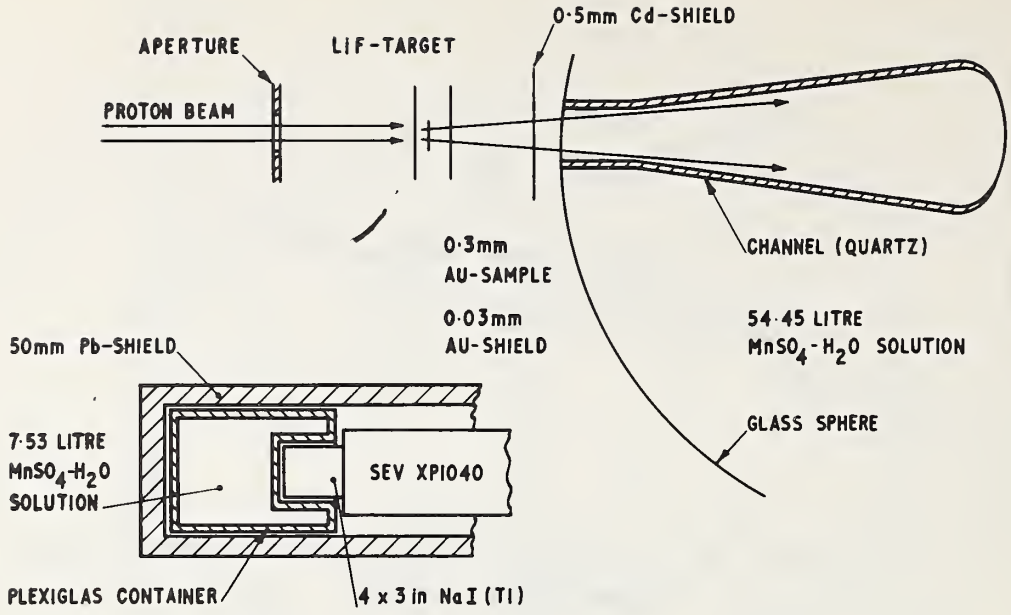

FIGURE 7. EXPERIMENTAL ARRANGEMENT FOR MEASUREMENT OF FLUX WITH A MANGANESE SULPHATE BATH USED BY PÖNITZ.

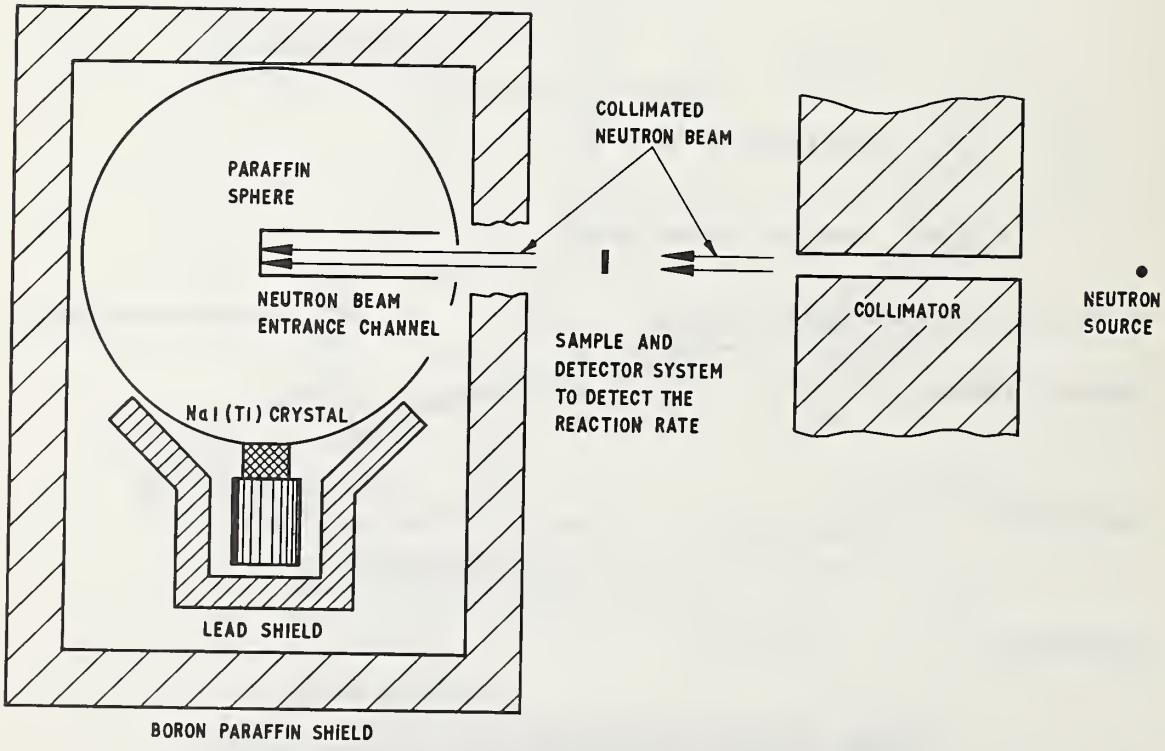

FIGURE 8. FLUX MEASUREMENTS WITH A "GREY" NEUTRON DETECTOR

DEVELOPMENTS IN STANDARD NEUTRON CROSS SECTIONS*

J. H. Gibbons

Oak Ridge National Laboratory
Oak Ridge, Tennessee 37830

Neutron cross section "standards" are reviewed with emphasis on reaction cross sections such as fission and capture. Special attention is given to $^{10}B(n,\alpha)^{7}Li^{*}$, ^{7}Li since this reaction is one of the best means of comparing intermediate and fast neutron cross sections with thermal values. Recent measurements of other "standard" cross sections are also discussed and recommendations for additional experiments are given.

When I finally stopped procrastinating about preparing for this conference I sat down with a bushel of reprints and preprints to try to re-acquaint myself with progress in standard neutron cross sections. My first surprise was that it has been two years - not one - since our first meeting. I guess this shows how fast time can fly when you're loafing.

My assigned job is to review developments in standard neutron cross sections. I can think of several people who are much abler than I to cover this subject and can only conclude that they were more nimble-footed than I in evading a commitment to speak. As far as I can tell, during the last couple of years we've seen almost as many evaluations as new results. Maybe these numbers should be about equal. Anyway, the several evaluations I refer to in this paper were of great help to me in my preparations. I must confess, though, that on several occasions I almost folded in some evaluated cross sections with experimental results when making my own summary. This is a marvelous circular route to ever more accurate and compatible results.

First let us consider what we mean by standard cross sections. My interpretation is that this term refers to those cross sections which satisfy two important conditions: (1) Their absolute value must be determined or determinable to a high degree of accuracy and hopefully by at least two independent techniques. (2) Their reaction characteristics must be such that they can be used conveniently and effectively in experiments in which they are used for normalization.

---

*Research sponsored by the U.S. Atomic Energy Commission under contract with the Union Carbide Corporation.

The potentially most accurately measurable cross sections are those obtainable by a transmission measurement since both neutron flux and detector efficiency cancel. Consequently our first highly accurate ($\lesssim$ 1%) cross section standards were total cross sections. We pass these over today, only noting that we continue to heavily depend upon the $^{1}H(n,n)$ cross section as a standard for fast neutron flux measurements for neutron energies above a few hundred kilovolts.

At lower energies (E_n < a couple hundred keV), where strongest current attention is now focussed, the hydrogen cross section standard is less effective (because of low-energy proton recoils) and we have to revert to standards involving exoergic reaction cross sections. On the basis of the criteria given above we can outline a spectrum of primary standards and identify the most likely candidates for a given energy range.

Neutron Energy	Best Primary Standard Cross Sections
Thermal	(1) $^{197}Au(n,\gamma)$, (2) $^{10}B(n,\alpha)^{7,7*}Li$, (3) $^{3}He(n,p)$, (4) $^{6}Li(n,\alpha)$.
0 to $\lesssim$ 200 keV (for relative flux)	(1) $^{10}B(n,\alpha\gamma)$, (2) $^{6}Li(n,\alpha)$, (3) $^{3}He(n,p)$.
23 - 30 keV (normalization point)	(1) $^{127}I(n,\gamma)$, (2) $^{197}Au(n,\gamma)$, (3) $^{235}U(n,f)$.
$\gtrsim$ 200 keV	(1) $^{1}H(n,n)$ [$^{235}U(n,f)$], (2) $^{10}B(n,\alpha\gamma)$ (up to ~ 400 keV).

Now, briefly, let's consider the developments over the past several years of our knowledge of these cross sections.

1. Thermal Energies

I've listed gold first as a thermal standard not only because its cross section at 2200 m/sec, 98.7 ± 0.3 (2σ) barns [1], is well known (to about ± 0.2%), but particularly because it activates with a convenient half-life, emits convenient decay products, and has a very well-known decay scheme. The absolute cross section is partially related to the boron absorption cross section (through pile oscillator experiments) but also has been independently obtained via a Breit-Wigner fit to the total cross section.

The ^{10}B reaction seems almost "wie von Himmel gefallen..." since it has a large thermal cross section, minimal resonance structure, a relatively large, positive Q-value, and most of the time emits prompt γ rays along with alpha particles. It can be used as a gas or solid or even in a liquid. Its thermal cross section (σ_a = 3835 ± 10 (2σ) barns) [1] is considered to be one of our best known cross sections. Also its alpha branching ratio [2,3] for thermal capture is now known to about 0.1%. We should note that recently it has been pointed out [3] that some confusion about this ratio existed because some people were reporting results for $(n,\alpha_o)/(n,\alpha\gamma)$ while others used $(n,\alpha_o)/(n,\alpha_o + n,\alpha\gamma)$. Similarly, the thermal cross section for $^{3}He(n,p)$ is known [4] to about 0.2%. The thermal cross section for $^{6}Li(n,\alpha)$ is less well-known, mostly because of uncertainty (about ± 3%) in the isotopic composition of samples [5]. My preference of standards for thermal cross section is boron since the cross section is well-known and because it lends itself to such a variety of useful physical forms. However, in most instances it is highly desirable to work with an activation reaction and in this case gold is an obvious choice. Other interesting secondary standards at 2200 m/sec have been based on the gold result. These include ^{59}Co (37.4 ± 0.15 barns) [6] and $^{235}U(n,f)$ [7] of 582.9 ± 6.4 barns. An excellent review of thermal fission constants was recently made by de Volpi [1].

2. $0 < E_n$ (keV) $\lesssim 100$

I choose this breadth of energy range because it turns out that fortunately there are convenient reactions that cover this entire span. As in the case of thermal neutrons, and for many of the same reasons, the boron reaction wins again in my judgement. Having stated my conclusion I shall now state my case. We are concerned in this section with absolute values to some degree but far more importantly with highly accurate relative cross sections versus energy in order to normalize neutron fluxes. There are two classes of candidates for this standard. First are the exoergic reaction cross sections using ^{3}He, ^{6}Li, and ^{10}B. These have relatively smooth, essentially non-resonant cross sections. The other candidate that must be mentioned is $^{1}H(n,n)$ through a secondary standard such as $^{235}U(n,f)$, but its applicability for E < 100 keV is marginal because of detector characteristics. Neutron energies in this range are so low that it is experimentally extremely difficult to utilize proton recoils from $^{1}H(n,n)$ for a quantitative measurement of neutron flux. The most valiant efforts have produced data down to about 40 keV [8] but they have not proved very successful for $E_n \lesssim 100$ keV or perhaps even higher. However, recent work by Bennet at Argonne [9] using pulse shape discrimination has raised hopes for use of this cross section down to a few kilovolts.

2.1 $^{3}He(n,p)$

The $^{3}He(n,p)$ cross section shape [4,10] is known in this energy range to ± 2%, perhaps slightly better. It should be noted that the

major reason for this small an error in the relative cross section is because the reaction was studied by the inverse reaction, $^{3}T(p,n)^{3}He$, using a flat response 4π neutron detector [11]. Recently Als-Nielsen [12] has correctly emphasized the value of Shapiro's calculation [13] that gave a reasonable interpretation of the non - 1/v behavior of $\sigma(n,p)$ for $E_n \gtrsim 2$ keV [14]. One drawback of this reaction as a standard is that it is difficult to build a neutron detector using ^{3}He gas that has both reasonable efficiency and fast time response, a prerequisite for work in the keV range. Fast time response is almost a must for work in the keV range since time-of-flight techniques are essentially mandatory to discriminate over background due to slower neutrons, especially when using a detector with a very large thermal and epithermal cross section.

2.2 $^{6}Li(n,\alpha)$

The $^{6}Li(n,\alpha)$ reaction continues to be investigated extensively [15,5,16,17]. For example, two papers will follow mine giving new cross section results in this energy range. As a result of these various investigations and theoretical fits [15] the shape of the reaction cross section for $E_n \lesssim 100$ keV is now known to about the same accuracy as $^{3}He(n,p)$, namely about ± 2%. It is also known now that the cross section is 1/v up to about 30 keV. Since one can build lithium-loaded scintillators this reaction is now used by some for flux standardization. However, the reaction cross section is about four times smaller than that for boron. This, along with a troublesome gamma-ray sensitivity and the limitation of $\lesssim$ 10% on Li content in the glass, restrict its usefulness in the higher keV range. One of the most disadvantageous factors is the relatively large scattering to capture probability in the scintillator, which causes a spreading of its fast time response and also induces significant multiple scattering corrections.

2.3 $^{10}B(n,\alpha\gamma)$

The reaction $^{10}B(n,\alpha\gamma)^{7}Li$ is a particularly valuable one since the prompt 478 keV γ-ray enables the use of a thick boron target, yet provides a fast time signature. The large reaction cross section (relative to scattering) decreases the time resolution-spoiling effects of neutron scattering. Furthermore, the reaction is a smoothly varying function of energy up to several hundred kilovolts and is very nearly 1/v to about 100 keV [3]. Almost as important as all of these features is the fact that the inverse reaction (via $^{7}Li(\alpha,n)$ and the $n\alpha_0/n\alpha\gamma$ ratio) can be accurately measured [3]. In recent years several experiments have been reported which bear on the subject [3,18-20] and have greatly increased our understanding of the cross section. At our last conference the knowledge of this reaction was insufficient enough to allow Bogart to speculate [21] that a relatively strong resonance existed in the cross section near 150 keV. Since that time high resolution studies of $^{7}Li(\alpha,n)$ and the ratio $(n\alpha_0)/(n,\alpha\gamma)$ have shown [3,20] the cross section to be smooth throughout this region, with no suggestion of a resonance at 150 keV. These studies on the shape of

the $(n,\alpha\gamma)$ cross section are so applicable to our concern that they bear a brief review. Besides, Dick Macklin and I made some of the measurements and this is one of the few rewards for being up on this platform. The experiment was two-fold. First we used an alpha-particle beam on thin metallic ^{7}Li targets and measured the neutron yield per alpha particle versus alpha energy for energies corresponding to $20 < E_n$ (keV) < 500 in the inverse reaction. Target thicknesses corresponded to a neutron energy spread of 5-15 keV in the inverse reaction. The largest target thickness correction factor (at 20 keV) was about 10%. The 4π graphite sphere neutron detector has an efficiency change of $\lesssim 0.3\%$ for neutrons from 20 keV to about 1 MeV [11]. Relative alpha current was readily monitored to better than 1%. We obtained from this experiment (Fig. 1), by normalizing ultimately to the thermal cross section, a curve of $\sigma(n,\alpha_o)$ vs. neutron energy. The second measurement was of the ratio $(n,\alpha_o)/(n,\alpha\gamma)$ by using face-to-face solid state counters viewing a thin boron foil (Fig. 2). Pulsed beam time-of-flight techniques were used to avoid problems due to thermalized neutrons. The ratio we obtained (Fig. 3, solid line) is in reasonable agreement with the rather broad spread of previous results. The accuracy of the latest measurement (about ± 2%) is much higher than previous measurements (about ± 8%). By combining the results of these two measurements ($\sigma(n,\alpha_o)$ and $(\alpha_o/\alpha\gamma)$) we arrived at the component $^{10}B(n,\alpha)$ cross sections (Fig. 1). Comparison of the summed (n,α) and $(n,\alpha\gamma)$ cross section with previous results is shown in Fig. 4. The results are all quite compatible, at least for $E_n \lesssim 100$ keV, with σ_a $^{10}B \propto 1/v$ to $< 2\%$. The separate results for $(n,\alpha\gamma)$ imply a cross section <u>less than 1/v extrapolation</u> by about 2% for $E_n \sim 100$ keV, with an uncertainty of about the same amount. In summary, for relative flux calibration in the energy range up to (and probably well beyond) 100 keV we have improved our lot over the last two years to the point that neutron fluxes can be normalized to better than 5%, and probably as accurately as 3%, through the $^{10}B(n,\alpha\gamma)$, $^{6}Li(n,\alpha)$, and $^{3}He(n,p)$ reactions.

3. Calibration Points in the 20-30 keV Range

While such reactions as $^{6}Li(n,\alpha)$, $^{10}B(n,\alpha\gamma)$, and $^{3}He(n,p)$ are convenient to normalize neutron flux over a range of energy, they do <u>not</u> serve well to normalize the absolute cross section value (e.g. at 30 keV). Standard cross section candidates suitable for this job need to have relatively large cross sections, to emit a typical capture gamma spectrum (e.g. gold, iodine) and/or activate with convenient half life with a well-known decay scheme (e.g. iodine, gold) or undergo fission in order to be of optimum use in experiments. In the low eV range where large and almost purely capturing resonances can occur (e.g. gold at 4.9 eV) one has a very convenient tie-point, but in the keV range where $\sigma_{sc} \gg \sigma_c$ this route is not possible.

There have been numerous attempts to establish an adequately accurate absolute standard cross section for the keV range. One route

has been via spherical shell transmission studies [22-24]. When appropriate Monte Carlo treatment of the relatively thick samples was invoked [23-24] we arrived at cross sections good to 5-10%. These were virtually all for ~ 23 keV neutrons, produced by an Sb-Be source. Other techniques have now been used, such as absolute counting of induced radioactivity in the sample and in the (p,n) target that produced the neutrons [25,26], or alternatively calibrating the integrated neutrons with a manganese bath measurement [26]. In two instances gold was studied by normalizing to the cross section at .0253 eV or 4.9 eV and extended to 30 keV using the shape of the boron cross section [27,28]. Last, having learned a number of pitfalls of the technique, recent absolute activation measurements using Sb-Be neutrons have been reported [29,30]. In short a large number of experiments, involving several independent techniques, have been performed to deduce some absolute cross sections. Two of the most promising results are ^{127}I and ^{197}Au. Recent reviews of these measurements, respectively by Robertson [29] and Pönitz, et al. [31,32] indicate absolute values accurate to about ± 3% and ± 2%. Apparently the most accurate single measurements are no better than 3%. It is gratifying to note that the results from the several independent techniques all are in good agreement. A great deal of credit is due our English, German, and Russian friends for their contributions to this work. Finally we have reached the state where measurements of relative cross section can be properly normalized. This will do wonders for the appearance of the cross section versus energy compilation, since most relative measurements differ from each other only in normalization.

An important, new measurement of σ_f (U-235) at 30 and 64 keV has been reported [32]. In one experiment the values were normalized to the Au(n,γ) cross section, but in a second experiment the cross section was measured by absolute fission counting and neutron flux counting by the associated radioactivity method, so this can be considered as a primary standard. The results are in reasonably good agreement with those of White [8] and Perkin, et al. [33] and give a σ_f (2.19 ± 0.6 b at 30 keV) that is even a few percent lower than that of the latest BNL compilation. Renormalization of activation experiments based on previous, considerably higher (~ 15% in the keV range) values for σ_f (235), has helped considerably in decreasing the apparent discrepancies between various capture results.

Although the sum total of capture measurements on gold and iodine near 30 keV would imply a slightly more accurate knowledge of the gold cross section rather than that of iodine there are strong reasons for retaining, if not even favoring the iodine cross section as a primary standard. The reason I make this claim is based mostly on cross section considerations. The capture cross section of a nucleus at say 100 keV can be more than 1000 times smaller than its thermal cross section. This means that a 0.1% contamination of thermal neutrons could change the observed capture rate by a factor of two at 100 keV. Pulsed beam techniques can essentially eliminate this problem but one doesn't always

have pulsed beam experiments. Therefore, other things being comparable, it is desirable to choose for a fast capture cross section standard one which has as small as possible thermal capture cross section and resonance integral (for a given fast capture cross section). Consider iodine vs. gold:

	Iodine	Gold
Thermal σ (b)	$\sim$ 6	$\sim$ 100
Resonance Integral (b·eV)	$\sim$ 140	$\sim$ 1600
30 keV σ (mb)	$\sim$ 760	$\sim$ 600

Clearly on this basis iodine is more desirable, since errors due to thermal and near-thermal neutron backgrounds should be more than two orders of magnitude less severe. Practice (i.e. various reports of capture cross sections) seems to bear this out. The iodine results have historically clustered along a relatively more narrow band than the results for gold. It's nice to have a choice in life and now we have two for σ_c standards near 30 keV. For non-time of flight experiments I strongly recommend iodine over gold.

4. $E_n \gtrsim 100$ keV

The energy range from a few keV to $\sim$ 100 keV used to be the neutron cross section favorite whipping boy a couple of years ago. Now clearly the new favorite is 100 to 200 keV! It may be that the relatively good agreement among results encountered for $E_n > 200$ keV may be due to the fact that virtually every measurement is normalized to the H(n,n) cross section (this automatically gives a low score for the Goldstein unhappiness coefficient), but more probably it's because absolute flux monitoring by hydrogen recoil is quite feasible for $E_n \gtrsim 200$ keV but becomes rapidly more difficult at lower energies. Suffice it to say that we remain relatively well satisfied with results for $E > 200$ keV but that the 100-200 keV range remains in a mess -- that is, we all too frequently encounter cross section values differing by up to 50% depending upon the experiment. In all fairness we should point out that one reason this region remains unimproved is because there are practically no new measurements! The most promising flux standards for this region are $^{10}B(n,\alpha\gamma)$ and $^{1}H(n,n)$ (usually through $^{235}U(n,f)$). $^{6}Li(n,\alpha)$ is much less desirable here because $d\sigma/dE$ is relatively large due to the resonance at 250 keV. We now think we know the relevant cross sections (^{1}H and ^{10}B) to a few percent so there is no reason why new cross sections cannot be normalized accurately. I must reiterate that errors due to background neutrons of degraded energy can do serious damage, so even experiments using "monoenergetic" neutrons from (p,n) reactions should incorporate time-of-flight gating. It is also timely to reexamine the $^{235}U(n,f)$ and $^{238}U(n,f)$ cross

sections (relative to $^{1}H(n,n)$) in the MeV range. In recent years we've paid little attention to these cross sections because those at lower energies were in such bad shape.

5. Conclusions

The extensive and painstaking absolute cross section work, for example on ^{197}Au and ^{10}B, has finally given sufficiently trustworthy standards ($\sim$ 3%) to call for a renormalization of older values, particularly those obtained by time-of-flight techniques. This, coupled with discarding of the suspect data, should give us a much less confusing set of cross section results. It would be highly desirable if these renormalizations and/or abandonment of earlier measurements would be performed by the original authors, spurred on by the evaluators.

There remain several standards measurements that should be very valuable:

1. The $(n,\alpha_o)/(n,\alpha\gamma)$ ratio for ^{10}B vs. E_n should be carefully checked for $50 < E_n$ (keV) $\lesssim 500$.

2. Cross section ratios vs. E_n should be measured for ^{10}B vs. $I(n,\gamma)$ ($E_n \gtrsim 10$ keV) and ^{10}B vs. ^{1}H (through $^{235}U(n,f)$) for $E \gtrsim 100$ keV in order to have a full cross-comparison of results.

3. The relatively consistent ($\sim$ 15%) difference between cross sections normalized to $^{235}U(n,f)$ and those normalized to other standards needs to be further explored. In particular, Pönitz's report [34] of σ_f (235) values 10-15% lower than White's in the upper keV range should be checked. If his results are correct the discrepancy in capture cross sections normalized to fission versus other standards would be further alleviated. It should also be obvious that such a lower value could adversely affect fast breeder hopes.

4. We need to renew our attention to standards and other cross sections in the upper neutron energy range, largely neglected in recent years.

Above all let us not forget that fast capture cross sections are never easy to measure accurately. Thus in closing I quote from a recent progress report I read a few months ago wherein a highly reputable and successful group refer to their work on this subject:
"--- work is continuing on attempts to find the cause of the 20% discrepancy between the two sets of $^{197}Au(n,\gamma)^{198}Au$ cross section measurements done in this laboratory ---."

6. References

1. A. de Volpi, Reactor and Fuel Processing Technology (in press) 1968.

2. A. J. Deruytter and P. Pelfer, J. Nucl. Energy A/B 21, 833 (1967).

3. R. L. Macklin and J. H. Gibbons, Phys. Rev. 165, 1147 (1968).

4. J. Als-Nielsen and O. W. Dietrich, Phys. Rev. 133, B925 (1964).

5. J. Spaepen, IAEA Proc. Conf. on Nuclear Data for Reactors, Paris, CN-23/119, October 17-21, 1966.

6. R. Vaninbroukx, Nucl. Sci. and Eng. 24, 87 (1966).

7. R. L. G. Keith, A. McNair, and A. L. Rodgers, EANDC(UK) 84S (1968).

8. P. H. White, J. Nucl. Energy A/B 19, 325 (1965).

9. E. Bennet, Nucl. Sci. and Eng. 27, 16 (1967).

10. R. L. Macklin and J. H. Gibbons, Int. Conf. on the Study of Nuclear Structure with Neutrons, Antwerpen, 1965, EANDC-50-S, Vol. I, paper 13.

11. R. L. Macklin, Nucl. Phys. 1, 335 (1957).

12. J. Als-Nielsen, "Neutron Cross Sections for ^{3}He in the Energy Range 0-10 MeV," CCDN-NW/6, September, 1967.

13. F. L. Shapiro, Soviet Phys., JETP 7, 1132 (1958).

14. L. Stewart, private communication (1967).

15. A. Bergström, S. Schwarz, and L. G. Strömberg, ENEA Report, CCDN-NW 3, October, 1966.

16. E. Fort and J. L. Leroy, IAEA Conference on Nuclear Data for Reactors, Paris, November 17-21, 1966, paper CN-23/67.

17. J. F. Barry, Conf. on Neutron Cross Sections and Technology, Washington, D.C., March 1966, CONF 660303, page 763.

18. S. A. Cox, Conf. on Neutron Cross Sections and Technology, Washington, D.C., March 1966, CONF 660303, page 701.

19. F. P. Mooring, J. E. Monahan, and C. M. Huddleston, Nucl. Phys. 82, 16 (1966).

20. K. M. Diment, AERE Report, AERE-R5224 (1967).

21. D. Bogart, Report NASA TMX-52.162 (1966).

22. H. W. Schmitt and C. W. Cook, Nucl. Phys. 20, 201 (1960).

23. T. S. Belanova, A. A. Van'kov, F. F. Mikehailus, and Yu. Ya. Staviskii, J. Nucl. Energy A/B 20, 411 (1966).

24. D. Bogart, NASA Report, NASA TMX-52235 (1966).

25. K. K. Harris, H. A. Grench, R. G. Johnson, F. J. Vaughn, J. H. Forziger, and R. Sher, Nucl. Phys. 69, 37 (1965).

26. W. Pönitz, J. Nucl. Energy A/B 20, 825 (1966).

27. M. C. Moxon and E. R. Rae, Nucl. Instr. and Methods 24, 445 (1963).

28. E. Haddad, R. B. Walton, S. J. Friesenhahn, and W. M. Lopez, Nucl. Instr. and Methods 31, 125 (1964).

29. J. C. Robertson, Nucl. Phys. 71, 417 (1965).

30. T. B. Ryves, J. C. Robertson, E. J. Axton, I. Goodier, and A. Williams, J. Nucl. Energy A/B 20, 249 (1966).

31. W. P. Pönitz, D. Kampe, and H. O. Menlove, EANDC(E) 84"S" (1967).

32. G. P. Knoll and W. P. Pönitz, J. Nucl. Energy A/B 21, 643 (1967).

33. J. L. Perkin, P. H. White, P. Fieldhouse, E. J. Axton, P. Cross, and J. C. Robertson, J. Nucl. Energy A/B 19, 423 (1965).

34. W. Pönitz, private communication (1968); see also the proceedings of this conference.

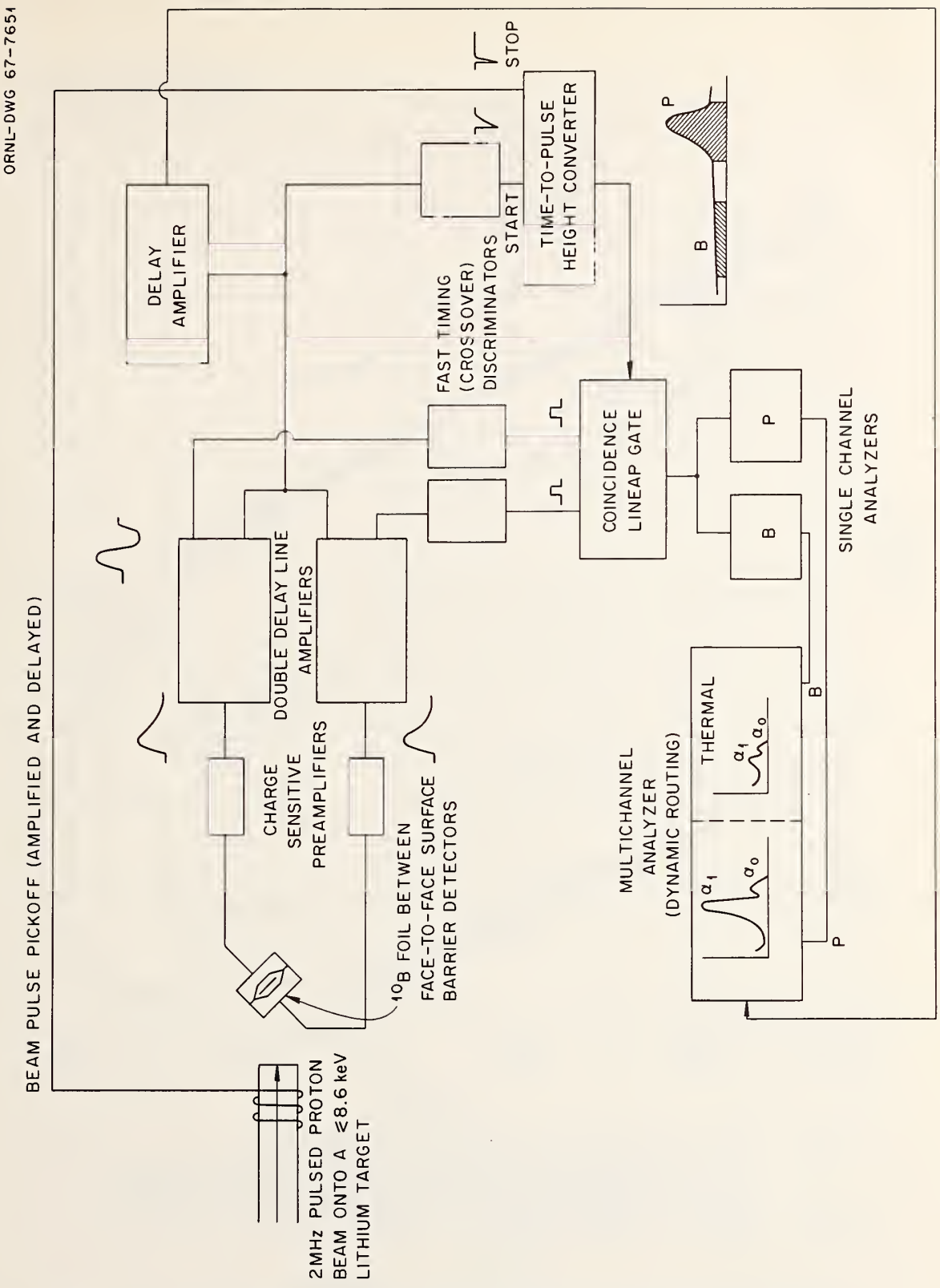

Fig. 1 - Boron (n,α) reaction cross sections versus energy. The shape of the lower curve was obtained via detailed balance from the total cross section for $^{7}Li(\alpha,n)^{10}B$ and its normalization from the thermal $^{10}B(n,\alpha_o)$ cross section. The upper curves were obtained using $(n,\alpha_o)/(n,\alpha\gamma)$ ratios.

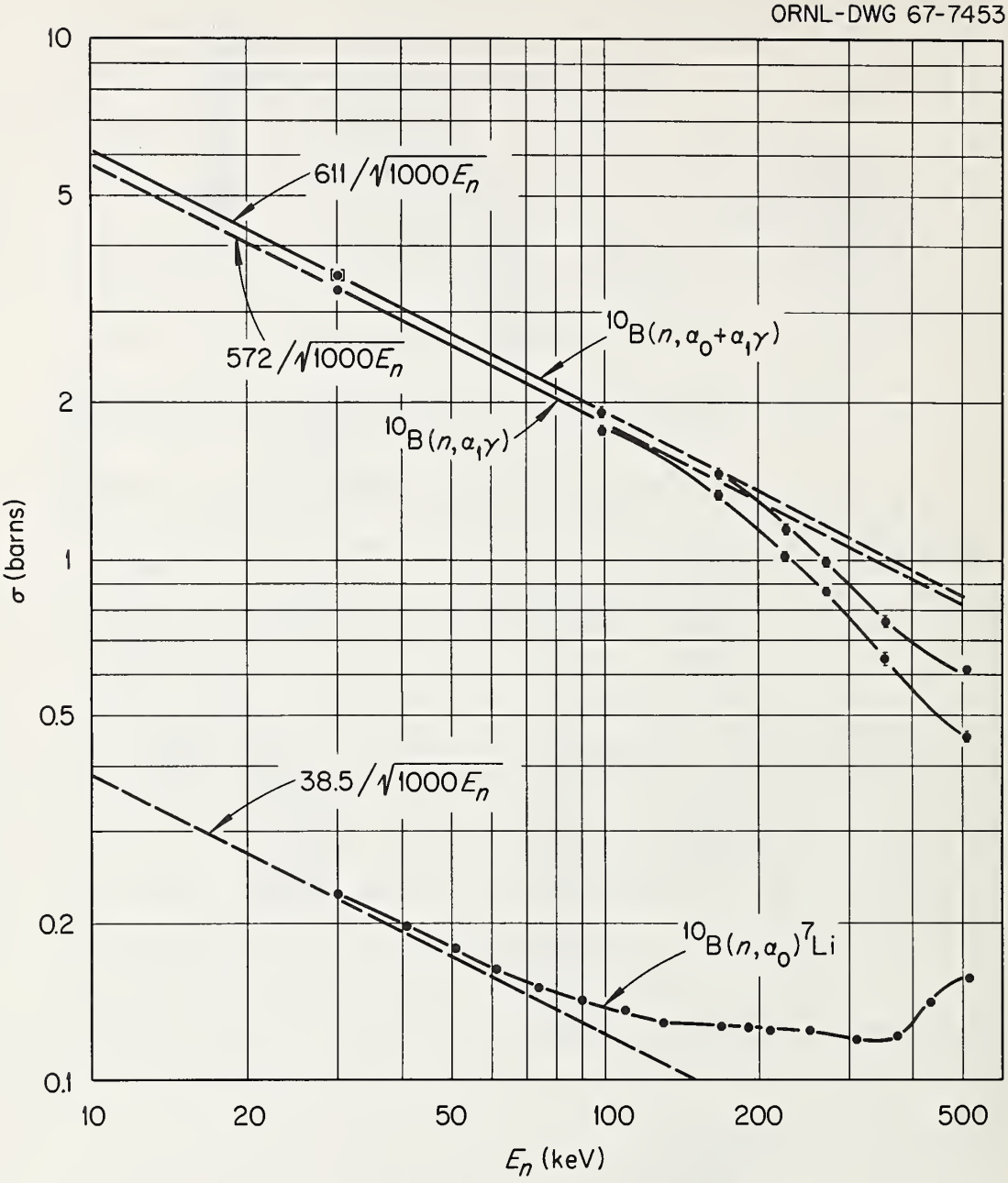

Fig. 2 - Block diagram of the experimental apparatus for ^{10}B: $(n,\alpha_0)/(n,\alpha\gamma)$ ratio measurements. A thin $^{7}Li(p,n)$ target provided the neutrons and time-of-flight techniques allowed discrimination of events due to off-energy neutrons.

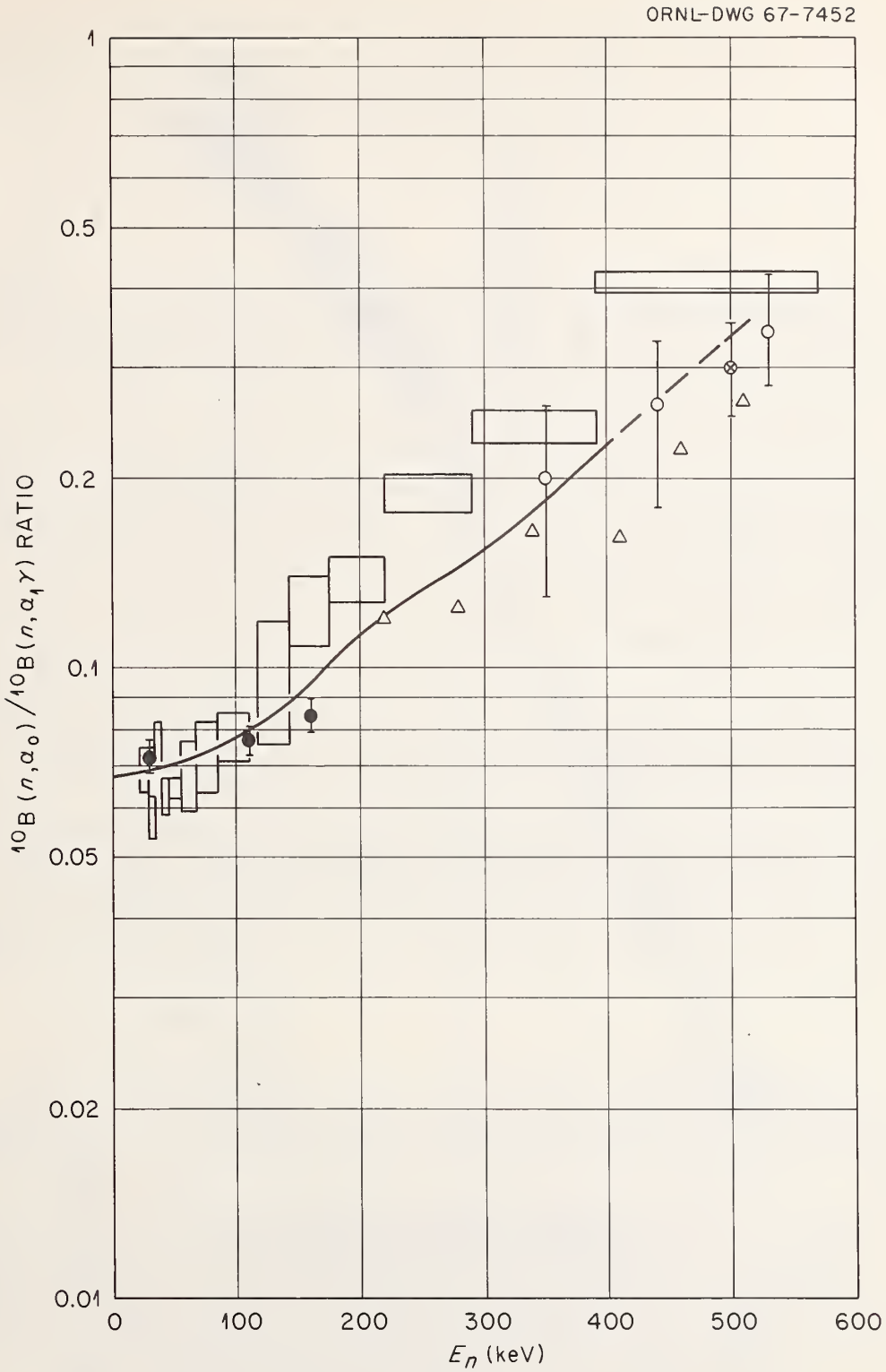

Fig. 3 - Results for the $(n,\alpha_0)/(n,\alpha\gamma)$ ratio versus neutron energy. The solid line represents the latest experimental results (ref. 3). Earlier, less accurate measurements are indicated by the symbols.

313-475 O-68—10

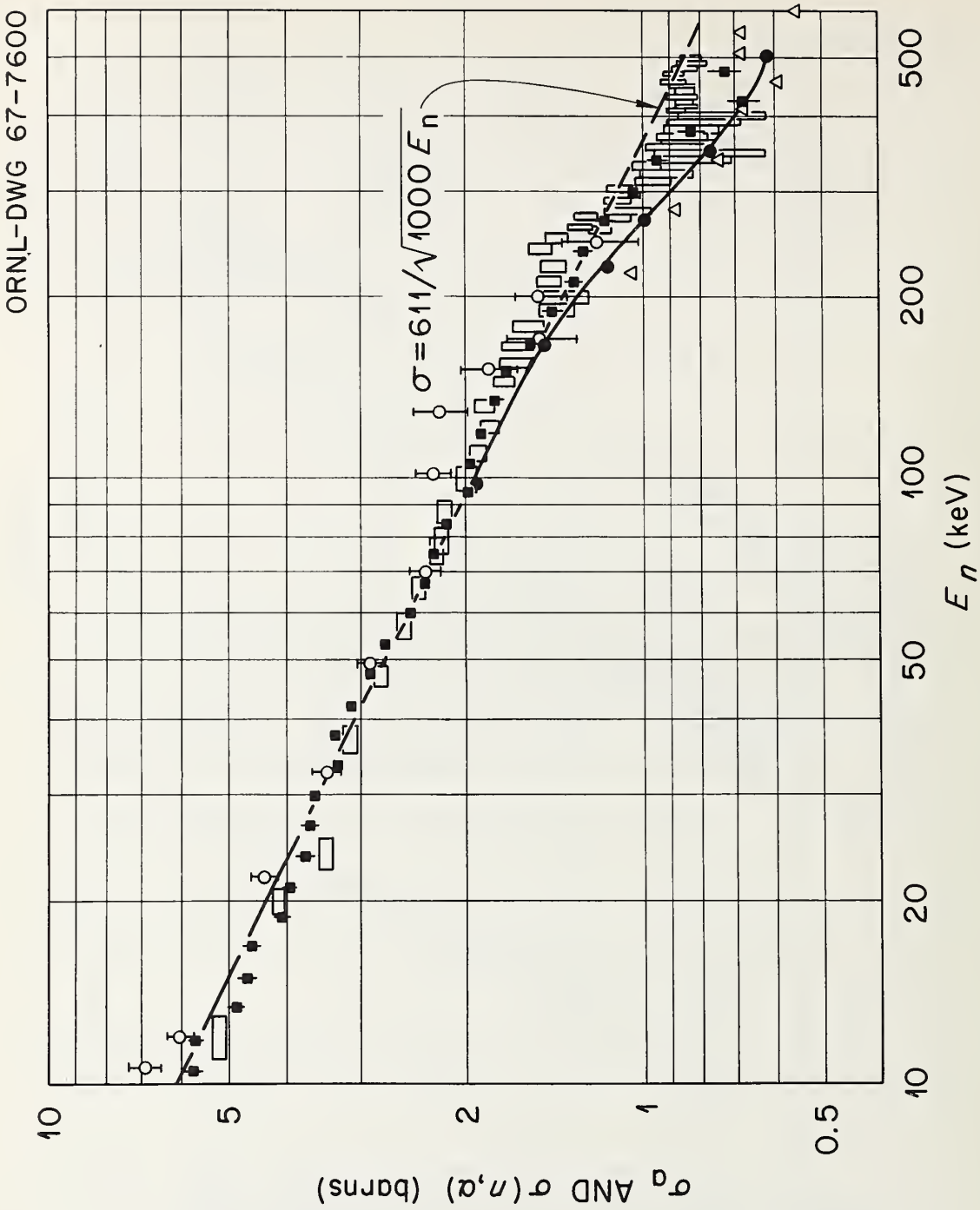

Fig. 4 - Summary of ^{10}B absorption and (n,α) cross section measurements. The data are consistent with a 1/v dependence to $E_n \gtrsim 100$ keV. The latest (n,α) measurements show a less-than-1/v cross section behavior for $E_n \gtrsim 150$ keV. These data do not preclude a small difference between absorption and (n,α) cross sections for $E_n \gtrsim 100$ keV.

Helium Production Cross Section Measurements

J. Weitman and N. Dåverhög

AB Atomenergi, Studsvik, Nyköping, Sweden

Abstract

Helium produced by (n,α) processes in structural materials irradiated in fast neutron fluxes will cause embrittlement of those materials. Reliable calculations of the helium production rate are hampered by lack of any accurate cross sections for important stainless steel components such as iron, chromium and nickel. A method suitable for the measurement of reactor spectrum integrated (n,α) cross sections in the sub-millibarn range has been developed. The method, which is general in so far as it does not depend on the existence of suitable activities in the product nuclei, relies on the high vacuum release and mass spectrometric absolute determination of small helium quantities, with a minimum detectable limit of 10^{12} He atoms per sample with the present equipment. Initially, the method was tested on boron loaded, thermal neutron flux irradiated stainless steel samples, for which the calculated and measured helium amounts could be compared. The first cross section measurements were performed on nickel, where the dominant $Ni^{58}(n,\alpha)$ reaction produces Fe^{55}, which only decays by electron capture to the ground state of Mn^{55}. The nickel samples were irradiated in a boron shielded rig in a MTR-type reactor to a fast neutron dose of about 10^{20} n/cm^2. the neutron flux being measured by the $Ti^{46}(n,p)Sc^{46}$, $Ni^{58}(n,p)Co^{58}$, and $Cu^{63}(n,\alpha)Co^{60}$ reactions. Considering effects of deviations from a fission flux we obtain a mean fission spectrum integrated helium production cross section of nickel of 4.2 mb, which is much higher than hitherto assumed in the literature. Our measured value is in good agreement with theoretical calculations performed at this laboratory. The Cranberg spectrum weighted theoretical excitation function exhibits a maximum around 5 MeV. Some 10%, or 0.5 mb, of the integral

$$\int^{\infty} \sigma_{n,\alpha}(E)\, f(E)\, dE$$

fall below 3 MeV and above 7 MeV, respectively. - Additional measurements on nickel as well as on iron, chromium and possibly other metals will follow.

The same method has been used as a very sensitive tool for B^{10} analysis. In this respect and in ease of interpretation it surpasses the pile oscillator technique. The method will also be adopted as a standard tool for materials dosimetry, the advantage of a helium accumulating dosimeter being that the integration process is not limited by radioactive decay, saturation or burn-up effects as is often the case in activation detectors.

During irradiation of materials in a reactor, helium atoms are formed by (n,α) reactions. The solubility of noble gases in materials such as stainless steel is practically negligible. At high temperatures the helium atoms migrate and form, due to their vanishing solubility, intra- and intergranular micro bubbles. The observation that these bubbles may, through a number of processes, decrease the ductility of irradiated materials has led to a considerable interest in the helium production cross sections. Elements of principal interest, forming in steel a matrix in which helium is uniformly distributed, are Fe, Ni, Cr. However, pointwise high concentrations of other materials may be present, such as TiN, TiO, and Ti_2S dispersions in titanium stabilized steels and MgO, CaO, and SiO_2 in slag inclusions (1). The local helium concentration in these heterogenities can be expected to be comparatively very high after a few years irradiation in a fast reactor. It is therefore also desirable to be able to calculate the helium production in these additional materials.

Presently, very little information is available about (n,α) excitation functions in the energy range of importance for reactors, that is roughly below 10 MeV. A recent compilation of fission spectrum averaged cross sections has been published by Alter and Weber (2). Their cross sections are largely based on a systematics by Roy and Hawton (3). These authors used the concept of a penetrability dependent effective energy, E_{eff}, introduced by Hughes (4), to correlate different $(\bar{\sigma}/A^{2/3})$-values, i.e., (n,p), (n,α), and (n,2n) cross sections normalized to a standard nucleus size. Unknown cross sections were determined from the lines representing the best possible fit to the few existing experimental points, thus avoiding Hughes assumption that the normalized $\bar{\sigma}$ values are proportional to the integral of the fission neutron spectrum above E_{eff}. The cross sections predicted by this approximate approach are expected to be correct within a factor of 3, at least for light and medium-weight elements, and within perhaps a factor of ten for heavy elements.

Among the stable and abundant isotopes of iron, chromium, and nickel, the $Ni^{58}(n,\alpha)Fe^{55}$ reaction is the most exoergic, having a Q-value of about 3 MeV. This reaction is thus energetically favourable, having a predicted mean fission cross section, according to Roy and Hawton, of 3.4 mb. The only measured value is the one by Schuman and Mewherter (5), based on radiochemical separation and subsequent counting of the Fe^{55} activity, obtained during irradiation in a receptacle slug in the BNL reactor. Schuman and Mewherter obtained a low value, 0.17 mb. Renormalization changes this value to about 0.5 mb, which still is low compared to both the Roy and Hawton prediction and to recent calculations by Eriksson (6) with a statistical model. Erikssons results for the Fe, Cr, and Ni isotopes are presented in an appendix to this paper. For the $Ni^{58}(n,\alpha)$ reaction Eriksson obtains 7.0 mb. The, as it seems, low experimental value might be explained by the approximate calibration procedure which was adopted for absolute determination of the X-ray activity, following the 2.6 year electron capture decay of Fe^{55}. However, the discrepancies for $Ni^{58}(n,\alpha)$, as well as a review of the sparse experimental information on (n,α) reactions in all principally important materials, indicated the need for direct measurements of the pertinent He-production cross sections.

In the following, a short description is given of a method, generally suitable for the determination of these cross sections. Also, our results for nickel are presented. Further measurements, involving iron, chromium and titanium are under way.

Though the majority of the possible (n,α) reactions in nickel are exoergic, the coulomb barrier around the nucleus inhibits α emission. The reaction rate with slow neutrons is therefore negligible, and the cross

section virtually has a threshold character, with a practical threshold in the MeV-region. When irradiating in a pile, the corrections for spectral deviations relative to the ideal fission spectrum are therefore small.

In our case, the irradiation was performed for a period of about 10 days in a rather central position of the Studsvik R2 reactor, which is of the MTR-type. The flux in the irradiation position was about 10^{14} $n/cm^2 \cdot sec$ and was monitored by the $Ni^{58}(n,p)Co^{58}$, $Ti^{46}(n,p)Sc^{46}$, and $Cu^{63}(n,\alpha)Co^{60}$ reactions. The irradiation rig was on all sides but one surrounded by normal fuel elements. In one of the outer diagonal positions bordering our rig, another rig, containing Al and small amounts of steel, was irradiated. Taking account of these irradiation conditions, we have made the reasonable assumption that the fast flux in our samples is nearly the same as in the fuel elements. Thus, when determining spectral corrections, we have used the form of neutron spectrum calculated for a pure fuel element array.

The irradiation rig is shown in Fig. 1. The nickel samples, about 20 in number, with a relative content of non gaseous impurities of less than 2×10^{-5}, are contained in sealed nickel cylinders, placed in an aluminum filler providing good thermal contact to the surrounding water coolant. The temperature rise in the rig due to γ-heating was less than $300^{\circ}C$. Helium diffusion from the samples could be of importance only at much higher temperatures. In the corner positions of the filler at each of five axial levels, a set of the above mentioned monitors was placed. From this, a good picture of the axial and radial fast flux distribution in the rig was obtained.

Except the sample cylinders and monitors, the rig contained 8 stainless steel samples, each with a known boron-10 content of 50 ppm by weight. After the irradiation, the helium content of these samples was determined by the same method as used for the nickel samples. As the inner part of the rig was canned in boral, containing several hundred mg boron per square centimeter, essentially only epithermal neutrons can penetrate into the samples, which was also proved by a chopper measurement of the boral transmission curve (7). From the small steel plates, it was shown that the probability for an (n,α) reaction in B^{10} during the irradiation was 3×10^{-3} per boron-10 nucleus. Assuming that 10% or 2 ppm of the total impurity content of the nickel samples is boron, we found that about 2×10^{14} He atoms per sample would be due to $B^{10}(n,\alpha)$-reactions. This corresponds to 2% of the total He amount of the nickel samples. The actual B^{10} content of the nickel samples should be even less than 2 ppm and therefore no correction for He produced by B^{10} is necessary. It was also shown that no other impurities with high (n,α) cross sections, such as Li^6, N^{14}, O^{17} could give any appreciable He contributions.

The amounts of helium produced were determined by a mass spectrometric technique, which will be only very shortly described in connection with Figs. 2a and 2b showing the experimental arrangement. The samples were transferred under vacuum from a magazine to a well outgased graphite crucible and within a few seconds heated to well above the melting point. No attempt was made to measure the temperature of the melt directly, but it is estimated to be in the range $1800\text{-}2000^{\circ}C$. The liberated gases are accumulated in a buffer volume, from which they are admitted through a needle valve to the ion source and the double focused spectrometer tube, which was constantly evacuated by a voltage stabilized oil diffusing pump. During the measurements, the total pressure in the spectrometer was always below 10^{-5} torr and generally around 2×10^{-6} torr, providing a constant pumping characteristic and negligible outscattering of helium ions from the focused beam. The steady state helium partial pressure in the

spectrometer depends on the (constant) pumping speed and the rate of He admission through the needle valve. This valve was continously adjusted to give an approximately constant spectrometer signal, which was recorded. The time to integrate the helium content in the accumulator could thus be easily determined from the record. Denoting the He inleakage rate by L and the spectrometer reading by S, we have

$$S(t) = C \cdot L(t) \tag{1}$$

where C is a proportionality constant and t time. The spectrometer was calibrated using a standard leak, with leak rate L_1, giving the signal S_1. The helium amount in the accumulator is thus determined from

$$n_{He} = \frac{L_1}{S_1} \int S(t)\, dt \tag{2}$$

The signal S(t) was generally choosen $\approx S_1$, thereby avoiding possible non-linearities in the spectrometer response. L_1 was accurately determined by a standard pipetting technique. The possibility of helium losses due to adsorption, gettering and other effects was investigated, by comparing a measured helium quantity, generally in the range 10^{14} - 10^{16} atoms and produced by irradiation of steel samples containing known ppm amounts of B^{10} in a known thermal flux, with the amount calculated. From these and other tests it was concluded that no appreciable helium losses occurred.

The monitor activities were measured by well known γ-spectrometric techniques to give the total number of reactions occurring during the irradiation,

$$n_M = N_M \iint \phi(E, t)\, \sigma_M dE dt.$$

If the small helium quantities due to many particle reactions, such as $(n, n'\alpha)$, and due to impurities are neglected, it is true that $n_X = n_{He}$. where n_X is the number of (n,α) reactions in nickel. The experimental information is summarized in the ratio

$$k = \left(\frac{n_X}{N_X}\right) : \left(\frac{n_M}{N_M}\right) = \frac{\iint \phi(E, t)\sigma_X\, dE\, dt}{\iint \phi(E, t)\sigma_M\, dE\, dt} = \frac{\int \phi(E)\sigma_X\, dE}{\int \phi(E)\sigma_M\, dE} \tag{3}$$

assuming that the energy and time dependence of the neutron flux are separable. From the known n and N values, the reaction probabilities $\left(\frac{n}{N}\right)_X$ and $\left(\frac{n}{N}\right)_M$ and k-values have been calculated and are given in Table I. The experimentally determined k-values are of course independent of any cross section assumptions. The limits of errors given in the mean k-values in Table I are due to statistical fluctuations. Systematic errors in the careful absolute calibrations of the mass and γ-spectrometers are estimated to 2% each, leading to a total experimental uncertainty of 3% in each of the mean k-values given.

The fission spectrum integrated (n,α) cross section $\bar{\sigma}_X$ can be determined from the k-values. Writing

$$\phi(E) = \phi_o \chi(E) + \Delta\phi(E) \qquad (4)$$

where $\chi(E)$ is the fission spectrum of U^{235}, $\int_o^\infty \chi(E)dE = 1$, and introducing the normalization energy E', such that

$$\phi_o = \frac{\phi(E')}{\chi(E')} \quad , \quad \Delta\phi(E') = 0 \quad , \quad E' = 6 \text{ MeV}$$

Eq. (3) can be transformed to

$$\bar{\sigma}_X = k\bar{\sigma}_M + \frac{kI_M - I_X}{\phi_o} = k\bar{\sigma}_M + \varepsilon(\sigma_M, \sigma_X) \qquad (5)$$

with

$$\bar{\sigma}_i = \int_o^\infty \sigma(E)\chi(E)dE \qquad i \equiv X \text{ or } M$$

and

$$I_i = \int_o^\infty \Delta\phi(E)\sigma(E)dE \qquad i \equiv X \text{ or } M$$

The values of $\bar{\sigma}_M$, the average cross sections of the monitoring reactions, have been taken from the literature. For $Ni^{58}(n,p)$ and $Ti^{46}(n,p)$ the recent values of Bresesti et al. (8) were chosen. For $Cu^{63}(n,\alpha)Co^{60}$, simply a mean value of the widely scattered data compiled by Liskien and Paulsen (9) has been adopted. This value, 0.47 mb, is in best agreement with the rather recent value 0.45 ± 0.05 mb given by Clare and Martin (10). The calculated spectral corrections are + 6.9%, - 1.2%, and - 3.9%, respectively, of the uncorrected values. The change in sign is due to the smaller slope of the assumed excitation function for the rather exoergic (n,α) reaction in nickel. The corrections have been obtained with the aid of Fig. 3. The $Ni^{58}(n,p)$ cross section was taken from (11) and the remaining cross sections from (6).

The very good agreement between the results based on different standards is of course partly fortuitous. Indirectly, however, it gives support to the standard cross sections chosen. For natural nickel, the calculated result according to (6) is 5.0 mb, to be compared with the present experimental value of 4.2 mb, Table II.

References

1. L. Ljungberg, to be published, ASTM Conference, San Francisco, June 1968.
2. H. Alter and C.E. Weber, Journal of Nuclear Materials, 16, 68-73 (1965).
3. J.C. Roy and J.J. Hawton, AECL-1181 (1960).
4. D.J. Hughes, Pile Neutron Research, Addison-Wesley, 1953.
5. R.P. Schuman and A.C. Mewherter, KAPL-1779 (1957).
6. J. Eriksson, AB Atomenergi, Studsvik, private communication.
7. Erik A. Johansson, AB Atomenergi, Stockholm, private communication.
8. A.M. Bresesti et al., Nucl. Sci. Eng. 29, 7-14 (1967).
9. H. Liskien and A. Paulsen, Nukleonik 8, 315-319 (1966).
10. D.M. Clare and W.H. Martin, J. Nuclear Energy A/B 18, 703 (1964).
11. BNL-325, Second Ed., Suppl. No. 2.

Calculated cross sections (mb) according to (6). Upper line gives $\sigma(n,p)$, lower line $\sigma(n,\alpha)$. Cross sections < 1 μb are set equal to zero

	Lab. energy MeV				Integrated cross-sections
	2	5	10	15	
^{50}Cr	3.6	221	368	320	32.8
	0.0	2.4	102	137	1.50
^{52}Cr	0.0	0.2	49.6	82.7	0.47
	0.0	0.004	22.3	51.8	0.15
^{53}Cr	0.0	1.4	25.1	40.7	0.47
	0.003	2.0	17.0	32.0	0.42
^{54}Cr	0.0	0.0	2.3	20.1	0.015
	0.0	0.0	4.0	13.5	0.024
^{56}Fe	0.0	0.7	93.4	133.5	1.02
	0.0	0.4	34.5	58.9	0.39
^{54}Fe	19.6	446.8	554.4	345.9	75.8
	0.0	1.8	53.8	79.7	0.84
^{57}Fe	0.0	1.7	44.7	65.5	0.77
	0.013	3.8	24.3	39.8	0.72
^{58}Ni	65.2	694.6	705.5	271.3	142.2
	0.7	41.06	116.0	46.7	6.96
^{60}Ni	0.0	6.8	170.0	202.6	3.14
	0.0	1.8	47.5	44.9	0.77

Table I

Samples					Monitors Observed reaction probabilities during irradiation			Results He-production probabilities normalized to monitor reaction probability		
No.	Weight in gram	Number of Ni-atoms $N_X \times 10^{-22}$	Measured number of He-atoms $n_X \times 10^{-16}$	Observed (n,α) reaction prob. in sample during irradiation $(\frac{n}{N})_X \times 10^7$	Monitor 1 $[Ni^{58}(n,p)Co^{58}]$ Observed no. of (n,p) reactions per Ni^{58}-atom $(\frac{n}{N})_{M-1} \times 10^7$	Monitor 2 $[Ti^{46}(n,p)Sc^{46}]$ Observed no. of (n,p) reactions per Ti^{46}-atom $(\frac{n}{N})_{M-2} \times 10^7$	Monitor 3 $[Cu^{63}(n,\alpha)Co^{60}]$ Observed no. of (n,α) reactions per Cu^{63}-atom $(\frac{n}{N})_{M-3} \times 10^7$	$k_1 = (\frac{n}{N})_X : (\frac{n}{N})_{M-1}$	$k_2 = (\frac{n}{N})_X : (\frac{n}{N})_{M-2}$	$k_3 = (\frac{n}{N})_X : (\frac{n}{N})_{M-3}$
1	2.4613	2.5246	0.8991	3.561	84.3	8.55	0.386	0.0422	0.416	9.23
2	2.4566	2.5197	0.9460	3.754	84.8	8.65	0.390	0.0442	0.434	9.63
3	2.4648	2.5281	0.9424	3.728	85.7	8.75	0.395	0.0435	0.426	9.44
6	2.4496	2.5126	0.9406	3.744	88.6	9.04	0.406	0.0423	0.414	9.22
7	2.4670	2.5304	0.9781	3.865	89.1	9.10	0.412	0.0433	0.425	9.38
13	2.4747	2.5383	0.9570	3.770	85.1	8.69	0.392	0.0443	0.434	9.61
15	2.4600	2.5232	0.9415	3.731	87.3	8.89	0.402	0.0427	0.420	9.28
16	2.4670	2.5304	0.9446	3.733	88.1	8.98	0.406	0.0424	0.416	9.19
17	2.4624	2.5257	0.9367	3.709	88.5	9.04	0.409	0.0419	0.410	9.01
23	2.4575	2.5207	0.8837	3.506	83.1	8.47	0.382	0.0422	0.414	9.18
25	2.4672	2.5306	0.9135	3.610	85.2	8.65	0.390	0.0424	0.417	9.26
26	2.4740	2.5376	0.9091	3.583	86.0	8.74	0.394	0.0416	0.410	9.09
27	2.4768	2.5405	0.9545	3.757	86.9	8.82	0.398	0.0432	0.426	9.44
							Mean k ——> values	$<k_1> =$ 0.0428 ± 0.0003	$<k_2> =$ 0.420 ± 0.003	$<k_3> =$ 9.31 ± 0.05

Table II

Monitor	Assumed fission spectrum average cross section of monitor $\bar{\sigma}_M$ (mb)	Average k value according to Table I $\langle k \rangle$	Uncorrected He-production cross section of nickel $\bar{\sigma}'_X = \langle k \rangle \bar{\sigma}_M$ (mb)	Spectral correction factor $\varepsilon(\sigma_M, \sigma_X) = \frac{kI_M - I_X}{\Phi_o}$ (mb)	Corrected mean He-production cross section of nickel $\bar{\sigma}_X = \langle k \rangle \bar{\sigma}_M + \varepsilon(\sigma_M, \sigma_X)$ (mb)
$Ni^{58}(n, p)$	91.5	0.0428	3.92	+ 0.27	4.19
$Ti^{46}(n, p)$	10.2	0.420	4.28	- 0.05	4.23
$Cu^{63}(n, \alpha)$	0.47	9.31	4.38	- 0.17	4.21

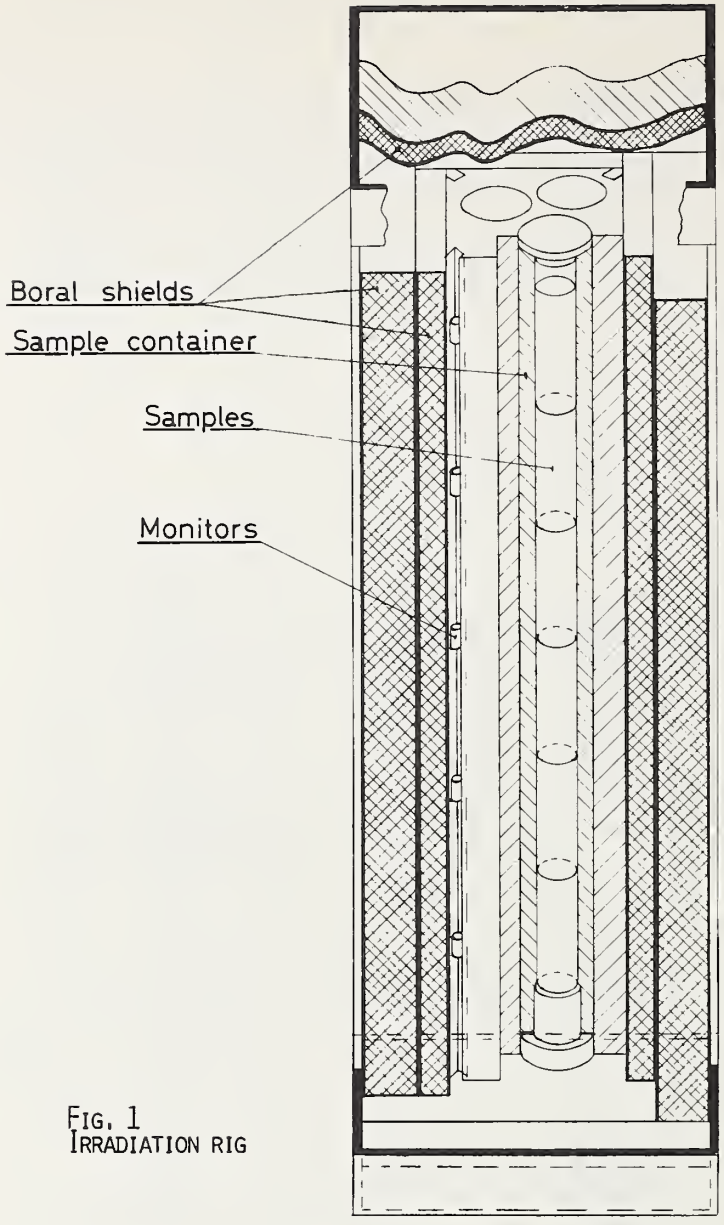

FIG. 1
IRRADIATION RIG

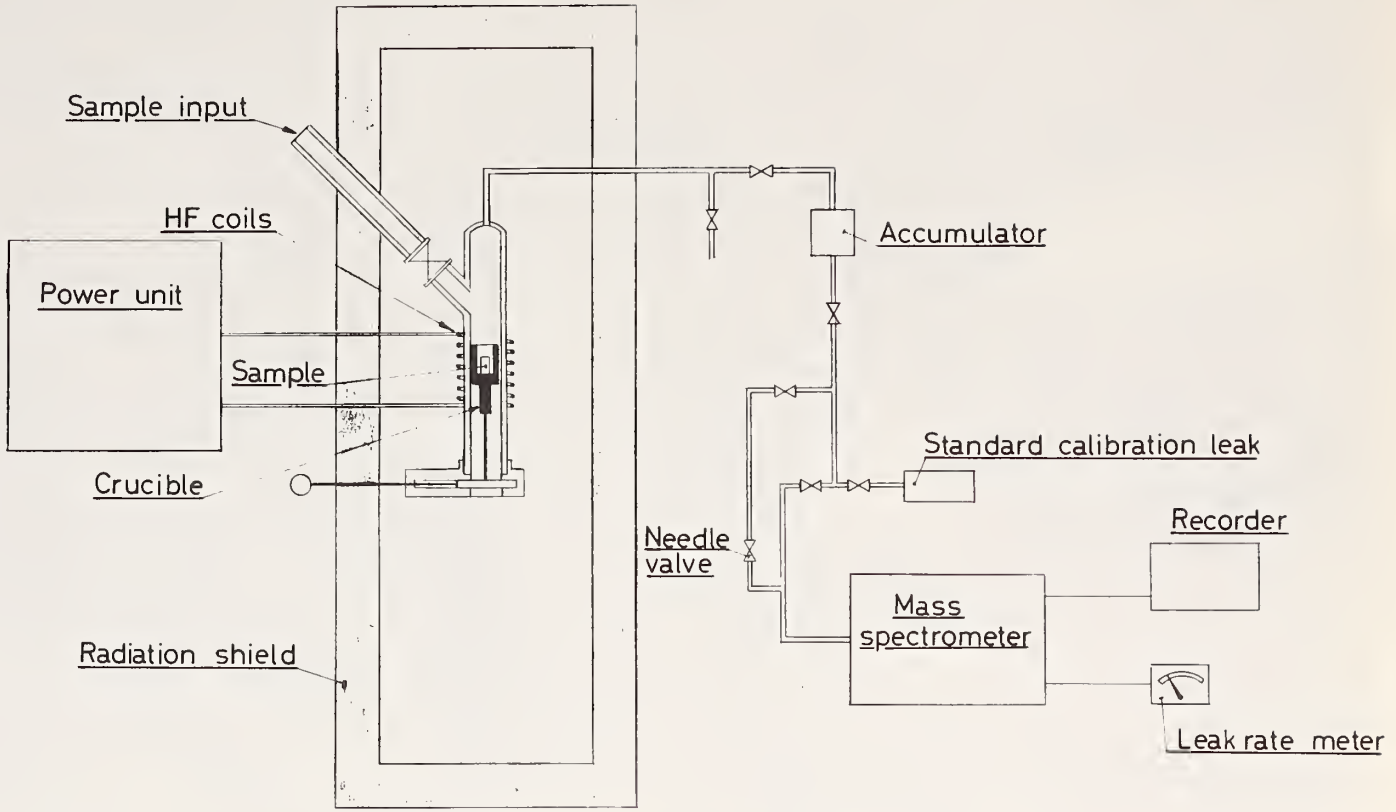

FIG. 2A. SCHEMATIC EXPOSITION OF THE EXPERIMENTAL ARRANGEMENT

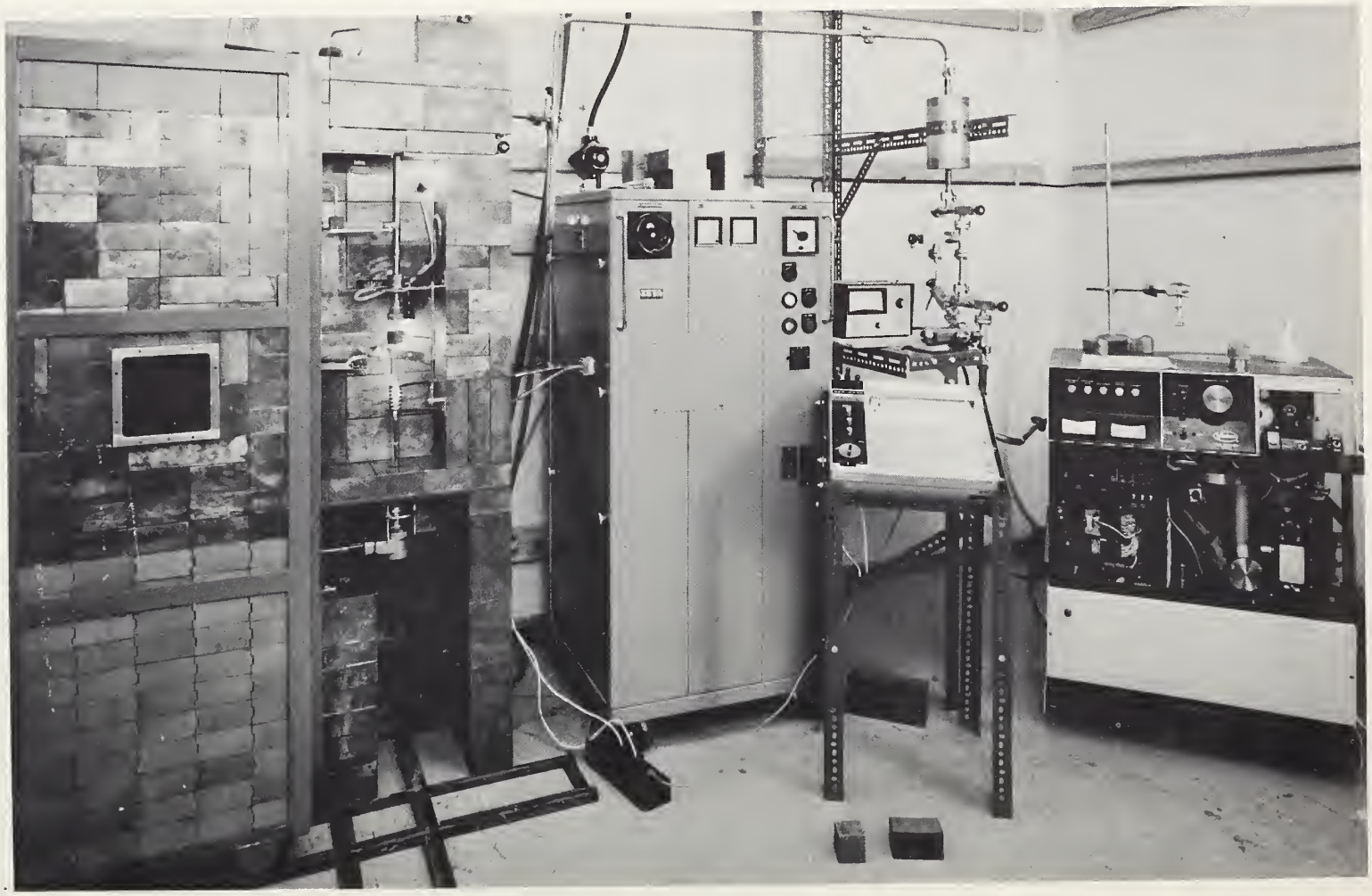

Fig. 2b.

Figure 3.

Flux in irradiation position

Cross sections for spectrum correction

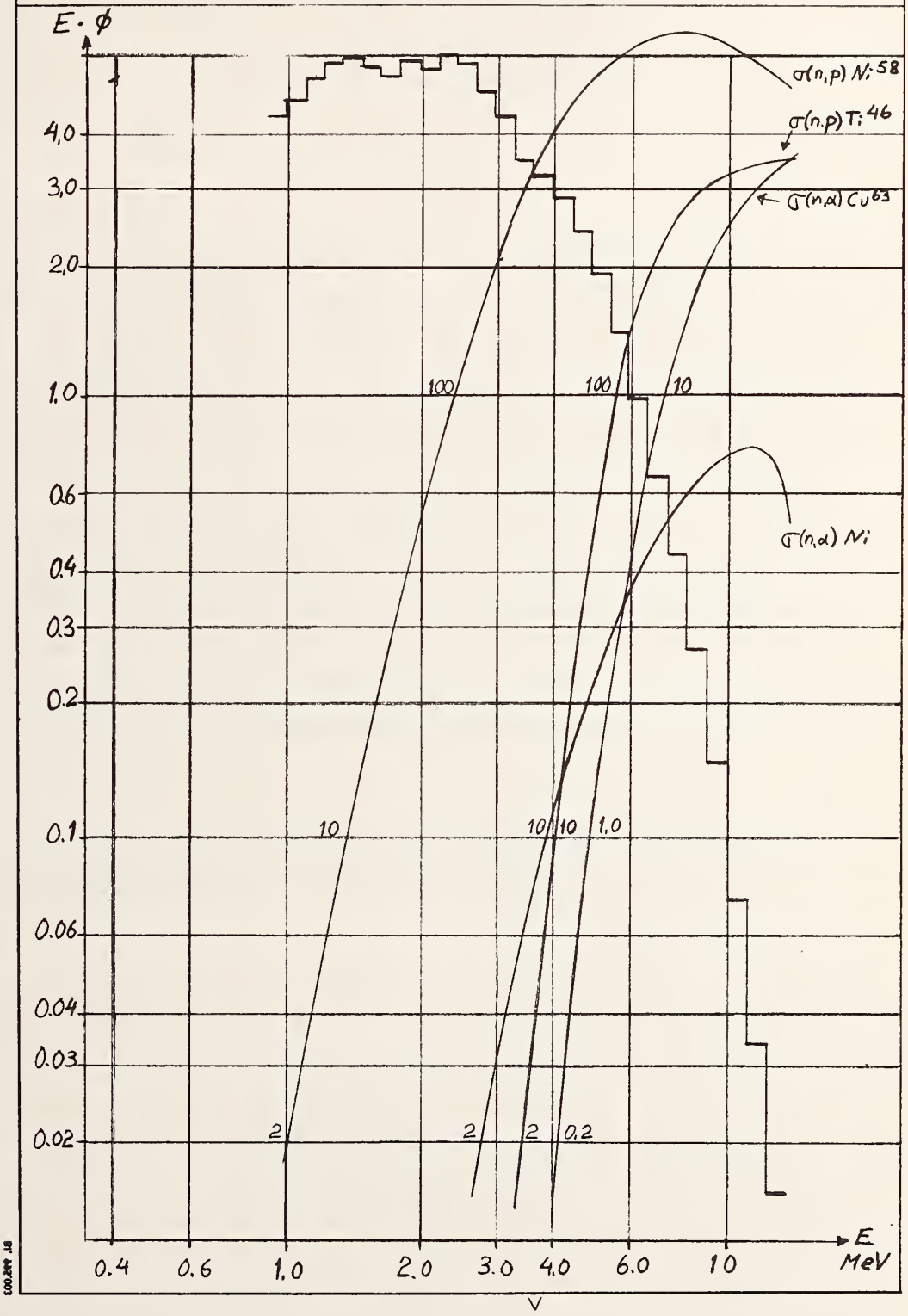

Measurement of Gamma-Ray Production Cross Sections Using a LINAC*

V. J. Orphan, A. D. Carlson, and C. G. Hoot

Gulf General Atomic Incorporated
San Diego, California 92101

ABSTRACT

A newly constructed facility which was designed especially for the measurement of gamma-ray production cross sections using a pulsed LINAC neutron source is currently being operated at Gulf General Atomic. The initial program for this facility is concerned with the measurement of epithermal capture gamma-ray spectra and yields for W, and the measurement of gamma-ray production cross sections by inelastic scattering in O and N. Later phases of the work will extend the capture gamma-ray spectra to U^{238}, Zr, and Fe, and the inelastic production to W and Fe. Large volume Ge(Li) detectors have been developed and are being used in these studies. In the case of capture gamma-ray work a gamma-ray spectrometer will be used which consists of a large Ge(Li) detector located inside a split NaI annulus. This system can be used in the pair spectrometer mode at high gamma-ray energies and in the Compton suppression mode at low gamma-ray energies. The principal considerations involved in using a LINAC for these measurements will be discussed together with the necessary extensions of previously used techniques. The experimental results obtained in the initial phase of the program will be presented.

---

*Work supported by Air Force Weapons Laboratory, Union Carbide Corporation and Defense Atomic Support Agency.

313-475 O-68—11

1. INTRODUCTION

An accurate knowledge of gamma-ray production cross sections over a wide neutron energy range (thermal to approximately 15 MeV) is essential for neutron shielding calculations. Although much gamma-ray production cross section data currently exist, in many cases these data were obtained with other objectives in mind and consequently do not fulfill all of the needs required to perform radiation transport calculations. Furthermore, serious gaps exist in gamma-ray production cross section data, especially at high energies.

The objective of a gamma-ray production cross section measurement is the determination of the cross section for the production of gamma rays by neutrons without attempting to identify the nuclear processes which produced the gamma rays. However, in favorable cases identification of the processes should be possible. In the eV and keV neutron energy range, gamma rays are produced by radiative neutron capture. Measurements have been, and are currently being made of resonance capture gamma-ray spectra using high-resolution Ge(Li) gamma-ray detectors and a variety of neutron sources such as: a fast neutron chopper and reactor,[1, 2] a monochromator and reactor,[3] and a pulsed LINAC neutron source.[4, 5] In the MeV neutron energy range, inelastic neutron scattering produces most of the gamma rays, although other processes, such as $(n, \alpha\gamma)$, also contribute. Previous and current measurements[6, 7] use a monoenergetic neutron source, usually a Van de Graaff accelerator.

This paper describes a newly constructed facility which was designed for the measurement of gamma-ray production cross sections using a pulsed LINAC neutron source and Ge(Li) gamma-ray detectors. An experiment planned for the measurement of capture gamma-ray production cross sections for neutrons from thermal to about 100 keV is described. In addition, a technique for measuring gamma-ray production cross sections over the neutron energy range of $\sim$ 100 keV to 15 MeV is discussed.

Some initial experimental results are presented.

2. DESCRIPTION OF EXPERIMENT

2.1 Capture Gamma-Ray Production Cross Sections

A schematic of the experimental arrangement which will be used to measure capture gamma-ray spectra is shown in Fig. 1. The Gulf General Atomic LINAC is used to produce a pulse of neutrons having a pulse width adjustable from 10 nsec to 4.5 μsec and a repetition rate of

up to 720 pps. A capture sample is placed at the terminus of a 15.5-meter neutron flight path in a collimated 6-in. diam neutron beam. The capture gamma-ray energies are measured with a Ge(Li) spectrometer and the corresponding neutron energies are determined by time of flight.

The Ge(Li) spectrometer consists of a large Ge(Li) detector located inside a split NaI annulus. This system can be used as a three-crystal pair spectrometer at high gamma-ray energies and in the Compton suppression mode at low gamma-ray energies. It is advantageous to use a pair spectrometer for capture gamma-ray production cross section measurements because its one-line response greatly simplifies the determination of gamma-ray yields. However, a disadvantage of the pair spectrometer is its lower (by about a factor of 5) counting efficiency than that of a singly-operated Ge(Li) detector. However, in taking data with an on-line computer, it is easy to record all three gamma-ray spectra - the singles Ge(Li) spectrum, the Compton-suppression spectrum, and the pair-spectrometer spectrum - simultaneously. Therefore, in those cases where the counting statistics in the pair spectrum are poor recourse to the singles spectrum will be possible. Even in these cases the pair spectrum should be useful for peak identification. As illustrated in Fig. 1 the Ge(Li) spectrometer is mounted on a movable carriage which allows the spectrometer to be pivoted about the capture sample (for angular distribution studies).

In initial experiments conducted to date, only a singly-operated Ge(Li) detector has been used. The 31 cm^3 coaxial Ge(Li) detector, which was fabricated in our laboratory, has a resolution of 3.7 keV (FWHM) at 662 keV and 4.7 keV (FWHM) at 2614 keV, when optimum low-noise electronics are used. When the Ge(Li) detector is used in a LINAC experiment, it is necessary to use electronics having special pulse-shaping optimized to minimize gamma flash interference; this results in a resolution loss of about 2 or 3 keV.

2.2 Gamma-Ray Production Cross Sections From High Energy Neutrons

Figure 2 shows, conceptually, the experimental arrangement to be used for measuring gamma-ray production cross sections with a LINAC in the MeV neutron energy range. The LINAC produces pulses of neutrons having a continuous spectrum of energies. By recording the time when a gamma-ray event is observed in the Ge(Li) detector relative to the LINAC pulse, the neutron time-of-flight, and hence the neutron energy, is determined. By using a 10 nsec neutron pulse width, a neutron energy resolution of about 2% at 10 MeV is possible for the 50-meter flight path.

A 50 cm o.d. ring sample with an area of about 1500 cm^2 will be used since it offers the optimum detector-to-sample solid angle, and hence seems to be the best configuration for enhancing the count rate. The Ge(Li) detector is placed at a back angle to reduce the intensity of gamma flash scattered off the sample into the detector, and it is shadow shielded from source neutrons and gamma rays. Initial experiments have been carried out using a disc sample viewed by a detector placed just outside the neutron beam and at a back angle of about 125^{o}.

2.3 Data Acquisition

A simplified block diagram of the data acquisition system is given in Fig. 3. This system is used for both of the two-parameter experiments described. For every gamma-ray event in the Ge(Li) detector two pulses are derived: a linear pulse (gamma-ray energy), and a timing pulse (neutron energy). The linear pulse is gated on after every LINAC pulse only for a time interval corresponding to neutron energies of interest. Currently, it is possible to gate the linear signal on about 1 μsec (corresponding to a 13 MeV neutron on the 50-m flight path) after the LINAC pulse without allowing the gamma flash pulse to pass through. The linear pulse is pulse-height analyzed using a 4096-channel ADC. A time analyzer, with available channel widths from 5 nsec to 80 nsec, is used to measure the time interval between the timing pulse from the Ge(Li) detector and a reference LINAC trigger pulse.

The digitized pulse height (h) and time-of-flight (t) information is stored in a CDC-1700 computer. The computer has been programmed to transfer on-line the two-parameter data (h, t) to a magnetic disk where it is stored in sequential fashion. Also, the computer maintains in its core memory an array of h for all t and an array of t for all h. Either of these arrays are available for live display on an oscilloscope during an experiment. At the conclusion of an experiment the CDC-1700 is used to sort the data stored on the disk. Pulse-height spectra corresponding to specified neutron energy intervals (time intervals) may be generated, scaled to a selected number of channels, displayed on an oscilloscope, and read out on punched paper tape. An important advantage of this method of treating two-parameter data is the flexibility it offers in choosing different neutron energy intervals. Furthermore, because the data are stored sequentially on the disk, data may be easily segregated according to the time it was accumulated. This allows one to easily exclude data taken during a period of gain shifting without disturbing previous data.

3. INITIAL RESULTS

3.1 Capture Gamma-Ray Spectra From W

Initial measurements have been made of the capture gamma-ray spectra from neutron capture in natural tungsten. The capture sample, a 4-3/4 in. diam x 0.3-in. thick piece of tungsten, was placed at an angle of 45° to the neutron beam at 15.5 meters and was viewed by a 31 cm^3 Ge(Li) detector located at 90° to the neutron beam and about 8 inches from the center of the sample. A 2-in. thick (4-in. square) piece of LiH was placed between the detector and the sample to reduce the background from scattered neutrons.

Figure 4 shows the capture gamma-ray yield for gamma-ray energies above $\sim$ 2.5 MeV as a function of neutron flight time. Lower energy resonances are identified in Fig. 4. With an electron pulse width of 1 μsec, the neutron energy resolution is .18% at 1 eV, 1.8% at 100 eV and 5.6% at 1000 eV. The "dip" at the peak of the lower energy resonances occurs because the Ge(Li) detector was viewing the back face of a thick sample. The gamma rays produced in the back portion of the sample are more efficiently detected than those produced in the front portion and the neutron flux near the resonance energies is depressed in the back portion of the sample. When the detector viewed the front face of the sample there was no dip and the resonance peak-to-background ratio improved. Six neutron energy intervals, for which capture gamma-ray spectra were generated, are delineated in Fig. 4.

Figures 5 and 6 show the capture gamma-ray spectra from about 4 MeV to 8 MeV for the six neutron energy intervals shown in Fig. 4. The energies, taken from Ref. 8, of some of the more prominent W resonance capture gamma rays are given above the peaks. The counting statistics for this 2.4-hour run are inadequate to permit the identification of many of the gamma ray lines. Much longer running times will be possible with our system when long-term gain stability is achieved by controlling the temperature of the electronics and by using a digital gain stabilizer.

As seen in Fig. 5, the gamma-ray energy resolution is constant at about 16 keV (FWHM) over the range of 4 MeV to 8 MeV. This is approximately the same resolution obtained for the high energy gamma rays resulting from thermal neutron capture in Cl when a moderated Pu Be neutron source is used. Hence, it may be concluded that there is no significant gamma-ray energy resolution degradation due to gamma flash interference for this range of neutron energies. Note that in Figs. 5 and 6, as has been pointed out previously,[2, 3, 4] the capture gamma-ray spectrum of natural W changes markedly from one neutron energy interval to another.

3.2 Gamma Rays From Neutron Inelastic Scattering in Natural Iron

The spectrum of gamma rays resulting from inelastic scattering in natural iron of neutrons with energies from 0.8 MeV to 13 MeV was studied using a 31 cm^3 Ge(Li) detector. The sample, a 12-in. diam x 1/2-in. thick disk of Fe was placed at 51 meters at an angle of 45^o with the incident neutron beam. The Ge(Li) detector, which was at an angle of about 125^o to the incident neutron beam, was about 18 in. from the center of the Fe sample. A 2-in. thick slab (4-in. square) piece of LiH was used to shield the Ge(Li) detector from sample-scattered neutrons. The LINAC was operated with a burst width of 100 nsec, a peak current of about 2 amps, an electron energy of 50 MeV, and a repetition rate of 360 pps.

Figure 7 shows the gamma-ray spectra from about 0.5 MeV to 2.2 MeV for six different neutron energy intervals obtained in a 2-hr run. The 0.845 MeV gamma ray from inelastic scattering in Fe^{56} is present in every spectrum. Note that the area under each 0.845 MeV gamma-ray peak in Fig. 7, normalized for the variation of incident neutron flux per unit energy, is proportional to the average 0.845 MeV gamma-ray production cross section over each neutron energy interval. Several other higher energy gamma rays from neutron inelastic scattering in Fe also appear in the spectra - especially as the neutron energy increases.

The gamma-ray energy resolution at 0.845 MeV is about 14 keV (FWHM) in the spectra shown in Fig. 7. The degraded resolution (from a value of about 6 keV (FWHM) with a radioactive source) is caused by the close proximity in time of the gamma flash. For a gamma ray produced by a 13-MeV neutron, the instantaneous count rate in the Ge(Li) detector is of the order of 10^6 cps. Therefore, it is not surprising that a loss of resolution results. Note that the positions of the 0.845 MeV gamma-ray peaks in Fig. 7 do not vary with neutron energy and hence, that time-dependent (or neutron energy-dependent) gain shifts caused by the gamma flash is not a problem. As seen in the first spectrum of Fig. 7 the principal background gamma-ray peak is the 0.695 MeV gamma ray from neutron inelastic scattering in Ge^{72}. Note also that the intensity of this background peak drops off sharply as the neutron energy increases. Background originating from sample-scattered neutrons striking the detector does not seem to be a serious problem. Additional detector shielding could easily be employed to reduce this background even further.

4. CONCLUSIONS

The use of a pulsed LINAC neutron source in conjunction with large volume Ge(Li) gamma-ray detectors provides an effective means of measuring gamma-ray production cross sections over a wide neutron energy range, from thermal to about 15 MeV. Unlike monoenergetic neutron sources, a LINAC allows the measurement to be made over the energy range in a single experimental run. Furthermore, the LINAC measurement permits flexibility in the choice of neutron energy intervals for which gamma-ray production cross sections are to be generated - the interval may be as large as is desirable and as small as the available counting statistics will allow.

4.1. REFERENCES

1. R. E. Chrien and M. Reich, Nucl. Instr. and Methods, 53, 93 (1967).

2. W. V. Prestwich and R. E. Coté, Phys. Rev. 160, 4, August 20, 1967.

3. Robert R. Spencer and Kenneth T. Faler, Phys. Rev. 155, 4, March 20, 1967.

4. E. R. Rae, et al., Phys. Rev. 155, 4, March 20, 1967.

5. K. J. Wetzel, C. K. Bockelman and O. A. Wasson, Nuclear Physics 92, 3 (1967).

6. G. H. Williams and I. L. Morgan, Nucl. Instr. and Methods 45, 313-318 (1966).

7. L. E. Beghian, F. Hofmann and S. Wilensky, Nucl. Instr. and Methods, 41, 141 (1966).

8. N. C. Rasmussen, Y. Hukai, T. Inouye, V. J. Orphan, "Thermal Neutron Capture Gamma-Ray Spectra of the Elements, " MITNE-85, (1967).

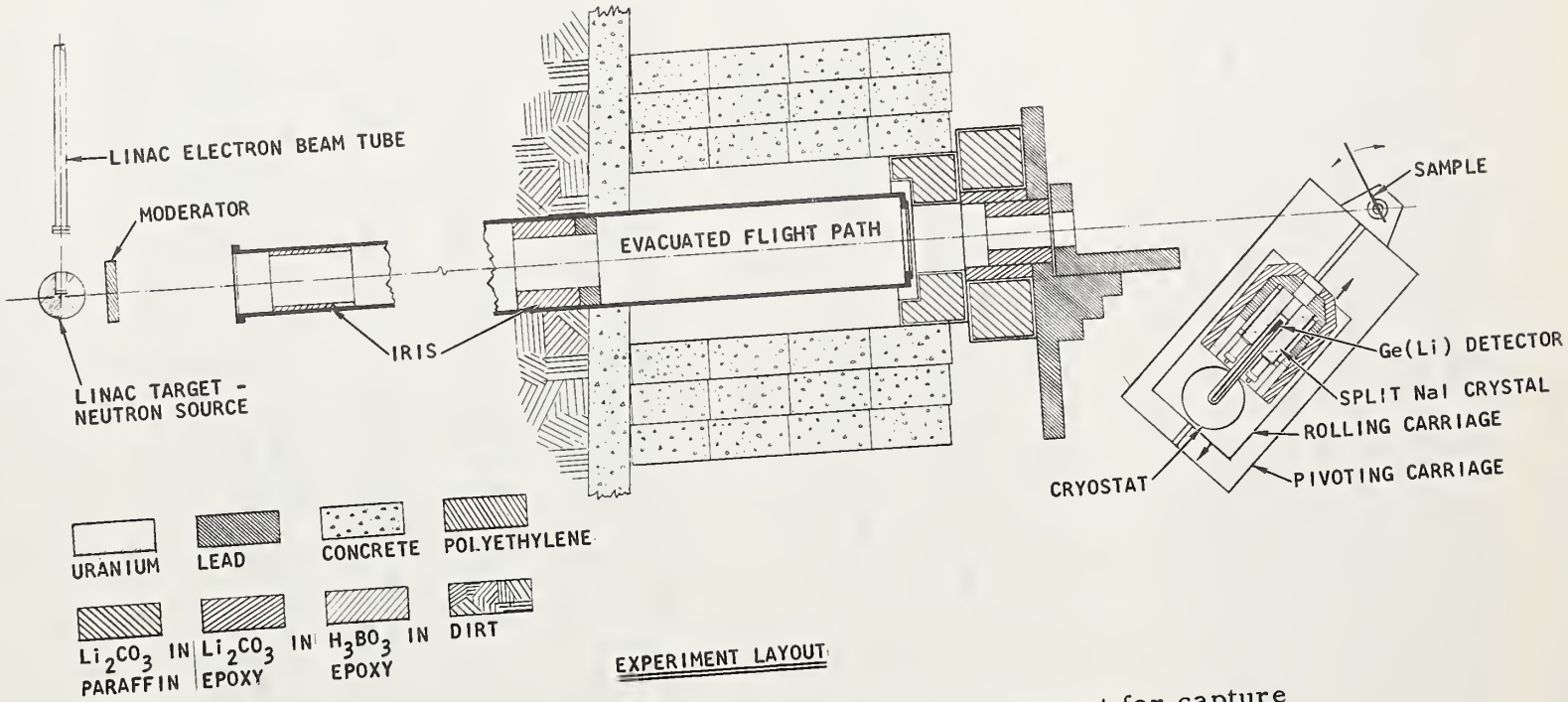

Figure 1. Schematic of experimental arrangement for capture gamma-ray experiment.

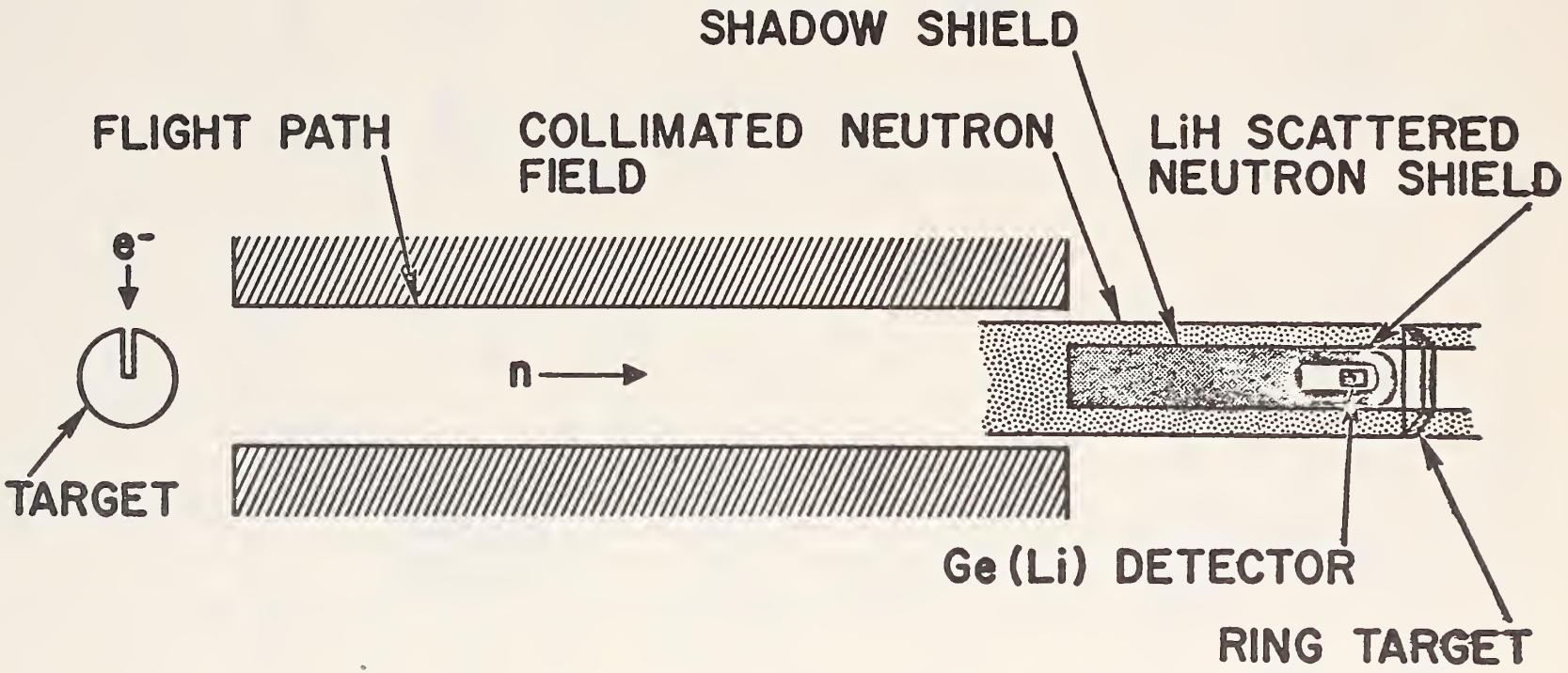

Figure 2. Conceptual schematic of apparatus for the measurement of gamma-ray production cross sections.

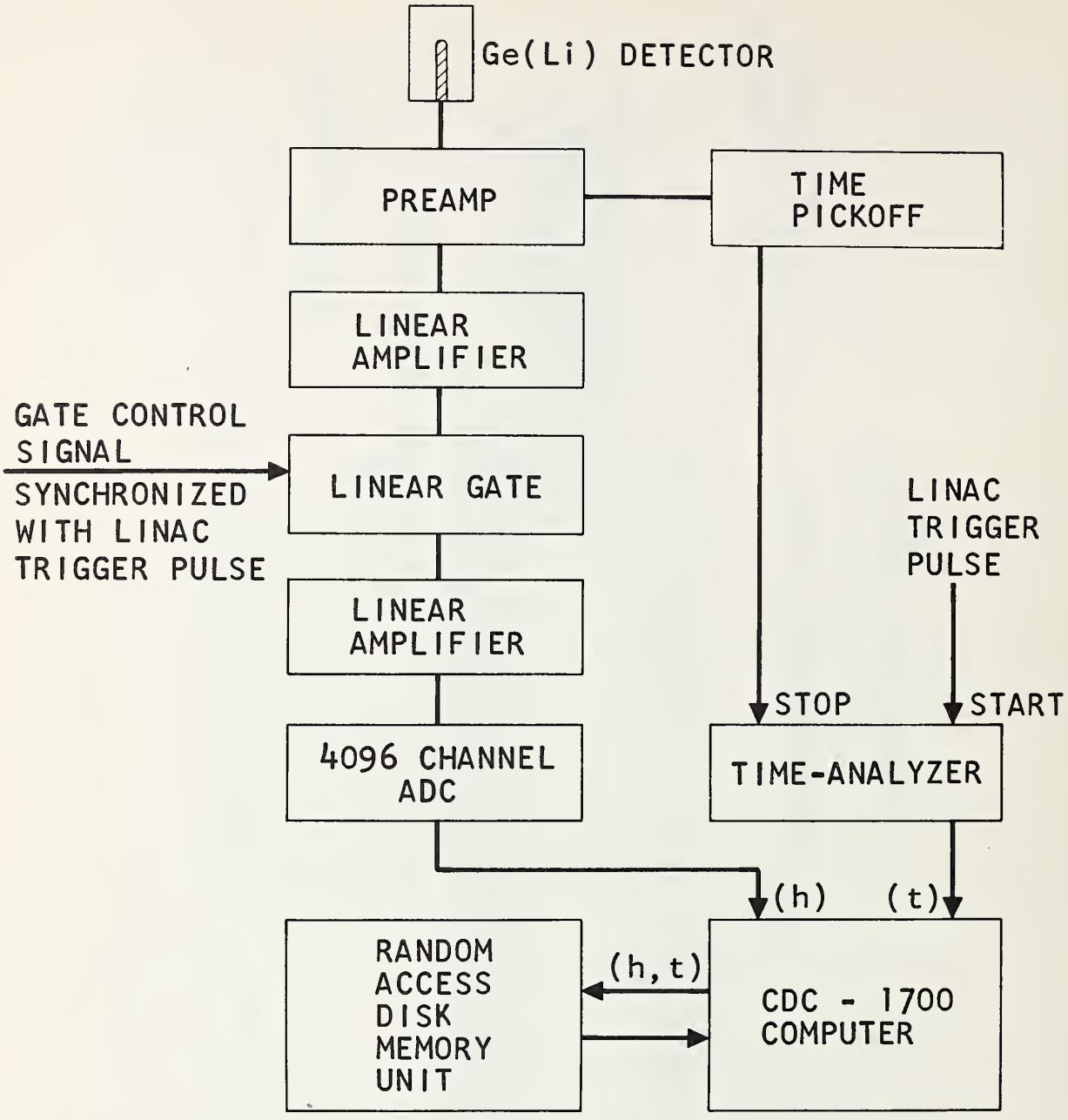

Figure 3. Simplified block diagram of data acquisition system.

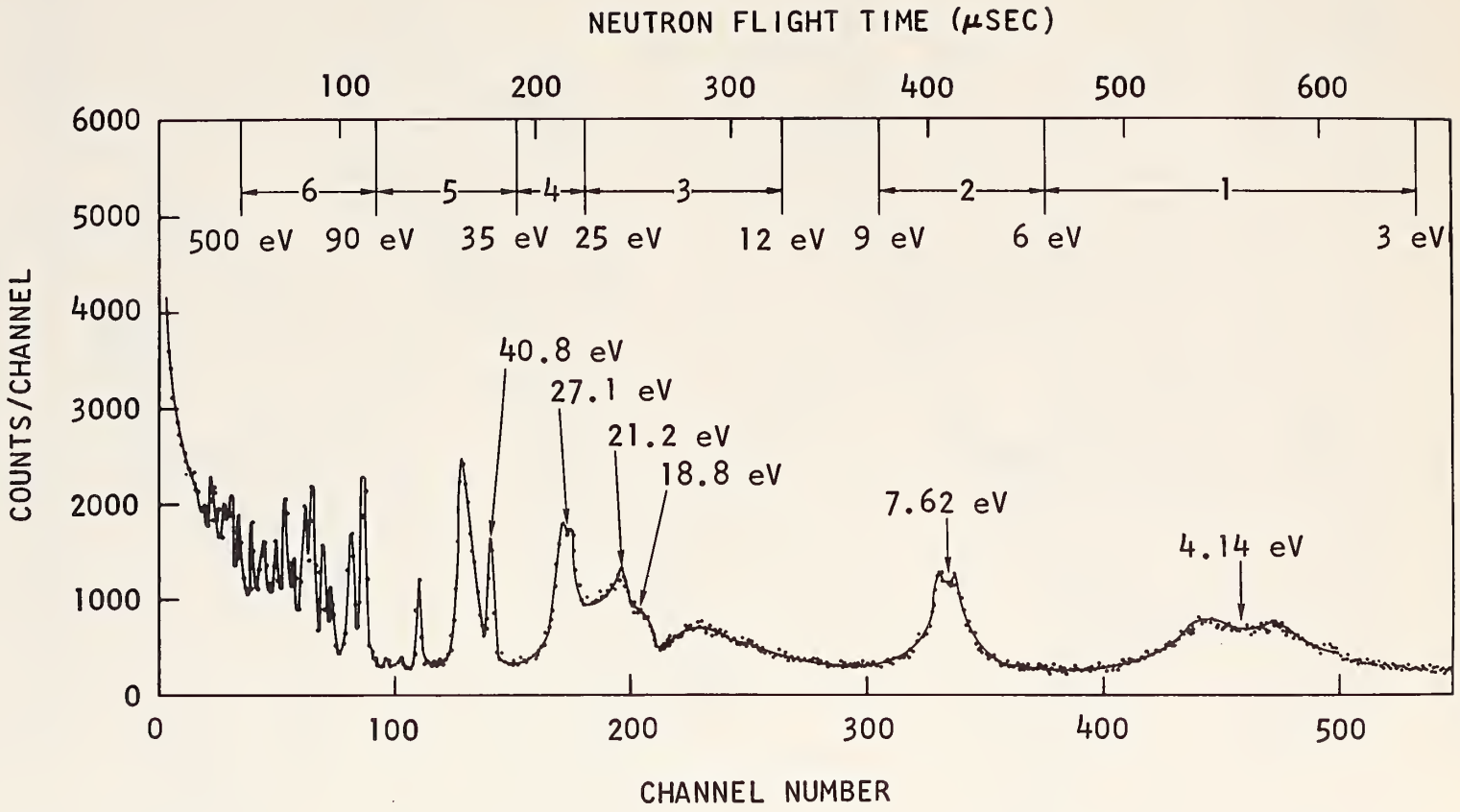

Figure 4. Capture gamma-ray yield for W as a function of neutron time of flight.

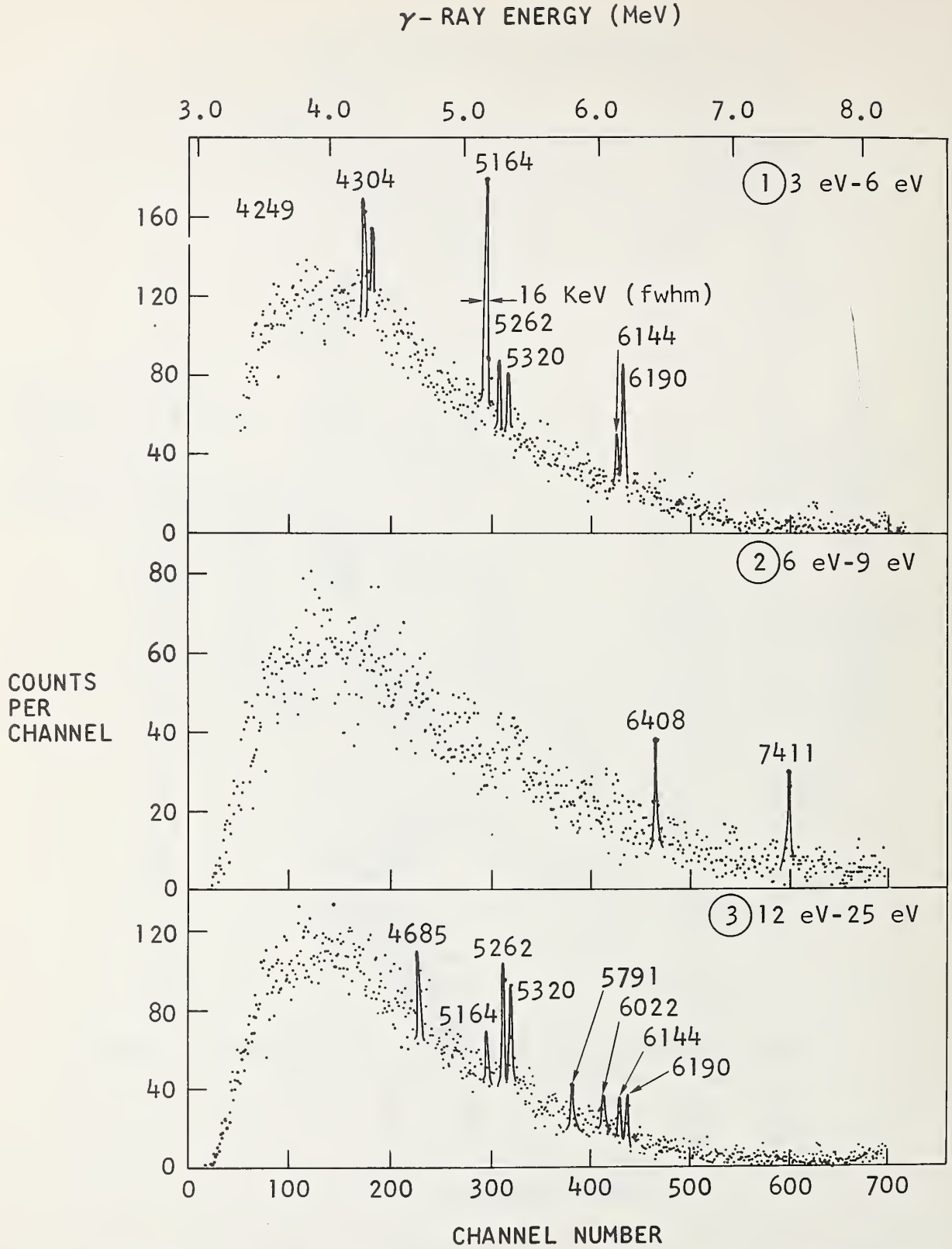

Figure 5. Tungsten capture gamma-ray spectra for three neutron energy intervals, 3-6 eV, 6-9 eV, and 12-25 eV (peak energies-keV).

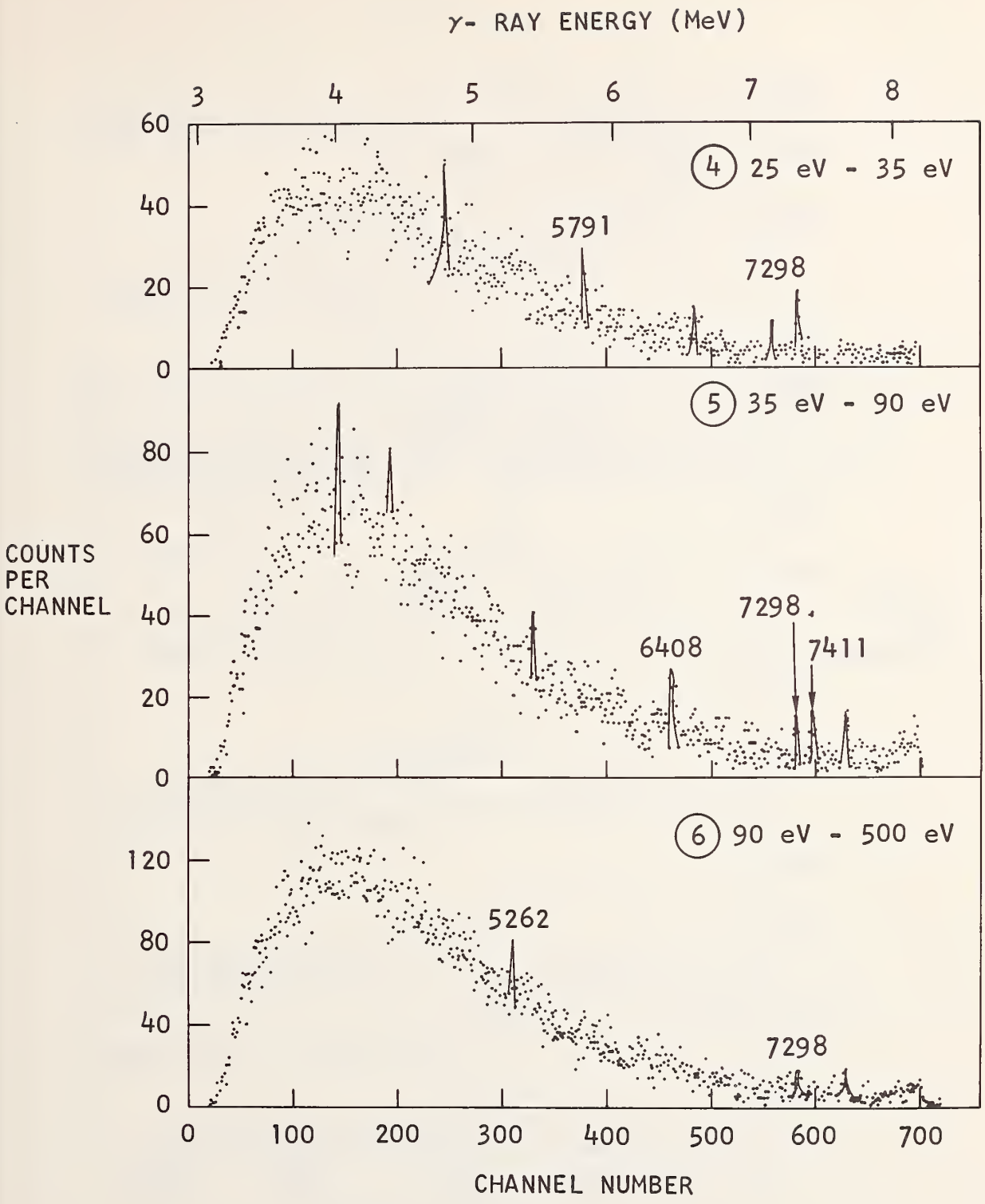

Figure 6. Tungsten capture gamma-ray spectra for three neutron energy intervals, 25-35 eV, 35-90 eV, and 90-500 eV (peak energies-keV).

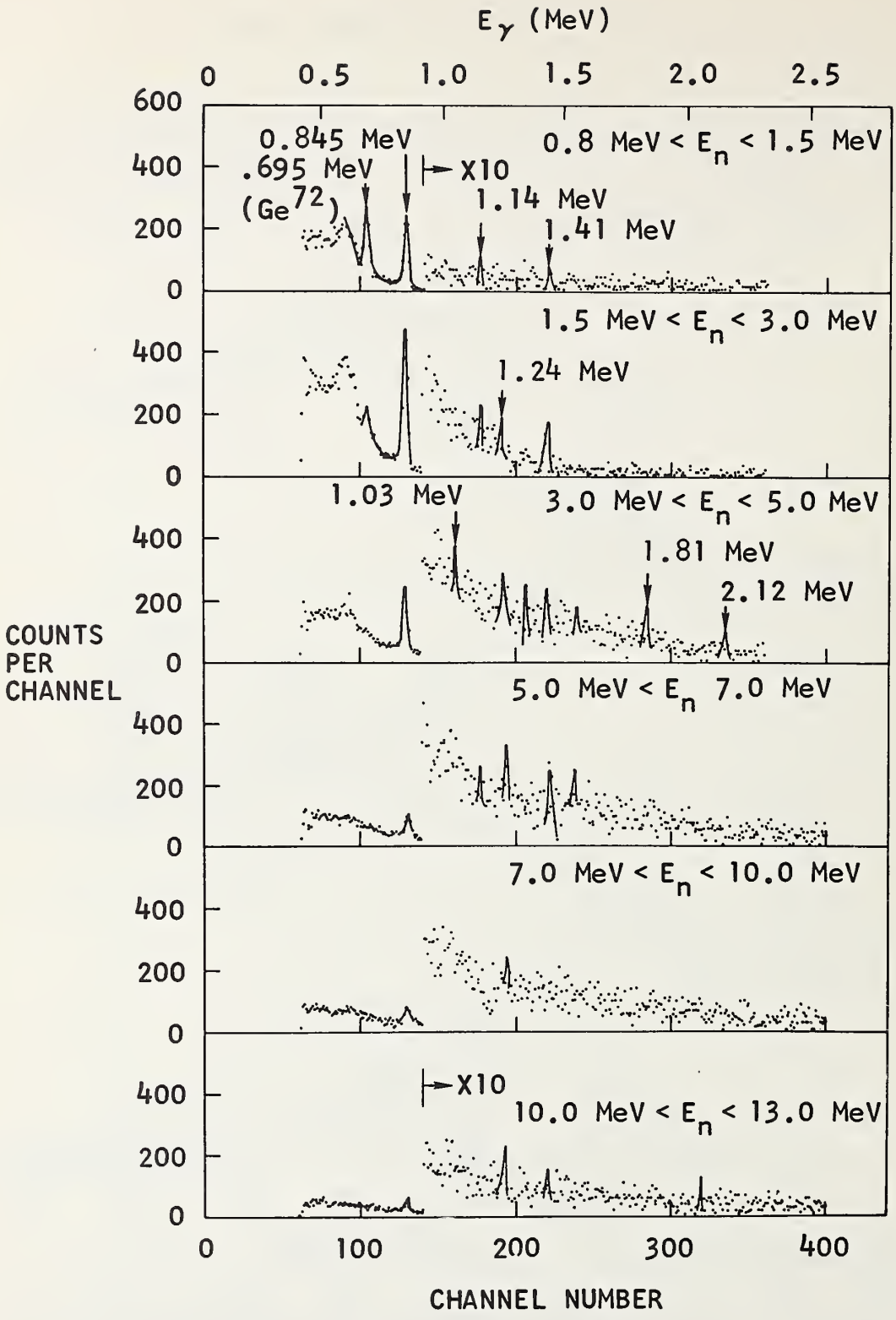

Figure 7. Gamma-ray spectra from about 0.5 to 2.2 MeV for inelastic scattering of neutrons of energies from 0.8 to 13 MeV.

Neutron Cross Sections of ^{6}Li in the Kilovolt Region*

J. A. Farrell

University of California, Los Alamos Scientific Laboratory, Los Alamos, N. M. 87544

and

W. F. E. Pineo

Duke University, Durham, North Carolina 22706

Abstract

The neutron total cross section of ^{6}Li has been measured in the neutron energy range 50 to 650 keV with the Duke University 3 MeV Van de Graaff accelerator using the $^{7}Li(p,n)^{7}Be$ reaction as a neutron source. The data have been fitted by least squares with the single-level Breit-Wigner formula plus a 1/V term. The $^{6}Li(n,\alpha)$ cross section has been computed from the resulting resonance parameters and compared with experiment.

* Work performed under the auspices of the U. S. Atomic Energy Commission.

1. Introduction

There still appears to be much uncertainty about the behavior of the $Li^6(n,\alpha)T$ cross section in spite of the efforts [1,2,3,4] that have been made to measure it. Since good direct measurements are difficult, we decided instead to measure the Li^6 neutron total cross-section and with the parameters obtained from the fit of this cross-section, calculate the $Li^6(n,\alpha)T$ cross-section.

2. Discussion of Experiment

Figure 1 shows the laboratory set-up used at Duke University for neutron cross section measurements. The details have been published elsewhere [5,6] so I will give only a brief description. The neutron source is the $Li^7(p,n)$ reaction using protons supplied by the Duke 3 MeV Van de Graaff accelerator. The machine energy is controlled by passing the singly ionized molecular beam H_2^+, through the electrostatic analyzer. Energy calibration is provided by the $Li^7(p,n)$ threshold. The proton beam H^+, is used to bombard the lithium target. Neutrons are selected by the neutron collimator through two 1/2° apertures located at 20° to the right and left of the proton beam direction. These apertures lead to the independent banks of BF_3 counters, each of which has its own electronics and scaler. The sample to be measured is placed over the left aperture and a count is taken for a preset count of the right aperture. The sample is then placed over the right aperture and the procedure repeated. The transmission is taken to be the geometric mean of the left bank and the right bank transmissions. Data are stored in Duke's on-line computer which writes them on magnetic tape and provides a digital readout of the cross section in the laboratory console area.

The samples that we used were prepared for us by Oak Ridge National Laboratory and consisted of two 3 x 5 inch lithium metal slabs enriched to 96.6% Li^6 and encased in thin silver foil. The N-values of the samples were .1431 nuclei/bn and .04755 nuclei/bn.

Data were first taken in five kilovolt steps over the region of 100 to 650 keV with the thicker of the two samples. We then mounted the thin sample and measured the cross-section over the resonance. A further run from 100-50 keV was made with the thick sample. The data were corrected for the 3.6 per cent Li^7 content of the samples, and the data below 100 keV were corrected for the presence of the low energy neutron group that results from the center of mass motion of the source reaction.

3. Analysis

Figure 2 shows both the data and the fit which we obtained. The data was fit assuming a 1/V law in the s-wave channel and a p-wave resonance term which is described by a single level Breit-Wigner formula. With these conditions, our fitted parameters are

$$\Gamma_n = 167.2 \text{ keV}$$

$$\Gamma_\alpha = 84.1 \text{ keV}$$

$E_o = 250.6$ keV

$R = 2.22$ fm

This fit was obtained by John Farrell at Los Alamos Scientific Laboratory and was checked at Duke using a program written from the R-matrix theory by David L. Sellin last summer.

Calculation of the $Li^6(n,\alpha)T$ Cross Section

The $Li^6(n,\alpha)$ cross section was calculated using Mr. Sellin's program, and Figure 3 shows our calculated cross section and the (n,α) data of Schwartz, Strömberg, and Bergström. Schwartz, et al.[1] made a relative measurement of the cross section using a Li^6 glass scintillator as a detector of $Li^7(p,n)$ neutrons. Their fit, from which they calculated the absolute cross section, was carried out by assuming a Breit-Wigner term in the p-wave channel, with a 1/V dependance of the S-wave cross section at the lower energies, which they extrapolated from the thermal value.

4. Conclusion

While we have not as yet been able to assign probable limits of error to our calculation, we should note that our fit to the total cross section did not seem to be too sensitive to the widths. It should also be noted that the widths are sensitive to the value chosen for the constant in the 1/V term since this will affect the choice of R and hence the penetrability. It will be helpful to obtain total cross section data in the region of 3-100 keV where we should be able to see the 1/V rise, and we plan to do this measurement in the very near future.

5. References

(1) S. Schwartz, L. C. Stromberg and A. Bergstrom, Nuclear Physics 63 (1965) 593.

(2) S. J. Bame and R. L. Cubitt, Phys. Rev. 114, (1959) 1580.

(3) F. Gabbard, R. H. Daves and T. W. Bonner, Phys. Rev. 114, (1959 201

(4) S. A. Cox, Conference Neutron Cross Section Technology, Washington, March 22-24, 1966, CONF-660303, page 701.

(5) C. D. Bowman, E. G. Bilpuch, and H. W. Newson, Annals of Physics, 17, 3 (March, 1962) 319.

(6). J. A. Farrell, E. G. Bilpuch, and H. W. Newson, Annals of Physics 37, 3 (May, 1966) p 367.

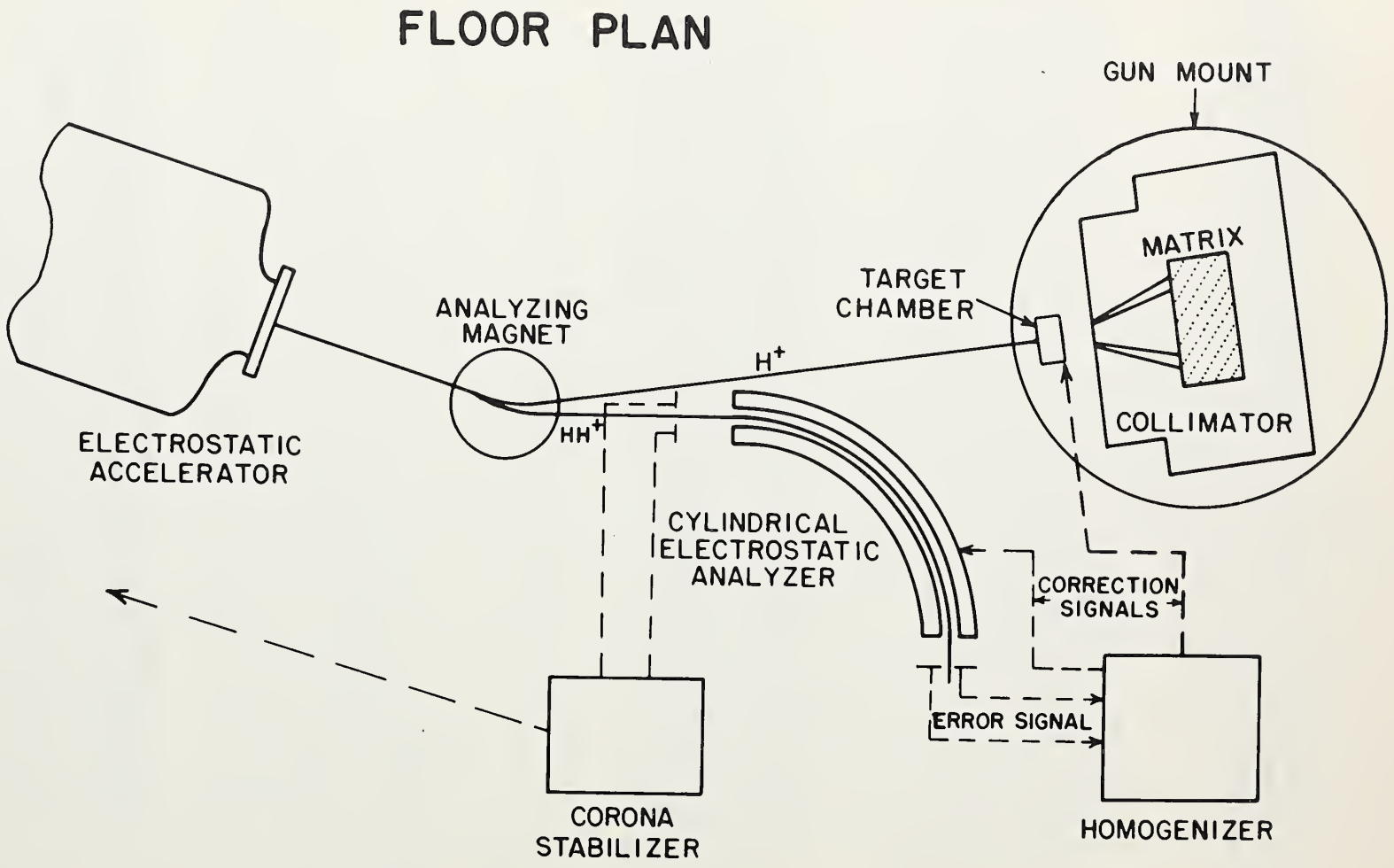

FIG. 1. FLOOR PLAN OF THE 3 MEV LABORATORY

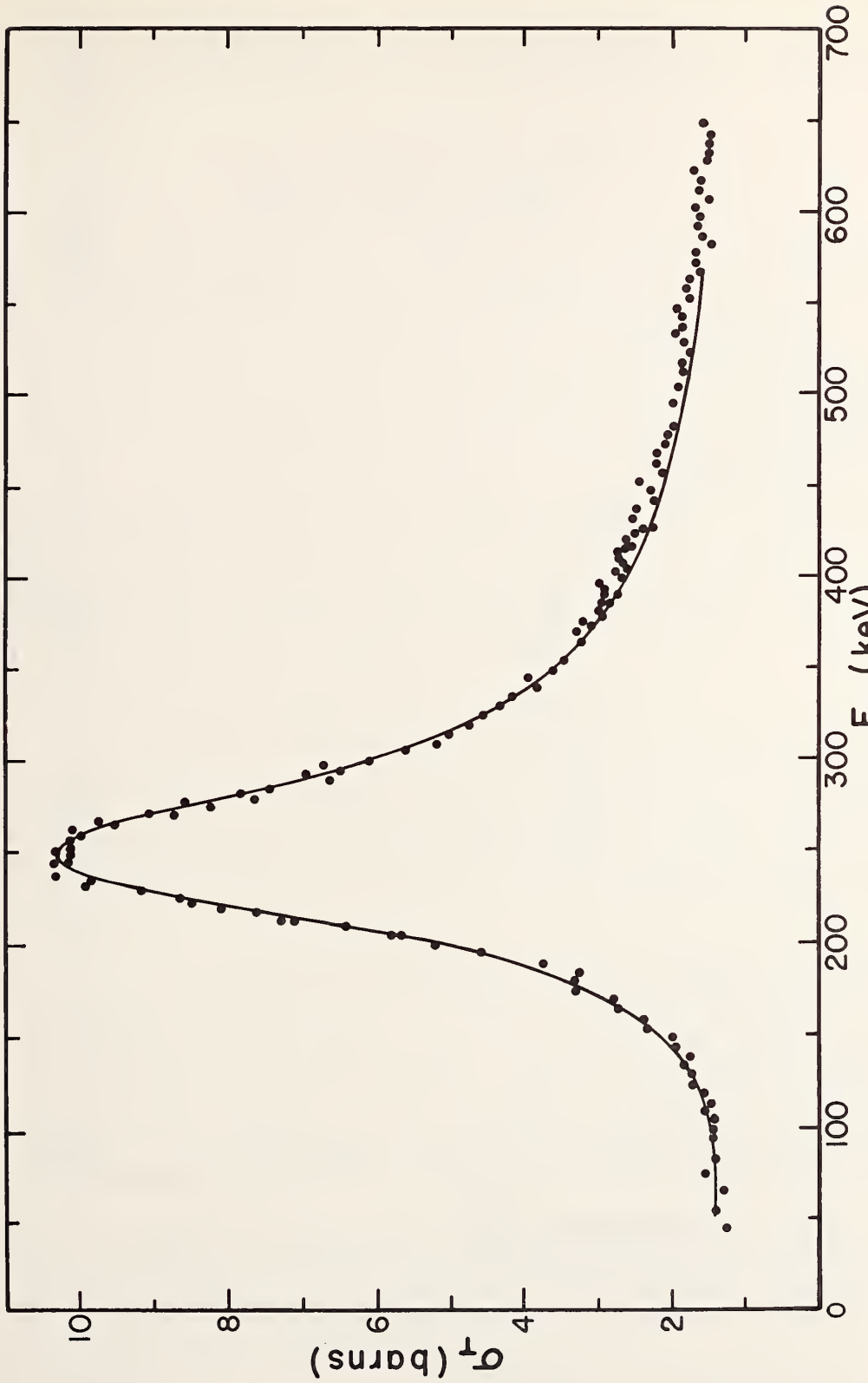

Fig. 2. Li^6 neutron total cross sections. The line is the fit to the data.

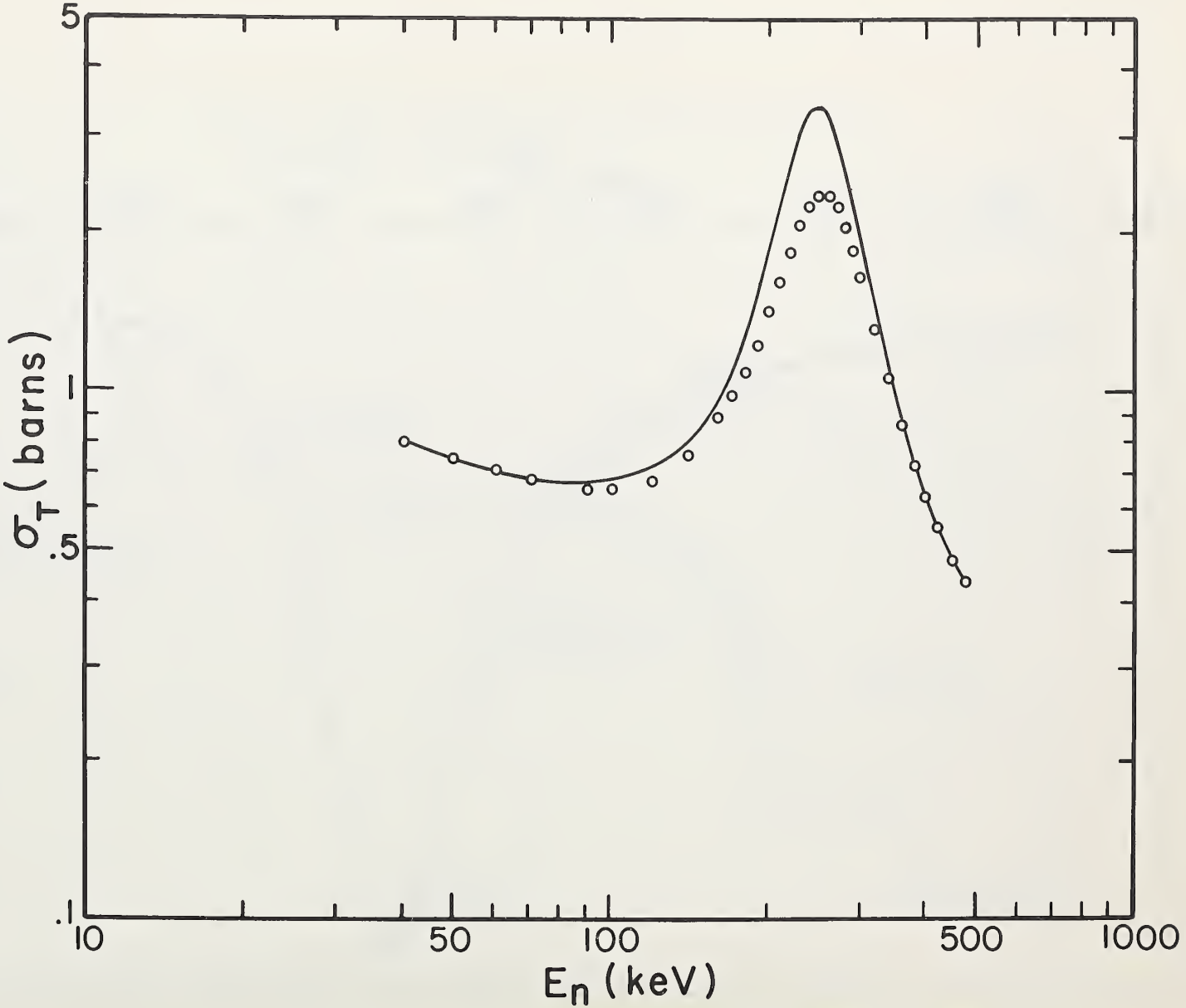

Fig. 3. $Li^6(n,\alpha)T$ cross section. The circles are the points of Schwartz, Stromberg, and Bergstrom.

Total Neutron Cross Sections of ^{6}Li, ^{7}Li and Lithium from 10 to 1236 keV*

C. T. Hibdon and F. P. Mooring
Argonne National Laboratory
Argonne, Illinois 60439

The total cross sections of ^{6}Li and natural lithium have been measured by the transmission method for neutrons in the energy range 10—1236 keV, and the total cross section of ^{7}Li was extracted from the results. Except for a range of energies near 250 keV, the neutron energy spread was ~2 keV. No structure other than a large resonance in the cross section of ^{6}Li at 250 keV and in the cross section of ^{7}Li at 260 keV was observed. These two resonances were investigated by both flat-detection and self-indication techniques, in each case with neutron energy spreads of ~1 keV and ~8 keV. The measured peak height of each of these resonances disagrees with the theoretical value for any possible value of J. Furthermore, the self-indication values of the cross sections are significantly higher than the flat-detection values. These facts, together with the results taken with the narrower resolution width (~1 keV), suggest that both resonances may possibly contain fine structure.

I. EXPERIMENTAL METHOD

The total neutron cross sections of ^{6}Li and natural lithium have been measured by the transmission method for neutrons in the energy range 10—1236 keV, and the total cross section of ^{7}Li was extracted from the results. Except for a range of energies near 250 keV, the neutron energy spread was ~2 keV. Near 250 keV the cross sections were investigated with good resolution (~1.3 keV) as well as with poor resolution (~8—9 keV).

A schematic representation of one arrangement of the neutron counter, long-counter monitors, and rotating target is shown in Fig. 1. The neutron counter consists of fifty $^{10}BF_3$ proportional counters embedded in a cylinder of paraffin which in turn is encased in a massive neutron shield. Neutrons, obtained from the $^{7}Li(p, n)$ reaction and transmitted by the transmission sample A, are scattered by the detector sample B into the array of 50 $^{10}BF_3$ counters. Backgrounds are measured with the detector sample removed.

With this neutron counter two types of transmission measurements are possible: (1) flat detection done with a detector sample B of a material (usually graphite) whose neutron scattering cross section is constant within the energy resolution of the incident neutron beam, and

*Work performed under the auspices of the U. S. Atomic Energy Commission.

(2) self-detection, performed with a detector sample of the same composition as the transmission sample A. The self-detection technique is used primarily to study narrow scattering resonances since it increases the sensitivity of the neutron counter for resonant neutrons.

The samples were lithium metal, either natural or enriched to 99.3% in ^{6}Li. The sample containers had 1-mil stainless steel end windows and the walls were nickel for the ^{6}Li samples and aluminum for the natural ones. Similar empty containers were used to correct for the effect of the thin steel windows. The thicknesses of the transmission sample were chosen to yield measured transmissions in the range 45—60% at each energy, and all measurements at any one energy were finished before changing to the next energy. A fresh lithium target for the neutron source was evaporated daily. An ASI-2100 digital computer was used to process the data as they were accumulated.

2. RESULTS

2.1 Cross Section Below 190 keV

Values for the cross sections from 10 keV to 176 keV are shown in Fig. 2. For these results the neutron counter was placed at an angle of 120° with respect to the direction of the incident proton beam. Values for the cross sections from 130 keV to 190 keV are shown in Fig. 3. For these results and for those obtained at higher neutron energies, the neutron counter was placed at 0° as shown in Fig. 1. For the energy range below 190 keV data were taken at 2-keV intervals, but the points shown in Fig. 2 above 45 keV represent cross sections obtained by averaging the measured results over 6-keV intervals. The statistical uncertainties (standard deviation) are about the size of the experimental points.

In the region of overlap of Figs. 2 and 3 the measured cross sections agree within statistical uncertainties. However, in the region from 10 keV to about 150 keV the values for the cross section of ^{6}Li shown in Fig. 2 fall from 0.1 to 0.3 barns below those shown in BNL-325 [1], while the values for natural lithium differ from those in BNL-325 by less than 0.1 barns. The present values for ^{7}Li below 150 keV agree within uncertainties with the values shown in BNL-325.

2.2 Cross Sections from 190 to 350 keV

Because a strong resonance occurs in the total cross section of both ^{6}Li and ^{7}Li near 250 keV, this energy region was investigated with better resolution (~1.3 keV). In addition, both flat- and self-detection techniques were employed near the peaks of the resonances. Each self-detection sample was 1.25 in. thick. The resonances in both isotopes was also investigated with poor resolution (~8.5 keV).

The results of the good-resolution studies are shown in Fig. 4. The values of the total cross section obtained by self-detection are shown in the inset. Because of possible energy shifts from day to day, each day's run overlapped the previous day's run sufficiently to determine that indeed no appreciable shift did occur. On the average, the cross section values obtained by self-detection are significantly higher than those obtained by flat detection.

Figure 5 shows the values of the total cross section of ^{6}Li obtained with poor resolution (~8.5 keV). Here open circles are the results obtained with flat detection and closed circles are those obtained with self detection. Again, especially near the peak of the resonance, the self-detection results are significantly larger than the flat-detection results. This can happen only if there is a significant variation of the cross section within the energy spread of the incident neutron beam.

The resolution used to obtain the results in Fig. 4 was sufficiently good that the peak height observed should be the true peak height in the cross section and hence could be used to determine the spin J of the excited state in the compound nucleus responsible for the resonance. However there is some ambiguity about the expected peak height because ^{6}Li shows a maximum in the capture cross section at this energy as well as in the total cross section. Thus the theoretical peak height includes the factor Γ_n/Γ, the ratio of the neutron width to the total width. Table I shows values for this ratio obtained from the results of several experimental groups. Using an average value $\Gamma_n/\Gamma = 0.67$, one then calculates expected peak heights (as described by Hibdon [2]) for various assumed values of J. These are shown in Table II. None of them agree with the

TABLE I. Values of Γ_n, Γ_a, and Γ used by different experimenters in fitting the large resonance in ^{6}Li.

Γ_n (keV)	Γ_a (keV)	Γ (keV)	Γ_n/Γ
114.0[a]	60.0	174.0	0.66
95.8[b]	50.3	146.1	0.66
114.0[c]	64.0	178.0	0.64
133.0[d]	55.0	188.0	0.71

TABLE II. Possible peak heights of the large resonance in ^{6}Li for various values of the spin J.

J		$\frac{5}{2}$	$-\frac{7}{2}$	$\frac{9}{2}$
σ_0	(b)	14.3	18.7	23.2
$\Gamma_n\sigma_0/\Gamma$	(b)	9.7	12.8	15.8

[a] C. H. Johnson, H. B. Willard, and J. K. Bair, Phys. Rev. 96, 985 (1954).

[b] H. B. Willard, J. K. Bair, J. D. Kington, and H. D. Cohn, Phys. Rev. 101, 765 (1956).

[c] J. B. Marion, G. Weber, and F. S. Mozer, Phys. Rev. 104, 1402 (1956).

[d] F. Gabbard, R. H. Davis, and T. W. Bonner, Phys. Rev. 114, 201 (1959).

results of the present measurements. In fact, agreement is impossible throughout the entire range of values for Γ_n/Γ shown in Table I.

Furthermore, the measured values near the maximum in the cross section seem to fluctuate systematically as the neutron energy is increased and are outside of statistical uncertainty. This fact together with the facts that the self-detection results give higher values for the cross section than do the flat-detection results and that the peak value of the cross section does not agree with any expected value suggests that this resonance may be complex and may possibly contain fine structure.

Figure 6 shows the results for natural lithium, measured with good resolution. The self-detection results are shown in the inset. Values for the total cross section of ^{7}Li were extracted from the data for natural lithium and ^{6}Li. These are shown in Fig. 7. The values determined from the self-detection technique are shown in the insert.

In other measurements of the cross section of natural lithium, the neutron source was a 9-keV-thick lithium target. These results are shown in Fig. 8, where open circles represent values obtained by flat detection and closed circles are values obtained by self detection. The solid and dotted lines in the figure represent theoretical peak heights for this maximum in the cross section for several values of J. Certainly the resolution used to obtain the results shown in Fig. 6 was adequate to completely resolve the resonance, but the measured height of the peak in the cross section does not agree with any of the possible values. The present results are in good agreement with earlier results [3].

In Figs. 6—8 the measured values for the cross section near the peak of the large resonance obtained by self-detection are higher than those obtained by flat detection. This fact, together with the lack of agreement between the measured peak height and possible values, suggests that this peak may possibly contain fine structure.

It should be noted that if the incident neutron beam contains a small fraction of neutrons whose energy is off resonance, an anomalously high self-detection cross section would be measured. For instance, for ^{6}Li the measured self-detection cross section could be explained if 5%—7% of the incident neutrons have energies for which the total cross section is 1.5 barns. From earlier studies [4] it is hard to see how such a large contaminant in the energy spectrum could be present, but the authors will further explore this possibility in the immediate future. However, the failure of the measured peak cross sections to agree with expected values cannot be explained in this manner.

2.3 The Cross Sections from 350 keV to 1236 keV

The cross sections of natural lithium, ^{6}Li, and ^{7}Li are shown in Fig. 9. Only flat-detection measurements were made in this energy region. Throughout the entire region the cross sections were determined at 2-keV intervals with an energy spread of ~2 keV. The values shown in Fig. 9 are the measured values averaged over 14-keV intervals. The statistical accuracy of the results shown in Fig. 7 is about ~0.4 times the diameter of the individual points.

Above 650 keV the neutron beam contains a second group of low-energy neutrons that arises from the formation of ^{7}Be in the 430-keV excited state. When the main group of neutrons has an energy near 800 keV, the low-energy component has an energy near 250 keV. Thus the strong resonances near 250 keV in both ^{6}Li and ^{7}Li reappear near 800 keV as spurious peaks in the total cross section.

3. REFERENCES

1. Neutron Cross Sections, compiled by D.J. Hughes, B.A. Magurno, and M.K. Brussel, Brookhaven National Laboratory Report BNL-325, 2nd ed. and Suppl. No. 2 compiled by J.R. Stehn, M.D. Goldberg, B.A. Magurno, and R. Weiner-Chasman 1964 (U.S. Government Printing Office, Washington, D. C.).
2. C. T. Hibdon, Phys. Rev. 114, 179 (1959).
3. C. T. Hibdon, Phys. Rev. 133, B353 (1964), Fig. 2.
4. C. T. Hibdon, Nucl. Instr. and Methods 17, 177 (1962).

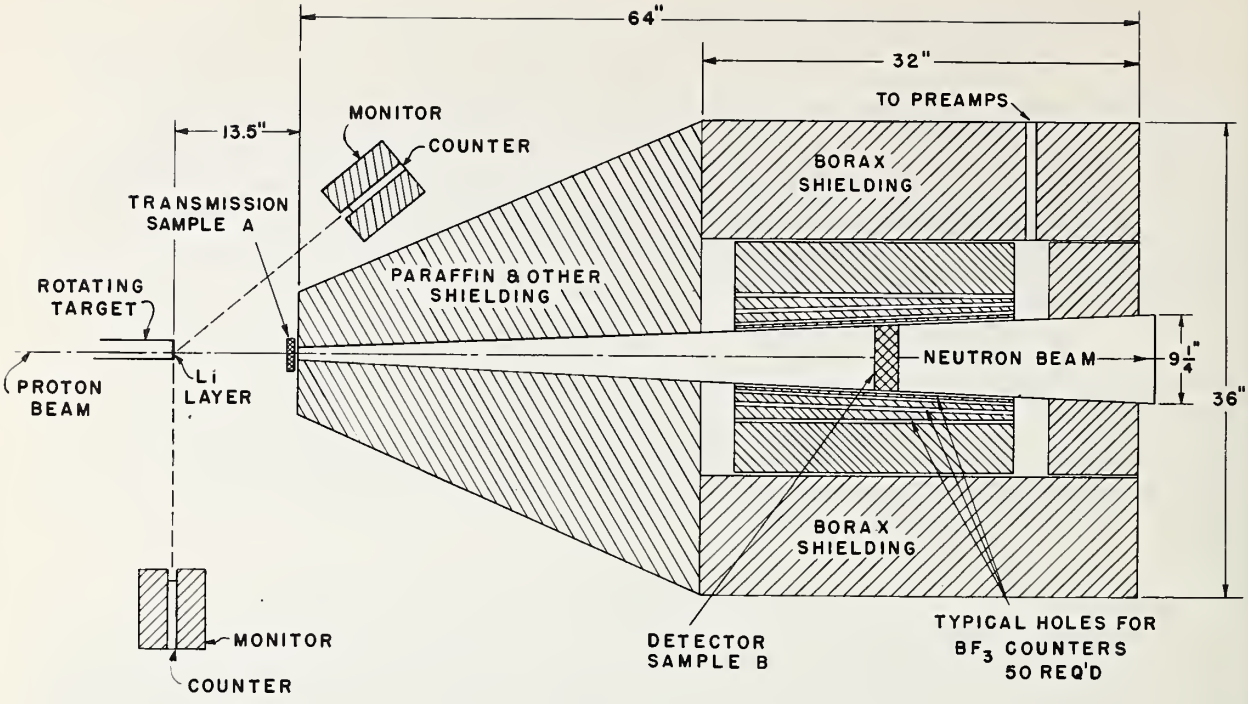

Fig. 1. Schematic arrangement of the lithium target, monitors, and neutron counter.

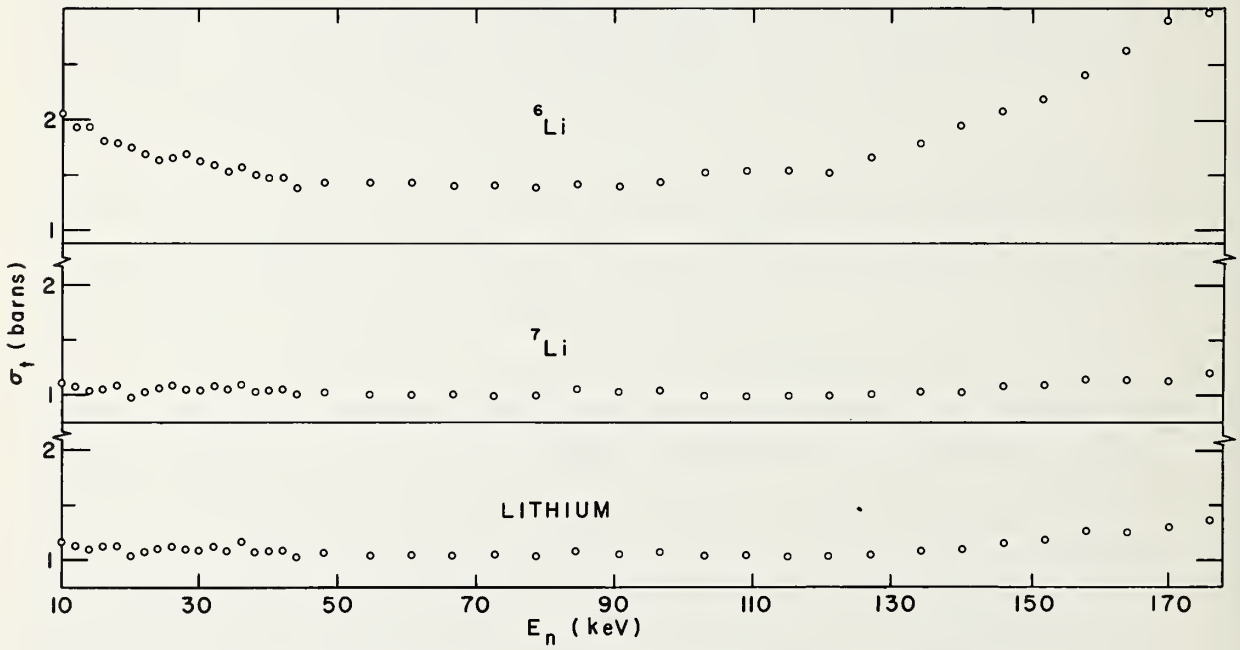

Fig. 2. Total neutron cross section of ^{6}Li, ^{7}Li, and natural lithium from 10 to 176 keV, measured at 120° with respect to the proton beam.

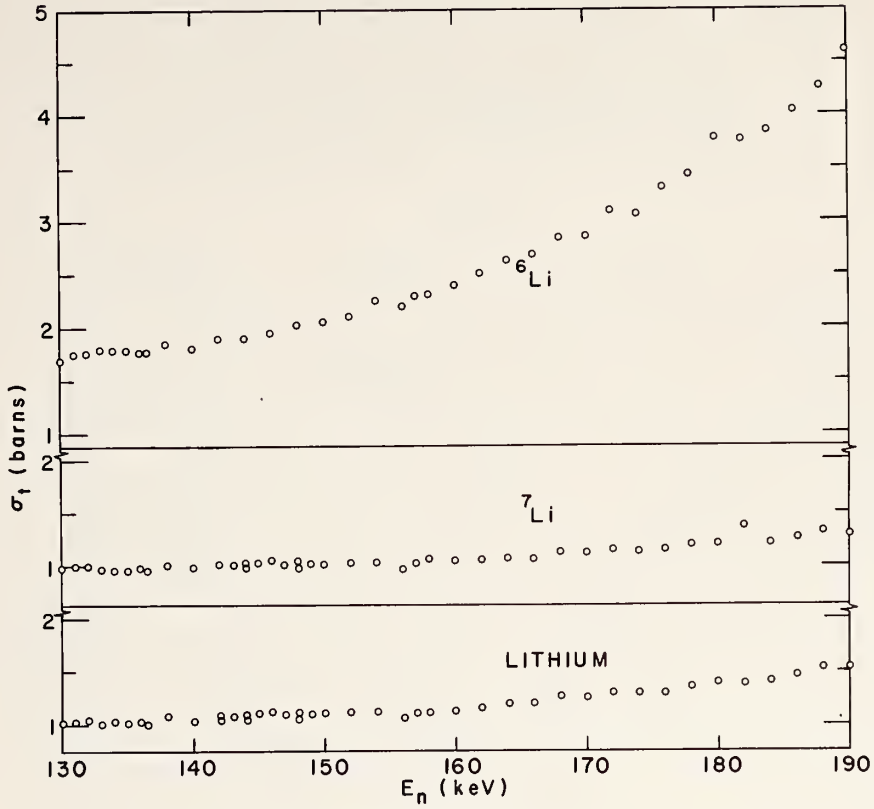

Fig. 3. Total neutron cross sections of ^{6}Li, ^{7}Li, and natural lithium from 130 to 190 keV, measured at 0° with respect to the proton beam.

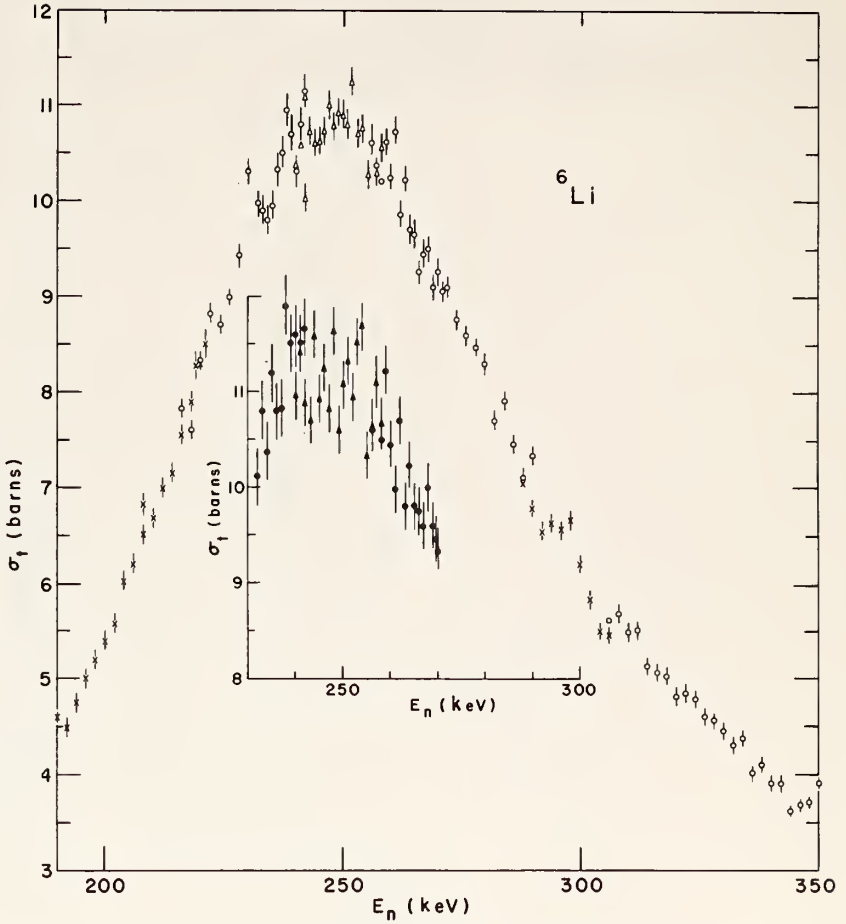

Fig. 4. Total neutron cross section of ^{6}Li from 190 to 350 keV. The inset shows the cross section obtained by self-detection.

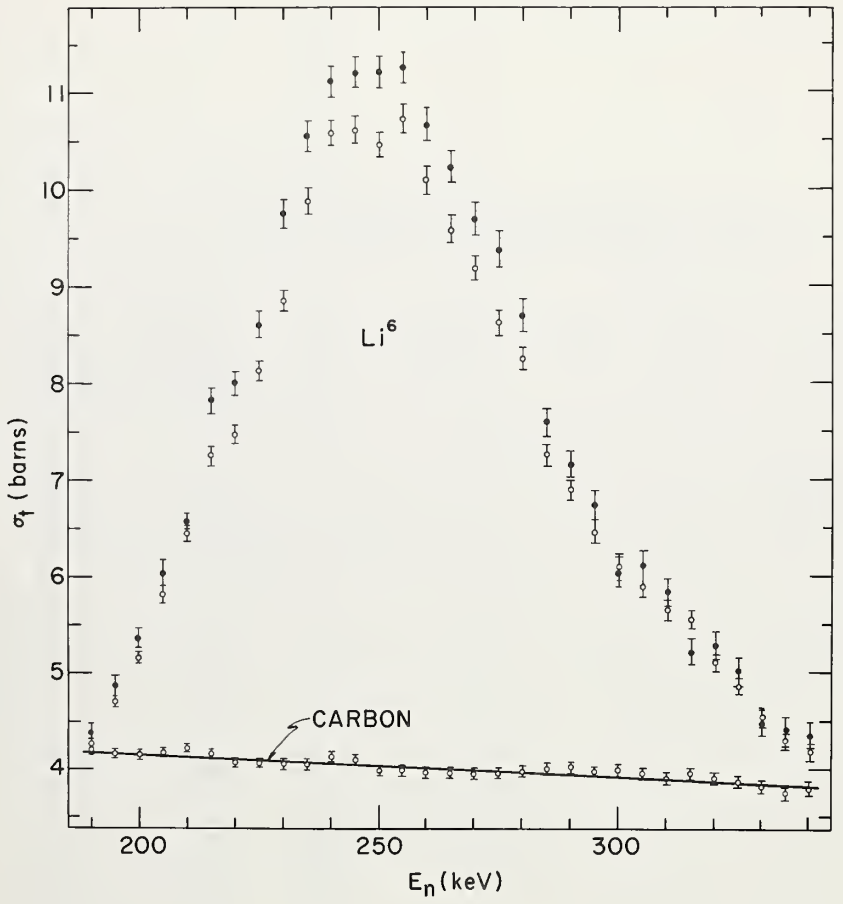

Fig. 5. Total neutron cross section of ^{6}Li from 190 to 340 keV with large neutron energy spread. Open circles show data obtained by flat detection, solid circles data by self-detection.

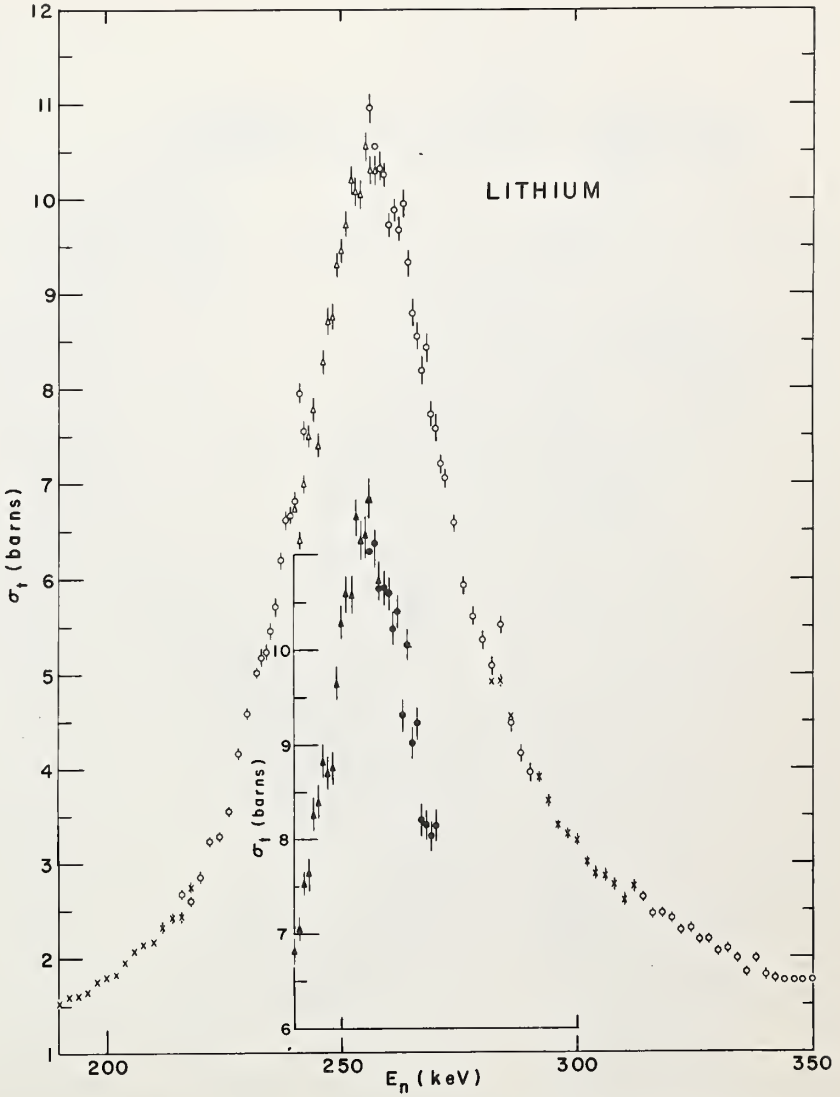

Fig. 6. Total neutron cross section of natural lithium from 190 to 350 keV. The inset shows data obtained by self-detection.

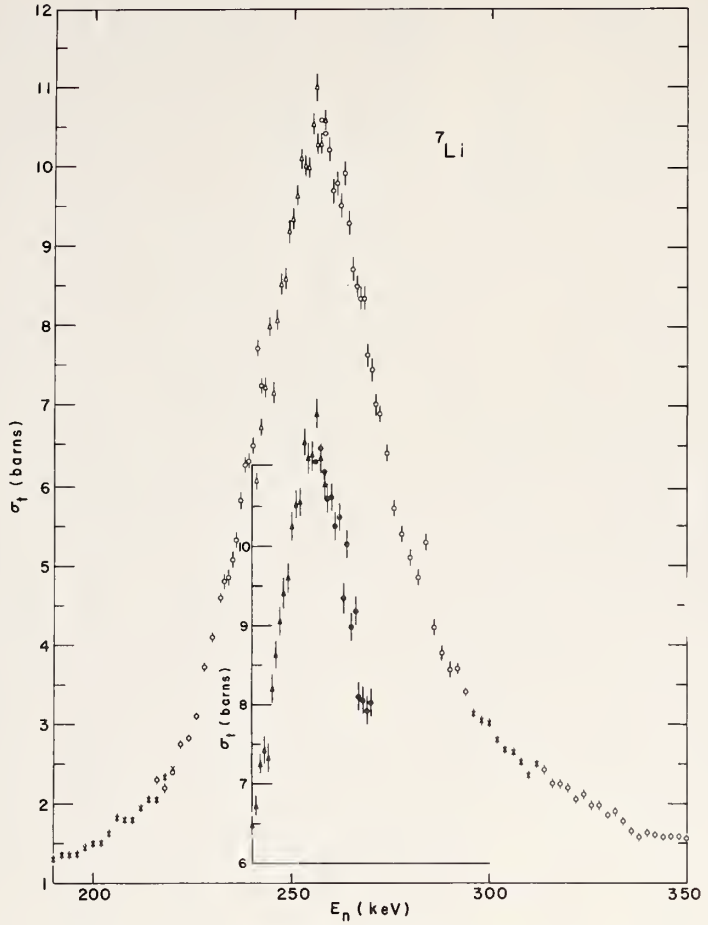

Fig. 7. Total neutron cross section of ^{7}Li from 190 to 350 keV. The inset shows data obtained by self-detection.

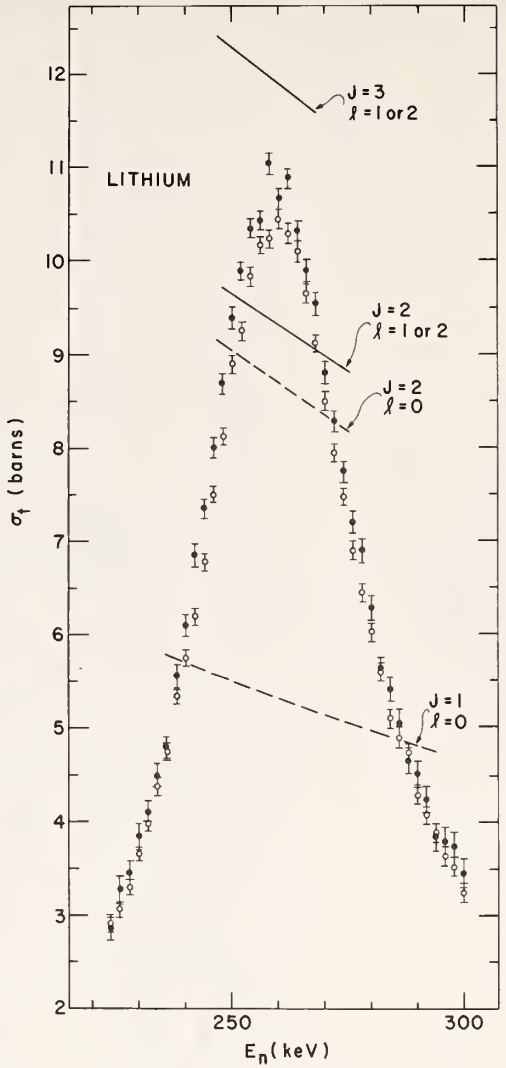

Fig. 8. Total neutron cross section of lithium from 224 to 300 keV, measured with a large neutron energy spread. Open circles show data obtained by flat detection, solid circles data by self-detection.

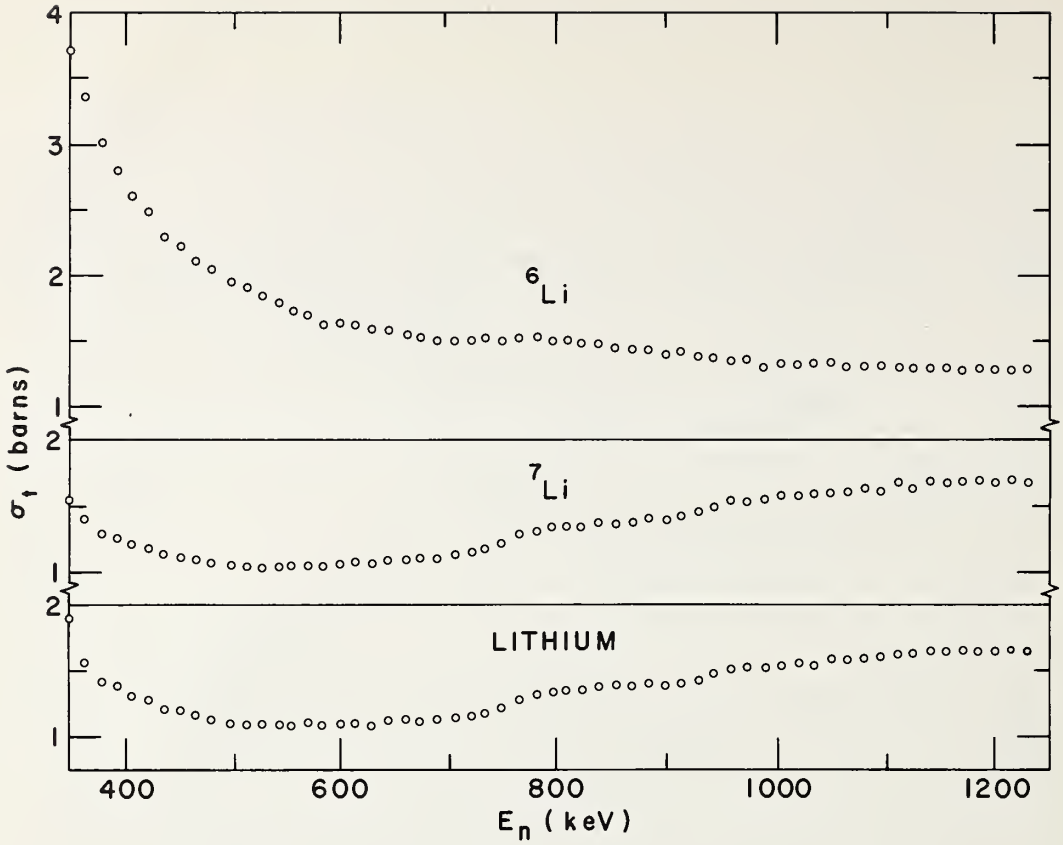

Fig. 9. Total neutron cross sections of ^{6}Li, ^{7}Li, and natural lithium from 350 to 1236 keV, measured by flat detection.

The non-elastic cross-section of beryllium for neutrons from 2.3 to 5.2 MeV

J.R.P. Eaton* and J. Walker
Physics Department
University of Birmingham
Birmingham 15
England

Abstract

The non-elastic cross-section of beryllium for neutrons has been measured with the sphere technique at seven energies between 2.3 and 5.2 MeV; neutrons were obtained from the T(pn) and D(dn) reactions with the 5 MeV electrostatic accelerator at A.E.R.E. Harwell. A ^{238}U fission chamber was used as a threshold detector and measurements were made with and without beryllium shells of different thicknesses around it. A Monte-Carlo calculation of the spectrum of neutrons elastically scattered in the beryllium enables a correction to be made for those neutrons taken below the detector threshold by elastic, rather than non-elastic, scattering. The comparison between the Monte-Carlo results and those given by using the analytical methods of Bethe, Beyster and Carter shows that a multi-group analysis is necessary. The measured cross-sections, corrected for the finite sizes of the detector and the source, are higher near threshold than earlier values.

1. Introduction

The neutron moderation and multiplication properties of beryllium have made it an interesting material in neutron technology. Multiplication ('fast effect'), which arises from the (n, 2n) reaction with fast neutrons, can produce an important (about 10%) contribution to the neutron multiplication of beryllium-moderated reactors and it has also been considered as a possible way of increasing the fluxes from neutron sources based on accelerators. The most recent published work on the fast effect in beryllium and beryllium oxide is by Amster and Perkins (1) and as they have given a fairly complete list of earlier work only limited reference will be made here; the report by Doherty (2) gives a set of preferred cross-sections for beryllium. The present work was started because the uncertainties in cross-sections, particularly for an energy range of about 3 MeV above threshold, caused variations in the calculated values of the fast effect from 1.03 to 1.19 (see, for example, Aline, Novak and Wolfe (3)) and because attempts to extract just the fast effect

---

*Now at Nuclear Design and Construction Ltd., Whetstone, Leics., England.

from measurements on multiplying assemblies were clearly made uncertain by the assumptions involved in the analysis. The approach used was to measure the non-elastic cross-section over the energy range 2.3 to 5.2 MeV by the sphere transmission technique (4) and then to obtain the (n, 2n) cross-section by subtraction of the known (n, α) one. This assumes that the (n, γ) and (n, n') reactions have negligible cross-sections and in this connection it is worth noting that measurements over part of the energy range by Day (5) Grace et al (6) and Scherrer et al (7) have failed to show gamma emission.

2. Measurements

The neutrons were produced from the D(d, n) and T(p, n) reactions by the 5 MV electrostatic accelerator at A.E.R.E. Harwell. Targets were 0.005 in. thick, 1 in. diameter gold foils with the deuterium or tritium in a 6.5 mg titanium layer. Seven neutron energies were used and are given in Table 1 together with the estimated uncertainty caused by energy loss of the bombarding particle in the target and uncertainty in the accelerating potential.

Table 1. Neutron Sources.

Neutron Energy MeV	Neutron reaction	Energy Spread MeV
2.3	T(p, n) He^3	0.050
2.7	"	0.050
3.2	"	0.045
3.7	"	0.045
4.2	D(d, n) He^3	0.085
4.7	"	0.075
5.2	"	0.065

Neutron counting rates in the threshold detector, a U-238 fission counter, were taken with and without a spherical beryllium shell around the counter to give the transmission ratio; in all cases the detector was at 0° to the bombarding beam. Table 2 gives the radii of shells and the distances from target to shell used at each neutron energy; the shells were formed from a nesting set of hemispheres. A general view of the experimental arrangement is shown in slide 1*. Here the target is at its minimum distance, 30 cm., from the shell. Also apparent is the long counter, placed about 5 m. from the source at 90° to the accelerated beam and used as a monitor; it had a common H.T. supply with the fission counter. A closer view of the fission counter in a pair of shells is shown in slide 2; the three small holes in the shells

*The photographs forming slides 1 and 2 are not included in the printed paper.

remained from earlier experiments and one was used for the detector stem in this case. The surface area of all the holes was always less than 1% of the total surface area of the sphere and no correction was made for them in the analysis. The density of the shells was assumed to be uniform and was obtained from the measured weights, accurate to 0.1%, and the radii.

The fission counter, manufactured by 20th Century Electronics Ltd, had the multi-electrode form of their type FC165 but the standard design was modified slightly to make the sensitive volume as near to the end as possible. Depleted uranium, with a 235:238 ratio of $(2.3 \pm 0.1) \times 10^{-4}$, was used in the 1 mg/cm^2 coating to minimise the response to low-energy neutrons and a cadmium sheath, 0.04 in. thick, was used as a thermal neutron shield. A comparison of counting rates in the fission chamber and the long counter gave the energy response of the fission chamber shown in Fig. 1 (slide 3) on the assumption of constant response for the long counter. This assumption should certainly be sound to high accuracy over the energy range 1 to 2 MeV, where the efficiency of the fission counter is rising from its threshold; for 2 to 6 MeV the U-238 fission cross-section is known to be constant (8).

For all transmissions, repeated measurements were made with the shells successively on and off. The counting rate from background neutrons (no neutron source) was always less than 0.01% of the rate during a run and scattering from the laboratory floor during a run was low because of the beam height of 9 ft. This and other sources of scattering were indeed found to be negligible by using a shadow shield of paraffin and cadmium for the direct radiation; an additional check on the negligible contribution from the shell support itself was obtained from runs with and without it beneath the fission chamber.

3. Analysis

Bethe, Beyster and Carter (4) have shown that it is convenient to calculate sphere transmission for the source, rather than the detector, at the centre and then to use the reciprocity theorem for the actual situation. They have given procedures based on different degrees of approximation such as the 'P' approximation which treats scattering as isotropic when linked with a transport cross-section, and the 'π' approximation which assumes this for all scatterings except the first where the actual scattering behaviour is used. In specific cases they also used Monte-Carlo calculations and in the present work the different methods have been compared for the ideal case of a central point source in a beryllium shell. Table 3 shows results for four shell thicknesses and an initial neutron energy of 3.25 MeV; the transmission gives the fraction of neutrons which have not suffered non-elastic collisions.

313-475 O 68—13

The π-analysis used is a little different from the Bethe, Beyster, Carter one in that elastic-scattering cross sections are used in place of elastic transport ones, and total cross-sections in place of transport ones. The one-group analysis assumes the same cross-sections for all collisions whereas the multi-group one uses four different sets for the initial neutrons and for those that have suffered one, two or more than two collisions. The group-average cross-sections were obtained by weighting the actual cross-sections with the energy spectrum after the appropriate number of collisions (9).

In the analysis of the experimental data, the spectrum of transmitted neutrons was computed by the Monte Carlo programme and, together with the response of the fission counter, allowed a correction to be made for neutrons scattered elastically, rather than inelastically, below the counter threshold. Corrections were also made for (a) finite size of the detector (correction about 0.1%), (b) finite distance from source to detector and (c) non-isotropic emission from source. Corrections (b) and (c) are partially compensating and give a net correction of about 1% at 30 cm separation and 0.1% at 100 cm separation. The response of the detector was checked to be almost independent of the direction of approach of the neutrons.

It was assumed that counts due to (n, 2n) secondary neutrons could be neglected; the justification depends on the nature of the (n, 2n) reaction at the energies involved and requires further investigation. A direct interaction model, for example, involving a virtual neutron outside Be^8 in its ground state (10) could contribute a small number of neutrons above the counter threshold. Measurements with a different threshold detector would clarify the point as would neutron spectrum measurements which have been made at an incident energy of 14 MeV (11) but not in any detail at lower energies.

4. Results on cross-sections and fast effect

The results from a multi-group π-analysis are shown in Table 4, column 2. Cross-sections for $Be^9(n, \alpha)$, taken or interpolated from Doherty's report (2), are in column 3 and the differences, giving cross-sections for the (n, 2n) reaction, are in column 4 where the estimated experimental errors have been increased by 10 mb. to allow for uncertainties in the (n, α) cross-section.

The fast effect can be calculated from

$$\int_0^\infty S(E) \left\{ \frac{\sigma_{ne}}{\sigma_t} - 2 \frac{\sigma_{n,\alpha}}{\sigma_t} \right\} dE$$

where σ_{ne} and σ_t are the energy-dependent non-elastic and total cross-sections respectively. S(E) is the slowing down spectrum and has been

computed for a fission source in a beryllium moderator by Hafele (12). This information together with the present results for δ_{ne} and Doherty's values for δ_t and $\delta_{n\alpha}$ gives 10 ± 1.5% for the fast effect.

We are grateful to the Science Research Council, London for financial support for apparatus and for a research studentship for one of us (J.R.P.E.), to A.W.R.E., Aldermaston for the loan of the beryllium and to A.E.R.E.. Harwell for the use of the electrostatic accelerator.

5. References

(1) H. Amster and S.T. Perkins, 1967, J. Nucl. Eng. 21, 263-270.

(2) G. Doherty, 1965, Atomic Energy Establishment, Winfrith report AEEW - M.513.

(3) P.G. Aline, P.E. Novak and B. Wolfe, 1960, Nucl. Sci. Eng. 7, 392-4.

(4) H.A. Bethe, J.R. Beyster and R.E. Carter, 1956, J. Nucl. Eng. 3, 207-223, 273-300; 1957, J. Nucl. Eng. 4, 3-25, 147-163.

(5) R.B. Day, 1956, Phys. Rev. 102, 767-787.

(6) M.A. Grace et al, 1951, Phys. Rev. 82, 969.

(7) V.E. Scherrer et al, 1954, Phys. Rev. 96, 386-388.

(8) Neutron cross-sections. Brookhaven National Laboratory report, B.N.L. 325.

(9) J.R.P. Eaton, Ph.D. thesis, University of Birmingham.

(10) T.H. Axford, K.C. Hines and J.P. Pollard, 1964, J. Nucl. Eng. 18, 131-139.

(11) Nuclear structure study with neutrons: Eds. Nève de Mévergnies et al, North Holland - Amsterdam 1966; R. Bouchez, p. 566, A.T.G. Ferguson, pp. 83-86.

(12) W. Hafele, 1959, Oak Ridge National Laboratory report ORNL 2779.

Table 2. Radii of shells and distances from source to detector.

E_n MeV	Inner radius cm	Outer radius cm	Distance from source to detector cm
2.3	13.46	14.99	113.5
2.7	"	"	"
3.2	13.46 11.94	" "	103.5) number to) of values 30.0)
3.7	as for 3.2 MeV	"	as for 3.2 MeV
4.2	"	"	"
4.7	13.46	"	113.5
5.2	13.46 11.94	" "	30 "

Table 3. Shell transmissions from different analyses.

Outer radius cm	One-group analysis			Multi-group analysis	
	P-analysis	π-analysis	Monte-Carlo	π-analysis	Monte-Carlo
12.69	0.938	0.940	0.943 ± .006	0.944	0.949 ± .006
13.46	0.865	0.869	0.878 ± .010	0.886	0.898 ± .010
14.99	0.721	0.725	0.741 ± .015	0.783	0.800 ± .015
16.51	0.588	0.591	0.614 ± .015	-	0.715 ± .015

Inner radius 11.94 cm. Density 1.814 gm/cc.
Initial neutron energy 3.25 MeV.

One standard deviation is quoted for the Monte-Carlo result.

Table 4. Cross-sections of beryllium at different neutron energies.

Neutron energy MeV	Non-elastic barns	(n, α) barns	(n, 2n) barns
2.3	0.09 $\pm$ .07	0.065	0.025 $\pm$ .08
2.7	0.59 $\pm$ .1	0.098	0.49 $\pm$ .11
3.2	0.64 $\pm$ .06	0.103	0.54 $\pm$ .07
3.7	0.64 $\pm$ .05	0.095	0.54 $\pm$ .06
4.2	0.72 $\pm$ .06	0.082	0.64 $\pm$ .07
4.7	0.72 $\pm$ .07	0.070	0.65 $\pm$ .08
5.2	0.73 $\pm$ .10	0.060	0.67 $\pm$ .11

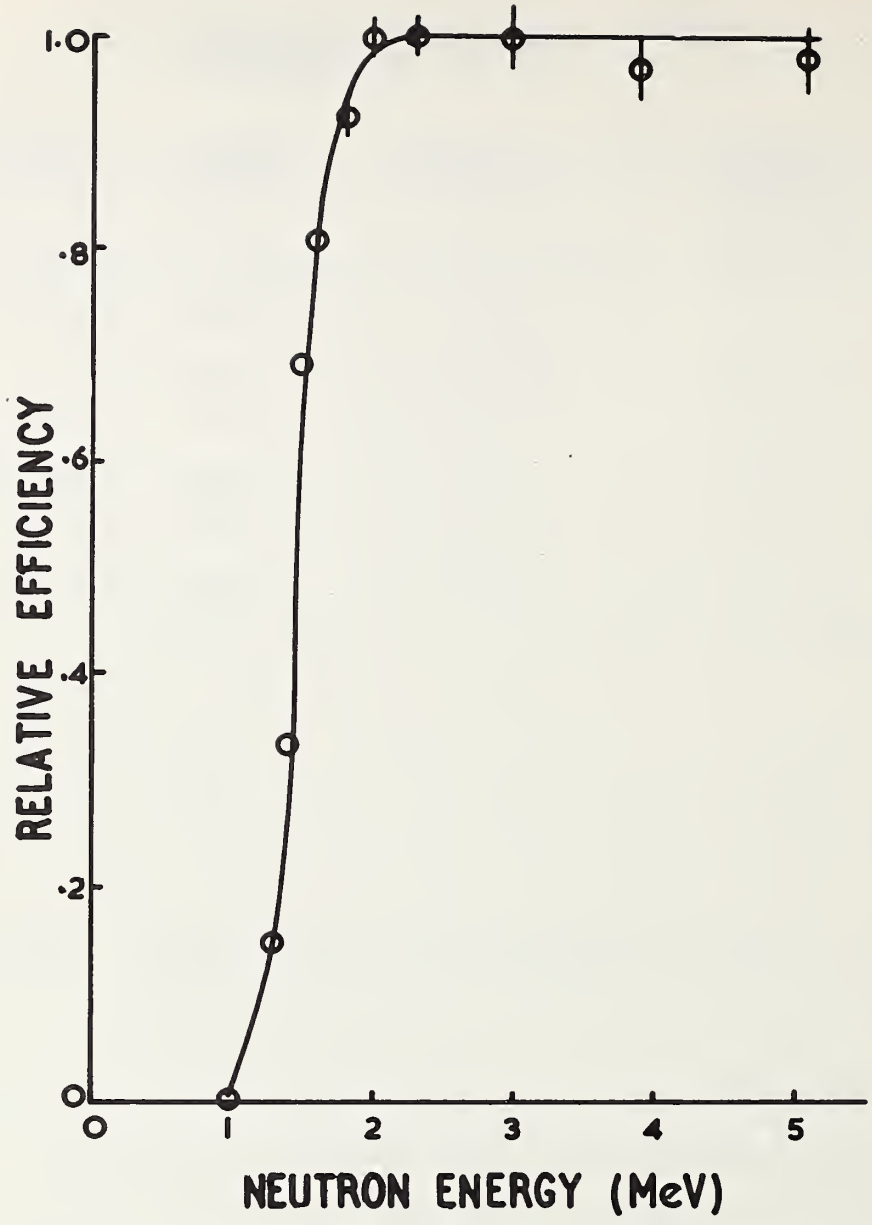

FIG.1. EFFICIENCY OF FISSION COUNTER AS A FUNCTION OF NEUTRON ENERGY

Fast Neutron Energy Measurements*

J. C. Davis and F. T. Noda

University of Wisconsin, Madison, Wisconsin 53706

Abstract: Neutron energies at which sharp resonances have been reported vary by as much as 200 keV for neutron energies around 7 MeV according to measurements at different laboratories. To investigate these differences the analyzing magnet of the Wisconsin Tandem Accelerator was recalibrated with an accuracy better than 0.1%. Energy loss and straggling were studied for Ni foils used as entrance windows for gas targets. The energies of some of the sharp structure in neutron total cross sections reported previously[1, 2] were measured with ^{7}Li(p, n) T(p, n), and D(d, n) neutrons. Neutron energies reported in ref. [1] should be increased from 1 keV at 3.4 MeV to 22 keV at 7 MeV and from 10 keV just above 7 MeV to 83 keV at 16 MeV. Energies reported in ref. [2] should be increased from 6 keV at 4.5 MeV to 15 keV at 6 MeV and from 24 keV just above 6 MeV to 88 keV at 14 MeV. Neutron energies are determined to about 0.1%.

An example of differences in neutron energies at which sharp structure in total cross sections is reported by various authors[1, 3, 4] is shown in fig. 1. Three recent measurements of the total cross section of C are plotted. The positions of the sharp structure differ by as much as 200 keV. The difference between energy scales in refs. [1] and [3] is particularly surprising, since D(d, n) neutrons were used in both experiments. Recent measurements of total cross sections of heavier elements carried out at our laboratory [2] with good resolution showed a systematic energy shift of the structure of the order of 20 keV between 6 MeV neutrons from the T(p, n) and D(d, n) reactions. The present work was undertaken with the aim of establishing a more accurate neutron energy scale in the MeV region.

As a first step the analyzing magnet which determines the energy of the charged particles used in neutron producing reactions was recalibrated. The calibration points were the thresholds of the (p, n)

---

* Work supported in part by the U.S. Atomic Energy Commission.

reactions on ^{7}Li, ^{9}Be, ^{13}C, ^{19}F, and ^{27}Al and those of the $D(^{16}O, n)$ reaction for charge states +3, +4, and +5. The value for the ^{9}Be threshold was taken from Bonner[5], values for the other thresholds were taken from Marion's review article[6]. Both object and image slits of the analyzer were set to 0.6 mm openings to limit the energy spread to 0.1% FWHM. Figure 2 shows the calibration constant of the magnet for different proton energies. The solid curve represents a least squares fit to the calibration points and is believed to have an accuracy of 0.07%. In earlier work at this laboratory the energy independent calibration constant shown by the dashed line had been used.

Secondly, the energy losses in the thin Ni foils which had been used as entrance windows on gas targets were determined by observing the sharp rise in the yield of the $^{7}Li(p, n)$ reaction with and without foils in the proton beam. From the shift in the threshold and in the peak of the rise curve both the most probable energy loss and the energy straggling in the foil may be obtained. The energy losses were found to be 10% to 20% larger than corresponds to the thickness quoted by the manufacturer. The energy straggling varied by ±25% from foil to foil indicating that some of the foils were not uniform in thickness.

The combination of recalibration of the magnet and measurement of energy loss in the foils reduces the difference between the energy scales for T(p, n) and D(d, n) neutrons noted by Carlson to below 10 keV, which is within the uncertainty of the energy measurement.

To establish a better neutron energy scale, the energies of narrow resonances in the C and O total cross sections were determined with neutrons from the $^{7}Li(p, n)$, T(p, n), and D(d, n) reactions. The neutron energy spread is <10 keV for $^{7}Li(p, n)$ neutrons, about 20 keV for neutrons from T(p, n), and about 25 keV for D(d, n) neutrons. The uncertainty in the neutron energies is about 0.1%. Typical transmissions as a function of neutron energy for a resonance in C and a resonance in O are shown in fig. 3; two different source reactions are used for each measurement. Table 1 shows measurements of the energies of four peaks in the C total cross section and four peaks in the O total cross section. The present measurements using different source reactions are compared with the earlier measurements at this laboratory, the latter both as originally quoted and corrected for the new energy calibration of the magnet. There appears to be a small difference between T(p, n) and D(d, n) neutrons of the order of the 0.1% uncertainty of the present measurements.

Table 1. Positions of peaks in MeV

Element	Neutron Source Reaction			Ref. [1] shifted	Ref. [1] original
	^{7}Li(p, n)	T(p, n)	D(d, n)		
C	4.935	4.937		4.94	4.93
	5.369	5.372		5.37	5.36
	6.295	6.293		6.29	6.27
		7.754	7.764	7.75	7.73
O		5.914		5.91	5.90
		6.394	6.398	6.41	6.39
		6.801	6.811	6.81	6.79
		7.196	7.204	7.19	7.18

Figure 4 shows a new measurement of the C total cross section between 7 and 8 MeV. The new data are compared to those shown in fig. 1, with the data of ref. [1] shifted by 15 keV to take into account the new magnet calibration. Although an effort was made to determine the neutron energies accurately, the cross sections were not measured with high precision. The agreement between the present energy determinations and the earlier measurements at this laboratory is satisfactory, but there remains a disagreement with results obtained elsewhere.

Work is in progress to determine neutron energy reference points at higher energies.

References

[1] D. B. Fossan, R. L. Walter, W. E. Wilson, and H. H. Barschall, Phys. Rev. 123, 209 (1961).

[2] A. D. Carlson and H. H. Barschall, Phys. Rev. 158, 1167 (1967).

[3] F. Manero, B. H. Armitage, J. M. Freeman, and J. H. Montague, Nuclear Phys. 59, 583 (1964).

[4] D. W. Glasgow and D. G. Foster, Jr., Bull. Am. Phys. Soc. 8, 321 (1963).

[5] T. W. Bonner, Nuclear Spectroscopy A (Academic Press, N. Y., 1960) p. 477.

[6] J. B. Marion, Revs. Mod. Phys. 38, 660 (1966).

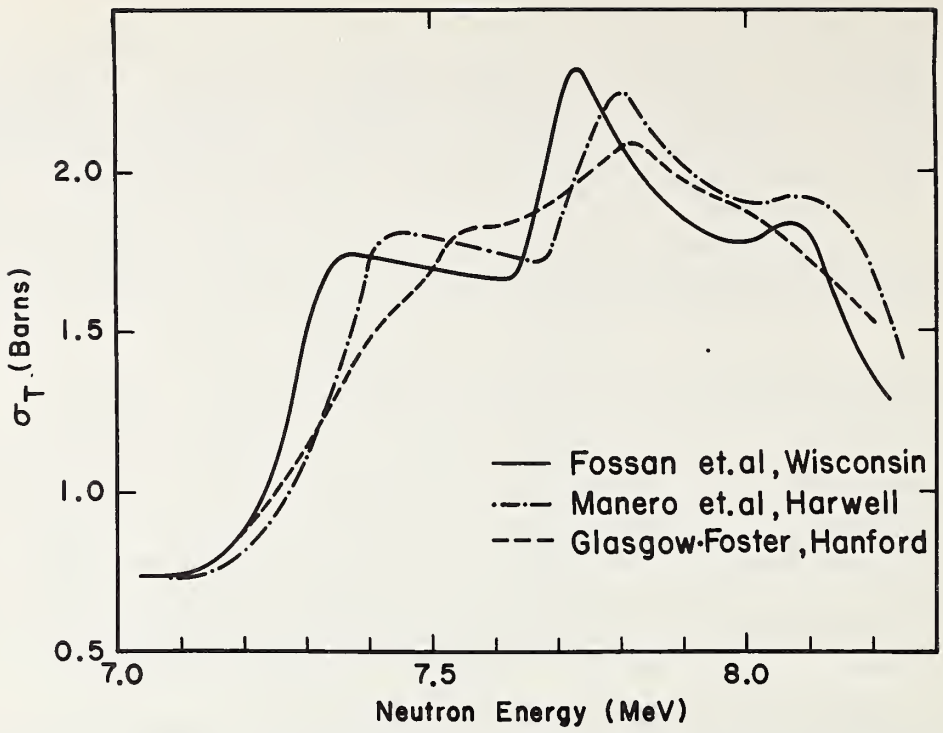

Total Cross Section of C

Figure 1

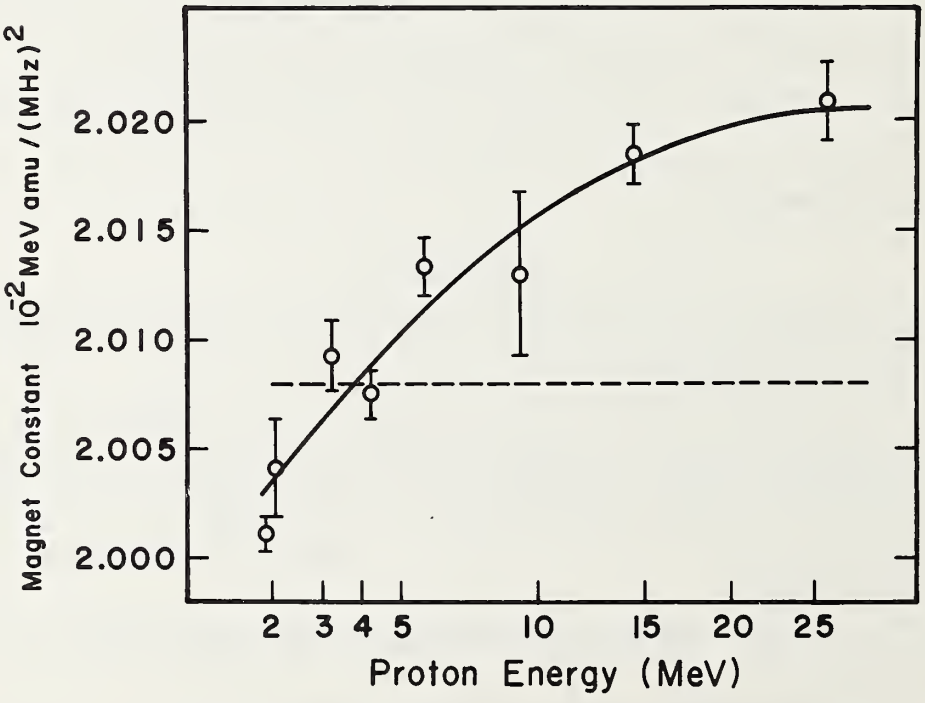

Analyzing Magnet Calibration Curve

Figure 2

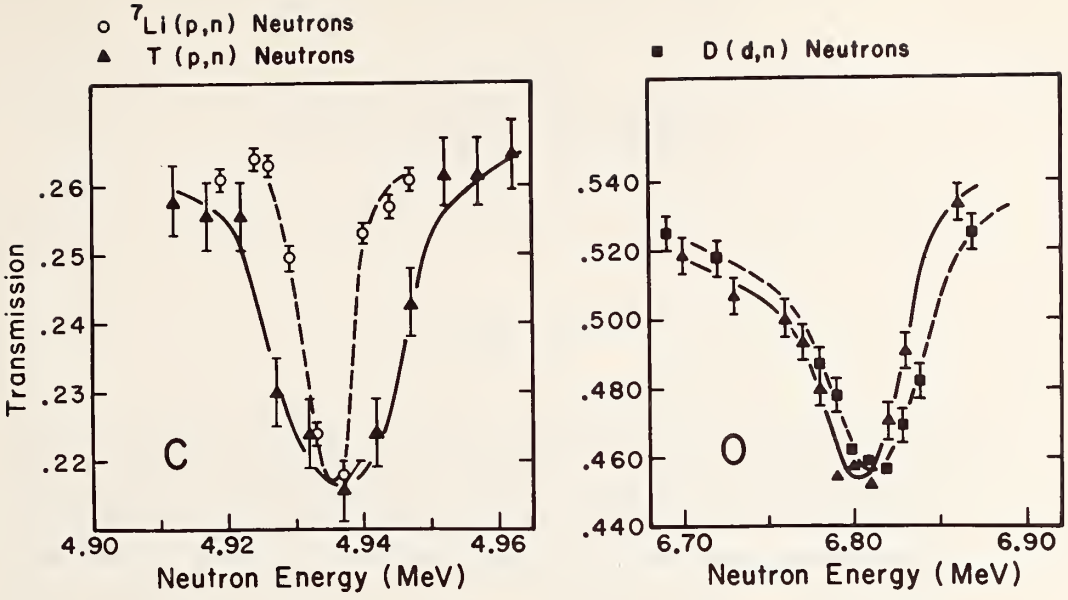

Transmission Measurements

Figure 3

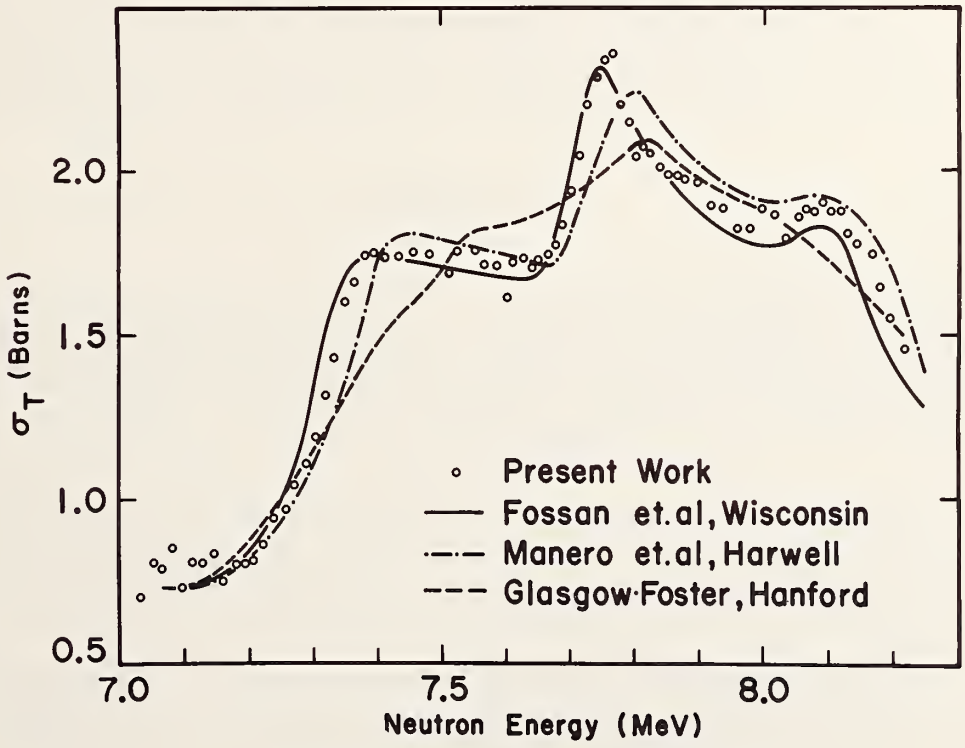

Total Cross Section of C

Figure 4

Experimental Techniques in Absolute Measurements of the Fission Neutron Yield*

A. De Volpi

Argonne National Laboratory
Argonne, Illinois 60439

ABSTRACT

From a recent study of current values of the fundamental fission parameters, underlying characteristics of the various neutron yield measurements have been isolated and examined for susceptibility to systematic error. One may classify these experiments into two categories, gated and non-gated, with variations in each group. Certain weaknesses of each method can be distinguished, and efforts made to evaluate or remedy the possible sources of error are examined. New published and unpublished data on $\nu(^{235}U)$ and $\nu(^{252}Cf)$ can be brought into the picture. An evaluation has been made of the prospects for improvements based on new techniques in neutron detection—particularly with the manganese bath. It is possible to develop some conclusions with respect to likely achievements in precision for these nuclear standards in comparison with other fission parameters.

1. INTRODUCTION

The neutron generation process in a reactor is related to either of two combined parameters, $\nu\sigma_f$ or $\eta\sigma_a$, specifying the neutron yield per absorption in fissionable material. Neither of these pairs is sufficient information because of structural effects, but each is a basis of calculational procedures. At present there are greater inconsistencies in reported data for both ν and σ_f than for both η and σ_a.

Although relationships between the neutron yield per fission, ν, and other nuclear data have long been recognized, desire for high precision has become more significant due to the strong influence of ν in various methods of in-core determination of breeding ratios for advanced reactors.

Underlying all ν values are the absolute measurements—mainly those of ^{235}U and ^{252}Cf. This survey concentrates on certain features of precision experiments for thermal fission of ^{235}U and spontaneous fission of ^{252}Cf.

---

*Work performed under the auspices of the U. S. Atomic Energy Commission.

Since ν inherently requires two absolute measurements—a fast-neutron emission rate and a fission-fragment rate—it is most susceptible to systematic errors in fully independent measurements. Historically, the first measurements were made by comparing the neutron rate against calibrated neutron sources. [1] Reference 2 demonstrates that in the past there were few ν measurements entirely independent of secondary calibration. Most measurements were relative either to calibrated or recalibrated neutron sources or normalized to ν of ^{252}Cf. As a result, present averages derived from least-squares fits are deduced mostly from the relationship $\nu = \eta(1 + \alpha)$.

2. MEASURING NEUTRONS/FISSION FOR ^{235}U

Absolute values of ν may be obtained by (a) evaluation of the critical mass in good geometry; (b) direct, ungated measurements of the separate neutron rates and fission rates; and (c) gated methods in which the product $\nu\varepsilon_n$ is the quantity derived—with neutron detection efficiency ε_n determined in an absolute experiment.

A precise measurement of ^{235}U critical mass in good geometry was published in 1960. [3] Aside from questions which arise concerning the status of multiplication theory, the experiment is effectively an evaluation of the product $\nu\sigma_f$.

There has been only one result for ^{235}U in the second category—ungated direct measurements. It was reported at the Paris Conference; [4] supplementary details were described at the Vienna Symposium. [5,6] The fission rates from two hemispherical ^{235}U counters were calibrated by a coincidence method using a low-efficiency neutron detector to find the fission-fragment counting efficiency. Neutron emission rates from the calibrated counters were determined in a manganese-bath system located in identical geometry at the reactor thermal column. Precision of 1.25% was obtained; the limiting factor was the inconsistency in the two averaged values. Subject to assumptions of uniformity and reproducibility of flux pattern, the hemispherical geometry should eliminate the angular correlation effects expected from fission counters with less than 100% fragment detection. The manganese-bath neutron efficiency was found from application of the 4π β/γ coincidence technique and use of the well-known hydrogen/manganese cross-section ratio. The neutron calibration was confirmed by comparison with the U. S. National Bureau of Standards source NBS-II.

Most measurements of neutron yield have used gated methods.

2.1 Gated Measurement Methods

Gated ν measurements require a fission counter, a fast-acting neutron detector, and electronic circuitry to record the number of single-channel and coincidence counts. In simplified form, the fission-counter rate F is proportional to the source rate S:

$$F = \varepsilon_f S \qquad (1)$$

where ε_f is the fission-counter efficiency. The neutron-channel rate N may contain the desired quantity ν in the form

$$N = \sum_{\nu} \left[1 - \left(1 - \varepsilon_n \right)^{\nu} \right] P(\nu) \, S \, , \tag{2}$$

where $P(\nu)$ is the neutron multiplicity distribution (if the neutron detector can count only one neutron per fission event) and ε_n is the detection efficiency per neutron. The summation is over all discrete values of ν.

At the other extreme, if the neutron detector can accumulate every possible neutron count per fission event, then the neutron rate is simply

$$N = \nu \varepsilon_n S \, . \tag{3}$$

For the latter case, the coincidence rate is

$$C = \nu \varepsilon_n \varepsilon_f S \tag{4}$$

and the coincidence/fission ratio gives

$$C/F = \nu \varepsilon_n \, . \tag{5}$$

Thus, if the neutron-detector efficiency can be found (over the fission-neutron energy spectrum), ν can be determined.

2.2 Detectors for Gated Measurements

Whether Eq. 2 or 3 applies depends on the nature of the neutron detector. If the neutrons from a single fission event can be sufficiently separated in time by slowing down in a moderator, then it is possible to detect nearly all neutrons of an event and Eq. 3 is used. Two types of detectors satisfy this requirement; the large liquid scintillators [7-10] and the boron pile. [11]

Equation 2 is appropriate when the neutron detector responds to a maximum of one neutron per fission—e.g., prompt neutron detectors of small physical size, where the first detectable reaction initiates a deadtime that prevents the remaining neutrons from producing multiple counts. This type of detector was used for fission-counter calibration by Porges and De Volpi. [5] If the neutron detector efficiency is low, Eq. 2 approaches $\nu\varepsilon_n\{1 - \varepsilon_n/2\}$. It is not unusual for a prompt-neutron detector of small volume to be less than 0.1% efficient.

Although Eq. 2 is primarily valid for small neutron detectors, it is also partially true for large detectors that have sufficient deadtime or ungated duration—relative to the neutron lifetime—to exclude some neutrons from a given fission event. If uncompensated, a reported ν value

would be too low. Because it is related to the neutron multiplicity, adjustment for this effect is not an automatic consequence of using the $\nu = 1$ or the standard source-calibration techniques.

2.3 Interactions

Validity of the coincidence equations requires that interactions between fission fragments and emitted neutrons are negligible. Two of the three recognized interactions [12] are certainly negligible: (a) the connection between ν and fission energy (e.g., fission-counter bias) [7,13]; and (b) the relationship between the direction of incident fission-inducing low-energy neutrons and the resulting fission; but it is not clear that the third interaction, (c) the orientation in direction between the fission fragment and its boiled-off neutron progeny, can be readily dismissed.

The strong correspondence between emitted fragment and associated neutrons was illustrated and discussed [2,5] in connection with fission cross-section measurements. In the usual equipment arrangement for the gated coincidence measurements of ν, a parallel-plate fission counter is placed perpendicular to the beam in a tube at the center of a "large" neutron detector. Sometimes these beam tubes have been several inches in diameter, resulting in escape apertures of up to 30 deg in one direction. If, at the same time, the fission-fragment counter has an efficiency significantly less than unity, it is possible for a small bias to be introduced into the experiment.

2.4 Angular Correlations

Since about 90% of the fission neutrons from ^{235}U are boiled off from the moving fission fragments, much of the fission-neutron kinetic energy appears to be derived from the momentum of the fragments. [14] This correlation in direction means that most of the neutrons are in an emission cone surrounding the direction of fragment movement. Fragment pairs with large velocity components perpendicular to the foil plane have the highest probability of ionization, while those emitted parallel to the foil plane have the highest probability of being absorbed in the foil coating.

If the neutron detectors used for the coincidence calibration of these fission counters were truly 4π, the correlation effect would vanish. However, in practice, the necessity for beam tubes through the neutron detector means that escape apertures range from 10 to 30%. In addition, the exit solid angle for fast neutrons may be as much as double the optical solid angle.

The degree of correlation is also highly dependent on the coating thickness. A thick coating leads to a reduced average coincidence rate and, thus, a fission-fragment efficiency which is too low. Maslin, et al., [15] noted a 12% decrease in coincidence efficiency when orientation to the beam of their 0.5 mg/cm^2 fission counter was changed from 45 to 90 deg. After evaluating this discrepancy with foils of 0.5, 0.1, and 0.14 mg/cm^2, they report a final error of 1% in σ_f.

Additional evidence concerning angular-correlation effects on coincidence measurements has been provided by Porges and De Volpi. [2] More recent data indicate that even a fission foil with 99.0% fragment efficiency leads to a 1% 0°/90°/180° effect for a neutron detector with 60% of 2π solid angle.

2.5 Efficiencies

The extrapolation of fission-fragment count rate to zero bias is subject to a number of errors for efficiencies less than 100%. These problems have been discussed by Maslin [15], White [16], and by Porges and De Volpi [2]. Comparison of fission-counter efficiencies against reported coating thickness indicates wide lattitude in practice. The problem is compounded by different techniques used for deposition, by varying oxidation states, and by degree of achievement of uniformity. Whether or not a distinct adjustment has been made for self absorption is often not clear in published reports.

Kenward reported a direct measurement of the prompt-neutron yield for ^{235}U using the coincidence technique. [17] The neutron detector consisted of a paraffin wax cylinder containing twelve BF_3 counters with a through-hole for the fission counter. A fission foil, mounted in a parallel-plate counter, was quite thick, 0.8 mg/cm^2, thus presenting a strong likelihood of problems in angular correlation even though the efficiency claimed was 94%. Normalization of neutron efficiency was based on a ^{240}Pu source calibrated by Richmond and Gardner. [18] While the strength was quoted with an error of 1.5%, its value was derived from comparisons with other sources that typically had 3% standard errors.

2.6 "Boron-Pile" Experiments

Colvin and Sowerby [19] have applied a boron pile as the neutron detector in a prompt coincidence-type neutron-yield experiment. The boron pile is a stack of graphite in which 240 BF_3 counters were implanted. This type of detector has nearly the same neutron efficiency (60%) as large liquid scintillators but is rather insensitive to gamma rays. The boron pile can be located next to a reactor, with a through-hole used for location of a fission counter. Four-millisecond gates are required for foreground and background measurements due to the long slowing-down times of neutrons in graphite. The efficiency of this neutron detector has been found by using a reaction with ν known to be 1, namely photodisintegration of the deuteron. This type of calibration is quite difficult and the lowest calibration energy is 200 keV. Because of the detector channel arrangement, there is a small anisotropy in neutron-detection efficiency.

2.7 Liquid-Scintillator Experiments

A large liquid scintillator was first calibrated with a n-p scattering experiment originated by Diven. [7] A 300-liter cadmium-loaded tank was used; neutron efficiency was roughly 80%. Values finally reported for the experiment are based on efficiency normalized by $\nu = 2.46 \pm 0.03$

313-475 O-68—14

(for ^{235}U) even though independent calibration was made through n-p scattering. The results of this latter calibration were rejected in favor of normalization because of lack of confidence in the precision of the method. If the result had been accepted, a ^{235}U neutron yield of 2.41 could have been obtained.

3. NEUTRON YIELD FROM ^{252}Cf

Because the neutron yield from the spontaneous-fission isotope ^{252}Cf can be determined in the absence of a reactor-connected background, it has been used rather extensively in evaluation of ν for ^{235}U. A number of measurements relying on both the gated and ungated techniques have been listed in Reference 2.

Most of the basic requirements of the measurements for ^{252}Cf are similar to those outlined for ^{235}U. As with ^{235}U, there are two groupings of values; some are around 3.78 and some about 3.70. The low ^{252}Cf values are associated with experimenters who derived low ^{235}U results.

A report by Moat [9] describes an evaluation of ^{235}U and ^{252}Cf neutron-yield values. The ^{252}Cf results follow from a separate experiment using calibrated ^{240}Pu as a neutron standard (somewhat similar to the work of Kenward [17]) and finding the fission rate by extrapolation to zero bias. The value obtained in this experiment, 3.70 ± 0.07, was revised in 1964 to 3.78 ± 0.07 by the same authors [20] who administered a correction for fission-neutron spectral differences of ^{252}Cf and ^{240}Pu. This result has again been revised downward to 3.683 following the 1966 recalibration of the ^{240}Pu source. [21] After finding a value of $\bar{\nu}$ for ^{252}Cf, the authors proceeded to calibrate a 100-liter cadmium-loaded liquid-scintillation counter for comparative measurements with ^{235}U.

One of the few internally consistent experiments reported with an absolute yield is by Hopkins and Diven. [8] They used a 800-liter cylindrical scintillation system to reduce fission escape to a nominal level. Efficiency for ^{252}Cf was about 85% following calibration by n-p scattering from 0.6-cm thick NE-102 plastic scintillator. D-D and D-T reactions were used to provide incident neutrons of 0-2, 3.9, and 6-8 MeV. The authors believe that a pileup correction is the limiting factor in accuracy (contributing 0.6% uncertainty to ν). The ^{252}Cf neutron spectrum reported by Bonner [22] was used for integration. (Compare with recent experiments by Meadows [23] and Condé and During. [29]) Relative values for ^{235}U and other nuclides were also obtained by Hopkins and Diven. [8]

Another key measurement was by Asplund. [10] One improvement this absolute measurement incorporated over similar prompt coincidence-type experiments was the use of pulse-shape discrimination to separate pulses due to recoil protons from those due to gamma rays. A spherical neutron counter containing 110 liters of cadmium-loaded scintillator was calibrated with D-D and D-T neutrons. It was possible to discriminate against Compton electrons down to 0.8-MeV proton-recoil energy. Neutron efficiency ranges from a little over 70% in the low-energy range down to

50% at 10 MeV. A parallel-plate fission counter providing a little more than 1 fission/sec was mounted in the beam tube.

An independent efficiency determination of the boron pile for ^{252}Cf was carried through by several methods; subsequent support for the single-neutron detection efficiency was obtained with calibration of the Harwell ^{240}Pu neutron source. [21]

The gated methods for determination of the neutron yield were examined at Paris by Colvin and Sowerby. [25] Although the boron-pile system has been dismantled, Colvin and Sowerby have been studying various effects which could lead to systematic errors in the different experiments, gated and ungated, as well as their own. They did not find any clearcut symptoms.

Two reports of ν by the ungated method were made at the Paris Conference. An intermediate result was derived by De Volpi and Porges [4] with a precision of 0.75%. For their measurements, two ^{252}Cf counters, one with parallel plate geometry and the other with hemispherical geometry, were calibrated for fragment efficiency by a prompt-coincidence method. Studies were made of a rather large 4-15% angular-correlation effect which was taken into account. These calibrated counters were placed in a manganese-bath system which, besides being independently standardized, was also compared with the U. S. National Bureau of Standards neutron source.

A second measurement quoted with similar precision has been reported by White and Axton. [26] One fission counter was calibrated for fission rate by small solid-angle fragment counting. Despite several initial problems in fission and neutron assay, high confidence has been realized because of the well-established manganese-bath system developed by Axton. [27]

A study made by H. Condé [28] highlights some additional features of the neutron yield experiments which may tend to explain the lack of internal consistency.

4. ATTAINABLE PRECISION

Estimates of attainable precision in ν are intertwined with the status of other absolute measurements of neutron cross sections. Certain general limitations in cross-section accuracy must be recognized. Attainable precision for average quantities such as nuclear cross sections is, first of all, bounded by proven techniques. This implies replication by other experimenters and critical scrutiny of measurement procedures, or at least cooperative exchange of samples, sources, equipment, or personnel. Attainable precision also is constrained by fitting processes currently applied to published data. At present, diverse experimenters located at distant laboratories, often applying different methods of measurement, must reconcile the data.

5. LIMITING FACTORS

In addition to the above general limits, precision depends on sample composition, neutron-energy resolution, and counting and calibration techniques.

Counting

There were indications at the Vienna Symposium on Standardization of Radionuclides [29] that counting facilities are in some selected cases approaching the 0.1% objective. This is true for small solid-angle counting of alpha emitters and particularly true for coincidence counting. Various physical effects requiring small corrections in the coincidence data have been thoroughly studied [30], and instrumental effects have been assimilated into available computer programs. [31] International calibrations of certain standard radioisotopes have been organized and analyzed by the International Bureau of Weights and Measures; 0.5% agreement has been obtained by a large number of laboratories in the past few years. [32]

Calibrations

Absolute neutron measurement techniques are also progressing. Despite only 1% agreement in source calibration for a dozen national laboratories through 1965, [33] improved manganese-bath calibration and monitoring methods [27] promise to reduce the error by an order of magnitude.

The various reference cross sections, especially $^{10}B(n,\alpha)$, $^{197}Au(n,\gamma)$, and $^{1}H(n,\gamma)$, continue to be re-evaluated by both old and new methods, especially with improved samples and better knowledge of supporting parameters such as half-life, branching ratios, and ancillary cross sections.

Current limitations in the accuracy of neutron counting by the manganese bath method include correction for resonance absorption in manganese, the hydrogen/manganese cross-section ratio, parasitic capture in oxygen and sulphur, fast neutron escape, absorption in the source, and chemical stability of the irradiated solution. Investigations into each of these factors has been carried out by many laboratories; it appears that convergence is approaching so that systematic errors need not exceed 0.1% for any correction other than the cross-section ratio—which is in the order of 0.25%.

6. CONCLUSIONS

Determination of the neutron yield per fission requires absolute counting measurements, which are avoided in other fission parameter determinations. However, reduced specifications for sample composition and for incident-neutron texture offset this liability. There also have been a number of improvements in neutron detection which are applicable to neutron-yield evaluation. Both British [25] and American [4] groups are pursuing better data and better agreement. Because the yields may

be determined by two widely different experimental methods, and because ^{252}Cf can be established as a convenient reference standard, it is likely that 0.33% accuracy is attainable in ν. This prognosis is further supported by preliminary data generated at our own laboratory.

7. REFERENCES

[1] SNYDER, T. M., WILLIAMS, R. W., Number of neutrons per fission for 25 and 49, USAEC Report LA-102 (1944).

[2] DE VOLPI, A., Current values of fundamental fission parameters, Reactor and Fuel Processing Technology (in press).

[3] ENGLE, L. B., et al., Reactivity contributions of various materials in TOPSY, GODIVA, and JEZEBEL, Nucl. Sci. Eng. 8 (1960) 543.

[4] DE VOLPI, A., PORGES, K. G., Direct and absolute measurements of average fission neutron yield from ^{235}U and ^{252}Cf, Proc. Conference on Nuclear Data, Paris, October 1966 (IAEA, Vienna: 1967), Vol. 1, pp. 297-306.

[5] PORGES, K. G., DE VOLPI, A., Absolute determination of fission fragment emission rates with a prompt neutron-fission coincidence method, Proc. Symposium on Standardization of Radionuclides, Vienna, October 1966 (IAEA, Vienna: 1967), p. 693.

[6] DE VOLPI, A., PORGES, K. G., ARMANI, R. J., Absolute calibrations of fission neutron source strength relying upon an improved manganese bath technique and absolute beta-gamma coincidence counting, Proc. Symposium on Standardization of Radionuclides, Vienna, October 1966 (IAEA, Vienna: 1967), p. 717.

[7] DIVEN, B. C., et al., Multiplicities of fission neutrons, Phys. Rev., 101 (1956) 1012.

[8] HOPKINS, J. C., DIVEN, B. C., Prompt neutrons from fission, Nucl. Phys., 48 (1963) 433.

[9] MOAT, A., et al., Some experimental determinations of the number of prompt neutrons from fission, J. Nucl. Energy, Parts A/B, 15 (1961) 102.

[10] ASPLUND-NILSSON, I., et al., An absolute measurement of $\bar{\nu}$ of ^{252}Cf, Nucl. Sci. Eng., 16 (1963) 124.

[11] COLVIN, D. W. SOWERBY, M. G., Boron pile $\bar{\nu}$ measurements, Proc. Symposium on Physics and Chemistry of Fission, Salzburg, March 1965 (IAEA, Vienna: 1965), Vol. II, p. 25.

[12] TERRELL, J., Prompt neutrons from fission, Proc. Symposium on Physics and Chemistry of Fission, Salzburg, March 1965 (IAEA, Vienna: 1965), p. 3.

[13] CONDE, Average number of neutrons from a fission of ^{235}U, Arkiv Fyskik, 29 (1965) 293.

[14] MILTON, J. C., FRASER, J. S., The energies, angular distributions and yields of the prompt neutrons from individual fragments in the thermal neutron fission of ^{233}U and ^{235}U, Canadian Report AECL-2163 (1965).

[15] MASLIN, E. E., et al., Absolute fission cross section of ^{235}U for 2200-m/sec neutrons, Phys. Rev., 139 (1965) B852.

[16] WHITE, P. H., Measurements of the ^{235}U neutron fission cross section in the energy range 0.04-14 MeV, J. Nucl. Energy, Pt. A/B, 19 (1965) 325.

[17] KENWARD, C. J., RICHMOND, R., SANDERS, J. E., A measurement of the neutron yield in thermal fission of ^{235}U, UKEA Report AERE R/R 212 (Rev.), (1958).
[18] RICHMOND, R., GARDNER, B. J., Calibration of spontaneous fission neutron sources, UKEA Report AERE R/R-2097 (1957).
[19] COLVIN, D. W., SOWERBY, M. G., Precision measurements of the mean number of neutrons per fission by the boron pile, Proc. Second U.N. Intern. Conference on the Peaceful Uses of Atomic Energy, Geneva, 1958 (United Nations, N. Y.,: 1958), Vol. 16, p. 121.
[20] MATHER, D. S., Average number of prompt neutrons from ^{235}U fission induced by neutrons from thermal to 8 MeV, Phys. Rev., 133 (1964) B1403.
[21] FIELDHOUSE, P., et al., Revision of the Harwell ^{240}Pu source strength and for ^{235}U and ^{252}Cf, J. Nucl. Energy, Pt. A/B, 20 (1966) 549.
[22] BONNER, T. W., Measurements of neutron spectra from fission, Nucl. Phys., 23 (1961) 116.
[23] MEADOWS, J. W., ^{252}Cf fission neutron spectrum from 0.003 to 15.0 MeV, Phys. Rev., 157 (1967) 1076.
[24] CONDÉ, H., DURING, G., Fission-neutron spectra of ^{235}U, ^{239}Pu, and ^{252}Cf, Proc. Symposium on Physics and Chemistry of Fission, Salzburg, March 1965 (IAEA, Vienna: 1965), Paper SM-60/49.
[25] COLVIN, D. W., SOWERBY, M. G., MC DONALD, R. I., Confirmatory experimental data on the Harwell boron pile $\bar{\nu}$ values, Proc. Conference on Nuclear Data, Paris, October 1966 (IAEA, Vienna: 1967), Vol. I, p. 307.
[26] WHITE, P. H., AXTON, E. J., Measurement of the number of neutrons per fission for ^{252}Cf, J. Nucl. Energy (to be published).
[27] AXTON, E. J., CROSS, P., ROBERTSON, J. C., Calibration of the NPL standard Ra-Be photoneutron sources by an improved manganese sulphate bath technique, J. Nucl. Energy, Parts A/B, 19 (1965) 409.
[28] CONDÉ, H., $\bar{\nu}$ of ^{252}Cf, Presented at the Panel of IAEA on Nuclear Standards Needed for Neutron Cross Section Measurements, Brussels, May 8-12, 1967.
[29] Symposium on Standardization of Radionuclides, Vienna, October 10-14, 1966 (IAEA, Vienna: 1967).
[30] BAERG, A. P., Measurement of radioactive disintegration rate by the coincidence method, Metrologia, 2 (1966) 23.
[31] DE VOLPI, A., PORGES, K. G., JENSEN, G., Computer code for reduction of coincidence counting data, J. Appl. Rad. Isotopes, 17 (1966) 277.
[32] Bureau International des Poids et Mesures, Panel Meeting: Discussion of four international comparisons of radionuclide solutions organized by the BIPM, October 15, 1966, Report by BIPM, dated April 24, 1967.
[33] NAGGIAR, V., Comparison internationale des mesures de taux d'emission de la source de neutrons Ra-Be (α,n) n° 200-1 du Conseil National de Richerches, Metrologia, 3 (1967) 51.

Review of Some Fast Neutron Cross Section Data†

Y. Kanda* and R. Nakasima**

*Tokyo Institute of Technology, Tokyo
**Hosei University, Tokyo , Japan

Abstract

Some of the existing cross section data which are usually adopted as standards in fast neutron experiments are reviewed. The compiled cross section data are those for $^{27}Al(n,\alpha)$, $^{56}Fe(n,p)$, $^{63}Cu(n,2n)$, and $^{65}Cu(n,2n)$ reactions in the energy ranging from threshold to 20 MeV. The raw data points are so much scattered that recommendation of the cross section value is difficult to make within the accuracy of 10%. This is mainly due to the ambiguity in determining the flux of neutrons and to the statistical fluctuations in the number of counts. In some cases, the inaccuracy in the neutron energy determination may lead to serious discrepancy. Discussions are presented in concern with the activation method and with the rejected data. Most probable excitation function is obtained for each reaction by means of the least squares method.

1. Introduction

Critical review of the reaction cross sections with fast neutrons is needed for the investigations of nuclear reaction theory and in connection with the use of some as standards in neutron flux measurements or in determining the cross section values of other reactions. Although extensive experimental works have been reported on (n,α), (n,p) and (n,2n) reactions for various kinds of element in the energy region from threshold to 20 MeV, the experimental points reported by different workers are so scattered that it is not easy to find out the reliable cross section values, and this is the main focus of the evaluation work aimed at by some members of the Japanese Nuclear Data Committee.

As the first report of the evaluation program, here we describe about the cross sections of $^{27}Al(n,\alpha)$, $^{56}Fe(n,p)$, $^{63}Cu(n,2n)$ and $^{65}Cu(n,2n)$ reactions. The cross sections of these reactions are adopted as useful standards in the measurements by means of the activation method, since the cross section values are large for 14 MeV neutrons and since the target fabrication is quite easy. Recently, Nagel[1] has evaluated these cross sections in connection with the neutron flux measurements. Nagel's work seems to be quite excellent but the details of the evaluation method are not mentioned. We describe our evaluation process in the next section. Comparison of our results with others is made in the final section.

---

† Work performed as one of the projects of the Japanese Nuclear Data Committee.

2. Method of evaluation

2.1. Compilation of the existing data

The literatures we surveyed are mainly those listed in CINDA 66, and several are also taken from the journals of recent issue; the all original literatures have been checked carefully. One problem in this stage is that the treatment of errors of cross sections and expressions of spreads of neutron energies are not uniform among the original papers. These are, however, used as they are, since it is impossible to recalculate on original values. Another problem is that the spread of neutron energy is not mentioned in some original papers. In our evaluation process, the spread has been estimated by checking the experimental conditions for a possible case, otherwise ±0.5 MeV has been assigned. So far as we reviewed, there is no systematic deviation due to the difference in the experimental means.

All data points are classified into three categories as to correspond to our evaluation process; (1) data obtained by absolute measurement, (2) excitation function data by either absolute or relative measurement, and (3) data by relative measurement at single energy point. There may be overlaps between categories (1) and (2). The numbers of the literatures we have referred to are shown in the following Table I according to the above classification.

Table I

Reaction	(1) Absolute	(2) Excitation function	(3) Relative
$^{27}Al(n,\alpha)^{24}Na$	12	13	5
$^{56}Fe(n,p)^{56}Mn$	7	6	6
$^{63}Cu(n,2n)^{62}Cu$	9	7	1
$^{65}Cu(n,2n)^{64}Cu$	5	5	6

2.2 Determination of the shape of the excitation function

Using the data of category (2), we determine the most probable shape of the excitation function at first. The process is shown schematically in Fig. 1. Looking at all available data we divide whole energy range into a few sub-regions, each from E_i to E_f, with slight overlap in order to fit at least five data points with a quadratic function of energy.

The explanation of Fig. 1 is following: One data set is chosen as the first reference data D_R and the least squares method leads to a quadratic functional form F_R, marked as (1) in the figure. Different functional form F_O, (2) in the figure, is obtained from other data D_O. The values of F_R and F_O at energy of E_N are used in normalizing D_O to D_R, and the normalized D_O is specified by D_{ON}. Again the least squares method is applied to both D_R and D_{ON}, and the standard deviation is calculated. By changing the normalization point E_N in step of 0.5 MeV, we look for the best normalization point $\hat{E}_N$ at which the standard deviation is minimum. Thus we find combined data

of $D_R(E)$ and $D_{ON}(E,\tilde{E}_N)$, and use this as the second reference data. The least squares fit to the second reference data is shown in the figure as (3). Repetition of the least squares fit and the normalization operations leads to a weighted average excitation curve in each sub-region of neutron energy. A typicla example of the curve obtained by these operations is also illustrated in Fig.1. It should be pointed out that the choice of the first reference data, $D_R(E)$ in Fig.1, does not affect the final shape of the excitation function. Thus we find the most probable shape of the excitation function for whole energy range by connecting each curve.

2.3. Determination of the absolute value of the cross section

Since almost all absolute measurements are made at energies between 14 and 15 MeV, we choose an energy point of 14.5 MeV in order to determine the absolute value of the cross section at this energy. The data at the other energy point, category (1) and some of category (2), are recalculated to shift to 14.5 MeV along the most probable shape of the excitation function or along own excitation curve when it was determined by absolute measurement. Thus the absolute value of the cross section at this energy point is determined as weighted mean, all cross section data being converted into those at 14.5 MeV.

By normalizing the most probable excitation function determined in the previous sub-section to the absolute value of the cross section at 14.5 MeV, we get evaluated cross sections in the whole energy range. These are tabulated in Table II in the next page with 0.5 MeV steps. In the Table, $\Delta\sigma$ corresponds to a band with confidence coefficient of 95% in t-distribution.

3. Discussions

All raw data points excluding a very few rejected ones, are shown in Fig.2 together with our evaluation curve for each reaction. The data of category (3) and some of category (2) are renormalized, if possible, to our evaluated values. Then most of the scattered data points approach to our evaluation curve although it is not illustrated here. It is not possible to discuss about each experimental work because of the limitation of pages, but about rejected data it should be mentioned that the treatment in getting the cross section value or in estimating the error is questionable. However our final result is not affected so much ($<$ 1%) even when they are included, since the number of data points rejected is quite few and the error is rather large.

As a whole, the followings are requested through the present evaluation work:

1) Further measurements should be done for $^{27}Al(n,\alpha)$ and $^{56}Fe(n,p)$ reactions in energy range from 8 to 12 MeV, and for $^{63}Cu(n,2n)$ and $^{65}Cu(n,2n)$ reactions near the threshold energy and above 15 MeV.

2) In the activation measurements, more reliable data on decaying product nucleus are wanted, particularly, on branching ratio in ^{64}Cu-decay.

In Fig.3, the evaluated excitation function for each reaction is compared with those presented in Nagel's report[1] and BNL-325. The

calculated (n,2n) cross sections by Pearlstein[2] are also shown in this figure.

The extension of such evaluation work to other reactions are planned as an activity of our group. Also the calculations by means of the statistical evaporation model are in our program in order to find out the systematic trend in level density parameters.

Table II

E_n (MeV)	$^{27}Al(n,\alpha)^{24}Na$		$^{56}Fe(n,p)^{56}Mn$		$^{63}Cu(n,2n)^{62}Cu$		$^{65}Cu(n,2n)^{64}Cu$	
	σ (mb)	$\pm\Delta\sigma$	σ (mb)	$\pm\Delta\sigma$	σ (mb)	$\pm\Delta\sigma$	σ (mb)	$\pm\Delta\sigma$
5.0	0.1	0.6	2.5	0.4				
.5	0.8	0.6	7.3	1.1				
6.0	1.7	0.5	14.4	2.2				
.5	6.9	0.5	22.5	2.4				
7.0	15.0	0.6	30.4	3.4				
.5	26.2	1.1	38.1	4.2				
8.0	40.2	1.6	45.6	5.0				
.5	57.3	2.5	52.8	5.9				
9.0	70.4	2.8	59.8	6.6				
.5	81.7	3.3	66.6	7.4				
10.0	91.4	3.7	73.2	8.1				
.5	99.3	4.0	80.4	8.9			50	10
11.0	108	4	88.2	9.8			156	7
.5	115	4	96.0	10.6			293	12
12.0	120	4	104	12	50	25	459	14
.5	123	4	109	12	173	14	600	14
13.0	124	4	113	13	281	18	719	16
.5	123	4	113	13	372	19	816	17
14.0	121	4	112	12	449	24	892	18
.5	116	4	106	12	509	26	942	19
15.0	109	4	97.5	10.5	554	28	975	20
.5	100	4	88.1	9.7	592	30	999	20
16.0	91.6	3.7	81.0	9.0	627	32	1019	20
.5	83.7	3.4	73.4	8.1	658	33	1037	20
17.0	76.1	3.0	67.9	7.5	684	34	1051	21
.5	68.9	2.8	62.8	6.9	705	35	1059	22
18.0	62.0	2.8	58.2	6.4	723	35	1058	24
.5	55.6	2.8	54.0	6.0	736	35	1056	24
19.0	49.6	2.8	50.3	5.0	745	36	1049	23
.5	44.0	2.7	47.0	5.1	750	36	1038	23
20.0	38.7	2.7	44.2	4.9	750	36	1020	23
.5	33.9	3.4	41.8	4.6				
21.0	29.4	4.5	39.8	3.4				

4. References

1) W. Nagel: Thesis, University of Amsterdam (1966)

2) S. Pearlstein: BNL-897 (1964) and Nucl. Data 3A 327 (1967).

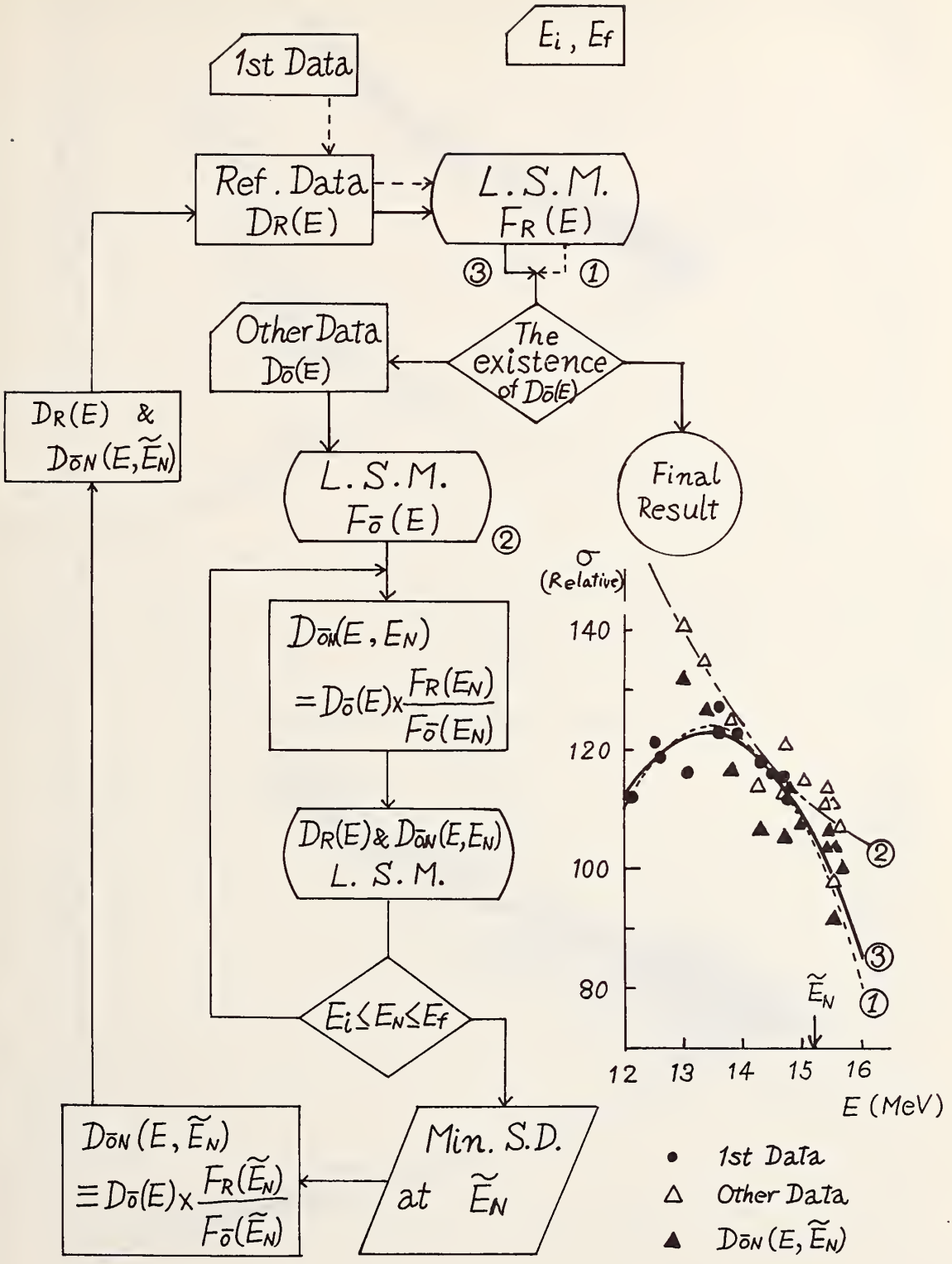
E_i , E_f
1st Data
Ref. Data
$D_R(E)$
L.S.M.
$F_R(E)$
③
①
Other Data
$D_{\bar{o}}(E)$
The existence of $D_{\bar{o}}(E)$
$D_R(E)$ & $D_{\bar{o}N}(E,\tilde{E}_N)$
L.S.M.
$F_{\bar{o}}(E)$
②
Final Result
$D_{\bar{o}N}(E,E_N) = D_{\bar{o}}(E) \times \frac{F_R(E_N)}{F_{\bar{o}}(E_N)}$
$D_R(E)$ & $D_{\bar{o}N}(E,E_N)$ L.S.M.
$E_i \leq E_N \leq E_f$
$D_{\bar{o}N}(E,\tilde{E}_N) \equiv D_{\bar{o}}(E) \times \frac{F_R(\tilde{E}_N)}{F_{\bar{o}}(\tilde{E}_N)}$
Min. S.D. at $\tilde{E}_N$
σ (Relative)
140
120
100
80
12
13
14
15
16
E (MeV)
$\tilde{E}_N$
1st Data
Other Data
$D_{\bar{o}N}(E,\tilde{E}_N)$

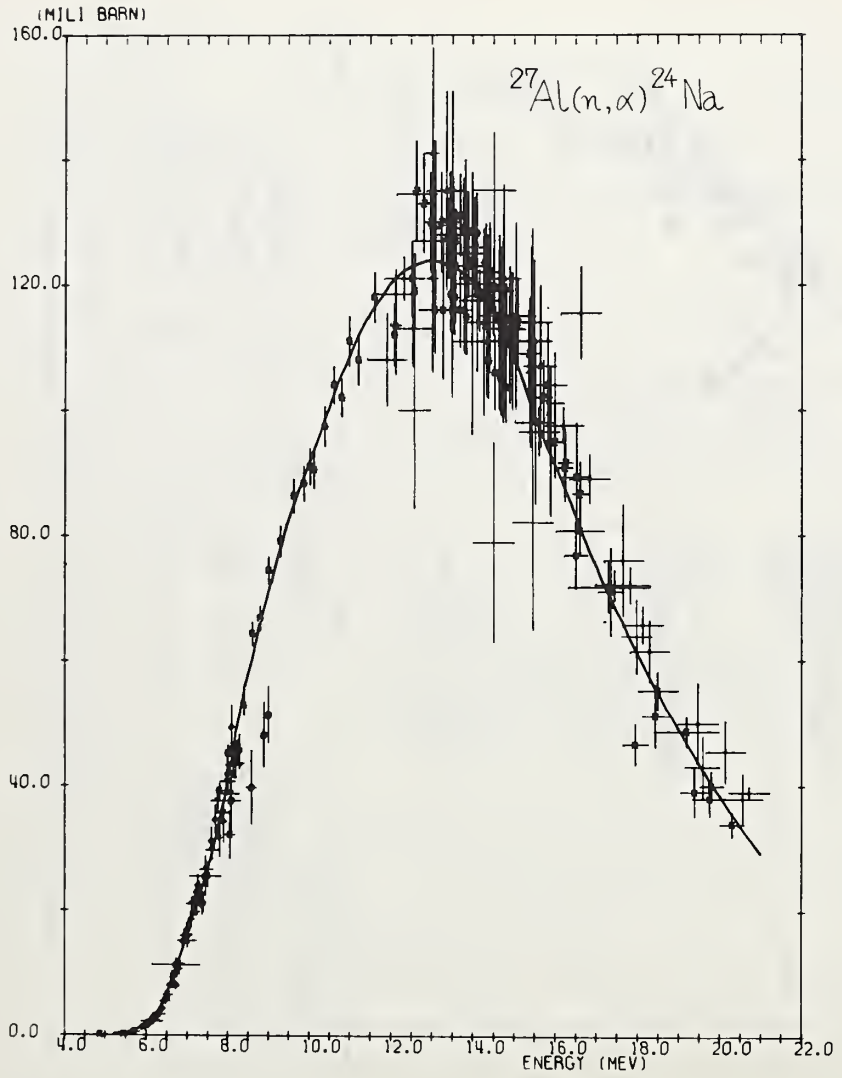
(MILI BARN)
160.0
120.0
80.0
40.0
0.0
$^{27}Al(n,\alpha)^{24}Na$
4.0
6.0
8.0
10.0
12.0
14.0
16.0
18.0
20.0
22.0
ENERGY (MEV)

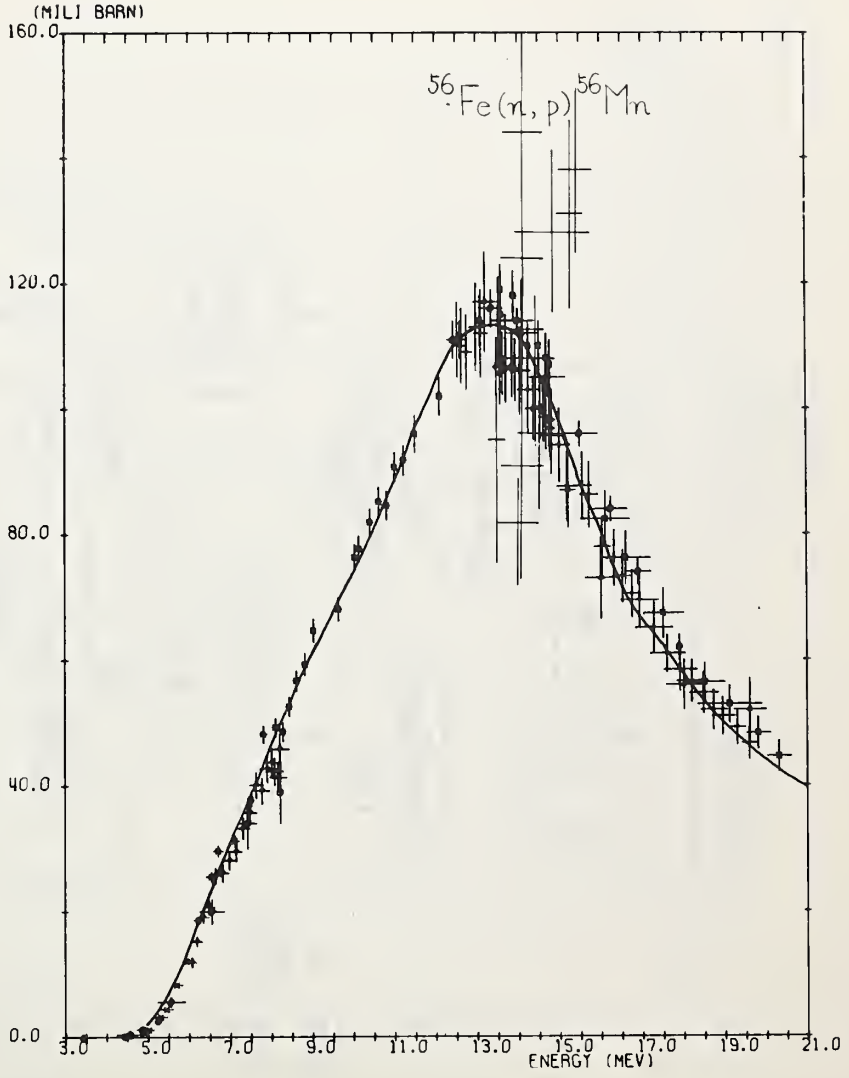
(MILI BARN)
160.0
120.0
80.0
40.0
0.0
$^{56}Fe(n,p)^{56}Mn$
3.0
5.0
7.0
9.0
11.0
13.0
15.0
17.0
19.0
21.0
ENERGY (MEV)

Fig. 2 A

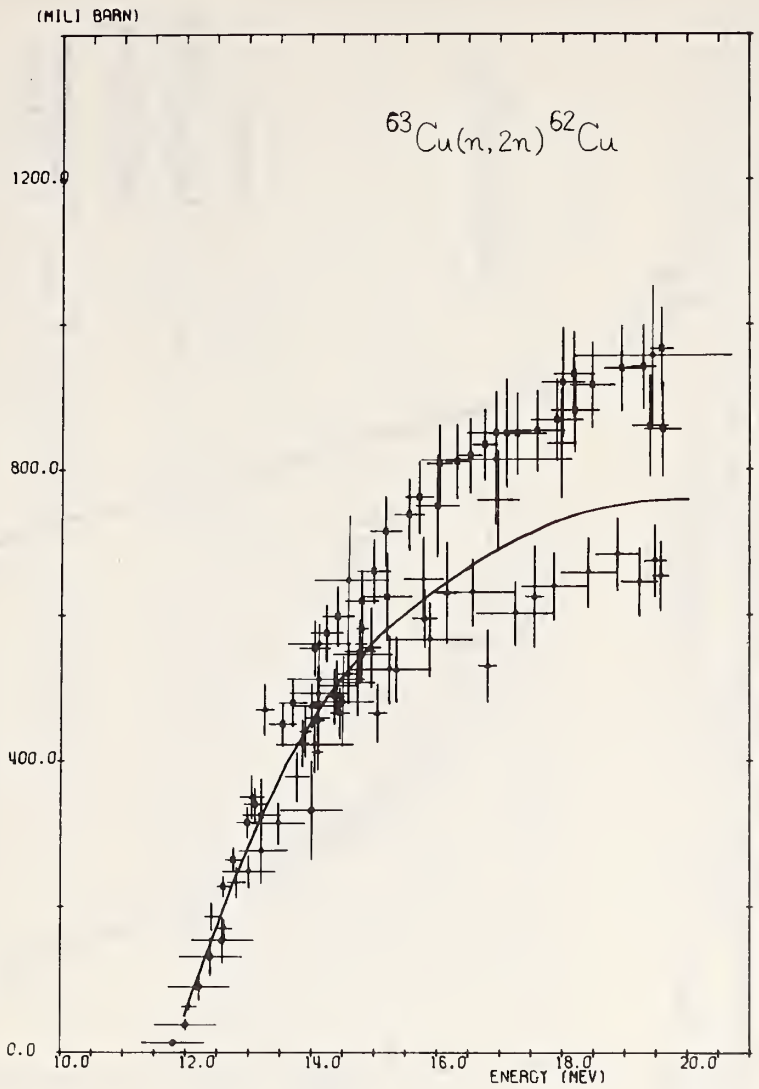
(MILI BARN)
$^{63}Cu(n,2n)^{62}Cu$
1200.0
800.0
400.0
0.0
10.0
12.0
14.0
16.0
18.0
20.0
ENERGY (MEV)

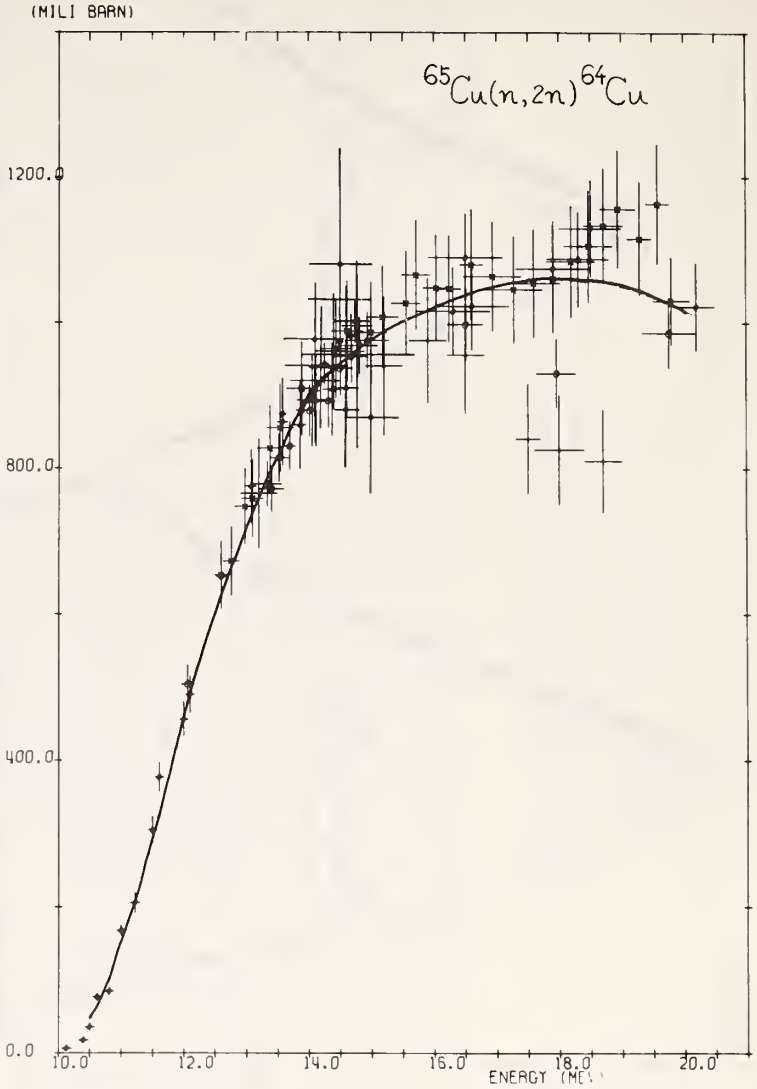
(MILI BARN)
$^{65}Cu(n,2n)^{64}Cu$
1200.0
800.0
400.0
0.0
10.0
12.0
14.0
16.0
18.0
20.0
ENERGY (MEV)

Fig. 2B

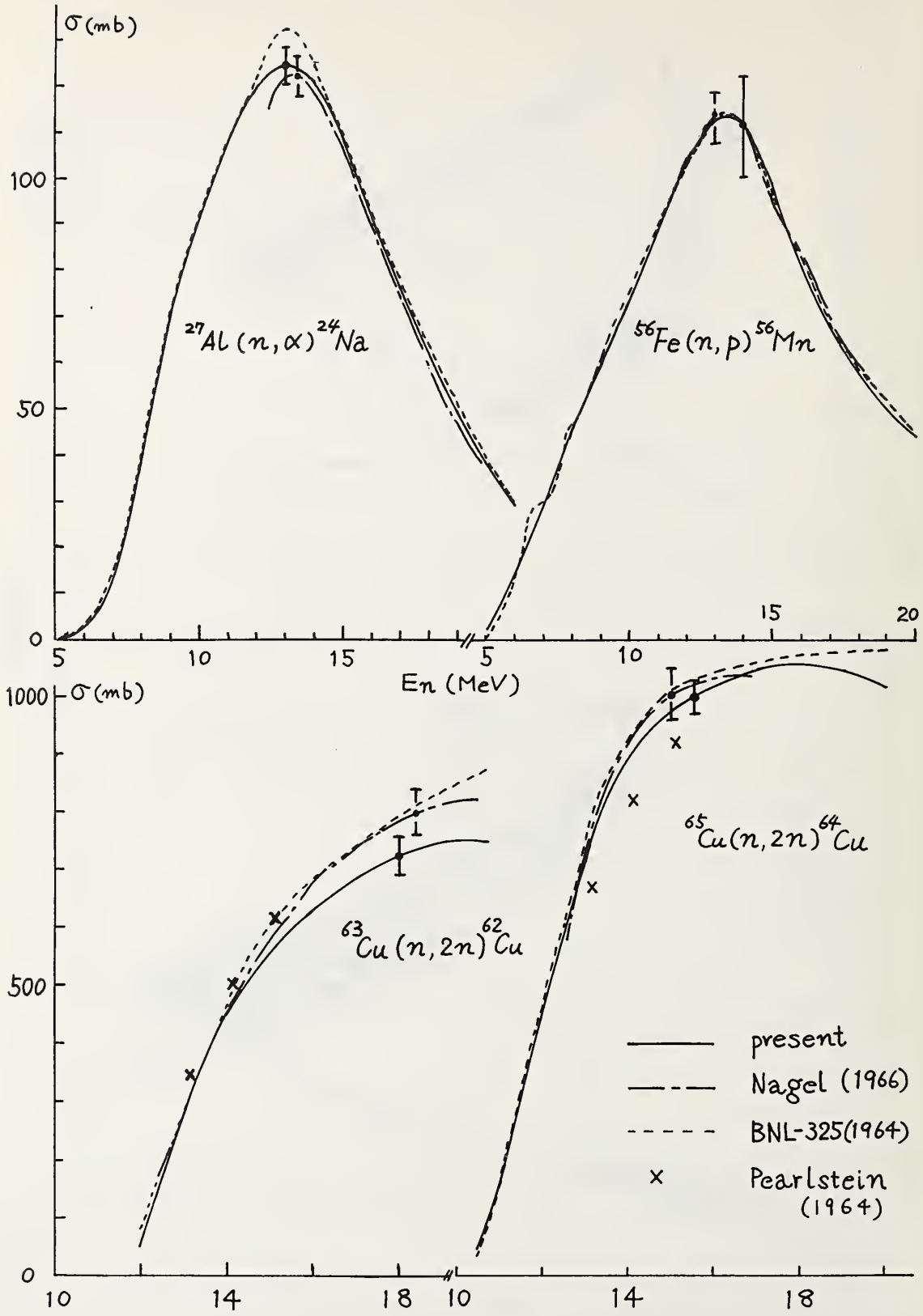
σ (mb)
100
50
0
$^{27}Al(n,\alpha)^{24}Na$
$^{56}Fe(n,p)^{56}Mn$
5
10
15
5
10
15
20
En (MeV)
σ (mb)
1000
500
0
$^{63}Cu(n,2n)^{62}Cu$
$^{65}Cu(n,2n)^{64}Cu$
present
Nagel (1966)
BNL-325(1964)
Pearlstein (1964)
10
14
18
10
14
18

Characteristics of Various Isotopes for Sandwich Foil Measurements of Neutron Spectra

T. J. Connolly*
F. de Kruijf**

Institüt für Angewandte Reaktorphysik
Kernforschungszentrum Karlsruhe, Germany

Abstract

The sandwich method involves activation of foils of a single isotope in multiple layers. The difference in specific activity of two such foils can be related to the neutron flux in the narrow energy interval or intervals in which self-shielding occurs. An analysis is made of several isotopes relative to their potential for yielding spectrum information in the 1 to 10^4 eV region via the sandwich technique. The analysis involves an approximate relationship giving the activation of individual foils in a multiple-layer stack as a function of the activation of single foils of different thicknesses. Activation in the latter foils is calculated by a standard effective resonance integral analysis. Input information includes both resolved and unresolved resonance parameters. The results give for each isotope the magnitude of the activation difference relative to the total activation of a single foil and also the distribution of this difference between individual resolved resonances and between resolved and unresolved resonances. Independent variables include individual foil thickness, number of foils per sandwich, and the neutron spectrum. Spectra representative of both thermal and fast reactors are included.

1. Introduction

Several workers [1,2,3,4,5] have developed the theory and technique of sandwich foil measurements of neutron spectra. In the application of this technique, a number of foils, usually three, of a given material are placed together and irradiated as a single foil. The thickness of the foils is chosen so that there is significant self-shielding in one or more resonances. The difference in the activity between the inside and outside foils, therefore, can be attributed to those energy regions in which the cross sections are shielded. If these energy regions are well defined, as in resolved resonances, and if the value of self-shielding can be computed with acceptable accuracy, then quantitative information about the flux at the energy regions in question is obtained. It is hardly necessary to add that in practice a good deal of painstaking calibration is required to achieve this goal.

---

* Nuclear Engineering Division, Stanford University.

** Reactor Institute Delft.

To date, multiple foil techniques have been applied mainly to neutron spectra in which $\varphi(E)$ follows closely a $1/E$ dependency [1, 5]. Weitzberg [4], however, has used the technique in two fast reactors in which $\varphi(E)$ deviated strongly from $1/E$. In the most common type of fast reactor (or fast critical assembly), namely, a sodium-cooled, metal or oxide fueled reactor, multiple foil schemes are not very attractive because such a small fraction of the activation takes place in the resolved resonance region, i.e., between 1 eV and a few keV. A principal reason for this study is that the steam-cooled reactor under investigation at the Kernforschungszentrum Karlsruhe has a significantly softer spectrum than liquid-metal-cooled fast reactors. In this spectrum, the fraction of activation of various isotopes in the resolved resonance region is greatly increased and, therefore, the possibility of obtaining spectral information from multiple foil techniques is enhanced.

The effectiveness of a given isotope as a spectral indicator in a given spectrum depends primarily on three factors: (1) the activity produced in the irradiation site of interest must be high enough to keep uncertainties introduced by the statistics of counting to an acceptably low value; (2) the difference in activation of two foils in a sandwich foil scheme must be large enough to permit an accurate measurement; (3) this difference in activation must be attributable quantitatively to resolved resonances whose parameters are known.

Some 24 isotopes have been evaluated in a rather extensive analytical investigation which included such variables as foil thickness, foils per sandwich, and neutron spectrum. Some of the results are summarized in this paper. The complete results are to be published in a Kernforschungszentrum Karlsruhe report [6A,B]. The calculations were based on resolved and unresolved resonance parameters provided by Dr. J. J. Schmidt.

2. Analysis of Sandwich Foil Measurements

In order to expedite the large number of calculations to be done, a simplified model of self-shielding in sandwich foils was adopted. It was postulated that the neutron capture rate at any interior point of an infinite slab is the superposition of two rates, one a unique function of the distance from one edge of the slab and the other a unique function of distance from the other edge. Such a model does not properly treat captures of neutrons which are scattered in the direction opposite to their impinging direction. In the present calculations, it was assumed that the flux impinging from both sides is identical. These assumptions lead to a relationship between the specific reaction rate in a given foil of a sandwich and the specific reaction rate in single foils of specified thickness. The relationship is

$$R(k,\ell) = \frac{1}{2}\left[kR(kt) - (k-1)R((k-1)t) + (\ell-k+1)R((\ell-k+1)t) - (\ell-k)R((\ell-k)t)\right],$$

where $R(k,\ell)$ is the specific reaction rate of the k^{th} foil (numbering from the outside) of a sandwich composed of ℓ foils of thickness t, and $R(nt)$, the specific reaction rate in a single foil of thickness nt. For example, the reaction rate of the center foil of a three-foil sandwich is

$$R(2,3) = 2R(2t) - R(t) \quad .$$

An expression for the difference in specific reaction rate or activation of any two foils in a sandwich can also be obtained.

$$D(k,\ell;m,n) = \frac{1}{2}\left[B'_k + B'_{\ell-k+1} - B'_m - B'_{n-m+1}\right] \quad ,$$

where

$$B'_n = nR(nt) - (n-1)R((n-1)t) \quad .$$

$D(k,\ell;m,n)$ designates the difference in the specific reaction rates of the k^{th} foil of an ℓ-foil sandwich and the m^{th} foil of an n-foil sandwich.

It is clear that only at neutron energies at which self-shielding occurs will there be a contribution to D. It was postulated that self-shielding occurred only in resonances and that the self-shielded portion of the reaction rate could, therefore, be represented.

$$R_s(nt) = \frac{N_a}{\rho_a} \sum_i I_i(nt) E_i \varphi(E_i) \quad ,$$

where $I_i(nt)$ is the effective capture integral of the i^{th} resonance centered at E_i. N_a and ρ_a are the number density and density, respectively, of the absorbing isotope. The equations for the activation difference of two foils can now be written.

$$D(k,\ell;m,n) = \frac{N_a}{\rho_a} \sum_i K_i(k,\ell;m,n)\varphi(E_i)$$

$$K_i(k,\ell;m,n) = \frac{1}{2}\left[B_{k,i} + B_{\ell-k+1,i} - B_{m,i} - B_{n-m+1,i}\right]$$

$$B_{n,i} = \left[nI_i(nt) - (n-1)I_i((n-1)t)\right]E_i$$

The flux is obtained from the measured activation difference by the equation

$$\varphi(E_j) = \frac{D\rho_a/N_a - \sum_{i \neq j} K_i \varphi(E_i)}{K_j}$$

The resonance integrals required in this analysis were performed using the TRIX program [7]. The calculation for foils is based on an equivalence relationship using a modified rational escape probability relationship. In all cases an option employing an intermediate resonance calculation technique adapted from Goldstein and Cohen [8] was used. Doppler broadening was included.

3. Results

The foregoing analysis was applied to 24 isotopes to determine their potential as spectral indicators in the sandwich technique. A portion of the results for 12 isotopes is presented in Table III. A principal quantity of interest, the activation difference, is defined as the difference in specific activation of two foils expressed as a fraction of the lower activity foil.

$$\delta = \frac{D(k,\ell;m,n)}{R(m,n)} .$$

When this quantity is low, the flux measurement is sensitive to random errors. Table I gives some of the isotope and foil properties on which the calculations were based. Table II gives four neutron spectra for which the detector responses were calculated. The spectrum designated SN3 is representative of a steam-cooled fast reactor. The other three spectra shown in Table II were devised to show the trends in sandwich-foil response as the spectrum varies from a 1/E spectrum to a very hard spectrum. Each of them has the same high energy spectrum but follows an E^A energy dependence below about 100 keV.

Table III gives the magnitude of the activation difference and also the distribution of the difference between a predominant resonance, other resolved resonances, and unresolved resonances. One interesting feature of these results is the fact that a much larger difference can be obtained between a single foil and the center foil of a sandwich than between the outer and center foil. In Table III, this is illustrated by the larger value of δ calculated for the 1,1;2,3 cases than for the 1,3;2,3 cases. This larger signal can be obtained only at the expense of some increase in experimental complexity, however. The variation (not shown in Table III) of the response, δ, with single-foil thickness was found to be similar to that observed by Ehret [1]. The value of δ has an initial rapid increase as foil thickness increases from zero and then levels off or decreases slightly. As would be expected, there is an attendant loss in selectivity of the response for the predominant resonance. Most of the activation differences given in Table III (exceptions are Cu 63, Cs 133, and Sm 152) are not far from the maximum. The activation difference can also be increased somewhat by increasing the number of foils per sandwich, as illustrated in the case of Au 197 in Table III. The trends in response with spectrum change are those one expects. As the spectrum hardens, the activation difference decreases and it tends to become distributed among several resonances. The responses indicated for the SN3 spectrum, however, do indicate promise for the method in steam-cooled fast reactors.

From these results it seems fair to conclude that several isotopes offer promise as spectral indicators in a wide range of neutron spectra. Considerable experimental development and standardization work will be required, however, to make the technique one of broad applicability.

4. References

1. G. Ehret, "Die Bestimmung Epithermischer Neutronenspektren mit Resonanzsonden (Sandwichmethode)", Atompraxis, 1, 393-400 (1961).

2. A. M. Judd, "Neutron Flux Measurements by Activation of Foils" Nuclear Instruments and Methods, 23, 29-35 (1963).

3. W. L. Zijp, "Review of Activation Methods for the Determination of Fast Neutron Spectra", RCN-37, May 1965.

4. A. Weitzburg, "Measurement of Epithermal Spectra in Fast Assemblies Using Resonance Sandwich Detectors", paper presented at Argonne Fast Reactor Conference, October 1965.

5. A. K. McCracken, "Techniques with Resonance Foil Sandwich Detectors", 168-178, Radiation Measurements in Nuclear Power, 1966.

6A. T. J. Connolly, F. de Kruijf, "An Analysis of Twenty-four Isotopes for Use in Multiple Foil (Sandwich) Measurements of Neutron Spectra below 10 keV", Kernforschungszentrum Karlsruhe, to be published.

6B. J. J. Schmidt, "Recommended Resolved and Statistical Resonance Parameters for Twenty-four Isotopes", Kernforschungszentrum Karlsruhe, to be published.

7. J. M. Otter, "The TRIX-1 Code, an Improved Analytical Calculation of Resonance Integrals", NAA-SR-MEMO 11538, July 1965.

8. R. Goldstein, E. R. Cohen, "Theory of Resonance Absorption of Neutrons", Nuclear Science and Engineering, 13, 132-140 (1962).

TABLE I

ISOTOPE AND FOIL PROPERTIES

			Foil Properties		
Isotope	Abundance (%)	Activity Half-life[1]	Phys/Chem Form	Abs. Dens. $N_a \times 10^{-24}$ (nuclei/cm^3)	Pot. Scat. Σ_p/N_a (barns)
Na 23	100	15.0 hr.	NaF	0.04	3.8
V 51	99.8	3.8 min.	Metal	0.0705	2.5
Mn 55	100	2.58 hr.	12% Ni	0.0714	5.8
Co 59	100	10.4 min.	Metal	0.089	6.5
Cu 63	69.1	12.8 hr.	Metal	0.05865	9.7
Ga 71	39.6	14.2 hr.	Metal	0.02	16.2
As 75	100	26.8 hr.	---	0.03	6.2
Se 80	49.8	18.0 min.	---	0.07	12.0
Br 81	49.5	35.9 hr.	KBr	0.00688	16.0
Mo 98	23.8	66.0 hr.	Metal	0.01525	22.7
Mo 100	9.62	14.3 min.	Metal	0.006175	56.0
Rh 103	100	4.4 min.	Metal	0.0726	5.1
Pd 108	26.7	13.6 hr.	Metal	0.0184	18.0
Cd 114	28.9	55.0 hr.	Metal	0.01337	15.6
In 115	95.7	54.0 min.	Metal	0.0366	11.1
Sb 121	57.2	2.8 day	---	0.0116	7.3
Cs 133	100	3.2 hr.	---	0.01	3.5
La 139	99.9	40.0 hr.	Metal	0.02668	3.2
Sm 152	26.6	47.0 hr.	---	0.008	13.1
W 186	28.4	24.0 hr.	Metal	0.018	39.0
Re 187	62.9	17.0 hr.	Metal	0.06	17.5
Ir 191	37.3	74.0 day	Metal	0.0292	29.0
Pt 198	7.2	30.0 min.	Metal	0.00476	148.0
Au 197	100	65.0 hr.	Metal	0.05904	10.8

[1] Activity regarded as most likely to be measured. Capture rate calculations included production of all isomers, however.

TABLE II

GROUP FLUXES USED IN CALCULATIONS

Group No.	Min. Energy (eV)	Group Flux (arb. units) Spectrum Designation SN3	A=-1	A=0	A=+1
1	6.5×10^{6}	1.326	1.326	1.326	1.326
2	$4.0 \times$ "	7.336	7.336	7.336	7.336
3	$2.5 \times$ "	16.98	16.98	16.98	16.98
4	$1.4 \times$ "	34.54	34.54	34.54	34.54
5	$0.8 \times$ "	48.94	48.94	48.94	48.94
6	$0.4 \times$ "	82.23	82.23	82.23	82.23
7	$0.2 \times$ "	75.83	75.83	75.83	75.83
8	$0.1 \times$ "	58.91	58.91	58.91	58.91
9	46,500	44.28	44.28	44.28	44.28
10	21,500	30.85	30.85	20.70	9.64
11	10,000	22.48	22.48	9.51	2.05
12	4,650	17.95	22.48	4.428	0.4428
13	2,150	13.65	22.48	2.07	0.0964
14	1,000	10.46	22.48	0.951	0.0205
15	465	6.760	22.48	0.4428	4.428×10^{-3}
16	215	4.337	22.48	0.207	9.64×10^{-4}
17	100	2.441	22.48	0.0951	2.05×10^{-4}
18	46.5	1.067	22.48	0.04428	4.428×10^{-5}
19	21.5	0.644	22.48	0.0207	9.64×10^{-6}
20	10	0.186	22.48	9.5×10^{-3}	2.05×10^{-6}
21	4.65	0.1009	22.48	4.428×10^{-3}	4.428×10^{-7}
22	2.15	0.1620	22.48	2.07×10^{-3}	9.64×10^{-8}
23	1.0	0.0388	22.48	9.51×10^{-4}	2.05×10^{-8}
24	0.465	0.01258	22.48	4.428×10^{-4}	4.428×10^{-9}
25	0.215	8.36×10^{-4}	22.48	2.07×10^{-4}	9.64×10^{-10}

TABLE III

MAGNITUDE OF ACTIVATION DIFFERENCE IN SANDWICH FOIL MEASUREMENTS

Isotope	Single Foil Thickness (cm)	Sandwich Type	Activation Diff., 100 δ (%) Spectrum SN3	A=-1	A=0	A=+1	Resonance Energy (eV)	Contribution to δ (%) Spectrum SN3	A=-1	A=0	A=+1
Na 23	0.05	1,1;2,3	14.0	4.8	8.3	2.6	2850	96.7	98.8	82.5	19.1
							Others[1]	3.3	1.2	17.5	80.9
							Unres.	----	----	----	----
		1,3;2,3	2.8	1.0	1.6	0.4	2850	97.5	99.1	86.4	24.8
							Others	2.5	0.9	13.6	75.2
							Unres.	----	----	----	----
Mn 55	0.0125	1,1;2,3	28.8	16.2	11.8	1.0	337	77.7	88.0	64.5	7.1
							Others	22.1	11.9	33.4	60.8
							Unres.	0.2	0.1	2.1	32.1
		1,3;2,3	8.5	4.7	3.4	0.1	337	75.7	86.6	64.9	15.3
							Others	24.2	13.4	34.7	68.6
							Unres.	0.1	0.0	0.4	16.1
Co 59	0.0125	1,1;2,3	48.4	29.5	13.9	0.7	132	98.6	99.8	89.4	6.0
							Others	1.4	0.2	10.6	94.0
							Unres.	----	----	----	----
		1,3;2,3	18.2	11.2	4.9	0.1	132	99.3	99.9	95.0	14.5
							Others	0.7	0.1	5.0	85.5
							Unres.	----	----	----	----

[1] "Others" refers to contribution from all other resonances treated as resolved in this work [6].

TABLE III (continued)

Isotope	Single Foil Thickness (cm)	Sandwich Type	Activation Diff., 100 δ (%) Spectrum SN3	A=-1	A=0	A=+1	Resonance Energy (eV)	Contribution to δ (%) Spectrum SN3	A=-1	A=0	A=+1
Cu 63	0.005	1,1;2,3	17.4	14.8	4.3	0.4	577	81.4	91.0	58.7	8.2
							Others	18.4	8.9	39.6	66.4
							Unres.	0.2	0.1	1.7	25.4
		1,3;2,3	4.2	3.7	0.9	0.1	577	87.6	94.1	71.2	15.9
							Others	12.3	5.9	27.8	61.0
							Unres.	0.1	0.0	1.0	23.1
Mo 98	0.02	1,1;2,3	18.1	20.8	3.4	0.4	429.4	14.0	16.0	9.5	0.8
							467.2	53.5	59.0	38.4	3.4
							Others	29.8	24.2	35.3	12.2
							Unres.	2.7	0.8	16.8	83.6
		1,3;2,3	4.9	5.4	0.8	0.0	429.4	9.2	10.5	7.2	1.2
							467.2	68.5	75.4	56.5	10.5
							Others	21.4	13.8	29.7	22.0
							Unres.	0.9	0.3	6.6	66.3
Cd 114	0.03	1,1;2,3	24.2	49.9	4.7	0.6	120.2	33.8	64.2	17.3	----
							394.1	23.4	18.1	15.9	----
							Others	19.5	9.9	18.0	----
							Unres.	23.3	7.8	48.8	95.2
		1,3;2,3	7.3	16.7	1.1	0.0	120.2	38.7	66.8	24.5	----
							394.1	29.1	20.4	24.6	----
							Others	16.5	7.6	19.2	----
							Unres.	15.7	5.2	31.7	83.7

TABLE III (continued)

Isotope	Single Foil Thickness (cm)	Sandwich Type	Activation Diff., 100 δ (%) Spectrum SN3	A=-1	A=0	A=+1	Resonance Energy (eV)	Contribution to δ (%) Spectrum SN3	A=-1	A=0	A=+1
In 115	0.0025	1,1;2,3	10.3	105.0	0.8	0.0	1.46	82.4	98.2	71.3	
							Others	8.2	1.7	9.4	
							Unres.	9.4	0.1	19.3	
		1,3;2,3	3.6	40.9	0.3	0.0	1.46	91.7	99.0	84.5	
							Others	6.0	1.0	8.5	
							Unres.	2.3	0.0	7.0	
Cs 133	0.005	1,1;2,3	8.0	35.2	1.4	0.0	5.9	40.2	90.2	35.6	
							Others	59.3	9.8	51.8	
							Unres.	0.5	0.0	2.6	
		1,3;2,3	1.5	8.6	0.2	0.0	5.9	53.9	94.1	50.3	
							Others	45.8	5.9	48.2	
							Unres.	0.3	0.0	1.5	
La 139[2]	0.025	1,1;2,3	14.6	36.0	2.0	0.0	72	100.	100.	100.	
		1,3;2,3	5.3	13.2	0.7	0.0	72	100.	100.	100.	
Sm 152	0.0125	1,1;2,3	37.9	100.0	6.9	0.2	8.0	53.5	96.1	48.5	0.3
							Unres.	46.5	3.9	51.5	99.7
		1,3;2,3	13.0	40.3	2.2	0.0	8.0	63.5	96.9	61.8	
							Unres.	36.5	3.1	38.2	

[2] The unresolved resonance parameters estimated for La 139 [6] gave what appeared to be unrealistically high self-shielding in the unresolved resonances. The unresolved resonance contribution was therefore omitted from the results presented here.

TABLE III (continued)

Isotope	Single Foil Thickness (cm)	Sandwich Type	Activation Diff., 100 δ (%) Spectrum SN3	A=-1	A=0	A=+1	Resonance Energy (eV)	Contribution to δ (%) Spectrum SN3	A=-1	A=0	A=+1
W 186	0.005	1,1;2,3	25.1	73.1	4.8	0.1	18.8	70.1	97.8	64.3	
							Others	27.7	2.2	27.7	
							Unres.	2.2	0.0	8.0	
		1,3;2,3	8.0	26.3	1.5	0.0	18.8	79.2	98.5	76.6	
							Others	20.0	1.5	20.0	
							Unres.	0.8	0.0	3.4	
Au 197	0.0025	1,1;2,3	18.7	101.2	3.3	0.1	4.9	46.3	95.2	32.0	
							Others	47.4	4.7	50.8	
							Unres.	6.3	0.1	17.2	
		1,3;2,3	5.6	40.6	0.9	0.0	4.9	62.4	96.8	51.1	
							Others	35.7	3.2	43.5	
							Unres.	1.9	0.0	5.4	
		1,1;3,5	28.3	151.3	4.9	0.2					
		1,5;3,5	9.2	64.7	1.4	0.0					
		1,1;4,6	36.1	190.1	6.2	0.2					

Advances in Accurate Fast Neutron Detection*

A. De Volpi and K. G. Porges

Argonne National Laboratory
Argonne, Illinois 60439

ABSTRACT

The manganese bath is presently the leading technique used to obtain the highest precision when neutrons in the energy range of 1 keV to 10 MeV are counted with accuracies in the order of 1%. Examples of such experiments are absolute measurements of the fission parameters ν and η. Recent improvements in the manganese bath, entailing continuous flow through an annular NaI(Tℓ) crystal, have resulted in greatly augmented efficiency, in our case producing 1.6×10^{-3} counts/neutron at a backbround level of about 30 counts/sec. One limitation, though, is in application to experiments involving fluctuating neutron backgrounds (nuclear reactors and accelerators). With a half-life of 2.58 h, the cycle time for full manganese irradiation and decay is in the order of two days. A study of possible substitutes with shorter half-lives demonstrates that the sulfate of vanadium (3.77-m half-life) satisfies the various chemical, isotopic, cross-section, and radiation requirements. Besides offering a one-hour full-cycle time, the vanadium bath has a figure of merit, in terms of relative efficiency per neutron, just about half that obtained from the manganese system. Supporting experiments have established the conditions required for use of vanadium.

1. INTRODUCTION

The manganese bath technique has been perfected in the past decade to the point where universally consistent results are obtained with 1% accuracy and precisions of a few-tenths of a percent. The method basically consists of surrounding a small source with a large moderator tank, allowing thermal neutron capture to take place primarily in dissolved manganese. The ^{56}Mn activity thus created is subsequently monitored as a measure of source strength.

The manganese bath is best suited for highly accurate source strength measurements of neutrons with energy spectra in the range of 1 keV to 10 MeV. Not only have standard neutron emitters been measured as an object

*Work performed under the auspices of the U. S. Atomic Energy Commission.

in themselves, but a number of nuclear parameters have been determined with the aid of the manganese bath. For example, some of the best values of η, neutrons per thermal absorption, and ν, neutrons per thermal fission or spontaneous fission, have been obtained by this method. [1-4]

Recent improvements in the manganese bath technique, entailing continuous flow monitoring, have improved the quality of such nuclear data and offer other opportunities for accurate fast neutron detection, [5] Moreover, certain extensions of the method involving the use of vanadium are subject to increased nuclear reactor and accelerator applications. In comparison with other measurement techniques, the water bath method is extremely insensitive to gamma-ray background.

2. MANGANESE BATH IMPROVEMENTS

Recent improvements of ^{56}Mn activity assessment center on continuous monitoring of gamma activity in place of intermittant sample withdrawal or dip counting after the source is withdrawn. By circulating the liquid in a closed loop past a sodium-iodide crystal, the activity may be followed without interruption from buildup to saturation and decay back to background. Calibration, as before, involves comparison of aliquots of ^{56}Mn added directly to the solution against aliquots counted in an absolute coincidence counting system.

Figures 1, 2, and 3 indicate details of the on-line counter used at this Laboratory. The detector here is a 15-cm annulus of 2.54-cm wall thickness. All pulses resulting from about 50-keV minimum transfer to light photons in the crystal are accepted by the electronic level discriminator. Temperature regulation of the counting system within $\pm 0.1°C$ is maintained by heating the solution. Stable plateau-type operation is obtained in high voltage, amplifier gain, and discriminator characteristic. For example, a slope of 0.01% count rate change per 0.1% change in phototube high voltage is maintained.

The annular configuration offers a good figure of merit, as demonstrated in Table I where the characteristics of three on-line systems are compared. The figure of merit chosen, essentially signal/$(\text{background})^{\frac{1}{2}}$, is normalized for manganese bath volume.

Performance of the system at this Laboratory has also been satisfactory. Corrections for finite pumping time are in the order of 0.5%. The background level is now about 29-counts/sec integral. With use of an upper level discriminator set at about 3 MeV equivalent, an additional 4-counts/sec background may be excluded by anticoincidence.

The overall efficiency for counting is about 0.4% per ^{56}Mn disintegration in the entire 537-liter system; this corresponds to about 0.2% efficiency per source neutron (at a $MnSO_4$ concentration of 400 g/liter).

Since background experience indicates reasonable stability, it is possible to consider counting neutron sources with emission rates of

10^4/sec at a precision of 0.1% in a normal cycle of two days. Sources as weak as 1000 counts/sec can be calibrated.

For reproducibility under these conditions, we have found it essential to maintain chemical stability by providing an excess of sulfate ions and by addition of a reducing agent.

3. SEARCH FOR OTHER SOLUTES FOR THE WATER BATH

One of the limitations of the manganese bath method is the time required for activation to saturation and subsequent decay to background level: in general, about ten half-lives (one day) are required to exceed 99.9% saturation and the same amount of time to retreat to background. Not only is a two-day cycle somewhat time-consuming from an experimenter's viewpoint, but it tends to mask the existence of short-term fluctuations in background. This latter deficiency is particularly noticeable when irradiations are conducted in the vicinity of a reactor or accelerator.

Additionally, there are some conceptual advantages to developing a neutron source calibration method which differs enough from the manganese system to serve as a cross check on the accuracy of such methods. Techniques of mechanical integration [7] and the so-called oil bath [8] have been used in a similar capacity, but none of these have yielded the precision or convenience obtainable from the manganese bath.

Louwrier [9] has attempted to substitute sodium as the activation component, finding agreement with the manganese bath to the extent of 1%. While providing an appropriate difference in the bath composition with regard to cross-section magnitude and shape, the production of ^{24}Na with its 15-h half-life clearly worsens the time/patience/stability/background factors.

An examination of the periodic table for suitable short-lived substitutes reveals very few other candidates. One prime requirement is that the element be nearly monoisotopic; other pertinent characteristics are solubility, cross section, half-life, radiation signature, cost, and availability. The only element, aside from manganese, which satisfies these general constraints is vanadium.

4. THE VANADIUM BATH

The characteristics of vanadium are compared with manganese, sodium, and other elements in Table II. ^{51}V is 99.76% naturally abundant; ^{50}V, the residual natural isotope, is essentially stable also. ^{51}V has a 4.9 thermal neutron capture cross section with firm 1/v behavior.

The decay scheme for ^{52}V is relatively simple with all beta decay populating the 1.4336-MeV excited state of ^{52}Cr. The resulting beta decay energy has an end point of 2.47 MeV. Thus, this isotope is unambiguously suited for beta-gamma coincidence calibration and for gamma-ray monitoring of thick solutions as well.

The short half-life is a double-edged blade. On one side, the 3.76-min period meets objectives of a fast-reacting neutron measurement system; on the other side, certain difficulties with regard to counting and calibration develop.

When methods of post-irradiation sampling or dip counting were used to survey the activity of the manganese bath systems, a brief decay isotope such as ^{52}V could not be handled. On-line monitoring, however, as developed by Axton [5] and extended in the manner described earlier in this article, allow consideration of vanadium. It has become necessary though to increase pumping rates to reduce the activity penalty due to transit through the pipes. Present pumping rates provide a mean delay of 130 sec compared to the 226-second half-life. Under these circumstances, dependence on stability of pumping rate remains a noticeable, but reduced factor. Thorough mixing, as well as examination of flow patterns, is also indicated.

The vanadium-manganese cross-section ratio is 4.9 b/13.25 b; also the number of gamma rays emitted per disintegration is in the ratio of 1/1.5. In addition to the cross section, the relative neutron counting efficiency is also affected by salt solubility. Thus, the count rate penalty incurred in use of vanadium is a factor of two to four, depending on whether maximum solubility is chosen or the more practical case of 200 g/liter. The figure of merit based on relative counts/neutron is given in Table II for both concentrations; this suggests that as long as signal strength remains much greater than background, then the vanadium bath provides nearly the same precision as the manganese system.

Because of the extremely high efficiency of the on-line monitor, the count rate penalty leads to a sacrifice in calibration capability only when sources less than 10^4/sec are to be counted. On the other hand, the entire irradiation requires only a haf hour—and decay to background another half hour. Thus, an experimental cycle of one hour can be followed with vastly improved systematic procedures for background subtraction.

Another difficulty associated with the use of vanadium is its limited availability and attendant high cost. There appears to be an abundant supply of vanadium-bearing ore, and refining methods are straightforward; so the present reason for high cost is basically low demand. If the demand increased enough to encourage vanadyl surfate pilot plant production, it is possible that these limitations will be diminished.

Three calibrations with vanadium have so far been conducted at this Laboratory. Proximity of a nuclear reactor is essential. Processing times have been reduced to 15 min for removal from the rabbit to insertion of aliquots in the bath—and nearly simultaneous introduction of a liquid-scintillator containing ^{52}V activity into a beta-gamma coincidence system. Adequate statistics can be obtained with the use of automatic counting equipment accumulating data in one-minute intervals.

Beta efficiency for liquid scintillator samples is about 99%. Sixty per cent efficiency has been obtained for 2.3 g of vanadyl sulphate dissolved in 11 ml of water and ethanol detecting the Cherenkov radiation. There is some evidence of possible difficulties during extended irradiations arising from what is probably uranium contamination left over from initial ore separation.

Other aspects involved in the use of vanadium are being evaluated. For example, based on a saturated solubility of 0.39066 ± 0.00064 g $VOSO_4$ per gram of aqueous solution, the vanadium/hydrogen atom ratio is being determined as a function of solution density.

Laboratories which lack nearby reactor irradiation facilities can make use of standard neutron sources for frequent and convenient calibration of the vanadium bath. For purposes of independent absolute calibration of neutron sources, it will be necessary to evaluate the vanadium/-hydrogen cross-section ratio by varying the concentration. [5]

5. EXPERIMENTS IN PROGRESS OR PLANNED

A number of experiments involving accurate fast neutron detection are in progress or planned for either the manganese or vanadium bath facility. The half-life of ^{252}Cf has been followed by neutron counting for a number of years, with results consistent with the data of Metta, et al. [10] The hydrogen/manganese cross-section ratio [5] is an important factor towards which we have been obtaining supporting data.

An example of another cross-section ratio which can be found with possibly high precision is shown in Fig. 4. This was a preliminary experiment to evaluate the technique of finding the boron/manganese thermal cross-section ratio by changing the boron/manganese atom ratio in the bath. The result for laboratory boron of unknown isotopic content is 57.7 ± 0.6%; we intend to use our supply of CBNM certified natural boron for the final experiment with associated improvements which offer the prospect of an error of ±0.1%.

Consideration has been given to a direct measurement of the hydrogen capture cross section by a dilution procedure in heavy water. Another effort directed towards accurate, even though redundant, data is determination of some thermal fission cross sections.

6. REFERENCES

[1] MACKLIN, R. L., et al., Manganese bath measurements of η of ^{233}U and ^{235}U, Nucl. Sci. Eng., 8 (1960) 210.

[2] SMITH, J. R., REEDER, S. D., FLUHARTY, R. G., Measurements of the absolute value of eta for ^{233}U, ^{235}U, and ^{239}Pu using monochromatic neutrons, USAEC Report IDO-17083 (1966).

[3] WHITE, P. H., AXTON, E. J., Measurement of the number of neutrons per fission for ^{252}Cf, J. Nucl. Energy (to be published).
[4] DE VOLPI, A., PORGES, K. G., Direct and absolute measurements of average fission neutron yield from ^{235}U and ^{252}Cf, Proc. Conference on Nuclear Data, Paris, October 1966 (IAEA, Vienna, 1967), Vol. 1, p. 297.
[5] AXTON, E. J., CROSS, P., ROBERTSON, J. C., Calibration of the NPL standard Ra-Be photoneutron sources by an improved manganese sulphate bath technique, J. Nucl. Energy, Parts A/B, 19 (1965) 409.
[6] CAPGRAS, A., Etalonnage de sources de neutrons (α,n), Proc. Symposium on neutron monitoring for radiological protection, Vienna, August 28-September 2, 1966 (IAEA, Vienna, 1967).
[7] DE JUREN, J. A., et al., Absolute calibration of the National Bureau of Standards photoneutron standard: I, J. Res. Nat. Bur. Standards, 55, No. 2 (1955) 63.
[8] FIELDHOUSE, P., et al., Revision of the Harwell ^{240}Pu source strength and for $\bar{\nu}$ for ^{235}U and ^{252}Cf, J. Nucl. Energy, Pt. A/B, 20 (1966) 549.
[9] LOUWRIER, P. W. F., Calibration of a radium (α,n) beryllium neutron source, Unpublished Thesis, Amsterdam, Netherlands (1966).
[10] METTA, D., et al., Nuclear constants of nine transplutonium nuclides, J. Inorg. Nucl. Chem., 27 (1965) 33.

Table I. CONTINUOUS MONITORING MANGANESE BATH SYSTEMS

System	Ref.	Crystal Size, cm	Crystal Volume, cm^3	B Background, c/s	Low Energy, keV	Upper Energy	Spec. BG[a,b], $\frac{c/m}{cm^3}$	ε Efficiency per ^{36}Mn Disint.	V System Volume, liter	Figure of Merit[c]
Axton, Cross, Robertson	[5]	5 × 5 cyl	100	5	40	∞	3.0	2.2×10^{-3}	75.7	0.074
			100	3	40	∞	1.8	2.2×10^{-3}		0.095
Capgras	[6]	7.5 × 7.5 cyl	340	0.82	740	950 keV	0.15		535[d]	
			340	3	50	∞	0.53			
De Volpi, Porges		15 × 15 annulus	1560	25	40	3.0 MeV	0.96	4.0×10^{-3}	538	0.43
			1560	30	40	∞	1.15	4.0×10^{-3}		0.40

[a] Background in the stated energy range divided by crystal volume.

[b] Best values quoted with optimum shielding are about 0.4 $(c/m)/cm^3$ for 90 keV → 3 MeV.

[c] Approximately (relative efficiency divided by square root of background) which is applicable when backgrounds are large compared to signal strength. The relative efficiency is the product εV.

[d] Estimated from data given in Ref. 6.

Table II. COMPARISON OF ACTIVATION ELEMENTS WITH MANGANESE

	$_{25}V$	$_{23}Mn$	$_{11}Na$	$_{45}Rh$	$_{53}I$	$_{49}In$
Primary active isotope	^{52}V	^{56}Mn	^{24}Na	^{104}Rh	^{128}I	^{116m}In
Abundance of primary isotope, %	99.76	100	100	100	100	95.7
Secondary isotope	^{50}V[a]	none	none	none	none	^{114m}In[b]
Appropriate soluble salt	$VOSO_4$	$MnSO_4$	$NaSO_4$	$Rh_2(SO_4)_3$	I_2O_2	$In_2(SO_4)_3$
Availability in chemically pure form	limited	readily	readily	costly	readily	readily
Solubility in cold water, g/liter	700	520	500	V.S.[c]	1874	V.S.[c]
Half-life of primary isotope	3.7 m	2.58 h	14.7 h	4.4 m[d]	25 m	54 m
Cycle time	1 h	2 d	2 wk	1 h	½ d	1 d
Gamma energy, MeV	1.4	0.85,1.8,2.1	2.7,1.4	0.052[e]	0.46	0.4,1.1,1.25
Useful gammas/disintegration	1	1.43	2	1	0.17	2
Beta end-point, MeV	2.7	0.7,1.0,2.8	1.4	—	2.1,1.7	1,0.87,0.60
Suitable for coincidence calibration	yes	yes	yes	no	no	maybe[f]
Cost, $/kg	6	0.25				
Activation cross section, barns	4.9	13.2	0.56	12	5.6	150
Relative sulphur cross section	0.10	0.038	0.89	0.125	0.0	0.005
Relative gamma counting efficiency	1	1	1	0.1	1	1
Relative neutron capture[g]	0.34-0.78[h]	1	0.2	1	0.85	1.2
Relative gamma/disintegration	0.67	1	1.3	0.67	0.11	1.3
Relative signal rates[i]	0.22-0.52	1	0.26	0.067	0.093	1.6
Figure of merit[j,k]	0.47-0.72	1	0.51	0.26	0.33	1.15

Table II (Contd.)

[a] ^{50}V is essentially stable, and the effect of an 80-barn cross section would be about half the absorption rate of sulphur.

[b] ^{114m}In has a 50-d half life, a 3.5% yield of detectable gammas, and an 8-barn thermal cross section. At constant irradiation this would produce a 0.12% effect in 1 y.

[c] V.S. = very soluble.

[d] Dominating.

[e] Low yield for other radiation.

[f] Due to effects of 52-barn cross section for 13s isomer which yield 3 MeV beta without a gamma transition.

[g] Based on cross section and concentration with manganese as a basis.

[h] The low value is for 200 g/liter $VOSO_4$; the high value is for 700 g/liter.

[i] (Gamma efficiency) × (gamma/disintegration) × (neutron capture)

[j] Based on (relative signal rates)$^{\frac{1}{2}}$ which is valid when background rates can be neglected.

[k] A penalty for decay enroute to the counter has not been applied.

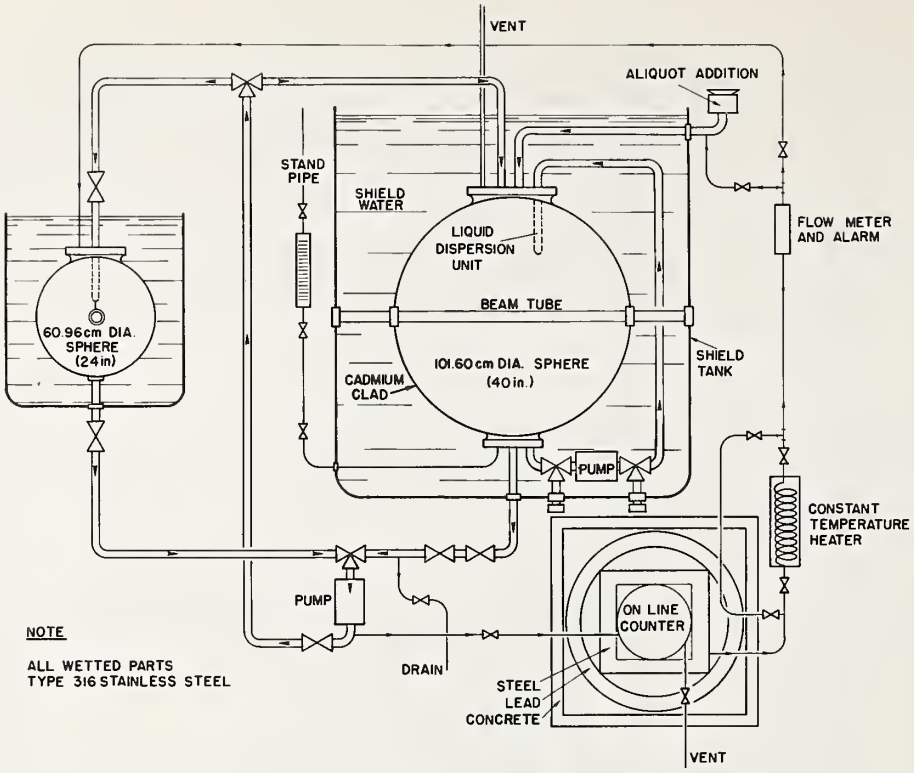

Fig. 1. Circulation system for manganese bath with continuous monitor.

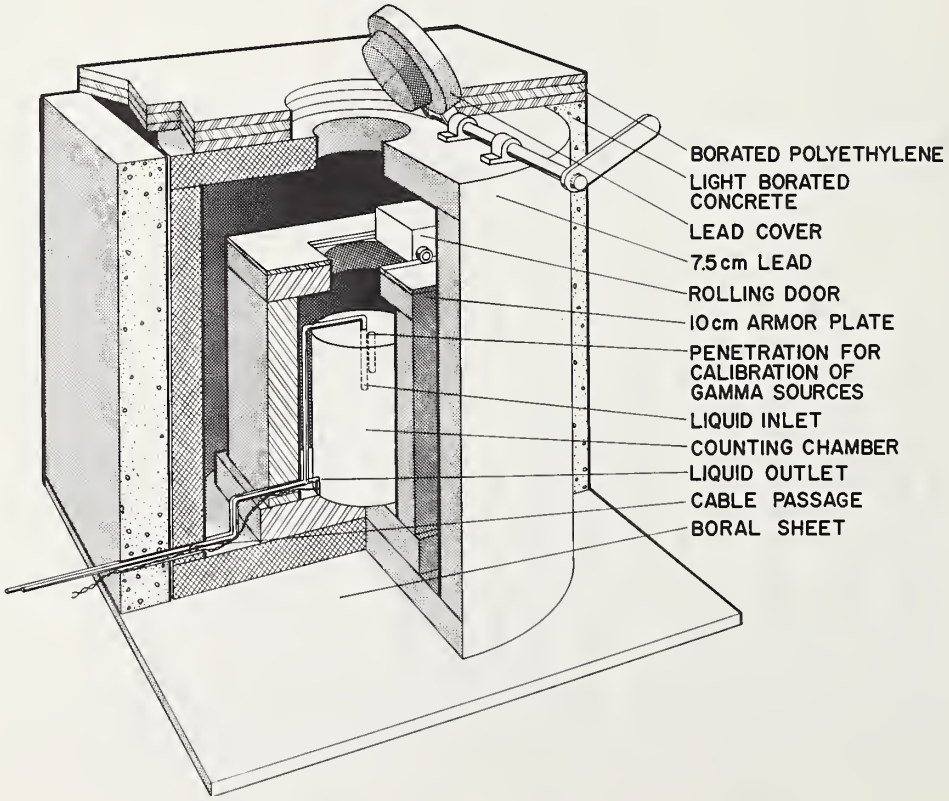

Fig. 2. Shielding arrangement for on-line counter used with manganese bath.

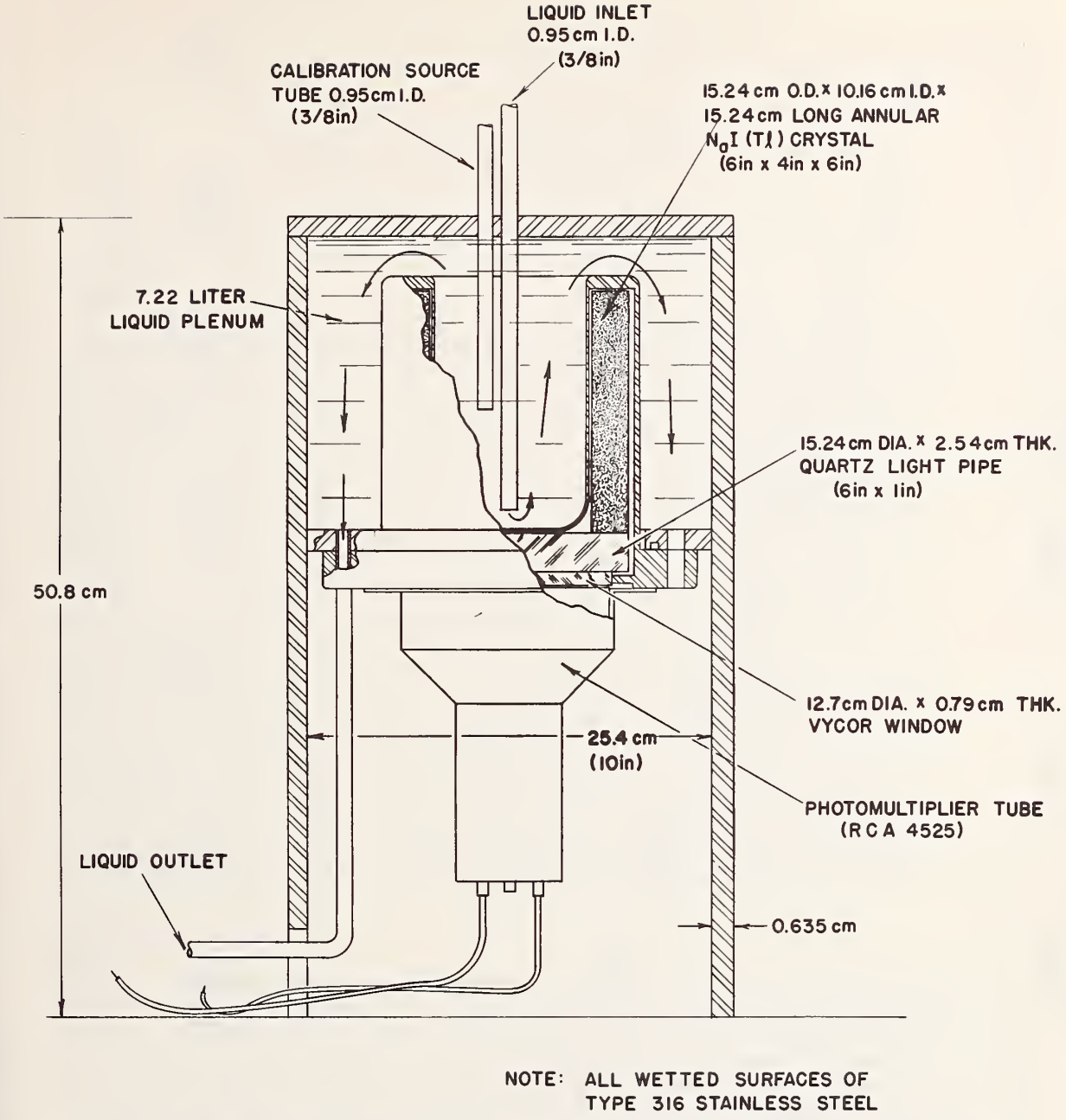

Fig. 3. Some construction details for annular sodium-iodide crystal used as gamma-ray detector of ^{56}Mn activity.

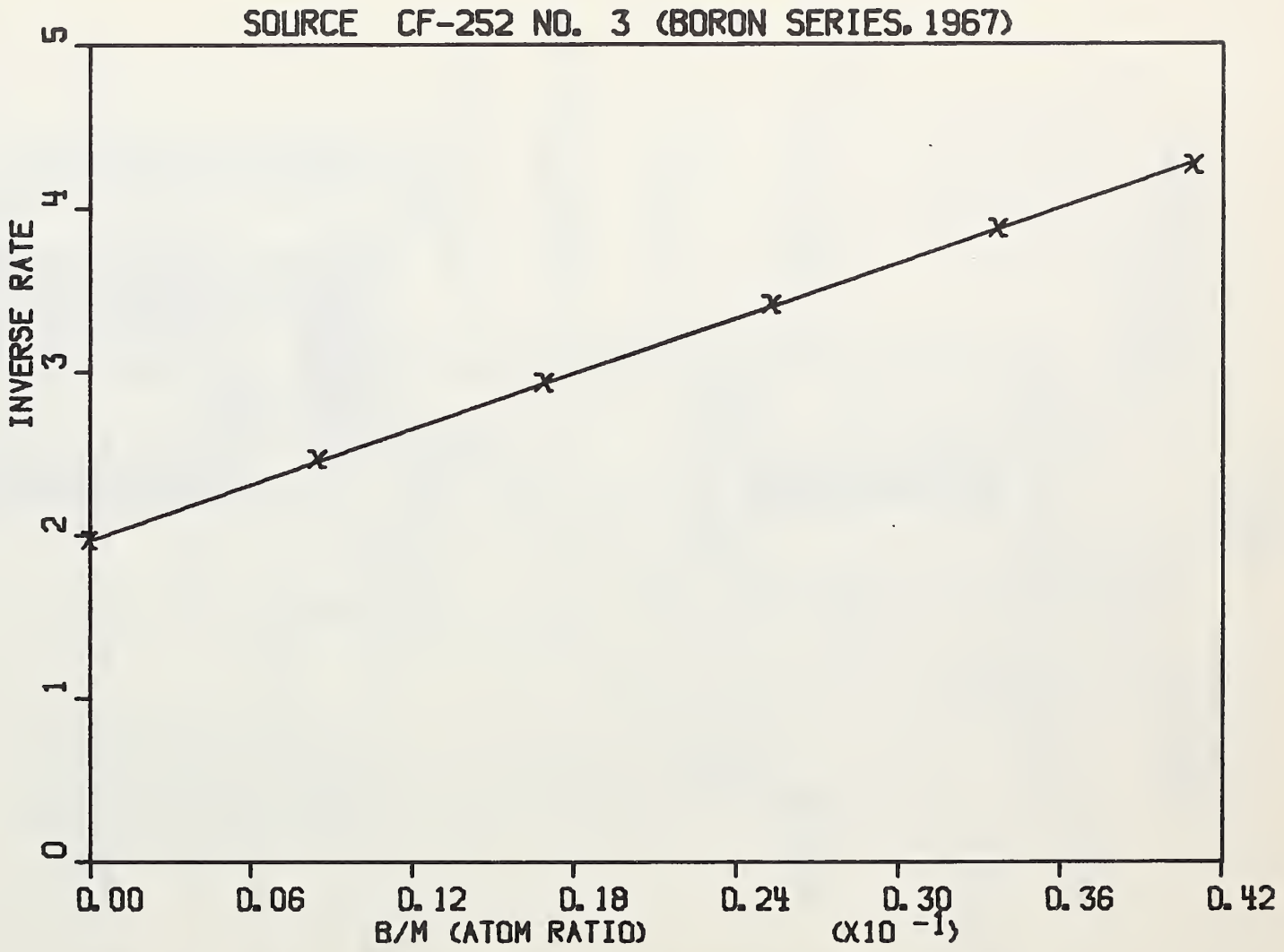

Fig. 4. The reciprocal count rate on the manganese bath plotted as a function of natural boron poison (atom ratio) added to the solution. The slope corresponds to the boron/manganese cross-section ratio.

Non Elastic and Some Inelastic Cross Sections in C^{12} and N^{14} at 15.3 Mev

Luisa F. Hansen, John D. Anderson,
Marion L. Stelts and Calvin Wong

University of California
Lawrence Radiation Laboratory, Livermore, California 94550

Abstract

Neutron cross sections in C^{12} and N^{14} have been measured at 15.3 Mev by means of the sphere transmission technique in conjunction with the time-of-flight facilities at Livermore. The carbon targets were solid spheres of 0.5, 1.3 and 3 mean free paths radius, while the nitrogen target was a spherical dewar of one mean free path. The analysis of the data has been done using the Livermore Monte Carlo Neutron Transport Program (SORS). To obtain agreement with the data, a revision of some of the cross sections and respective angular distributions was required, which resulted in a dramatic improvement in the quality of the fits to the measured time spectra. Very good agreement with the experimental results in C^{12} has been obtained with a SORS calculation that includes a σ_t = 1340 mb, σ_{ne} = 550 mb, an (n,n') cross section of 200 mb to the 4.43 Mev and 100 mb to the 9.6 Mev levels. The angular distribution for the 4.43 Mev level was taken from the literature, while the 9.6 Mev angular distribution was assumed to be isotropic. For N^{14} fair agreement between the calculations and the measurements was obtained for the following cross sections: σ_t = 1570 mb and σ_{ne} = 706 mb. The (n,n') cross sections to the first 6 excited levels inclusive was 200 mb, while 446 mb accounted for the rest of the (n,n') cross sections. The non-elastic cross sections obtained for C and N, corrected for multiple scattering, were (554 ± 30) mb and (600 ± 30) mb, respectively.

1. Introduction

Pulsed integral experiments performed with good time resolution permit the study of the non-elastic and inelastic differential neutron cross sections for a given incident neutron energy in great detail. In the present work, we have undertaken the study of neutron cross sections in C and N for 15 Mev incident neutrons. A spherical geometry was chosen for the target to reduce the complexity of the calculations to a one dimensional problem. The resolution of the measurements was such that they were sensitive not only to the magnitude of the elastic and inelastic cross sections, but also to the shape of the respective angular distribution. In order to obtain detailed agreement between calculated and measured time spectra, it was necessary to remove many of the simplifying assumptions regarding the magnitude and shape of the neutron cross sections.

---

*Work performed under the auspices of the U. S. Atomic Energy Commission.

Not only are these integral measurements sensitive to the total and differential cross sections, but they are also a very attractive tool for checking input cross sections and assumptions in neutron transport codes.

2. Experimental Set Ups

The measurements were made using the time-of-flight facilities at Livermore [1,2]. There are ten detectors at 15° intervals between 3° and 135° with a 10.3 meter flight path. The neutron detectors are 2" x 2" cylindrical plastic scintillators. The bias of the counters was set at 1.6 Mev which allowed us to obtain inelastic cross sections for excitation energies as high as 12 Mev in the target nucleus. The neutron beam was obtained from the $T(d,n)\alpha$ reaction. A third harmonic D_3^+ beam from the 90-inch variable energy cyclotron of around 1.5 Mev swept at $f_o/2$ produced deuterons of 0.5 Mev which struck a tritium loaded target and produced neutron bursts of nominal energy 15 Mev at 0° with a 2 mHz repetition rate. The neutron production at the tritium target was monitored with a solid state detector which counted the α's emitted at 174° from the deuteron beam-line. This enabled us to extract absolute cross sections from the measurements. The carbon targets were solid spheres of 0.5, 1.3 and 3 mean free paths radius, while the nitrogen target was a spherical dewar of one mean free path. All these targets were centered at the tritium target.

3. Experimental Results and Discussion

A typical time-of-flight spectrum is shown in Fig. 1. The data was analyzed using SORS[3]; the output of the program was modified in such a way that it gave for each neutron leaving the target sphere and arriving at the detector position its x,y,z coordinates, its direction cosines, velocity and time of arrival. All of this information was stored on a magnetic tape. A separate edit program was written to fold in the detector efficiency and time resolution of the system. In Fig. 2 is shown the calculated spectrum using SORS. The experimental spectrum from Fig. 1, corrected for background and converted to absolute time of flight, is also shown. The calculation assumed an elastic cross section of 831 mb and non-elastic cross section of 554 mb, [the (n,α) and (n,p) cross section was 90 mb while the total (n,n') cross section was 464 mb]. On the other hand, the published neutron cross sections for C between 14 and 15 Mev neutrons are as follows[4]: Elastic, (790 ± 50) mb; non-elastic, (550 ± 50) mb; inelastic, (220 ± 30) mb to the 4.43 Mev level, 96 mb to the 9.6 Mev level, and 124 mb for excitation of the 10.84, 11.1 and 11.81 Mev levels. The sum of the cross section to the inelastic levels is 440 mb which is in good agreement with the 464 mb used in SORS. The difference of ~20 mb could be

attributed to the excitation of the 7.6 Mev level[5]. The large discrepancy in magnitude and shape between the calculated and measured time spectrum can be explained as follows:

I. The large discrepancy in magnitude by a factor of 2 to 4 between 22.5 and 32.5 shakes (10^{-8} sec) is due to the fact that in the neutron transport code only one inelastic level is considered. In the case of C, the total inelastic cross section of 464 mb was assigned to the 4.43 Mev level. Furthermore, the shape of the calculated time spectrum in this region was incorrect due to the fact that an approximate shape was assumed for the angular distribution of the neutrons to the 4.43 Mev level (a two-step histogram in which 75% of the neutrons were between 0 and 90°.

II. The discrepancies in the region between 20 to 22.5 sh. and 25 to 27.5 were found to be the result of two simplifying assumptions used in the calculations: (a) the (d,t) reaction is isoergic and (b) it is isotropic. Once the proper energy and angular dependence were taken into account, the agreement for the above regions was improved.

III. In order to fit the region beyond 32.5 sh., the neutron inelastic cross section to the 9.6 Mev level was inserted into the neutron cross section library. The angular distribution was taken to be isotropic[5] with a total cross section of 100 mb.

IV. The discrepancy in the height of the elastic peak was due to a poor estimate of the 0° cross section. A revision of the neutron elastic angular distribution input in the library was required to bring it in better agreement with experimental measurements at 14.8 Mev [6,7]. Also, the cross section at 0° was calculated according to the Wick's limit[8] which raised the value from 550 to 750 mb/sr. These changes in the elastic angular distribution brought the calculated height for the elastic peak in better agreement with the measurements.

The overall effect of the changes introduced in Steps I, II, III and IV on the predictions of SORS can be seen in Fig. 3. This calculation was done with the following values for the cross sections: elastic = 829 mb, non-elastic = 550 mb, $\sigma_{4.43\ \text{Mev}}$ = 200 mb with the proper angular distribution taken from the literature[6,7] and $\sigma_{9.6}$ = 100 mb. The shaded area corresponds to an energy interval between 7.6 and 6.3 Mev neutrons, and two effects can be contributing to the discrepancy in this area: (1) A small contribution could be

due to inelastic scattering to the 7.66 Mev level[5], (2) the rest is the result of the minimum in the carbon total cross section which has been smoothed out in the input cross sections.

The discrepancy beyond 45 sh., although not much larger than the statistical accuracy of the measurements, is real. It results from the contribution of low energy neutrons coming from higher inelastic levels which were not included in our calculation. This effect is better seen for the C sphere of 3 mean free path radius. Figure 4 shows SORS predictions calculated as in Fig. 3 (curve a). If the 120 mb cross section corresponding to the 10.8-11.1 and 11.8 Mev levels is added to the 9.6 Mev level cross section, the results are given by curve b. As the 9.6 Mev level contribution is expected at around 35 sh., (neutrons inelasticly scattered from the 9.6 Mev level at forward angles) the counts in this region are therefore overestimated by 30 to 50%. However, beyond 40 sh., the agreement with the measurements is improved, since some of these low energy neutrons come from inelastic scattering from higher excited levels which are crudely accounted for by inclusion into the 9.6 Mev level. Beyond 50 sh., the neutron spectrum is being modified by the detector bias, such that the contributions from the backward angle scattering from higher levels is not seen.

The non-elastic cross sections corrected for multiple scattering were 571 mb and 538 mb for the 0.5 and 1.3 mean free path radius spheres, respectively. For the largest carbon sphere, a value of 550 mb gave good agreement with the measurements. The value of (554 $\pm$ 30 mb) obtained from these measurements is in good agreement with previously reported values[9,10].

4. Nitrogen Measurements

The measured time of flight spectrum from nitrogen bombarded with 15.3 Mev neutrons for a one mean free path target thickness is shown in Figure 5. The predicted spectrum using SORS is also shown. The calculations were done using the following cross section: elastic, 864 mb; non-elastic, 706 mb, which was distributed as follows: 646 mb account for the neutron inelastic cross sections, 40 mb, 15 mb and 5 mb account for the (n,α), (n,p), and (n,2n) cross sections, respectively. The (n,n') cross section is distributed as follows: a total of 200 mb were assigned to the sum of the cross sections from the 3.95 Mev, 5.10 Mev, 5.75 Mev, 7.07 Mev and 7.95 Mev levels, with the cross sections for each level given according to the following ratios with respect

to the total sum: .240, .238, .283, .166, and .079. The cross section for the 2.31 Mev level was assumed negligible.

The same angular distribution shape was taken for all the inelastic levels: slightly forward peaked, with the ratio of the cross sections 0 - 90° to 90° - 180° equal to 1.5. This is a very close representation of the measurements[11]. At the present time, a revision of the cross sections and angular distribution of the elastic scattering input in the Code is in progress to explain the discrepancies between measurements and calculations.

5. Conclusions

The resolution of the neutron time of flight spectra, obtained from these integral measurements, was such that it enabled us to extract values for some of the inelastic neutron cross sections. For carbon, the cross sections to the 4.43 and 9.6 Mev levels were determined with an accuracy of 10% and 30% respectively, i.e., $\sigma_{4.43\ \text{Mev}} = 220 \pm 20$ mb and $\sigma_{9.6\ \text{Mev}} = 100 \pm 30$ mb. The non-elastic cross section has been determined with a 5% uncertainty: (554 ± 30) mb. Furthermore, the measurements were sensitive to the shape of the angular distributions to the ground state and first excited level in C.

For the nitrogen, where the levels are much closer, the resolution was insufficient to identify the neutron groups. However, once the discrepancies between calculations and measurements are resolved, it will be possible to obtain a value for the neutron inelastic cross section for the sum of the first 6 excited levels plus the average cross section to the levels above 7.95 Mev excitation energy.

Using pulsed sphere techniques, it is clear that one can obtain integral inelastic cross sections. Under favorable conditions, differential information can also be obtained.

6. REFERENCES

1. B. D. Walker, J. D. Anderson, J. W. McClure and C. Wong, Nucl. Instr. Methods 29, 333 (1964).

2. R. Swenson and C. Wong UCRL-7905T and Proc Karlsruhe Conf. Automatic Acquisition and Reduction of Nuclear Data (1964).

3. Ernest F. Plechaty, private communication.

4. Neutron Cross Sections, BNL 325, Sup. No. 2, (1964).

5. R. Bouchez, J. Duclos and P. Perrin, Nucl. Phys. 43, 623 (1963).

6. J. D. Anderson, C. C. Gardner, J. W. McClure, N. P. Nakada and C. Wong, Phys. Rev. 111, 572 (1958).

7. Robert W. Peelle, Phys. Rev. 105, 1311, (1957).

8. G. C. Wick, Phys. Rev. 75, 1459 (1949).

9. Malcolm H. MacGregor, William P. Ball and Rex Booth, Phys. Rev. 108, (1957).

10. Arun Challerjee and A. M. Ghose, Phys. Rev. 161, 1181, (1967).

11. Harry Lutz, private communication.

TIME OF FLIGHT NEUTRON SPECTRUM FROM C^{12} BOMBARDED WITH 15.28 MeV NEUTRONS

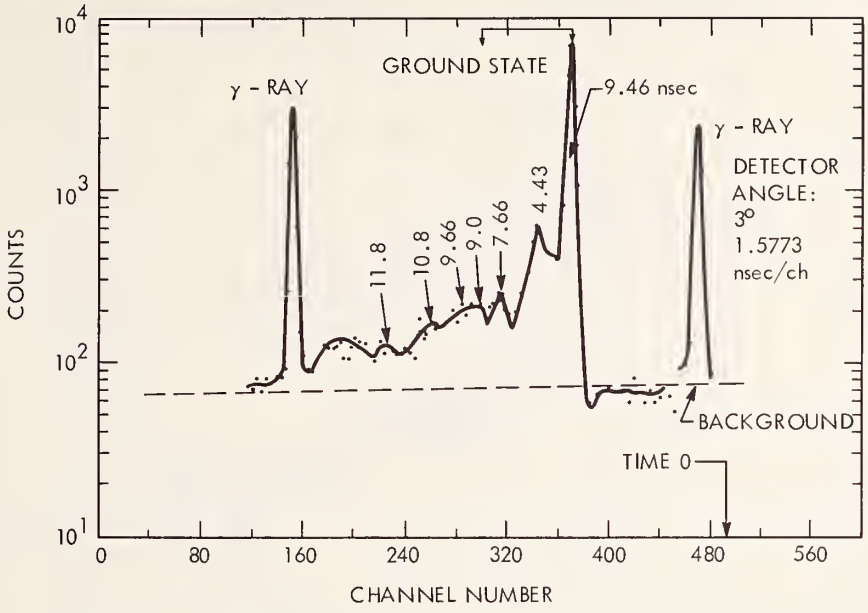

Fig. 1. Neutron time of flight spectrum from C^{12} bombarded with nominal 15 Mev neutrons. The positions at which the excited levels in C begin to contribute are indicated.

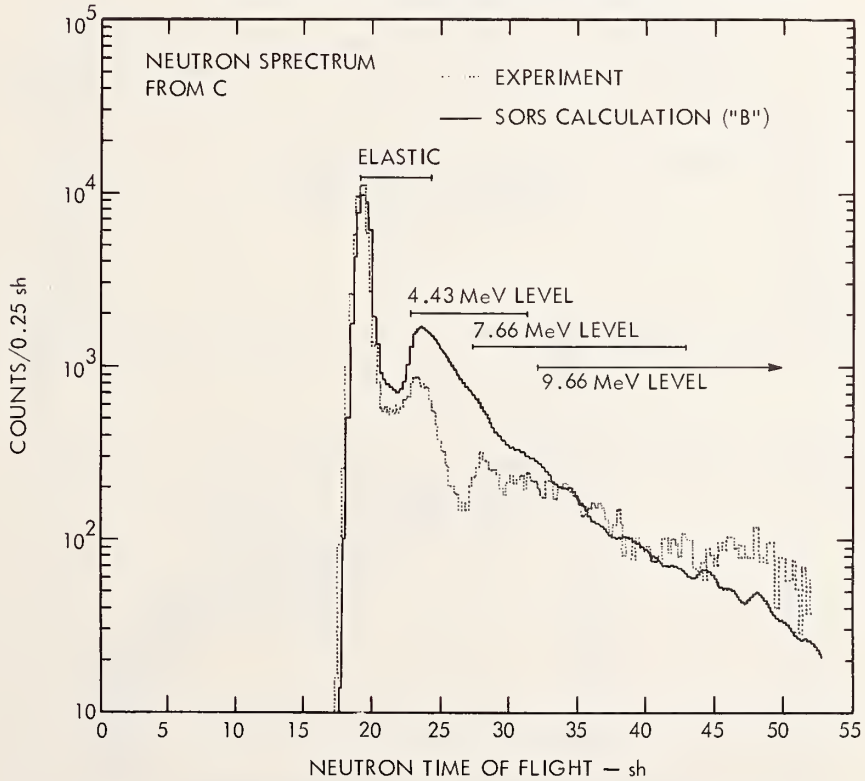

Fig. 2. Comparison of calculated and measured neutron time of flight spectrum using common neutron transport assumptions. See text for explanation of discrepancy.

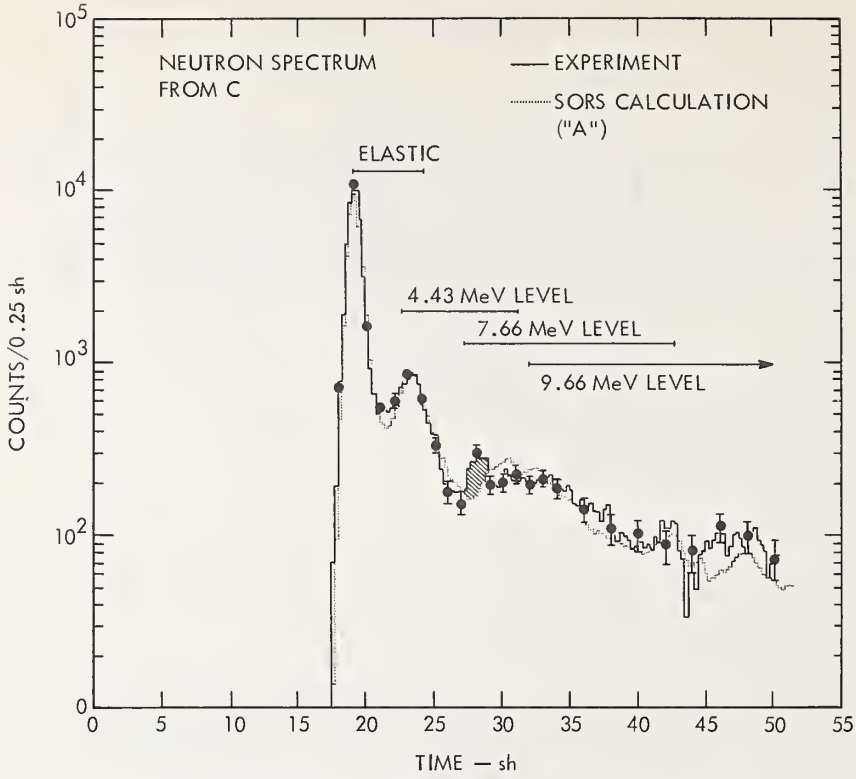

Fig. 3. Comparison of computed and measured neutron time of flight spectrum using the revised SORS neutron transport calculation.

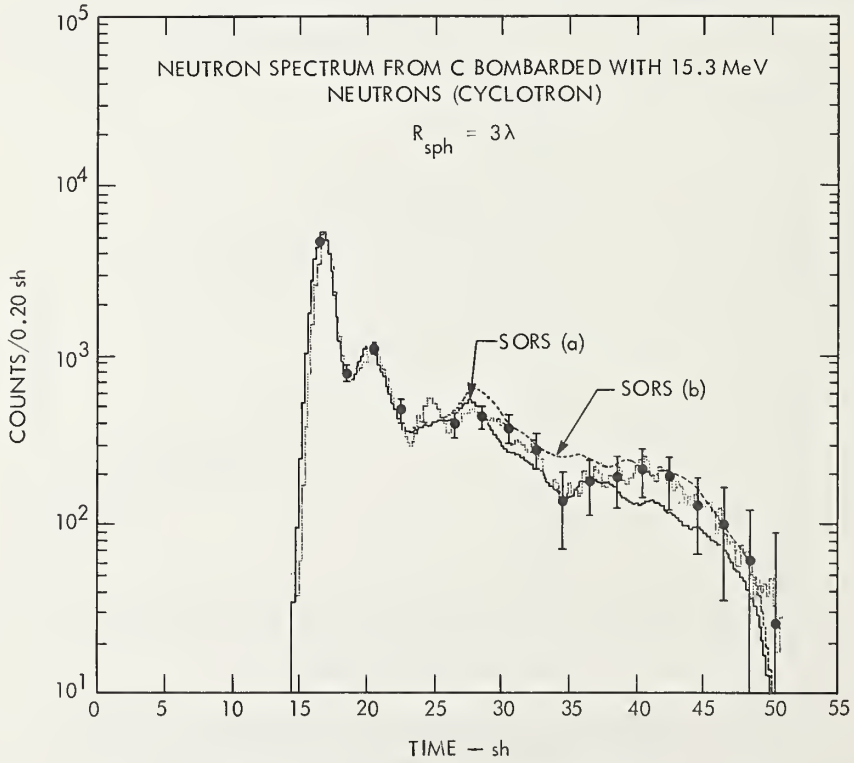

Fig. 4. Comparison of computed and measured neutron time of flight spectrum as a function of the input cross sections for the 9.6 Mev level: SORS(a) $\sigma_{9.6\ Mev}$ = 100 mb and SORS(b) $\sigma_{9.6\ Mev}$ = 220.

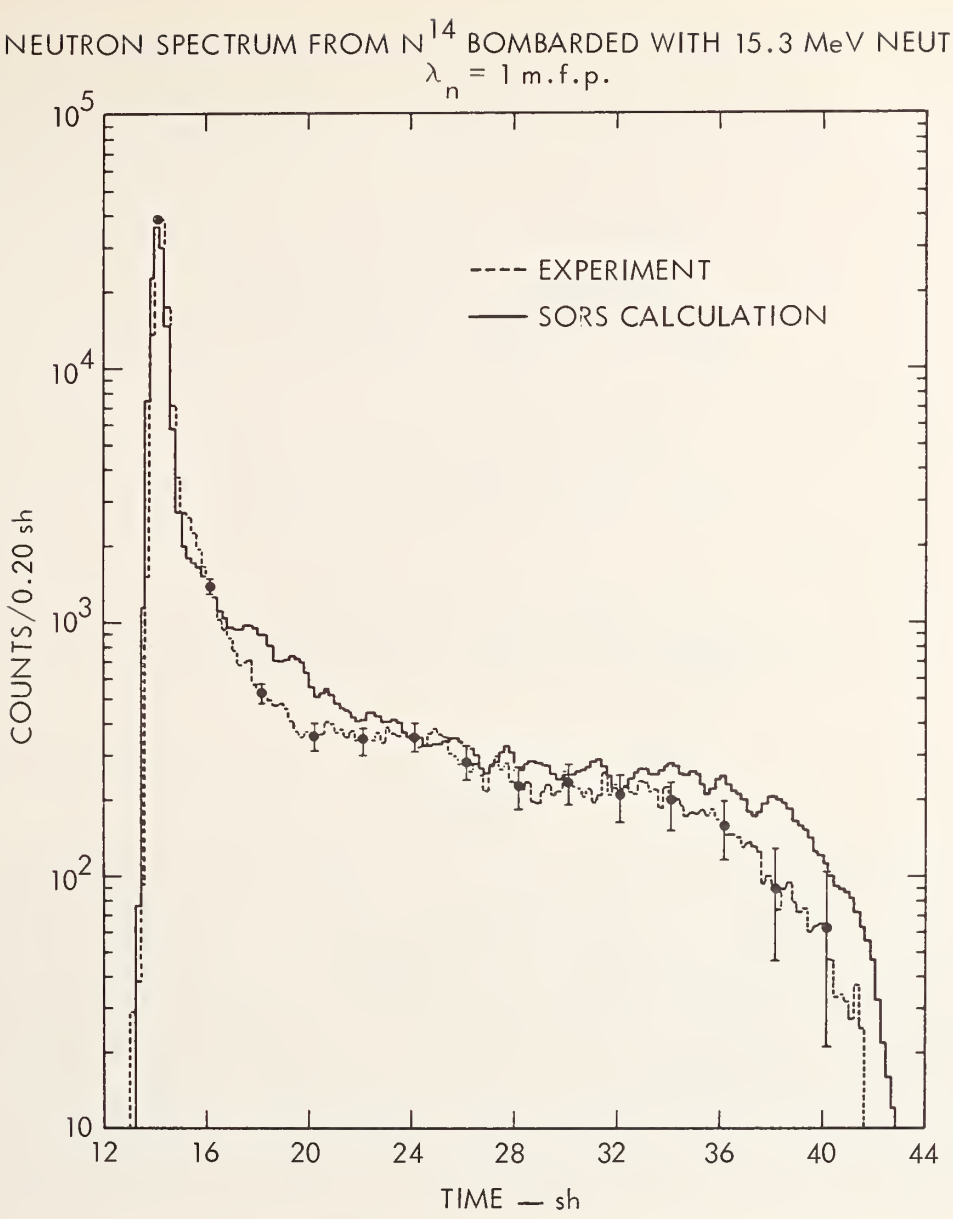

Fig. 5. Comparison of computed and measured time of flight spectrum for N^{14}.

NEUTRON DIFFERENTIAL CROSS SECTION EVALUATION BY A MULTIPLE FOIL ACTIVATION ITERATIVE METHOD*

W. N. McElroy and J. A. Ulseth

Battelle Memorial Institute
Pacific Northwest Laboratory
Richland, Washington 99352

S. Berg

TRW Systems Group of TRW, Inc.
Redondo Beach, California 90277

G. Gigas and T. B. Crockett

Atomics International
A Division of North American Rockwell Corp.
Canoga Park, California 91311

ABSTRACT

A multiple foil activation iterative method is being studied and used to evaluate differential cross sections for reactions useful for determining fast reactor neutron flux spectra. This multiple foil activation method involves irradiation of a selected set of detectors (usually 10 to 15), measurement of resultant activities, and determination of appropriate iterative solution differential flux spectra for dissimilar reference neutron environments. These reference spectra, and corresponding measured activities for foils of a single reaction, are used in an inverted iterative process to obtain the evaluated differential cross section curve. Results are presented of the application of this method to the preliminary evaluation of differential cross section data for $^{27}Al(n,\alpha)^{24}Na$, $^{58}Ni(n,p)^{58}Co$, and $^{54}Fe(n,p)^{54}Mn$.

This paper is based, in part, on work performed under United States Atomic Energy Commission Contracts AT(45-1)-1830 and AT(11-1)-GEN-8, and has been assigned BMI Report Number BNWL-SA-1527.

313-475 O-68—17

1. INTRODUCTION

The multiple foil activation iterative method, in addition to providing experimental measurement of neutron flux spectra, affords a procedure for independent determination and evaluation of foil reaction differential cross section data. The method provides a direct experimental means of adjusting existing differential cross section data to attain consistency with integral activity measurements. This consistency is, in general, lacking in current differential cross section evaluations.

A manual iterative method for determining neutron flux spectra by foil activation has been previously reported.[1] A fully-automated computer code (SAND-II)* has been developed to perform the spectral analysis by an iterative method qualitatively similar to that described.[2]

Foil activation data for different types of neutron environment have been analyzed to establish: (1) the reliability of neutron flux spectrum and fluence determination by calculations (diffusion, transport, and Monte Carlo techniques), spectrometry, and foil activation methods; (2) the effect of spectral variations on calculated spectrum-averaged cross sections used to report fluxes and fluences.

In each of the 11 environments studied, a set of foil detectors, including low and high energy neutron reactions, was irradiated. Measured activities for each foil set were used as input to the code to obtain an appropriate solution flux spectrum.[3]

For each environment, the integral neutron flux solution over the energy range from 10^{-10} to 18 MeV should be accurate to within ±10 to 30%.[2] The differential flux spectral solutions are expected to have larger errors, and reflect fluctuations resulting from the errors in foil reaction cross sections and measured activities. The use of a large number of foils with overlapping energy regions of sensitivity, and subsequent examination of the solution differential spectral structure, has helped to distinguish the true structure from that which may be caused by cross section and activity measurement errors.

The mathematical procedure involved in the determination of spectra from the monitor activation and the differential activation curve can be inverted to define the shape of the activation curve if the neutron spectra are determined. The spectra can be determined independently or may be determined in the same experiment by the activation of other monitor materials whose activation cross sections are known. The success of the spectral determination effort prompted this investigation of cross section determination.

---

* *The SAND-II (Spectrum Analysis by Neutron Detectors-II) code has been written in Fortran IV for the CDC 6600 and Univac 1108 computers. The code uses a discrete energy interval model of 620 intervals over the energy range, 45 per decade up to 1 MeV, and 170 from 1 to 18 MeV.*

The discussion that follows includes a brief review of the multiple foil activation method and of the technique by which foil reaction cross section data may be evaluated using this method. Preliminary results are reported in which the authors have used the iterative method to evaluate the differential cross section data for the $^{27}Al(n,\alpha)^{24}Na$, $^{58}Ni(n,p)^{58}Co$, and $^{54}Fe(n,p)^{54}Mn$ reactions.

2. MULTIPLE FOIL ACTIVATION ITERATIVE METHOD

The absolute magnitude and shape of the differential cross section for the foil reaction being studied can be established by (1) irradiating a detector [such as iron foils for the $^{54}Fe(n,p)^{54}Mn$ reaction] in each of "m" different neutron environments, (2) determining the corresponding values of saturated activity, and (3) solving the system of activation integral equations:

$$A_j = \int_o^\infty \sigma^{[K]}(E)\ \phi_j(E) \quad (j = 1,\ldots m).* \tag{1}$$

In equations (1), A_j is the measured value of saturated activity for the j^{th} environment, $\phi_j(E)$ is the corresponding differential flux, and $\sigma^{[K]}(E)$ is the foil reaction differential cross section solution [evaluated $\sigma(E)$] at the K^{th} iteration. The "m" different spectra might be provided, for example, by placing different absorbers and scatterers in the path of a well-collimated beam from a high intensity reactor or other neutron source.

Successful application of this procedure requires a reasonable determination of the form and absolute magnitude of the "m" differential spectra. This information can be acquired with a combination of the multiple foil activation iterative method and existing neutron spectrometry. (In the present work, only results based on the multiple foil activation method are used.) Spectrometry can provide detailed spectral structure, and the multiple foil method, using a comprehensive set of foil detectors, can determine the absolute magnitude and verify overall shape.

The current iterative procedure used to solve equations (1) requires an initial differential cross section approximation $\sigma^{[O]}(E)$** and measured

---

* *In practice, an exponential term appears in the integral to account for attenuation by cover materials such as cadmium; it is omitted throughout this paper as a matter of convenience.*

** *A smooth fit to previous experimental data and/or theoretical predictions can be used as input -- only the relative shape of the differential cross section curve needs to be specified since the iterative procedure determines the absolute magnitude.*

values of A_j and $\phi_j(E)$ as input. The computer code CAND-II (Cross section Analysis by Neutron Detectors-II) is being used to perform the numerical steps of iteration. [This code differs from SAND-II, used to determine the $\phi_j(E)$'s, only in the format used for the tabulated cross section input and output.]

3. CROSS SECTION EVALUATION

Studies are in progress to investigate the reliability of the iterative procedure in determining $\sigma^{[K]}(E)$ solutions for foil reactions of interest for use in fast reactors. The sensitivity of the solutions to uncertainties in reference spectrum shape and activity measurements and to the selection of different reference spectra is being studied. Eleven measured reference spectra [$\phi_j(E)$'s determined by the SAND-II code, $j = 1,...11$] with corresponding measured activities [A_j] for several reactions are being used. CAND-II solutions $\sigma^{[K]}(E)$ have been obtained for the reactions $^{54}Fe(n,p)^{54}Mn$, $^{58}Ni(n,p)^{58}Co$, and $^{27}Al(n,\alpha)^{24}Na$ using both reasonable input forms [$\sigma^{[O]}(E)$ determined by selecting a best fit curve to existing differential data] and unreasonable input forms [$\sigma^{[O]}(E)$ assumed to be a constant, a straight line, etc.]. The outputs, using these different input forms, define an envelope of solutions which help to establish the reasonableness of the best fit solution.

Preliminary results for the $^{27}Al(n,\alpha)^{24}Na$, $^{58}Ni(n,p)^{58}Co$, and $^{54}Fe(n,p)^{54}Mn$ reactions are presented in Figures 1, 2, and 3, respectively. The shaded area in each figure represents the envelope of solutions $\sigma^{[K]}(E)$ based on all the initial approximations, $\sigma^{[O]}(E)$, listed in the figure legends. These results are derived from the use of a total of 7, 9, and 11 reference spectra, respectively. Because three of the spectra used are very similar, the results shown in Figures 1, 2, and 3 are in effect based on 5, 7, and 9 spectra, respectively. [A meaningful solution for equations (1) requires a large number of distinct $\phi_j(E)$'s.] The most reasonable solution for each reaction should be from the $\sigma^{[O]}(E)$ representing a best fit through all available differential data. The CAND-II solution based on this best fit input is identified by the solid curve in each figure. Most of the monoenergetic differential cross section measurements reported in BNL-325 as well as the current BNL evaluated cross section curve[4] are also shown in Figures 1, 2, and 3.

The solution envelope broadens at higher energies for each of the reactions shown in Figures 1, 2, and 3. This indicates lower reliability for the differential solution with increasing energy and is associated with the lack of high energy neutrons, and lack of adequate differences among the 11 reference spectra.* Although the CAND-II solutions based on the best fit inputs should be the best evaluations, they are only approximately correct in differential form because the reference spectra

---

* *For these tests, no real effort was made to select neutron environments that were different enough in the high energy region to provide more nearly unique solutions -- that is, smaller solution envelopes.*

were not dissimilar enough. Nevertheless, the iterative process does adjust the input differential form and magnitude so as to produce consistency with the integral activity measurements -- a necessary condition that is not currently satisfied for most cross section evaluations reported in Reference 4.

Table I provides tabulations of the new $^{54}Fe(n,p)^{54}Mn$, $^{58}Ni(n,p)^{58}Co$, and $^{27}Al(n,\alpha)^{24}Na$ evaluated differential cross sections. Calculated values of fission-averaged cross sections based on these tabulated data for four forms of the fission spectrum are presented in Table II for reference purposes.

4. CONCLUSIONS

Preliminary results indicate that the multiple foil activation iterative method can provide reliable evaluated differential cross sections for neutron reactions, including those of interest in fast reactor flux and fluence measurements. Results for three threshold reactions support these conclusions and further demonstrate that the method produces consistent results even when the spectra used are not very dissimilar. Evaluations based on the multiple foil activation method should be particularly useful for determining spectrum-averaged cross sections of individual foil reactions used for flux and fluence monitors.

Without the continued assistance and encouragement of C. Weber, H. Morewitz, and C. Bingham of Atomics International, this work could not have been accomplished. Since the work reported herein is based on cooperative studies, the authors wish to acknowledge the contributions and assistance of L. Beller, H. Alter, S. Carpenter, and C. Dunford of Atomics International, E. Tochilin of U. S. Naval Radiological Defence Laboratory, R. Armani of Argonne National Laboratory, J. Walker, L. Morrison and C. Mehl of Sandia Corporation, W. Biggers, G. Hansen, and J. Grundl of Los Alamos Scientific Laboratory, and R. C. Barrall of Stanford University. They provided important additional information which helped to establish the accuracy of the foil activation measurements and the iterative neutron flux spectral results.

5. REFERENCES

1. W. N. McElroy, S. Berg, and G. Gigas, "Neutron Flux Spectral Determination by Foil Activation," Nuclear Science and Engineering 27, 533 (March 1965).

2. W. N. McElroy, S. Berg, T. B. Crockett, and R. G. Hawkins, "A Computer-Automated Iterative Method for Neutron Flux Spectra Determination by Foil Activation," Volumes I, II, III, and IV, AFWL-TR-67-41 (September 1967).

3. W. N. McElroy, S. Berg, T. B. Crockett, and R. J. Tuttle, "Measurement of Neutron Flux Spectra by a Multiple Foil Activation Iterative Method and Comparison with Reactor Physics Calculations and Spectrometer Measurements," invited paper, Special Session on Comparison of Fast Reactor Spectrum Measurements, American Nuclear Society, Chicago, Illinois, BNWL-SA-1475 (November 1967).

4. J. R. Stehn, et al., "Neutron Cross Sections," BNL-325, Second Edition, Supplement No. 2 (1965-1966).

5. H. Liskien and A. Paulsen, "Compilation of Cross-Sections for Some Neutron Induced Threshold Reactions," EUR 119.e, European Atomic Energy Community, Euratom (1963).

TABLE I

EVALUATED DIFFERENTIAL CROSS SECTION DATA

Neutron Energy (MeV)	Cross Section (Barns) $^{54}Fe(n,p)^{54}Mn$	Cross Section (Barns) $^{58}Ni(n,p)^{58}Co$	Neutron Energy (MeV)	Cross Section (Barns) $^{27}Al(n,\alpha)^{24}Na$
1.0	0.00*	0.00*	4.6	0.00*
1.1	2.35×10^{-3}	1.86×10^{-3}	4.8	2.19×10^{-5}
1.2	4.25	3.55	5.0	6.47
1.3	6.41	5.44	5.2	1.04×10^{-4}
1.4	9.03	1.08×10^{-2}	5.4	1.78
1.5	1.22×10^{-2}	1.83	5.6	4.68
1.6	1.68	2.38	5.8	9.73
1.7	2.31	3.18	6.0	1.79×10^{-3}
1.8	3.11	4.31	6.2	3.07
1.9	4.00	5.51	6.4	4.74
2.0	4.86	6.76	6.6	7.78
2.2	6.21	8.84	6.8	1.21×10^{-2}
2.4	7.33	1.17×10^{-1}	7.0	1.69
2.6	8.88	1.58	7.1	1.92
2.8	1.20×10^{-1}	2.09	7.2	2.13
3.0	1.53	2.46	7.3	2.10
3.1	1.67	2.46	7.4	2.22
3.2	1.81	2.35	7.5	2.68
3.3	1.99	2.34	7.6	3.11
3.4	2.16	2.33	7.7	3.14
3.5	2.32	2.36	7.8	3.12
3.6	2.48	2.62	7.9	3.59
3.7	2.66	3.07	8.0	4.31
3.8	2.86	3.53	8.1	4.43
3.9	3.00	3.82	8.2	4.24
4.0	3.09	3.98	8.3	4.24
4.5	3.94	4.98	8.4	4.68
5.0	4.84	5.79	8.5	4.98
5.5	5.38	6.33	9.0	6.66
6.0	5.78	6.63	9.5	7.76
6.5	5.93	6.72	10.0	8.70
7.0	6.20	6.71	10.5	9.56
7.5	6.38	6.58	11.0	1.04×10^{-1}
8.0	6.48	6.37	12.0	1.20
8.5	6.51	6.21	13.0	1.32
9.0	6.58	5.94	14.0	1.26
9.5	6.55	5.86	15.0	1.06
10.0	6.38	5.66	16.0	8.63×10^{-2}
11.0	6.19	5.29	17.0	7.33
12.0	5.71	4.91	18.0	6.15
13.0	5.53	4.48		
14.0	4.91	3.86		
15.0	3.85	2.73		
16.0	3.15	1.96		
17.0	2.63	1.16		
18.0	2.26	4.47×10^{-2}		

* *Assigned Value*

TABLE II

CALCULATED FISSION AVERAGED CROSS SECTIONS FOR

Fe, Ni, AND Al

$\phi^f(E)$ - Fission Form[2]	$\bar{\sigma}^f$ - Fission Averaged Cross Section (mb)*		
	$^{54}Fe(n,p)$	$^{58}Ni(n,p)$	$^{27}Al(n,\alpha)$
Watt	95.1	121	0.663
Frye	93.2	118	0.606
Cranberg	89.8	113	0.683
Grundl Adjusted	116.0	147	0.676

---

*

$$\bar{\sigma}^f = \frac{\int_0^\infty \sigma(E)\ \phi^f(E)\ dE}{\int_0^\infty \phi^f(E)\ dE}$$

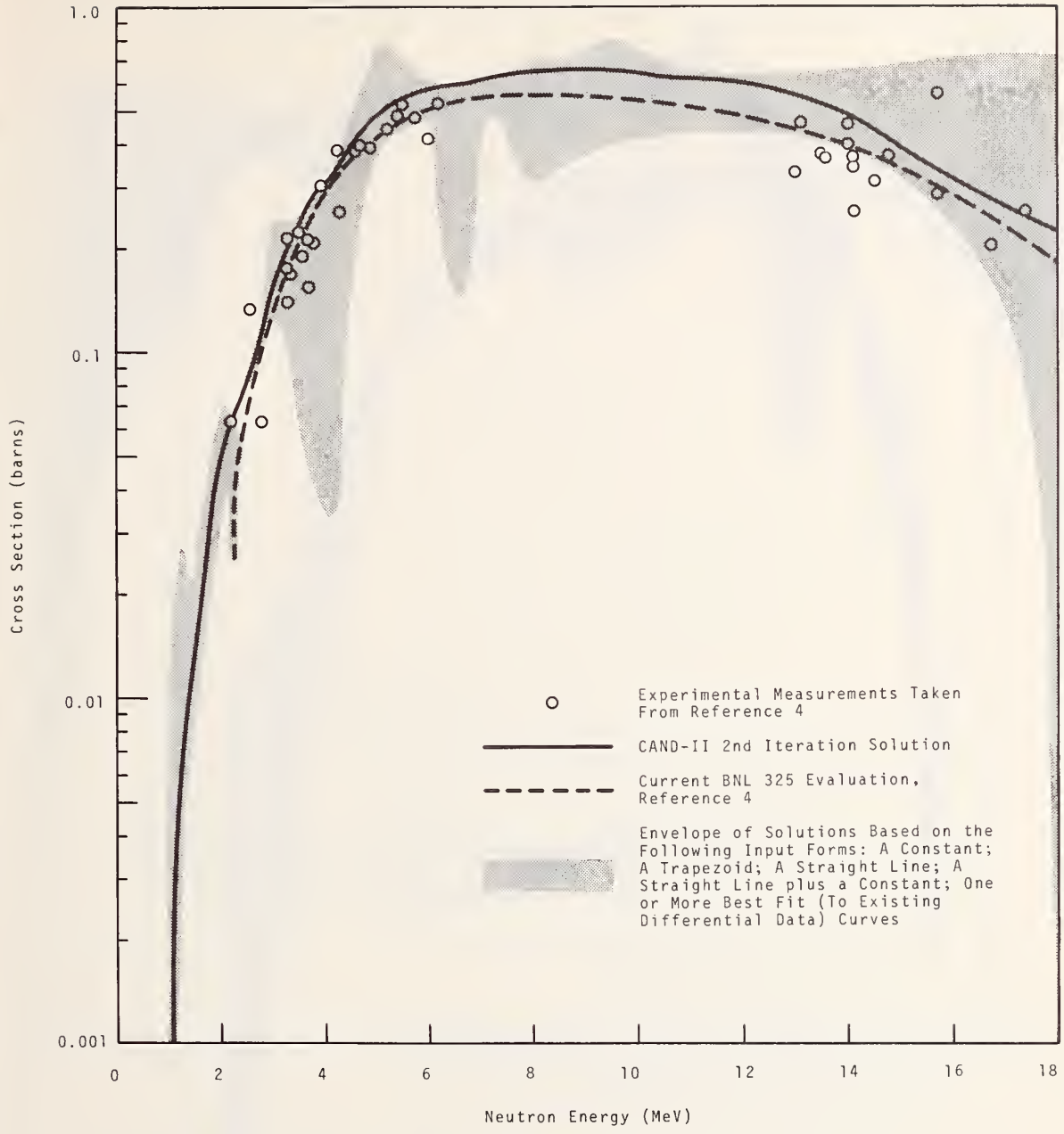

FIGURE 1
CAND-II Solution for $^{54}Fe(n,p)^{54}Mn$ Reaction Cross Section

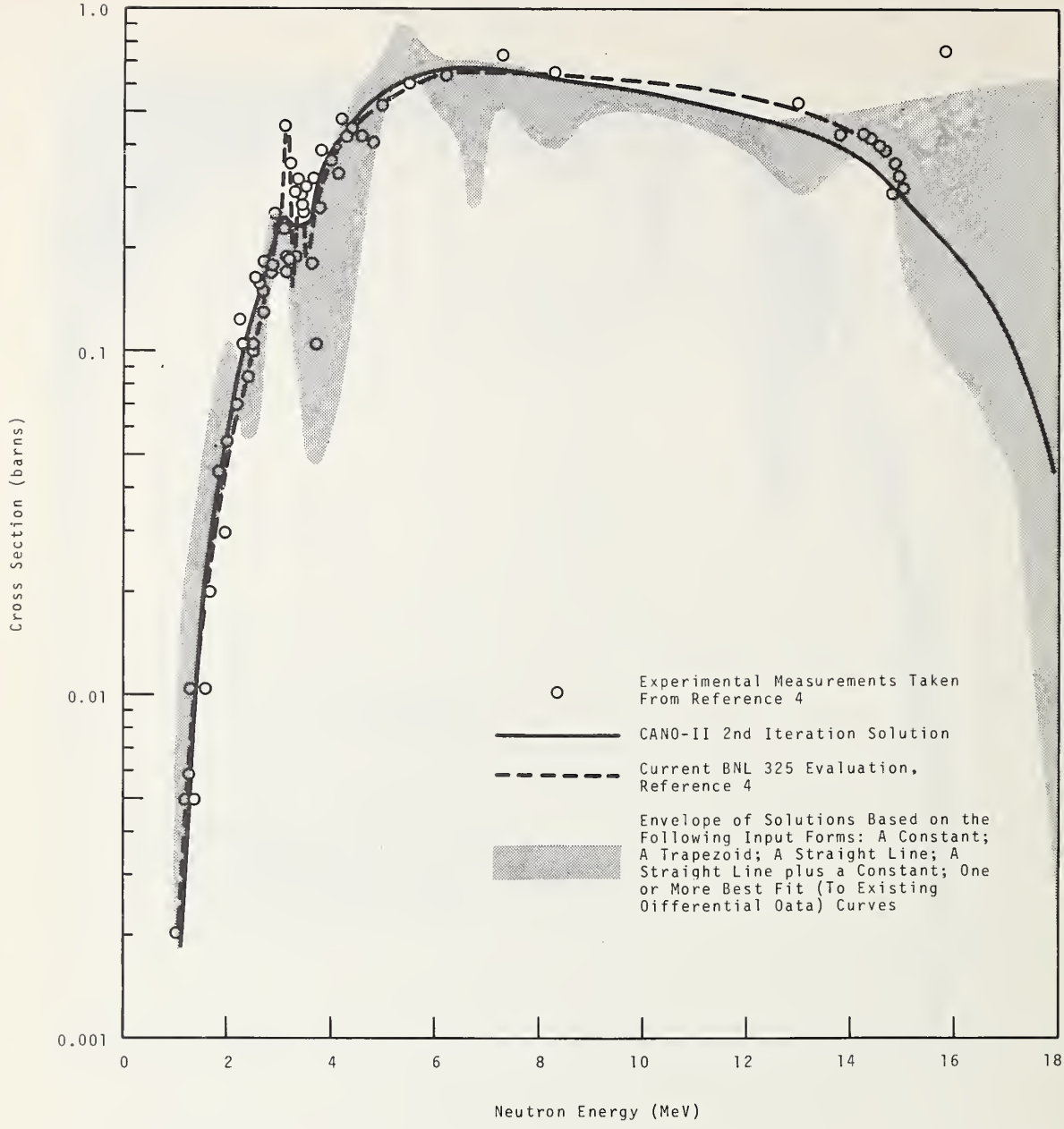

FIGURE 2

CAND-II Solution for $^{58}Ni(n,p)^{58}Co$ Reaction Cross Section

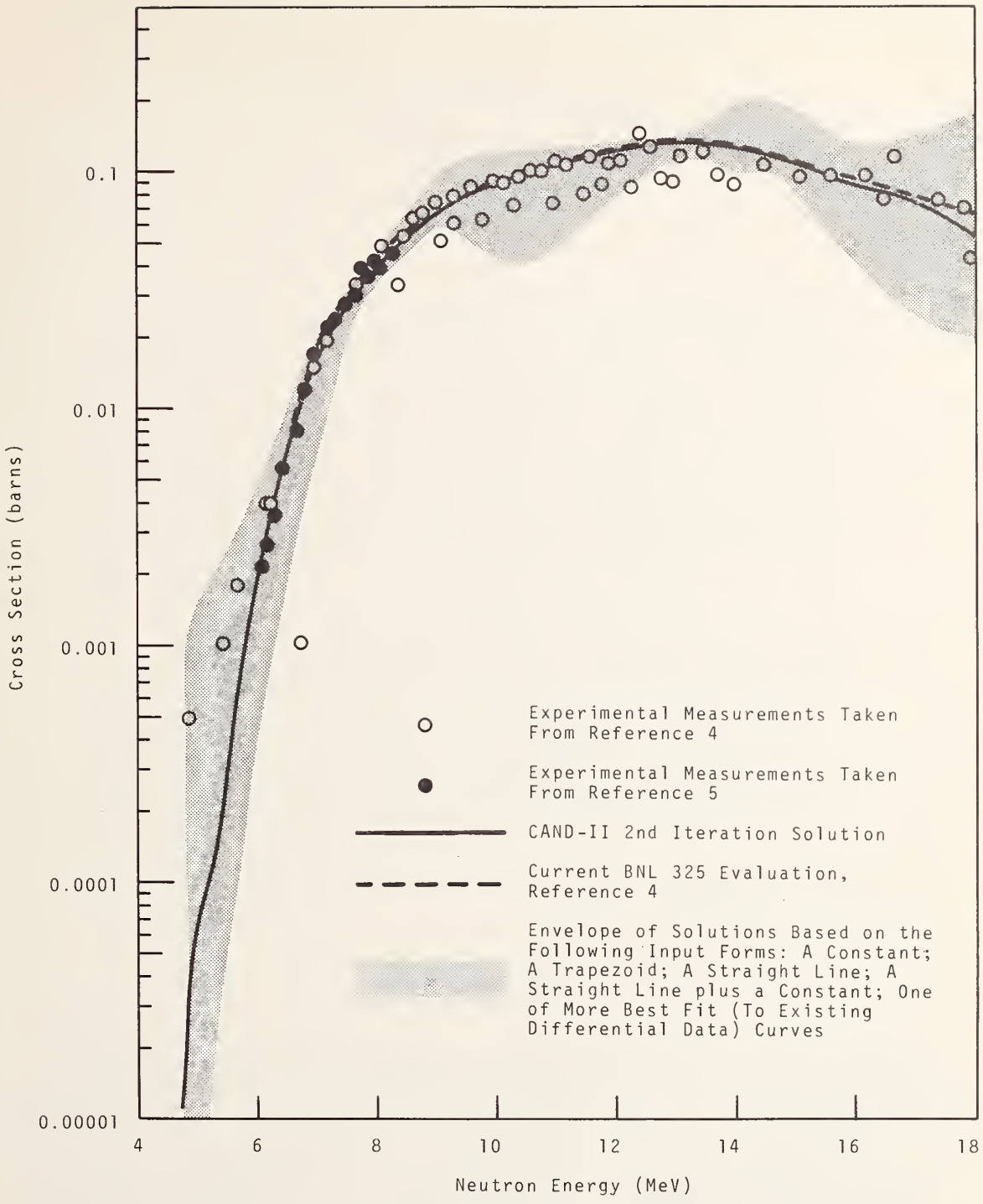

FIGURE 3

CAND-II Solution for $^{27}Al(n,\alpha)^{24}Na$ Reaction Cross Section

Spatially Continuous Neutron Flux Plotting with Spark Chambers*

K. G. Porges, W. W. Managan and W. C. Kaiser

Argonne National Laboratory
Argonne, Illinois 60439

ABSTRACT

Wire spark chambers yielding signals from which the spark location may be inferred within 0.1 cm have been recently developed for high energy physics experiments. With the addition of a fission foil, a single wire counter of this general type may be incorporated in a long tube of modest diameter, suitable for insertion in an available reactor or critical assembly instrument channel, and used to obtain the neutron flux profile with continuous spatial resolution. In addition to the advantages of resolution and speed, this device is relatively temperature and radiation insensitive and may thus be permanently sited to allow repeated flux profile measurements.

The fission foil is self-calibrating: alpha tracks due to the natural alpha activity of the fissionable coating may be registered simply by increasing the applied voltage. The space resolution obtainable with such an instrument can be kept to a few millimeters by optimizing the geometry, such that only fission fragments emitted within a certain small angle to the foil normal are registered. The deionization time required after each spark limits the maximum count rate to the order of 10^3/sec.

Preliminary results, obtained with a prototype instrument are presented.

1. INTRODUCTION

The measurement of the spatial distribution of the neutron flux in a reactor or critical assembly is one of the principal tools of design and diagnostics, allowing direct comparisons with theoretical predictions.

Traditional techniques of flux profile plotting, activation and subsequent counting of foils or wire on one hand, and probing with a displaceable counter on the other, each have certain inherent problems which the system described here was designed to resolve.

Foil activation, while potentially very precise, requires two shutdowns, for insertion and for withdrawal; even where automatic counting equipment and a computer program are available, the time lag between

*Work performed under the auspices of the U. S. Atomic Energy Commission.

acquisition and production of the flux plot is considerable; irradiation times required where fluxes are weak may be quite long. Probing with a small fission detector, either a gas counter or a junction device, has the drawback of requiring very constant power levels as well as detector efficiency during what may be a long run. Mechanical positioning is critical; signals must be highly amplified and intermittent noise sources often present at reactor sites can be difficult to cope with. There have been some attempts to deploy a larger number of counters in order to expedite matters; however, this adds the possibility of cross-talk to the electronic problems mentioned above and further requires intercalibration of detector efficiencies.

To cope with the problem of fitting cables from each detector into available channels (which should be narrow to make the measured flux representative), detectors may be interconnected with delay lines and the time between a pulse and its echo reflected from the far end of the line used to sort pulses into channels.

This logically leads to the development of a continuous coaxial fission chamber, loaded with ferrite to slow down the propagation velocity of pulses along the anode. Such a chamber would in principle yield a continuous flux survey, but could not provide space resolution better than about 2 cm, limited partly by technically possible delay/risetime ratios which determine the resolution for strictly localized input, and partly through the considerable range of fission tracks which spread the input.

The fission spark chamber described here has an inherent position resolution of about 1 mm and can overcome the range-induced uncertainty by means discussed below. Its main drawback is the limited input rate, in the order of 10^3/sec maximum, due to the slow dispersal of the plasma developed in each spark. Even with this limitation, the time required for data acquisition is seen to be significantly shorter than that required by other methods. The detection efficiency function can be calibrated, as described below, in one count. When on-line computation is available, the efficiency function can be folded into the experimental distribution to obtain a flux plot within a matter of 5-min running time, at a space resolution of about 2 mm.

2. PRINCIPLE OF OPERATION

Wire spark chambers are inherently capable of discrimination between densely and less densely ionizing events. As shown by Bowman and Hill,[1] fission fragments, the most densely ionizing of all particles, are thus readily registered under conditions where any other ionizing event, including alpha particles, is unable to release a spark. On the other hand, the voltage may be raised until alpha particles are counted. Since most fissionable deposits have some natural alpha activity (for ^{235}U, this arises mainly from ^{234}U admixture), any means which can locate sparks along the wire not only allow inference of the fission rate in a long fissionable deposit parallel to the wire in the presence of a neutron flux, but also provides a plot of the local alpha emission of the deposit; hence, an

efficiency calibration curve, in the absence of external neutrons, at raised voltage.

As regards methods of spark location, timing the arrival of an acoustic wave along the wire through magnetostriction [2] is currently exploited to considerable extent in multiwire arrangements; a less frequently applied method relies on the resistive-reactive division of currents along the anode wire between the spark and either end. [3] Attempts to use acoustic timing were abandoned as the signal was found to depend critically on the state of annealing. It was necessary to put considerable tension on the long (approximately one-meter) wire to reduce the amplitude of mechanical vibrations; the tension destroyed annealing, resulting in a critical loss of signal. Moreover, the problem of confusion between inputs arises when mean intervals between counts become comparable with the acoustic transit time, about 200 μsec for 1 m.

The resistive division method requires very careful grounding and attention to the reactance, for which purpose best results are obtained by feeding leads from either end of the wire through a common transformer core in the opposite sense. [3] With a chamber destined to fit into blind channels in a critical assembly or reactor, access to the far end of the chamber is restricted and it is practically necessary to take signals only from one end. The use of resistance wire for the anode largely removes the dependence on reactance and grounding, while introducing some nonlinearity which can be minimized by chossing a relatively low resistivity and introducing series resistance between charging capacitor and cathode. To the extent to which the capacitor recharges fully between discharges, the current pulse from one end of the anode is proportional to the location of the spark. This signal can be readily taken out via ferrite core transformer and stretched with a capacitative shunt to microsecond length. The resulting pulses are of suitable shape and size to be directly processed by a multichannel analyzer. Spatial resolution of the spark is necessarily a matter of the number of channels available and was about 2 mm for the prototype unit described below.

In addition to the method of spark location, the dispersion of fission tracks also contributes some uncertainty, which must be minimized by proper choice of parameters. If we may suppose that the probability of spark formation depends on equilibrium between rate of charge multiplication in the immediate vicinity of the wire and rate of charge removal through recombination, sparking will require a minimum input energy $T = [(dE/ds)\ \Delta r]$, where Δr is the radius of the multiplication region, determined by the applied voltage. Keeping this minimum above the maximum which can be delivered by alpha particles will prevent registering the latter. For fission tracks, one may define an approximate energy deposition rate

$$dE/ds \sim (E)^{\frac{1}{2}}$$

from which one finds, after some manipulation, that the fission foil-anode distance $\underline{a}$ should be chosen according to

$$\underline{a} = R\left[1 - R(dE/ds)_{min}/E_0\right]$$

where E_0 = fragment energy, R = fragment range, and $(dE/ds)_{min} \geq T/\Delta r$.

With this choice, the light fission fragment is just countable, at a space resolution determined only by range and energy straggling and the spark formation probability distribution near threshold. The effect of straggling can be further reduced by introducing a collimator consisting of a row of small holes drilled into a plate. With this arrangement, the detection efficiency of the chamber is evidently low. This is, in fact, desirable for reactor measurements, where it may otherwise be a problem to keep count rates within the limits dictated by the rate of dispersal of the plasma generated in the spark. As it happens, the deionization deadtime is of the same order as the deadtime of conventional multichannel analyzers and thus imposes a limitation which is more apparent than real.

3. PERFORMANCE TESTS

A test spark chamber of 30-cm length was bench tested to verify the predicted resolution. The anode was made of 0.005-in. diameter nichrome of about 10 Ω/ft ; the cathode was a steel bar, into which a groove of circular cross section and 0.125-in. diameter has been milled. With the anode at -2700 V, pulses were fed through simple passive circuits to an 800-channel analyzer. An analyzer display obtained by displacing a collimated ^{252}Cf source repeatedly by 2 cm is shown in Fig. 1. Peak position is plotted against displacement in Fig. 2. From this preliminary investigation, it is apparent that the linearity is satisfactory. The full width at half maximum of the peaks averages at about 1.7 mm. A chamber of 100-cm length and 1-cm diameter, for insertion in a critical assembly test channel, is under construction.

4. SUMMARY

The use of spark counters for purposes of flux plotting appears to have the advantageous feature of rapid, on-line data acquisition as well as continuous space resolution. If a spark counter can be designed to fit into a narrower channel, it may be possible by this means to look for relatively small structure effects in critical assemblies, otherwise very difficult to measure. The rapid rate of data acquisition, on the other hand, makes this instrument a good candidate for space-time-dependence measurements. Finally, the rugged and temperature-insensitive nature of such a counter should allow its permanent siting in a reactor, permitting periodic flux profiles to be taken for diagnostic purposes.

The help of R. J. Armani, who supervised electroplating of the 36-in. long fission foils for the prototype counter, is gratefully acknowledged.

5. REFERENCES

[1] BOWMAN, C. D., HILL, R. W., Nucl. Instr. Methods, 24 (1963) 213.
[2] GIANELLI, G., Nucl. Instr. Methods, 31 (1964) 79.
[3] CHARPAK, G., FAVIER, I., MASSONNET, L., Nucl. Instr. Methods, 24 (1963) 501.

313-475 O-68—18

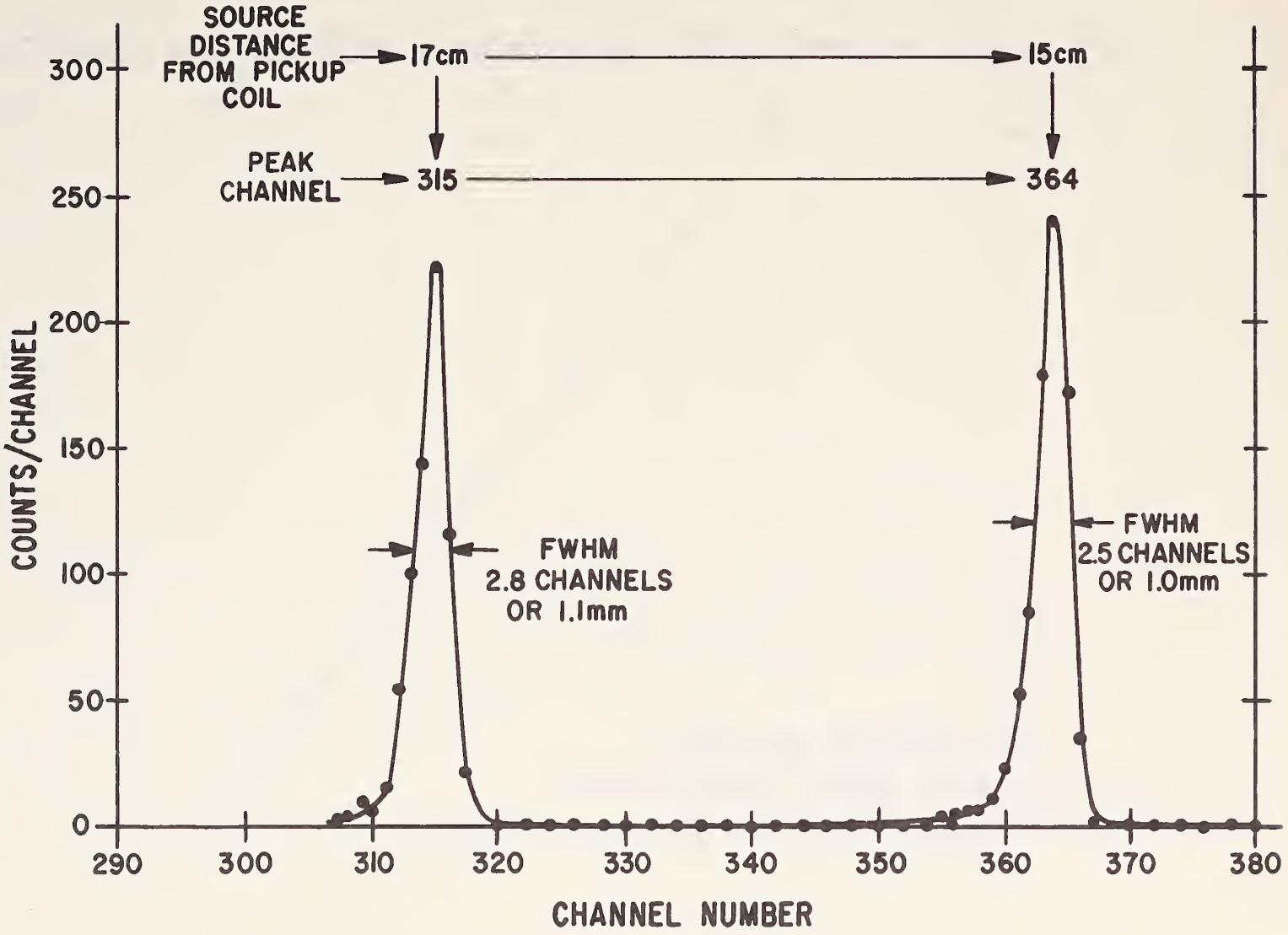

Fig. 1. Typical MCA Pulse-Height Data Counts/Channel Versus Channel Number (Scale: 2.5 Channels/mm).

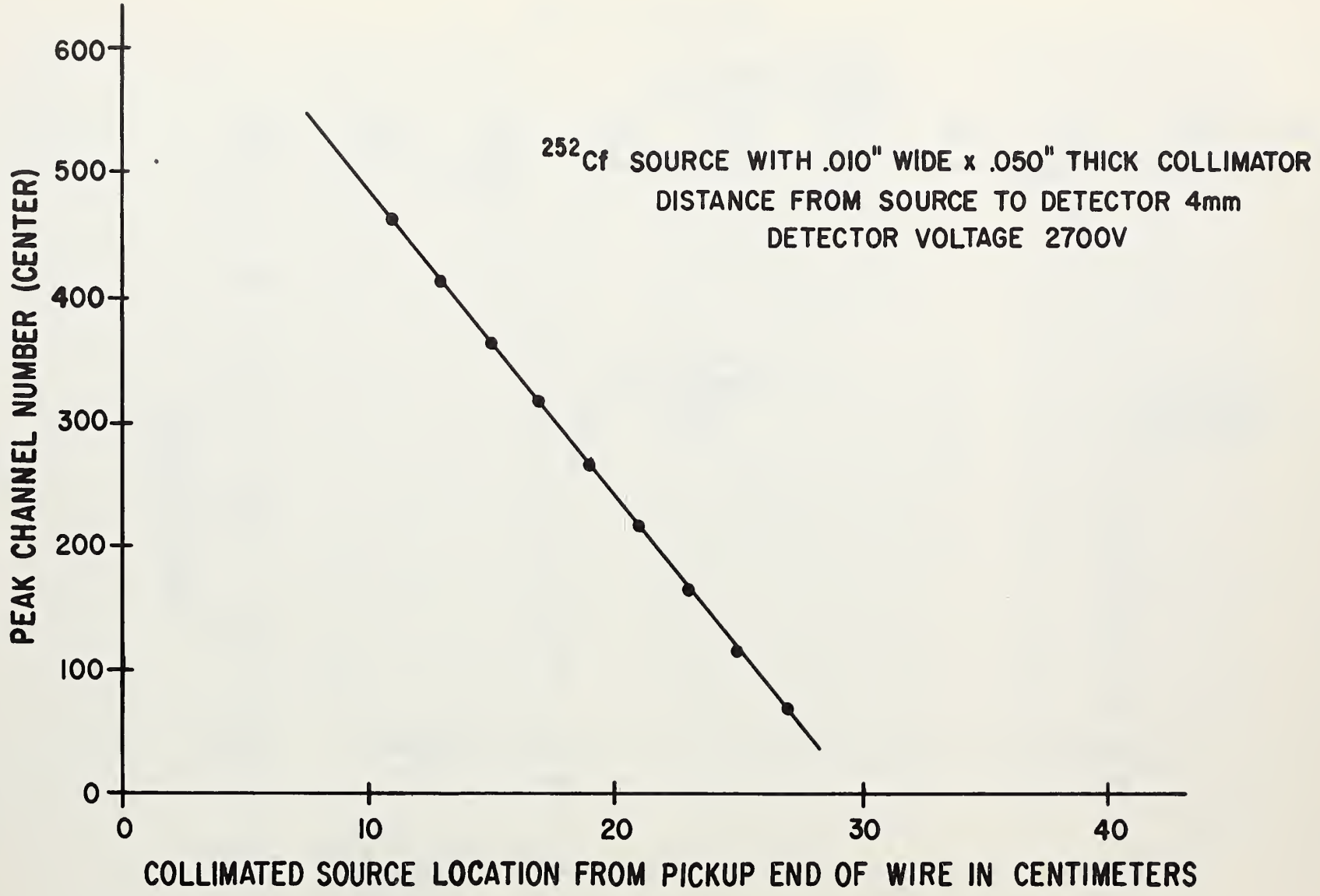

252

Fig. 2. Linearity Plot: MCA Peak Position Versus Source Position from Pickup Coil.

THE MANGANESE-55 RESONANCE ACTIVATION INTEGRAL*

Rudolph Sher
Brookhaven National Laboratory, Upton, N. Y. 11973**

The infinite dilution resonance capture integral of Mn^{55} has been carefully remeasured, using cadmium ratio techniques. The measurement was done in beam geometry at the BNL Graphite Reactor. Corrections for scattering effects in the Cd filters and the contribution to the activation of non-beam neutrons were made. The 1/E-ness of the spectrum was verified by means of previous fast-chopper data taken at the same beam. The result for the resonance integral was 14.4 ± 0.5 barns, based on a Au resonance integral value of 1565 ± 30 barns. There have been about a dozen previous measurements of the Mn resonance integral, with values ranging from 11 to 18 barns. The present result agrees well with two measurements in which particular care was taken to determine the neutron spectrum; because of the high value of the principal resonance energy in Mn (336 ev), the measured integral is particularly sensitive to spectral effects, and it is suggested that this is what is chiefly responsible for the large spread of values previously determined.

---

* Supported by AEC.

** Permanent address: Department of Mechanical Engineering, Stanford University, Stanford, California. 94305

The infinite dilution resonance activation integral of Mn-55 from 0.5 eV has been carefully remeasured in beam geometry at the BNL Graphite Reactor, using cadmium ratio techniques. The result, including the 1/v part, is 14.41 ± 0.48 barns, based on the Au resonance integral of 1565 ± 30 barns and the Mn 2200 m/sec cross section of 13.3 ± 0.1 barns. The neutron spectrum was determined to be closely 1/E, and corrections for Cd filter effects and self-shielding were applied according to the method of Pearlstein and Weinstock.[1]

The experiment was done in a beam which used to serve the BNL fast chopper. This beam is internally split into two parallel beams, each approximately 1/4 in. x 3 in. with a center-to-center distance of about one inch. The neutron flux in the beam is about 10^8 n/cm^2/sec. 0.387-inch diameter foils were mounted on an aluminum wheel attached by a small belt drive to an electric motor. The foils were mounted on a one-inch diameter circle; the wheel shaft was centered between the beams. With this arrangement, each foil "saw" one or the other of the beams more than 50% of the time during a rotation of the wheel.

In each irradiation four foils were used, two Mn and two Au. The four foils were mounted 90° apart on the wheel, and one foil of each type was cadmium-covered on both sides. The thickness of the Cd covers was 0.047 in. The "bare" foils had aluminum covers of approximately the same thickness.

The foils were Al-Mn and Al-Au alloys, with nominal 2% (weight) Mn and 0.5% Au content. The Mn density was about 1.3 mg/cm^2; the Au was about 0.33 mg/cm^2. In a separate foil calibration experiment, all the foils were irradiated on a wheel in a thermal column, and relative Mn and Au contents determined.

All counting was of gamma-ray activity; two NaI scintillation counters were employed. For Mn, the discriminators were biased just below the 840 keV peak; for Au, just below the 412 keV peak. In order to allow the Al activity to die out, the Mn counts were begun about two hours after the end of the irradiation. The usual background and dead-time corrections were applied to the data to obtain relative count rates, corrected to an arbitrary zero of time. In all, three runs were taken, using three different sets of Mn and Au foils. Two other runs were done to determine the effects of scattered neutrons on the activations.

In addition to the standard corrections, the following possible sources of error were investigated and found to be absent or negligible:
(1) Mn-54 activity in the Mn foils arising from the (n,2n) reaction. This has a gamma-ray energy closely equal to that of Mn-56, but a half-life of about 300 days, as compared to the Mn-56 half-life of 2.58 hours. Counts taken on the Mn foils a day or two after irradiation showed no detectable activity above background.
(2) Scattering effects in the Mn foils, i.e., activity resulting from non-beam neutrons (but not including scattering effects in the Cd filters). Two runs were made to investigate these; in the first run, two foils were irradiated on the wheel. One had a Cd cover in front only, and the

other had a Cd cover in back only. The difference in the "Cd ratio" thus obtained is essentially a measure of the activation arising from thermal neutrons scattered back into the foils, and it was determined that about 2.5% of the total activation is caused by these neutrons. In the second run, one Mn foil was irradiated in the beam, and another irradiated adjacent to the first, out of the beam. Both foils were cadmium covered, front and back. The ratio of the out-of-beam activity to the in-beam activity was again close to 2.5%. It thus appears that the fraction of thermal-neutron activation due to scattered neutrons is equal to that of epithermal neutrons, and the Cd ratio is therefore unaffected.

The Cd ratios obtained in the three runs, corrected for the relative Mn and Au contents determined in the calibration run, are listed in Table I below.

TABLE I

CADMIUM RATIOS

	Run 1	Run 2	Run 3	Average
Mn	40.31	40.55	39.72	40.19 ± 0.40
Au	3.53	3.52	3.58	3.54 ± 0.04

The corrections for cadmium-filter effects were made according to the method of Pearlstein and Weinstock.[1] Because of the thinness of the samples, the principal corrections arose from scattering in the Cd. The corrections in the Cd ratios amounted to about 8% for Au and 6% for Mn (assumed to be a 1/v-detector).

The cadmium-cutoff corrections were estimated from the data of Pearlstein and Weinstock[1] for the Au foils; for the Mn foils the results of Stoughton and Halperin[2] were used. The cutoff for Mn is 0.549 eV, while that for Au is 0.618 eV. When corrected for all these effects, the result for the Mn resonance integral is 14.41 ± 0.35 barns. The error includes the uncertainties in the 2200 m/sec cross sections and Au resonance integral.

The 1/E-ness of the neutron spectrum was determined from fast chopper data in the beam supplied by R. Chrien. The method is based on the fact that the curves $C_1(t)$ and $C_2(\alpha t)$ of count rate vs. time measured with a thin BF_3 counter with the chopper running at two speeds whose ratio is α (and no sample) are congruent only if the spectrum is 1/E. By this means it could be estimated that the maximum error in the Mn-55 resonance integral arising from non-1/E-ness is 2%, which raises the overall error in the result to ± 0.48 barns.

There have been about a dozen previous measurements of the Mn-55 resonance integral; when corrected to a cadmium-cutoff energy of 0.5 eV, standard values of the Mn 2200 m/sec cross section (13.3 ± 0.1 barns), the Au 2200 m/sec cross section (98.8 ± 0.3 barns), and the Au resonance integral (1565 ± 30 barns), the results range from about 11 barns to about 18 barns (see Table II). Many of the published descriptions of these measurements are too incomplete to enable one to guess at possible sources of this large spread of values, but it is likely that in many cases, the spectrum deviated from the 1/E shape. Because the Mn resonance energy is so high (336 eV) compared to that of Au, even small deviations from 1/E-ness can cause large errors in the Mn resonance integral. For example, a spectrum whose shape is $1/E^{1.01}$ will lead to a measured Mn resonance integral which is 5% low, or about 0.4 barns. Of the previous experiments, only Dahlberg et al., and Walker seem to have carefully investigated the neutron spectrum, and the close agreement of the present result with their values suggests that spectral effects are indeed responsible for a major part of the large variation in the reported values. In addition, some of the measurements may have been subject to large and uncertain self-shielding and scattering corrections.

REFERENCES

1. Pearlstein, S., and Weinstock, E. V., Nuclear Sci. Eng., 29, 28 (1967).

2. Stoughton, R. W., and Halperin, J., Nuclear Sci. Eng., 15, 314 (1963).

TABLE II

SUMMARY OF

MANGANESE-55 RESONANCE INTEGRAL MEASUREMENTS

Author	Result	Method	Reference
This work	14.4 ± 0.5	Cd ratio (beam)	
Kohler and Schmelz	13.6 ± 0.5	Absolute counting of Cd-covered Au and Mn foils	Nukleonik, 9, 270 (1967)
Louwrier and Aten	15.0 ± 1.4	Cd ratio in $MnSO_4$ tank	J.Nucl.Energy, 19, 267 (1965)
Vidal	16.3	Pile osc.	CEA-R 2486 (1965)
Baumann	18.1	Cd ratio	WASH-1046 (1964)
Axton	14.8 ± 1.5	Cd ratio	J.Nucl.En., 17, 125 (1963)
Berneth and Schumann	14.1	Cd ratio	WASH-1041 (1962)
Dahlberg et al.	14.3 ± 0.6	Cd ratio (beam)	J.Nucl.En., 14, 53 (1961)
Feiner	15.3 ± 0.6	Cd ratio	KAPL-2000-16 (1961)
Walker et al.	14.1 ± 0.8	Cd ratio (beam)	Can.J.Phys., 38, 57 (1960)
Tattersall et al.	15.5 ± 5.0	Pile osc.	J.Nucl.En., 12, 32 (1960)
Klimentov and Griazev	11.7 ± 1.5	Danger coeff.	J.Nucl.En., 9, 20 (1959)
Macklin and Pomerance	10.8	Pile osc.	1955 Geneva Conf. 5, 96 (1956)
Harris et al.	11.8	Cd ratio	Phys. Rev., 79, 11 (1950)

Session C

THE NEED FOR AND USE OF NEUTRON DATA IN REACTOR DESIGN APPLICATIONS

Chairman

D. R. HARRIS
Bettis Atomic Power Laboratory

USE OF NEUTRON DATA IN THERMAL REACTOR POWER PLANT DESIGN

R. J. French, Manager
Core Engineering
Westinghouse Electric Corporation
APD - PWR Plant Division
Pittsburgh, Pennsylvania 15230

In terms of the utilization of neutron cross section data, I would like to direct myself to those areas in which an improvement in the accuracy of data can be demonstrated to result in an improvement in the economic performance of the pressurized water reactor core. The basis for this demonstration would be the determination that an expenditure of a given amount of money could result in an improvement in the economic performance of the reactor core commensurate with that expenditure.

The basic data considered in this paper consist of the microscopic reaction rate cross sections, the neutrons produced per fission, the capture-to-fission ratio, the material yields per fission, and the decay constants for the various materials including the fissionable materials uranium-235 and the various isotopes of plutonium as well as the fertile material uranium-238. In addition, the characteristics of the structural material and those of the moderating material must be considered. It must be recognized that these characteristics alone are not of practical value and they must be considered together with a theoretical model to develop a basis for the prediction of practical engineering characteristics.

In addition to the uncertainties which result from errors in the basic data as well as simplifications in the model for analysis, one must consider the uncertainties which arise from variation in material characteristics, variations as a result of manufacturing tolerances as well as variations which result from differences in operational mode. As an example of variations which result from materials characteristics in manufacturing deviations, one can consider the effect of fuel enrichment, dimensional tolerances, fuel impurities, structural impurities, and the uncertainties which result from variations in water density throughout the pressurized water reactor core. One should also consider the variations due to operational considerations such as control rod programming, load follow, the effects of xenon oscillations, the effects of power shaping control rods, the effects of stretch-out operation, the effects of materials limitations, and the auxiliary considerations of the reprocessing costs involved. To put these matters into proper perspective, the factors which affect the economics of pressurized water reactor core performance can be grouped into two parts: those which affect power capability of the core, and those which affect the fuel performance in terms of burnup, fissile material depletion, and fertile material conversion.

The application of a basic theory is of value in determining an optimum design and the extrapolation of performance from that presently known. Beyond this, the actual operating experience is adequate to determine economic performance. In terms of optimization, it may very easily be concluded that a considerable number of years of experience would be necessary to determine from the variations in reactor design what the optimum configuration should be. In addition, a considerable number of years of experience would be required before one could determine if the presently warranted performance could actually be achieved. Although the penalties may vary from fuel or reactor plant contract to contract, it is clear that the uncertainties in the prediction of the capabilities of fuel performance at the actual burnups under consideration do, in fact, impose an uncertainty on the electric utility industry and, therefore, upon the economy in general. This uncertainty will reflect itself in the rate at which the electric utility industry will, or should, increase the percentage of installed power given to the nuclear industry.

I would now like to draw the observation that the material constants which are of greatest importance to the designer of a power reactor core vary considerably as a result of the operational experience which the designer does not have at the time he is to make a design decision. The state-of-the-art strongly affects the areas of interest and the areas in which the designer is prepared to recommend the expenditure of effort and money for the development of increased accuracy of basic data. As macroscopic operational experience becomes available, the requirement for high precision or accuracy in many of the basic physics characteristics becomes of substantially reduced value.

With this background commentary, I would like to begin with a discussion of the state-of-the-art in the development of the understanding of the performance of the pressurized water reactor core. I would like to begin with the postulation of as simple an analytic model as possible which does, in fact, exhibit all the physical characteristics which we consider to be important in the evaluation of the engineering characteristics of the core. With this postulated model, and a given set of basic data, we attempt to fit the available critical experiments. A large number of these have been developed over quite a number of years as a function of the important parameters of core design. From the critical experiments it is possible to demonstrate a correct functional variation of the analysis according to basic parameters.

Figure 1 illustrates in a concise form the ability of a simple analytic prediction to correlate the critical experiments available for slightly enriched uranium-235-fueled critical assemblies. Here we have given an example of the fit of the data as a function of the moderating ratio (the hydrogen-to-uranium number density ratio). The lack of an obvious trend as a function of this variable is encouraging in that it permits us to conclude that variations in water density as a function of temperature or power level should be properly predicted. In addition, we have correlated the data as a function of pellet diameter, enrichment, clad thickness of material, and

boric acid concentration in the moderator. From these correlations, it is possible to conclude that we have a considerable amount of confidence in the prediction of the variation of characteristics of the reactor core as a function of these variables. On the basis of this information, we have hopes of being able to extrapolate the critical facility data to the hot operating reactor condition. In addition, it is possible to assume that the effect of the depletion of U-235 during energy generation can be properly described by this method.

Table 1 illustrates the data which have been developed during the startup of reactor cores and are to be compared to predictions based upon the extrapolations of critical data. Specifically, we have shown the comparison of the predicted and measured critical boron concentration. The values are presented for the clean condition at zero power, the full-power condition, and the condition with the short-term saturable fission product poisons xenon and samarium built in. These values tend to confirm the conclusion that the critical data have provided us with a system from which it is possible to predict beginning-of-life data in operating reactor systems.

It is concluded that the uncertainties resulting from basic data are now reduced to the point where they are not significant relative to the uncertainties from other characteristics such as manufacturing tolerances and impurities.

In addition to the problem of predicting the beginning-of-life condition, one is vitally concerned with the predictions of the effects of fuel depletion in addition to those of the destruction of U-235. One is concerned with the production of plutonium and its effect of neutron multiplication and the effect of the fission product poisons which are inherent in the fission process.

Figure 2 illustrates the results of a series of critical experiments conducted under the auspices of the ESADA group in which it was possible to evaluate the criticality effects of plutonium with variations in the important isotope, plutonium-240. With separate critical experiments to evaluate the consequences of the variation in U-235 enrichment and the concentration of plutonium as well as its specific isotopes, the time-honored equivalent fission product cross section which is generally varied arbitrarily to force a correct burnup prediction for actual operating experience has a distinct chance of avoiding the serious compensations of errors which might otherwise occur.

It is of substantial interest to note that operating reactor experience is available as a function of energy generation in pressurized water reactor cores which can be employed for the above mentioned normalization to the equivalent fission product cross section. We now have good data out to about 10,000 MWD/MTU. Although this falls substantially short of the proposed operating limits now in existence, it does provide a good base from which extrapolations to the nearly optimum values can be made. It is of interest to note that this information is available for reactor cores fueled with the fissile material, uranium-235, as well as the fissile isotopes of

plutonium, since similar information is available for the operation of the Saxton power reactor in which a considerable fraction of the assemblies is fueled with plutonium.

Figure 3 illustrates the results of the core follow program for the Selni reactor first core. The data are presented on the basis of critical boron concentration as a function of lifetime. It can be seen that these data provide important information in terms of predicting the performance of pressurized water reactor cores as energy is generated. The fact that information is available for plutonium fueled reactor cores gives one further confidence in the normalization process.

An additional body of information which is of considerable importance in the prediction of reactor performance is the assembled results of the Yankee Core Evaluation Program which, among other information, has determined the variation of the fissionable and fertile isotopes with burnup as a function of position within the reactor core for the first core of the Yankee power reactor. Figure 4 presents a summary of such information for specific fuel rod locations in the Yankee reactor. In a similar vein, it is intended that the Saxton Plutonium Program will give the same information for the plutonium recycle core.

It can be seen from the above that we have developed a large body of information which makes it possible to check both the significance of basic reactor physics data and the models employed in engineering analysis to enable predictions which are of significance in the long term evaluation of pressurized water reactor cores.

The preceding information formulates the basis of what we refer to as the present state-of-the-art in the development of the pressurized water core. Essentially all this information, as well as many other tests for reactivity coefficients, control rod worths, etc., is embodied in the correlations against the predicted model and results in the model embodying all the experience which is presently available. With this then as the background, we wish to consider how uncertainties remaining in basic data result in uncertainties in extrapolation which are of significance both in terms of optimization of the reactor power plant and the uncertainties in the commitment of the nuclear industry. It is pertinent at this time to consider the presently current commitments in terms of reactor power plants as well as fuel contracts.

Table 2 illustrates total Westinghouse commitments. These commitments represent at this time approximately one-third of the total commitments within this country. If one were to assume an uncertainty in the performance of this fuel, specifically two and a half million kilograms of uranium and presume that it were to be burned to an average of 30,000 MWD/MTU which resulted in an error of 1% in the fuel cost, it would lead to a total uncertainty of 10 million dollars. On the basis of total commitments at this time, it can be seen clearly that small uncertainties can lead to a large commitment in total dollar investment and would lead one to conclude that considerable investment in the resolution of uncertainties might well be appropriate.

To clarify the picture as it now exists, consider Figure 5 which is a cartoon illustrating the present situation wherein we have experience up to approximately 10,000 MWD/MTU. The present projection is for a discharge burnup of the order of 30,000 MWD/MTU. This value is probably very near the optimum value to be considered if one considers the situation in terms of three cycle operation and assumes that simple averaging is valid. It is clear from the figure that there will be a region of fuel at the end of each cycle with 10,000 MWD/MTU burnup, a region with 20,000 and a region with 30,000 MWD/MTU. If the burnup curve is linear, it can be seen that these three values would average to a neutron multiplication of unity which is, in fact, the definition of end-of-life. At this point it becomes clear then that we are able to normalize the calculations to a burnup of 10,000 MWD/MTU and that the spreading dashed lines illustrate the growth of uncertainty as we extrapolate beyond this point of experience. Although this appears to be a grossly oversimplified representation of the situation, it does tend to give a remarkably accurate summary of the situation. For example, the assumption of averaging neutron multiplication within the core turns out to be quite good for the simple reason that there is a strong desire to achieve very uniform power distributions by means of non-uniform loading.

Clearly then, on the basis of the large amount of operational experience, critical experiment experience and spent core analysis, we are in a position to state that our basic interests lie in the area where factors become important beyond 10,000 MWD/MTU burnup or there is a relatively large shift in significance beyond 10,000 MWD/MTU in burnup. In either case, the result could very well be a compensating error which leads to errors in extrapolation beyond present values. Immediately, one is concerned with the evolution of fission product poisoning where the concentrations of the fission product poisons are changing beyond the normalization point at 10,000 MWD/MTU — one considers the higher isotopes in plutonium, for example, plutonium-241 and -242 as well as transuranic isotopes generated in very small quantities. With respect to these last mentioned materials, it should be kept in mind that there can be potential economic interest as the result of their potential use as a heat source for space power packs.

Finally, one must be concerned with the generation of many of the isotopes from the point of view that they represent serious radioactivity problems which must be considered during reprocessing and refabrication of fuel. There is a distinct possibility that the economics of reprocessing and refabrication can be significantly affected by the concentrations of these materials.

At this point I would like to present for your considerations some bench marks which will permit you to assess the significance of various factors which result in errors in the thermal water reactor core design. For example, if there is an error in the neutron multiplication which averages to 1% in k at the end of life, it requires an adjustment in the U-235 feed enrichment equal to 0.14 w/o to compensate for this error. This can immediately be converted to an uncertainty of 0.065 mils per kilowatt hour which is approximately 4% of the fuel cost. This can be extrapolated to a total

uncertainty of approximately 40 million dollars on the present Westinghouse commitments. Or, to consider the same uncertainty of 1% in neutron multiplication at the end of life for a single 800 megawatt plant, the compensation in enrichment necessary to overcome this error would require a change in enrichment with the resulting change in cost of approximately $400,000 per year.

Permit me now to consider more specifically the consequences of uncertainties in the fission product cross section. If there is an average error in the fission product cross section equal to 1%, this will result in an error in the neutron multiplication of 0.088%. From the previous figures one can conclude that this 1% error in fission product will result in an error 0.012 w/o enrichment or 0.0057 mils per kilowatt hour. In our 800 megawatt plant, a 1% error in fission product cross section is equivalent to an error in annual expenditure of about $35,000.

We have performed an extensive series of analyses with the fission product depletion code, CINDER, developed by the Bettis Atomic Power Laboratory for this purpose. We have employed this code to assess the variation of the effective fission product cross section as well as the sensitivity of this value to the basic physics constants of the various contributors to the fission product poisoning.

Table 3 gives a tabulation of the more important contributors to the fission product cross section as a function of burnup. It is quite logical to expect that the major uncertainties in the prediction of the fission product cross section and its extrapolation would lie within this group. By the assumption that the uncertainties in any of the basic constants will lead to a linearly-dependent error in the gross fission product cross section, one can perform a statistical combination of uncertainties to assess the total uncertainty in the final value as well as the relative contribution of uncertainty by the various nuclides.

Table 4 presents a tabulation of the resulting uncertainties in the gross fission product cross section. It can be seen from this table that relatively few of the nuclides tend to contribute a large fraction of the uncertainty that we now must suffer. It is interesting to observe that if no normalization process were involved, which is the basis for the data on Table 4, we would expect an uncertainty of approximately 3-1/2% in the final fission product poison in the three-cycle core which would represent an error of approximately $100,000/year in an 800 megawatt plant. This is approximately a 1% uncertainty in the fuel cost.

Let us consider now the fact that we are normalizing the fission product cross section at 10,000 MWD/MTU and that we have hopes, therefore, of reducing the uncertainty resulting from uncertainties in the basic data which go into the fission product cross section. We can expect that the important contributors to the uncertainty are likely to be different than those tabulated in Table 4. Table 5 presents a tabulation of the uncertainties resulting from the normalized case. It can be seen here that the total uncertainty is reduced approximately by a factor of five through this

process of normalization. The important nuclides can be limited to xenon-131, promethium-148 (the metastable state), and promethium-147. It is possible to conclude that the area where further work is desirable lies in the improvement in accuracy of yields and cross section data for these materials.

I would like now to return and consider some of the other factors involved with uncertainties that are likely to obtain as burnup data are developed beyond 10,000 MWD/MTU. At this time let us consider the transuranic isotopes, specifically the plutonium isotopes and their progeny which are likely to become significant during high burnups. It is significant to state here that the consideration of plutonium as a source of fuel material for utilization in thermal water reactors is one of major importance. To a large extent, the present success of the nuclear industry is based upon the assumption that the value of the discharged plutonium can be justified on the basis of present day technology. There is a presumed worth for the discharged plutonium which certainly cannot be justified unless it is possible to recycle this plutonium either in the projected fast breeder reactors or in a recycle sense in presently existing thermal water reactors. There are a number of programs, most notably at this time the Edison Electric Institute Program, which are actively endeavoring to assist in the development of the information necessary to recycle plutonium into present day water reactors. Of prime consideration is the performance of the plutonium as a fuel material as well as the considerations relating to the manufacture of plutonium-loaded fuel rods and the strategies for employing these in water reactors. Here, in itself, lies a major uncertainty in the economics of the thermal water reactor which can be affected only slightly, perhaps, by the uncertainties in the basic data involved.

Consider Figure 6. We show a chain diagram which illustrates the evolution of nuclides as a result of interaction with neutrons and illustrates some of the more important materials for consideration in high burnup fuel. Of course, the higher isotopes of plutonium are important but we conclude also that higher nuclides americium and curium can be of substantial importance. There is the problem of radioactivity which can be of importance in fuel reprocessing as well as the potential benefit from materials such as plutonium-238 in which there is a potential for isotopic energy generators.

The Yankee Spent Core Program has developed some information concerning the concentrations of these higher isotopes which are presented in Table 6. Although at this time it is difficult to anticipate the reactivity uncertainty in the prediction of these higher isotopes, their total effect is of the order of 0.4%. The present value of neptunium-237, perhaps unrealistically high, can be computed to have a very substantial impact on the fuel cycle cost (as much as a half mil per kilowatt hour).

Finally, I would like to comment quickly on the related problem of the generation of uranium-232 in high burnup reactor fuel. Figure 7 illustrates the chain of reactions which can lead to the generation of U-232. Information from the Yankee Spent Core Program indicates that the present penalties proposed by the Commission for recycling uranium through the diffusion plant could lead to a cost increment in the fuel cycle of the order of 0.017 mils per kilowatt hour.

In summary, it is concluded that the factors which most significantly affect plant design are those which become important or change significantly at high burnup. Increased accuracy in nuclear data for materials that could become valuable (such as plutonium-238) or which could adversely affect fuel reprocessing (uranium-232) is clearly needed. One could expect the information derived from post irradiation evaluation programs to be especially useful.

TABLE 1

CORE STARTUP CRITICAL DATA

	INDIAN POINT	SELNI	SENA	SCE	CYW
Cold					
Critical Boron (ppm)					
Predicted	1949	1910	2040	2380	2133
Measured	1897	1800	1885	2250	2040
Difference	52	110	155	130	113
Boron Worth (ppm/% Δk)					
Predicted	114	109	111	108	106
Measured	125	100	111	101	109
Hot Zero Power					
Critical Boron (ppm)					
Predicted	1976	1910	2110	2570	2335
Measured	1893	1840	1972	2524	2305
Difference	83	70	138	46	30
Boron Worth (ppm/% Δk)					
Predicted	134	135	146	146	132
Measured	127	139	120	128	122

TABLE 2

CURRENT COMMITMENTS

Number of Plants	35
Amount of Fuel (including extra regions)	2.5×10^6 KgU

TABLE 3

CONTRIBUTIONS TO GROSS FISSION PRODUCT CROSS SECTION

Nuclide	BURNUP 8,000 MWD/MTU	16,000 MWD/MTU	34,000 MWD/MTU
Nd-143	11.52%	11.78%	10.56%
Sm-149	12.91	10.33	6.52
Sm-151	8.92	6.99	6.46
Pm-148m	9.61	7.65	4.71
Pm-147	9.72	7.78	4.84
Xe-131	5.73	6.12	6.10
Rh-103	6.73	8.38	9.15
All Others	34.86	40.97	51.66
Total	100.00%	100.00%	100.00%

TABLE 4

UNCERTAINTIES IN GROSS (EFFECTIVE THERMAL) FISSION PRODUCT CROSS SECTION

BURNUP (MWD/MTU)	STANDARD DEVIATION (BARNS/FISSION)
2,000	7.07
4,000	7.75
8,000	6.47
14,000	4.43
20,000	3.15
35,000	1.79
40,000	1.46

TABLE 5

UNCERTAINTY IN NORMALIZED FISSION PRODUCT CROSS SECTION

BURNUP (MWD/MTU)	STANDARD DEVIATION (BARNS/FISSION)
20,000	1.32
40,000	1.41

NOTE: NORMALIZATION DONE AT 10,000 MWD/MTU

TABLE 6

INVENTORY OF HIGHER ISOTOPES IN YANKEE FUEL

	BURNUP		
Nuclide	10,000 MWD/MTU	20,000 MWD/MTU	31,000 MWD/MTU
Pu-242	0.021 kg/MTU	0.145 kg/MTU	0.331 kg/MTU
Np-237	0.109	0.272	0.535
Pu-238	0.012	0.065	0.169
Am-241	0.067	0.180	0.307
Am-243			
Cm-242	0.0011	0.0065	0.0226
Cm-244			

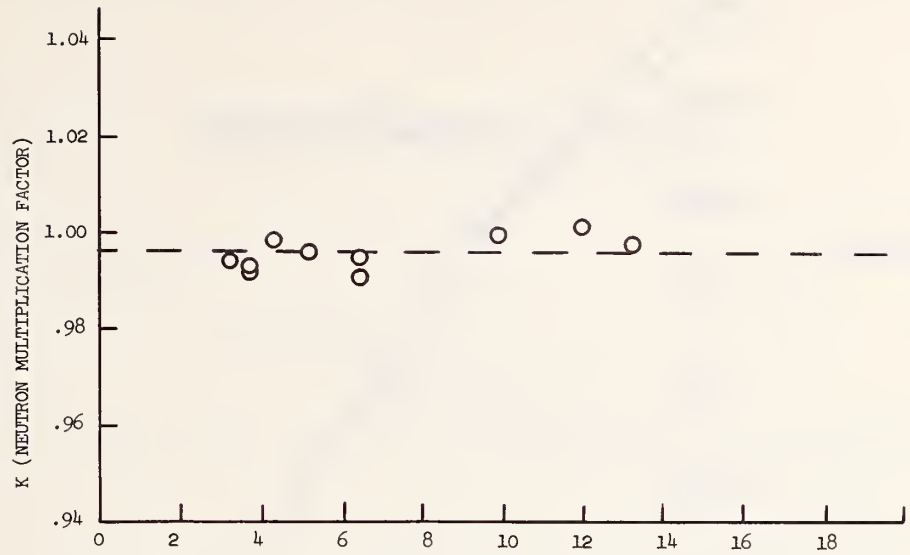
1.04
1.02
1.00
.98
.96
.94
K (NEUTRON MULTIPLICATION FACTOR)
0
2
4
6
8
10
12
14
16
18
N^H/N^U (ATOM RATIO)

FIG. 1

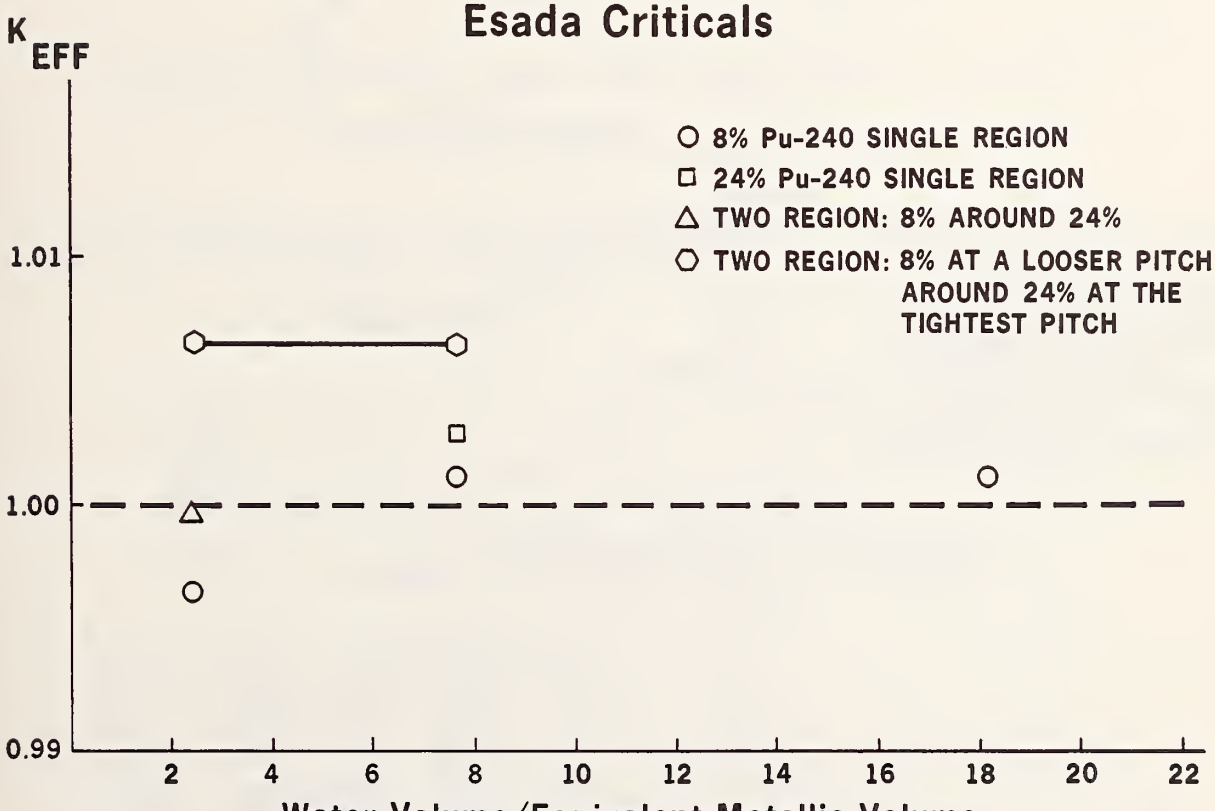
Esada Criticals
K_{EFF}
8% Pu-240 SINGLE REGION
24% Pu-240 SINGLE REGION
TWO REGION: 8% AROUND 24%
TWO REGION: 8% AT A LOOSER PITCH AROUND 24% AT THE TIGHTEST PITCH
1.01
1.00
0.99
2
4
6
8
10
12
14
16
18
20
22
Water Volume/Equivalent Metallic Volume

FIG. 2

Selni Cycle I (Measured Boron Concentration vs. Burnup)

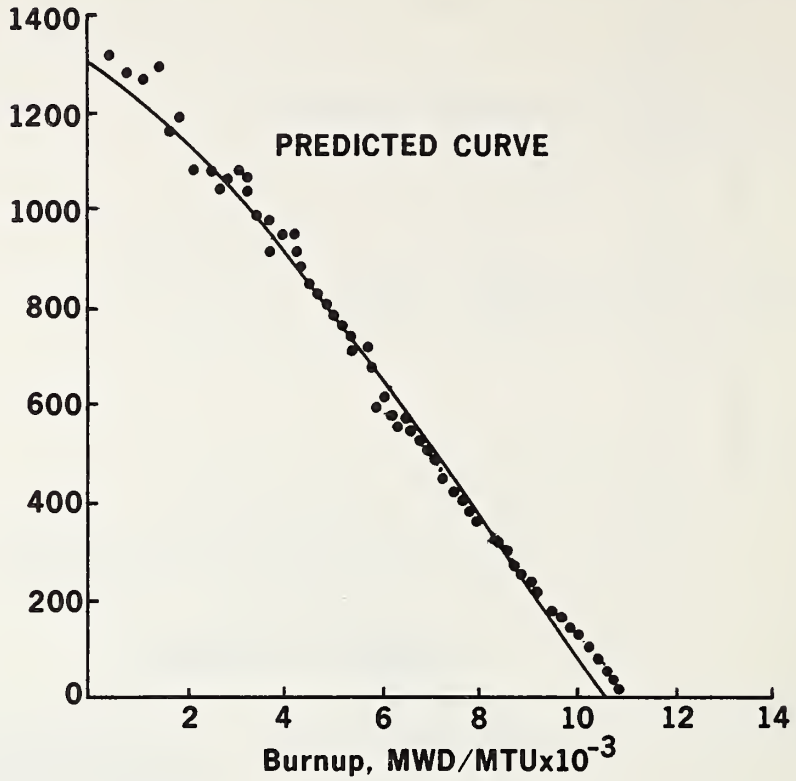

FIG. 3

Uranium and Plutonium Isotopic Inventory of the Yankee Core I Fuel

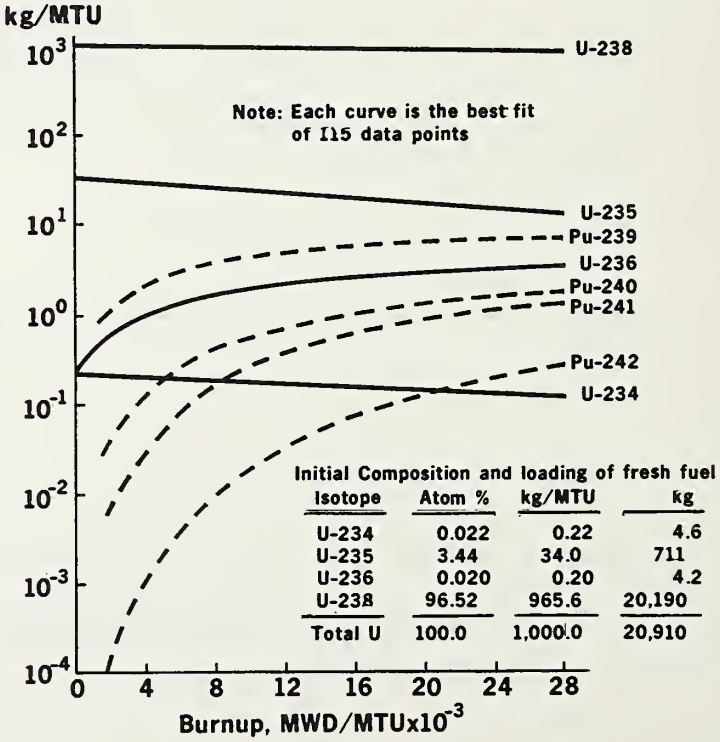

Initial Composition and loading of fresh fuel

Isotope	Atom %	kg/MTU	kg
U-234	0.022	0.22	4.6
U-235	3.44	34.0	711
U-236	0.020	0.20	4.2
U-238	96.52	965.6	20,190
Total U	100.0	1,000.0	20,910

FIG. 4

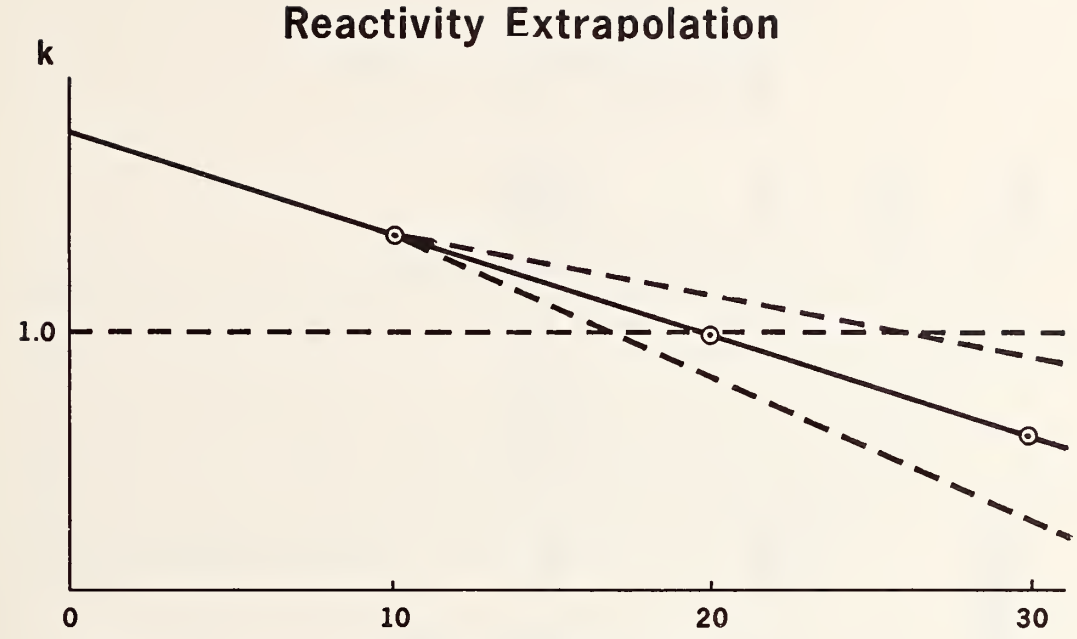
Reactivity Extrapolation
k
1.0
0
10
20
30
Burnup, MWD/MTU x 10 -3

FIG. 5

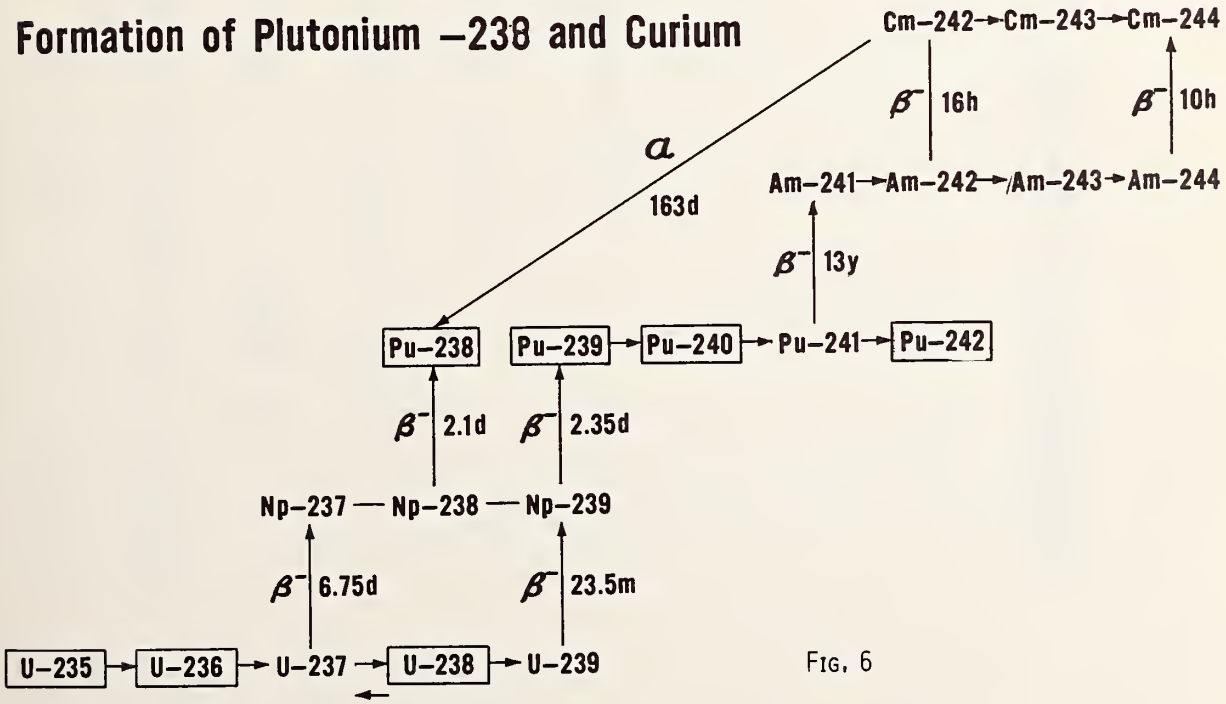
Formation of Plutonium –238 and Curium
Cm–242→Cm–243→Cm–244
β⁻ 16h
β⁻ 10h
α
163d
Am–241→Am–242→Am–243→Am–244
β⁻ 13y
Pu–238
Pu–239→Pu–240→Pu–241→Pu–242
β⁻ 2.1d
β⁻ 2.35d
Np–237 — Np–238 — Np–239
β⁻ 6.75d
β⁻ 23.5m
U–235→U–236→U–237→U–238→U–239

FIG. 6

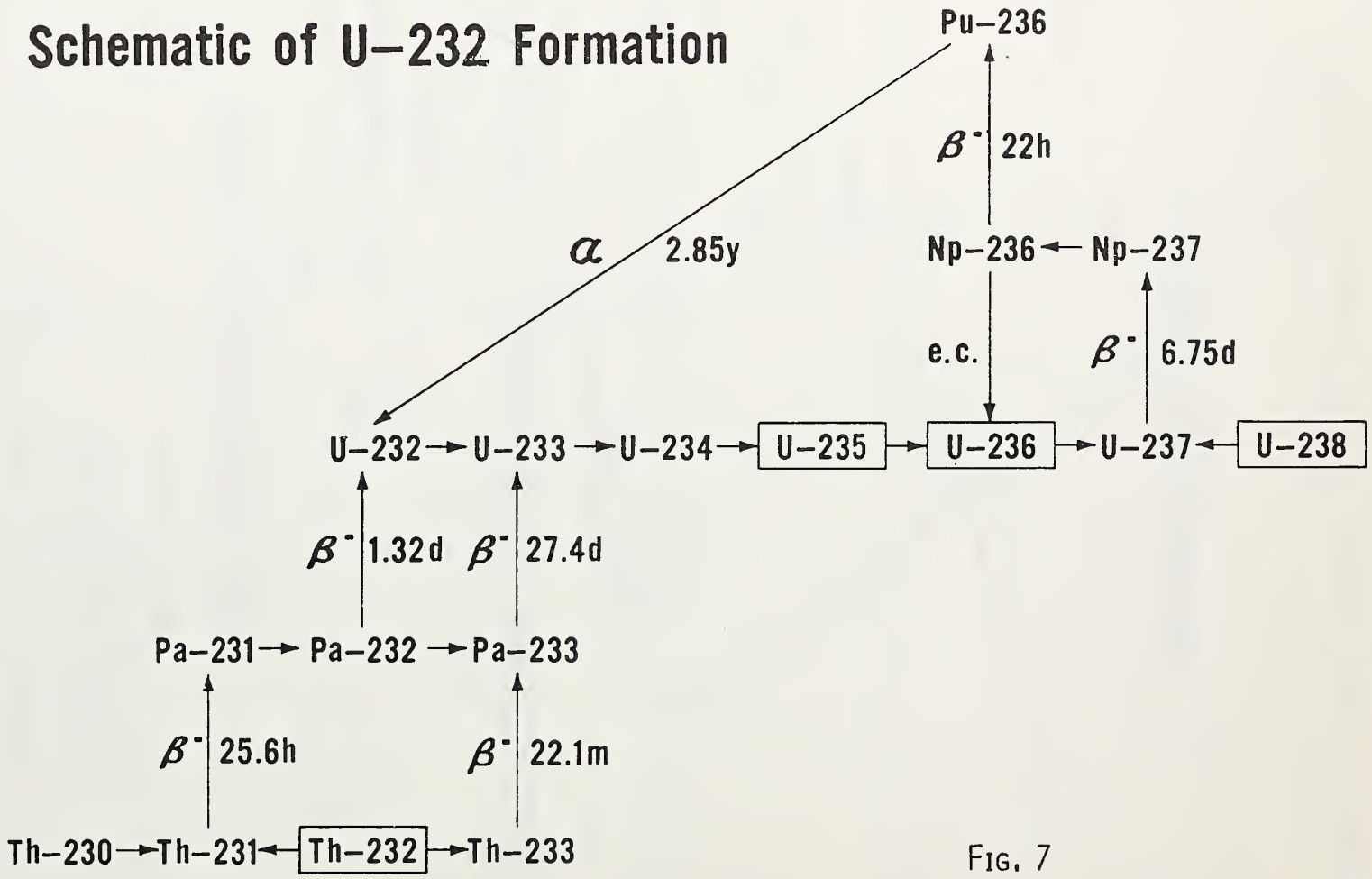
Schematic of U–232 Formation
Pu–236
β⁻ 22h
α 2.85y
Np–236
Np–237
e.c.
β⁻ 6.75d
U–232
U–233
U–234
U–235
U–236
U–237
U–238
β⁻ 1.32d
β⁻ 27.4d
Pa–231
Pa–232
Pa–233
β⁻ 25.6h
β⁻ 22.1m
Th–230
Th–231
Th–232
Th–233

FIG. 7

SENSITIVITY OF REACTIVITY CHARACTERISTICS TO CROSS SECTION UNCERTAINTIES FOR PLUTONIUM-FUELED THERMAL SYSTEMS*

By

U. P. Jenquin, V. O. Uotinen, C. M. Heeb

Battelle Memorial Institute
Pacific Northwest Laboratory
Richland, Washington 99352

ABSTRACT

Uncertainties in reactivity characteristics due to cross-section uncertainties are estimated for plutonium-fueled thermal reactor systems. The reactivity characteristics considered are: reactor multiplication, boron worth, moderator and fuel temperature coefficients, and void coefficient. Under the assumptions used in the analysis, appreciable uncertainties in reactor multiplications are due to uncertainties in the values of the resonance integrals and the normalizations of the thermal cross sections, as well as uncertainties in the shape of the ^{239}Pu thermal cross sections. Uncertainties in moderator coefficients are due mainly to uncertainties in the shape of the ^{239}Pu thermal cross sections.

INTRODUCTION

In the course of correlating calculated with measured reactor physics data, the question of the adequacy of the nuclear data usually arises. In some cases, the discrepancies between calculated and measured data can be accounted for by the cross-section uncertainties. This report shows to what extent the theoretical predictions of various reactivity characteristics are influenced by uncertainties in the nuclear data. Discrepancies due to inaccuracies in the theory itself will not be discussed.

The study has been restricted to the nuclear data σ_a and $\nu\sigma_f$ for the fissile and fertile isotopes of the reactor systems analyzed. The normalization and shapes of the thermal cross sections and the values of the resonance integrals are considered.

In Section I, the theoretical methods utilized in the analysis are discussed. In Section II the techniques used to determine the sensitivity of the reactivity characteristics to cross-section changes are explained and the results presented. In Section III, estimates of cross-section uncertainties are discussed. The uncertainties in the various reactivity characteristics are related to the cross-section uncertainties in Section IV.

---

* This paper is based on work performed under United States Atomic Energy Commission Contract AT(45-1)-1830.

I. THEORETICAL METHODS

Four critical experiments were selected for analysis to cover the range of plutonium-fueled H_2O-moderated reactor systems typical of large power reactor plants (UO_2-PuO_2) and compact reactor systems (Al-Pu). A description of each system is given in Table I. Hereafter, they will be referred to by the identification in Column 1. The first three systems are uniform lattices of cylindrical fuel rods in H_2O moderator. The MTR system[1] is an arrangement of fuel plates separated by H_2O moderator. In addition, this system contains numerous aluminum structural plates and H_2O gaps between these plates.

The theoretical methods consist of using the computer codes HRG,[2] THERMOS,[3] and TEMPEST[4] to obtain multigroup cell homogenized cross sections for use in multiplication calculations with the HFN[5] code. For the first three systems, the unit lattice cell with reflecting boundaries is assumed to consist of three cylindrical regions of fuel, clad, and moderator. For the MTR system the corresponding regions are slabs.

Nonthermal effects are computed using the HRG code which solves the time independent Boltzmann equation with isotropic sources of neutrons using the B-1 approximation. A fission spectrum for ^{239}Pu was assumed for weighting of fast cross sections. Resonance absorption in the fissile and fertile isotopes is treated according to the methods developed by Adler, Hinman, and Nordheim.[6] The corrections for absorber lump interaction used in the resonance computation within the HRG code, were calculated by the Carlvik method[7] for the rod lattices and by the Bell method[8] for the MTR slab system. The cladding was considered as part of the moderator for the calculation of lattice heterogeneity corrections.

Thermal effects are computed using THERMOS which solves the space-energy Boltzmann equation. The moderator scattering kernel was computed for each temperature by GAKER which is a subsidiary code to THERMOS and is based on the Nelkin model for H_2O.[9] All other thermal scatter-transfers were based on a gas model scattering kernel for the constituent materials.

The cell average thermal transport cross sections, $\bar{\Sigma}_{tr}$, are obtained from computations using the TEMPEST code. Flux and volume weighted atom densities are used as input to the code and the Wigner-Wilkins spectrum is utilized. The thermal diffusion coefficient is obtained from $1/3\ \bar{\Sigma}_{tr}$. For the MTR system, a site revised version of THERMOS[10] was used to calculate transport cross sections.

The multigroup cross sections for the homogenized lattice cell are edited to four energy groups. The boundaries for these groups are selected to isolate the effects of the major resonances of ^{239}Pu, ^{240}Pu, and ^{238}U cross sections. The upper energies of the groups are 10 MeV, 11.7 KeV, 2.38 eV, and 0.683 eV.

The reactor systems are assumed to be one dimensional cylinders consisting of two regions, a homogeneous core and a reflector. The reflector was assumed to be at the same temperature and of the same composition as the moderator except for the MTR system in which case the composition was beryllium. The four group constants for the homogenized lattice obtained from the fine

structure calculations, along with four group constants for the reflector (computed using the HRG and TEMPEST or THERMOS codes), are utilized in computing lattice multiplication values, k_{eff}, assuming one dimensional-multigroup diffusion theory using computer code HFN. A radial description of the reactor system is used in the HFN code. The code computes the radial neutron distribution in each energy group. The axial neutron distribution is approximated using energy-independent transverse bucklings.

II. SENSITIVITY CALCULATIONS

To determine how sensitive the reactor multiplication values are to isotopic cross section changes, the HFN calculations were repeated with the group cross section, $\nu\bar{\Sigma}_f$ or $\bar{\Sigma}_a$, arbitrarily increased by 10% in groups 1, 2, or 3 or by 1% in group 4. The difference in multiplications between the perturbed and unperturbed cases divided by the percentage change in group cell average cross section gives the sensitivity of the neutron multiplication to the cell average cross section for each energy group. Each fissile or fertile isotope contributes a fractional amount to the cell average cross section. Multiplying by this fractional amount gives a sensitivity coefficient of reactivity in terms of isotopic group average cross sections. We then assume the change in the macroscopic group average value for each isotope results from a change in the group average microscopic value for that isotope. The results for each reactor system at 20°C are given in Table II. The neutron multiplications are most sensitive to changes in the thermal cross sections. Since ^{239}Pu is the dominant isotope in terms of reactivity in all of the systems, the sensitivities in group 4 are largest for ^{239}Pu. The fuels which contain uranium are composed primarily of ^{238}U, thus, the sensitivity of neutron multiplications to changes in the group 2 ^{238}U cross section is quite significant. Results were presented at the First Conference on Neutron Cross Section Technology[11] for systems similar to the L_x Mixed Oxide and the H_x Mixed Oxide systems.

To determine how sensitive the other reactivity characteristics are to isotopic cross section changes, the parameter is calculated for the normal case and again for the case where a particular group cross section has been perturbed. The difference between the two values divided by the percentage change in the group cross section gives the sensitivity of the reactivity characteristic to the group cross section. This sensitivity is divided into isotopic group sensitivities in the same manner as the multiplication sensitivities were. The results (Tables III-VI) show that the reactivity characteristics are most sensitive to the thermal cross sections. Again, the largest sensitivities are for ^{239}Pu in the thermal group and ^{238}U in the nonthermal groups.

Thus far, the THERMOS calculations utilized ^{239}Pu thermal cross sections contained in the BNW Master Library.[12] These data are based upon the fitting of Leonard[13] with the 2200 m/sec constants normalized to values of the 1965 IAEA evaluation.[14] This evaluation does not provide information on the shape and the uncertainty in the shape of the evaluated data. In the absence of these data, we have used the ^{239}Pu absorption and fission cross section data from Schmidt's compilation[15] to illustrate the sensitivity of the reactivity characteristics to differences in the shape of these cross sections. The Schmidt data were used in THERMOS calculations and the cell average cross sections were again generated. Since the 2200 m/sec constants are nearly

identical to those of the IAEA evaluation (σ_a is 0.25% larger, σ_f is 0.02% smaller) and the same value of ν was used for both sets, differences in reactivity characteristics represent differences in the shapes of the cross sections. Figure 1 shows the differences between the two sets of data in the form of η as a function of energy. The difference in η as a function of energy is very important in situations where the energy of the peak of the thermal flux is shifting, i.e., moderator temperature changes. The neutron multiplication is also quite sensitive to the shapes of the cross sections because the multiplication is essentially proportional to η for the cell. The difference between the calculated reactivity characteristics using each set of data is shown in Table VII.

III. CROSS SECTION UNCERTAINTY ESTIMATES

We shall restrict ourselves to only the uncertainties in basic nuclear data for ^{235}U, ^{238}U, ^{239}Pu, ^{240}Pu, and ^{241}Pu. Further, we consider only the data for resonance and thermal neutron energies. The resonance data considered are the absorption and fission integrals for infinite dilution. The thermal data considered are the 2200 m/sec values of all of the isotopes and the shape of the ^{239}Pu cross sections.

Resonance Data

It was assumed that the infinitely dilute resonance integrals of the pertinent fissile and fertile isotopes are uncertain by 5%. Based upon previous reviews[16,17] of these resonance integral data, a 5% uncertainty may be an optimistic estimate of the status of these data.

To arrive at the uncertainty in reactor multiplications due to uncertainties in resonance cross sections, we assume that the magnitude of the relative uncertainty in the effective resonance integral, I_{eff}, is that of the value for the infinitely dilute resonance integral, I_∞. Based upon this assumption the uncertainty in I_{eff} is then related to the average cross section using the relationship $I_{eff} = \bar{\sigma}\ \Delta U$ where the lethargy increment ΔU arises in assuming a 1/E neutron flux variation with energy.

As stated previously, the group structure was selected so as to separate the major resonances of the ^{239}Pu, ^{240}Pu, and ^{238}U cross sections. The major portion of the resonance integrals for ^{235}U, ^{238}U, and ^{239}Pu are contained in group 2. Nearly all of the ^{240}Pu resonance integral is contained in group 3. Since most of the resonance integral for these nuclides is within group 2 for ^{235}U, ^{238}U, and ^{239}Pu and group 3 for ^{240}Pu, the uncertainties in the effective resonance integrals were assumed to be totally within these groups. The uncertainties in resonance integrals which have been conceived as the uncertainty in group average cross sections (group 3 for ^{240}Pu and group 2 for the other nuclides) are combined with the corresponding sensitivities to obtain uncertainties for the reactivity characteristics.

2200 m/sec Constants

The uncertainties in the 2200 m/sec constants for the fissile isotopes are those given in the IAEA evaluation.[14] They are 0.4% for ^{235}U absorption and fission cross sections, 0.5% for ^{239}Pu absorption and fission cross sections, and 2.0% for ^{241}Pu absorption and 1.0% for ^{241}Pu fission cross sections. For

the fertile isotopes ^{238}U and ^{240}Pu we have chosen the uncertainties to be 2.0% and 3.0% respectively. Analogous to the resonance data, these uncertainties have been combined with the calculated sensitivities to obtain estimates of the uncertainties in the reactivity characteristics.

Shape of the ^{239}Pu Thermal Cross Sections

As stated earlier, the effect of the shape of the ^{239}Pu thermal cross sections was determined by choosing two sets of cross sections and comparing the calculated reactivity characteristics using each set. It is probably reasonable to assume that uncertainties in the shape of the cross sections are of the order of the differences in the two sets of cross sections used in the calculations. The calculated differences which were presented in Section II will be represented as uncertainties in Section IV.

IV. UNCERTAINTIES IN THE REACTIVITY CHARACTERISTICS

Neutron Multiplication

Uncertainties in the neutron multiplication due to uncertainties in the cross sections are tabulated in Table VIII for each isotope in each system. The uncertainty due to the shape of the ^{239}Pu cross sections represents uncertainties in both the absorption and fission cross sections.

Since ^{239}Pu is the dominant isotope from a reactivity standpoint in all of these systems, it was expected to have the largest contributions to the uncertainty in the neutron multiplication. Based on the assumptions used in the calculations, the largest uncertainty in neutron multiplications is due to the shape of the ^{239}Pu cross sections. However, in going to systems with harder spectrums, uncertainties due to resonance integral data become larger and uncertainties due to the thermal data become smaller.

Temperature Coefficient

Uncertainties in all of the reactivity coefficients are represented as the difference of the coefficient calculated with perturbed (i.e., increased by 10%) cross sections and the coefficient calculated in the normal manner. The calculated uncertainties are very small; however, since the coefficients are small, the percentage error can be appreciable.

Uncertainties in the average temperature coefficients are presented in Table IX. Values smaller than $0.1 \times 10^{-5}/°C$ are listed as zero. The uncertainties due to uncertainties in the resonance integrals and 2200 m/sec constants are small and about the same for all systems. Since the temperature coefficients are large and negative ($\sim -10 \times 10^{-5}/°C$), all of these uncertainties yield less than a 10% uncertainty in the temperature coefficient. For a system which is close to optimum moderation in terms of reactivity, uncertainties of the order of $0.5 \times 10^{-5}/°C$ could yield very large percentage uncertainties in the temperature coefficient.

As indicated in Table IX, the shape of the ^{239}Pu thermal cross sections affects the value of the temperature coefficient a great deal. The percentage uncertainty in the temperature coefficient is between 10 and 20% for the systems

considered. The thermal neutron spectrum shifts to higher energies with increasing temperature, thus the change in η^{239} as a function of energy is very important.

The sensitivities of the moderator temperature coefficient between 20 and 220°C are comparable to the sensitivities of the temperature coefficient between 20 and 72°C, thus the uncertainties are comparable and will not be presented.

Other Reactivity Characteristics

The only important resonance integral data to consider with regard to the Doppler (fuel temperature) coefficient are those of ^{238}U, ^{239}Pu, and ^{240}Pu. The absolute uncertainty in the Doppler coefficient is between 0.3 and 0.5×10^{-5}/°C for ^{238}U, 0.1 and 0.2×10^{-5}/°C for ^{239}Pu, and 0.0 and 0.1×10^{-5}/°C for ^{240}Pu. These are significant uncertainties because the Doppler coefficients are quite small, between 1.0 and 2.0×10^{-5}/°C. The percentage uncertainties are: 20-25% for ^{238}U, 5-15% for ^{239}Pu, and 0-5% for ^{240}Pu.

The void coefficient (density change) is similar to the moderator temperature coefficient except that the temperature of the system remains constant. As the temperature of a system increases and/or a system becomes more undermoderated, the importance of the temperature decreases while the importance of the moderator density increases. Thus, uncertainties in the void coefficient are similar to uncertainties in the moderator coefficient for the systems considered.

The boron worth is essentially only a thermal effect because the boron cross section is 1/v in shape. The uncertainty in the boron worth for the Saxton system was found to be about 0.5% due to uncertainties in the 2200 m/sec constants for ^{239}Pu and about 1.5% due to uncertainties in the shape of the ^{239}Pu cross sections. These uncertainties would be expected to be larger in systems where the thermal neutron spectrum is softer.

V. CONCLUSIONS

Significant uncertainties in the neutron multiplication occur because of uncertainties in the resonance integral data, uncertainties in the 2200 m/sec constants, and uncertainties in the shape of the ^{239}Pu thermal cross sections. The assumed uncertainties in resonance integral data result in significant uncertainties in the neutron multiplication. Reducing the uncertainties in the resonance integral data to less than 5% for ^{238}U and ^{239}Pu would be desirable.

The uncertainty in k_{eff} due to uncertainties in the 2200 m/sec constants is sufficiently small to give relatively accurate values of k_{eff}. However, the shape of the thermal cross sections must also be known accurately to predict k_{eff} accurately, as indicated by the effect presented for ^{239}Pu cross sections. We have assumed the two effects to be independent of each other. In reality, the values for the evaluated 2200 m/sec constants are correlated to the shapes of the cross sections.[18] Therefore, uncertainties in the 2200 m/sec constants are related to uncertainties in the shapes of the cross sections. Because of the importance of the shapes of the cross sections in calculating neutron multiplications, we recommend that the evaluator provide these data along with the uncertainties, in addition to values and uncertainties in 2200 m/sec constants.

Moderator temperature coefficients are very sensitive to the shapes of the ^{239}Pu cross sections. A reduction in the uncertainties of the shapes of the cross sections for the fissile nuclides would lend increased confidence in calculating moderator temperature coefficients. The uncertainties in calculated Doppler coefficients are large because of the uncertainties in the resonance integral data. From a reactor safety standpoint, these coefficients are important, thus uncertainties in the resonance integral data for ^{238}U and ^{239}Pu should be reduced.

VI. REFERENCES

1. D. D. Lanning and G. J. Busselman. Phoenix Fuel Program Progress Report, BNWL-635. Pacific Northwest Laboratory, Richland, Washington, November, 1967.

2. J. L. Carter, Jr. "Computer Code Abstracts, Computer Code-HRG," Reactor Physics Department Technical Activities Quarterly Report, July, August, September, 1966, USAEC Report BNWL-340, Pacific Northwest Laboratory, Richland, Washington, October 15, 1966.

3. H. C. Honeck. THERMOS - A Thermalization Transport Theory Code for Reactor Lattice Calculations, USAEC Report BNL-2526, Brookhaven National Laboratory.

4. R. H. Shudde. Unpublished Data. North American Aviation Corporation, September 1960.

5. J. R. Lilley. Computer Code HFN-Multigroup Multiregion Neutron Diffusion Theory in One Space Dimension, USAEC Report HW-71545, Hanford Atomic Products Operation, General Electric Co., Richland, Washington, November 1961.

6. F. T. Adlier, G. W. Hinman, and L. W. Nordheim, "The Quantitative Evaluation of Resonance Integrals," paper No. 1988, Proceedings of the Second United Nations Conference on the Peaceful Uses of Atomic Energy, Vol. 16, pp. 155, 1958.

7. I. Carlvik. "The Dancoff Correction in Square and Hexagonal Lattices," Nucl. Sci. and Eng., 29, p. 3, September 1967.

8. G. I. Bell. "A Simple Treatment for Effective Resonance Absorption Cross Sections in Dense Lattices," letter to the Editor, N.S.E. 5, 75-77, (1959).

9. M. Nelkin. "Scattering of Slow Neutrons by Water," Phys. Rev., 119, pp. 741-746. 1960.

10. D. R. Skeen and L. J. Page. The Battelle Version of the THERMOS Code, BNWL-516. Pacific Northwest Laboratory, Richland, Washington, September 1967.

11. R. C. Liikala, W. L. Purcell, and J. R. Worden. "Sensitivity of Reactor Multiplication Values to Cross Section Uncertainties for Thermal Systems," Proceedings of the Conference on Neutron Cross Section Technology, pp. 75-87, March 1966.

12. K. B. Stewart. BNW Master Library, BNWL-CC-325. Pacific Northwest Laboratory, Richland, Washington, September 1965.

13. B. R. Leonard, Jr. A Review of the Neutron Cross Sections of Pu^{239} Below 1 eV, TNCC(US)-58, August 1959.

14. C. H. Westcott, et al. "A Survey of Values of the 2200 m/s Constants for Four Fissile Nuclides," Atomic Energy Review, 3, p. 2. 1965.

15. J. J. Schmidt. Neutron Cross Sections for Fast Reactor Materials, Part 1: Evaluation, KFK-120 (E ANDC-E-35U), February 1966.

16. R. C. Liikala and W. L. Purcell. "Correlation of Effective Cross Sections," Plutonium Utilization Program Annual Report Fiscal Year 1967, USAEC Report BNWL-624, Pacific Northwest Laboratory, Richland, Washington, January 1968.

17. F. G. Dawson, et al. "Analysis of Plutonium Fueled Light Water Reactors," IAEA Symposium on the Use of Plutonium as a Reactor Fuel, Brussels, Belgium, March 1967.

18. B. R. Leonard, Jr. Private Communication.

19. Taylor, E. G., et al. Saxton Plutonium Program Critical Experiments for the Saxton Partial Plutonium Core, EURAEC-1493, WCAP-3385-54, Westinghouse Electric Corp., December, 1965.

20. V. O. Uotinen and L. D. Williams. "Experiments and Calculations for H_2O-Moderated Assemblies Containing UO_2-2 wt% PuO_2 Fuel Rods," Trans. Am. Nucl. Soc., vol. 10, No. 1, p. 186. 1967.

TABLE I

DESCRIPTION OF THE REACTOR SYSTEM (1,19,20)

Identification	Lattice type and spacing (in.)	Fuel Diameter, (in.)	Fuel Constituents	Plutonium Composition % 239/240/241/242
Saxton (19)	□ 0.56	0.337	UO_2-6.6 wt% PuO_2	90.6/8.5/0.9/0.0
L_x Mixed Oxide (20)	Δ 0.85	0.505	UO_2-2.0 wt% PuO_2	91.7/7.6/0.7/0.0
H_x Mixed Oxide (20)	Δ 0.85	0.505	UO_2-2.0 wt% PuO_2	71.7/23.5/4.1/0.7
MTR (1)	plates 0.198	0.040	Al-20 wt% Pu	65/23/8/4

TABLE II

SENSITIVITY OF NEUTRON MULTIPLICATION TO CROSS SECTION CHANGES

Multiplication Sensitivity, $\frac{dk}{k}$/% Change in $\bar{\sigma}$, (10^{-3}/%$\Delta\bar{\sigma}$)

System	Group	Absorption					Fission				
		^{235}U	^{238}U	^{239}Pu	^{240}Pu	^{241}Pu	^{235}U	^{238}U	^{239}Pu	^{240}Pu	^{241}Pu
Saxton	1	0.01	0.25	0.09	0.04	-	0.02	0.38	0.25	0.01	-
	2	0.11	0.97	0.71	0.04	-	0.13	-	1.00	-	-
	3	0.02	0.03	0.13	0.47	-	0.02	-	0.02	-	-
	4	0.33	0.20	6.71	0.16	-	0.40	-	7.57	-	-
L_x Mixed Oxide	1	0.01	0.30	0.03	-	-	0.02	0.46	0.09	-	-
	2	0.14	1.09	0.32	0.01	-	0.17	-	0.46	-	-
	3	0.03	0.04	0.05	0.30	-	0.04	-	0.08	-	-
	4	1.04	0.61	5.82	0.11	-	1.35	-	7.21	-	-
H_x Mixed Oxide	1	0.01	0.33	0.03	-	-	0.03	0.50	0.08	0.01	0.01
	2	0.14	1.14	0.27	0.04	0.03	0.18	-	0.41	-	0.06
	3	0.03	0.04	0.04	0.52	-	0.04	-	0.07	-	-
	4	1.15	0.68	5.05	0.39	0.32	1.57	-	6.55	-	0.46
MTR	1	-	-	0.11	0.02	0.02	-	-	0.16	0.03	0.02
	2	-	-	0.67	0.10	0.11	-	-	0.88	-	0.16
	3	-	-	0.08	0.74	0.01	-	-	0.14	-	0.01
	4	-	-	7.47	0.56	0.81	-	-	6.48	-	0.79

TABLE III

SENSITIVITY OF TEMPERATURE COEFFICIENT TO CROSS SECTION CHANGES

Temperature Coefficient Sensitivity, $\Delta\left(\frac{1}{k}\frac{dk}{dT}\right) \Big/ \%$ Change in $\bar{\sigma}$, $(10^{-6}/^{o}C/\%\Delta\bar{\sigma})$

System	Group	Absorption					Fission				
		^{235}U	^{238}U	^{239}Pu	^{240}Pu	^{241}Pu	^{235}U	^{238}U	^{239}Pu	^{240}Pu	^{241}Pu
Saxton*	1	-	0.01	-	-	-	-	0.04	0.03	-	-
	2	0.02	0.14	0.10	0.01	-	0.08	-	0.63	-	-
	3	0.01	0.01	0.04	0.15	-	0.02	-	0.19	-	-
	4	0.11	0.07	2.32	0.05	-	0.12	-	2.35	-	-
L_x Mixed Oxide*	1	-	0.05	-	-	-	0.01	0.12	0.02	-	-
	2	0.05	0.37	0.11	-	-	0.13	-	0.35	-	-
	3	-	-	0.01	0.03	-	-	-	0.01	-	-
	4	0.11	0.07	0.63	0.01	-	0.11	-	0.58	-	-
H_x Mixed Oxide*	1	-	0.06	-	-	-	0.01	0.13	0.02	-	-
	2	0.03	0.25	0.06	0.01	0.01	0.13	-	0.29	-	0.05
	3	-	-	-	0.04	-	0.01	-	0.01	-	-
	4	0.11	0.06	0.48	0.04	0.03	0.13	-	0.53	-	0.04
MTR**	1	-	-	-	-	-	-	-	0.01	-	-
	2	-	-	-	-	-	-	-	0.58	-	0.11
	3	-	-	0.01	0.08	-	-	-	0.62	-	0.07
	4	-	-	1.06	0.08	0.12	-	-	9.84	-	1.19

* 20 to 72°C for the fuel and moderator

** 20 to 50°C for the moderator, 20 to 115°C for the fuel

TABLE IV

SENSITIVITY OF MODERATOR TEMPERATURE COEFFICIENT TO CROSS SECTION CHANGES

Temperature Coefficient Sensitivity, $\Delta\left(\frac{1}{k}\frac{dk}{dT}\right)\Big/$% Change in $\bar{\sigma}$, $(10^{-6}/{}^{o}C/\%\Delta\bar{\sigma})$

System	Group	Absorption					Fission				
		^{235}U	^{238}U	^{239}Pu	^{240}Pu	^{241}Pu	^{235}U	^{238}U	^{239}Pu	^{240}Pu	^{241}Pu
Saxton*	1	0	0.02	0.01	0		0	0.09	0.06	0	
	2	0.02	0.17	0.13	0.01		0.02		0.12		
	3	0.01	0.01	0.05	0.16		0		0		
	4	0.15	0.09	3.01	0.07		0.18		3.48		
L_x Mixed Oxide*	1	0	0.08	0.01	0		0.01	0.27	0.05	0	
	2	0.04	0.31	0.09	0		0.10		0.27		
	3	0	0.01	0.01	0.06		0.02		0.04		
	4	0.14	0.08	0.77	0.02		0.11		0.58		
H_x Mixed Oxide*	1	0	0.13	0.01	0	0	0.02	0.31	0.05	0.01	0
	2	0.06	0.45	0.11	0.02	0.01	0.12		0.27		0.04
	3	0	0.01	0.01	0.10	0	0.02		0.03		0
	4	0.15	0.09	0.67	0.05	0.04	0.15		0.61		0.04

* 20 to 220°C for the moderator, fuel is at 20°C.

TABLE V

SENSITIVITY OF DOPPLER COEFFICIENT TO CROSS SECTION CHANGES

Doppler Coefficient Sensitivity, $\Delta\left(\frac{1}{k}\ \frac{dk}{dT}\right)\Big/$% Change in $\bar{\sigma}$, $(10^{-6}/{}^{o}C/\%\Delta\bar{\sigma})$

System	Group	Absorption					Fission				
		^{235}U	^{238}U	^{239}Pu	^{240}Pu	^{241}Pu	^{235}U	^{238}U	^{239}Pu	^{240}Pu	^{241}Pu
Saxton *	1	0	0.004	0.001	0.001		0	0.001	0	0	
	2	0.006	0.057	0.042	0.002		0.008		0.061		
	3	0	0	0	0		0.001		0.008		
	4	0.008	0.005	0.163	0.004		0.010		0.197		
L_x Mixed Oxide*	1	0	0	0	0		0	0.007	0.001	0	
	2	0.011	0.086	0.025	0.001		0.009		0.025		
	3	0.002	0.002	0.003	0.018		0		0.001		
	4	0.005	0.003	0.028	0		0.008		0.042		
H_x Mixed Oxide*	1	0	0	0	0	0	0	0.008	0.001	0	0
	2	0.011	0.088	0.020	0.003	0.002	0.008		0.019		0.003
	3	0.001	0.002	0.002	0.021	0	0		0.001		0
	4	0.004	0.002	0.018	0.001	0.001	0.007		0.031		0.002

* 20 to 1500°C for the fuel, moderator is at 220°C.

TABLE VI

SENSITIVITY OF BORON WORTH AND VOID COEFFICIENT TO CROSS SECTION CHANGES

Boron Worth Sensitivity, $\Delta\left(\frac{1}{k}\ \frac{dk}{d(ppm*)}\right)$ / % Change in $\bar{\sigma}$, (10^{-6}/ppm/%$\Delta\bar{\sigma}$)

System	Group	Absorption					Fission				
		^{235}U	^{238}U	^{239}Pu	^{240}Pu	^{241}Pu	^{235}U	^{238}U	^{239}Pu	^{240}Pu	^{241}Pu
Saxton*	1	0	0.01	0	0		0	0.01	0	0	
	2	0	0.03	0.02	0		0		0.02		
	3	0	0	0	0		0		0		
	4	0.03	0.02	0.61	0.01		0.04		0.68		

Void Coefficient Sensitivity, $\Delta\left(\frac{1}{k}\ \frac{dk}{d(\%\ Void)}\right)$ / % Change in $\bar{\sigma}$, (10^{-6}/% Void/%$\Delta\bar{\sigma}$)

L_x Mixed Oxide**	1	0	1.1	0.1	0		0.2	4.0	0.8	0	
	2	0.5	3.8	1.1	0		1.4		4.0		
	3	0.1	0.1	0.1	0.8		0.2		0.5		
	4	1.6	1.0	9.1	0.2		1.7		9.2		
H_x Mixed Oxide**	1	0.1	1.6	0.1	0	0	0.2	4.7	0.7	0.1	0
	2	0.7	5.4	1.3	0.2	0.1	1.8		4.0		0.6
	3	0	0.1	0.1	1.0	0	0.2		0.4		0
	4	2.1	1.2	9.1	0.7	0.6	2.4		9.9		0.7
MTR***	1			0.1	0	0			0.9	0.2	0.1
	2			0.6	0.1	0.1			1.6		0.3
	3			0.4	4.0	0			0.4		0
	4			47.8	3.6	2.2			12.3		1.5

* Atoms of natural boron per million molecules of H_2O, 0 to 1000 ppm.

** 0 to 20% void at 220°C, fuel is at 1500°C.

*** 0 to 30% void at 50°C, fuel is at 115°C.

TABLE VII

DIFFERENCES IN REACTIVITY CHARACTERISTICS
USING TWO DIFFERENT SETS OF ^{239}Pu THERMAL CROSS SECTIONS

Reactivity Characteristic	System			
	Saxton	L_x Mixed Oxide	H_x Mixed Oxide	MTR
Neutron Multiplication, $\frac{dk}{k}$ (10^{-3})	+6	+5	+4	+19
Temp. Coeff. (20-72°C), $\frac{1}{k}\frac{dk}{dT}$ (10^{-5}/°C)	+1.6	+2.3	+2.1	
Mod. Coeff. (20-220°C), $\frac{1}{k}\frac{dk}{dT}$ (10^{-5}/°C)	+0.8	+1.7	+1.6	
Boron Worth (0-1000ppm), $\frac{1}{k}\frac{dk}{ppm}$ (10^{-5}/ppm)	-1.0			
Void Coeff. (0-20%), $\frac{1}{k}\frac{dk}{\%\ Void}$ (10^{-3}/% Void)		+0.42	+0.37	

TABLE VIII

UNCERTAINTIES IN NEUTRON MULTIPLICATION DUE TO UNCERTAINTIES IN ISOTOPIC CROSS SECTIONS

Isotope and Cross Section	Uncertainty in k_{eff}, 10^{-3}		
	Resonance Integral Data	2200 m/sec Constants	Shape of ^{239}Pu Thermal Cross Section
Saxton			
^{235}U absorption	1	<1	
^{235}U fission	1	<1	
^{238}U absorption	5	<1	
^{239}Pu absorption	4	3	6
^{239}Pu fission	6	4	
^{240}Pu absorption	2	<1	
L_x Mixed Oxide			
^{235}U absorption	1	<1	
^{235}U fission	1	<1	
^{238}U absorption	6	1	
^{239}Pu absorption	2	3	5
^{239}Pu fission	2	4	
^{240}Pu absorption	2	<1	
H_x Mixed Oxide			
^{235}U absorption	1	<1	
^{235}U fission	1	<1	
^{238}U absorption	6	1	
^{239}Pu absorption	1	2	4
^{239}Pu fission	2	3	
^{240}Pu absorption	3	1	
^{241}Pu absorption	0	<1	
^{241}Pu fission	0	<1	
MTR			
^{239}Pu absorption	3	4	19
^{239}Pu fission	4	3	
^{240}Pu absorption	4	2	
^{241}Pu absorption	<1	2	
^{241}Pu fission	1	1	

TABLE IX

UNCERTAINTIES IN TEMPERATURE COEFFICIENT DUE TO UNCERTAINTIES IN ISOTOPIC CROSS SECTIONS

Isotope and Cross Section	Uncertainty in Temperature Coefficient, $\frac{1}{k}\frac{dk}{dT}$ (10^{-5}/°C)		
	Resonance Integral Data	2200 m/sec Constants	Shape of ^{239}Pu Thermal Cross Sections
Saxton			
^{235}U absorption	0	0	
^{235}U fission	0	0	
^{238}U absorption	0.1	0	
^{239}Pu absorption	0	0.1	1.6
^{240}Pu fission	0.3	0.1	
^{240}Pu absorption	0.1	0	
L_x Mixed Oxide			
^{235}U absorption	0	0	
^{235}U fission	0.1	0	
^{238}U absorption	0.2	0	
^{239}Pu absorption	0.1	0	2.3
^{239}Pu fission	0.2	0	
^{240}Pu absorption	0	0	
H_x Mixed Oxide			
^{235}U absorption	0	0	
^{235}U fission	0.1	0	
^{238}U absorption	0.1	0	
^{239}Pu absorption	0	0	2.1
^{239}Pu fission	0.1	0	
^{240}Pu absorption	0	0	
^{241}Pu absorption	0	0	
^{241}Pu fission	0	0	
MTR			
^{239}Pu absorption	0	0.5	
^{239}Pu fission	0.3	0.5	
^{240}Pu absorption	0	0	
^{241}Pu absorption	0	0	
^{241}Pu fission	0	0.1	

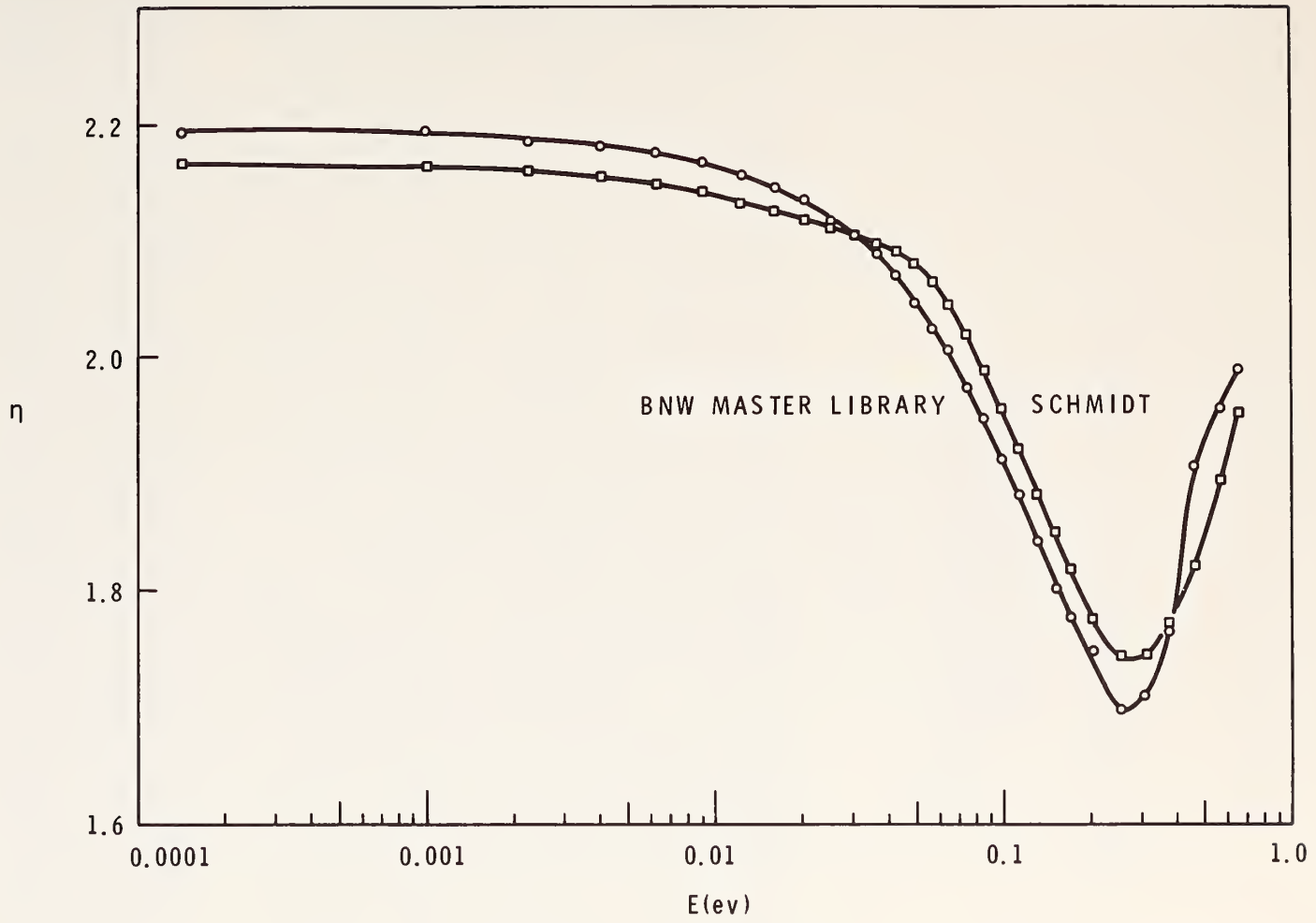

FIGURE 1
Variation of Eta with Energy for ^{239}Pu

SIGNIFICANCE OF NEUTRON DATA TO FAST REACTOR POWER PLANT DESIGN*

P. Greebler, B. A. Hutchins, and B. Wolfe

General Electric Company
Nuclear Energy Division
Advanced Products Operation
Sunnyvale, California 95125

ABSTRACT

An evaluation of the sensitivity of physics parameters and fuel costs of fast power reactors indicates that combined current data uncertainties produce about a ±0.15 mill/kwh uncertainty in fuel cost for a sodium-cooled fast reactor whose design has not been severely limited by requirements on the sodium void and Doppler reactivity effects. The uncertainty in physics parameters and fuel cost for steam-cooled fast reactors is about the same as for sodium coolant. Fissile breeding with steam-cooled fast reactors is jeopardized by the possibility of appreciably adverse nuclear data, whereas adequate breeding gain appears assured for sodium-cooled systems. For a sodium-cooled reactor that must satisfy stringent sodium void and Doppler reactivity requirements, the combined data uncertainties produce about a ±0.25 mill/kwh uncertainty in fuel cost. The current large uncertainty in the Pu-239 alpha value below 15 keV is the largest single contributor to the over-all fuel cost uncertainty, with the uncertainties in U-238 radiative capture cross sections and Pu-239 $\bar{\nu}$ being next in importance. A set of targets for nuclear data accuracy is recommended, on the basis of the calculated sensitivity of fuel cost to specific data uncertainties, which would reduce the calculated fuel cost uncertainty to about ±0.03 mill/kwh.

Design modifications and associated development programs to improve fuel and heat transfer-fluid flow performance will be required, even for a sodium-cooled fast reactor, in the event of appreciably adverse nuclear data, if specific performance targets, such as low fissile doubling time (∿10 years), are to be achieved. The uncertainties in performance, date of introduction, and need for additional development of fast reactors due to data uncertainties have large enough economic implications for the total reactor economy to justify an intensive effort to reduce these uncertainties.

---

* Work performed in part under Contract AT(04-3)-189
Project Agreement 10 between the
Atomic Energy Commission and
General Electric Company

1 INTRODUCTION

As fast reactor designers, we are concerned about nuclear data uncertainties for two reasons. One is the uncertainty that it produces in our projections of fast breeder reactor power costs, mainly in the plutonium credit and plutonium inventory components of the fuel cost. A large economic uncertainty results from these data uncertainties because they tend to obscure the role fast breeders will play in the future reactor economy. A second concern is for the design of the early-generation fast breeder power plants and the uncertainty in reactivity coefficients and other reactor performance characteristics associated with the data uncertainties.

There have been several studies of the sensitivity of fast reactor physics parameters to uncertainties in nuclear data.[1-6] Uncertainty in current fuel cost projections of sodium-cooled fast power reactors due to nuclear data uncertainties was discussed in Reference 6. This paper will cover an extension of the work described in that earlier presentation, including consideration of steam-cooled as well as sodium-cooled fast reactors. A summary will first be given of the significant points made in the earlier presentation on the status of data uncertainties and their effect on projected fuel costs, and on the indicated requirements for nuclear data measurements to reduce the cost uncertainties. Consideration will then be given to core design alternatives that may be adopted in order to satisfy advanced performance targets in the event of adverse nuclear data, and to an assessment of the resulting uncertainties in the projected reactor economy.

Data uncertainty ranges used for the sensitivity studies are indicated in Tables I and II. These were evaluated from the sources of References 7 through 31 and are fully discussed in the earlier paper.[6] ENDF/B data[7] was used for the base cross-section data. For the most important data uncertainties, the principal references are the following:

Pu-239 alpha - Schomberg, Sowerby and Evans[8]; the ENDF/B evaluation[11]; Hopkins-Diven[12]; and the ORNL measurements of deSaussure, et al[13].

Pu-239 σ_f - Dubrovina and Shigin[14]; Smith, Henkel and Nobles[15]; White, et al[16]; and Henkel[17].

Pu-239 $\bar{\nu}$ - Mather, et al[18]; and Colvin and Sowerby[19].

U-238 σ_c - Macklin, Pasma and Gibbons[20]; Moxon, et al[21]; Barry, Bunce, and White[22]; Leipunski, et al[23]; and Bercqvist[24].

2. SODIUM-COOLED FAST REACTOR PARAMETERS

Table III shows physics parameters and fuel cost of two sodium-cooled, oxide-fueled, 1000 MW(e) fast reactors which were used as models for the determination of the sensitivity of the fuel cost to uncertainties in nuclear data.

The low leakage reactor has a 2-1/2 foot core height. This was selected on the basis of thermal-hydraulics and economics considerations, with secondary consideration given to the sodium void reactivity problem. It has a very good neutron economy as indicated by the breeding ratio of almost 1.4 and the less than 10-year fissile doubling time. The fuel cost is calculated to be 0.5 mill/kwh. The cost components most sensitive to the nuclear data uncertainties are the plutonium credit and the plutonium inventory, and these are based on a fissile plutonium value of $10/gm, a 10% per annum fuel use charge, and an 80% load factor. The Doppler coefficient (-T dk/dT) with coolant out of the core is just under 0.004, and total loss of sodium results in a 1.2% reactivity increment. Since we do not yet fully understand the limitations on the design that may be imposed by the sodium voiding reactivity effect, we classify this reactor for purposes of discussion as being an "advanced design".

The second reactor, having a 1.5 ft core height, is a more conservative safety design with regard to the sodium voiding reactivity problem. It was a requirement for this reactor that the reactivity change due to total sodiumvoiding be zero (or negative) and, further, that the negative Doppler coefficient with sodium out be at least 0.004. This requires a core with a high neutron leakage, in this case produced by having a core of only 18-inches in height. It also requires the addition of a small amount of moderating material, 3.4 v/o BeO, to degrade the neutron spectrum. Imposing these stringent safety criteria penalizes the neutron economy, as noted from the higher fissile inventory, lower breeding ratio, longer doubling time, and higher fuel cost, compared with the low leakage reactor. These requirements for the Doppler and sodium void coefficients also affect the sensitivity of the fuel cost to the nuclear data uncertainties.

3. FUEL COST COMPONENTS - EXAMPLES OF SENSITIVITY TO SPECIFIC DATA UNCERTAINTIES

Table IV shows the breakdown in fuel cost for the two reactors. Note that for the advanced core -- the one with the 2.5 ft height and with no BeO -- the plutonium credit almost cancels the fissile inventory cost; whereas this is not the case for the less advanced reactor and, hence, accounts for most of the difference in total fuel cost. The three right-hand columns show the changes in the calculated fuel cost components for the advanced reactor when we use three different cross-section variations which are the extreme highs in their respective uncertainty ranges. The high Pu-239 alpha below 15 keV produces a very large reduction in the plutonium credit which is associated with the loss of breeding ratio. Most of the cross-section uncertainties

mainly affect the plutonium credit component of the fuel cost, with the variation in the plutonium inventory cost associated with the associated change in fissile "enrichment" generally being considerably smaller. An exception to this rule is the fission cross section of the dominant fissile isotope, Pu-239, whose variation primarily affects the inventory cost component, as shown in the next to the last column of Table IV. Variations in the radiative capture cross sections of the fertile isotopes produce opposing effects on the credit and inventory cost components. The right-hand column of Table IV shows that using high U-238 capture cross sections between 1 and 100 keV improves the plutonium credit by an amount that substantially overrides the penalty in the plutonium inventory cost.

Note that the fabrication and recovery costs in Table IV are affected only in the third significant decimal place. This is due to small variations in the power distribution that result in small changes in the ratio of blanket fuel to core fuel, in addition to small changes in fissile material losses during processing.

4. SENSITIVITY RESULTS FOR LOW LEAKAGE REACTOR

Table V continues to show the sensitivity of the advanced reactor to data uncertainties. The uncertainty range in total fuel cost (minimum and maximum values) is shown corresponding to each of several important nuclear data uncertainties, and for the combined effect of all of the data uncertainties. The adjacent column g i v e s the uncertainty ranges in the fissile doubling time. The bottom row shows the base values which were calculated using the ENDF/B cross-section data.

The assumptions made on the energy correlation of the data uncertainties and the method used to get the combined effect of the various uncorrelated contributions were described in the earlier paper.[6] The uncertainty in the fuel cost on the high side from the base value is about 0.15 mill/kwh; 0.25 mill/kwh for the full uncertainty span. The uncertainty span in doubling time is about a factor of two. The uncertainties in alpha and $\bar{\nu}$ of Pu-239 and in the U-238 capture cross section are the largest individual contributors to these uncertainties, with fission product capture and Pu-239 fission being the next most important. Other data uncertainties that contribute significantly include cross sections for U-238 inelastic scattering and fission, steel and tantalum (the control rod material) capture, Pu-240 fission and capture, and Pu-241 fission.

In order to arrive at these uncertainty ranges, available measured data and data evaluations were used to select the very highest and the very lowest reasonable values for each data parameter within each assumed correlated energy interval. Thus the uncertainty ranges here are considered to be near maximum uncertainties -- much nearer to two or three standard deviations than to one.

5. SENSITIVITY RESULTS FOR HIGH LEAKAGE REACTOR

Table VI shows the sensitivity to data uncertainties of the high leakage reactor in which stringent requirements are imposed on the sodium void and the Doppler reactivity effects. In this case, the BeO content has to be adjusted in order to satisfy these requirements as the cross-section data varies. The right-hand column lists the ranges of BeO content corresponding to the ranges of listed data uncertainties. In this case, the Pu-239 alpha uncertainty, which produces a 30% uncertainty in the calculated Doppler coefficient and a 2$ uncertainty in the calculated sodium voiding reactivity, results in a large uncertainty in the required amount of BeO which, in turn, considerably enlarges the fuel cost uncertainty, and also that of the doubling time, relative to the advanced low-leakage reactor.

6. ACCURACY GOALS FOR NEUTRON DATA MEASUREMENTS

Table VII lists nuclear data measurements needed for fast reactor computations, with the first four being the most important. The indicated accuracies are desired over the different parts of the neutron energy spectrum in order to reduce the fuel cost uncertainty associated with each kind of data to the amount listed in the right-hand column. These fuel cost uncertainties are for the low-leakage advanced sodium-cooled reactor, since longer-term accuracy goals for cross-section measurements are being considered here. Note the very high precision required of $\bar{\nu}$ to get its cost uncertainty to less than 0.02 mill/kwh. The Pu-239 σ_f and U-238 σ_c are desired at the next higher precision. The Pu-239 alpha value below 15 keV should be given the highest priority, even though it does not ultimately require the highest precision, because its present uncertainty is so large. If cross-section measurers can provide the data accuracies requested here, it will be possible to design plutonium-fueled fast power reactors with only a $\pm$0.03 mill/kwh uncertainty in fuel cost due to data uncertainties.

7. SENSITIVITY RESULTS FOR STEAM-COOLED FAST REACTORS

The earlier reported sensitivity studies considered only the two sodium-cooled reactors that were discussed above. Results of calculations on steam-cooled fast reactors show a fuel cost sensitivity to data uncertainties which is similar to that for sodium-cooled fast reactors. However, the breeding ratio in excess of unity is considerably lower with steam coolant than with sodium and the doubling time sensitivity is correspondingly higher. Table VIII shows changes in several physics parameters of two steam-cooled 1000 MW(e) fast reactors produced by increasing the Pu-239 alpha below 15 keV from the base values to the high end of the uncertainty range. The steam-cooled reactors are designed for 1500 and 2400 psi steam pressure. Results for the low-leakage, sodium-cooled reactors are also given for comparison. Although the increase in fissile inventory and the reduction of

breeding ratio is virtually the same for all three reactors, thereby resulting in the same increment of fuel cost, the advanced sodium reactor continues to have a fairly low doubling time, whereas the 1500 psi steam reactor becomes a very marginal breeder and the 2500 psi steam reactor is reduced to a non-breeding advanced converter system. It is also noted that the loss of coolant reactivity for the steam-cooled reactors is more sensitive to the Pu-239 alpha uncertainty than is the case for the sodium-cooled reactor.

8. ENGINEERING DESIGN ALTERNATIVES TO COUNTERACT ADVERSE DATA

If subsequent measurements of cross sections indicate that data is on the adverse side of the uncertainty range, a number of design modifications may be considered which would still satisfy certain performance targets. For illustration by a relatively simple example, the advanced sodium-cooled reactor concept (no severe limitations imposed by the sodium void reactivity effect) will be considered with alternatives in core and fuel design that would yield a doubling time of 10 years even if the very high Pu-239 alpha values considered in this sensitivity study turned out to be correct.[1]

As indicated in Table VIII the pessimistic Pu-239 alphas increase the doubling time to 13.5 years. Engineering design modifications that may be considered to counteract such adverse data and return the doubling time to 10 years include the following:

1. Different fuel material (not oxide) such as carbide which (if developed to its full potential) could appreciably reduce fissile inventory because of its higher thermal conductivity and also increase the breeding ratio because of its higher density of fertile and fissile atoms.

2. Sodium-bonded fuel which would reduce fissile inventory because of improved heat transfer from fuel surface to coolant.

3. Smaller fuel rod diameter to reduce fissile inventory and/or higher oxide density to increase breeding ratio.

4. Higher fuel volume fraction to increase breeding ratio and reduce inventory. This can be achieved through advances in fuel spacer and subassembly enclosure design that result in lower fuel rod pitch-to-diameter ratio and in lower steel and sodium content.

---

1. Other combinations of pessimistic data could be considered for this purpose. For example, a combination of lower U-238 capture cross sections and not quite so high Pu-239 alphas would produce about the same effect on breeding and economics as the very high Pu-239 alphas alone.

These design modifications require advances in fuel technology and demand higher performance of the coolant in core heat removal (such as higher flow velocity and/or larger temperature rise across the core to accommodate an improved fuel heat transfer and/or a tighter fuel lattice) with consequent increased severity on material requirements to withstand larger coolant pressure differentials across the core and/or higher coolant outlet temperatures. Development programs in sodium technology must, correspondingly, be extended to assure that reactor operation under these more stringent requirements does not result in unacceptable risks to the potential utility reactor operators.

Table IX shows core design parameters which would result from the high Pu-239 alpha values below 15 keV for the original low-leakage design and for two alternate designs which are chosen to yield 10-year doubling times with the high Pu-239 alpha values. In order to achieve this condition, the fuel was sodium-bonded to the clad in one case, and the fuel rod diameter reduced from 0.25 to 0.225 inches for the other alternate. The fuel rod pitch-to-diameter ratio was reduced for both alternates, permitting a slightly higher fuel volume fraction with a lower sodium content and no increase in the steel content. The alternate designs have the base design characteristics of 2.5 ft core height, 18-inch thick blankets, oxide fuel density at 90% theoretical density, steel clad thcknesses based on the gaseous fission-product vent-to-coolant approach, 300°F coolant temperature rise across the core, and a peak central fuel temperature slightly below the melting point.

Sodium bonding or the smaller fuel rod diameter each permit an increase in fuel specific power leading to a reduction in the fissile inventory by about 20%; the higher fuel volume fraction and lower sodium fraction increase the breeding ratio from 1.28 to 1.31. The tighter lattice and higher heat transfer from fuel to coolant require about a 35 ft/sec sodium flow velocity for the alternate designs, compared with 28 ft/sec for the base design. This results in coolant core pressure drops of about 200 psi for the alternate designs.

9. ECONOMIC IMPLICATIONS OF FAST REACTOR DATA UNCERTAINTY

The previous sections have indicated that the uncertainty in power cost due to nuclear data uncertainties amounts to approximately 0.25 mill/kwh For calibration it is worth noting that this uncertainty represents about a $2 million per year operating uncertainty for a 1000 MW(e) plant.[2] It also

2. The nuclear data uncertainties affect mainly the fuel cost, but they also produce a small uncertainty in capital cost because of resultant uncertainties in design requirements such as number of control rods, shielding thicknesses, and containment pressure in a Doppler-controlled design basis accident. These capital cost factors are estimated to add about another 0.03 mill/kwh to the power cost uncertainty span associated with the nuclear data uncertainties. The power cost uncertainty span arising from approximations in current neutronics computation methods -- other than data -- is estimated to be about 0.05 mill/kwh.

313-475 O-68—21

represents a total fuel cost differential of $35 billion over a 35-year period between 1985 and 2020 using one projective buildup of fast breeder electrical generating capacity.(32) The total cost of power from mature fast breeder reactors has been generally estimated to be in the neighborhood of 3 to 4 mill/kwh(33) so that the large dollar figures indicated above are due to the very large usage of electricity rather than to a large percentage increase in the cost of electricity.

The uncertainty span in doubling time translates into a difference of 1 million tons in cumulative ore requirements (natural U_3O_8 over the same 35 year period) which would lead to a potential additional cost differential of the order of $30 billion.(34)

The previous discussion has indicated that specific goals such as low doubling time (which would alleviate the ore requirements mentioned above) can be achieved if one alters the design in the direction of requiring improved performance from the reactor fuel and system. This route of course entails added risk to the achievement of predicted reactor performance and/or requires additional development work prior to the commitment of the reactor. It may entail additional costs in power generation.

In their state of asymptotic development, it is predicted that the fast reactor may have an inherent cost advantage over competing reactor types of the order of 1/2 to 1 mill/kwh, or more, due primarily to its potential for very low fuel costs. However, because of first-of-a-kind fabrication costs and the need to develop a stable and large scale sodium components industry, the initial achievement of even break-even economics, compared to other power sources, will be a challenge. The large-scale introduction of fast breeders depends upon their achieving this economic parity with competing forms of nuclear and fossil power sources. The uncertainty in economic performance clouds the target designs necessary to reach economic parity and obscures the need for the development programs which might hasten the economic introduction of fast reactors. The date of introduction of fast reactors is of some importance since fast reactors are expected to be the most economical users of plutonium, a biproduct of all reactor operation. By 1980, it is estimated that there will be approximately 100 metric tons of plutonium recovered from civilian power reactors, by 1985 approximately 300 tons, and by 1990 600 tons.(35) The value of the plutonium used in a fast breeder has been estimated at approximately $10/gram or more as compared to estimates closer to $5/gr for the value of plutonium if it were used in a thermal reactor.(36) Thus, a five year reduction in the date of introduction of breeders can result in significant cumulative savings to the economy.

In summary, it appears that uncertainties in economics and performance due to present nuclear data uncertainties are not large enough to affect the ultimate development of economic fast breeders. They do produce significant uncertainties in the performance of the breeders, their date of introduction and the urgency and cost incentives for additional development work. The economic implications are large enough to justify an intensive effort to reduce these uncertainties.

TABLE I

DATA UNCERTAINTIES

Material	Data Type	Energy	Percent Change High	Percent Change Low
1. Pu-239	α	See Table II		
	σ_f	15 keV	+15.0	- 8.0
		50 keV	+25.0	0
		500 keV	+10.0	0
		2 MeV	+ 3.0	- 3.0
		4 MeV	0	- 6.0
		10 MeV	0	0
	$\bar{\nu}$	0 to 10 MeV	+ 1.6	- 2.5
	Nuclear Temperature	Fission Neutron Spectrum	+ 7.0	- 7.0
	σ_{inel}	0.1 to 10 MeV	+80.0	0
2. U-238	σ_c	1 keV	0	0
		4 keV	+20.0	-20.0
		10 keV	+25.0	-25.0
		100 keV	+20.0	-15.0
		1 MeV	+15.0	0
		4 MeV	+15.0	0
	σ_f	2 MeV	0	-15.0
		4 MeV	+ 8.0	- 8.0
		6 MeV	+ 2.0	0
		10 MeV	0	0
	σ_{inel}	100 keV	0	0
		500 keV	+15.0	-15.0
		1 MeV	+10.0	-10.0
	σ_{inel}, Nuclear Temperature	2 to 10 MeV	+25.0	-25.0
3. Pu-240	σ_c	100 eV	+20.0	-15.0
		10 KeV to 1 MeV	+40.0	-25.0
	σ_f	100 to 300 keV	+30.0	-30.0
		1 MeV	+10.0	-10.0
		10 MeV	+ 5.0	- 5.0
	σ_{inel}	(Same as for U-238)		

TABLE I

DATA UNCERTAINTIES (Continued)

Material	Data Type	Energy	Percent Change High	Percent Change Low
4. Pu-241	α	100 eV to 10 MeV	+25.0	-25.0
	σ_f	100 eV to 10 MeV	+25.0	-25.0
5. Pu-242	σ_c	(Same as Pu-240)		
	σ_f	(Same as Pu-240)		
6. Fission Products	σ_c	100 eV to 10 MeV	+50.0	-30.0
7. Ta	σ_c	100 eV to 10 MeV	+30.0	-25.0
8. Fe, Cr, Ni	σ_c	100 eV to 10 MeV	+50.0	-30.0
	σ_{inel}	800 keV to 10 MeV	+15.0	-15.0
9. Na	σ_c	100 eV to 10 keV	+75.0	-30.0
		10 keV to 10MeV	+30.0	-25.0
	σ_{elas}	100 eV to 10 MeV	+20.0	-20.0
10. Be	$\sigma_{n,2n}$	2 to 10 MeV	+20.0	-20.0

TABLE II

UNCERTAINTIES FOR PU-239 ALPHA VALUES

E	High Values[a] $\frac{\Delta\alpha}{\alpha}$ (%)	$\frac{\Delta\sigma_c}{\sigma_c}$ (%)	$\frac{\Delta\sigma_f}{\sigma_c}$ (%)	Low Values $\frac{\Delta\alpha}{\alpha}$ (%)	$\frac{\Delta\sigma_c}{\sigma_c}$ (%)	$\frac{\Delta\sigma_f}{\sigma_f}$ (%)
0.2 keV	0	0	0	-10	-10	0
0.6 keV	+ 50	+ 50	0			
1.0 keV	+100	+ 60	-20			
3.0 keV	+110	+ 90	-10			
5.0 keV	+140	+105	-15			
10.0 keV	+ 80	+ 60	-10			
15.0 keV	+ 20	+ 20	0	-20	-20	
2.0 MeV	+ 20	+ 20	0	-20	-20	0

[a] Due to the difference approach used in one of the methods for obtaining the high α values below 15 keV,(8) the σ_f values were lowered and σ_c values simultaneously raised to conform to those required to obtain high α values.

TABLE III

1000 MW(e), Na-COOLED, FAST REACTORS

	Low Leakage	High Leakage	Comments
Power (MWt)	2500	2500	
Core Height(ft)	2.5	1.5	Blankets-18" Axial;12" Radial
Core Diameter (ft)	8.0	10.8	
In-Pile Fissile Pu (kg)	2360	2710	Add 30% out-of-pile
Breeding Ratio	1.38	1.28	
Doubling Time (yr)	9.2	14.7	
Fuel Cost (mills/kwh)	0.50	0.70	$10/gm fissile Pu.[a]
Doppler-Na Out ($-T\frac{dk}{dT}$)	0.0038	0.004	3.4 v/o BeO in high leakage reactor
Coolant Loss Reactivity (Δk)	+0.012	-0.001	
Core Volume Composition Fuel/Na/Steel/BeO/Ta	42.4/ 39.2/ 17.7/0/ .7	36/40/ 20/3.4/ 0.6	

[a] Also 10% fuel inventory interest rate, 80% load factor, $200/kg fabrication for 2.5 ft core and $230/kg for 1.5 ft core, $30/kg fabrication for axial blanket and $25/kg for radial blanket, $55/kg for reprocessing, 1.15×10^5 MWD/Te average fuel burnup.

TABLE IV

COMPONENT FUEL COSTS (MILLS/KWH)

	Base Values		2.5 ft Core		
	1.5 ft Core	2.5 ft Core	High Pu-239 α 0.2 to 15 keV	High Pu-239 σ_f 15 to 300 keV	High U-238 σ_c 1 to 100 keV
Pu Credit	-0.30	-0.40	-0.29	-0.41	-0.47
Pu Inventory	0.50	0.44	0.45	0.41	0.46
Fabrication	0.25	0.24	0.241	0.237	0.242
Recovery	0.19	0.17	0.171	0.168	0.171
Fabrication Cap.	0.06	0.05	0.05	0.05	0.05
Total	0.70	0.50	0.62	0.46	0.45

TABLE V

COST AND DOUBLING TIME UNCERTAINTY RANGES (2.5 ft CORE)

Data Uncertainty	Fuel Cost (mills/kwh)	Doubling Time (yr)
Pu-239 Alpha (0.2 to 15 keV)	0.48 to 0.62	8.8 to 13.5
Pu-239 σ_f (15 to 300 keV)	0.46 to 0.50	8.4 to 9.2
Pu-239 $\bar{\nu}$ (0 to 10 MeV)	0.45 to 0.58	8.1 to 11.5
U-238 σ_c (1 to 100 keV)	0.45 to 0.55	8.0 to 10.9
U-238 σ_{inel} (0.1 to 2 MeV)	0.49 to 0.51	9.0 to 9.4
Fis. Product σ_c (0 to 10 MeV)	0.48 to 0.54	8.7 to 10.1
All Data Uncertainties	0.41 to 0.66	7.2 to 14.2
Base Values (ENDF/B)	0.50	9.2

TABLE VI

UNCERTAINTY RANGES (1.5 FT CORE)

Data Uncertainty	Fuel Cost (mills/kwh)	Doubling Time (yr)	v/o BeO
Pu-239 Alpha (0.2 to 15 keV)	0.66 to 0.90	13.0 to 40.0	2.7 to 6.2
Pu-239 σ_f (15 to 300 keV)	0.68 to 0.70	14.4 to 14.7	3.1 to 3.6
Pu-239 $\bar{\nu}$ (0 to 10 MeV)	0.65 to 0.78	12.5 to 19.9	3.3 to 3.6
U-238 σ_c (1 to 100 keV)	0.65 to 0.75	12.0 to 19.3	3.0 to 3.8
U-238 σ_{inel} (0.1 to 2 MeV)	0.69 to 0.71	14.4 to 15.0	3.2 to 3.6
Fission Product σ_c (0 to 10 MeV)	0.66 to 0.76	13.2 to 18.3	2.9 to 4.3
All Data Uncertainties	0.61 to 0.94	10.1 to 42.0	2.2 to 6.5
Base Values (ENDF/B)	0.70	14.7	3.4

TABLE VII

TARGETS FOR DATA ACCURACY

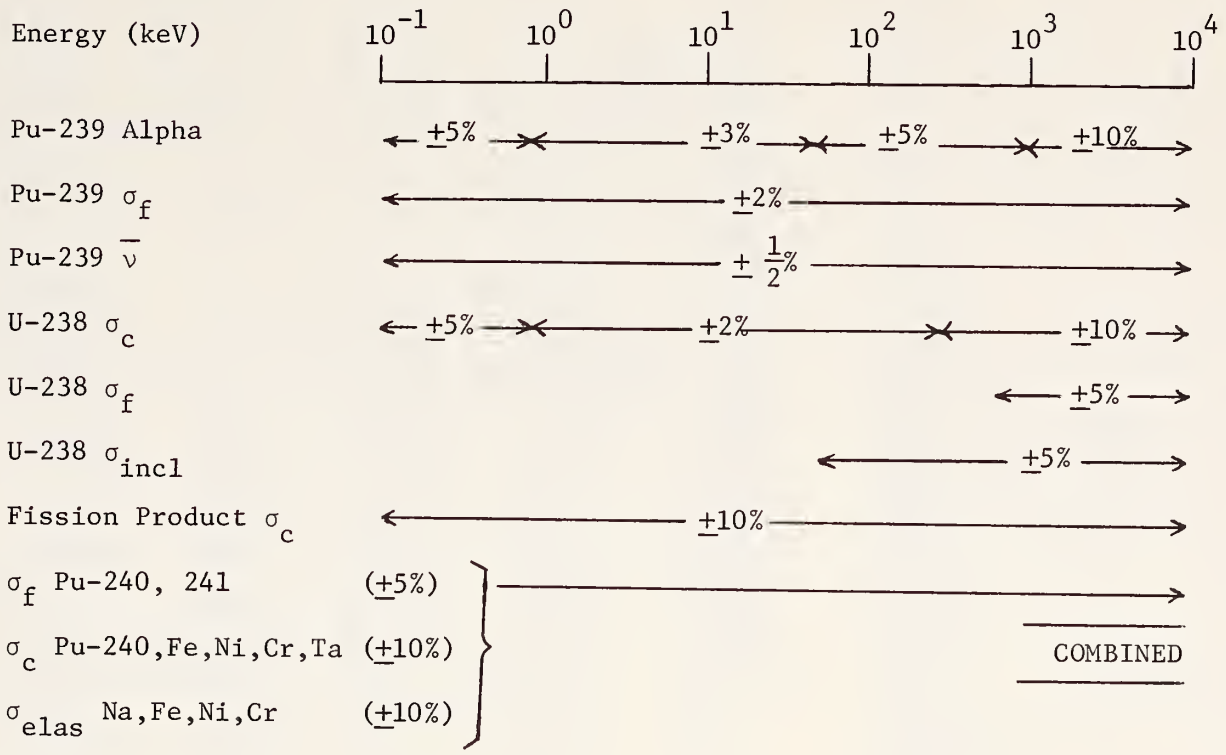

Mills/kwh Uncertainty
±0.01
±0.01
±0.015
±0.01
±0.005
±0.005
±0.005
±0.015
±0.03

TABLE VIII

EFFECTS OF HIGH PU-239 ALPHA BELOW 15 keV -- STEAM VERSUS SODIUM COOLANT

	1500 psi Steam 15" Core Height	2500 psi Steam 20" Core Height	Sodium 30" Core Height
In-Pile Fissile Inventory (Kg)	3000→3080	2420→2500	2360→2430
Breeding Ratio	1.17→1.07	1.1→1.0	1.38→1.28
Doubling Time (yr)	28→82	41→∞	9.2→13.5
Fuel Cost mills/kwh	0.88→1.00	0.85→0.97	0.50→0.62
Coolant Loss Reactivity (Δk)	0.012→0.020	0.023→0.031	0.012→0.018

TABLE IX

CORE DESIGN CHANGES TO COUNTERACT HIGh PU-239 ALPHAS

	Base Design	Sodium Bonded	Small Rod Diameter
Fuel Rod Diam. (Inch)	0.25	0.25	0.225
Sodium Bonded	No	Yes	No
Rod Pitch-to-Diam.	1.25	1.20	1.20
Fuel/Sod/Steel (v/o)	42/39/18	44/37/18	44/37/18
Core Diam. (ft)	8.0	7.15	7.15
Pressure Drop (psi)	80	190	210
In-Pile Fissile Pu (Kg)	2430	2020	2020
Breeding Ratio	1.28	1.31	1.31
Doubling Time (Yr)	13.5	10	10
Fuel Cost (mill/kwh)	0.62	0.51	0.54

REFERENCES

1. T. P. Moorhead, "The Effects of Errors in Cross-Section Data on Calculations for a Large Dilute Fast Reactor", Paper SM-18/15, Proceedings of the Seminar on Physics of Fast and Intermediate Reactors, Vienna, 1961, Vol. II, p. 111, Vienna, 1962.

2. P. Greebler, C. L. Cowan, G. L. Gyorey, B. A. Hutchins, C. L. Fies, and J. R. Sueoka, "Calculated Nuclear Reactor Parameters and Their Uncertainties in a 1000 MW(e) Fast Ceramic Reactor", GEAP-4471, General Electric Company (July, 1966).

3. P. Greebler and B. A. Hutchins, "User Requirements for Cross Sections in the Energy Range from 100 eV to 100 keV", GEAP-4472, General Electric Company (June, 1966).

4. R. D. Smith, "Nuclear Data Requirements for Fast Reactor Design and Operation", Paper CN-23/52, Conference on Nuclear Data - Microscopic Cross Sections and Other Data Basic for Reactors, Paris, October 17-21, 1966. Also, private communication from J. L. Rowlands for other sensitivity studies conducted in the U.K..

5. P. Greebler, G. L. Gyorey, B. A. Hutchins, and B. M. Segal, "Implications of Recent Fast Critical Experiments on Basic Fast Reactor Design Data and Calculational Methods", Proceedings of the International Conference on Fast Critical Experiments and Their Analysis, ANL (October, 1966).

6. P. Greebler, B. A. Hutchins, and R. B. Linford, "Sensitivity of Fast Reactor Economics to Uncertainties in Nuclear Data", Presented at the Meeting of the American Nuclear Society, Chicago (November, 1966). To be published in Nuclear Applications.

7. "ENDF/B Summary Documentation", ENDF Newsletter, Vol. 3, No. 2, Brookhaven National Laboratory, National Neutron Cross Section Center (October 2, 1967). This reference contains summary documentation for about one-half of the ENDF/B materials.

8. M. G. Schomberg, M. G. Sowerby, and F. W. Evans, "A New Method of Measuring Alpha (E) for ^{239}Pu", IAEA Symposium on Fast Reactor Physics and Related Safety Problems, SM-101/41, Karlsruhe, Germany, October 30-November 3, 1967.

9. J. R. Stehn, M. D. Goldberg, R. Wiener-Chasman, S. F. Mughabghab, B. A. Magurno, and V. M. May, "Neutron Cross Sections", BNL 325, 2d Edition, Supplement No. 2, Vol. III, (Z = 88 to 98), Brookhaven National Laboratory (February, 1965).

10. J. J. Schmidt, "Neutron Cross Sections for Fast Reactor Materials Part I: Evaluation", KFK 120, Kernforschungszentrum, Karlsruhe, (February, 1966).

11. P. Greebler, P. G. Aline, and B. A. Hutchins, "Evaluation and Compilation of ^{239}Pu Cross-Section Data for the ENDF/B Files", GEAP-5272, General Electric Company, (December, 1966).

12. J. C. Hopkins and B. C. Diven, "Neutron Capture to Fission Ratios in ^{233}U, ^{235}U, ^{239}Pu", Nuclear Science Engineering 12, 169 (1962).

13. A. Lottin, L. W. Weston, G. deSaussure, and J. H. Todd, "Ratio of Capture to Fission in ^{239}Pu at keV Neutron Energies", Proceedings of the International Conference on Fast Critical Experiments and Their Analysis; ANL-7320, Argonne National Laboratory, 22 (1966).

14. S. M. Dubrovina and V. A. Shigin, "Fission Cross-Sections of ^{231}Pa and ^{239}Pu in the 1.5 to 1500 keV Energy Range", Dokl. Akad Nauk SSSR 157, 561 (1964).

15. R. K. Smith, R. L. Henkel, and R. A. Nobles, "Neutron-Induced Fission Cross-Sections for ^{233}U, ^{235}U, ^{238}U, and ^{239}Pu from 2 to 10 MeV", Bull. Am. Phys. Soc. 2, 196 (1957).

16. P. H. White, J. G. Hodgkinson, and G. J. Wall, "Measurement of Fission Cross-Sections for Neutrons of Energies in the Range 40-500 keV", Proc. Conf. on Physics & Chemistry of Fission, IAEA, Salzburg, Austria, EANDC(UK) 535 (1964).

17. R. L. Henkel, "Summary of Neutron-Induced Fission Cross-Sections", LA-2114, Los Alamos Scientific Laboratory, (1957).

18. D. S. Mather, P. Fieldhouse, and A. Moat, "Measurement of the Prompt ν for the Neutron-Induced Fission of ^{232}Th, ^{233}U, ^{234}U, ^{238}U, and ^{239}Pu", Nucl. Phys. 66, 149 (1965).

19. D. W. Colvin and M. G. Sowerby, "Boron-Pile $\bar{\nu}$ Measurements", Proc. Conf. of Physics and Chemistry of Fission, IAEA, Salzburg, Austria, SM-60/44 (1964).

20. R. L. Macklin, P. J. Pasma, and J. H. Gibbons, "Neutron Capture", AEC Nuclear Cross-Section Advisory Group, WASH-1046, p. 88-90, (1964

21. M. C. Moxon, E. R. Rae, R. Batchelor, P. A. Egelstaff, and A. T. G. Ferguson, "Neutron Interactions with Reactor Materials", Third Geneva Conf., A/CONF. 28/P/167 (1964).

22. J. F. Barry, J. Bunce, and P. H. White, "Cross-Section for the Reaction ^{238}U (n, γ) ^{239}U in the Energy Range 0.12-7.6 MeV", J. Nucl. Energy 18, 481 (1964).

23. A. I. Leipunski, O. D. Kazachkovsky, G. Y. Artyukhow, A. I. Baryshnikou, T. S. Belanova, V. N. Galkou, Y. Y. Stavissky, E. A. Stumbur, and L. E. Sherman, "Measurements of Radiative Capture Cross-Sections for Fast Neutrons", Second Geneva Conf., A/CONF. 15/P/2219 (1958).

24. I. Bercqvist, "Fast Neutron Radiative Capture Cross-Sections in Ag, Ta, W, Au, Hg, and U", Arkiv Fysik, 23, 425 (1963).

25. R. Batchelor, Proc. Phys. Soc. (London), A 69, 214 (1964).

26. E. Barnard, A.T.G. Ferguson, W. R. McMurray, I. J. vanHeerden, "Scattering of Fast Neutrons by ^{238}U", International Conf. on Study of Nuclear Structure with Neutrons, Antwerp, Belgium, EANDC-50-S, P/26 (1965).

27. K. Parker, "Neutron Cross-Sections of ^{235}U and ^{238}U in the Energy Range 1 keV - 15 MeV. Part I, Best Cross-Sections for ^{238}U Based on Microscopic Experimental and Theoretical Data Available at December, 1961", AWRE-O-79/63, (1964).

28. W. B. Henderson, P. A. DeCorrevont, and J. W. Zwick, "Evaluation and Compilation of Ta-181, W-182, W-183, W-184, and W-186 Cross-Section Data for the ENDF/B File", GEMP-448, General Electric Company, November 11 (1966).

29. M. C. Moxon, "The Neutron Capture Cross-Section of Iron and Cobalt", International Conf. of Study of Nuclear Structure with Neutrons, Antwerp, Belgium, P/88 (1965).

30. R. L. Macklin, P. J. Pasma, and J. H. Gibbons, "Resonance Neutron Capture and Transmission in Sulfer, Iron, and Lead", Phys. Rev. 136, B 695 (1964).

31. R. L. Macklin, J. H. Gibbons, "Capture Cross-Section Studies for 30-220 keV Neutrons Using a New Technique", Phys. Rev. 159, 1007 (1967).

32. R. J. Dietrich, "Uranium Requirements for Nuclear Power", Nuclear News, Vol. 10, N. 9 (September, 1967).

33. K. P. Cohen, G. L. O'Neill, "Safety and Economic Characteristics of a 1000 MWe Fast Sodium-Cooled Reactor Design". Conference of Safety, Fuels and Core Design in Large, Fast Power Reactors, Argonne National Laboratory, ANL-7120, October 11-14 (1965).

34. "World Uranium and Thorium Resources" Organization for Economic Cooperation and Development and European Nuclear Energy Agency (August, 1965).

35. M. C. Beckman, H. A. Wagner, "Plutonium Recycle in U.S. Thermal Reactors", Symposium on Plutonium Fuel Technology, Phoenix, Arizona, October (1967).

36. P. M. Murphy, "The Influence of Plutonium on the Design of Advance Reactors", Twelfth Annual Meeting of American Nuclear Society, Denver, Colorado, June 20-23 (1966).

FISSION PRODUCT CROSS-SECTION AND POISONING IN FAST REACTORS

V. Benzi

Centro di Calcolo del C.N.E.N. - Bologna , Italy

ABSTRACT

The neutron cross-sections for radiative capture by fission product nuclei can be estimated in the unresolved resonance region by using the statistical model and the experimental data available. These estimates can be used to define pseudo-fission-product cross-sections which are very useful for fast reactors calculations concerning long term reactivity changes, breeding gain, etc.. The properties of these pseudo-fission-product cross-sections are discussed both for U-235 and Pu-239. It is shown that for energies above $\sim$ 1 KeV the natural elements Pd and Pt can be reasonably adopted as mock-fission-products for U-235 and Pu-239 respectively, as far as neutron absorption is concerned.

1. INTRODUCTION

The estimate of the loss of neutrons due to the gross fission-products poisoning is of great importance for the assessment of fuel cycle costs (1,2,3). In connection with such a problem, the concept of pseudo-fission-product (PFP) has been extensively used for thermal (4,5,6,7,8) as well as fast reactors (9,10). For thermal reactors the adoption of the Westcott's model permits an easy solution of the problem by using thermal absorption cross-sections and resonance integrals, two quantities which have been measured for a great number of fission-product nuclei. For fast reactors, however, the situation is less satisfactory since the energy dependence of the capture cross-sections over the energy range from the resonance region up to some MeV is required, whereas the data available are rather scarce. For this reason an extensive use of theoretical estimates, based essentially on the statistical model is required to fill the large gaps existing in the experimental data.

2. PFP CROSS-SECTIONS

Some results on fission-product cross-sections above 1 KeV obtained using experimental data and theoretical methods have been reported elsewhere (11). From these results, the "radiative capture cross-section" $\bar{\sigma}_{n\gamma}$ at energy E>1 KeV of a fresh PFP due to a fission induced by a neutron of energy E can be obtained putting

$$\bar{\sigma}_{n\gamma}(E;E'') = \Sigma_i \, y_i(E'') \sigma_{n\gamma}^{(i)}(E)$$

where y_i and $\sigma_{n\gamma}^{(i)}$ represent the yield and cross-section of the i-th fission-product. In Figs. 1 and 2 the $\bar{\sigma}_{n\gamma}$ for thermal fission of U-235 and Pu-239 obtained in this way are shown. To obtain these curves, the fission-products with short lifetime have been replaced by their decay products. It will be noted that $\left[\bar{\sigma}_{n\gamma}(E)\right]_{Pu-239} \simeq 1.25 \left[\bar{\sigma}_{n\gamma}(E)\right]_{U-235}$.

3. FLUX-TIME BEHAVIOUR

As the irradiation of the fuel increases, the quantity $\bar{\sigma}_{n\gamma}$ would be expected to change. If the short-life nuclei are assumed to decay immediately, for a flux ϕ (assumed constant in time), at time t we have

$$\bar{\sigma}_{n\gamma}(E;t;\phi) = \Sigma_k N_k(t;\phi)\sigma_{n\gamma}^{(k)}(E)$$

where $N_k(t;\phi)$ is the concentration of the k-th fission-product (primary or secondary). To estimate the magnitude of the irradiation effects on $\bar{\sigma}_{n\gamma}$, a (PuO_2+UO_2) fueled reactor with a 3350 litres core was considered. The following composition of the core was assumed: $Pu/(Pu+U_{238})$=17.7% ; (PuO_2+UO_2)=35% ; SS=15% ; Na=50% . The last three figures refer to the volume fraction. A 26-group calculation was performed to obtain the energy dependence of the neutron spectrum, and the $\sigma_{n\gamma}^{(i)}(E)$ were averaged over this spectrum, to produce a set of single-group constants. Then the $N_k(t;\phi)$ were obtained by solving the appropriate balance equation system, with the condition $N_k(t=0)=y_k(E^{**})$. The differences found between the "fresh" and "irradiated" PFP were quite small for reasonable values of flux-time, being less than 10% for $\phi t=5\times10^{23}\ cm^{-2}$. This suggests that for reactors with a neutron spectrum which does not differ too greatly from the one here considered and for a flux-time up to $\sim10^{23}\ cm^{-2}$, the macroscopic group cross-section of the PFP in the j-th group at time t is simply given by

$$[\bar{\Sigma}_j(t)] \approx [\bar{\sigma}_j] \int_0^t N_{fiss}(t')dt'$$

where $[\bar{\sigma}_j]$ is the group cross-section of the fresh PFP and $N_{fiss}(t')dt'$ is the number of fissions in a volume element of the core during a time interval $(t',t'+dt')$. The above expression does not apply in the resolved resonance region; however the reaction rates of the fission-products in this energy region were found negligible for the reactor here considered. To give an idea of the order of magnitude of the poisoning effects, the one-group values found for σ_f and $\sigma_{n\gamma}$ of Pu-239 and $\bar{\sigma}_{n\gamma}$ were 1.854, 0.078 and 0.087 barns respectively.

4. THE REMOVAL OF GASEOUS FISSION-PRODUCTS

It is rather difficult to estimate the reactivity effects due to fission products in a vented fuel element, because the balance equations governing the growth and decay of the nuclei are complicated by the presence of a leakage term. To get an idea of the influence of venting on neutron economics, the balance-equation system previously considered was solved assuming yield, cross-section and decay constant equal to zero for all the fission-products which are isotopes of Kr, Rb, I, Xe and Cs. With this assumption, which is equivalent to the instantaneous removal of the gaseous fission products from the fuel, the one-group cross-section of PFP, is reduced by about 15% but remains rather insensitive to the irradiation time.

5. THE EFFECT OF THE YIELD ENERGY-DEPENDENCE

Because the fission-product yields depend on the energy of the neutron causing the fission, it would be necessary to consider the average yields

$$\bar{y}_i = \int y_i(E')\phi(E')dE' / \int \phi(E')dE'$$

to obtain the PFP cross-section in a given reactor

$$\bar{\sigma}_{n\gamma}(E) = \Sigma_i \bar{y}_i \sigma_{n\gamma}^{(i)}(E)$$

Unfortunately, the energy dependence of the yields has not been extensively investigated, nor are the existing theories on the fission process able to predict such a dependence accurately. An upper limit can be estimated by using the yields for fission induced by ∿14 MeV neutrons in U-235, for which experimental data exist. The $\bar{\sigma}_{n\gamma}$ so obtained compared with the case of thermal fission shows an increase which reaches a maximum value of ∿10% at low energies.

6. MOCK FISSION-PRODUCTS

Mock fission-products are frequently used in fast reactor physics to simulate the effects of fission-product capture on reactivity. Natural Pd and Pt seem to be suitable for this purpose, if the neutron spectrum is not very soft or very hard. This is shown in Figs. 1 and 2, in which the existing experimental data on $\sigma_{n\gamma}$ for Pd and Pt, respectively, are plotted. Above ∿150 KeV there are not experimental measurements for Pd, but an estimate of $\sigma_{n\gamma}$ can be obtained by means of the statistical model and the data available for single isotopes. The results obtained in this way are represented by triangles in Fig. 1. For natural Pt there are experimental data up to 1 MeV, which are shown in Fig. 2. Both elements can be used for simulating the capture cross-sections of gross fission-products of U-235 or Pu-239, if one takes into account the relationship $[\bar{\sigma}_{n\gamma}]_{Pu-239} \simeq 1.25 [\bar{\sigma}_{n\gamma}]_{U-235}$.

7. CONCLUSIONS

For reactors with neutron spectra comparable with the one considered in this paper, it seems that the following conclusions can be drawn:

i) the pseudo-fission-product concept can reasonably be accepted for flux-times up to about $\sim 10^{23} cm^{-2}$. This permits a very simple estimate of the time-dependence of the group-capture cross-sections of the gross fission-product;

ii) the complete removal of the gaseous fission-products gives a reduction in the total capture cross-section of about 15%. This figure, which is smaller than the uncertainties affecting the estimate of $\bar{\sigma}_{n\gamma}$, corresponds to a small effect as far as reactor reactivity is concerned;

iii) the energy dependence of the fission-product yields does not seem greatly to affect the estimate of $\bar{\sigma}_{n\gamma}$;

iv) as far as the capture cross-sections are concerned, natural Pd and Pt can reasonably be used as mock fission-products for U-235 and Pu-239 respectively.

8. REFERENCES

(1) J.R. Dietrich: ANS Trans. 9, No. 2, p. 548, November 1966

(2) W.B. Lewis: Proc. F.A.S.T. Symposium on Nuclear Energy 1966, edited by C.N.E.N. (1967)

(3) W.B. Lewis: I.A.E.A. Symposium on Heavy Water Power Reactors, Paper SM 99/37 (Vienna 1967)

(4) D.G. Hurst: CRRP-659 and Addendum (AECL-346)(1956)

(5) W.H. Walker: CRRP-913 (AECL-1054)(1960)

(6) E.A. Nephew: ORNL-2869 (UC-81)(1960)

(7) V. Benzi and A. Chiarini: Energia Nucleare, 9, 266, 1962

313-475 O-68—22

(8) V. Benzi and A. Chiarini: Energia Nucleare, 12 , 44 , 1965

(9) M.M. Levine: Proc. Physics of Fast and Intermediate Reactors, vol. II, Paper I.A.E.A. (Vienna) (1962)

(10) M. Marseguerra and E. Menapace: C.N.E.N. Symposium on Fast Reactor, Roma 1963 (1967)

(11) V. Benzi and M.V. Bortolani: Nuclear Data for Reactors, vol. I, p. 537, I.A.E.A. (Vienna) (1967)

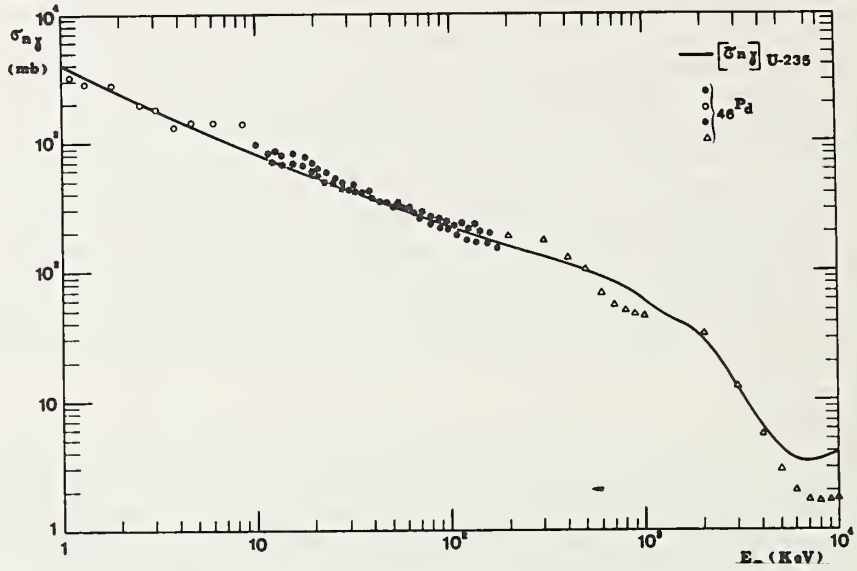

Fig. 1 - The PFP cross-section for U-235 (full line).
The points and triangles are experimental and theoretical capture cross-sections of natural Pd.

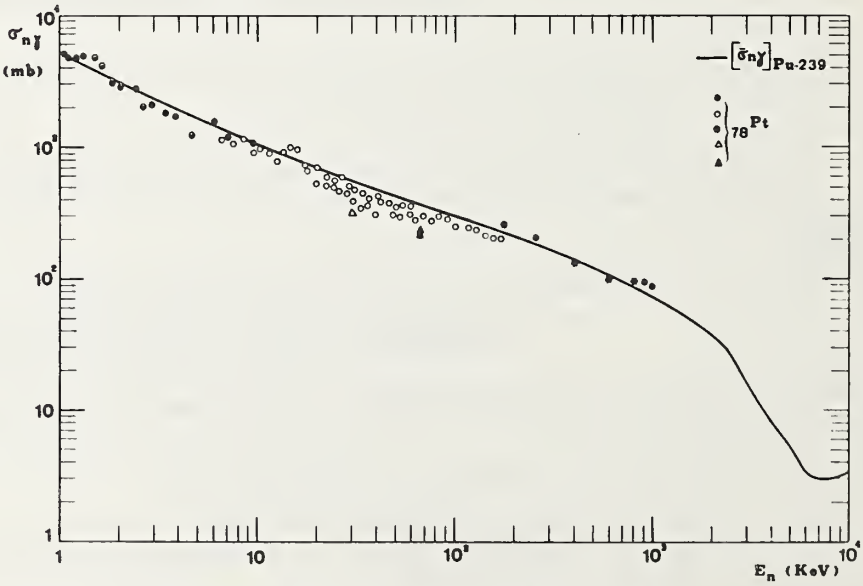

Fig. 2 - The PFP cross-section for Pu-239 (full line).
The points are experimental cross-sections of natural Pt.

The $(n,\gamma n')$ and Fission Reactions as Possible Sources of Low Energy Neutrons in Fast Critical Assemblies

K. Parker, E. D. Pendlebury, J. P. Shepherd and P. Stanley

Atomic Weapons Research Establishment, Aldermaston, Berks, England

Abstract

At the Washington Conference on Neutron Cross Section Technology, March 22-24, 1966, Moldauer presented calculations of the $(n,\gamma n')$ cross section of several nuclides including U238. In this process neutron re-emission follows a fairly low energy gamma ray transition in the compound nucleus and there results a continuous spectrum of relatively low energy neutrons peaking at an energy typically several tens of keV. It has been suggested that this reaction could enhance the low energy portion of calculated fast reactor spectra and this paper describes a simple investigation of this possibility. It was also convenient and logical to consider possible uncertainties in the low energy tail of the fission spectrum at the same time since many more neutrons will have fission reactions in a reactor system than $(n,\gamma n')$ reactions.

1. Introduction

A number of measurements on zero energy fast reactor systems suggest that the spectrum is being wrongly calculated in the energy range below 100 keV and more particularly below 10 keV. Typical is the boron perturbation measurement [1] where the discrepancies between measured and calculated values seem too large to be explained by uncertainties in the ^{10}B absorption cross section alone but could be explained if the calculated spectrum is too hard due to underestimation of the low energy flux.

At the Washington Conference on Neutron Cross Section Technology, March 22-24, 1966, Moldauer [2] presented calculations of the $(n,\gamma n')$ cross section of several nuclides including ^{238}U. In this process neutron re-emission follows a fairly low energy gamma ray transition in the compound nucleus and there results a continuous spectrum of neutrons peaking at an energy typically several tens of keV. After making a number of simplifying assumptions Moldauer calculates a $^{238}U(n,\gamma n')$ cross section of 166 mb at 1 MeV which is somewhat larger than the directly observed (n,γ) cross section but much smaller than the conventional (n,n') inelastic scattering cross section.

It has been suggested that this process could enhance the low energy portion of the calculated fast reactor spectra and this note describes a simple investigation of this possibility. It was convenient and logical to consider possible uncertainties in the low energy tail of the fission spectrum at the same time since many more neutrons will have fission reactions in a reactor system than $(n,\gamma n')$ reactions.

2. Outline of Calculations

The systems Vera 3A[3] and Zebra 1 [4] were chosen as suitable for calculation since they contain a high proportion of ^{238}U (the driving material is 32% enriched uranium in Vera 3A and 12% enriched uranium in Zebra 1).

The neutron spectrum at the centre of Vera 3A was calculated with three different sets of cross sections,

(i) using adjusted group cross sections derived from recent DUNDEE/PENICUIK calculations [5] to make them consistent with experimental critical sizes. Specifically the following data files were used,

^{235}U : 1041	^{236}U : 173	Cr : 1017
^{238}U : 1005	C : 1006	Ni : 1019
^{234}U : 174	Fe : 1036	H : 1010

Data file numbers of the form 1000 + X imply that the constants are adjusted from those derived from data file X. Reference [6] contains further details of the data files used. Of interest here is the fact that in the data files 41 and 5 for ^{235}U and ^{238}U the inelastic scattering cross sections are those of AWRE Reports O-82/63 [7] and O-79 [8] respectively whilst the fission spectrum - from the same sources - for both nuclides is given by

$$f(E) = 0.45270 \exp(-E/0.965) \sinh\{(2.29\,E)^{\frac{1}{2}}\}$$

where f(E) dE is the fraction of neutrons emitted in (E,E+dE).

In the adjustment process [5] most of the group inelastic cross sections in ^{238}U - to individual levels and to the continuum - were reduced significantly with corresponding increases in the elastic cross section. The implication of the adjustment process here is that DFN 5 data for ^{238}U gives too soft a spectrum and there is a hardening when the data are adjusted. In ^{235}U on the other hand the changes in the inelastic cross sections imply some softening of the spectrum in the adjustment process.

(ii) Using the same data as in (i) except for the total and (n,n') continuum reactions in ^{238}U (DFN 1005). The contribution of the (n,γn') reaction was introduced by calculating the appropriate group cross sections and transfer matrices, adding them to the similar quantities for the (n,n') continuum reaction and increasing the total cross section to maintain neutron conservation. The resulting group cross sections for ^{238}U have data file number 4005. Details of the calculation of the (n,γn') transfer matrix are given in Section 3.

(iii) Using the same data as in (i) except that for ^{235}U and ^{238}U the fraction of fission neutrons in all groups with upper energy below 80 keV is increased by a factor of 2 and the increase compensated by a uniform percentage reduction (~1% in fact) in the fraction for all higher energy groups. The resulting group cross sections for ^{235}U and ^{238}U have data file numbers 5041 and 5005 respectively.

Table 1 shows the old and new fission spectra and also gives the salient features of the group cross section set (32 group set 11) used in all these calculations.

All the calculations were carried out using the S_n program STRAINT [9] with the S_4 isotropic option making the diagonal transport correction [10] to take into account the effect of anistropic scattering.

Similar calculations, but only using the data as described in (i) and (ii) above, were carried out on Zebra 1.

3. Calculation of the Group Cross Section and Transfer Matrix for the $(n,\gamma n')$ Reaction

Figure 5 of Moldauer's paper gives a calculated excitation function for the $^{238}U(n,\gamma n')$ reaction between 0.2 and 1.2 MeV. In the derivation several approximations are made and the values given are probably subject to quite large errors. At 1.2 MeV Moldauer's curve is still rising rapidly but must eventually turn over and fall due to increased competition from particle emission. Moreover, for higher incident energies the spectrum of secondary neutrons will be harder and of less interest in the present context.

In the present calculations the reaction was neglected for energies greater than 1.6 MeV and less than 0.13 MeV and for energies between 1.2 and 1.6 MeV a constant cross section of 320 mb was assumed. Group cross sections were calculated from the formula

$$\sigma_g = \int_g \sigma(u)\, du \Big/ \int_g du$$

where the integrals are over lethargy u in group g.

Moldauer's figure 6 gives the spectrum of secondary neutrons at an incident energy of 1 MeV. Consideration of the qualitative average first gamma ray spectrum in his figure 1 suggests that it is a reasonable approximation to take a normalised spectrum having the same shape as that of figure 6 for the distribution of E/E_o, where E_o is any incident neutron energy. This means that the frequency function for E/E_o is given by

$$p(E/E_o) = 6\, q(E/E_o)$$

where $q(E)$ is Moldauer's function which is normalised to 166 mb for $E_o = 1$ MeV.

In the light of the approximations made so far it is reasonable to take all secondary neutrons from the reaction in group g to have a spectrum corresponding to that for incident neutrons of energy $\bar{E}_g$ where $\bar{E}_g$ is the energy corresponding to the mean lethargy in group g (see Table 1). The resulting transfer matrix is given in Table 2.

4. Results and Discussion

The dimensions and compositions of Vera 3A and Zebra 1 were taken to be those of the equivalent spherical critical systems given in references [3] and [4]. The inverse reactivity B was calculated in each

case along with the spectra, in particular the spectra at the centre of the systems. The fact that B is not quite equal to unity has a negligible effect on the spectra.

It is interesting to compare the B values with the different data. These are given in the table below. It will be seen that the effect

System	B-Values		
	Ordinary data	(n,γn') modification	Fission Spec. modification
Vera 3A	1.0048	1.0031	1.0041
Zebra 1	1.0029	1.0042	-

on B of the data modification is negligible. In the case of Zebra 1 the (n,γn') reaction has the opposite effect to that in Vera 3A. The "ordinary data" are those referred to in Section 2, paragraph (1), and are in fact the PENICUIK adjusted data. Zebra 1 was not used in the adjustment procedure and it is interesting to see how satisfactorily close to unity the B value is for that system.

In the case of Vera 3A the (n,γn') modification has a negligible effect on the core spectrum and the fission spectrum modification has an even less effect. Hence the calculation on Zebra 1 with the fission spectrum modification was not carried out. The effect of the (n,γn') reaction on the core spectrum in Zebra 1 is greater than the effect in Vera 3A but it is still negligible. The effects on the spectra at the core centres in the 2 cases are illustrated in Figures 1 and 2.

A useful measure of the change in spectra is the effect on the average ^{10}B (n, abs) cross section. This is given for DFN 13 ^{10}B data in the table below, where the average values of the $^{235}U(n,f)$ cross section, based on DFN 1041 data, are also given for comparison. The effect is small in all cases.

System	$^{10}B(n,abs)$ cross section in barns			$^{235}U(n,f)$ cross section in barns		
	Ordinary data	(n,γn') mod.	Fiss. Spec mod.	Ordinary data	(n,γn') mod.	Fiss. Spec mod.
Vera 3A	1.51	1.54	1.54	1.56	1.58	1.57
Zebra 1	1.17	1.22	-	1.42	1.44	-

5. Conclusions

Bearing in mind that the (n,γn') reaction is believed to be overestimated in the data used in the calculations reported in this note, there does not appear to be any justification for a significant expenditure of effort, either theoretical or experimental, to study it in any more detail at the present time. The same also applies to the low energy end of the fission spectrum. As far as the latter is

concerned it is worth mentioning the recent measurements by Meadows [11] where the ^{252}Cf spontaneous fission spectrum was measured down to 2.8 keV. In the range 2.8-100 keV a least squares fit to the spectrum gives

$$f(E) = k\, E^{n} \exp(-E/1.501)$$

where $n = 0.54 \pm 0.08$ as against the normal value of 0.5 for this type of functional dependence on energy.

6. References

[1] W. G. Davey, ANL-6682 (1963)

[2] P. A. Moldauer, Conference on Neutron Cross Section Technology, Washington, March 1966, CONF-660303, Book 2 p.613

[3] M. H. McTaggart, H. Goodfellow, W. J. Patterson and J. W. Weale, AWRE Report No. R5/66 (1966)

[4] A. R. Baker, International Conference on Fast Critical Experiments and their Analysis, Argonne, October 1966, ANL-7320 p.116

[5] Pamela C. E. Hemment and E. D. Pendlebury, International Conference on Fast Critical Experiments and their Analysis, Argonne, October 1966, ANL-7320 p.88

[6] Susan M. Miller and K. Parker, AWRE Report No. O-55/65 (1965)

[7] K. Parker, AWRE Report No. O-82/63 (1963)

[8] K. Parker, AWRE Report No. O-79/63 (1964)

[9] R. D. Wade, AWRE Report No. O-12/63 (1963)

[10] E. D. Pendlebury and L. H. Underhill, IAEA Conference on the Physics of Fast and Intermediate Reactors, Vienna, August 1961, Vol. II, p.73

[11] J. Meadows, Wash 1068, p.17 (1966)

Table 1

Feature of the 32 Group Set 11 Group Constant Set and the Modified Fission Spectrum

Group Number	Upper Boundary	Width in Lethargy	Energy at Mean Weighted Lethargy	Proportion of Standard Fission Spectrum in Group	Proportion of Softer Fission Spectrum
1	14.6 MeV	0.07833	14.05 MeV	0.00004	0.00004
2	13.5	0.07696	12.99	0.00008	0.00008
3	12.5	0.1278	11.73	0.00033	0.00033
4	11.0	0.1466	10.22	0.00111	0.00110
5	9.5	0.1719	8.718	0.00364	0.00360
6	8.0	0.2076	7.211	0.01147	0.01135
7	6.5	0.2624	5.701	0.03455	0.03420
8	5.0	0.3857	4.123	0.10784	0.10675
9	3.4	0.3483	2.857	0.14825	0.14675
10	2.4	0.4055	1.960	0.19145	0.18951
11	1.6	0.3747	1.327	0.15697	0.15538
12	1.1	0.3438	0.9263	0.11201	0.11088
13	0.78	0.3494	0.6550	0.08195	0.08112
14	0.55	0.3964	0.4511	0.06134	0.06072
15	0.37	0.3528	0.3102	0.03424	0.03389
16	0.26	0.3677	0.2163	0.02218	0.02196
17	0.18	0.3254	0.1530	0.01216	0.01204
18	0.13	0.4855	0.1020	0.01033	0.01023
19	80 keV	0.6208	58.65 keV	0.00601	0.01202
20	43	0.6702	30.76	0.00253	0.00506
21	22	0.7885	14.83	0.00102	0.00204
22	10	0.9163	6.325	0.00034	0.00068
23	4	0.9163	2.530	0.00009	0.00018
24	1.6	0.9008	1.020	0.00002	0.00004
25	0.65	0.9163	0.4111	0.00001	0.00002
26	0.26	0.8602	0.1691	0.00000	0.00000
27	0.11	0.9628	67.97 eV	0.00000	0.00000
28	42 eV	1.030	25.10	0.00000	0.00000
29	15	1.003	9.083	0.00000	0.00000
30	5.5	1.012	3.317	0.00000	0.00000
31	2.0	1.609	0.8944	0.00000	0.00000
32	0.4 (Thermal Group)	-	0.03876	0.00000	0.00000

Table 2

Group Cross Sections and Transfer Matrix for the $(n,\gamma n')$ Reaction

Initial Group	Total $(n,\gamma n')$ Cross Section	Final Groups													
		12	13	14	15	16	17	18	19	20	21	22	23	24	25
11	310.1	18.6	52.7	58.9	49.6	40.3	43.4	24.8	9.3	6.2	6.2	0	0	0	0
12	136.8	0	8.2	24.6	24.6	21.9	15.7	15.7	12.3	5.5	5.5	1.4	1.4	0	0
13	72.2	0	0	5.4	12.6	13.0	10.8	10.8	9.4	4.3	3.6	1.4	0.7	0	0
14	35.6	0	0	0	2.5	6.1	6.1	7.5	6.1	3.6	2.1	1.1	0.4	0.4	0
15	20.1	0	0	0	0	1.4	3.0	4.8	4.7	2.9	1.8	0.8	0.4	0.2	0
16	10.9	0	0	0	0	0	0.5	2.5	3.2	2.3	1.3	0.7	0.3	0.2	0
17	5.85	0	0	0	0	0	0	0.7	1.8	1.6	1.0	0.5	0.2	0.1	0.1
18	2.11	0	0	0	0	0	0	0	0.4	0.7	0.5	0.3	0.1	0	0

All cross sections are in millibarns

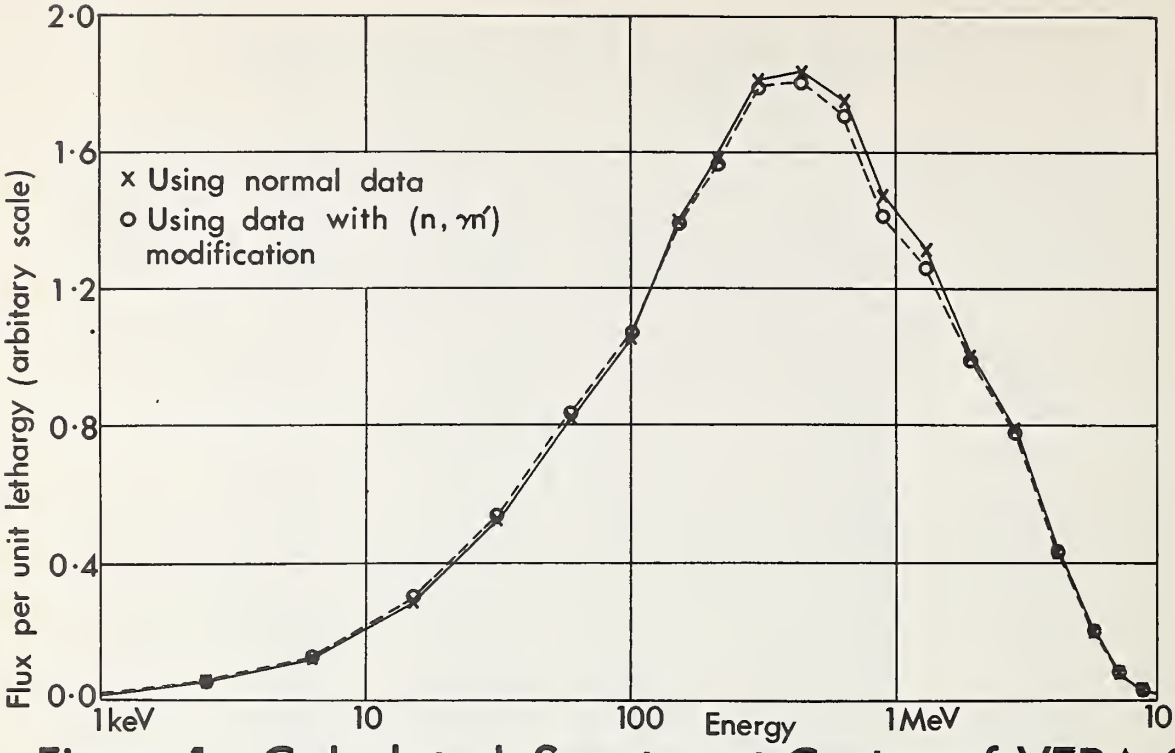

Figure 1 Calculated Spectra at Centre of VERA 3A

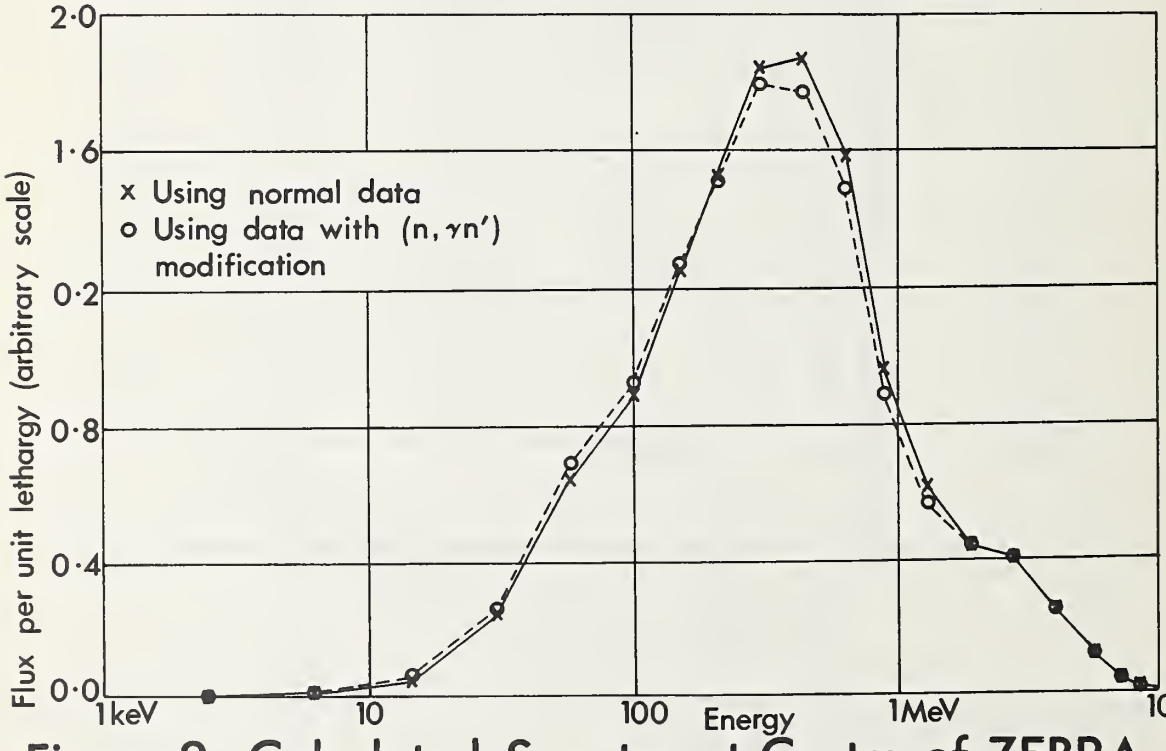

Figure 2 Calculated Spectra at Centre of ZEBRA 1

Fissile Doppler Effect Measurement Data and Techniques*

C. E. Till and R. A. Lewis

Argonne National Laboratory

Argonne, Illinois 60439

ABSTRACT

Reactivity measurements in critical assemblies of the Doppler effect in fissile materials ideally measure a quantity of direct interest -- the difference between the fission and absorption components directly in the flux and adjoint spectra of interest. In practice, however, the Doppler effect can be obscured by the effect of thermal expansion of the material. The systematics of the reactivity effects of expansion for ^{233}U, ^{235}U, ^{239}Pu and ^{241}Pu are discussed. It is shown that the differences in their cross section variation with energy cause their expansion effects to differ markedly from each other in magnitude, in variation with sample density and with spectrum. Methods of minimizing the effects of sample expansion on Doppler effect measurements by spectrum and sample density considerations are discussed. Residual expansion effects are evaluated by use of samples with differing expansion properties. Precise experimental Doppler effect data in fast reactor spectra are presented that demonstrate excellent consistency in the Doppler effect inferred from samples expanding in different ways. An analyses is presented showing the degree of agreement given by various cross section averaging treatments of the ^{235}U resonance parameters.

1. THE REACTIVITY EFFECTS OF EXPANSION OF A SAMPLE OF FISSILE MATERIAL

Within the context of group-diffusion theory, the reactivity worth of a sample of fissile material can be written exactly as

$$\frac{\Delta k}{k} = \left(\frac{N_0 M_s}{AD}\right) \sum_i \phi_i' \sum_j \left(\chi_j \nu_i \sigma_{f_i} + \sigma_{i\to j}\right) \phi_j^* - \sigma_{t_i} \phi_i^* \qquad (1)$$

where $N_0 = 6.03 \times 10^{23}$, M_s = sample mass, A = atomic mass, D = integral over the reactor volume of $\sum_j \chi_j \phi_j^* \sum_i \phi_i \nu_i \Sigma_{f_i}$, ϕ_i' = perturbed flux in group i in the sample, ϕ_j^* = unperturbed reactor adjoint flux in group j. All cross sections, σ, are defined per fissile atom, and the subscripts f, i→j and t denote fission, group-transfer and total cross section, respectively. Written in this form, the changes in worth due to sample expansion are all contained in the changes in ϕ_i' as the sample expands, and it is in the calculation of ϕ_i' that approximations enter. A simple and reasonably accurate expression for ϕ_i' is based on an expression of neutron balance and the reciprocity

*Work performed under the auspices of the U. S. Atomic Energy Commission.

relationship, leading to [1]

$$\phi_i' = P_{c_i} \sum_{k \neq i} \frac{\left(\Sigma_{k\to i} + \chi_i \nu_k \Sigma_{f_k}\right) \phi_k' + \left(1 - P_{c_i}\right) \Sigma_{t_i} \phi_i}{\Sigma_{t_i} - P_{c_i}\left(\Sigma_{i\to i} + \chi_i \nu_i \Sigma_{f_i}\right)} \qquad (2)$$

where P_{c_i} = flat-source probability of a neutron born in the sample in group i making its first collision in the sample, ϕ_i is the unperturbed (reactor) flux in group i, and all cross sections are those for the fissile sample.

At low energies where $\chi_i \to 0$ and $\Sigma_{k\to i} \to 0$, $k \neq i$, for heavy elements, it can be shown [1] that for small sample expansions $\delta k \approx = -\left(\frac{N_0 M_s}{AD}\right) \phi \left([\nu-1]\, \sigma_f^2\right) \delta(N\bar{\ell})$, $\bar{\ell}$ = mean chord length in the sample.

At high energies, where significant numbers of neutrons are born in the fission process, corresponding approximations give $\delta k_i \approx \left(\frac{N_0 M_s}{AD}\right) \chi_i \phi \nu(\nu-1)\, \sigma_f^2\, \delta(N\bar{\ell})$.

As $\delta(N\bar{\ell})$ is negative, these expressions show that, as expected, the expansion effects are positive at low energies and negative at fission neutron energies. Further, however, the magnitude of the expansion effects will vary from isotope to isotope approximately proportionally to $\nu(\nu-1)\, \sigma_f^2$ at high energies and $(\nu-1)\, \sigma_f^2$ at low energies.

Figure 1 shows the reactivity effect of expansion for various fissile isotopes as a function of sample density, calculated from Eqs. (1) and (2) for a nominal 1 in. diameter cylindrical sample at the center of ZPR-6, Assembly 5 (a 2600 ℓ full-scale mockup of a UC fast power reactor) [2]. The figure illustrates the large differences in the expansion effects of various fissile isotopes caused mainly by the differences in ν and σ_f. It also shows that the shape of expansion reactivity vs. sample density curve differs from isotope to isotope. Most noticeably, ^{239}Pu in this spectrum has a larger expansion effect than ^{241}Pu at low densities but the ^{241}Pu expansion effect increases more rapidly with sample density, until at metal densities the ^{241}Pu effect is considerably higher. The reason is that the ^{239}Pu σ_f below 100 keV is smaller than the other isotopes, and as the expansion effect is proportional to σ_f^2, ^{239}Pu has a relatively small (positive) contribution from the low-energy range subtracting from the dominant negative effect at high energies. ^{241}Pu, however, has a relatively large (positive) contribution from the low-energy range because of its higher σ_f. As the sample density increases, the flux in the sample in the low-energy region decreases, and the positive contribution is suppressed. The progressive decrease in its importance relative to the high-energy contribution causes the net expansion effect to increase more rapidly with density in ^{241}Pu than in ^{239}Pu, causing a crossing of the two curves at about PuO_2 densities.

The expansion coefficients of the various isotopes are sensitive in varying degrees to both the flux and adjoint spectrum. Quite realistic changes in the material compositions of the reactor can change the magnitude of the expansion coefficient very significantly, and in some cases can even

cause it to change sign. To give a basis for the discussion of these effects, calculated expansion effects for the various isotopes are compared between ZPR-6 Assembly 5 [2], and ZPR-9 Assemblies 14 and 17 [3]. Both the latter assemblies have considerably softer spectra than Assembly 5, and the variation in the adjoint flux with energy is considerably different between the two. Comparisons of the calculated flux and adjoint spectra at the center of the three assemblies are given in Figs. 2 and 3, respectively.

The changes in material compositions between the three assemblies are related in the following way. Starting with the Assembly 5 composition, Assembly 14 was constructed by removing a fraction of the ^{238}U and replacing it with polyethylene and graphite to substantially soften the original spectrum. For Assembly 17, the remainder of the ^{238}U plates were removed and replaced with graphite which softened the flux spectrum further, but more importantly, considerably altered the shape of the adjoint function at fission energies.

Figures 1, 4 and 5 show the very different behavior of the expansion effects in the three assemblies. Not only do the expansion effects for several of the isotopes change sign between assemblies, but they also change sign as the sample density changes within a given assembly. (The abscissa in all three figures are easily generalized to other sample diameters, as it is the product of the atom density, N, and the mean chord length, ℓ, that is meaningful.)

The explanation of the sign changes as a function of sample density in the two softer spectrum assemblies is the following: In those isotopes with high cross sections in the low-energy region, the very substantial shift of flux to low energies can cause the positive reactivity effects in the low-energy region to overbalance the negative effects at high energy, resulting in a net positive expansion effect. As the density of the sample increases, however, the large low-energy flux depressions in the sample cause the positive contribution to lessen in comparison to the high-energy self-multiplication contributions. The result is a change in sign from positive to negative as the density increases.

The behavior of the expansion coefficients of the two uranium isotopes, in changing sign from Assembly 4Z to Assembly 14 at oxide densities, and reversing sign again in Assembly 17, is to be understood on the following basis. The major change from Assembly 5 to Assembly 14 was a very substantial softening of the real flux spectrum. The removal of a fraction of the ^{238}U also changed the reactor fission cross section somewhat at high energies and the reactor absorption cross section at low energies, but the adjoint spectrum has the same general shape in Assembly 14 as it had in Assembly 5. The very substantial shift in flux to low energies caused the positive reactivity effects in the low-energy region to overbalance the negative effects at high energy, resulting in a net positive expansion effect. When the remainder of the ^{238}U was removed in going to Assembly 17 (a small amount of ^{238}U actually remained, due to the 7% or so present in the enriched uranium fuel) the removal of fission in ^{238}U at high energies, and the removal of absorption at low energies, as well as a general increase in leakage due to the smaller assembly, caused the adjoint function to become a monotonically decreasing function of energy. The effect of this on the expansion corrections can be understood by reference to Eq. (1). This

equation shows that the flux change in any energy group is weighted by the algebraic sum of three terms -- the self-multiplication term which is weighted by the fission neutron adjoint, the removal term which is weighted by the adjoints at energies below those of the group under consideration, and the absorption term which is weighted by the adjoint of the group itself. At the highest energies then, the effect of a monotonically decreasing adjoint flux with energy is to increase the self-multiplication term somewhat, and increase the removal term somewhat as well, in comparison to the absorption term. Thus a given flux change in the high-energy region is weighted somewhat more heavily, and the negative reactivity effect of expansion is therefore increased. The reverse is true at low energies. The self-multiplication term is decreased relative to the absorption term, and the removal term is small compared to the other two terms. The result is a decrease in weighting given to any flux changes at lower energies, and therefore a decrease in the positive contributions to the expansion effect. The calculated changes in the fluxes and adjoints in the three assemblies chosen for illustration, are sufficient to cause the sign changes.

The foregoing considerations illustrate the sensitivity of the expansion effect to reactor fluxes and adjoints, and illustrate the necessity for experimental verification of expansion corrections. Secondly, however, they also illustrate the possibility of utilizing the very different behavior of the expansion effect in the various isotopes with changes in fluxes and adjoints, to aid in the evaluation of the expansion effects themselves. Thirdly, the effects predicted for ^{233}U and the plutonium isotopes in fast spectra demonstrate the need for caution in identifying measured reactivity effects due to heating as Doppler effects until a thorough evaluation of the expansion effects has been made. Finally, the magnitude of these effects, particularly in the plutonium isotopes suggests that they may play a useful part in some reactor power coefficients.

2. EQUIPMENT AND TECHNIQUES

The experimental approach to the problem of separation of thermal expansion effects from Doppler effect in fissile element Doppler effect measurements is based on the use of constrained-expansion reduced-density samples. The expansion effect decreases more rapidly with reduction in sample density than does the Doppler effect, and advantage is taken of this in the sample design. The residual expansion effects are evaluated by the use of three different element types, each with approximately the same sample density -- one type in which the sample is allowed to expand freely (denoted FE), a second in which axial expansion is not allowed (NE), and a third in which axial expansion is not allowed, and the radial expansion is constrained as well (NNE). A fourth element type, containing ^{235}U metal, has also been used to check the results. The proof of the method lies in the consistency of the results given by the various element types, when the known differences in expansion properties are taken into account.

Reference [4] gives a complete description of the equipment and techniques used. Briefly, however, a Doppler element, as described above, is oscillated repetitively in and out of the critical assembly while a small servo-controlled calibrated boron rod holds the reactor critical. The

difference in the average position of the calibrated rod, sample-in minus sample-out, gives the reactivity worth of the sample relative to the reference sample-out configuration. Repeating this procedure with the sample at various temperatures traces the reactivity change of the sample with increasing temperature.

The three types of Doppler elements that are used to evaluate expansion properties have the following characteristics in common: Cylindrical 1-in. diameter, 12-in. long, reduced density UO_2 samples are contained in a sealed 50-mil wall, nickel-alloy heater tube. The elements differ in the design of the heater tube. In the FE elements, the heater tube material is Inconel and the end caps are simply welded in. In the NE elements, the material is also Inconel but a piston and bellows arrangement at each end allow a constant axial length of UO_2 to be held as the temperature is increased. In the NNE elements, the heater tube material is Invar, allowing essentially zero radial expansion as well, from room temperature to approximately 200°C. Above this the radial expansion of the NNE elements almost parallels that of the NE element.

As shown above, the reactivity effects of expansion are related through the flux changes to changes in P_c, and hence to changes in Σa (Σ, the total macroscopic cross section of the sample, a, the sample radius). Reference [4] (or [5]) shows that the changes in Σa (or $N\bar{\ell}$) with temperature are related to the coefficient of linear expansion of the sample, α_s, and of Invar, α_I, by the following expressions:

For FE elements, $\delta(\Sigma a)/\Sigma a = -2\ \alpha_s \Delta T$ (3a)

For NE elements, $\delta(\Sigma a)/\Sigma a = -3/2\ \alpha_s \Delta T$ (3b)

For NNE elements, $\delta(\Sigma a)/\Sigma a = -\alpha_I \Delta T$ (3c)

Equations (1), (2) and (3) allow the reactivity effects of expansion to be calculated for each of the element types.

In the measurements to be described below, a 1 in. diameter ^{235}U metal sample was also used, and the discontinuous change in volume as the metal passes through the α-β phase change can be used to calibrate the expansion effect in this element.

3. EXPERIMENTAL RESULTS

Experimental data has been obtained for ^{235}U in four different assemblies each designed to have the same central spectrum (where the Doppler element is positioned). The assemblies were Assembly 5 and Assembly 4Z on ZPR-6, and Assemblies 11 and 12 on ZPR-9. The assemblies are mockups of a large dilute carbide fast reactor, and are described elsewhere [2], [3], [4]. The aim of this section is to give a consistent intercomparison of the data from the various element types on the different assemblies, so that some judgment can be made of the consistency and reliability of the ^{235}U Doppler effect data.

Figure 6 shows the experimental results for Assembly 4Z, in which five different ^{235}U Doppler element types were used, before expansion corrections are made. Figure 7 shows the same results, corrected for expansion on the basis described above, showing the way the expansion corrections bring the 1 in. diameter UO_2 results for the three elements with differing expansion

properties into agreement. The metal result is somewhat higher, and the half-inch oxide result considerably lower, as theory predicts.

Figures 8 and 9 show the results for the 1 in. diameter UO_2 samples in each of the three assemblies. Each figure shows the uncorrected experimental data in the lower portion of the figure, and the Doppler effect, corrected for expansion, in the upper portion. The purpose of displaying the results in this form is to demonstrate the degree of consistency of the data in the various assemblies.

The Assembly 5 data, shown in Fig. 8, are the most precise of the data taken on the four assemblies and should be weighted most heavily. Assembly 5 was the full-scale version of the carbide mockup, and very considerable care was taken with the measurement preparation, and the integrated power levels at which the measurements were done were increased to give the high precisions shown. The expansion effects are sufficiently small in these reduced density oxide samples that only in this assembly are the differences between the constrained expansion samples and the freely expanding sample unambiguously outside statistics. The figure shows the way that the expansion corrections bring the results of the two different types of elements precisely into line.

Figures 6 and 7 showing the Assembly 4Z results, also demonstrate the consistency of the results given by the various types of elements, although the precisions on these measurements were somewhat less.

The results from Assemblies 11 and 12 on ZPR-9, shown in Fig. 9, show considerably more scatter. Assemblies 11 and 12 were small zone assemblies, in which it is known that complete spectral equilibration was not achieved, and one may conclude from the results that they are reasonably consistent with the more precise results from the assemblies on ZPR-6, but the precisions are poor enough that no very precise conclusions may be drawn.

It is concluded that the precise data of Assembly 5, and the overall consistency of the data on the other assemblies, particularly that on Assembly 4Z, demonstrates that the expansion effects in the assemblies for the reduced density oxide samples are relatively small, and that their magnitude has been accurately established. The set of experiments therefore represent a reliable reference against which calculations of the ^{235}U Doppler effect for spectra typical of large dilute power reactors can be checked.

4. COMPARISONS WITH CALCULATION

The basic data available at the present time which can be used in ^{235}U Doppler calculations in spectra such as that found in ZPR-6 Assembly 5 consist of low-energy resolved resonance data (below 60 eV) and infinite-dilution capture and fission cross section data. Unresolved resonance parameters have been generated for the Doppler range, 100 eV to 10,000 eV, by estimating average resonance spacing from resolved data and adjusting the strength function to fit the infinite-dilution data. Lacking any way to estimate multi-level parameters in this range, the unresolved parameters and the framework in which they are used have been based on single-level Breit-Wigner line forms despite the fact that ^{235}U s-wave spacing is estimated to

be in the range of 1-2 eV and the Doppler width at 1000 eV and 1000°K is about 1.2 eV. This procedure is probably adequate for the estimation of resonance self-shielding in the generation of group cross sections in the Doppler range because this self-shielding is quite small and the results are insensitive to the unresolved parameters. Due to resonance overlap, however, the application of these unresolved parameters to Doppler calculations is very uncertain. Hwang [6], for example, has found significant effects due to ^{235}U self-overlap.

It would seem impossible, on the basis of present basic data, to do a definitive ^{235}U Doppler calculation for comparison to the measurements. However, survey calculations have been made to determine the degree of sensitivity of the ^{235}U Doppler effect calculated for the 1 in. diameter enriched UO_2 sample to assumptions of group cross section sets, resonance spacing, and resonance overlap. The basic calculation was made using perturbation theory, Schmidt unresolved parameters [7], conventional isolated-resonance theory [8], ENDF/B [9] and MCC [10] for the group cross sections, and diffusion theory to generate the spectra; the result was +0.174 Ih/kg-^{235}U for a temperature change from 293°K to 1100°K in the 1 in. ^{235}U O_2 sample. This number is relatively insensitive to various proposed changes in the present ENDF/B data; e.g., ignoring the smooth ^{238}U σ_c values (presumably p-wave) below 3920 eV raises the calculated ^{235}U Doppler value by 5%, introduction of the new ^{238}U σ_c data [11] between 100 and 500 keV (12% lower than ENDF/B) raises the value by 7%.

There have been evaluations of the ^{235}U unresolved data which have set the average s-wave level spacing higher than the 1.06 eV estimated by Schmidt while retaining about the same strength function (about 10^{-4}). For example, spacings of 1.72 for J = 3 and 1.34 for J = 4 have been in use at Argonne for some time. The larger spacing produces a larger Doppler effect, about 6% higher than the value given above, although the change is mitigated by changes in Γ_γ and Γ_f values. Rough calculations have been done on a range of resonance spacings from 1 to 2 eV, holding all other parameters fixed, which indicate an increase of about 60% in the Doppler effect at 2.0 eV spacing over that at 1.0 eV spacing.

An estimate of the possible effect of resonance overlap on the Doppler effect within the context of a model in which single-level line forms are overlapped has been obtained by calculating the Doppler effect in single average ^{235}U resonances throughout the Doppler range with and without adjacent ^{235}U resonances present. The calculations used Schmidt parameters (except that the level spacing was varied) and the RABBLE code [12]. All resonances had average parameters and were equally spaced. Resonances within ±10 times the Doppler width at 1100°K were considered in the overlap calculations. The effect of overlap in these calculations was very large. At 1.0 eV level spacing a reduction in the Doppler effect of a factor of 10 was obtained in the overlapped case relative to the case in which overlap was ignored; at a 2.0 eV spacing overlap reduced the calculated value by a factor of 4.

It may be concluded that, primarily due to the overlap problem, calculation of the ^{235}U Doppler effect to better than a factor of 2 or 3 is not possible at the present time.

313-475 O 68—23

Summary -- ^{235}U Doppler Calculations, 293°K to 1100°K
1 in. Diam $^{235}UO_2$ Sample, ZPR-6 Assembly 5,
Diffusion Theory, Perturbation Theory

Measured Value = +0.08 Ih/kg-^{235}U

RESONANCES ASSUMED ISOLATED

Group Cross Section Set	Resonance Parameters	$\delta\rho$ Ih/kg-^{235}U	Ratio $\frac{\delta\rho \text{ Schmidt}}{\delta\rho \text{ Hwang}}$	Ratio $\frac{\delta\rho}{\delta\rho \text{ ENDF/B}}$
1. ENDF/B-MC^2	Schmidt Hwang	+0.174 +0.185	0.941	---
2. ENDF/B-MC^2 With Reduced ^{238}U σ_c Grps 6-8	Schmidt Hwang	+0.187 +0.198	0.944	1.075
3. ENDF/B-MC^2 Without Smooth ^{238}U σ_c Below 3920 eV	Schmidt Hwang	+0.183 +0.193	0.948	1.051

ESTIMATED OVERLAP EFFECT -- Schmidt Parameters Except for Resonance Spacing

Resonance Spacing (eV)	Ratio -- With Overlap/Isolated
1.0	0.07
1.5	0.12
2.0	0.25

5. REFERENCES

1. C. E. Till, "Fissile Doppler Effect Measurement and the Effect of Thermal Expansion," Reactor Physics Division Annual Report, July 1, 1966 to June 30, 1967, ANL-7310 (to be published).

2. R. A. Karam et al., "Measured Physics Parameters in a Large U-C Fast Core, Assembly 5 of ZPR-6," Reactor Physics Division Annual Report, July 1, 1966 to June 30, 1967, ANL-7310 (to be published).

3. R. Pond and C. E. Till, "Doppler Effect Measurements in CH_2-Softened Spectra; ZPR-9 Assemblies 13-17," Reactor Physics Division Annual Report, July 1, 1966 to June 30, 1967, ANL-7310 (to be published).

4. C. E. Till, R. A. Lewis and R. N. Hwang, "ZPR-6 Doppler Measurements and Comparisons with Theory," Proceedings of the International Conference on Fast Critical Experiments and Their Analysis, October 10-13, 1966, ANL-7320, 319.

5. C. E. Till, R. A. Lewis and E. F. Groh, "U-235 Doppler Effect Measurement Data and Techniques," Reactor Physics Division Annual Report, July 1, 1966 to June 30, 1967, ANL-7310 (to be published).

6. R. N. Hwang, "An Improved Method of Doppler Effect Calculation for Fissile Materials in the Intermediate Energy Region," Proceedings of the Conf. on Breeding, Economics, and Safety in Large Fast Power Reactors, October, 1963, ANL-6792, 727-745.

7. J. J. Schmidt, "Resonance Properties of the Main Fertile and Fissionable Nuclei," National Topical Meeting on Reactor Physics in the Resonance and Thermal Regions, San Diego, California, 1966 (also KFK-120).

8. L. Dresner, "Resonance Absorption in Nuclear Reactors," Pergamon Press (1960).

9. S. Pearlstein, "Evaluated Nuclear Data File/B, Cross Section Evaluation Working Group," Brookhaven National Laboratory, (no comprehensive reference available at this time).

10. B. J. Toppel, A. L. Rago and D. M. O'Shea, "MC^2 - A Code to Calculate Multigroup Cross Sections," ANL-7318 (June 1967).

11. H. O. Menlove and W. P. Poenitz, "Absolute Radiative Capture Cross Section for Fast Neutrons in ^{238}U," Nucl. Sci. Eng. (to be published).

12. P. H. Kier and A. A. Robba, "RABBLE, A Program for Computation of Resonance Absorption in Multiregion Reactor Cells," ANL-7326 (April 1967).

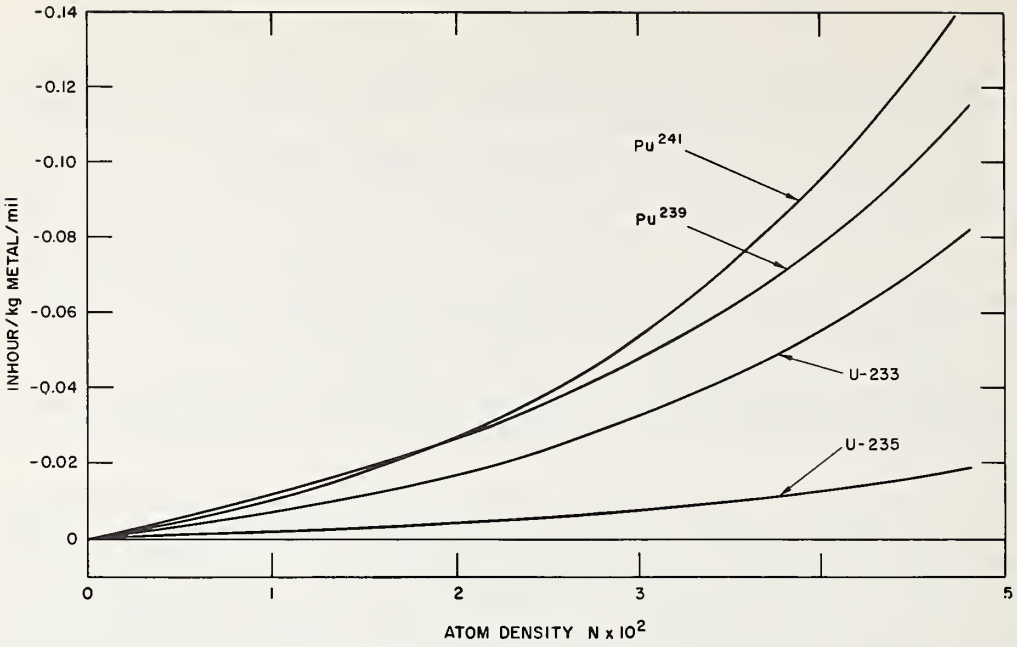

Fig. 1 "Reactivity Effects of Expansion for 1 in. Diameter Cylindrical Samples of Various Isotopes in Assembly 5, ZPR-6."

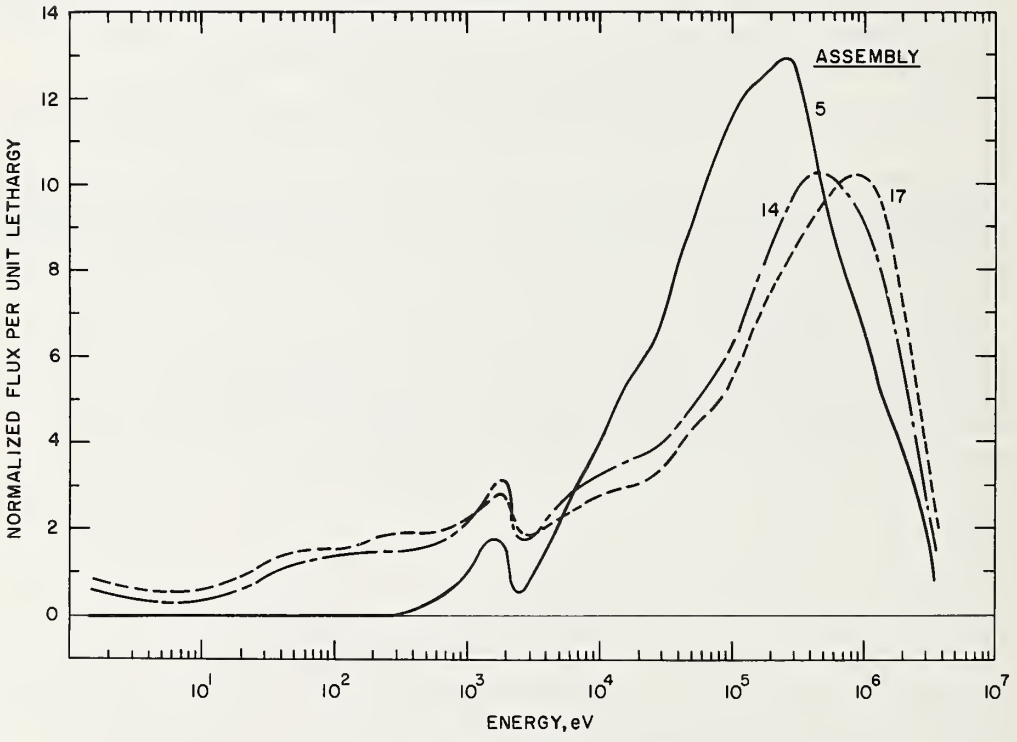

Fig. 2 "Comparison of the Real Flux Spectra in Assemblies 14 and 17, ZPR-9, and Assembly 5, ZPR-6."

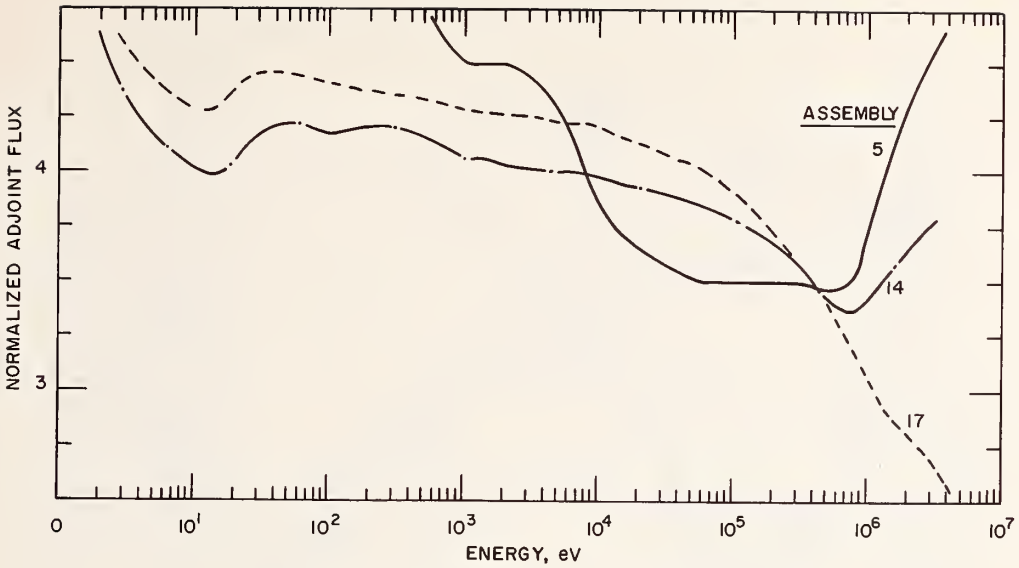

Fig. 3 "Comparison of the Adjoint Spectra in Assemblies 14 and 17, ZPR-9, and Assembly 5, ZPR-6.

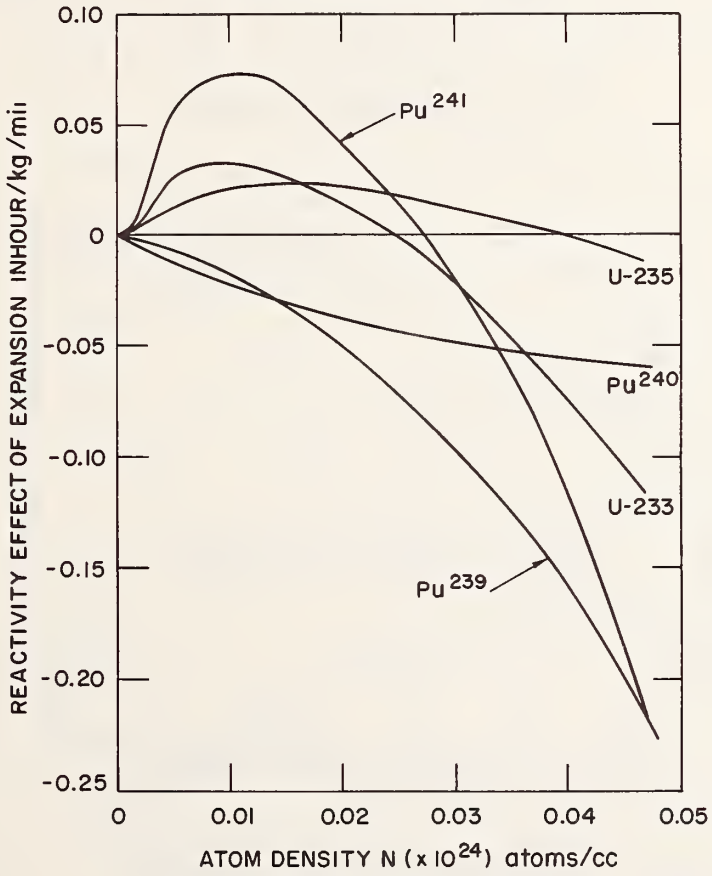

Fig. 4 "Reactivity Effects of Expansion for 1 in. Diameter Cylindrical Samples of Various Isotopes in Assembly 14, ZPR-9."

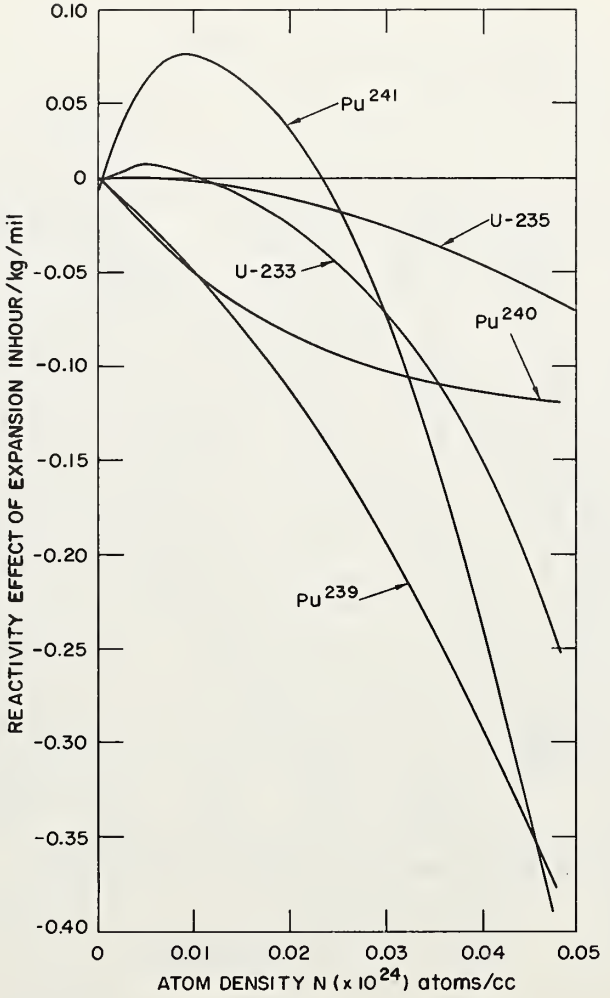

Fig. 5 "Reactivity Effects of Expansion for 1 in. Diameter Cylindrical Samples of Various Heavy Isotopes in Assembly 17, ZPR-9."

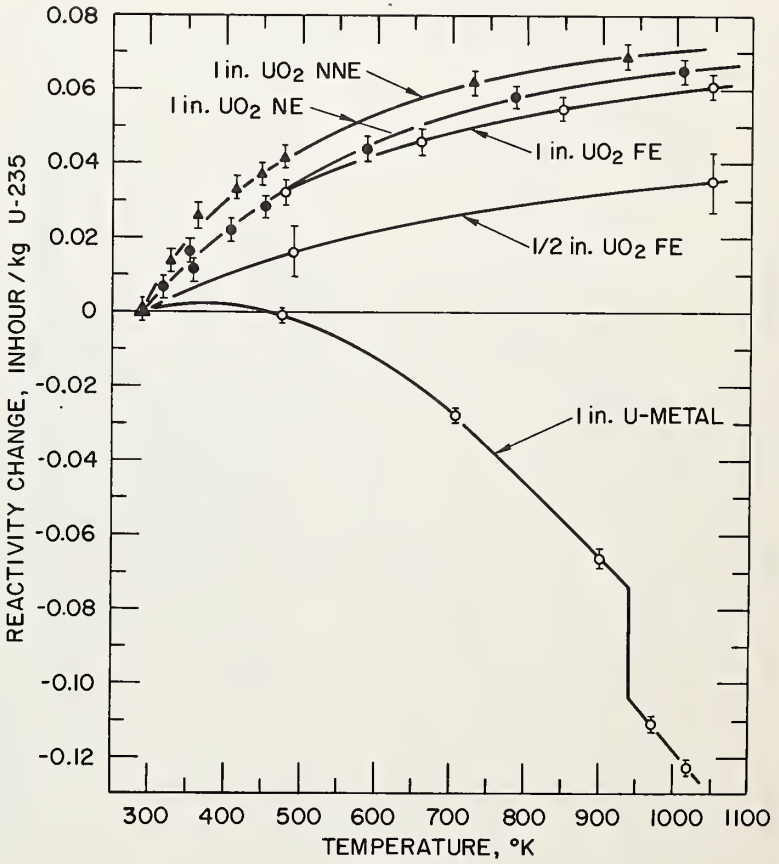

Fig. 6 "Assembly 4Z, ZPR-6, U-235 Experimental Data, Reactivity Change on Heating."

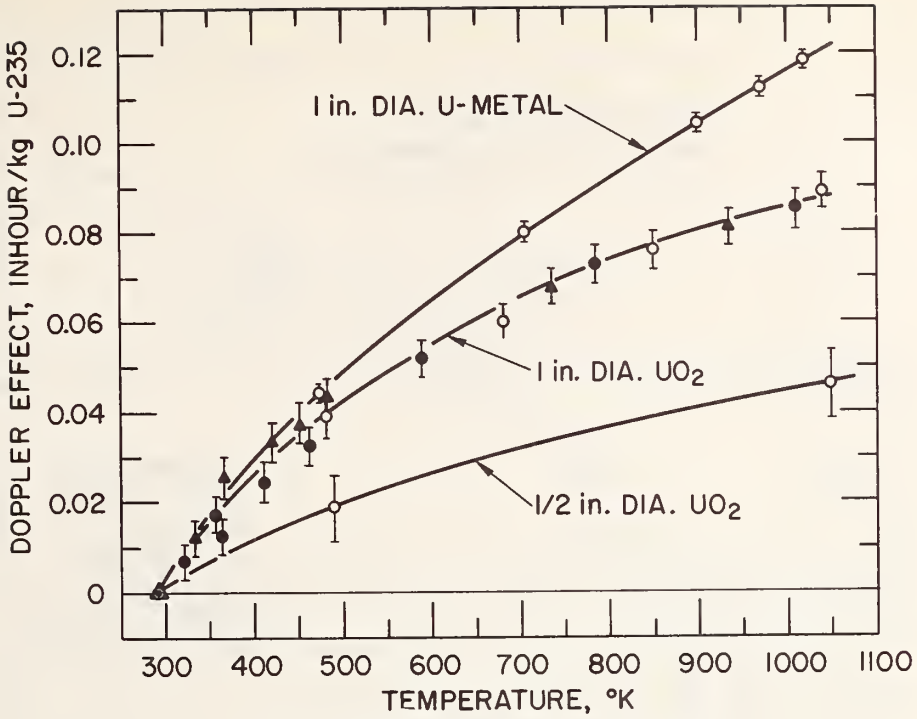

Fig. 7 "Assembly 4Z, ZPR-6, U-235 Doppler Effect Corrected for Expansion."

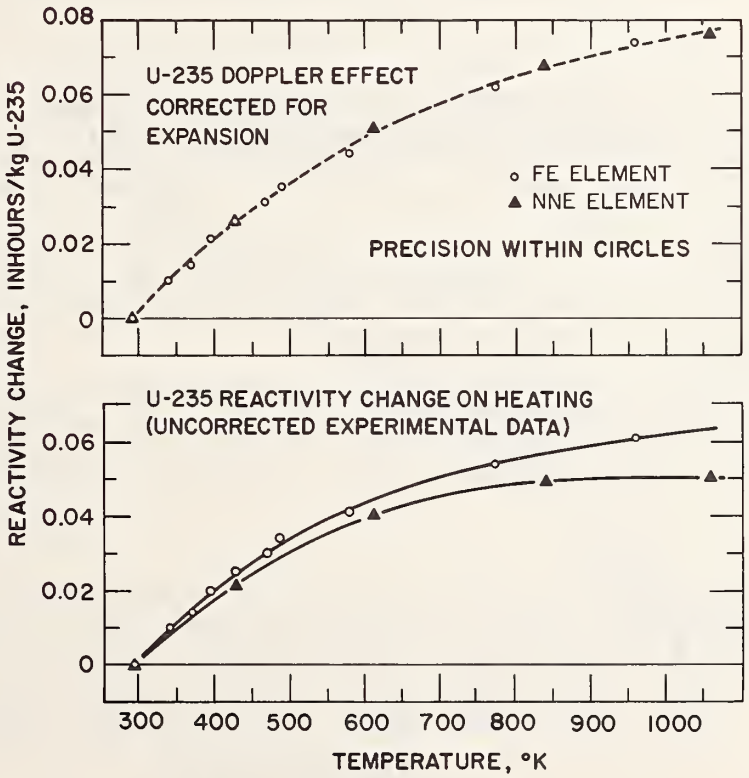

Fig. 8 "Assembly 5, ZPR-6, U-235 Doppler Effect Corrected for Expansion (upper portion) and U-235 Reactivity Change on Heating (lower portion), 1 in. Diameter UO_2 Samples."

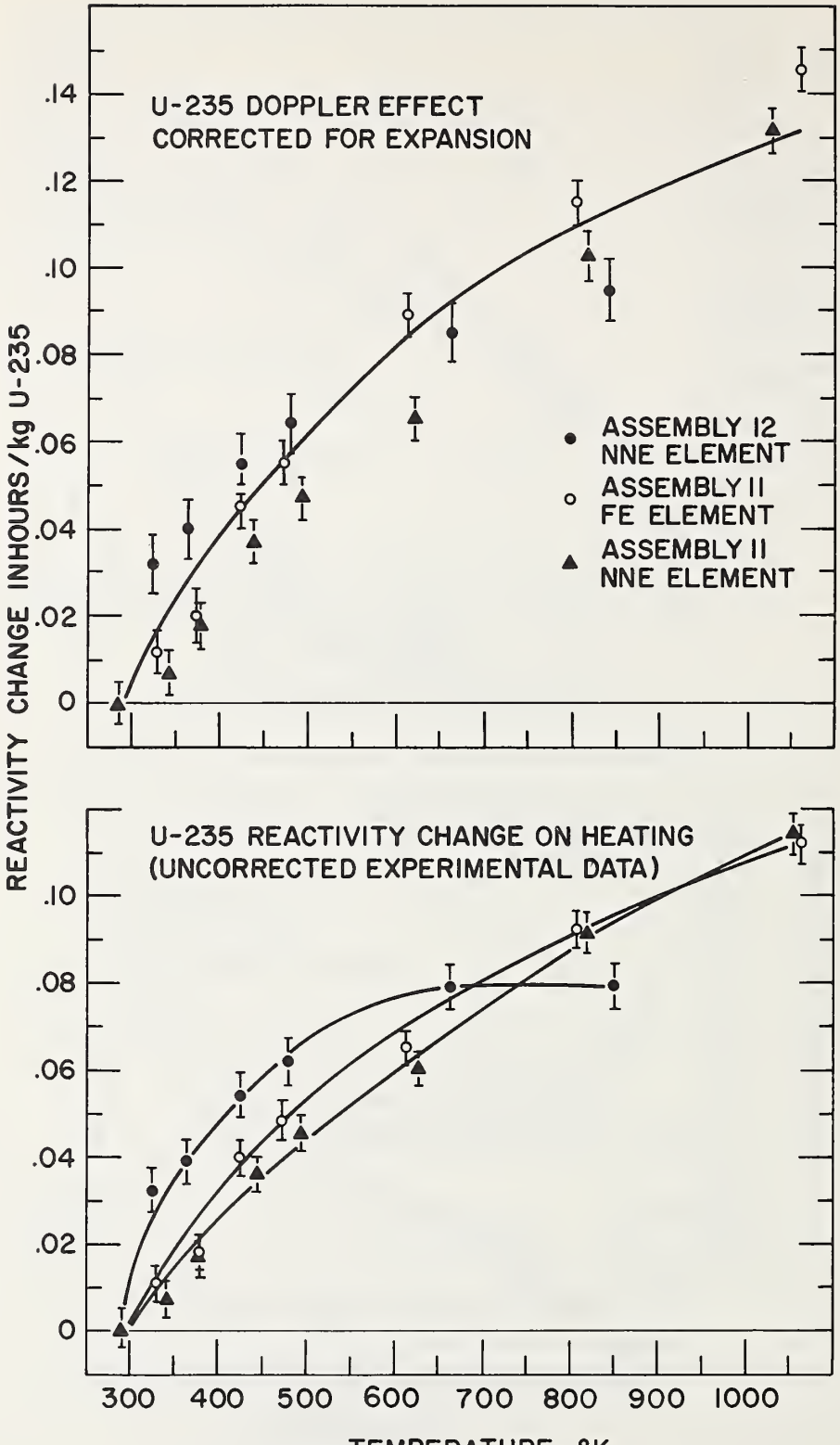

Fig. 9 "Assemblies 11 and 12, ZPR-9, U-235 Doppler Effect Corrected for Expansion (upper portion) and U-235 Reactivity Change on Heating (lower portion), 1 in. Diameter UO_2 Samples."

AN EXAMINATION OF METHODS FOR CALCULATING THE DOPPLER COEFFICIENT IN FAST BREEDER REACTORS

M. W. Dyos
C. R. Adkins*
T. E. Murley

Advanced Reactors Division
Westinghouse Electric Corporation
Madison, Pennsylvania 15663

*Permanent Address: Carnegie-Mellon University, Pittsburgh, Penna.

Abstract

The importance of the Doppler coefficient of reactivity on fast breeder reactor safety dictates that it should be predicted with as much accuracy as possible. The approximations that are usually made in computing the Doppler coefficient are: (I) the isolated narrow resonance approximation is used, (II) interference scattering is neglected, (III) overlap effects between different resonances and overlap between more than two sequences are neglected, (IV) heterogeneity is treated through an equivalence relationship and (V) the unresolved resonances are assumed to be uniformly spaced in energy.

The work reported here removes all of these restrictions. Furthermore, since the unresolved resonance region contributes significantly to the Doppler coefficient in fast reactors, this region is treated more rigorously through the generation of individual pseudo resonances using random sampling techniques within the framework of a single level Breit-Wigner formalism. A procedure is used which ensures that the pseudo resonance parameters yield resonance integrals that are consistent with broad group measured data. The resonance structure of each isotope is then complete over the energy range of interest for Doppler calculations. This resonance data is used in conjunction with an ultra fine group integral transport theory code.

The purpose of this paper is to examine the validity of the usual approximate methods by comparing with this more refined method of calculation. A numerical comparison is made for a plutonium-uranium carbide fuelled, sodium cooled fast breeder reactor.

1. Introduction

The extreme importance of the Doppler coefficient of reactivity on fast breeder reactor safety dictates that it should be computed as accurately as possible. Moreover, since a considerable portion of

Doppler coefficient results from neutron interaction in the unresolved resonance region, it is important that the approximate methods, which are currently in use, be compared with more sophisticated calculational methods to determine their validity over a wide range of fuel compositions.

The purpose of the work reported here is to give the results of calculations using sophisticated methods of calculating the Doppler coefficient within the framework of a single level Breit-Wigner formalism. These results will then be compared with calculations made using the approximate methods. It is hoped to shed light on the validity of the approximate methods and enable the development of even better approximate calculational schemes, which can be used in routine design analysis.

2. Method of Calculation

The accurate calculation has been made using the integral transport theory code RABBLE[1], which solves the slowing down equation in a set of coupled spatial regions. The flux in each region is taken to be spatially flat and the regions are linked together through the use of collision and transmission probabilities. The unresolved resonance region has been treated in detail by constructing statistical resonances with the PSEUDO code[2]. The construction of statistical resonances is made in a manner which ensures that the statistical resonance parameters yield pointwise cross sections that are in agreement with low resolution measurements[3]. Statistical resonances have been constructed for both s- and p- wave resonances and for the accessible spin states of the compound nucleus associated with these values of orbital angular momentum. Details of the isotopes and energy ranges for which statistical resonances have been constructed are given in Table 1. The RABBLE code has been modified to permit the more accurate treatment of p wave resonances. This has been achieved using an expression which permits the "symmetric" p-wave line shape function to be expressed in terms of the well known line shape functions for s-wave resonances[4]. It is worth noting that the p-wave neutrons in U-238 and Pu-240 contribute about 48 percent and 18 percent respectively to the unresolved infinitely dilute capture resonance integrals below 15 KeV. Since these contributions are significant their contributions to the Doppler coefficient have been examined in detail.

A comparative calculation was made using the MC^2 code[5]. The approximations that are employed in the code, in that part of the energy in which a resonance calculation is performed, are:

(I) the isolated narrow resonance approximation is used,

(II) overlap effects between different resonances and overlap between more than two sequences are neglected,

(III) interference scattering is neglected in the unresolved resonance region,

(IV) the unresolved resonances are taken to be uniformly spaced in energy,

(V) heterogeneity is treated through an equivalence relationship, and

(VI) higher angular momentum neutrons are treated as s wave resonances with a modified reduced neutron width.

To ensure consistency between the data used in the RABBLE and MC^2 calculations in the unresolved resonance region a preliminary run was made of MC^2 to obtain the infinitely dilute capture and fission resonance integrals over the unresolved resonance regions shown in Table 1. These infinitely dilute resonance integrals were obtained from the pointwise data for U-238[6], Pu-239[7] and Pu-240[8] evaluated for the ENDF/B data files from low resolution experimental data. The PSEUDO code, using the method described in Reference (3), predicted infinitely dilute resonance integrals in the unresolved resonance region which were consistent with the results obtained from the MC^2.

The most serious approximation made in the RABBLE calculation would seem to be the use of the Breit-Wigner single level formula for the resonances of the fissile materials (Pu-239 in this calculation). However, it has been shown at Argonne[9] and by Otter[10] that multilevel effects are not important for Pu-239 in the energy range used in this calculation. The results of the RABBLE calculation can be used with confidence.

3. Numerical Calculation

The Doppler coefficient of reactivity has been computed for a typical fuel rod in a (Pu, U)C fuelled LMFBR. The fuel rod had a diameter of 0.625 cm. The calculations were performed for a two region cell in which the sodium bond, clad and sodium coolant were smeared into an outer region. Details of the cell geometry and number densities in each region are given in Table 2. The RABBLE calculations, using five spatial regions, showed that there was very little fine structure in the spatial distribution of the flux.

The calculated Doppler coefficient represents a change in the average fuel temperature from 1000°K to 1560°K while the temperature of the coolant in the outer region remained constant at 750°K. The RABBLE calculation gave the Doppler coefficient as -5.17×10^{-6} $\Delta k/k/°C$, whereas, the MC^2 calculation gave a value of -2.17×10^{-6} $\Delta k/k/°C$. Reasons for this large discrepancy are discussed in the next section.

4. Discussions of Results

It can be seen from Table 3 that U-238 makes the dominant contribution (94.3 percent) to the Doppler coefficient. The overall Doppler coefficient as a function of energy is shown in Figure 1 as computed by RABBLE and MC^2. Also shown in the figure is the flux per unit lethargy as computed by the MC^2 code. Figure 1 shows that for the fuel rod composition used in this study the majority of the Doppler coefficient arises in the vicinity of the sodium resonance at 2.85 KeV. Above the peak of the sodium resonance the cross sections computed by RABBLE and MC^2 are in close agreement at both the temperatures considered. There is, however, a considerable difference in the Doppler coefficient which can be attributed to the more accurate treatment of resonance capture, in the unresolved resonance region, as computed by the RABBLE code through the use of statistical resonances. It was observed that the p-wave neutrons made a 50 percent contribution to the capture cross section for U-238 in the unresolved resonance region but their contribution to the Doppler coefficient was only 10 percent in the unresolved resonance region and 2 percent overall. It is concluded that because of their small importance the treatment of p-wave resonances in the MC^2 code is adequate. It may be true, however, that the Doppler broadening of p-wave resonances makes a significant contribution to the Doppler coefficient at lower fuel temperatures, as for example the measurement of the Doppler coefficient in a critical assembly.

Below the peak of the sodium resonance large differences in the calculated Doppler coefficients between RABBLE and MC^2 are observed (see Figure 1). It would be expected that the two calculations would agree in this energy range due to the dominance of U-238 for which the resonance parameters are resolved. Identical resonance parameters were used for U-238 in this energy region for both calculations. Part of this discrepancy can be explained in terms of the spatial dependence of the neutron slowing down source which is not precisely treated in MC^2. The spatial dependence of the slowing down source in MC^2 is treated through an equivalence relation but is treated exactly, within the framework of integral transport theory, in the RABBLE code. The slowing down source in the fuel is greatly affected by the large sodium resonance in the region external to the fuel. The effect of the equivalence relationship in MC^2 in the vicinity of the sodium resonance is to increase the effective potential scattering cross section, decrease the resonance self shielding and diminish the Doppler effect in a particular energy group. The slowing down source in the fuel is greatly affected by neutrons scattered in the sodium resonance, external to the fuel region, which then enter the fuel region at a lower energy. This spatial effect cannot be adequately treated by an equivalence relationship, especially when the fuel region produces a scattering source which is a rapidly varying function of energy. It is, therefore, possible that the differences in the Doppler coefficient below the peak of the sodium resonance can be attributed to the differences in the treatment of neutron slowing down in the respective codes.

In addition, there will be other, but smaller, effects which could contribute to the differences in the calculated Doppler coefficient for the two methods. These effects are the use, in the MC^2 code, of the narrow resonance approximation and the overlap of the resolved resonance region for U-238 with the unresolved resonance regions of Pu-239 and Pu-240. Of particular importance is the better treatment of Pu-239 and Pu-240 in the RABBLE code through the use of statistical resonances.

It can be seen from Table 3 that Pu-240 has a small but positive Doppler coefficient. This can be explained by the fact that because of its low concentration the increase in the capture cross section is more than offset by the decrease in the flux at the higher temperature. A similar effect is also seen in iron, carbon and sodium where the cross sections are independent of the fuel temperature.

5. Conclusions

Calculations of the Doppler coefficient in liquid metal fast breeder reactors, in which a major part of the Doppler coefficient arises in the vicinity of the sodium resonance at 2.85 KeV can only be made with confidence when a spatial treatment of the slowing down source is used. P-wave effects make only a very small contribution to the overall Doppler coefficient at temperatures in the vicinity of 1000°K, but a significant contribution to the capture and fission cross sections. The statistical method for constructing resonance parameters in the unresolved resonance region is important for the accurate prediction of the Doppler coefficient in the unresolved resonance region.

It is very difficult to separate out the individual effects arising from the use of the narrow resonance approximation, limited resonance overlap effects, the neglect of interference scattering in the unresolved resonance region and the uniform spacing of resonance levels in the unresolved resonance region, but these effects must be investigated in detail in future work.

6. References

(1) P. H. Kier and A. A. Robba, "RABBLE, A Program for Computation of Resonance Absorption in Multi-Region Reactor Cells," ANL-7326 (1967).

(2) M. W. Dyos, C. R. Adkins and S. Dolinar, "Modifications to the PSEUDO Code for the Construction of Statistical Resonances in the Unresolved Resonance Region," WCAP-7130, November 1967.

(3) M. W. Dyos, "The Statistical Treatment of Resonance Absorption in the Unresolved Resonance Region," invited paper to be presented at Am. Nucl. Soc. Annual Meeting, Toronto, June 1968.

(4) M. W. Dyos, "The Doppler Broadened Line Shape Function for P-Wave Resonances," Trans. Am. Nucl. Soc., 264, 10, June 1967.

(5) B. J. Toppel, A. L. Rago and D. M. O'Shea, "MC^2, A Code to Calculate Multigroup Cross Sections," ANL-7138, June 1967.

(6) W. A. Wittkopf, D. H. Roy and A. Z. Livolsi, "U-238 Neutron Cross Section Data for ENDF/B," BAW-316, May 1967.

(7) P. Greebler, P. Aline and B. Hutchins, "Evaluation and Compilation of Pu-239 Cross Section Data for the ENDF/B Files," GEAP-5272, December 1966.

(8) P. A. Pitterle and M. Yamamoto, "Evaluated Neutron Cross Sections of Pu-240 for the ENDF/B Files," APDA-TM-43, January 1967.

(9) W. M. Manning and S. Lawroski, "Reactor Development Progress Report, September 1967," ANL-7382 (October 1967).

(10) J. M. Otter, "Calculation of Pu-239 Resonance Cross Sections Using Fission Widths from Channel Fission Theory," Atomics International Report, NAA-SR-12515 (October 1967).

TABLE 1. ENERGY RANGES AND ISOTOPES FOR WHICH STATISTICAL RESONANCES HAVE BEEN CONSTRUCTED

ISOTOPE	ANGULAR MOMENTUM AND SPIN (ℓ,J)	ENERGY RANGE (KeV)	NUMBER OF RESONANCES
U-238	(0,1/2)	3.9-15.0	607
U-238	(1,1/2)	3.9-15.0	597
U-238	(1,3/2)	3.9-15.0	1213
Pu-239	(0,0)	0.292-3.0	313
Pu-239	(0,1)	0.298-3.0	863
Pu-240	(0,1/2)	0.679-15.0	891
Pu-240	(1,1/2)	0.679-15.0	883
Pu-240	(1,3/2)	0.679-15.0	1483

TABLE 2. DETAILS OF FUEL CELL FOR DOPPLER COEFFICIENT CALCULATIONS

	REGION 1	REGION 2
OUTER RADIUS (CM.)	0.3124	0.4826
C (Atoms/barn-cm.)	0.0095	-
Na. (Atoms/barn-cm.)	-	0.0124
Fe (Atoms/barn-cm.)	-	0.0091
U-238 (Atoms/barn-cm.)	0.0077	-
Pu-239 (Atoms/barn-cm.)	0.0014	-
Pu-240 (Atoms/barn-cm.)	0.0004	-
INITIAL TEMPERATURE (°K)	1000	750
FINAL TEMPERATURE (°K)	1560	750

TABLE 3. FRACTIONAL CONTRIBUTIONS TO THE DOPPLER COEFFICIENT

ISOTOPE	FRACTIONAL CONTRIBUTION TO THE DOPPLER COEFFICIENT
U-238 s-wave	-0.925
U-238 p-wave	-0.018
Pu-239	-0.092
Pu-240 s-wave	+0.010
Pu-240 p-wave	+0.001
Fe	+0.020
Na-23	+0.004
C	0.0

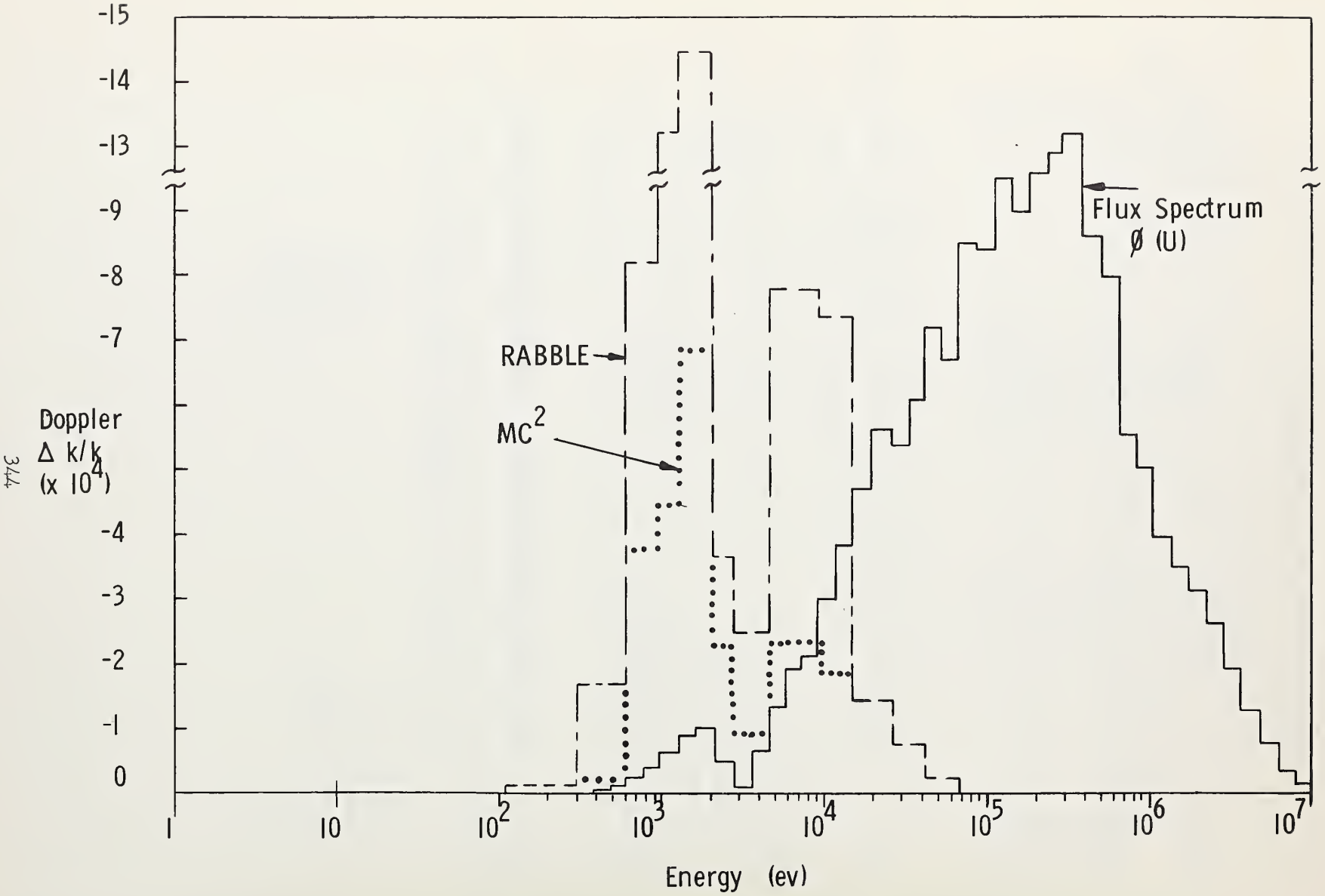

Fig. 1. Calculated Doppler Coefficients

INFLUENCE OF NEUTRON DATA IN THE DESIGN OF OTHER TYPES OF POWER REACTORS*

A. M. Perry

Oak Ridge National Laboratory
Oak Ridge, Tennessee 37830

ABSTRACT

The effects of cross-section uncertainties on estimates of breeding performance and of power cost for a molten-salt breeder reactor are shown to be small. Uncertainty in breeding ratio due to cross-section uncertainties is less than ±0.02, and the uncertainty in power costs is less than ±0.03 mills/kwhr(e). Similarly small effects are shown for the high-temperature gas-cooled reactor. The need for further refinements in nuclear data is related primarily to the calculation of temperature coefficients of reactivity.

1. INTRODUCTION

I have been asked to remark on the influence of nuclear data in the design of "other power reactors" — that is, other than fast breeder reactors and water-moderated thermal reactors. I take this to mean the impact on reactor design and economics of uncertainties in neutron cross sections; and among other power reactors, I shall direct your attention primarily to two thermal reactors operating on the thorium-^{233}U fuel cycle, namely the molten-salt breeder reactor (MSBR) and the high-temperature gas-cooled reactor (HTGR).

In considering the effects of cross-section uncertainties on reactor design and performance, a distinction must be made among (a) those effects which become apparent in operation of the first fuel loadings of the first reactors, and for which adjustments can be made in subsequent fuel loadings of the same reactors; (b) those effects which, though apparent in operation of the first few reactors, can only be allowed for in the design of subsequent reactors; and (c) those effects which, following more or less inevitably from the facts of nature, will continue to influence the economics of nuclear power in future generations of reactors. While the first two classes of effects are of some economic importance in the short run, it is the last class which appears to involve potentially very large sums of money. It is easily seen, for example, that a difference of 0.01 mills/kwhr(e) represents a cost difference of $70,000/year for a single 1000 Mw(e) reactor operating at a plant factor of 0.8. Continuing this line of reasoning, with the help of current estimates of future nuclear-

*Research sponsored by the U. S. Atomic Energy Commission under contract with the Union Carbide Corporation.

313-475 O-68—24

electric capacity in the United States, one finds that a difference in power cost of 0.01 mills/kwhr(e) implies a cost differential of $5 million per year by 1975, $20 million per year by 1985, and perhaps $80 million per year by the year 2000, with a cumulative cost differential by the year 2000 of nearly $1 billion. I think it would be a mistake, however, to conclude from this sort of exercise that an uncertainty of 0.01 mills/kwhr(e) in predicted power cost, associated with neutron cross-section uncertainties, represents a potential saving of this magnitude to be realized by improving the accuracy of cross-section measurements. In the first place, improved values of cross sections may lie on either side of the present most-probable values. Secondly, the cross-sections themselves are not uncertain — only our knowledge of them is; and to the extent that the design parameters (though not the calculated power cost) of a fully optimized reactor are insensitive to small variations in assumed cross-sections, the true cost cannot be altered by refining the nuclear data.

Nonetheless, since both the AEC and the power companies, as well as reactor designers, must make decisions based in part on estimates of power generation costs, it may still be of interest to see what uncertainties in reactor performance and in cost of power are associated with present uncertainties in nuclear data.

The cost of power is customarily divided into capital costs, representing the fixed investment in plant, the more-or-less fixed operating and maintenance costs, and the fuel-cycle cost, which is roughly proportional to the amount of energy generated. The elements of the fuel cost, all of which are in some degree sensitive to nuclear data, are the inventory costs, i.e., the carrying charges on the value of fuel materials allocated to the plant, the costs of fabricating, shipping, storing, and reprocessing the reactor fuel, and the cost of the fuel materials consumed. Fabrication and processing costs, per unit energy generated, are essentially inversely proportional to the amount of energy extracted from each fuel element before it must be discharged from the reactor. Although in some types of reactors the limiting exposure of fuel is determined by physical properties and radiation damage, rather than by nuclear reactivity, one in any case designs a reactor to minimize the excess reactivity invested, and therefore an error in predicting the fuel reactivity as a function of exposure may result in early discharge of the fuel, and in higher fabrication and processing costs. However, the economic penalty associated with such an error should be confined to the first few cores, since adjustments in fuel loading would be made in subsequent cores to achieve the desired exposure. Such adjustments do, however, influence the amount of fissionable material allocated to the plant, and hence the inventory cost. The burnup cost, finally, varies linearly with the conversion ratio, and is given (for a net electrical efficiency of 0.45) by

$$C_B = 0.1\ c(1+\alpha)(1-B)\ \text{mills/kwhr(e)}\ ,$$

where c is the value of the feed material ($/g), α is the average capture/fission ratio of the fissile material in the core, and B is the conversion ratio. If B is greater than unity, C_B is a production credit.

Effects of cross-section uncertainties on capital costs are less easily identified, but may, for example, include the following:

a) The excess reactivity of the loaded core may be somewhat greater than anticipated. Allowance for this possibility must be made in the design, and may involve a slightly greater control capability than would otherwise be necessary. In addition, deeper insertion of control rods may influence the power distribution, implying slightly conservative design with respect to the average power density. Alternatively, flexibility in the initial loading may be provided, perhaps involving small additional expense in first-core fabrication cost or in additional power outage for refueling operations.

b) Power-density distributions in large cores are very sensitive to local variations in reactivity. Allowance for cross-section uncertainties may require conservative thermal-hydraulic design of the core, or (as is more likely) may require provision for very close monitoring of the power distribution and for adjusting local reactivity by fuel management, control-rod manipulations, or both.

c) Large cores also exhibit a tendency toward unstable flux oscillations, which also requires monitoring and control capabilities, to an extent which depends fairly strongly on the temperature coefficients of reactivity. These, in turn, may be subject to some uncertainty as a result of cross-section uncertainties. Here again, it is primarily the complexity of the flux-sensing and control devices that may be affected.

d) Shielding calculations may be subject to appreciable error because of uncertainty in secondary gamma-ray production by neutron capture in various components of the reactor and shield, leading to the need for additional conservatism in design.

e) Neutron activation of various components, and subsequent handling problems, can be affected by cross sections of minor constituents or trace elements whose cross sections are not well known.

2. INFLUENCE ON FUEL-CYCLE ANALYSIS

With these qualitative effects in mind, we turn first to an evaluation of the uncertainties in fuel-cycle analysis for the MSBR and the HTGR that are attributable to cross-section uncertainties. The analysis of these effects for the MSBR was performed at the Oak Ridge National Laboratory, while most of the information relating to the HTGR was kindly furnished by H. B. Stewart of Gulf General Atomic, Incorporated. In each case, the procedure used was to carry out equilibrium fuel-cycle calculations with the best available cross sections, and to repeat these calculations with perturbed cross-section sets representing what we believe to be the probable errors in each important cross section. The perturbations were applied taking one nuclide at a time, and in each such calculation the fuel concentration was adjusted to maintain the optimum fuel exposure. This allows for the sort of adjustment in fuel loading that could be made

immediately in the MSBR or in subsequent core loadings for the HTGR. It also allows for such secondary effects as shifts in neutron spectrum, changes in $^{235}U/^{233}U$ absorption ratio, changes in ^{236}U absorptions, changes in the amount of fuel available for recycle, etc., all of which may follow as a consequence of the altered cross sections.

The use of equilibrium fuel-cycle calculations for this purpose is justified by the fact that in both reactor types the fuel cycle, even though started up with ^{235}U (or Pu), approaches equilibrium composition in about 5 years.

3. Molten-Salt Breeder Reactor

For purposes of the present discussion, a brief and quite general description of the MSBR concept should suffice. It is a graphite-moderated reactor, operating on the thorium-^{233}U fuel cycle. Fuel, as UF_4, and fertile material, as ThF_4, are dissolved in a molten mixture of LiF and BeF_2 which circulates through the reactor core and through external heat exchangers. The UF_4 and ThF_4 may be carried in the same salt stream, as is the case in the concept currently under most active study at ORNL, or in separate salt streams. In the latter case, the fertile stream also surrounds the core on all sides as a blanket region, reducing the loss of neutrons by leakage to a very low level. In either case, addition of fuel and removal of fission products are performed continuously by circulating a small portion of the main salt stream to chemical-processing equipment which is an integral part of the reactor plant. Typically, about five fuel inventories would be processed for fission-product removal in the time required to burn up one inventory, so that fission-product poisoning is small. In addition, processes appear to be available for removing Pa from the salt stream on a much faster cycle, i.e., less than 5 days.

Detailed neutronic calculations show that the breeding capabilities of the two concepts are very similar, and a choice between them will be based primarily on engineering and chemistry considerations, rather than on differences in neutronic behavior. A summary of important MSBR characteristics is shown in Table 1.

The distribution of neutron captures is very nearly the same in either MSBR design. The distribution shown in Table 2 is for a two-stream reactor, and gives an indication of the relative importance of various neutron absorbers. The figures are normalized to one absorption in fissile uranium ($^{233}U + ^{235}U$) and hence give directly the loss in breeding ratio associated with captures in any element. (The excess of neutron productions over neutron absorptions shown in Table 2 is not a consequence of poor convergence in the equilibrium fuel-cycle calculation, but rather of the fact that the FLIP/FLOP two-dimensional synthesis used in these calculations, while accounting for neutron absorptions in the axial blanket, neglects neutron productions in that region — an error of approximately 0.2% in the neutron balance. This leads to an underestimate of

Table 1. Selected Characteristics of MSBR

	Two-Streams	One-Stream
Reactor power, Mw(e)	250[a]	1000
Core height/diameter, ft	10/8	14/14
Power density, kw/liter	40	40
Specific fissile inventory, kg/Mw(e)	1.0	1.0
Breeding ratio	1.07	1.07
Annual fuel yield, %/yr	5	5
Fuel doubling time, yr	14	14
Fuel-cycle cost, mills/kwhr(e)	0.5	0.3–0.5[b]

[a] One of four reactors in a 1000 Mw(e) station.

[b] No reliable estimates of fuel processing cost are available as yet for this concept.

Table 2. Typical Neutron Balance — MSBR

Nuclide	Absorptions	Productions
^{233}U	0.9262	2.0733
^{235}U	0.0738	0.1474
^{232}Th	0.9880	0.0040
^{234}U	0.0793	0.0010
^{233}Pa	0.0005	
^{236}U	0.0078	0.0001
^{237}Np	0.0007	
^{6}Li	0.0070	
^{7}Li	0.0255	
Be(n,γ)	0.0030	
Be(n,α)	0.0049	
Be(n,2n)	0.0130	0.0260
F(n,γ)	0.0225	
F(n,α)	0.0100	
Graphite	0.0441	
Xe	0.0050	
^{149}Sm	0.0076	
^{151}Sm	0.0022	
Other fission products	0.0174	
Delayed neutrons	0.0030	
Structure	0.0013	
Leakage	0.0039	
	2.2467	2.2518

~0.005 in the breeding ratio. This limitation of the synthesis procedure is being eliminated in a new version of the program.)

Because of the operating flexibility of fluid fuel reactors, which allows criticality to be maintained by adjustment of fuel concentration, we are not primarily concerned with the problem of maintaining criticality per se. We are concerned instead with the fraction of source neutrons that is available for absorption in fertile materials, and with the uncertainty in this fraction arising from uncertainties in nuclear data.

There are, in fact, comparatively few nuclides in the MSBR for which cross-section uncertainties lead to appreciable uncertainty in the breeding performance of the reactor, and ^{233}U is the only nuclide whose cross-section uncertainties produce as much as 0.01 uncertainty in the breeding ratio. Here the important quantity is the average value of η, averaged over the entire reactor spectrum. This quantity may be uncertain for at least three reasons: (1) the value of η at 2200 m/sec, η_o, is uncertain by perhaps as much as 1/2%, (2) the variation of η, relative to η_o, as a function of energy in the range below 0.5 ev is not known well enough to establish $\bar{\eta}/\eta_o$ (in a thermal spectrum with kT ~ 0.1 ev) to better than 1/2%, and (3) $\bar{\eta}$ in a 1/E spectrum above 0.5 ev is subject to an uncertainty of about 1%. Altogether, we estimate that these independent uncertainties produce an overall uncertainty in $\eta(^{233}U)$, in a typical MSBR spectrum, of about ±0.012, which is by far the largest single contributor to the uncertainty in the neutron balance and hence in the power cost.

The value adopted for η_o, i.e., 2.293 ± 0.01, is somewhat higher than that recommended by Westcott et al. [1] (2.284 ± 0.008). We believe that the absolute measurements of η_o made by J. R. Smith [2], which were reported as very tentative at the time of the Westcott evaluation should now be given greater weight.

The ambiguity in the epithermal η is, fortunately, not so significant now as it has been until recently. The ambiguity arose from a discrepancy that appeared to exist between average epithermal α values as deduced from differential fission and total cross section measurements on the one hand, and from direct integral measurements of α on the other hand. The differential measurements yielded a value of α [3], averaged over a 1/E spectrum above 0.5 ev, of about 0.23. This value is subject to appreciable uncertainty, however, because σ_c must be deduced by subtraction of σ_f and σ_s from the measured σ_T. Furthermore, an adequate statistical analysis of the probable error in $\bar{\alpha}$, as derived from the differential cross sections, has not been made. The integral $\bar{\alpha}$ measurements are performed by measuring the ^{234}U and fission-product concentrations in irradiated ^{233}U samples. Results of the three most recent measurements of this type are as follows:

Halperin	$\bar{\alpha}$ = 0.171 ± 0.017	Ref. [4]
Esch and Feiner	$\bar{\alpha}$ = 0.175 ± 0.008	Ref. [5]
Conway and Gunst	$\bar{\alpha}$ = 0.175 ± 0.006	Ref. [6]
Average	$\bar{\alpha}$ = 0.175 ± 0.005	

We believe that the close agreement among these independent measurements and the inherently greater accuracy of the direct integral α measurement support the lower value of α in the epithermal energy range.

Recent work by L. W. Weston et al., of ORNL, and R. W. Ingle et al., of RPI, using the RPI Linac, has provided simultaneous fission and capture cross-section measurements over the energy range 0.02–1000 ev [7]. An average $\alpha(>0.5$ ev) may be deduced, primarily from these measurements, which is in much better agreement with the integral measurements, i.e., 0.183 ± 0.017. We somewhat conservatively assign a value of 0.18 ± 0.01, recognizing that there may still be unknown systematic errors in either method. It may be noted that an uncertainty of 0.01 in $\alpha(>0.5$ ev) generates an uncertainty of about 0.006 in the breeding ratio, for a typical MSBR configuration.

A similar discrepancy between differential cross-section measurements and direct α measurements in the epithermal region has existed for ^{235}U. Recent α values deduced by de Saussure, Gwin, and Weston [8] from their measurements of fission and capture cross sections for ^{235}U are in much closer agreement with the integral α measurements for ^{235}U than any values previously derived from differential cross-section measurements, and we believe that this troublesome discrepancy is essentially resolved.

In addition to the related uncertainties in η and in α, there is also an uncertainty in the value of $\nu = \eta(1 + \alpha)$. This is not of any direct consequence in the subcadmium energy range, since η is an independently measured quantity. In the epicadmium range, however, η is deduced from α and ν, and must reflect uncertainties in both of these quantities. It is difficult to assess the uncertainty in ν because of what appear to be systematic discrepancies between determinations by various methods. Nonetheless, we presently believe it is unlikely that ν lies outside the range 2.50 ± 0.01, including delayed neutrons. The combined effect of the uncertainties in $\overline{\alpha}$ and in ν is an uncertainty of about 1% in $\overline{\eta}$, in the energy range $E > 0.5$ ev.

Uncertainty in the value of η averaged over the thermal neutron spectrum is important because ~70% of the absorptions in ^{233}U occur in the subcadmium neutron range. Direct measurements of $\eta(E)/\eta(0.025$ ev) have been made by several investigators since the early 1950's. The existing measurements are not in good agreement with each other or with values deduced from differential cross section measurements, nor do they have the very high precision required to determine $\langle \eta/\eta_o \rangle_{avg}$ to an error as small as that in η_o itself [$\eta_o = \eta(0.025$ ev)].

The problem is illustrated by the data shown in Fig. 1, where the open symbols (and the black symbols below 0.1 ev) represent direct relative η measurements, normalized to $\overline{\eta} = 2.293$ in the range 0.01 to 0.07 ev, while the black symbols above 0.1 ev are deduced from $\eta = 2.50/(1 + \alpha)$, with α taken from the fission and capture cross-section measurements of Weston et al. Results of other similar measurements, not shown in Fig. 1, exhibit considerably more scatter, especially above 0.2 ev. Equally important, there has been until recently considerable ambiguity about the

depth and location of the dip in η between 0.1 and 0.2 ev. Here again, the measurements of Weston et al. have appreciably reduced the uncertainty in $\eta(E)$ below 1 ev, although the points shown represent preliminary unpublished data, which are still subject to possible revision. With these recent developments, it does not appear that the value of η, averaged over an MSBR spectrum below 1 ev, is uncertain by more than about ±0.012, excluding the uncertainty in η_o, or about ±0.015 including the uncertainty in η_o. Small as it seems, this remains the principal source of uncertainty (~ ±0.012) in the breeding ratio of an MSBR so far as cross sections are concerned.

The ^{235}U cross sections are known with about the same precision as those of ^{233}U, but are of far less importance, since less than 10% of the fissile-material absorptions are in ^{235}U.

Uncertainties in cross sections of ^{234}U and ^{236}U are of minor consequence, since these materials reach equilibrium concentrations rather quickly. The ^{234}U is a fertile material, while ^{236}U is a poison. The equilibrium absorption rate in each depends primarily on the capture-to-fission ratio of the fissile precursors, ^{233}U and ^{235}U; however, there is some small dependence on the ^{234}U and ^{236}U cross sections because some of the material is extracted from the fuel stream, along with the fissile isotopes, as excess production.

One of the most abundant materials in the MSBR, and one of the most important parasitic neutron-absorbers, is fluorine. As is true of other light elements, the resonances of fluorine are predominantly scattering resonances, and the radiative capture widths are difficult to determine accurately. The capture widths are not known to better than ±30%, and the high-energy (n,α) cross sections are equally uncertain. These uncertainties affect the estimated breeding gain to the extent of about 0.004; while not large in an absolute sense, this is a non-trivial fraction of the breeding gain, and it would further enhance our confidence in performance estimates for molten-salt reactors to have improved accuracy in these cross sections of fluorine. A more accurate determination of the resonance capture integral would itself be an appreciable help in reducing the limits of uncertainty in the fluorine absorption rate.

Uncertainties in remaining cross sections, including Li, Be, C, Pa, and fission products, appear collectively to contribute an uncertainty in breeding ratio of less than 0.01.

The effective cross sections of thorium may be subject to some uncertainty, arising to some extent from uncertainties in resonance parameters, but primarily from methods of computation of resonance self-shielding, and from variations in geometry of the salt passages. Variations and uncertainties in passage geometry may well contribute the greatest uncertainty in thorium absorption rate. Further analysis of this possibility is required, but is likely to lead to requirements on the mechanical design of MSBR cores, rather than to the need for further measurements of cross sections or resonance integrals. In any case, the thorium concentration in the salt can be adjusted within rather wide limits, governed primarily by its influence on the melting point of the salt.

The various cross-section uncertainties that contribute at all significantly to the uncertainty in the estimated breeding performance of the MSBR are summarized in Tables 3 and 4 for the heavy and light elements respectively. Also shown are the corresponding uncertainties in fuel-cycle cost. Both of these effects were calculated by performing complete equilibrium fuel-cycle analyses for each altered set of cross sections. Thus such secondary effects as changes in $^{235}U/^{233}U$ absorption ratio and in ^{236}U absorption rate, shifts in spectrum, and the small revisions in fissile concentration required to maintain an optimum fuel processing rate are all fully taken into account.

Table 3. Effect of Heavy-Element Cross-Section Uncertainties on MSBR Performance

Nuclide	Quantity	Assigned Value	Assigned Uncertainty	δBR	δFCC [mills/kwhr(e)]
^{233}U	η_o	2.293	±0.010	0.008	0.013
	$(\bar{\eta}_T/\eta_o)$	~1	±0.5%	0.009	0.015
	ν	2.50	±0.01	0.003	0.005
	α_F	0.18	±0.01	0.006	0.010
^{235}U	η_o		±0.010	0.001	0.001
	$(\bar{\eta}_T/\eta_o)$	~1	±0.5%	0.001	0.001
	ν	2.43	±0.01	--	--
	α_F	0.50	±0.02	<0.001	0.001
^{234}U	$\bar{\sigma}_a$		±10%	<0.001	0.001
^{236}U	$\bar{\sigma}_a$		±15%	<0.001	0.001

Since the uncertainties listed in Tables 3 and 4 are all independent, we have combined them by taking the square root of the sum of the squares as the overall uncertainty in breeding ratio or in fuel-cycle cost attributable to cross-section uncertainties. The resulting values,

$$[\Sigma(\delta B)_i^2]^{1/2} = 0.016$$

and

$$[\Sigma(\delta FCC)_i^2]^{1/2} = 0.026 \text{ mills/kwhr(e)} ,$$

Table 4. Effect of Light-Element Cross-Section Uncertainties on MSBR Performance

Nuclide	Assigned Cross Section Uncertainty, %	δBR	δFCC [mills/kwhr(e)]
F(n,α)	±30	0.003	0.005
F(n,γ)(resonance)	±30	0.002	0.003
F(n,γ)(thermal)	±7	0.001	0.002
Be(n,α)	±10	0.001	0.002
Be(n,γ)	±10	--	--
Be(n,2n)	±15	0.002	0.003
^{7}Li	±10	0.003	0.004
C	±10	0.004	0.006
FP (thermal)	±10%	--	--
FP (resonance)	±30	0.003	0.005

reflect primarily the uncertainty in the average thermal η of ^{233}U. (If all the assessed cross-section uncertainties are added up in the same direction, the result is $\Sigma(\delta B)_i = 0.05$ and $\Sigma(\delta FCC)_i = 0.08$. We regard this, however, as an extremely improbable combination of circumstances.)

In performing these calculations, as I remarked earlier, the fuel-cycle calculations were repeated with altered cross sections, and with the fuel processing rate held fixed at the optimum value for the nominal cross sections. We have also attempted to reoptimize the reactor design with the altered cross sections, taking all deviations in one direction, first for the ^{233}U cross sections alone, and subsequently for all cross sections. Though the optimization procedure is allowed to seek best values for such diverse parameters as salt volume fractions in the core and blanket, salt reprocessing rates, and several others of lesser importance, no significant revisions of core design parameters or of reactor performance were found. We conclude, therefore, that small revisions in nuclear data would not appreciably affect reactor design, nor alter the conclusions listed in Tables 3 and 4.

While these uncertainties in breeding ratio and in fuel-cycle cost, arising from uncertainties in nuclear data, are indeed small, the question arises whether in the very long run the uncertainties in breeding performance imply significant differences in the amount of natural uranium that would have to be mined to maintain a fuel supply for a rapidly expanding nuclear power economy. In order to get some insight into this question, we have calculated the amount of uranium that would have to be mined to satisfy the fuel requirements for a particular postulated pattern or reactor construction and operation. For this purpose, we suppose that only water-moderated reactors would be built prior to 1975, while thereafter molten-salt breeder reactors would begin to capture the market for new reactors, giving rise to the curve of installed capacity vs time shown in Fig. 2. (The total nuclear capacity projection shown is slightly more

conservative than the one used in current AEC system evaluation studies, but should serve well enough to illustrate the point.) In this analysis, the plutonium produced in the water reactors is assumed to be recycled, while fissile material produced by the breeder reactors in excess of their own requirements — if any — was made available to the water reactors as needed.

We have performed this calculation for each of five cross-section sets, e.g., the nominal set, two sets combining all favorable or all unfavorable deviations of the ^{233}U cross sections, and two sets combining all favorable or all unfavorable deviations of the cross sections for all nuclides. The results of these calculations are shown in Fig. 3, in which the dashed line represents the cumulative U_3O_8 requirement for the water reactors, while the solid lines represent the combined requirement for the converters and the breeders.

Figure 3 shows that the long-term resource requirements for the postulated mix of water reactors and MSBR's could ultimately differ by more than a factor of two, if all the cross sections should differ from the nominal values in the same direction and by the extreme amounts represented by curves D and E. Thus, the uranium requirement could range from less than 800,000 short tons of U_3O_8, representing an investment in the neighborhood of $10 billion, to upwards of 2,000,000 tons of U_3O_8, possibly costing $50 billion or more. However, even if the U_3O_8 price were to rise to $30/lb, as suggested by the extreme curve E (corresponding to an increment of nearly $10/g in the cost of enriched ^{235}U), the additional increment in the fuel-cycle cost for the MSBR (beyond the short term effects already cited) would not exceed 0.10 mills/kwhr(e).

These calculations were performed several months ago, prior to our most recent evaluation of the uncertainties in η for ^{233}U, and involve a somewhat greater deviation of η from nominal than we presently think likely, i.e., a deviation of +0.024, on the favorable side, and −0.020 on the adverse side, compared with the uncertainty of ±0.012 cited above. Thus, curves D and E must be regarded as highly improbable combinations of cross sections, and even curves B and C represent deviations in breeding ratio greater than the combined statistical uncertainty of ±0.016 cited above. This does not, of course, exclude the possibility that factors other than cross sections could cause additional deviations of the breeding ratio from the calculated value.

4. High-Temperature Gas-Cooled Reactor

The effects of cross section uncertainties on estimated fuel-cycle costs for the HTGR are quite similar to those already cited for the MSBR. Both types of reactors have a graphite moderator, both are intended to operate on the thorium-^{233}U fuel cycle (though either may be started up with plutonium, and the HTGR could quite conceivably use a low-enrichment uranium cycle), and both have well-thermalized spectra with about 70% sub-cadmium captures in the fuel. Since the HTGR has a conversion ratio less than 1, enriched ^{235}U fuel is required, along with recycled ^{233}U, resulting in a somewhat higher ratio of fuel absorptions in ^{235}U. The principal differences in neutron balance between the two concepts are the absence of

the Li and F (though not necessarily of the Be) from the HTGR, and the much longer fuel exposure in the HTGR, resulting in greater fission-product poisoning. In order to distribute fuel fabrication and reprocessing costs over as much energy production as possible, the HTGR tends to operated most economically at a fuel exposure of about 1.5 fifa (fissions per initial fissile atom loaded in the reactor). This yields a conversion ratio of about 0.8–0.85; about 75% of fuel absorptions are in ^{233}U, if the bred uranium is recycled. Thus, the importance of ^{233}U and ^{235}U cross sections in the HTGR is similar to their importance in the MSBR.

Since the HTGR is a solid fuel reactor, the initial fuel composition is fixed at the time of manufacture; hence the attainable exposure for the fuel is subject to some initial uncertainty owing, in part, to cross-section uncertainties. This effect, expected to be small in any event, should be confined to early cores of the first reactors.

Perhaps the chief distinction between the HTGR and the MSBR is the role played by fission products, which account for 0.10 absorptions per absorption in fuel, excluding ^{135}Xe and ^{149}Sm, or 0.15 including Xe and Sm. Greater attention must therefore be paid to the cross sections of the various fission products.

Equilibrium fuel-cycle calculations have been performed by Gulf General Atomic for a typical 1000 Mw(e) HTGR, allowing the cross sections of the various nuclides present in the core to be perturbed one at a time from their nominal values. The calculations were done for the partial recycle mode in which bred ^{233}U is recycled once, but partially burned ^{235}U, containing most of the ^{236}U in the reactor, is not recycled. The separation is accomplished by incorporating fissile and fertile materials in separate coated fuel particles in making up the fuel elements. Table 5 shows results obtained by Gulf General Atomic [10] for the effect on fuel-cycle costs of individual cross-section uncertainties. The overall uncertainty, obtained by taking the square root of the sum of the squares, is only ±0.02 mills/kwhr(e), again a very small uncertainty compared with other sources of uncertainty in calculating power costs.

To put these cost uncertainties in perspective, one may compare them with some other sources of uncertainty.

A difference of \$1/kw (e) in the capital cost (\$1 million for a 1000 Mw(e) plant) corresponds to 0.02 mills/kwhr(e) in the power cost. (Capital-cost estimates customarily include a 10% contingency, reflecting an uncertainty of ~0.2 mills/kwhr(e) in power cost.)

A difference of 1¢/10^6 Btu in the cost of fossil fuels corresponds to a difference of about 0.08 mills/kwhr(e) in the cost of power from a conventional power plant. (The U. S. average cost for coal is around 25¢/10^6 Btu, with costs deviating as much as 10¢ in either direction depending on the location of the plant.)

A difference of \$1/g in the price of ^{235}U makes a difference of about 0.025 mills/kwhr(e) in the fuel burnup cost for a reactor with an electrical

Table 5. Effect of Cross-Section Uncertainties on Fuel-Cycle Costs for a Typical HTGR

Nuclide	A_i/A_f [a]	$\delta\sigma/\sigma$ (%) [b]	δFCC [mills/kwhr(e)]
^{233}U	0.74		0.015
^{235}U	0.26		0.003
^{233}Pa	0.019	10,15	0.009
^{236}U	0.008	15,20	0.003
^{135}Xe	0.043	10,20	0.0013
^{143}Nd	0.022	4,20	0.0008
NSAG [c]	0.018	(10)	0.0022
^{147}Pm	0.012	20,30	0.003
^{149}Sm	0.012	5,15	--
^{151}Sm	0.012		--
^{131}Xe	0.011	20,15	0.0011
^{103}Rh	0.010	5,10	0.0005
^{133}Cs	0.009	7,10	0.0009
Eu	0.008		--

[a] Absorptions per neutron absorbed in fuel.

[b] The first figure listed is the percentage uncertainty in the thermal cross section, the second in the resonance integral.

[c] Low-cross-section aggregate of remaining fission products.

efficiency of 42% and a conversion ratio of 0.8 — and a comparable additional difference in the inventory charge.

A difference of 10% in the estimated fuel fabrication and processing costs corresponds to 0.03–0.04 mills/kwhr(e) in fuel-cycle cost for a typical HTGR, and about 0.02 mills/kwhr(e) for the MSBR.

OTHER EFFECTS OF CROSS-SECTION UNCERTAINTIES

It does not appear, therefore, that cross-section uncertainties are an important source of uncertainty in the fuel-cycle cost, either for an MSBR or for an HTGR.

Does this mean that improved cross-section information would be of no value in the design of these reactors? I don't think so. It is true that the selection of fuel design and of fuel-cycle parameters would be very little affected by improved nuclear data. But there are aspects of

reactor design where improved nuclear data, coupled with information from other sources such as critical experiments, could help to reduce design uncertainties and consequently to reduce the design margins necessary to allow for such uncertainties. Several such aspects were mentioned in the introduction. Chief among them are the various temperature coefficients of reactivity, particularly those related to the thermal neutron spectrum and to the Doppler coefficient of resonance capture in thorium.

The problem is illustrated by some calculations performed by Gulf General Atomic for a typical HTGR spectrum. Figure 4 shows several different assumptions on the energy dependence of η for ^{233}U in the energy range below 1 ev. Curve A represents a data set in use at General Atomic from 1962 to 1966, and was based on a multilevel fit for the low-lying resonances. Curve B was based on all experimental data available up to July 1967. Curve C takes strongly into account the recent unpublished data of Weston et al. Since the thermal-neutron spectrum at operating temperature has its peak at about 0.15 ev, it is easy to see that the rise in η from 0.15 to about 0.4 ev can have an important influence on the temperature coefficient. This is even more true at the higher temperatures of interest in the analysis of power transients. Figure 5 shows the results obtained by Gulf General Atomic for the average values of η as a function of moderator temperature. Other things being equal, a change of η of 0.01 over a 1000° temperature range would contribute about 5×10^{-6} $\delta k/k/°C$ to the temperature coefficient. While not large, this is nonetheless appreciable compared with the expected magnitude of the temperature coefficient.

It does not seem likely, in fact, that uncertainties in temperature coefficients can be wholly resolved by probable improvements in cross-section measurements, and much reliance will have to be placed in temperature-dependent reactivity measurements. Measurements of this type, involving various mixtures of C, Th, ^{233}U, and ^{235}U, are presently planned for the High-Temperature Lattice Test Reactor at Pacific Northwest Laboratories.

In the MSBR, since most of the energy from fission is deposited in the circulating fuel itself, rather than in the graphite moderator, the prompt temperature coefficient is dominated by thermal expansion of the salt, rather than by shifts in the thermal neutron spectrum. Thus, the effects just described, while present, are of relatively lower importance.

In summary, it does not appear that uncertainties in neutron cross-sections can give rise to significant uncertainties in fuel-cycle performance or in power cost, either for the MSBR or for the HTGR. Nonetheless, it would be helpful to the designers of these reactors to have improved cross-section data for a few important nuclides.

For both reactor types, the cross sections of ^{233}U continue to remain the most important. Cross-section and η variations in the thermal and near-thermal neutron energy range will continue to be analyzed closely, in conjunction with temperature-dependent reactivity measurements.

For the HTGR, cross sections of several of the fission-products poisons, e.g., ^{143}Nd, ^{103}Rh, ^{133}Cs, and especially ^{147}Pm need to be known with greater accuracy.

For the MSBR, the resonance (n,γ) cross section and the high-energy (n,α) cross section of fluorine particularly are needed to better accuracy.

Many of the effects of cross-section uncertainties for the MSBR were calculated by C. W. Craven, Jr. I am particularly indebted to H. B. Stewart, M. K. Drake, and R. Traylor, of Gulf General Atomic, for making available to me the results of their studies relating to the HTGR.

6. REFERENCES

[1]. C. H. Westcott et al., A Survey of Values of the 2200 m/s Constants for Four Fissile Nuclides, Atomic Energy Review, 3(2): 3–60, IAEA (July 1965).

[2]. J. R. Smith and E. Fast, Techniques for Determining Eta for the Thermally Fissionable Isotopes, USAEC Report IDO-17173, Phillips Petroleum Company, April 1966, and subsequent private communications.

[3]. Based primarily on the measurements of Moore et al. (M. S. Moore, L. G. Miller, and O. D. Simpson, Phys. Rev., 118, 714 (1960).

[4]. J. Halperin et al., The Average Capture/Fission Ratio of ^{233}U for Epithermal Neutrons, Nucl. Sci. Eng., 16(2): 245 (June 1963).

[5]. L. J. Esch and F. Feiner, Survey of Capture and Fission Integrals of Fissile Materials, paper presented at the National Topical Meeting — Reactor Physics in the Resonance and Thermal Regions, February 1966, San Diego, California.

[6]. D. E. Conway and S. B. Gunst, Integral Measurements of the Epithermal Neutron Capture-to-Fission Cross-Section Ratios of ^{233}U, USAEC Report WAPT-TM-613, Bettis Atomic Power Laboratory, June 1967.

[7]. L. W. Weston et al., Measurement of the Neutron Fission and Capture Cross Sections for ^{233}U in the Energy Region 0.4–1000 ev, USAEC Report ORNL-TM-1751, Oak Ridge National Laboratory, April 26, 1967, and subsequent private communications.

[8]. G. de Saussure et al., Measurement of α, the Ratio of the Neutron Capture Cross Section to the Fission Cross Section, for ^{235}U in the Energy Region from 3.25 ev to 1.8 kev, USAEC Report ORNL-3738, Oak Ridge National Laboratory, April 1965, and subsequent private communications.

[9]. H. Palevsky et al., Direct Measurement of the Energy Variation of η of ^{233}U, ^{235}U, and ^{239}Pu, J. Nucl. Energy, 3, 177 (1956).

[10]. H. B. Stewart, Gulf General Atomic, private communication to A. M. Perry, Oak Ridge National Laboratory, January 1968.

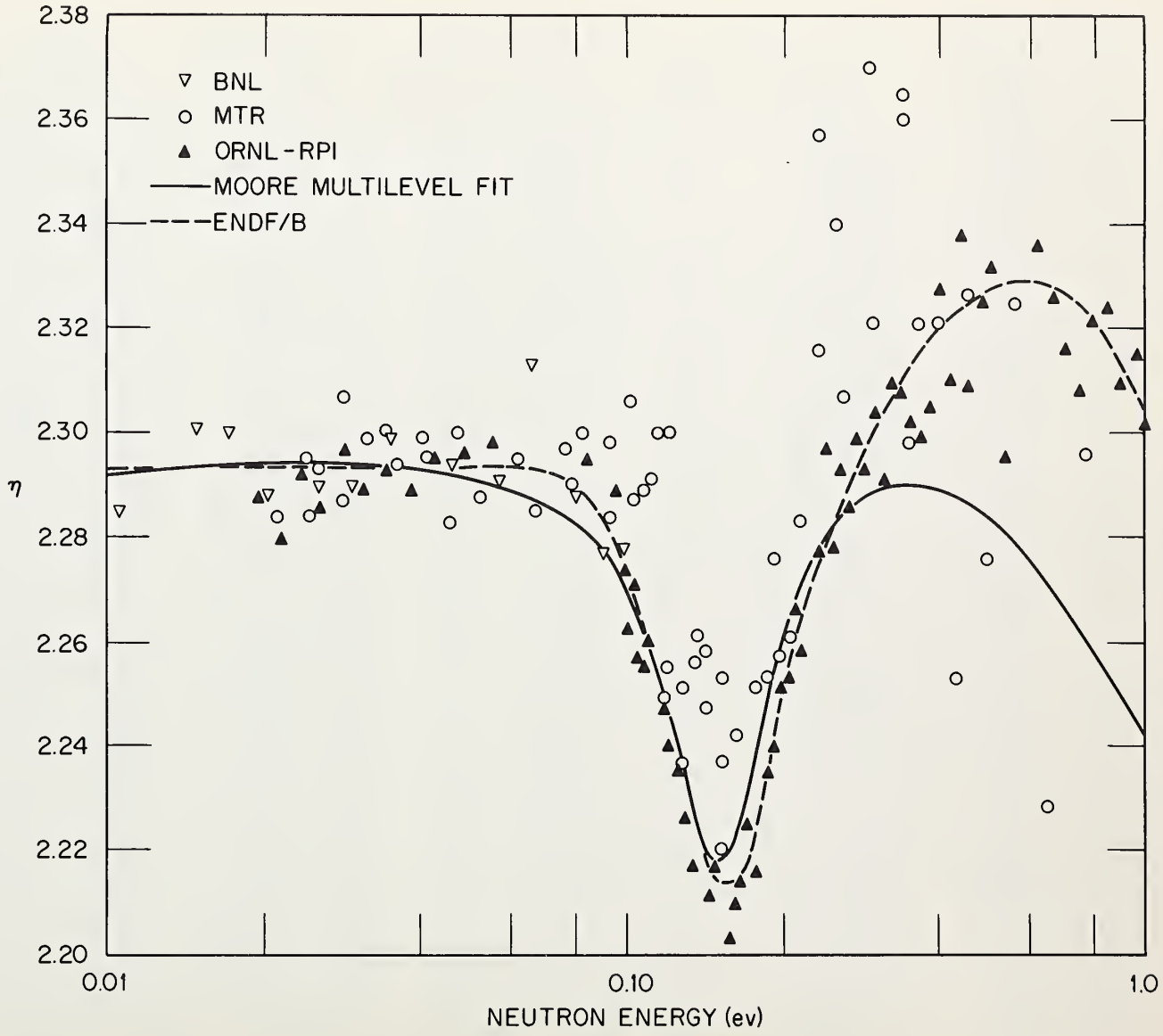

Fig. 1. Energy Dependence of Eta of ^{233}U, 0-1 ev. (BNL: Ref. 9; MTR: Ref. 8; ORNL-RPI: Ref. 7; Moore: Ref. 3.)

313-475 O-68—25

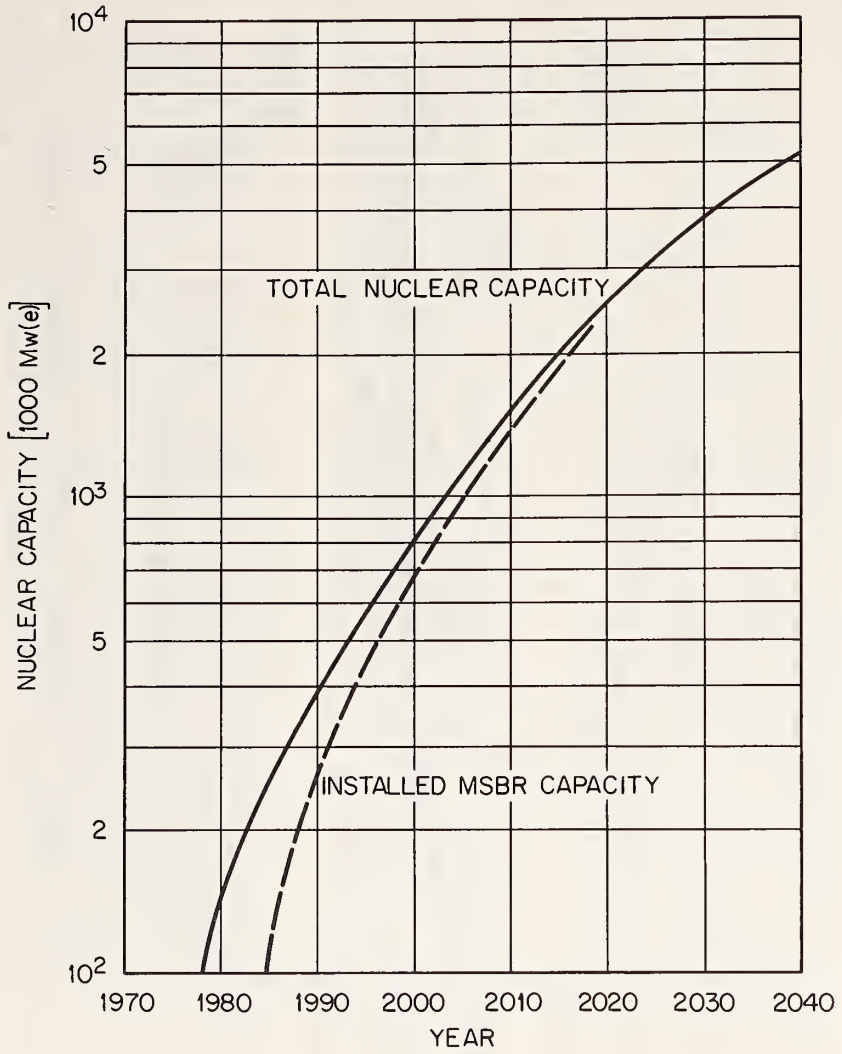

Fig. 2. Estimate of Nuclear Electrical Capacity.

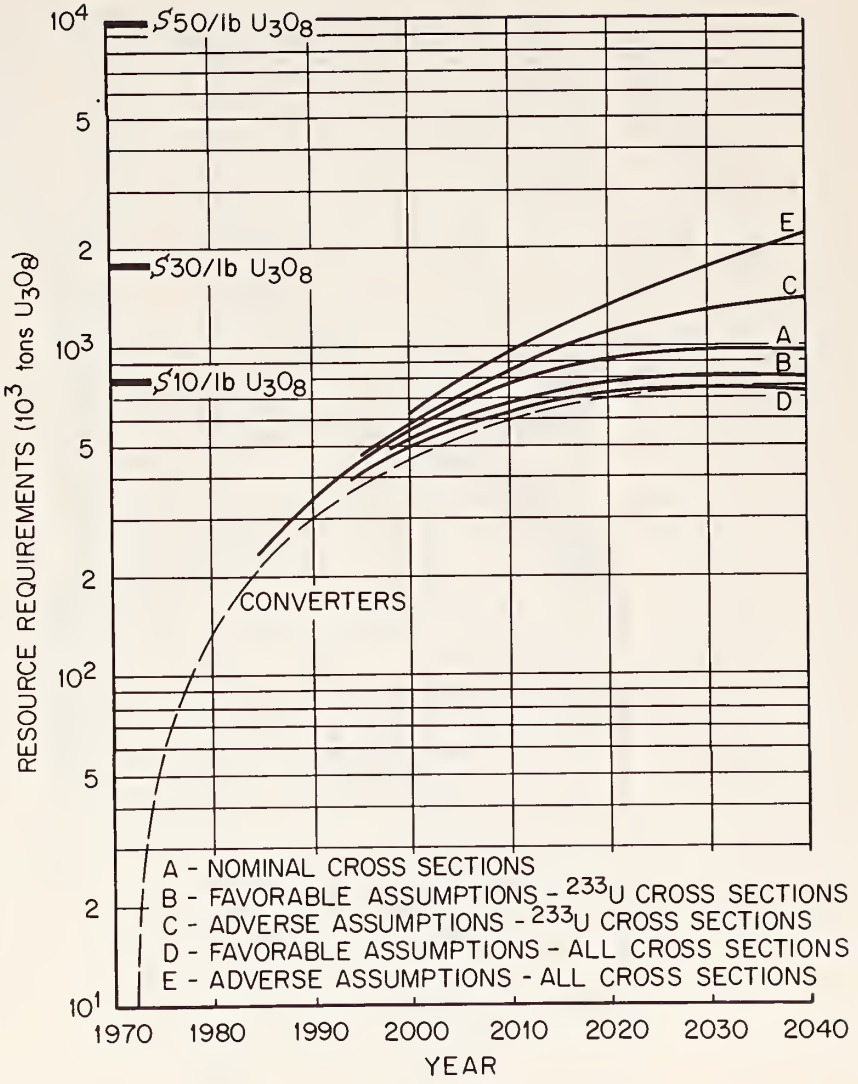

Fig. 3. Cumulative Uranium Requirements.

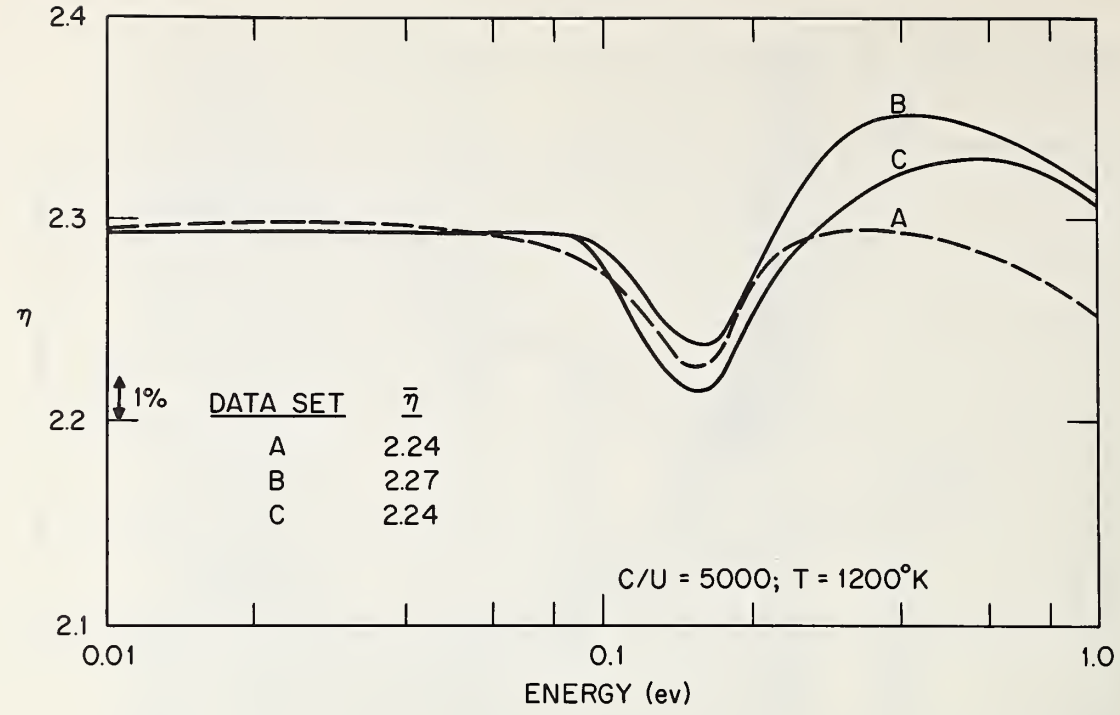

Fig. 4. Assumed $\eta(E)$ for ^{233}U, Alternate Data Sets.

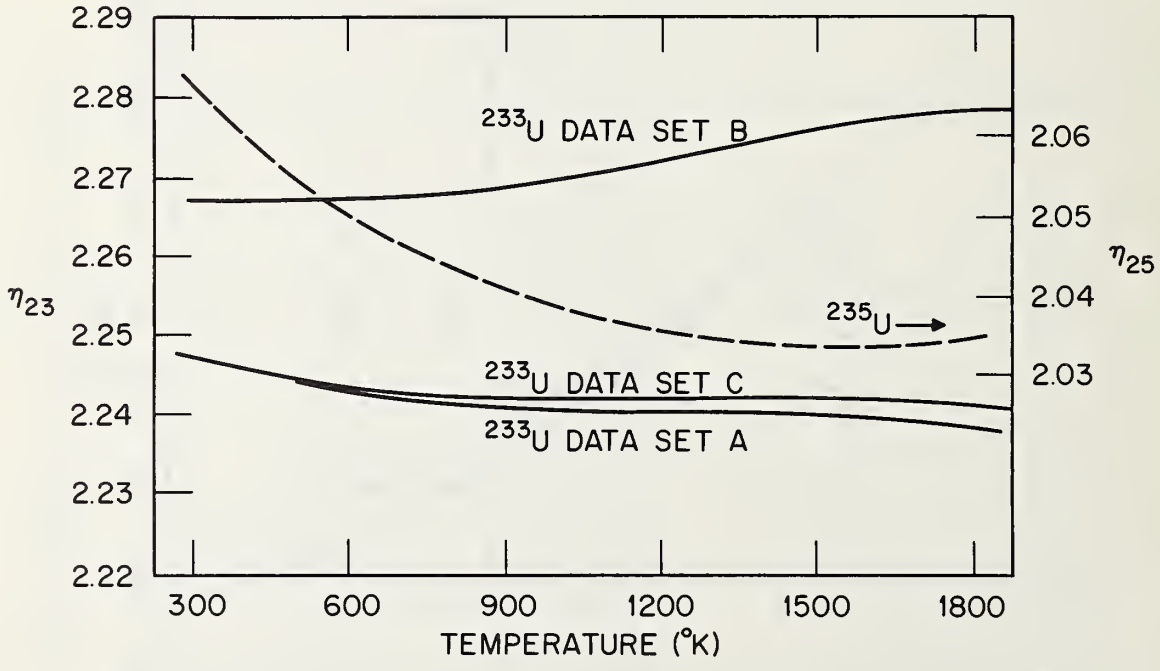

Fig. 5. Spectrum-Averaged η for ^{233}U, Alternate Data Sets.

EFFECTS OF CROSS-SECTION UNCERTAINTIES IN COMPACT SPACE POWER REACTORS*

P. S. Brown, J. L. Watts, and R. J. Doyas
Lawrence Radiation Laboratory, University of California
Livermore, California 94550

Abstract

The effects of cross-section uncertainties have been studied in compact (20 kWe to 10 MWe) space power reactors. Three systems were considered having core sizes of 12, 78, and 525 liters and median fission energies of 560, 380, and 200 keV, respectively. Each core contained UN fuel, W-Re-Mo alloy cladding, and Li coolant within a Ta pressure vessel and BeO reflector. The cross sections of each material were perturbed 10%, and downscatter terms of each scattering matrix were increased 50%. Reactivity effects were computed for these perturbations with the ZOOM diffusion code with tight convergence. The size of perturbations was varied to demonstrate linearity. Because of hardness of the spectra, the perturbations had significant effects only above 10 keV. The additivity of groupwise and materialwise cross-section changes was examined to determine interaction between the various perturbations. Calculations were done to determine the sensitivity of the spectrum shape, fission ratios, reactivity worths, and neutron lifetime to cross-section uncertainties, and to evaluate whether measurement of such parameters in critical experiments can be useful in testing cross-section data.

1. Introduction

Lawrence Radiation Laboratory is studying several space reactor designs with power levels ranging from 20 kWe to 10 MWe. Because of low allowable burnups, operational reactivity losses will be small; hence, it is not planned to provide much variable reactivity control, possibly as little as 1%. The amount of shim reactivity that can be provided may be limited, and it is therefore desirable to predict criticality to high accuracy. In fact, it appears that some of the smaller systems may be criticality limited, even with fully enriched U^{235} fuel. This study was undertaken to determine how cross-section uncertainties affect the neutronics of the reactors under consideration.

Core volumes differ by more than an order of magnitude among the various systems. It is therefore necessary to study a range of core sizes. Three reactors were considered in this study (Table I). Each contains UN fuel, clad with an alloy of 45 a/o tungsten, 25 a/o rhenium, and 30 a/o molybdenum. The cylindrical cores are contained in tantalum pressure vessels and are reflected radially with BeO, 5 cm thick. Lithium is the coolant.

2. Method

Reactivity and other effects were evaluated by comparing tightly converged ZOOM [1] computations using perturbed and unperturbed cross sections. ZOOM is a diffusion code that was found to calculate values of k_{eff} differing from transport results by only a few percent, even for the smallest system considered. It was estimated that ZOOM would be sufficiently accurate for calculating the various effects of cross-section

*Work performed under the auspices of the U. S. Atomic Energy Commission.

perturbations, including those involving changes in leakage.

The following cross-section perturbations were made: 10% reductions in σ_a, σ_f, ν, and the average cosine of the scattering angle $\bar{\mu}$; 10% increase in σ_s, and a 50% increase in the off-diagonal terms of the transfer matrix $\mu_{i\to j}$ (balanced by a decrease in the diagonal term $\mu_{i\to i}$ to preserve normalization to unity). When smaller perturbations were made, the results were found to be quite linear, thus permitting interpolation for smaller changes and extrapolation for reasonably larger changes. The cross sections were obtained from the Howerton Evaluated Library [2] and were weighted into the 16-group Hansen-Roach [3] structure using a single fast reactor spectrum typical of the three reactors.

The additivity of groupwise and materialwise perturbations on a given cross section was generally found to be quite good (~10%). Likewise, the additivity of perturbations among the different cross sections was found to be good even when all the cross sections were perturbed simultaneously. The major non-additive effects were encountered when downscatter was increased 50%, thereby affecting the shape of the spectrum appreciably.

3. Results

Space does not permit listing the individual effects of cross section perturbations in each material. However, the reactivity effects of perturbing the macroscopic cross sections over the entire energy range are given in Table II. The trends are as expected, the effects of $\Delta\Sigma_c$ being greatest in the large reactor with the softest spectrum and the effects of $\Delta\Sigma_s$ and $\Delta\bar{\mu}$ being greatest in the small reactor with the highest leakage. The $\mu_{i\to j}$ perturbation may have a positive or negative effect, as explained below.

The energy dependent effects of the above macroscopic perturbations are given in Table III. Owing to hardness of the neutron spectra, the lower eight groups contributed negligibly to the neutron balance, and cross section perturbations had appreciable effects only above about 10 keV. Hence, only the upper eight groups are listed. The results have been divided by the group lethargy widths to provide a better picture of the energy trends. The trends are consistent with what might be expected from perturbation theory expressions, and from the behavior of the regular spectra (Fig. 1) and adjoint fluxes (Fig. 2) in the three reactors. The groupwise reactivity effects of $\Delta\Sigma_c$ correspond approximately to the shape of $\phi(u)$, with the importance of the lower groups enhanced by the increase of Σ_c with decreasing energy. Two peaks in the $\Delta\nu$ and $\Delta\Sigma_f$ values are evident in the larger reactors, one corresponding to U^{235}, the other to U^{238} fissions. The reactivity effects of $\Delta\Sigma_s$ are generally positive because of a decrease in leakage. However, in some groups the Δk_{eff} is negative since increasing the value of Σ_s increases the scatter of neutrons to an energy of lower importance. The negative result occurs in more groups in the large reactor, where the leakage is relatively small and the adjoint spectrum decreases more rapidly with decreasing energy. The reactivity effects of increasing the $\mu_{i\to j}$ from each group i are positive or negative, depending upon the sign and relative magnitude of the difference $(\phi_j^+ - \phi_i^+)$ for downscatter to group j. Because of the adjoint spectrum shapes, the total effect (all groups i at once) can be positive or negative (Table II). The effects of perturbing $\bar{\mu}$ are especially big in the

upper groups where the scattering is highly anisotropic.

Estimates have been made of the actual cross-section uncertainties and their possible effects. It appears that over the energy range of importance in the three reactors, representative pointwise uncertainties for these materials are of the order of ±20% in σ_c, ±2% in ν, ±3% in σ_f, ±20% in σ_s, and ± 30% in $\bar{\mu}$. In regard to uncertainties in energy transfer, it is estimated that the $\Delta\mu_{i\to j}$ is about ±10% for elastic scattering (corresponding to the ±30% uncertainty in $\bar{\mu}$). For inelastic scattering, a ±50% uncertainty in nuclear temperature θ is assumed. Hand perturbation calculations have shown that a 50% decrease in θ produces almost the same reactivity effect as a 50% increase in the inelastic $\mu_{i\to j}$ in the small reactor, and the same effect as a 6% increase in $\mu_{i\to j}$ in the large reactor. The reason for the different relationship between $\Delta\theta$ and $\Delta\mu_{i\to j}$ in the two reactors is attributable to the different adjoint spectrum shapes.

Using the above representative uncertainties, the absolute values of all groupwise and materialwise effects have been added to give a maximum effect for each cross section and for all cross sections combined (Table IV). It should be noted that in Table IV, inelastic scattering accounts for over 80% of the uncertainty in $\mu_{i\to j}$ in the large and medium reactors, and about 65% in the small reactor.

The results in Table IV are rather extreme and unrealistic in that no credit has been taken for cancellation of effects among the materials, different cross sections, or energy groups. Assuming no correlation of effects among materials, cross sections or energy groups, and assuming the groupwise and pointwise cross section uncertainties to be the same, the individual groupwise and materialwise reactivity effects have been statistically averaged by taking the square root of the sum of the squares (Table V). In reality it is not legitimate to take so much credit for cancellation of effects, since some compounding of errors should occur because of normalization of cross section data amongst materials and between different cross sections, or incorrectly normalizing a cross section curve at a particular energy. On the other hand, the uncertainties in group cross sections should be smaller than the pointwise uncertainties. The approach one uses to characterise such uncertainties is highly subjective, and if desired, the results in Table V can be scaled up or down for other assumed uncertainties. The uncertainties used in Tables IV and V are representative of the "average" uncertainties that might be encountered for the materials considered. Admittedly, it would be better to estimate the uncertainty at each energy for each material cross section; however, the amount of labor involved would be about as great as that in setting up an evaluated library.

Several conclusions may be drawn from Table V. First, none of the reactors is particularly sensitive to uncertainties in the downscatter matrix. This is not surprising since the adjoint spectra do not vary much over the energy range of importance in the three reactors. When the results are treated statistically, inelastic scattering accounts for about 97% of the uncertainty in $\mu_{i\to j}$ in the small and medium reactors and 71% in the large reactor. The biggest source of uncertainty in the small reactor is scattering (a leakage effect). The biggest source of uncertainty in the medium and large reactors, which have softer spectra and a higher concentration of materials which capture neutrons, is capture. The uncertainty in k_{eff} resulting from the combined estimated

cross section uncertainties is about ±2% for all three reactors (or ±4% within 95% confidence limits). A considerable improvement in the accuracy of the cross section data would be needed to reduce the uncertainty in a calculated k_{eff} to below one percent, irrespective of uncertainties from computational methods.

The signs of the macroscopic changes described above (Table II) were chosen to produce softer spectra. The resultant effects of these changes on median fission energy (MFE) are given in Table VI. It is apparent that large perturbations in scattering (Σ_s and $\mu_{i\to j}$) have an appreciable effect on the spectrum. Fission ratios were also found to be very sensitive to these perturbations, with the various threshold fission ratios changing by 20 to 40% when all the reactor cross sections were simultaneously perturbed. If actual cross section uncertainties are used and allowance is made for cancellation of effects, the sensitivity of the fission ratios (and MFE's) will be appreciably less. Their measurement could, however, be used to verify that gross errors in the cross section data (particularly inelastic scattering) do not exist. It is interesting to note that with all cross sections (except ν) perturbed as in Table VI, the reactivity effects in the small, medium, and large reactors are only 0.002, -0.0137, and -0.0424, respectively. Thus, although the spectrum may be in considerable error, the value of k_{eff} is changed only a small amount.

The uncertainty in neutron lifetime ℓ resulting from the combined estimated cross section uncertainties (Table V) is less than ±5% for the three reactors. This uncertainty is small compared to the disagreements that are usually reported for fast reactor lifetime measurements, possibly because this study deals with thinly reflected systems. The main change in ℓ comes from σ_s uncertainties in the small reactor (a leakage effect), from σ_c and σ_s uncertainties in the medium reactor, and from σ_c uncertainties in the large reactor. Uncertainties in energy transfer appear to have relatively little effect on ℓ.

The reactivity worths of various materials were found to be very sensitive to spectrum changes resulting from cross section perturbations in the reactor materials, as well as to perturbations in the cross sections of the reactivity samples themselves. It will be very difficult to determine whether the discrepancy between calculation and experiment is due to an incorrectly calculated spectrum or to sample cross section errors. Furthermore, if the error is definitely due to sample cross sections, it may be impossible to determine which cross sections are incorrect, except for a few cases in which one cross section contributes almost entirely to the reactivity worth (e.g. a strong absorber or fissile material).

4. Conclusions

Some of the major conclusions to be drawn from this study are: (1) Using "estimated" cross-section uncertainties, the value of k_{eff} can be calculated on the average to about ±2% for these small systems; (2) Cross-section uncertainties below about 10 keV have negligible effect; (3) The primary sources of error are scattering in the smaller systems and capture in the larger systems; (4) Because of flatness of the adjoint spectra, uncertainties in elastic and inelastic downscatter have relatively little effect; (5) The spectrum may be grossly in error, and yet the value of k_{eff} may be exact in view of the way reactivity errors cancel;

(6) Neutron lifetimes and fission ratios are not very sensitive to the estimated cross-section uncertainties. The value in measuring these quantities would be to verify the absence of gross errors in the data; (7) It will be difficult, if not impossible, to determine the source of discrepancies between calculated and measured reactivity worths.

The authors wish to acknowledge the helpful comments and suggestions of Dr. R. J. Howerton.

5. References

1. E. H. Canfield, et al., "ZOOM-II, One-Dimensional, Multi-Group, Neutron Diffusion Theory Reactor Code with Linearly-Anistropic Corrections to Neutron Leakage for the CDC-3600 and CDC-6600 Computers," to be published.
2. R. J. Howerton, Lawrence Radiation Laboratory, unpublished.
3. Reactor Physics Constants, ANL-5800, Table 7-2 (1963).

Table I. Description of Reactors.

	Small	Intermediate	Large
Core volume (liters)	12.2	78.0	524.9
Fuel volume fraction	0.74	0.60	0.45
Fuel enrichment (a/o-U^{235})	83.0	53.0	31.5
Median fission energy (keV)	560	380	200

Table II. Δk_{eff} Due to Macroscopic Cross-Section Perturbations.

Reactor size	Σ_c(-10%)	ν(-10%)	Σ_f(-10%)	Σ_s(+10%)	$\mu_{i\to j}$(+50%)	$\bar{\mu}$(-10%)
Small	0.01308	-0.09690	-0.06291	+0.03354	+0.00667	+0.00949
Medium	0.02959	-0.09932	-0.06404	+0.02005	-0.00780	+0.00598
Large	0.03867	-0.10123	-0.06521	+0.00885	-0.02781	+0.00308

Table III. $\Delta k_{eff}/\Delta u$,[a] Effects of Group Macroscopic Cross-Section Changes.

Gp	Σ_c(-10%)	ν(-10%)	Σ_f(-10%)	Σ_s(+10%)	$\mu_{i\to j}$(+50%)	$\bar{\mu}$(-10%)	E_{lower}
				Small			
1	.000701	-.00866	-.00628	.002492	-.002241	.002027	3 MeV
2	.001316	-.02211	-.01534	.009400	.002996	.003272	1.4 MeV
3	.001412	-.02304	-.01553	.009999	.003587	.002605	900 keV
4	.002494	-.02498	-.01643	.010909	.005801	.002550	400 keV
5	.003387	-.01686	-.01186	.005952	.001538	.000585	100 keV
6	.001662	-.00749	-.00309	.000429	-.000830	.000042	17 keV
7	.000441	-.00084	-.00044	-.000062	-.000150	.000010	3 keV
8	.000042	-.00004	-.00002	-.000006	-.000006	.000000	550 eV
				Intermediate			
1	.000930	-.00765	-.00517	.000160	-.006510	.001100	
2	.002056	-.01910	-.01239	.002771	-.009116	.001956	
3	.002664	-.01769	-.01154	.005246	-.001756	.001340	
4	.005107	-.02216	-.01445	.007022	.001386	.001782	
5	.009527	-.02228	-.01420	.005516	.005719	.000517	
6	.003800	-.00952	-.00546	-.000677	-.001038	.000052	
7	.000664	-.00111	-.00069	-.000028	-.000137	.000001	
8	.000039	-.00007	-.00003	.000000	-.000003	.000000	
				Large			
1	.00082	-.00566	-.00369	-.001150	-.00746	.00042	
2	.00165	-.01375	-.00854	-.001273	-.01336	.00079	
3	.00224	-.01032	-.00652	-.000194	-.00265	.00052	
4	.00472	-.01507	-.00890	.004080	.00095	.00092	
5	.01034	-.02476	-.01559	.004070	.00016	.00053	
6	.00786	-.01637	-.01029	.000570	-.00332	.00007	
7	.00146	-.00212	-.00154	-.000030	-.00033	.00000	
8	.00006	-.00007	-.00006	.000000	.00000	.00000	

[a]Results normalized to equal lethargy widths.

Table IV. Maximum Effects (Δk_{eff}) of Estimated Cross-Section Uncertainties.

Reactor size	σ_c(20%)	ν(2%)	σ_f(3%)	σ_s(20%)	$\mu_{i\to j}$ (see text)	$\bar{\mu}$(30%)	Combined Δk_{eff}
Small	0.0262	0.0194	0.0189	0.0671	0.01365	0.0285	0.174
Medium	0.0592	0.0197	0.0192	0.0410	0.01525	0.0179	0.172
Large	0.0773	0.0202	0.0196	0.0241	0.00433	0.0090	0.155

Table V. Statistically Averaged Effects (Δk_{eff}) of Estimated Cross-Section Uncertainties.

Reactor size	σ_c(20%)	ν(2%)	σ_f(3%)	σ_s(20%)	$\mu_{i\to j}$ (see text)	$\bar{\mu}$(30%)	Combined Δk_{eff}
Small	0.00702	0.00784	0.00786	0.01206	0.00316	0.00660	0.0193
Medium	0.01572	0.00814	0.00777	0.00736	0.00354	0.00351	0.0213
Large	0.01726	0.00900	0.00834	0.00466	0.00116	0.00192	0.0218

Table VI. Values of Median Fission Energy (keV) with Various Macroscopic Cross-Section Perturbations.

Reactor size	Unpert.	Σ_f(-10%)	Σ_c(-10%)	Σ_s(+10%)	$\mu_{i\to j}$ (+50%)	$\bar{\mu}$ (-10%)	All Σ's changed
Small	560	545	545	525	408	560	347
Medium	380	358	362	340	253	380	209
Large	200	190	186	178	133	200	105

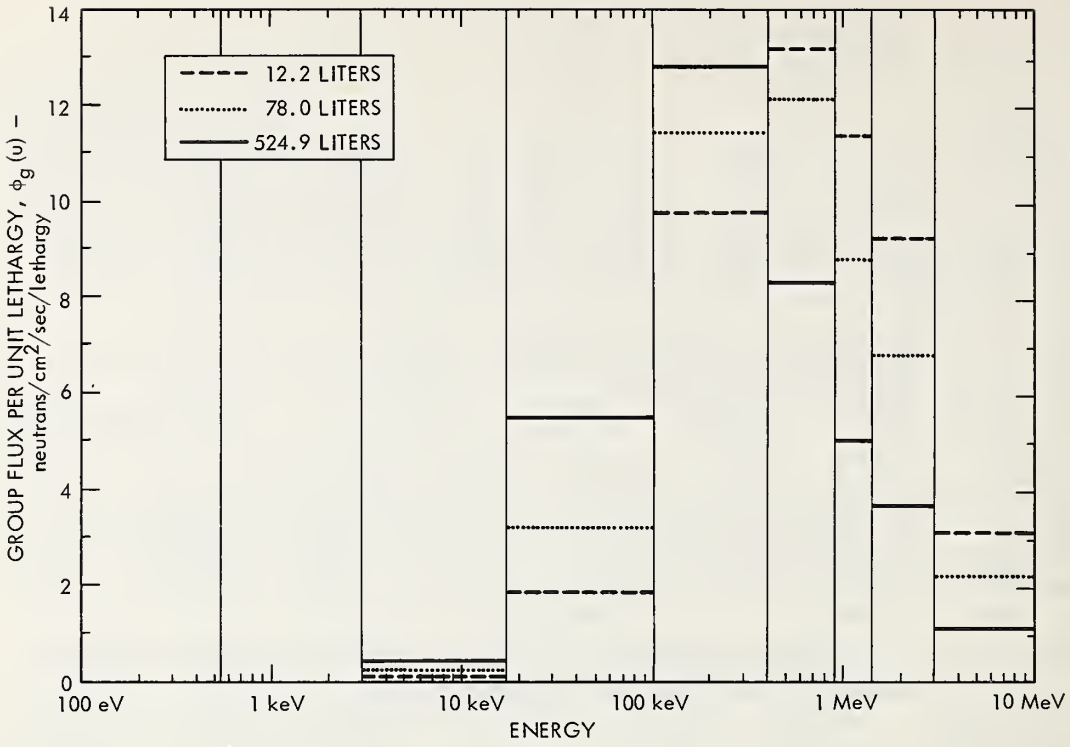

Figure 1. Neutron spectra in the small, intermediate, and large reactors.

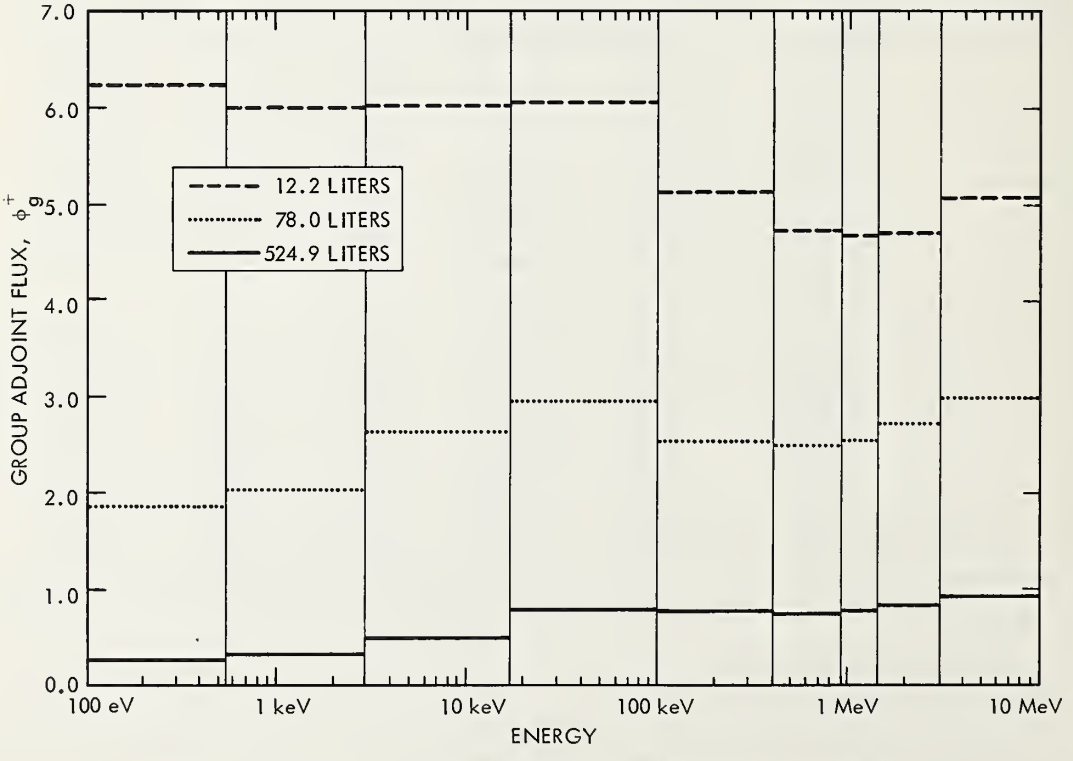

Figure 2. Adjoint group fluxes in small, intermediate, and large reactors.

NEW CROSS SECTION NEEDS FOR ZIRCONIUM HYDRIDE SNAP REACTORS*

Eric H. Ottewitte

Atomics International
Canoga Park, California 91304

ABSTRACT

A zirconium hydride SNAP reactor consists of hydrided rods of U-Zr alloy surrounded by rotatable beryllium reflector drums. The current direction of SNAP reactor designs is toward reliable long-term (1 to 5 years) operation and additional safety features. These designs may require poison-backings on the reflector drums (for some applications) plus a variety of new burnable poisons.

Candidate poison-backings include europium and other rare earths as well as B_4C. Both absorption and scattering cross sections are important, particularly in the kev range. Candidate burnable poisons include Gd-157, Sm-149, Cd-113, Gd-155, Hf-177, Ir-191, Eu-151, Dy-162, Sm-152, and Dy-163. The absorption cross sections below 10 ev are particularly important.

One of the desired safety features in future zirconium hydride reactors is subcriticality in water in the event of a launch abort. This might be achieved through spectral shift if the burnable poison has a low-lying (below 0.1 ev) resonance. A large number of stable or long-lived isotopes which have not been measured for low-lying resonances are indicated.

1. INTRODUCTION

A zirconium hydride SNAP reactor consists of hydrided rods of U-Zr alloy surrounded by rotatable beryllium reflector drums. The current direction of SNAP reactor designs is towards reliable long-term (1 to 5 years) operation and additional safety features. Designs for both "unmanned" (involving the presence of instruments, etc.) and "manned" (involving the presence of humans) missions are being made.

Additional emphasis is placed on some of the conventional SNAP material cross section components, and the cross section needs for a wide variety of new isotopes is indicated.

2. BURNABLE PREPOISONS

Multi-year operation of a SNAP reactor requires the use of burnable prepoisons to match the reactivity loss rate. Reactivity is lost by hydrogen moderator loss from the fuel, by fuel burnup, and by fission product

*This work performed under AEC Contract AT(04-3)-701

poisoning. The mismatch between the reactivity loss rate and the prepoison burnout rate imposes increased control drum requirements, thereby limiting some SNAP reactor applications. Therefore, it is important to have as wide a variety of prepoisons to choose from as possible, and to know their effective absorption cross-sections well. The absorption cross sections below 10 ev are particularly important to the thermal SNAP reactor.

Prediction of the prepoison burnout rate is subject to several uncertainties:

1) cross-section uncertainties in the parent isotope
2) cross-section uncertainties in the daughter product (cross-sections of appreciable magnitude for the daughter products will cause a slower effective rate of poison burnout. An example of this is Eu-151. Two-thirds of the Eu-151 captures lead to a relatively stable metastate of Eu-152 which has about the same cross-section.)

All stable and nonstable isotopes were examined on the basis of available thermal cross-section and resonance integral information. (The CINDA indices were very useful here.) Isotopes in the gaseous and liquid state and those which produce gases were eliminated. Table I lists stable and radioactive isotopes which could not be evaluated because insufficient cross-section information exists. Table II lists those which could be evaluated and evidenced potential, in order of effective cross-section. Included also are estimates of isotope cost. The economically feasible isotopes (and important daughters) of interest for up to five-year SNAP reactor lifetime applications are given in Table III.

All the others in Table II are useful in combination with a fast burning low-resonance absorber (for intrinsic subcriticality). They may also prove useful by themselves if additional cross-section measurements and/or further analysis should increase their effective cross-section.

3. INTRINSIC WATER SUBCRITICALITY (IWS)

The problems associated with preventing accidental criticality in a SNAP reactor are more severe than for an earthbound reactor. Over-the-road transport and potential launch abort over the ocean could accidentally result in infinite water reflector and water flooding of the core.

As SNAP reactors are undermoderated, the addition of water to the reactor core results in a reactivity increase due to reduced neutron leakage and to softening of the neutron energy spectrum (Figure 1). (The spectral shift effectively transports neutrons to energies where the U-235 eta is higher.) It appears that a method of eliminating this core reactivity increase and thereby achieving subcriticality in water ("intrinsic" water subcriticality, IWS) would be to add an absorber which has a resonance prominent in a water-moderated spectrum, but not in the normal operational ZrH-moderated spectrum. From Figure 1, one observes that for the spectrum to shift into a low-lying resonance, the resonance energy should lie below 0.1 ev.

Figure 2 plots for each isotope the lowest resonance energy recorded in the current BNL-325. Excluding the inert gas Xe-135, only four isotopes were found with thermal resonances at 0.1 ev or lower:

Isotope	E_o(ev)
Sm-149	0.0976
Gd-155	0.0268
Gd-157	0.0314
Lu-176	0.104

Sm-149 and Lu-176 are marginally close to 0.1 ev, and therefore less attractive. Figure 3 illustrates the Gd-155 and Gd-157 cross-sections compared to a 1/v absorber. Of these two, Gd-157 burns out too fast for most reactor applications, posing impossible reactivity control requirements. Thus Gd-155 is the reference IWS absorber.

The Gd-155 worth lies predominantly in thermal absorption. The uncertainty in this worth is about 5% based on the most recent evaluations (Table IV). This uncertainty is not important at this time.

Gd-155 also burns out too fast for some reactor applications. Thus a wider variety of low-resonance absorbers featuring lower cross-sections is desired. Such isotopes might be found among the unmeasured long-lived radioisotopes, and stable isotopes obscured by many sister element isotopes (e.g., the seven stable isotopes of Yb). An attempt was made to find additional candidates by correlating lowest-resonance energies with atomic mass number, A (Figure 2). The lowest-lying resonances were found in the even-odd and odd-even isotopes. A literature search for isotopes located at the curve low points yielded Eu-155 with a resonance around 0.1 ev. However, Eu-155 is too radioactive to be useful. Hopefully, additional studies and new cross-section measurements will uncover more suitable substitutes which would increase the number of burnable poisons which are also useful for IWS.

4. REFLECTOR CONTROL DRUM OPTIMIZATION

Some manned mission applications may require complete (4π) shielding of the reactor. In order to reduce the total system weight, it is desirable to change from void-backed reflector drums (control by neutron leakage) to poison-backed reflector drums (control by neutron absorption). For the reflective material BeO is equivalent to Be in reactivity worth, and preferred for other engineering reasons. For the poison material, a Eu_2O_3-metal matrix appears to be the preferred poison backing. Other poisons considered were boron compounds, tantalum, and other rare earths.

The relative importance of the Be and Eu cross section components upon this critical parameter, control drum worth, is explored by means of first-order perturbation theory in Tables V and VI. The components of highest worth require the most accuracy.

Another "reaction" of importance here is the zirconium transport cross section, between 500 ev and 10 Mev. Table VII shows that its first order worth is 26% $\Delta k/k$. (Zirconium constitutes 35 atom % of the core). Uncertainties here produce uncertainties in core leakage and, thereby, in drum control.

TABLE I

STABLE AND NEAR STABLE ISOTOPES OF POTENTIAL USE AS BURNABLE POISONS: NO AVAILABLE NUCLEAR DATA

Radioactive Isotopes	t 1/2 (yr)
Al-26m	7.4×10^5
Si-32	700
Ca-41	7.7×10^4
Ti-44	47
Fe-60	10^5
Ni-59	10^4
Ni-63	92
Se-79m	10^4
Mb-91m	long
Mo-93	10^4
Tc-97	10^6
Tc-98m	10^6
Sn-126	10^5
Ba-133m	7.2
La-137	10^4
La-138	stable
Pm-145	18
Sm-146	10^8
Gd-148	85
Gd-150	10^5
Gd-154	stable
Tb-157	150
Tb-158m	150
Dy-154	10^6
Ho-163	10^3
Yb-170	stable
Yb-171	stable
Yb-172	stable
Yb-173	stable
Hf-182	10^6
Os-186	stable
Os-187	stable
Os-188	stable
Pt-193	<500
Pb-202	10^5
Pb-205	10^7
Pb-210	22
Bi-208	10^5
Po-209	10^3
Th-229	7300

TABLE II

EVALUATED BURNABLE POISONS

Isotope	SNAP Spectrum Weighted Cross Section (b)	Cost			t 1/2 (yr)
		$/mg	Isotope Form	$/mg Oxide	
Pd-107	13	NA*			10^6
Gd-156	13	0.9	oxide		S†
Ac-227	28	NA			21.2
Nb-94	30	NA			10,000
Hf-179	30	1.55	oxide		S
In-113	49	12.0	oxide		S
Eu-154	49	NA			16
Hf-176	51	6.0	oxide		S
Dy-160	66	2.4	oxide		S
Ir-193	79	20.00	Ir	~$3	S
Eu-153	84	1.00	oxide		S
Dy-164	85	0.25	oxide		S
Au-197	91	elem. §			S
Hf-178	92	0.50	oxide		S
Pa-231	94	5.6	oxide		32,480
Rh-103	99	elem.			S
Lu-176	100	43.00	oxide		S
Dy-161	108	1.50	oxide		S
Ag-109	109	0.60	Ag		S
Re-185	112	1.60	Re		S
Dy-163	113	1.40	oxide		S
Sm-152	173	0.35	oxide		S
Dy-162	192	0.15	oxide		S
In-115	197	0.45	oxide		S
Yb-168	384	32.0	oxide		S
Te-123	390	20	Te	~$20	S
Eu-151	443	1.0	oxide		S
Ir-191	454	30.0	Ir	~$4	S
Hf-177	462	1.5	oxide		S
Sm-151	526	NA			90y
Gd-155	908	1.4	oxide		S
Gd-113	1142	0.90	oxide		S
Sm-149	1719	0.70	oxide		S
Gd-157	3239	0.6 to 1.2	oxide		S

*NA: not commercially available

†S: stable

§elem.: 100% natural abundance in element, costs should be small compared to a separated isotope

TABLE III

PERTINENT PREPOISON CROSS-SECTIONS FOR UP TO FIVE-YEAR LIFE SNAP REACTORS

Parent Isotope	Important Daughter Isotopes
Gd-157	None; the parent isotope's cross-section is very high
Sm-149	Ibid
Cd-113	Ibid
Gd-155	Ibid
Hf-177	Hf-178, Hf-179
Ir-191	Ir-192, Ir-193, Pt-192
Eu-151	Eu-152 to Eu-156, Gd-152, Gd-154 to Gd-156
In-115	In-116, Sn-116
Dy-162	Dy-163
Sm-152	Sm-153, Eu-154
Dy-163	Dy-164, Dy-165, Ho-165

TABLE IV

GADOLINUM-155 2200 M/S ABSORPTION VALUES REPORTED

Date	Cross Section (1000b)	Reference
9-60	60.6 ± 0.5	N.S. and E8, 183
1-60	56.2 ± 1.0	BNL-325 (1960)
7-59	88.7	Phys. Rev. 115, 424
58	66 ± 2	A/Conf. 15 P/11
7-58	61 ± 5	BNL-325 (1958)
57	87.2	Phys. Rev. 105, 196
50	78	Phys. Rev. 77, 634

TABLE V

BERYLLIUM RELATIVE CONTRIBUTIONS (%Δk/k) TO CONTROL DRUM WORTH (FIRST-ORDER PERTURBATION OF TRANSPORT-THEORY CALCULATIONS)

Group	Lower Group Energy	σ_a	σ_{Tr}	$\sigma_{g\to g+1}$
1	3.0 Mev	-0.0011	+0.0097	-0.0005
2	1.4 Mev	-0.0027	+0.0329	-0.0008
3	0.9 Mev	0.0000	+0.0128	-0.0058
4	0.4 Mev	0.0000	+0.0003	-0.0016
5	0.1 Mev	0.0000	-0.0017	-0.0094
6	17 kev	0.0000	-0.0053	-0.0017
7	3 kev	0.0000	+0.0014	-0.0093
8	550 ev	0.0000	+0.0002	-0.0074
9	100 ev	0.0000	+0.0013	-0.0041
10	30 ev	0.0000	+0.0042	-0.0041
11	10 ev	0.0000	+0.0130	-0.0017
12	3 ev	0.0000	+0.0223	-0.0004
13	1 ev	0.0000	+0.0216	+0.0003
14	0.4 ev	0.0000	+0.0234	+0.0040
15	0.1 ev	0.0000	+0.0662	-0.0005
16	0.009 ev	0.0000	+0.0469	
Total		-0.0038	+0.7456	-0.0431

TABLE VI

EUROPIUM RELATIVE CONTRIBUTIONS (%Δk/k) TO CONTROL DRUM WORTH (FIRST-ORDER PERTURBATION OF TRANSPORT-THEORY CALCULATIONS)

Group	Lower Group Energy	σ_a	σ_{Tr}	$\sigma_{g\to g+1}$
1	3.0 Mev	0.000	0.000	0.000
2	1.4 Mev	0.000	0.000	0.000
3	0.9 Mev	0.000	0.000	0.000
4	0.4 Mev	0.000	0.000	0.000
5	0.1 Mev	0.002	0.000	0.000
6	17 kev	+0.002	0.000	0.000
7	3 kev	+0.010	0.000	0.000
8	550 ev	+0.031	0.000	0.000
9	100 ev	+0.097	0.000	0.000
10	30 ev	+0.193	-0.005	0.000
11	10 ev	+0.310	-0.024	0.000
12	3 ev	+0.711	-0.091	0.000
13	1 ev	+0.762	-0.110	0.000
14	0.4 ev	+2.263	-0.469	0.000
15	0.1 ev	+2.217	-0.707	0.000
16	0.009 ev	+3.215	-0.722	
Total		+9.811	-2.128	-0.001

TABLE VII

REACTIVITY WORTH (%Δk/k) OF ZIRCONIUM CROSS SECTION COMPONENTS (FIRST-ORDER PERTURBATION OF TRANSPORT-THEORY CALCULATIONS)

Group	Lower Group Energy	σ_a	σ_{Tr}	$\sigma_{g\rightarrow g+1}$
1	3.0 Mev	-0.009	3.11	-0.058
2	1.4 Mev	-0.030	4.93	-0.035
3	0.9 Mev	-0.026	2.87	-0.032
4	0.4 Mev	-0.062	3.42	-0.808
5	0.1 Mev	-0.083	2.35	-0.174
6	17 kev	-0.069	1.57	-0.014
7	3 kev	-0.036	1.50	-0.007
8	550 ev	-0.032	3.45	-0.004
9	100 ev	-0.475	0.42	-0.004
10	30 ev	-0.017	0.28	-0.006
11	10 ev	-0.014	0.41	-0.007
12	3 ev	-0.013	0.45	-0.006
13	1 ev	-0.015	0.41	-0.006
14	0.4 ev	-0.017	0.34	-0.008
15	0.1 ev	-0.046	0.61	-0.002
16	0.009 ev	-0.062	0.35	
Total		-1.007	26.46	-1.170

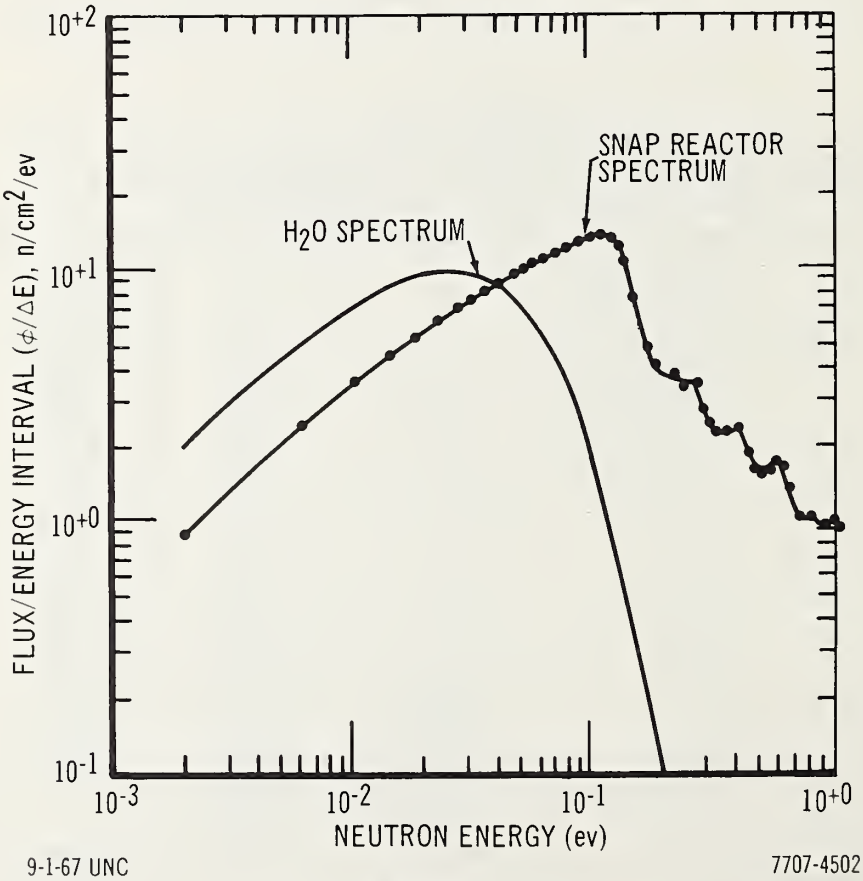

Figure 1

Comparison of Thermal Neutron Spectra

Figure 2

AN EMPIRICAL STUDY OF THE LOWEST KNOWN RESONANCE ENERGIES

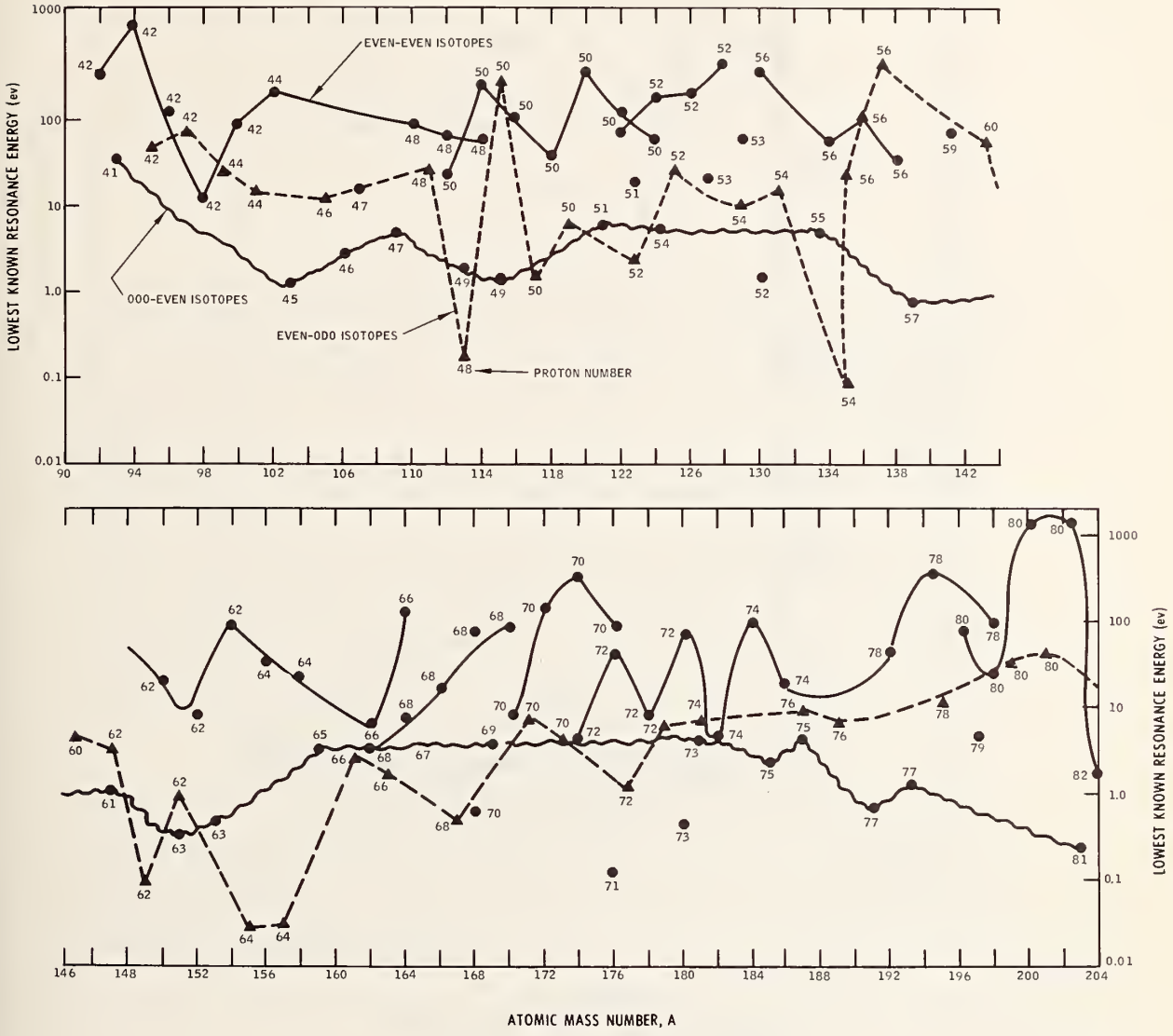

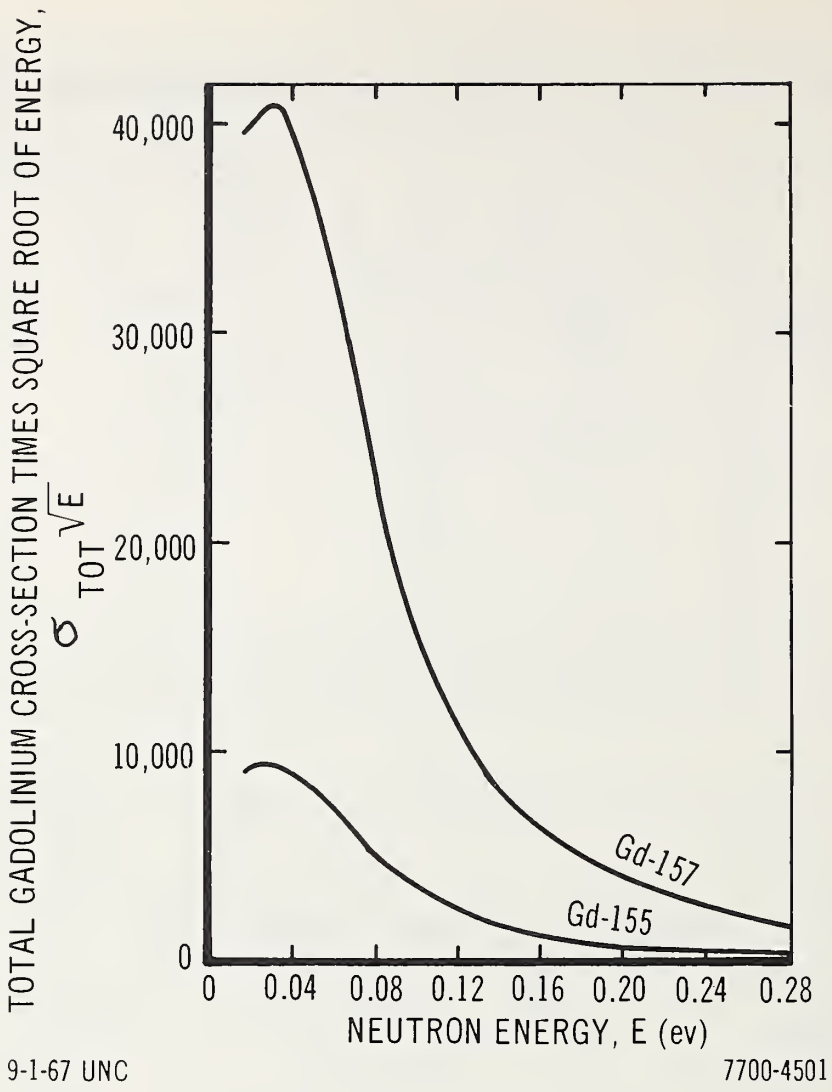

Figure 3
Total Gd-155 and -157 Cross Section Times the Square Root of Energy

FISSPROD, A FISSION PRODUCT PROGRAM FOR THERMAL REACTOR CALCULATIONS

MRS. F.E. LANE & W.H. WALKER
ATOMIC ENERGY OF CANADA LIMITED
CHALK RIVER, ONTARIO, CANADA

ABSTRACT

FISSPROD calculates the concentrations of about 200 fission product nuclides by setting up and solving a matrix equation. The nuclides are arranged in order of increasing A and Z to give a lower triangular matrix with non-zero elements near the diagonal, permitting concentrations to be calculated one at a time. The present input includes all ground state and metastable nuclides with half-lives exceeding $\sim$ 5 hrs between masses 76 and 166. For each nuclide any or all of the reactions represented by the following data can be calculated: thermal cross section and resonance integral for neutron capture to the metastable and ground states of the next higher mass isotope; decay constant for β-decay to the metastable and ground states of the next lower charge isobar; decay constant for an isomeric transition (metastable states only); and yields in the thermal neutron fission of U-233, U-235, Pu-239 and Pu-241 and fast fission in U-238.

Comparisons of FISSPROD calculations with pile oscillator determinations of fission product cross sections in irradiated U-233, U-235, and Pu-239 have been made. The calculated cross sections are lower than measured values for MTR-irradiated U-235, but within the estimated errors, and are appreciably greater than values obtained at Chalk River.

The role of absorption by fission products in calculations of the reactivity of thermal reactors was reviewed at the 1966 Paris Conference [1] by one of the authors. In this paper we describe the evaluation of fission product data and the computation of neutron absorption by fission products, and compare computed and experimental results.

1. FISSION PRODUCT DATA EVALUATION

Results of fission product data evaluation at Chalk River, which has been in a state of sporadic activity since the last publication [2], are now in draft form and will be published shortly as AECL-3037. Cross sections are presented in the Westcott formalism [3]. Yields have been updated and extended to include fast fission in Th-232. The cross section evaluation covers many of the same nuclides as the latest volumes of BNL-325 [4] and will be published not because of any startling disagreements, since these are non-existent, but because it treats the data from quite a different point of view and provides the basis for FISSPROD input data. BNL-325 recommended resonance parameters have been used wherever applicable to fission products to calculate resonance integrals. In many cases these give the preferred values for the integral. Details of the resonance integral calculations and their results will appear separately in an AECL report.

2. THE COMPUTER PROGRAM, FISSPROD

FISSPROD was originally intended as a detailed fission product computer program providing outputs on which to base models of pseudo-fission product cross sections which were more sophisticated and would give a more accurate representation of absorption by fission products than the one in use at Chalk River [2,5]. These improved models have not been developed because FISSPROD calculations have shown that for CANDU-type reactors the original model, updated to 1964 [2], is quite accurate. However FISSPROD has proved particularly useful for comparisons of input data with measurements of fission product absorption in irradiated samples. It is this application that will be discussed here in some detail.

FISSPROD was written for CRNL's G-20 computer in an Algol-like language, APEX, and is described in detail in AECL-3038. It treats all fission products with half-lives exceeding about 5 hours, including isomeric states, as a group interrelated by neutron capture, β-decay and isomeric transition. Each nuclide is characterized by three parameters, (A,Z,E), where A is the mass number, Z is the charge and E is the isomeric state (0 ≡ ground state, 1 ≡ metastable state). The allowed modes of formation of (A,Z,E) are:

- Fission, either cumulative (if $T_{\frac{1}{2}}$<5 hours for all precursors) or direct
- Neutron capture, either in (A-1,Z,0) or (A-1,Z,1)
- β-decay, either from (A,Z-1,0) or (A,Z-1,1)
- Isomeric transition to (A,Z,0) from (A,Z,1).

If nuclides and yields are listed in order of increasing A and Z then all these transmutations yield a nuclide further down the list. This gives a lower triangular matrix with non-zero elements near the diagonal, permitting concentrations to be calculated one at a time by a coupled system of first order differential equations with constant coefficients. The equations are solved explicitly rather than by numerical integration.

The general form of the equation for the i-th nuclide in the list is

$$\frac{dx_i(\psi)}{d\psi} + x_i(\psi) \sum_{j>i} m_{ji} = y_i(\psi) + \sum_{k<i} m_{ik}\, x_k(\psi) \qquad (1)$$

where $x_i(\psi)$ is the concentration of the i-th nuclide at irradiation $\psi=\Phi t$,

m_{ij} represents the dependence of i-th nuclide on the preceding nuclides from which it may be formed by the modes listed above,

and $y_i(\psi)$ is a yield function of the form $(\alpha_i + \beta_i e^{-\sigma_a})$ where

σ_a is the absorption cross section of the fissile atom, and α_i and β_i depend on the yield of the i-th nuclide and fission cross section.

For neutron capture the Westcott convention is used [3]. In this case

$$m_{ij} = \hat{\sigma}_{ij} = \overset{o}{\sigma}_{ij} + \frac{2}{\sqrt{\pi}} \left(r\sqrt{T/T_o}\right) I_{ij}$$

where $\overset{o}{\sigma}$ is the 2200 m/sec cross section (velocity v_o)

I is the reduced resonance integral (not including the 1/v extrapolation of $\overset{o}{\sigma}$)

r is the epithermal index

T is the neutron temperature

and $T_o = 293.6°K$, or $20.44°C$, is the "temperature" of a 2200 m/sec neutron.

For decay $m_{ij} = \lambda_{ij}/\Phi$ where Φ is the conventional flux, nv_o

For brevity let $\sigma_i = \sum_{j>i} m_{ji}$.

The right-hand side of Eq. (1) is a sequence of exponential functions in $\sigma_a\psi$, $\sigma_1\psi$ ------ $\sigma_{i-1}\psi$. As the integration proceeds the solution for $x_i(\psi)$ takes the same general form, and introduces an exponential function in $\sigma_i\psi$ to the sequence

Thus $$\frac{dx_i}{d\psi} + \sigma_i x_i = A + \sum_{k=o}^{i-1} a_k e^{-\sigma_k\psi} \quad (\sigma_o=\sigma_a)$$

gives $$x_i = C + \sum_{k=o}^{i-1} c_k e^{-\sigma_k\psi}.$$

This is true provided σ_i does not equal any of the preceding σ_k. If $\sigma_i = \sigma_j$ then the new exponential term has the form $\psi e^{-\sigma_i\psi}$ and the general form for x_i is

$$x_i(\psi) = C + \sum_{k=o}^{i} c_k \psi^{n_k} e^{-\sigma_k\psi} \quad (n_k \geq 0)$$

Finally to avoid loss of accuracy, exponential terms with very small values of $\sigma_i\psi$ are represented by a 35-term power series in ψ. The final form for $x(\psi)$ is

$$x_i(\psi) = \sum c_k f_k(\psi)$$

where $f_k(\psi) = \psi^k \quad o \leq k < 34$ and $f_k(\psi) = \psi^{n_k} e^{-\sigma_k \psi} \quad k > 34$.

Thus the differential equation (1) is represented by a vector of coefficients a_k together with the lists σ_k and n_k, while the solution is given by the same lists and a vector of coefficients, c_k.

3. ABSORPTION BY FISSION PRODUCT IN SAMPLES IRRADIATED IN MTR & NRU

Only two sets of measurements of gross fission product cross sections in samples of irradiated fissile material have been published in sufficient detail to permit an accurate comparison with FISSPROD. This has been done previously [1] for the results of Okazaki et al [6] on samples of ^{233}U, ^{235}U and ^{239}Pu irradiated in NRU. We have made a FISSPROD comparison with the results of Gunst et al [7] that were obtained by reactivity measurements in RMF and ARMF of a ^{235}U sample irradiated in MTR to about 2.5 n/kb. Additional details of the irradiation and flux measurements are given in England's fission product study, WAPD-TM-333 [8], and it is on the basis of this information that the comparison with FISSPROD has been made.

The flux convention used by England [8] is 4-group with the fourth group, Φ_4, comprising the Maxwellian distribution and epithermal component up to 0.625 eV and the third, Φ_3, the epithermal from 0.625 eV to 5.5 keV. Conversion to the conventional flux nv_o, and epithermal index, r, of the Westcott convention [3] follows from equating reaction rates, i.e.

$$[g_4\sigma_4 + \sigma_3(\Phi_3/\Phi_4)]\Phi_4 = [\overset{o}{\sigma} + (2/\sqrt{\pi})(r\sqrt{T/T_o})I]\, nv_o$$

Here g_4 is the effective cross section in a Maxwellian spectrum (20.44°C) of a 1/v absorber with $\overset{o}{\sigma}$ = 1.0 barns; $\overset{o}{\sigma}$, I, r and T are defined above. Using some additional numerical values given in reference [9],

$$nv_o = \Phi_4\, g_4 + .04354(\Phi_3/\Phi_4)$$

and $$(r\sqrt{T/T_o})^{-1} = 10.255\, g_4(\Phi_4/\Phi_3) + 0.4465.$$

In the MTR irradiation samples were moved every three weeks. Thermal and epithermal flux monitors were replaced at each shift so that there is a complete record of flux changes throughout the 20 3-week periods from initial insertion to removal for the last set of reactivity measurements. This includes two 3-week periods when the sample was out for interim testing. The conventional fluxes and $r\sqrt{T/T_o}$ values for each period derived from the data shown in WAPD-TM-333 are given in Fig. 1.

The FISSPROD calculations are based on an interim CRNL evaluation of fission product data which has only minor differences from latest values. A single set of ^{235}U cross sections was used based on T=126°C and r=.026 ($\hat{\sigma}_a$ = 653 b, $\hat{\sigma}_f$ = 554 b). Both the results of the reactivity measurement and the WAPD-TM-333 calculations exclude the ^{135}Xe and ^{149}Sm component formed

directly in fission (or by β-decay of precursors formed directly in fission) but include the capture products. However ^{135}Xe and ^{149}Sm, in addition to their capture products, are included when formed by neutron capture. In FISSPROD this can be done by comparing complete listings of nuclide contributions for a specific irradiation with the appropriate yields (y_{135} and y_{149}) first given their correct value, then set to zero. This is not practical when very many points are calculated as in Fig. 1 (∿ 115). For this reason the plot in Fig. 1 is for $y_{135} = y_{149} = 0$, but includes ^{236}U and its capture products since these differ from the ^{135}Xe and ^{149}Sm capture products by less than a barn.

The most prominent feature of the curve is the high initial value of the fission product capture cross section which diminishes quite rapidly during the first few irradiation periods. Nuclide by nuclide concentrations printed out at the beginning and end of each out-of-pile period and after the initial 3-week period indicate that this is due almost entirely to ^{105}Rh and ^{151}Sm. This effect can be understood in terms of a simple model: if a nuclide is formed directly in fission but is not destroyed by capture or decay then the capture cross section is $y\hat{\sigma}$ barns/fission and is constant for all irradiations (for ^{235}U $y\hat{\sigma}$ equals ∿ 170 b/f for ^{105}Rh and 56 b/f for ^{151}Sm). It is apparent that hold-up by a precursor (both ^{105}Ru and ^{151}Pm are included in FISSPROD) and destruction of the nuclide will combine to keep the barns/fission below this level and to give the roughly exponential decrease observed. The ^{105}Rh contribution at the end of the first irradiation period is 18 b/fission and after 7 is just 1.8 barns/fission. For ^{151}Pm the corresponding values are 34.5 and 3.6 barns/fission.

The fine structure of the curve is due to changes in the concentrations of large cross section fission products, mainly ^{105}Rh, ^{151}Sm and the ^{149}Sm formed by capture, accompanying changes in the flux level. ^{143}Nd and ^{147}Pm and its capture products also contribute. The increase after removal from the reactor is mainly due to the increase in ^{149}Sm formed by 53 hr ^{149}Pm.

The computer time to obtain the points plotted in Fig. 1 and the 7 detailed print-outs was 16 minutes.

Table I compares FISSPROD calculations with the results of Gunst et al and those of Okazaki et al. Results of England's fission product calculations [8] are also included. The FISSPROD calculations exclude primary ^{149}Sm and may therefore be compared directly to the MTR results. Results for the NRU samples have also been corrected for ^{149}Sm. Earlier comparisons with the MTR results [1,6] did not make this correction.

The experimental values of Gunst et al are in reasonable agreement with calculation but, as noted previously [1], those of AECL-2510 are about 10 b low for $\hat{\sigma}_0$ and 50-80 barns high for I.

4. SUMMARY

FISSPROD determines the concentration of up to 200 fission product nuclides, including isomeric states, by solving explicitly a coupled system of differential equations with constant coefficients. The input fission product data has been reviewed and is believed to permit calculations that are accurate to about 3% [1]. A detailed calculation for comparison with experimentally-determined values of fission product absorption in irradiated fissile materials differs from one set of results [7,8] by the sum of the errors (10%) or less but differs from a second [6] by 20% or more. Additional measurements under closely controlled irradiation conditions would be very useful.

5. REFERENCES

[1] WALKER, W.H. Proceedings of the Paris Conference on Nuclear Data for Reactors I, 521 (1966).

[2] WALKER, W.H. Atomic Energy of Canada report No. AECL-2111 (1964).

[3] WESTCOTT, C.H., WALKER, W.H., ALEXANDER, T.K. Proc. 2nd ICPUAE 16, 70 (1958).

[4] GOLDBERG, M.D., MUGHABGHAT, S.F., MAGURNO, B.A., PUROHIT, S.N., MAY, V.M. Brookhaven National Laboratory report No. BNL-325, 2nd edition, Supp. 2 Vols IIA, IIB, IIC (1966).

[5] WALKER, W.H. Atomic Energy of Canada report No. AECL-1054 (1960).

[6] OKAZAKI, A., DURHAM, R.W., LOUNSBURY, M. Atomic Energy of Canada reports AECL-2510 and AECL-2506 (1966).

[7] GUNST, S.B., CONNOR, J.C., McGARRY, E.D., CONWAY, D.E., & STEIN, S. Bettis Atomic Power Laboratory report WAPD-T-1468 (revised) (1962).

[8] ENGLAND, T.R. Bettis Atomic Power Laboratory report WAPD-TM-333 (1962).

Table I - Comparison of Measured and Calculated Fission Product Absorption Cross Sections*

Reactor	Source	U-235 Depletion	σ_o	RI(0.12 eV)	** I
		percent	- barns per fission -		
MTR	Exp.	-	55±4	210±30	
	WAPD-TM-333	64	54	236	
	FISSPROD	62.7	50	~235	192
MTR	Exp.	-	47±3	190±30	
	WAPD-TM-333	81	48	220	
	FISSPROD	79.4	45	~220	179
NRU	Exp	74'	34.4±3.2		259±47
	FISSPROD	74.0	44.7		179
	Exp	78	34.5±3.0		223±44
	FISSPROD	77.7	43.7		175

*^{149}Sm produced by decay of ^{149}Pm which was formed directly in fission is not included.

**RI(.12eV) = I + the contribution of the 1/v extrapolation of σ_o in the epithermal flux above .12eV.

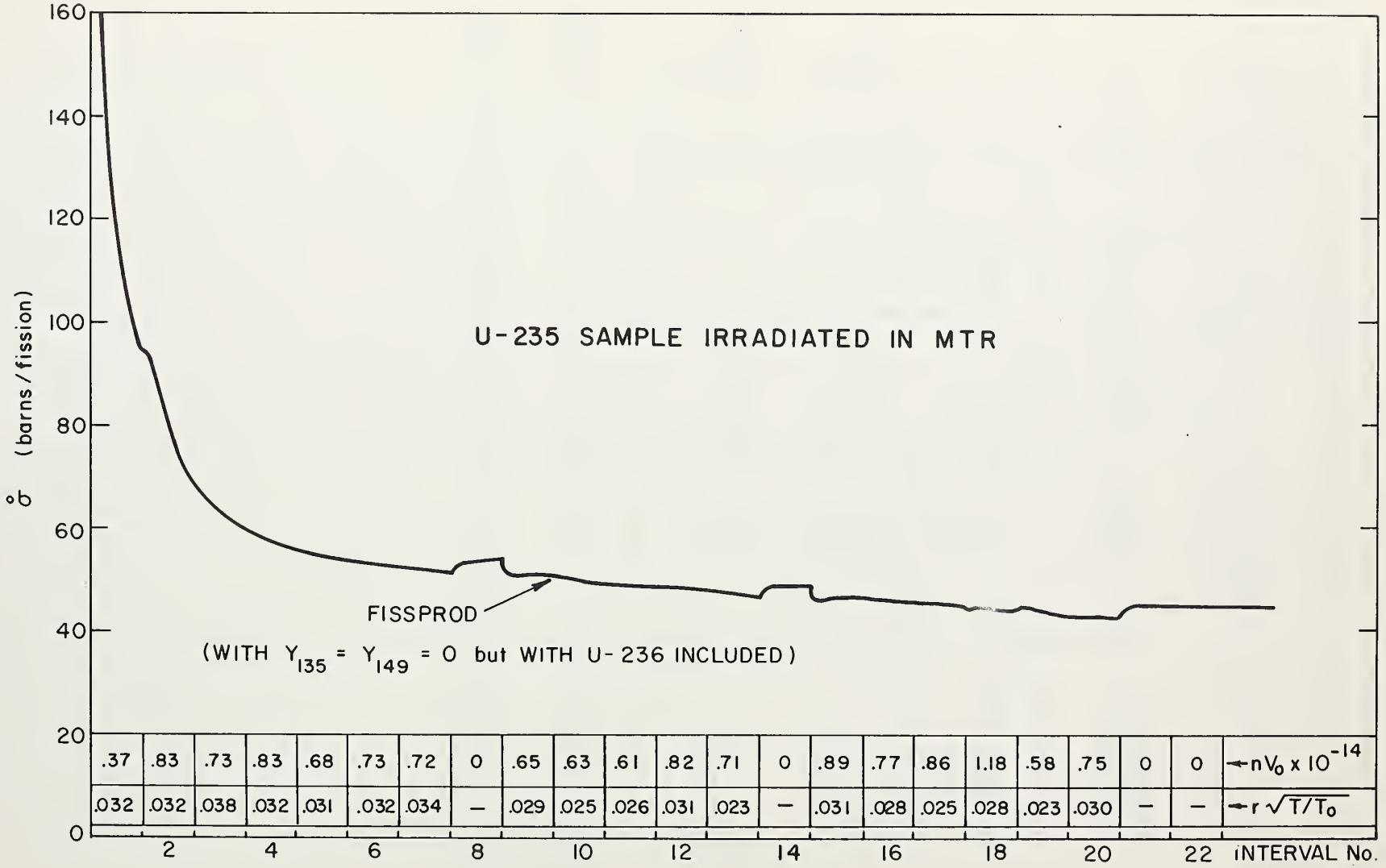

.37	.83	.73	.83	.68	.73	.72	0	.65	.63	.61	.82	.71	0	.89	.77	.86	1.18	.58	.75	0	0	$\rightarrow nV_0 \times 10^{-14}$
.032	.032	.038	.032	.031	.032	.034	–	.029	.025	.026	.031	.023	–	.031	.028	.025	.028	.023	.030	–	–	$\rightarrow r\sqrt{T/T_0}$

Fig. 1 Calculated changes with irradiation in the absorption cross section of fission products from U-235 irradiated in MTR. The flux and epithermal component for each three-week interval are also shown.

EFFECTS OF UNCERTAINTIES IN NUCLEAR DATA ON EXPERIMENTAL & CALCULATED REACTOR BURNUP*

By

D. E. Christensen, R. C. Liikala, R. P. Matsen and D. L. Prezbindowski

Battelle Memorial Institute
Pacific Northwest Laboratory
Richland, Washington 99352

ABSTRACT

Inaccuracies in the basic nuclear data information results in uncertainties in the experimental determination and the theoretical prediction of reactor burnup. The experimental determination of reactor burnup requires measuring the number of fissions that occur and the changes in the fuel isotopic composition as a function of exposure. These data are also utilized to deduce ratios of effective cross sections. A fundamental quantity required in the determination is the content of a fission monitor (e.g., ^{137}Cs, ^{148}Nd, etc.,) . Uncertainties in yield, half lives, and branching ratios of the monitor lead to uncertainties in the number of fissions. This results in uncertainties in determining the isotopic composition of the fuel and the ratios of effective cross sections as a function of exposure. The measured isotopic composition changes along with the deduced ratios of effective cross sections are used to compare to theoretically predicted values to check the accuracy of the theoretical methods. The theoretical prediction of reactor burnup is based upon the use of cross sections. Uncertainties in the basic cross sections lead to uncertainties in calculated results. Results are given for plutonium fuel (Al-Pu) irradiation experiments conducted in the Plutonium Recycle Test Reactor (PRTR).

1. INTRODUCTION

Integral measurements have played an important role in cross-section evaluation. The validity of a cross section set is often based upon analysis of critical experiments and resonance integral measurements. Irradiation experiments provide data which are, in general, a more sensitive test of the adequacy of cross section sets. The resonance integral and critical assembly experiments test mainly one quantity, such as η for the principal fissile nuclide in the fuel in a critical assembly and cover a limited range

* This paper is based on work performed under United States Atomic Energy Commission Contract AT(45-1)-1830.

of conditions. The irradiation experiment provides data which test the relative reaction rates of all isotopes present in the fuel and cover a wide range of conditions.

This paper deals with the limitation that uncertainties in nuclear data place upon the experimental determination and theoretical prediction of burnup. Our approach here is to utilize the ratios of effective cross sections as characterizing burnup. We give results for irradiation experiments of aluminum-plutonium alloy fuels (Al-Pu) which were conducted in the Plutonium Recycle Test Reactor (PRTR). The first part of this paper considers the limitations on the experimental determination of burnup due to uncertainties in the nuclear data that are used in the analysis. The second part of this paper gives results of an analysis of the effects of uncertainties in basic cross sections on the calculated burnup for these experiments.

2. EXPERIMENTAL ANALYSIS

2.1. Methods

The experiment includes the measurement of the fuel concentration and isotopic compositions at various exposures during the irradiation. The experimenter can choose how to measure the exposure. One method is based upon assuming values for the flux-averaged capture to fission cross-section ratios for the fissile nuclides present in the fuel. Another method is to measure the content of a fission product which is yielded directly in fission. This fission product, which may be stable or radioactive, serves to monitor the number of fissions that have occurred. Some experiments include both methods in determining the number of fissions. In either case, nuclear data (i.e., cross sections, yields, and half lives) are required to deduce the exposure obtained in the irradiation.

The latter of the above methods was used in the experimental analysis[1,2] of the Al-Pu fuel irradiation experiments in the PRTR. The monitor chosen was ^{137}Cs. The measured ^{137}Cs activity is converted to plutonium fissions assuming certain values for the yield of ^{137}Cs from fissions in plutonium and the half life of ^{137}Cs. Since the values of the yield and half life are uncertain, the experimental isotopic compositions and exposures will be uncertain. The effect of these uncertainties are best observed in the ratios of effective cross sections which are derived from the isotopic composition data. The methods of deriving ratios of effective cross sections from the experimental data have been presented previously.[2,3,4]

One of the methods[4] (which we limit ourselves to) for deriving ratios of effective cross sections is build around the use of the least squares fitting code, LIKELY.[5] Briefly, the analysis consists of fitting the measured isotopic concentrations with the burnup equations in closed form. The results of the analysis are a set of values for the following set of

ratios of effective* cross sections $\hat{\alpha}^{49}$, $\hat{\sigma}_a^{40}/\hat{\sigma}_a^{49}$, and α^{41} where the superscripts 49, 40, and 41 refer to ^{239}Pu, ^{240}Pu, and ^{241}Pu respectively. The quantities $\hat{\alpha} = \hat{\sigma}_c/\hat{\sigma}_f$ are the ratios of the capture to fission cross sections for the indicated plutonium isotopes. The one standard deviations associated with the fitting process are also assigned to these quantities by the LIKELY code.

2.2. Error Analysis

The reliability of the results (ratios of effective cross sections) is affected by the uncertainty in the yield (Y) and half life (T) of ^{137}Cs because these values are used in deducing the plutonium concentration. The values assumed for these quantities in the analysis were Y = 0.0648 ± 0.0019|6| and T = 29.68 ± 0.30 years.|7| The yield of ^{137}Cs from fission in isotopes other than ^{239}Pu was assumed to be the same as for ^{239}Pu fission. Certain parameters were also required to be held fixed during the fitting process. The fixed parameters, their values and assumed uncertainties were $\hat{\sigma}_a^{41}/\hat{\sigma}_a^{49} = 1.20 \pm 0.05$, $\hat{\sigma}_a^{42}/\hat{\sigma}_a^{49} = 0.0878 \pm 0.006$, and $\lambda^{41}/\hat{\sigma}_a^{41}\phi = 0.050 \pm 0.025$ where λ^{41} is the decay constant for ^{241}Pu and ϕ is the average total neutron flux from the beginning to the end of the irradiation. The uncertainty in each of these parameters (i.e., Y, T, $\hat{\sigma}_a^{41}/\hat{\sigma}_a^{49}$, etc.) contributes to the uncertainty of the fitted ratios (let us collectively call them "X" according to

$$\sigma^{**}_{x,P} = \frac{\partial x}{\partial P}\,\sigma(P) = \frac{\Delta x}{\Delta P}\,\sigma(P) = \frac{x_2 - x_1}{P_2 - P_1}\,\sigma(P) \qquad (1)$$

where $\sigma_{x,P}$ is the uncertainty in x caused by a one standard deviation uncertainty, $\sigma(P)$, in the parameter P. Assuming that uncertainties in the parameters are uncorrelated, the variance of x due to all effects is

$$\sigma^2(x) = \sigma_o^2 + \sum_{i=1}^{N} \sigma^2_{x,P_i} = \sigma_o^2 + \sum_{i=1}^{N} \left(\frac{\partial x}{\partial P_i}\right)^2 \sigma^2(P_i) \qquad (2)$$

where σ_o is the one standard deviation uncertainty in x due to the least squares fitting process.

---

*Effective Cross Section, $\hat{\sigma}^i_x = \dfrac{\int_{E=o}^{\infty}\int_{V} \sigma^i_x(E)\phi(\underline{r},E)\,dE\,d\underline{r}}{\int_{E=o}^{\infty}\int_{V} \phi(\underline{r},E)\,dE\,d\underline{r}}$

** Meaning standard deviation not cross section.

The quantities $\frac{\partial x}{\partial P} = \frac{x_2 - x_1}{P_2 - P_1}$ are evaluated by obtaining the least squares fitted value of x for two slightly different values of the parameter while holding the remaining parameters at their nominal values. Since the experimental data depends upon Y and T, a new set of data must be generated when Y or T is changed to a slightly different value. This new set of data is then least squares fitted to obtain the new value of x that is necessary to evaluate the partial derivative $\frac{\partial x}{\partial P}$. The formation of $\frac{\partial x}{\partial P}$ for the second type of parameter (e.g., $\hat{\sigma}_a^{41}/\hat{\sigma}_a^{49}$) requires no change in the data. All that is necessary in this case, is to least squares fit the data for two slightly different values of the parameter. The results of equations 1 and 2 for the plutonium data are shown in Table I. The fuel elements in the PRTR irradiations were 19 rod clusters. The results given in Table I are for the data obtained from the outer 12 rods of the cluster.

An examination of the numbers in Table I shows that the term $\frac{\partial x}{\partial Y}\sigma(Y)$ is, in one of the cases, the largest contributor to $\sigma(x)$. This is because the ^{137}Cs thermal fission yield from ^{239}Pu is not yet accurately known. Values of this fission yield that have been reported in the literature range from $0.0540 \pm .0039$|8| to $0.0672 \pm .0014$.|9| A recent evaluation of the yield data has been made by Rider, et al.|10| In view of the general lack of agreement between the measured values and the results of this recent evaluation, the value of $Y = .0648 \pm .0019$ that we have used to analyze the data appears to be reasonable. A significant improvement in the accuracy of the yield of ^{137}Cs (say reducing the uncertainty to 1%) would considerably increase our confidence in the least squares fitted values obtained from these plutonium irradiation experiments.

3. THEORETICAL ANALYSIS

3.1. Methods

A number of calculational studies of these PRTR burnup experiments have been performed and reported.|2,3,11,12,13,| The most recent study|3,13| attempted to correlate the ratios of effective cross sections directly. The calculated ratios $\hat{\alpha}^{49}$ and $\hat{\alpha}^{41}$ based upon the best available evaluation of 2200m/sec constants were about one standard deviation away from experimental values and the ratio $\hat{\sigma}_a^{40}/\hat{\sigma}_a^{49}$ was about seven standard deviations away from the experimental values. In a calculation, errors may be due to either the method of calculation or the cross-section data. Detailed analyses were made to determine the errors in calculated results due to assumption used in the analysis and approximations inherent in the theory itself. The net result of these studies was that the use of approximations and inaccurate methods led to about a 1% uncertainty in $\hat{\alpha}^{49}$ and about a 10% uncertainty in $\hat{\sigma}_a^{40}/\hat{\sigma}_a^{49}$. The following is an assessment of the effects of cross-section uncertainties in the calculated ratios of effective cross sections. A knowledge of the effects of cross-section errors is important not only for large differences between calculated and experimental results but also for small differences, since a small difference can arise as a result of a fortuitous cancellation of errors of cross section and model, in which case an improvement in either cross section or calculational model could yield poorer results.

The theoretical methods utilized are based upon the neutron transport equation. The neutron spectrum was computed for a PRTR cell containing an Al-Pu fuel element at various exposures. The thermal neutron spectrum (below 0.683 eV) neutron spectrum was computed using the THERMOS code.|15| The nonthermal (>.683 eV) neutron spectrum was computed using the HRG code.|16| The cross sections for the THERMOS and HRG codes were obtained from the BNW Master Library.|17| The thermal cross sections for ^{239}Pu and ^{241}Pu were normalized to the IAEA evaluation.|14| All of the plutonium isotope cross sections in which this analysis is based upon are given in Reference|13|.

The cross sections considered uncertain were the infinite dilution resonance integrals and 2200m/sec constants for the plutonium isotopes and the shape of the thermal cross sections for ^{239}Pu. The effects of cross-section uncertainties were calculated using the same assumptions of the previous analysis.|3,13| Under these assumptions, the effective cross section is computed by the relationship

$$\hat{\sigma} = \frac{\bar{\sigma}_1 \left(\frac{\bar{\Sigma}_{a2}}{\bar{\Sigma}_{1\to 2}} \right)_{cell} + \bar{\sigma}_2 \left(\frac{\bar{\Phi}_{2\ fuel}}{\bar{\Phi}_{2\ cell}} \right)}{\left(\frac{\bar{\Sigma}_{a2}}{\bar{\Sigma}_{1-2}} \right)_{cell} + \left(\frac{\bar{\Phi}_{2\ fuel}}{\bar{\Phi}_{2\ cell}} \right)} \qquad (3)$$

where: subscripts 1 and 2 refer to nonthermal and thermal energy groups

$\bar{\Sigma}_{a2}$ is the cell averaged absorption in group #2

$\bar{\Sigma}_{1\to 2}$ cell averaged transfer cross section from group 1 to 2.

$\bar{\Phi}_{2\ fuel}$ = average flux per unit volume in group #2 in the fuel

$\bar{\Phi}_{2\ cell}$ = average flux per unit volume in group #2 in the cell

$\bar{\sigma}_1$ = cross section averaged over the epithermal spectrum

$\bar{\sigma}_2$ = cross section averaged over the thermal spectrum.

Equation (2) was then used to estimate the effects of perturbations in $\bar{\sigma}_1$ and $\bar{\sigma}_2$ upon $\hat{\sigma}$.

3.2. Effects of Uncertainties

3.2.1. Resonance Integral and 2200m/sec Constants

For this analysis, we have assumed that the resonance integrals of the plutonium isotopes are uncertain by 5%. Based upon previous reviews|13,18| of these resonance integral data, a 5% uncertainty may be an optimistic estimate of the status of these data. Nonetheless, we shall utilize these uncertainty estimates to illustrate the effect on calculated ratios of effective cross sections. The uncertainties in the 2200m/sec constants are those given in the IAEA evaluation|14| for ^{239}Pu and ^{241}Pu and our estimates for ^{240}Pu and ^{242}Pu.|13| To determine the effect of these estimated cross-section uncertainties on the effective cross section, we assume the relative uncertainties in resonance integrals I and 2200m/sec constants are directly related to $\overline{\sigma}_1$ and $\overline{\sigma}_2$ of equation (3). Also, the cross section perturbations are small enough that the bracket quantities are not significantly affected. The uncertainties in the effective cross sections calculated under these assumptions are given in Table II for the resonance integral data and for the 2200m/sec constants. These results pertain to the outer 12 rods of the 19 rod cluster and are for a plutonium fractional depletion (β) of 0.003 except for ^{240}Pu and ^{242}Pu where data on the exposure dependence are given.

We will utilize the results of our previous analyses|3,13| to put these uncertainties in proper context. As an illustration, the calculated values of $\hat{\alpha}^{49}$, $\hat{\alpha}^{41}$ and $\hat{\sigma}_a^{40}/\hat{\sigma}_a^{49}$, were respectively about 4, 9, and 20% different from those deduced from the experiment. As stated above, inaccurate methods yield about a 1% error in $\hat{\alpha}^{49}$ and $\hat{\alpha}^{41}$ and about a 10% error in $\hat{\sigma}_a^{40}/\hat{\sigma}_a^{49}$. The data presented in Tables II and III indicates that $\hat{\alpha}^{49}$ and $\hat{\alpha}^{41}$ are significantly affected only by uncertainties in the 2200m/sec values. Assuming the errors in σ_{a2200} and σ_{f2200} are uncorrelated then the associated errors in $\hat{\alpha}^{49}$ and $\hat{\alpha}^{41}$ are about 2.3 and 8.0% respectively. The error in $\hat{\sigma}_a^{40}/\hat{\sigma}_a^{49}$ due to uncertainties in resonance integral and 2200m/sec data for ^{240}Pu is at most 5%, assuming the errors in I_∞ and σ_{2200} act in the same direction. Thus, we note that the assumed uncertainties in 2200m/sec constants for ^{239}Pu and ^{241}Pu result in larger uncertainties in $\hat{\alpha}^{49}$ and $\hat{\alpha}^{41}$ than do the uncertainties in the theoretical methods. The reverse is true for the ratio $\hat{\sigma}_a^{40}/\hat{\sigma}_a^{49}$ (i.e., ∿5% error due to cross-section inaccuracies and ∿10% error due to methods).

3.2.2. Shape of the ^{239}Pu Thermal Cross Sections

We next consider the effect of the shape (i.e., energy variation below 1.0 eV) of the ^{239}Pu absorption and fission cross sections in the calculated effective cross sections. Cross-section evaluations are frequently based upon "eyeball" fits through data compilations. Thus the accuracy with which the shape of the cross section is known is somewhat subjective. We have taken the curves of the ^{239}Pu thermal cross section data from Schmidt's compilation|19| and normalized these data to the 2200m/sec constants of the IAEA evaluation|14|. These cross sections were used in a THERMOS calculation and the effective cross sections were again generated. The results are compared to those which are based upon the ^{239}Pu data* in the BNW Master Library|17| in Table IV.

* The shapes of these data are the mathematically smooth curves derived by Leonard from simultaneous fitting of $\sigma_f(E)$, $\sigma_a(E)$, and $\eta(E)$ as described in detail in TNCC(US)-58|Ref 20|.

The differences in the shape of the ^{239}Pu cross sections give rise to a significant effect on the ratios, viz, $\hat{\alpha}^{49}$ changes by 3.6%, $\hat{\sigma}_a^{41}/\hat{\sigma}_a^{49}$ changes by 1.7%, and $\hat{\sigma}_a^{40}/\hat{\sigma}_a^{49}$ changes by 1%. The ratio $\hat{\alpha}^{41}$ remained the same since the ^{241}Pu data we use are based upon $\alpha^{41}(E)$ being almost constant throughout most of the thermal energy region. We do not know what errors to assign to the shapes assumed for the plutonium cross sections. However, we feel the cross-section data for ^{239}Pu which are based upon the fitting of Leonard|20| (those contained in the BNW Master Library) are the best available information on the shape of these cross sections.

The results of this analysis point out the importance of knowing accurately, both the magnitude of the 2200m/sec constants and the shape of the thermal cross sections. Leonard|21| has pointed out to us that in evaluating the best values of the 2200m/sec constants the shape of the thermal cross sections must be carefully considered. Most evaluations of 2200m/sec constants include data obtained from integral experiments and the shape of the cross section must be "known" to interpret these integral measurements. Thus, for the sake of consistency it seems reasonable to expect the evaluator of 2200m/sec constants to supply information (tabulations) on the shape of the thermal cross sections (e.g., $\sigma\sqrt{E}$ vs E) as well as the 2200m/sec values.

Earlier in this paper we stated that ratios of effective cross sections are a more sensitive test of cross section data uncertainties than are reactivity measurements (i.e., critical assembly experiments). To illustrate the relative sensitivity, we show in Table V the effect of the shape of the ^{239}Pu cross sections on some thermal parameters. The reactivity $\overline{\eta}f$, would be affected by about 0.8%, the thermal utilization by 0.4%, and the thermal disadvantage factor by 0.4%. These changes are small contrasted to those in the ratios of effective cross sections.

In summary of the theoretical analysis, we have shown that calculated ratios are affected by uncertainties in basic cross-section data. For the experiments considered in this paper, the uncertainties in thermal cross sections led to the largest uncertainty in calculated results. The shape of the thermal cross section for ^{239}Pu has been shown to have a significant effect on the effective cross sections.

4. CONCLUSIONS

The accuracy in the experimental determination and the theoretical prediction of burnup for plutonium fuels irradiated in the PRTR are limited by inaccuracies in basic nuclear data. A precise measurement $\pm$1% error) of the yield of ^{137}Cs from fissions in plutonium would significantly improve the accuracy of, and confidence in, the experimental values obtained in the analyses. For other fuels|3,22| which have higher concentrations of ^{241}Pu than that studied in this paper, the yield of ^{137}Cs from ^{241}Pu fissions must be known. Thus, a precise measurement of the yield of ^{137}Cs from ^{241}Pu fission will be of value. An accurate theoretical correlation of these experiments will require more precise thermal cross-section data. Particular attention should be given to resolving the shape of the thermal cross sections

for all the plutonium isotopes as well as improving the precision of the 2200m/sec constants. We recommend that future evaluations of 2200m/sec cross sections include results for the shape of the cross sections in the thermal energy region.

The authors thank W. L. Purcell for his assistance in performing the theoretical analysis. Some clarifying discussions concerning cross-section evaluation were held with Dr. B. R. Leonard, Jr.

5. REFERENCES

1. D. E. Christensen, E. B. Reppond, and W. A. Reardon. Burnup Data from Low Exposure Plutonium-Aluminum Fuel, BNWL-CC-904. Pacific Northwest Laboratory, Richland, Washington, 1966.

2. W. A. Reardon and D. E. Christensen. "Atom Ratios and Effective Cross-Section Ratios in Highly Depleted Plutonium-Alloy Fuel," Nucl. Sci. and Eng., 30, p. 222. 1967.

3. L. C. Schmid, D. E. Christensen, B. H. Duane, R. C. Liikala, and R. P. Matsen. "Experimental and Theoretical Methods Used for Burnup Analyses at Battelle Northwest," Proceedings of the Joint International Conference on the Physics Problems in Thermal Reactor Design. London, England, June 1967.

4. R. P. Matsen. "A New Technique for the Determination of Ratios of Effective Cross Sections from Burnup Data," to be published in Nucl. Sci. and Eng.

5. B. H. Duane. Maximum Likelihood Nonlinear Correlated Fields (Battelle Northwest Program LIKELY). USAEC Report BNWL-390. Pacific Northwest Laboratory, Richland, Washington, 1965.

6. H. R. Fickel and R. H. Tomlinson, Can. J. of Physics, 37, p. 926. 1959.

7. S. G. Gorbics, N. E. Kuntz, and A. E. Nash. Nucleonics, 21, p. 63. 1963.

8. D. A. Marsden and L. Yaffe. Can. J. Chem., 43, p. 249. 1965.

9. B. F. Rider, et al. Accurate Nuclear Fuel Burnup, 20th Progress Report, USAEC Report GEAP-5403. General Electric Co., Pleasanton, Calif. 1966.

10. B. F. Rider, et al. A Survey and Evaluation of Thermal Fission Yields for U-235, Pu-239, U-233, and Pu-241, USAEC Report GEAP-5356. General Electric Co., Pleasanton, Calif. September 1967.

11. L. J. Page. Theory Experiment Correlation of Burnup Data from Al-1.8 wt% Pu Fuel (Initially 6 at% Pu-240), USAEC Report BNWL-393. Pacific Northwest Laboratory, Richland, Washington, 1967.

12. G. Sofer, et al. "Plutonium Production and Burnup Calculation Methods for Light Water Moderated Reactors," Symposium on Nuclear Materials Management, Vienna, Austria, September 1965.

13. R. C. Liikala and W. L. Purcell. "Correlation of Effective Cross Sections," Plutonium Utilization Program Annual Report Fiscal Year 1967, USAEC Report BNWL-624, Pacific Northwest Laboratory, Richland, Washington, January 1968.

14. C. H. Westcott, et al. "A Survey of Values of the 2200 m/s Constants for Four Fissile Nuclides," Atomic Energy Review, 3, p. 2. 1965.

15. H. C. Honeck. THERMOS-A Thermalization Transport Theory Code for Reactor Lattice Calculations, USAEC Report BNL-2526. Brookhaven National Laboratory.

16. J. L. Carter, Jr. "Computer Code Abstracts, Computer Code-HRG," Reactor Physics Department Technical Activities Quarterly Report - July, August, September, 1966, USAEC Report BNWL-340, Pacific Northwest Laboratory, Richland, Washington, October 15, 1966.

17. K. B. Stewart. BNW Master Library, USAEC Report BNWL-CC-325, Pacific Northwest Laboratory, Richland, Washington, September 1965.

18. F. G. Dawson, et al. "Analysis of Plutonium Fueled Light Water Reactors," IAEA Symposium on the Use of Plutonium as a Reactor Fuel, Brussels, Belgium, March 1967.

19. J. J. Schmidt. "Neutron Cross Sections for Fast Reactor Materials, Part 1: Evaluation," KFK 120 (EANDC-E-35U), February 1966.

20. B. R. Leonard, Jr. "Survey of the Status of Low Energy Cross Sections of Fissile Nuclides," Neutron Physics, Proceedings of the Symposium held at Rensselaer Polytechnic Institute, May 1961, Academic Press, New York, 1962, and TNCC(US)-58.

21. B. R. Leonard, Jr., (Private communication).

22. D. F. Christensen, E. B. Reppond and W. A. Reardon. Burnup Data from High Exposure Plutonium-Aluminum Fuel, BNWL-CC-905. Pacific Northwest Laboratory, Richland, Washington, 1966.

TABLE I

ERROR ANALYSIS RESULTS

Ratio	Value X	Standard Deviation in X Due to Fitting Process	^{137}Cs Yield (Y)	^{137}Cs Half life (T)	Uncertainty in X due to Assumed Uncertainties in Fixed Parameters			Collective Standard Deviation
					Fixed Parameter #1	Fixed Parameter #2	Fixed Parameter #3	
		σ_o	$\frac{\partial X}{\partial Y}\sigma(Y)$	$\frac{\partial X}{\partial T}\sigma(T)$	$\frac{\partial X}{\partial(\hat{\sigma}_a^{41}/\hat{\sigma}_a^{49})}\sigma(\hat{\sigma}_a^{41}/\hat{\sigma}_a^{49})$	$\frac{\partial X}{\partial(\hat{\sigma}_a^{42}/\hat{\sigma}_a^{49})}\sigma(\hat{\sigma}_a^{42}/\hat{\sigma}_a^{49})$	$\frac{\partial X}{\partial(\lambda^{41}/\hat{\sigma}_a^{41}\phi)}\sigma(\lambda^{41}/\hat{\sigma}_a^{41}\phi)$	$\sigma(X)$
$\hat{\alpha}^{49}$	0.4425	0.0032	0.0143	0.0049	0.0030	0.0000	0.0017	0.0161
$\hat{\alpha}^{41}$	0.3312	0.0054	0.0074	0.0026	0.0197	0.0052	0.0113	0.0252
$\left.\frac{\hat{\sigma}_a^{40}}{\hat{\sigma}_a^{49}}\right\|_{\beta=0}$*	0.5821	0.0058	0.0114	0.0039	0.0028	0.0000	0.0016	0.0138
$\left.\frac{\hat{\sigma}_a^{40}}{\hat{\sigma}_a^{49}}\right\|_{\beta=0.1238}$	0.4745	0.0034	0.0071	0.0025	0.0063	0.0000	0.0036	0.0110
$\left.\frac{\hat{\sigma}_a^{40}}{\hat{\sigma}_a^{49}}\right\|_{\beta=0.235}$	0.4369	0.0026	0.0050	0.0019	0.0074	0.0000	0.0042	0.0104
$\left.\frac{\hat{\sigma}_a^{40}}{\hat{\sigma}_a^{49}}\right\|_{\beta=0.3639}$	0.4159	0.0023	0.0048	0.0017	0.0081	0.0000	0.0046	0.0109
$\left.\frac{\hat{\sigma}_a^{40}}{\hat{\sigma}_a^{49}}\right\|_{\beta=0.4852}$	0.4081	0.0022	0.0045	0.0016	0.0084	0.0000	0.0048	0.0110

*Where β denotes the fractional depletion of plutonium

TABLE II

EFFECTS OF UNCERTAINTIES

IN RESONANCE INTEGRALS I_∞ ON EFFECTIVE CROSS SECTIONS

Pu Isotope	% Uncertainty in I_∞^*	% Uncertainty in $\hat{\sigma}$	
		Absorption, $\hat{\sigma}_a$	Fission, $\hat{\sigma}_f$
239	5.0	0.12	0.11
240	5.0	2.58 for β = 0.003 1.15 for β = 0.485	--
241	5.0	0.17	0.18
242	5.0	3.82 for β = 0.003 3.04 for β = 0.485	--

*Both Fission and Absorption Integrals were assumed to be 5% uncertain

TABLE III

EFFECTS OF UNCERTAINTIES

IN 2200 m/sec CONSTANTS σ_{2200}, ON EFFECTIVE CROSS SECTIONS

Pu Isotope	% Uncertainty in σ_{2200}	% Uncertainty in $\hat{\sigma}$	
		Absorption, $\hat{\sigma}_a$	Fission, $\hat{\sigma}_f$
239	0.5(σ_a and σ_f)	0.49*	0.49
240	3.0	1.45 for β = 0.003 2.31 for β = 0.485	--
241	(2.0 σ_a),(1.0 σ_f)	1.93**	0.96
242	20.0	4.71 for β = 0.003 7.84 for β = 0.485	--

* A 0.5% uncertainty in $\hat{\sigma}_a^{49}$ corresponds to $\sim$ a 1.5% uncertainty in $\hat{\sigma}_c^{49}$.

** A 1.9% uncertainty in $\hat{\sigma}_a^{41}$ corresponds to $\sim$ a 6.7% uncertainty in $\hat{\sigma}_c^{41}$.

TABLE IV

INFLUENCE OF THE SHAPE OF THE ^{239}Pu CROSS SECTIONS ON EFFECTIVE CROSS SECTIONS AND THEIR RATIOS

Pu Data	Effective Cross Sections						
	^{239}Pu			^{241}Pu	^{240}Pu		
	$\hat{\sigma}_a$	$\hat{\sigma}_f$	$\hat{\alpha}$	$\hat{\sigma}_a$	$\hat{\sigma}_a$	$\hat{\sigma}_a^{41}/\hat{\sigma}_a^{49}$	$\hat{\sigma}_a^{40}/\hat{\sigma}_a^{49}$
Schmidt	493.0	341.8	0.442	596.0	232.8	1.21	0.472
BNW Master Library	497.9	341.6	0.458	592.1	233.0	1.19	0.468

TABLE V

INFLUENCE OF THE SHAPE OF THE ^{239}Pu CROSS SECTIONS ON REACTIVITY, THERMAL UTILIZATION, AND THERMAL DISADVANTAGE FACTORS

Pu Data	Reactivity $(\bar{\eta}f)^*$,	Thermal Utilization, f	Disadvantage Factor, $\bar{\Phi}_{Fuel}/\bar{\Phi}_{Cell}$
Schmidt	1.679	0.9397	0.7526
BNW Master Library	1.664	0.9403	0.7499

* Ratio of Cell Averaged Values $(\nu\bar{\Sigma}_f/\bar{\Sigma}_a)$Thermal

RATIO OF PHOTON TO NEUTRON FISSION RATES IN FAST REACTORS*

E. J. Dowdy, W. H. Kohler, R. T. Perry and N. B. Poulsen
Nuclear Engineering Department, Texas A&M University
College Station, Texas 77840

ABSTRACT

The large inventory of fuel in fast power reactors combined with the relatively low neutron fission cross sections have prompted this evaluation of the relative photofission to neutron fission rates in such reactors. The photofission cross section of the fuel (especially Pu^{239}) is relatively large and strongly energy dependent in the gamma ray energy range of 6-10 MeV, a range in which there is a copious supply of gamma rays arising from fission and from neutron radiative capture in the reactor materials. We have calculated the ratio of the photofission rate to neutron induced fission rate in representative fast reactors. The multigroup neutron cross-sections used in the computations were obtained from the set of Bondarenko, et al.[1] and the group fluxes from AIM-6[2]. First flight gamma ray fluxes were used in computing the photofission reaction rates from the measured[3] photofission excitation functions for the fuel materials, except for Pu^{241} and Pu^{242} for which no references for photofission are listed in CINDA[4]. In every case, the ratio of photofission to neutron induced fission was calculated to be less than 1×10^{-3}.

1. INTRODUCTION

With the continuing quest for improved accuracy in reactor calculations, it occurred to us that a reconsideration of the importance of photofission was in order. This was felt to be particularly true for calculating fast reactor fission rates because of the relatively small neutron fission cross-section and the large inventory of fuels, some of which have an appreciable photofission cross section for the hard gamma rays produced in fission and radiative capture. Consequently, we have calculated relative photofission rates in some fast reactors in an attempt to determine the importance of photofission so that a suggestion might be offered for inclusion of this effect in calculations or so that justification might be given for neglecting it.

Since only prompt gamma rays have energies above the fission threshold and prompt gamma ray generation is determined by the neutron flux, we have calculated the ratio of photofission rates to neutron induced fission rates so that we need know only the neutron spectrum and not the absolute neutron fluxes.

*Supported in part by grants from the Texas A&M University Research Council.

In the following section, the method used for computing the ratio is presented. This is followed by presentation of results for several fast reactors and a qualitative examination of the ratio for assemblies differing in composition from those included in this study.

2. METHOD OF CALCULATION

The threshold for photofission in any fuel material is on the order of 5.0 MeV so that only gamma rays with energies greater than this were considered. Such hard gamma rays originate as prompt gamma rays from both fission and radiative capture of neutrons. Thus, if second order effects are ignored, the photofission rate is determined completely by the neutron group fluxes. Specifically, if $S^k(\vec{r})$ is the number of gamma rays produced per unit volume per unit time in the k^{th} gamma ray energy group at the point $\vec{r}$, then

$$S^k(\vec{r}) = \sum_{j,\ell} \left\{ \left[F_\ell^k \Sigma^j_{\ell,\mathrm{FISS}} + C_\ell^k \Sigma^j_{\ell,(n,\gamma)} \right] \phi^j(\vec{r}) \right\}$$

where F_ℓ^k and C_ℓ^k are the k^{th} gamma ray group intensities in the prompt fission gamma ray spectrum and the radiative capture gamma ray spectrum, respectively, of the ℓ^{th} reactor material, $\Sigma^j_{\ell,\mathrm{FISS}}$ and $\Sigma^j_{\ell,(n,\gamma)}$ are the corresponding macroscopic fission and radiative capture cross sections of the ℓ^{th} material for neutrons in neutron group j, and $\phi^j(\vec{r})$ are the neutron group fluxes.

Interactions of high energy gamma rays in high Z materials are dominated by pair production so that any interaction can be considered as removing a gamma ray from consideration in computing photofission rates. Hence, we require only the uncollided gamma ray fluxes, or the first flight fluxes. The first flight flux of gamma rays in the k^{th} group at the point $\vec{r}'$ is

$$\Phi^k(\vec{r}') = \int_{\vec{r}} S^k(\vec{r}) \, \frac{\exp\left\{ -\mu_t^k \, |\vec{r}' - \vec{r}| \right\}}{4\pi(\vec{r} - \vec{r}')^2} \, d\vec{r}$$

where μ_t^k is the total linear attenuation coefficient of the core mixture for k^{th} group gamma rays.

For convenience, we have restricted our calculations to regions of the reactors where there are negligible neutron flux gradients. The desired ratio of photofission rate to neutron induced fission rate then takes the relatively simple form

$$\frac{\sum_{k,\ell} \Sigma^k_{\ell,(\gamma,f)} \Phi^k_1(\vec{r})}{\sum_{j,\ell} \Sigma^j_{\ell,FISS} \phi^j(\vec{r})} = \frac{\sum_{k,\ell} \Sigma^k_{\ell,(\gamma,f)} \frac{S^k}{\mu^k_t}}{\sum_{j,\ell} \Sigma^j_{\ell,FISS} \phi^j(\vec{r})}$$

where $\Sigma^k_{\ell,(\gamma,f)}$ is the macroscopic photofission cross-section of the ℓ^{th} material for k^{th} group gamma rays and S^k is the (assumed) constant rate of generation of k^{th} group gamma rays at the point $\vec{r}$.

The gamma ray energy range (5 - 10 MeV) was divided into 10 groups of equal width. Due to the paucity of data on the dependence of the (n,γ) spectra on neutron energy, we have assumed that the spectra are independent of neutron energy and have used thermal neutron capture spectra[5,6]. The capture gamma ray spectra turn out to be relatively unimportant in the final analysis as the radiative capture rate is only a small contribution to the hard gamma ray generation rate. Similarly, the gamma ray spectra from fission[7] was assumed to be independent of the energy of the neutron causing fission. The self-shielded neutron group cross sections were obtained from the set of Bondarenko, et al.[1], the group fluxes gotten from AIM-6[2] calculations, the gamma ray attenuation coefficients gotten from Grodstein's compilation[8], and the photofission cross sections are those of Katz, et al.[3].

3. RESULTS AND DISCUSSION

In table 1, the reactors included in this study are listed along with the composition of each and the computed ratio of photofission rate to neutron induced fission rate.

The ratio is seen to be very small for all cases, leading us to conclude that even in the most exact calculations, photofission can be safely ignored. In general, the generation of hard gamma rays is due mainly to fission and radiative capture in the fuels, other materials being relatively unimportant. Although we have not included in the photofission calculations the heavier isotopes formed during operation of high powered fast reactors, their relative fissionability[9] indicates that the photofission cross-sections would be less than for Pu^{239}.

In comparing the five cases presented, the following trend in the ratio is noted. For a fixed neutron spectrum, reducing the amount of fissile material increases the ratio (compare Zebra 1 core and reflector). Dilute

plutonium fueled assemblies will have a larger ratio than heavily loaded assemblies. (Na-1 and ZPR-3(48) are dilute and have a correspondingly larger ratio than Vera 9A, which is heavily loaded.) In blanket regions, the ratio is expected to be relatively large, but an estimate of the magnitude would still be less than 10^{-3}.

4. REFERENCES

1. Bondarenko, I. I., Editor, Group Constants for Nuclear Reactor Calculations, Consultants Bureau, New York (1964).

2. Flatt, H. and D. C. Baller, NAA Program Description (1961).

3. Katz, L., A. P. Baerg and F. Brown, Second Geneva Conference on Peaceful Uses of Atomic Energy 15, 188 (1958).

4. CINDA 67, TID-24049.

5. Groshev, L. V., V. N. Lutsenko, A. M. Demidov and V. I. Pelekhov, Atlas of γ- Ray Spectra from Radiative Capture of Thermal Neutrons, Pergamon Press, New York (1959).

6. ANL-5800, Second Edition, p. 632.

7. ANL-5800, Second Edition, p. 630.

8. Grodstein, G. W., NBS Circular 583 (1957).

9. Hyde, E. K., The Nuclear Properties of the Heavy Elements V. III - Fission Phenomena, Prentice-Hall, Englewood Cliffs, N. J. (1964), p. 51.

TABLE 1
Calculated Values of the Ratio of Photon to Neutron Fission Rates

ASSEMBLY	Composition, nuclei-cm^{-3} x 10^{-22}								RATIO
	Pu^{239}	Pu^{240}(A)	U^{235}	U^{238}	Cr	Fe	Ni	Others	
Zebra 1 (reflector)			0.0301	4.099	0.091	0.350	0.036		0.17×10^{-3}
(core)			0.4655	3.433	0.082	0.447	0.032		0.46×10^{-4}
Na-1	0.085	0.049		0.522	0.332	0.936	0.365	(O) 1.313, (Na) 1.22	0.76×10^{-4}
ZPR-3(48)	0.164	0.011	0.0016	0.741	0.266	0.990	0.131	(C) 2.08, (Na) 0.623 (Al) 0.011, (Mo).021	0.62×10^{-4}
Vera 9a	1.0687	0.0544			0.158	0.609	0.066	(C) 3.422, (Al) .001 (Cu) 1.125	0.48×10^{-4}

(A) Sum of Pu^{240}, Pu^{241}, Pu^{242}.

CRITICALITY AND CENTRAL REACTIVITY CALCULATIONS USING ENDF/B DATA*

by

R. J. LaBauve and M. E. Battat

University of California
Los Alamos Scientific Laboratory
Los Alamos, New Mexico 87544

ABSTRACT

A series of criticality calculations has been performed for selected experimental assemblies to test the Category I, ENDF/B neutron data. These assemblies include JEZEBEL (plutonium core), TOPSY (enriched uranium core with natural uranium reflector), and ZPR-3 Assembly 48 (plutonium fuel, soft spectrum). Central reactivity worths were also computed for several materials of interest in fast reactor design. In the course of obtaining multigroup constants for input to the Los Alamos Scientific Laboratory codes used in these calculations, several ENDF/B retrieval and processing codes were employed. These include DAMMET, a code for rearranging and altering the mode of the standard BCD ENDF/B library tape; ETOE, a code for preparing an MC^2 library tape; and MC^2, a code for generating multigroup constants from microscopic neutron data. Calculational results have been compared with experiment as well as results obtained using other nuclear data libraries.

*Work done under the auspices of the United States Atomic Energy Commission.

1. INTRODUCTION

Calculations have been performed for three selected critical experiments, using the Category I, Evaluated Nuclear Data File/B (ENDF/B) library data.[1] The experiments selected for study were:

1. a bare plutonium-metal assembly - JEZEBEL[2]
2. a uranium-reflected ^{235}U metal assembly - TOPSY[2]
3. a dilute plutonium-fueled assembly surrounded by a depleted uranium reflector - ZPR-3 Assembly 48[3]

For all three systems, critical masses and central reactivity worths were computed; in addition, central activation ratios were calculated for ZPR-3 Assembly 48. These calculations were compared both with experiment and results obtained by C. B. Mills[4] using the UKAEA and LRL neutron data contained in the LASL library.

2. CALCULATIONS

For the Category I, ENDF/B library data, multigroup constants were generated using the following sequence of processing codes: DAMMET[5] - a code for merging and changing the mode of the ENDF/B data, and ETOE[6] - a code to generate a library for MC^2[7] - a multigroup constants code. For these calculations, the MC^2 options specified were (1) all fine-group treatment, (2) P-1 fundamental mode calculation, and (3) homogeneous calculation using core composition. The inelastic scattering secondary energy distributions for carbon, chromium, and nickel were inferred from the ANL MC^2 library because these ENDF/B data were expressed in a form not compatible with MC^2. The number of broad groups used were 13, 17, and 25 for JEZEBEL, TOPSY, and ZPR-3 Assembly 48, respectively.

Critical mass calculations were performed with the DTF-IV[8] (multigroup transport) code for spherical geometry and S_8 option. Regular and adjoint fluxes and currents from these transport problems were subsequently used in perturbation calculations of small sample central reactivity worths.

3. RESULTS AND CONCLUSIONS

Calculated central spectra for the various experiments are given in Table I. For ZPR-3 Assembly 48, the computed and measured spectra are also compared. Calculated and experimental critical masses are shown in Table II. Central reactivity worths for selected materials - using ENDF/B, UKAEA, and LRL neutron data - are compared with experimental values in Tables III (JEZEBEL), IV (TOPSY), and V (ZPR-3 Assembly 48). Central activation ratios for ZPR-3 Assembly 48 are given in Table VI.

Insofar as the ENDF/B data are concerned, the following observations can be made from these tabulated results:

1. Reduction of the $^{238}U(n,\gamma)$ cross sections above 200 keV would give better agreement with experiment.

2. The ^{6}Li and ^{7}Li data need to be re-examined. In the case of ^{7}Li, the large discrepancy may be due to the inadequate representation of the secondary energy distribution data given in ENDF/B.

3. The carbon and sodium data give poor results in the ZPR-3 Assembly 48 spectrum.

4. In general, the iron, chromium, and nickel are too absorptive for the systems studied.

TABLE I

CALCULATED AND MEASURED CENTRAL SPECTRA
Percent of Total Flux - ENDF/B Cross Sections

E_{lower}	$\phi_{calculated}$			$\phi_{experiment}$
	JEZEBEL	TOPSY	ZPR3/48	ZPR3/48*
6.065 MeV	2.36	1.23	0.42	
3.679	9.04	5.72	1.71	
2.231	16.27	12.29	3.81	
1.353	18.73	16.22	5.47	
0.821	17.73	16.60	7.31	
0.498	14.37	15.77	9.90	10.85
0.302	9.95	13.27	11.94	11.36
0.183	5.69	8.87	12.01	10.85
0.111	3.04	5.14	10.15	10.31
67.4 keV	1.75	2.74	8.88	8.97
40.9		1.31	7.20	7.13
24.8	0.86	0.65	6.77	5.83
15.0		0.13	5.64	4.76
9.12		0.04	3.42	3.85
5.53	0.19		2.08	2.80
3.35			1.40	1.82
2.03			0.42	1.27
1.23			0.85	
748 eV			0.43	
454			0.14	
214			0.05	

*Normalized as follows:
Sum of measured fluxes = sum of corresponding calculated fluxes

TABLE II

CALCULATED AND EXPERIMENTAL CRITICAL MASSES
ENDF/B CROSS SECTIONS

(JEZEBEL Pu contains 4.5% ^{240}Pu. TOPSY U is enriched to 94.1% ^{235}U.)

System	Calculated (kg)	Experiment (kg)
JEZEBEL	15.65 Pu	16.28 Pu
TOPSY	15.9 U	17.4 U
ZPR-3/48	339 ^{239}Pu*	272 ^{239}Pu**

*Calculated homogeneous sphere (R_{core} = 49.78 cm) = 337.1 kg.
Homogeneous cylinder = 337.1/0.927 = 363.6
Heterogeneous cylinder = 363.6 - 25.0 = 338.6
k_{eff} = 0.975 for R_{core} = 47.42 cm.

**Heterogeneous cylindrical mass.

TABLE III

JEZEBEL - CENTRAL REACTIVITY WORTHS
cents/mole

Material	ENDF/B*	UKAEA*	LRL*	Experiment
Fe	- 27.2 (1020)	- 22.2 (2036)		- 21.5
Ni	- 60.1 (1021)	- 54.6 (2046)		- 48.0
^{235}U	929. (1044)	821. (2030)	798. (923)	804.
^{238}U	87. (1047)	103. (2005)	98. (8926)	114.
^{239}Pu	1763. (1051)	1557. (2329)	1591. (942)	1592.
^{240}Pu	1091. (1053)	983. (2201)	855. (943)	1038.

*Numbers in parentheses are material identification numbers.

TABLE IV

TOPSY - CENTRAL REACTIVITY WORTHS
cents/mole

Material	ENDF/B*	UKAEA*	LRL*	Experiment
^{6}Li	- 70.2 (1005)	- 72.8 (2214)		- 130.4
^{7}Li	0.004 (1006)	3.0 (2215)		7.9
Be	9.1 (1007)	8.9 (2008)		9.2
Fe	- 2.4 (1020)	- 2.7 (2036)		- 2.2
Mo	- 6.7 (1025)		- 5.8 (420)	- 3.5
^{235}U	212.7 (1044)	216.8 (2030)	207.3 (923)	208.4
^{238}U	25.4 (1047)	21.5 (2005)	28.7 (8926)	26.7
^{239}Pu	392.5 (1051)	396.4 (2329)	403.4 (942)	402.6
^{240}Pu	221. (1053)	210. (2201)	168. (943)	286 $\pm$ 14

*Numbers in parentheses are material identification numbers.

TABLE V

ZPR-3 ASSEMBLY 48 - CENTRAL REACTIVITY WORTHS
cents/mole

Material	ENDF/B*	UKAEA*	LRL*	Experiment**
C	- 0.21 (1010)	- 0.04 (2006)	- 0.21 (61)	- 0.017
Na	- 0.19 (1059)	- 0.07 (2182)		- 0.046
Cr	- 0.279 (1018)			- 0.149
Fe	- 0.287 (1020)	- 0.18 (2036)		- 0.204
Ni	- 0.443 (1021)	- 0.32 (2046)		- 0.325
Mo	- 1.78 (1025)		- 0.49 (420)	- 1.27
^{235}U	26.8 (1044)	23.3 (2030)	23.9 (923)	24.1
^{238}U	- 2.02 (1047)	- 1.87 (2005)	- 1.56 (8926)	- 1.80
^{239}Pu	35.4 (1051)	31.9 (2329)	35.0 (942)	32.2
^{240}Pu	6.56 (1053)	2.94 (2201)	- 7.0 (943)	5.87

*Numbers in parentheses are material identification numbers.

**Values given in Ref. 3 were expressed as central perturbation cross sections. These were converted to cents/mole.

TABLE VI

ZPR-3 ASSEMBLY 48
CENTRAL ACTIVATION RATIOS RELATIVE TO ^{235}U FISSION
ENDF/B CROSS SECTIONS

(1.0-cm radius central region)

Type	Calculated	Experiment
^{238}U fission	0.0332	0.0307
^{238}U (n,γ)	0.158	0.138
^{239}Pu fission	0.960	0.976
^{240}Pu fission	0.248	0.243

4. REFERENCES

1. "Category I, ENDF/B Data Tape Numbers 114, 115, 116, 117, and 999," as distributed by Brookhaven National Laboratory (1967).

2. L. B. Engle et al., "Reactivity Contributions of Various Materials in Topsy, Godiva, and Jezebel," Nuclear Sci. and Eng. 8, 543 (1960).

3. W. G. Davey, "Intercomparison of Calculations for a Dilute Plutonium-Fueled Fast Critical Assembly (ZPR-3 Assembly 48)," ANL-7320 (1966).

4. C. B. Mills, "Master Data Tape Cross Sections vs Critical Experiments," private communication (1968).

5. J. Felberbaum (ed.), "Description of the ENDF/B Processing Codes CHECKER, CRECT, DAMMET, and Retrieval Subroutines," ENDF-110 (1967).

6. D. M. Green and T. A. Pitterle, "ETOE, A Program for ENDF/B to MC^2 Data Conversion," APDA-TM No. 44 (1967).

7. B. J. Toppel et al., "MC^2, A Code to Calculate Multigroup Cross Sections," ANL-7318 (1967).

8. K. D. Lathrop, "DTF-IV, a FORTRAN-IV Program for Solving the Multigroup Transport Equation with Anisotropic Scattering," LA-3373 (1965).

TRANSURANIUM CROSS SECTIONS WHICH INFLUENCE FBR ECONOMICS

Eric H. Ottewitte

Atomics International
Canoga Park, California 91304

ABSTRACT

Many of the cross-section uncertainties pertinent to FBR physics are well known: particularly $\sigma_{n,\alpha}$(U-238), $\sigma_{n,\alpha}$(Pu-240), α(Pu-239), and fission product absorptions. This paper describes a quantitative evaluation of the effect on fuel cycle costs of FBR transuranium isotope production, specifically, isotopes U-232 through Cm-244. The results show that many transuranium isotopes besides U-238 and Pu-239 through Pu-242 may influence the FBR economics. The modes by which this may occur are isotope sales (Np-237, Am, and Cm-244), alpha-emitter radiological safety considerations in the design of reactor and reprocessing plants, gamma and neutron shielding requirements in fuel fabrication, alpha-radiation destruction of reprocessing solvent and ion-exchange media. Cross-section needs for these phenomena are assigned relative importance from the quantitative results.

1. INTRODUCTION

To determine their effect on fuel cycle costs, a quantitative evaluation of FBR transuranium isotope production was made. The potential significance of the isotopes considered is given in Table I. Burnup calculations were made in which the isotopes were allowed to build up over successive cycles, eventually reaching equilibrium levels. Figure 1 describes the branches included in the burnup chain. Table II presents the resulting equilibrium transuranium concentration levels. The results indicate that many transuranium isotopes besides U-238 or Pu-239 through Pu-242 may influence the FBR economics. The significance of these concentration levels is explored in terms of isotope recovery and sales, fuel reprocessing, fuel fabrication, and the radiological safety of alpha emitters.

2. TRANSURANIUM ISOTOPE RECOVERY AND SALES

The motivation to recover the transuranium isotopes comes from the projected demand and estimated price for some of these isotopes, and the desire to lower FBR fuel cycle costs by improving the fuel reprocessing plant's high investment-to-annual revenue ratio (5/1). The projected demand for all isotopic power fuel appears to go beyond the anticipated production (especially for Pu-238). Industry apparently has enough confidence in the field of isotopic power and radiation applications to invest appreciable funds: americium is to be recovered at Hanford; the NFS plant will add facilities to recover neptunium now and possibly americium and curium later.

For commercial FBR's the opportunity for isotope production appears to be limited to those isotopes which are chemically separable by-products of normal electrical power generation. Recovery of neptunium should yield essentially pure Np-237. The americium containing Am-241 and Am-243, and the curium containing Cm-242 and Cm-244, will be valuable without isotopic separation (see Table I).

Applying profit estimates (Table III) to the sale of the calculated isotope production (Table II), one obtains a decrease in electricity costs of 0.07 mills per kwhr. This is about 9% of the predicted FBR fuel cycle costs or about 1/7 of the Pu-239 + Pu-241 credit. This savings agrees with similar isotope revenue estimates of one or two tenths of a mill per kwhr, given at the 1967 Augusta Conference on Nuclear Fuel Reprocessing. Thus, from Tables II and III, the cross sections which lead to the production of Am-241, Am-243, Np-237, Cm-244, and Cm-242 are important, in that order, to the understanding of transuranium isotope recovery and sales. With this information, the industry can plan for recovery capability and develop certain isotope markets, so as to obtain maximum additional revenues.

3. FUEL REPROCESSING

Fuel reprocessing consists of (1) dissolving the fuel elements, (2) extracting the fission products, (3) extracting the plutonium and uranium separately, and (4) purifying the uranium stream with silica gel and the plutonium stream by ion exchange. High levels of radioactivity present during these processes can reduce the efficiency of plutonium recovery by damaging the solvent and extractant chemicals and the ion exchange resins. Studies of these phenomena are currently underway at ORNL. The alternative solutions to this problem are as follows:

1) Allow the fuel to cool for a longer period of time. Fuel cooled for one hundred days still has up to two megacuries beta-gamma radiation per handling batch. However, this step increases fuel inventory charges.

2) Keep the radiation exposure of the chemicals used to an acceptable minimum by either discarding them sooner, cleaning them up more thoroughly after use, utilizing them more efficiently by using a continuous operation process rather than a batch process, or diluting the plutonium concentration via uranium recycle.

Each alternative involves some other compromise. Thus, the level of radioactivity in the fuel influences the reprocessing plant costs.

To select the economically optimum process and plant design, it becomes important to understand the sources and components of this radioactivity. Table IV presents the radioactivity levels 120 days after discharge from a 100-MWD/kg, 1000-Mwe FBR. Note that the transuranium activity is predominantly alpha. Since the alpha energy of 5 Mev is totally absorbed, the transuranium activity is very important throughout the fuel recovery process in terms of radiolytic damage. Thus the cross-sections which are important here are those which lead to Pu-241, Cm-242, and Am-243 production, in that order.

4. SHIELDING REQUIREMENTS FOR THE PROCESSING OF MIXED $(U,Pu)O_2$ IN AN FBR FUEL FABRICATION FACILITY

The basic aim of the fuel fabrication plant is to economically fabricate the high activity Pu fuels expected from LWR or FBR equilibrium recycle. This is expected to account for 32% of the fuel cycle cost (before Pu credit). One of the factors which will significantly influence process design philosophy is the shielding requirements which will be imposed by the heavy isotopes of high exposure, Pu-containing fuels. It appears that the major radiation hazards after aqueous reprocessing will be due to Pu isotopes, with a negligible contribution from fission products. It is probable that neutron shielding requirements (the neutrons arise from spontaneous fission and alpha-n reactions with light elements) will be more stringent than those due to gamma radiation.*

Although heavily shielded structures used in conjunction with manipulator operations could provide maximal radiation protection, such a philosophy is not favored since it would make fuel fabrication extremely expensive. The favored approach, to cope with radiation hazards, is to provide a minimal degree of shielding, and to automate the process and equipment so that a minimum amount of operator handling is required.

Some of the many factors to be considered in designing an FBR fuel fabrication process are:

1) Choice of shielding materials for gamma and neutron protection

2) Location of shielding, i.e., around the equipment within the glove box or on the exterior of the glove box. The former procedure is tentatively preferred for several reasons including: (a) less shielding is required when the shielding is close to the source, (b) shielding of the equipment can provide protection to the hands in contrast to shielding on the enclosure, (c) most of the shielding requirements will be for neutron rather than gamma radiation; such shielding may be similar to paraffin, or polyethylene, which would result in poor box visibility. Some other important considerations in the design of internally shielded glove boxes are: (1) possible requirement for wider boxes to accommodate internal shielding and (2) probable requirement for shielding hardware which is easily disassembled, to allow access for equipment maintenance.

3) Degree (or thickness) of shielding, i.e., whether to provide thick and costly shielding which can provide full eight-hour protection to an operator, or only a small fraction of such shielding to accommodate the expected time that an operator will spend performing a particular operation. For maintenance requirements the bulk of the source material could be removed, or if necessary, maintenance personnel could be rotated to assure safe exposure limits.

4) Type of glove box, i.e., conventional with operator availability from two opposite glove box faces, or one-sided glove boxes where operations are intended through only one glove box window, while the opposite side of the glove box is designed for maintenance.

*This assumes no recycle of uranium, a situation characteristic of the near-term future. If uranium is recycled, the gamma shielding problem becomes significantly worse, due to the gamma activity of thallium-208, a decay product of uranium-232.

Table V illustrates typical shielding requirements for an FBR fuel fabrication plant. One concludes from this that it is important to the fuel fabrication plant designer to fully understand the nature and the magnitude of the radiation levels to be expected.

Table VI shows which isotopes are the main contributors to these shielding requirements. The different energy gamma rays from these contributors will vary the relative importance of these isotopes somewhat as the shielding thickness varies. The need for adequately anticipating the Pu-238 production should be noted.

5. ALPHA-EMITTER RADIOLOGICAL SAFETY DESIGN

The designer of a reactor, fuel fabrication plant, or fuel reprocessing plant must consider the possibility of airborne plutonium in an accident. Significant controversy still exists with respect to the maximum permissible concentration (MPC) of plutonium. Specifically the question exists whether, even though plutonium is insoluble, small particles of plutonium may act as if they were soluble in the blood. If so, high efficiency plutonium filters may be required to reduce the airborne plutonium from a hypothetical accident.

Calculations based on the data in Table II indicate that the alpha hazard from Pu-238 is of the same magnitude as from Pu-239, Pu-240, and Pu-241.

6. CONCLUSIONS

Table VII summarizes the transuranium isotopes which may be of importance to FBR fuel cycle costs. Cross-section components which lead to their production (Figure 1) affect the general FBR program and warrant attention.

TABLE I

BURNUP CHAIN MEMBERS AND THEIR POSSIBLE SIGNIFICANCE

FP	Fission product pairs produced in every fission The concern here was to introduce the fission product reactivity effect.
FPP	Products of fission product absorption, i.e., FP (n,γ) FPP. The concern here was to account for the depletion of the FP reactivity effect as high absorbers burn into low absorbers. To effect this, FPP was represented with zero-magnitude cross-sections.
U^{232}	Alpha emitter which might affect fuel fabrication or radiological safety.
U^{237}	Radioactive product of the U^{238} (n, 2n) reaction which might affect discharge fuel storage time, radiological safety, or fuel reprocessing.
U^{238}	Feed material.
U^{239}	Highly radioactive product of U^{238} (n,γ) reaction which might affect discharge fuel storage time, radiological safety, or fuel reprocessing. U^{239} is included with its "granddaughter" Pu^{239} in the cycle mass balances.
Np^{236}	Radioactive product of Np^{237} (n,2n) reaction which might affect discharge fuel storage time, radiological safety, design, or fuel reprocessing.
Np^{237}	U^{237} daughter which has a high market value as target material for Pu^{238} production. Thus Np^{237} sale may influence FBR economics. Sufficient Np^{237} is produced to also have a small but observable effect on reactivity.
Np^{238}	Radioactive product of Np^{237} (n,γ) reaction, which might affect discharge fuel storage time, radiological safety, fuel reprocessing, and contamination of Np^{237}.
Np^{239}	U^{239} daughter and Pu^{239} precursor which might affect fuel reprocessing (continuous decay into recoverable plutonium), discharge fuel storage time, radiological safety, and contamination of Np^{237}. Np^{239} is also included as Pu^{239} in the cycle mass balances.
Pu^{236}	Np^{236} radioactive (alpha-emitting) daughter which might affect radiological safety or fuel fabrication.
Pu^{238}	Alpha-emitting Np^{238} daughter which might affect radiological safety, or fuel fabrication. High costs preclude its separation from regular discharge fuel and subsequent resale. Equilibrium composition (maybe 1%) might affect reactivity. Although fissionable, Pu^{238} also constitutes a fertile fuel, Pu^{238} (n,γ) Pu^{239}. It was treated as a fertile in the breeding ratio definition (an almost insignificant effect).
Pu^{239}	Main fissile fuel.
Pu^{240}	Main fertile fuel.
Pu^{241}	Main fissile fuel.
Pu^{242}	Product of Pu^{241} (n,γ) reaction which affects reactivity.
Pu^{243}	Radioactive product of Pu^{242} (n,γ) reaction which might affect discharge fuel storage time, radiological safety, or fuel reprocessing.
Am^{241}	Pu^{241} daughter which has potential use as a heat and gamma source and as target material for Cm^{242}.
Am^{242}	Radioactive product of Am^{241} (n,γ) reaction which might affect radiological safety.
Am^{243}	Pu^{243} daughter which has potential use as a target for Cm^{244}.
Am^{244}	Radioactive product of Am^{243} (n,γ) reaction which might affect radiological safety.
Cm^{242}	Am^{242} daughter which has potential use as a heat source: by itself and as a parent of Pu^{238}.
Cm^{243}	Radioactive product of Cm^{242} (n,γ) reaction which might affect radiological safety, discharge fuel storage time, or fuel reprocessing.
Cm^{244}	Product of Am^{244} decay (primarily) and of Cm^{243} (n,γ) reaction. Cm^{244} has potential use as a heat source and as a target material for higher isotopes. Might also affect fuel reprocessing and radiological safety.

TABLE II

ISOTOPIC BUILDUP LEVELS IN RECYCLED FUEL AT TIME OF DISCHARGE FROM A 100-MWD/kg, 1000-MWE FBR

Isotope	Reactor-Averaged Concentration (per Metric Ton Mix)		Plutonium Isotopic Composition (%)
FP	29.98	kg	
U-232	13.8	mg	
U-237	3.02	g	
U-238	908.7	kg	
U-239	1.24	g	
Np-236	0.034	mg	
Np-237	175	g	
Np-238	0.112	g	
Np-239	179.	g	
Pu-236	0.46	mg	5.94×10^{-6}
Pu-238	246.	g	0.32
Pu-239	40.36	kg	71.8
Pu-240	17.15	kg	23.4
Pu-241	2.265	kg	2.90
Pu-242	1.196	kg	1.53
Pu-243	0.052	g	
Am-241	176	g	
Am-242	0.064	g	
Am-243	96.5	g	
Am-244	0.014	g	
Cm-242	16.2	g	
Cm-243	0.257	g	
Cm-244	6.50	g	
			100.0

TABLE III

ESTIMATED POTENTIAL ISOTOPE SALE REVENUES FROM A 100-MWD/kg, 1000-MWE FBR

Byproduct	Sale Price ($/g)	Processing Costs ($/g)	Net Profit* ($/g)	Discharge Masses (kg/cycle)	kwhrs Operation	Net Savings (mills/kwhr)
Np-237	50	27	23	1.8	3500	0.012
Am	100	58	42	3.5	3500	0.042
Cm-244	400	148	252	0.13	3500	0.009
Cm-242	(130)			0.25	3500	<0.009**
						0.07

*W. A. Rodger, S. L. Reese, S. S. Stanton, "Multi-Purpose Plant for the Recovery of Neptunium and Other Isotopes," New York State Atomic and Space Development Authority (1967)

**Cm-242 has value as a heat source as well as a source of pure Pu-238 (through decay). Using a Pu-238 sale price, the net savings might be about that for Cm-244.

TABLE IV

RADIOACTIVITY IN FUEL 120 DAYS AFTER DISCHARGE FROM A 100-MWD/kg, 1000-MWE FBR

Isotope	Decay Mode	Half Life	Equilibrium Discharge Composition $\left(\frac{gm}{MT\ Mix}\right)$	Radiation Level After 120 Days of Cooling	
				Curies per kg of Discharge Isotope	Kilocuries per kg of Fuel Mix
U-232	α	73.6 y	0.014	2.09×10^{4}	0.0
U-237	α	6.75 d	3.0	356	0.0
U-238	α	4.5×10^{9} y	909 kg	3.35×10^{-4}	0.0
U-239	β	23.5 m	1.2	2×10^{-5}	0.0
Np-236	α	22 h (57%)	0.000034	5.5	0.0
Np-237	β	2.14×10^{6} y	175.	0.706	0.0
Np-238	β	2.10 d	0.112	224.	0.0
Np-239	β	2.35 d	179	310.	0.0
Pu-236	α	2.85 y	0.0046	5.04×10^{5}	0.0
Pu-238	α	89 y	246.	1.68×10^{4}	4.1
Pu-239	α	24,400 y	40.4 kg	61.38	2.5
Pu-240	α	6760 y	17.2 kg	221.	3.8
Pu-241	α	13 y	2.3 kg	1.13×10^{5}	260.0
Pu-242	α	379,000 y	1.2 kg	3.89	0.0
Pu-243	β	4.98 h	0.05	0.1	0.0
Am-241	α	458 y	176	3.25×10^{3}	0.6
Am-242	β,γ	16 h (81%)	0.064	0.6	0.0
Am-243	α	8000 y	96.5	1.85×10^{5}	17.9
Am-244	β,γ	26 m	0.014	2.7×10^{-5}	0.0
Cm-242	α	162.5 d	16.2	2.1×10^{6}	34.0
Cm-243	α	35 y	0.257	4.2×10^{4}	0.0
Cm-244	α	18.4 y	6.50	7.95×10^{4}	0.5

TABLE V

SHIELDING CRITERIA FOR FBR FUEL FABRICATION FACILITY

	Required* Lead (γ shielding) at 18 Inches from Source	Required* Polyethylene (Neutron shielding) at 18 Inches from Source
50 Liters $Pu(NO_3)_4$ Solution	0.35 in.	14 in.
Filtered $Pu(C_2O_4)_2$ Precipitate Bearing 10 kg Pu	0.34	6
Granulated UO_2-PuO_2 (2.0 gms/cc) Bearing 10 kg Pu	0.34	2
Sintered $(U, Pu)O_2$ Pellets (9.9 gms/cc) Bearing 10 kg Pu	0.30	2
Five Assembled Fuel Elements	0.24	12

*Requirements based on a dose rate of 3.3 mrem/hr at 18 inches.

TABLE VI

ISOTOPIC CONTRIBUTIONS TO RADIATION LEVELS DURING FUEL FABRICATION

Isotope	Gamma Dose Surface Rads/hr (% Contribution)	Neutron/sec Per Gram U + Pu (% Contribution)
U-232	2.%	.02%
Pu-236	0.2%	0.006%
Pu-238	46.%	11.%
Pu-239	10.%	7.%
Pu-240	20.%	74%
Pu-241	21.%	0%
Pu-242	0.1%	8%

TABLE VII

TRANSURANIUM ISOTOPES OF IMPORTANCE
TO FBR FUEL CYCLE COSTS

Consideration	Important Isotopes
Isotope Sales	Am-241, Am-243, Np-237, Cm-244, and Cm-242
Radiolytic Damage in Fuel Reprocessing	Pu-241, Cm-242, Am-243
Fuel Fabrication	Pu-240, Pu-238
Alpha-Emitter Radiological Safety	Pu-238, Pu-239, Pu-240, Pu-241

313-475 O-68—29

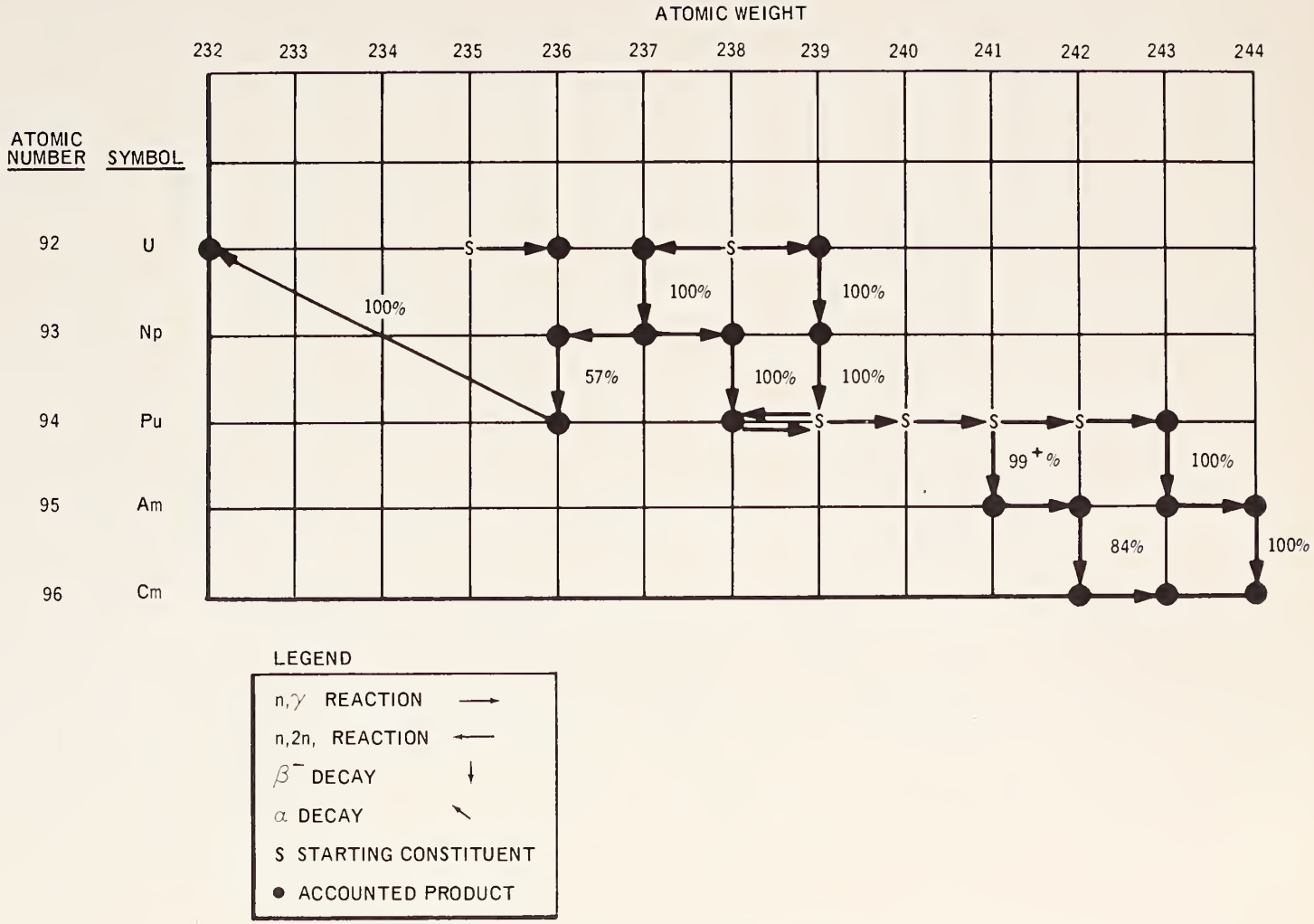

Figure I. Branches of Interest in FBR Fuel Burnup

Session D

MEASUREMENT AND ANALYSIS OF TOTAL AND PARTIAL CROSS SECTIONS FOR FISSILE AND FERTILE NUCLEI

Chairman

A. HEMMENDINGER
Los Alamos Scientific Laboratory

SECOND CONFERENCE ON NEUTRON CROSS SECTIONS
AND TECHNOLOGY (Washington, March 1968)

INVITED PAPER

MEASUREMENTS ON FISSILE NUCLEI: EXPERIMENTAL RESULTS AND INTERPRETATION

A. Michaudon

Centre d'Etudes Nucléaires de Saclay - France -

This paper presents some aspects of the interaction of resonance neutrons with fissile nuclei. This subject has been covered many times during the last few years on the occasion of several Conferences, for example :

- The Symposium on Physics and Chemistry of Fission (1965) [1]
- The International Conference on the Study of Nuclear Structure with Neutrons (1965) [2]
- The 1966 Washington Conference on Neutron Cross Section Technology [3]
- The 1966 Paris Conference on Nuclear Data [4]

The Proceedings of these 4 Conferences provide a wealth of detailed information as well as general surveys which will be used as a base for this presentation. In addition, we shall include, when it is possible, some recent results, even when they are not published yet.

For convenience, we have divided this paper into three parts :

- measurements on fissile nuclei ;
- analysis and interpretation of the data ;
- subthreshold fission .

1. NEUTRON CROSS SECTION MEASUREMENTS ON FISSILE NUCLEI

The measurements on fissile nuclei can be divided into two categories :

- neutron cross section measurements,
- measurements of certain properties of certain modes of decay (fission, for example) of the compound nucleus states.

The second class of measurements is interesting as it can provide a more thorough understanding of the fission process since each resonance has a well defined spin and parity. A study over several resonances can show up the average behaviour as well as fluctuations of certain properties of fission for one spin state and the way they differ from one spin state to another. In fact, as we shall see later, hardly any spin assignments have been made for the fissile nuclei except for Pu^{239}. For some of them, such as U^{233} and Pu^{241}, not a single spin has yet been determined. For these nuclei (U^{233}, Pu^{241}, etc...) the fission process has been studied in the resonances with the hope that it would be significantly different for the two spin states; if so, its properties may be used for the spin determination.

In this paragraph, we shall treat only the subject of neutron cross section measurements. The 2nd category of measurements will be considered in the next paragraph, while interpreting the data.

The slow neutron total cross section of a fissile nucleus is the sum of three partial cross sections :

- fission,
- radiative capture,
- elastic scattering.

Most of the intense neutron sources now available deliver narrow bursts of fast neutrons which are moderated to increase the neutron flux at low energy. In this case, the resolution is mainly determined by the slowing down time of the neutrons in the moderator and also by the angle between the normal to the moderator and the flight path, when it is not perpendicular to it.

There are neutron sources, where the duration of fast neutron production cannot be neglected, when compared to the moderation time. This happens, when there is a multiplication of the fast neutrons either with a booster of constant reactivity (Harwell) or with a pulsed reactor which is just below prompt criticality during the multiplication process (Dubna). For the first case, the relaxation time is about 100 ns (for a multiplying factor of 10), and for the second case the duration of the neutron burst is rather long ($\sim$4 μsec).

The time resolution of a nuclear explosion is limited mainly by the moderation time ; but in a manner which is different from the "classical" sources [8] . The fast neutrons are produced within 100 ns. The moderator is then submitted to a very high pressure and a very high temperature which lead to the following consequences :

- the neutron are thermalised at a rather high energy. The maxwellian distribution peaks at about 60 eV and it dominates the $\frac{1}{E}$ tail up to about 200 eV; this results in a very wide time distribution of the moderated neutrons, which has a FWHM of 3.8 μ sec.
- for energies above thermalisation, the moderation time is six times shorter than with a moderator at atmospheric pressure; this is due to its high compression.
- there is a cut off at about 25 eV in the low energy tail of the spectrum of the emitted neutrons since, the moderator is moving during the slowing down process.

These considerations will be useful when we examine the quality of some neutron cross section measurements.

Let us start with the total cross section which is the easiest to measure. Among the most recent total cross section measurements, is that of Pu^{239} carried out both at Harwell [9] and at Saclay [10 , 11] with 120 and 103 meter flight paths respectively. Though the flight path for the Harwell measurement is slightly longer than for Saclay's, yet the resolution is slightly better in the 2nd case (2.5 ns/m compared to 1 ns/m). This comes from the fact than a narrow burst of 50 ns has been used at Saclay, which is not possible at Harwell, as we have noticed above. In addition to this, the Saclay measurements have been performed on samples cooled down to the liquid nitrogen temperature to reduce the Doppler effect which, at low energy, is more important than the resolution. The advantage of reducing the Doppler width is illustrated in fig. 1; this resonance at 41.4 eV which is, in fact, a doublet, can be resolved only by cooling the sample.

In order to determine the resonance parameters of a fissile nucleus, at least two independent measurements must be performed. Together with the total cross section, the fission cross section is generally measured. With "classical" neutron sources (with the exclusion of nuclear explosions), the type of fission fragment detector which can be used depends strongly on the natural radioactivity of the element to be studied. When the natural radioactivity is not very high, as for U^{235}, for example, a classical ionisation chamber can be used. In a measurement performed at Geel [12] 3.4 g of U^{235} has been used in a multiplate ionisation chamber and still a larger amount can be put in such a detector. For nuclei of higher radioactivity, (U^{233}, Pu^{239}, Pu^{241}) α pile-up becomes very important and a faster detector is needed. The most frequently used is a gas scintillator. Measurements with a such a detector have been performed at Harwell [13] where the gas circulated through the cell which contained 40 mg of

Pu^{239}, and at Saclay [14] where the gas was kept in a sealed chamber which contained 300 mg of Pu^{239}. An even bigger detector has been constructed at Saclay with 1 g of Pu^{239}. [32]

A good detector for fissile nuclei having a large α activity is a spark chamber, which has an excellent discrimination against α rays, and which has been used for several measurements at Livermore [15] .

The quantity of fissile element used can be greatly increased by employing multiplate or multicell detectors without deteriorating the resolution due to the distance uncertainty, by recording separately the pulses coming from deposits having different flight path lengths. This technique is now feasible because of the large number of digits available in modern analysers.

With a nuclear explosion, the overwhelming intensity and the very short duration of the experiment permit measurements on very small and very radioactive elements [8] . The fission fragments are detected in a solid state detector, and they are produced with such an intensity that in place of the number of counts, the current in the detector is recorded as a function of the time of flight.

The fission cross section can also be measured by detecting the fission neutrons, assuming that the average number of fast neutrons, $\bar{\nu}$, emitted per fission is constant in the resonance region. The sensitivity of the detector to γ-rays can be reduced by using the pulse-shape discrimination technique [16] . With such an arrangement, the quantity of fissile element being used can be much larger than with the fission fragment detection system. However, when the sample is thick, multiple scattering corrections must be made.

The resolution of fission cross section measurements depends on the quantity of fissile element which can be used in the detector. With 300 mg of Pu^{239} the fission cross section of this nucleus has been measured at Saclay (flight path of 19 meters) with an overall resolution of 11 ns/m at 100 eV and 6 ns/m at 5 keV [14]. The figures 2, 3 and 4 show a comparison between this measurement and the one which has been carried out at Los Alamos with a flight path of 185 meters [17] . One can see that though the flight path is nearly ten times longer, the resolution of the Los Alamos experiment at 75 eV and 200 eV is not so good as the Saclay one. This illustrates the effect of the large moderation time of a nuclear explosion at these energies.

As the resolution of fission cross section measurements increases,

the Doppler effect becomes relatively more and more important. Till recently, not a single experiment had been performed on a cooled sample for this type of measurement. The difficulties associated with such a measurement have been overcome at Saclay where a measurement is being performed with a gas scintillator containing 1 g of Pu^{239} at the liquid nitrogen temperature. The scintillating gas is helium with a small admixture of nitrogen which acts as a wavelength shifter. The quantity of Pu^{239} is divided into 12 cells situated at three different flight path lengths. The pulses delivered by cells having different flight path lengths are recorded separately on a magnetic tape. Preliminary results obtained with a flight path of 50 meters and a nominal resolution of 1 ns/m are shown in figures 2, 3, 4. One can see an improvement compared to the results obtained previously. The results could be still better with linear accelerators, now under construction, which will be more powerful than the old Saclay machine. This comparison illustrates that for "classical" measurements, a linear accelerator can be as good, if not better, than a nuclear explosion.

Between resonances, the fission cross section measured with a nuclear explosion is much lower and can be determined with a better accuracy than with a "classical" neutron source. The most striking example is for Pu^{239} around 30 eV where the cross section, as measured by the Los Alamos group, is as low as 0.01 ± 0.01 barn. This is, because the background with a nuclear explosion is much lower since there is only one burst and therefore no neutron overlap. With a classical neutron source, the overlap of neutrons is reduced by the use of filters (B^{10} for example) which are not 100% efficient. The background is generally determined using the "black resonance" technique, which can bring about a systematic error, if the detector is sensitive not only to fission but also to the incident neutrons (this has been verified at Saclay with a gas scintillator). If this happens, the background is underestimated and the cross section, especially between resonances, is overestimated. In the low cross section region, it is probably safer to rely on the measurements made with a nuclear explosion.

The radiative capture cross section of a fissile nucleus is more difficult to measure, since the detector must be able to differenciate the γ-rays coming from radiative capture from those emitted during the fission process. Therefore, for a capture cross section measurement, also fission needs to be detected; this is why, usually, both the capture and the fission cross sections are measured simultaneously. Their ratio, $\alpha = \frac{\sigma \text{ capt}}{\sigma \text{ fis}}$, is of great importance for the design of fast reactors.

Several methods can be used to know whether a γ-ray pulse is

due to fission or radiative capture :

- one consists in using a large tank of liquid scintillator which detects all γ-rays emitted by the sample placed in a multiplate ionisation chamber at the center of the tank [18] . This technique has been used for U^{235} with an amount of fissile element as high as 7.65 g of U^3O^8. The pulses delivered by the tank in coïncidence with those of the fission chamber are due to fission. When they are in anticoïncidence, they are mainly due to radiative capture. Of course the separation between the two events is not so clear cut and some corrections must be made before. the capture and fission cross sections are actually obtained.
- in the technique used at Dubna [19] , the γ-rays are also detected in a large liquid scintillator, but it is loaded with cadmium in order to detect the fission neutrons which are captured after moderation in the liquid scintillator itself. The mean lifetime of a fast neutron sent into the detector is about 8 μ sec. A pulse from the detector followed by another pulse several μ sec after, is considered as being due to fission ; if not, it is supposed to be caused by a capture event. This technique works for low counting rates and a wide time resolution. Otherwise, the corrections become rather important.
- the Harwell group [20] uses a modified version of the Geel detector [21] which is itself derived from the system developped by Moxon and Rae [22] . This is a liquid scintillator divided into two parts by means of a specially shaped aluminium separator, each part being viewed by its own photomultiplier. A fission neutron is detected through a recoiled proton which, by pulse shape discrimination, can be distinguished from electrons produced by γ-ray interactions. For fission detection, each half of the detector works separately. A γ-ray event, on the contrary, gives electron pulses in both halves which are in coïncidence. Fig. 5 shows provisional results on α for Pu^{239} measured with this detector, together with the previous data obtained from other laboratories. The Harwell results confirm the rather high value of α in the keV region which was calculated before from the total and fission cross sections and which is of primary importance for the design of fast reactors.

At low energy, where the partial cross sections can be measured with a good resolution, the set consisting of capture and fission cross sections is better and more reliable than the one that includes the total and fission cross sections. At higher energy, in the unresolved resonance region, the first set is also preferable ; but between these two extremes ,

when one wants to increase the range of analysis of individual resonances, the 2nd set may prove superior because the total cross section is usually measured with a better resolution then any other partial cross section.

The elastic scattering cross section is generally obtained as a by-product from the total cross section. The potential scattering cross section, σ_p , is deduced from the value of the cross section in the valleys, taking into account the contribution of neighbouring resonances. The compound elastic scattering cross section can be calculated from the neutron widths of the resonances. Nevertheless, the measurement of the elastic scattering cross section can be very useful, in favourable cases, when determining the spins of the resonances. The area $\frac{\pi}{\Sigma} \sigma_0 \Gamma_n$ of a resonance observed in scattering , when combined with the parameters obtained from the analysis of transmission data, may lead to the value of the statistical factor g. Also resonance-resonance interference in scattering is much simpler to analyse than for the fission process since the scattering process has only one exit channel. Thus, this effect is free from the ambiguities which are associated with the fission process which may have more than one exit channel and for which two resonances having the same spin state may not interfere if their fission vectors are orthogonal in the space of the exit channels.

The scattering cross section is difficult to measure not only because of the γ -rays emitted by fission and by radiative capture, but also and mainly because of the fission neutrons. The smaller the ratio Γ_n/Γ_γ or Γ_n/Γ_f , the more difficult this measurement becomes. The contribution of unwanted radiations (γ -rays, fast neutrons) can be either eliminated or measured by different methods;

- in a now rather old measurement on Pu^{239}, Fraser and Schwartz [23] detected the scattered neutrons with a set of BF^3 proportional counters, practicaly insensitive to γ -rays, but sensitive to fast neutrons, whose contribution was evaluated by difference between two measurements : one with a B^4C sleeve between the sample and the detector, and the other without this sleeve.
- in a more recent experiment on U^{235} performed with the crystal spectrometer installed at the Belgian reactor BR2, Poortmans et al. [24] used proportional He^3 counters as a detector of scattered neutrons. This detector has also the advantage of being insensitive to γ -rays, but, in addition to this, fission neutrons give rise to pulses which are larger than those due to scattered neutrons. Their contribution can therefore be largely removed by a simple amplitude discrimination. On the other hand, this detector has a very poor time resolution which reduces its usefulness for time of flight experiments.

- at Harwell [25], the neutron scattering detector is a set of Li^6 glasses which is also sensitive to γ-rays and fast neutrons. In a measurement on Pu^{239}, the contribution of γ-rays is measured by a set of natural Li glasses and that of fast neutrons by a stylbene crystal. Therefore,there is a double correction to be made on the data before obtaining the actual scattering cross section.
- lastly, we should mention the "bright line" method in which the contribution of γ-rays and fast neutrons is removed with time of flight. This technique has been used in several laboratories, particularly at Livermore [26]. Nevertheless, it has a few disavandtages [27] which will not be considered here.

2. ANALYSIS AND INTERPRETATION OF THE DATA

The experimental results are analysed in order to obtain as much information as possible on resonance parameters of interest in nuclear physics (average values, statistical distributions, correlations, etc...) and also on parameters which can reproduce accurately the measured cross sections. This second aspect of the analysis is of particular importance for the design of reactors since, once accurate theoretical cross sections are obtained, they can be used to compute apparent cross sections, broadened by Doppler effect, at various temperatures. In that case, it is not necessary that the parameters used in the calculations should have any physical significance; the only important thing is that they should reproduce correctly the experimental results.

Nevertheless, this last kind of analysis is not completely satisfactory. First, experimental results are very often of interest in nuclear physics and must be exploited with the greatest care possible to extract the maximum of information on the interaction of slow neutrons with nuclei and especially on the fission process Secondly, this information may be useful, when calculating cross sections in energy ranges or for nuclei for which there are no measurements.

The interpretation of the results is guided by the A. Bohr theory [27] in which the properties of the fission process are determinated by transition states at the saddle point (large deformations) which have a spectrum similar to that of the first excitated states at equilibrium in the same compound nucleus (small deformations). When fission is induced by s-wave neutrons in an even-odd fissile nucleus of spin I and parity π, then the spin of the resonances(seen in the cross sections a function of energy) is either $J = I + \frac{1}{2}$ or $J = I - \frac{1}{2}$ with the same parity π as before. For each value of spin and parity there may be either one or several transition

states or exit channels available, completely or partially open.

Let us examine some properties of the fission process which, according to the theory of Bohr, may depend on the spin state of the resonances :

1) The average value of the fission width $\langle \Gamma_f \rangle_{J\pi}$:

For given spin and parity J^π there may be one or several exit channels i having fission barrier heights $E_{fi}^{J\pi}$. For each channel i, the mean partial fission width $\langle \Gamma_{fi} \rangle_{J\pi}$ is given by the Hill and Wheeler formula [28] :

$$2\pi \frac{\langle \Gamma_{fi} \rangle_{J^\pi}}{\langle D \rangle_{J^\pi}} = P_i = \left\{ 1 + \left[\exp\left[- 2\pi \left(\frac{E - E_{fi}^{J^\pi}}{\hbar\omega} \right) \right] \right] \right\}^{-1} \quad (1)$$

in which :

$\langle D \rangle_{J\pi}$ is the average spacing of resonances having spin and parity J^π
P_i is the penetration factor for the channel
E is the excitation energy of the compound nucleus,
$\hbar\omega$ is the circular frequency of the inverted harmonic oscillator which describes the shape of the fission barrier ($\hbar\omega \sim 500$ keV).

For all the channels i belonging to the same J^π, the average value of the total fission width $\langle \Gamma_f \rangle_{J\pi}$ is given by the relation :

$$2\pi \frac{\langle \Gamma_f \rangle_{J^\pi}}{\langle D \rangle_{J^\pi}} = \sum_i P_i = N_{eff} \quad (2)$$

N_{eff} is the effective number of channels. It is equal to the number of exit channels when all of them are completely open ($P_i = 1$ for all i's).

2) Fluctuations of the fission widths :

When the number of exit channels is ν and when the partial fission width $\langle \Gamma_{fi} \rangle_{J\pi}$ is the same for all the channels i, then the distribution of the total fission widths Γ_f obeys the classical χ^2 law P_ν with ν degrees of freedom. The variance of such a distribution is $2/\nu$, which shows that the distribution becomes narrower as ν increases.

This case happens either when there is only one single channel open ($\nu = 1$) whatever the height of the fission barrier $E_{fi}^{J\pi}$ may be, or when there are several exit channels with equal values of E_{fi} (equal values of P_i).

In most cases, when the spin J is associated with several exit channels, each one having a different value of P_i, then the distribution P_ν defined above is no longer valid. If the total fission width Γ_f is the sum of ν partial widths Γ_{f_i}, then the apparent value, ν_{app} of the total fission width distribution will be smaller than ν ($\nu_{app} < \nu$). The value of N_{eff} will also be smaller than ν ($N_{eff} < \nu$)

The study of the fluctuations of the fission widths belonging to different spin states is even more complicated.

3) Mass distribution of the fission fragments :

This mass distribution is very asymmetric for fission induced by slow neutrons. Nevertheless, the amount of asymmetry, or more exactly the peak to valley ratio of the distribution, may depend on the fission channel which is considered. As we consider transition states of collective character only, fission through states belonging to quadrupole vibration bands is expected to be more symmetric than through octupole vibration ones.

Some of other properties of the fission process related to the mass distribution of the fission fragments are :

4) Kinetic energy of the fission fragments : this is smaller for symmetric than for asymmetric fission.

5) Mean number of neutrons $\bar{\nu}$ emitted per fission : this is more important for symmetric than for asymmetric fission.

6) The probability of emission and the spectrum of long range α particles.

Vandenbosch [29] has proposed a model of the fissioning nucleus at scission which explains when and how the properties 3) to 6) are correlated. A complete discussion of this model would be beyond the scope of this paper.

7) Fission fragment anisotropy when fission is induced by non polarized neutrons in aligned nuclei :

J. W. T. Dabbs has shown that such an anisotropy occurs for U^{235} aligned using the crystal $UO_2Rb(NO_3)_3$ cooled to very low temperature [30]. Under these conditions, the anisotropy of the fission fragments is opposite to that of the α-rays emitted by natural radioactivity. The amount of anisotropy may be defined by the coefficient A_2/T (T is the absolute temperature of the sample) of the 2nd order Legendre polynomial which describes the angular distributions of the fission fragments. The coefficient A_2 has been calculated by J. W. T. Dabbs in the case of U^{233} and U^{235} for the spins and exit channels which can be reached in these nuclei by " S " wave neutrons (Table I, fig. 6). This coefficient can have widely different ....

values, but it depends more on the channel (here, the channel is defined by the quantum number K) than on the spin J. This is a general statement that the properties of the fission process depend more on the channels that on the spins. They depend on the spins if the exit channels for the two spins have different properties.

The spins of neutron resonances in fissile nuclei are not well known. For some of them, such as U^{233} ou Pu^{241}, not a single resonance spin has been determined.

The complete subject of spin determination of resonances in fissile nuclei has been treated in detail at the Paris Conference [31] : therefore, there is no need to cover this subject again in the present paper.

We shall now examine in detail the available data, we have, on two very different nuclei : U^{235} and Pu^{239} which are, by far, the best known up to now. Pu^{241} has been discussed in detail by M.S. Moore at the last Washington Conference [7] . As for U^{233}, despite the fission cross section measured by the Los Alamos group [33] it is not well known yet and its resonance structure is so complicated that it is difficult to interpret.

2.1. U^{235}

Its spin is 7/2 and its parity is negative. Therefore "s" wave neutrons induce 3^- and 4^- resonances. At the saddle point, transition states of the same spin and parity are found in octupole collective excitations having K = 0 (3^- state only) or K = 1 and K = 2 (for both 3^- and 4^- states). One expects that the K = 0 band should be lower in energy than the two other ones.

For quite a long time, the lowest threshold for fission was thought to be 0.6 MeV below the neutron binding energy,for it was at this energy that the threshold of the reaction U^{235} (d , pf) was observed [34] . At the Salzburg Conference, D. Eccleshall and M.J.L. Yates [35] reported their results on the reaction U^{234} (t, pf). Although the same compound nucleus is excited in both reactions, the lowest threshold for fission was by 0.5 MeV lower than the first one. According to the results of the (t, pf) reaction, the lowest fission threshold in the compound nucleus U^{236} lies about 1 MeV below the neutron binding energy.

This discrepancy has been explained by M.J. Specht et al [36] who measured and analysed the fission fragment anisotropy in the reaction U^{235}(d, pf). They demonstrated that the mechanism of the (d, pf) reaction excites preferably negative parity states and, therefore, octupole bands in

the compound nucleus U^{236}. According to this hypothesis, the fission threshold which lies at - 0.6 MeV (relative to the neutron binding energy) would not be of the ground state, but of the lowest octupole band (presumably K = 0). We recall that the K = 0 band contains the 3^- state; but not the 4^- one, in contradiction to the K = 1 and K = 2 bands which contain both. No information is available on the energies of these last two bands.

The most recent results on resonances observed in the fission cross section of U^{235} have been obtained at BCMN (Euratom, Geel) where the measurements have been carried out with two different detectors and a flight path of 60 meters for both of them [12]. The analysis of this cross section, with the Breit-Wigner single level formalism, combined with the Saclay results on transmission [37, 38], leads to the value of Γ_f for 78 resonances below 150 eV. The distribution of these fission widths is shown in fig. 7; it is consistent with the distribution of a χ^2 family having ν = 4 degrees of freedom. There is no evidence of a break in the experimental distribution which could suggest the existence of two families having different values of the mean fission width.

The average value of those 78 fission widths is :

$$\langle \Gamma_f \rangle = 53 \text{ meV} \qquad (3)$$

Those results, though performed on a larger number of resonances in fission, are nevertheless in excellent agreement with the previous Saclay results [37, 38]. The value of N_{eff} deduced from this average fission width is :

$$N_{eff} = 2\pi \frac{\langle \Gamma_f \rangle}{\langle D \rangle} = 0.3 \qquad (4)$$

Such a low value of N_{eff} would imply that subthreshold fission plays an important part in the slow neutron induced fission of U^{235}.

In fact, the estimation of the average fission width derived from resonance analysis may be at fault due to the following reasons :

- among the resonances which are actually observed, only a limited number of them can be fully analysed (less than half), the others appear in complicated structures where they are difficult to locate and a fortiori to analyse.
- it has been demonstrated that about 20% of the resonances are not visible at all in U^{235} cross section even with excellent resolution [39]. Those resonances which are systematically missed have small neutron widths and correspond to small level spacings.

The resonances which are not included in the statistics for the two reasons mentioned above, have certainly a mean fission width larger than that of the ones analysed. The average fission width which is calculated from the analysis of individual resonances (formula 3) is therefore underestimated. Also, if some broad resonances, as one of those which are probably missed, are included in the distribution shown in fig. 7, then the apparent value of ν may be decreased by a large factor. The effect of quasi-resonances will be discussed in paragraph II.3.

There are very few resonances for which the spin has been determined. Two methods have been used up to now :

- transmission of polarised neutrons though samples of polarised U^{235} nuclei [40]. Using this method, V. Sailor has shown that the resonances at 0.29 eV and 1.14 eV are of different spin states and that the one at 2.03 eV is probably of the same spin state as the first one. Though absolute values of the spins must be confirmed, it seems that the resonance at 0.29 eV (and perhaps the one at 2.03 eV) has spin 3 , while the one at 1.14 eV, has spin 4 (table II, fig. 8).
- measurement of the elastic scattering cross section. It is particularly difficult to interpret in the case of U^{235}. This is due to the low values of both the neutron widths and the level spacings and also to the fact that the two possible values of g are very close to each other ($g_1 = 7/16$ and $g_2 = 9/16$) and therefore hard to distinguish. Despite these difficulties, the measurement has been carried out and analysed at Mol [24] and the spins of the resonances at 8.8 eV and 12.4 eV have been determined (table II, fig. 8).

Now we have at our disposal only 5 resonances with some information about their spins (we have already mentioned the ambiguity associated with 3 of them), we can have a rough estimate of the mean fission width for the two spin states :

$$\langle \Gamma_f \rangle = 64 \text{ meV} \quad \text{for } J = 3 \qquad (5)$$

$$\langle \Gamma_f \rangle = 70 \text{ meV} \quad \text{for } J = 4 \qquad (6)$$

The mean fission width does not seem to vary much from one spin state to another.

The peak-to-valley ratio of the mass distribution of the fission fragments in the resonances has been measured twice by Cowan et al. using a nuclear explosion as a pulsed neutron source [41] . The ratio of the activities of Ag^{111} relative to Mo^{99} has been obtained for 17 resonances from 8.8 eV to 40 eV, for which it shows variations ranging from + 22% to - 50% when compared to thermal neutron fission. From the

values of this ratio, it is possible to separate the resonances into two groups : 4 in the 1st group (higher value of the ratio Ag^{111}/Mo^{99}) and 13 in the second one. The mean fission widths for these two groups are also very close ($\langle \Gamma_f \rangle$ = 63 meV for the 1st group and $\langle \Gamma_f \rangle$ = 52 meV for the second one.)

As we have seen before, such a grouping will exist if the properties of the exit channels are different. It may correspond to the two spin states if the exit channels which are different in properties, have also different spin states.

In the case of U^{235}, the state 3^- is found in the 3 exit channels K : 0, 1 and 2; while the state 4^- only in the last two channels (K = 1 and 2) Therefore, properties that are different for the 2 spin states will occur if the K = 0 band is different from the two other ones.

In the case of the peak-to-valley ratio of the mass distribution of the fission fragments, the nearly constant value of $\langle \Gamma_f \rangle$ for the two groups would mean that the 3 octupole bands are very close in energy.

There is another method to determine the spins of the resonances which has been used several times for non-fissile nuclei [42] . The method consists in studying the multiplicity of the capture γ-rays emitted in the resonances. In favourable cases, this multiplicity is sufficiently different for the two spin states that it can be measured and used for spin determinations. In actual practice, one uses two NaI (Tl) crystals facing each other with the sample placed in between them, and one records separately the following two counting rates : one given by pulses above a bias of about 3 MeV (singles) and the second given by coincidence between pulses above a lower bias (500 KeV to 1 MeV) in the two crystals (coincidences). The greater the multiplicity, the higher the ratio R of the "coincidences" compared to the "singles".

This method was never applied to fissile elements because of the background and of the effects of radiation emitted during fission (γ-rays and fast neutrons). Nevertheless, an attempt has been made at Saclay on U^{235} [43] . Since the bulk of fission γ-rays have an energy lower than 1 MeV [44] an effort was made to minimise their contribution by setting appropriate biases : about 4.5 MeV for the "singles" and about 1.1 MeV for the "coincidences". The measurement was therefore carried out as for a non fissile element, but interposing about 1 cm of lead between the sample of U^{235} and the crystals. The ratio R defined above is plotted in fig. 9 for 24 resonances. There is clearly a separation of the resonances into two groups which can tentatively be explained as due to the two spin states.

The group with the higher value of R would correspond to the spin 4. With this assumption, there is agreement with the spin values determined by Poortmans (Table II, fig. 8, réf. 24).

The mean values of the fission widths for the resonances of these two groups are :

High value of R (spin 4 ?) $\langle \Gamma_f \rangle = 27.2$ meV (7)
Low value of R (spin 3 ?) $\langle \Gamma_f \rangle = 66.7$ meV (8)

The ratio of these two mean fission widths is 2.45 in good agreement with theoretical predictions [6] . But on the other hand, the absolute value of the average fission width is still lower than the one calculated from the channel theory of fission. If, according to J.E. Lynn [6] the average value of N_{eff} for the two spin states is 1.5, the mean fission width should be 260 meV.

Can the levels which remain unanalysed explain this large discrepancy ?

One method can be used to take into account all the resonances, analysed as well as not analysed ones. Its consists in averaging the cross sections over energy intervals wide enough to include many resonances. For instance, the measurements of G. de Saussure [46] of the ratio of capture to fission cross sections ($\alpha = \sigma_{capt.}/\sigma_{fis.}$) show that the value of α is around 0.5 at low energy (fig. 10).

To obtain such a low value of α , J.E. Lynn [6] has proposed a scheme of the transition states in which there are 2 fully open channels for the spin 3^- and one for the spin 4^- . This leads to an average value of N_{eff} for the 2 spin states which is equal to 1.5 and therefore to the value $\langle \Gamma_f \rangle = 265$ meV, as already mentioned above. It is to be noted that the ratio $\langle \Gamma_\gamma \rangle / \langle \Gamma_f \rangle$, in that case, is 0.17, much lower than the observed value $\alpha = 0.5$. This is ignoring the effect of fluctuations of the widths, already noticed a long time ago [47] , which plays an important part when calculating average cross sections. To be more specific, one needs to know the quantities $\left\langle \frac{\Gamma_n \Gamma_\gamma}{\Gamma} \right\rangle$ and $\left\langle \frac{\Gamma_n \Gamma_f}{\Gamma} \right\rangle$ to calculate the average capture and fission cross sections, respectively. The quantities between the brackets can be written as follows :

$$\left\langle \frac{\Gamma_n \Gamma_\gamma}{\Gamma} \right\rangle = S_c \quad \frac{\langle \Gamma_n \rangle \langle \Gamma_\gamma \rangle}{\langle \Gamma \rangle} \tag{9}$$

$$\left\langle \frac{\Gamma_n \Gamma_f}{\Gamma} \right\rangle = S_f \quad \frac{\langle \Gamma_n \rangle \langle \Gamma_f \rangle}{\langle \Gamma \rangle} \tag{10}$$

In the absence of correlations, the statistical factors S_c and S_f can be calculated, knowing the distributions for the widths Γ_n, Γ_f and Γ_γ. The factor S_f is slightly lower then unity, but the other factor S_c can have values much high than unity (as high as 2 or even 3) for large fission widths and low values of ν.

The high values of $\langle \Gamma_f \rangle$ needed to obtain $\alpha = 0.5$, cannot explain the behaviour of the cross sections in the resonance region. We have already noticed the big discrepancy between $\langle \Gamma_f \rangle = 265$ meV (calculated from α) and $\langle \Gamma_f \rangle = 53$ meV (formula 3) obtained from resonance analysis even if this last value is underestimed, as we discussed previously.

Even the simulated cross sections calculated by J.E. Lynn [45] are not satisfactory in that respect. For example the observed values of N_{eff} and ν deduced from the simulated cross sections are 0.53 (instead of 0.3 deduced from experiments) and 2.7 (instead of 4) respectively. In addition, the proportion of missed levels in the calculated cross sections is certainly larger than 20%, as deduced from measurements. The proposed explanation according to wnich the resonances at low energy would be an extreme statistical sample is not as strong as before, since G. de Saussure's measurements have shown that the value of α below 100 eV is very close to other values measured at higher energy.

Therefore, it seems that there is a disagrement between the average value of α on one side and the behaviour of the cross sections at low energy, on the other. The disagrement may be apparent only, if one notices that the calculations of α (either with the S_c and S_f factors or with simulated cross sections) have been made with the hypothesis that all the parameters are completely independent, that is to say, in the absence of correlations. Yet, correlations have been found in the cross sections [48, 37, 38] which, in this respect, are worth a further study. This question will be raised again in paragraph III.

Several measurements on the kinetic energy of the fission fragments [49] and on ternary fission [49, 50] showed variations from resonance to resonance. The Saclay results on ternary fission [50] seem to be confirmed by recent measurements carried out with the Euratom linac at Geel [51].

Lastly, fission fragment anisotropy measurements with non-polarised neutron beams and aligned U^{235} nuclei have been reported by Dabbs [30] and they are shown in fig. 11. It is worth noticing that, nowhere, the value K = 0 is reached, though this band, which is supposed to be the lowest in energy, should give the highest contribution to the fission cross section. Also, the two spin 3 resonances studied by Dabbs have either K = 2 (at 0.29 eV) or K = 1 (at 8.8 eV) [52], but clearly not K = 0 alone.

This measurement is now being performed at the Saclay linac, with the same equipment, in order to determine the average value of K for a larger number of resonances and also for clusters of unresolved resonances which are probably broader than the average and in which, according to currently accepted channel theory, the value K = 0 would have a larger probability to be found. It can be noticed in table I, fig. 6, that the band K = 0 corresponds to the largest anisotropy and therefore does not need any knowledge about the spins. Preliminary measurements with a flight path of 5 meters, showed that the counting rate in the big 19.3 eV resonance is about 500 counts per hour. [80]

2.2 Pu^{239}

Its spin is 1/2 and its parity is positive. Therefore "S" wave neutrons induce 0^+ and 1^+ resonances. At the saddle point, 0^+ transition states of simple collective character are found in the ground state and in the quadrupole β vibration (which is often excluded from the scheme of transition states as this mode is supposed to lead to fission). There are no 1^+ transition states of simple collective character.

The lowest threshold observed in the reaction Pu^{239} (d, pf) lies at - 1.6 MeV (relative to the neutron binding energy). According to H. Specht [36], this is certainly the lowest threshold corresponding to the ground state 0^+, since the mechanism of the reaction excites predominantly positive parity levels in the compound nucleus Pu^{240} (and not negative parity one as with U^{235}).

The measurement and the analysis of fission fragment anisotropy in this reaction, carried out by Britt et al [53] have shown that, at the saddle point, the 2 quasi-particule states are 2.6 MeV above the ground state, that is to say 1 MeV above the neutron binding energy. Therefore, their contribution to fission is negligible.

The total and fission cross sections have been measured and analysed with the Breit Wigner single level formalism [54]. The fission width has been determined for nearly one hundred resonances below 250 eV. The distribution of these fission widths is shown in fig. 12. It is clear that there is a break in the distribution which can be fitted with the sum of 2 distributions having the following properties :

Family of narrow resonances : $\langle \Gamma_f \rangle = 41$ meV , $\nu = 1$ (11)

Family of wide resonances : $\langle \Gamma_f \rangle = 1.5$ eV , $1 \leq \nu < 2$ (12)

Examples of wide resonances appearing in the total cross section are shown in fig. 13 and fig. 14.

The spin determination of Pu^{239} resonances is not so difficult as for U^{235} [31] . Among the most recent results, let us recall elastic scattering measurements carried out at Harwell [25] and at Livermore [26] . When combined with transmission data, these results can be used to determine the spins of a fairly large number of resonances. We can notice that the analysis of both the total and fission cross sections can also be used to determine the spins of several resonances [31, 54] . The known spins of Pu^{239} resonances are displayed in table III, fig. 15. Generally, the recent measurements (columns 4, 5 and 7 of the table) agree quite well. If we confine ourselves to the results of Asghar, which are the most complete, the mean fission widths for the two spin states are :

$$\text{spin } 1^+ : \langle \Gamma_f \rangle = 30 \text{ meV} \tag{13}$$

$$\text{spin } 0^+ : \langle \Gamma_f \rangle = 425 \text{ meV} \tag{14}$$

They are different, and the difference noticed here is certainly underestimated if we remark that large spin 0 resonances are more difficult to analyse and that the largest of them are certainly not analysed in the scattering measurements.

The mass distribution of the fission fragments in Pu^{239} resonances has been measured by Cowan et al [56] in the same manner as for U^{235}. There are much larger variations of the peak-to-valley ratio of the mass distribution for Pu^{239} than for U^{235}. With these variations, it is very easy to split the resonances into two groups; the one having the highest amount of symmetric fission is expected to belong to the 0^+ state, the other to the 1^+ state. With this assumption, the results obtained by Cowan are shown in table III, fig. 15 (column 6). They agree quite well with direct spin 1 determinations, except for the resonance at 47.6 eV. The discrepancy at 59.22 eV may be apparent only, since at this energy, there is a cluster of poorly resolved resonances and the contribution of neighbouring resonances (particularly the large one at 60.94 eV) is perhaps not correctly evaluated. It is not possible to verify the results of Cowan with direct spin 0 determinations. Nevertheless, it is worth noticing that the mean fission width of spin 0 resonances (as determined by Cowan) is very high ($\langle \Gamma_f \rangle = 1.75$ eV) and is in excellent agreement with the value found using formula 12.

Therefore, the three types of results considered until now, namely :

- distribution of the fission widths,
- direct determination of the spins of the resonances,
- mass distribution of fission fragments

lead to the conclusion that there exist two families of resonances in Pu^{239}:

one, having $J = 1^+$, $\langle \Gamma_f \rangle = 41$ meV and $\nu = 1$ (15)

the other, having $J = 0^+$, $\langle \Gamma_f \rangle = 1.5$ eV and $1 < \nu < 2$ (16)

The effective numbers of channels for these two families are :

$N_{eff} = 0.08$ for $J = 1^+$ (17)

$N_{eff} \sim 1$ for $J = 0^+$ (18)

The 2nd value of N_{eff} is in agreement with the channel theory, in which one channel is fully open, and perhaps a 2nd one is partially open.

The 1st value of N_{eff} can be used to calculate the energy of the 1^+ channel with the help of formula 1 . Assuming that $\hbar\omega = 0.5$ MeV, one finds :

$$E_{1^+} - E_B = 0.2 \text{ MeV} \quad (19)$$

E_{1^+} is the energy of the 1^+ channel,

E_B is the neutron binding energy.

A similar result is obtained when fitting the variation of α as a function of energy between 15 KeV and 100 KeV [57] as measured by Lottin et al. [58] .

If, according to Britt et al. [53] , 2 quasi-particule states are 1 MeV above E_B , then the 1^+ channel does not belong to this category of states. This is why Griffin has postulated that this 1^+ state is a combination of two octupole vibrations ($K = 0^-$ and $K = 1^-$) which may be lower in energy [59] . With this hypothesis, the exit channels for the two spin states are very different: ground state and perhaps quadrupole vibrations for $J = 0^+$, and octupole vibrations for $J = 1^+$. This explains why the properties of the fission process (such as the mass distribution of the fission fragments) which depend mainly on the exit channels, can be so different for the two spin states in Pu^{239} (which is not the case for U^{235}).

Melkonian has measured the total kinetic energy of the fission fragments and has found variations which are also correlated with the spins of the resonances [49] .

Up to now we have considered only the single-level analysis of the cross sections. This type of analysis is certainly valid for the narrow spin 1^+ resonances : but it must be used with caution for the large spin 0 resonances. Derrien has already pointed out the interest in using the multilevel formalism for the study of complex structures such as the one around 83 eV [54] . A multilevel analysis of this structure has been carried out at Harwell [60] and the result is shown in fig. 16. In order to fit the fission cross section, 5 resonances are needed with the multilevel formalism instead of 6 with the single level one [54] ; but, with the former, 2 exit channels for the spin 0 resonances need to be used.

A multilevel analysis over a much wider energy internal (between 14 and 90 eV) has been carried out by Farrell [61] on the fission cross section measured with a nuclear explosion as the neutron source. This analysis will certainly be presented with more details by Farrell in his invited paper [62] . Nevertheless, a few points may be worth considering :

- in the same structure at 83 eV, a good fit is obtained with 5 resonances also, but the two spin 0 resonances have only one exit channel, the same for both of them; this is in contradiction with the Harwell multilevel fit .
- throughout the whole energy range, from 14 eV to 90 eV, there are 15 spin 0 resonances and 3 of them only have their fission width in the 2nd exit channel. Among those three resonances, the one at 77.80 eV is not actually observed, and the other at 66.75 eV has been wrongly attributed to Pu^{239} [54] . At this energy, there is a Pu^{240} resonance which perturbed the total cross section and also the fission cross section when measured with a fairly thick sample [63] . To increase the confusion at this energy, there is an unusual long tail of the nearby 65.7 eV resonance and, lastly, the Los Alamos measurements are also perturbed by an impurity resonance due to the Pt used as a backing foil [64] .
- from the number of spin 1 resonances and the distribution of their spacings, Farrell has estimated that 30% of them, at least, are missed, which would have small fission widths but not necessarily small neutron widths. This is very unlikely to appear for the following reasons : they cannot be missed because they are close to the observed spin 1 resonances since this is preluded by level repulsion; they cannot be missed because they are close to large spin 0 resonances or because they are distributed at random since, as they would be narrow and not necessarily have small neutron widths, they should show up in transmission if not in fission, but this is not observed in the experimental results. Below 250 eV, only 3 resonances are seen in transmission and not in fission and it is because they have small neutron widths [54]
  Let us recall, in this respect, that the smallest fission width observed, even in the most recent Saclay measurements, is 3 meV which corresponds remarkably well to the theoretical calculations of the width due to the (n, γ_f) process [65] which, in all these measurements, is counted with the simple (n, f) reactions.

In favourable cases, as Pu^{239}, where the proportion of missed levels is small, where the observed resonances easily break up into two families having different spins and different values of the average fission width, where many spins have been measured directly and where the resonances

are rather well separated, we have seen the difficulties associated with the interpretation of multilevel fits which cannot be considered as unique.

The situation is less favourable for U^{235}. Since 20% of the levels are missed an assymmetry in the shape of a resonance can be explained by a hidden level as well as by an interference effect. This renders multilevel fits still more ambiguous. For example, Vogt [66] and Shore et al. [67] from a multilevel fit on a restricted energy range have assigned spins for the first U^{235} resonances. They were found later to be in contradiction with polarisation measurements [40].

The situation for U^{233} and Pu^{241} is still worse. In these nuclei, level overlap is so important that 30% or more of the resonances are missed and not a single spin has been determined yet. Therefore the interpretation of multilevel fits is hypothetical. They can probably reproduce the measured cross sections, but the physical significance of the parameters is rather illusory.

2.3. QUASI RESONANCES

The first quasi-resonance appeared in the 1st run of a computer when Lynn carried out calculations of simulated cross sections of U^{233} [68]. Strong interference between two closely spaced broad resonances caused a very sharp peak to appear which was called a quasi-resonance. In the same article, simulated cross sections of U^{233} (calculated with simple hypotheses coming from channel theory) showed how their analysis could lead to erroneous statistical distributions of the parameters. But if we still take the case of U^{233}, it is not clear what the main distorting effect is : simple resonance overlap or interference which, in extreme situations, can give rive to quasi-resonances.

Prior to Lynn's calculations, simulated cross sections of U^{235} had been carried out at Saclay to verify the proportion of missed levels determined from cross section measurements [37-38]. But the interference effect, expected to be of small importance had been neglected. This simplification is based on a simple calculation which shows that, among the 20% of missed levels, only 7% of them are of the same spin state as that of the close-by levels which hide them. This small proportion is simply due to the repulsion of levels having the same spin and parity.

It is interesting to know more about the importance of missed levels relative to interference. This is the reason, why we carried out calculations of simulated cross sections with exactly the same parameters as those used by Lynn for U^{233} [68] but with a different set of random numbers. In particular, the effective number of exit channels was

N_{eff} = 3 x 1 for one spin state and N_{eff} = 1 + 2 x 0.1 = 1.2 for the other. The simulated total and fission cross sections have been calculated between 0 and 25 eV (that is to say for 100 resonances) in two cases : with and without interference. In the 2nd case, the cross sections reduce to a sum of Breit-Wigner single-level formulas. The cross sections are very similar in both cases which demonstrates that interference plays a small part in that particular case. A fortiori, no quasi-resonances are observed. Therefore one is led to the conclusion that the difference between the parameters which are used in the calculations and those which come from resonance analysis is due, not to interference, but to the common-place effect of resonance overlap.

Another example, where interference is expected to be rather important, is that of spin 0 resonances in Pu^{239}. In the same manner as for U^{235}, the total and the fission cross sections of Pu^{239} have been simulated from 0 to 250 eV. The fission width distribution has been chosen equal to that described in formulas (15) and (16). For the spin 0 resonances, the calculations have been made both with $\nu = 1$ and $\nu = 2$. Not a single quasi-resonance has been observed in these simulated cross sections.

The probability of observing a quasi-resonance can be estimated by calculating the probability P that the sum of the fission widths of neighbouring resonances of same spin and parity is greater than k times their spacing ($\Gamma_{f_1} + \Gamma_{f_2} > k D$) [45] .

$$P_1(x) = 1 - x\sqrt{\pi}\ \exp(x^2)\left[1 - \theta(x)\right] \tag{20}$$

$$P_1(x) \xrightarrow[x \to \infty]{} \frac{1}{2x^2}\left[1 - \frac{3}{2x^2} + \frac{15}{4x^4} \cdots\right] \tag{21}$$

$$P_2(x) = 1 - 8x^2\, P_1(2x) \tag{22}$$

$$P_2(x) \xrightarrow[x \to \infty]{} \frac{3}{8x^2}\left[1 - \frac{5}{8x^2} + \cdots\cdots\right] \tag{23}$$

In these formulas :

P_1 is the probability defined above when the fission width distribution obeys a χ^2 law having $\nu = 1$ degree of freedom;

P_2 is defined in the same way as P_1, but for $\nu = 2$;

$$x = \frac{k}{\sqrt{\pi}}\ \frac{\langle D \rangle}{\langle \Gamma_f \rangle}\ ; \tag{24}$$

$\langle D \rangle$ is the mean level spacing of the resonances for the spin state considered;

$\langle \Gamma_f \rangle$ is the mean fission width for the same set of resonances;

$\theta(x)$ is defined as $\theta(x) = \frac{2}{\sqrt{\pi}} \int_0^x e^{-t^2} dt$ (25)

In table IV, fig. 17, the probabilities are calculated for the spin 0 resonances of Pu^{239} with $\kappa = 1$ and $k = 2$. Together with P, the probability Q that the criterion $\Gamma_{f_1} + \Gamma_{f_2} > k D$ is not fulfilled for the spin 0 resonances below 250 eV, has been calculated.

The values of Q in table IV, show that the criterion $\Gamma_{f_1} + \Gamma_{f_2} > D$ is certainly too severe when calculating the probability of observing quasi-resonances. The criterion $\Gamma_{f_1} + \Gamma_{f_2} > 2 D$ would probably be more appropriate. With this last condition, the probability of observing a spin 0 quasi-resonance in Pu^{239} is 3% at the most.

Let us try now to study the quasi-resonance phenomenon in a more general way, even for high values of N_{eff} which are not met in actual practice [57] . To be more specific, let us take the case of one spin (J) sequence only, so that the overlap between resonances having different spins is ignored. This simplification will not alter the effect of interference since resonances having different spins do not interfere. For the single spin sequence under study, let us assume that there are ν fission exit channels which are fully open. Then N_{eff} is equal to :

$$N_{eff} = \nu = 2\pi \frac{\langle \Gamma_f \rangle}{\langle D \rangle} \qquad (26)$$

For large values of N_{eff}, interference will distort the shape of the resonances and some of them will be missed. The apparent values of the mean fission width ($\langle \Gamma_f \rangle_{app}$) and of the average level spacing ($\langle D \rangle_{app}$) can be used to calculate the apparent value of the effective number of exit channels ($(N_{eff})_{app}$).

$$(N_{eff})_{app} = 2\pi \frac{\langle \Gamma_f \rangle_{app}}{\langle D \rangle_{app}} \qquad (27)$$

For small values of N_{eff}, interference plays a negligible part and N_{eff} is very close to $(N_{eff})_{app}$. But as the value of N_{eff} increases, two opposite effects appear at the same time. First, as the resonances become broader, their overlap is greater and interference effect should increase; secondly, the number ν of exit channels increases (in this simplified case, we have assumed $\nu = N_{eff}$) and this should diminish the effect of interference.

In order to know what the final result is, we have calculated a set of simulated cross sections from parameters selected at random but obeying the known statistical distributions [57] . For each cross section, there was a well defined value of N_{eff}. The parameters used in the calculations have been determined with the following hypotheses :

- all the resonances have the same spin, therefore, the level spacing distribution obeys the Wigner law. The average level spacing is set arbitrarily equal to 1 eV.
- the neutron width distribution obeys the Porter-Thomas law.
- the strength function is equal to 10^{-4}. This value is obtained experimentally for most of the fissile nuclei.
- the total radiation width is small (Γ_γ = 1 meV)
- the average fission width is equal to $\langle \Gamma_f \rangle = N_{eff} \langle D \rangle / 2\pi$
- the fission width distribution obeys a χ^2 law having N_{eff} degrees of freedom
- the number of dimensions ν of the exit channel space should be equal to N_{eff}. But the computer code used in the calculations cannot treat the case of a channel space having more than three dimensions. This limitation in the capacity of the code led to the following conditions for the calculations :

$$\nu = N_{eff} \quad \text{when } N_{eff} \leq 3 \tag{28}$$

$$\nu = 3 \quad \text{when } N_{eff} > 3 \tag{29}$$

These conditions exagerate the effect of interference for values of N_{eff} greater than 3.

The calculations have been carried out with and without the interference effect included, using 10 different values of N_{eff} ranging from 1 to 50. The cross sections with interference effect included have been calculated using the formalism of Vogt [66] . Without interference, the cross section reduces to a sum of Breit-Wigner single level formulas.

In fig. 18, the total cross section, calculated without interference in the extreme case of N_{eff} = 50, is displayed. Only a few "bumps" show up where there are as many as fifty levels to start with. When the same parameters are used to compute the cross section with interference, then, many quasi-resonances appear as can be seen in fig. 19.

Each of these cross sections (with and without interference) has been analysed with the single-level formalism.

The variation of $(N_{eff})_{app}$ as a function of N_{eff} is plotted in fig. 20 for the following three cases :

- without interference (curve A),
- with interference ($\nu = N_{eff}$ when $N_{eff} \leq 3$, $\nu = 3$ when $N_{eff} > 3$) (curve B),
- with interference (qualitative extrapolation to the case of $\nu = N_{eff}$ (curve C).

This figure shows that $(N_{eff})_{app}$ is very close to N_{eff} when it has a small value ($N_{eff} < 2$). For increasing values of N_{eff}, the apparent value of $(N_{eff})_{app}$ does not vary much and does not reach a value higher than about 5.

For the fissile nuclei usually studied, the two values $(N_{eff})_{app}$ and (N_{eff}) are very chose to each other. For U^{235}, in particular, where the observed value of N_{eff} is about 0.25, it is very unlikely that taking into account interference effects can lead to a much higher value of N_{eff}.

To summarise this paragraph, one should say that it seems that the effect of interference and of quasi-resonances has sometimes been largely overestimated. Interference can explain certain shapes of resonances (especially in the wings) but, in the usual cases met with in practice, it cannot distort in an important manner the distributions of the parameters which are much more sensitive to the superposition of the cross sections belonging to the two spin states.

It would be of great interest to measure cross sections of nuclei, for which high values of N_{eff} would be expected (low fission barrier height compared to the neutron binding energy). As these nuclei have a short life time, the nuclear explosion is an outstanding neutron source for such measurements.

3. SUBTHRESHOLD FISSION

Various aspects of subthreshold fission have been discussed by Rae at the Salzburg Conference [5]. It was pointed out that the thermal neutron fission cross section of several non-fissile nuclei, even-even or odd-even, is anomalously low. With the exception of Am^{241}, the measured cross sections are much lower than the ones calculated with the following formula :

$$\sigma_{nF}\ (\text{thermal}) \approx \frac{\langle \Gamma_F \rangle}{\langle \Gamma_F \rangle + \langle \Gamma_\gamma \rangle}\ \sigma_{abs}\ (\text{thermal}) \qquad (30)$$

in which $\langle \Gamma_f \rangle$ is given by the Hill and Wheeler formula.

Back in 1956, Wheeler had pointed out this anomaly for Pu^{240} and had suggested that either the fission width of the 1st resonance at 1 eV was exceptionally low or fission induced by "S" wave neutrons was inhibited [69]. This last assumption was confirmed later by the following results :

- the fission widths of the resonances below 120 eV are small and lower than 0.6 meV [70]

- the Pu^{240} fission cross section measured between 30 KeV and 2 MeV by de Vroey et al. [71] is relatively constant and egal to about 100 mb between 30 KeV and 300 KeV. The shape of the cross section, as it is measured, is very similar to the one calculated with " s " wave neutron fission inhibited, but "p" wave one allowed. The small and constant value of the cross section between 30 KeV and 300 KeV would come from the fact that the increase in $\langle \Gamma_f \rangle$ as a function of energy is compensated by the decrease in the "p" wave cross section for the formation of the compound nucleus.
- the calculations by Johansson [72] of the positions of the shell-model states for very large deformations have shown that negative parity states (such as 1/2 - and 3/2 -) lie lower in energy than the 1/2 + state. These calculations provided a theoretical background for the measurements quoted above.

All this is discussed in the paper by Rae [5].

Just after the Salzburg Conference, the Pu^{240} fission and capture cross sections were measured with a nuclear explosion [73]. Many individual resonances were observed both in fission and in capture. If the explanation mentionned above is correct, an anticorrelation should be observed between Γ_n and Γ_f. This comes from the fact that a p-wave resonance which should therefore have a small neutron width, should, on the contrary, have a large fission width. Such an anticorrelation is not apparent in the experimental results.

In fact, the situation is more complicated as we shall see now.

In view of having more information on the shape of the fission barrier, and also to elucidate the low value of the thermal neutron fission cross section, the total and fission cross sections of Np^{237} have been measured at Saclay [74, 75, 76].

The total cross section does not show any anomaly and is quite similar to that of nearby odd A nuclei.

The fission cross section has been measured several times since it has an unusual behaviour. It was measured first with a gas scintillator [74] and a flight path of 12.4 meters. A grouping effect of the resonances was clearly observed [74] which was confirmed by a 2nd measurement carried out with an ionisation chamber and a flight path of 6 meters [75].

Lastly, the same cross section was measured in much better conditions with an improved gas scintillator and an overall resolution of 18 ns/m at 100 eV [76].

We shall now examine some properties of this cross section [76].

First, it is entirely different from the total cross section and from the fission cross sections of other nuclei measured up to now. Instead of showing a regular pattern, it is composed of high peaks (or structures) at definite energies : 40 eV - 118 eV - 198 eV, etc... up to 4 keV (fig. 21). There are 17 such peaks below 1 keV, with a mean level spacing of about 60 eV.

The first structure at 40 eV is composed of several intense resonances which were resolved and analysed. All the parameters (spin excluded, but fission width Γ_f included) of these resonances have been determined. Curve B (in fig. 22) shows the cumulative sum of the fission widths as a function of energy up to 80 eV (the estimation of Γ_f for resonances not seen in fission will be discussed later). The resonances situated between 35 eV and 46 eV contribute 90% to the total sum $\sum_0^{80} \Gamma_f$, though they represent only 14% of the total number of resonances observed in transmission below 80 eV. The next peak at 118 eV, and the others at higher energies, cannot be completely resolved into several resonances (if several) because of the lack of resolution. No anomaly is observed; neither in the curve A (fig. 22) at 40 eV and 118 eV, nor above, in the total cross section, at the energies of the peaks.

Between peaks, in the fission cross section, only a few weak resonances appear and these can be analysed; the others, although observed in transmission, do not emerge above the background. Nevertheless, it is possible find an upper limit $\Gamma_{f\,max}$ of the fission width for these resonances, when they are at low energy. Arbitrarily, the fission width Γ_f is then set equal to $\frac{1}{2}\Gamma_{f\,max}$ (with an error of $\frac{1}{2}\Gamma_{f\,max}$).

Curve B (in fig. 23) represents the distribution of the fission widths for all the resonances observed in transmission below 80 eV. This histogram is definitely inconsistent with one single distribution of a χ^2 family. It is necessary to assume there are at least two distributions, one with $\langle \Gamma_f \rangle = 0.009$ meV and $\nu = 1$ (small fission resonances) the other with $\langle \Gamma_f \rangle = 0.4$ meV and $\nu = 1$ (large fission resonances). The parameters of the family of small resonances are approximate since only half of them were actually observed in fission. In addition to these two families, there is a large fission width (resonance at 39.9 eV) which is still outside the distribution. The ratio of the number of resonances in each family is 0.18, which is different from the ratio of the number of resonances supposed to belong to the two possible spin states.

The experimental fission cross section has been compared to a

"simulated" one, calculated from a set of parameters selected at random but obeying the usual statistical distributions. In particular the "simulated" fission width distribution was assumed to be the same as the one shown in fig. 23 and described above.

Both the experimental and the "simulated" fission cross sections were then averaged with a rectangular weighting function (10 eV wide) every 10 eV. Between 0 and 160 eV, the variance of the averaged values of the experimental fission cross section is $\sim$ 3 times higher than that of the "simulated" one. This comparison confirms the presence of an intermediate structure which clearly appears in the neutron subthreshold fission cross section of Np^{237}. It does not seem that the formation of the compound nucleus through "doorway states" can explain this structure in fission since it does not show up in the total cross section. This implies that the coupling of the compound nucleus states to fission exit channels is stronger at some discrete energies. It thus seems that only a more thorough understanding of the fission process can explain this structure.

Recently, Strutinsky [77] has calculated the deformation energy for heavy nuclei and large deformations, taking into account shell-model corrections to the liquid drop model. It is, then, possible to obtain not only one but two or even three fission barriers. The first and lowest minimum corresponds to the stable nucleus at equilibrium (small deformations). The second minimum corresponds to deformations $\beta \approx 0.5$ to 0.6. According to Strutinsky, "this second minimum may be of importance for the fission process as it provides a possibility for the formation of an intermediate quasi-stationary state in the fissioning nucleus. The fission width will strongly depend on the properties of this state".

The coupling of the compound nucleus states to the fission exit channels which is more intense at some discrete energies and which has been observed may be just the coupling through those intermediate quasi-stationary states explicitly mentioned by Strutinsky.

It is interesting to remember the concept of "doorway states" imagined by the M.I.T. group [79] as intermediate states between the coupling of the entrance channel to the compound nucleus states. Now, it seems that fission has probably shown one of the best examples of another type of intermediate state between the coupling of the compound nucleus states, not to the entrance channel, but to the exit channels.

Keeping this theory in mind, the need to measure the spins of the resonances in the structure at 40 eV is therefore obvious. It is also worth noticing that the spacing distribution of the big peaks observed in fission below 1.6 keV obeys the Wigner law (1 population only) as if they were

coupled to one spin state only (fig. 24). Nevertheless, this last result needs more precision because of the difficulty of correctly identifying structures composed of several individual resonances.

We can notice that at zero neutron energy, the intermediate structure in the fission cross section of Np^{237}, presents a minimum, which can explain the low value of the thermal neutron fission cross section. This explanation renders unnecessary the arguments developped by Rae for Pu^{240} [5]

Another example of grouping effect of resonances in fission has been observed in Pu^{240} and will be presented at this conference [78] .

If this phenomenon of intermediate structure in subthreshold fission is a general one, it may be observed also in the fission cross section of fissile nuclei when the contribution of transition states above the neutron binding energy is of some importance. This is the case for the 1^+ channel in Pu^{239} and very probably for the 4^- channel in U^{235}. In the paragraph II, we discussed the existence of correlations which may come from a kind of intermediate structure just as the fall above 600 eV of the Pu^{239} fission cross section which causes such a high value of α at that energy.

4. CONCLUSION

A complete treatment of the neutron cross section measurements should include a detailed comparison of the data, especially from the point of view of their accuracy and the discrepancies among various measurements. This aspect of the subject has been ignored in this paper.

We shall try now to summarise briefly what has been covered in this paper :

- the greater accuracy and resolution in the measurements is mainly apparent in partial cross sections. For instance, the resolution of the Pu^{239} fission cross section is becoming comparable to that of the total one. This permits the analysis of a much larger number of resonances than before.

- the increase in intensity of the pulsed neutron sources permits a more and more detailed study of certain modes of decay of the compound nucleus states (certain properties of fission, for example) which were reserved before to thermal neutron sources.

- among all fissile nuclei, Pu^{239} has been, by far, the most thoroughly studied during these last few years and its cross sections are now understood better.

- there are apparent inconsisfencies in U^{235} cross sections which will probably be removed by polarisation and K. value measurements in the resonances.

- interference should be taken into account in the analysis but its

importance should not be over-stressed in the usual cases.

- Fission cross section measurements of non-fissile or "exotic" nuclei, (in their ground state or isomeric state (if any), such as U^{232}, U^{234}, U^{235} *($1/2^+$) transplutonium elements, etc ... should provide examples of the fission process in more extreme cases and therefore help to understand its properties more thorougly.

- probably, the most interesting phenomenon mentioned here, is the intermediate structure observed in the substhreshold fission of Np^{237} and Pu^{240}. It is interesting, not only because of the insight it provides into the fission process and the mechanism of nuclear reactions ; but also for the consequences it may have for the fission cross sections of fissile nuclei. In this respect, correlations should be studied more carefully and should also be introduced into the simulated cross sections, when necessary.

The author wishes to thank all those who have transmitted to him their results before their publication. He feels very indebted to M . ASGHAR for interesting and stimulating discussions and for his kind and efficient help, when preparing this manuscript in english.

5. REFERENCES

[1] Proceedings of the Symposium on Physics and Chemistry of Fission (Salzburg, March 1965) I. A. E. A. Vienna (1965).

[2] Proceedings of the International Conference on the Study of Nuclear Structure with Neutrons (Antwerp, July 1965) North Holland Publishing Co Amsterdam (1966).

[3] Proceedings of the Conference on Neutron Cross Section Technology (Washington, March 1966) CONF - 660303 - TID 4500.

[4] Proceedings of a Conference on Nuclear Data for Reactors (Paris, October 1966) I. A. E. A. Vienna (1967).

[5] E. R. Rae ref. 1 - Vol. 1 - p. 187 .

[6] J. E. Lynn ref. 4 - Vol. 2 - p. 89.

[7] M. S. Moore and O. D. Simpson ref. 3 - Vol. 2 - p. 840 .

[8] B. D. Diven ref. 2 - p. 441 .

[9] C. A. Uttley ref. 2 - p. 535 -

[10] J. Blons et al. ref. 2 - p. 564 .

[11] J. Blons et al. C. R. Acad. Sc. 262 (1966), 79 .

[12] M. G. Cao et al. to be published in Journ. of Nucl. En.

[13] G. D. James ref. 1 Vol. 1 - p. 235 .
International Conference on Fast Critical Experiments and their Interpretation (Argonne, October 1966).

[14] G. de Saussure et al. ref. 1 Vol. 1 p. 205 .
C. R. Acad. Sc. 259 (1964) 3498.

[15] C. D. Bowman and G. F. Auchampaugh ref. 4 Vol. 2 p. 149 .

[16] F. D. Brooks. Proceedings of a Symposium on Neutron Time of Flight Methods (July 1961) Euratom (Brussels 1961) p. 389.

[17] E. R. Shunk et al. Report LA-DC 7620 .

[18] G. de Saussure et al. ref. 4 Vol. 2 p. 233
ORNL-TM-1804 .

[19] U. V. Ryabov et al. ref. 1 Vol. 1 p. 287 .

[20] M. G. Schomberg et al. AERE-PR/NP 12 p. 6 .

[21] G. Carraro and H. Weigman EANDC (E)76 "U" p. 133 .

[22] M. C. Moxon and E. R. Rae Nucl. Inst. Meth. 24 (1963) 445 .

[23] J. S. Fraser and R. B. Schwartz Nucl. Phys. 30 (1962) 269 .

[24] F. Poortmans et al. ref. 3 p. 755
ref. 4 p. 211 .

[25] M. Asghar ref. 4 Vol. 2 p. 185
Nucl. Phys. A 98 (1967), 33 .

[26] G. D. Sauter and C. D. Bowman UCRL 14200
UCRL 70408
Phys. Rev. Let. 15 (1965) 761 .

[27] A. Bohr Proceedings of the International Conference on the Peaceful Uses of Atomic Energy - Geneva (1955) Vol. 2 p. 151 United Nations (New-York).

[28] D. L. Hill and J. A. Wheeler Phys. Rev. 134 (1964) B 952 .

[29] R. Vandenbosch Nucl. Phys. 46 (1963), 129 .

[30] J. W. T. Dabbs ref. 1 Vol. 1 p. 39 .

[31] A. Michaudon ref. 4 Vol. 2 p. 161 .

[32] J. Blons private communication .

[33] D. W. Bergen et al. ref. 3 Vol. 2 p. 895 .

[34] J. A. Northrop et al. Phys. Rev. 115 (1959), 1277 .

[35] D. Eccleshall and M. J. L. Yates ref. 1 Vol. 1 p. 77 .

[36] H. J. Specht et al. Phys. Rev. Let. 17 (1966) 1187 .

[37] A. Michaudon C. E. A. Report 2552 (1964) .
Thesis (May 1964)

[38] A. Michaudon et al. - Comptes rendus du Congrès International de Physique Nucléaire (Paris 1964) Vol. 2 p. 712
- Nucl. Phys. 69 (1965) 545 .

[39] A. Michaudon et al. Phys. Let. 7 (1963), 211.

[40] V. Sailor et al. B. A. P. S. II, 11 (1966) 29 .

[41] G. A. Cowan et al. Phys. Rev. 122 (1961) 1286 .
Phys. Rev. 130 (1963) 2380 .

[42] C. Coceva et al. Phys. Let. 16 (1965), 159 .

[43] M. Asghar et al. to be published .

[44] H. Maier-Leibnitz et al. ref. 1 Vol. 2 p. 113 .

[45] J. E. Lynn ref. 2 p. 125 .

[46] G. de Saussure et al. ref. 4 Vol. 2 p. 233 .
Report ORNL TM-1804 .

[47] A. M. Lane and J. E. Lynn Proc. Phys. Soc. A 70 (1957), 557 .

[48] P. Egelstaff Journ. Nucl. En. 7 (1958), 35 .

[49] E. Melkonian et al. ref. 1 Vol. 2 p. 355 .

[50] A. Michaudon et al. Nucl. Phys. 69 (1965) 573 .

[51] Nève de Mevergnies private communication .

[52] J. W. T. Dabbs private communication .

[53] H. C. Britt et al. Phys. Rev. Let 11 (1963) R 502 .

[54] H. Derrien et al. ref. 4 Vol. 2 p. 195 .

[55] E. Vogt Phys. Rev. 118 (1960) 724 .

[56] G. A. Cowan et al. Phys. Rev. 144 (1966) 979 .

[57] A. Michaudon, Invited paper presented at the Meeting of the French Physical Society (Bordeaux, March 1967) : published in Journ. de Phys. (Supt Jan. 1968) .

[58] A. Lottin et al. International Conference on Fast Critical Experiments and their Analysis , (Argonne, October 1966).

[59] J. J. Griffin ref. 1 Vol. 1 p. 23 .

[60] G. D. James, to be published in Journ. Nucl. En. .

[61] J. A. Farrell Report LA-DC-8528 .

[62] J. A. Farrell Invited paper, this Conference .

[63] B. H. Patrick et al. ref. 4 Vol. 2 p. 117 .

[64] E. R. Shunk et al. ref. 3 Vol. 2 p. 979 .

[65] J. E. Lynn Phys. Let. 18 (1965), 31 .

[66] E. Vogt Phys. Rev. 112 (1958), 203 .

[67] F. J. Shore and V. L. Sailor Phys. Rev. 112 (1958), 191 .

[68] J. E. Lynn Phys. Rev. Let. 13 (1964) 412 .

[69] J. A. Wheeler Physica XXII (1956) 1103 .

[70] F. D. Brooks and J. E. Jolly AERE PR/NP 6 (1963) 13 .

[71] M. de Vroey et al. ref. 1 Vol. 1 p. 281 .

[72] S. A. E. Johansson Nucl. Phys. 12 (1959) 449 .

[73] D. H. Byers et al. ref. 3 Vol. - p. 903 .

[74] D. Paya et al. ref. 4 Vol. 2 p. 128 .

[75] D. Paya et al. Proceedings of the Meeting of the French Physical Society (March 1967). Journal de Physique (Sup^{t} to Jan. 1968) .

[76] A. Fubini et al. submitted to Phys. Rev . Let. .

[77] V. M. Strutinsky Nucl. Phys. A 95 (1967), 420 .

[78] E. Migneco and J. Theobald - This Conference .

[79] H. Feshbach, A. K . Kerman and R. H. Lemmer "Intermediate Structure and Doorway States in Nuclear Reactions". MIT Report.

[80] J. W. T. Dabbs private communication

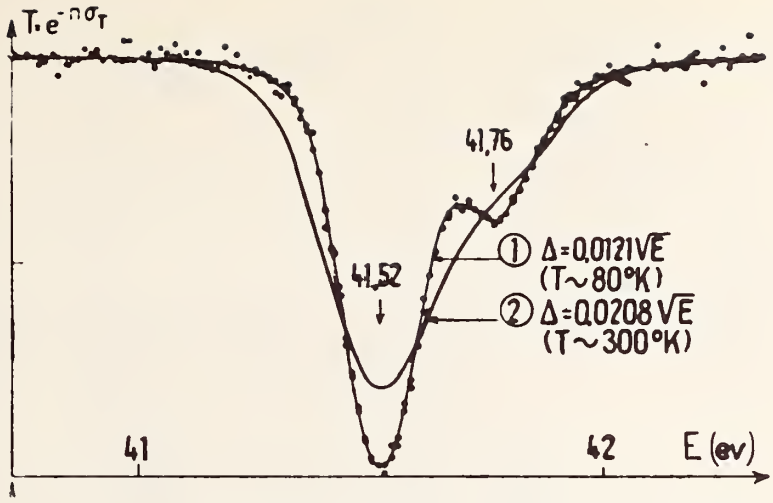

Fig. 1 Group of two close resonances in Pu^{239} resolved in a transmission experiment carried out with a sample cooled down to the liquid nitrogen temperature [10 , 11]

1 - Single-level fit to the measured cross section ;

2 - Shape of the transmission curve as it would appear in a measurement with a sample at room temperature.

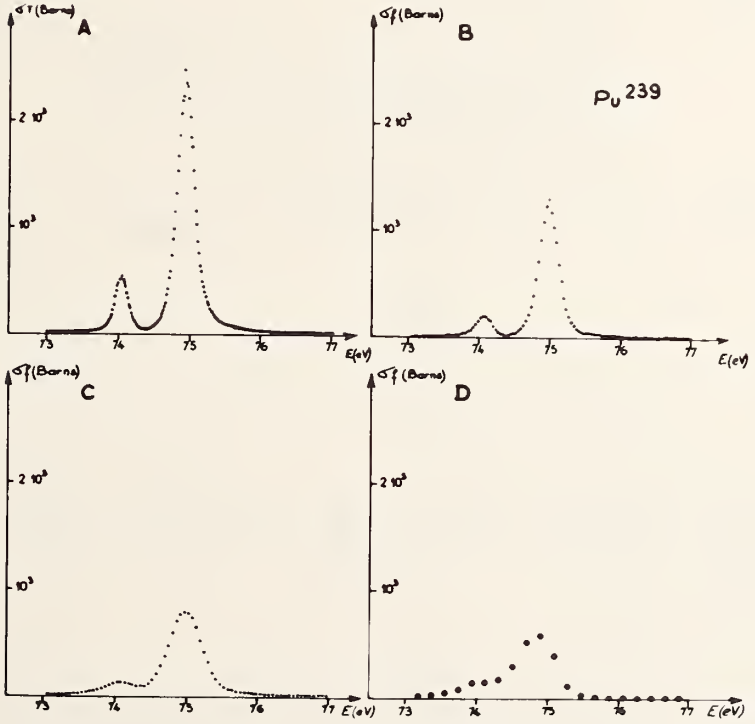

Fig. 2 - Various measured cross sections of Pu^{239} between 73 and 77 eV

A - Total cross section [54]
B - Fission cross section (preliminary Saclay results) [32]
C - Fission cross section (old Saclay results) [14]
D - Fission cross section (Los Alamos) [17]

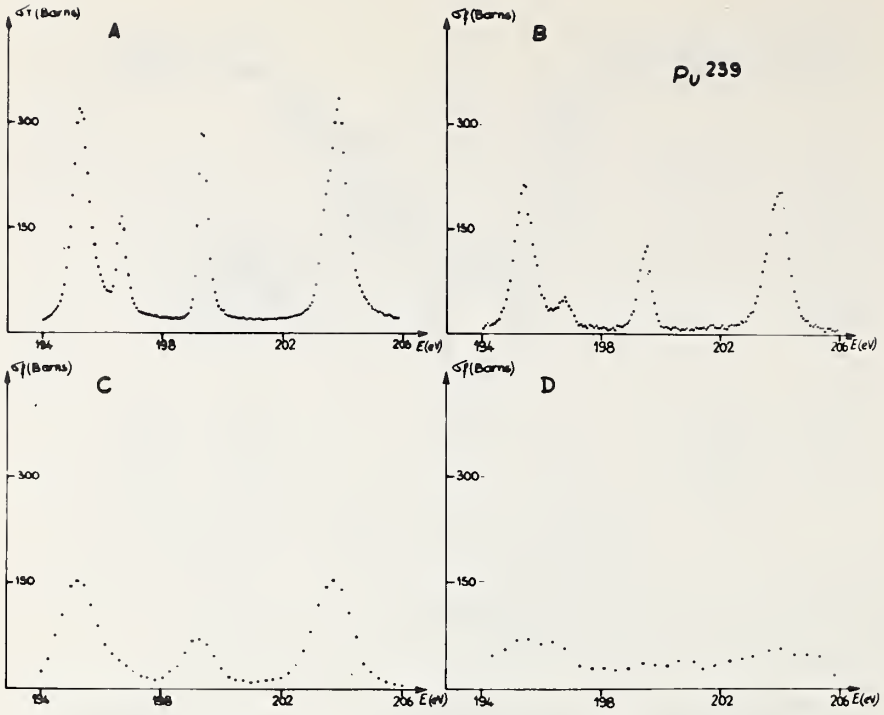

Fig. 3 - Various measured cross sections of Pu^{239} between 194 and 206 eV

A - Total cross section [54]
B - Fission cross section (preliminary Saclay results) [32]
C - Fission cross section (old Saclay results) [14]
D - Fission cross section (Los Alamos) [17]

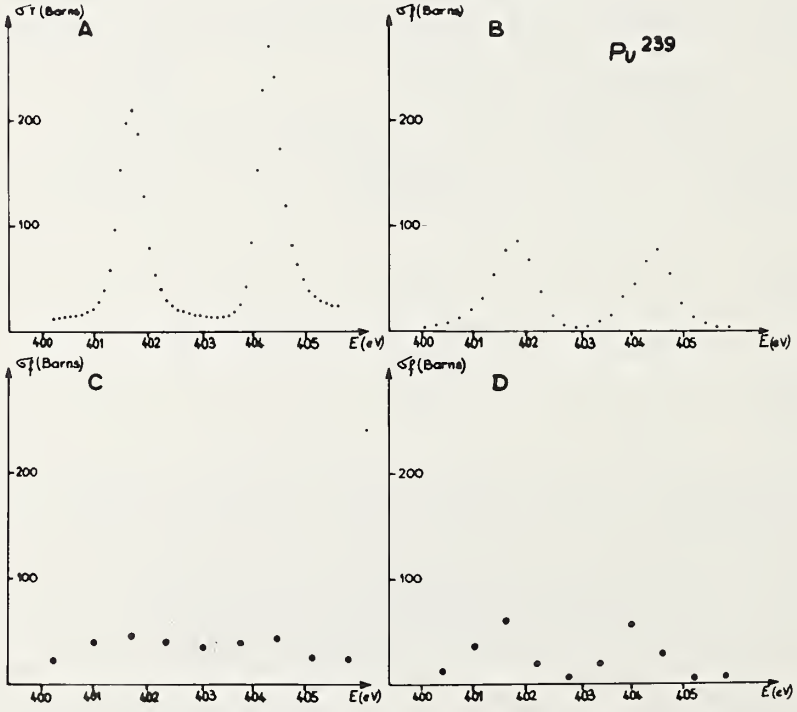

Fig. 4 - Various measured cross sections of Pu^{239} between 400 and 405 eV

A - Total cross section [54]
B - Fission cross section (preliminary Saclay results) [32]
C - Fission cross section (old Saclay results) [14]
D - Fission cross section (Los Alamos) [17]

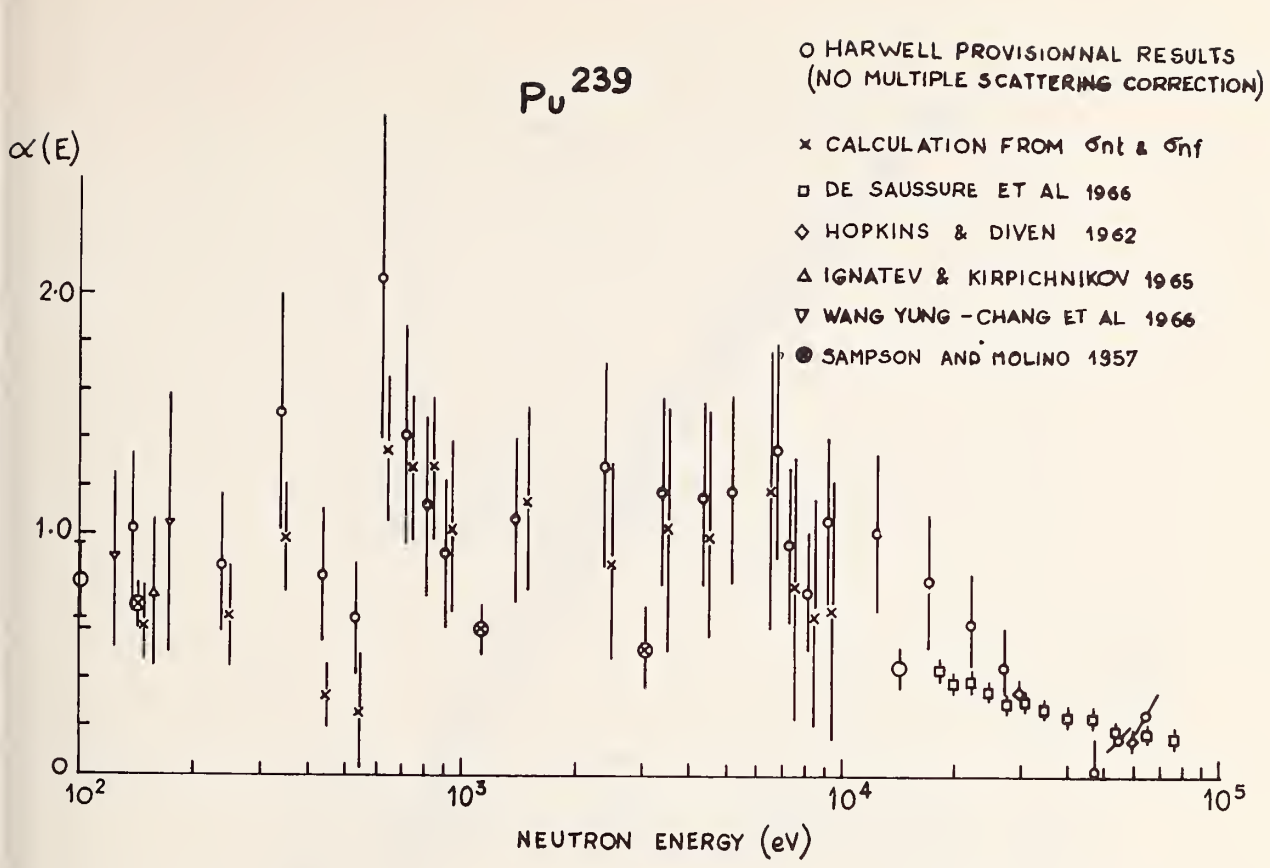

Fig. 5 - Measurements of α carried out at Harwell and comparison with other measurements (E. R. Rae, private communication)

TABLE I

K \ J	U^{233}		U^{235}	
	2^+	3^+	3^-	4^-
0	+ 0.074		+ 0.077	
± 1	+ 0.037	+ 0.055	+ 0.058	+ 0.065
± 2	- 0.037	0	0	+ 0.031
± 3		- 0.092	- 0.096	- 0.027
± 4				- 0.108

Fig. 6 - Calculated values of A_2 (in °K) corresponding to various J, K values for U^{233} and U^{235} [30]

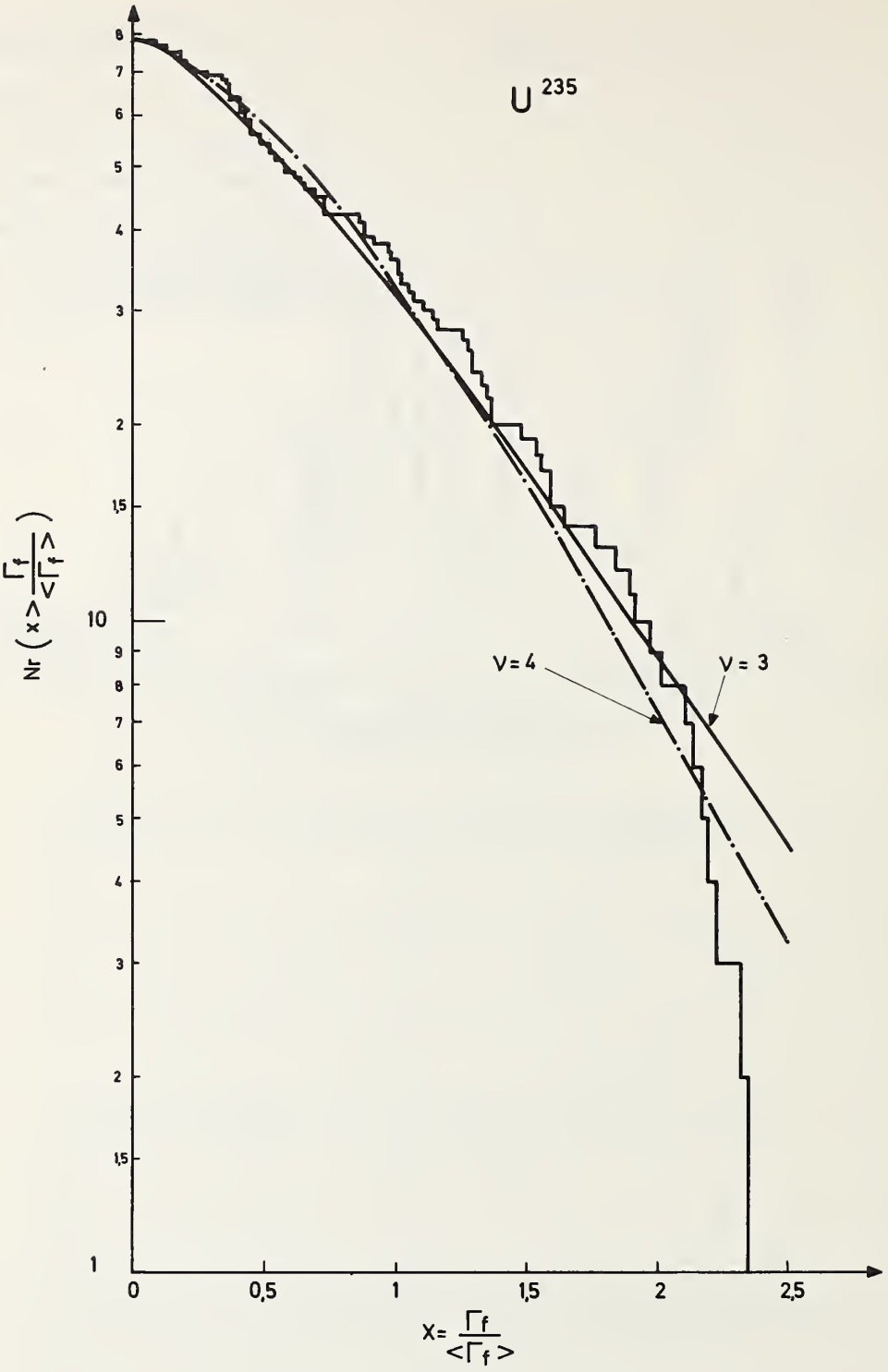

Fig. 7 - Fission width distribution of U^{235} resonances [12]

TABLE II

SPINS OF U^{235} NEUTRON RESONANCES

Energy (eV)	Γ_f (meV)	J_1	J_2
0.29	100	x	
1.14	115		x
2.03	10	(x)	
8.8	82	J = 3	
12.4	24		J = 4

Fig. 8 - Spins of U^{235} resonances.
The spins of the resonances at 0.29, 1.14 and 2.03 eV are determined from polarisation measurements [40]
The spin of the resonances at 8.8 and 12.4 eV are determined from resonance scattering measurements [24]

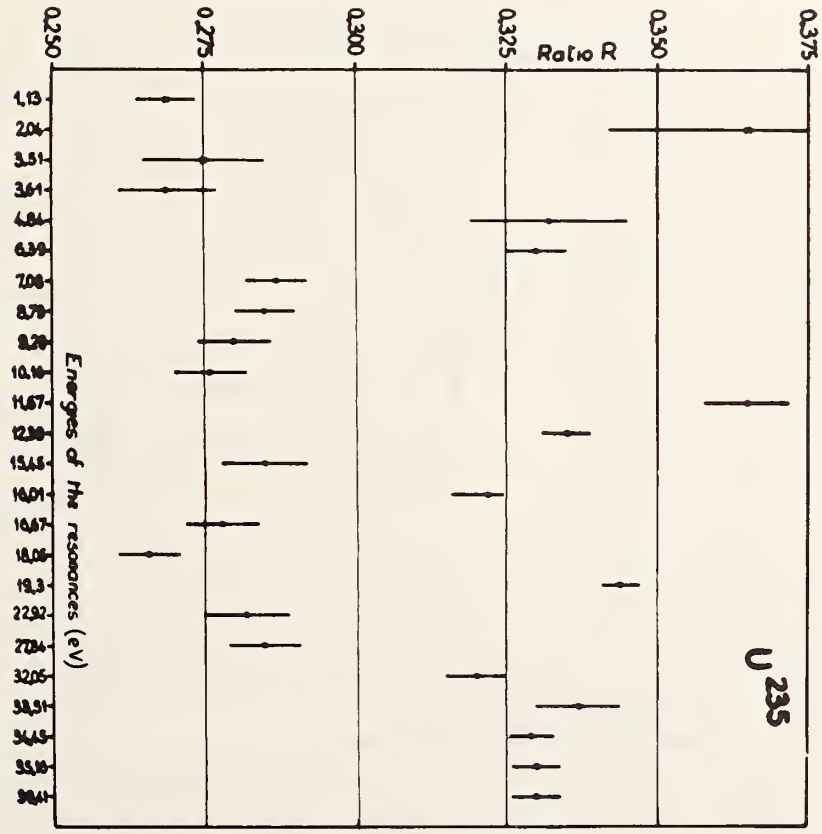

Fig. 9 Multiplicity of the γ-rays in U^{235} resonances. The ratio R of "coïncidences" to "singles" (defined in the text) is plotted for 24 resonances [43]

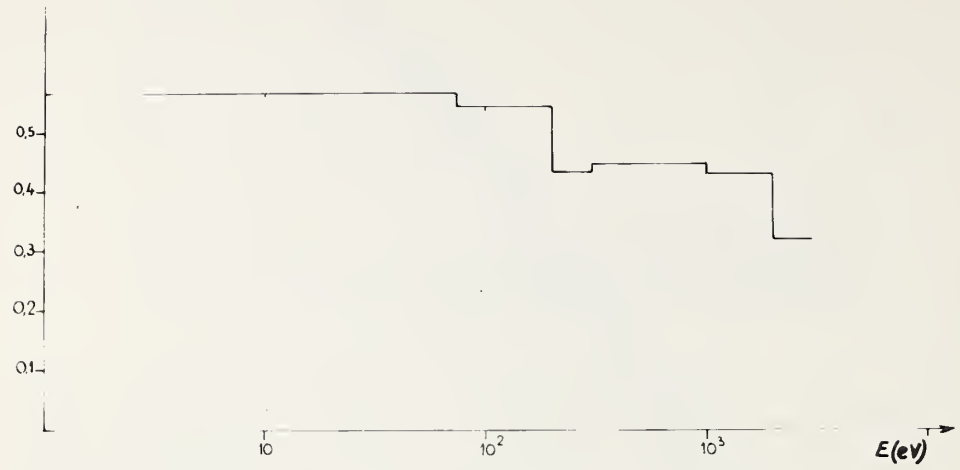

Fig. 10 Values of α of U^{235} obtained for different energy ranges from the measurements , by de Saussure [46]

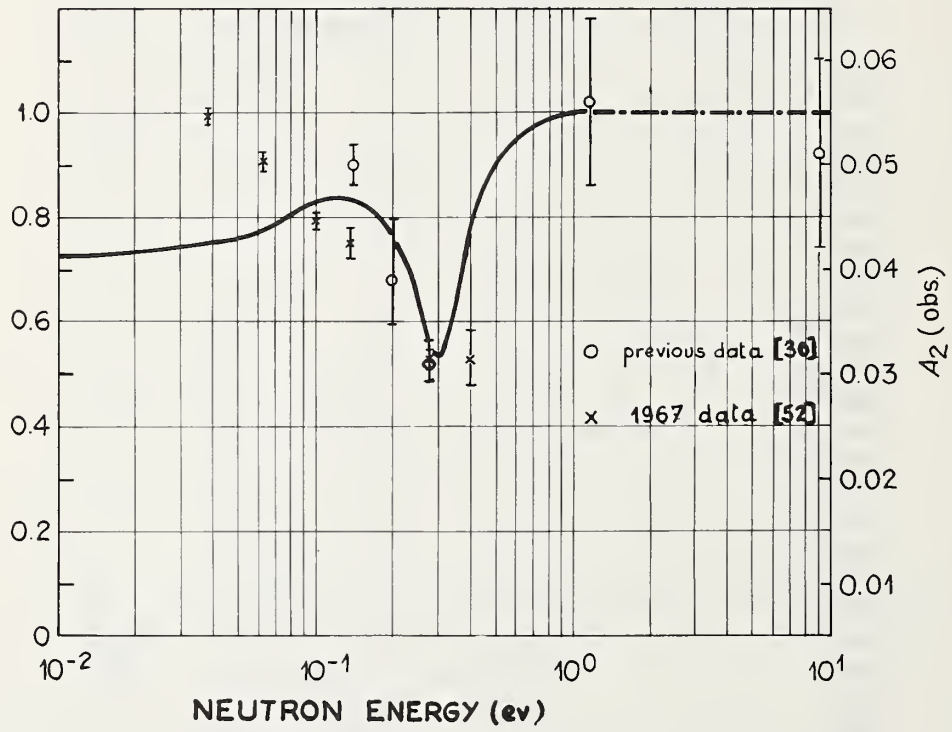

Fig. 11 The observed value of A_2 for U^{235} [30, 52]. The solid curve is derived from a multilevel fit [30].

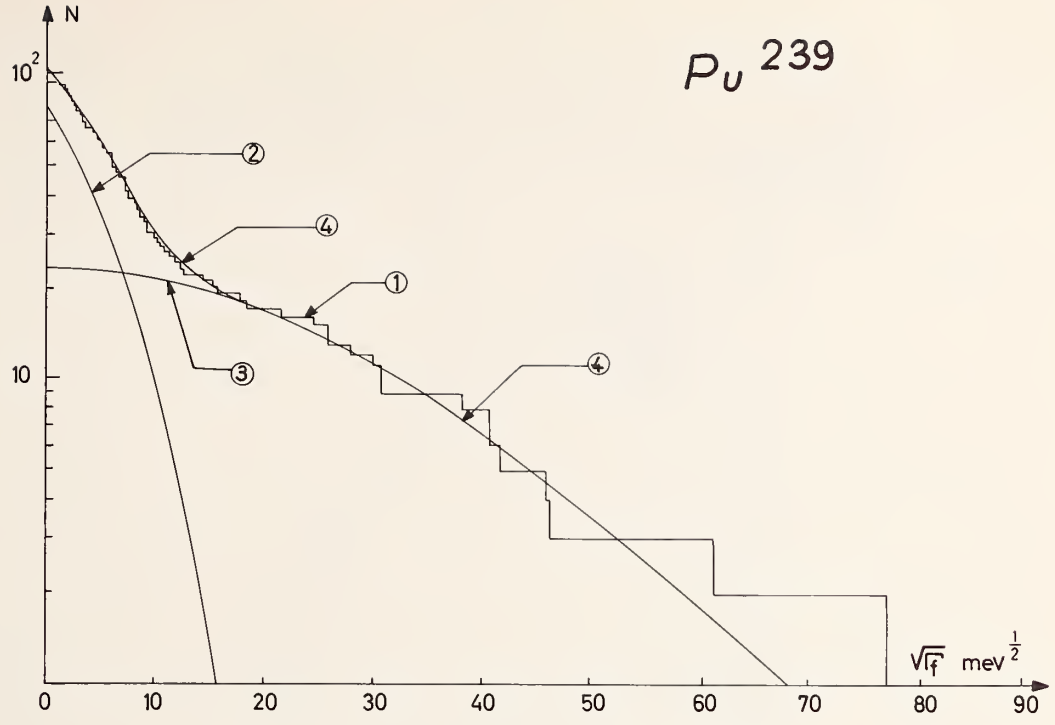

Fig. 12 Fission width distribution of Pu^{239} resonances [54]

1 - Experimental distribution .
2 - χ^2 distribution with $\langle \Gamma_f \rangle$ = 41 meV and ν = 1 (72 levels) .
3 - χ^2 distribution with $\langle \Gamma_f \rangle$ = 1,3 eV and ν = 2 (24 levels) .
4 - Sum of distributions (3) and (4) .

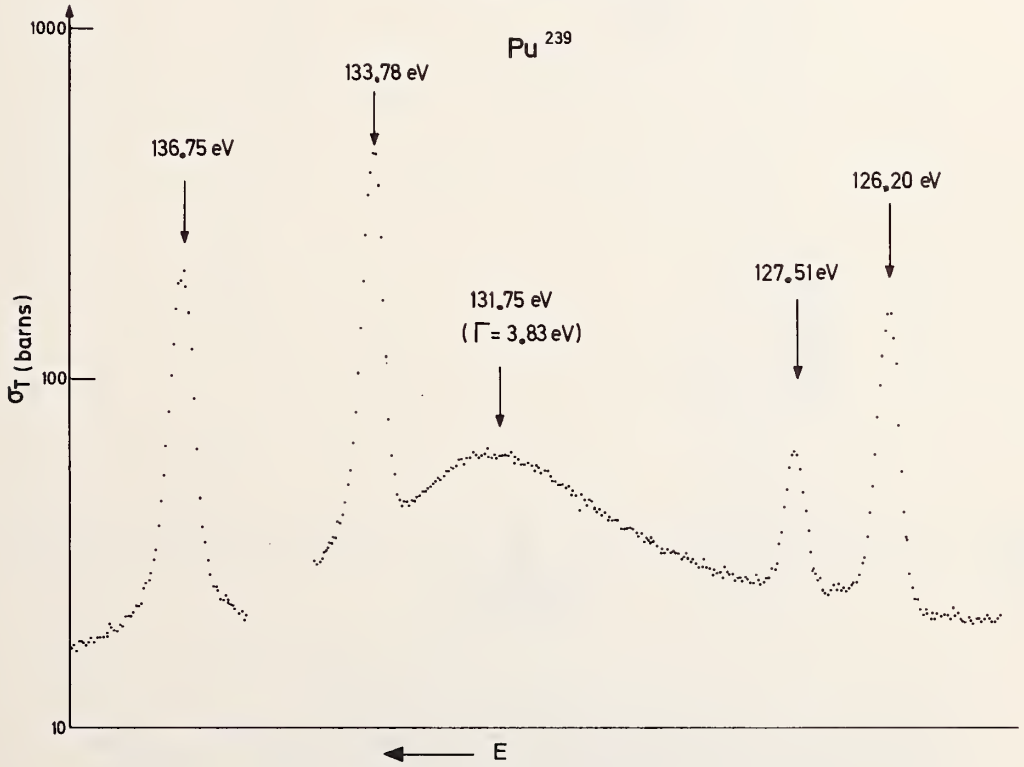

Fig. 13

The measured total cross section of Pu^{239} between 125 and 138 eV [54] .
There appears clearly a broad resonance at 131. 75 eV having a
total width of 3. 83 eV.
(The break at 135 eV corresponds to an impurity resonance in Pu^{240}).

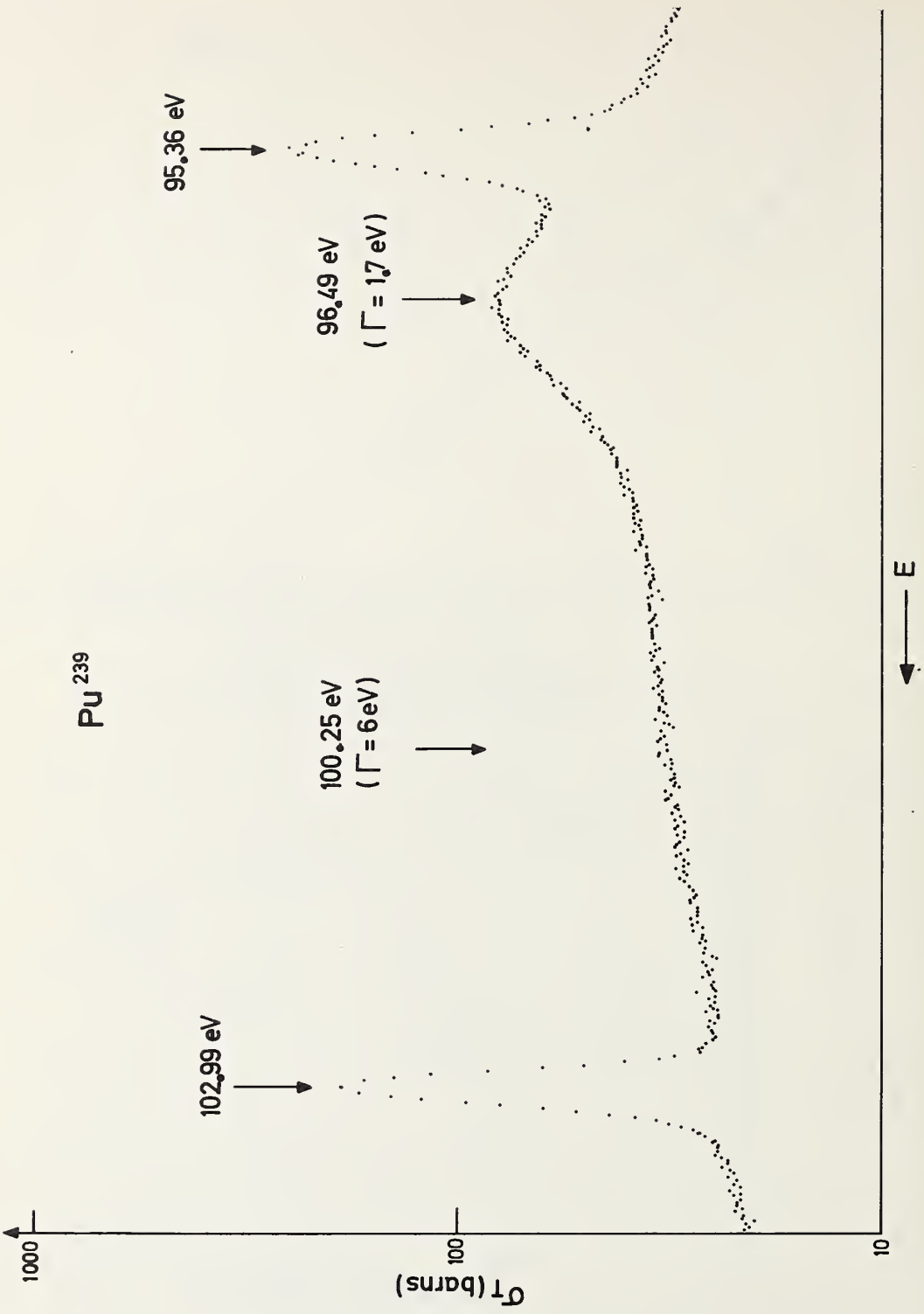

Fig. 14

The measured total cross section of Pu^{239} between 94 and 104 eV [54]. There appear two broad resonances : one at 96.49 eV (Γ = 1,7 eV) and another at 100.25 eV (Γ = 6 eV).

TABLE III

SPINS OF Pu^{239} NEUTRON RESONANCES

Energy (eV)	Spin J						Γ_f
	Vogt réf 55	Fraser réf 23	Sauter réf 26	Asghar réf 25	Cowan réf 56	Derrien réf 54	(meV) réf. 54
(1)	(2)	(3)	(4)	(5)	(6)	(7)	(8)
- 1.2	J_1 [a]						
0.3	J_2 [a]						60
7.82	J_1 [a]	1	1				47
10.93	J_1 [a]	1	1				143
11.5						0 [d]	~ 500
11.89		1	1				24
14.31			1				67
14.69		0	1	1			30
15.42			0 [a]		(1)	0 [d]	650
17.66		1	1	1	1		34
22.28		0	1	1	1		62
26.29				1	1		55
32.38			0 [b]		(0)		110
35.43			1 [b]				5
41.42 }		1 [c]	1 [c]	1 [c]	1 [c]		3
41.66 }							54
44.48		0	1	1	1		5
47.60			0	0	1		240
49.71					0	0 [d]	690
50.08				1	1		12
52.60			1	1	1		9
55.63				(0)			22
57.44					0	0 [d]	~ 500
58.84					0	0 [d]	~ 1100
59.22				0	1		133
60.94					0	0 [d]	~ 6000
65.71				1	1	(1) [f]	74
74.05				1			32
74.95			1	1	1	1 [e]	84
81.76					0	0 [d]	~ 2000
85.48				0			17

Energy (eV)	Spin J		Γ_f
	Asghar réf 25	Derrien réf 54	(meV) réf. 54
(1)	(5)	(7)	(8)
90.75	1	1 [e]	17
95.36	0		37
96.49		0 [d]	~ 1670
100.25		0 [d]	~ 6000
103	0		13
105.3	1		6
106.67	1	1 [f]	26
116.03	0		215
118.83	1	1 [e]	43
126.2	0		
131.75	0	0 [d]	~ 3300
133.78	1		7
136.75	0		88
146.25	1	(0) [f]	13
147.44		0 [d]	~ 1000
157.08	0	0 [d]	630
164.54	1	1 [e]	8
167.1	1	(1) [f]	74
171.08		0 [d]	~ 1000
177.22	1		5
184.87		0 [d]	~ 1500
195.36	0		350
196.7	1		59
199.4	1	1 [e]	90
203.93	0		
207.37	1	(1) [f]	7
211.1		0 [d]	800
216.5	(1)	(0) [f]	10
220.2		1 [f]	4
223.2			~ 2
227.8		0 [d]	~ 6000
231.40	1	1 [e]	4
234.3	0		14
239.1	1	(0) [f]	17
242.9	0	1 [f]	58
248.86	1	1 [e]	6
251.2	1	1 [e]	14
256.11	1		
262.37	0		
272.62	1		
275.57	1		
279.59	0		
282.92	1		
288.59	1		
301.81	(1)		

Fig. 15 The spins of Pu^{239} resonances :

a - Spin determined completely or partially by a multilevel fit,
b - Two weak scattering resonances [26 , 31],
c - Doublet not resolved in the measurement,
d - Spin 0 attributed from the large value of the fission width ;
e - The other value of the spin leads to a value of Γ_γ which is either impossible or is very unlikely;
f - Spin determined from the assumption that Γ_γ is independant of the spin and does not vary from resonance to resonance.

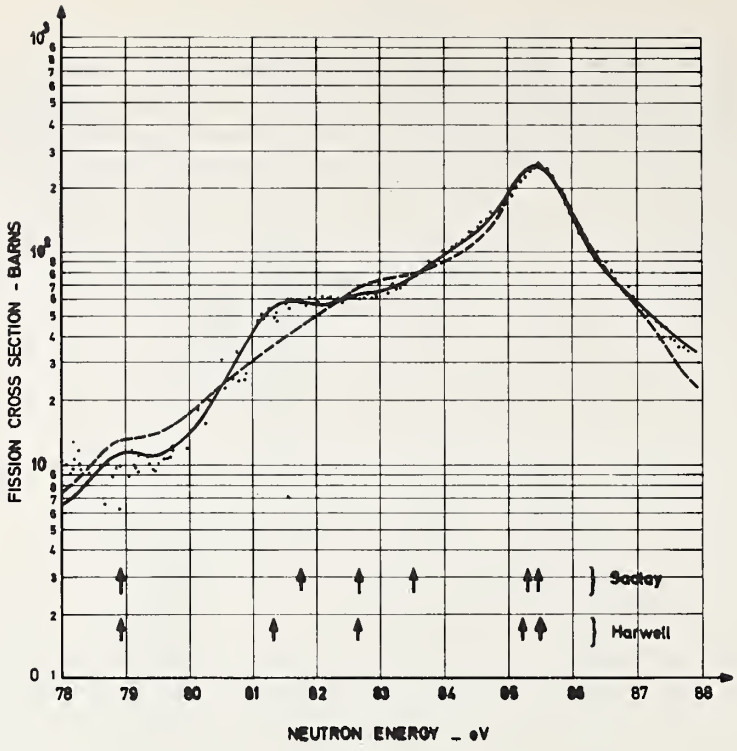

Fig. 16

The multilevel fit of the fission cross section of Pu^{239} in the region of 83 eV [60]
The arrows indicate the positions of the resonances used in the multilevel fit (Harwell) [60] and in the single-level fit (Saclay) [54]
The solid curve refers to the multilevel fit with 2 fission channels for the spin 0 resonances.
The dashed curve represents the best multilevel fit with one fission channel only for the spin 0 resonances.

TABLE IV

Pu^{239}

	P_1	Q
k = 1	9.10^{-2}	$11.5.10^{-2}$
k = 2	$3.5.10^{-2}$	0.45
	P_2	Q
k = 1	$11.5.10^{-2}$	6.10^{-2}
k = 2	$2.7.10^{-2}$	0.52

Fig. 17

P_1 is the probability that the sum of the fission widths of two neigbouring spin 0 levels in Pu^{239} is greater than k times their spacing (one fission channel)
P_2 is defined as P_1 but for two fission channels.
Q is the probability that the criterion $\Gamma_{f_1} + \Gamma_{f_2} > k\,D$ is not observed for spin 0 resonances situated in an energy range of 250 eV.

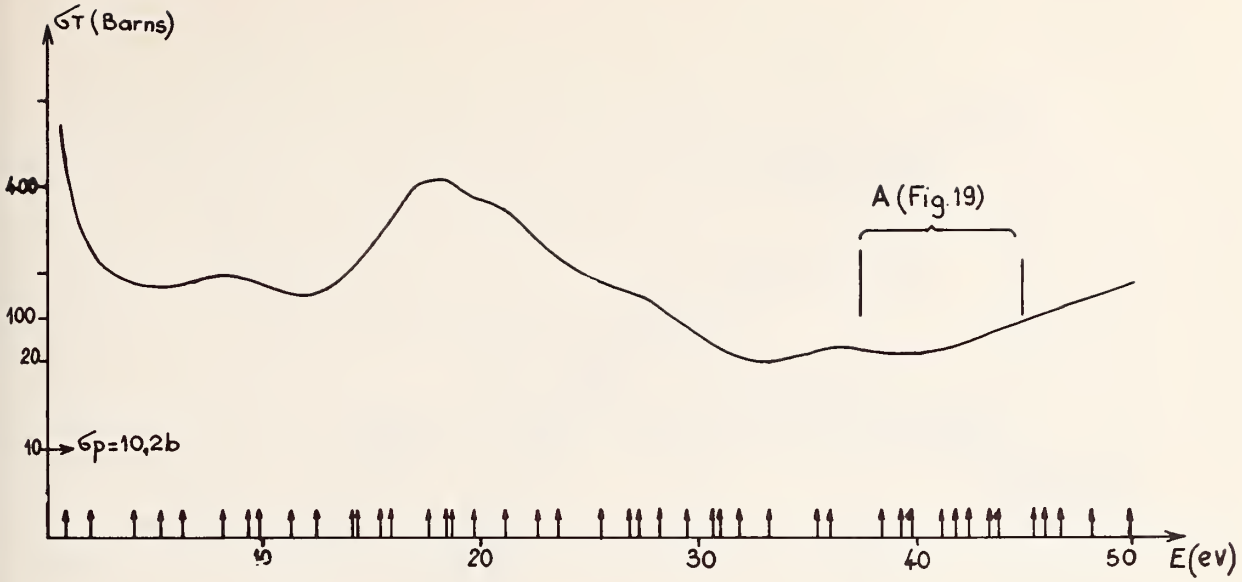

Fig. 18

Simulated total cross section below 50 eV calculated without interference and with $N_{eff} = 50$. The arrows indicate the positions of the levels used in the calculations. The portion A, calculated with the same parameters but with the interference included, is shown in Fig. 19

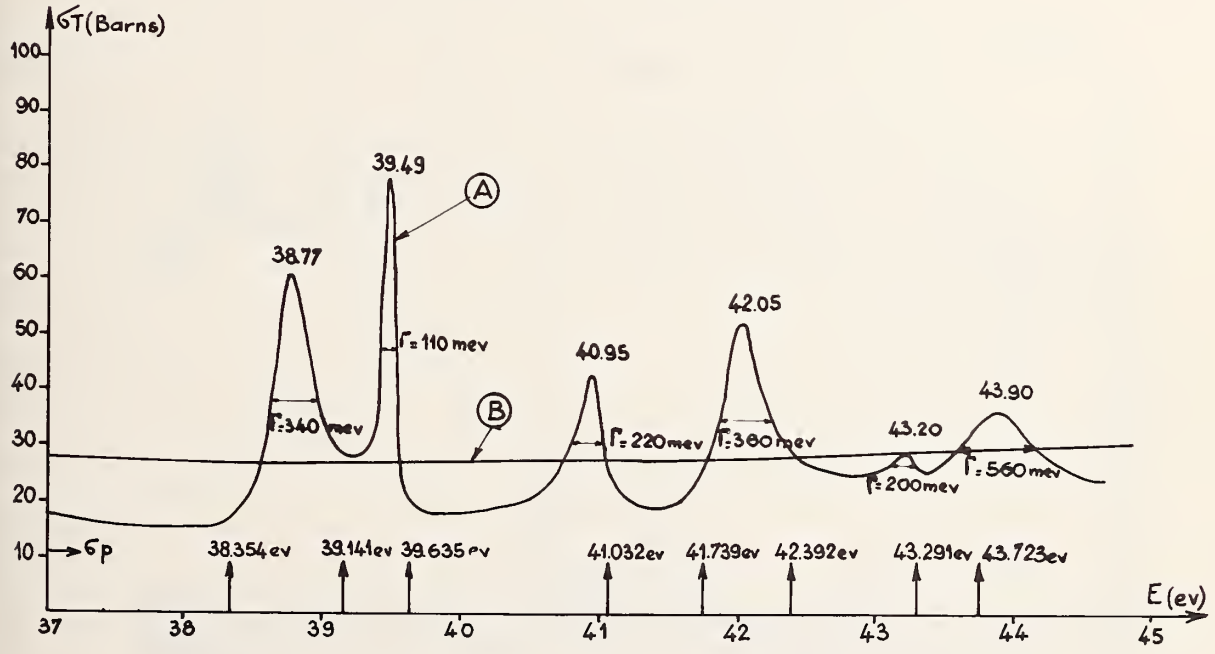

Fig. 19 - The simulated total cross section calculated between 37 and 45 eV with $N_{eff} = 50$:

A - with interference. There are 6 quasi-resonances with energies and widths written for each of them.

B - without interference (this is a portion of the curve in Fig. 18)

The arrows with the energies indicate the positions of the levels used in the calculation.

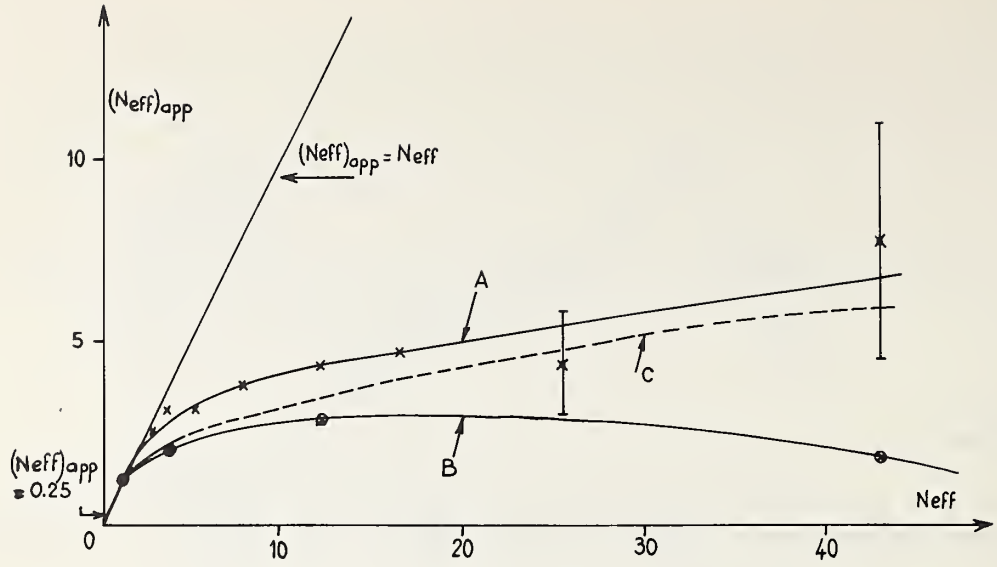

Fig. 20 The variation of the apparent number of exit channels as a function of the true one N_{eff}

A - without interference

B - with interference included $\nu = N_{eff}$ when $N_{eff} \leq 3$
$\nu = 3$ when $N_{eff} > 3$

C - with interference (qualitative extrapolation to the case of $\nu = N_{eff}$)

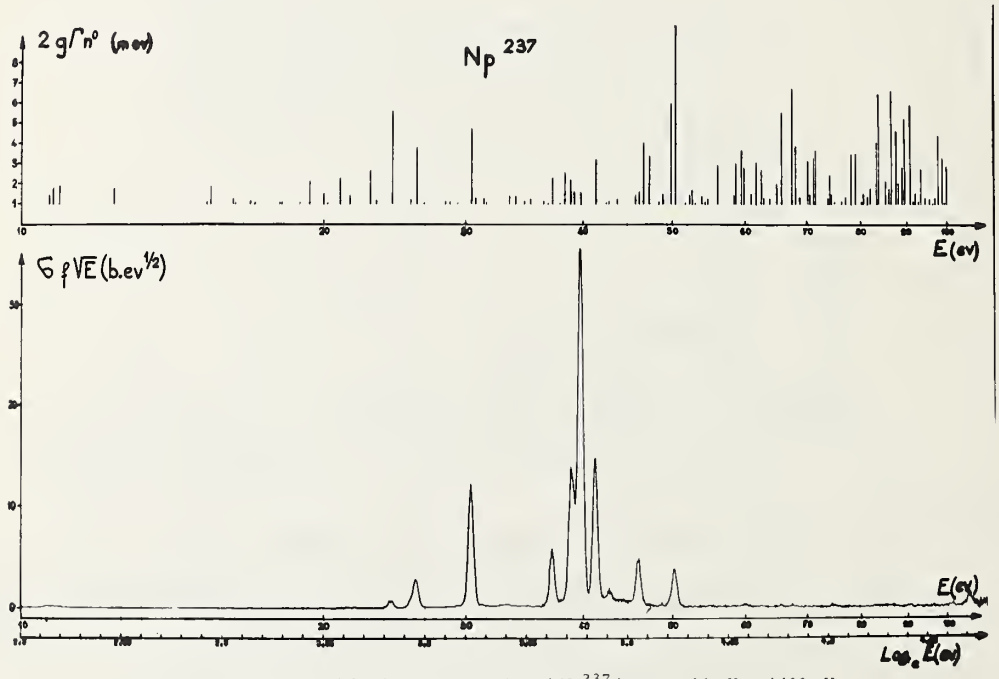

Fig. 21 The observed fission cross section of Np^{237} between 10 eV and 100 eV
The upper part of the figure shows the positions of the resonances as observed in transmission. For each resonance, the height of the bar is proportional to the reduced neutron width $2g\Gamma_n^{\circ}$

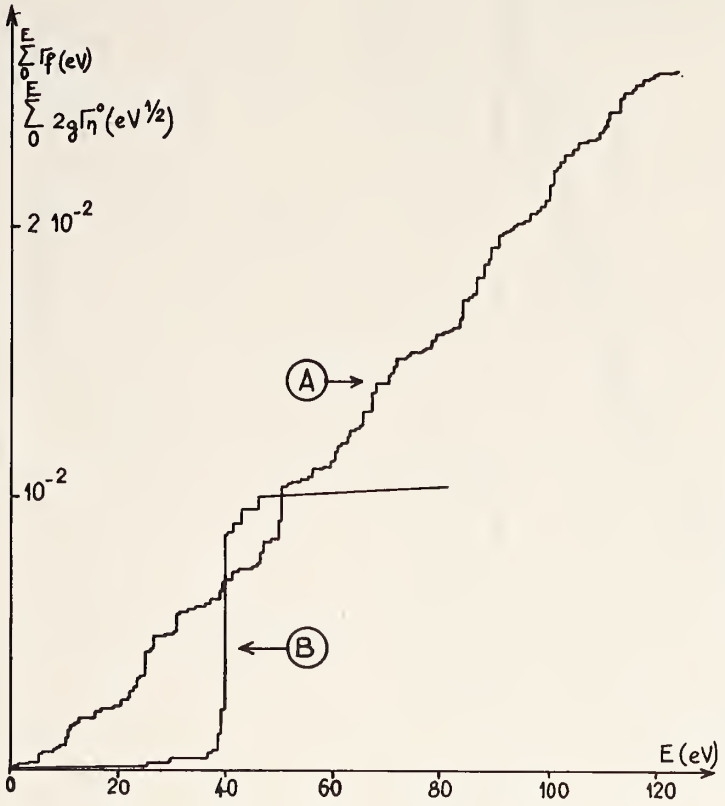

Fig. 22

Curve A shows the cumulative sum of the reduced neutron widths $2g\Gamma_n^\circ$ for the resonances situated below E (ev) as a function of E.
Curve B shows, in the same manner, the cumulative sum of the fission widths.

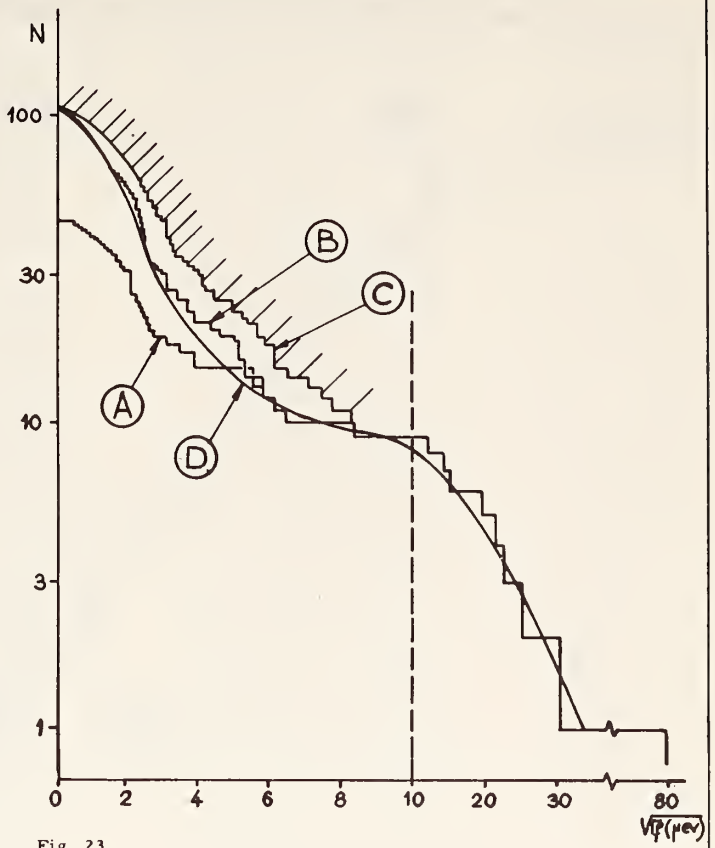

Fig. 23

Fission width distribution of the resonances situated below 80 eV. N is the number of resonances having a value of $\sqrt{\Gamma_f}$, greater than the abscissa.

A - resonances actually observed in the fission cross section.

B, C - all the resonances observed in transmission below 80 eV.

For the resonances not seen in fission, Γ_f is set equal either to 1/2 $\Gamma_{f\,max}$ (curve B) or to $\Gamma_{f\,max}$ (curve C). The dashed area is forbidden.

D - theoretical distribution
Note the change of scale at $\sqrt{\Gamma_f} = 10$ ($\mu eV^{1/2}$) and the break between 30 and 80 (μeV)

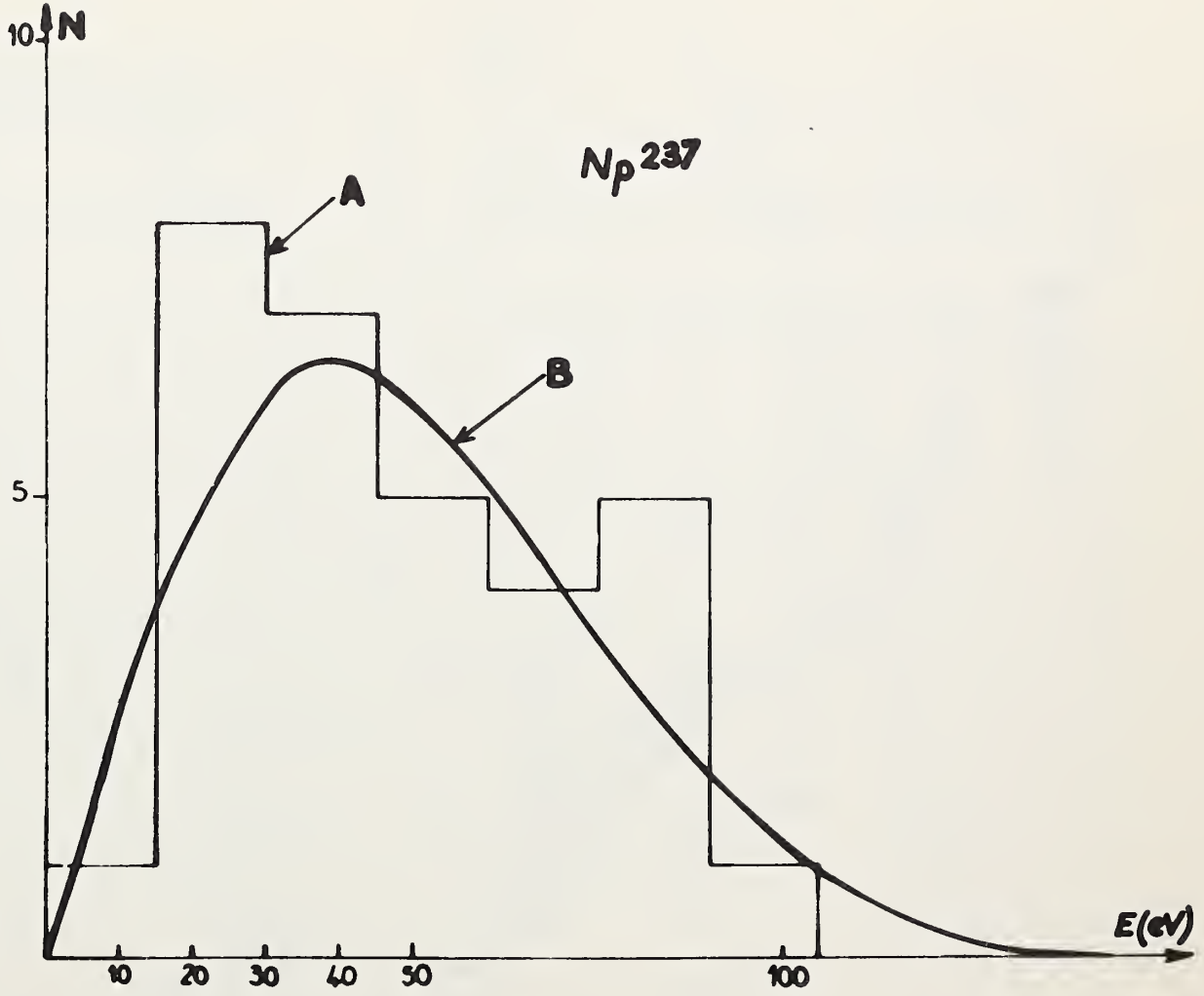

Fig. 24 The level spacing distribution of the big peaks structure observed in the fission cross section of Np^{237} below 1.6 KeV.

NORMALIZATION OF RELATIVE ^{235}U FISSION CROSS-SECTIONS IN THE RESONANCE REGION

A. J. Deruytter[+] and C. Wagemans[++]

Central Bureau for Nuclear Measurements, EURATOM, Geel (Belgium)

Studiecentrum voor Kernenergie, Mol (Belgium)

Abstract

Measurements were performed with the Linac of the CBNM in view of extending the Linac fission cross-sections down to below thermal energy for a direct normalization to the previously determined absolute 2200 m/s-reference cross-section. The measurements are performed at a well-collimated short flight-path (about 8 meter) with low repetition rate and long burst-time of the Linac. The comparison of induced reaction-rates in a back-to-back U-235- and B-10-foil is made simultaneously with two sets of solid-state detectors and registered in two halves of a 4096 channels time-of-flight analyser.

1. Introduction

Although it is possible with a linear electron accelerator for neutron production to measure relative fission cross-sections down to thermal energy (0.0253 eV) and hence to normalize these cross-sections directly to the thermal value, for a lot of practical reasons (low repetition frequency, short flight path, interpretation of background) it is generally not done that way. More often the cross-section curves are normalized with respect to a resonance integral determined from crystal spectrometer or chopper measurements around a reactor, that are normalized to the 2200 m/s-value. In many cases the data of Shore and Sailor (1) are used; these are normalized to the data of Leonard (2) that are finally normalized to the "world value" for σ_f (2200 m/s) of U-235. One previous direct normalization was reported by Bowman et al. (3). In this experiment we measure simultaneously the fission spectrum and the neutron spectrum with solid state detectors on each side of a back-to-back U-235- and B-10-layer. From the counting-rate ratios σ_f curves are calculated and normalized to a 2200 m/s-value of 587.3±3.5 barn. From this normalized curve a few resonance integrals are calculated with the corresponding error. We propose to use for further normalization the resonance integral

$$\int_{7.8\ \mathrm{eV}}^{11\ \mathrm{eV}} \sigma_F(E)\, dE$$

for reasons discussed in the text.

[+] CBNM, Euratom, Geel (Belgium)

[++] Nationaal Fonds voor Wetenschappelijk Onderzoek (Belgium)

2. Experimental Procedure

Two series of measurements of σ_f were performed: (1) energy-region 140 eV $> E_n >$ 0.009 eV (useful region 0.009 eV to 10 eV) (2) energy-region 0.15 eV $< E_n <$ 140 eV (useful region 0.4 eV to 21 eV) which yield a large region of overlapping that serves to interconnect both runs. In the first run we use large burst widths (2 μs) and low repetition-rates (50 pps) to avoid overlapping of successive bursts in the low energy region. The shape of the neutron spectrum measured via B-10(n, α)-reaction rates did not change when we lowered the repetition frequency to 12 Hz, so it was safe to use 50 Hz attractive in view of the higher counting-rates. In the second run we wanted somewhat better resolution to extend the measurements to about 21 eV neutron energy. Convenient Linac parameters were 50 ns burst width and 400 Hz repetition-frequency. In table 1 pertinent data are given concerning Linac parameters, multichannel analyser programs and neutron filters used. In the first series of measurements also runs were performed with Cd in the beam to evaluate background due to badly timed epi-Cd neutrons in the beam. The flight-path used has a length of 8.00 m from the 2.5 cm thick polyethylene moderator back-face to the back-to-back source. In the wall of the accelerator building a specially designed collimator is introduced to reduce the beam diameter to 60 mm. The beam after passage through the detection chamber goes through an evacuated aluminium tube with thin entrance window and is stopped about 20 m behind in a concrete beam-catcher(see fig. 1).

The detection chamber is an evacuated cylindrical chamber with thin entrance and exit windows and large dimensions (diameter is 27 cm). In the center of this chamber a back-to-back layer of B-10 and U-235 is mounted. On each side the layer is viewed by Au-Si surface-barrier detectors (1 mm thick Si and 30 μg/cm^2 Au). On the boron-side each detector has a separate preamplifier and the signals are only mixed after passage through a separate fast discriminator; on the fission side 4 detectors are connected in parallel with one preamplifier. The Si-crystals have a diameter of 2 cm and are mounted in a thin aluminium frame to reduce the amount of scattering material. The signals of the fast discriminators are mixed for each reaction type and fed into two halves of a 4096 channel time-of-flight analyser with accordeon system so that the fission-spectrum and the B-10 (n, α)Li-7 spectrum are recorded simultaneously. The neutrons pass first through the B-10-layer, for which absorption a small correction is applied to the fission data.

The U-235 layer was prepared by electrospraying uranylacetate on a thin aluminium plate (0.1 mm thick). The thickness of the layer is 2.5 mg/cm^2 on a diameter of 8 cm, and the isotopic composition of the U is 99.505 atom % U-235; 0.168% U-234; 0.301% U-238 and 0.026% U-236. The B-10 deposit is an elemental boron layer prepared by evaporation (electron bombardment) in vacuum with a thickness of 103 μg/cm^2, an isotopic enrichment of 92% and a diameter of 80 mm.

Each series of measurements consists of several direct runs separated by background runs to detect eventual changes in background during the measurement. Each direct run is a simultaneous recording of the B-10(n, α)Li-7 counts (discriminator set to register only the α -particles) and the U-235(n,f) fragments (discriminator set to detect only fission fragments) in two halves of

the TOF-analyser. For each background run the appropriate additional filters are put in the beam, and again fission and B-counts are registered.

3. Treatment of the Data, Results and Discussion

With the background filters in the beam we obtain for the "black" resonances a number of channels where over 99.9% of the incident resonance energy neutrons are absorbed; the remaining counting-rate is due to room background neutrons and "off-energy" beam neutrons. The average of these channels is considered as the background at the energy of the black resonance. Typical backgrounds are in the second type run for the Ta resonance (4.3 eV) 3%, Rh (1.25 eV) 0.6% for the B-10(n,α)-reaction and for the fission rate respectively: 15% and 1%. In the first type of run are the backgrounds for Ta and Rh 2% and 1% for the boron reaction and 3% and 1.5% for the fission reactions. In the direct runs and background runs two filters are used in common: Co and W in the first series, Cd and Co in the second one to normalize the background runs in time to the direct runs. The influence of the other background filters on the counting-rates in the permanent background resonances is indeed very small. The background-law is established by interpolation between the black resonances.
In the first type of measurements we also determined the background with a Cd filter in the beam yielding the contribution to the counting rate in the thermal region of "off-time" higher energy neutrons ($E_n > 0.4$ eV) and of room background neutrons. This contribution was found to be 0.006% for the fission spectra and 0.035% for the neutron spectrum at thermal energy. Once the background law is established the direct neutron spectrum (B-10 reactions) is corrected for it and then converted in a counting rate vs energy spectrum. With the method of least squares this spectrum is fitted with an expression

$$y = \sum_{i=1}^{n} a_i \, E^{i-1}$$

that is then used to obtain the $\sigma_F \sqrt{E}$ spectrum from the fission spectrum previously corrected for background in the same way as the neutron spectrum. The programs used were taken from (4). This $\sigma_F \sqrt{E}$-spectrum (ratio of corrected fission and fitted neutron spectrum) is then normalized to the 2200 m/s-value of σ_f determined with a chopper at the belgian BR2 reactor (communication D-4 at this conference) $\sigma_f^0 = 587.3 \pm 3.5$ barn. To normalize the series of measurements II to the first group of measurements I we determine k from a relationship:

$$k \int_{1.8\ eV}^{10\ eV} \sigma_F(E)\, dE = \int_{1.8\ eV}^{10\ eV} \sigma_F^{norm}(E)\, dE$$

where $\sigma_F^{norm}(E)$ are the normalized fission cross-sections of measurement I and $\sigma_F(E)$ the values from the second group of data treated in a similar way as described before (ratio of corrected fission data and fitted neutron spectrum).

In order to compare our results with previous results obtained by other ways of normalization and or with other detection techniques we summarized the results of several authors in table 2. These results are partly taken from (5). The differences between the integrals from different experiments are in some cases as high as 15%. Our values differ with a normalization via the results of Shore and Sailor by 3%.

As almost all relative fission cross-sections measured with a Linac come down in energy below 8 eV a resonance integral that can be considered useful for further normalization of U-235 fission cross sections is:

$$\int_{7.8\ \mathrm{eV}}^{11\ \mathrm{eV}} \sigma_F(E)\, dE$$

because it contains a large resonance (high counting-rate) and a relatively large timing error (+ 0.5 eV) does not considerably affect this integral because of the small cross-sections at the limits of the integral.

The value for this integral from our normalisation procedure is 222.0±2.0 barn-eV. The error results mainly from the value of σ_f^0. This result is still preliminary.

Acknowledgements

The authors wish to thank Dr. J. Spaepen (CBNM), Dr. Nève de Mévergnies (SCK, Mol) and Prof. J. Verhaeghe (University of Ghent) for fruitful discussions, Mrs. M. G. Cao and Mr. U. Meloni (CBNM) for their help with computations, Mr. E. Mies and Mr. L. Van Steelandt (SCK, Mol) for their technical help.

Special thanks go to Mr. C. Allard and Mr. J. M. Salomé for the excellent Linac operation.

One of us (C. Wagemans) wishes also to thank the "Nationaal Fonds voor Wetenschappelijk Onderzoek" for financial support.

4. References

(1) F. Shore, V. Sailor, Phys. Rev. 112, 1, p 191 (1958)

(2) Leonard, Seppi, Friesen, Hanford Atomic Products Operation, General Electric Company (1954) unpublished.

(3) C. Bowman et al., Conf. on Neutron Cross-Section Technology, Book 2, p 1004, March 1966, Washington D. C.

(4) M. G. Cao, Rapport EUR 3652. f

(5) Paper D-3 presented at this Conference.

TABLE 1

Energy Region	Linac Parameters	Neutron filters		Analyser Program	
		common filters	background filters	E(eV)	Δt_{ch}
I. 0.009 - 140 eV useful region: 0.01 - 10 eV	2 μs, 50 Hz 45 MeV, i_{av}=30 μA 1.4 kW	Co, W also run with Cd	Ta, Rh	140 - 125 125 - 23 23 - 2.5 2.5 - 0.75 0.75- 0.009	640 ns x 1 x 8 x 1 x 2 x 8
II. 0.15 - 140 eV useful region: 0.4 - 21 eV	50 ns, 400 Hz 53 MeV, i_{av}=30 μA 1.6 kW	Cd, Co	W, Ta, Rh	140 - 125 125 - 23 23 - 7.8 7.8 - 2.5 2.5 - 0.15	160 ns x 1 x 8 x 1 x 2 x 8

TABLE 2

Comparison of fission integrals - $\int \sigma_F(E)\, dE$ (barn - eV)

Energy Interval (eV)	Brooks	de Saussure	Mostovaya	Bowman	Ryabov	Michaudon		CBNM i. ch.	CBNM Liq. Sc.	Our results Solid state detector
5 -7.4	57.0	62.2	66.41	) 292.1	61.72	61.4				59.0±0.6
7.4-10	201.0	219.2	233.0	)	194.6	216.4	212.4	210.1	210.2	206.0±2.0
10 - 15	197.7	216.7	226.9	220.0	205.9	218.7	213	202.9	206.3	212.0±2.0

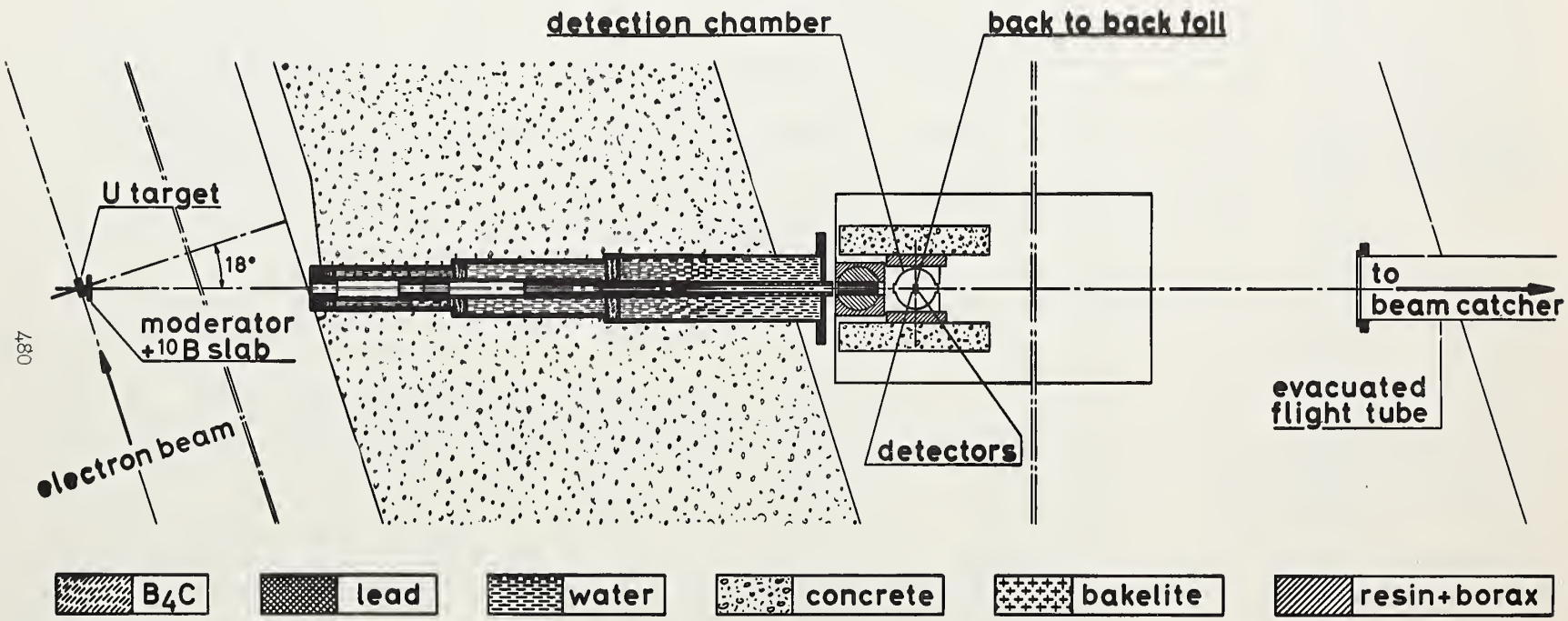

480

Fig. 1: Experimental set-up and collimation in the short flight-path 17 of the Geel-Linac.

FISSION CROSS SECTION MEASUREMENT ON U-235

M. G. Cao, E. Migneco, J. P. Theobald, J. A. Wartena and J. Winter

Central Bureau for Nuclear Measurements

EURATOM, Geel, Belgium

Abstract

The cross section of the U-235(n,f) reaction has been measured with a high energy resolution for neutrons between 6 eV and 3 keV.
A fission fragment and a fission neutron detector were used simultaneously. Resonance parameters for 78 levels between 6 and 150 eV are given. The statistical distributions of Γ_f, Γ_γ and α have been studied.

1. Introduction

The fission cross section of U-235 in the epithermal neutron energy range has been remeasured with the aim to reduce the background contribution as much as possible and to increase the energy resolution. This permits us to eliminate the main source of discrepancy in previous experiments (1, 3) and to give parameters for a higher number of resonances in the energy range between 50 and 150 eV.
Two independent detectors systems have been used in the time-of-flight spectrometer: an ionisation chamber as fission fragment and a liquid scintillator tank as fission neutron detector.

2. Experimental Technique

Fast neutrons produced in the mercury cooled natural uranium target by the electron beam of the CBNM linear accelerator are slowed down by a 2.8 cm thick polyethylene sheet of 20 cm x 20 cm. The spectrum of the moderated neutrons as determined with a $^{10}BF_3$ counter shows in good approximation an energy dependence like $E^{-0.887}$ in the considered energy range. The experimental set-up is shown in fig. 1.

The detectors

The fission neutron detector (fig. 2) consists of four liquid scintillation chambers forming a hollow cylinder with outer diameter 38 cm, inner diameter 16 cm, inner length 18 cm, outer length 38 cm. The metallic U-235 sample is placed in the middle of this cylinder. It is a disc of 12 cm diameter and a thickness of about 100 mg/cm^2 in the neutron energy range up to 41 eV and of about 200 mg/cm^2 for higher energy ranges. The isotopic composition of the sample is: U-234: 0.72%, U-235: 93.1%, U-236: 0.17%, U-238: 5.9%. The detector is filled with liquid scintillator NE 213. The sample is shielded from the liquid by a 5 mm thick hollow cylinder of Li-6 to avoid fission induced by backscattered neutrons. Each chamber is viewed by a 58 AVP photoelectron multiplier connected with a pulse shape discriminator, the output of which delivers the signal of a recoil proton in the energy range between 350 keV and 1.8 MeV. The four P.S.D.'s are linked with six two-input coincidence stages. The electron time resolution is 30 nsec FWHM, the coin-

cidence resolution 40 nsec (fig. 3).

The fission fragment detector (fig. 4) is a sequence of circular ionization chambers with a sensitive area of 26 cm diameter and an interelectrode distance of 4 mm. The electrodes are 35 μ thick aluminium foils spanned on rigid aluminium rings. In each chamber one electrode forms the backing of an electrosprayed uran-uranyl acetate layer with a content of 800 μg U/cm^2 on an area of 26 cm diameter. The isotopic composition of the uranium is: U-234: 0.168%, U-235: 99.505%, U-236: 0.026%, U-238: 0.301%. The layer thickness is about 1.5 mg/cm^2. The filling gas of the chambers is argon plus 5% CO-2 under 450 Torr pressure. The voltage applied to the chambers is 500 V. In the energy range up to 41 eV a sequence of six ionization chambers in the higher range eight chambers are used. This "multiple ionization chamber" is housed in a cylindrical aluminium box with a window of 0.6 mm thickness in the neutron beam. Each two chambers are combined to a unit with a common middle electrode which is connected with an amplifier. The time resolution of one chamber unit is between 40 and 50 nsec FWHM. The total time resolution of the detector is 100 nsec FWHM (fig. 5).

The neutron spectrum has been measured and controlled by a bank of $^{10}BF_3$ proportional counters placed 1 m behind the fission detectors.

The multichannel time-of-flight analyzers used during this experiment are: Two 4096 channel analyzers equipped with an "accordeon" and a 65 536 channel analyzer system consisting of a sequence of: fast logic units, a 10 nsec time coder, a derandomizer and a magnetic tape recorder. Both analyzer systems have a maximum time resolution of 10 nsec/channel. The time-of-flight analyzers are started with an electronic signal produced by the passage of the electron burst just before the linac target.

3. Measurements

The simultaneous measurements with the two detectors are performed in three runs of the following characteristics:

Neutron energy range	1st run 4.7 - 47 eV	2nd run 30 - 300 eV	3rd run >240 eV
Linac beam energy	50 MeV	50 MeV	50 MeV
Peak beam current	0.45 A	1.2 A	1.5 A
Burst frequency	100 Hz	150 Hz	400 Hz
Burst width	300 nsec	80 nsec	50 nsec
Channel width	(4.7-8 eV) 640nsec (8 -26.3eV) 320nsec (26.3-43eV) 160nsec (43 -47eV) 1280nsec	80 nsec	80 nsec
Number of channels	4096	16 384	4096
Polyethylene moder.	20 x 20 x 2.8 cm^3		
Permanent background samples	Au, Mo	W, Mn	Mo
Samples for the background spectrum	Au, Mo	W, Mo, Co, Mn, Bi	Mo, Mn, Bi, Na
Cut-off-filter	Cd	B(nat)	B-10
Detector distance	60.58 m	60.58 m	60.58 m

These sets of parameters are the same for both detectors.

4. Results

The fission cross section has been calculated from the data coming out of the time-of-flight analyzer by application of the following formula:

$$\sigma_f(E) \quad \sqrt{E} = K \frac{N_f(E) - (BG)_f(E)}{N_n(E) - (BG)_n(E)}$$

σ_f: fission cross section (barn); E: incoming neutron energy (eV); K: normalization constant (barn – eV); N_f: fission yield; $(BG)_f$: background count in the fission detector; N_n: neutron rate; $(BG)_n$: background count in the neutron detector. The functions BG(E) and $N_n(E)$ have been determined by fitting the data with smooth analytical curves.

The normalization constant K is calculated by equalizing the integrals $\int_{8eV}^{10eV} \sigma_f(E)dE$ of these data and the data obtained by Shore and Sailor (2), which are normalized with the value $\sigma_f(0.025\ eV) = 582$ b for thermal neutrons. The different runs are matched by equalizing the integrals $\int \sigma_f(E)dE$ over the overlapping energy ranges.

The comparison of these data with those of other laboratories (BNL 325 III) show, that our fission cross section is in general higher in the peaks of resonances and lower in the valleys between them (Figs. 6, 7, 8, 9, 10). This effect is a consequence of the higher energy resolution in this experiment and the special care that has been taken to avoid as much as possible scattering material in the neutron beam near the detectors.

The integrals of the fission cross section over several given neutron energy ranges for different experiments are shown in table 1.

The results of Michaudon (3) and Ryabov (4) agree quite well with our data. The integrals differ within a few percent with alternating sign up to 200 eV. The integrated data of Brooks (5) are systematically lower, while those of de Saussure (6) are slightly higher. Two integrals disagree with values of other laboratories. The comparison of the data collected with the two different detector systems demonstrates in general a good agreement. This can be seen in table 1, which shows in the last columns the fission cross section integrals over large energy ranges for both experiments. The integrals over the single resonances fluctuate within 3% except for a few resonances for which a correction for self absorption and multiple scattering inside the metallic uranium sample of the liquid scintillator has still to be applied. The error on σ_f in the highest resonance peaks (at 8.8; 12.4; 19.3 eV...) is 1% due to counting statistics, in the residual cross section between the resonances about 20%. Here the error on the background determination is of importance.

5. Evaluation of the Resonance Parameters

The parameters of the fission resonances from the ionization chamber data have been determined up to 150 eV with the shape analysis computer program 032 S of Saclay.

For the Doppler width Δ the dependence $\Delta = 0.021 \cdot \sqrt{E_r} \cdot eV^{-1/2}$ has been used.

The resolution function has been calculated taking into account the following contributions: detector thickness, flightpath inclination, moderation time, channel width, burst width, detector jitter. The final resolution function was assumed to be a gaussian with a variance equal to the sum of the variance of the single contributions.

The Γ and Γ_n values applied are results from the experiments of Michaudon (7, 8).
For energies higher than 50 eV only such resonances have been analyzed which have a total Γ width of less than 200 meV to avoid contributions of overlapping levels. A term for residual fission between the resonances has been neglected. 78 resonances have been analyzed and the results are given in table 2.
In contrast with other experiments (7) we do not find a correlation between the values of Γ_γ and Γ_f. The calculated correlation coefficients are:

$$\rho(\Gamma_\gamma, \Gamma_f) = \frac{\langle \Gamma_\gamma \Gamma_f \rangle - \langle \Gamma_\gamma \rangle \langle \Gamma_f \rangle}{\sqrt{\mathrm{Var}(\Gamma_\gamma)\ \mathrm{Var}(\Gamma_f)}} \simeq 10^{-5}$$

In particular there is no evidence that large Γ_f values are combined with large values of Γ_γ.
The mean values of Γ_f and Γ_γ are: between 6 - 50 eV $\overline{\Gamma_f}$ = 48.5±2.2 meV, $\overline{\Gamma_\gamma}$ = 40.8±1.8 meV; between 50 - 150 eV $\overline{\Gamma_f}$ = 57.2±2.0 meV, $\overline{\Gamma_\gamma}$ = 49.0±1.6 meV and for the total range from 6 - 150 eV $\overline{\Gamma_f}$ = 53.2±1.5 meV, $\overline{\Gamma_\gamma}$ = 45.2±1.2 meV.
The statistical distribution of the Γ_f values has been fitted with the formula for the X^2 distribution (fig. 11, 12).
For resonances in the range between 6 and 50 eV the best fit was obtained with ν = 3.8±1.7 degrees of freedom, while between 50 and 150 eV as well as for the total range from 6 to 150 eV ν = 4±1.2 delivers the best approximation.
The Γ_γ values in the energy range between 6 and 50 eV fluctuate considerably less than it was deduced from other experiments (7). As a matter of fact the number ν of degrees of freedom calculated with the formula

$$\left\langle \left(\frac{\Gamma_\gamma}{\langle \Gamma_\gamma \rangle} \right)^2 \right\rangle - 1 = \frac{2}{\nu}$$

is 41 instead of 32.
In the energy range between 50 and 150 eV the fluctuations increase and ν is calculated to be 31. Because of the fact that we cannot verify a correlation between Γ_γ and Γ_f no resonance classification for the two spin families can be tried following a grouping in the Γ_γ distribution, but the distribution of $\alpha = \Gamma_\gamma / \Gamma_f$ (fig. 13) shows a slight evidence for a resonance grouping in the following sense:
If we devide the resonances into two groups with $0 < \alpha < 0.6$ and $1.0 < \alpha < \infty$ we find, that the first type of resonances has a Γ_f value of 100 meV while the second type has Γ_f = 27 meV. Resonances with $0.6 < \alpha < 1.0$ remain unclassified. If one assumes that this grouping is also valid for the two spin families one finds Γ_f^{3-} = 100 meV and Γ_f^{4-} = 27 meV.
In the first group we find 22 resonances, in the second 38, 15 remain unclassified.
Theoretical considerations of Bazazyants and Gordeev (9) predict the values Γ_f^{3-} = 81 meV and Γ_f^{4-} = 32.5 meV.

6. Conclusions

The σ_f values we have obtained are in good agreement with the data of Michaudon (3). The ratio of the cross section in the peaks of the resonances to that between them has been increased. A fit of data with the single level formalism has been reached without assuming a contribution of residual fission.
The data obtained with the fission fragment detector agree within a few percent with the results of the fission neutron detector. The deviations can be

quantitatively explained by self absorption and multiple scattering effects for big resonances and by bad counting statistics for small ones. The statistical properties of the resulting resonance parameters can be summarized as follows:

1) We cannot verify a correlation between the Γ_f and Γ_γ values.
2) The X^2 distribution of Γ_f shows that $\nu \simeq 4$. For the Γ_γ values we find $\nu \simeq 40$ for resonances below 50 eV and $\nu \simeq 30$ for resonances between 50 and 150 eV.
3) In the distribution of α we find a grouping of resonances with Γ_f = 100 meV below α = 0.6 and with Γ_f = 27 meV higher than α = 1.0.

We thank Dr. J. Spaepen for his continuous support and Mr. K. H. Böckhoff for his help during the experiment and the evaluation of the data. The authors are especially indebted to Dr. Michaudon and Mr. Derrien from the CEA Saclay for the computer program and their experimental and theoretical data given to them before publication. Mr. Merla was during the time of this experiment our technical assistent. His contributions to this work are highly acknowledged. We feel great gratitude to all who have helped us to realize these measurements: Mr. De Keyser and Mr. Van der Veen for the excellent data handling electronics, Dr. Lauer, Dr. Verdingh and Mr. Van Audenhove for the prepation of samples, Mr. Schreiber for the construction of all mechanical parts and the detectors, Mr. Meloni for his help during the evaluation and last but not least Mr. Allard and Mr. Salomé for the linac operation.

7. References

(1) C. D. Bowman et al., Phys. Rev. 130 (1963) 1482;
(2) S. F. Shore and V. L. Sailor, Phys. Rev. 112 (1958) 191
(3) A. Michaudon, Rapport CEA - R 2552 (1964)
(4) U. V. Ryabov et al., Symposium on Physics and Chemistry of Fission, Salzburg, Proceedings (1965) 287
(5) F. D. Brooks, Symposium on Neutron Time-of-Flight Methods, Saclay Proceedings (1961) 131
(6) G. De Saussure et al., Conference on Nuclear Data for Reactors, Paris, Proceedings (1967) 233
(7) A. Michaudon, Nucl. Phys. 69 (1965) 545
(8) A. Michaudon, private communication
(9) N. Bazazyants and I. V. Gordeev, Atomnaya Energiya 13 (1962) 321

TABLE 1

COMPARISON OF FISSION INTEGRALS

$\int \sigma_f(E)\,dE$ (BARN-EV)

ENERGY INTERVAL (EV)	BROOKS	DE SAUSSURE		MOSTOVAJA	BOWMAN	RJABOV	MICHAUDON		OUR DATA (IONIZ. CH.)		(LIQ.SCI.)
5 - 7.4	57.0	62.2		66.41		61.72	61.4				
7.4 - 10	201.0	219.2		233.0	292.1	194.6	216.4	212.4	210.1		210.2
10 - 15	197.7	216.7		226.9	220.0	205.9	218.7	213	202.9		206.3
15 - 20.5	278.8	315.6		326.5	332.6	278.7	310.9	286.8	291.4		290.7
20.5 - 33	417	415.6	447.2	487.2	457.7	419.4	459.8	427.1	411.2		421
33 - 41	416	495.0	492	548	517.5	459	484.0	445	471.7		476
41 - 60	830	918.0	925	1015	968.6	816		839	843.1		860
60 - 73	250		310	348	302.6	275		301	288.6	263.8	290.4
73 - 100	580		666	750		693		631	613.8	645.7	614.5
100 - 113	184		216	247		231		230	199.8	217.1	193
113 - 200	1584		1876			1775		1798	1750.5	1726.1	1642
200 - 300			2082			2056		2059		1767.9	
300 - 1000			8106			8111		8106		6974	
1000 - 3000			13220			13240		13310		13278	
3000 - 10000			27370			26130		27850			
10000 - 20000			46840			32250		26690			

TABLE 2

U 235 RESONANCE PARAMETERS

E_o(eV)	Γ_T(meV)	Γ_n(meV)	Γ_f(meV)	Γ_γ(meV)	$\alpha=\Gamma_\gamma/\Gamma_f$	$\sigma_o\Gamma_f$(barn.eV)
6.39 ± 0.0007	45. ± 3.	0.26 ± 0.015	9. ± 1.	36. ± 2.	4.18 ± 0.	10.1 ± 0.2
7.08 ± 0.0007	64. ± 5.	0.13 ± 0.006	27. ± 3.	36. ± 3.	1.33 ± 0.	9.8 ± 0.1
8.79 ± 0.0008	133. ± 13.	1.18 ± 0.050	84. ± 9.	47. ± 6.	0.56 ± 0.01	109.9 ± 0.8
9.29 ± 0.0027	160. ± 40.	0.20 ± 0.040	115. ± 37.	45. ± 26.	0.39 ± 0.03	19.9 ± 0.4
10.20 ± 0.0016	95. ± 10.	0.06 ± 0.006	46. ± 7.	49. ± 7.	1.07 ± 0.01	3.9 ± 0.1
11.65 ± 0.0008	40. ± 5.	0.59 ± 0.040	4. ± 1.	35. ± 4.	8.21 ± 0.01	7.0 ± 0.1
12.39 ± 0.0012	69. ± 6.	1.29 ± 0.060	28. ± 3.	40. ± 4.	1.41 ± 0.01	54.6 ± 0.7
12.85 ± 0.0023	83. ± 13.	0.04 ± 0.015	72. ± 29.	11. ± 27.	0.16 ± 0.03	3.5 ± 0.1
13.69 ± 0.0067	75. ± 38.	0.04 ± 0.015	32. ± 22.	43. ± 27.	1.34 ± 0.04	1.6 ± 0.5
14.51 ± 0.0023	52. ± 8.	0.13 ± 0.010	14. ± 2.	38. ± 6.	2.83 ± 0.01	2.9 ± 0.1
15.40 ± 0.0021	98. ± 15.	0.25 ± 0.020	53. ± 9.	44. ± 8.	0.83 ± 0.01	11.4 ± 0.2
16.08 ± 0.0019	56. ± 7.	0.37 ± 0.020	18. ± 3.	37. ± 5.	2.01 ± 0.01	9.8 ± 0.2
16.69 ± 0.0023	138. ± 15.	0.28 ± 0.020	97. ± 13.	41. ± 8.	0.42 ± 0.01	15.2 ± 0.3
18.07 ± 0.0091	160. ± 20.	0.36 ± 0.030	116. ± 20.	44. ± 15.	0.38 ± 0.02	18.6 ± 1.6
19.31 ± 0.0010	105. ± 10.	3.10 ± 0.150	60. ± 6.	42. ± 5.	0.69 ± 0.01	118.8 ± 1.0
20.61 ± 0.0038	92. ± 10.	0.19 ± 0.020	54. ± 8.	38. ± 7.	0.71 ± 0.01	6.9 ± 0.2
21.08 ± 0.0013	70. ± 6.	1.58 ± 0.100	25. ± 3.	43. ± 4.	1.72 ± 0.01	34.7 ± 0.4
22.94 ± 0.0015	92. ± 10.	0.45 ± 0.030	52. ± 7.	40. ± 6.	0.77 ± 0.01	14.2 ± 0.2
23.42 ± 0.0020	37. ± 4.	0.69 ± 0.060	6. ± 1.	30. ± 3.	5.20 ± 0.01	6.0 ± 0.2
27.82 ± 0.0010	128. ± 15.	0.72 ± 0.050	68. ± 9.	59. ± 8.	0.86 ± 0.01	17.8 ± 0.1
28.38 ± 0.0026	140. ± 30.	0.16 ± 0.020	111. ± 28.	29. ± 15.	0.26 ± 0.02	5.8 ± 0.1
29.64 ± 0.0030	73. ± 10.	0.18 ± 0.010	30. ± 5.	42. ± 6.	1.39 ± 0.01	3.3 ± 0.1
30.59 ± 0.0045	150. ± 15.	0.21 ± 0.020	101. ± 14.	49. ± 11.	0.48 ± 0.01	6.0 ± 0.2
30.86 ± 0.0026	60. ± 6.	0.52 ± 0.050	19. ± 3.	40. ± 4.	2.05 ± 0.01	7.1 ± 0.2
32.07 ± 0.0009	100. ± 10.	1.95 ± 0.150	53. ± 7.	45. ± 6.	0.84 ± 0.01	41.8 ± 0.3
33.53 ± 0.0029	62. ± 8.	1.92 ± 0.120	23. ± 3.	37. ± 5.	1.64 ± 0.01	27.1 ± 0.7
34.39 ± 0.0024	85. ± 10.	2.20 ± 0.200	38. ± 6.	44. ± 7.	1.16 ± 0.01	37.3 ± 0.6
34.83 ± 0.0076	110. ± 30.	0.90 ± 0.200	84. ± 30.	25. ± 20.	0.30 ± 0.02	25.5 ± 1.2
35.20 ± 0.0031	175. ± 25.	4.50 ± 0.300	126. ± 20.	45. ± 11.	0.36 ± 0.01	118.3 ± 2.0
39.41 ± 0.0010	95. ± 10.	2.50 ± 0.020	55. ± 6.	38. ± 4.	0.69 ± 0.01	47.3 ± 0.3
41.88 ± 0.0024	90. ± 10.	1.45 ± 0.010	21. ± 2.	67. ± 8.	3.17 ± 0.01	10.5 ± 0.2
42.70 ± 0.0068	64. ± 6.	0.29 ± 0.030	17. ± 3.	47. ± 5.	2.81 ± 0.01	2.3 ± 0.1
43.39 ± 0.0020	66. ± 7.	0.68 ± 0.050	21. ± 3.	44. ± 5.	2.07 ± 0.01	6.5 ± 0.1
47.95 ± 0.0056	76. ± 8.	0.84 ± 0.060	21. ± 3.	54. ± 6.	2.59 ± 0.01	6.2 ± 0.4
49.43 ± 0.0036	60. ± 6.	0.75 ± 0.080	22. ± 3.	37. ± 4.	1.71 ± 0.01	7.1 ± 0.2
50.14 ± 0.0069	54. ± 7.	0.25 ± 0.020	25. ± 4.	29. ± 4.	1.19 ± 0.01	2.9 ± 0.1
50.49 ± 0.0026	122. ± 13.	1.13 ± 0.030	61. ± 7.	60. ± 7.	0.97 ± 0.01	14.5 ± 0.2
51.72 ± 0.0241	50. ± 8.	0.27 ± 0.030	10. ± 3.	39. ± 7.	3.76 ± 0.01	1.4 ± 0.2
53.46 ± 0.0024	164. ± 25.	0.64 ± 0.050	104. ± 18.	59. ± 12.	0.56 ± 0.02	9.8 ± 0.1
55.08 ± 0.0029	121. ± 12.	3.28 ± 0.080	58. ± 6.	60. ± 6.	1.04 ± 0.01	36.7 ± 0.6
56.50 ± 0.0023	147. ± 15.	4.89 ± 0.350	93. ± 12.	49. ± 9.	0.53 ± 0.01	70.6 ± 0.8
58.06 ± 0.0032	65. ± 10.	1.36 ± 0.080	30. ± 5.	33. ± 6.	1.09 ± 0.01	14.2 ± 0.4
58.70 ± 0.0018	160. ± 20.	1.42 ± 0.100	109. ± 16.	49. ± 10.	0.45 ± 0.01	21.3 ± 0.2
60.85 ± 0.0048	170. ± 40.	0.51 ± 0.030	123. ± 30.	46. ± 13.	0.38 ± 0.02	7.8 ± 0.2
61.18 ± 0.0067	173. ± 50.	0.45 ± 0.050	113. ± 35.	60. ± 22.	0.53 ± 0.03	6.2 ± 0.2
64.31 ± 0.0061	60. ± 7.	1.25 ± 0.060	6. ± 1.	52. ± 6.	8.22 ± 0.01	2.7 ± 0.1
65.82 ± 0.0083	60. ± 30.	0.31 ± 0.060	36. ± 19.	24. ± 14.	0.65 ± 0.02	3.7 ± 0.2
66.38 ± 0.0082	67. ± 20.	0.37 ± 0.040	38. ± 12.	29. ± 10.	0.75 ± 0.01	4.1 ± 0.2
72.40 ± 0.0015	130. ± 30.	3.20 ± 0.400	68. ± 18.	59. ± 17.	0.88 ± 0.02	29.6 ± 0.5
74.57 ± 0.0046	118. ± 12.	2.96 ± 0.200	56. ± 7.	60. ± 8.	1.07 ± 0.01	24.1 ± 0.9
77.53 ± 0.0052	121. ± 10.	1.02 ± 0.080	66. ± 8.	54. ± 7.	0.81 ± 0.01	9.3 ± 0.2
78.11 ± 0.0058	140. ± 15.	1.02 ± 0.080	100. ± 14.	39. ± 9.	0.38 ± 0.01	12.1 ± 0.3
79.69 ± 0.0089	120. ± 12.	0.69 ± 0.030	82. ± 10.	37. ± 6.	0.45 ± 0.01	7.7 ± 0.3
80.37 ± 0.0082	170. ± 30.	0.74 ± 0.030	144. ± 27.	25. ± 9.	0.17 ± 0.01	10.1 ± 0.3
81.46 ± 0.0067	110. ± 10.	0.89 ± 0.030	81. ± 8.	28. ± 5.	0.35 ± 0.01	10.3 ± 0.3
89.85 ± 0.0093	138. ± 20.	0.66 ± 0.050	87. ± 14.	51. ± 10.	0.59 ± 0.01	5.9 ± 0.2
90.44 ± 0.0047	63. ± 6.	4.83 ± 0.200	10. ± 1.	48. ± 5.	4.88 ± 0.01	10.8 ± 0.2
92.60 ± 0.0049	98. ± 15.	2.53 ± 0.200	45. ± 8.	50. ± 9.	1.11 ± 0.01	16.2 ± 0.3
94.12 ± 0.0044	75. ± 15.	4.00 ± 0.300	9. ± 2.	62. ± 13.	6.70 ± 0.02	6.7 ± 0.2
100.40 ± 0.0076	135. ± 20.	0.66 ± 0.040	71. ± 11.	64. ± 11.	0.90 ± 0.01	4.4 ± 0.1
101.00 ± 0.0069	92. ± 10.	1.00 ± 0.050	27. ± 3.	64. ± 7.	2.40 ± 0.01	3.7 ± 0.1
101.90 ± 0.0164	107. ± 20.	0.36 ± 0.030	70. ± 15.	36. ± 10.	0.52 ± 0.01	3.0 ± 0.2
103.00 ± 0.0047	120. ± 12.	2.52 ± 0.300	78. ± 12.	39. ± 10.	0.50 ± 0.01	20.5 ± 0.4
103.60 ± 0.0074	146. ± 20.	2.07 ± 0.100	72. ± 11.	72. ± 11.	1.00 ± 0.02	12.7 ± 0.3
107.60 ± 0.0080	77. ± 7.	4.12 ± 0.010	19. ± 2.	53. ± 5.	2.75 ± 0.01	12.5 ± 0.4
108.10 ± 0.0316	120. ± 18.	0.44 ± 0.040	67. ± 14.	52. ± 12.	0.78 ± 0.02	2.9 ± 0.3
108.90 ± 0.0118	97. ± 10.	1.26 ± 0.040	38. ± 4.	58. ± 6.	1.54 ± 0.01	5.8 ± 0.3
111.20 ± 0.0350	103. ± 15.	0.48 ± 0.020	23. ± 4.	79. ± 12.	3.44 ± 0.02	1.2 ± 0.1
111.70 ± 0.0064	98. ± 10.	1.13 ± 0.040	46. ± 5.	51. ± 6.	1.10 ± 0.01	6.1 ± 0.1
115.30 ± 0.0318	73. ± 17.	0.44 ± 0.060	33. ± 10.	39. ± 11.	1.19 ± 0.02	2.2 ± 0.3
124.80 ± 0.0093	182. ± 27.	2.20 ± 0.300	118. ± 24.	61. ± 19.	0.52 ± 0.02	14.8 ± 0.4
130.10 ± 0.0260	82. ± 12.	1.69 ± 0.015	12. ± 2.	68. ± 10.	5.67 ± 0.02	2.5 ± 0.2
132.80 ± 0.0415	64. ± 10.	1.20 ± 0.400	19. ± 14.	43. ± 16.	2.23 ± 0.04	3.5 ± 2.3
133.60 ± 0.0112	99. ± 14.	4.47 ± 0.500	51. ± 9.	43. ± 9.	0.84 ± 0.01	22.4 ± 0.9
136.40 ± 0.0118	124. ± 12.	3.15 ± 0.200	50. ± 6.	70. ± 8.	1.40 ± 0.01	12.1 ± 0.5
137.60 ± 0.0077	59. ± 7.	3.10 ± 0.300	23. ± 4.	33. ± 5.	1.43 ± 0.01	11.3 ± 0.3
139.20 ± 0.0142	45. ± 7.	0.47 ± 0.060	22. ± 5.	23. ± 5.	1.05 ± 0.01	2.1 ± 0.1
147.40 ± 0.0061	73. ± 8.	2.70 ± 0.150	34. ± 4.	37. ± 5.	1.10 ± 0.01	10.9 ± 0.3

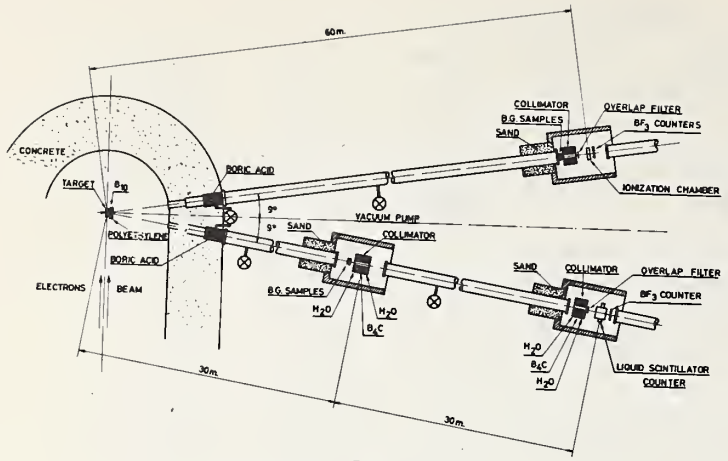

FIG. 1

Experimental set-up.

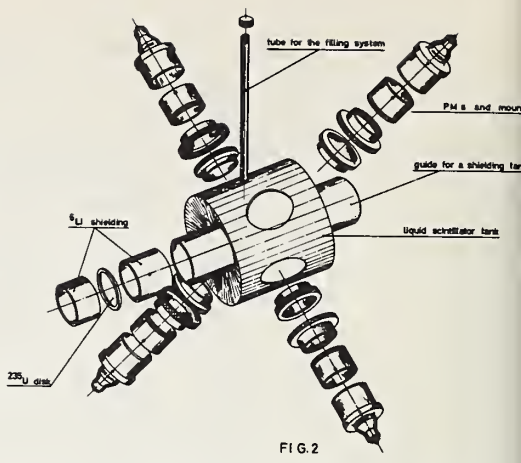

FIG. 2

Liquid scintillation neutron detector.

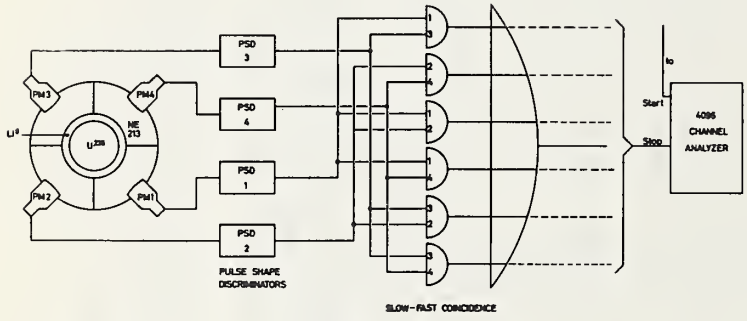

FIG. 3

Electronic block diagram for the fission neutron detector.

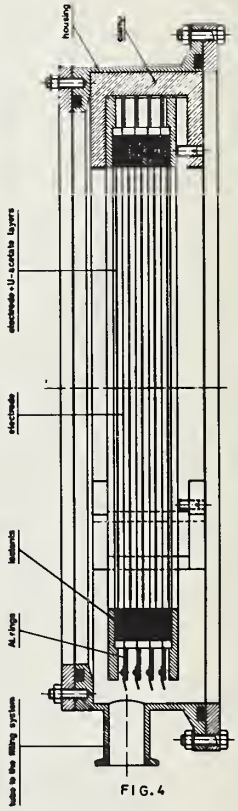

FIG. 4

Multiplate ionization chamber.

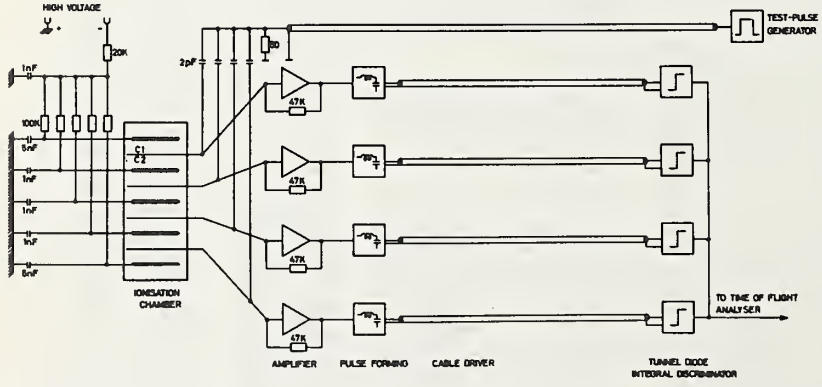

FIG. 5

Electronic block diagram for the fission fragment detector.

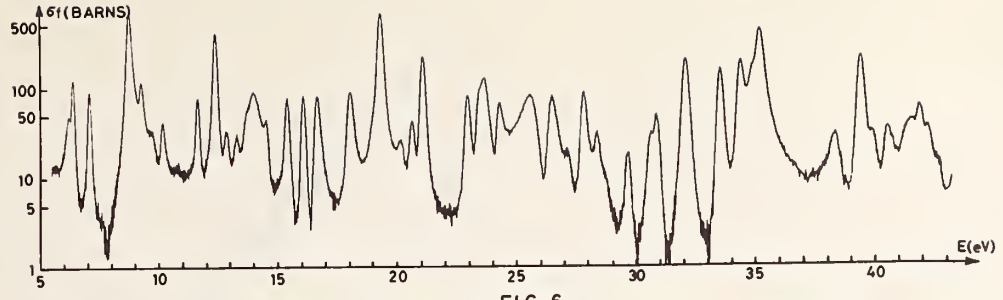

FIG. 6
The fission cross section of U-235 between 6 and 45 eV.

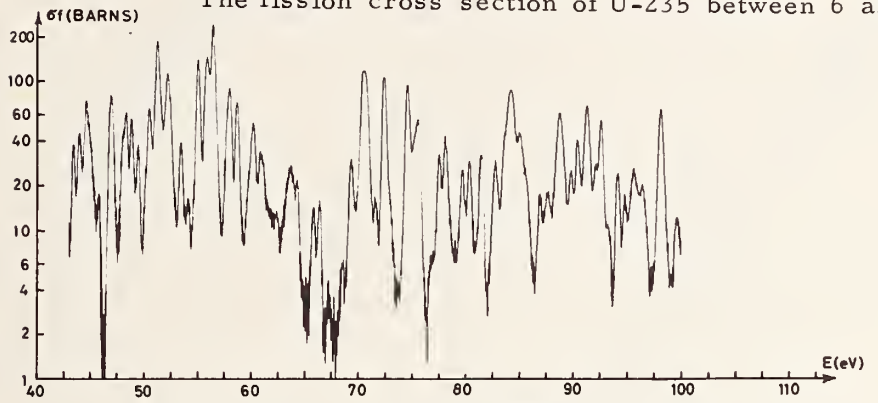

FIG. 7
The fission cross section of U-235 between 60 and 100 eV.

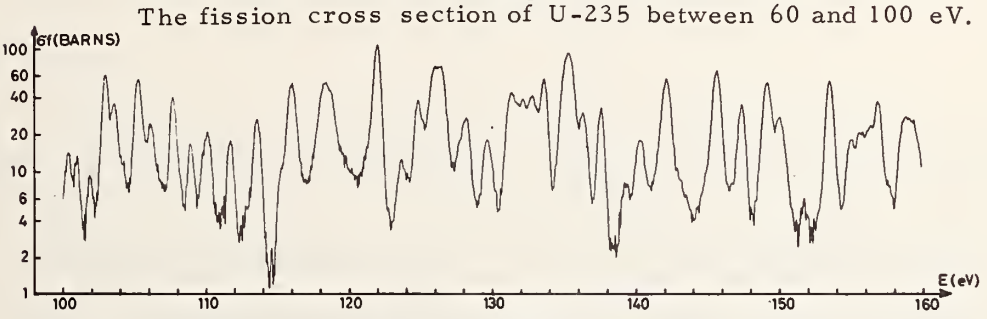

FIG. 8
The fission cross section of U-235 between 110 and 160 eV.

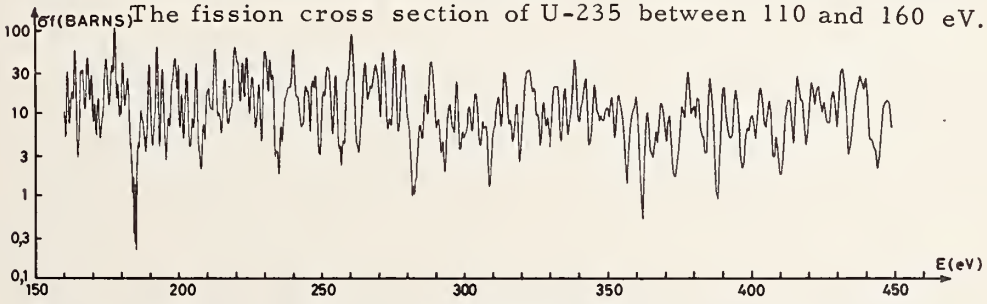

FIG. 9
The fission cross section of U-235 between 150 and 450 eV.

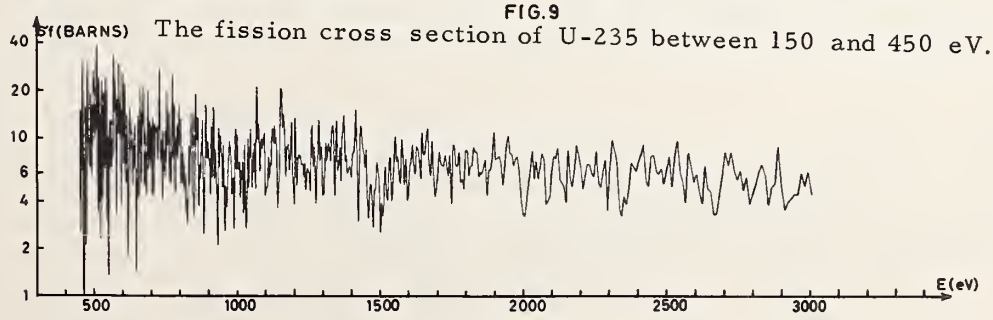

FIG. 10
The fission cross section of U-235 between 450 eV and 3 KeV.

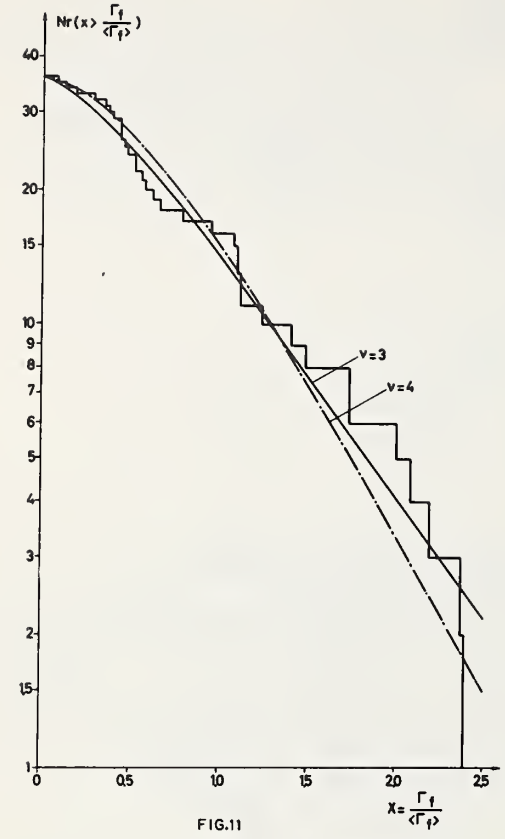

FIG.11

X^2 distribution of $\Gamma_f/\langle\Gamma_f\rangle$ for resonances between 6 and 50 eV.

FIG. 12

X^2 distribution of $\Gamma_f/\langle\Gamma_f\rangle$ for resonances between 6 and 150 eV.

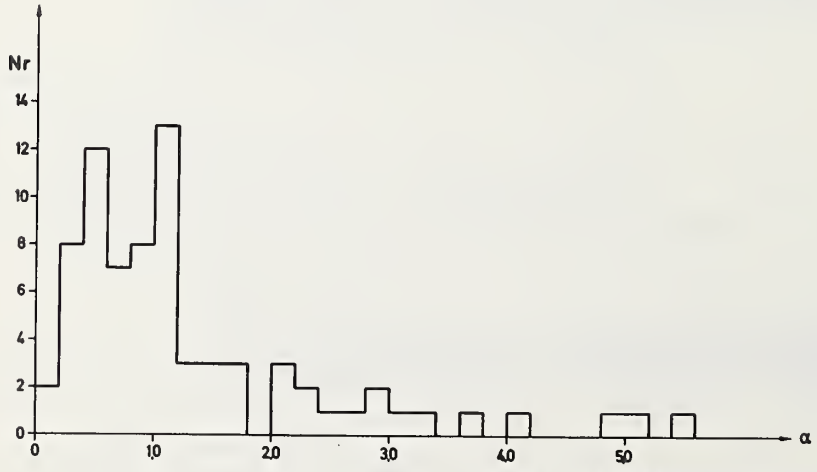

FIG.13 Statistical distribution of α .

PRECISE 2200 M/S FISSION CROSS-SECTION OF ^{235}U

A. J. Deruytter, J. Spaepen and P. Pelfer[+]
Central Bureau for Nuclear Measurements
EURATOM, Geel (Belgium)

Abstract

A new precise measurement of the 2200 m/s fission cross-section of U-235 was performed with a slow chopper at the BR2-reactor (energy-range from 0.005 eV to 0.1eV). Simultaneous recordings of pulse-height and time-of-flight spectra of successively compared U-235F-4-layers and standard natural boron-layers were made. The detection of the B-10(n, α)Li-7 and U-235(n,f) reaction fragments is made with excellent pulse-height resolution in low geometry with a surface-barrier detector. The relative B-10 contents of several standard boron-foils were checked by their neutron induced reaction rates. The absolute B-10 contents were determined from direct weighing in vacuum combined with careful chemical and isotopic analysis of witness foils. The fission foils were checked by α- and fission fragment counting.

A discussion with regard to previous results is included.

1. Introduction

The most serious criticism about direct precise thermal fission cross section measurements with choppers (1) or crystal spectrometers (2) is the insufficient knowledge of the efficiency of the 2π (2) or 4π (1) geometry ionization chambers used in such experiments. Indeed in such differential measurements rather thick fissile layers (about 0.5 mg/cm^2) were used in view of counting statistics and the resulting pulse-height spectra show appreciable low-energy-tailing. Because of the insufficient knowledge of the range-energy relations for fission fragments at the end of their range the interpretation of the number of pulses lost below the discriminator-setting is rather uncertain. The same remark applies for the boron ionization chambers when B-10(n, α)Li-7 is used as the reference cross-section. Here insufficient resolution of the charged particle spectrum hampers the separation of the Li-7 and α-particle peaks and consequently the accurate knowledge of the efficiency. In this respect solid state detectors had not been fully exploited.

Other extremely important items for such precise measurements are the homogeneity, isotopic composition, chemical purity and accurate knowledge of the weight of the natural boron and fissile foils. In this respect the CBNM (Euratom) has started a few years ago a long-term project to improve the quality of such standard foils.

In the present experiment the neutron induced counting-rates of high quality foils of elemental natural boron and evaporated U-235F-4 layers have been compared in identical low geometry and neutron beam with a solid state detector. Neutron energy selection is done with a slow chopper and simultaneous pulse-height and time-of-flight spectra are recorded.

[+]Euratom Research Fellow

2. Experimental Procedure

2.1. Neutron beam and energy selection

The beam is extracted from a tangential beam-hole T-7 of the belgian BR2-reactor. The geometry of the beam-tube is shown in fig. 1. The fine collimation is performed by crossed soller slits. This fine collimator is followed by a slow chopper that can be rotated with a speed up to 12000 revolutions per minute yielding two neutron bursts per revolution. The chopper is made of a stack of Al and Cd slits respectively 1 mm and 0.1 mm thick with dimensions: 137 mm by 59 mm. In the present measurements the rotor turned at 92 revolutions per second yielding a burst width of about 25 μsec. Behind the fine collimator and before the chopper a very stable beam monitor with solid-state detector is installed. The flight-path of the neutrons after the rotor is 2003.6±0.2 mm from the rotor axis to the detection layer and it is shielded with B_4C, borax and lead.

2.2. Detection chamber

The detection chamber is an evacuated aluminium container of cylindrical shape with thin entrance and exit windows. The detector used is a Au-Si surface-barrier detector with a circular sensitive surface of 22 mm diameter. A series of brass-collimators with different opening diameters can be put in front of the detector. The sample changer inside the detection chamber has a 4 position maltesian cross design (3).

2.3. Targets

2.3.1. A set of natural boron targets was prepared by evaporation (electron bombardment) in vacuum on gold coated quartz backings of 0.7 mm thickness and 40 mm diameter. The deposit itself has a diameter of 38 mm and several layer-thicknesses were prepared. During the evaporation witness layers are prepared to be used for chemical and isotopic analysis.

The 4 layers used in the present experiment were B64, B69, B73 and B74. In table 1 we compare the results of direct weighing in vacuum, after correction for chemical and isotopic analysis with the neutron induced counting-rates with the samples mounted in the sample changer in the geometry of the fission experiment. A typical spectrum of the B-10(n, α) Li-7 reaction products is shown in fig. 2 for B74. Based on the proportionality of the counting-rate and the amount of B-10 in the foil a fit of the type $y = a\,x$ is calculated through the four points. The relative measurements of counting-rates are in excellent agreement with the absolute weights in the range of weights from 30 to 70 μg natural boron/cm^2. The average deviation from the straight-line fit is only 0.2% (table 1).

For the evaluation of the fission cross-sections the B-10 weights are taken from the straight-line fit (table 1).

2.3.2. A set of 4 targets was prepared by evaporation of U-235F-4 on gold-coated quartz backings (identical to the backings of the boron layers). The isotopic composition of the NBS 930-material used is 93.336±0.010 atom % U-235; 1.0812±0.0020% U-234; 0.2027±0.0006% U-236; 5.380± 0.005% U-238.

The main error on the specific activity is caused by the value of the U-234 α half-life.

For this quantity we use the result of Spernol and Lauer (4) of $(2.443 \pm 0.005) \times 10^5$ yrs. This value is the result of precise α-counting ($< 0.2\%$) and potential coulometry (0.1%). This result is not final and work is continuing. The calculated specific activity for NBS 930-material is $(2.5697 \pm 0.0076) \times 10^6$ dps/g. A typical fission spectrum of the layer U4 is shown in fig. 3.

These four layers were carefully examined by low geometry counting by Spernol et al. CBNM and the weights were deduced using the previously calculated specific activity. Results and accuracies are summarized in table 2. Then these layers were mounted in the sample changer and their α-rates and fission rates successively measured in the geometry of the fission cross-section measurement. The agreement with the previous data was good.

2.4. Electronic Equipment

The neutron time-of-flight analysis is made with a 100 channels time-of-flight analyser with a variable initial delay and variable channel widths. The signals from the detector are fed into a 512 channels Nuclear Data pulse-height analyser after proper amplification. Automatically a gain switch is operated when a natural boron or a uranium-foil moves in the counting-position. The entrance discriminator of the PH-analyser also serves for the TOF analyser so that a pulse is only analysed in time when it is registered in the PH-analyser. In this way we have a simultaneous picture of the pulse-height and time-of-flight spectrum and the efficiency corrections (overlapping, low energy-tailing) can be calculated on the real spectra.

3. Method and Analysis

From the counting-rates of a boron and a fissile foil in an identical neutron beam the relationship (1) for the fission cross-section σ_f^1 in the neutron velocity channel around v_1 can be deduced assuming $\sigma_f v$ to be constant and $\sigma_B v = \sigma_B^0 v_0$ in the considered channel

$$\sigma_f^1 = \frac{\varepsilon_B}{\varepsilon_f} \frac{N_B}{N_U} \sigma_B^0 v_0 \frac{C_f}{C_B} \frac{1}{v_1} \qquad (1)$$

ε_B is the efficiency for the detection of the B-10(n, α)Li-7 reaction and ε_f the efficiency for detecting a fission reaction; N_B is the number of B-10 atoms on the standard foil and N_U the number of U-235 atoms in the fissile layer; σ_B^0 is the 2200 m/s reference absorption cross-section of B-10 and v_0 is the standard velocity of 2200 m/s; C_f and C_B are the counting rates in the considered velocity channel for the fission and epi-Cd and room-background neutrons. The estimated corrections on C_f and C_B for scattered neutrons resulting in incorrect timing are about $\cdot 10^{-4}$, and only the difference of the corrections enters in (1).

4. Results and Discussion

The purely geometrical factors for the detection of α-particles and fission fragments are closely the same. The reproducibility of the four positions of the sample changer has been checked and the maximum displacement of the center was inferior to 0.02 mm between the four positions. The distance between detector collimator and layer diaphragm is measured with a precision of 0.005 mm (geometry precision: 2×10^{-4}). The agreement of the α-rates of the fissile targets measured by Spernol et al. (CBNM) and in our equipment as well as the comparison of the same U-target in different positions of the sample changer permits us to accept 0.1% error for the geometry reproduction in the experiment. The border regions of evaporated targets are extremely small (< 0.1 mm) and effects on the ratio of geometry factors are negligible ($< 5 \times 10^{-4}$) except when the border profiles would be very different and that is not to be expected from layers prepared by basically the same technique.

For the B-10(n, α)Li-7 reaction only the α-particles are detected, whereas for the U-layers two fission fragments can be detected per reaction and so the detection efficiency for the fission reaction is twice that for B-10 (n, α).

Possible effects on the geometry factor of multiple scattering in the backing and Coulomb Scattering of α-particles and fission fragments have been examined. Based upon the results of Engelkemeir and Walton (5) and White (6) it can be concluded that an error of 0.1% on $\frac{\varepsilon_B}{\varepsilon_f}$ due to the difference in scattering is an upper-limit.

The efficiencies used for the calculation of σ_f have been deduced from spectra such as figs. 2 and 3, taking into account the very small overlapping of α and Li-7 peaks in the B-10 (n, α)-reaction and the low-energy-tailing in the fission spectra.

The precision of an efficiency ratio for a particular uranium and a particular boron-layer will be composed of 0.1% for the purely geometrical reproducibility 0.1% for the difference in scattering behaviour plus the relative errors on the geometries calculated from the spectra (maximum 0.05% error) yielding a typical total error of 0.15% (quadratic sum).

The value of σ_B^0 is taken equal to 3834±5 barn (relative precision = 0.13%). This value is a weighted average of the results of Prosdocimi and Deruytter (7) (8) (9), Als Nielsen and Dietrich (10) and Safford et al. (11).

The determination of v_1 is done with the slow chopper. The calibration of the time-of-flight scale is made by determination of the sharp cut-offs in the total cross-section of polycrystalline samples of α-iron and Be by a transmission measurement. The precision reached on the time-of-flight scale is 0.2% (12).

The remaining factors in equation (1) are C_f and C_B. The layers used until now for comparison are for B-10(n, α): B64 and B74 and for U-235: U4 and U5. The results are analysed statistically and σ_f^0 (2200 m/s) is obtained from a weighted straight-line fit (σ_f, τ) where we use only the values obtained for the 20 channels around the reference value covering an energy-range from 0.063 to 0.014 eV. The fit and the measured values of σ_f in this range are shown in fig. 4. The resulting purely statistical error on σ_f^0 is then combined with the previously discussed

errors on the other terms in equation (1) to yield the final error of 0.60%. In table 7 these errors are listed in abbreviated form.

After a small correction was applied for the difference in efficiency for binary and ternary fission the value for the fission cross-section of U-235 obtained from this work in its present stage is 587.3±3.5 barn (0.063 eV to 0.014 eV). When only the region around thermal energy (0.0302 to 0.0213 eV) is used a value of 584.9±4.5 barn is obtained. (Statistical error 0.56%).

This result has still to be considered as preliminary. We want a new check of the time-of-flight scale, an improved comparison of the UF_4-layers via fission fragment counting, intercomparisons of four layers of elemental boron and UF_4 (instead of two), a confirmation of the half-life of U-234 and improved counting statistics.

The result depends in fact directly upon the value adopted for the U-234 half-life which is provisionally found by Spernol et al. to be 1.6% lower than the previous best value.

If we would accept a best value for $T_{1/2}$ (U-234) of (2.470±0.020) x 10^5 yrs calculated from previous results (13) (14) (15) and the new provisionally result of Spernol et al. (4) a fission cross-section of 581.0±5.4 barn would result from our measurement (energy-region 0.063 eV to 0.014 eV).

The agreement with the new value of Keith (16) based on his new determination of the U-233 half-life is very good although this measurement was an integral one (inside thermal column). Also the agreement with the mean value used by Westcott et al. (17) as input data for their least squares analysis of the U-235 data of 583.5±4.2 barn is excellent.

The authors thank Drs. H. Moret and H. Eschbach for the preparation and weighing of the boron foils; Drs. G. H. Debus and P. Debièvre for the isotopic analysis; Drs. K. Lauer, Y. Le Duigou and V. Verdingh for the chemical analysis.

The automatization of the equipment and the adaptation of the analysers to the read-out system was performed by E. Mies (S. C. K., Belgium). We further thank Mr. L. Vansteelandt (S. C. K. Belgium) and his group for the mechanical maintenance of the slow chopper.

The authors wish also to thank Dr. G. C. Hanna (Chalk River, Canada) and Prof. Havens W. W. Jr. (Columbia University, New York) for valuable discussions.

5. References

(1) A. J. Deruytter, J. of Nucl. En. 15, 165 (1961)

(2) G. J. Safford and E. Melkonian, Phys. Rev. 113, 1285 (1959)

(3) H. Moret, Nucl. Instr. and Meth. 14, 2 (1962)

(4) A. Spernol and K. F. Lauer (CBNM, Euratom) private communication.

(5) D. Engelkemeir and G. N. Walton AERE R 4716 (1964)

(6) P. H. White, private communication (1967) (EANDC UK 87 "AL")

(7) A. J. Deruytter, G. H. Debus, K. Lauer, H. Moret and A. Prosdocimi Report EUR. 12. e (1962)

(8) A. Prosdocimi and A. J. Deruytter, J. of Nucl. En. A/B 17 (1963) 83

(9) G. H. Debus and P. Debièvre, J. of Nucl. En. A/B 21, 373 (1967)

(10) J. Als Nielsen and O. Dietrich, Phys. Rev. 133 B925 (1964)

(11) G. J. Safford et al. Phys. Rev. 119, 1291 (1960)

(12) A. J. Deruytter et al. Neutron time-of-flight Methods (Editor J. Spaepen) p. 275 (1961)

(13) E. H. Fleming, A. Ghiorso and B. B. Cunningham, Phys. Rev. 88, 642 (1952)

(14) C. A. Keinberger, Phys. Rev. 87, 520 (1952)

(15) P. H. White, G. J. Wall and F. R. Pontet, J. of Nucl. En. A/B 19, 33 (1965)

(16) R. L. G. Keith, A. McNair and A. L. Rodgers, EANDC (UK) 84 "S"

(17) C. H. Westcott, K. Ekberg, G. C. Hanna, N. J. Pattenden, S. Sanatani and P. M. Attree, Atomic Energy Review, 3, N° 2 (1965)

TABLE 1

	^{10}B weights (μg)	Counting rates (58 measurements)	^{10}B weights (μg) (straight-line fit)
B64	146.01 ± 0.60	99,179 ± 55	146.28 ± 0.38
B69	92.19 ± 0.49	62,299 ± 36	91.89 ± 0.24
B74	98.48 ± 0.54	67,194 ± 40	99.11 ± 0.26
B73	77.88 ± 0.43	52,537 ± 40	77.49 ± 0.20

TABLE 2

Low geometry α-measurements

Layer number	Accuracy in %				Amount uranium in μg
	Statistical (= 3σ)	Geometry Factor	Scattering	$\sqrt{\sum \delta_i^2}$	
U1	0.05	0.20	0.03	0.2	1612.2 ± 5.8
U3	0.04	0.20	0.03	0.2	854.9 ± 3.1
U4	0.06	0.20	0.03	0.2	1703.8 ± 6.1
U5	0.04	0.20	0.03	0.2	3449.3 ± 12.3

TABLE 3

Cause of error	Relative error on σ_f^0 in %
number of B-10 atoms (Section 2.3.1.)	0.25
number of U-235 atoms (Section 2.3.2.)	0.36
$\varepsilon_B/\varepsilon_f$ (Section 4)	0.14
σ_B^0 (Refs. 7, 8, 9, 10 and 11)	0.13
v_1 (Ref. 12)	0.20
data combined for B64, B74, U4 and U5 in the 20 channels around 2200 m/s (fit Fig. 4)	Total error = 0.60% ($\sqrt{\sum \delta_i^2}$)

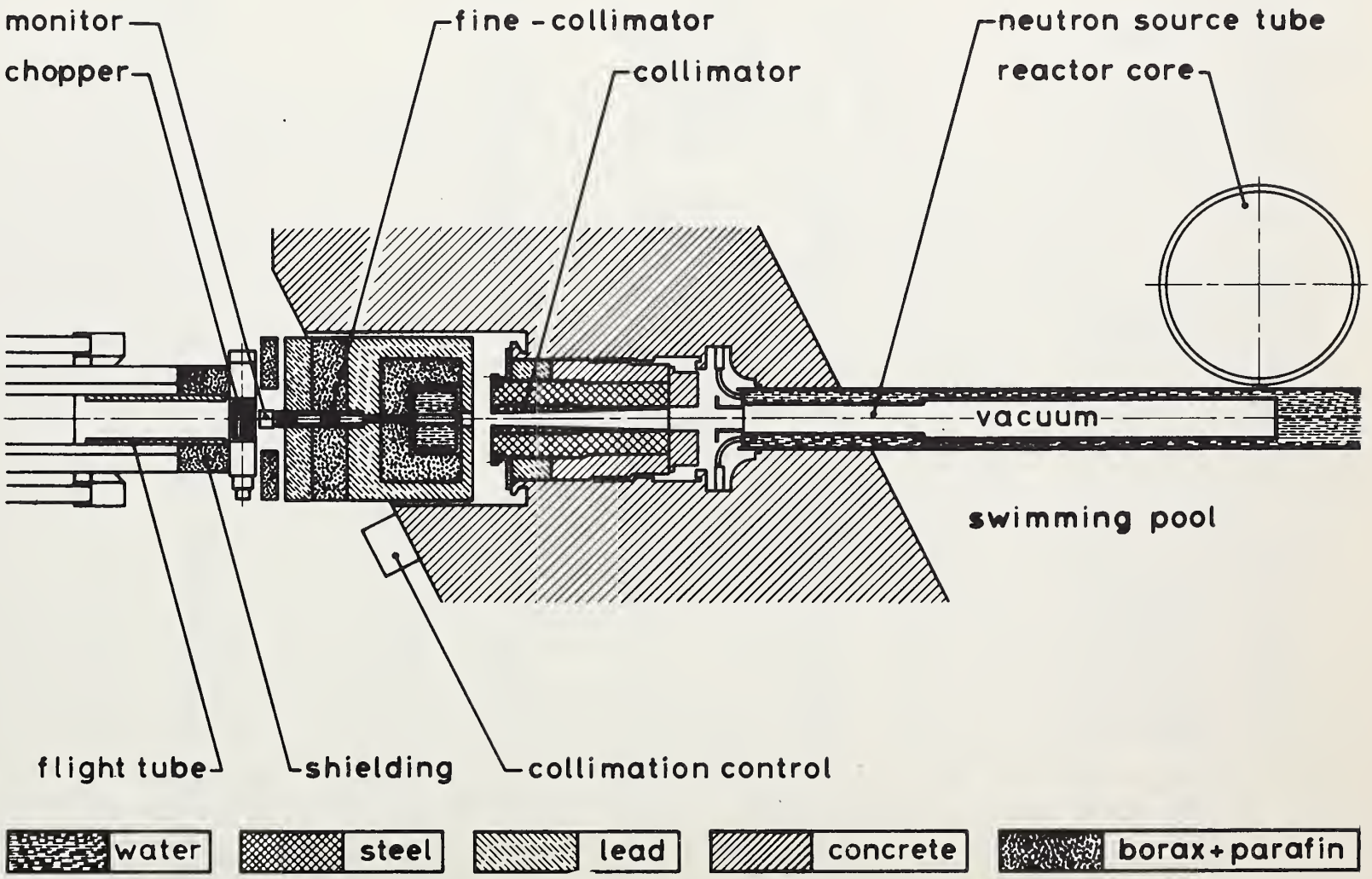

Fig. 1: The collimation in the tangential beam-hole T7 of the Belgian BR2-reactor.

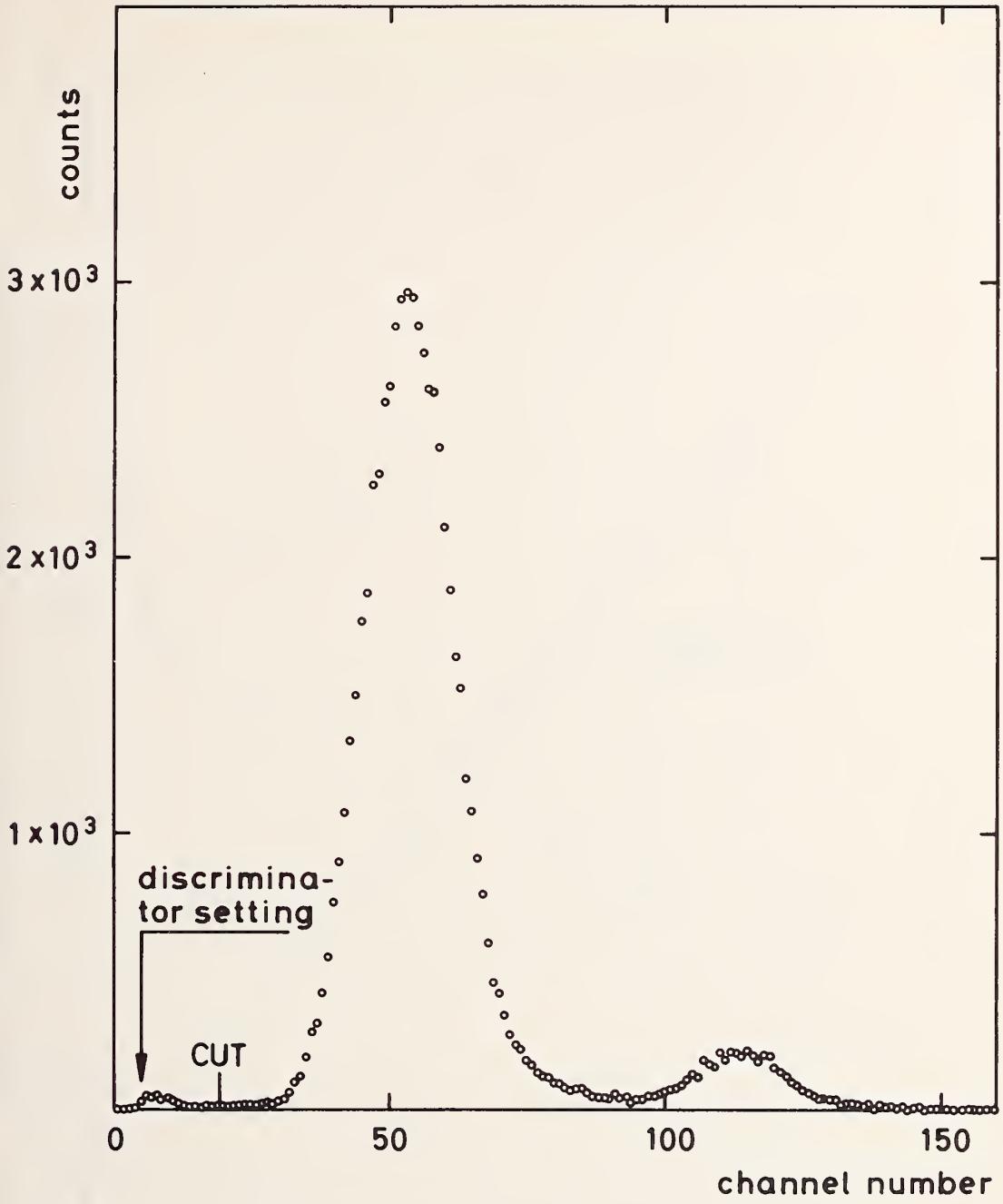

Fig. 2: A typical spectrum of the α-particles from the B-10(n, α)Li-7 reaction in layer B74. The discriminator-setting of the PH-analyser is indicated as well as the cut in the spectrum separating α-particles and Li-7 fragments.

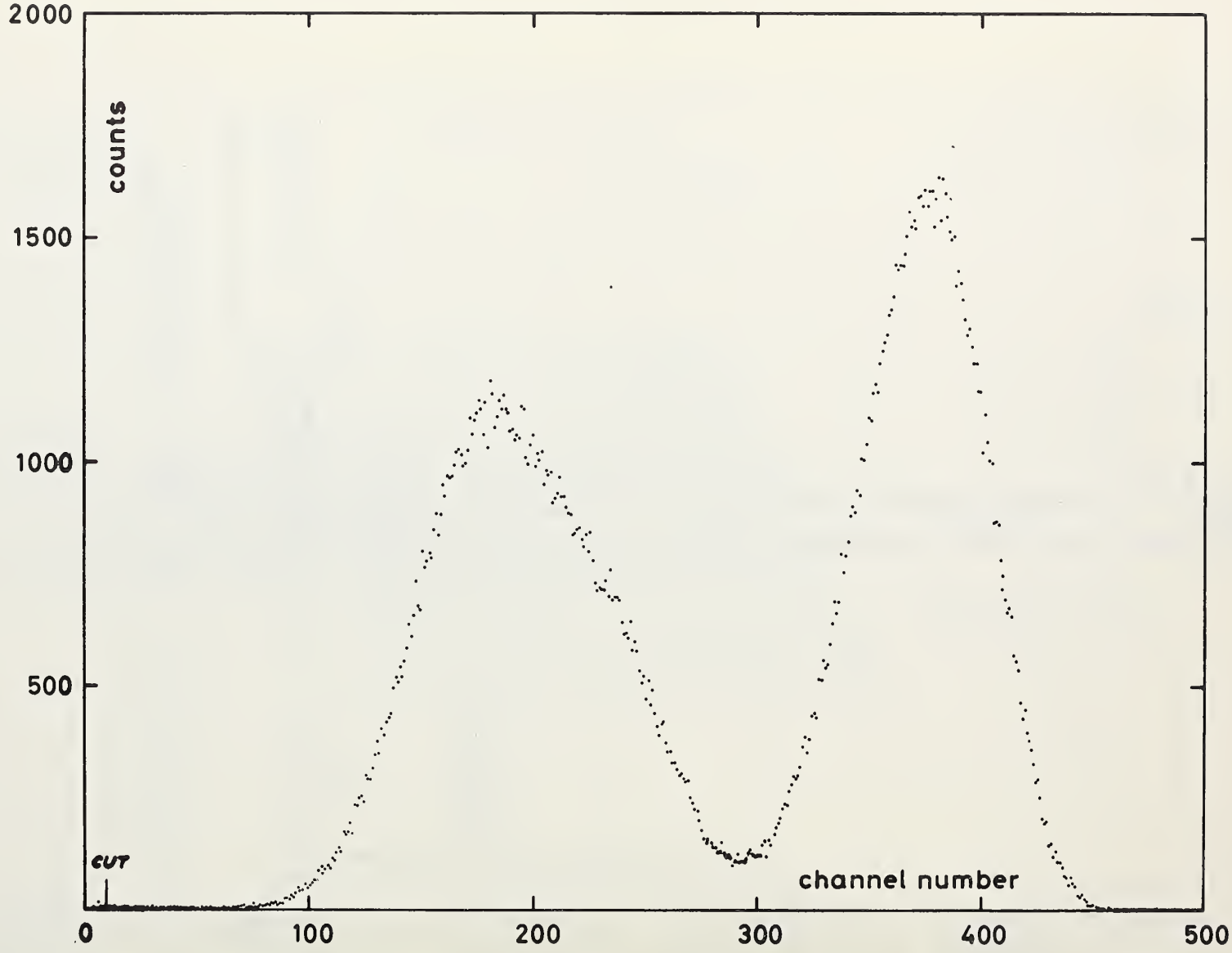

Fig. 3: A typical spectrum of the thermal neutron induced fission fragment spectrum of layer U4.

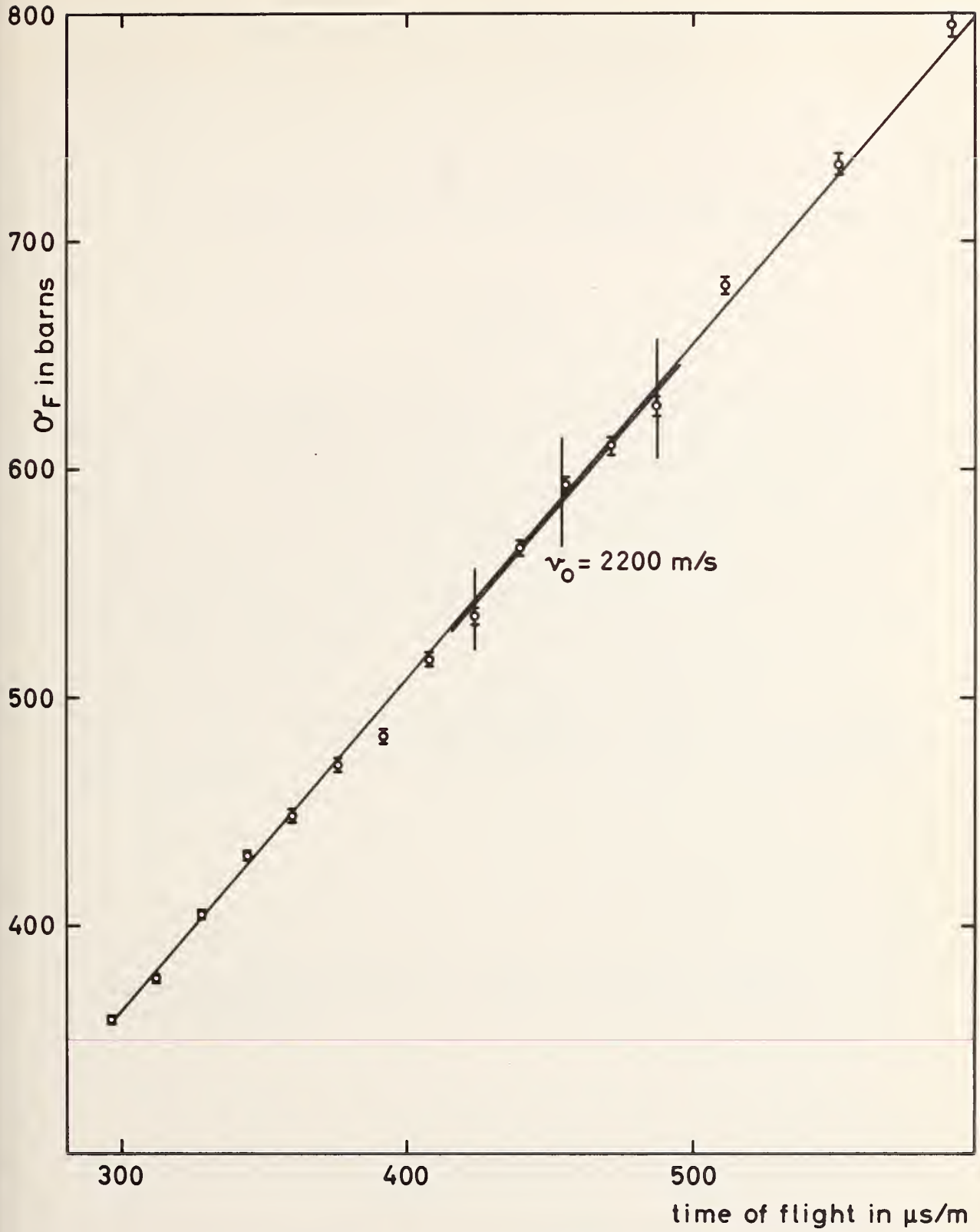

Fig. 4: The fission cross-section of U-235 as a function of time-of-flight. Straight line fits for the whole TOF-range and for the 5 channels around 2200 m/s are also shown.

Measurement of the U^{235} Fission Cross Section In the keV Energy Range*

W. P. Poenitz

Argonne National Laboratory, Argonne, Illinois 60439

ABSTRACT

The energy dependence of the fission cross section of U^{235} was measured in the range 30 - 1500 keV. This dependence is important due to the increasing emphasis on fast reactors and due to the significance of this cross section as a standard in cross section experiments. The energy dependent shape was measured using a specially collimated beam of pulsed-monoenergetic neutrons derived from the $Li^7(p,n)Be^7$ reaction. The fission events were measured by means of a gas scintillation counter using a time-of-flight technique for background suppression. The relative neutron flux was measured using a beam catcher detector which had a flat efficiency curve in the energy range under consideration. The measured cross section shape was normalized at 30 keV to a cross section value taken from a recent absolute measurement by Knoll and Poenitz. The experimental results agree with some other measured cross section shapes in this energy range but tend to disagree at higher energies with the cross section values measured relative to the hydrogen scattering cross section by about 15 percent.

---

* This work performed under the auspices of the U.S. Atomic Energy Commission.

313-475 O-68—34

1. INTRODUCTION

For several years there has been an increasing emphasis on fast reactor physics calculations. As a consequence, there is an increasing demand for highly accurate fission cross section data in the intermediate and fast energy region. To meet this demand a program of fission cross section measurements for several fissile nuclei was started at ANL. The main emphasis was on U^{235} and Pu^{239} where an accuracy of 1 - 2% in the keV range was anticipated. This paper presents a first shape measurement for U^{235} in the energy range 30 - 1500 keV. Figure 1 indicates that such a measurement seems to be highly desirable. There are two sets of data available which cover the range considered here and are given with error bars of 1.3 - 3.0% (Allen and Ferguson, [1]) and 2.5 - 3.0% (White [2]), respectively, but disagree in absolute values as well as in shape by as much as 20%. Recent measurements at 23 keV by Perkin et al. and at 30 keV by Knoll and Poenitz performed with completely independent methods as well as older measurements by Dorofeev and Dobrinin [5] at 23 keV and by Michaudon et al. [6] below 20 keV support the lower value measured by White at 40 keV. On the other hand, other measured cross sections [7, 8] show a energy dependence similar to that measured by Allen and Ferguson. In addition, we calculated fission cross sections of U^{235} from measurements of the ratio of the gold 197 capture cross section to the U^{235} fission cross section [10-15] and several independent measurements of the gold cross section [16-19] which agree with the shape measured by Allen and Ferguson and result in much lower values at higher energies.

2. EXPERIMENTAL PROCEDURE

The experiment consists of relative measurements of the fission events in a U^{235} sample and the neutron flux strength of the collimated monoenergetic pulsed neutron beam striking this sample. The time-of-flight method was applied to the measurements of the fission events which were detected with a gas scintillation counter. Therefore, it was possible to discriminate against events caused by low energy background neutrons which were detected with much higher efficiency than the keV energy neutrons (resonance integral: 274 barn, thermal cross sections: 577 barn [20]). The experimental arrangement is shown in Fig. 2.

2.1. The Neutron Source

The $Li^7(p,n)Be^7$ reaction was used as a neutron source. Thin Li-metal targets were used ranging from 10 keV thickness at low energies to 80 keV thickness at high energies. The target thickness was determined from the forward yield rise curve at the threshold of the $Li^7(p,n)Be^7$ reaction. The proton beam was pulsed with 3.33 MHz and a pulse half width of about 10 nsec. A neutron beam was collimated

by means of a 60-cm long Li-loaded paraffin collimator with a cylindrical form at the neutron target side and a cone form at the detector side. The neutron source was enclosed in a 150 × 150 × 150 cm cube of shielding material to reduce the room background to a low level. Measurements were performed at neutron emission angles of 0, 75, and 81 degrees in respect to the proton beam direction. This configuration allows cross section measurements in the region 20 - 1500 keV. The proton energy was determined by an electrostatic analyzer for the H_2^+-beam.

2.2. The Fission Counter

The fission counter (see Fig. 2) was designed to minimize the necessary corrections for the present experiment. On 50 cm^2 area 4 mg/cm^2 fissile material were painted on each side of a Ni-foil backing. The material consists of 0.0277 ± 0.0003 percent U^{234}, 98.37 ± 0.1 percent U^{235}, 0.0565 ± 0.0006 percent U^{236}, and 1.54 ± 0.01 percent U^{238}. The fission counter has two 0.018 cm thick bronze foils as neutron beam entrance and exit windows. Argon with 15 percent nitrogen as a wave length shifter was used as a scintillation gas. The pressure was about 0.9 atmosphere. The counter was silverplated to increase the light reflection from the walls. The fission events were analyzed according to their energy and time information and recorded in a two dimensional matrix using an on-line computer system [22].

2.3. The Neutron Monitor

The neutron flux monitor consists of a plexiglas tank of a cube-shape of about 76 cm side length filled with water. A 9 cm diameter channel serves as entrance channel for the neutron beam and leads to approximately the center of the tank. At the center of one side of the tank a 12.5 cm diameter, 7.5 cm high NaI(Tl) detector was located to count the 2.2-MeV γ-rays from the neutron capture process in hydrogen. The efficiency of the detector is essentially constant as long as the leakage of neutrons is small. A small correction for different γ-ray attenuation due to the energy dependent change of the neutron field in the water tank can be calculated with high accuracy. The efficiency curve for the counter used in the present experiment is shown in Fig. 3. Details about this counter are given in Ref. [21]. The γ-ray spectra measured by the NaI(Tl)-detector were recorded with a multi-channel analyzer. The 2.2 MeV photopeak was used for the determination of relative neutron flux.

3. EVALUATIONS AND RESULTS

Three different energy thresholds were set in the two dimensional energy-time matrix (in which the fission events were recorded) to receive time spectra. From these spectra "general" background spectra (α-pile up) and effects due to room background neutrons were subtracted. The former was normalized according to the measuring time, the latter was measured with the collimator closed by a brass plug and normalized using a long counter. A straight line was fitted through the residual background outside the peak in the time-of-flight spectra. This was used to subtract the residual background under the peak in the time-of-flight spectra. Two different time-ranges were used for the calculation of the number of fission events. In one case the thresholds were set to just enclose the fission peak caused by the monoenergetic keV neutrons, in the other case the threshold at the low energy side was changed to much lower energy values. The results using different energy or time thresholds were always in agreement within the statistical error. The background subtraction employed for the neutron counter spectra was the same as for the fission spectra. Corrections were made for the following:

1) The second neutron group occuring above 2.378 MeV incident proton energy (max. correction 1.0 percent).

2) The scattering of neutrons in the bronze windows of the fission counter, in the nickel backing of the fission foil and in the air between the fission and neutron counters (max. correction 2.1 percent).

3) The efficiency of the neutron counter (max. 6.1 percent).

4) Dead time of the multi-channel analyzer recording the 2.2-MeV capture γ-ray spectra (max. 1.0 percent).

No corrections were necessary for the change in the efficiency of the fission counter due to the change in the momentum carried by the neutrons as we counted forward and backward fission fragments.

The present measurements were normalized at 30 keV to a recent measured value of 2.19 ± 0.06 barn by Knoll and Poenitz [4]. This value seems to be in good agreement with results by Perkin et al. [3], Dorofeev and Dobrynin [5] at 23 keV and by White [2] at 40 keV. The results are given in Table 1. The first column gives the average neutron energy, the second gives the resolution where ΔE_n means the target thickness. The errors in the cross section values are from different sources;

1) In the high energy range (400 - 1500 keV) where the statistical error is about 1.5 percent and the accuracy of the shape is about 2 - 3%, the error is mainly due to the uncertainty in the normalization factor.

2) In the lower energy range where the values were measured at 75 and 81 degrees, the error is mainly due to less statistical accuracy. The results are shown in Fig. 4 where an eye-guide curve is drawn through the measured points. This curve may not be too well defined in the energy range 90 - 300 keV where no measured values are available.

4. CONCLUSIONS

The most important result of the present measurement of the cross section shape of U^{235} seems to be the disagreement with all other measured values in the range 300 - 1500 keV if one normalizes to a value of 2.19 barn at 30 keV. The shape measured in the present experiment agrees, however, with the shapes measured by Allen and Ferguson[1], Henkel [7], and Gorlov [8]. It agrees further with the prediction for the fission cross section of U^{235} given by the capture cross section of gold and measurements of the ratio σ_γ (Au)/σ_f (U^{235}). The present measurements are also consistent with previously performed neutron capture cross section measurements of U^{238} [27]. The absolute fission cross section of U^{238} at 2.5 MeV measured by Smith, Henkel, and Nobels [23] (revised value: .51 + .03 barn, which agrees with the result of .48 + .06 barns, measured by Allen and Ferguson) and a ratio of $\sigma_f(U^{238})/\sigma_f$ (U^{235}) $\approx$ .43 [ref. 24,25,26,28] gives a value of 1.18 barn which is lower by about 11% than the presently assumed cross section in this energy region [20], but would agree with the results given in Table 1. It should be emphasized that the present lower data for U^{235} would affect also the Pu^{239} fission cross section as one can assume that the ratios of these cross sections are relatively well known. The accuracy of the present data is to be considered to be preliminary as the present stage of the experiment does not reflect the ultimate capability of the method and measurements applying several other independent methods are in preparation.

The author wishes to thank the members of the Applied Nuclear Physics Section for their help in the preparation of this experiment.

5. REFERENCES

1. W. D. Allen and A. T. G. Ferguson, Proc. Phys. Soc. Lond. A70, 575, (1957).
2. P. H. White, J. Nucl. Energy, A/B 19, 325 (1965).
3. J. L. Perkin et al., J. Nucl. Energy A/B 19, 423 (1965).
4. G. F. Knoll and W. P. Poenitz, J. Nucl. Energy A/B 21, 643 (1967).
5. G. A. Dorofeev and Y. P. Dobrynin, J. Nucl. Energy II, 5, 217 (1956).
6. A. Michaudon et al., CEA-1093 (1959).
7. R. L. Henkel, LA 2122, (1957).
8. G. V. Gorlov et al., J. Nucl. Energy A12, 79 (1960).
9. C. L. Bailey et al., LA 150, (1944).
10. A. E. Johnsrud et al., Phys. REv. 116, 927 (1959).
11. S. A. Cox, Phys. Rev. 122, 1280 (1961) and private communication.
12. J. A. Miskel et al., Phys. Rev. 128, 2717 (1962).
13. B. C. Diven et al., Phys. Rev. 120, 556 (1960).
14. J. F. Barry, J. Nucl. Energy A/B 18, 491 (1964).
15. F. J. Vaughn et al., Bull. Am. Phys. Soc. 11, 5 , 753 (1966).
16. K. K. Harris et al., Nucl. Phys. 69, 37 (1965).
17. W. P. Poenitz, J. Nucl. Energy A/B 20, 825 (1960).
18. W. P. Poenitz et al., J. Nucl. Energy, (to be published).
19. See references cited in ref. 18.
20. J. R. Stehn et al., BNL-325, Second Edition, Supplement No. 2 (1965).

21. W. P. Poenitz, Nucl. Instrument & Methods, 58, 39, (1968).

22. J. F. Whalen et al., Nucl. Instrument & Methods 39, 185 (1966).

23. R. K. Smith et al., Bull. Am. Phys. Soc. 2, 196 (1957).

24. P. H. White, G. P. Warner, J. Nucl. Energy

25. G. N. Smirenkin et al., Atomnaya Energiya, 18, 4, 366 (1962).

26. W. E. Stein et al., CONF-660303, 623 (1966).

27. H. O. Menlove, W. P. Poenitz, Nucl. Science & Engineering, (to be published).

28. R. W. Lamphere, Phys. Rev. 104, 1654 (1956).

Table 1 RESULTS FOR THE FISSION CROSS SECTION OF U^{235}

$\bar{E}_n$/keV	$\Delta E_n/E_n$	σ/barn
30 ± 2	0.30	2.19 ± .06 *
55 ± 3	0.18	1.81 ± .09
76 ± 3	0.20	1.66 ± .10
267 ± 5	0.03	1.03 ± .08
280 ± 5	0.05	1.26 ± .15
285 ± 5	0.05	1.19 ± .09
290 ± 20	0.27	1.07 ± .06
400 ± 20	0.20	1.01 ± .05
496 ± 10	0.04	1.03 ± .05
695 ± 20	0.12	1.00 ± .05
850 ± 20	0.09	.99 ± .05
1040 ± 20	0.08	1.10 ± .05
1150 ± 20	0.07	1.09 ± .05
1470 ± 20	0.05	1.11 ± .06

* This is the result of Knoll and Poenitz[4], used for normalization of the present shape measurements.

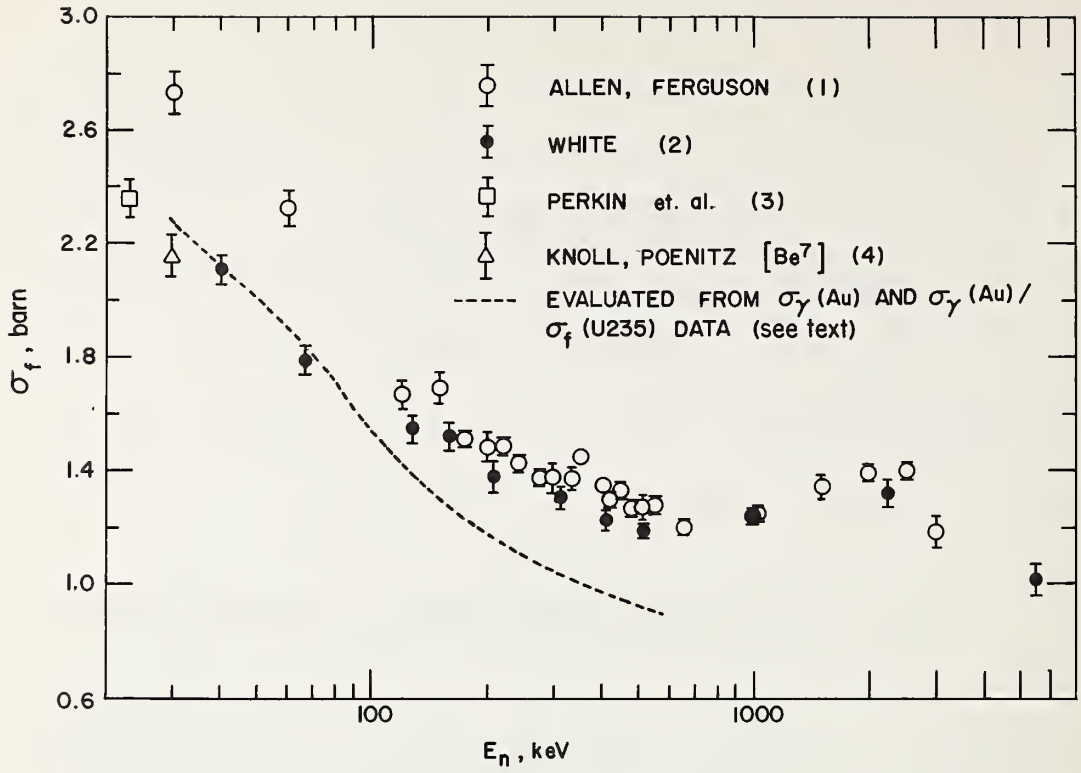

Fig. 1 Some fission cross sections in the 10 - 10000 keV region.

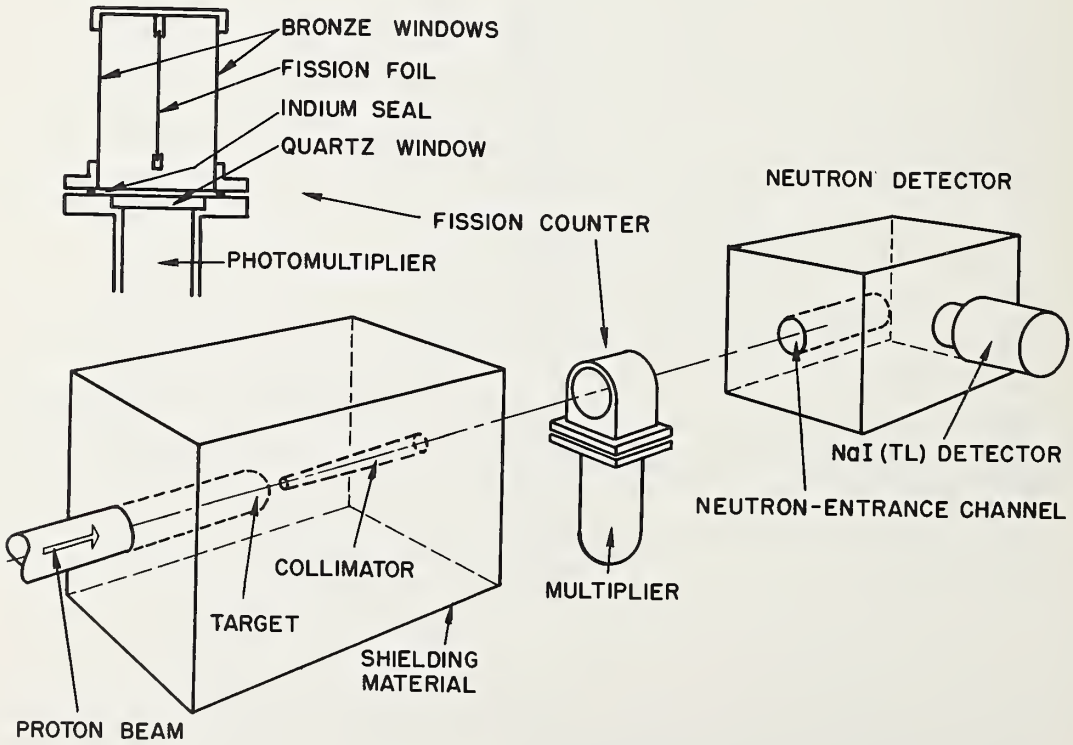

Fig. 2 Experimental set-up

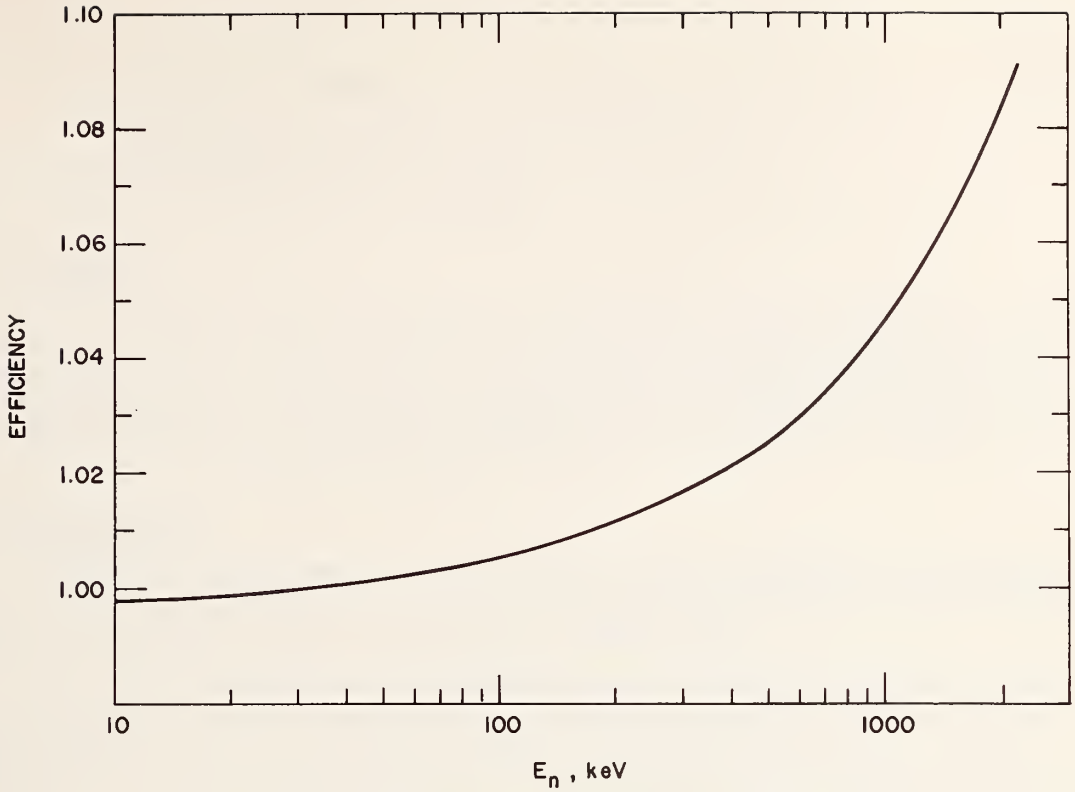

Fig. 3 Efficiency of the Neutron-Beam-Catcher Detector

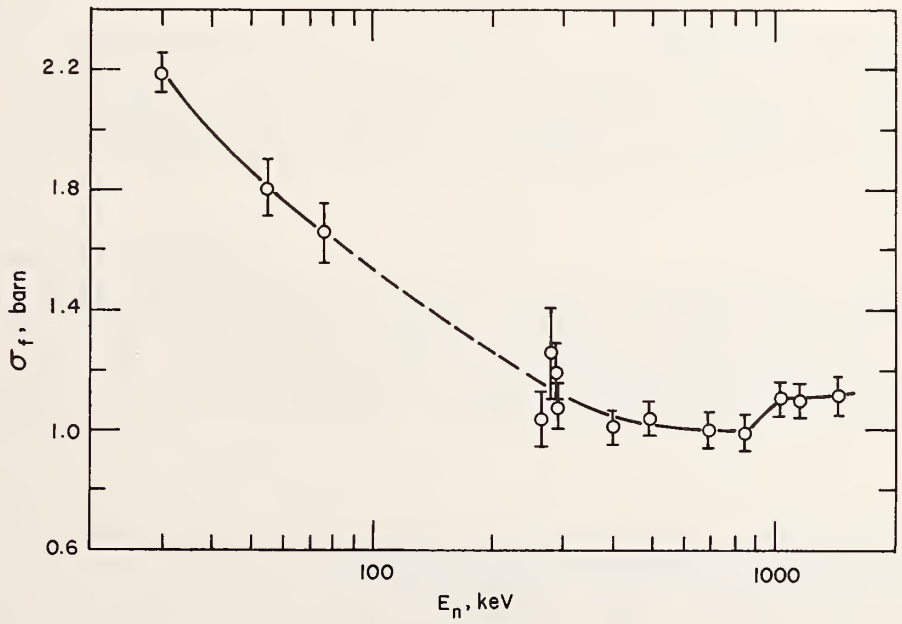

Fig. 4

The fission cross section of U^{235}. Present results, normalized at 30 keV to 2.19 barn [ref. 4].

SCATTERING CROSS SECTION OF Pu-240

M. G. Cao, E. Migneco, J. P. Theobald, J. A. Wartena
Central Bureau for Nuclear Measurements
EURATOM, Geel, Belgium

Abstract

The scattering cross section of Pu-240 has been measured between 18 eV and 2.5 keV with a boron-10-loaded liquid scintillation detector. The Γ_n values of 14 resonances between 20.45 and 287.1 eV have been determined and the scattering resonance areas as well as the Γ_n values compared with other measurements (3) (4).

1. Introduction

In the last years the cross sections of neutron induced reactions on Pu-240 found the interest of reactor designers (1) and got a new significance in the field of theoretical nuclear physics (2).

For many resonances in the investigated energy range the parameters Γ_n and Γ_γ have been determined from transmission, radiative capture and scattering data (3, 4, 5). The scattering experiment has been reported by Asghar et al. (3). These authors used Li-6 glass scintillator detectors and measured contributions from capture γ-radiation with natural Li or Li-7 glass scintillators.

In the experiment to be described here, a boron-10-loaded liquid scintillator detector NE 321 A has been used. A pulse shape discriminator selects the pulses from the B-10($n\alpha$) reaction from those due to γ-radiation and recoil protons. So the contribution of resonant radiative capture is eliminated and the background from spontaneous fission is reduced.

2. Experimental Technique

The experimental geometry and the neutron collimation is shown in figure 1. The time-of-flight spectrometer with the CBNM linear accelerator as a pulsed neutron source have been described in the paper D-3 of this Conference. The characteristic parameters of the experiment are given in table 1.

3. Sample

The sample prepared at the Los Alamos Scientific Laboratory is a disc of 7.62 cm diameter and a thickness of $4.105.10^{-4}$ atoms per barn. It is canned in an aluminium container which yields a mass ratio Al/Pu of about 1.2. The isotopic composition of the Pu as determined at L. A. S. L. is Pu-238: 0.004±0.002%, Pu-239: 1.43±0.02%, Pu-240: 97.92±0.04%, Pu-241: 0.52±0.03% and Pu-242: 0.12±0.01%.
The plutonium itself is alloyed with 1.15% Al. All chemical impurities are negligible except the 190 ppm Mn in the Al-canning. (The big 337 eV resonance of Mn is visible in the scattering yield spectrum).

4. Detectors

The detector consists of four boron-10-loaded liquid scintillators with a diameter of 11 cm and a thickness of 1 cm viewed laterally by four XP 1040 photo-electron multipliers (fig. 2). The axis of the detectors lie in the plane of the sample disc. The distance of the sample center from the detector surface is 5.75 cm.
Because of the high natural activity of the sample the front side of the liquid scintillator is shielded with 4 mm of iron. The background due to slow neutrons is reduced by surrounding the total detector system with boron loaded plastic (not to be seen in fig. 1).
A bloc diagram of the pulse shape discriminator (PSD) is shown in fig. 2. The principle of this circuitry which determines the zero crossing of a specially shaped pulse has been described by Roush et al. (6). The two RCL shapers which are used deliver a pulse crossing zero after about 200 ns. The time difference of the crossing points for different ionizing particles is of the order of several ten nanoseconds. The dynamic amplitude range of the apparatus is 1 to 300, the time uncertainty of the zero crossing is 3 ns for the entire dynamic range. The dead time is 2.5 μ s, and a pile-up pulse after more than 250 ns does not disturb the PSD. These characteristics guanrantee a clear analysis of the light pulses from the liquid scintillator. Such an analysis is shown in fig. 3. The test scintillator is NE 321 A with the cylinder dimensions 12 mmx33mm $\emptyset$. It is placed on the cathode center of a XP 1040 photo-electron multiplier. In the test-scintillator liquid 3 nC of 241 Am is solved giving α-particles of about 6 MeV. An Am-Be source with a polyethylene moderator delivers slow and fast neutrons and γ rays impinging on the scintillator.

The horizontal scale of fig. 3 representing the pulse amplitude is 2 MeV/scale unit for α particles, 400 keV/unit for recoil protons and 75 keV/unit for electrons. The vertical scale represents the time of zero crossing. The unit is 30 ns.
The spots characterize pulses from electrons (indicated by γ) recoil protons (indicated by n, p), and α particles from Am-241 (indicated by α). The spots representing B-10(n, α) Li-7, Li-7* reactions fall into an area limited by four thresholds defined by the dotted lines in the figure. The same threshold setting is used in the Pu-240 scattering experiment.

5. Measurement

The measurement has been performed in two runs covering the neutron energy ranges 18-360 eV and 36-3000 eV. The neutron spectrum has been determined and controlled with a bank of BF_3 counters. For the measurement and normalization of the background the "black resonance technique" has been applied.
In order to normalize the Pu-240 scattering cross section, the scattering yield of tungsten, for which the Γ_n values of some resonances are fairly well known (7) has been recorded simultaneously with that of Pu-240 in a special run. In this measurement the Pu-240 disc was sandwiched with a 0.101 g/cm^2 tungsten foil.
The energy dependence of the detector efficiency has been determined relative to that of a BF_3 counter, for which a $1/\sqrt{E}$-dependence has been assumed.

The results are in a good agreement with a Monte Carlo calculation by Bollinger and Thomas (8).

6. Results and Analysis

The time-of-flight spectrum of the scattering yield is shown in figures 4a and b. The procedure of the reduction of these data with an IBM 1401 computer is published elsewhere (9).
The multiple scattering and self-absorption effects in the observed scattering areas of the resonances have been corrected with an analytical computer program (10), in those cases where these effects are small. For larger corrections the correction factors of Asghar (3) have been used. In order to justify this, it was verified that for the resonance at 41.62 eV the Monte Carlo calculation of Harwell gives with our parameters a factor very close to that of Asghar.
For these calculations the Γ_n values of (4) and the Γ_γ values of (5) have been used.
The correction for multiple scattering is in this case a coarse approximation because the detector is considered as having a 4π geometry. Furtheron its time resolution is neglected against the Doppler broadening, which is only correct for resonances smaller than about 40 eV.

After these corrections the resonances have been analysed with a single level area method. The results are shown in table 2, where for comparison the scattering areas of (3) and the Γ_n values of the transmission experiment (4) are presented.

The agreement of the scattering areas with Asghar's results is rather good, also when our values are in general slightly higher. But our Γ_n values are systematically smaller than the results of the transmission experiment (4). This discrepancy can hardly be explained by the error in the multiple scattering correction.

The authors are grateful to Dr. J. Spaepen and Mr. K. H. Böckhoff for their support. They are indebted to Mr. Moxon, Harwell for his help in the calculation of the multiple scattering corrections.

7. References

(1) Compilation of EANDC requests EANDC 55 "U" (1966)

(2) H. WEIGMANN, submitted to Zeitschrift für Physik

(3) M. ASGHAR, M. C. MOXON and N. J. PATTENDEN, Paris Conference on Nuclear Data for Reactors, October 1966, Paper CN-23/31

(4) Paper D-7 of this conference

(5) Paper D-9 of this conference

(6) M. L. ROUSH, M. A. WILSON, W. F. HORNYAK, University of Maryland Report 367 (1964)

(7) Neutron cross sections, BNL 325 II C (1966)

(8) L. M. BOLLINGER and G. E. THOMAS, Rev. of Sc. Instr. 28, 489 (1957)

(9) M. G. CAO, report EUR 3652. f (1967)

(10) P. RIBON, private communication (1967)

TABLE 1

	1st run		2nd run
Neutron energy	18 eV - 360 eV		36eV-3keV
Linac beam energy		50 MeV	
Linac peak current		2 A	
Burst frequency		400 Hz	
Burst width		45 ns	
Analyser channel width	320ns(3 - 5 eV) 160ns(18-112eV) 80ns(112-360eV)		80 ns
Number of channels		4096	
Moderator dimensions		$20x20x2.8cm^3$ (polyethylene)	
Permanent background samples	Mn, Au		Na
Samples for the background spectrum		Na, Mn, Co, W, Au	
Overlap filter		B nat.	
Flight path length		30.93 m	

TABLE 2

E_0 (eV)	Area of ref. 3	Area (b. eV)	Γn meV	Γn of ref. 4
20.45	24.7	28.8	1.8 ± 0.3	2.7 ± 0.3
38.32	734	690	15.1 ± 1.9	19.2 ± 0.9
41.62	523	529	13.9 ± 1.8	16.8 ± 0.9
66.62	1540	1813	45.0 ± 6.0	55.9 ± 2.2
72.78	470	478	18.3 ± 2.3	22.0 ± 1.0
90.77	124	135	9.3 ± 1.2	13.5 ± 0.6
105.00	765	826	36.4 ± 4.7	45.5 ± 2.5
121.60	95	135	11.5 ± 1.5	14.5 ± 0.9
135.30	128	150	13.8 ± 1.8	18.5 ± 1.1
151.90		99.6	11.0 ± 1.4	14.2 ± 1.0
162.70		77.2	9.5 ± 1.2	8.6 ± 1.0
185.80		92.1	11.9 ± 1.5	16.3 ± 1.2
260.50		102	16.2 ± 2.0	23.2 ± 1.2
287.10		1362	117.1 ± 1.5	138.2 ± 7.0

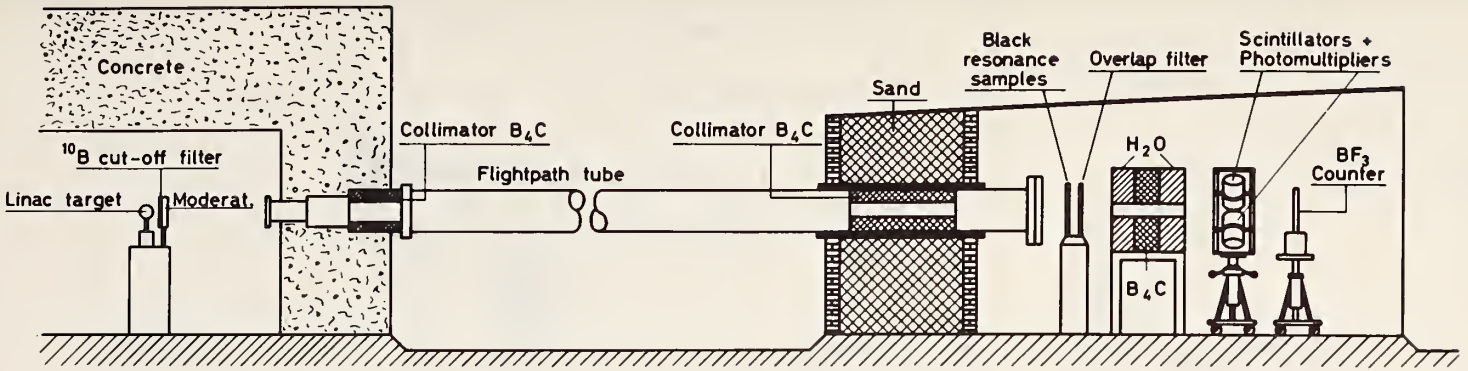

Fig.1. Experimental set-up

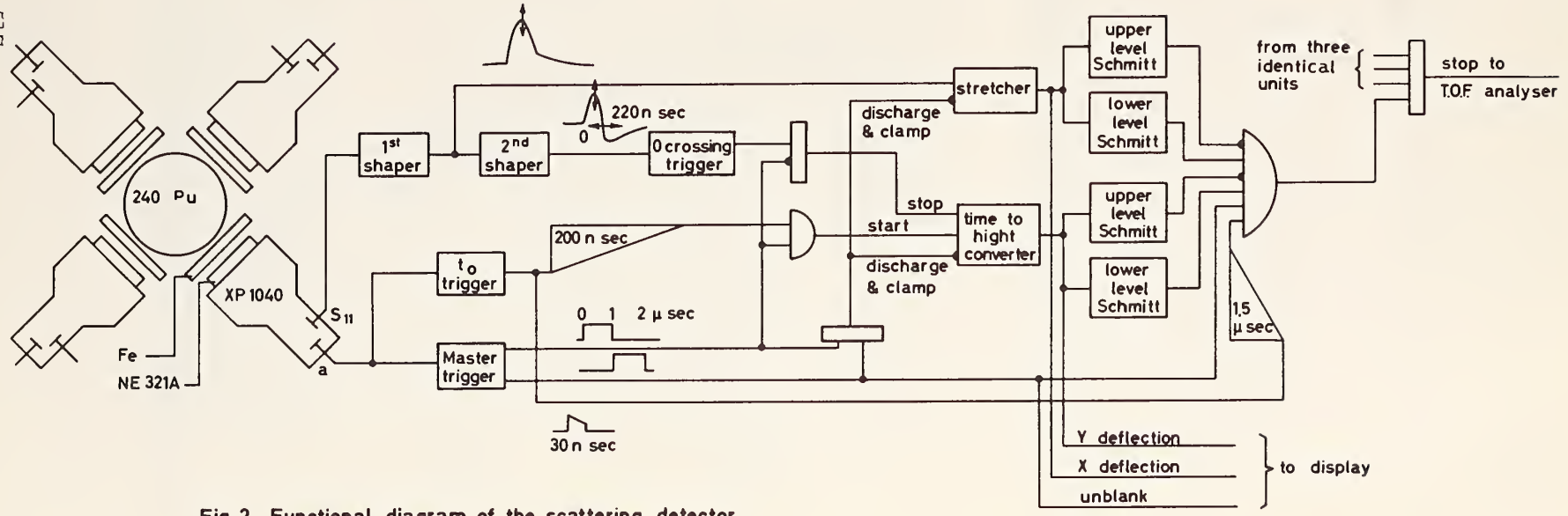

Fig. 2. Functional diagram of the scattering detector

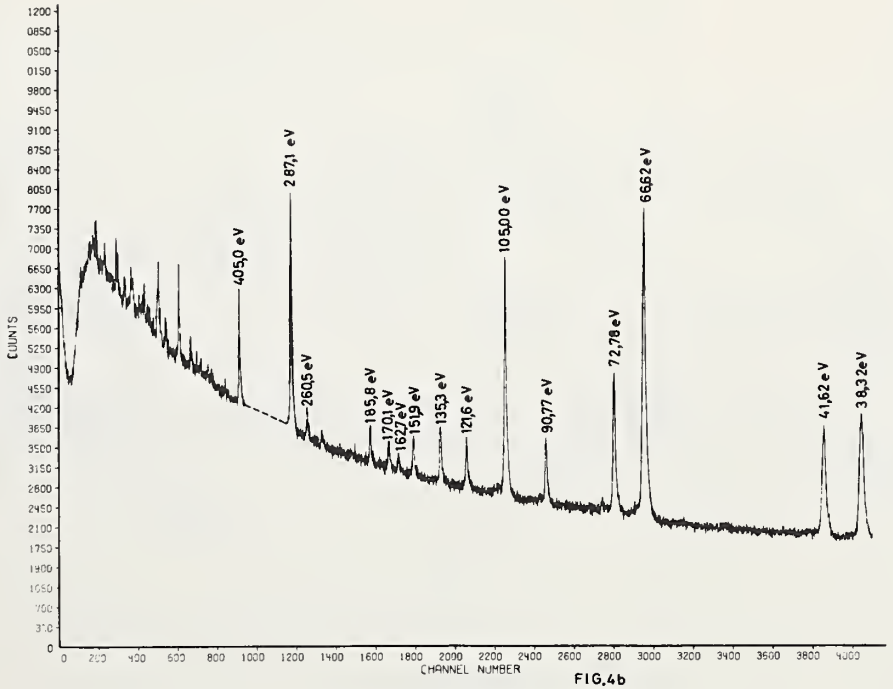

FIG.4b

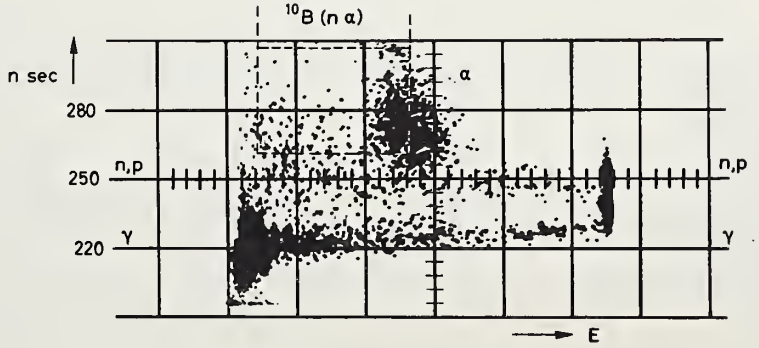

Fig. 3. Display pattern of the test scintillator

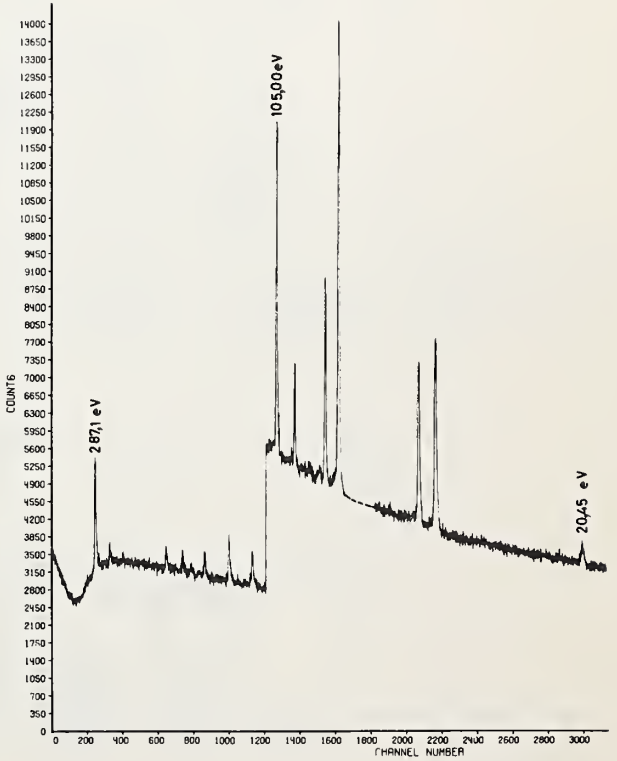

FIG. 4a

Fig. 4a and 4b:
Scattering yield (T. O. F. spectrum)

FINAL RESULTS ON THE NEUTRON TOTAL CROSS SECTION OF Pu-240

W. Kolar and K. H. Böckhoff
Central Bureau for Nuclear Measurements
EURATOM, Geel, Belgium

Abstract

The neutron total cross section of Pu-240 has been measured with high resolution in the energy range 20 eV - 5.7 keV. Up to this energy 264 resonances were detected and analysed with respect to Γ_n using the area program of Atta and Harvey. For 32 resonances between 38 eV and 820 eV the full set of resonance parameters E_r, Γ_n and Γ_γ could be evaluated by combining the results of the transmission experiment with those of a capture experiment (8). For the 102 resonances up to 1500 eV a mean level spacing of $\langle D \rangle = 14.7$ eV was obtained. Presuming that all resonances in that range are of the s-type, the strength function yields $S_o = (1.05 \pm 0.16) \cdot 10^{-4}$.

1. Introduction

Up to recently the results (1-3) of total and partial cross section measurements on Pu-240 were strongly limited both in quality and quantity due to the lack of sample material. With the supply of about 74 g of highly enriched Pu-240 by the U. S. A. E. C. it was possible to achieve more accurate and more complete cross section data.
Total, capture and scattering cross section measurements were performed at Harwell with one part of the new sample batch and resonance parameters were derived from a combined analysis which yielded a complete resonance description for most of the resonances between 20 eV and 288 eV. Besides that, resonance energies and neutron widths were deduced up to neutron energies of 949 eV (4).
About simultaneously with these experiments, transmission measurements were performed at Euratom Geel with the CBNM linear accelerator using another part of the Pu-240 sample batch (5). For the major part of the resonances between 20 eV and 800 eV resonance energies and neutron widths were determined applying shape analysis (6).
The work to be described here concerned the determination of the total cross section and the neutron widths of the resonances in the energy range between 20 eV to 5.7 keV for which the entire sample batch of 74 g could be used.

2. Samples

Seven plutonium disks with a total weight of 73.9 g Pu-240 were available. The samples (diameter 7.62 ± 0.013 cm) prepared and analysed by Los Alamos Scientific Laboratory, consist of a plutonium-aluminium alloy (1.15% Al by weight) sealed in aluminium of 0.25 mm thickness. The plutonium concentration varies for the different samples between 97.8 and 98.75%. For the calculations a mean value of 98.3 ± 0.5% was taken.

The isotopic composition[1] of the plutonium samples is: Pu-238: 0.004±0.002%, Pu-239: 1.43±0.02%, Pu-240: 97.92±0.04%, Pu-241: 0.52±0.03%, Pu-242: 0.12±0.01%.

3. Measurements and analysis of the results

A description of the experimental arrangement, the data acquisition and treatment is given in (5) and (7). Fig. 1 shows as an example the observed total cross section (not corrected for Doppler and resolution broadening) for the energy range from 340 eV - 740 eV.
264 resonances have been analysed between 20 eV and 5.7 keV using the area program of Atta and Harvey (6).
The results are shown in table I. Since for the energies up to 750 eV several independent measurements were performed the listed values of the reduced widths Γ_n^0 are weighted averages. Those values marked with an asterisk have been determined by combination of transmission and capture (8) results.
The errors of the area analysis results of Γ_n^0 were obtained from the following individual components:
a) Statistical errors. These are considered by the area program itself.
b) Error due to the uncertainty in the choice of the boundaries for the different resonances. Practically for all resonances area analysis with two different integration ranges ("window"-widths) has been performed. The differences of the Γ_n^0 values varied from resonance to resonance, but in general they did not exceed the statistical error limits. Therefore this error was assumed to be in the same order of magnitude as the statistical error.
c) Error due to the uncertainty in sample thickness. This contributed with 0.6% to the Γ_n^0 values.
The total error of the parameters as quoted in table I combines the above mentioned errors and considers also the results obtained with different sample thicknesses. The error contributions due to Doppler width and baseline uncertainty are not taken into account. The Doppler width calculation presumed the validity of the gas model and made the hypothesis that for the Pu-240-Al-alloy the effective temperature is equal to the ambient temperature. A possible small error due to instabilities of the monitors and the electronics is neglected.

4. Statistical properties

Fig. 2 shows for the energy range up to 1.5 keV the observed numbers of levels versus $x = (\Gamma_n^0)^{1/2}$ together with the theoretical distribution for $\nu = 1$ degrees of freedom. The solid curve is normalised to the detected 102 levels while the broken curves are normalised to 115 resp. 120 levels. As these two last curves give a better fit to the experimental data one may conclude that about 20 levels could not be detected.
The experimental distributions of the nearest-neighbour (P^0) resp. the next-nearest-neighbour spacings (P^1) are shown in fig. 3 and 4. For comparison the random distributions resp. the distributions of the Gaussian orthogonal ensemble (9) (10) as predicted from the theory are included.

---

[1] as determined by L. A. S. L.

There was no possibility to discriminate between s and p-waves because of the small sample thickness. It was assumed that all observed resonances were s-wave resonances. In this way the value of the s-wave strength function was found to be $S_0 = (1.05 \pm 0.16) \cdot 10^{-4}$.
The mean level spacing as calculated from the experimental results is $\langle D \rangle = 14.7$ eV. If one takes into account that about 20 levels could not be detected the mean level spacing reduces to $\langle D \rangle \sim 12.5$ eV. The difference is an indication of the possible error.

5. References

(1) Neutron Cross Sections, Rep. BNL 325 2nd. ed. Suppl. Nr. 2
(2) D. H. Byers, B. C. Diven, M. G. Silbert, rep. LA DC 7623 (1966)
(3) A. Michaudon, Resonance energies up to 372 eV, private communication (1966)
(4) M. Asghar, M. C. Moxon, N. J. Pattenden, Conference on "Nuclear data for reactors" October 1966, Paper CN-23/31
(5) K. H. Böckhoff, A. De Keyser, H. Horstmann, W. Kolar and H. Martin, Proceedings of the Conference on "Nuclear data for reactors" October 1966, Vol. II 135
(6) S. E. Atta, J. A. Harvey, Rep. ORNL-3205 (1961)
(7) W. Kolar, K. H. Böckhoff, Journal of Nucl. En. , in press
(8) H. Weigmann and H. Schmid, Journal of Nucl. En. , in press and Paper D-9 of this Conference
(9) P. B. Kahn and CH. E. Porter, Nucl. Phys. 48 (1963) 385
(10) CH. E. Porter, Nucl. Phys. 40 (1963) 167

TABLE I

Pu-240 resonance parameters: reduced neutron widths

E_0(eV)	Γ_n^0(meV)	E_0(eV)	Γ_n^0(meV)
20.45 ± 0.01	0.60 ± 0.07*	596.8 ± 0.20	2.35 ± 0.10
38.32 ± 0.02	3.10 ± 0.15*	608.1 ± 0.20	0.92 ± 0.06
41.62 ± 0.02	2.60 ± 0.14*	632.5 ± 0.20	0.53 ± 0.05
66.62 ± 0.05	6.85 ± 0.27*	437.5 ± 0.20	0.46 ± 0.05
72.78 ± 0.05	2.58 ± 0.12*	665.1 ± 0.20	7.64 ± 0.31*
90.77 ± 0.06	1.42 ± 0.06	678.6 ± 0.20	1.00 ± 0.07
92.51 ± 0.06	0.31 ± 0.02	712.1 ± 0.30	0.050 ± 0.023
105.00 ± 0.07	4.45 ± 0.24*	743.3 ± 0.30	0.037 ± 0.026
121.6 ± 0.10	1.32 ± 0.08*	750.0 ± 0.24	2.49 ± 0.12
130.7 ± 0.15	0.013 ± 0.005	758.9 ± 0.25	0.22 ± 0.03
135.3 ± 0.10	1.59 ± 0.10	778.3 ± 0.30	0.04 ± 0.03
151.9 ± 0.12	1.14 ± 0.08	782.2 ± 0.30	0.10 ± 0.04
162.7 ± 0.13	0.67 ± 0.08	791.0 ± 0.25	0.85 ± 0.05
170.1 ± 0.14	1.05 ± 0.09	810.5 ± 0.25	7.52 ± 0.35
185.8 ± 0.16	1.19 ± 0.09	819.9 ± 0.26	3.84 ± 0.19
192.0 ± 0.20	0.014 ± 0.009	845.6 ± 0.27	0.35 ± 0.03
199.6 ± 0.17	0.066 ± 0.007	854.9 ± 0.27	1.64 ± 0.09
239.2 ± 0.15	0.79 ± 0.05	876.5 ± 0.27	0.47 ± 0.04
260.5 ± 0.15	1.44 ± 0.07	891.5 ± 0.27	3.16 ± 0.15
287.1 ± 0.17	8.16 ± 0.41*	903.9 ± 0.28	0.73 ± 0.05
304.9 ± 0.20	0.41 ± 0.04	908.9 ± 0.28	2.62 ± 0.13
318.3 ± 0.15	0.29 ± 0.03	915.3 ± 0.28	1.19 ± 0.07
320.7 ± 0.15	1.08 ± 0.06	943.5 ± 0.30	4.00 ± 0.18
338.4 ± 0.15	0.31 ± 0.03	958.4 ± 0.30	2.31 ± 0.12
346.0 ± 0.15	0.89 ± 0.04	971.3 ± 0.30	2.58 ± 0.13
363.7 ± 0.15	1.70 ± 0.07	979.2 ± 0.32	0.23 ± 0.05
372.0 ± 0.17	0.72 ± 0.04	1001.8 ± 0.32	3.10 ± 0.16
405.0 ± 0.20	5.39 ± 0.25*	1024.1 ± 0.42	0.16 ± 0.05
419.0 ± 0.20	0.30 ± 0.03	1041.6 ± 0.35	0.39 ± 0.06
445.8 ± 0.30	0.075 ± 0.014	1045.7 ± 0.35	0.12 ± 0.05
449.8 ± 0.20	0.78 ± 0.06	1072.6 ± 0.35	3.34 ± 0.17
466.5 ± 0.22	0.14 ± 0.03	1099.8 ± 0.35	2.54 ± 0.26
473.3 ± 0.22	0.19 ± 0.02	1115.7 ± 0.5	0.08 ± 0.05
493.9 ± 0.22	0.26 ± 0.05	1128.8 ± 0.4	1.49 ± 0.09
499.3 ± 0.25	0.86 ± 0.06	1133.8 ± 0.4	0.20 ± 0.06
514.3 ± 0.25	0.95 ± 0.07	1142.7 ± 0.4	1.20 ± 0.08
526.1 ± 0.40	0.040 ± 0.021	1159.6 ± 0.4	0.65 ± 0.06
530.8 ± 0.40	0.030 ± 0.017	1185.5 ± 0.4	4.57 ± 0.23
546.4 ± 0.25	1.33 ± 0.09	1190.8 ± 0.4	3.33 ± 0.17
553.2 ± 0.25	0.79 ± 0.06	1208.9 ± 0.4	1.81 ± 0.11
566.3 ± 0.30	1.32 ± 0.07	1228.0 ± 0.4	0.29 ± 0.06
584.1 ± 0.45	0.05 ± 0.02	1236.5 ± 0.4	0.32 ± 0.06

E_0(eV)	Γ_n^0(meV)	E_0(eV)	Γ_n^0(meV)
1254.7 ± 0.4	2.17 ± 0.13	2198.2 ± 0.8	2.77 ± 0.22
1281.4 ± 0.4	0.12 ± 0.06	2240.6 ± 0.8	0.72 ± 0.16
1300.3 ± 0.4	6.79 ± 0.35	2256.6 ± 0.8	2.83 ± 0.23
1328.1 ± 0.4	10.13 ± 0.51	2277.9 ± 0.8	8.94 ± 0.55
1345.0 ± 0.5	0.71 ± 0.08	2290.7 ± 0.9	4.36 ± 0.36
1350.9 ± 0.6	0.23 ± 0.07	2303.3 ± 1.2	0.36 ± 0.15
1362.9 ± 0.6	0.20 ± 0.08	2334.4 ± 0.9	0.76 ± 0.16
1377.0 ± 0.5	1.74 ± 0.12	2350.9 ± 0.9	0.65 ± 0.17
1389.0 ± 0.6	0.38 ± 0.07	2365.8 ± 0.9	4.95 ± 0.35
1401.2 ± 0.6	0.14 ± 0.08	2373.4 ± 0.9	---
1408.6 ± 0.6	0.29 ± 0.07	2386.1 ± 0.9	0.38 ± 0.15
1426.1 ± 0.5	0.97 ± 0.10	2405.0 ± 0.9	0.51 ± 0.15
1429.0 ± 0.5	0.40 ± 0.08	2416.0 ± 0.9	1.32 ± 0.18
1450.2 ± 0.5	1.67 ± 0.14 [1]	2434.3 ± 0.9	4.16 ± 0.31
1462.9 ± 0.5	0.55 ± 0.09	2459.4 ± 0.9	0.52 ± 0.17
1481.2 ± 0.7	0.24 ± 0.08	2470.8 ± 0.9	0.92 ± 0.16
1540.7 ± 0.5	2.57 ± 0.16	2485.3 ± 0.9	0.42 ± 0.17
1549.5 ± 0.5	3.98 ± 0.22	2521.0 ± 1.0	2.18 ± 0.22
1563.7 ± 0.5	2.90 ± 0.20	2538.6 ± 1.0	5.70 ± 0.40
1575.3 ± 0.5	3.18 ± 0.19	2549.2 ± 1.0	1.58 ± 0.24
1609.6 ± 0.6	0.87 ± 0.10	2575.3 ± 1.0	0.94 ± 0.19
1621.4 ± 0.6	0.71 ± 0.09	2639.5 ± 1.0	8.29 ± 0.83
1643.0 ± 0.6	2.65 ± 0.17	2652.4 ± 1.0	0.71 ± 0.16
1662.6 ± 0.6	1.59 ± 0.13	2692.8 ± 1.0	6.64 ± 0.50
1687.9 ± 0.6	0.80 ± 0.10	2717.7 ± 1.0	0.78 ± 0.19
1724.1 ± 0.6	2.01 ± 0.16	2739.2 ± 1.0	3.38 ± 0.34
1741.6 ± 0.6	0.60 ± 0.10	2748.4 ± 1.0	1.95 ± 0.25
1763.7 ± 0.6	1.23 ± 0.11	2817.6 ± 1.1	0.78 ± 0.19
1771.4 ± 0.8	0.23 ± 0.12	2843.5 ± 1.1	2.94 ± 0.30
1779.0 ± 0.6	11.7 ± 0.6	2859.7 ± 1.1	0.51 ± 0.21
1841.2 ± 0.7	2.93 ± 0.21	2882.0 ± 1.1	0.55 ± 0.22
1852.7 ± 0.7	0.80 ± 0.13	2895.6 ± 1.1	1.11 ± 0.22
1872.7 ± 0.7	1.79 ± 0.16	2905.0 ± 1.1	2.13 ± 0.26
1901.6 ± 0.7	4.80 ± 0.29	2938.0 ± 1.1	2.43 ± 0.28
1916.6 ± 0.7	0.82 ± 0.14	2968.6 ± 1.1	1.55 ± 0.25
1943.3 ± 0.9	0.18 ± 0.11	2980.5 ± 1.2	1.98 ± 0.37
1949.1 ± 0.7	1.87 ± 0.17	2986.2 ± 1.2	0.23 ± 0.15
1956.2 ± 0.7	5.90 ± 0.36	2994.7 ± 1.2	1.02 ± 0.21
1973.1 ± 0.7	1.53 ± 0.17	3004.0 ± 1.2	1.39 ± 0.24
1991.5 ± 0.7	2.57 ± 0.21	3018.0 ± 1.2	2.12 ± 0.33
1998.3 ± 0.7	0.12 ± 0.09	3029.0 ± 1.2	0.38 ± 0.20
2016.7 ± 0.7	1.17 ± 0.17	3054.7 ± 1.2	0.85 ± 0.27
2022.9 ± 0.7	1.23 ± 0.17	3077.4 ± 1.2	2.31 ± 0.34
2033.4 ± 0.7	2.25 ± 0.21	3088.0 ± 1.2	0.63 ± 0.31
2055.6 ± 0.8	1.51 ± 0.17	3112.7 ± 1.2	0.68 ± 0.25
2082.8 ± 0.8	2.16 ± 0.21	3172.5 ± 1.3	3.99 ± 0.41
2110.7 ± 1.0	0.30 ± 0.12	3192.5 ± 1.3	6.17 ± 6.2
2154.0 ± 1.1	0.31 ± 0.15	3237.5 ± 1.3	1.26 ± 0.26
2182.0 ± 0.8	1.83 ± 0.18	3268.5 ± 1.3	2.34 ± 0.35

[1] probably two resonances

E_0(eV)	Γ_n^0(meV)		E_0(eV)	Γ_n^0(meV)
3332.0 ± 1.3	0.25 ± 0.17		4599 ± 1.9	1.11 ± 0.44
3423.0 ± 1.4	0.59 ± 0.21		4615 ± 2.0	3.85 ± 0.93
3458.0 ± 1.4	1.16 ± 0.23		4646 ± 2.0	2.18 ± 0.66
3465.5 ± 1.4	5.84 ± 0.58		4721 ± 2.0	7.43 ± 1.10
3493.5 ± 1.4	1.11 ± 0.23		4745 ± 2.0	3.56 ± 0.73
3555.0 ± 1.4	1.52 ± 0.26		4755 ± 2.0	0.82 ± 0.41
3567.5 ± 1.4	2.71 ± 0.34		4766 ± 2.0	0.22 ± 0.22
3595.0 ± 1.4	0.47 ± 0.22		4771 ± 2.0	0.32 ± 0.29
3657 ± 1.5	4.85 ± 0.50		4779 ± 2.0	0.49 ± 0.36
3665 ± 1.5	0.90 ± 0.32		4792 ± 2.0	1.93 ± 0.49
3702 ± 1.5	0.84 ± 0.28		4812 ± 2.1	2.48 ± 0.50
3723 ± 1.5	0.98 ± 0.33		4823 ± 2.1	0.91 ± 0.36
3800 ± 1.6	1.64 ± 0.38		4894 ± 2.1	0.85 ± 0.39
3844 ± 1.6	1.23 ± 0.32		4958 ± 2.1	4.13 ± 0.78
3852 ± 1.6	1.59 ± 0.33		4969 ± 2.1	2.23 ± 0.70
3872 ± 1.6	0.74 ± 0.31		4993 ± 2.2	1.30 ± 0.49
3900 ± 1.6	3.35 ± 0.43		5072 ± 2.2	7.15 ± 0.70
3917 ± 1.6	2.61 ± 0.37		5113 ± 2.2	1.30 ± 0.49
3954 ± 1.6	1.47 ± 0.33		5134 ± 2.2	0.58 ± 0.41
3975 ± 1.7	1.62 ± 0.35		5148 ± 2.2	0.70 ± 0.49
3990 ± 1.7	0.47 ± 0.29		5162 ± 2.2	0.55 ± 0.41
4031 ± 1.7	1.71 ± 0.33		5194 ± 2.2	4.26 ± 0.75
4084 ± 1.7	1.88 ± 0.36		5215 ± 2.3	2.21 ± 0.54
4100 ± 1.7	4.02 ± 0.44		5249 ± 2.3	7.24 ± 0.97
4122 ± 1.7	7.74 ± 0.63		5279 ± 2.3	1.93 ± 0.62
4134 ± 1.7	1.05 ± 0.36		5299 ± 2.3	3.71 ± 0.62
4149 ± 1.7	4.11 ± 0.45		5334 ± 2.3	2.78 ± 0.69
4161 ± 1.7	1.39 ± 0.38		5350 ± 2.3	2.09 ± 0.68
4203 ± 1.8	6.75 ± 0.66		5367 ± 2.3	0.96 ± 0.55
4221 ± 1.8	1.05 ± 0.32		5393 ± 2.4	1.14 ± 0.57
4270 ± 1.8	2.43 ± 0.41		5417 ± 2.4	3.47 ± 0.68
4288 ± 1.8	4.83 ± 0.61		5489 ± 2.4	0.67 ± 0.54
4329 ± 1.8	4.58 ± 0.53		5499 ± 2.4	1.17 ± 0.54
4376 ± 1.8	1.24 ± 0.45		5510 ± 2.4	4.78 ± 0.94
4386 ± 1.8	0.48 ± 0.36		5522 ± 2.5	2.32 ± 0.61
4398 ± 1.9	1.17 ± 0.37		5544 ± 2.5	7.82 ± 1.2
4422 ± 1.9	0.91 ± 0.36		5574 ± 2.5	10.2 ± 1.2
4433 ± 1.9	0.71 ± 0.33		5592 ± 2.5	2.77 ± 0.80
4458 ± 1.9	1.52 ± 0.40		5615 ± 2.5	0.83 ± 0.67
4570 ± 1.9	3.26 ± 0.67		5681 ± 2.5	1.40 ± 0.66
4588 ± 1.9	7.76 ± 0.89		5692 ± 2.5	1.21 ± 0.61

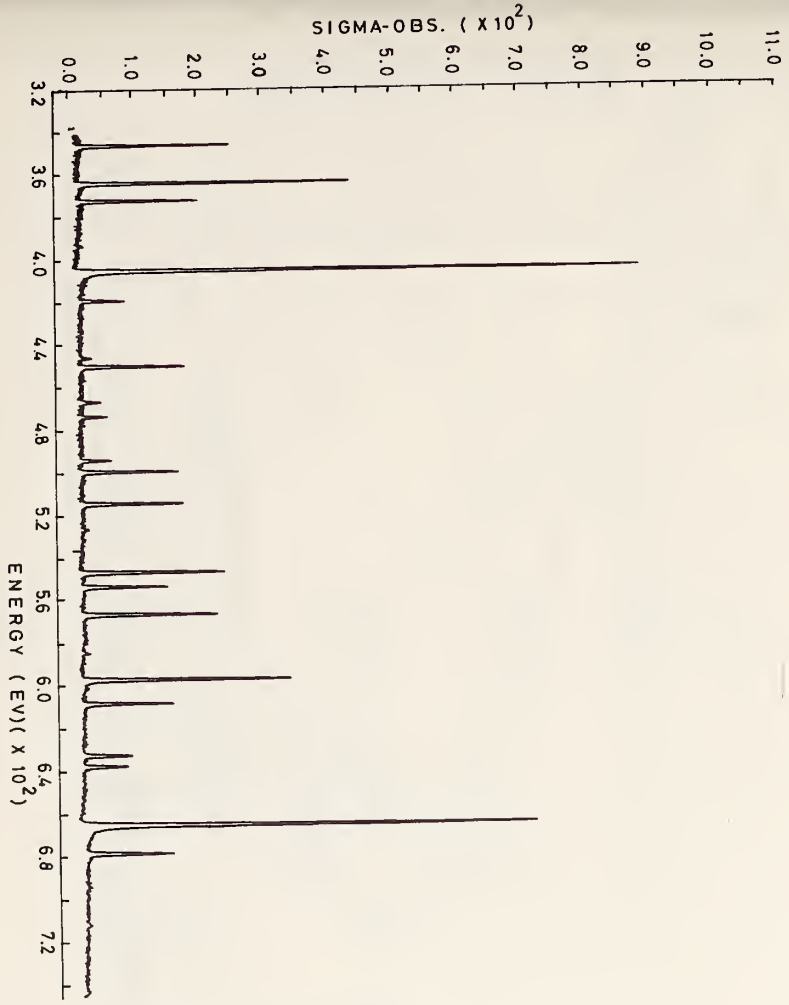

Fig. 1: Observed total cross section versus neutron energy E. (Not corrected for Doppler and resolution broadening).

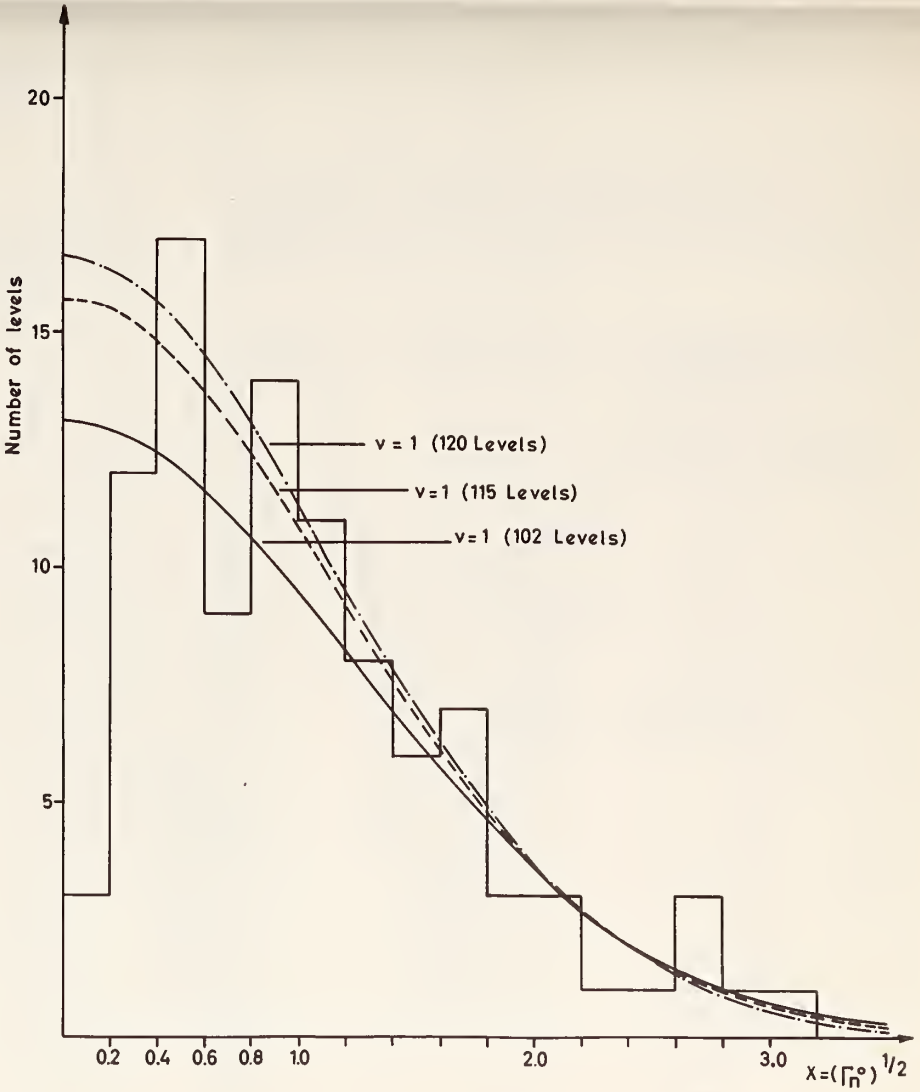

Fig. 2: Histogram of the observed numbers of levels versus $x = (\Gamma_n^0)^{1/2}$. The theoretical distributions for $\nu = 1$ are normalised to 102, 115 resp. 120 levels (see also text).

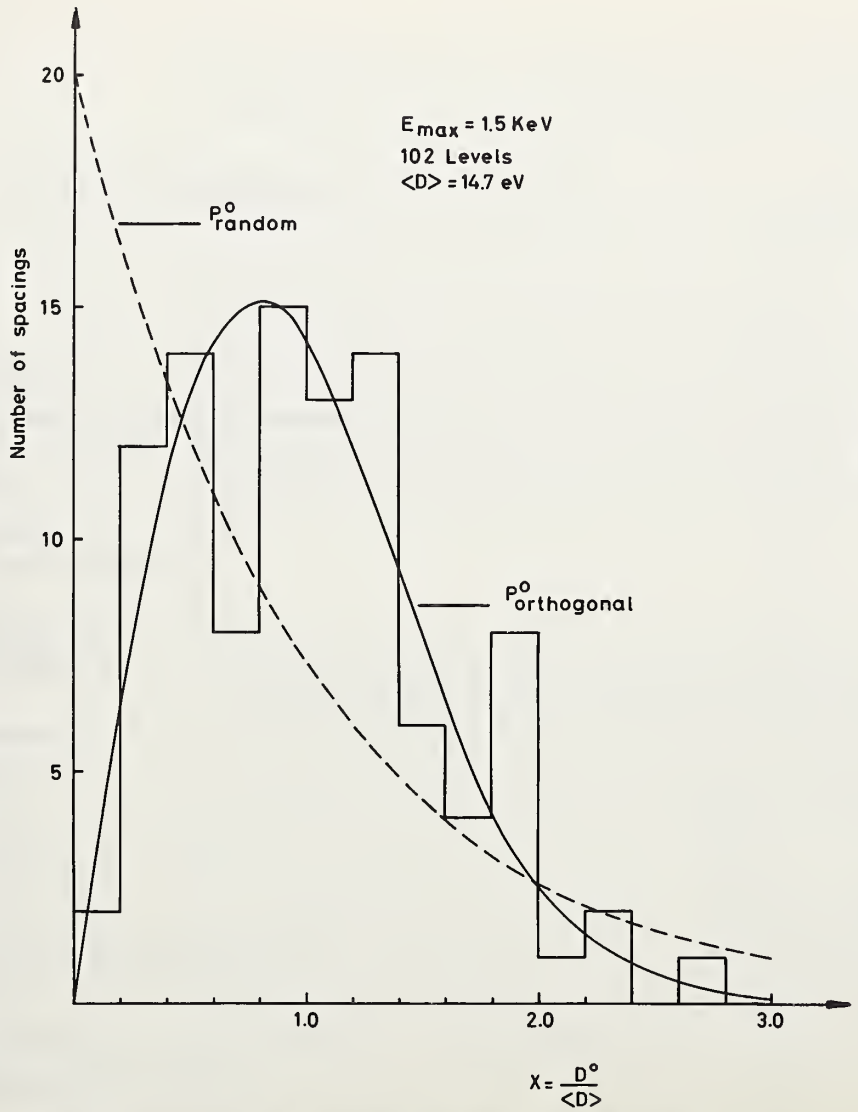

Fig. 3: Histogram of the observed distribution of nearest-neighbour spacings. The theoretical distributions correspond to random resp. the distribution of the Gaussian orthogonal ensemble.

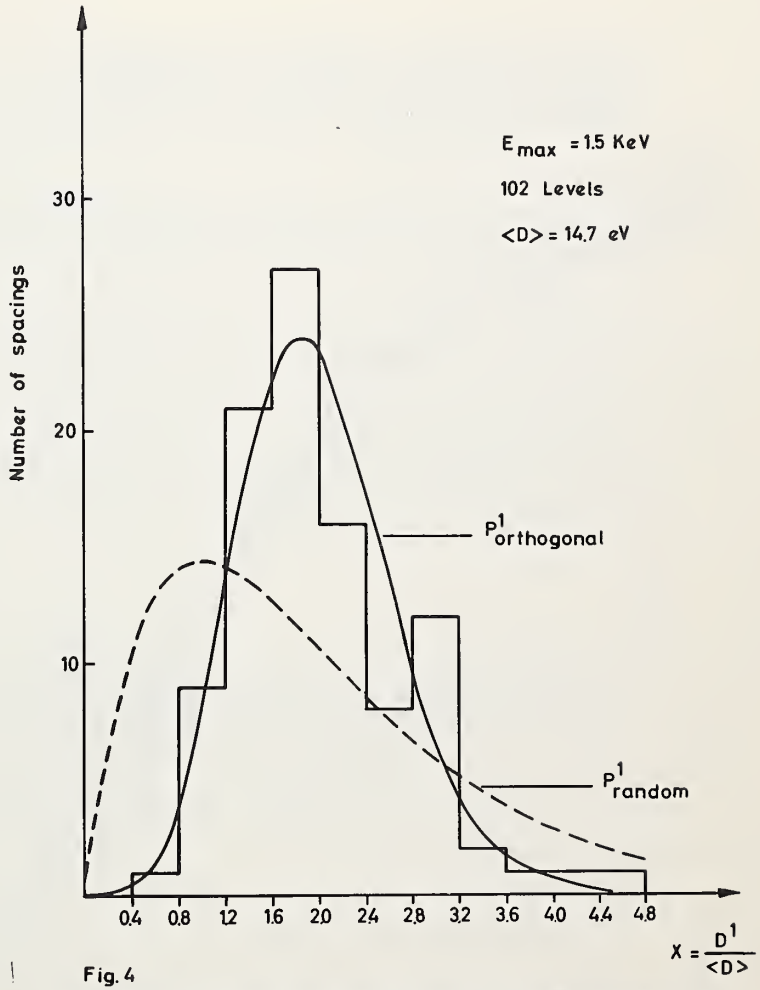

Fig. 4

Histogram of the observed distribution of next-nearest-neighbour spacings. The theoretical distributions correspond to random resp. the distribution of the Gaussian orthogonal ensemble.

RESONANCE GROUPING STRUCTURE IN NEUTRON INDUCED SUBTHRESHOLD FISSION OF Pu-240

E. Migneco and J. P. Theobald

Central Bureau for Nuclear Measurements

EURATOM, Geel, Belgium

Abstract

The subthreshold fission cross section of Pu-240 has been measured in the energy range between 200 eV and 8 keV.
The fission spectrum obtained shows a periodical appearance of groups of resonances with particularly high fission widths.
The mean fission cross section is higher than the calculated value for p-wave fission.

1. Introduction

In 1956 Wheeler (1) has pointed out the anomaly in the fission width of the 1 eV resonance of Pu-240. He has deduced from the very low value of Γ_f at 1 eV the possibility that s-wave fission is forbidden.

Recently De Vroey et al. (2) tend to confirm this assumption. This problem has been discussed in detail by Rae (3).

The presented paper describes an experiment on subthreshold fission of Pu-240 by means of a high resolution time-of-flight spectrometer.

2. Experimental set-up

The CBNM linear electron accelerator has been used as a pulsed neutron source.
The fission events have been detected by a fission neutron liquid scintillation detector (Fig. 1), which was described in detail in a previous paper (4).
The neutron flight path is 30.57 m. The geometry and the collimation of the set-up is shown in fig. 2.
The parameters of the time-of-flight spectrometer are the following:

Linac beam energy	55 MeV
Peak beam current	1.4 A
Burst frequency	400 Hz
Burst width	50 ns
Analyser channel width	40 ns
Number of channels	4096
Dimensions of the polyethylene moderator	20x20x2.3 cm^3
Cut-off filter	B-10

The background as determined with the "black resonance" technique is negligible relative to the high time independent spontaneous fission background of Pu-240.

The incoming neutron spectrum has been measured with a bank of BF_3 counters at about 60 m from the Linac target.
The Pu-240 sample prepared and analyzed by L. A. S. L. has a diameter of 7.620 + 0.013 cm. It contains 54.3347 g Pu with a Pu-240 concentration of 97.93 + 0.05%. The Pu-239 contamination is 1.38 + 0.02%. The rest is Pu-238, Pu-241 and Pu-242. The sample is alloyed with 1.2% Al. It consists of 5 discs, each of which is packed into a thin aluminium canning.

3. Results

The measured fission cross section is shown in fig. 3. This curve has been obtained from the experimental spectrum after subtraction of the spontaneous fission background determined by fitting the experimental count between the resonances.
The spectrum has been normalized equalizing the $\int \sigma_f(E)dE$ of the Pu-239 impurity resonances at 203.46 eV, 203.93 eV and 195.36 eV with the value given by Derrien et al. (5). The error introduced by this normalization is + 8%.
The systematical error introduced by the different $\bar{\nu}$ (the mean number of neutrons per fission event) and the different fission neutron spectra of the reactions Pu-239(n, f) and Pu-240(n, f) has been neglected, because of the absence of data for Pu-240.
The efficiency of the pulse shape γ-discriminator has been tested with U-238 and Th-232 samples in an identical experiment. No significant contribution of the high neutron capture resonances was detected.
The resonances were analyzed with a single level area analysis program, which applies corrections for self screening and multiple scattering.
This computer program is a modified version of GACA (7).
The resonances at 1.408 keV and 1.402 keV have not been resolved. Their analysis is performed under the assumption, that their total widths are equal.
The input parameters Γ_n and $\langle\Gamma_\gamma\rangle$ = 23.2 meV are taken from measurements by Kolar and Böckhoff (6) and Weigmann and Schmid (8).
The results are shown in table I.

4. Discussion

The mean fission width in the energy range between 450 eV and 4 keV turns out to be 3.5 meV, when one uses the number of resonances given in ref. 6. This value can be compared with the average value of Γ_f calculated with formula for s-wave neutrons

$$\langle\Gamma_f\rangle = \frac{D}{2\pi} \exp\left(-\frac{2\pi E_F}{\hbar\omega}\right)$$

where D = 14.9 + 0.8 eV is the mean level spacing (6) E_F is the threshold energy of 710 keV and $\hbar\omega$ = 650 keV is a measure for the potential barrier thickness. The calculated value is 2.5 meV. If one takes into account the large error on the experimental value, the agreement is satisfactory.
This fact as well as the results of the Petrel experiments (9), are in contradiction with assumption, that s-wave fission is highly forbidden. The

Petrel experiments show a mean fission cross section, which does not decrease at neutron energies below 10 keV, what one would expect for a p-wave fission cross section. The presented measurement supports these Petrel results.
Transmission measurements of Kolar and Böckhoff moreover show in some total cross section resonances, with a high Γ_f value, interference effects which indicate an s-wave resonance (6).
The Γ_f values for the resonance group between 750 and 820 eV agree well with the estimated values given by Weigmann and Schmid (8). These authors observed unusual high Γ_γ values in that energy range and deduced a contribution of subthreshold fission γ's to their results.
The group structure in the fission spectrum of Pu-240 is the most surprising result of this investigation. It seems to indicate a new form of intermediate state mechanism in fission, which can be explained in the following way (10, 11, 12).
The nuclear potential energy V as a function of a suited deformation parameter η (10) shows besides the ground state minimum a second minimum at a certain deformation η_1. The potential energy $V(\eta_1)$ is of the order of 2 MeV. (Fig. 4).
The normal compound nuclear states in the zero deformation potential have at about 5.4 MeV neutron binding energy a high level density D = 15 eV, where for the intermediate states in the second potential minimum at the η_1 deformation corresponds an excitation energy of 5.4 - 2 MeV and in consequence a low level density D = 650 eV. The latter levels can be considered as excited states of a hypothetical deformed shape isomer.
The enhancement effect on some compound nuclear states is a consequence of a mixing of these states with the intermediate states at neighboured energies.

We thank Dr. J. Spaepen for his interest and Mr. K. H. Böckhoff for his support and many advices during this experiment. The authors are very much indebted to Dr. H. Weigmann for suggestions and interesting discussions. We feel gratitude to Mr. J. Wartena, who has constructed the electronic equipment and to Drs. M. G. Cao and H. Schmid for their help in the data evaluation.

5. References

(1) J. A. Wheeler, Physica 22 (1956) 1103

(2) M. De Vroey and al., Proceedings of a Symposium on Physics and Chemistry of Fission, Salzburg 1965, Vol. 1

(3) E. R. Rae, Proceedings of a Symposium on Physics and Chemistry of Fission, Salzburg 1965, Vol. 1

(4) M. G. Cao, E. Migneco, J. P. Theobald, J. A. Wartena and J. Winter, Fission cross section measurements on U-235 (to be published in J. of Nucl. Energy), Paper D-3 of this Conference

(5) H. Derrien, J. Blons and al., Nuclear data for reactors, Vol. II, Paris 1966

(6) W. Kolar and K. H. Böckhoff, Resonance Parameters of Pu-240, Part I: Neutron Widths (Submitted to J. of Nucl. Energy), Paper D-7 of this Conference

(7) F. M. Fröhner and al., CA-5816

(8) H. Weigmann and H. Schmid, Resonance Parameters of Pu-240, Part II: Radiative Widths (Submitted to J. of Nucl. Energy), Paper D-9 of this Conference

(9) D. H. Byers and al., Fission cross section from Petrel, LA-3586

(10) V. M. Strutinsky, Nucl. Phys. A95. 2(1967) p. 420

(11) H. Weigmann (private communication)

(12) E. Lynn (private communication)

TABLE I

E_r keV	$\Gamma_n \pm \Delta\Gamma_n$ meV	$\Gamma_f \pm \Delta\Gamma_f$ meV	$g\frac{\Gamma_n \Gamma_f}{\Gamma}$ meV
3.3810	34.5 ± 12.1	126.9 ± 43.9	23.72
3.0640	128.0 ± 38.4	12.3 ± 1.7	9.63
2.7470	102.0 ± 13.3	10.7 ± 1.3	8.03
2.6960	345.0 ± 27.6	93.9 ± 11.7	70.10
2.0530	68.5 ± 6.9	1.9 ± 0.2	1.39
2.0330	101.5 ± 10.2	7.2 ± 0.9	5.54
1.9560	261.0 ± 18.3	24.5 ± 3.0	20.71
1.9160	35.9 ± 5.7	42.3 ± 7.3	14.98
1.8420	125.8 ± 10.1	10.1 ± 1.2	7.99
1.4260	36.7 ± 3.7	4.0 ± 0.5	2.30
1.4080	10.9 ± 6.5	60.0 ± 38.3	6.95
1.4020	5.2 ± 1.0	60.0 ± 16.2	3.53
0.8200	110.0 ± 5.5	1.0 ± 0.1	0.82
0.8100	213.0 ± 10.7	9.6 ± 1.2	8.32
0.7910	23.9 ± 1.4	12.9 ± 1.7	5.14
0.7820	3.0 ± 0.9	132.0 $^{+\text{undef.}}_{-85}$	2.50
0.7500	68.2 ± 3.4	7.8 ± 1.0	5.36

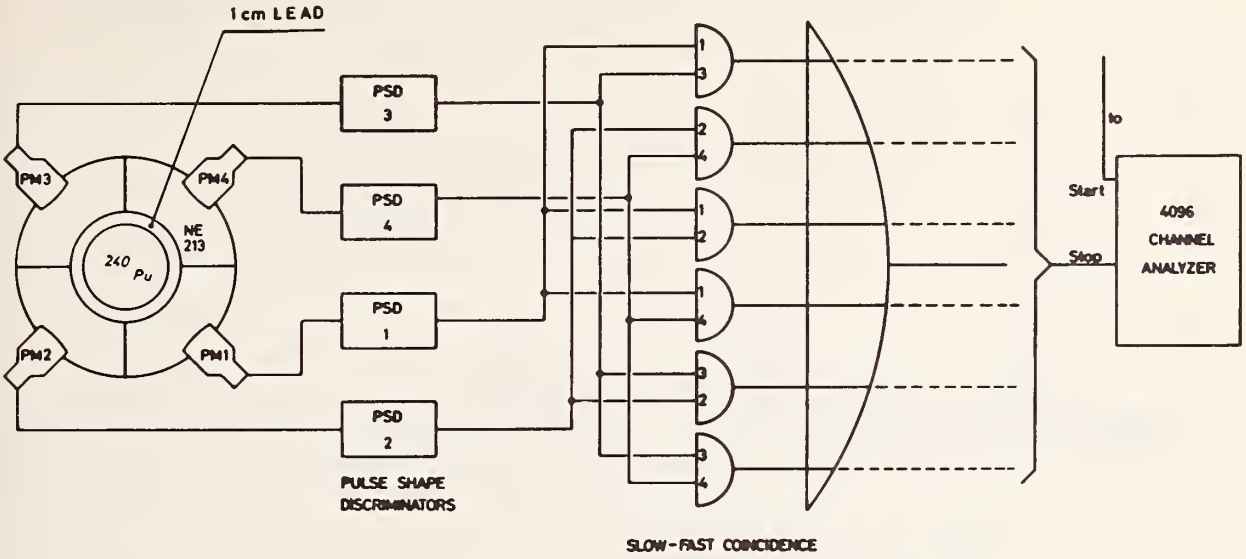

Fig. 1: The fission neutron liquid scintillator detector.

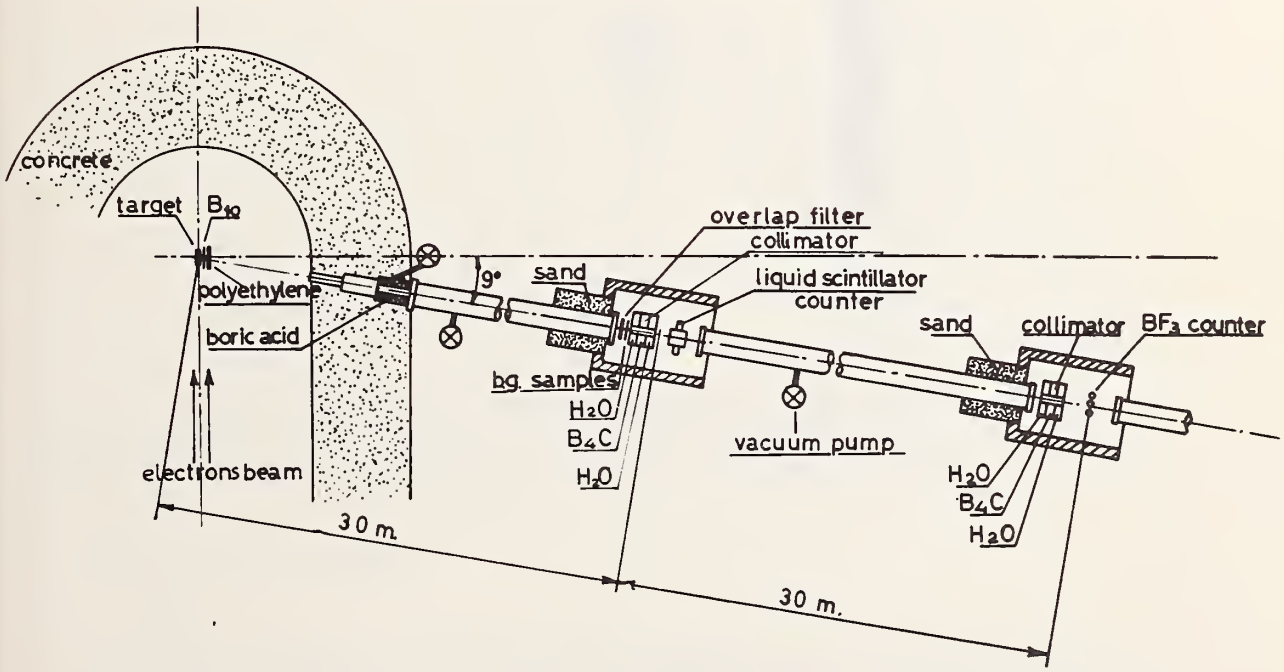

Fig. 2: The experimental set-up.

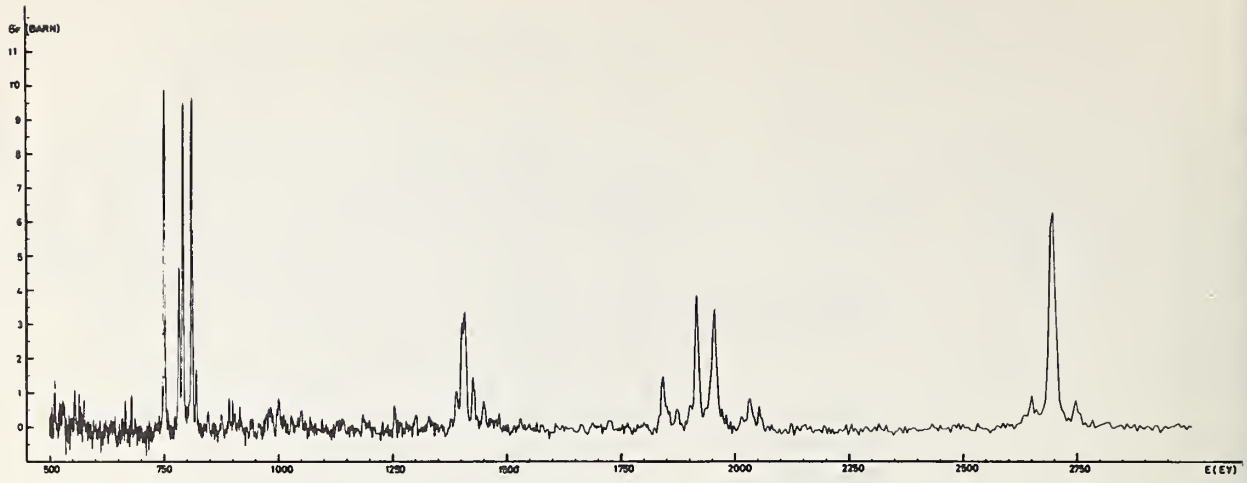

Fig. 3: The subthreshold fission cross section of Pu-240 between 500 eV and 3000 eV.

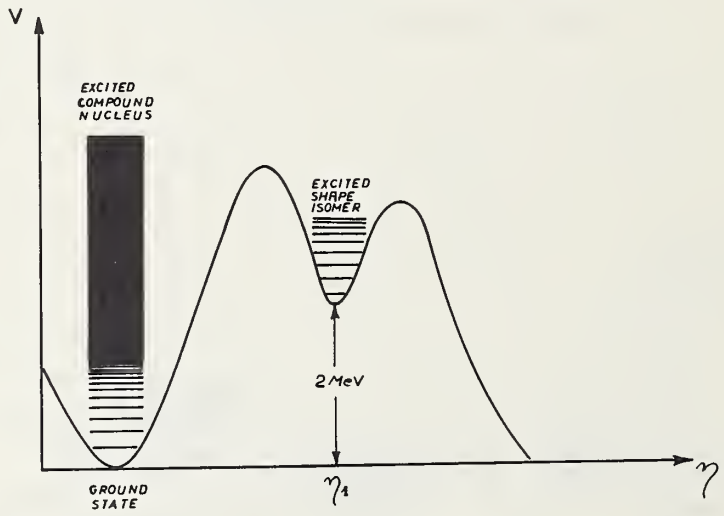

Fig. 4: The nuclear potential energy V as a function of the deformation parameter η (qualitative figure).

NEUTRON CAPTURE MEASUREMENTS IN THE RESONANCE REGION: Cu and Pu-240

H. Weigmann, J. Winter and H. Schmid
Central Bureau for Nuclear Measurements
EURATOM, Geel, Belgium

Abstract

Radiative neutron capture in natural Cu has been studied in the neutron energy range from 200 eV to 16.5 keV. An area analysis of the data yields information on resonance parameters: For large resonances ($\Gamma_n \gg \Gamma_\gamma$) with known isotopic assignment values of Γ_γ or, if the spin of the resonance is unknown, $2g\Gamma_\gamma$ are obtained. In some cases, it was possible to assign the spin of the resonance from the measured $2g\Gamma_\gamma$ assuming a fairly constant radiation width. For a number of small resonances ($\Gamma_n \ll \Gamma_\gamma$) with unknown isotopic assignment, values of $4ag\Gamma_n$ (a = isotopic abundance) have been determined. The radiative widths obtained for 32 resonances in Pu-240 in the neutron energy range between 38 eV and 820 eV are also given, yielding a mean value of $\overline{\Gamma_\gamma} = (23.2 \pm 2.0)$ meV. The observation of unusual large radiative widths for some resonances is explained by the presence of subthreshold fission.

1. Measurements

Neutron capture measurements on Cu and Pu-240 have been performed at detector stations of 30 m and 60 m distance from the target of the CBNM 60 MeV electron linac. The experimental set up (1) and the capture γ-ray detector (2) employed have been described previously. Nominal resolutions between 6 nsec/m and 1 nsec/m have been used. The energy spectrum of the neutrons at the detector station was measured with a B-10 slab viewed by a NaI crystal; the B-10(n,α)Li-7, Li-7$^+$ cross section is assumed to vary as 1/v in the energy range of interest. An absolute calibration of the product detector efficiency times neutron flux constant was obtained by observing neutron capture events in "black" resonances with known parameters; the resonances in Ag at 5.2, 16.3 and 51.4 eV as well as the 20.46 eV resonance in Pu-240 were used for this purpose. The parameters of the latter resonance have been taken from Asghar et al. (3).
In fig. 1 as an example of the raw data a time-of-flight spectrum is shown which was obtained from a $3.37\ 10^{-2}$ atom/b sample of natural Cu at the 60 m flight path station. The steps in the spectrum are due to changes in channel width (40, 80 and 160 nsec, respectively) of the 4096 channel analyser.

2. Results and Discussion

2.1. Copper

An area analysis of the observed resonances was carried out by means of the "GACA" program of Fröhner and Haddad (4). The calculations were performed on the IBM 360/65 computer at Ispra, the data and results being transmitted with the aid of the teleprocessing system connecting Geel and Ispra.

The results are presented in table I. Input data, which have been taken from ref. (5 - 9) are given in brackets. The errors indicated in the table contain both, experimental uncertainties which are mainly due to the error in absolute flux calibration, and the uncertainty in the input data. The information which can be obtained from capture area analysis depends on the ratio of Γ_n to Γ_γ (the following subsections correspond to the indications given in column 8 of table I):

(i) For strong resonances ($\Gamma_n \gg \Gamma_\gamma$) the isotopic assignments as well as the neutron widths of which are mostly known in the case of Cu, the area analysis yields values of the radiative width Γ_γ or, if the spin of the resonance is unknown, of $2g\Gamma_\gamma$. The results obtained for 21 resonances are given in column 7 of table I. From the Γ_γ-values for resonances with known (8) spin the following mean values of the radiative width may be inferred:

isotope (resonance spin)	$\overline{\Gamma_\gamma}$	number of resonances
Cu-63 (both spin values)	0.51 ± 0.05	7
Cu-63 (J = 1)	0.60 ± 0.06	2
Cu-63 (J = 2)	0.48 ± 0.05	5
Cu-65 (both spin values)	0.34 ± 0.04	5

For Cu-65 the radiative width of the resonance at 229 eV (8) has been included, the one of the resonance at 4.391 keV which is probably an unresolved dublett has been excluded. The errors only reflect the experimental uncertainties, they do not contain the expected spread of individual radiative widths around their mean value which may be quite large (even about 40%) in this region of the periodic table as experimentally observed by Moxon (10). In view of this expected large spread, the difference observed in $\overline{\Gamma_\gamma}$ between resonances with J = 1 and J = 2 in Cu-63 may well be accidental. For some of the resonances with as yet unknown spin it is possible to deduce the resonance spin from the values obtained for $2g\Gamma_\gamma$ in the resonance analysis. The criterion used here is that for the opposite choice of the spin value a radiative width would be obtained which differs from the above mean value by more than 40%. The resonance spins obtained are given at the end of column 3 in table I. If we adopt for the 8.363 keV resonance the isotopic assignment of ref. (8) (in ref. (8) this resonance appears at 8.549 keV and is stated to be due to Cu-65), we would obtain a radiative width of at least (0.9 + 0.1) eV which is completely incompatible with the above mean value for this isotope. Therefore, we infer that this resonance is due to Cu-63.

(ii) There are some resonances of intermediate strength the neutron widths as well as the isotopic assignments of which are unknown. For these, therefore, we can only determine the quantity $4ag\Gamma_n\Gamma_\gamma/\Gamma$ which is given in column 4 of table I.

Using the same argument as given at the end of (i) it may be inferred that three of them (those at 8.650 keV, 14.115 keV and 14.637 keV) are due to Cu-63. For the other three resonances of this group we can draw no conclusion because a small value of the quantity $4ag\Gamma_n\Gamma_\gamma/\Gamma$ may be due to a small neutron width (of the order of magnitude or smaller than Γ_γ).

(iii) Especially at low neutron energies a large number of very weak resonances ($\Gamma_n \ll \Gamma_\gamma$) is observed. Some of these (marked with an asterisk) have not been observed before and for all of them the isotopic assignment is unknown. Using $\Gamma_\gamma = (0.42 \pm 0.4 / 0.2)$ eV for these resonances the quantity $4ag\Gamma_n$ quoted in column 5 of table I was obtained.

These data, together with the values of $4ag\Gamma_n$ taken from ref. (5, 7, 8) for the stronger resonances up to 9.2 keV neutron energy (above that energy there are many resonances with unknown neutron width), have been used to calculate a "reduced width distribution" (precisely: a distribution for the quantity $4ag\Gamma_n^0$). The integral distribution is shown in fig. 2 together with two theoretical curves (Porter-Thomas distributions): The broken line gives the theoretical distribution if one assumes that all of the 36 resonances are s-wave. The full line represents the theoretical reduced width distribution for only the 22 stronger resonances, the remaining 14 resonances being assumed to be p-wave. From a detailed comparison and an inspection of the values of $ag\Gamma_n^1$ for the weak resonances it is concluded that $14 \pm \frac{1}{2}$ of the small resonances are due to p-wave interaction. From these, we obtain a value for the p-wave strength function for natural Cu of

$$S_1 = (0.30 \begin{smallmatrix} + 0.18 \\ - 0.14 \end{smallmatrix}) \cdot 10^{-4} ,$$

where the error contains besides the interpretation uncertainty (12, 13 or 15 of the weak resonances may be p-wave), also the statistical uncertainty on the quantity $\Sigma ag\Gamma_n^1$ as obtained from a limited number of levels.

2.2. Plutonium-240

Radiative widths obtained for 36 resonances by combining the capture area analysis with transmission area analysis (11) are given in table II. Excluding the last four resonances for which an extraordinarily high value of Γ_γ is observed (see below), a weighted mean value of

$$\bar{\Gamma}_\gamma = (23.2 \pm 2.0) \text{ meV}$$

is obtained. It is in good agreement with a preliminary value of $\bar{\Gamma}_\gamma = (21 \pm 2)$ meV obtained by Asghar et al. (7).

There are however, four resonances at the upper limit of the analysed energy range for which an extraordinarily high value of Γ_γ is observed. This has been interpreted as being due to the presence of subthreshold fission in these resonances. Of course if fission is present, it will be detected via the prompt γ-radiation associated with the fission process: thus, the observed area under a resonance will be proportional to

$$\frac{\Gamma_n(\Gamma_\gamma + \varepsilon\Gamma_f)}{\Gamma} ; \quad \varepsilon = \frac{E_f}{B}$$

instead of $\Gamma_n\Gamma_\gamma/\Gamma$ for a resonance without fission (E_f is the total γ-ray energy of the prompt fission γ's; B is the neutron binding energy for Pu-240). In fact, in a recent measurement of the subthreshold fission cross section by Migneco and Theobald (13) it has been verified that a strong fission component is present in just these four resonances (and also in some groups of resonances at higher neutron energies).

We are grateful to Dr. J. Spaepen for his continuous interest in this work and to Mr. K. H. Böckhoff for interesting discussions and for his support during these measurements.

Table 1: Resonance Parameters of Cu obtained from Area Analysis

(values in brackets were used as input data)

E_0(keV)	Isotope	J	$4ag\Gamma_n$ (meV)	Γ_n(eV)	Γ_γ(eV)	remarks
0.229	[65]			$2g\Gamma_n=(22.2\pm1.5).10^{-3}$	[0.24±0.02]	(iii)
0.400			0.49±0.05			(iii)
0.576	[63]	[2]		[0.86±0.03]	0.485±0.040	(i)
0.648			17.8±1.0			(iii)
0.804			6.9±0.6			(iii)
0.991			23.6±1.4			(iii)
1.359			12.0±1.0			(iii)
2.037	[63]	[1]		[43.5±2.0]	0.57±0.07	(i)
2.211[x]			29.4±3.2			(iii)
2.319[x]			17.9±2.1			(iii)
2.527	[65]	[2]		[16.8±1.8]	0.36±0.04	(i)
2.640	[63]	[2]		[4.5±0.5]	0.58±0.05	(i)
2.851[x]			46±5			(iii)
3.304[x]			38±4			(iii)
3.498[x]			36±4			(iii)
3.583[x]			29±3			(iii)
3.918	[65]	[1]		[24±2]	0.47±0.05	(i)
4.391	[65]	[2]		[7±1]	0.91±0.07	(i), (iv)
4.434[x]			38±5			(iii)
4.486	[65]	[1]		[16±2]	0.33±0.04	(i)
4.852	[63]	[1]		[14±2]	0.62±0.06	(i)
5.250[x]			30±5			(iii)
5.385	[63]	[2]		[40±4]	0.44±0.05	(i)
5.819	[63]	[2]		[10.4±1.0]	0.46±0.04	(i)
6.290			67±10			(iii)
6.448	[65]	[2]		[26±3]	0.35±0.04	(i)
6.845			$4ag\Gamma_n\Gamma_\gamma/\Gamma$(eV) = 0.19±0.03			(ii)
7.009[x]			38±6			(iii)
7.090	[63]			[$2g\Gamma_n$=0.74]	$2g\Gamma_\gamma$=0.34±0.03	(i)
7.568						(v)
7.931						(v)
8.363	63		[4680]		$4ag\Gamma_\gamma$=0.70±0.08	(i)
8.650	63		$4ag\Gamma_n\Gamma_\gamma/\Gamma$(eV) = 0.37±0.05			(ii)
9.191	[63]	[2]		[36.6±3.7]	0.42±0.04	(i)
9.775						)
9.847						) (vi)
9.946						)
10.340[x]			$4ag\Gamma_n\Gamma_\gamma/\Gamma$(eV) = 0.21±0.04			(ii)
10.655[x]						) (vi)
10.860						)
12.172			$4ag\Gamma_n\Gamma_\gamma/\Gamma$(eV) = 0.14±0.03			(ii)

Table 1 (continued)

E_0(keV)	Isotope	J	$4ag\Gamma_n$ (meV)	Γ_n(eV)	Γ_γ(eV)	remarks
12.576	[63]			[$2g\Gamma_n$=17.2±1.5]	$2g\Gamma_\gamma$=0.56±0.07	(i)
12.933						)
13.001						)(vi)
13.221						)
13.753	[63]	1		[$2g\Gamma_n$=49.3]	$2g\Gamma_\gamma$=0.33±0.08	(i)
14.115[x]	63		$4ag\Gamma_n\Gamma_\gamma/\Gamma$(eV)= 0.42±0.07			(ii)
14.286	[65]	1		[$2g\Gamma_n$=52]	$2g\Gamma_\gamma$=0.23±0.04	(i)
14.637	63		$4ag\Gamma_n\Gamma_\gamma/\Gamma$(eV)= 0.42±0.07			(ii)
15.170	[63]	2		[$2g\Gamma_n$=34.7]	$2g\Gamma_\gamma$=0.64±0.07	(i)
15.880	[63]	2		[$2g\Gamma_n$=22.1]	$2g\Gamma_\gamma$=0.71±0.09	(i)
16.159	[65]	2		[$2g\Gamma_n$=44]	$2g\Gamma_\gamma$=0.72±0.10	(i)
16.368	[63]	1		[$2g\Gamma_n$=13.8]	$2g\Gamma_\gamma$=0.42±0.06	(i)

(i), (ii), (iii): see corresponding subdivision of chapter 3, text.

(iv): there is some indication in the shape of this resonance that it is an unresolved dublett; this would explain the extremely high Γ_γ.

(v): unresolved dublett.

(vi): insufficiently resolved group of resonances.

Table 2: ^{240}Pu resonance parameters: Radiative widths

E_0(eV)	Γ_γ(meV)	E_0(eV)	Γ_γ(meV)
38.34	20.0 ± 2.0	372.3	21.5 ± 3.0
41.64	21.8 ± 2.0	405.0	26.0 ± 2.3
66.66	23.5 ± 2.0	419.0	---
72.83	21.0 ± 2.0	450.2	26.5 ± 3.0
90.78	19.5 ± 2.0	466.4	---
92.50	---	473.2	---
105.05	26.0 ± 2.5	494.2	---
121.67	21.5 ± 2.0	499.6	21.5 ± 2.5
135.2	24.5 ± 2.5	514.6	25.5 ± 3.0
151.7	21.5 ± 2.0	546.8	25.0 ± 2.5
162.9	20.0 ± 3.0	553.5	24.5 ± 3.0
170.3	22.0 ± 2.0	566.6	21.5 ± 2.0
186.1	22.0 ± 2.0	597.2	25.0 ± 2.5
199.6	---	608.4	21.0 ± 2.5
239.3	21.5 ± 2.5	632.6	25.0 ± 3.5
260.7	24.0 ± 2.3	637.8	22.0 ± 3.0
287.3	26.0 ± 2.0	665.5	26.5 ± 2.5
305.1	---	678.9	26.0 ± 3.5
318.5	---	(750.5	49 ± 4)
320.9	21.0 ± 2.5	(759.6	---)
338.7	---	(791.4	80 + 16)
346.2	21.5 ± 2.5	(811.0	45 ∓ 4)
364.0	25.0 ∓ 2.5	(820.4	30 ∓ 3)

3. References

(1) H. Weigmann and H. Schmid, Nucl. Phys. A104 (1967) 513

(2) H. Weigmann, G. Carraro and K. H. Böckhoff, Nucl. Instr. and Meth. 50 (1967) 265

(3) M. Asghar, M. C. Moxon and N. J. Pattenden, Conf. Nuclear Data (Paris 1966) CN-23/31

(4) F. H. Fröhner and E. Haddad, Nucl. Phys. 71 (1965) 129

(5) M. D. Goldberg et al., BNL 325, second ed., suppl. 2

(6) J. B. Garg, J. Rainwater and W. W. Havens, Jr., CR 1860 (1964)

(7) R. Wagner, W. M. Good and D. Paya, Conf. Nucl. Struct., Antwerp (1965), paper 99
W. M. Good, D. Paya and R. Wagner, ORNL 3778 (1964) p 69

(8) J. Julien, S. de Barros, P. L. Chevillon, V. D. Huynh, G. Le Poittevin, J. Morgenstern, F. Netter and C. Samour, Conf. Nucl. Struct., Antwerp (1965), paper 80
P. L. Chevillon-Pitollat, CEA-R 3128 (1967)

(9) R. E. Coté, L. M. Bollinger and J. M. LeBlanc, Phys. Rev. 111 (1958) 288

(10) M. C. Moxon, Conf. Nucl. Struct., Antwerp (1965), paper 88

(11) W. Kolar and K. H. Böckhoff, Journ. Nucl. Energy, to be published, and this conference, paper D-7

(12) M. Asghar, private communication

(13) E. Migneco and J. P. Theobald, submitted to Nucl. Phys., and this conference, paper D-8

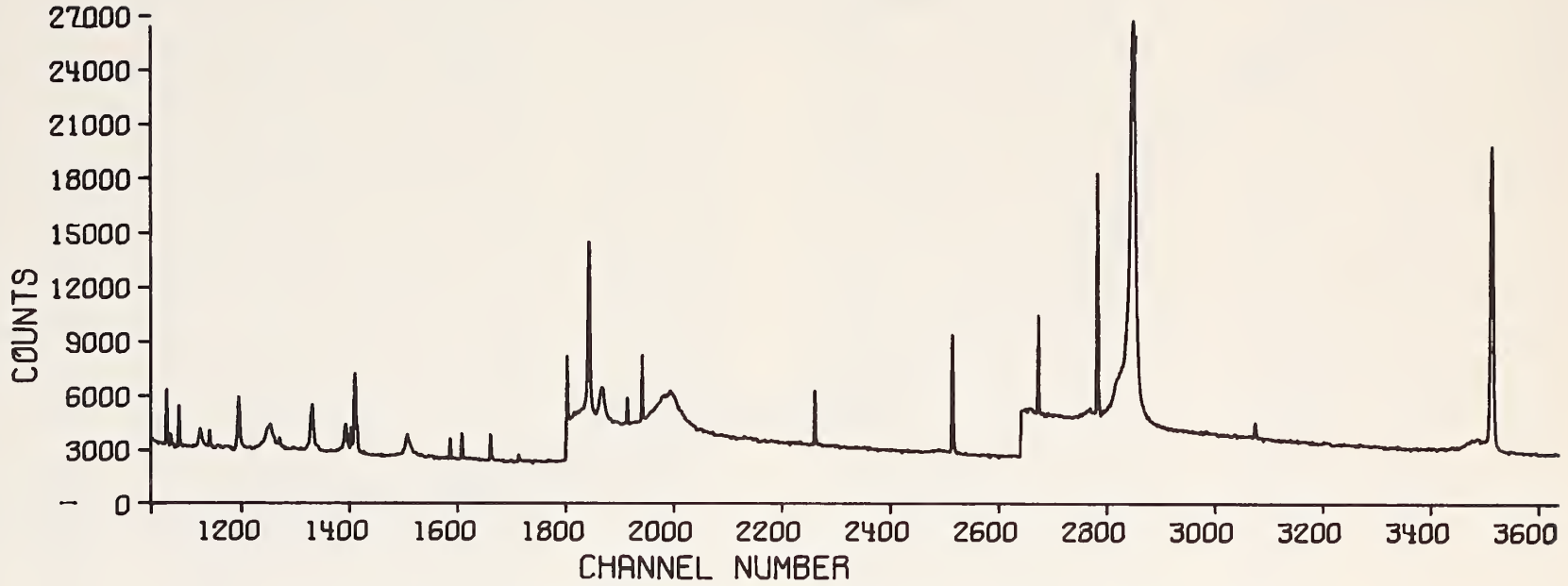

Fig. 1: Time-of-flight spectrum obtained from a $3.37\ 10^{-2}$ atom/b sample of natural Cu at the 60 m flight path station; the neutron energy range is from about 7.3 to 0.2 keV.

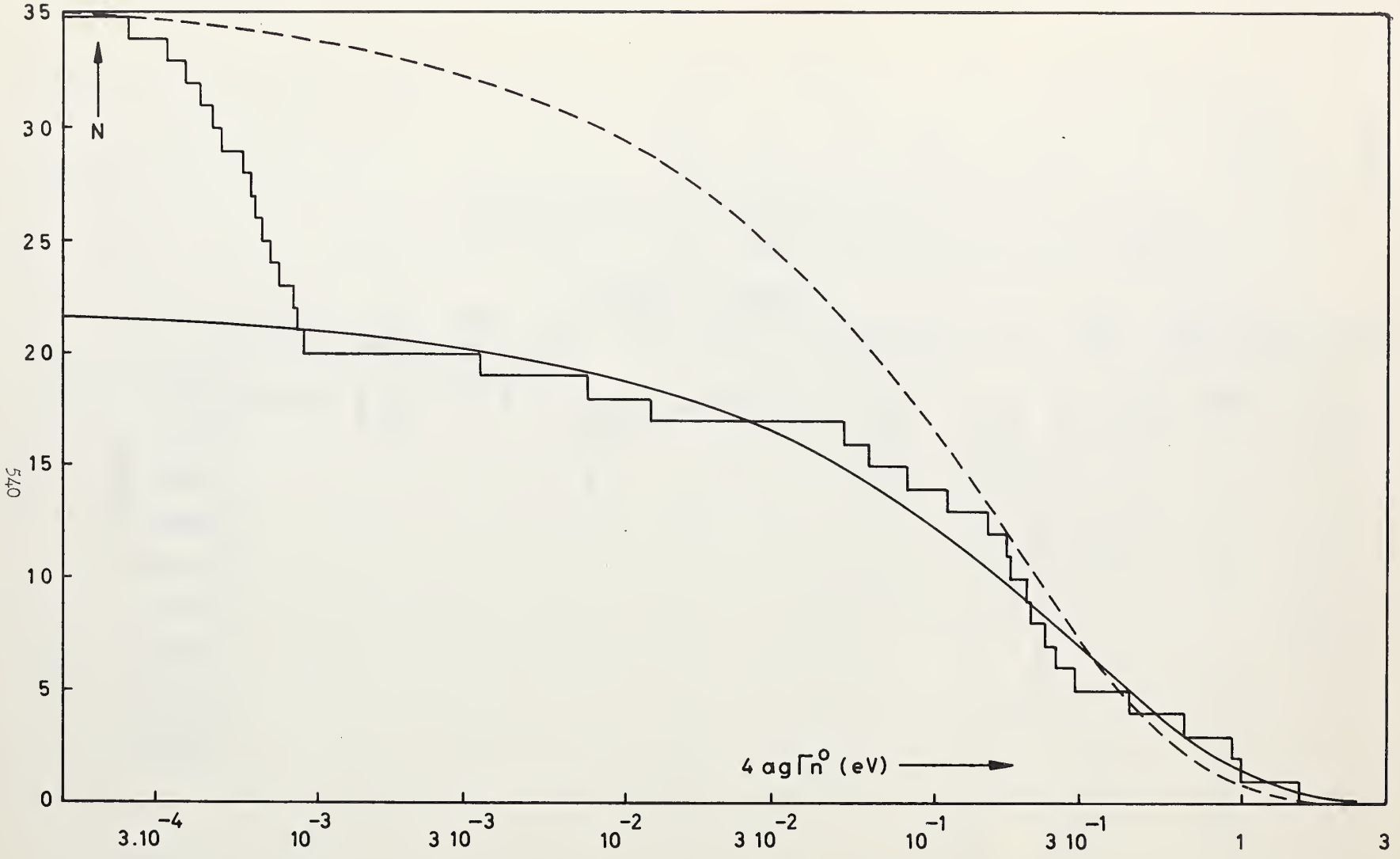

Fig. 2: Integral reduced width distribution: Number N of resonances for which $4ag\Gamma_n^\circ$ is larger than abscissa. Theoretical (Porter-Thomas) distributions are under the assumptions that none (broken line) or 14 (full line) of the small resonances are p-wave.

NEUTRON SCATTERING CROSS SECTIONS OF U^{233}, U^{235}, AND Pu^{241} FROM 1 TO 30 eV*

G. D. Sauter
Dept. of Applied Science, University of California
Davis, California 95616

and

C. D. Bowman
University of California, Lawrence Radiation Laboratory
Livermore, California 94550

Abstract

Scattering measurements of U^{233}, U^{235}, and Pu^{241} have been made at the Livermore linear electron accelerator using the 4π neutron source technique. Scattering cross sections, corrected for effects of sample thickness, have been obtained for neutron energies between 1 and 30 eV. For Pu^{241}, the scattering cross section and published fission data have been simultaneously fitted with Reich and Moore's multilevel formula. A good fit to both cross sections could only be obtained by allowing a sizeable fluctuation in the capture widths. Spin assignments were made for all resonances in the 1-30 eV interval. The resulting resonance parameters are presented. The results of a similar fit to U^{233} were less successful and no spins were obtained. The U^{235} scattering cross section was not sufficiently detailed for meaningful multilevel analysis.

1. Introduction

The neutron scattering cross sections of U^{233}, U^{235}, and Pu^{241} for neutron energies from 1 to 30 eV have been measured at the Livermore electron linear accelerator. The measurements were carried out using a 4π neutron source in a time-of-flight technique [1]. Spin values for neutron resonances in Pu^{241} have been obtained from the data.

The experimental arrangement is shown in Fig. 1. The principal feature of the 4π neutron source technique is the spherical carbon shell. When a pulse of high-energy (about 30-MeV) electrons strikes the tungsten target embedded in the shell, the resulting bremsstrahlung γ radiation creates a burst of high-energy neutrons via (γ, n) interactions with the tungsten. Some of these neutrons scatter back and forth in the moderating shell. After many successive scatters, these neutrons have not only been slowed down to the energies of interest, but have also "forgotten" their point of origin and are uniformly distributed around the shell. Monte Carlo calculations have indicated that the inner surface of the moderating shell is a uniformly distributed 4π neutron source to within 5% for all neutron energies below 1 keV. For energies below 200 eV, the time t_o (μ sec) after the electron pulse for maximum intensity of neutrons of energy E(eV) is $t_o = 2.0/E^{1/2}$. The full width at half maximum intensity τ (μ sec) is given by $\tau = 1.8/E^{1/2}$.

Neutrons from the inner surface of the shell are scattered by a thin sample placed in the center of the spherical cavity. Scattered neutrons

*Work supported by U. S. Atomic Energy Commission, National Science Foundation, and Control Data Corporation.

emerging from the sample in a particular direction pass through a small hole in the shell and reach the boron-loaded liquid scintillator neutron detector. A second hole in the shell, diametrically opposite the first hole, prevents the detector from "seeing" any part of the carbon shell. Thus the only direct neutron source seen by the detector is the scattering sample. Since the sample-to-detector flight time of fission neutrons and gamma rays is much shorter than that of the scattered neutrons of interest, the background associated with fission and capture events is separated in time from the scattered neutrons. By appropriately gating the detector, it can be made insensitive to capture and fission effects.

For a thin scattering sample, it can be readily shown [1] that the neutron detection rate is proportional to the scattering cross section of the sample and the energy dependent neutron flux incident on the sample. This flux can be determined from a measurement with a sample having a known scattering cross section, such as carbon. The two measurements can then be combined to yield the desired scattering cross section. (For further experimental details, see [1].)

2. Plutonium-241

The two Pu^{241} samples thicknesses were 1.14×10^{20} and 2.34×10^{20} atoms/cm^2. When corrected for sample thickness effects, the two measurements yielded scattering cross sections which agreed very closely (to within 5% at the peaks of the largest resonances). The resulting scattering cross section for Pu^{241} between 3 and 32 eV is shown in Figs. 2 and 3.

When the variation of the neutron scattering cross section with energy is known, attempts can be made to deduce the spins of the various resonance levels, using either area analysis or shape analysis. Area analysis, based on the single-level Breit-Wigner formula, has been successfully used in the case of Pu^{239} [2], where most of the resonances are sufficiently isolated from each other. For Pu^{241}, there appear to be only three levels for which area analysis is applicable, those at 13.38, 14.72, and 17.83 eV. We have area analyzed our data for these three levels. The scattering area of an isolated resonance is given by $2\pi^2\lambda^2 g\Gamma_n^2/\Gamma = 4.09 \times 10^6\ g\Gamma_n^2/E_o\Gamma$ barn-eV, where Γ_n and Γ are expressed in eV. From a measured scattering area, one can find $g\Gamma_n^2/\Gamma$ and g for a level, using known values for $g\Gamma_n$ and Γ and the relation $g = (g\Gamma_n)^2/\Gamma\ /(g\Gamma_n^2/\Gamma)$. For the 13.38, 14.72, and 17.83 eV resonances, our data yield values for the scattering areas of 14.6, 29.0, and 18.2 barn-eV respectively. Using published values for $g\Gamma_n$ and Γ [3], we then calculated g values of 0.36, 0.58, and 0.41 respectively. These indicate that the spins probably are J=2 (g = 0.417) for the 13.38 and 17.83 eV levels and J=3 (g = 0.583) for the 14.72-eV level.

We have also simultaneously fitted our Pu^{241} scattering data and the Pu^{241} fission cross section obtained by Moore et al.[4], using the multilevel cross section formula of Reich and Moore [5] with one fission channel per spin state. This shape analysis is based on the following concept. Accurate values for $g\Gamma_n$ and Γ are known from earlier fission and total cross section measurements. Since the peak cross section of a scattering resonance is proportional to $g\Gamma_n^2/\Gamma^2$, the analysis of the scattering data should yield an accurate value of the product $g\Gamma_n^2$ which is independent of the value of spin assumed in the shape analysis. (We will demonstrate this independence below.) With known values of $g\Gamma_n^2$ and $g\Gamma_n$,

the g value (and hence the spin) can be determined as $g = (g\Gamma_n)^2/(g\Gamma_n^2)$.

Assuming the spin values suggested by Moore et al. [4], we varied the values for Γ_n, Γ_f, and Γ_γ for the various levels until we obtained the best stimultaneous fit for the scattering and fission data between 2 and 32 eV. For each resonance we then computed $g\Gamma_n^2$ and calculated g, using published values [3] for $g\Gamma_n$. The calculated g values were consistent with the initially assigned values except for the group of resonances between 12.78 and 17.83 eV. The spin for each of these resonances was opposite that suggested by Moore et al. Next we repeated the fitting process assuming all spins opposite to those of Moore et al. For this fit, which yielded calculated cross sections that were nearly identical with those of the first fit, the computed values of $g\Gamma_n^2$ changed very little from those of the first fit. The g values determined in this case were again consistent with those proposed by Moore et al. except for the group of resonances between 12.78 and 17.83 eV. Finally, we carried out the fitting process for a third time using the spins suggested by Moore et al. for all resonances except those between 12.78 and 17.83 eV, for which the opposite values were used. Again the calculated cross sections were nearly identical with those of the previous fittings, and the computed values of $g\Gamma_n^2$ changed only slightly. The g values determined were the same as those obtained from the two previous fittings. Furthermore, the g values for the 13.38, 14.72, and 17.83 eV levels in all three fittings were consistent with those determined independently by area analysis. The results of the fitting procedure for Pu^{241} are shown in Table 1. The resonance parameters shown are those obtained in the final fitting. Figure 2 and 3 show the experimental fission [4] and scattering cross section data. The solid curves are the cross sections calculated from the multilevel formula using the resonance parameters listed in Table 1.

As a result of our Pu^{241} analysis, we conclude that the spins of the excited levels formed by low energy neutron absorption in Pu^{241} are those shown in Table 1. These agree with the values suggested by Moore et al. for all levels except the group between 12.78 and 17.83 eV, where our values are opposite to his in every case. Of the 20 levels considered here, we find 7 levels with J=2 and 13 levels with J=3. The average fission width of the J=2 levels is 511 mV and 192 mV for the J=3 levels. These values support the prediction of the Bohr-Wheeler theory [6,7] that the J=2 levels should have a larger average fission width.

3. Uranium-233

The two U^{233} sample thicknesses were 4.83×10^{20} and 9.42×10^{20} atoms/cm^2. For neutron energies above 15 eV, the data from the thicker sample were of poor quality, due to the effects of the large gamma flash created when each electron pulse is stopped by the tungsten target in the carbon shell. Thus for energies above 15 eV, only the thin sample data were used. For neutron energies below 15 eV, the two measurements, when corrected for the effects of sample thickness, again yielded scattering cross sections which agreed very closely. The measured neutron scattering cross section for U^{233} between 1 and 31 eV is shown in Figs. 4 and 5.

The scattering resonances in U^{233} appear too small and too closely spaced to make area analysis feasible. We attempted a shape analysis by trying to simultaneously fit our scattering data and the fission data of Nifenecker [8], again using the multilevel formula of Reich and Moore

with one fission channel per spin state. We could not obtain an acceptable simultaneous fit. Inasmuch as this same simultaneous fitting procedure was successful for Pu^{241}, this failure indicates that more than one fission channel per spin state is required to describe U^{233}. We have also attempted to simultaneously fit the capture and fission data of Weston et al. [9]. Again our failure to obtain a satisfactory result indicated a single fission channel per spin state is not sufficient.

We have fitted Weston's capture data alone, using the multilevel formula. We held all capture widths Γ_γ constant at 45 mV and adjusted $g\Gamma_n$ and Γ_f for each level. Some of the resulting values of $g\Gamma_n\Gamma_\gamma$ and Γ are listed in Table 2. Figs. 4 and 5 show the measured and calculated capture cross sections. Using the Γ values obtained from the capture fit, we have attempted to fit the scattering data using the single channel multilevel formula. The resulting cross section is shown in Figs. 4 and 5. The fit is adequate only for energies less than 6 eV, as shown by the solid line. The dashed line above 6 eV represents the best fit we could obtain. The values of $g\Gamma_n^2$ resulting from the fit for levels below 6 eV are listed in Table 2. As for Pu^{241}, we computed values of g for these levels from our values of $g\Gamma_n^2$ and values [3] of $g\Gamma_n$ obtained from other experiments. These computed g values were too far from the true values (0.583 or 0.417) to be meaningful. The discrepancy is related to a significant difference in our results for the neutron width in comparison with other measurements. We illustrate this by calculating alternate approximate values of $g\Gamma_n$ from our data. We obtained the square root of the product of our $g\Gamma_n^2$ value and an assumed value, g = 0.5. These alternate $g\Gamma_n$ values are shown in Table 2. We have no explanation for the large difference between our values and the previously measured values for $g\Gamma_n$.

4. Uranium-235

The sample thicknesses used for the U^{235} measurements were 2.84×10^{20} and 4.18×10^{20} atoms/cm^2. After corrections for effects of sample thickness, the scattering cross sections determined from the two measurements are in satisfactory agreement. The resulting scattering cross section for U^{235} between 1 and 31 eV is shown in Fig. 6. The arrows in the figure indicate the positions of known resonances in U^{235}. We have not attempted any area or shape analysis of this data.

5. Conclusions

From our measurements on U^{233}, U^{235}, and Pu^{241}, we have determined the neutron scattering cross sections for these nuclides for neutron energies below 31 eV. For Pu^{241}, we have deduced the spins of 20 levels between 2 and 32 eV. These spins are the same as those suggested by Moore et al. [4] except for all the levels in the group between 12.78 and 17.83 eV. Although no spin assignments could be made for U^{233}, we have obtained values for Γ and $g\Gamma_n\Gamma_\gamma$ for the resonances between 1 and 31 eV.

We gratefully acknowledge the help of G. F. Auchampaugh, who supplied the multilevel code used in the analysis, and the support of the National Science Foundation and the Control Data Corporation in providing the digital computer facilities.

6. References

1. G. D. Sauter and C. D. Bowman, Nucl. Instr. Methods 55, 141 (1967).

2. G. D. Sauter and C. D. Bowman, Phys. Rev. Letters 15, 761 (1965).

3. J. R. Stehn et al., Neutron Cross Sections, BNL 325, 2nd ed., Supp. 2, Vol. III (1965).

4. M. S. Moore, O. D. Simpson, T. Watanabe, J. E. Russell, and R. W. Hockenbury, Phys. Rev. 135, B945 (1964).

5. C. W. Reich and M. S. Moore, Phys. Rev. 111, 929 (1958).

6. A. Bohr, Proc. Intern. Conf. on Peaceful Uses of Atomic Energy, Geneva 2, 151 (1956).

7. J. A. Wheeler, Physica 22, 1103 (1956).

8. H. Nifenecker, J. Phys. (Paris) 25, 877 (1964).

9. L. W. Weston, R. Gwin, G. deSaussure, R. W. Ingle, R. R. Fullwood, and R. W. Hockenbury, ORNL-TM-1751, April 1967 (unpublished).

Table 1. Resonance Parameters for Pu^{241}

E_o(eV)	Γ_γ(mV) (a)	Γ_n(mV) (a)	Γ_f(mV) (a)	$g\Gamma_n$ (b)	$g\Gamma_n^2$(mV^2) (a)	(c)	(d)	g (e)	Assigned J
4.27	39	0.58	32+	0.33	0.195	0.195	0.216	0.56	3
4.57	25	0.47	142-	0.21	0.092	0.093	0.096	0.48	2
5.92	40	2.87	1330-	1.22	3.44	3.44	3.46	0.43	2
6.91	40	0.58	105-	0.35	0.196	0.196	0.194	0.62	3
8.57	30	0.61	85+	0.48	0.220	0.214	0.228	1.05	3
9.50	25	0.155	120-	0.092	0.014	0.016	0.016	0.61	3
10.20	35	1.85	990+	0.75	1.43	1.24	1.45	0.39	2
12.74	40	0.65	250-	0.39	0.248	0.240	0.241	0.62	3
13.39	57	3.15	36-	1.10	4.13	4.15	4.13	0.29	2
14.70	35	4.98	145+	3.07	14.5	15.6	13.8	0.65	3
15.98	40	1.32	475-	0.76	1.01	1.06	1.04	0.57	3
16.68	35	1.63	350+	0.61	1.12	0.930	0.950	0.33	2
17.86	80	4.35	37+	1.60	7.90	7.55	7.45	0.32	2
20.63	34	0.29	59+	0.17	0.048	0.042	0.048	0.61	3
22.88	60	1.10	335-	0.63	0.710	0.770	0.770	0.56	3
23.97	60	1.42	185+	0.79	1.18	1.10	1.22	0.54	3
26.30	30	3.60	315-	2.21	7.52	7.00	7.90	0.65	3
28.77	60	6.40	690+	2.42	17.1	18.4	15.1	0.34	2
29.33	35	0.49	70+	0.35	0.140	0.138	0.148	0.87	3
30.90	40	2.32	320+	1.44	3.15	3.18	3.46	0.65	3

(a) Values obtained from final fitting, using spins suggested by Moore et al. [4] except for those resonances between 12.74 and 17.86 eV, where opposite spins were used.

(b) From Stehn et al. [3].

(c) Values obtained from fitting using spins suggested by Moore et al.

(d) Values obtained from fitting using spins opposite those of Moore et al.

(e) Computed from $g = \left(g\Gamma_n\right)^2 / \left(g\Gamma_n^2\right)$, using $g\Gamma_n^2$ values from final fitting.

Table 2. Resonance Parameters for U^{233}

E_o(eV)	(a) Γ(mV)	(a) $g\Gamma_n\Gamma_\gamma$(mV^2)	$g\Gamma_n^2$(mV^2)	(b) $g\Gamma_n$(mV)	LRL (c) $g\Gamma_n$(mV)
1.59	645	3.9	0.0051	0.087	0.050
1.74	255	6.6	0.15	0.151	0.28
2.29	95	4.1	0.063	0.090	0.18
3.61	180	2.8	0.046	0.071	0.15
4.72	995	8.7	0.31	0.14	0.39

(a) Obtained from our fit to U^{233} capture data [9].

(b) Taken from Ref. [3].

(c) Computed from the values in column four from the relationship, $g\Gamma_n = (0.5\ g\Gamma_n^2)^{1/2}$.

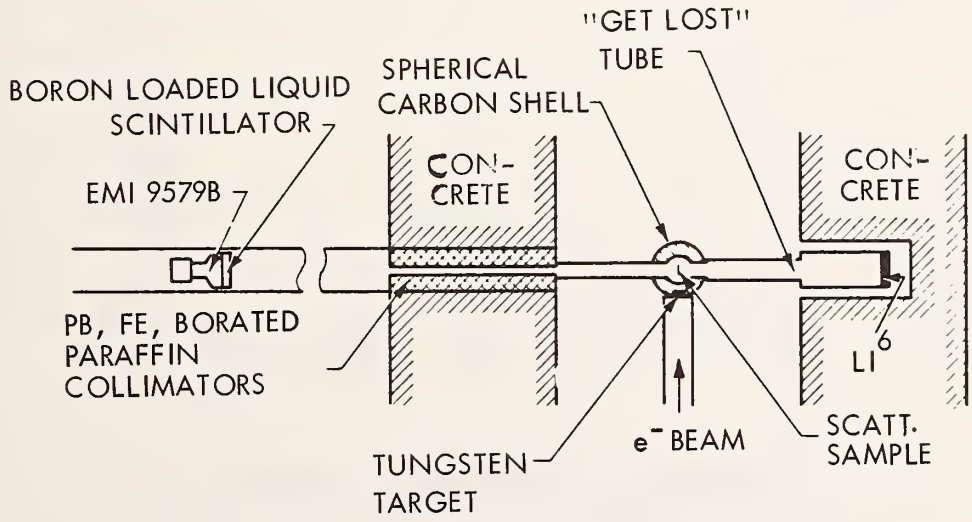

Figure 1. Plan view of the experimental arrangement. The drawing is not to scale. The sample-to-detector flight path is 18.1 m.

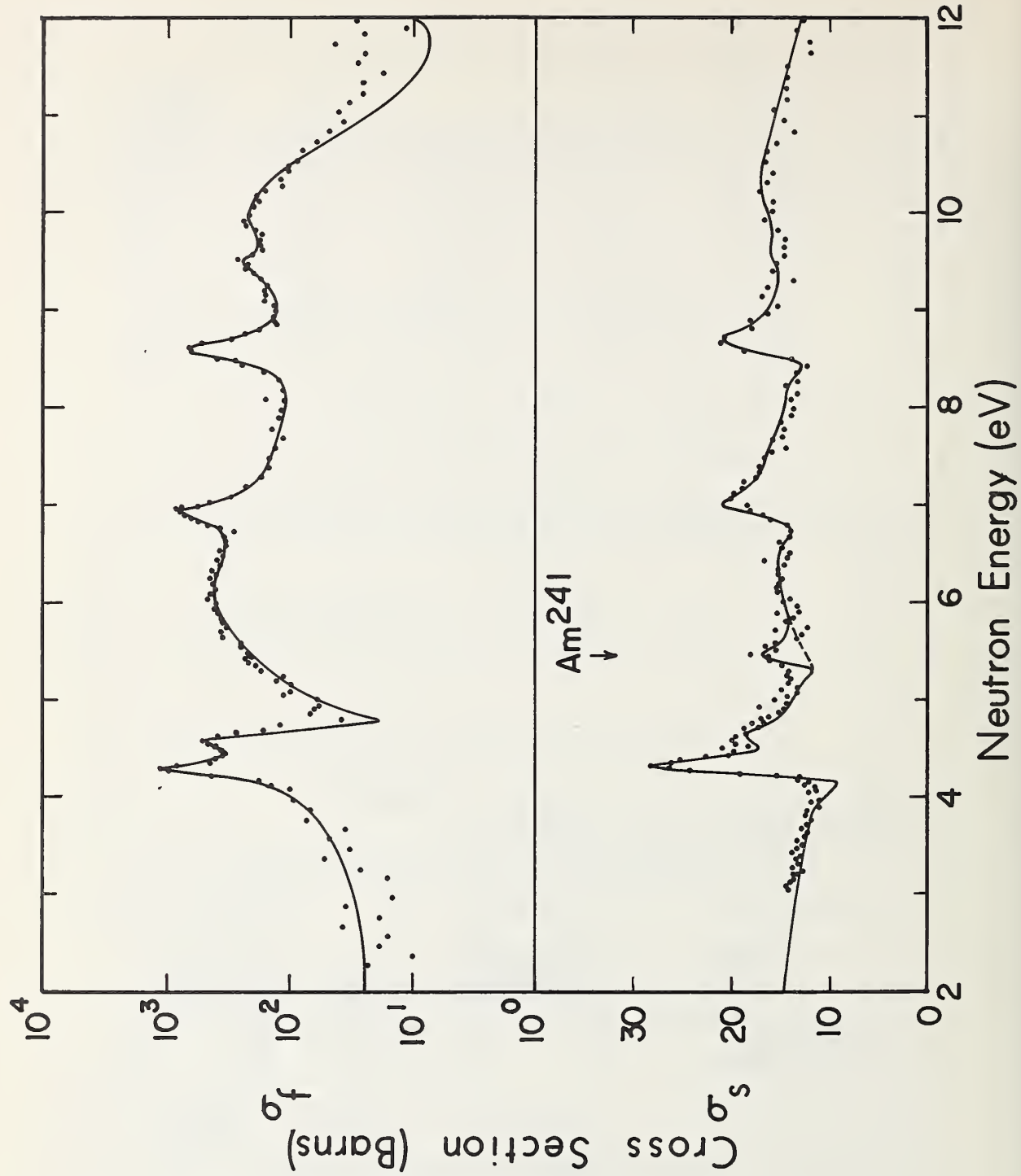

Figure 2. The neutron scattering and fission cross sections of Pu^{241} from 2 to 12 eV. The solid curve is the simultaneous multi-level fit using the parameters of Table 1.

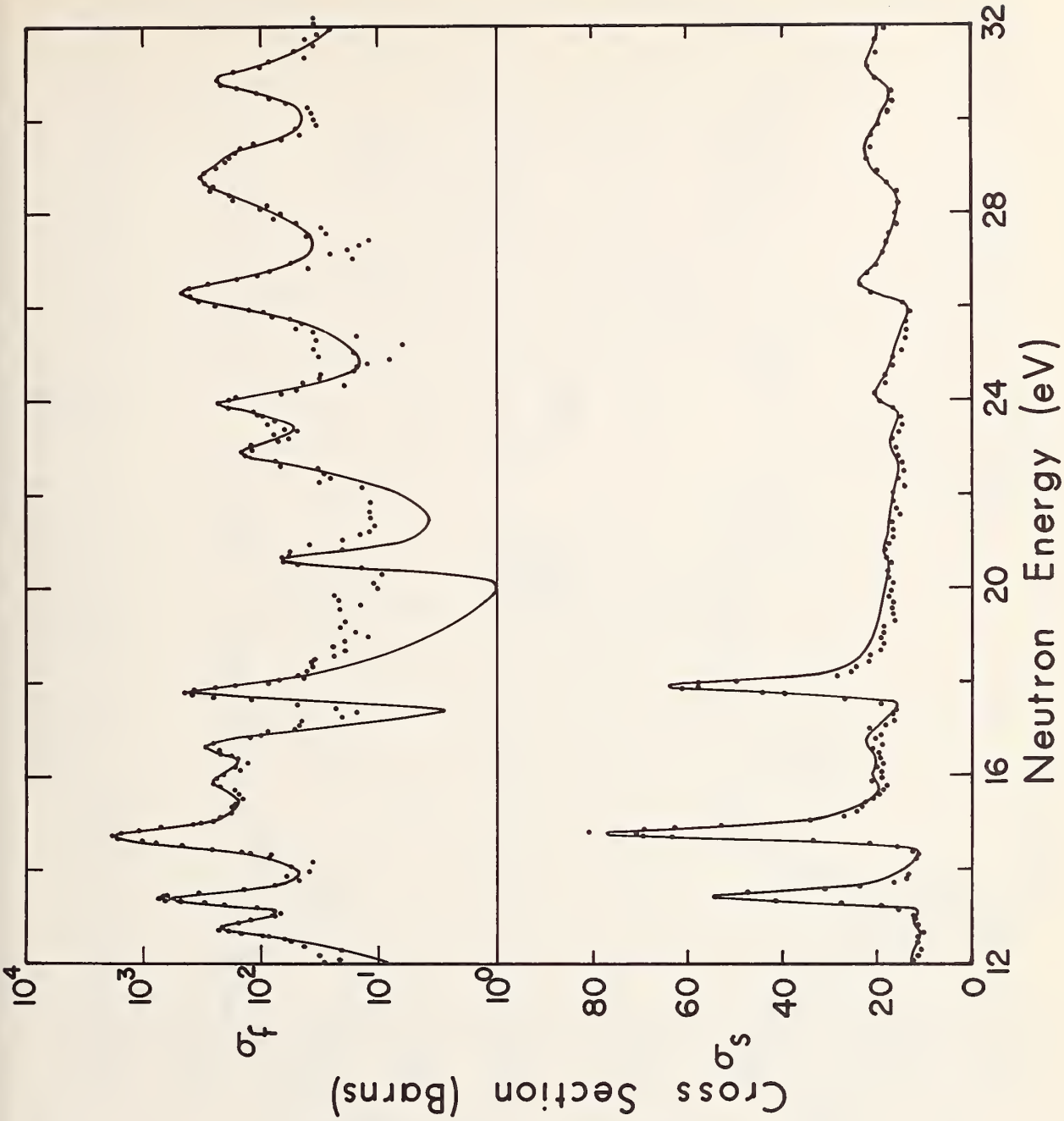

Figure 3. The neutron scattering and fission cross sections of Pu^{241} from 12 to 32 eV. The solid curve is the simultaneous multi-level fit using the parameters of Table 1.

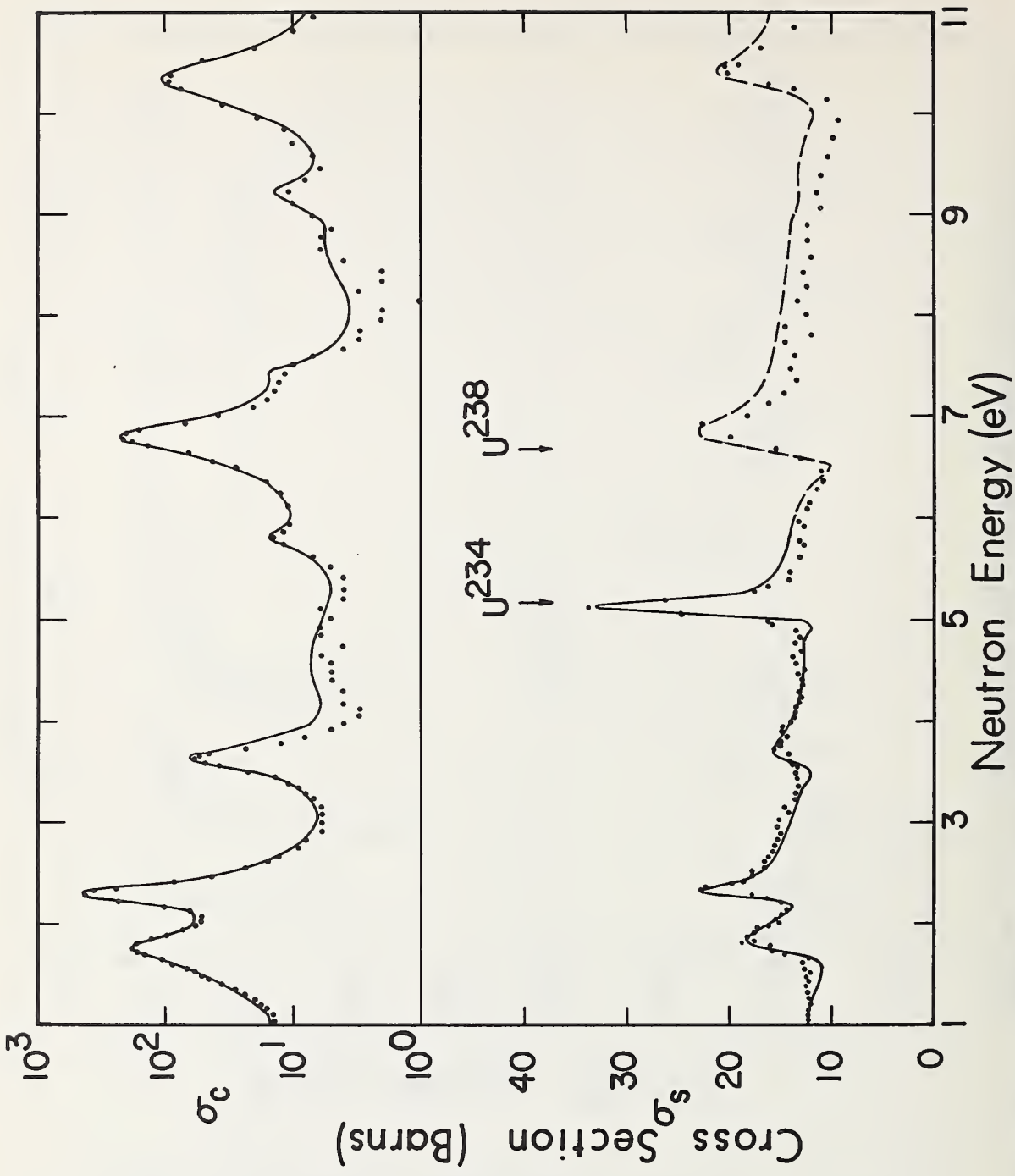

Figure 4. The neutron scattering and capture cross sections of U^{233} from 1 to 11 eV. The solid and dashed lines are the multilevel fits described in the text.

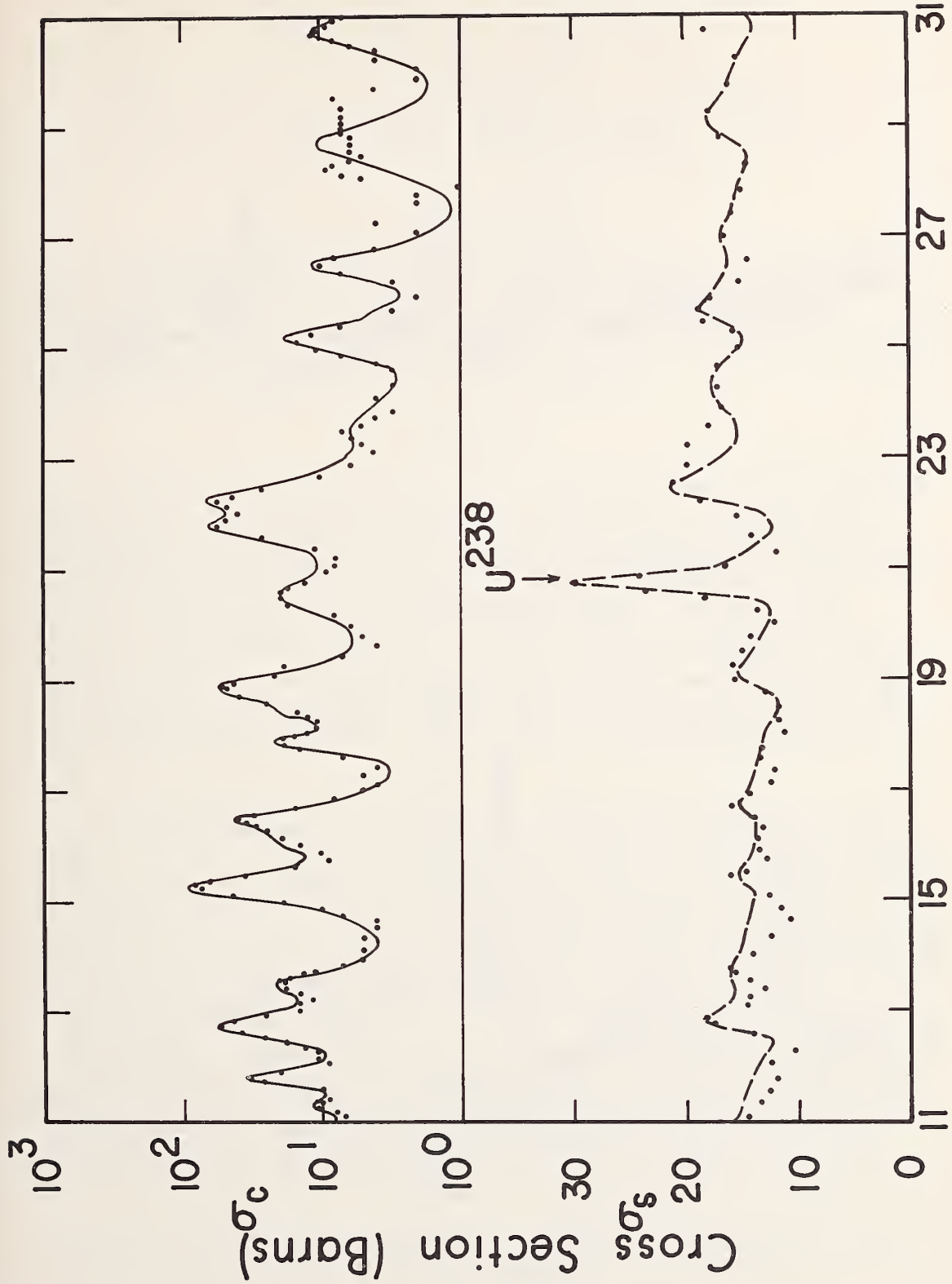

Figure 5. The neutron scattering and capture cross sections of U^{233} from 11 to 31 eV. The solid and dashed lines are the multi-level fits described in the text.

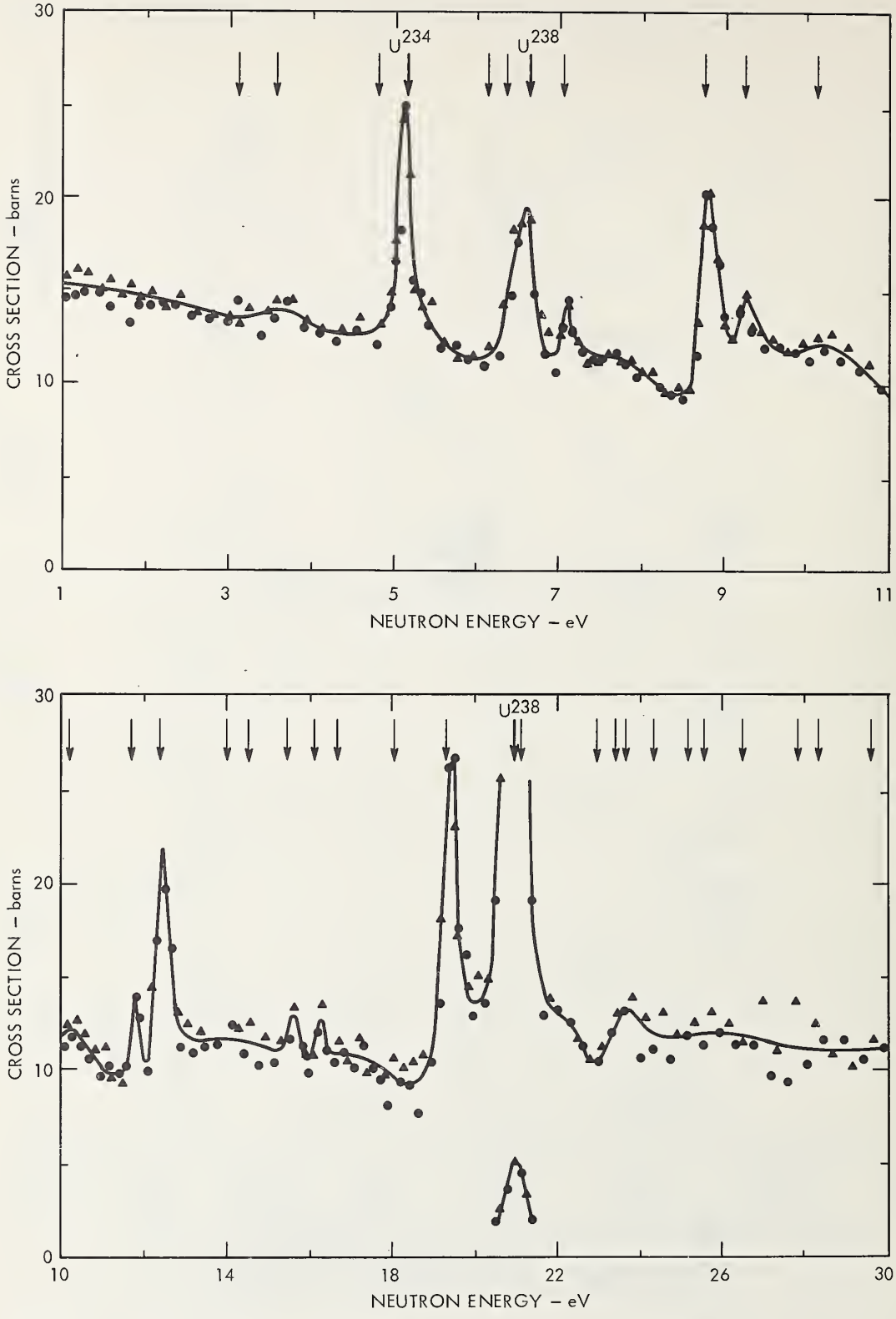

Figure 6. The neutron scattering cross section of U^{235} from 1 to 31 eV. The solid line is only to guide the eye.

Fission Cross Section Measurements: Present and Potential Capabilities*

J. A. Farrell
University of California, Los Alamos Scientific Laboratory
Los Alamos, New Mexico 87544

Abstract

The current techniques of measuring the neutron cross sections of the fissionable nuclei are discussed and compared along with possible improvements in the future. The different methods of determining resonance parameters from the cross section data are considered. Recent experiments that have yielded information on the properties of the deformed transition nucleus are also discussed.

1. Introduction

The neutron cross sections of the fissionable nuclei are the basic data used in all reactor calculations so that it is not surprising that laboratories throughout the world have devoted much effort to their measurement. As a result, most of the "easy" measurements have now been made, not once, but several times. An examination of cross section requests reveals that the desired measurements fall into two general groups: increased accuracy in the cross sections of the common fissile nuclei such as ^{235}U and ^{239}Pu; and less accurate measurements of the cross sections of short lived nuclei such as ^{233}Pa and ^{237}U for which little or no data now exists. In addition, there has been a shift in the neutron energy range of interest due to the increased importance of fast reactors.

Besides the practical engineering applications of fission cross section measurements, there is much to learn about the physics of the fission process. The primary data to be inferred from the cross sections are the resonance parameters or their averages but these are difficult to determine for the thermal fissioning nuclei because the ratio of the resonance widths to the spacing between resonances is too large. Besides the study of resonance parameters, there have been several recent experiments that have yielded information about the quantum numbers of the states of the highly deformed transition nucleus.

It is the purpose of this paper to discuss the current methods of cross section measurement and analysis and the outlook for the future. The discussion will include the measurement of the total, scattering, and capture cross sections as well as the fission cross sections of fissionable nuclei as these are necessary for a complete understanding of the properties of the nucleus.

---

* Work performed under the auspices of the United States Atomic Energy Commission.

2. Cross Section Measurements

There are a number of different neutron sources that have been used to measure the neutron cross sections of fissionable nuclei. The most common are the nuclear reactor with a fast chopper or crystal spectrometer, the Van de Graaff accelerator, the electron linac, the underground nuclear explosion, and sources using radioactive isotopes. Of these, the chopper, linac, and nuclear explosive are inherently pulsed devices in which the neutron energy is determined by measuring the flight time over a known distance. The Van de Graaff may be used either pulsed or with a continuous beam and the other sources are continuous. The crystal spectrometer is a low energy device and the fast chopper with its relatively long burst width is useful to perhaps 10 eV before the resolution becomes too poor. The Van de Graaff, on the other hand, is most effective at neutron energies above a few tens of kilovolts. At present, for the measurement of neutron cross sections over a broad energy range, the two leaders in the field are the electron linac (and I include here proton synchrocyclotrons, which have similar characteristics) and the underground nuclear explosion. Both produce a short burst of neutrons of sufficient intensity to permit a long flight path and therefore good energy resolution.

For fissionable nuclei, there are four neutron cross sections of interest: total, fission, capture, and scattering. Total cross sections can be measured in the same manner as nonfissionable nuclei and are the easiest to measure accurately by making a simple sample in-sample out transmission measurement so that it is not necessary to measure either the neutron flux or detector efficiency. Also, since the source is observed directly, counting rates are much higher than for a partial cross section measurement. Because of the high counting rates, it is possible to use long flight paths with electron linacs such as those at Saclay, Harwell, and RPI to achieve a very high energy resolution. Total cross sections can also be measured with a nuclear explosion as the neutron source but the accuracy is less. Because of the single pulse, the transmission must be determined by measuring the neutron flux before and after the beam has passed through the sample so that additional errors are introduced from uncertainties in the flux measurements. For neutron energies above about 100 keV, the Van de Graaff is superior in resolution and is also capable of taking useful data with very small samples because of the small size of the source.

Fission cross sections are relatively easy to measure as fission fragments are heavy and energetic so that they are easy to detect. However, it is necessary to measure the neutron flux and detector efficiency as well as the number of target nuclei and this introduces additional errors into the measurements. In practice, errors less than ± 5% are difficult to attain although accuracies better than this are badly needed. The best known fission cross section is ^{235}U. Figure 1 shows a comparison of several representative measurements between 10 keV and 10 MeV.[1-6] The bar enclosed in a circle indicates the size of a 5% error. It can be seen that over most of the energy range the discrepancies are greater than this. Two percent accuracy is approached only between 10 keV and 100 keV where the measurements of Perkin et al.,[1] White,[2] and Knoll and Pönitz[5] obtain the same values with quite different techniques. Obtaining an accuracy of 1% will be a long and costly project. New methods of sample

foil assay need to be developed as present techniques seem to be limited to about ± 1%. The most promising way of achieving a 1% or better measurement seems to be a measurement at one or more fixed energies using radioactive sources such as Sb-Be.[7] If an energy insensitive detector could be designed, it would then be possible to extend this accuracy over a considerable energy range.[8] If a 1% or better measurement of the ^{235}U can be made, the cross sections of the other fissile isotopes can be measured relative to it to a similar degree of accuracy.

The major advances in cross section measurements with linacs in the past few years have not been so much improvements in the accelerators themselves as in the detectors and data acquisition systems. The neutron flux from existing linacs is not sufficient for flight paths of more than 30 or 40 meters so that energy resolution is not as good as in total cross section measurements. In practice, the resolution is good enough to permit resonance shape analysis to perhaps 40 eV. A detector that permits increased flight paths has been developed at Harwell.[9] The fission neutrons are counted instead of the fission fragments and this permits the use of much thicker fission samples which offsets the reduced flux. However, because of the thick sample, the data must be corrected for multiple scattering in the sample and the scattering cross section must be known or estimated in order to obtain the fission cross section. A different sort of detector that is in use at the Lawrence Radiation Laboratory at Livermore is the spark chamber.[10] The chamber permits fission cross section measurements from thermal energy to several MeV. The detector is insensitive to both the alpha radioactivity of the sample and the gamma flash from the accelerator and it is therefore possible to measure the cross sections of fairly radioactive samples such as ^{232}U and ^{238}Pu. Since the measurements extend down to thermal energies, they may be normalized to the usually well known cross sections at this energy and accurate determinations of the neutron flux, detector efficiency, and number of target nuclei are not needed.

For the simple measurement of fission cross sections for neutron energies from 20 eV to several hundred keV, the underground nuclear explosion is probably superior to any other method. The technique has been adequately described elsewhere.[11] The intense flux permits flight paths as long as 300 meters and below 1 keV, the background is almost nonexistent making it possible to measure very low cross sections. Figure 2 shows fission cross section of ^{239}Pu measured by this method[12,13] along with a multilevel fit with the Reich-Moore multilevel formula.[14] The cross section in the minimum at 30 eV was measured to be less than 0.01 barn and several other valleys between resonances are less than 0.25 barn. The low cross section between resonances is of considerable importance in multilevel fitting as it is a result of interference between resonances. These very low valleys in ^{239}Pu have since been confirmed at Harwell.[9]

The biggest advantage of the nuclear explosion is that the very high flux makes it possible to measure the cross sections of highly radioactive samples and samples for which only small amounts of material are available. These measurements can be done in no other way. Measurements are planned for the fission cross section of ^{237}U which has a half life of about a week. The use of a sample with such a short life requires careful timing

between the preparation of the sample and the experiment. The sample will be flown in and installed a few hours before the shot. Another type of measurement that the nuclear explosion can do well is the fission cross sections of the even-even nuclei below threshold where the cross sections are very small. Measurements have already been made on ^{240}Pu[15] and are planned on all of the even uranium isotopes. A disadvantage of the nuclear explosion is that it is not possible to do any sort of pulse height analysis since there are some thousands of events within the resolving time of the apparatus. The data is recorded by photographing an oscilloscope display of the current from the solid state detectors along with a reference trace containing the timing information. The photograph of the trace must then be digitized using a projection microscope or automatic film reader. While some difficulties have been encountered with distortions in the film reading, the overall accuracy of the measurements can approach 5%. The cross section measurements are made relative to the ^{235}U fission cross section at high energies and the $^{6}Li(n,\alpha)$ cross section at low energies. Due to heating of the moderator by shock and neutrons and the motion of the moderator, the nuclear explosion is limited to neutron energies above 10 to 20 eV.

In the important energy range from 100 keV to a few tens of kilovolts, no present source is capable of making adequate measurements. Instrumental resolution and Doppler broadening are both wider than the resonance structure so that the experimental cross section is highly dependent on experimental technique. Cooled samples will reduce the Doppler broadening but there still remains the problem of improving instrumental resolution.

Another interesting experiment performed with the nuclear explosion source is the "wheel" experiment of Cowan.[16] The neutron beam is collimated by a slit and the sample is a moving wheel which provides the time resolution. Individual resonances are then characterized by bands of fission products on the wheel. The resonances are cut out and subjected to radiochemical analysis. Cowan found that the resonances of ^{239}Pu could be divided into two groups with different symmetry of the fission product masses. He was further able to identify these groups with the two possible spin states of the compound nucleus. This is a promising method of assigning spins at at least the more prominent resonances of a fissionable nucleus.

The capture cross sections of fissionable nuclei are more difficult to measure because of the intense gamma ray background associated with fission which is commonly ten times greater than the capture gammas. Perhaps the best method of measuring capture cross sections is to have a large gamma ray detector surrounding a fission fragment detector. If the fission detector could be made 100% efficient, the capture gammas could be separated from the fission gammas by requiring them to be in anticoincidence with events in the fission detector. A scheme of this sort is in use at the RPI linac in conjunction with a group at Oak Ridge National Laboratory.[17] Of course, the fission chamber is not 100% efficient so that a correction must be made for a fission gamma ray background. An important advantage of this arrangement is that simultaneous measurements are made of both the fission and capture cross sections with the same resolution and energy calibration. Figure 3 shows some typical

data on ^{235}U taken by this method. The curve is a least squares fit to the data using the Adler multilevel formula.[18] In order to record both cross sections as well as the flux simultaneously, the ORNL-RPI group uses two on line computers for data storage.

Capture cross sections are measured with the nuclear explosion by using a Moxon-Rae type of detector.[19] Since the detector also records the gamma rays associated with fission, a large correction must be made to the raw data to obtain the capture cross section. Again, the technique is at its best with highly radioactive samples which can be measured by no other method. Figure 4 shows the apparatus for handling a radioactive capture sample. The sample is kept enclosed in the lead pig until 15 sec before shot time so that the radiation does not damage the detectors. Immediately after the shot, the sample is again withdrawn into the pig. A trial of the technique was made on the Persimmon experiment in the spring of 1967 with the mildly radioactive isotope ^{147}Pm. The data is still being analyzed but a provisional capture cross section is shown in Fig. 5.[20] On an experiment in the near future the capture and fission cross sections of ^{233}Pa will be measured using the same sample handling apparatus. The activity of the capture sample is 30,000 curies but the neutron flux will be high enough to overcome this.

The neutron scattering cross sections of the fissionable nuclei are perhaps the most difficult partial cross sections to measure and are the most important for resonance analysis. The scattering cross section is very small because the fission widths are generally much larger than the neutron widths and there is a large fast neutron background of fission neutrons. Scattering measurements are important because they furnish the most convenient method of assigning spins to individual resonances. Sauter and Bowman[21] at Livermore have separated the scattered neutrons from the fission neutrons by time-of-flight by placing the sample close to the source and the detector at the end of a 14 m flight path. Asghar[22] at Harwell has adapted the detector mentioned earlier[9] for scattering measurements by employing a stilbene crystal and pulse shape discrimination to record only the scattered neutrons. The flight path is 60 m so that the resolution is good. Sauter and Bowman and Asghar have both assigned spins to the low energy resonances with complete agreement.

3. Resonance Parameters

Until recently most resonance parameters have been obtained by analyzing the cross section in terms of a sum of single level Breit-Wigner formulas. The parameters could be determined from area analysis of the cross section data which is independent of instrumental resolution. In view of the many different pairs of fission fragments, it seemed obvious that fission was a many channel process and that there would be no interference between resonances. It has since become apparent that there is interference between resonances corresponding to only a few fission channels. Perhaps the most obvious case is in ^{239}Pu which is shown in Fig. 2 where the cross section is nearly zero in places because of destructive interference between levels. A theoretical description of fission as a few channel process was first given by A. Bohr.[23] It is apparent that to properly fit the cross sections some sort of multilevel

treatment is desirable. Three forms of multilevel formulas have been applied to the analysis of fission cross sections: the Adler formula,[18] the Reich-Moore formula,[14] and the Vogt method.[24] The Adler formula is the simplest to use and is most amenable to least squares fitting as it represents each level as the sum of a symmetric and antisymmetric Breit-Wigner term but the physical meaning of the widths is not clear. Both the Vogt and Reich-Moore approaches are based on the R-Matrix theory[25] with a few simplifying assumptions. In the Reich-Moore approach, the number of fission channels is fixed and the dimensions of the matrix to be inverted are one more than the number of fission channels. In the Vogt approach, the level matrix is inverted with dimensions equal to the number of resonances but the number of fission channels is not specified and, in fact, may be estimated from the parameters of the fit. However, there are many more parameters than in the Reich-Moore formula and the computation time is an order of magnitude greater if many resonances are included. In practice, it is usually necessary to make further simplifying assumptions in using the Reich-Moore formula such as restricting the number of fission channels to one per spin state. Lynn[26] has argued that because $\Gamma \tilde{=} D$, so many levels are missed that the measured average parameters are in error. Figure 6 shows a mock fission cross section with parameters generated from the appropriate statistical distributions. The average widths and spacings are about what one would expect for ^{233}U and there are three fission channels per spin state. The solid curve is the fission cross section calculated according to the Reich-Moore formula, the dotted surve is a single level calculation. The arrows indicate the positions of the resonances. Within the energy range shown there are 40 actual resonances but if one simply counts peaks, only about 25 are actually seen. The main reason for missing levels is the overlap of two levels in different spin states. The rest have been missed because of small Γ_n/Γ_f. None appear to have been missed because of interference as all the levels seen in the single level cross section are also seen in the multilevel. Bergen[27] has attempted to fit this data with the multilevel formula under the simplifying assumptions usually made in such treatments: only one fission channel per spin state (rather than the three actually present) and a constant capture width. The work is still in progress but the fit reproduces the cross section quite well except for a few trouble spots. The average error in Bergen's fission widths is about 15 to 20% and he has correctly assigned the spins for 68% of the levels. The misassigned levels are mostly those with small fission widths for which the interference is small. It is obvious that a single level treatment of a cross section such as this would be completely erroneous although a reasonable representation of the data can be obtained by adding enough levels. The next step will be to try the fit again using the proper spin assignments.

An accurate determination of all the resonance parameters can be made only by simultaneously fitting all of the partial cross sections, although in most cases the variation in the capture width may be neglected. The work with the mock cross sections shows that some meaningful results can be obtained with multilevel fitting if one is careful. It is inevitable that a substantial fraction of the resonances will be missed but in certain cases it is possible to determine the number missed from the distortion of the statistical distributions. For example, Fig. 7 shows the distributions of the level spacings for the two spin states in ^{239}Pu[13] fitted with Wigner distributions.[28] The solid curve is the

distribution for no missing levels and the dashed curve is the same distribution but with 30% missed at random. Similarly, a histogram of widths will be distorted if the levels are systematically missed because of small widths.

To get useful resonance parameters, it is almost essential to have reliable spin assignments. While relative spin assignments can be made by observing the interference between resonances, the absolute spins must be determined in some other way. The only thermal fissioning nucleus for which adequate spin assignments are known at present is ^{239}Pu for which scattering measurements,[21,22] multilevel fitting,[13] and radiochemical analysis of the fission products[16] give almost complete agreement.

4. Properties of the Transition Nucleus

In 1955, A. Bohr[23] has suggested that at the saddle point, most of the energy of the fissioning nucleus is in the form of potential energy of deformation so that fission proceeds through only a few states, the so-called transition states. The spectrum of these states is expected to be similar to the first few excited states of the target nucleus, that is, a series of vibrational bands. Two recent experiments have yielded information on the quantum numbers of these transition states.

Britt et al.,[29] have measured fission fragment angular correlations for the (d,pf) reaction on ^{233}U, ^{235}U, and ^{239}Pu which give information on the compound nuclei ^{234}U, ^{236}U, and ^{240}Pu. The theoretical treatment of the data is outside the scope of this talk but by comparing the angular correlations with the predictions of a simplified model, it is possible to determine the quantum numbers and excitation energies of the first few vibrational bands of the transition nucleus.

Similar information from a quite different experiment has been obtained by Loveland et al.,[30] by measuring fission fragment angular distributions for the (n,f) reaction on the threshold fissioner ^{234}U. Again by comparing the data with the predictions of a simplified microscopic model they were able to assign quantum numbers to the states of the transition nucleus.

5. Future Prospects

The advent of fast solid state electronics and small digital computers has made possible much more sophisticated experiments involving multiparameter analysis. Most large accelerators now have on line computers for use in data acquisition. Experiments will probably become more automated as experience with on line computers increases. The EURATOM linac at Geel is in operation and the number of papers at this conference attests to its effectiveness. New machines are under construction at Oak Ridge and Livermore. The Oak Ridge linac is a high current, short pulse machine for the measurement of fission cross sections to higher energies than has been feasible in the past.

Future measurements with nuclear explosives will be concentrated primarily on the cross sections of short lived isotopes and isotopes available in small quantities that can be measured in no other way.

It seems possible to measure scattering cross sections but this is still in need of development. More sophisticated experiments than the measurement of cross sections will be attempted such as the measurement of angular distributions and a $\bar{\nu}$ experiment.

While the technique of measuring cross sections by means of a vacuum flight path to the surface has been well developed, there are other possibilities for using the nuclear explosion that are also being explored. One is the use of a short flight path with the entire apparatus underground. This would permit even higher fluxes for measurements on very small samples. A first attempt at this technique was unsuccessful but there is no reason to believe that it will not work. Another possible experiment involves a very long flight path in a horizontal tunnel with an unmoderated source for high resolution in the kilovolt region. A test experiment of this method is in progress.

6. References

[1] J. L. Perkin, P. H. White, P. Fieldhouse, E. J. Axton, P. Cross, and J. C. Robertson, J. Nucl. Energy 19, 423 (1965).

[2] P. H. White, J. Nucl. Energy 19, 325 (1965).

[3] R. K. Smith and S. McGuire, private communication (1966).

[4] B. C. Diven, Phys. Rev. 105, 1350 (1957).

[5] G. F. Knoll and W. P. Ponitz, EANDC(E)74S.

[6] W. D. Allen and A. T. G. Ferguson, Proc. Phys. Soc. A70, 573 (1955).

[7] R. Batchelor, EANDC(UK)79A.

[8] R. F. Taschek, EANDC(US)100A.

[9] B. H. Patrick, M. G. Schomberg, M. G. Sowerby, and J. E. Jolly, in Proceedings of the Paris Conference on Nuclear Data for Reactors, (1966) (IAEA, Vienna, 1967), Vol. 2, p. 127.

[10] C. D. Bowman and G. F. Auchampaugh, in Proceedings of the Paris Conference on Nuclear Data for Reactors, (1966) (IAEA, Vienna, 1967), Vol. 2, p. 149.

[11] W. K. Brown, B. C. Diven, and P. A. Seeger, Arkiv Fysik 36, 47 (1967).

P. A. Seeger, A. Hemmendinger, and B. C. Diven, Nucl. Phys. A96, 605 (1967).

A. Hemmendinger, B. C. Diven, W. K. Brown, A. Ellis, A. Furnish, and E. Shunk, Los Alamos Scientific Laboratory Report LA-3478, Part I (1968).

P. A. Seeger and D. W. Bergen, Los Alamos Scientific Laboratory Report LA-3478, Part II (1967).

[12] E. R. Shunk, W. K. Brown, and R. LaBauve, in Proceedings of the Conference on Neutron Cross Section Technology, Washington, D. C., (1966).

[13] J. A. Farrell, Phys. Rev. 165, 1371 (1968).

[14] C. W. Reich and M. S. Moore, Phys. Rev. 111, 929 (1958).

[15] D. H. Byers, B. C. Diven, and M. G. Silbert in Proceedings of the Washington Conference on Neutron Cross Section Technology (1966).

[16] G. A. Cowan et al., Phys. Rev. 144, 979 (1966).

[17] G. deSaussure, L. W. Weston, R. Gwin, R. W. Ingle, and J. H. Todd in Proceedings of the Paris Conference on Nuclear Data for Reactors, (1966) (IAEA, Vienna, 1967), Vol. 2, p. 233.

[18] D. B. Adler and F. T. Adler, Proceedings of the Conference on Breeding in Large Fast Reactors, Argonne 1963, ANL 6792, p. 695.

[19] M. C. Moxon and E. R. Rae, Nucl. Inst. and Meth. 24, 445 (1963).

[20] J. Beery, private communication (1968).

[21] G. D. Sauter and C. D. Bowman, Phys. Rev. Letters 15, 761 (1965).

[22] M. Asghar in Proceedings of the Paris Conference on Nuclear Data for Reactors, (1966) (IAEA, Vienna, 1967), Vol. 2, p. 185.

[23] A. Bohr, Proceedings of the First United Nations International Conference on the Peaceful Uses of Atomic Energy, Vol. 2, 151 (1955).

[24] E. Vogt, Phys. Rev. 112,203 (1958) and 118,724 (1960).

[25] A. M. Lane and R. G. Thomas, Rev. Mod. Phys., 30, 257 (1958).

[26] J. E. Lynn in Proceedings of the Paris Conference on Nuclear Data for Reactors, (1966), (IAEA, Vienna, 1967), Vol. 2, p. 89.

J. E. Lynn, Phys. Rev. Letters, 13, 412 (1964).

[27] D. W. Bergen, private communication (1958).

[28] E. P. Wigner, Columbia University Report No. TID-7547, 1957, p. 49 (unpublished).

[29] H. C. Britt, private communication (1968).

[30] W. Loveland, J. R. Huizenga, A. Behkami, and J. H. Roberts, Phys. Letters 24B, 666 (1967).

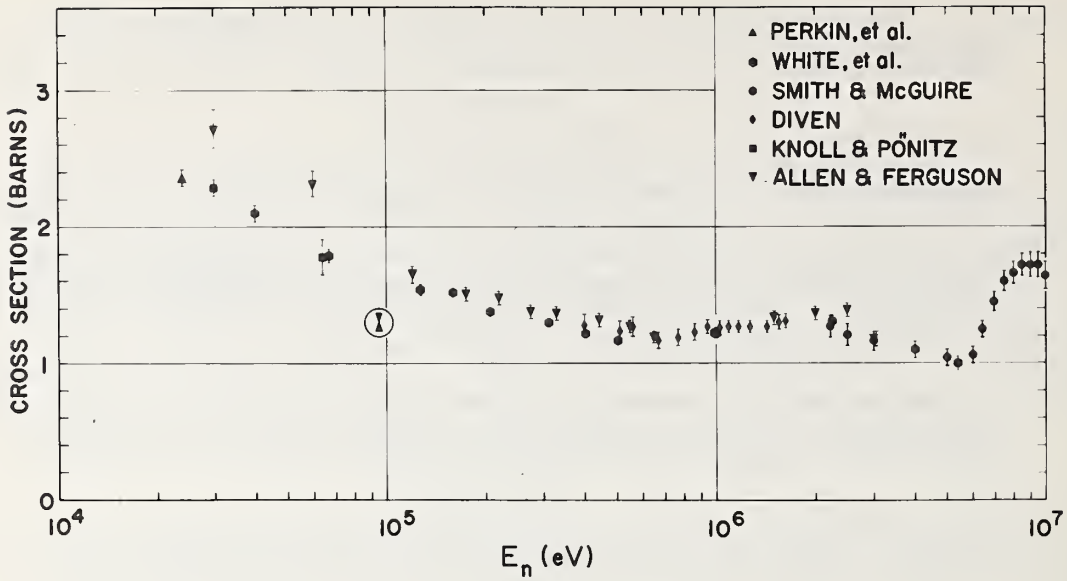

Fig. 1. A comparison of measurements of the ^{235}U fission cross section from 10 keV to 10 MeV taken from Refs. 1-6. The bar enclosed in a circle indicates the size of a ± 5% error bar.

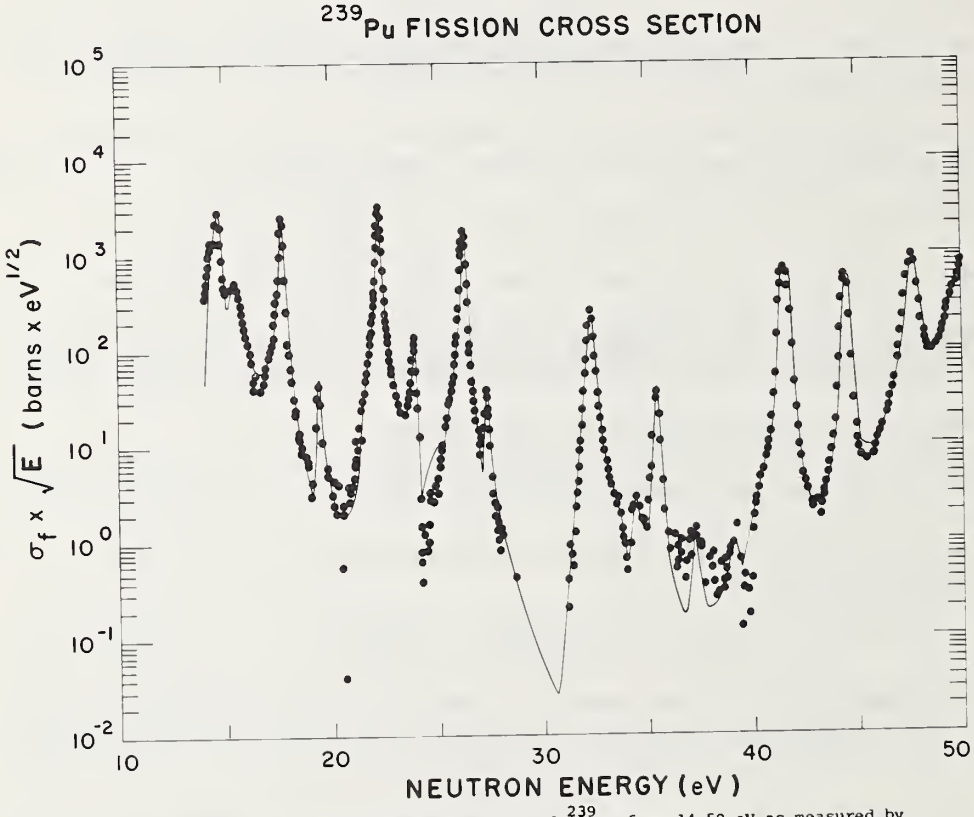

Fig. 2. The fission cross section of ^{239}Pu from 14-50 eV as measured by a nuclear explosion.[12,13] The solid curve is a multilevel fit to the data.

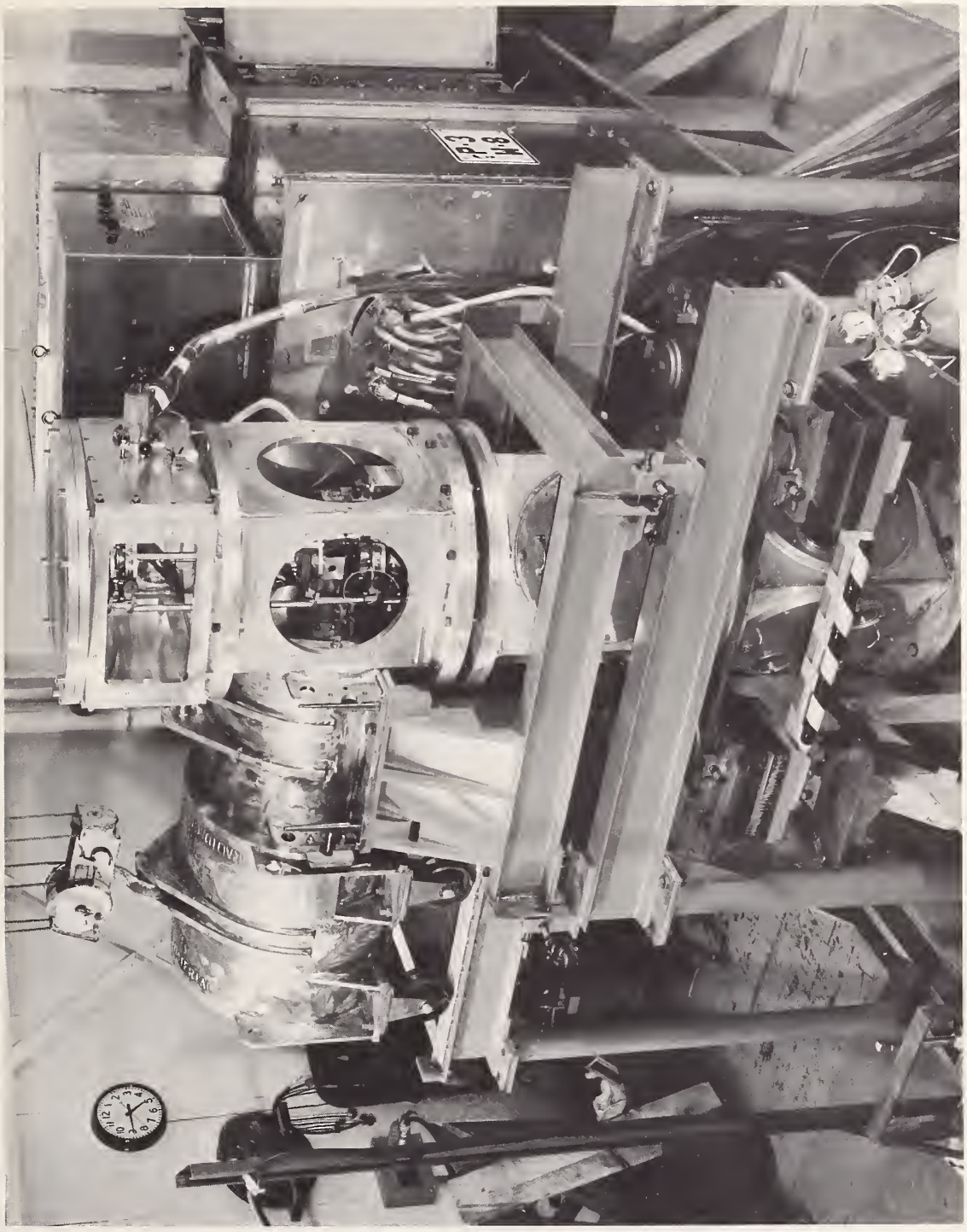

Fig. 3. The radioactive sample equipment used for nuclear explosion cross section measurements. At the left, on wheels, is the shipping container for the sample which is removed before the experiment and replaced by a pneumatic piston which pushes the sample from the storage chamber next to the shipping container into the fission chamber on the right.

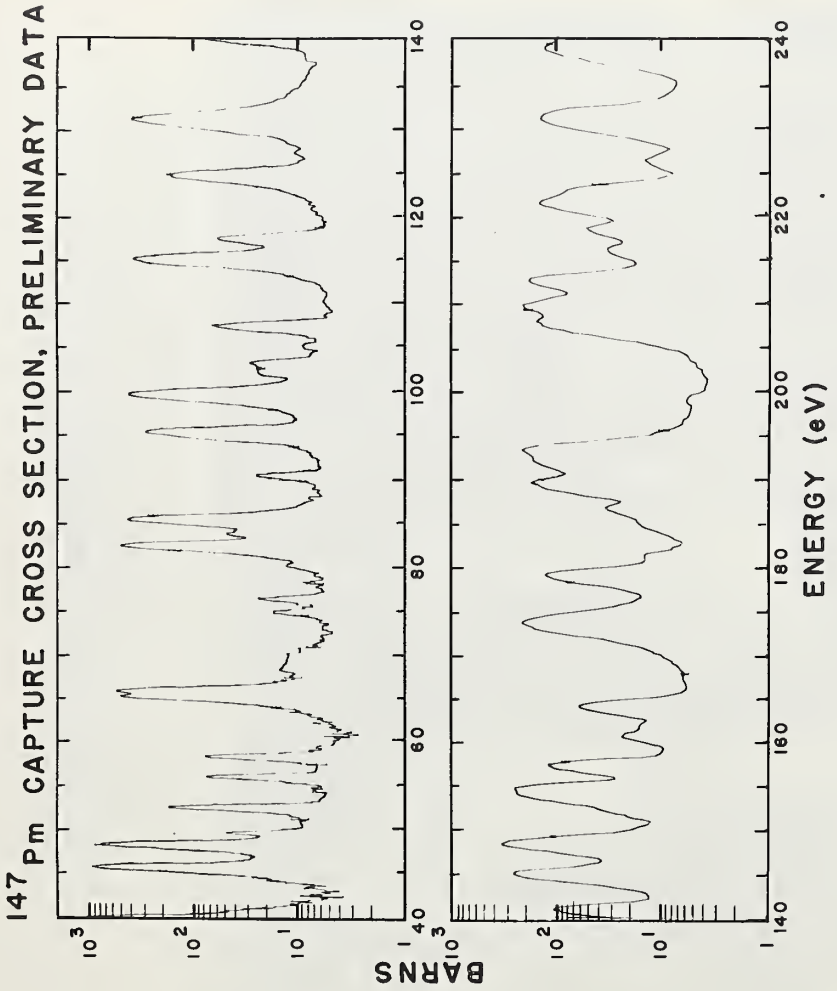

Fig. 4. A preliminary measurement of the capture cross section of the fission product ^{147}Pm using the equipment in Fig. 3.

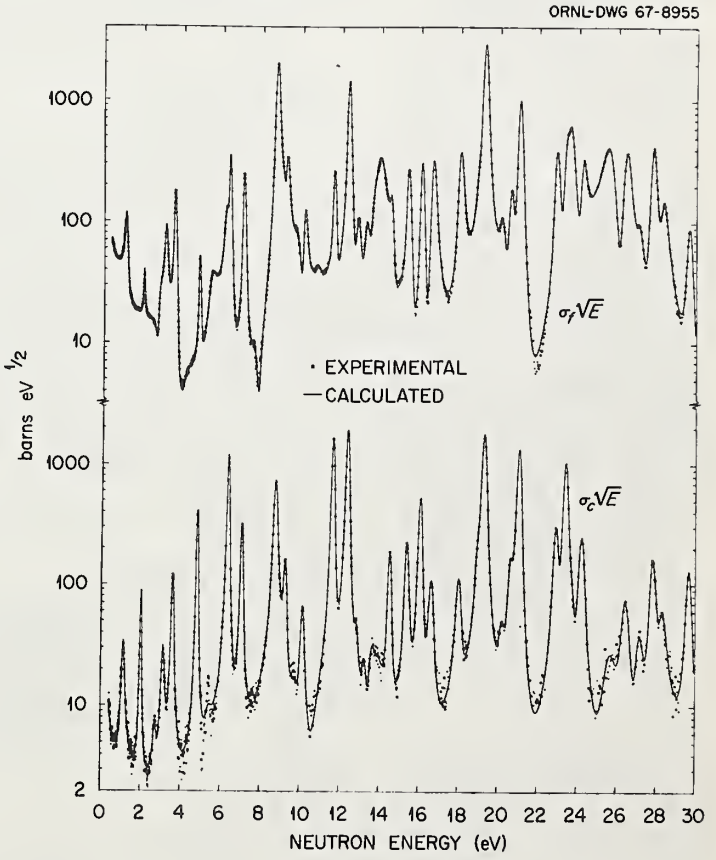

Fig. 5. A simultaneous measurement of the fission and capture cross sections of ^{235}U by the ORNL-RPI groups.[17] The curve is a simultaneous multilevel fit.

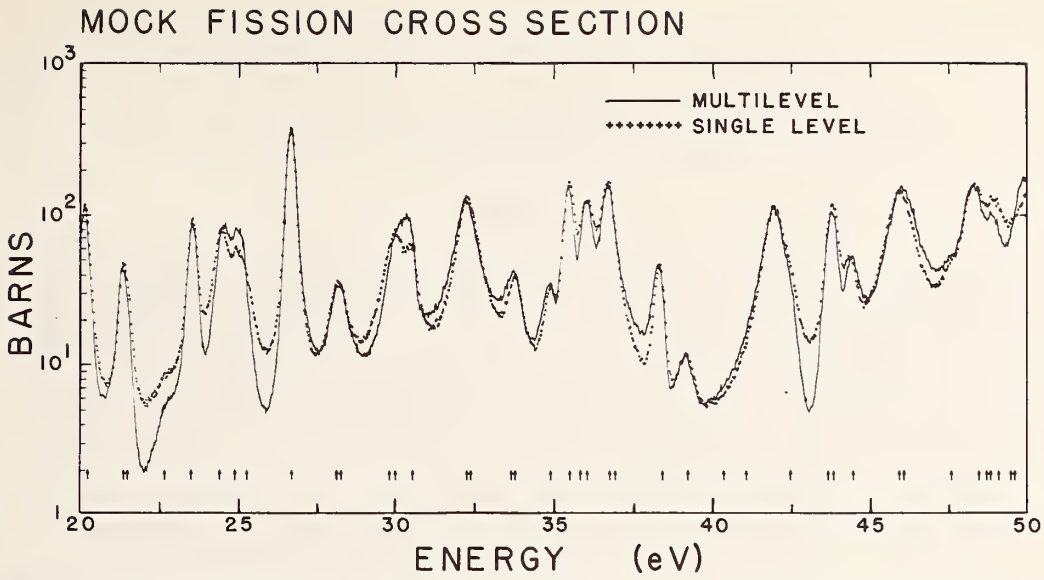

Fig. 6.

A mock fission cross section computed from resonances generated from the appropriate statistical disxributions. The average parameters chosen are about what one would expect for ^{233}U with two open and one partially closed fission channels for the 2^+ spin state and one open, two partially closed channels for the 3^+ spin state. The neutron widths are chosen so that the strength function is 10^{-4} and the capture widths are distributed with 44 degrees of freedom with an average of 40 meV.
The arrows indicate the positions of resonances. The solid curve is a multilevel calculation, the points are calculated from a sum of single levels. A 3% Gaussian random error has been added to the calculation to simulate experimental statistical error.

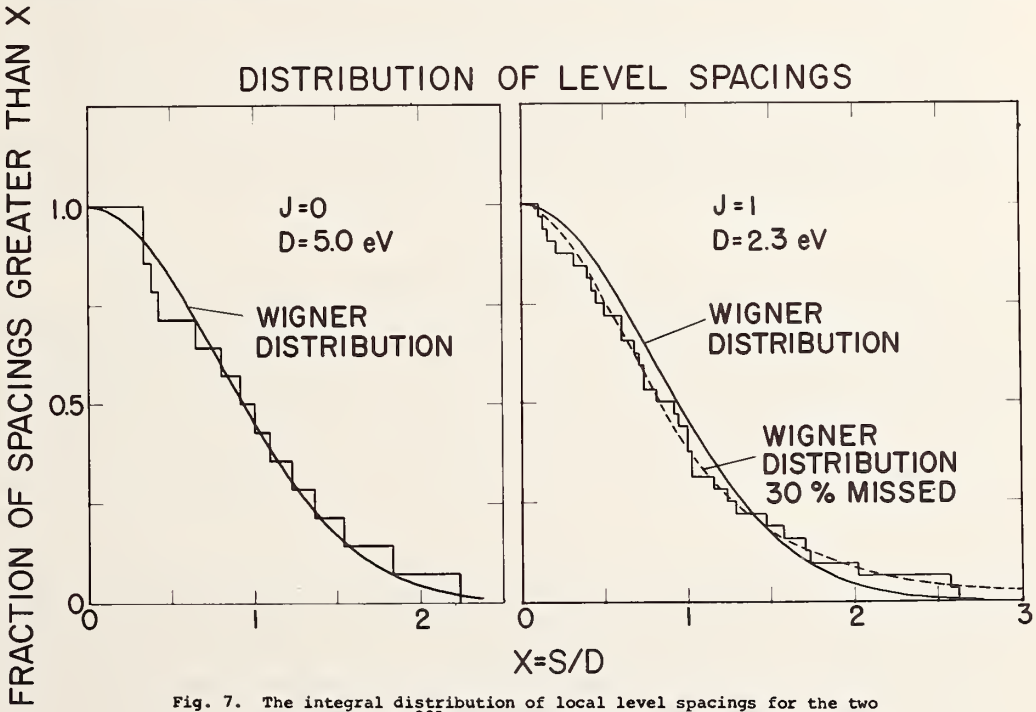

Fig. 7. The integral distribution of local level spacings for the two spin states of ^{239}Pu measured over an energy range of 14 to 90 eV.[13] The solid curves are Wigner distributions,[28] the dashed curve indicates the effect on the distribution of missing 30% of the levels at random.

Neutron Induced Fission Cross Section Measurements in ^{244}Cm *

R. R. Fullwood, J. H. McNally, and E. R. Shunk
Los Alamos Scientific Laboratory, University of California
Los Alamos, New Mexico 87544

Abstract

The neutron induced fission cross section in ^{244}Cm was measured in March 1967 using a 305.2 m flight path and a nuclear explosive as the pulsed neutron source. This paper is a report of these measurements at a laboratory angle of $55^{o} \pm 16$ using manually digitized film readings and covering a neutron energy range from 2 MeV to 20 eV. A 205 μg sample of 95% ^{244}Cm was used. The fission threshold is observed to occur at about 710 keV and sub-threshold fission is clearly seen. Because of uncertainties in the quantity of curium and because of the low signal level, the standard deviation of the cross section is claimed to be ± 30% except in the valleys between resonances where no information is obtained.

1. Experimental Procedure

Neutron cross section measurements performed using a time-of-flight spectrometer and a nuclear explosive source (NES) are quite similar to any other time-of-flight experiments using multiply pulsed sources (MPS). The basic difference is that the flux in the NES experiments exceeds that in the MPS experiments by about 10^{13}. The techniques for the NES experiments have been described elsewhere.[1] It is, however, appropriate to compare these measurements with MPS measurements from the point of view of the errors associated with the techniques. The basic difference is that the NES technique is a continuous or analogue measurement while the MPS technique is largely digital.

Figure 1 shows a diagrammatic comparison of the two methods. With some exceptions both methods are relative measurements, relative to some presumably known cross section. The MPS measurements have in many cases depended upon knowing the cross section being measured at some neutron energies especially thermal. The NES experiments because they do not go down to room temperature thermal and because it was planned that they be used to measure material where little or no data existed, normalize the measurement to $^{6}Li(n,\alpha)$ up to 10 keV neutron energy and to $^{235}U(n,f)$ above 10 keV.

Up to the detectors the two techniques are identical. If anything the NES technique has the advantage because the high flux allows rather ideal detector geometries. In the detectors a basic difference occurs. In the MPS technique, the fission rate is measured by counting pulses using some discriminator as a decision-making device. This is not a clear decision depending upon the detector. In the NES case the reaction rate is deduced from the rate of charge liberation in the detector which depends on the rate of energy deposition and the ionization potential in the silicon detectors. Since the measurement is relative to the standard which is being measured at the same time, common factors such as the ionization potential cancel. The energy release in the

---

* Work performed under the auspices of the U. S. Atomic Energy Commission.

fission fragments is approximately the same in ^{244}Cm and ^{235}U and has been measured [2] and calculated. [3] The experimental value of 185.5 MeV is used here. Implicit also in the normalization is that the fission is dominantly binary and that the angular distribution of the unknown and ^{235}U as a function of energy for the measurement are the same within the stated error.

The solid state detectors have a dead space from which charge cannot be collected but which reduces the fission fragment energy absorbed in the active region. This thickness is determined by measuring the energy deposition in the detector due to bombardment by a well collimated beam of alpha particles from ^{239}Pu. By rotating the detector with respect to the beam, the thickness is determined. The fission fragment energy is corrected for absorption in this thickness by range-energy formulae. This was measured to be 2.7 μM of silicon; the error in this correction is ± 2%.

The relative solid angle between the reference and unknown is measured by alpha counting a 3 μg sample of ^{239}Pu of the diameter of the beam in the locations of the two foils. This ratio is checked by geometry calculations.

After the signal becomes digitized in the MPS experiment, the accuracy is considered absolute within counting losses and counting statistics. This is not the case for the NES; the gain of the system can and does slowly change but by introducing calibration signals within several milliseconds of the time of measurement and recording both the signal and the calibration on the same film the relative error is eliminated. What remains is the analogue memory read-out error, i.e., the error in the digitization of the film. For the data reported here, the reading was done by New Mexico State University on Benson Lehner film readers. The typical rms reading error is ± 4% at low levels.

Another type of error that is not eliminated by the calibrator is a frequency dependent effect. Each element in the system has been studied to insure a flat response (within ± 2%) from 3 MHz to 300 Hz for the signal amplitudes appropriate to the measurement. Cable reflections could appear as satellite resonances occurring 3 μsec (1000 ft of signal cable) after a real resonance. This is prevented by matching the cables on both ends and thus reducing the reflections to less than 0.05%.

The curium sample was prepared by R. L. Folger and coworkers of the Savannah River Plant. The sample was deposited on a platinum backing foil of 7.6 ± 0.12 μm. They assayed the sample at 95% ^{244}Cm, 1.7% ^{245}Cm, 3.2% ^{246}Cm, 0.16% ^{243}Am, and smaller amounts of other Cm isotopes. The quantity of curium was determined by three different methods: the difference in aliquots before and after electrodeposition gave 292 μg and neutron counting with a calibrated detector gave 260 μg. The third method using alpha counting in a geometry of 2.34×10^{-6} steradians was performed by M. G. Silbert (LASL) and gave 205 μg assuming a half-life of 18.11 years. The data were normalized using the last number. The sample size was 1.6 cm diameter and thus was completely contained in the beam diameter of 1.93 cm defined by a steel collimator of 2 m length.

The energy measurement is determined by recording the gamma flash and time marks derived from a standard accurate to 0.001%. These data have not been corrected for hold up time in the moderator which would constitute a small effect. The data have been corrected for center of mass effects but not for resolution broadening due to the moderator nor for Doppler broadening.

2. Discussion of Results

A background measurement is performed by measuring the signal from a backing of the same thickness of that holding the fission sample. The resulting signal goes from 0.1 mV at low energies to about 100 mV at 1 MeV. The fission signal unfortunately was low being 1.6 mV at the 23 eV resonance and practically zero between resonances resulting in an excessive background subtraction.

Table I presents the mean cross section and the limits of integration for resonances for which the mean cross section is greater than 0.1 barns. The energy of the resonance is computed as the weighted mean. The standard deviations quoted are purely statistical as determined by the signal level which is related to the number of fissions. Probably the integrals extend over several resonances especially at the higher energies but the signal levels are so low that they are not clearly resolved. It should be noted that a comparison with the total cross section measurement of Coté et al.,[4] shows good agreement on the energy of the resonances. Figure 2 presents the data above 100 keV and clearly shows the threshold at 710 keV. The data tend to lie above that of Barton and Koontz[5] but within the uncertainties of the measurement. There have also been the evaluations of Dunsford[6] giving 2.05 barns at 3 MeV and of Prince[7] giving 2.57 barns.

Future work would include data at the 90° angle, the automatic reading of the film, further analysis of the sample, and possibly some attempt to extract resonance parameters at low energy.

The authors wish to acknowledge the fact that this work is due to the efforts of many people, in particular the W-8 and P-3 staffs and especially A. Hemmendinger and B. C. Diven.

3. References

[1] B. C. Diven, Proceedings of the International Conference on the Study of Nuclear Structure with Neutrons, Antwerp, Belgium, July 1965, North Holland Pub. Co., Amsterdam; A. Hemmendinger et al., LA-3478 Part I; P. Seeger and D. W. Bergen, LA-3478 Part II; W. K. Brown et al., Arkiv für Fysik, 36, 6, pp. 47-55, 1966.
[2] A. Smith, et al., Geneva Conference Proceedings (1958) Paper P/690.
[3] V. E. Viola Jr., Nuc. Data, 1, pp. 391-410, Dec. 1965.
[4] R. E. Coté, R. F. Barnes, H. Diamond, Phys. Rev. 134, B1281-1284, June 1964.
[5] Private communication.
[6] C. L. Dunford, AI-65-190, Nov. 1965.
[7] A. Prince, GEMP-411, Feb. 1966.

Table I

Low Energy Fission Cross Section Data for ^{244}Cm

Neutron Energy (eV)	$\overline{\sigma_f}$ (barns)	Width of Integral (eV)	Coté, et al [4] (eV)
23.0	58.4 ± 11	.40	22.9
35.2	45.8 ± 7	.40	35.0
53.0	2.3 ± .4	.25	52.8
70.4	3.0 ± .4	.49	69.9
73.3	2.0 ± .3	.51	
74.2	1.9 ± .3	.59	
86.4	8.0 ± .9	1.49	86.0
96.7	7.3 ± .4	.86	96.0
113.3	1.7 ± .2	.4	
121.3	3.3 ± .2	.8	
133.5	4.6 ± .4	1.4	133
141.2	2.0 ± .2	2.1	
151.5	1.6 ± .2	1.2	
156.1	.4 ± .05	.7	
172.0	1.0 ± .2	1.5	
182.3	3.2 ± .2	2.3	182
190.0	0.5 ± .05	.9	
198.1	4.6 ± .03	2.3	197
211.1	1.5 ± .14	2.0	211
223.3	2.5 ± .09	2.5	222
231.4	.78 ± .09	1.9	231
265.7	.86 ± .08	3.5	273
287.5	1.10 ± .09	1.8	
305	.97 ± .07	2.4	
330	.72 ± .08	3.8	
345	.34 ± .4	2.9	
354	1.57 ± .1	5.4	
364	1.45 ± .09	7.0	360
387	1.07 ± .08	6.2	
397	.35 ± .04	9.3	
420	1.0 ± .05	17.2	419
443	.5 ± .05	7.6	445
470	1.36 ± .09	8.3	
495	0.69 ± .06	4.0	
519	1.06 ± .08	7.5	516
616	.48 ± .04	20.7	
650	.87 ± .08	13.4	
777	.24 ± .02	41.3	768
815	1.08 ± .05	33.8	
864	.75 ± .05	32.2	
926	.50 ± .03	42.0	
1172	.15 ± .01	116.0	
1409	.24 ± .02	95	

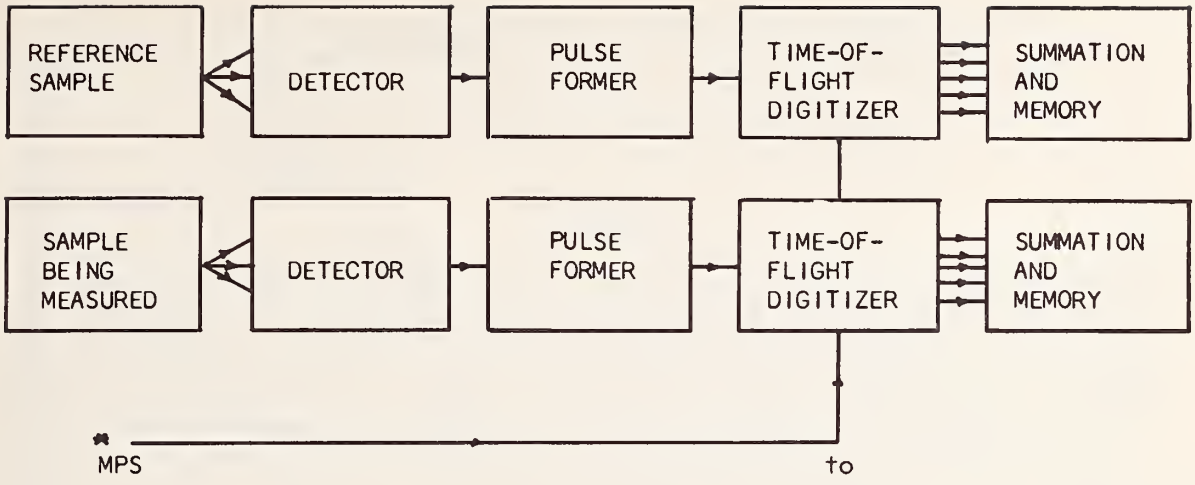

MULTIPLY PULSED SOURCE (MPS) EXPERIMENT

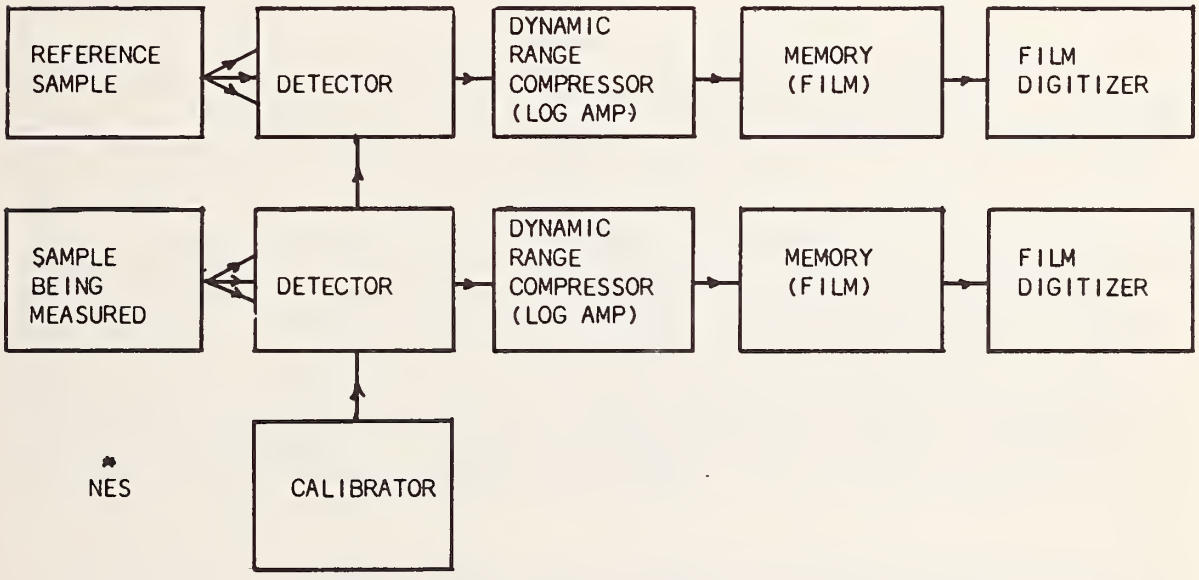

NUCLEAR EXPLOSIVE SOURCE (NES) EXPERIMENT

Fig. 1. Comparison of Multiply Pulsed Source (MPS) and Nuclear Explosion Source (NES) Experiments.

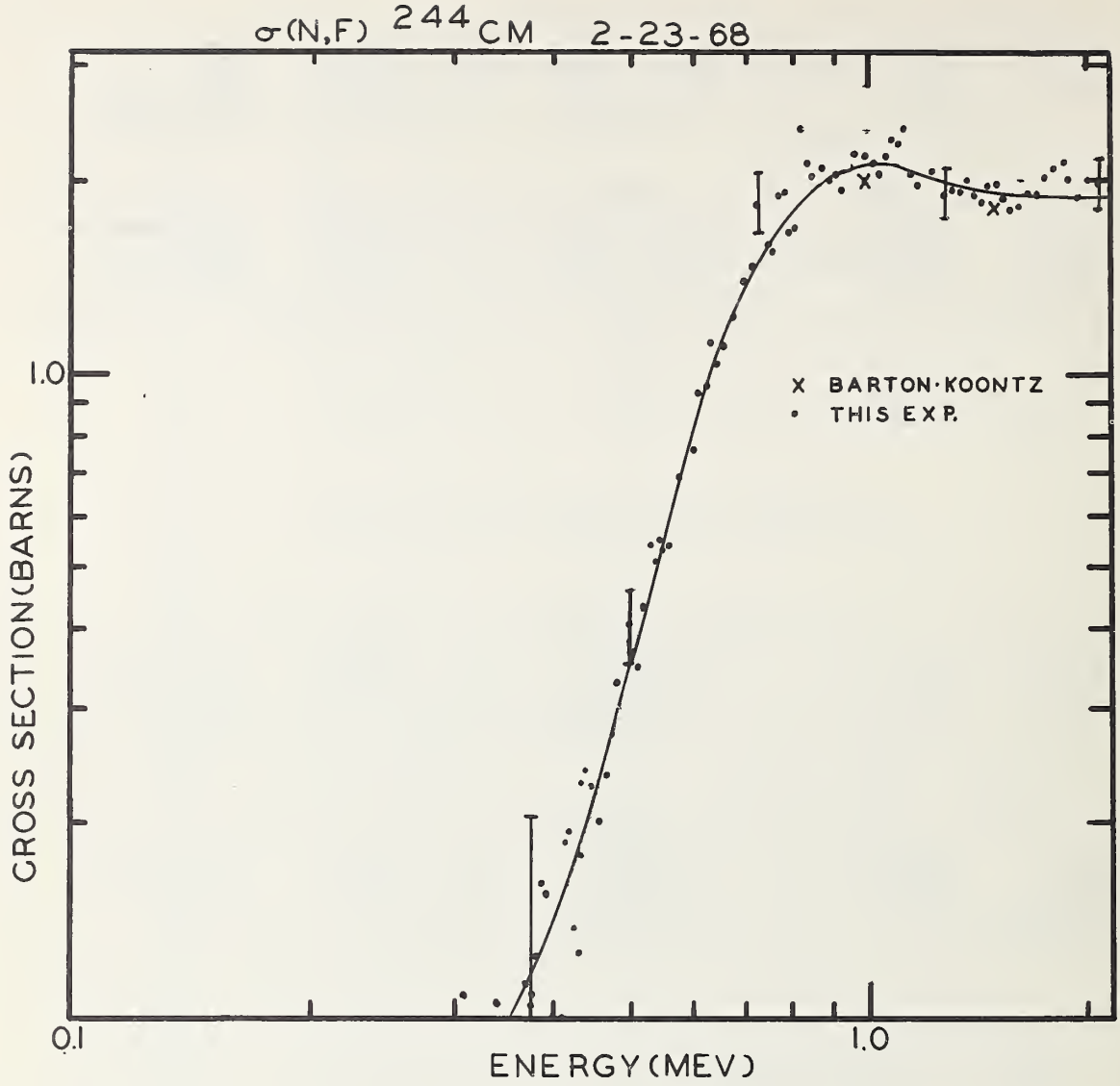

Fig. 2. Fission Cross Section ^{244}Cm.

^{238}U Neutron Capture Results from Bomb Source Neutrons*

N. W. Glass, A. D. Schelberg, L. D. Tatro and J. H. Warren
University of California, Los Alamos Scientific Laboratory
Los Alamos, New Mexico 87544

Abstract

Results on neutron capture in ^{238}U from 30 eV to 2050 eV neutron energy are presented. The data were obtained by neutron time-of-flight utilizing the pulse source of neutrons from the Petrel nuclear explosion. The total radiation width, Γ_γ, has been determined for 62 $\ell = 0$ levels with $\bar{\Gamma}_\gamma = [19.1 \pm 0.6 \text{ (stat.)} \pm 1.4 \text{ (syst.)}] \times 10^{-3}$ eV. There appears to be a significant variation in the value of Γ_γ from resonance to resonance. Approximately 200 weak resonances have been found which can be ascribed to p-wave levels. Analysis of these weak resonances, assuming $\ell = 1$, gives results consistent with: an average reduced neutron width of $(3.7 \pm 0.7) \times 10^{-3}$ eV; an average level spacing of 7.0 ± 0.5 eV; and a strength function of $(1.8 \pm 0.3) \times 10^{-4}$.

1. Introduction

Neutron capture measurements on ^{238}U were made using a neutron beam to the surface from the Petrel underground nuclear device detonation. Descriptions of the use of nuclear detonations for cross section measurements have been given [1], and the experimental details and recording methods for these measurements have been previously described [2].

The sample configuration used on Petrel resulted in a self-indication type measurement [3] from which, in principle, $g\Gamma_n$ and Γ_γ (in the single-level Breit-Wigner formula) could be determined for resolved resonances by area analysis. Preliminary analysis, however, indicated that for resonances where $\Gamma_\gamma/(\Gamma_n + \Gamma_\gamma)$ is appreciably less than unity, the transmission measurements of other workers [4, 5, 6] yielded more precise values of $g\Gamma_n$, in terms of quoted errors, than values obtained from this self-indication measurement. Therefore, in the analysis of the Petrel data, emphasis has been given to the determination of Γ_γ for the stronger resonances and to the determination of $g\Gamma_n$ for weak resonances.

A principal objective of these measurements and analyses was the determination of Γ_γ for enough s-wave resonances to give a statistically significant distribution of Γ_γ. On general grounds, Γ_γ is not expected to vary widely for resonances with the same spin of the compound nucleus. Since the ground state spin of ^{238}U is $I = 0$, the spin of the compound nucleus formed by all s-wave capture is $J = 1/2$.

An additional objective was the determination of the properties of the population of weak resonances formed by p-wave neutron capture. The detection threshold for weak resonances is lower in a good resolution capture measurement than in a transmission measurement with comparable resolution, since the potential scattering term does not add an effective background.

*Work performed under the auspices of the U. S. Atomic Energy Commission

2. Analysis for Resonance Parameters

2.1. Determination of Radiation Widths

A portion of the data for the first ^{238}U sample in the beam is shown in Fig. 1. The experimental areas under each resonance were determined from a running sum of the data points made in the course of computer processing.

The transmission measurements of Garg, et al [4] on ^{238}U using a 200 meter flight path with the Nevis cyclotron are perhaps the most extensive yet published in terms of the number of levels resolved and analyzed for Γ_n. They derived Γ_n for all of the levels for which it seemed feasible to extract Γ_γ from these capture data. Their listed values of Γ_n and quoted uncertainties were used, then, in the determination of Γ_γ from the Petrel data.

The calculated capture area of a resonance for a sample of finite thickness, with no multiple scattering and subsequent capture contribution, is given by

$$A_o = \frac{1}{n}\int_{E_1}^{E_2} \frac{\sigma_\gamma}{\sigma_t}\left(1-e^{-n\sigma_t}\right) dE \text{ (eV-barns)} \qquad (1)$$

where: n = sample thickness in atoms/barn, and σ_γ and σ_t are capture and total cross sections given by the single-level Breit-Wigner formulae with Doppler-broadening [4].

When multiple scattering effects are included, the capture area can be expressed by

$$A = A_o + A_1 + A_2 + - - - = A_o\left(1 + \frac{A_1}{A_o} + \frac{A_2}{A_o} + - - -\right)$$

where A_o is given by (1). A_1 is the contribution to the area from single scatters and capture. A_2 is the contribution from two successive scatters and capture etc. If $A_1 \ll A_o$, some improvement over the first two terms only is obtained by the approximation

$$A = A_o\left[1 + \frac{A_1}{A_o} + \left(\frac{A_1}{A_o}\right)^2 + \left(\frac{A_1}{A_o}\right)^3 + - - -\right] = \frac{A_o}{1 - \frac{A_1}{A_o}} .$$

A_o and A_1 were computed[1] on an IBM 7030 computer for each resonance with the appropriate Γ_n and trial values of Γ_γ until the computed area, A, matched the measured area, thus determining Γ_γ for the resonance. Statistical errors were determined from quoted errors in Γ_n, uncertainties and scatter in the measured areas from separate readings and detectors, and estimated uncertainties in the multiple scattering corrections.

2.2. Determination of Neutron Widths

For the weaker levels, $\Gamma_\gamma/\Gamma \sim 1$, and $g\Gamma_n$ can be determined uniquely from the capture area. Values of $g\Gamma_n$ were determined by the same computer program as was used for determining the Γ_γ's. The measured and computed

---

[1]We are indebted to H. A. Grench for these programs.

areas were matched by varying the input values of $g\Gamma_n$ and using $\Gamma_\gamma = 20 \times 10^{-3}$ eV. The results are insensitive, as expected, to the value of Γ_γ used. The data from all detectors and samples were utilized for the detection and confirmation of the weak resonances and for the determination of $g\Gamma_n$.

3. Results and Discussion

The results of this investigation are listed in Tables I and II. Table I includes resonances which have been identified and measured in previous work [4, 5, 6, 7]. Columns 3 and 4 are taken from these sources. Above 20 eV, all data in Columns 5 through 11 are from this work; however, for resonances where Γ_γ is derived from these measurements, the values of $g\Gamma_n$ and $\Delta g\Gamma_n$ listed in Columns 3 and 4 were utilized. The resonances assumed as $\ell = 1$, by Garg, et al [4] are also so assumed here. The additional weak resonances found in this work are listed in Table II. These are all assumed to be $\ell = 1$. The resonances marked by asterisks are less certain. The energies of the prominent resonances are taken from Garg, et al and were used to establish the energy scale for the other resonances. It was possible to establish an independent energy scale from the timing measurements, however, there were very few inconsistencies with the resonance energies of Garg, et al, and their source position uncertainty was less.

Since the values of Γ_γ and $g\Gamma_n$ will reflect systematic errors both in the neutron flux determination and gamma-ray detector calibrations, the data were analyzed for consistency with the results of Garg, et al [4], and with those of Ashgar, et al [5]. The weighted average of the ratios of Γ_n (this work)/Γ_n (Garg) for the independently determined resonances from 80.8 eV to 1797.7 eV is 1.027 ± 0.035. Similarly, the weighted average ratio Γ_n (this work)/Γ_n (Ashgar) for resonances from 80.8 eV to 790.9 eV is 0.9585 ± 0.040. Other consistency checks involving the minimization of the dispersion of the Γ_γ distribution were made. On the basis of these various checks, a ± 5% systematic error on the calibrations has been assigned.

3.1. Radiation Widths

The weighted mean value $\bar{\Gamma}_\gamma$, determined by maximum likelihood [8,9] analysis for 62 resonances from 36.7 eV to 2031 eV is

$$\bar{\Gamma}_\gamma = [19.1 \pm 0.6 \text{ (stat.)} \pm 1.4 \text{ (syst.)}] \times 10^{-3} \text{ eV with a}$$

dispersion

$$\sigma_n = [3.3 \pm 0.5 \text{ (stat.)} \pm 0.35 \text{ (syst.)}] \times 10^{-3} \text{ eV.}$$

A variation in Γ_γ from resonance to resonance thus appears quite real. This conclusion is strengthened by the fortuitous appearance of a pair of resonances at 937 eV and 958 eV with similar Γ_n's but capture yields differing such that $\Gamma_\gamma(937)/\Gamma_\gamma(958) = 1.7 \pm 0.1$.

The distribution of Γ_γ is shown in Fig. 2. Fits of two Chi-squared distributions [8] are shown. One fit (solid line) is obtained by assuming a distribution about the mean, $\bar{\Gamma}_\gamma$, and determining the number of degrees of freedom. This results in $\nu = 44 \pm 8$ degrees of freedom. Another

approach is to consider the total radiation widths to consist of a constant plus a fluctuating part arising from high energy gamma-ray transitions which vary in intensity from resonance to resonance. Thus $\Gamma_\gamma = \Gamma_\gamma^0 + \Gamma_\gamma^1$, and by taking $\Gamma_\gamma^0 = 12 \times 10^{-3}$ eV, the analysis gives $\nu = 3.7 \pm 0.7$ degrees of freedom for the fluctuating part. The fit is fairly reasonable for either case, hence no choice can be made on the basis of the experimental distribution.

Rosen, et al [3] quote a value $\bar{\Gamma}_\gamma = (24.6 \pm 0.8) \times 10^{-3}$ eV for 32 levels to 1 Kev, and Ashgar, et al [5] measured $\bar{\Gamma}_\gamma = (23.74 \pm 1.09) \times 10^{-3}$ eV for 27 resonances to 823 eV. For resonances from 36 to 823 eV from this work, $\bar{\Gamma}_\gamma = (20.6 \pm 1.7) \times 10^{-3}$ eV.

An apparent variation of Γ_γ with neutron energy can be observed in Fig. 3. The appearance of this quasi-structure and its possible relationship to intermediate structure could be significant.

3.2. Neutron Widths

On the basis of an assumed Porter-Thomas [8] distribution ($\nu = 1$) of $\ell = 0$ reduced neutron widths, Garg, et al [4] concluded that 24 weak resonances for neutron energies up to 2 Kev were probably p-wave. Five of the weak resonances listed by Garg, et al are not clearly visible in this work, although in most cases there are weak resonances found nearby. Thomas and Bollinger [7] found 12 weak resonances from 4.41 eV to 173 eV which they attributed to p-wave interactions. All except the 57.9 eV resonance are identified above 20 eV. There are approximately 170 additional weak resonances found in this work.

A plot of the number of weak resonances attributed to $\ell = 1$ is illustrated in Fig. 4. The plot is consistent with a mean level spacing, $\bar{D}_1$, of 7.0 eV with an increasing number of missed resonances above a few hundred eV. If the 2J + 1 dependence [10] of the level density, with no parity dependence, is assumed; then

$$2\bar{D}\ (\ell=1,\ J=3/2) \geq \bar{D}\ (\ell=1,\ J=1/2) = \bar{D}\ (\ell=0,\ J=1/2) \qquad (2)$$

and

$$\bar{D}_1 = \left([\bar{D}\ (\ell=1,\ J=1/2)]^{-1} + [\bar{D}\ (\ell=1,\ J=3/2)]^{-1} \right)^{-1}$$

$\bar{D}\ (\ell=0,\ J=1/2) \approx 20.8$ eV from Garg, et al [4] and confirmed by these measurements. Hence, by calculation, $\bar{D}_1 \geq 6.9$ eV.

The measured value of $\bar{D}_1$ (Fig. 4, Table III) is thus completely consistent, although it cannot be regarded as rigorous verification of (2) since it is possible a considerable number of weak levels have been missed below a few hundred eV.

The p-wave strength function is defined [3] as

$$S_1 = \frac{\Sigma_p g\Gamma_n^1}{(2\ell+1)\ \Delta E} = \frac{\overline{g\Gamma_n^1}}{(2\ell+1)\ \bar{D}_1}$$

where $g\Gamma_n^1 = g\Gamma_n\ E_o^{-1/2}\ (X_o^2 + 1)\ X_o^{-2}$ and $X_o = kR$, R is the nuclear radius.

Using $R = 8.4 \times 10^{-13}$ cm [3], $g\Gamma_n^1 = g\Gamma_n E_o^{-3/2} (E_o + 3 \times 10^5)$ where E_o is the resonance energy in eV. Since $g = 1/2\ (2J+1)\ (2I+1)^{-1}$ and $I = 0$, $J = 1/2$ or $3/2$ for $\ell = 1$, g will be 1 or 2 for p-wave resonances. There is no way here to separate the two p-wave populations, hence they must be lumped together.

The measured values of S_1, $\overline{g\Gamma_n^1}$ and $\overline{D}_1$ are listed in Table III. The distributions of $g\Gamma_n^1$ are shown in Fig. 5. Also shown are Porter-Thomas ($\nu = 1$) distributions and the distributions corresponding to $\nu = 2$ degrees of freedom. The fit appears better for $\nu = 2$. However, many of the resonances with $g\Gamma_n^1 < 4$ mv are close to the detection threshold and there is a possible bias toward larger values of $g\Gamma_n^1$ within the measurement uncertainty. The dotted lines in the histogram bars of Fig. 5(a) show the result if the values $g\Gamma_n^1 - \Delta g\Gamma_n^1$ are substituted when $g\Gamma_n^1 < 4$ mv. This results in a somewhat more reasonable fit to $\nu = 1$, although the fit is nearly as good for $\nu = 2$.

After considering and analyzing many aspects of the data, the following conclusions are drawn with corollary restrictions:

(1) Average $\ell = 1$ strength function, $S_1 = \dfrac{\Sigma g\Gamma_n^1}{(2\ell + 1)\ \Delta E} = (1.8 \pm 0.3) \times 10^{-4}$

(2) Average $\ell = 1$ level spacing, $\overline{D}_1 = 7.0 \pm 0.5$ eV

(3) Average $\ell = 1$ reduced neutron width, $\overline{g\Gamma_n^1} = (3.7 \pm 0.7) \times 10^{-3}$ eV

These conclusions are subject to the restrictions that:

(1) A Porter-Thomas distribution correctly represents the $\ell = 0$ reduced neutron widths.

(2) The level density has a $2J + 1$ dependence such that

$$\frac{\overline{D}(J = 1/2,\pi^+)}{\overline{D}(J = 1/2,\pi^-)} \leq 1 \quad \text{and} \quad \frac{\overline{D}(J = 1/2,\pi^+)}{D(J = 3/2,\pi^-)} \leq 2.$$

These restrictions appear to be experimentally verified. Restriction (1) is obviously necessary since it is the basis for assignment of $\ell = 1$ levels. Restriction (2) is necessary since a lower bound on D_1 cannot be unequivocally defined from the data as represented in Figs. 4 and 5.

4. Conclusion

The measurements on neutron capture in ^{238}U in the resonance region by bomb source neutrons have yielded good quality data. The neutron energy resolution and sensitivities obtained are considerably enhanced over hitherto available laboratory methods. New quantitative results have been obtained on: (1) the fluctuation of total radiation widths of resonances with the same spin of the compound nucleus; and (2) the population of levels formed by p-wave neutron capture.

5. References

[1] A. Hemmendinger, Phys. Today 18, 17 (1965).
W. K. Brown, B. C. Diven, and P. A. Seeger, Arkiv For Fysik, 36, No. 6, 47, (1967).

[2] N. W. Glass, J. K. Theobald, A. D. Schelberg, J. H. Warren and L. D. Tatro, Proceedings of the Conference on Neutron Cross Section Technology, Washington, D. C., 766, March 1966.

[3] J. L. Rosen, J. S. Desjardins, J. Rainwater, and W. W. Havens, Jr., Phys. Rev. 118, 687 (1960).

[4] J. B. Garg, J. Rainwater, J. S. Petersen, and W. W. Havens, Jr., Phys. Rev. 134, B985 (1964).

[5] M. Ashgar, C. M. Chaffey, and M. C. Moxon, Nucl. Phys. 85, 305 (1966).

[6] F. W. K. Firk, J. E. Lynn, and M. C. Moxon, Nucl. Phys. 41, 614 (1963).

[7] G. E. Thomas and L. M. Bollinger, Paper No. 96 in Nuclear Structure Study with Neutrons (North-Holland Publishing Co., Amsterdam, 1966).

[8] C. E. Porter and R. G. Thomas, Phys. Rev. 104, 483 (1956).

[9] M. Ashgar, C. M. Chaffey, M. C. Moxon, N. J. Pattenden, E. R. Rae, and C. A. Uttley, Nucl. Phys. 76, 196 (1966).

[10] J. A. Harvey, Page 23 in Neutron Time-of-Flight Methods (European Atomic Energy Community, Brussels, 1961).

TABLE I

1	2	3	4	5	6	7	8	9	10	11
ENERGY (eV)	ℓ	$g\Gamma_n$	$\Delta g\Gamma_n$	Γ_γ	Stat. $\Delta\Gamma_\gamma$	Syst. $\Delta\Gamma_\gamma$	$g\Gamma_n$	$\Delta g\Gamma_n$	Γ_n^0	$g\Gamma_n^1$
4.41	1	0.00011								(3.6)
6.68	0	1.52	0.02						(0.59)	
10.25	(1)	0.0015								(13.7)
11.32	1	0.00036								(2.8)
19.6	1	0.00097								(3.4)
21.0	0	8.9	0.8							
36.7	0	31.2	0.9	20.9	4.3	1.8				
45.2	1	0.00083					0.001	0.0005		0.99
63.4	1	0.0055					0.0048	0.002		2.9
66.3	0	25.3	1.0	17.35	3.0	1.6				
80.8	0	2.07	0.18				1.96	0.1	0.22	
83.8	1	0.007					0.0064	0.001		2.5
89.4	1	0.076	0.01				0.085	0.003		30.0
93.3	1	0.003					0.004	0.002		1.3
102.8	0	65.0	2.0	24.9	4.1	1.7				
116.9	0	35.8	1.5	23.3	3.6	2.0				
124.4	1	0.0142					0.019	0.005		4.1
145.8	0	0.85	0.33				0.84	0.04	0.070	
152.6	1	0.037					0.031	0.005		4.9
158.9	1	0.0104					0.013	0.003		2.0
165.5	0	3.5	0.4	16.2	11.4	6.0				
173.0	1	0.0334					0.03	0.005		4.0
190.3	0	150.0	3.0	18.5	5.6	1.0				
208.6	0	56.4	5.8	23.8	3.6	1.7				
237.4	0	27.7	1.6	31.4	3.5	3.5				
242.8	1	0.16	0.03				0.15	0.02		12.0
264.0	1	0.23	0.03				0.24	0.03		16.8
273.7	0	25.1	1.6	26.1	2.3	2.8				
291.1	0	15.4	1.7	31.4	8.0	5.3				
311.1	0	0.99	0.07				1.02	0.06	0.058	
347.9	0	82.0	7.3	17.9	1.5	1.1				
376.9	0	1.135	0.08				0.87	0.1	0.045	
397.6	0	6.0	1.0				6.3	0.6	0.32	
410.2	0	19.3	1.0	14.4	1.4	1.3				
434.2	0	8.1	1.5				10.5	0.6	0.50	
454.4	1	0.43	0.11				0.45	0.10		14.0
463.3	0	5.16	0.43				5.8	0.2	0.27	
478.7	0	3.1	0.7				4.4	0.5	0.20	
488.9	1	0.44	0.11				0.62	0.12		17.3
518.6	0	43.2	2.3	22.4	1.5	1.7				
535.5	0	37.0	2.3	24.9	1.5	2.2				
556.0	1	0.47	0.24				0.85	0.28		19.6
580.2	0	27.0	0.7	24.4	3.8	2.4				
595.2	0	82.0	4.9	20.8	1.6	1.3				
619.9	0	28.4	1.0	19.8	2.1	1.7				
624.2	1	(0.42)	(0.17)				0.8	0.1		15.5
628.7	0	4.0	0.5				4.8	0.8	0.19	
661.2	0	116.0	7.0	18.8	1.5	1.1				
677.0	1	0.52	0.26				0.83	0.42		14.2
693.2	0	34.0	1.3	16.5	1.1	1.3				
708.5	0	18.6	2.7	13.4	2.9	1.2				
721.8	0	1.3	0.3				0.95	0.15	0.035	
729.9	1	0.8	0.3				0.60	0.20		9.2
732.3	0	1.35	0.14				1.4	0.2	0.052	
743.0	1	0.55	0.14				0.3	0.1		4.5
765.1	0	6.6	1.1	11.7	8.0	1.8	5.6	0.8	0.20	
779.1	0	1.7	0.2				1.4	0.2	0.050	
790.9	0	5.1	0.6				5.8	0.3	0.21	
821.6	0	59.0	3.0	20.0	2.5	1.4				
846.6	1	0.60	0.15				0.6	0.1		7.4
851.0	0	56.0	3.0	20.1	1.6	1.4				
856.2	0	81.0	4.4	23.1	1.5	1.5				
866.5	0	4.1	0.6				4.9	0.5	0.17	
891.3	1	0.9	0.3				0.67	0.15		7.6
905.1	0	45.0	1.5	18.4	1.8	1.3				

TABLE I. See Text. Widths are in units of 10^{-3} eV.

TABLE I (continued)

1	2	3	4	5	6	7	8	9	10	11
ENERGY (eV)	ℓ	$g\Gamma_n$	$\Delta g\Gamma_n$	Γ_γ	Stat. $\Delta\Gamma_\gamma$	Syst. $\Delta\Gamma_\gamma$	$g\Gamma_n$	$\Delta g\Gamma_n$	Γ_n^0	$g\Gamma_n^1$
909.6	0	0.9	0.3				1.3	0.3	0.043	
925.2	0	8.5	0.6	41.0	30.0	15.0	10.4	1.0	0.34	
932.5	1	0.3	0.3				0.16	0.16		1.7
936.9	0	147.0	15.0	20.9	1.6	1.3				
958.4	0	158.0	15.0	12.3	1.6	0.7				
991.8	0	347.0	16.0	16.9	1.3	0.9				
1000.3	0	1.3	1.3				Missing			
1011.3	0	1.9	0.6				1.9	0.4	0.060	
1023.0	0	6.4	1.3	12.5	7.0	2.0	5.6	0.7	0.175	
1029.1	0	3.2	1.0				2.0	0.3	0.062	
1033.2	1	0.6	0.6				0.8	0.1		7.3
1053.9	0	75.0	16.0	16.1	1.3	1.0				
1068.0	0	0.65	0.65				1.0	0.2	0.031	
1070.5	1	0.3	0.3				Missing			
1081.1	1	0.65	0.3				1.8	0.5		15.3
1094.8	1	0.65	0.3				2.0	0.5		16.7
1098.3	0	15.0	3.3	20.2	7.3	2.6				
1103.2	1	0.65	0.3				1.9	0.5		15.6
1108.9	0	30.0	1.7	16.9	1.3	1.4				
1131.5	0	2.2	0.7				3.6	0.7	0.11	
1140.4	0	220.0	17.0	15.2	1.6	0.8				
1167.5	0	80.0	5.0	15.9	1.2	1.0				
1177.6	0	63.5	5.1	17.7	1.3	1.1				
1195.0	0	92.0	10.0	19.0	1.4	1.2				
1210.9	0	9.0	1.7	14.0	8.3	1.9				
1245.1	0	231.0	18.0	21.6	3.5	1.2				
1267.0	0	26.7	1.8	28.3	6.0	3.1				
1273.2	0	28.6	1.8	33.0	7.0	3.8				
1298.4	0	2.9	1.1				3.8	0.8	0.11	
1317.2	0	4.0	0.7				4.3	0.4	0.12	
1331.0	0	1.1	0.7				1.7	0.7	0.047	
1393.0	0	138.0	19.0	20.0	2.6	1.2				
1405.1	0	76.9	7.5	20.8	1.9	1.3				
1410.0	1	1.1	1.1				0.5	0.2		3.0
1417.0	1	1.1	0.8				3.2	1.0		18.2
1419.6	0	9.0	4.0				7.0	2.0	0.19	
1427.7	0	30.2	3.8	22.3	3.0	2.0				
1444.1	0	21.7	3.8	15.2	2.7	1.3				
1473.8	0	78.7	7.7	18.8	1.8	1.2				
1523.1	0	215.0	19.0	16.4	1.5	0.9				
1546.0	1	0.8	0.8				3.5	1.0		17.5
1550.0	0	1.2	0.8				3.0	1.0	0.076	
1565.0	0	2.0	0.4				4.8	0.5	0.12	
1598.2	0	320.0	20.0	17.6	1.8	0.9				
1622.9	0	84.6	12.0	13.5	2.0	0.8				
1638.2	0	40.5	5.0	17.1	2.2	1.2				
1662.1	0	163.0	20.0	15.5	1.5	0.9				
1688.3	0	78.0	12.0	17.4	2.3	1.1				
1696.3	1	(0.8)	(0.8)				0.5	0.2		2.2
1709.4	0	56.0	6.0	23.4	2.6	1.7				
1723.0	0	13.7	1.7	20.6	6.0	2.9				
1744.0	0	1.7	0.4				1.77	0.24	0.042	
1755.8	0	63.0	21.0	19.4	2.5	1.3				
1782.3	0	464.0	42.0	31.2	2.2	1.7				
1797.7	0	2.1	0.8				2.6	0.5	0.061	
1808.3	0	17.0	4.0	13.6	4.1	1.3				
1845.6	0	13.3	2.0	11.8	4.3	1.2				
1902.3	0	21.0	4.0	12.1	4.1	1.0				
1917.1	0	21.8	2.2	14.7	4.0	1.2				
1968.7	0	576.0	44.0	21.0	5.0	1.1				
1974.7	0	468.0	45.0	14.0	6.0	0.7				
2023.6	0	202.0	23.0	18.0	4.0	0.9				
2031.1	0	50.0	5.0	12.0	5.0	0.8				

TABLE II

ENERGY (eV)	$g\Gamma_n$	$\Delta g\Gamma_n$	$g\Gamma_n^1$	ENERGY (eV)	$g\Gamma_n$	$\Delta g\Gamma_n$	$g\Gamma_n^1$	ENERGY (eV)	$g\Gamma_n$	$\Delta g\Gamma_n$	$g\Gamma_n^1$
* 47.5	0.0008	0.0008	0.74	542.1	0.16	0.04	3.8	1233.4	0.6	0.3	4.2
* 49.5	0.0005	0.0003	0.43	550.5	0.10	0.04	2.3	1236.3	0.7	0.4	4.9
* 56.4	0.0006	0.0002	0.43	560.2	0.045	0.01	1.0	1251.1	0.9	0.2	6.2
* 72.8	0.010	0.005	4.9	566.5	0.033	0.01	0.74	1263.0	0.3	0.2	2.0
* 74.4	0.0027	0.001	1.3	585.2	0.10	0.03	2.1	1279.5	0.4	0.1	2.6
* 91.0	0.006	0.006	2.1	598.2	0.11	0.04	2.3	1285.4	0.5	0.1	3.3
98.2	0.0048	0.001	1.5	* 602.2	0.15	0.15	3.1	1289.4	0.4	0.1	2.6
111.4	0.0085	0.0015	2.2	606.2	0.27	0.05	5.5	1311.7	0.3	0.2	1.9
121.4	0.006	0.003	1.4	614.7	0.16	0.05	3.2	1326.0	0.4	0.1	2.5
127.4	0.006	0.003	1.3	633.1	0.14	0.04	2.7	1338.0	0.24	0.10	1.5
133.3	0.0125	0.004	2.5	636.5	0.12	0.03	2.3	1347.0	0.34	0.06	2.1
136.0	0.006	0.003	1.1	664.8	0.13	0.04	2.3	1363.4	1.1	0.4	6.6
* 137.5	0.0035	0.0035	0.65	668.2	0.23	0.10	4.0	1369.9	0.33	0.10	2.0
* 196.4	0.015	0.015	1.6	681.1	0.06	0.03	1.0	1381.0	0.5	0.3	3.0
* 200.5	0.027	0.010	2.9	685.2	0.06	0.03	1.0	1387.4	0.40	0.15	2.3
201.5	0.038	0.010	4.0	688.2	0.08	0.03	1.3	1399.4	0.40	0.20	2.3
215.5	0.042	0.010	4.0	697.5	0.16	0.10	2.6	1422.8	0.36	0.06	2.0
218.8	0.03	0.01	2.8	704.8	0.10	0.03	1.6	* 1438.3	0.5	0.5	2.8
239.9	0.053	0.010	4.3	711.0	0.30	0.10	4.8	1447.3	1.0	0.4	5.5
* 240.9	0.063	0.063	5.1	713.9	0.25	0.05	3.8	1454.8	0.4	0.1	2.2
252.5	0.026	0.01	2.0	716.9	0.10	0.05	1.6	1467.5	0.25	0.25	1.3
253.9	0.10	0.02	7.5	734.8	0.15	0.03	2.3	1482.7	0.38	0.10	2.0
257.6	0.03	0.01	2.2	739.8	0.09	0.04	1.4	1488.6	0.5	0.2	2.6
* 262.6	0.046	0.015	3.3	756.5	0.38	0.1	5.5	1494.5	0.6	0.2	3.1
275.3	0.16	0.02	10.6	787.4	0.3	0.1	4.1	1506.4	0.6	0.2	3.1
282.5	0.13	0.04	8.3	* 797.4	0.13	0.13	1.7	1513.3	1.2	0.3	6.2
287.3	0.2	0.1	12.4	807.5	0.33	0.08	4.3	* 1520.2	0.6	0.6	3.1
294.5	0.06	0.02	3.6	808.5	0.4	0.1	5.3	1527.1	1.1	0.4	5.6
306.3	0.05	0.02	2.8	828.8	0.4	0.1	5.1	1534.5	0.6	0.2	3.0
315.9	0.05	0.01	2.7	834.8	0.16	0.06	2.0	* 1539.8	0.7	0.7	3.5
318.6	0.03	0.005	1.6	* 860.0	0.15	0.15	1.8	1555.8	0.4	0.1	2.0
322.8	0.044	0.004	2.3	871.6	0.18	0.08	2.1	1568.9	2.0	0.5	9.8
332.2	0.05	0.01	2.5	881.5	0.18	0.10	2.1	1579.6	0.4	0.1	1.9
337.5	0.11	0.03	5.4	893.2	0.18	0.08	2.0	1593.0	2.0	0.5	9.6
352.3	0.20	0.02	9.1	914.2	0.30	0.15	3.3	1611.6	0.4	0.1	1.9
354.5	0.05	0.02	2.3	918.2	0.20	0.05	2.2	1646.8	0.4	0.2	1.8
366.4	0.05	0.02	2.1	* 928.3	0.11	0.11	1.2	1673.2	0.2	0.1	0.89
373.7	0.07	0.02	2.9	940.7	0.6	0.3	6.3	1682.3	0.4	0.2	1.8
387.2	0.04	0.02	1.6	962.3	0.4	0.3	4.0	* 1719.3	0.6	0.6	2.6
395.5	0.07	0.01	2.7	965.2	0.6	0.2	6.0	* 1728.5	0.35	0.35	1.5
400.5	0.04	0.02	1.5	978.3	0.9	0.2	8.9	1735.8	0.5	0.2	2.1
413.5	0.05	0.02	1.8	985.0	0.35	0.1	3.4	1768.6	0.5	0.2	2.0
415.5	0.05	0.02	1.8	1003.5	0.21	0.04	2.0	* 1803.5	0.5	0.5	2.0
* 423.0	0.05	0.05	1.7	1041.1	0.25	0.1	2.3	1822.4	1.1	0.2	4.2
440.0	0.31	0.06	10.1	1047.0	0.5	0.1	4.7	1833.5	0.8	0.3	3.0
448.4	0.08	0.02	2.5	1063.0	1.0	0.2	8.7	* 1854.6	0.4	0.4	1.5
458.4	0.08	0.02	2.5	1074.0	0.9	0.2	7.7	1866.5	2.9	0.5	10.8
467.4	0.13	0.03	3.9	1119.3	0.6	0.1	4.8	1880.4	1.8	0.5	6.7
485.3	0.11	0.04	3.1	1150.0	0.23	0.10	1.8	1893.3	1.9	0.5	6.7
494.6	0.05	0.01	1.4	1154.0	0.9	0.1	6.9	1914.0	3.5	1.0	12.5
499.1	0.12	0.02	3.2	1158.7	0.8	0.1	6.1	1925.2	1.6	0.5	5.7
511.1	0.10	0.02	2.6	1184.8	0.2	0.1	1.5	1933.3	0.4	0.2	1.4
523.6	0.27	0.04	6.8	1203.0	0.45	0.10	3.3	1943.4	1.0	0.2	3.5
528.2	0.07	0.03	1.7	1218.8	1.0	0.2	7.1	1953.5	4.5	1.5	15.6
532.2	0.08	0.03	2.0	1224.6	0.7	0.5	4.9	1990.3	1.2	0.6	4.2
								2000.1	0.5	0.1	1.7
								2051.1	2.0	0.5	6.4

TABLE II. See Text. Widths are in units of 10^{-3} eV. The existence of resonances by asterisks is less certain

TABLE III

Neutron Energy (eV)	No. of Levels	$\overline{g\Gamma^l}$ ($\times 10^{-3}$ eV)	$\bar{D}_l$	$S_l = \frac{1}{2l+1}\frac{\overline{g\Gamma^l}}{\bar{D}_l}$
0 - 200	27	3.64 ± 1.11	7.41	$(1.64 \pm 0.50) \times 10^{-4}$
0 - 400	55	4.33 ± 0.66	7.27	$(1.99 \pm 0.38) \times 10^{-4}$
0 - 600	79	4.40 ± 0.56	7.59	$(1.93 \pm 0.30) \times 10^{-4}$
0 - 800	103	4.34 ± 0.47	7.77	$(1.86 \pm 0.26) \times 10^{-4}$
800 - 2051	96	4.71	13.03	1.2×10^{-4}

313-475 O-68—39

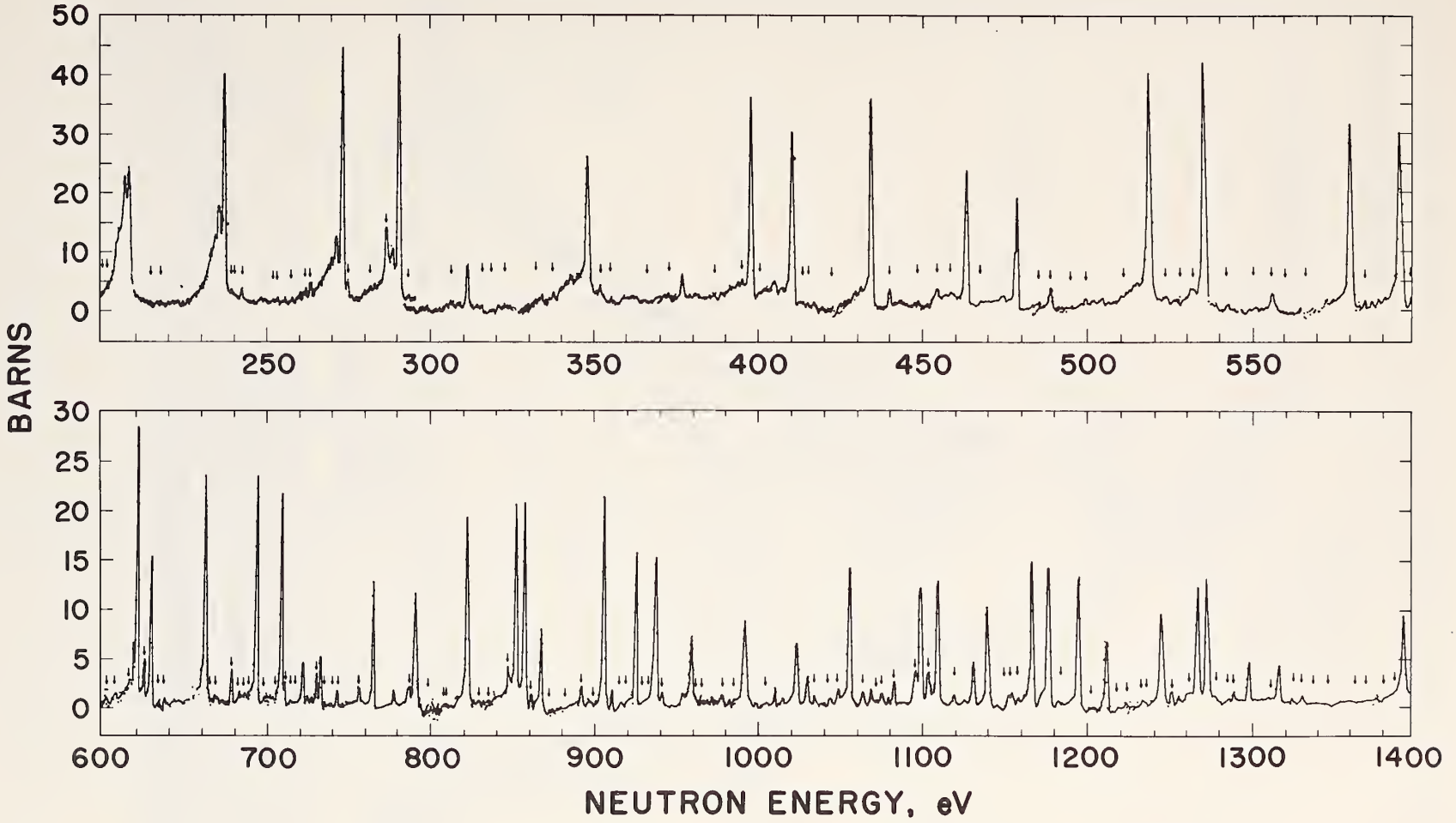

Fig. 1. A portion of the experimental capture data from the first ^{238}U sample in the neutron beam from the Petrel event. The small arrows indicate locations of weak resonances which are assigned $\ell = 1$. Data from more sensitive detectors and the thick sample were used in the confirmation and measurement of these resonances.

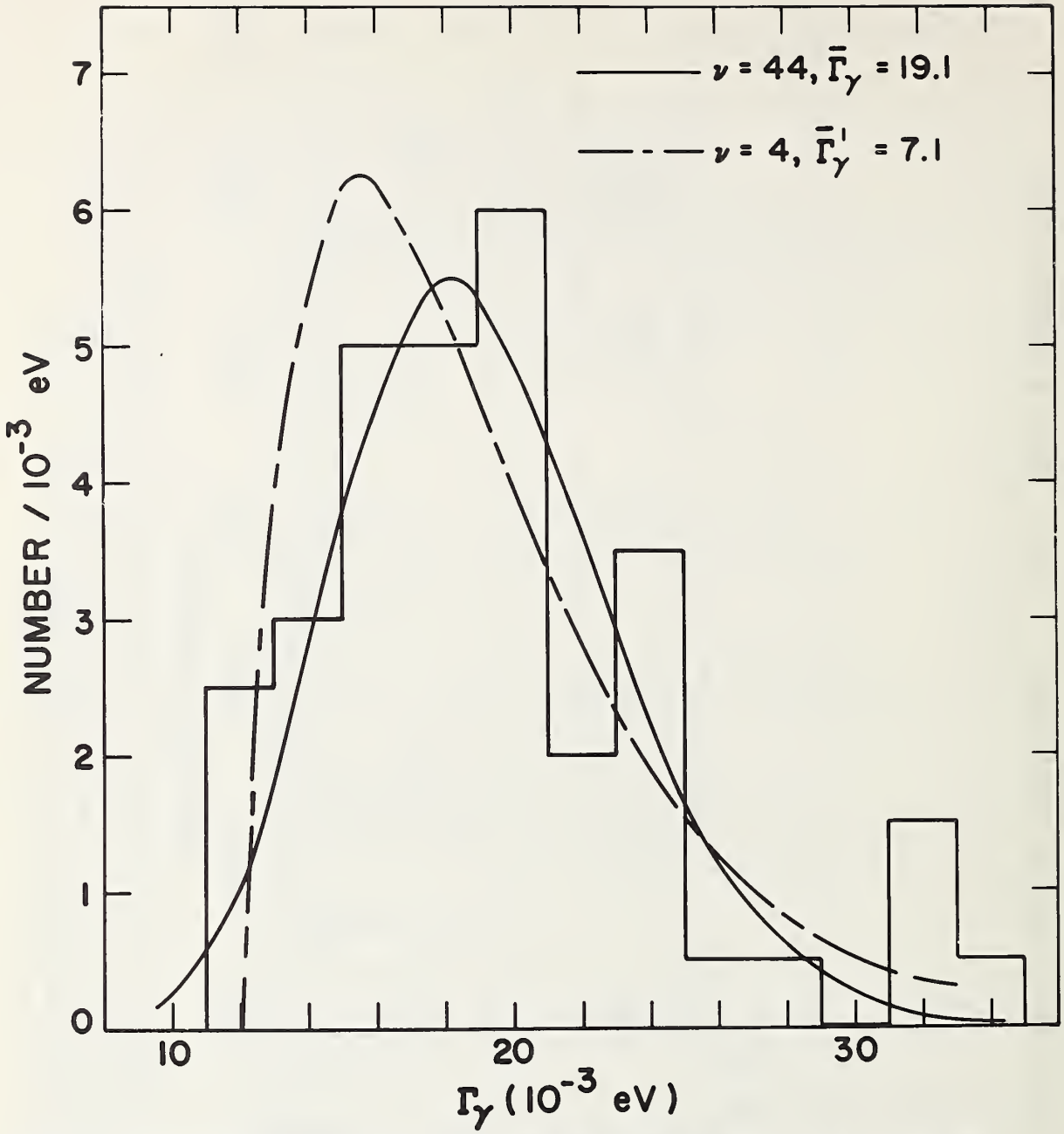

Fig. 2. The distribution of Γ_γ for resonances from 36.7 eV to 2031 eV neutron energy for capture in ^{238}U. The solid line is a Chi-square distribution with 44 degrees of freedom about the mean, $\bar{\Gamma}_\gamma = 19.1 \times 10^{-3}$ eV. The dashed line is a Chi-square distribution with 4 degrees of freedom about the mean of an assumed fluctuating part of $\bar{\Gamma}_\gamma^1 = 7.1 \times 10^{-3}$ eV where $\Gamma_\gamma = \Gamma_\gamma^0 + \Gamma_\gamma^1$ and $\Gamma_\gamma^0 = 12 \times 10^{-3}$ eV.

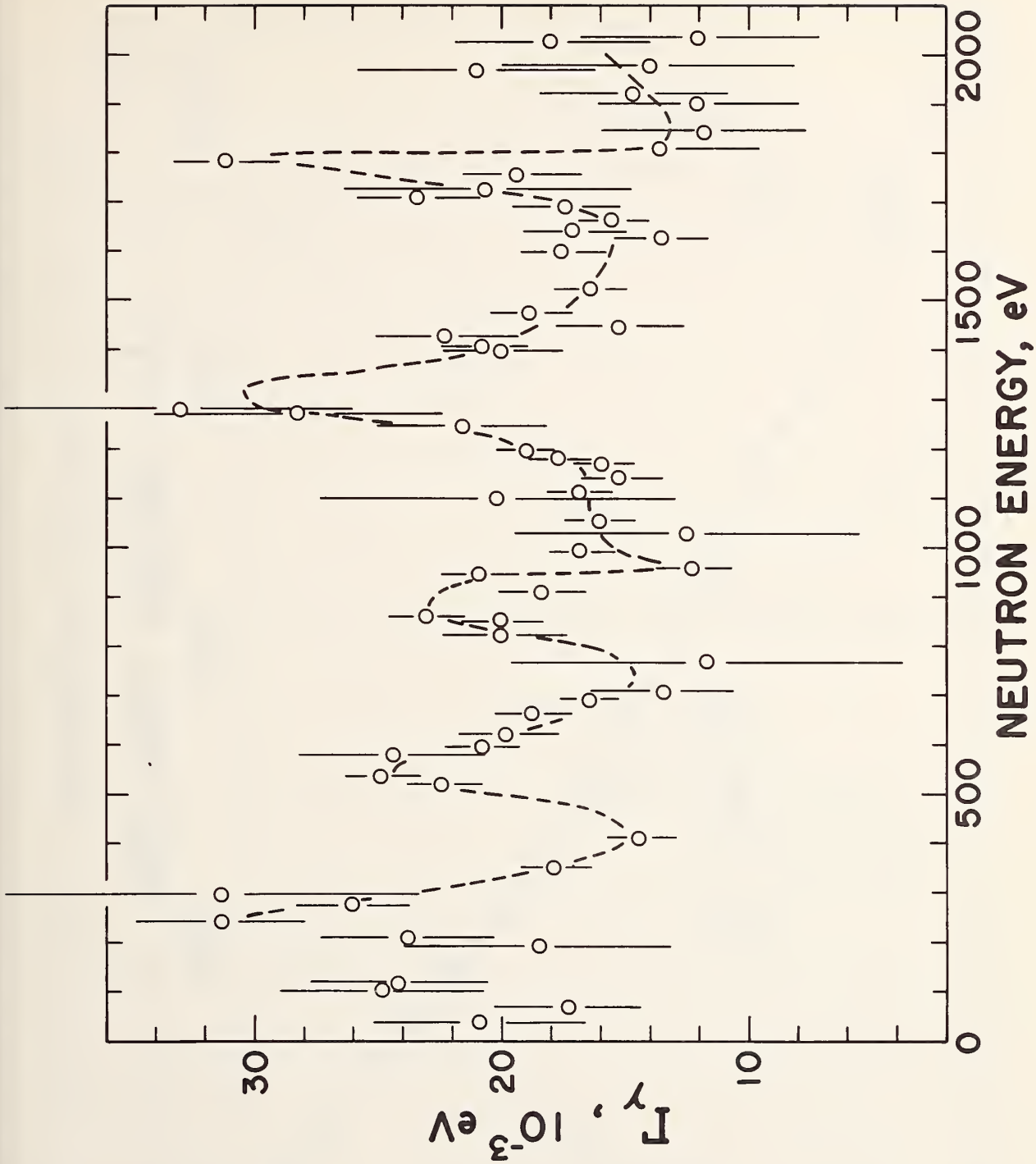

Fig. 3. Radiation widths versus neutron energy. The dashed line is a guide to the eye to emphasize possible structure. Error bars are statistical only.

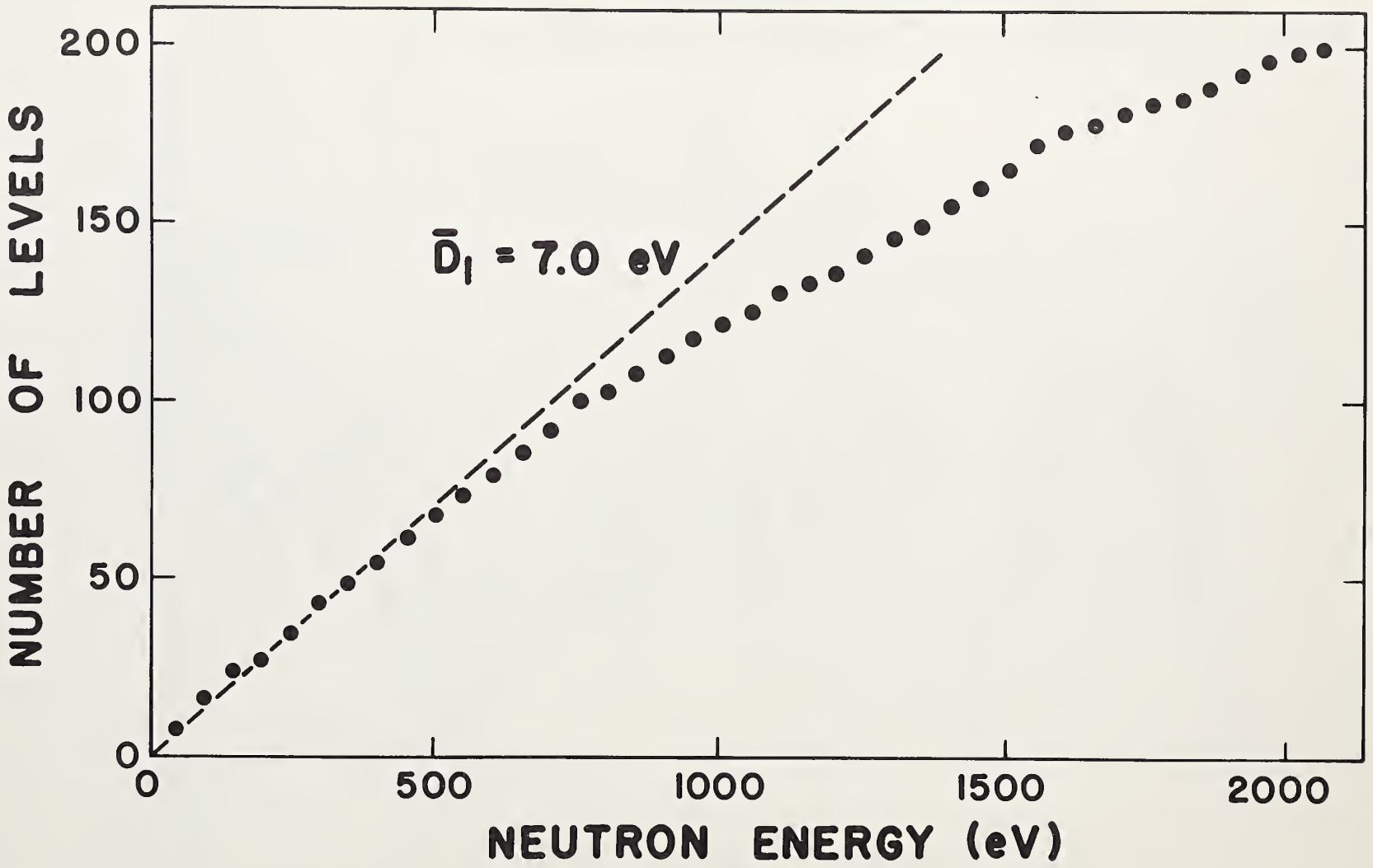

Fig. 4. Cumulative number of levels assigned $\ell = 1$ as a function of neutron energy.

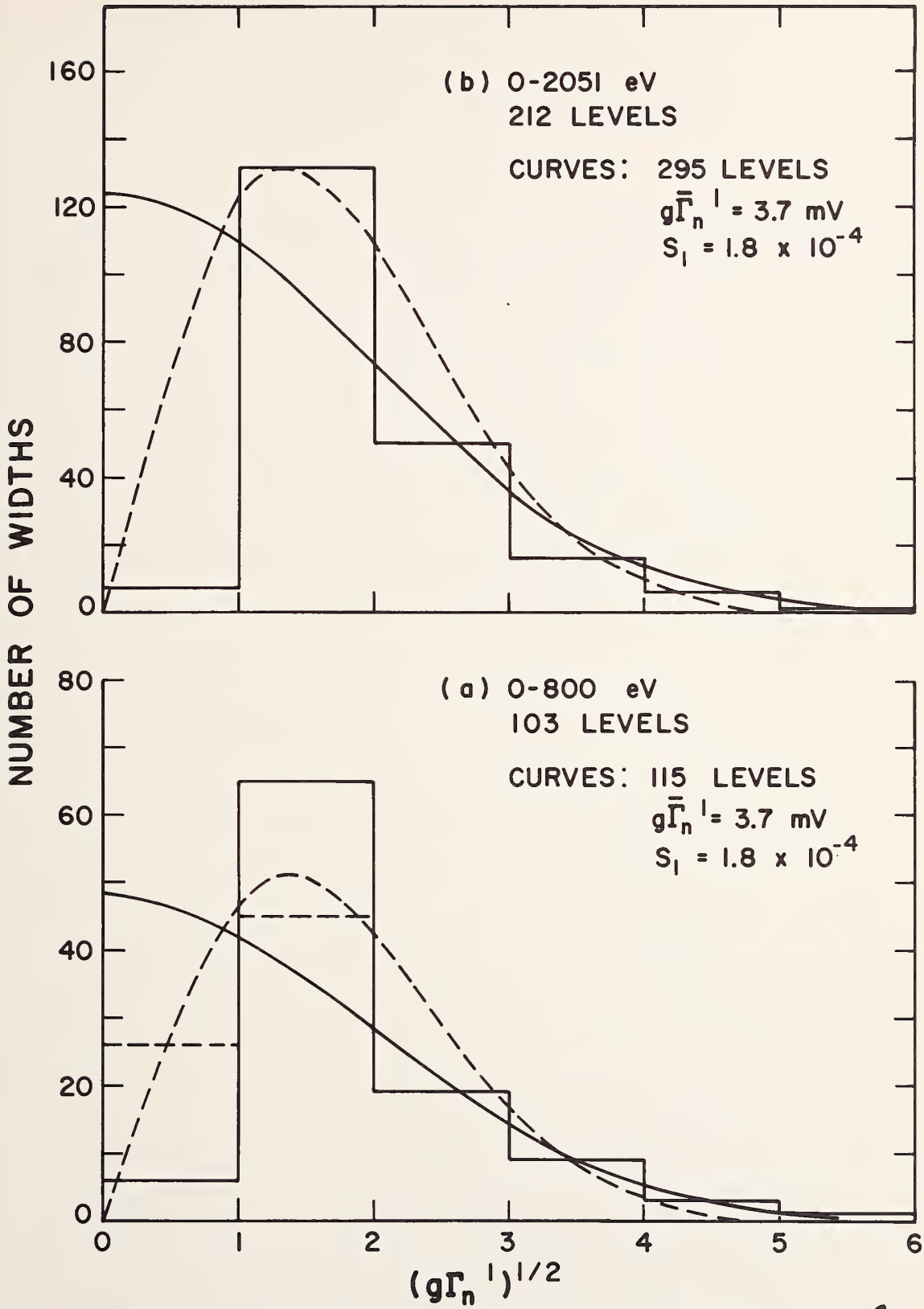

Fig. 5. The distribution of reduced neutron widths assumed to be $\ell = 1$. The solid lines are Porter-Thomas distributions and the dashed lines are Chi-squared distributions with $\nu = 2$ degrees of freedom.

Measurement of the Absolute Value of Eta for ^{241}Pu by the Manganese Bath Method*

by J. Richard Smith and S. Darrel Reeder
Idaho Nuclear Corporation, Box 1845, Idaho Falls, Idaho 83401

Abstract

The absolute value of eta for ^{241}Pu has been measured using the manganese bath technique. The MTR crystal spectrometer provided monoenergetic neutrons for measurements at 0.0253 eV and 0.060 eV. Purity of the monochromatic beam was insured by the operation of a mechanical neutron filter in the Bragg beam. The measurement consisted of comparing the ^{56}Mn activity induced in the solution by the neutron beam with the activity induced by fission neutrons emitted when the low-energy beam was absorbed in the fissile sample. The ^{241}Pu was produced by the Oak Ridge Calutron Group, reduced to metal by Dow Chemical Company, then rolled into foils and canned in aluminum by Oak Ridge. Additional manganese bath measurements were also made on ^{233}U, ^{235}U, and ^{239}Pu at both neutron energies to complete a detailed intercomparison of the four fissile isotopes. A least-squares analysis is being made of the experimental data to determine the best values of eta, the eta ratios, and their associated errors.

*Work performed under the auspices of the U. S. Atomic Energy Commission.

Measurement of the Absolute Value of Eta for ^{241}Pu by the Manganese Bath Method

by J. Richard Smith and S. Darrel Reeder
Idaho Nuclear Corporation, Box 1845, Idaho Falls, Idaho 83401

1. Introduction

Although production and storage problems present a formidable obstacle to the utilization of ^{241}Pu as a primary reactor fuel, this isotope shows promise of a lively career as a secondary fuel. There is a sort of poetic justice in the fact that parasitic absorption in ^{240}Pu is partially compensated by the birth of a fissile daughter, ^{241}Pu. The nuclear properties of the second generation isotope have a great influence on the neutron economy of plutonium fuel systems. The fission parameters are particularly important, and these have been the object of a considerable number of experimental investigations in recent years. There has nevertheless continued a notable scarcity of information concerning eta, the number of fission neutrons produced per absorption. Only a few measurements have been made [1,2], and these were in reactor spectra. The recent experiment of Fast and Aber [2] produced a precise measurement of the ratio of eta for ^{241}Pu to that of ^{235}U, evaluated at 2200 m/sec. This measurement was nevertheless done in a pile spectrum, and the authors point out the currently uncertain state of the spectral corrections.

It seemed advantageous to have an absolute measurement of eta for ^{241}Pu, using monochromatic 0.0253 eV neutrons. Such measurements were previously made of eta for ^{233}U, ^{235}U, and ^{239}Pu, using the manganese bath technique in conjunction with the MTR crystal spectrometer [3]. It was suggested that these same techniques could be used to measure eta for ^{241}Pu, provided a suitable sample could be obtained.

2. Experimental Arrangement

The experimental equipment and techniques are described in a previous report [3], and will be only briefly outlined here. The arrangement is illustrated in Figure 1, where the tank is shown aligned in the 0.0253 eV position. The Bragg beam produced by the (0002) reflection of beryllium is passed first through a mechanical neutron filter to remove neutrons from all but the primary Bragg reflection. Then it is trimmed to size by a collimator having adjustable apertures. Next it passes through a manganese-aluminum alloy monitor foil, where it produces a ^{56}Mn activity to which the solution activity can be compared. The use of the monitor foil makes the experiment less sensitive to reactor fluctuations and irradiation history. Finally the neutrons pass through a helium-filled channel which admits them to the center of the bath. Here they are either absorbed directly in the solution or in a fissile sample. In the former case the absorption of the neutron beam induces in the solution a level of ^{56}Mn activity proportional to the number of neutrons in the beam. In the latter case the absorption produces in the sample fission neutrons whose absorption

in the solution gives rise to a ^{56}Mn activity proportional to the number of fission neutrons produced. The ratio of the two activities is proportional to eta, and becomes that parameter after the application of several small corrections.

In operation the tank is covered with 0.020 in. Cd and then surrounded by a 1 ft wall and roof of borated paraffin. An additional 1 ft wall of the borated paraffin isolates the shielded tank from the crystal spectrometer and the path of the main reactor beam. This shielding reduces the irradiation background to about 1% of the open beam activity value at 0.0253 eV.

The experiment was performed at two energy points. One of these was chosen to be 0.0253 eV, the unhappy standard energy for comparison of low energy cross sections. The other was chosen to be that point giving the highest Bragg beam intensity, while remaining several minutes of arc removed from the deep dips that occur in Bragg spectra due to competition between the planes of the crystal [4]. The beryllium crystal used in the current experiment was different from that used previously, though from the same original melt. The maximum intensity point appeared at 0.06 eV for this crystal, compared with 0.057 eV used previously. At 0.06 eV the ^{56}Mn activities produced during the experiment are about double those encountered at 0.0253 eV.

After the two energy points had been chosen, the Bragg beam at each point was studied by time of flight to detect the presence of higher or lower order neutrons. The speed and angle of the mechanical neutron filter were set to reduce the fraction of undesired neutrons to less than 0.1% of the first-order peak intensity. At the two primary energy points, and in a wide neighborhood of each, transmission measurements were made on all the samples used in this experiment.

Counting of ^{56}Mn activities in a 5-gallon sample of solution and in the monitor foil was done on a pair of 3 in. x 3 in. NaI(Tl) scintillation counters. An integral count of gamma rays having energies above approximately 25 keV was made. This yielded the highest possible counting rate, with excellent stability. The observed decay of the samples accurately followed the ^{56}Mn half life, giving a routine check of the purity of the activity.

3. ^{241}Pu Samples

Since this experiment depended strongly on the availability of the ^{241}Pu samples, mention must be made of the construction of these. They were produced by an interlaboratory effort, most of which was centered in Oak Ridge National Laboratory. The calutron group directed by Leon Love produced 13.49 grams of Pu assaying 99.82% ^{241}Pu.* In addition, 18.62 grams of the feed material, assaying 83.93% ^{241}Pu* was made available for a backup foil to thicken the sample. These were reduced to metal (in separate batches two weeks apart) by W. V. Connor

*Post-separation assay

of Dow Chemical Company and returned to Oak Ridge. There the group under Ed Kobisk rolled the samples to size and canned them in 0.008 in. Al for use in the manganese bath sample holder.

The finished samples are pictured in Figure 2, and pertinent information appears in Table I. Samples are numbered in the order of manufacture. Samples I and II (99% ^{241}Pu) were received together, while Sample III arrived about a month later. All the data at .0253 eV and nearly all the data at .060 eV were obtained using these samples. Since Sample II is thinner than Sample I it was placed first in the beam, to decrease the fast multiplication correction for the whole sample. The normal order of samples, then, was II-I-III. It may be noted that only 6 grams of the 99% ^{241}Pu got into the first two samples. An effort was made to recover the remainder, with Sample IV resulting from this effort. The latter foil arrived in time for a few runs to be made at 0.060 eV.

4. Corrections to the Experiment

A number of corrections must be applied to the experimental data to deduce the correct value of eta. Many of these are characteristic of the experimental equipment, and were determined during the course of the previous experiments. Some corrections are characteristic of the sample, and must be redetermined for each sample used. These are fast multiplication, indirect multiplication, transmission, and impurities. Indirect multiplication results from the absorption in the sample of neutrons scattered back from the solution. It is suppressed by surrounding the sample with cadmium, except for the side facing the beam. The protective cadmium is in the form of cylindrical spacers placed flush against the interior faces of the sample foils, with a 0.020 in. Cd disk added at the back of the assembly. The cadmium spacers affect the fast multiplication and the indirect multiplication in different ways. Longer spacers separate the foils further and so decrease the fast multiplication, but they also increase the absorptive loss to cadmium. To test the validity of these corrections the sample geometry was varied as outlined in Table II. The bulk of the data were obtained using the first two orientations listed, and the results reported here are based entirely upon these runs. The results for the two sets of spacers agreed to within 0.1% at both energies, contributing to our confidence that these corrections ought not to be far wrong.

Those sample orientations in which the low-assay foil is placed first, alone, or omitted were designed to test the effectiveness of the impurity and transmission corrections. These have not been completely fed into the analysis, but in their incomplete form they suggest a possible uncertainty of perhaps 0.4% in the impurity correction. This figure is expected to shrink under further investigation, but for the present we must include it in the error estimate of the values quoted in this paper.

Another correction on which we must for the present relax the error estimate is that for excess resonance absorption in manganese. Our previous calculation assumed the above-1/v resonance absorption

integral to be 8.0 barns and did not consider resonance self-shielding in the solution. Recent work on the resonance integral of manganese indicates that the above-1/v contribution may be in the neighborhood of 10.5 barns [5]. Use of the higher number would lower all our eta values by about 0.3%. On the other hand, application of Axton's self-protection correction [6] would cut this apparent shift by half. It is likely that both these modifications are appropriate and that our eta values are high by a little less than 0.2%. The status of this correction is not considered firm enough at present to warrant adoption at this stage of the analysis.

In the course of the present experiment additional data were taken on ^{233}U, ^{235}U, and ^{239}Pu, in order to be sure the conditions of the previous experiment were being repeated and to allow a simultaneous intercomparison of the four eta values. The agreement between runs to the same type was very gratifying. The results of all these data, combined with the results of the previous measurement, will be published when this analysis is complete.

5. Conclusions

The preliminary values of eta for ^{241}Pu are displayed in Table IV. These values are based on an incomplete analysis of a portion of the data collected, and may shift by a few tenths of a per cent when analysis is complete.

The authors would like to express their appreciation to Messrs. L. O. Love and E. H. Kobisk of Oak Ridge National Laboratory and to W. V. Connor of Dow Chemical Company for the processing of the ^{241}Pu and production of the samples used in this experiment. Thanks are also due to Mr. M. B. Hendricks for his assistance in collecting the data and to Mr. C. L. Miller for maintenance of the equipment used in the experiment.

6. References

[1] GAERTTNER, E. R. et al., Nucl. Sci. and Engr. 3, 758 (1958).

[2] FAST, E. and ABER, E. F., USAEC Report IN-1060 (1967).

[3] SMITH, J. R., REEDER, S. D., and FLUHARTY, R. G., USAEC Report IDO-17083 (February 1966).

[4] SPENCER, R. R. and SMITH, J. R., Nucl. Sci. and Engr. 8, 393 (1960).

[5] VIDAL, R. and ROULLIER, F., IAEA Report INDC/156, Paper No. CN-23/73 (1966).

[6] AXTON, E. J. and RYVES, T. B., J. Nucl. Energy 21, 543 (1967).

Table I

Description of Samples

Sample Number	Weight	Thickness	^{241}Pu*
I	4.5015 g	.0129 in.	99.21
II	1.5141 g	.0045 in.	99.21
III	14.4715 g	.0373 in.	83.82
IV	2.757 g	.0079 in.	≈99 (assay not received yet)

Overall diameter of clad samples is 1.46 in. Flange depth .098 in.

*Assay of foil trimmings

Table II

Sample Orientations Used

		Number of Runs	
Order of Samples	Spacers Used	.0253 eV	.060 eV
II-I-III	5/8 in. & 1/2 in. Cd	8	9
II-I-III	1 1/16 in. & 7/8 in. Cd	6	4
II-I-III	None	3	2
III-I-II	None	3	1
IV-II-I-III	5/8 in., 5/8 in., & 1/2 in. Cd	0	3
IV-II-I	5/8 in. & 1/2 in. Cd	0	2
III	None	0	2

Table III

Corrections to the Experiment

Correction	Value at .0253 eV	.060 eV
Fast Multiplication		
Short Spacers	1.0149 ± 0.0020	1.0181 ± .0020
Long Spacers	1.0133 ± 0.0020	1.0167 ± 0.0020
Transmission		
Initial	.99813 ± .00010	.98374 ± .00020
Final	.99806 ± .00010	.98315 ± .00020
Indirect Multiplication		
Short Spacers	.9880 ± .0010	.9880 ± .0010
Long Spacers	.9815 ± .0010	.9815 ± .0010
Impurities		
Initial	.9898 ± .005	.9791 ± .005
Final	.9856 ± .005	.9736 ± .005
Scattering	.9987 ± .0012	.9983 ± .0012
Resonance Absorption in Mn	1.0098 ± .004	1.0098 ± .004
Oxygen and Sulfur Absorption	.9941 ± .0010	.9941 ± .0010
Structural Absorption	1.0107 ± .002	1.0107 ± .002
Duct Streaming	.9997 ± .0002	.9997 ± .0002
Leakage	.9985 ± .0010	.9985 ± .0010
Total Correction $(\eta^*/\eta)^\dagger$		
Short Spacers	1.0123 ± .0073	1.0002 ± .0073
Long Spacers	1.0040 ± .0073	.9922 ± .0073
η^*, uncorrected experimental value		
Short Spacers	2.1939 ± .0040	2.2032 ± .0040
Long Spacers	2.1765 ± .0040	2.1847 ± .0040

†Does not include impurity correction, which was applied to individual runs

Table IV

Eta for ^{241}Pu

Energy (eV)	Eta
0.0253 eV	2.17 ± 0.02
0.060 eV	2.20 ± 0.02

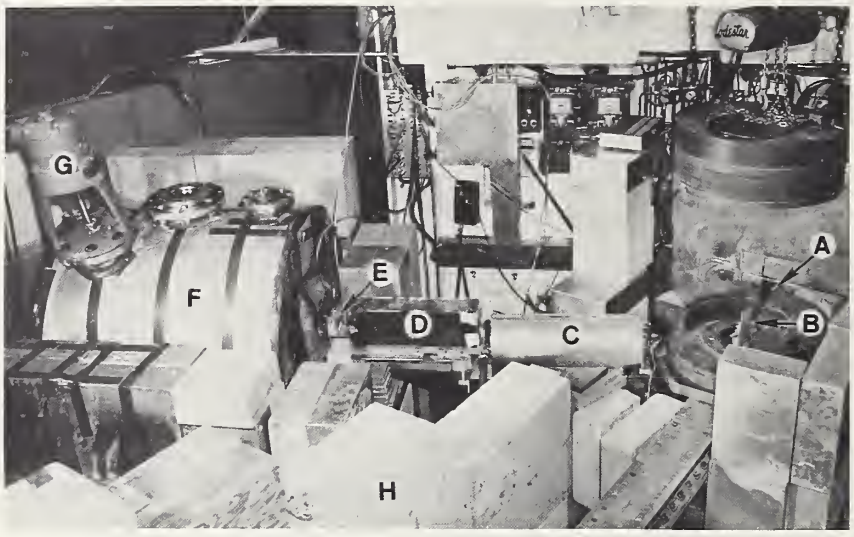

Figure 1 - Manganese bath apparatus at the MTR crystal spectrometer. The setup shown admits neutrons of 0.0253 eV energy to the bath. The essential elements are (A) reactor beam hole, (B) beryllium crystal, (C) mechanical neutron filter, (D) variable-aperture collimator, (E) monitor foil, (F) manganese bath tank, (G) mixer, and (H) shielding.

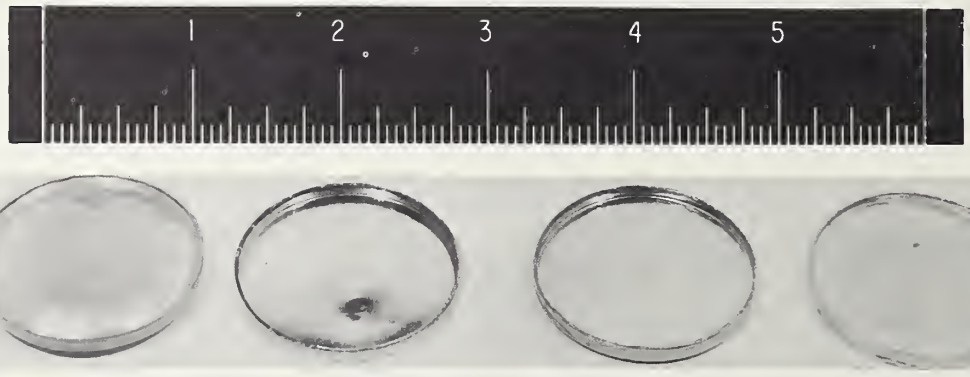

Figure 2 - ^{241}Pu foils used in the experiment. From left to right they are IV, II, I, III (see Table I). The data described in this paper were obtained using the three foils on the right.

TECHNIQUES FOR FISSION CROSS-SECTION MEASUREMENTS FOR ELEMENTS WITH HIGH α AND SPONTANEOUS FISSION ACTIVITY*

Philip G. Koontz and David M. Barton, University of California, Los Alamos Scientific Laboratory, Los Alamos, New Mexico 87544

ABSTRACT

Some considerations involved in measuring the neutron-induced fission cross section of high specific activity alpha emitters are discussed and a technique using solid state detectors combined with fast solid state circuits described. Amplitude discrimination alone can be used to distinguish between alpha and fission events and the alpha pile-up controlled by resolving individual pulses. This technique can be extended to isotopes with a high specific activity from spontaneous fission by using time discrimination. A Mobley buncher on a Van de Graaff accelerator with time coincidence is used to discriminate against the random spontaneous fission events. The results obtained for ^{238}Pu (3.8×10^7 alpha/min/μg) and ^{244}Cm (1.8×10^8 alpha/min/μg - 232 fiss/min/μg spontaneous fission) for several neutron energies are presented to illustrate the discussion.

The problem of measuring fissions from a material with a high alpha activity came up when we were asked to measure the neutron-induced fission cross section for ^{238}Pu at several neutron energies. The method chosen is a measurement of ^{238}Pu relative to that of ^{235}U, using a foil changer and neutron monitors, at a discrete energy neutron beam supplied by a Van de Graaff or a Cockroft-Walton accelerator. Since it is essential to distinguish between the alpha pile-up of the high-activity foil (3.8×10^7 α/min/μg) and the low-energy fission pulses, special techniques must be used.

One such technique is shown in Fig. 1. The detector is a diffused junction silicon crystal and gives pulses ~ 10-15 nsec long. These pulses are amplified by a solid state pre-amplifier and amplifier, with a rise time of ~ 1 nsec designed to drive a 50 Ω line. These pulses are fed into a fast discriminator, which opens a 20 nsec gate, allowing the same pulse, delayed by the proper amount, to pass through the gate. It is then stretched to a few microseconds, amplified by a slow amplifier before entering a P.H.A. (pulse height analyzer) and a slow discriminator which drives the scalers. Thus only the comparatively few fission or alpha pile-up pulses that are larger than the fast discriminator bias setting will pass through the 20 nsec gate and enter the slow system for analyses. The bottom part of Fig. 1 shows a fission pulse height spectrum for ~ 100 μg foil of ^{235}U and ~ 50 μg foil of ^{238}Pu, both taken with the same fast discriminator bias. If the bias had been lowered to show the alpha peak from ^{235}U, the single alpha events would have appeared at about Channel 8, indicating a significant pile-up of some three alphas in one 20 nsec gate on the ^{238}Pu curve. The scaler

* Work performed under the auspices of the U. S. Atomic Energy

discriminator for counting fissions was typically set at about Channel 29. These curves were taken with the partial collimation obtained by placing the detector about 1 cm from the ~ .25-in.-diam foil deposit, giving approximately 1/10 of 2π counting geometry. This spacing gave an appreciable improvement in fission pulse height resolution as well as decidedly fewer low-energy fission pulses in comparison to a close spacing between foil and detector, approximating a 2π geometry. The shift in the peaks for ^{238}Pu toward higher energies relative to those for ^{235}U agrees with known energies for the two atoms. A sketch of the foil changer and other details of the experiment can be found in the October 20, 1967, issue of the Physical Review.

A second request for us to measure the fission cross section for ^{244}Cm accentuates the problem, because the 18-yr half-life indicates an alpha activity about five times that of ^{238}Pu. In addition, the spontaneous fission rate for ^{244}Cm is high. If the cross sections are comparable for the two elements, the spontaneous fission rate will be many times higher than the fission rate induced by the neutron flux available from the Van de Graaff generator at the 3.0 MeV energy, as an example. The Mobley magnet buncher at the Van de Graaff offers a possible means of reducing the relative background of spontaneous fissions by requiring a time coincidence between an induced fission and a buncher pulse before the pulse can be recorded.

Figure 2 shows the circuit used in conjunction with the buncher. The detector and fast amplifier are the same as above. The pulse is split, one part going through a suitable delay as before into the linear gate, and the other through an adjustable attenuator, amplifier, and discriminator into a fast coincidence circuit. A pulse from the buncher through an adjustable delay is divided, one part going to the other half of the coincidence circuit. The buncher pulse repeats every 500 nsec. A pulse from the coincidence circuit indicates that the signal is greater than some desired pulse height such as alpha pile-up and that it is in time with a buncher pulse. The coincidence pulse opens the 20 nsec gate and allows the same signal pulse to come through, be stretched, amplified, counted by the scaler, and recorded in the P.H.A. The same coincidence pulse starts a T.A.C. (time to amplitude) circuit which is stopped by the other part of the buncher pulse coming through a suitable delay. After appropriate amplification, the T.A.C. pulse can go into the P.H.A. or into a S.C.A. (single channel pulse height analyzer) whose output can be used for externally gating the P.H.A. and also a scaler. Figure 3 shows a time display of the T.A.C. pulses. Assume that we have only random spontaneous fission and alpha pile-up pulses in coincidence with the buncher pulses, which we would have with a vacuum in the target. Assume that both the signal pulse and the buncher pulse are each 10 nsec wide. The coincidence pulse out, which starts the T.A.C. circuit, would come at the time of the leading edge of the later pulse, delayed by the inherent delay in the coincidence circuit. Thus all spontaneous fission pulses earlier than the buncher pulse would give a coincidence pulse at the same time relative to the buncher stop pulse and then would come at the same time on the

T.A.C. time display on the P.H.A., resulting in a peak in the higher channels. The random fissions occurring later than the buncher, within the coincidence time, will give coincidence pulses that vary in time, as shown by the flat portion of the curve in Fig. 3. The area under the flat portion is the same as the area under the peak. It would be desirable to have the timing adjusted so that the neutron-induced fissions arrive in the flat part of the spontaneous fission curve as indicated in Fig. 3. Then the lower and upper bounds of the S.C.A. could be adjusted as shown, which limits the time resolution, and the S.C.A. pulses can be used to externally gate the P.H.A. and to drive the scalers in the lower part of the circuit.

It is obvious that the timing of the circuits is very important. In Fig. 2, the part of the circuit in the control room rack can be adjusted quite easily with the aid of a fast pulser and a scope. The pulse from the pulser is split at A, fed into the circuits as shown at B and C. The points D and E are observed with the scope and the arrival times of the pulses adjusted by Delay (1). Then the points F and G are observed and the arrival times adjusted by Delay (2). The value of the T.A.C. circuit in channels/nsec can be adjusted by Delay (3) and the gain of the amplifier. Then Delay (4) must be adjusted with real signal and buncher pulses for optimum timing. The position of neutron-induced fission pulses as shown in Fig. 3 offers a convenient check as already mentioned.

The early data with ^{244}Cm was taken with the electronics as shown in Fig. 2, but certain difficulties appeared. The gate scaler records all coincident events within the narrow time limits set by the S.C.A. If the fast discriminator is adjusted to pass a few alpha pile-ups, some will be recorded together with the fission events, from both the spontaneous fission and the neutron-beam-induced fission. In theory, the random background of both alpha pile-up and spontaneous fission can be eliminated by a background run of the same length of time with a vacuum target, provided there is no drift of the fast discriminator amplifier system, but a slight drift may change the rate of alpha pile-ups, and the net number of gates is subject to error. In practice, these may be detected by looking at the pulse height data from the externally gated P.H.A. for both runs. The fission scaler records only those pulses above some chosen pulse height, but it does record all of the random spontaneous fissions occurring within the wider time of the coincident circuit, leading to a higher percentage of random background.

The difficulties have been eliminated by the changes in the circuit as shown in Fig. 4. Basically this consists of the addition of a dual linear gate to restrict the fission scaler to record pulses within the time specified by the S.C.A. and retaining the pulse height discrimination which it had previously. It also permits the use of the P.H.A., either internally or externally gated, to examine the pulse heights or the time display of the T.A.C. circuit, since the linear gate can be bypassed with a switch.

If the effective time resolution as determined by the S.C.A. is 5 nsec and the time between pulses is 500 nsec, data is taken for only 1% of the time, and 99% of the random background is eliminated. A check run did indeed show this to be the case. However, this is not the entire story -- the ratio of the area under the random curve to the area under the induced fission peak is a measure of the background. The area of the neutron-induced fission peak increases with the neutron flux available. For very high beam current, the buncher technique may not be required to produce a suitably low background. In a run at 14 MeV at the Cockroft-Walton with a steady beam of 700 μA, and the circuitry of Fig. 1 as used with ^{238}Pu, the steady spontaneous fission background was a third or a fourth of the total fission counts.

One other difficulty is the radiation damage to the solid state detector, particularly by the intense alpha bombardment by the ^{244}Cm. A bombardment of a few hours (perhaps 5 or 6) by the ^{244}Cm represents the useful life of a detector.

The following table gives some resulting cross sections at energies 1.0, 1.5, 3.0, and 14.9 MeV together with the cross sections used for ^{235}U.

Energy (MeV)	Cross section in barns		
	^{235}U	^{238}Pu	^{244}Cm
1.0	1.22	2.08	2.0
1.5	1.26	2.20	1.8
3.0	1.16	2.23	1.8
14.9	2.13	2.67	2.6

The results for ^{238}Pu, as mentioned, were published in the October 20, 1967, Physical Review. The results for ^{244}Cm are preliminary and have not been published. The ^{244}Cm value at 14.9 MeV was obtained at the Cockroft-Walton using a beam current of ~ 700 μA without bunching.

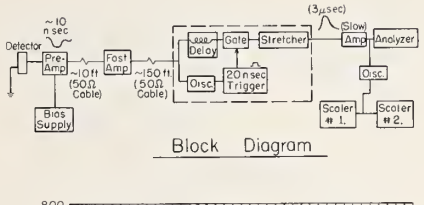

Fig.1 Block Diagram and Fission Pulse-Height Spectrum for Fission Cross-Section for ^{238}Pu.

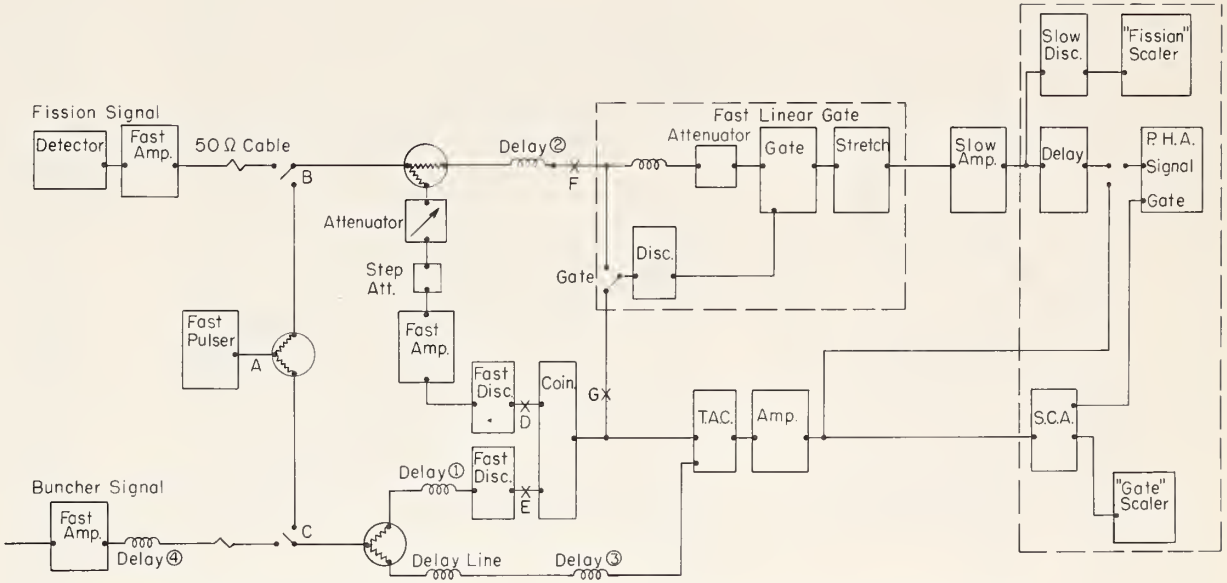

Fig.2. Block Diagram for ^{244}Cm Fission Cross-Section Measurement.

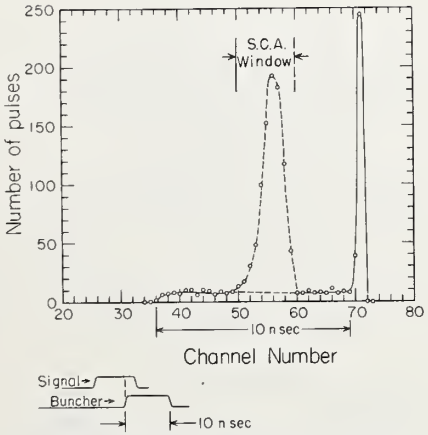

Fig 3. Time Display of Random Background and Neutron-Induced Fission Pulses.

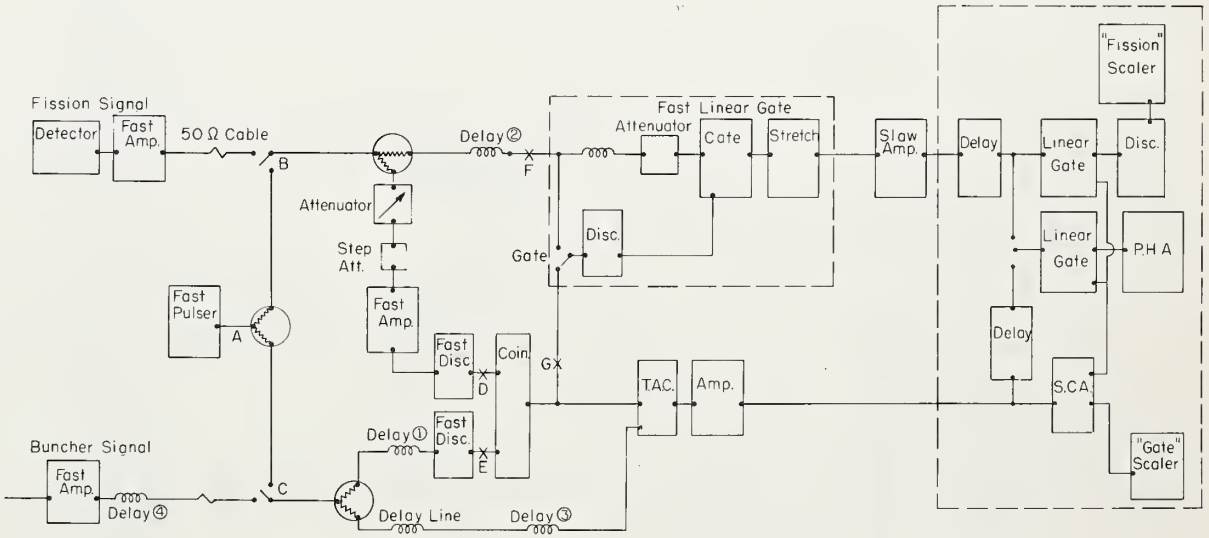

Fig. 4. Modified Circuit for ^{244}Cm Fission Cross-Section Measurement.

Fragment Angular Distributions for Monoenergetic Neutron-Induced Fission of Pu^{239}*

J. R. Huizenga and A. N. Behkami
University of Rochester and Argonne National Laboratory

J. W. Meadows, Jr.
Argonne National Laboratory
Argonne, Illinois 60439
E. D. Klema
Northwestern University
Evanston, Illinois 60201

Abstract

Fission fragment angular distributions have been measured for the fission of Pu^{239} induced by monoenergetic neutrons of energies 150, 400, 475, 550, 600, 700, 800, 900, 1000, and 1200 keV (energy resolution ± 25 keV). The fission fragments were detected with solid state silicon detectors at six angles simultaneously, namely, 3.7°, 24.0°, 37.2°, 54.7°, 72.3° and 90.0°. The relative sizes of the detectors were determined in an identical configuration with thermal neutrons. For various sets of optical model neutron transmission coefficients, the values of K_o^2 (the projective K of the total angular momentum I on the nuclear symmetry axis is assumed to have a Gaussian distribution, and K_o^2 is the squared standard deviation of the Gaussian) were calculated from the experimental angular distribution at each neutron energy. The excitation energy dependence of K_o^2 will be discussed in terms of the nuclear pairing energy of the highly deformed transition nucleus.

1. Introduction

Detailed analysis of the energy dependence of the fission fragment anisotropy from the Pu^{239}(d,pf) reaction has given some evidence[1] of structure in a plot of K_o^2 as a function of excitation energy for the transition nucleus Pu^{240}. The parameter K is the projection of the total angular momentum I on the nuclear symmetry axis, and the K distribution is assumed to have a Gaussian form characterized by K_o^2,

$$F(K) \alpha \exp(-K^2/2K_o^2) \qquad (1)$$

From the energy position of one of the breaks in the K_o^2 curve, the magnitude of the pairing energy gap 2Δ in the highly deformed transition nucleus Pu^{240} was estimated to be 2.6 MeV.[1] This value is approximately twice the pairing energy of Pu^{240} in its ground state shape.

*Work supported by the U. S. Atomic Energy Commission.

Some question has been raised about the interpretation of the various breaks in the energy dependent K_o^2 curve.[2] In particular, is it possible that some of the observed structure is related to the (d,p) reaction mechanism? Due to the important implications of such a deformation dependent pairing energy on nuclear structure in general, we have re-investigated this problem by way of the Pu^{239}(n,f) reaction. The angular distribution of fission fragments has been studied as a function of neutron energy for neutron energies in the 100 to 1200 keV range. The purpose of this study is to elucidate the excitation energy dependence of K_o^2 in order to obtain evidence on the pairing energy of the transition nucleus Pu^{240}.

2. Experimental Procedure

Monoenergetic neutron beams were produced from the Li^7(p,n)Be^7 reaction. Protons were accelerated in the Argonne Reactor Physics Van de Graaff and bombarded a lithium target prepared by vacuum evaporation. The neutron energy spread, which is related to the lithium target thickness, was $\pm$ 25 keV.

The neutrons impinged on a Pu^{239} target (99.7% isotopically pure) prepared by a painting technique on a 0.001 inch aluminum backing foil.[3] The Pu^{239} target has a thickness of 0.5 mg/cm^2 and an areal size of 1/8 inch in diameter.

The fission fragments from the Pu^{239}(n,f) reaction were detected at six angles simultaneously with surface barrier solid state detectors. The six detectors were each centered at one of the following angles θ to the neutron beam axis, 3.7°, 24.0°, 37.2°, 54.7°, 72.3° and 90.0°, respectively. The detectors, of approximately 0.62 cm diameter, were located 7.30 cm from the target.

The collimating system restricted the image of the proton beam spot on the lithium target to a diameter less than 1/8 inch. With the angular spread in the neutron beam direction and the above detector arrangement, the overall angular resolution was approximately 7°.

3. Experimental Results

The fission fragment angular distributions for the Pu^{239}(n,f) reaction were measured at average neutron irradiation energies of 150, 400, 475, 550, 600, 700, 800, 900, 1000 and 1200 keV. The beam spread was $\pm$ 25 keV. The data for each energy were gathered in a series of runs in order to check the overall consistency of the data at each energy. A summary of the results is given in Table I; and, for two energies, 400 and 900 keV, the angular distributions are plotted in Figs. 1 and 2.

After mounting the Pu^{239} target in the vacuum chamber, the relative areas of the six detectors were determined by irradiation with thermal neutrons. With s-wave neutron capture, the angular distribution is isotropic. Since the relative detector areas were determined with the target in an identical geometrical position as that of the various runs, all corrections due to possible irregularities in target thickness, exact positioning of target, etc. cancel.

Since the fission cross section of Pu^{239} for thermal neutrons is much larger than it is for 100-1200 keV neutrons, the possibility of contamination by thermal neutron induced fission was investigated. The effect of such a contamination is to lower the anisotropy and to give too large values of K_o^2. However, at selected neutron energies, the fission rate was measured with the detector chamber alternately bare and covered with 0.020 inch of cadmium. An upper limit of 5% of the fission events is due to thermal neutron fission. The contribution to fission from scattered neutrons is small and was neglected.

The fraction of fission events produced by neutrons from the $Li^7(p,n)Be^{7*}$ reaction which leaves Be^7 in its first excited state is zero for $E_n \leq 500$ keV. At the higher energies, the fraction is not negligible; however, the anisotropy is quite insensitive to neutron energy and, therefore, we have neglected to make a correction for the second neutron group.

4. Theory

The fissioning transition nucleus is completely characterized by the quantum numbers I (total angular momentum), M (projection of I on a space fixed axis to be designated as the neutron beam direction), and K (defined in section I). If it is assumed that the fragments separate along the nuclear symmetry axis, the angular distribution is uniquely determined by the above quantum numbers.[4] [5]

If a compound state (K,M) fissions through a transition state I, the angular distribution is given by the square of the rotational part of the collective wave function,

$$W(\theta) \alpha \left| D^I_{M,K} (\theta) \right|^2 \qquad (2)$$

Therefore, the fission fragment angular distribution offers a direct source of information on the spectrum of quantum states associated with the transition nucleus.

The fission fragment angular cross section is given by[6]

$$W(\theta) = 2\pi \sum_{\ell} \sum_{J} \sum_{I} \sum_{M} P(\ell J; IM)\ W(I,M;\theta) \qquad (3)$$

where the first term is a partial probability of formation of a state (I,M) of the compound nucleus from a particular (ℓ,J) combination,

$$P(\ell,J;IM) = \frac{\sum_{\sigma,\mu} (2\ell+1)\ T_{\ell}^{J}(E)\ |C^{\ell,s,J}_{o,\sigma,\sigma}|^2\ |C^{J,I_o,I}_{\sigma,\mu,M}|^2}{(2s+1)\ (2I_o+1) \sum_{J,\ell,\sigma} (2\ell+1)\ T_{\ell}^{J}(E)\ |C^{\ell,s,J}_{o,\sigma,\sigma}|^2} \qquad (4)$$

and the second term gives the angular distribution of the fission fragments emitted from the compound state (I,M),

$$W(I,M;\theta) = \sum_{k} \frac{\exp(-K^2/2K_o^2)\ [|D^{I}_{MK}(\theta)|^2]}{\sum_{k} \exp(-K^2/2K_o^2)} \qquad (5)$$

The transmission coefficients $T_{\ell}^{J}(E)$ are derived from the optical model with spin-orbit interaction, where $J = \ell+s$ and s is the neutron spin with projection σ on the space fixed axis. The target spin and its projection on the space fixed axis are denoted by I_o and μ, respectively. The quantities $C^{\ell,s,J}_{o,\sigma,\sigma}$ and $C^{J,I_o,I}_{\sigma,\mu,M}$ are Clebsh-Gordan coefficients. The symmetric top wave functions $D^{I}_{MK}(\theta)$ are given by[5]

$$D^{I}_{MK}(\theta) = \{(I+M)!(I-M)!(I+K)!(I-K)!\}^{1/2} \sum_{X} \frac{(-1)^X (\sin\ \theta/2)^{K-M+2X} (\cos\ \theta/2)^{2I-K+M-2X}}{(I-K-X)!(I+M-X)!(X+K-M)!X!} \qquad (6)$$

where the sum is over X = 0, 1, 2, 3... and contains all terms in which no negative value appears in the denominator of the sum for any one of the quantities in parenthesis.

5. Results of Calculations and Discussion

Computer calculations were utilized to search for a value of K_o^2 in eqs. 3, 4, and 5 which minimized the difference between the theoretical and experimental fission fragment angular cross sections (χ^2 criterion). Examples of such comparisons are shown for two energies in Figs. 1 and 2 for three values of K_o^2. The determined values of K_o^2 at each neutron energy are plotted in Fig. 3. These values were computed with Perey-Buck neutron transmission coefficients.[7] Calculations were performed also

with Bjorklund-Fernbach neutron transmission coefficients[7] with very similar results.

The values of K_o^2 are of the order of 4 to 5 for neutron energies up to 600 keV. Values of this magnitude may be associated with collective excitations. At higher neutron energies, the values of K_o^2 increase markedly. The association of this break in the energy dependent K_o^2 curve with the introduction of contributions from two quasi-particle states in the K spectrum gives a pairing energy 2Δ of 2.2 ± 0.1 MeV (based on $B_f = 4.90$ MeV). This value is considerably larger than the same quantity for the Pu^{240} ground state nucleus and agrees within experimental error with a revised measurement[8] from the Pu^{239}(d,pf) reaction.

6. References

1) H. C. Britt, W. R. Gibbs, J. J. Griffin and R. H. Stokes, Phys. Rev. 139, B354 (1965).

2) H. C. Britt, R. W. Newsome, Jr., and R. H. Stokes, Symp. Recent Progress Nucl. Phys. with Tandems, Heidelberg, July (1966). J. R. Huizenga, International Nuclear Physics Conference (Becker, Goodman, Stelson and Zucker, eds.), Academic Press, New York (1967).

3) Prepared by A. J. Gorski.

4) A. Bohr, Proceedings of the International Conference on the Peaceful Uses of Atomic Energy, Geneva (1955) (United Nations, New York, 1955), Vol. 2, p. 151.

5) J. A. Wheeler, Fast Neutron Physics, Part II (J. B. Marion and J. L. Fowler, eds.), Wiley (Interscience), New York (1963).

6) W. R. Gibbs and J. J. Griffin, Phys. Rev. 137, B807 (1965).

7) E. H. Auerbach and F. G. J. Perey, Brookhaven National Laboratory Report, BNL-765, July (1962).

8) F. A. Rickey and H. C. Britt, Bull. of Am. Phys. Soc. 13, 36 (1968).

Table I

Fission Fragment Angular Distributions for the Pu^{239}(n,f) Reaction at Several Neutron Energies

E_n (keV)	W(θ) Experimental					
	3.7°	24.0°	37.2°	54.7°	72.3°	90.0°
150±25	1.066±0.014	1.041±0.014	1.056±0.015	1.001±0.014	0.990±0.014	1.000±0.012
400±25	1.142±0.021	1.090±0.016	1.101±0.017	1.056±0.016	1.014±0.016	1.000±0.013
475±25	1.108±0.012	1.090±0.013	1.058±0.012	1.009±0.012	1.040±0.013	1.000±0.010
550±25	1.128±0.013	1.116±0.014	1.090±0.014	1.019±0.013	1.019±0.013	1.000±0.011
600±25	1.148±0.011	1.112±0.012	1.083±0.011	1.052±0.011	1.033±0.012	1.000±0.011
700±25	1.113±0.014	1.080±0.015	1.048±0.015	1.014±0.014	1.000±0.015	1.000±0.012
800±25	1.132±0.012	1.104±0.012	1.079±0.012	1.035±0.011	1.033±0.012	1.000±0.010
900±25	1.111±0.012	1.101±0.012	1.071±0.012	1.057±0.012	1.002±0.012	1.000±0.010
1000±25	1.123±0.015	1.099±0.015	1.082±0.015	1.028±0.014	1.002±0.015	1.000±0.012
1200±25	1.122±0.013	1.104±0.014	1.066±0.014	1.027±0.013	0.993±0.014	1.000±0.011

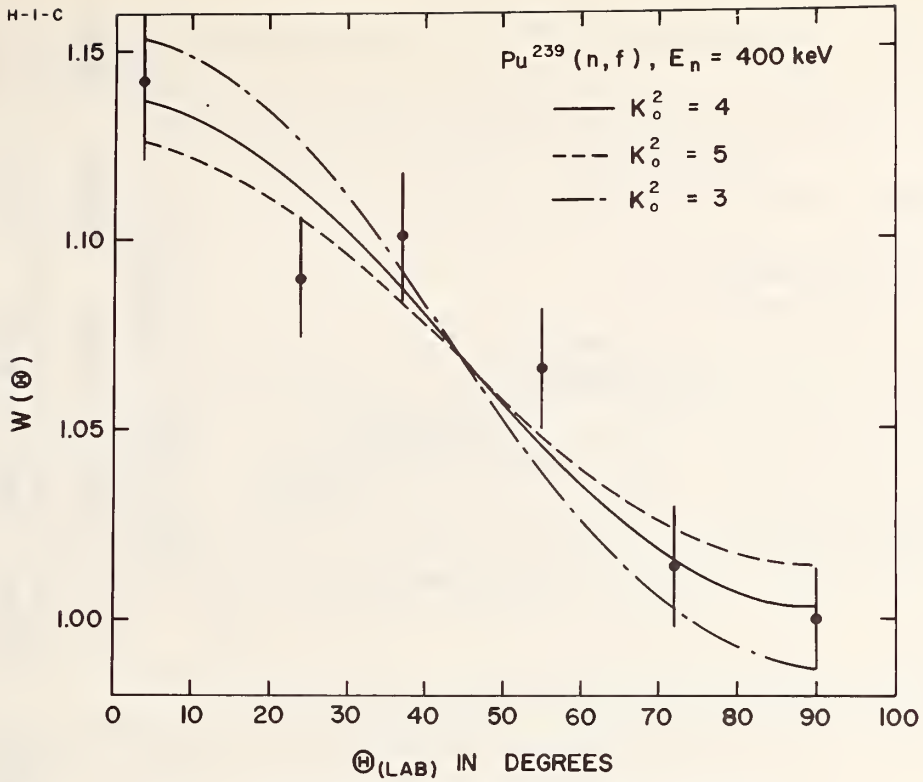

Fig. 1 Experimental and theoretical fission fragment angular distributions for neutron induced fission of Pu^{239}. The different lines correspond to the use of different values of K_o^2 in the theoretical calculations.

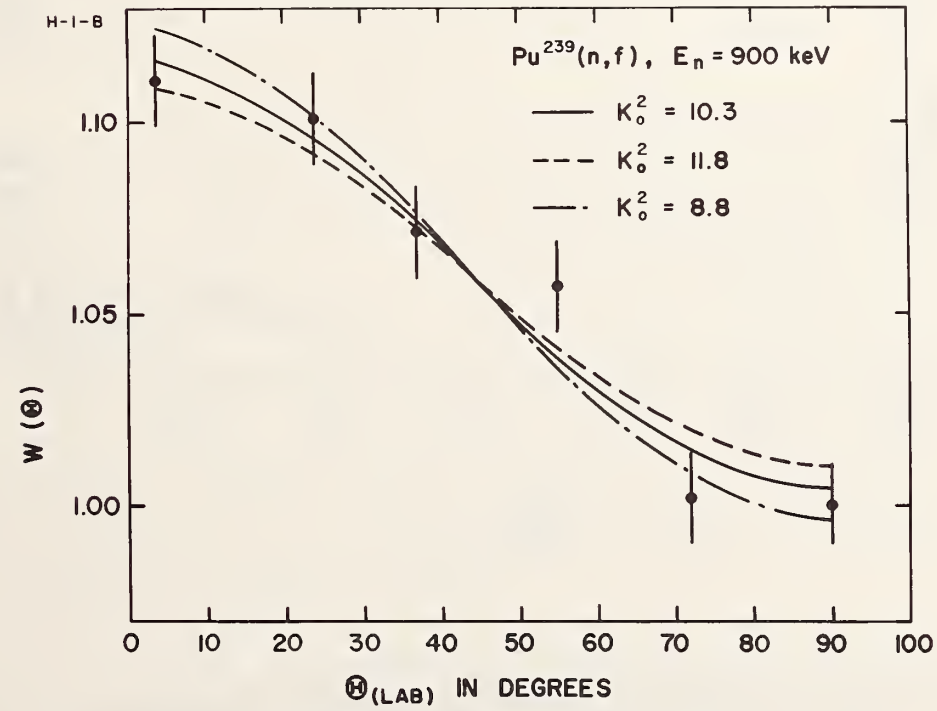

Fig. 2 Experimental and theoretical fission fragment angular distributions for neutron induced fission of Pu^{239} The different lines correspond to the use of different values of K_o^2 in the theoretical calculations.

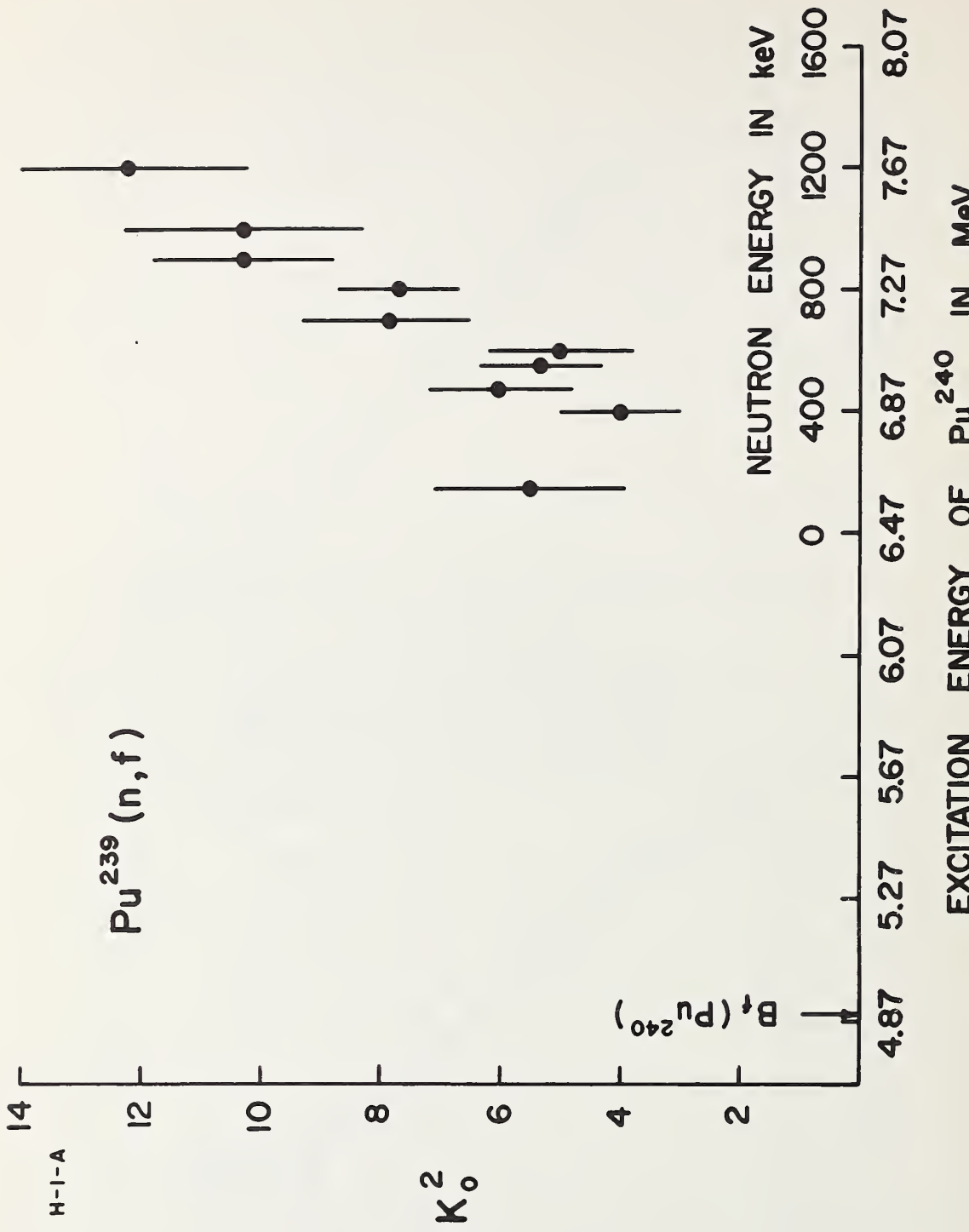

Fig. 3 Energy dependence of K_0^2 deduced from the experimental data as outlined in the text.

FISSION CROSS-SECTION OF ^{232}Th FOR THERMAL NEUTRONS

M. NEVE de MEVERGNIES and P. del MARMOL

C.E.N. - S.C.K. - MOL (Belgium)

The knowledge of the subthreshold fission cross-section of ^{232}Th is of interest for reactor physics and for fission physics. There is only one measurement with thermal neutrons quoted in the literature, namely the one by KORNEEV, SKOBKIN and FLEROV [1] . These authors used a Sb-Be photoneutron source, surrounded by paraffin for slowing down the 30 keV neutrons, and a fission chamber as detector ; they obtained $\sigma_f = (60 \pm 20)\,\mu$ b. We have remeasured this quantity, using a solid state track detector and a purer thermal neutron spectrum.

The ^{232}Th deposits were prepared by BCMN - EURATOM (Geel) : an organic complex of 3.2 mg/cm^2 thickness, containing (47 $\pm$ 1) % of ^{232}Th, was fixed by electrospraying on an Al disk of 0.5 mm thickness and 10 mm diameter.

As fission detector, we used a polycarbonate known as Makrofol-E which registers the tracks of fission fragments [2] ; these tracks are made visible by etching with NaOH (6 N) at 60°C for about 30 min., and are counted by means of a microscope (x 250 or x 500).

The Makrofol disks were held tightly against the Th deposits in an Al or Cd box and were irradiated in the vertical thermal column of the BR1 graphite reactor operating at medium power (i.e. between 400 kW and 1 MW). It is very important to have low gamma and fast neutron fluxes at the irradiation position, so as to minimize the "background" due to photo- and fast neutron - fissions. In our case, the Al or Cd sample-box was placed, respectively, in a graphite or B_4C container, located itself in a lead cylinder of 10 cm diameter, and 10 cm height. At the irradiation position, the unperturbed thermal flux is 2.5 x 10^9 n/cm^2 sec., for 1 MW reactor power, and the ratio of thermal to epithermal fluxes is 3.85 x 10^5 (corresponding to a Cadmium ratio of 1.10^5 for Au). In spite of this high value, the number of fissions recorded with the sample and Makrofol detector inside the Cd-B_4C container amounted to about 10 % of the number recorded with the Al-graphite container.

Three irradiations were performed, two in the Al-graphite container, and one in the Cd-B_4C container ; the integrated thermal fluxes at the surface of the containers amounted, respectively, to 8.63 x 10^{13}, 3.07 x 10^{13} and 1.01 x 10^{15} n/cm^2.

The main errors on the results came from the uncertainty on the Th-content of the deposits ($\sim$ 2%) and the statistics of the track counting. These two errors were combined and arbitrarily multiplied by a factor of two so as to take into account any systematic error.

The following fission cross-sections were obtained :

Run n° 1	:	37 ± 2 μb
Run n° 2	:	46 ± 5 μb
Weighted average	:	39 ± 4 μb

This result is in rough agreement with the value (60 ± 20 μb) quoted in [1]

It may be of interest to compare this value with the one deduced from the well-known formula for the penetrability below the fission barrier. For neutron energies far below the barrier, this formula can be written as :

$$\bar{\Gamma}_f = \frac{D}{2\pi} \exp\left(\frac{-2\pi E_f}{\hbar\omega}\right) \qquad (1)$$

where $\bar{\Gamma}_f$ = average fission width
D = average level spacing
E_f = fission threshold energy
$\hbar\omega$ = 650 keV

For thermal neutrons, one has :

$$\sigma_f \text{ (therm.)} = \frac{\bar{\Gamma}_f}{\bar{\Gamma}_f + \bar{\Gamma}_\gamma} \sigma_{abs} \text{ (therm.)}$$

where $\bar{\Gamma}_\gamma$ = average radiation width.

Combining (1) and (2) and using the following numerical values from ref. [4] and [5] : D = 18.6 eV
$\bar{\Gamma}_\gamma$ = 21.5 meV
σ_{abs} (therm.) = 7.4 + 0.1 b
E_f = 1.35 MeV

one obtains : σ_f (therm.) = 2.1×10^{-3} b.

i.e. a value about 50 times larger than the measured one. This disagreement is similar to the one mentioned by E. RAE [3] in the case of other nuclei and probably points to the inadequacy of relation (1) far from the threshold energy.

REFERENCES

[1] KORNEEV, SKOBKIN and FLEROV, Sov. Ph. JETP 10 (1960), 29

[2] R.L. FLEISCHER, P.B. PRICE and R.M. WALKER in Ann. Rev. Nucl. Sc. Vol. 15, pg. 1, 1965

[3] E. RAE, Physics and Chemistry of Fission, Vol. I, pg. 187, edited by I.A.E.A., Vienna, 1965

[4] M. ASGHAR et al. - Nucl. Phys. 76 (1966), 196

[5] D.J. HUGHES and R. SCHWARTZ, AEC-Report BNL-325, 1958, and J.R. STEHN et al. - AEC-Report BNL-325, 2d Edit., Vol. III, 1965

A SINGLE LEVEL ANALYSIS OF ^{233}U CROSS SECTIONS*

M. J. Schneider
Westinghouse Astronuclear Laboratory
Pittsburgh, Pennsylvania 15236

ABSTRACT

Experimental cross sections for neutrons on ^{233}U have been fitted with a single level Breit-Wigner least squares analysis from 0.4 to 61.4 eV. The total cross section measurements by Pattenden and Harvey, and the simultaneously measured capture and fission cross sections of Weston, et al., were used. All three cross sections were fit simultaneously. Doppler broadening and experimental resolution were accounted for by using an effective sample temperature greater than its actual temperature. Sixty-three resonances were found in this energy range, and with them the data can be well reproduced. Resonance curves, plots of alpha vs. energy, the resonance parameters, and brief statistical analyses of them are presented. Some disagreement is found between the present parameters and those recommended in BNL-325.

1. INTRODUCTION

This note describes a recent analysis of published experimental data on the $n + ^{233}U$ reaction. The low energy fission, capture, and total cross sections have been simultaneously fitted with a series of non-interfering Breit-Wigner resonances ("single level fit"). The fit was done from 0.4 to 61.4 eV, using the CDC-6600 computer and a fitting code, SPURS, written at Westinghouse Astronuclear Laboratory. The analysis was done on the following data:

From the SCISRS[1] data file, the results of the Pattenden and Harvey measurement[2,3,4] of the total cross section of ^{233}U were selected. The simultaneously measured capture and fission cross sections of Weston, et al.[6,7] were also used. These data were obtained directly from the experimenters at Oak Ridge National Laboratory. They not only represent the first simultaneous measurement of these two cross sections for ^{233}U, but also, one of the few measurements of its resonance capture cross section. Weston, et al. normalized their data to the total cross sections of Pattenden and Harvey, both in magnitude and in energy scale.

---

*The Nuclear Engine for Rocket Vehicle Application Program (NERVA) is administered by the Space Nuclear Propulsion Office, a joint office of the U.S. Atomic Energy Commission and the National Aeronautics and Space Administration. Aerojet-General Corporation as prime contractor for the engine system and Westinghouse Electric Corporation as subcontractor for the nuclear subsystem, are developing a nuclear propulsion system for deep space travel.

2. THE FITTING

The chief goal of the fitting was to compile a set of single level resonance parameters for ^{233}U. The fitting code does not have the power to add or subtract resonances, but only to juggle their parameters. The insertion of resonances thus represents a conscious decision on the part of the analyst. Resonances were inserted where they were known to exist from other analyses, or where there was some other indication that they were actually present. Resonances were not added solely because the fit disagreed with the experimental curve. It is believed that the largest of these disagreements, particularly in the fission curve, are caused by multilevel interference effects [8].

The statistical spin factor, g, was taken to be 1/2 for all resonances. On the recommendation of Moore and Simpson, [10] a constant potential scattering of 12.6 barns was assumed.

Other assumptions made in the fitting procedure were: (1) all neutrons have $\ell = 0$; (2) the fission and capture cross sections include no interference between resonances; (3) interference between potential and resonance scattering can be satisfactorily accounted for; (4) the sample nucleii have a Maxwellian velocity distribution, and thus Doppler broadening of resonance peaks may be included[9] ; (5) experimental resolution may be taken into account by defining an "effective temperature" of the sample, greater than its actual temperature[9].

The assumption that in the capture cross section no interference will be seen between resonances is justified theoretically[8], but for the fission cross section one does expect interference. The assumption is justified, then, by the accuracy with which the single level parameters can reproduce the actual cross section curves. It is felt that agreement between the two is close enough to be quite adequate for reactor applications.

The energy resolution of all measurements was a well known function of neutron energy. SPURS was designed so that for a given run, the fission and capture data could be given at one effective temperature, and the total cross section data at another. This is to allow for cases like these, where the fission and capture data have one resolution and the total cross section data another. The resolutions were averaged over each energy interval for which SPURS was run. Each interval was small enough to minimize the disagreement between the average and the extremes of resolution, but large enough so that SPURS could fit several resonances at one time.

The fitting code has provision for a relaxation factor on all parameters. For the i'th iteration, if the distance between experimental and calculated points is minimized by, e.g., $\Gamma_f^{(i+1)} = \Gamma_f(i) + \Delta\,\Gamma_f$, the code will take $\Gamma_f^{(i+1)} = \Gamma_f(i) + r\,\Delta\,\Gamma_f$, where r is the relaxation factor, inserted to prevent overshooting or rapid divergence: $0 < r \leq 1$. The code allows convergence to be checked after each iteration.

The code iterates on the parameters of up to seven resonances simultaneously and can fit data at 200 energy points in one run. The initial parameters for the n'th run are the final parameters of the n-1'th run. After each set of runs, calculated and experimental data points can be plotted with the CalComp plotter for comparison. The set of uns from .4 to 25 eV, with five iterations and data at 1425 energy points, took 1/2 hour Central Processor time on the CDC-6600.

The zero' th guess at the parameters of ^{233}U was taken from Stehn, et al.[14] (BNL-325). For the resonances for which BNL-325 gives no parameters, zero' th guesses were done by eye and usually needed more iterations than those resonances at which guesses were more educated.

SPURS gives the analyst the option of weighting the experimental data so that either the peaks or the valleys (or neither) in the resonance curve are given greater importance when fitting. The present work was done with inverse weighting, i.e. more importance was given to data in the valleys. This procedure can be justified by noting that with no weighting, the peaks would have greater importance, since a 20 percent error at high cross section values gives a greater contribution to the sum of the distances between experimental and calculated data points than a 20 percent error at low cross sections. Another argument in favor of inverse weighting is the fact that resolution errors lead to smaller absolute errors in the valleys, than in the peaks. Consequently, one would want to give more weight to valley data.

The fitting code was re-run for a group of resonances until either (1) it gave a good reproduction of the experimental curve, or (2) increments in all parameters were small ($\approx$1%), or perhaps (3) convergence couldn' t be improved with repeated iteration.

Careful attention was paid to the last increments in all parameters before iterating was stopped and the parameters were accepted as approved. All resonances for which any parameter failed to converge within 15 percent (i.e. in which the final increments were larger than 15 percent) were suspect. There were 39 resonances for which all parameters converged to within 15 percent of their final values. For 36 all parameters converged to within 5 percent.

3. RESULTS

3.1. Below 10 eV

The experimental data and fitted curves are shown in Figures 1 through 7. To correct for negative energy resonances, the code allows a 1/v correction term to be added to the resonance cross section so that, e.g.,

$$\sigma_{fis}(E) = \sigma^{res}_{fis}(E) + C^{corr}_{fis} \times \sqrt{\frac{.0253}{E}}$$

where

$$C^{corr}_{fis} = \sigma_{fis}(.0253) - \sigma^{res}_{fis}(.0253).$$

With the final fitted parameters, the 1/v corrections needed to bring the thermal cross section into agreement with the BNL-325 recommendations were

Fission: C^{f}_{corr} = 436.2 barns

Capture: C^{c}_{corr} = 33 barns.

The first area of sizable disagreement between curve and data points is in the region around 3 eV. The shape of the valley of the fission curve is not well reproduced by the present fit. This is presumed to be a multilevel interference effect, which would be expected in fission, but not in capture. The present fit has its poorest performance in minima, but Lynn[11] has shown that it is in the minima that interference effects can have their greatest relative influence. It is also possible that the approximation of a 1/v correction to account for negative energy resonances may be contributing to errors in the valleys.

For the 1.55 eV resonance, which is overshadowed by the stronger 1.78 eV peak, parameterization is much more difficult. This is one resonance for which disagreement with the accepted parameters is greater than 50 percent. It is possible that interference is playing a role here even though the present parameters reproduce the data well.

In an attempt to come closer to reproducing the height of the peak at 3.6 eV, it was fitted with two closely spaced resonances. The results were not as good as with one resonance and the attempt was abandoned. The peak at 4.7 eV was fitted under the assumption that it was due to two resonances. The general shape of the peak has been fairly well reproduced, but when iterating was stopped, the final change in the most poorly converged parameter of these two resonances was 31 percent. Another disagreement between the present work and other parameter sets is seen for this peak at 4.8 eV, which was attributed to two resonances, due to its irregular contour. Some of the area thus has been given to a smaller resonance and the parameters of the larger one have been sharply altered. For the resonances at 8.75 and 9.30 eV, it appears that interference effects play a large role and the present parameters vary widely from other determinations.

3.2. 10-30 eV

The Oak Ridge capture data show a prominent peak at 11.8 eV, but this peak appears neither in the fission curve nor in the total curve. The experimenters at Oak Ridge have concluded [12] that this peak is probably due to some impurity associated with the aluminum backing in the fission chamber. It should be mentioned, however, that Nifenecker did use a small resonance in this region in his analysis of the fission cross section [13].

In the 10-30 eV region, the present fit again does not get all the way down into the deepest valleys in the fission and total cross section data, presumably for the reasons mentioned above. A resonance was added at ~13.5 eV because of a definite bump in the fission curve adjacent to the 13.8 eV peak. This led to large variation from the generally recommended parameters for the bigger resonance. The resonance at 26.5 eV did not converge too well. The worst of its parameters had final increment 40 percent. All other resonances from 12.7 to 32 eV converged to within 10 percent.

3.3. 30-60 eV

Above 30 eV the total cross section data are of poorer resolution, but are still useful. Individual points of the capture cross section data frequently fall below zero in this region (but not below -2 barns). The fluctuations of the capture data get worse also. Only the fission data remain sharp. In one instance, an attempt was made to do a double fit on the fission and total data only, ignoring the measured capture cross section. The attempt was halted, however, when the resulting parameters gave capture cross sections that were in clear disagreement with the measurements. Confidence was retained in the data because the disagreement was not violent. Moreover, the necessity for using all three cross sections was emphasized (assuming one has faith in them).

One would hope that the use of an effective temperature to account for the poor resolution of the total data, and the application of a least squares fit in counteracting the fluctuations of the capture data, would have led to parameters in which one could have confidence. Such was not the case. All resonances between 32.5 and 42.5 eV have parameters which failed to converge to within 15 percent of their final values. Although the present parameters in this range have less confidence attached to them, they reproduce moderately well the fission and total data input.

There are troublesome places where several resonances overlap closely; the region between 32.8 and 34.5 eV was fitted with three resonances. Between 39 and 41 eV, the experimental fission data form a flat plateau which was fitted with four resonances. The breakdown of Breit-Wigner theory for closely spaced resonances [8] hindered the fit here. The present parameters can reproduce the data well, particularly for fission. Whether they reflect the actual physical situation is open to doubt. Parameters of the 63 resonances that were found for ^{233}U are listed in Table 1 along with an indication of the degree of reliability of the parameters for each resonance. In addition, the present parameters are compared with those recommended in BNL-325 [14]. There have been mentioned several instances where the disagreements are greater than 50 percent.

If the fitted alpha (capture ÷ fission) curve is plotted on top of the experimental points, agreement between the two is good except where the fit does not reach the valleys of the fission curve. At higher energies, the alpha points scatter widely, reflecting the fluctuations of the capture data.

3.4. Parameter Statistics

Some brief calculations were done to see how the present fission, capture, and reduced neutron width distributions compare with Porter-Thomas [5] predictions. The results are shown in Figures 5 through 7. Distributions were made for all 64 resonances (including the 11.8 eV peak later discarded).

Porter and Thomas found that the reduced neutron widths obey a χ^2 distribution with $\nu = 1$:

$$P(x, \nu)dx = \frac{1}{\sqrt{2\pi x}} e^{-1/2x} dx \text{ for } \nu = 1 \text{ where } x = \frac{\Gamma_n^o}{\langle \Gamma_n^o \rangle} .$$

Figure 5 shows that the present 64 Γ_n^o's obey a distribution with $\nu = 2$. From this distribution one may conclude that this analysis has missed a number of resonances, as is typical of this sort of fit. If the convergence criterion is imposed, the 39 most reliable Γ_n^o's obey a distribution with $\nu = 3$, showing that resonances with small Γ_n^o have less reliable parameters.

Very small resonances, those in the wings of others, and those that are closely spaced and tend to join are the most likely to be obscured in the resonance curve, and thus missed in the fit [15]. The relative magnitudes of Γ_n, Γ_f, and Γ_c for ^{233}U are such that (a) The height of the capture curve at resonance is proportional to Γ_n and Γ_c, but (b) the height of the fission curve at resonance is proportional to Γ_n/Γ_f. Resonances tend to join as Γ_f/D increases, where D is the resonance spacing. Since all three causes of missed resonances lead to omission of those with large Γ_f, it is expected that the present distribution of Γ_f (fig. 6) has ν smaller than it really should be.

Figure 7 shows the capture width distribution for 64 resonances. It is seen that this distribution does not follow a χ^2 curve for any value of ν. The spread of capture widths contrasts with the Γ_c = constant assumption of other workers [13, 16].

It is felt that the results of this analysis should benefit reactor calculations, and that the simultaneous measurement and simultaneous triple fit processes provide important insights into ^{233}U cross sections and resonance parameters.

4. REFERENCES

1. J. M. Friedman and M. Platt, "SCISRS Sigma Center Information Storage and Retrieval System", Brookhaven National Laboratory, BNL-883(T-357) (July, 1964).

2. N. J. Pattenden and J. A. Harvey, "The Resonance Energy Cross Section of U^{233}", Proceedings of the International Conference on Nuclear Structure, 882 (1960).

3. N. J. Pattenden and J. A. Harvey, Nuclear Science and Engineering 17, 404 (1963).

4. N. J. Pattenden and J. A. Harvey, "Tabulation of the Neutron Total Cross Section of U^{233} from 0.07 to 10,000 eV Measured with the ORNL Fast Chopper", Oak Ridge National Laboratory, ORNL-TM-556 (April, 1963).

5. C. E. Porter and R. G. Thomas, Physical Review 104, 483 (1956).

6. L. W. Weston, et. al., "Measurement of the Neutron Fission and Capture Cross Sections for ^{233}U in the Energy Region 0.4 to 1000 eV", Oak Ridge National Laboratory, ORNL-TM-1751 (April, 1967).

7. G. deSaussure, et. al., "Measurement of the Neutron Capture and Fission Cross Sections and of their Ratio Alpha for ^{233}U, ^{235}U and ^{239}Pu", Proceedings of the IAEA Conference on Nuclear Data for Reactors, International Atomic Energy Agency (1966), Vol. II, p. 233.

8. E. Vogt, Physical Review 112, 203 (1958).

9. D. W. Drawbaugh and G. Gibson, "Preparation of Microscopic Cross Sections of U^{235} for Reactor Calculations", Conference on Neutron Cross Section Technology, U.S.A.E.C., CONF 660303 (1966), Vol. II, p. 939.

10. M. S. Moore and F. B. Simpson, Nuclear Science and Engineering 13, 18 (1962).

11. J. E. Lynn, "Quasi-Resonances and the Channel Theory of Neutron-Induced Fission", Proceedings of the International Conference on the Study of Nuclear Structure with Neutrons, North Holland Publishing Company (1966), p. 125.

12. G. deSaussure, Private Communication.

13. H. Nifenecker, LeJournal de Physique 25, 877 (1964).

14. J. R. Stehn, et. al., "Neutron Cross Sections", Brookhaven National Laboratory, BNL-325, 1965 2nd ed., Suppl. 2, Vol. III p. 92-233-1.

15. J. J. Schmidt, Resonance Properties of the Main Fertile and Fissionable Nucleii", Reactor Physics in the Resonance and Thermal Regions, Proceedings of the National Topical Meeting of the American Nuclear Society, San Diego, February 7, 1966, M.I.T. Press (1966).

16. D.W. Bergen and M.G. Silbert, Physical Review 166, 1178 (1968).

TABLE I

RESULTS OF PRESENT WORK AND COMPARISON WITH PARAMETERS RECOMMENDED IN BNL-325

E_o (eV)			$2g\Gamma_n \times 10^5$ (eV)		$\Gamma_c \times 10^3$ (eV)		$\Gamma_f \times 10^3$ (eV)	
BNL-325	This Work	Quality of Fit	BNL-325	This Work	BNL-325	This Work	BNL-325	This Work
.17	.17	d	.02	.02	40.	40.0	60.	60.
1.55	1.453	a	17.	7.64*	50.	24.9	600.	432.
1.78	1.786	a	31.	34.2	40.	49.2	220.	222.
2.30	2.284	a	18.	17.6	40.	39.9	46.	49.9
3.66	3.62	a	14.1	10.9	53.	38.6	180.	130.
4.81	4.662	c	28.	10.9	70.	2.36*	800.	463.
-	4.981	c	-	5.46	-	12.8	-	372.
5.95	5.89	a	15.	16.7	80.	42.9	300.	389.
-	6.577	a	-	19.0	-	28.3	-	322.
6.82	6.797	a	89.	75.6	53.	36.3	140.	99.8
7.60	7.466	c	4.1	1.36*	48.	30.0	150.	48.4*
8.75	8.662	c	6.	.83*	40.	7.18	500.	29.2*
9.30	9.276	c	11.	9.87	50.	37.7	200.	225.
10.45	10.347	a	155.	158.	80.	45.1	260.	243.
11.5	11.244	a	20.	22.5	(45.)	20.5*	350.	460.
12.9	12.747	a	140.	139.	(45.)	39.2	260.	286.
13.8	13.501	b	41.	10.2*	(45.)	56.8	320.	113.*
-	13.709	a	-	15.8	-	11.4	-	114.
15.5	15.344	a	90.	82.4	(45.)	51.9	170.	121.
16.4	16.125	a	120.	70.3	(45.)	27.6	600.	329.
16.7	16.495	a	41.	60.6	(45.)	30.8	100.	127.
18.1	17.926	a	30.	20.0	(45.)	26.9	160.	82.8
18.6	18.394	a	17.	16.2	(45.)	52.9	120.	183.
19.1	18.908	a	170.	167.	(45.)	45.0	270.	256.
20.8	20.542	a	110.	83.9	(45.)	56.7	420.	336.
22.1	21.783	a	90.	103.	(45.)	50.4	180.	184.
22.5	22.267	a	330.	375.	(45.)	47.4	370.	452.
24.	23.692	a	100.	93.0	(45.)	23.3	600.	915.
25.5	25.228	c	100.	84.5	(45.)	41.4	330.	333.
26.0					(45.)			
27.0	26.488	c	-	69.1	(45.)	55.1	-	567.
-	28.205	a	-	70.9	-	70.4	-	762.
29.2	28.974	a	160.	118.	(45.)	20.0*	460.	379.
-	29.450	a	-	12.3	-	33.7	-	86.1
31.2	30.648	a	80.	60.6	(45.)	46.4	400.	265.
-	31.391	b	-	44.4	-	8.60	-	497.
32.3	31.918	a	110.	94.7	(45.)	40.3	200.	204.
-	32.914	c	-	20.1	-	59.5	-	302.

TABLE I - Cont'd.

E_o (eV)			$2g\,\Gamma_n \times 10^5$ (eV)		$\Gamma_c \times 10^3$ (eV)		$\Gamma_f \times 10^3$ (eV)	
BNL-325	This Work	Quality of Fit	BNL-325	This Work	BNL-325	This Work	BNL-325	This Work
-	33.260	c	-	37.6	-	4.28	-	802.
34.9	34.274	c	170.	274.	(45.)	5.49*	700.	1264.
-	35.357	c	-	27.6	-	.101	-	572.
-	35.936	c	-	14.7	-	82.6	-	262.
37.1	36.450	c	90.	71.5	(45.)	40.1	270.	130.*
38.0	37.352	c		47.1	(45.)	18.5		239.
-	39.164	c	-	26.0	-	13.2	-	241.
40.2	39.673	c	-	48.5	-	3.83	-	470.
-	40.363	c	-	70.6	-	36.7	-	651.
41.3	40.944	c	-	26.8	-	32.1	-	91.1
43.2	42.516	c	-	66.6	-	37.7	-	168.
44.2	43.397	a	-	18.5	-	10.9	-	65.5
-	44.420	c	-	7.76	-	.035	-	266.
47.1	46.018	a	-	35.6	-	53.7	-	95.6
47.9	47.097	a	-	55.4	-	18.2	-	281.
49.3	48.601	a	-	205.	-	78.1	-	177.
-	50.308	c	-	41.5	-	2.13	-	700.
51.4	50.853	c	-	4.30	-	.902	-	141.
-	51.854	e	-	.07	-	.0005	-	1.04
54.0	53.032	a	-	58.5	-	14.1	-	213.
-	53.950	a	-	148.	-	51.0	-	486.
55.2	54.683	a	-	104.	-	33.9	-	204.
57.0	56.130	a	-	456.	-	70.8	-	975.
58.3	57.436	a	-	268.	-	18.1	-	787.
-	58.384	a	-	90.1	-	25.0	-	321.
-	61.300	b	-	214.	-	79.7	-	712.

* = difference greater than 50 percent.
() = assumed to be so by experimenter.
a = good fit, converged to within 5 percent.
b = good fit, converged to within 15 percent.
c = poor convergence, but experimental data reproduced satisfactorily.
d = not fit, parameters taken from BNL-325.
e = poor convergence, data poorly reproduced.

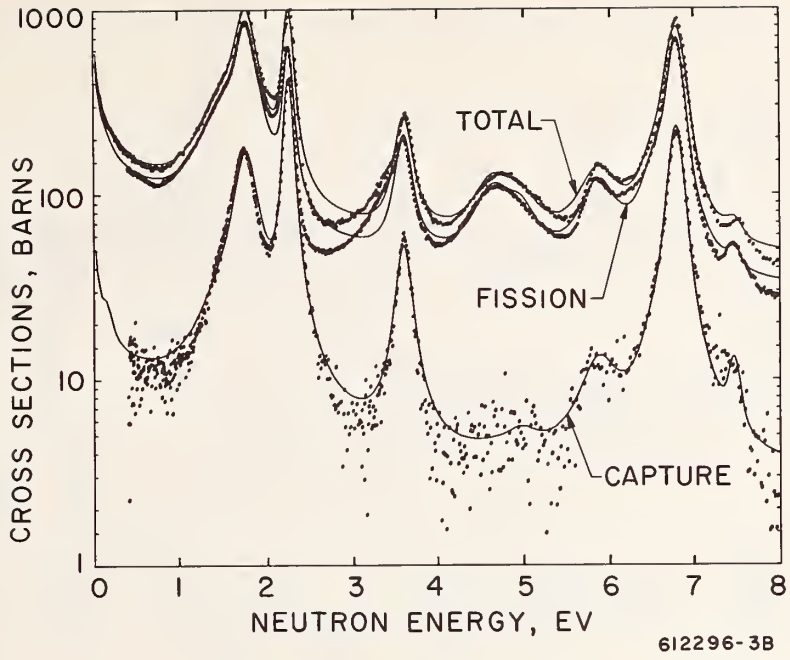

Figure 1. Experimental data and fitted curves for the fission, capture and total cross sections of ^{233}U from 0 to 8 eV.

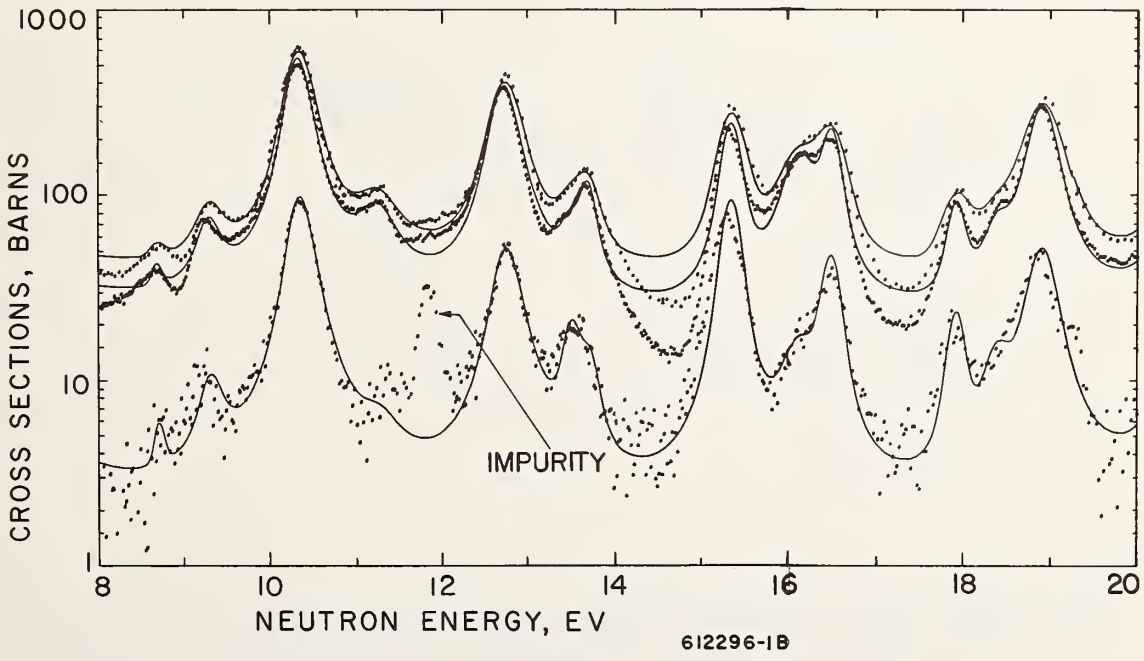

Figure 2. Experimental data and fitted curves for ^{233}U cross sections from 8 to 20 eV.

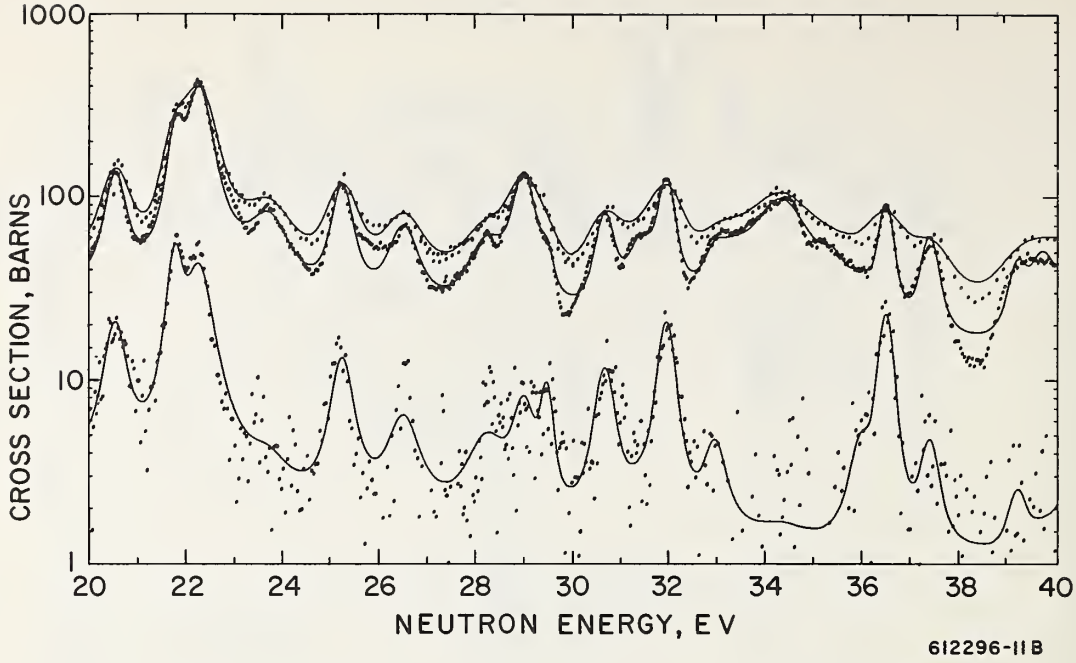

Figure 3. Experimental data and fitted curves for ^{233}U cross sections from 20 to 40 eV.

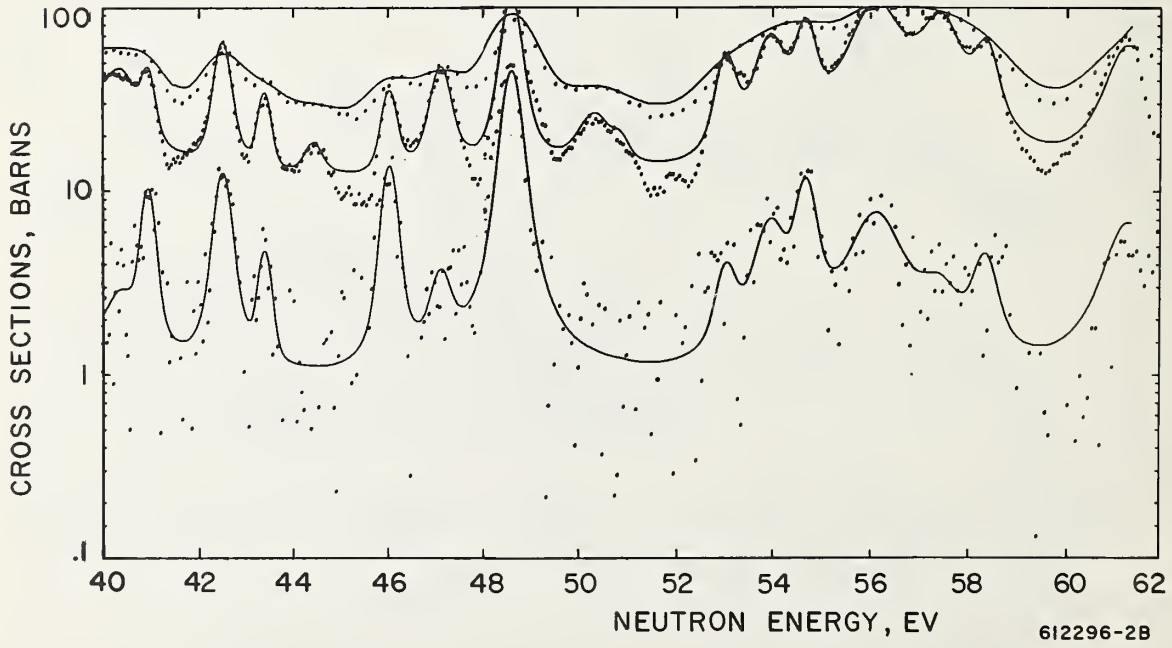

Figure 4. Experimental data and fitted curves for ^{233}U cross sections from 40 to 62 eV.

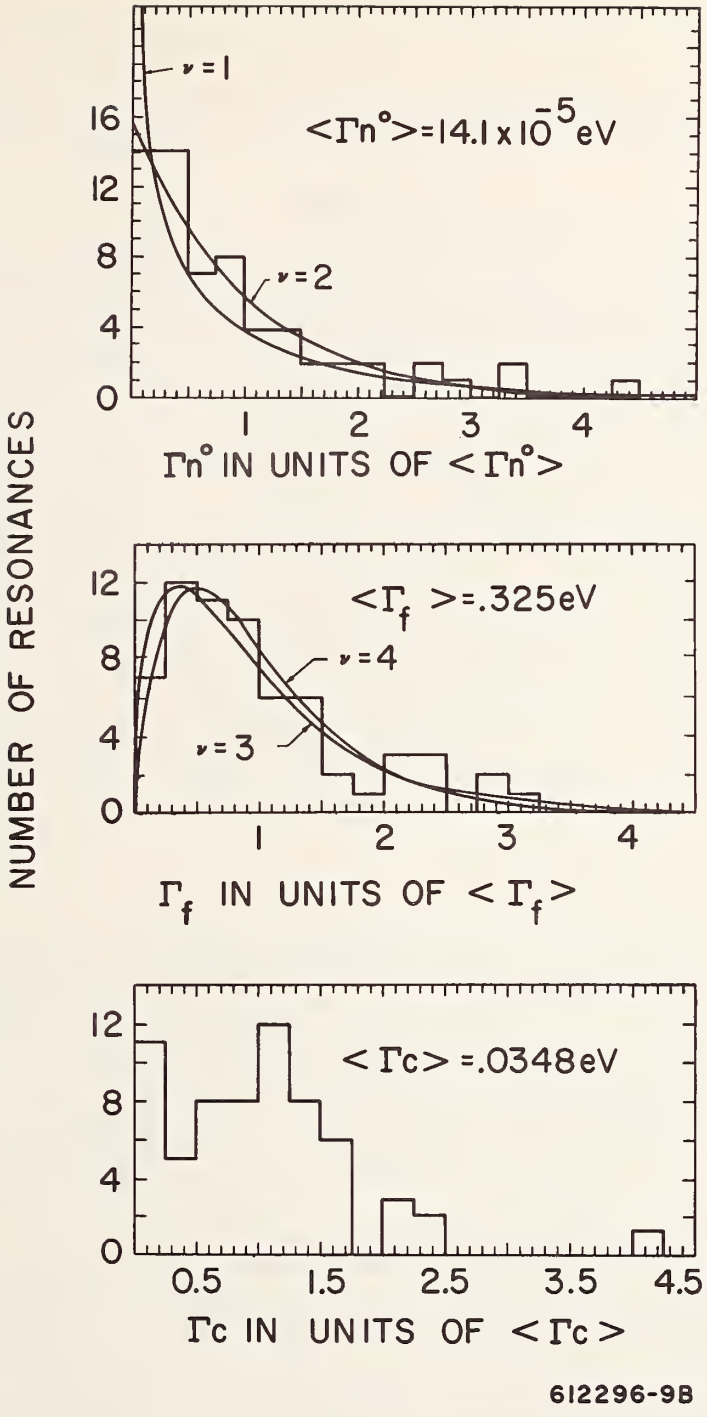

Top: Figure 5. Reduced neutron width distribution for ^{233}U--64 resonances.
Middle: Figure 6. Fission width distribution for ^{233}U--64 resonances.
Bottom: Figure 7. Capture width distribution for ^{233}U--64 resonances.

Relative Fission Cross Sections of ^{236}U, ^{238}U, ^{237}Np, and ^{235}U*

W. E. Stein, R. K. Smith, and H. L. Smith, University of California, Los Alamos Scientific Laboratory, Los Alamos, New Mexico 87544

Abstract

Fission cross-section ratios $^{236}U/^{235}U$, $^{238}U/^{235}U$, and $^{237}Np/^{235}U$ have been measured with pulsed, monoenergetic neutrons in the energy range 1.0 to 5.0 MeV with time-of-flight background discrimination. Vacuum evaporated fissile deposits (~ 0.5 mg/cm^2) were placed back to back between two 9.5 cm^2 surface barrier detectors. Slow and fast output signals were obtained simultaneously from each detector by means of separate electronic systems. Slow, linear pulses which exceeded a lower bound set to reject alpha particles were identified as fission events. The fraction of fragment pulses below this bias, determined from an extrapolation of the pulse-height spectrum, was ~ 1.2%. Only those fission events which occurred during and a few nanoseconds after the neutron burst were recorded. This time interval, determined by the measured time resolution (1.3 nsec FWHM) and the time walk of the smallest pulses (~ 2 nsec), was typically 6 nsec. Fission events induced by scattered neutrons which occur at later times were excluded. Characteristics of this detector system and preliminary data were reported earlier [1]. Present results include additional data on $^{238}U/^{235}U$ and $^{237}Np/^{235}U$ and new data on $^{236}U/^{235}U$.

1. Introduction

Accurate values of neutron induced fission cross sections of ^{236}U, ^{238}U and ^{237}Np relative to that of ^{235}U are of considerable importance in the calculation and evaluation of the performance of nuclear chain reacting systems. Relative fission cross sections of these isotopes are used as spectral indices in the measurement of neutron spectra in critical assemblies. They also provide a check on the credibility of available absolute fission cross sections. In addition the isotopes ^{238}U and ^{235}U are possible major constituents of a nuclear reactor.

Relative values obtained from published cross sections lack the precision presently required. In many cases discrepancies of 10-15% exist between various sets of experimental data. There are comparable disagreements in the dependence of relative cross sections on neutron energy.

The present experiment was initiated to provide more accurate values of the desired relative cross sections in the neutron energy range of 1.0 to 5.0 MeV. Since a description of the method and preliminary data have been presented earlier [1], emphasis in this paper will be placed on the presentation of new data and on the evaluation of various sources of error associated with these measurements. The latter effort not only provides

*Work performed under the auspices of the U. S. Atomic Energy Commission

the uncertainties assigned to the present data, but also indicates where improvements can be made in future measurements.

2. Experimental Method and Apparatus

The experiment consisted of counting fission fragments emitted by each of two known masses of fissile deposits placed back-to-back and irradiated with pulses of monoenergetic neutrons. Neutron bursts of approximately one nanosecond duration and repetition rate of 2×10^6 pulses/sec were obtained from the Los Alamos electrostatic accelerator, Mobley buncher, and the $T(p,n)^3He$ reaction.

Fissile deposits were prepared by vacuum evaporation of the oxide compounds onto 5×10^{-3} inch thick, 1.875 inch diameter platinum disks. Deposits were one inch diameter and ranged in thickness from 0.5 to 0.7 mg/cm^2. Details of preparation and assay of these fissile sources have been presented by H. L. Smith and J. P. Balagna [2].

Fission fragments were detected and recorded by means of 9.5 cm^2 surface barrier detectors [3] and a fast-slow electronic system. Slow, linear pulses with amplitudes above a lower bound which was set to reject alpha particles were identified as fission fragment pulses. The fraction of fragment pulses below this bias, determined from an extrapolation of the pulse-height spectrum, was 1.2% with a maximum deviation of ± 0.5%. Only those fission events which occurred during and a few nanoseconds after the neutron burst were recorded. Fissions induced by scattered neutrons which traversed a longer flight path and reached the detector at later times were rejected.

Details of the detector characteristics and estimates of the background eliminated by fast timing have been previously presented [1]. Briefly stated, measurements with this relatively low mass detector indicate that the background correction for $^{238}U/^{235}U$ at 2.5 MeV would be about 3 to 5%. This background is expected to vary with accelerator operating conditions, neutron energy, and even the configuration of other nearby equipment. It is therefore advantageous to eliminate by fast timing the extraneous counts that actually exist during each particular cross section measurement, rather than to make corrections based on an independent set of background measurements.

3. Measurements

3.1. Procedure

The detector was positioned approximately 8.5 cm from the center of the tritium target with the centers of the fissile deposits on the proton beam axis. Detector efficiencies were determined from the ratio of the measured alpha particle rate and the known disintegration rate of the

fissile deposit. Fission counts from each detector were recorded for a particular neutron energy and specified integrated accelerator current. A number of runs was made for each detector orientation. Typical pulse-height and time spectra from each surface barrier detector were recorded for both orientations.

Each of the recorded counts was corrected for the extrapolation to zero pulse height, proper time interval, separation of the fissile deposits, detector efficiency, and center of mass motion coupled with fragment anisotropy. For each run the ratio of corrected counts was computed and a preliminary cross-section ratio was obtained by including the ratio of fissile deposit masses and the ratio of atomic weights. These provisional cross-section ratios were further corrected for the attenuation of the neutron flux in the platinum backings and for inelastic neutron scattering in the region of the detector not excluded by timing. For each neutron energy the statistically weighted average of the cross-section ratio was obtained for each detector orientation. The final relative cross section was found from an average of these values for the two detector orientations. It is to be noted that, if statistically comparable data were obtained for each orientation, the corrections for foil separation and neutron attenuation would cancel in the final average.

3.2. Discussion of Errors

The uncertainties assigned to these results were separated into two categories. First, relative or point-to-point errors have been evaluated in order to define the shape or dependence of the relative cross sections on neutron energy. Table I gives the quantities or corrections which have been considered in the determination of these uncertainties. The values listed are the estimated standard errors in percent of the final cross-section ratio. The second class of uncertainties are those which contribute to the absolute error. These have been evaluated and are listed in a similar format in Table II.

Errors associated with items marked † could be reduced possibly a factor of two in future measurements by providing sufficient counting time, thinner fissile deposits, and improved data recording techniques. Uncertainties assigned to the center of mass-anisotropy and inelastic scattering corrections were derived from the errors associated with the data used to obtain these corrections. Whenever possible similar sets of data taken at different times were carefully compared for both shape and absolute value. The consistency items in both tables reflect a generous estimate of the discrepancies between various sets of similar data.

3.3. Results and Discussion

The measured relative fission cross sections $^{236}U/^{235}U$, $^{238}U/^{235}U$, and $^{237}Np/^{235}U$ are listed in Table III and shown in Figs. 1-3. The

associated uncertainties shown in these figures are relative standard errors. Absolute or overall errors which include for example uncertainties in the masses of the fissile deposits (see Table II) are estimated to be 2.2% for $^{236}U/^{235}U$ and $^{238}U/^{235}U$, and 2.6% for $^{237}Np/^{235}U$.

The present results for $^{236}U/^{235}U$ are shown as solid circles in Fig. 1. Open circles are the data from Table II of Lamphere [4] for which an estimated absolute error of 1.5% was assigned. Since these two sets of data differ consistently by about 5% over the entire energy range common to both experiments, there appears to be a real disagreement between these two experiments.

Results from this experiment for $^{238}U/^{235}U$ along with the data of Lamphere [4], Jarvis [5], and Smith, Henkel, and Nobles [6] are shown in Fig. 2. Again the data of Lamphere are consistently higher than the present results. In this case the discrepancy varies from about 6% at the lower energies to about 8% near 3.0 MeV. The square at 2.5 MeV represents the value of 0.425 ± 1.5% reported by Jarvis. Ratios formed from the results of Smith, Henkel, and Nobles which have been corrected recently for neutron scattering are also shown in Fig. 2 by the symbol x. Excellent agreement is found between the results of this experiment and the values of Jarvis and Smith, et al.

$^{237}Np/^{235}U$ results from this experiment are given in Fig. 3. Comparison data are not shown in this figure. Ratios formed from the data of Henkel [7], which are the results most often quoted for this energy range, are consistently lower than the present values by about 13%. If however the cross-section ratios for $^{237}Np/^{238}U$ are computed from the results of this experiment, a direct comparison can be made with the measurements of Schmitt and Murray [8]. Within the errors assigned to both measurements and in the energy region common to these two experiments, good agreement is found in such a comparison.

The authors are indebted to J. G. Povelites for the preparation of the fissile deposits, to G. E. Hansen and J. A. Grundl for the evaluation of most of the corrections used in this work, and to the operating personnel of the Van de Graaff accelerator.

4. References

[1] W. E. Stein, R. K. Smith, and J. A. Grundl, Proceedings of the Conference on Neutron Cross Section Technology, Washington, D.C., March 1966.

[2] H. L. Smith and J. P. Balagna, ibid.

[3] Oak Ridge Technical Enterprises Corporation, Oak Ridge, Tenn.

[4] R. W. Lamphere, Phys. Rev. 104, 1654 (1956).

[5] G. A. Jarvis, USAEC Report LA-1571, Los Alamos Scientific Laboratory, July 1953.

[6] R. K. Smith, R. L. Henkel, and R. A. Nobles, Bull. Am Phys. Soc. 2, 196 (1957).

[7] R. L. Henkel, USAEC Report LA-2122, Los Alamos Scientific Laboratory, June 1957.

[8] H. W. Schmitt and R. B. Murray, Phys. Rev. 116, 1575 (1959).

TABLE I. Quantities or corrections considered in the evaluation of the relative standard errors. Values listed are in percent of the final cross-section ratio.

Item	$^{236}U/^{235}U$	$^{238}U/^{235}U$	$^{237}Np/^{235}U$
Statistics (typical)†	0.5	0.5	0.4
Relative time interval†	0.3	0.3	0.3
Center of mass and anisotropy	0.3	0.4	0.3
Inelastic Neutron scattering	0.4	0.5	0.3
Relative consistency	0.5	0.5	0.6
Total relative standard error (typical)	0.9	1.0	0.9

Table II. Quantities or corrections considered in the evaluation of the absolute standard errors. Values listed are in percent of the final cross-section ratio.

Item	$^{236}U/^{235}U$	$^{238}U/^{235}U$	$^{237}Np/^{235}U$
Relative errors	0.9	1.0	0.9
Pulse-height extrapolation†	0.6	0.6	0.6
Absolute time interval†	0.4	0.4	0.4
Ratio of detector efficiencies†	0.8	0.6	1.7
Isotopic abundance	0.1	0.1	0.1
Absolute consistency	0.6	0.6	0.6
Subtotal of absolute standard error (typical)	1.5	1.5	2.1
Ratio of fissile deposit masses	1.5	1.5	1.5
Total absolute error	2.2	2.2	2.6

†See section 3B of text.

Table III. Relative fission cross sections. Uncertainties are relative standard errors.

Energy(MeV)	$^{236}U/^{235}U$	$^{238}U/^{235}U$	$^{237}Np/^{235}U$
1.00	0.271 ± 0.005	---	1.21 ± 0.01
1.25	0.465 ± 0.007	---	---
1.50	0.527 ± 0.005	0.220 ± 0.003	1.28 ± 0.01
1.75	---	---	1.30 ± 0.01
2.00	0.596 ± 0.005	0.403 ± 0.004	1.31 ± 0.01
2.25	0.639 ± 0.006	0.415 ± 0.004	1.32 ± 0.01
2.50	0.666 ± 0.006	0.417 ± 0.004	1.33 ± 0.01
2.75	0.666 ± 0.006	0.418 ± 0.004	1.35 ± 0.01
3.00	0.681 ± 0.006	0.422 ± 0.004	1.35 ± 0.01
3.25	0.696 ± 0.006	0.432 ± 0.005	1.36 ± 0.01
3.50	0.717 ± 0.006	0.452 ± 0.005	1.36 ± 0.01
3.75	0.729 ± 0.007	0.465 ± 0.005	---
4.00	0.735 ± 0.007	0.474 ± 0.004	1.35 ± 0.01
4.25	0.743 ± 0.006	0.478 ± 0.005	---
4.50	0.759 ± 0.007	0.489 ± 0.006	1.38 ± 0.01
4.75	0.750 ± 0.007	0.487 ± 0.005	---
5.00	0.750 ± 0.007	0.481 ± 0.005	---

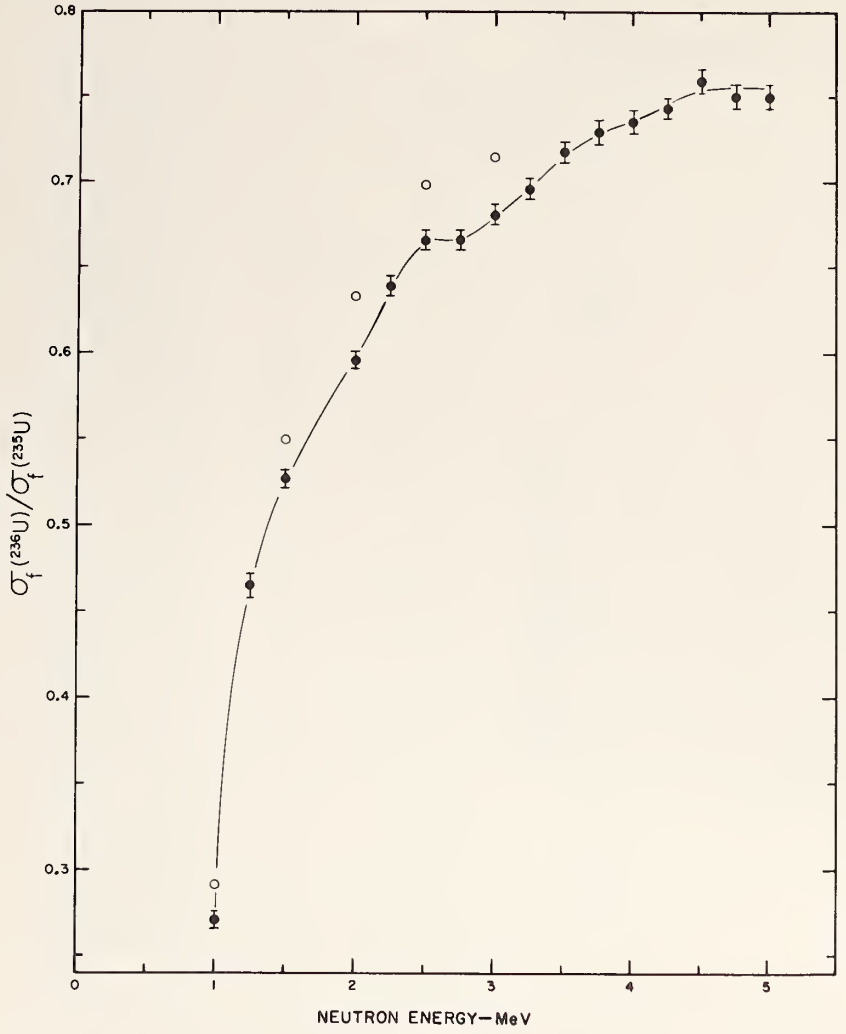

Fig. 1. $\sigma_f(^{236}U)/\sigma_f(^{235}U)$ vs neutron energy. Open circles are data of Lamphere [4]. Solid points are the results of this experiment. Uncertainties are relative standard errors.

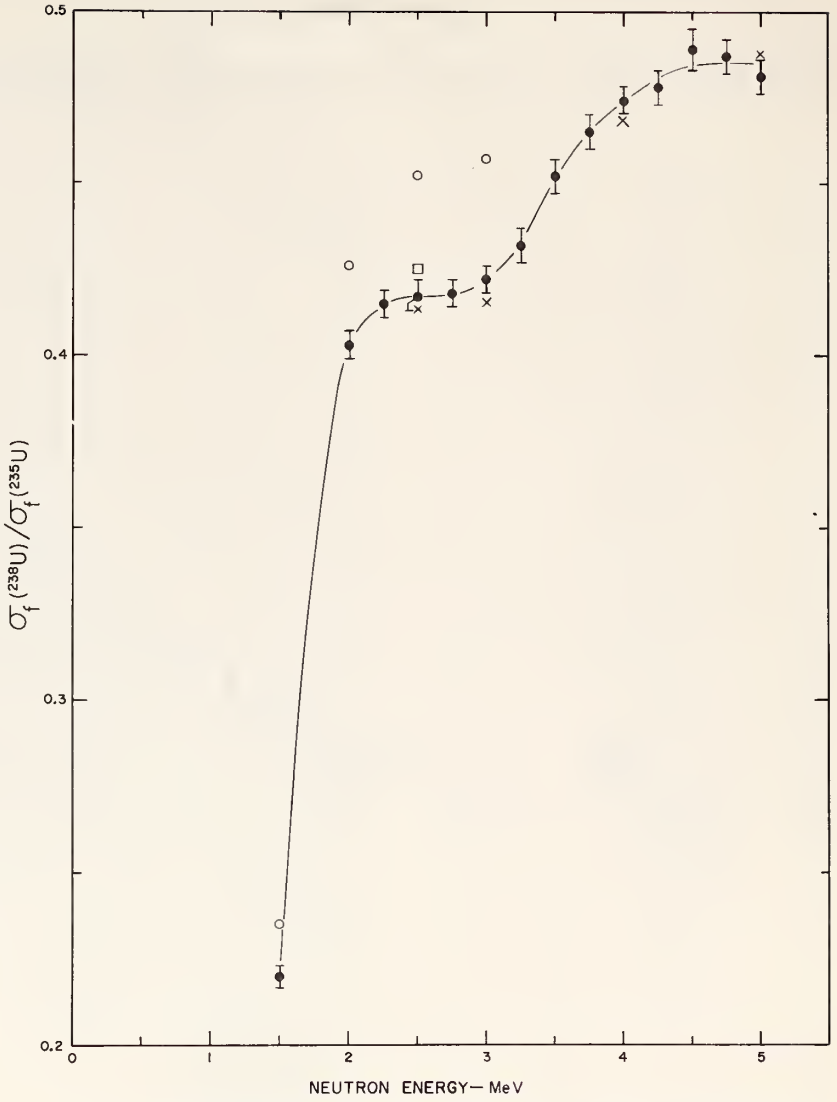

Fig. 2. $\sigma_f(^{238}U)/\sigma_f(^{235}U)$ vs neutron energy. Symbols are as follows: open circles, Lamphere [4]; square, Jarvis [5]; x, Smith, Henkel, and Nobles [6] corrected for neutron scattering; and solid circles, results of this work. Uncertainties are relative standard errors.

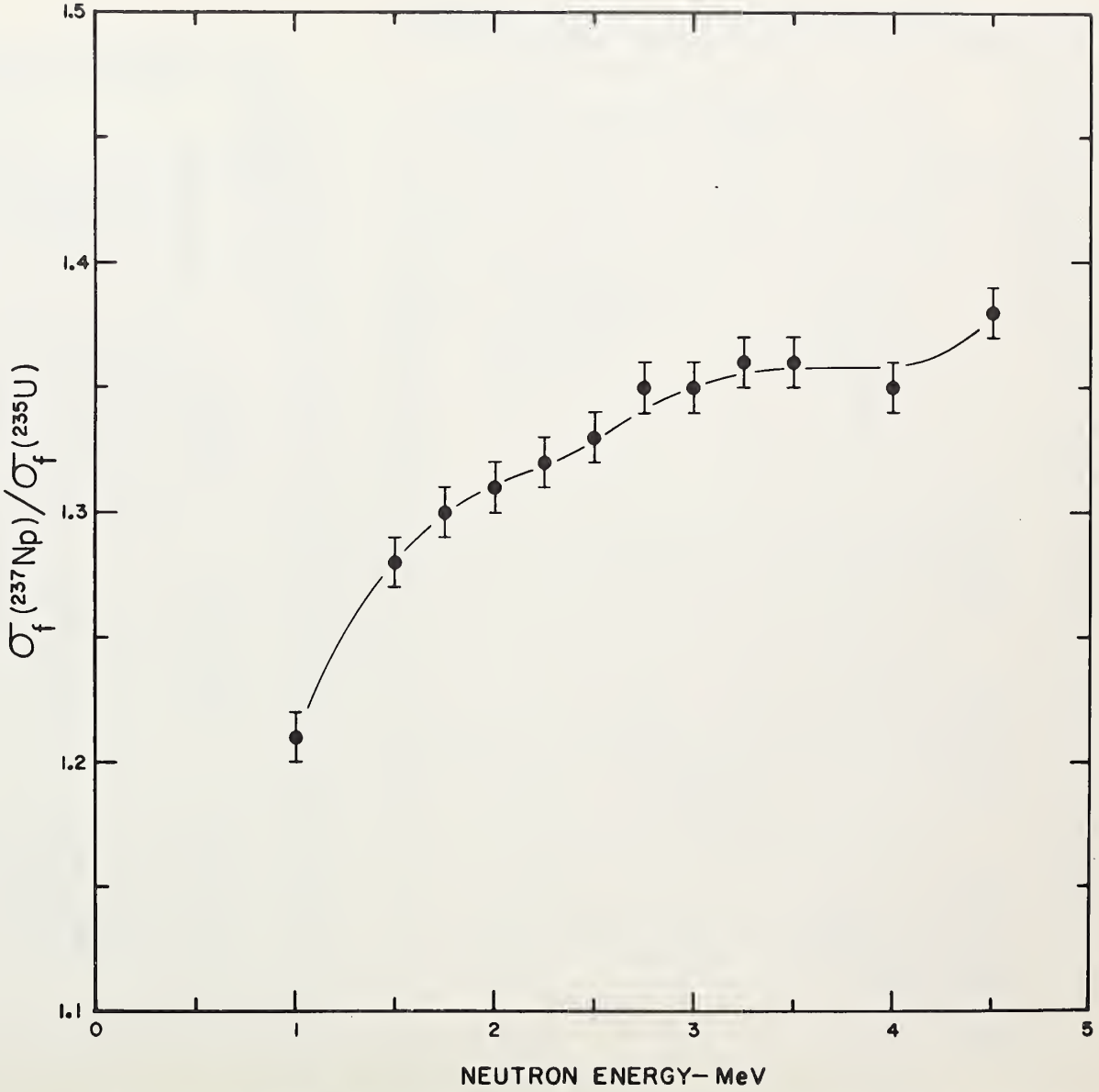

Fig. 3. $\sigma_f(^{237}Np)/\sigma_f(^{235}U)$ vs neutron energy. Solid circles are the results of this work with relative standard errors.

LOW ENERGY U-235 $\bar{\nu}$ MEASUREMENTS*

S. Weinstein+ and R. C. Block

Division of Nuclear Engineering and Science
Rensselaer Polytechnic Institute
Troy, New York 12180

A method has been developed for high resolution measurements of the variation of $\bar{\nu}$ with incident neutron energy. The system utilizes the Rensselaer LINAC as a source of neutrons, a multiplate ionization chamber to detect fission fragments, and a 0.75 meter gadolinium-loaded liquid scintillation tank to detect the prompt fission neutrons. The data is processed and stored in a PDP-7 on-line computer, with up to 12 values of multiplicity allowed for both fission and background events associated with each time-of-flight channel. For the energy region from 0.012 eV to 40.0 eV we have found that, to within 0.25%, the values of $\bar{\nu}$ for U-235 do not differ from the value at 0.0253 eV.

*Work supported by the U. S. Atomic Energy Commission under Contract AT(30-3)328.

+In partial fulfillment of S. Weinstein's doctoral thesis.

1. INTRODUCTION

The prediction of both criticality and breeding ratio in reactors depends upon the energy dependence of eta, the number of fission neutrons emitted per neutron captured in the fissile nuclide. Since

$$\text{eta} = \frac{\bar{\nu}}{1+\alpha} \qquad \text{where} \qquad \alpha \equiv \left[\sigma_c/\sigma_f\right] \quad \text{fissile}$$

it is usually assumed that the energy variation in eta is primarily a reflection of the variation in α, and that the value of $\bar{\nu}$ is a very slowly varying linear or quadratic function of the energy of the neutron that induced the fission. Questions about the adequacy of the latter assumption for the resolved resonance region can be raised as a result of recent experiments involving the energy dependence of fission fragment kinetic energies,[1,2] and of fission mass yields.[3,4] The experiment that is being reported here has as its objective the determination of the energy dependence of $\bar{\nu}$ for U-235 to an overall accuracy of about 0.25% for the major resonances below 40 eV and over the range from 1.0 eV to 0.01 eV.

2. EXPERIMENTAL ARRANGEMENT

Figure 1 is a sketch of the major components of the experiment. The neutron pulse is produced in a water-cooled tantalum target by the electron pulse from the RPI LINAC, and is partially moderated and reflected toward the detector by a 1.0 in. polyethylene disk (M). The neutrons travel approximately 25 meters to the detector through an evacuated flight tube. The detector (FC) is a 28 plate fission ionization chamber containing 4.5 grams of very pure (99.9%) U-235. The chamber is situated at the center of the flight tube of a 0.70 meter diameter scintillation tank. Both the fission chamber and the tank are on loan by the Oak Ridge National Laboratory. The liquid scintillant in the tank is primarily xylene, containing 0.5 wt.% gadolinium. The scintillations in the tank are viewed by four 58 AVP photomultiplier tubes (P) whose photocathode faces are directly immersed in the liquid.

3. EXPERIMENTAL PROCEDURE

A fission in the chamber is accompanied by three events:

a. the emission of highly ionizing fission fragments in the fission chamber.
b. the emission of prompt fission gamma rays.
c. the emission of ν prompt fission neutrons.

A coincidence between the fragment pulse from the fission chamber and the prompt gamma pulse from the tank is taken as an indication that a fission has occurred. This coincidence pulse opens a 30 microsecond gate to a fast scaler that counts the number of fission neutrons emitted. Most of the prompt fission neutrons enter the scintillation tank and, after many collisions with the hydrogen in the scintillant, are thermalized. The thermalized neutrons diffuse in the liquid and are preferentially absorbed by the gadolinium with a mean time for absorption of 10 microseconds. The fast scaler thus stores the number of gadolinium capture gamma events during a 30 microsecond gate following the fission event.

The fast scaler gate can also be opened by a background sampling pulse, either from a random pulse generator or a periodic generator whose frequency is not synchronized with the LINAC. This precedure samples the number of background counts per gate over the time-of-flight interval.

The data is sorted in a logic-timing circuit and routed to a PDP-7 computer. The computer stores the data in a three dimensional storage array, with 256 time-of-flight channels for each of 12 values of neutron multiplicity (from 0 through 11) for both the fission events and the background events.

4. RESULTS

The value of $\bar{\nu}$ in time-of-flight channel i is given by

$$\bar{\nu}_i = \frac{1}{\epsilon}\left[\frac{\sum_n n(FG)_{n,i}}{\sum_n (FG)_{n,i}} - \frac{\sum_n n(BG)_{n,i}}{\sum_n (BG)_{n,i}}\right]$$

where n is the detected multiplicity, with possible values from 0 to 11

$(FG)_{n,i}$ is the number of fission gates corresponding to a multiplicity n in time-of-flight channel i.

$(BG)_{n,i}$ is the number of background gates corresponding to a multiplicity n in time-of-flight channel i.

ϵ is the overall efficiency of the system for detecting U-235 fission neutrons.

In the U-235 measurement reported here the value of ϵ was found to be 0.660, based on a 2200 meter/sec value of 2.414 for U-235 prompt $\bar{\nu}$.

Figure 2 is a plot of the energy variation of $\bar{\nu}$ for U-235 in the energy range from 1.0 to 0.01 eV, and Fig. 3 a plot of the same quantity determined for each resolved

resonance from 40 to 1.2 eV. The values have been corrected for background events and for accidental coincidences due to alpha particle pile-up in the fission chamber. They have not yet been corrected for dead-time losses in the 10 MHZ fission neutron scaler.

The analysis for the data shown in Figs. 2 and 3 have been carried to the point where nearly all of the possibly important sources of systematic errors have been shown to be insignificant or have been corrected for. A thorough statistical analysis has not as yet been performed with all of the data, but it does appear that these results are consistent with the hypothesis that, to $\pm$ 0.25%, the fission neutron multiplicity induced by neutrons in the energy range from 0.01 to 40 eV has a constant value. However, we now estimate that the application of the dead-time correction would be reflected as an additional 0.1 to 0.2% variation in the observed energy dependence of the neutron multiplicity. Accurate corrections for this effect are now being made.

Recently we have started a cooperative experiment with ORNL to measure $\bar{\nu}$ and α for Pu-239 and U-233. The fission ion chambers have been supplied by Oak Ridge and contain about 1.5 grams of Pu-239 and 1.0 gram of U-233. In these $\bar{\nu}$ experiments we hope to extend the energy range of the measurements to 10 keV and possibly 40 keV.

5. REFERENCES

(1) M. S. Moore and L. G. Miller, "Channel Effects in the Kinetic Energy of Fragments of Fission Induced by Low-Energy Resonance Neutrons," in The Proceedings of the Symposium on Physics and Chemistry of Fission, IAEA, Salzburg, March 22-26, 1965, Vol. I, p. 87.

(2) E. Melkonian and G. K. Mehta, "Variation of Fission Fragment Kinetic Energy Distribution, Mass Distribution, and Yield of Long-Range Alpha Particles in the Resonance Neutron Induced Fission of U-235 and Pu-239," in The Proceedings of the Symposium on Physics and Chemistry of Fission, IAEA, Salzburg, March 22-26, 1965, Vol. II, p. 355.

(3) K. T. Faler and R. L. Tromp, "Variation in U-235 Mass Yields at Neutron Energies Below 0.5 eV," Phys. Rev., Vol. 131 (1963) No. 4, p. 1746.

(4) G. A. Cowan, et al., "Symmetry of Neutron-Induced U-235 Fission at Individual Resonances II," Phys. Rev., Vol. 130 (1963) No. 6, p. 2380.

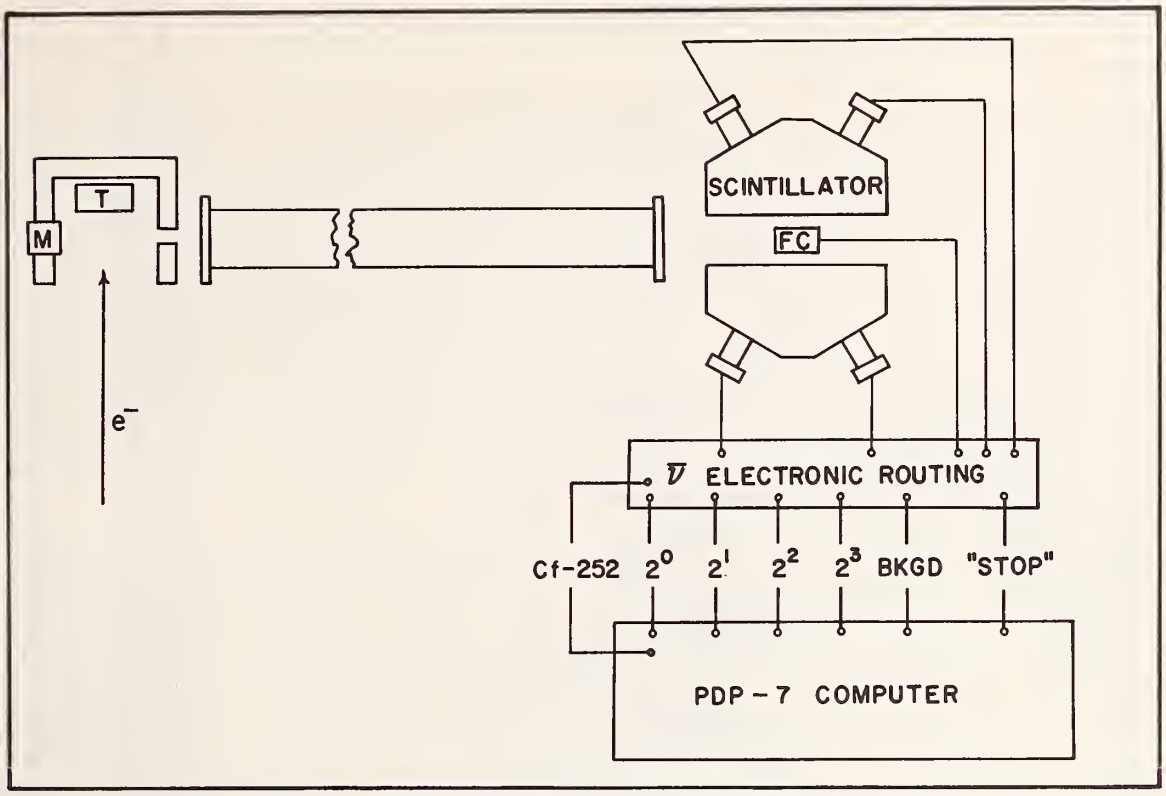

MAJOR COMPONENTS OF $\overline{\nu}$ EXPERIMENT

FIGURE 1

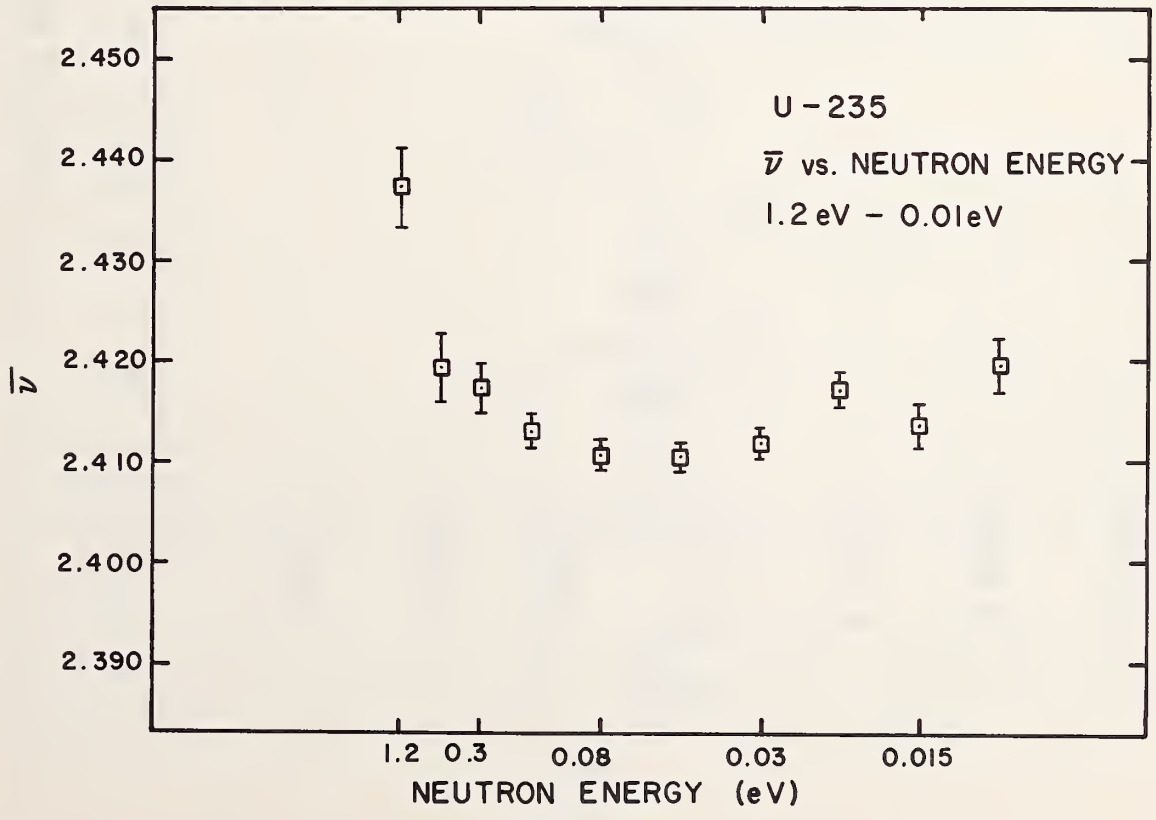

FIGURE 2

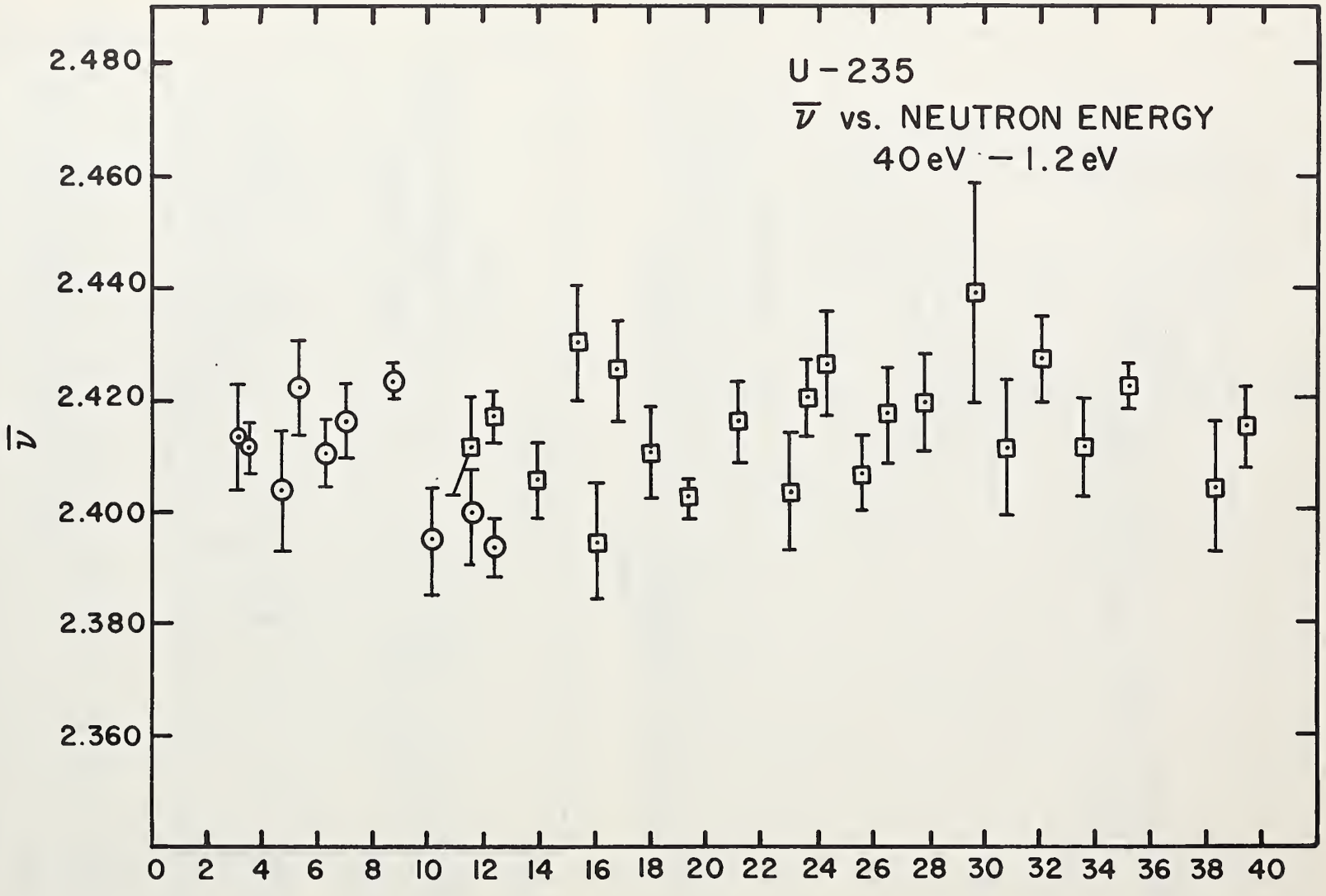
U-235
$\overline{\nu}$ vs. NEUTRON ENERGY
40 eV — 1.2 eV
$\overline{\nu}$
2.480
2.460
2.440
2.420
2.400
2.380
2.360
0 2 4 6 8 10 12 14 16 18 20 22 24 26 28 30 32 34 36 38 40
NEUTRON ENERGY (eV)

FIGURE 3

AUTHOR INDEX